

Preface

The Nineteenth American Peptide Symposium (APS) was held in San Diego, California on June 18-23, 2005. More than 1,000 scientists, accompanying persons, and exhibitors from all over the world attended the conference, and as Editor of the Proceedings of the 19th APS, I am very pleased to share the state-of-the art research projects and ideas that were presented during this event.

The symposium began with a special session focused on protein design co-sponsored by the Protein Society and the American Peptide Society to encourage discussion between two complementary fields of science. For example, the contribution in this book by Dr. Etzkorn on the mechanism of peptidyl-prolyl isomerase clearly shows how short peptides can be used as tools to investigate the biology of larger protein. This session organized by Dr. Jeff Kelly, President-Elect of the Protein Society and co-Chair of the 19th APS was a great success and opened future opportunities for interactions between the two societies.

The increasing active participation of young investigators to the field of peptide research was clearly seen with the outstanding lectures at the Bert Schram Young Investigator mini-symposium sponsored by the Escom Science Foundation and chaired by Dr. John P. Mayer and Dr. Alain Fournier (a number of which are described in this Proceedings), and the large number of poster entries for the Young Investigator's Poster Competition (organized by Dr. DeAnna Long).

As demonstrated by the contributions to this Proceedings, the topics of the Symposium covered cutting-edge research presented by a wide range of distinguished speakers. As outlined by the contribution by Dr. Richard Houghten, recipient of the Merrifield Award, as well as the Goodman Memorial Session, the progresses in peptide and peptidomimetic chemistry are driven by the need to develop novel therapeutics or tools to understand biological natural events. Novel approaches to generate peptides by biological means were also presented at this symposium. Other increasing topics included quorum sensing, post-translational modifications of peptides, peptide quaternary structures in material science and disease, and proteomics.

I wish to thank all authors of the contributions for their efforts and their willingness to participate to this book, and Michael Chorev and Donna Freher-Lyons for their assistance in the preparation of this book. Lastly, I wish to give special thank to my husband and daughter for their support and encouragement in preparing the Proceedings of the 19th American Peptide Symposium

Sylvie Blondelle

Message from the President of the American Peptide Society

The 19th American Peptide Symposium was another successful addition to the American Peptide Society's series of biennial symposia. An international group of 980 registrants from 33 countries contributed to the high quality program that is documented in this volume. Thank you to all of the lecturers and poster presenters for your excellent contributions. Congratulations to co-chairs Jeffery Kelly and Tom Muir along with their staff and the organizing and program committees for a successful meeting. Thank you also to all of our sponsors and exhibitors. And finally, thank you to Past President Roger Freidinger for his oversight of this effort.

The American Peptide Society recognized the achievements of outstanding scientists involved in peptide science through several awards and special sessions at the symposium. Richard Houghten of the Torrey Pines Institute for Molecular Studies was the recipient of the 2005 R. Bruce Merrifield Award, which recognizes outstanding career achievements in peptide science. Richard described his pioneering work on combinatorial chemistry in his lecture "From Tens to Trillions: Advances in Synthetic Combinatorial and Diversity Oriented Methods over the Past 20 Years." Robin Offord of the University of Geneva presented the Makineni lecture, which honors long time peptide science supporter Rao Makineni, and described his research on medicinal chemistry applied to a synthetic protein. The Dr. Bert L. Schram Young Investigators Mini-symposium that started off the meeting on Saturday and the Young Investigators Poster Competition highlighted the accomplishments of young scientists in our field. The Society presented 59 Travel Awards, totaling \$31,000, to young scientists from all over the world so that they could present their research at the symposium. The Murray Goodman Memorial Session honored our good friend and colleague, a leader who influenced our field and the people in it in so many ways – through his research, his mentoring, his service to the Society as President, and as Founding Editor of *Biopolymers (Peptide Science)*. Murray will be greatly missed by his friends and colleagues.

American Peptide Society activities go beyond those at the symposium. American Peptide Society members receive *Biopolymers (Peptide Science)*, the official society journal which publishes both original research and review articles, in print and electronic forms as part of their membership so that they can keep abreast of advances in our field in between symposia. All Society members are invited to submit manuscripts to the journal. The American Peptide Society is now a full member of the Federation of American Societies for Experimental Biology (FASEB). Our membership in FASEB increases the visibility of our Society in the biomedical research community, provides the benefits of FASEB membership to our members and allows our participation in FASEB public affairs initiatives. Other activities and special discounts for Society members are described on the society website www.americanpeptidesociety.com.

We're looking ahead to the 20th American Peptide Symposium that will be held June 26-30, 2007 in Montreal. Co-chairs Emanuel Escher and William Lubell are working hard on assembling an exciting program with the theme "Peptides for

Youth.” I look forward to working with you in American Peptide Society activities and seeing you in Montreal in 2007.

My best wishes for success in your peptide activities!

Jane V. Aldrich
University of Kansas

19th American Peptide Symposium

**June 18-23, 2005
San Diego, California**

Co-Chairs

Jeffery W. Kelly, Ph.D.

Scripps Research Institute
Department of Chemistry, MB 12
10550 N. Torrey Pines Road
La Jolla, CA 92037
jkelly@scripps.edu

Tom W. Muir, Ph.D

Rockefeller University
Synthetic Protein Chemistry Lab
1230 York Avenue, MC 223
New York, NY 10021
muirt@rockvax.rockefeller.edu

Scientific Program Committee

Samuel H. Gellman, Ph.D., University of Wisconsin - Madison

Richard A. Houghten, Ph.D., Torrey Pines Institute for Molecular Studies

Jeffery W. Kelly, Ph.D., Scripps Research Institute

William D. Lubell, Ph.D., University of Montreal

Hisakazu Mihara, Ph.D., Tokyo Institute of Technology

Tom W. Muir, Ph.D., Rockefeller University

Symposium Organizing Committee

Donna M. Freher-Lyons, American Peptide Society

Richard A. Houghten, Ph.D., Torrey Pines Institute for Molecular Studies

Jeffery W. Kelly, Ph.D., Scripps Research Institute

Tom W. Muir, Ph.D., Rockefeller University

Student Affairs Committee

J. Ryan Holder, Ph.D. (Co-Chair) Amgen, Inc.

DeAnna W. Long, Ph.D. (Co-Chair), Peptides International

John Blankenship, University of Montreal

Florence Brunel, Ph.D. The Scripps Research Institute

Audrey Kelleman, University of California, San Diego

Jason Moss, The Scripps Research Institute

Krista Wilson, University of Florida

Mini-Symposium Committee

Alain Fournier, Ph.D. (Co-Chair), INRS - Institute Armand Frappier

John P. Mayer, Ph.D. (Co-Chair), Eli Lilly & Company

J. Ryan Holder, Ph.D., Amgen, Inc.

DeAnna W. Long, Ph.D., Peptides International, Inc.

Travel Grant Committee

Phil Dawson, Ph.D. (Chair), The Scripps Research Institute

David Andreu, Ph.D., Universitat Pompeu Fabra

Alain Fournier, Ph.D., INRS - Institute Armand Frappier

John P. Mayer, Ph.D., Eli Lilly & Company

Marcey L. Waters, Ph.D., University of North Carolina

Volunteer Staff

Maia Carnevali

Aikomari Guzman

Rebecca Harbach

David Hitt

Audrey Kelleman

Ryan Lamer

Kevin Oliver

Becci Perea

Jenni Peterson

Mika Tomioka

Aaron Wohlrab

List of the 19th American Peptide Symposium Sponsors

Platinum Level Sponsor

SynPep Corporation

Gold Level Sponsor

PolyPeptide Laboratories, Inc.

Silver Level Sponsors

Bachem

Eli Lilly & Company

UCB Bioproducts, Inc.

Mercury Level Sponsors

AAPPTeC

American Peptide Company

Amersham Health/GE Healthcare

C S Bio Co.

Cambridge Research Biochemicals

Merck Research Laboratories

Midwest Bio-Tech, Inc.

NeoMPS, INC.

New England BioLabs Inc.

Senn Chemicals USA

Sinopep Pharmaceutical Inc.

Copper Level Sponsors

Amgen, Inc.

Biomol International

Chemicon International Inc.

ESCOM Science Foundation

Genentech

Hoffmann-La Roche Inc.

Novo Nordisk A/S

Peptides International, Inc.

Sussex Research

Synthetech, Inc.

Contributors

Chemistry Today

PharmaChem

RSP Amino Acids LLC

List of the 19th American Peptide Symposium Exhibitors

AAPPTeC	Intavis
Abgent	IRIS Biotech GmbH
AC Scientific, Inc.	Japanese Peptide Society
Activotec Ltd.	John Wiley & Sons
Advanced ChemTech	Jupiter Bioscience Limited
Akzo Nobel / Eka Chemicals	Midwest Biotech Inc.
American Peptide Company	MP BioMedical
American Peptide Society	NeoMPS (Groupe SNPE)
AnaSpec, Inc.	Peptides International, Inc.
Australian Peptide Association	Peptisyntha, Inc.
BACHEM	Polymer Laboratories, Ltd.
Bentham Science Publishers Ltd.	PolyPeptide Laboratories, Inc.
BioBlocks Inc.	Protein Society
Bio-Synthesis, Inc.	Protein Technologies, Inc.
C S Bio Co.	Rapp Polymere GmbH
C.A.T GmbH & Co.	Roche Colorado
Cambridge Research Biochemicals	Rohm and Haas Company
CBL-PATRAS SA	Senn Chemicals USA
CEM Corporation	SciGene
Chem Impex	Sigma Aldrich
CPC Scientific, Inc.	Springer
Elim Biopharmaceuticals, Inc.	SynPep Corporation
EMD Chemicals Inc.	Synthetech, Inc.
EMD Biosciences, Inc.	Tianjin Nankai Hecheng Sci.
European Peptide Society	& Tech. Co., Ltd.
Fluorous Technologies, Inc.	UCB Bioproducts SA
Genzyme Pharmaceuticals	VersaMatrix A/S
Georg Thieme Verlag KG	Waters Corporation
GL Biochem (Shanghai) Ltd.	YMC Co., Ltd. /
Global Peptide Services, LLC	Seika Corporation of America

The American Peptide Society

The American Peptide Society (APS), a nonprofit scientific and educational organization founded in 1990, provides a forum for advancing and promoting knowledge of the chemistry and biology of peptides. The approximately one thousand members of the Society come from North America and from more than thirty other countries throughout the world. Establishment of the American Peptide Society was a result of the rapid worldwide growth that has occurred in peptide-related research, and of the increasing interaction of peptide scientists with virtually all fields of science.

The American Peptide Society is a Sustaining Associate Member of the Federation of American Societies for Experimental Biology (FASEB). Our affiliation with FASEB increases the visibility of our Society in the biomedical research community and allows our participation in any FASEB public affairs initiatives.

Biopolymers (Peptide Science) is the official journal of the American Peptide Society. A full year subscription to this journal is automatically included with membership in the APS. The journal publishes both original articles and reviews covering all aspects of peptide science. Eminent peptide scientists Lila Gierasch and Charles Deber serve as the journal editor and current trends editor, respectively, and they welcome your manuscript submissions. Members also have free access to the Society's continually evolving web site where the latest information on American Peptide Society activities and developments in peptide science may be found. Free professional position and resume posting is offered at the site. Membership in the American Peptide Society is open to scientists throughout the world who are interested in the chemistry or biology of peptides and small proteins. The American Peptide Society strongly believes in supporting the young scientists entering our field. Reduced membership rates for students and postdoctoral fellows are provided. Information on the American Peptide Society is available at the society website www.americanpeptidesociety.com.

American Peptide Symposia

Symposium Year	Chair (s)	Location
1st 1968	Saul Lande <i>Yale University</i> Boris Weinstein <i>University of Washington-Seattle</i>	Yale University New Haven, CT
2nd 1970	F. Merlin Bumpus <i>Cleveland Clinic</i>	Cleveland Clinic Cleveland, OH
3rd 1972	Johannes Meienhofer <i>Harvard Medical School</i>	Children's Cancer Research Foundation, Boston, MA
4th 1975	Roderich Walter <i>University of Illinois Medical Center – Chicago</i>	The Rockefeller University and Barbizon Plaza Hotel New York, NY
5th 1977	Murray Goodman <i>University of California San Diego</i>	University of California - San Diego, San Diego, CA
6th 1979	Erhard Gross <i>National Institutes of Health</i>	Georgetown University Washington, DC
7th 1981	Daniel H. Rich <i>University of Wisconsin- Madison</i>	University of Wisconsin- Madison, Madison, WI
8th 1983	Victor J. Hruby <i>University of Arizona</i>	University of Arizona Tucson, AZ
9th 1985	Kenneth D. Kopple <i>Illinois Institute of Technology</i> Charles M. Deber <i>University of Toronto</i>	University of Toronto Toronto, Ontario, Canada
10 th 1987	Garland R. Marshall <i>Washington University School of Medicine</i>	Washington University St. Louis, MO
11 th 1989	Jean E. Rivier <i>The Salk Institute for Biological Studies</i>	University of California-San Diego, San Diego, CA
12 th 1991	John A. Smith <i>Massachusetts General Hospital</i>	Massachusetts Institute of Technology, Cambridge, MA
13 th 1993	Robert S. Hodges <i>University of Alberta-Edmonton</i>	Edmonton Convention Center Edmonton, Alberta, Canada
14 th 1995	Pravin T.P. Kaumaya <i>The Ohio State University</i>	The Ohio State University Columbus, OH
15 th 1997	James P. Tam <i>Vanderbilt University</i>	Nashville Convention Center Nashville, TN
16 th 1999	George Barany <i>University of Minnesota</i> Gregg B. Fields <i>Florida Atalantic University</i>	Minneapolis Convention Center Minneapolis, MN
17 th 2001	Richard A. Houghten <i>Torrey Pines Institute for Molecular Studies</i>	Town and Country Resort Hotel San Diego, CA

18 th	2003	Michal Lebl <i>Spyder Instruments and Illumina</i>	Marriott Copley Place Boston, MA
		Michael Chorev <i>Beth Israel Deaconess Medical Center</i>	
19 th	2005	Tomi K. Sawyer <i>ARIAD Pharmaceuticals</i>	Town and Country Resort Hotel San Diego, CA
		Jeffery Kelly <i>Scripps Research Institute</i>	
		Tom Muir <i>Rockefeller University</i>	

The Merrifield Award

Endowed by Rao Makineni (1997)

Sponsored by the Pierce Chemical Company (1977-1995)

Richard A. Houghten



Dr. Richard A. Houghten, founder and President of Torrey Pines Institute for Molecular Studies, received his doctorate in organic chemistry from the University of California, Berkeley, in 1975. Following positions at the University of California, San Francisco, and Mount Sinai School of Medicine, he joined the Scripps Research Institute in 1981. Torrey Pines Institute for Molecular Studies began operations in 1989 with eight employees. Now in its 17th year, it has become internationally recognized for its scientific contributions in a wide range of fields, including chemistry, multiple sclerosis, diabetes, immunology, infectious disease, heart disease, cancer vaccines and pain management. The

institute has grown to include over 65 scientists, technicians and administrative staff, all of whom work in an environment that emphasizes personal and professional growth by encouraging the development of independent research ideas as well as the development of collaborative efforts with scientists throughout the world. Dr. Houghten's scholarly contributions include over 500 publications and 60 issued patents. He also founded the journal, *The Journal of Peptide Research* and is active on several other editorial boards.

In addition to Torrey Pines Institute for Molecular Studies, Dr. Houghten founded three commercial businesses, one of which became a publicly-traded biotechnology company. His achievements have been recognized in the form of numerous honors and awards. Most recently, his contribution to the field of peptide science was acknowledged by the 2004 Ralph F. Hirschmann Award in Peptide Chemistry. Other honors received include the Vincent du Vigneaud Award for Excellence in Peptide Science (2000) and the UCSD Connect Athena Pinnacle Award for Empowering Women in the Workplace. His acceptance of the Athena Pinnacle Award in 1999 further distinguishes Dr. Houghten and his dedication to the mentoring and advancement of women scientists in the work place.

Dr. Houghten's scientific contributions include the "tea bag" approach, which was originally utilized to facilitate the synthesis of peptides. The tea bag method, in which solvent permeable packets are used during the synthesis process, has now resulted in not only the synthesis of millions of peptides, but also the synthesis of millions of low molecular weight compounds. In collaboration with his long time associates and colleagues at Torrey Pines Institute for Molecular Studies, he has also developed approaches in combinatorial chemistry which are invaluable for the rapid identification of individual compounds from millions to billions of others (positional

scanning), the use of existing combinatorial libraries to generate entirely new diversities of compounds (libraries from libraries), the cross-referencing of library screening results with gene data bases in order to fine-tune the direction towards which further testing moves for a given disease target (biometrical analysis), and novel volatilizable solid supports.

2005 – Richard A. Houghten, Torrey Pines Institute for Molecular Studies

2003 – William F. DeGrado, University of Pennsylvania, School of Medicine

2001 – Garland R. Marshall, Washington University Medical School

1999 – Daniel H. Rich, University of Wisconsin – Madison

1997 – Shumpei Sakakibara, Peptide Institute, Inc.

1995 – John M. Stewart, University of Colorado – Denver

1993 – Victor J. Hruby, University of Arizona – Tucson

1991 – Daniel F. Veber, Merck Sharp & Dohme, Inc.

1989 – Murray Goodman, University of California, San Diego

1987 – Choh Hao Li, University of California, San Francisco

1985 – Robert Schwyzler, Swiss Federal Institute of Technology

1983 – Ralph F. Hirschmann, Merck Sharp & Dohme, Inc.

1981 – Klaus Hofmann, University of Pittsburgh, School of Medicine

1979 – Bruce Merrifield, The Rockefeller University

1977 – Miklos Bodansky, Case Western Reserve University

The Makineni Lecture Award

Endowed by PolyPeptide Laboratories, Inc., and Murray and Zelda Goodman
Sponsored by the American Peptide Society

Robin E. Offord



Professor E. Robin Offord began in nuclear physics but soon changed to biology. He first worked at the Medical Research Council Laboratory, Cambridge, U.K. (1962-1966), in the group Frederick Sanger where he obtained his Doctorate and collaborated with, among others, César Milstein and Aaron Klug. He taught and researched at Oxford from 1966 – 1980 (University Lecturer in Molecular Biophysics, Tutor, Christ Church), when he left to become Director of the Département de Biochimie Médicale at Geneva. He was also

President of Basic Medicine in Geneva from 1994 to 2000. Prof. Martin Rodbell (Nobel Prize 1994) was a visiting member of his group for two years in the early 1980s. In 2004 he became the founding Director of a new Department in the Medical Faculty, the Department of Structural Biology and Bioinformatics. Prof. Offord has written, co-authored, or edited 6 books and is the author or co-author of 180 published scientific papers, mainly in various fields of protein science. He is co-inventor on several granted Patents.

Prof. Offord was one of the pioneers of the technique of protein semisynthesis. He was responsible for the first of the so-called anti-HIV “fusion inhibitors” and building on this he and his colleagues have designed and made a series of semisynthetic and synthetic proteins which are among the most powerful anti-HIV substances currently known. One of them is the first to give full protection against infection in macaques. His Geneva research group receives support from the United States National Institutes of Health for this work as an overseas applicant, as well as support from the Swiss Government.

Prof. Offord has been adviser to governments in several countries, and to international organizations. He is currently adviser to the Netherlands Government on proteomics, to the UN International Trade Centre, and a member of the Geneva government’s Council for Regional Economic Development. He has been a Journal Managing Editor, member of many Editorial Boards and has consulted for many major pharmaceutical and biotechnology firms. He has been a co-founder of a number of start-ups. He was a co-founder of the Swiss Institute for Bioinformatics and is Chairman of the Advisory Board of Eclosion, Geneva’s new life-sciences incubator. He shared the “Man of the Year 2002” award of the Swiss financial newspaper ‘L’agefi’. He is Secretary of the American Peptide Society.

Achievement Award for Scientific and Administrative Excellence

The American peptide Society initiated this new award in 2005 to recognize and honor those who have made outstanding scientific and administrative contributions in the promotion and advancement of research in peptide science that resulted in the advancement of public health.

Rao S. Rapaka

Dr. Rao S. Rapaka was recognized for the depth of his range of scientific knowledge of the neuro-biochemistry of peptide science and his twenty-five years of continuous contributions to organizing dozens of mini-symposia, review articles, and focused journal special editions in this field.

Dr. Rapaka received his training in medicinal and peptide chemistry in the laboratories of a number of leading scientists including Professors Eugene Jorgensen (University of California) and Dan W. Urry (University of Alabama Medical Center). His research career started with a study of the role of stereochemical factors that influence the pressor activity of angiotensin via the synthesis and structure-activity relationships of strategically designed analog of angiotensin II. He showed the critical part that stereochemical factors played on the conformation of the peptide chain. This early success laid the foundation for many of his other significant contributions to important peptides. For example, Dr. Rapaka demonstrated that hydroxylation was a very critical step for the stability and activities of collagen polypeptides. Upon studying analogs of the protein elastin, Dr. Rapaka demonstrated that coacervation was due to hydrophobic interactions between certain amino acid side chains. Using Fourier Transform-Infrared methods, not only he showed the β -turn and β -sheet conformations of enkephalins but he also found that ethanol abolishes these conformations for [Met⁵]-enkephalinamide, thus abolishing the opioid receptor recognition for μ - and δ -receptor interaction.

The breadth of his contributions is exemplified in over 100 publications and 18 research monographs. Through his long tenure at the NIH Dr. Rapaka has initiated a large number of grants and research contracts in organic syntheses and medicinal chemistry, and promoted new research areas and technologies enhancing both medicinal chemistry and drug discovery. Furthermore, Dr. Rapaka administers a National program of "Drug Supply and Related Research Services" and manages a medicinal chemistry program at NIDA. His current areas of interest are lipid maps and isolation of new bioactive endogenous lipid ligands.

Peptide Society Travel Grants

The Travel Award Committee's mission was to administer financial support for travel and housing expenses in order to provide a broad opportunity for young investigators to participate in a major scientific event, meet leaders and colleagues in the field, and present their research projects to the scientific community.

Awardees:

Kalpana Bhargara (University of North Carolina)
Damien R. Boeglin (University of Montreal)
Malene Brandt (Royal Veterinary & Agriculture University)
James P. Cain (University of Arizona)
Andrea Caporale (University of Padova)
Pradip Chakraborty (University of Gottingen)
Arvind K. Chappa (University of Kansas)
Jeffrey D. Copps (Creighton University)
Sonya Cressman (University of British Columbia)
Nadia J. Edwin (Louisiana State University)
Marcus A. Etienne (Louisiana State University)
Wei-Jie Fang (University of Kansas)
Fabrice Galaud (University of Montreal)
Sharon Gilead (Tel Aviv University)
Krisztina Heredi-Szabo (Creighton University)
Frank W. Kotch (University of Wisconsin-Madison)
Vinod V. Kulkarni (University of Arizona)
Ulrike Kusebauch (Max Planck Institute of Biochemistry)
Teresa Lama (University of Naples Federico II)
Mian Liu (University of Minnesota)
Erica S. Lovelace (University of Queensland)
Luciana Malavolta (Universidade Federal de Sao Paulo)
Chris R. Manz (Duke University)
Fernanda F. Marques (University of Michigan)
Larry R. Masterson (University of Minnesota)
Remco Merckx (Utrecht University)
Christopher M. Micklitsch (University of Delaware)
Byoung J. Min (University of Arizona)
Barbara Mulinacci (University of Florence)
Michael C. Owen (Creighton University)
Ilaria Paoloini (University of Florence)
Angela Peck (University of Kansas)
Ravil R. Petrov (University of Arizona)
Magdalena J. Przydzial (University of Michigan)
Beili Quan (Indiana University at Bloomington)
Karthikan Rajagopal (University of Delaware)
Soumendra Rana (Indian Institute of Technology, Bombay)
Cesar Manuel Remuzgo Ruiz (University of Sao Paulo)
Rebecca A. Roof (University of Michigan)

Deborah M. Rothman (Massachusetts Institute of Technology)
Ronak Rughani (University of Delaware)
Giuseppina Sabatino (University of Florence)
Lillian Sando (University of Queensland)
Rajesh Sankaranarayanan (University of Arizona)
Yu Tian (Center of Advanced Biotechnology & Medicine)
Aleksandar Todorovic (University of Florida)
Simona Tomaselli (University of Naples Federico II)
Isabelle van den Eynde (Vrije Universiteit Brussel)
Karolien van Rompaey (Vrije Universiteit Brussel)
Dirk-Jan van Zoelen (Utrecht University)
Miquel Vila-Perello (Universitat Pompeu Fabra)
Aude Violette (CNRS – IBMC, Strasbourg)
Xin Wang (University of Kansas)
Jia Wang (Louisiana State University)
John K. Whitehead (Louisiana State University)
Ekaphol Wooden (University of Arizona)
Weiming Xu (Rutgers University)
Tatyana V. Yakovlev (University of Kansas)
Hailin Zheng (Weizmann Institute of Science)

Bert Schram Young Investigators' Mini-Symposium

The Bert Schram Young Investigator Mini-Symposium was the opening session of the meeting and as in previous years was generously supported by ESCOM Science Foundation. The session was chaired by John Mayer (Eli Lilly) and Alain Fournier (University of Quebec).

We were fortunate to have an excellent selection of graduate students as well as postdoctoral fellows from the world-wide peptide community. In the spirit of the symposium the speakers were chosen to reflect the diverse scientific disciplines within the peptide community. First Place was awarded to Matthew Hartmann (Massachusetts General Hospital/Harvard Medical School), Second Place (a tie) to Deborah Rothman (MIT) and Florence Brunel (Scripps Research Institute) and Honorable Mention to Barbara Mulinacci (University of Florence). We wish all participants continued success in their careers.

Participants

John Blankenship (University of Montreal)
Florence Brunel (The Scripps Research Institute)
Jaimes Cain (University of Arizona)
Luis J. Cruz (University of Barcelona)
Christina Foerg (Swiss Federal Institute of Technology Zurich)
Evgenia Glukhov (Hospital of Sick Children Toronto)
Matthew Hartmann (Massachusetts General Hospital/Harvard Medical School)
Remco Merckx (Utrecht University)
Barbara Mulinacci (University of Florence)
Beili Quan (Indiana University)
Karthikan Rajagopal (University of Delaware)
Deborah Rothman (Massachusetts Institute of Technology)
Miquel Vila-Perello (Universitat Pompeu Fabra)
Hope Wilson (California Alliance for Minority Participation)
David Zoeteway (University of Guelph)

Young Investigators' Poster Competition

On behalf of the Student Affairs Committee, we would like to thank all the people involved with the Young Investigator Poster Competition held at the 19th American Peptide Symposium. This year's Young Investigator Poster Competition featured over 60 poster presentations. We would like to send a special thank you to our sponsor, CS Bio, the volunteer judges, and the Symposium organizing committee for the 19th APS. Thank you to all the students and post-doctoral associates for their participation and for their excellent presentations to make this event a success. On behalf of the American Peptide Society, Congratulations to all of our winners!

Award Winners

First Place:

Melissa Shults (Massachusetts Institute of Technology - B. Imperiali)

Second Place:

Dirk-Jan van Zoelen (Utrecht Institute for Pharmaceutical Sciences - R.M.J. Liskamp)

Third Place:

Brian Lohse (Riso National Laboratory - R. Berg)
Justin Murray (University of Wisconsin - S. Gellman)
Ronak Rughani (University of Delaware - J. Schneider)

Honorable Mention:

Pradip Chakraborty (Institute for Organic and Biomolecular Chemistry - U. Diederichsen)
Marcus Lynch (Ohio State University - Pravin Kaumaya)
Hinke Malda (Eindhoven University of Technology - T. Hackeng)
Christopher Micklitsch (University of Delaware - J. Schneider)
Audrey Kelleman (University of California San Diego - M. Goodman and M.S. Van-Nieuwenhze)
Michael Owen (Creighton University Medical Center – S. Lovas)
Krista Wilson (University of Florida- C. Haskell-Luevano)

We give a BIG thank you to over 30 volunteer judges for the mini-symposium and poster competition who generously donated their time and expertise during the competition.

Judges:

Jungmo Ahn	Robert P. Hammer	Maria Kempe
Michael Carrasco	Jie Han	Michal Lebl
Ralph Casale	Deborah L. Heyl-	William Lubell
Krys Darlak	Clegg	Claudio Mapelli
Jesse Dong	Thomas Hoeg-Jensen	John McMurray
Alain Fournier	Ryan Holder	Hisakazu Mihara
Paolo Grieco	Pravin T.P. Kaumaya	Yuji Nishiuchi

Laszlo Otvos
Annamaria Papini
David Perrin
Christian Renner

Paolo Rovero
Mark Spaller
Kripa Srivastava
Wilfred van der Donk

Sandy Vigil Cruz
Cody, Wayne
Liang Zeng Yan

Abbreviations

μ	hydrophobic moment	AGRP	Agouti-related protein
[θ]	mean residue ellipticity	AHL	N-acylhomoserine lactone
A	active site	Aib	α -aminoisobutyric acid
$\alpha\alpha$ AAs	C $^{\alpha,\alpha}$ -disubstituted amino acids	AIDS	acquired immune deficiency syndrome
aa	amino acid	Alloc	allyloxycarbonyl
AAA	amino acid analysis	AMBER	assisted model building and energy refinement
Aad	α -aminohexanedioic acid	AMC	amino-4-methyl coumarin
AAH	amphiphilic α -helix	AMPs	antimicrobial peptides
A β	amyloid β -protein; amyloid β -peptide	AMPB	(4-aminomethyl)phenylazobenzoic acid
Ab7	2-amino-7-bromoheptanoic acid		
Aba	4-amino-1,2,4,5-tetrahydro-2-benzazepine-3-one	AMPP	[3-(3-aminomethyl-phenylazo)-phenyl]-acetic acid
Abc	4'-aminomethyl-2,2'-bipyridine-4-carboxylic acid	AN	electron acceptor
ABP	arterial blood pressure	Ang	angiotensin
ABPP	activity-based protein profiling	Ang II	angiotensin II
Abu	\square -amino- <i>n</i> -butyric acid	ANPP	4-anilino- <i>N</i> -phenethyl-piperidine
Abz	o-aminobenzoyl	AnV	Annexin-A5
AC	adenyl cyclase	Aoe	2-amino-8-oxo-9,10-epoxy decanoic acid
Ac	acetyl; acyl		
Aca	adamantanecarboxyl-; ϵ -amino acaproic acid	APB	(4-amino)phenylazobenzoic acid
ACAB	4,4'-azobenzene-dicarboxylic acid-(4-iodo-but-2-ynyl)-bis-amide	APC	antigen presenting cell
ACC	adrenocortical carcinoma; 7-amino-4-carbamoylmethylcoumarin	4Aph	4-aminophenylalanine
Ac5c	1-aminocyclopentane carboxylic acid	Apo A-I	apolipoprotein A-I
Ac $_n$ c	1-aminocycloalkane-1-carboxylic acid	ApoCaM	Ca-free calmodulin
ACE	angiotensin-converting enzyme	APP	amyloid β -precursor protein
Ach	1-amino-1-cyclohexane carboxylic acid	APX	ascorbate peroxidase
Acm	acetamidomethyl	Aq.	aqueous
ACN	acetonitrile	AR	anomalous reflection
ACP	acyl carrier protein	Ar	aromatic residue
Acpc	1-aminocyclopropane-1-carboxylic acid	ARDS	acute respiratory distress syndrome
ACTH	adrenocorticotropin; adrenocorticotrophic hormone	Asu	2-amino suberic acid
AD	Alzheimer's disease	ASP	agouti signal protein
Ad	adenovirus	AT $_1$	Ang II receptor
Adc	10-aminodecanoic acid	aTc	anhydrotetracycline
ADCC	antibody dependent cell-mediated cytotoxicity	ATCC	American Type Culture Collection
ADNP	activity-dependent neuroprotective protein	ATL	adult T-cell leukemia
Ae9	2-amino-9-alkenoic acid	Atmp	4-amino-2,2,6,6-tetramethylpiperidine
AEM	affinity enhancing motifs	ATP	adenosine triphosphate
Aens	2-amino-(<i>n</i> -1)-alkenoic acids	ATR-IR	attenuated total reflection infra red spectroscopy
AFM	atomic force microscopy	AUC	area under the curve
Agl	aminoglycine	AVP	arginine vasopressin
		BAL	backbone amide linker
		BBB	blood brain barrier
		Bbs	4-tert-butyl-benzenesulfonyl
		BD	healthy blood donor serum; blood donors

BEMP	2-tert-butylimino-2-diethylamino-1,3-dimethylperhydro-1,3,2-diazaphosphorine	Cit	2-amino-5-ureido-n-valeric acid
BHI	brain heart infusion	CLEAR	cross-linked ethoxylate acrylate resin
BHQ	Black Hole Quencher	CLL	chronic lymphocytic leukemia
BIA	biospecific interaction analysis	CM	chloroform-methanol
Biot	biotinyl	CN	cinchonine
Bip	biphenylalanine, 4-phenyl-phenylalanine; β -(4-biphenyl)alanine	CNBr	cyanogen bromide
BK	bradykinin	CNS	central nervous system
BNP	brain natriuretic peptide	Col	collagen
Boc; <i>t</i> Boc	<i>tert</i> -butoxycarbonyl	COSY	correlated spectroscopy
Bom	benzyloxymethyl	CoV	coronavirus
BOP	(benzotriazol-1-yloxy)-tris(dimethylamino)phosphonium hexafluorophosphate; benzotriazolylloxy-hexamethylphosphoramidate	CPDs	cyclobutane pyrimidine dimers
Bpa	<i>p</i> -benzoylphenylalanine	CpG	α -cyclopentylglycine
BSA	bovine serum albumin	CPP	cell penetrating peptide
BTC	bis(trichloromethyl)carbonate	cPPL	crude porcine pancreatic lipase
BTX	batrachotoxin	CPWR	coupled plasmon waveguide resonance
tBu	<i>t</i> -butyl	CRDs	cysteine-rich domains
Bz	benzoyl	CRPs	collagen-related peptides
Bzl	benzyl	CsA	Cyclosporin A
CaM	calmodulin	CSD	chemical shift deviation
CAMM	computer assisted molecular modeling	CSI	chemical shift indice; chemical shift index
cAMP	cyclic adenosine-3',5'-monophosphate	CSPG	chondroitin sulfate proteoglycan
CAMs	constitutively active mutants	CTC	chlorotrityl chloride
CAR	coxackie-adenovirus receptor	CTF	C-terminal fragment
CBD	chitin binding domain	CTL	cytotoxic T-lymphocyte
Cbm	carbamoyl	CVFF	consistent valence force field
Cbz	carbobenzyloxy; benzyloxycarbonyl	2D	two dimensional
CCK	cyclic cystine knot; cholecystokinin	3D	three dimensional
CCR	CC chemokine receptor	DA	dopaminergic
CD	circular dichroism; cinchonidine	Da	Dalton
c3diPhe	1-amino-c-2,t-3-diphenylcyclopropane-r-1-carboxylic acid	Dab	2,4-diaminobutyric acid
CD ₃ OH	methan- <i>d</i> ₃ -ol	DabcyI	(4-[4-(dimethylamino)phenylazo]benzoyl (D-Ala ² , MePhe ⁴ , Gly-ol ⁵)enkephalin; H-Tyr-D-Ala-Gly-NMePhe-Gly-ol
CE	capillary electrophoresis	DAMGO	2,3-diaminopropionic acid
CecB2	cecropin B2	Dap; DAP	4',6-diamidino-2-phenylindole
CF	5(6)-carboxyfluorescein	DAPI	diaminosuberlic acid
CFDA	carboxyfluorescein diacetate	DAS	dibenzyl glycine
cfu	colony forming units	Dbzg	1,8-diazabicyclo[5.4.0]-undec-7-ene
CGRP	calcitonin gene related peptide	DBU	N,N'-dicyclohexylcarbodiimide
Cha	cyclohexylalanine	DCC	dichloromethane
Chg	α -cyclohexylglycine	DCM	1-(4,4-dimethyl-2,6-dioxocyclohexylidene)ethyl
CHL	cholesterol	Dde	DNA-directed immobilization
CHO	Chinese hamster ovary	DDI	diethylamine
CHROBA	chromism-based assay	DEA	diethyl azodicarboxylate
cHx	cyclohexyl	DEAD	diethylglycine
		Deg	P1R lacking EC
		deINT-P1R	desferal
		DFO	deuteroheamin-His-peptides
		DhHP	3-(2,6-dimethyl-4-hydroxyphenyl)-propanoic acid
		Dhp	

DIAD	diisopropyl azodicarboxylate	DSC	differential scanning calorimetry; N,N-disuccinimidyl carbonate
Dibal-H	diisobutylaluminum hydride	DSLET	H-Tyr-D-Ser-Gly-Phe-Leu-Thr-OH
Dibg	diisobutylglycine	DTNP	2,2 dithiobis(5-nitropyridine)
DIC, DIPCDI	N,N'-diisopropyl carbodiimide	DTPA	N,N-bis[2-[bis(carboxyethyl)amino]ethyl]; diethylene triaminepentaacetic acid
DIEA, DIPEA	N,N-diisopropylethylamine	Dts	dithiasuccinoyl
DKP	2,5-diketopiperazine	DTT	dithiothreitol
DLS	dynamic light scattering	Dyn	dynorphin
DM	dodecyl maltoside		
Dmab	4{N-[1-(4,4-dimethyl-2,6-dioxo-cyclohexylidene)-3-methylbutyl]-amino} benzyl	E	exosite
DMAP	N,N-dimethylaminopyridine	EADI	(<i>E</i>)-alkene dipeptide isostere
DMB	2,4-dimethoxybenzyl	EC	N-terminal extracellular domain
DME	dimethoxyethane, glyme	EC ₅₀	50% effective concentration
DMEM	Dulbecco's modified Eagle's medium	ECD	extracellular domain; electronic circular dichroism
DMF	N,N-dimethylformamide	ED ₅₀	median effective dose
Dmmb	2-mercapto-4,5-dimethoxy benzyl	Eda	ethylenediamine; enediyne amino acid
DMP	Dess-Martin periodinane	Edans;EDANS	5-[(2'-aminoethyl)amino] naphthalenesulfonic acid
dmpa	dimethoxyphenylacetyl	EDC	1-(3-dimethylaminopropyl)-3-ethyl carbodiimide hydrochloride
DMPC	1,2-dimyristoyl- <i>sn</i> -glycero-3-phosphocholine; dimyristoyl phosphatidylcholine	EDL	extensor digitorum longus
DMPG	1,2-dimyristoyl- <i>sn</i> -glycero-3-[phospho-rac-(1-glycerol)]; dimyristoyl phosphatidylglycerol	EDT	1,2-ethanedithiol
DMS	dimethyl sulfide	EDTA	ethylenediamine-tetraacetic acid
DMSO	dimethyl sulfoxide	ee	enantiomeric excesses
DMT, Dmt	2',6'-dimethyltyrosine	EGF	epidermal growth factor
DMT-MM	4-(4,6-dimethoxy-1,3,5-triazin-2-yl)-4-methylmorpholinium chloride	EGFP	enhanced green fluorescent protein
DN	electron donor	EGFR	EGF receptor
DNA	deoxyribonucleic acid	ELISA	enzyme linked immunosorbance assay
Dnp, DNP	2,4-dinitrophenyl	EM	electron microscopy
DOPC	dioleoyl-DL-3-phosphatidylcholine	EMSA	electrophoretic mobility shift assays
DOR	δ-opioid receptor	eNOS	endothelial nitric oxide synthase
DOTA	1,4,7,10-tetraazacyclododecane-N,N',N'',N'''-tetraacetic acid	Env	envelope glycoprotein
DPDPE	cyclo[D-Pen2,D-Pen5]enkephalin	Eoc	ethoxycarbonyl
DPH	phenytoin	ePC	egg yolk phosphatidylcholine
DPhPC	diphytanoyl phosphatidylcholine	EPL	expressed protein ligation
DPLCE	D-Pen2, Cys4 enkephalin	EPO	erythropoietin
DPPA	diphenylphosphoryl azide	EPR	electron paramagnetic resonance
DPPC	1,2-dipalmitoyl- <i>sn</i> -glycero-3-phosphatidylcholine	eq	equivalent
DPPG	dipalmitoyl phosphatidylglycerol	ES	electrospray
DPPIV	dipeptidyl amino peptidase IV	ES-MS	electrospray mass spectrometry
DPPS	dipalmitoyl phosphatidylserine	ESI	electrospray ionization
Dpr	diaminopropionic acid	ESI-MS	electrospray ionization mass spectrometry
DQF-COSY	double-quantum filtered-correlated spectroscopy	ESR	electron spin resonance
		ET3N	triethylamine

EtOH	ethanol	GnRH	gonadotropin-releasing hormone
EtSH	ethyl sulfide	GPCR	G-protein-coupled receptor
F5c	2,3,4,5,6-pentafluorocinnamoyl	GPC	gel permeation chromatography
FACS	fluorescence-activated cell sorting	GPI	guinea pig ileum
FAD	familial Alzheimer's disease	Grb2	growth factor receptor-bound protein 2
FAF	familial amyloidosis-Finnish type	GRF	growth hormone releasing factor
FAM	carboxyfluorescein	GRPs	glycine-rich proteins
FBS	fetal bovine serum	GSH	reduced glutathione
FGF	fibroblast growth factor	GSSG	oxidized glutathione
FIB	focused ion beam	GSTI	glutamine synthetase
FITC	fluorescein isothiocyanate	GTP	translational inhibitor
FKBP	FK506 binding protein	GTT	guanosine triphosphate
Flu	fluorescein 5-carboxyl		glucose tolerance test
Fmc	fluorenyl-9-methylcarbonyl	HA	hemagglutinin
fMLP	formyl-Met-Leu-Phe	HABA	4'-hydroxyazobenzene-2-carboxylic acid
Fmoc	9-fluorenylmethoxycarbonyl	HAP	histo-aspartic protease
FN	fibronectin	HAT	histone acetyl transferase
Fol	1,2 aminoalcohol	hAT1	human angiotensin II type 1
FP	phenylalaninol	HATU	<i>N</i> -[(dimethylamino)-1 <i>H</i> -1,2,3-triazolo[4,5- <i>b</i>]pyridin-1-yl-methylene]- <i>N</i> -methylmethanaminium hexafluoro phosphate <i>N</i> -oxide
FPLC	fusion peptide		hemoglobin
FPP	Fast Performance Liquid Chromatography	Hb	<i>O</i> -benzotriazolyl- <i>N,N,N',N'</i> -tetramethyluronium hexafluoro phosphate; <i>N</i> -[1 <i>H</i> -benzotiazol-1-yl-(dimethylamino)methylene]- <i>N</i> -methylmethanaminium hexafluoro phosphate- <i>N</i> -oxide
FPR	farnesyl diphosphate	HBV	hepatitis B virus
FRB	formyl peptide receptor	HCV	hepatitis C virus
FRB	FKBP-rapamycin binding domain	Hcy	homocysteine
FRET	fluorescence resonance energy transfer	HDAC	histone deacetylase
Fsa	Fourier-transform ion cyclotron resonance	HDL	high-density lipoprotein
FTICR	Fourier transform infrared	HDX	hydrogen/deuterium exchange
FTIR		HE	high exhaustion
gA	gramicidin; gramicidin A	HEK	human embryonic kidney
GA	gibberellin	HER	human epidermal growth factor receptor
Gal	galactose	HF	hydrogen fluoride
GAS	group A streptococcal	HFA	hexafluoroacetone
gB	glycoprotein B	HFIP	hexafluoroisopropanol
Gd(III)DTPA	gadolinium(III)	HG	human gastrin
	diethylenetriamine pentaacetic acid	HGP	hairless guinea pig
GdnHCl	guanidinium hydrochloride	HI	human insulin
GFC	gel filtration chromatography	hIAPP	human islet amyloid polypeptide
GFP	green fluorescent protein	HIF-1 α	hypoxia inducible factor 1 α
GGPP	geranylgeranyl diphosphate	hIL-8	human interleukin 8
GH	growth hormone	HIV	human immunodeficiency virus
GHRP	growth hormone-releasing peptide	HIP	heparin interacting protein
GHS	growth hormone secretagogue	HLA	human leukocyte antigen
GI	gastro-intestinal		
GIF	growth inhibition factor		
GlcNAc	<i>N</i> -acetylgalactosamine		
gln II	glutamine synthetase II		
GLP-1	glucagon-like peptide 1		
Gm	gomesin		

Hmb	N-(2hydroxy-4-methoxy)	Hyp	hydroxyproline; trans-4-
HMBA	4-hydroxymethylbenzoic acid resin		hydroxyproline
HMC	hydroxymethylcarbonyl	I Amp	4-(N-isopropyl)-
hMCR	human melanocortin receptor		aminomethylphenylalanine
HMEC	human mammary epithelial cells	IBMX	3-isobutyl-1-methylxanthine
HmSer	α -hydroxymethylserine	IC ₅₀	50% inhibition concentration
HAM/TSP	HTLV-1 associated myelopathy/tropical spastic paraparesis	i.c.v.	intracerebroventricular
		Idp	3-isopropyl-3-(2,6-dimethyl-4-hydroxyphenyl)propanoic acid
HmVal	α -hydroxymethylvaline	IEX	ion exchange chromatography
HN	humanin	IFN	interferon
HNE	4-hydroxy-trans-2,3-nonenal	Ig	immunoglobulin
¹ H-NMR	proton nuclear magnetic resonance	IGF	insulin-like growth factor
HOAt	1-hydroxy-7-azabenzotriazole	Igl	α -(2-indanyl)glycine
HOBt	1-hydroxybenzotriazole	IL	interleukin
HONB	N-hydroxy-5-norbornene-2,3-dicarboximide	Im	immunity protein
HOObt	3,4-dihydro-3-hydroxy-4-oxo-1,2,3-benzotriazine	IMPACT	intein-mediated purification with an affinity chitin-binding tag
HoPhe	homophenylalanine	IN	HIV-1 integrase
Hor	hydroorotyl	Ind	indoline-2-carboxylic acid
HOSu	N-hydroxysuccinimide	Indo	indomethacin
HP	hot plate	iNOS	inducible nitric oxide synthetase
Hpi	3a-hydroxy-pyrrolo[2,3-b]indole	Inp	isonipecotic acid
HPLC	high performance liquid chromatography	i.p.	intraperitoneal
HPMVEC	human pulmonary microvascular endothelial	IP	inositol phosphate
hPrP	human prion protein	IPA	isopropyl alcohol
Hpt	haptoglobin	iPrOH	isopropanol
hPTH	human parathyroid hormone	IPTG	isopropyl- β -D-thiogalactopyranoside
HPV	human papilloma virus		internally quenched fluorogenic substrate
Hpx	hemopexin-like	IQFS	
HR	heptad repeat; hydrophobic repeat	IR	infrared spectroscopy; insulin receptor
HR-MAS	high resolution-magic angle spinning	I/R	ischemia/reperfusion
HRMS	high resolution mass spectroscopy	ITC	isothermal titration calorimetry
Hse	homoserine	i.v.	intravenous
HSQC	heteronuclear single-quantum coherence/correlation	ivDde	1-(4,4-dimethyl-2,6-dioxocyclohex-1-ylidene)-3-methylbutyl
HSV-1	herpes simplex virus type 1	K a	association equilibrium constant
HTLV-1	human T-cell lymphotropic/leukemia virus type 1	Kd	dissociation equilibrium constant
HTS	high-throughput screening	KLH	keyhole limpet hemocyanin
hUCP-1	human uncoupling protein 1	KOR	kappa opioid receptors; Kaiser resin
HUVEC	human umbilical vein endothelial cells		
Hva	homoveratryl	L aa	lipoaminoacid
Hvn	homovanillyl	LAC	β -lactamase
hV1bR	human vasopressin pituitary receptor	LAH	lithium aluminum hydride
hV2R	human vasopressin kidney receptor	LB	Luria-Bertani
Hyl	5-hydroxylysine	LC	lung cancer
		LCAT	lecithin-cholesterol acyltransferase

LC/ESI-MS	liquid chromatography/electrospray ionization mass spectrometry	Mdm2	murine double minute 2
LCFA	long chain fatty acids	Mdp	C ^α -methyl DOPA; 3-methyl-3-(2,6-dimethyl-4-hydroxyphenyl)-propanoic acid
LC-MS,		ME	2-mercaptoethanol
LC/MS/MS	liquid chromatograph/tandem mass spectrometry	Me	methyl
LCP	lipidic core peptide; lipid core peptide	MeCN	acetonitrile
LDA	lithium diisopropylamide	MeOH	methanol
ldp	3-isopropyl-3-(2,6-dimethyl-4-hydroxyphenyl)propanoic acid	Mesna	mercaptoethanesulfonic acid
LDL	low density lipoprotein	MFS	major facilitator superfamily
LDMS	laser desorption mass spectroscopy	MHC	major histocompatibility complex
LH	luteinizing hormone	MHS	6-maleimidohexanoic acid N-hydroxysuccinimide ester
LIF	laser induced fluorescence detection	MIC	minimum inhibitory concentration
LINCL	late-infantile neuronal ceroid lipofuscinosis	MIP-1	macrophage inflammatory proteins 1
LMMP	longitudinal muscle with myenteric plexus	MM	molecular mechanics
LMP	low melting point	MMP	matrix metalloproteinase
Lol	leucinol	Mmt	4-methoxytrityl
LPO	lipid peroxidation	Mnpe	N-2-mercapto-1-(2-nitrophenyl)ethyl
LPS	lipopolysaccharide	MO	molecular orbital
LVDP	left ventricular developed pressure	Mob	4-methoxybenzyl
LVP	lysine vasopressin	MOG	myelin oligodendrocyte glycoprotein
mAb	monoclonal antibody	MOR	mu opioid receptors
MALDI	matrix-assisted laser desorption/ionization	MP	mastoparan
MALDI-TOF	matrix-assisted laser desorption/ionization time-of-flight	MPA	methionine proximity assay
MAP	multiple antigen peptide	MPER	membrane-proximal external region
MAPS	microwave assisted peptide synthesis	MR	magnetic resonance
MAPK	mitogen-activated protein kinase	MRI	magnetic resonance imaging
Mapoc	4-dimethylaminophenacyloxy-carbonyl	MRSA	methicillin-resistant <i>Staphylococcus aureus</i>
MaUCP-1	golden hamster UCP-1	MS	mass spectrometry; multiple sclerosis
MBC	minimal bactericidal concentration	MSA	methanesulfonic acid
MBHA	<i>p</i> -methylbenzhydramine	Msc	β-methylsulfonyl ethoxycarbonyl
MBP	maltose binding protein; myelin basic protein	MsCl	methanesulfonyl chloride
Mca	(7-methoxycoumarin-4-yl)acetyl	MSH	melanocyte stimulating hormone; melanotropin
MCP-1	monocyte chemoattractant protein 1	MSNT	2,4,6-mesitylene-sulfonyl-3-nitro-1,2,4-triazolide
mCPBA	3-chloroperbenzoic acid	MTBD	7-Methyl-1,5,7-triazabicyclo-[4.4.0]dec-5-ene
MC	melanocortin; microencapsulated	MTII	Ac-Nle-c[Asp-His-D-Phe-Arg-Trp-Lys]-NH ₂
MCR	melanocortin receptor	Mtt	4-methyltrityl
MD	molecular dynamics	MTT	3-[4,5-dimethylthiazol-2-yl]-2,5-diphenyltetrazolium bromide
MDA	malondialdehyde	MVD	mouse vas deferens
		MVF	measles virus fusion protein
		MW	molecular weight
		MW-SPPS	microwave-assisted solid-phase peptide synthesis
		Myr	myristoyl

NA	neuraminidase	Nva	norvaline
NABH(OAc)₃	sodium triacetoxyborohydride	OBOC	one-bead one-compound
NADPH	nicotinamide adeninedinucleotide phosphate, reduced form	OC2Y	O-(2,6-dichlorobenzyl)-tyrosine
Nal	naphthylalanine	OHDA	hydroxydopamine
D-Nal-2	D-3-(2-naphthyl)alanine	Oic	octahydroindolyl-2-carboxylic acid
NBA	nucleobase amino acid	OMe	methoxy
NBS	N-bromosuccinimide	OMPC	outer membrane protein complex
NC	nociceptin; nucleocapsid	<i>o</i> NBS	<i>o</i> -nitrobenzenesulfonyl
NCL	native chemical ligation	<i>o</i> NPS	<i>o</i> -nitrophenylsulfonyl
NE	norepi-nephtrine	OPfp	pentafluorophenyl ester
N-ECD	N-terminal extracellular domain	Orn	ornithine
NEP	nephtrilysin	Osu	N-hydroxysuccinimide ester
NET	norepinephrine transporter	OT	oxytocin
NFAT	nuclear factor of activated T-cell	OTR	oxytocin receptor
NHMe	N-methylamide	OXL	5(4H)-oxazolone
NHS	N-hydroxysuccinimide	<i>Pa</i>	pseudomonas aeruginosa
Nif	niflumic acid	PA	partial agonist; anthrax protective antigen
NIR-FT	near-infrared, Fourier-transform	PAD	partial alloc deprotection
NIR-FT-Raman	Near Infrared Fourier Transformed Raman spectroscopy	PAGE	polyacrylamide gel electrophoresis
NK-R	neurokinin receptor	Pal	(3-pyridinyl)alanine
Nle	norleucine	D-3-Pal	D-3-(3-pyridyl)alanine
Nleu	N-isobutyl glycine	PAL	peptide amide linker 5-(4-Fmoc-aminomethyl-3,5-dimethoxy phenoxy)valeric acid; photoaffinity labeling
NLS	nuclear localization signal	PAM	phenylacetamidomethyl resin
Nma	2-(N-methylamino)benzoyl; N-methylanthranyl, N-methylalanine	PAO	<i>p</i> -aminophenylarsen(III)oxide
NMM	N-methylmorpholine; N-methylmorpholine	PAP	pulmonary artery pressure
NMP	N-methylpyrrolidinone	Pbf	2,2,4,6,7-pentamethyl-dihydrobenzofuran-5-sulfonyl
NMR	nuclear magnetic resonance	PBLA	poly-β-benzyl-L-aspartate
NO	nitric oxide	PBLG	poly-γ-benzyl-L-glutamate
nOct	<i>n</i> -octanoyl	PBMC	peripheral blood mononuclear cells
NOE	nuclear overhauser effect; nuclear overhauser enhancement	PBS	phosphate-buffered saline
NOESY	nuclear overhauser enhanced spectroscopy	PC	prostate cancer
Npa	2-nitrophenylacetyl	PCs	proprotein convertases
NPN	N-phenyl-naphtylamine	PCIBLA	poly(β-p-chlorobenzyl L-aspartate)
NPY	neuropeptide Y	Pcn	(E)-α-phenylcinnamoyl
5-Npys	5-nitropyridylsulfide	PCR	polymerase chain reaction
Npys	5-nitro-2-pyridinesulfonyl	PD	Parkinson's disease
Ns	2-nitrobenzenesulfonyl	Pd	palladium
NSAIDs	non-steroidal anti-inflammatory drugs	PDGF	platelet derived growth factor
NSB	non-specifically bound	PDI	protein disulfide isomerase
Nsc	2-(4-nitrophenylsulfonyl)ethoxy-carbonyl	PDMS	polydimethylsiloxane
NT	neurotensin	PDB	protein data bank
NTI	naltrindol	PEG	polyethylene glycol
NTS	nuclear targeting signal peptide	PEGA	polyethylene glycol polyacrylamide
		PEM	protein epitope mimetics
		Pen	penicillamine
		PES	potential energy surface

PET	positron emission tomography	PTHR	parathyroid hormone receptor
PFG	pulsed field gradient	<i>p</i> -TsOH	<i>p</i> -toluenesulfonic acid
PFGSE	pulsed-field-gradient spin-echo	PTX	pertussis toxin
Pfp	pentafluorophenyl ester	pTyr	phosphotyrosine
PFP	protein fingerprint	PVAc	polyvinylacetate
PFTase	protein farnesyltransferase	PWR	plasmon waveguide resonance
PG	protecting group	PyAOP	(7-azabenzotriazol-1-yloxy)- tris(pyrrolidino)phosphonium hexafluorophosphate
PH	pleckstrin homology	PyBOP	(benzotriazol-1-yloxy)- tris(pyrrolidino)phosphonium hexafluorophosphate
Phg	phenylglycine		
PhSH	thiophenol		
Pht	phthaloyl		
PI	phosphatidylinositol		
PICUP	photo-induced cross-linking of unmodified proteins	QDs	quantum dots
Pin1	protein interacting with NIMA 1	QCM	quartz crystal microbalance
Pip	L-pipecolic acid	QSAR	quantitative structure-activity relationships
pip	D-pipecolic acid		
PKA	cAMP-dependent kinase A	RCAM	ring-closing alkyne metathesis
PKC	protein kinase C	RCM	ring-closing metathesis; ring- closing alkene metathesis
Plm	plasmepsin	RDC	residual dipolar coupling
PMA	phorbol-12-myristate 13-acetate	rDNA	recombinant desoxynucleic acid
Pmc	2,2,5,7,8-pentamethylchroman- 6-sulfonyl	Rg	radius of gyration
PMN	polymorphonuclear leukocyte	RGA	reporter gene assay
Pms	2-[phenyl(methyl)sulfonyl] ethoxy carbonyl	RGD	Arg-Gly-Asp
pNA	<i>p</i> -nitroaniline	RI, r.i.	retro-inverso
PNA	peptide nucleic acid	RIS	radioimmunosciintigraphy
<i>p</i> NBS	<i>p</i> -nitrobenzenesulfonyl	RIT	radioimmunotherapy
Pns	phenylnorstatine	rLys turn	reverse lysine turn
<i>p</i> NZ	<i>p</i> -nitrobenzyloxycarbonyl	rms	root mean square
p.o.	oral administration	RMSD, rmsd	root mean square deviation
POMC	proopiomelanocortin	RNase	ribonuclease
POPC	1-palmitoyl-2-oleoyl- <i>sn</i> - glycero-3-phosphocholine	RNAP	RNA polymerases
POPG	1-palmitoyl-2-oleoyl- <i>sn</i> -3- [phospho -rac-(1-glycerol)]	ROE	rotating frame nuclear Overhauser effect
POPE	1-palmitoyl-2-oleoyl- <i>sn</i> - glycero-3-phospho- ethanolamine	ROESY	rotating frame nuclear Overhauser enhanced spectroscopy
POPNA	pyrrolidine-based oxy-peptide nucleic acid	ROMP	ring-opening metathesis
PPLA	poly(β -phenethyl L-aspartate)	rOTR	rat oxytocin receptor
PPlase	peptidyl-prolyl isomerase	RP	reversed-phase
PPT	polypurine/polypirimidine tract	RP-HPLC	reversed-phase HPLC
P1R	PTH receptor-1	rt/RT	room temperature
PR8	A/Puerto Rico/8/34 influenza virus strain	RT-PCR	reverse transcriptase-polymerase chain reaction
Pra	propargylglycine	RU	resonance units
PRP	platelet rich plasma	rUT	rat urotensin receptor
PrP ^C	cellular prion protein	rV1aR	rat vasopressin vasopressor receptor
ps	picosecond	rV1bR	rat vasopressin pituitary receptor
PS	polystyrene; poly(styrol); phosphatidylserine	rV2R	rat vasopressin kidney receptor
PSP	phosphoserine phosphatase	SA	simulated annealing
PS-SCL	positional scanning SCL	SAR	structure activity relationship
PTC	primary tumor cell; phase transfer catalysis	SARS	severe acute respiratory syndrome
PTH	parathyroid hormone		

SARS-CoV	SARS coronavirus	TBDMS	<i>tert</i> -butyldimethylsilyl
Sc, sc, s.c.	subcutaneous	TBDMSCl	<i>tert</i> -butyldimethylsilylchloride
SCAM	substituted cysteine accessibility method	TBS	<i>t</i> -butyldimethylsilyl
Sce	<i>Saccharomyces cerevisiae</i>	TBTU	2-(1H-benzotriazol-yl)-1,1,3,3-tetramethyluronium tetrafluoroborate
SCLC	small cell lung cancer	<i>t</i> Bu	<i>tert</i> -butyl
SCLs	synthetic combinatorial libraries	TCE	tetrachloroethane
SD	standard deviation; substitution degrees	TCEP	tris(carboxyethyl)phosphine
SDF-1	stromal-derived cell growth factor 1	Tcp	tetrachlorophthaloyl
SDS	sodium dodecyl sulfate	TCP	trityl chloride polystyrene
SEC	size exclusion chromatography	TCR	T cell receptor
Sec	selenocysteine	TD	tetramerization domain
SEER	sequence-enabled reassembly	TEA	triethylamine
SEM	scanning electron microscopy	TEM	transmission electron microscopy
SFTI	sunflower trypsin inhibitor	TES	triethylsilane
SH	src homology domain	TF	tail-flick
SHU 9119	Ac-Nle-c[Asp-His-D-Nal(2')-Arg-Trp-Lys]-NH ₂	TFA	trifluoroacetic acid
SICLOPPS	split intein circular ligation of peptides and proteins	Tfa	trifluoroacetyl
siRNA	small interfering RNA	TFE	trifluoroethanol
SM	sphingomyelin	TFMSA	trifluoromethanesulfonic acid
SO	superoxide	TfOH	triflic acid
SOD	superoxide dismutase	Tft	4,4,4-trifluorothreonine
SP	substance P	TG	tentagel
SPA	scintillation proximity assay	THF	tetrahydrofuran
SPECT	single photon emission computed tomography	Thi	β -(2-thienyl)-alanine
SPPS	solid-phase peptide synthesis	THP	triple-helical peptide; tetrahydropyranyl
SPR	surface plasmon resonance	ThT	thioflavin T
SPS	solid phase synthesis	Thz	thiazolidine-4-carboxylic acid; thiazolidyl
Sps	2-(4-sulfophenylsulfonyl)-ethoxycarbonyl	Tic	1,2,3,4-tetrahydroisoquinoline-3-carboxylic acid
Stat3	signal transduction and activator of transcription 3	TIPS; TIS	triisopropyl silane
STD-NMR	saturation transfer difference NMR	TLC	thin layer chromatography
Ste2p	α factor pheromone receptor	TM	transmembrane, transmembrane helix
STM	short transmembrane segment; scanning tunnelling microscopy	TM, TMD	transmembrane domain; transmembrane helix
STMs	signal transduction modulators	TMA	trimetic acid; tissue microarray
SUIM	suberimidyl	Tmob	2,4,6-trimethoxybenzyl
Suc	succinyl	TMR	tetramethylrhodamine
SV40	simian virus 40	TMS	trimethylsilyl
T α 1	thymosin α 1	TMSBr	trimethylsilylbromide
TAC	triazacyclophane	TMSOTf	trimethylsilyloxy
T-ag	tumor antigen	TMT	trifluoromethanesulfonate
TAPP	H-Tyr-D-Ala-Phe-Phe-NH ₂	TNF	β -methyl-2',6'-dimethyltyrosine
TASP	template-assembled synthetic protein(s)	TNTU	tumor necrosis factor
TAT	transactivating transcriptional activator		2-(5-norbornene-2,3-dicarboximido)-1,1,3,3-tetramethyluronium tetrafluoroborate
TBAF	tetra- <i>n</i> -butylammonium fluoride	TOAC, Toac	2,2,6,6-tetramethylpiperidine-1-oxyl-4-amino-4-carboxylic acid
Tbc	tetrahydro- β -carboline	TOCSY	total correlation spectroscopy
		Tos	tosyl
		TP5	thymopentin
		TPP I	tripeptidyl-peptidase I

Tris	tris(hydroxymethyl) aminomethane
Trt	trityl
Tsoc	triisopropylsilyloxy
U _{69,593}	(5 α ,7 α ,8 β)-(-)-N-methyl-N-[7-(1-pyrrolidinyl)-1-oxaspiro[4.5]dec-8-yl]benzeneacetamide
U-II	urotensin-II
UCP	uncoupling proteins
UDP-GlcNAc	uridine diphosphate N-acetylglucosamine
USDA	United States Deptment of Agriculture
UT	urotensin II receptor
UTI	urinary tract infection
UV	ultraviolet spectroscopy
UVR	ultraviolet radiation
UV-Vis	ultraviolet-visible spectroscopy
V _{1a-R}	V _{1a} receptor
V _{1aR}	vasopressin vasopressor receptor
V _{1bR}	vasopressin pituitary receptor
VCD	vibrational circular dichroism
VDAC	voltage dependent anion-selective channel
VEGF	vascular endothelial growth factor
VesCPs	<i>Vespa</i> chemotactic peptides
VIP	vasoactive intestinal peptide
VLDL	very low density lipoprotein
VMA	vacuolar membrane ATPase
vMIP-II	viral macrophage inflammatory protein II
VP	vasopressin
VPhe	2,3-cyclopropyl phenylalanine
V _{2R}	vasopressin kidney receptor
VRE	vancomycin-resistant enterococci
vWF	Willebrand factor
W _{ang}	p-benzyloxubenzyl alcohol resin
WGA	wheat germ agglutinin
WSCD	water-soluble carbodiimide
WT	wild type
X _{aa} , X _{xx}	any amino acid
Z	benzyloxycarbonyl; pyroglutamic acid
ZF	zinc finger

Contents

Preface	i
Message from the President of the American Peptide Society	ii
Committees of the 19 th American Peptide Symposium	iv
Symposium Sponsors	vi
Symposium Exhibitors	vii
The American Peptide Society	viii
American Peptide Symposia	ix
The Merrifield Award	xi
The Makineni Lecture Award	xiii
Achievement Award for Scientific and Administrative Excellence	xiv
Peptide Society Travel Grants	xv
Bert Schram Young Investigators' Mini-Symposium	xvii
Young Investigators' Poster Competition	xviii
Abbreviations	xx
Contents	xxx

Merrifield Award Lecture

From Tens to Trillions - Advances in Synthetic Combinatorial Chemistry of Peptides, Peptidomimetics and Heterocyclic Compounds Derived from Peptides <i>Richard A. Houghten</i>	3
--	---

Goodman Memorial

Peptides in the Days of Photonics <i>Christian Renner and Luis Moroder</i>	17
It All Started in Brooklyn, NY, Forty-five Years Ago! <i>Claudio Toniolo</i>	22
Short Transmembrane Peptide Sequences as Nucleation Sites for Globular Protein Folding <i>Arianna Rath, Linda Lee, Rachel M. Johnson and Charles M. Deber</i>	26
Synthesis and In Vitro Opioid Activity Profiles of Novel Cyclic Enkephalin Analogs <i>Peter W. Schiller, Grazyna Weltrowska, Irena Berezowska, Carole Lemieux, Nga N. Chung and Brian C. Wilkes</i>	31
A Photo-Controlled β -Hairpin <i>Markus Löweneck, Shou-Liang Dong, Tobias E. Schrader, Wolfgang J. Schreier, Wolfgang Zinth, Luis Moroder and Christian Renner</i>	36
Structure-Function Relationship Studies of Analogs of PTH(1-11) Fragment Containing Combinations of Aib and (α Me)Nle <i>Andrea Caporale, Nereo Fiori, Elisabetta Schievano, Michael Chorev, Stefano Mammi and Evaristo Peggion</i>	38
Membrane Associated Structure of a Ghrelin Agonist as Determined by NMR <i>Dale F. Mierke, Andrea Piserchio, John Eynon, Jundong Zhang, John E. Taylor, Heather Halem, Michael D. Culler and Jesse Z. Dong</i>	40
Scaffold, Dendritic and Metal-Assisted Assembly of Collagen-Like Biomaterials <i>Weibo Cai, Sen Wai Kwok, Joseph P. Taulane and Murray Goodman</i>	42

Peptide and Protein Synthesis Strategies

Positional Scanning for Peptide Secondary Structure by Solid Phase Synthesis with	47
---	----

Aza-Amino Acids and Freidinger Lactams <i>Damien R. Boeglin, Mandar S. Bodas, Fabrice Galaud and William D. Lubell</i>	
Synthesis of Cyclic Peptides via Transition Metal Catalyzed C-C Bond Formation <i>Dirk T. S. Rijkers, Hefziba T. ten Brink, Nourdin Ghalit, Jan Tois and Rob M. J. Liskamp</i>	50
Solid Phase Synthesis of Phosphorylated Cis and Trans 3-Peptidyl-4-(4'-hydroxyphenyl)- β -Lactams <i>David R. Coleman IV, Kumar K. Kaluarachchi and John S. McMurray</i>	53
Switch on Amyloid β Peptide Self-Assembly by Enzyme-Triggered Acyl Migration <i>Sonia Dos Santos, Arunan Chandravarkar, Bhubaneswar Mandal, Richard Mimna, Karine Murat, Lydiane Saucède, Marie-Stephanie Camus, Gabriele Tuchscherer and Manfred Mutter</i>	56
ROMP of Norbornyl Oligopeptides: A Versatile Synthetic Method for Exploring Receptor Topology <i>Younjoo Lee, Keith Baessler and Nicole S. Sampson</i>	59
Native Chemical Ligation at Aromatic Residues <i>Sylvie Tchertchian, Fred Opligger, Marianne Paolini, Sonia Manganiello, Sylvain Raimondi, Benoît Depresle, Nicolas Dafflon, Hubert Gaertner and Paolo Botti</i>	61
Robotic Synthesis of Soluble Peptide Arrays <i>Wen Lin and James G. Boyd</i>	64
Covalent Capture: Application to Peptides Possessing Auxiliary Groups for Extended Chemical Ligation <i>Nikolett Mihala and Keith Rose</i>	66
Asymmetric Induction on a Racemic Amine by Chiral Dipeptide 5(4H) Oxazolones from C $^{\alpha}$ Methyl Phenylglycine <i>Alessandro Moretto, Cristina Peggion, Fernando Formaggio, Marco Crisma, Bernard Kaptein, Quirinus B. Broxterman and Claudio Toniolo</i>	68
Poly(ethylene glycol) (PEG) Modifications and Conformational Analysis of Thymosin α 1 <i>Keliang Liu, Jiankun Qie, Jinbo Ma, Liangyou Wang, Wenxia Zhou, Chunhui Qi, Xiunan Zhao, Jianquan Zheng and Sijian Dong</i>	70
Suppression of Side Reactions Associated with Use of the Benzyloxymethyl Group on Histidine <i>Kumiko Yoshizawa-Kumagaye, Takehiro Ishizu, Shuji Isaka, Masaji Tamura, Rumi Okihara, Yuji Nishiuchi and Terutoshi Kimura</i>	72
Peptide Synthesis in Water: 2-(4-Sulfophenyl- sulfonyl)ethoxycarbonyl Group and Coupling Reagents <i>Keiko Hojo, Mitsuko Maeda and Koichi Kawasaki</i>	74
Efficient Synthesis in Solid-Phase of Freidinger-like Lactams by Microwave Irradiation <i>Teresa Lama, Pietro Campiglia, Luigia Auriemma, Isabel Gomez-Monterrey, Alfonso Carotenuto, Ettore Novellino and Paolo Grieco</i>	76
Synthesis of Monocyte Chemoattractant Protein 1 (MCP-1) Analogs via Native Chemical Ligation <i>Tami L. Raguse, Nicole Stowell, Reannon Holland, Thomas Bodenshtein, Steven C. Pomerantz, Jennifer F. Nemeth, Anuk Das, Marian Kruszynski and George A. Heavner</i>	78
NMR Analysis of a Multi-domain Peptide of the <i>Saccharomyces cerevisiae</i> Alpha Factor Receptor <i>Racha Estephan, Jacqueline Englander, Boris Arshava, Jeffrey M. Becker and Fred Naider</i>	80
Further Studies on an Alternative Approach to Prepare Esterified Protected Peptides	82

under Mild Conditions <i>Patricia B. Proti, Pedro V. de Oliveira and M. Terêsa M. Miranda</i>	
A Long Range S,N-Acyl Migration by Silver Ion Assistance in Thioester Ligation <i>Yi-An Lu and James P. Tam</i>	84
The C-Terminal Fragment of Acanthoscurrin is a Difficult Sequence <i>César Remuzgo, Gustavo F. S. Andrade, Maria L. A. Temperini, Sirlei Daffre And M. Terêsa M. Miranda</i>	86
A Novel Approach to Resin-based Cysteine Alkylation <i>Bin Yang and Richard D. DiMarchi</i>	88
Deprotection of the p-Methoxybenzyl Group of Selenocysteine by Neighboring Group Participation <i>Katharine M. Harris and Robert J. Hondal</i>	90
Overcoming Challenges in Automated Long Peptide Synthesis – A Multi-pronged Approach <i>Yingwei He, Guodi Lu, John Mountzouris and Chun Wu</i>	92
Synthesis and Biological Evaluation of Antagonist Analogs of the Peptide Hormone Oxytocin <i>Jake L. Stymiest, Bryan F. Mitchell, Susan Wong and John C. Vederas</i>	94
Development of Wang Resin Supported Evans-type Oxazolidinone for Asymmetric Reaction <i>Tomoya Kotake, Yoshio Hayashi, S. Rajesh, Tooru Kimura and Yoshiaki Kiso</i>	96
A Convenient Synthetic Method for Monodehydro-2,5-diketopiperazines <i>Yoshio Hayashi, Akiko Oda, Yuri Yamazaki, Yuka Okuno and Yoshiaki Kiso</i>	98
Solid-Phase Synthesis of Azole-Based Peptides and Peptidomimetics <i>Eric Biron and Horst Kessler</i>	100
Efficient Synthesis of N-Methylamino Acids Compatible with Fmoc Solid-Phase Peptide Synthesis <i>Eric Biron, Jayanta Chatterjee and Horst Kessler</i>	102
The “O-Acyl Isopeptide Method” for the Synthesis of Alzheimer’s Disease-Related Amyloid β Peptide (A β) 1–42 <i>Youhei Sohma, Maiko Kimura, Yousuke Chiyomori, Yoshio Hayashi, Atsuhiko Taniguchi, Masato Sasaki, Tooru Kimura and Yoshiaki Kiso</i>	104
The “O-Acyl Isopeptide Method” for the Synthesis of Difficult Sequence- Containing Peptides: Application to the Synthesis of Alzheimer’s Disease-Related Amyloid β Peptide (A β) 1–42 Mutants <i>Yousuke Chiyomori, Youhei Sohma, Maiko Kimura, Yoshio Hayashi, Fukue Fukao, Atsuhiko Taniguchi, Tooru Kimura and Yoshiaki Kiso</i>	106
Enhancing Atom Economy of SPS: Recoverable and Reusable Building Blocks for Depsipeptide Synthesis <i>Jan Spengler, Javier Ruiz-Rodríguez, Tommaso Cupido, Klaus Burger and Fernando Albericio</i>	108
1-N-Methyl-Histidine as a Side-Product in Backbone N-Methylated PTH Analogs <i>Zhanna Potetinova and Gordon E. Willick</i>	110
Combinatorial Approach in the Synthesis of a Small Library of β -Turn Structures Based on Thiazolidine Moiety <i>Alfonso Carotenuto, Teresa Lama, Orazio Mazzoni, Pietro Campiglia, Ettore Novellino, Alessia Bertamino, Maria V. Diurno, Isabel Gomez-Monterrey, Luigia Auriemma and Paolo Grieco</i>	112
Solid-Phase Peptide Synthesis Using ChemMatrix [®] , a Polyethylenglycol (PEG)-based Solid <i>Fernando Albericio, Nuria Bayo, Silvia A. Camperi, Osvaldo Cascone, Simon Côté, Luis J. Cruz, Abdelhamid Errachid, Robert Furic, Fayna García-Martín, Yesica García-Ramos, Nancy B. Iannucci, Mariela M. Marani, Mateu Pla-Roca,</i>	114

<i>Martina Quintanar-Audelo, Josep Samitier and Judit Tulla-Puche</i>	
<i>p</i> -Nitrobenzyloxycarbonyl (pNZ) as an Alternative to Fmoc for the Protection of Amines in Solid-Phase Peptide Synthesis	116
<i>Albert Isidro-Llobet, Pilar E. López, Judit Guasch-Camell, Mercedes Álvarez and Fernando Albericio</i>	
Synthesis and NMR Analysis of CCR5 and CXCR4 Peptides Containing Tyrosine Sulfate	118
<i>Tatsuya Inui, Patricia Cano-Sanchez, Boris Arshava, Inbal Ayzenshtat, Jacob Anglister and Fred Naider</i>	
Steroid-Peptide Conjugates	120
<i>Witold A. Neugebauer, Jérôme Côté, Audrey Fortier, Ghassan Bkaily, Levon Avedanian, Danielle Jaques and Fernand Gobeil Jr.</i>	
Influence of Natural Loop Residues or Oligolysines on the Biophysical Properties of Transmembrane Domains of a G Protein-Coupled Receptor	122
<i>Patricia Cano-Sanchez, Tatsuya Inui, Beatrice Severino, V. V. Suresh Babu, Boris Arshava, Jeffrey M. Becker and Fred Naider</i>	
Design, Synthesis and Analysis of Constrained B-Cell Epitope from HER-2 Protein	124
<i>Sharad V. Rawale and Pravin T. P. Kaumaya</i>	
Synthesis of the Four Stereoisomers of N-Fmoc-O-t-Bu-4,4-trifluorothreonine	126
<i>Zhong-Xing Jiang and Yihua Bruce Yu</i>	
Synthesis of N ^α -Fmoc-N ^ε -[(2-nitrophenyl)acetyl]-lysine (Fmoc-Lys(Npa)-OH) and its Applications in Solid-Phase Peptide Synthesis	128
<i>Aimin Song, Lucy Wu, Xiaobing Wang and Kit S. Lam</i>	
A MS-based Encoding Method for OBOC Combinatorial Branched Peptide Libraries	130
<i>Xiaobing Wang and Kit S. Lam</i>	
Sequential Chemical Ligation for Polypeptide Synthesis by the Combination of the Thioester Method and the Extended Chemical Ligation Using a Photoremovable Auxiliary	132
<i>Toru Kawakami, Masahiro Tsuchiya, Ken'ichiro Nakamura and Saburo Aimoto</i>	
Solid-Phase Synthesis of a Mucin Glycopeptide Segment from CD43 for NMR and Crystallization Studies	134
<i>Mian Liu, George Barany and David Live</i>	
SPPS of Bacterial Addressed Peptides and PNAs Overcoming the Resistance against Antibiotics	136
<i>Rüdiger Pipkorn, Waldemar Waldeck and Klaus Braun</i>	
Convergent Synthesis of the Cysteine-rich Mdm2 RING Finger Domain	138
<i>Zoe Vasileiou, Dimitrios Gatos and Kleomenis Barlos</i>	
Evaluation of Polyamide-Polystyrene Block Polymers in Peptide Synthesis and Biochemistry	140
<i>Spyros Markos, Antonios Saravanos, Michael Batistatos, Alexios Aletras, Dimitrios Gatos and Kleomenis Barlos</i>	
New Nomenclature for Complex Cyclopeptides	142
<i>Jan Spengler, José-Carlos Jiménez, Klaus Burger, Ernest Giralt and Fernando Albericio</i>	
New Approaches for Native Chemical Ligation	144
<i>Dana Baas, Daniel G. Mullen and George Barany</i>	
Microwave-Assisted Solid-Phase Peptide Synthesis (MW-SPPS) on CLEAR Supports	146
<i>Anne L. Carenbauer, Matthew R. Cecil, Andrzej Czerwinski, Krzysztof Darlak, Mirosława Darlak, DeAnna Wiegandt Long, Francisco Valenzuela and George Barany</i>	
Microwave Assisted Peptide Synthesis – A Tool to Replace Classical SPPS?	148
<i>Andreas Rybka and Hans-Georg Frank</i>	

Fast and Versatile Peptide Backbone Modifications Using Microwave Energy <i>Daniel Raichman and Gerardo Byk</i>	150
Microwave-Assisted Synthesis of Multivalent Dendrimeric Peptides using Cycloaddition Reaction ('Click') Chemistry <i>Dirk T. S. Rijkers, G. Wilma van Esse, Remco Merckx, Arwin J. Brouwer, Hans J. F. Jacobs, Roland J. Pieters and Rob M. J. Liskamp</i>	152
Efficient Synthesis of Disulfide Bridge Containing Peptides: Melanin Concentrating Hormone (MCH) and Brain Natriuretic Peptide (BNP) <i>Jianjun Jiang, Brian D. Dayton, Sevan J. Brodjian, Bryan C. Tieman, Susan E. Brophy and Paul L. Richardson</i>	154
Rapid Solution-phase Synthesis of a 20-mer Peptide According to the DioRaSSP® Method <i>Ivo F. Eggen, Frits T. Bakelaar, Paul B.W. Ten Kortenaar, Knut Adermann, Wolf-Georg Forssmann and Axel Schulz</i>	156
A New Efficient Post-Assembly Strategy for the Synthesis of Sulfated Peptides <i>John A. W. Kruijtzter, Johan Kemmink and Rob M. J. Liskamp</i>	158
Auxiliary Group-Assisted Peptide Thioester Preparation Based on On-resin N-S Acyl Shift Triggered by TFA Treatment <i>Megumi Sumida, Ken'ichiro Nakamura, Toru Kawakami, Thomas Vorherr and Saburo Aimoto</i>	160
Evaluation of Solid Supports and Solvent Conditions for Use with Microwave- Assisted Solid-Phase Peptide Synthesis <i>Sandra C. Vigil-Cruz, Angela M. Peck and Jane V. Aldrich</i>	162
Efficient Recombinant Production of the 16 Amino Acid Peptide AOD9604 <i>Allan W. Hey, Angelo Guidolin, Reza Zareie, Kathryn Smith, Ela Knapik and Stan Bastiras</i>	164
Chemical Synthesis of the Gsti Protein by a NCL Method on a X-Met Site <i>Daniela Marasco, Angela Saporito, Paolo Botti, Eduardo Patriarca, Rossella Fasulo, Alessandro Spasiano, Carlo Pedone, Ettore Benedetti and Menotti Ruvo</i>	166
N,O-Acyl Shifts: Unexpected Side-Reaction and Beneficial Tool in Fmoc-Chemistry <i>Louis A. Carpino, Calin D. Sferdean, Irene Coin, Sandra Tremmel, Eberhard Krause, Michael Bienert and Michael Beyermann</i>	168
Magnetic CLEAR Beads for Solid-Phase Synthesis of Peptides and Affinity Ligands <i>Pottayil G. Sasikumar and Maria Kempe</i>	170
An Efficient and Facile Synthesis of Tyrosine-Sulfate-Containing Peptides: Synthesis of the N-Terminal Peptide of CCR5 and Its Analog <i>Hasmik Sargsyan, Boris Arshava, Patricia Cano, Tatsuya Inui, Jacob Anglister and Fred Naider</i>	172
Interaction of DPH with the Local Anesthetic Receptor Site in D1-S6 of the Na ⁺ Channel by NMR and Molecular Modeling <i>Bih-Show Lou and Ta-Hsien Lin</i>	174
The Structural Determinants of GPCR Binding and Activation: Insights from Mutagenesis and Molecular Modeling Studies of the Human Angiotensin II Type 1 (hAT1) Receptor <i>Marie-Eve Beaulieu, Pierre Lavigne and Emanuel Escher</i>	176
Protein Epitope Mimetics. A New Approach to Target Protein-Protein Interactions <i>Frank Otto Gombert, Jan Willem Vrijbloed and Daniel Obrecht</i>	178
Application of Phenylphosphate Mimetics to the Design and Synthesis of Olefin Metathesis-Derived Grb2 SH2 Domain-Binding Macrocycles <i>Sang-Uk Kang, Zhen-Dan Shi, Rajeshri Kariki, Jason Phan, Karen M. Worthy, Lakshman K. Bindu, Marc Nicklaus, David S. Waugh, Robert J. Fisher and Terrence R. Burke, Jr.</i>	180
Radiolabeled Peptides as CXCR4 Ligands	182

<i>Ettore Benedetti, Giancarlo Morelli, Raffaella Della Moglie, Stefania De Luca, Luigi Aloj, Andrea Ciarmiello, Secondo Lastoria, Claudio Arra, Amelia D'Alessio and Laura Tarallo</i>	
Aza-peptides with Multiple Aza-amino Acids, Synthesis and Preliminary Conformational Analysis of Glu-azaAla-Ala-azaAla-Leu-azaAla-Lys-azaAla-NH ₂	184
<i>Damien R. Boeglin, Mallem H.V. Ramana Rao, Jean-Philippe Demers and William D. Lubell</i>	
Design and Synthesis of Bicyclic Internal β -Turn Mimetics and their Applications toward Biologically Interesting Ligands	186
<i>Byoung J. Min, Xuyuan Gu, Ravil R. Petrov, Yeon Sun Lee and Victor J. Hruby</i>	
Synthesis and Incorporation of Freidinger Lactam Analogs in GHRP-6	188
<i>Fabrice Galaud, Annie Demers, Huy Ong and William D. Lubell</i>	
Microwave-assisted Synthesis of N-glycosylated Building Blocks	190
<i>Ilaria Paolini, Francesca Nuti, Giuseppina Sabatino, Mario Chelli and Anna M. Papini</i>	
Parallel Solid-Phase Synthesis of Mucin-Like Glycopeptides from an α -GalN3 O-Linked Threonine Building Block	192
<i>Mian Liu, David Live and George Barany</i>	
Synthesis of Silyl Ether Linkers for Solid-Phase Peptide Synthesis	194
<i>Cassidy M. Dobson, George Barany and Rita S. Majerle</i>	
Synthetic Routes to, and Mechanistic Understanding of, Dithiasuccinoyl (Dts)-Amines and Chlorocarbonyl Carbamoyl Disulfanes	196
<i>Michael J. Barany, Megan M. Corey, Michael C. Hanson, Rita S. Majerle, Robert P. Hammer and George Barany</i>	
Peptide-Derived (Sulfonyl)Azides as Versatile Synthons in Chemoselective Bioconjugations	198
<i>Remco Merkx, Dirk T. S. Rijkers, Arwin J. Brouwer, Johan Kemmink and Rob M. J. Liskamp</i>	
Chemically Synthesized Annexin-A5-Based Probes for Molecular Imaging	200
<i>Cheng-Bin Yim, Anouk Dirksen, Chris P.M. Reutelingsperger and Tilman M. Hackeng</i>	
Unequivocal Synthesis of (Z)-Alkene or (E)-Fluoroalkene Dipeptide Isosteres via DKP Mimetics to Probe Structural Requirements of Peptide Transporter	202
<i>Ayumu Niida, Shinya Oishi, Makiko Mizumoto, Yoshikazu Sasaki, Kenji Tomita, Hirokazu Tamamura, Akira Otaka, Tomohiro Terada, Ken-ichi Inui and Nobutaka Fujii</i>	
Development of New Photoremovable Amino Protecting Group and its Application toward Chemical Synthesis of 7TM-GPCR	204
<i>Satoshi Ueda, Akira Otaka, Hirokazu Tamamura and Nobutaka Fujii</i>	
Multivalent Peptide Dendrimers: Native Chemical Ligation as a Synthetic Tool	206
<i>Hinke Malda, Tilman M. Hackeng, Marcel H. P. van Genderen and Egbert W. Meijer</i>	
Synthesis and Use of C-terminally Biotinylated Peptidomimetics with High Grb2 SH2 Domain-binding Affinity	208
<i>Zhen-Dan Shi, Benedetta Peruzzi, Pathirage G. Dharmawardana, Tiffany Leech, Ettore Appella, Karen M. Worthy, Lakshman K. Bindu, Robert J. Fisher, Donald P. Bottaro and Terrence R. Burke, Jr.</i>	
Total Solid Phase Synthesis of a Marine Cyclodepsipeptide IB-01212	210
<i>Luiz J. Cruz, Marta Martínez, Julia Pérez, Marta Trujillo, Librada M. Cañedo, Ricard Rodríguez, Ernest Giralt and Fernando Albericio</i>	
Interference with Protein-Protein Interactions Involved in Protease Inhibitor Complex Formation	212
<i>Dirk-Jan van Zoelen¹, Maarten R. Egmond², Roland J. Pieters¹ and</i>	

<i>Rob M. J. Liskamp</i>	
Sequence-Enabled Reassembly (SEER) Peptides for the Detection of DNA Sequences	214
<i>Aik T. Ooi, Cliff I. Stains, Jason R. Porter, Indraneel Ghosh and David J. Segal</i>	
A Mild Acidic Method for the Selective Deprotection of N1-trityl-3a-hydroxypyrrolo[2,3-b]indole Derivatives	216
<i>Jonathan P. May and David M. Perrin</i>	
Enantiomerically Pure H-Arg(Z)2-aldehyde Diethylacetal: A Useful Building Block in the Synthesis of Peptide Aldehydes	218
<i>Fritz Dick, Juergen Gerhardt, Barbara Jakobi, Beat Sax, Joachim Schwindling and Christian Staehelin</i>	
Chlorotrityl Chloride (CTC) Resin as a Convenient Reusable Protecting Group	220
<i>Fayna García-Martín, Nuria Bayo, Luis J. Cruz, James Bohling and Fernando Albericio</i>	
Synthesis and Purification of Multiphosphorylated Peptides	222
<i>Vladimir V. Kalashnikov, Yongping Tang and Jeanick H. Pascal</i>	
Dealing with the Aggregation Problem of Polyglutamine Peptides: Synthesis Strategies	225
<i>Myriam Létourneau, Martin Viau, Ariane Sirois, Yvan Boulanger and Alain Fournier</i>	

Biosynthesis of Bioactive Peptides

Synthesis and Biological Assessment of Insulin-Like Analogs with Differential Activity at the Insulin and IGF-1 Receptors	229
<i>Richard D. DiMarchi, Jie Han, Amy Hoffman, Vasily M. Gelfanov, Wayne Kohn, Radmila Micanovic and John P. Mayer</i>	
Biosynthesis of the Cyclotide Kalata B1 using Protein Splicing Tools	235
<i>Richard Kimura, Krish Krishnan and Julio A. Camarero</i>	
Exploration and Elaboration of Reported Insulin Superagonism through Site-Selective Replacement at TyrB26	237
<i>David L. Smiley, Ma Boaquan, Vasily M. Gelfanov and Richard D. DiMarchi</i>	
Synthesis of an RNase B 30-124 Glycoform by Native Chemical Ligation	239
<i>Christian Piontek, Stefano Mezzato, Daniel Varon, Nelson Lombana, Manuela Schaffrath, Andreas Martin, Franz-Xaver Schmid and Carlo Unverzagt</i>	

New Themes in Anti-Microbials and Quorum Sensing

Threaded Rings and Complex Topologies in Antimicrobial Peptides: Nature's Engineering Templates	243
<i>David J. Craik, K. Johan Rosengren, Lillian Sando and Shane S. Simonsen</i>	
A Minimalist Approach to Antimicrobial Proteins with Thionin as a Template	248
<i>Miquel Vila-Perelló, Sabrina Tognon, Andrea Sánchez-Vallet, Antonio Molina and David Andreu</i>	
Discovering Additional Chemical and Biological Functions for 3-Oxo-N-Acylhomoserine Lactones	252
<i>Gunnar F. Kaufmann, Rafaella Sartorio, Sang-Hyeup Lee, Claude J. Rogers, Michael M. Meijler, Jason A. Moss, Bruce Clapham, Andrew P. Brogan, Tobin J. Dickerson and Kim D. Janda</i>	
Comparing Antimicrobial and Membrane Permeabilizing Activity of Peptides Derived from Human Cationic Proteins	255
<i>Susana Sánchez-Gómez, Guillermo Martínez de Tejada, José Leiva-Leon, Ignacio Moriyón, Dagmar Zwegytick, Karl Lohner and Sylvie E. Blondelle</i>	

Preliminary NMR Analysis of ProP440-500 the C-Terminal Cytoplasmic Domain of Bacterial Osmosensory Protein ProP	258
<i>David L. Zoetewey, David N. M. Jones, Janet M. Wood and Robert S. Hodges</i>	
Synthesis and Conformation of Analogs of the Antiviral Peptide Halovir A	261
<i>Andrea Dalla Bona, Cristina Peggion, Fernando Formaggio, Bernard Kaptein, Quirinus B. Broxterman and Claudio Toniolo</i>	
Total Synthesis in Solution and Preliminary Conformational Analysis of TOAC-Labeled Alamethicin F50/5 Analogs	263
<i>Micha Jost, Cristina Peggion, Fernando Formaggio and Claudio Toniolo</i>	
A Lipid Monolayer Made Permeable to Tl(I) Ions by the Lipopeptaibol Trichogin GA IV	265
<i>Chiara Baldini, Cristina Peggion, Ester Falletta, Maria Rosa Moncelli, Rolando Guidelli and Claudio Toniolo</i>	
A Universal Influenza B Peptide Vaccine	267
<i>Paolo Ingallinella, Elisabetta Bianchi, Xiaoping Liang, Marco Finotto, Michael Chastain, Jiang Fan, Tong-Ming Fu, Hong Chang Song, Melanie Horton, Daniel Freed, Walter Manger, Emily Wen, Li Shi, Roxana Ionescu, Colleen Price, Marc Wenger, Emilio Emini, Riccardo Cortese, Gennaro Ciliberto, John Shiver and Antonello Pessi</i>	
Design, Synthesis and Analysis of a Cysteine-Deleted Analog of the Antimicrobial Peptide Tachyplesin-I	269
<i>Deborah L. Heyl, Kiran Kumar Gottipati, Sreeja Sreekumar, Sathan Thennarasu and Ayyalusamy Ramamoorthy</i>	
Progress toward Total Solid-Phase Synthesis of Cyclic Lipodepsipeptide Antibiotic Fusaricidin A	271
<i>Rekha Rawat, Ralph T. Martello, Pierre Y. Jean-Charles and Predrag Cudic</i>	
Biological and Structural Characterization of a New Linear Gomesin Analog	273
<i>Marcos A. Fázio, Laurence Jouvensal, Françoise Vovelle, Philippe Bulet, M. Terêsa M. Miranda, Sirlei Daffre and Antonio Miranda</i>	
Monomeric Analogs of Halocidin	275
<i>Xavier Doisy</i>	
Fragment of Human Lysozyme Conjugated on the N-terminus and Displaying Antibacterial Properties	277
<i>Xavier Doisy</i>	
Synthesis and Raman Spectroscopy Studies of the Antimicrobial Peptide Cecropin B2	279
<i>Susanne Ladefoged Nielsen and Xavier Doisy</i>	
Alamethicin Interaction with Lipid Membranes: A Spectroscopic Study on Synthetic Analogs	281
<i>Lorenzo Stella, Marcello Burattini, Claudia Mazzuca, Antonio Palleschi, Mariano Venanzi, Cristina Peggion and Claudio Toniolo</i>	
Design of Bactericidal Self-Assembling Cyclic D,L- α -Glycopeptides	283
<i>Shai Rahimipour, Leila Motiei and Reza M. Ghadiri</i>	
HB-50: A Pre-Clinical Study of a Prophylactic for Wound Infection	285
<i>Scott M. Harris, Lijuan Zhang, Jody Parente, George T. Rodeheaver and Timothy J. Falla</i>	
Designer Multifunctional Antimicrobial Peptides Kill Fluoroquinolone-Resistant Clinical Isolates	287
<i>Laszlo Otvos, John D. Wade, Feng Lin, Barry A. Condie, Christine Snyder, Jorg Hanrieder and Ralf Hoffmann</i>	
Solution Structures of Stomoxyn and Spinigerin, Two Antimicrobial Peptides from Insects	289
<i>Celine Landon, Herve Meudal, Nathalie Boulanger, Philippe Bulet, Reto</i>	

<i>Stöcklin and Françoise Vovelle</i>	
Rational Design of α -Helical Antimicrobial Peptides	291
<i>Yuxin Chen, Michael Guarnieri, Michael Vasil and Robert S. Hodges</i>	
Dimer Formation of Novel Cationic Antimicrobial Peptides in Membrane Environments	293
<i>Evgenia Glukhov and Charles M. Deber</i>	

Post-Translational Modifications of Peptides and Proteins

Enzymatic Incorporation of Prenyl Azides into Peptides and Proteins: Tools for Selective Protein Labeling	297
<i>Juhua Xu, Stepan Lenevich, Jason Boggs, Daniel G. Mullen, George Barany and Mark D. Distefano</i>	
N-Alkylaminooxy Amino Acids as Versatile Derivatives for "Post-Translational" Modifications of Synthetic Peptides	300
<i>Michael R. Carrasco</i>	
Improved Synthesis of 5-hydroxylysine (Hyl) Derivatives	303
<i>Mare Cudic, Janelle L. Lauer-Fields and Gregg B. Fields</i>	
Synthesis and Biological Assessment of Sulfonic Acid-Based Glucagon Antagonists	305
<i>Bin Yang, Vasily M. Gelfanov and Richard D. DiMarchi</i>	
Thioester Bond Liability: Study on Natural Influenza and Model Acylpeptides	307
<i>Marina V. Serebryakova, Larisa V. Kordyukova, Boris V. Vaskovsky and Ludmila A. Baratova</i>	
Chemical Synthesis of MUC2 Tandem Repeat Model Carrying Multiple O-GalNAc Moieties	309
<i>Hironobu Hojo, Yoshiyuki Matsumoto, Yoshiaki Nakahara, Yusuke Suzuki, Minoru Suzuki and Akemi Suzuki</i>	
Site Specific Introduction of Unnatural Amino Acids at Sites Critical to Insulin Receptor Recognition and Biological Activity	311
<i>Beili Quan, David L. Smiley, Vasily M. Gelfanov and Richard D. DiMarchi</i>	

Towards Peptides as Potential Therapeutics

Target-Based Proteolytic Profiling for Characterizing Cancer Progression	315
<i>Janelle L. Lauer-Fields, Dmitriy Minond, Diane Baronas-Lowell, Michael J. Chalmers, Scott A. Busby, Patrick R. Griffin, Hideaki Nagase and Gregg B. Fields</i>	
From Simple Consensus Peptides to High Affinity Ligands: A Stepwise Diversity Oriented Strategy for the Acquisition of Potent Signaling Inhibitors	320
<i>David S. Lawrence</i>	
Cyclic Modular β -Sheets	325
<i>James S. Nowick, Justin O. Brower, Omid Khakshoor, Wade A. Russu and R. Jeremy Woods</i>	
Apolipoprotein A-I Mimetic Peptides	329
<i>G. M. Anantharamaiah, Mohamad Navab, Sreenivas T. Reddy, Susan Hama, Greg Hough, Mayakonda N. Palgunachari, Manjula Chaddha, Geeta Datta, David W. Garber and Alan M. Fogelman</i>	
Understanding BBB Transport using Glycosylated Enkephalins and Endorphins	332
<i>Dhana Muthu, Isabel Alves, Charles M. Keyari, Larisa Yeomans, Richard D. Egleton, Jean M. Bidlack, Henry I. Yamamura, Victor J. Hruby, Edward J. Bilsky and Robin Polt</i>	
Design and Study of Novel Peptide Inhibitors against the SARS-Coronavirus Spike Protein	335

<i>Zhe Yan, Brian Tripet and Robert S. Hodges</i>	
Screening Biosynthetic Peptide Libraries for Antimicrobial Activity	338
<i>Lisa O. Nilsson, Mostafa Louassini and Ernesto Abel-Santos</i>	
Cellular Delivery and Design of Proprotein Convertase Inhibitors	341
<i>Ajoy Basak, Xiaolei Hao, Ying Feng, Dayani Mohottalage, Farzaneh Lotfipour and Sarmistha Basak</i>	
Mechanism of Interaction between the (17-31) Binding Domain of PTH and the PTH Receptor	344
<i>Thomas Dean, Ashok Khatri, Zhanna Potetinova, Gordon Willick and Thomas J. Gardella</i>	
[3,3]-Sigmatropic Rearrangements, and Chiral Aziridines for the Asymmetric Synthesis of Novel Amino Acids	347
<i>Hongchang Qu, Lu Liu, Xuyuan Gu and Victor J. Hruby</i>	
A Library of Cysteine-Biotin Derivatives Useful for Pretargeting Avidin-Biotin Radioimmunosciintigraphy	349
<i>Cristina Bolzati, Andrea Caporale, Davide Carta, Liliana Cofano, Elisabetta Schievano, Francesco Tisato, Fiorenzo Refosco, Evaristo Peggion and Giuliano Bandoli</i>	
A Methionine Scan of Region [168-176] of the Parathyroid Hormone Receptor 1 – The “Magnet Effect”	351
<i>Angela Wittelsberger, Beena E. Thomas, Dale F. Mierke and Michael Rosenblatt</i>	
A New Approach to the Synthesis of Polycyclic Dipeptide Derivatives as Potential Antitumoral Agents	353
<i>Teresa Lama, Orazio Mazzoni, Pietro Campiglia, Alessia Bertamino, Ettore Novellino, Maria V. Diurno, Isabel Gomez-Monterrey, Antonio Mazzella di Bosco and Paolo Grieco</i>	
A Purification Strategy for Synthetic Peptides that Utilizes pH to Optimize Selectivity	355
<i>Andrew F. Coffey, Linda L. Lloyd, Keeley J. Mapp, Louise E. Rochell and Alasdair MacDonald</i>	
Agonist Activation of the Angiotensin II Type 1 Receptor Alters the Spatial Proximity of Transmembrane Domain 7 to the Ligand Binding Pocket	357
<i>Dany Fillion, Gaétan Guillemette, Richard Leduc and Emanuel Escher</i>	
An Asymmetric Synthesis of (R)- and (S)-o-cyano-phenylalanine Leading to Chiral Constrained Phenylalanine Dipeptide Mimetics	359
<i>Karolien Van Rompaey, Isabelle Van den Eynde, Steven Ballet and Dirk Tourwé</i>	
Analogues of Multifunctional Ligands for Opioid and CCK Receptors	361
<i>Ekaphol Wooden, Vinod Kulkarni, Yeon S. Lee, Richard S. Agnes, Christine Salibay, Peg Davis, Shou-Wu Ma, Josephine Lai, Frank Porreca and Victor J. Hruby</i>	
Antigen Effects of Peptide Nucleic Acids on HIF-1 α Expression	363
<i>Zhanna Zhilina, Amy Ziembra, Lenka Stankova, Stacey Wood, Meghan Boros and Scot Ebbinghaus</i>	
Novel Glyco-lipid-arsenicals (III) with Anti-proliferative Effects on MCF-7 Human Breast Cancer Cells	365
<i>Norbert Wimmer, Jodie A. Robinson, Nagaraj Gopisetty-Venkatta, Sarah J. Roberts-Thomson, Gregory R. Monteith and Istvan Toth</i>	
Antisense PNA and PNA-peptide Conjugates for the Modulation of β -globin Gene Splicing	367
<i>Alessandra Romanelli, Soccorsa Pensato, Erminia Di Niola, Giordana Feriotto, Francesca Salvatori, Giulia Breveglieri, Laura Zaccaro, Michele Saviano, Roberto Gambari, Carlo Pedone and Ettore Benedetti</i>	
β -Amino Acid Analogues of an Insect Neuropeptide	369

<i>Pawel Zubrzak, Howard J. Williams, Geoffrey M. Coast, Gloria Reyes-Rangel, Eusebio Juaristi, Janusz Zabrocki, Allison Strey and Ronald J. Nachman</i>	371
Branched Neurotensin for Tumor Targeting	
<i>Chiara Falciani, Monica Fabbrini, Barbara Lelli, Luisa Lozzi, Alessandro Pini and Luisa Bracci</i>	
CCK/MSH Analogs and Derivatives for Imaging and Incorporation in Multimeric Ligands	373
<i>Rajesh Sankaranarayanan, Fang Gao, Jatinder S. Josan, Heather Handl, Josef Vagner, Robert J. Gillies and Victor J. Hruby</i>	
Cellular Uptake of Pyrrolidine-Based Oxy-Peptide Nucleic Acid	375
<i>Mizuki Kitamatsu, Rino Matsuzaki and Masahiko Sisido</i>	
Chemical Biology and Biomedical Application of Synthetic Molecules Targeted to Apoptosis Regulated by the Bcl-2 Family	377
<i>Jun Wang, Dongxiang Liu, Krishna Kumar, Aihua Nie, Yohichi Kumaki, Pak-Nei Hon, R. Wayne Fritzsche, Jing An, John C. Reed and Ziwei Huang</i>	
Comparative Immunogenicity of Common and Rare HIV Mutant Peptides	379
<i>Sylvie E. Blondelle, Rosa Moya, Kim Schroder and Darcy B. Wilson</i>	
Conformational Studies of Agouti-Related Protein (AGRP)-Melanocortin Chimeric Peptides	381
<i>Andrzej Wilczynski, Krista R. Wilson, Joseph W. Scott, Arthur S. Edison and Carrie Haskell-Luevano</i>	
C-Terminal Ether Analogs of NN703	383
<i>Kjeld Madsen, Peter Andersen, Michael Ankersen, Bernd Peschke, Birgit Sehested and Jan Soerensen</i>	
Cyclic Statine-based Peptides as Inhibitors of β -Secretase	385
<i>Alessandra Barazza, Marion Götz, Christian Renner, Michael Willem and Luis Moroder</i>	
Design and Structure Determination of a Selenium Labeled Antimicrobial Peptide	387
<i>Xiaomei Zhou, Phat L. Tran, Joe Fralick and Ted W. Reid</i>	
Design and Synthesis of Encoded One-bead One-compound Peptidomimetic Libraries for Identification of $\alpha_4\beta_1$ Integrin Ligands	389
<i>Ruiwu Liu, Li Peng, Jan Marik and Kit S. Lam</i>	
Design and Synthesis of Histone Deacetylase Inhibitors by Side Chain Modification of 2-Amino-(n-1)-alkenoic Acids	391
<i>Mohammed P. I. Bhuiyan, Tamaki Kato and Norikazu Nishino</i>	
Design of a Library of Histone Deacetylase Inhibitors Based on Chlamydocin	393
<i>Norikazu Nishino, Mohammed P. I. Bhuiyan, Yoshinori Hirashima, Louis A. Watanabe, Priti Soni, Tamaki Kato, Tomonori Nishino and Minoru Yoshida</i>	
Design of an Antibody for Early Detection of Ovarian Cancer	395
<i>Danielle Carbin, Sharad Rawale, Carl Morrison, Jeffrey Fowler, Larry Maxwell and Pravin T. P. Kaumaya</i>	
Design, Synthesis and Applications of Cell-penetrant Peptides as Signal Transduction Modulators	397
<i>John Howl, Michelle Farquhar and Sarah Jones</i>	
Novel MTII/AGRP Hybrid Analogs that Lead to Selective Ligands for the Human Melanocortin Receptors	399
<i>Minying Cai, Alexander Mayorov, Kevin Chandler, Christopher Cabello, Dustin Tanaka, Dev Trivedi and Victor J. Hruby</i>	
Design, Synthesis, and Evaluation of Gluten Peptide Analogs as Selective Inhibitors of Human TG2	401
<i>Olga Fierro, Stefania Albrizio, Alfonso Carotenuto, Gabriella Caliendo, Daniela Guarino, Paolo Grieco, Pietro Campiglia, Teresa Lama and Ettore Novellino</i>	

Novel Blue- and Red-Shifted Internally Quenched Fluorogenic Substrates for Continuous Monitoring of SARS-CoV 3CLpro	403
<i>Pamela Hamill, Martin Richer, Derek Hudson, Hongyan Xu and François Jean</i>	
Discovery and Optimization of a TRAIL R2 Agonist for Cancer Therapy	405
<i>Yvonne M. Angell, Ashok Bhandari, Anjan Chakrabarti, M. Nuria De Francisco, Amy N. Duguay, Brian T. Frederick, Karen Leu, Kerstin Leuther, Xianfeng Li, Kalyani Penta, Sunila Piplani, Reuben Sana, Erik A. Whitehorn, Pete J. Schatz, Kevin Yin and Christopher P. Holmes</i>	
Development of Peptide Vaccines against HPV-16 Associated Cervical Cancer and Group A Streptococci	407
<i>Peter M. Moyle, Aniko Horváth, Levente Karpáti, Colleen Olive, Nadia Barozzi, Norbert Wimmer, Michael Good and Istvan Toth</i>	
Disulfide as a Constraint to Build Super Potent and Selective Melanocortin-4 Receptor (MC4R) Agonists	409
<i>Liang Zeng Yan, David Flora, Patrick Edwards, David L. Smiley, Paul J. Emmerson, Hansen M. Hsiung, Robert Gadski, JeAnne Hertel, Mark L. Heiman, Saba Husain, Thomas P. O'Brien, Steven D. Kahl, Lianshan Zhang, Richard D. DiMarchi and John P. Mayer</i>	
Effect of Dimerization and Tetramerization on the Potency of HIV-1 Integrase Inhibitory Peptides	411
<i>Krzysztof Krajewski, Christophe Marchand, Yves Pommier and Peter P. Roller</i>	
The Effects of Stable Bradykinin Receptor 2 Agonist B9972 on Pulmonary Vasculature <i>in vitro</i> and <i>vivo</i>	413
<i>Laimute Taraseviciene-Stewart, John M. Stewart, Lajos Gera, Nana Burns, Robertas Scerbavicius and Norbert F. Voelkel</i>	
Etk/Bmx Tyrosine Kinase Peptide Substrates and Inhibitors Derived from the Autophosphorylation Site of the Enzyme	415
<i>Ching-Yi Hsieh, Jan Marik, Jenny Kung, Coleen Sweeney, Kit S. Lam and Hsing-Jien Kung</i>	
Fluorescence Resonance Energy Transfer Substrates for Determining Cathepsin B pH Specificity	417
<i>Paolo Ruzza, Luigi Quintieri, Alessio Osler, Andrea Calderan, Barbara Biondi, Maura Floreani, Andrea Guiotto and Gianfranco Borin</i>	
Ghrelin Attenuates Burn-induced Cachexia	419
<i>Ambikaipakan Balasubramaniam, Rashika Joshi, Chunhua Su, Lou Ann Friend and James H. James</i>	
High Affinity High Specificity $\alpha 4 \beta 1$ Integrin Targeting Peptidomimetics for Lymphoid Cancers	421
<i>Li Peng, Ruiwu Liu, Xiaobing Wang, Jan Marik, Yoshikazu Takada and Kit S. Lam</i>	
Highly N-Methylated Somatostatin Analogs: Synthesis, Biological Activity and Structure-Activity Relationship Studies	423
<i>Eric Biron, Daniel Langenegger, Daniel Hoyer and Horst Kessler</i>	
Highly Sensitivity FRET Substrate for Assay of HCV Protease	425
<i>Xiaohe Tong, Ling Sheng, Xiaofen Zhong, Yi Tang, Junge Lu, Zhenjun Diwu and Anita Hong</i>	
Identification and Characterization of Synthetic Peptide Substrates and Small Molecule Inhibitors of Non Receptor Tyrosine Kinase Etk	427
<i>Lauren Lee, Ruiwu Liu, Nianhuan Yao, Jan Marik, Ching-Yi Hsieh, Hsing-Jien Kung and Kit Lam</i>	
Identification of High Affinity Anti-MCP-1 Antibodies using Synthetic Proteins	429
<i>Marian Kruszynski, Ping Tsui, Jinqun Luo, Anuk Das, Nicole Stowell, Michael Brigham-Burke, Jennifer F. Nemeth, Li Yan, Heena Beck, Jil Carton, Raymond</i>	

<i>Sweet, George A. Heavner, Michael Bardroff, Daniela D. Ducata, Ute Jager and Robert Rauchenberger</i>	
Mapping Cell Binding using Collagen III “Toolkit”	431
<i>Nicolas F. Raynal, Tony Peachey and Richard W. Farndale</i>	
Modeling of $\alpha 1$ Adrenergic Receptors: the Application in the Design of Selective $\alpha 1B$ -Adrenergic Antagonists	433
<i>Slavica Erić, Tomaž Šolmajer, Marko Oblak, Miha Kotnik and Danica Agbaba</i>	
Characterization of the Interaction of HIP Analog Peptide with Heparin	435
<i>Jing Wang and Dallas Rabenstein</i>	
New Urotensin-II Analogs Modified at Position 4	437
<i>Paolo Grieco, Pietro Campiglia, Alfonso Carotenuto, Teresa Lama, Ettore Novellino, Paolo Rovero and Guido Iaccarino</i>	
New Urotensin-II Analogs with a Constrained Trp-7 Side Chain	439
<i>Alfonso Carotenuto, Paolo Grieco, Pietro Campiglia, Teresa Lama, Ettore Novellino, Paolo Rovero and Guido Iaccarino</i>	
Novel GnRH Antagonists Derived from Degarelix: Exploration of the GnRH Antagonist Pharmacophore	441
<i>Manoj P. Samant, Doley J. Hong, Glenn Croston, Catherine Rivier and Jean Rivier</i>	
Novel Neuroprotective Neurotrophic NAP Analogs Targeting Iron Toxicity and Oxidative Stress in Neurodegenerative Diseases	443
<i>Hailin Zheng, Dan Blat, Moussa B.H. Youdim, Lev M. Weiner, Dudy Dangoor, Ilana Gozes and Mati Fridkin</i>	
One-bead One-compound: Different Type of Screening Assays for Anti-bacterial Adhesion	445
<i>Yanlei Liu, Li Peng, Xiaobing Wang, Kit S. Lam and Joseph W. Leung</i>	
Peptide - Mediated Delivery of siRNA via Noncovalent Complexes and Covalent Conjugates	447
<i>Renata T. Witkowska, Mohammad Ahmadian, James W. Dattilo, Lafe J. Purvis, Sasha J. Mayer, Lishan Chen, Yuching Chen, Kunyuan Cui, Ken W. Farber, Sharin E. Roth, Michael E. Houston, Paul H. Johnson and Steven C. Quay</i>	
Peptides Reproducing the ApoA-I 141-164 Region: Studies on Hpt Recognition	449
<i>Luca D. D'Andrea, MariaStefania Spagnuolo, Angela De Stefano, Marianna Morra, Alessandro Carlucci, Annarita Del Gatto, Pasqualina Caso, Carlo Pedone, Paolo Abrescia and Ettore Benedetti</i>	
Peptidomimetic Inhibitors of Platelet Adhesion as Potential Novel Antiplatelet Agents	451
<i>Vivienne Buckley, Elise Bernard, Edelmiro Moman, Lorraine Coleman, Dermot Kenny and Marc Devocelle</i>	
Peptidyl-based Delivery Systems as a Strategy for the Therapeutic Intervention of Human Astrocytoma and Medulloblastoma	453
<i>Sarah Jones and John Howl</i>	
Photolabeling with N-Terminal Urotensin II Photoprobes Identifies Methionine 288 of Rat Urotensin Receptor as a Contact Point	455
<i>Brian J. Holleran, Christophe Proulx, Marie-Eve Beaulieu, Emanuel Escher and Richard Leduc</i>	
Protein Kinase C Isoform (PKC) Peptide Activator/Inhibitors Exert Cardioprotective Effects in Polymorphonuclear Leukocyte (PMN)-induced Ischemia/Reperfusion (I/R) Injury	457
<i>London H. Young, Aisha Phillipson, Didi Omiyi, Norrell Atkinson, Manoj Jivani, Jovan Adams, Ellen E Peterman, Philip Taormina II, Richard J. Brue and Margaret Harvey</i>	
Rational Design of Small Molecules for a Novel Class of Anti-Cancer Drugs	459

using a Phenylalanine Library	
<i>Lajos Gera, Daniel C. Chan, Laimute Taraseviciene-Stewart, Vitalija Simkeviciene, Paul A. Bunn, Jr. and John M. Stewart</i>	
Repair of Photodamaging Effects on Human Melanocytes by 4-Phenylbutryl-His-D-Phe-Arg-Trp-NH ₂ . A Superpotent Analog of α -Melanocortin	461
<i>James J. Knittel, Leonid N. Koikov, Pilgrim Jackson, Glenn Milhauser, Ana Luisa Kadekaro, Renny J. Kavanagh and Zalfa Abdel-Malek</i>	
RGD Peptide-Labeled Quantum Dots for Integrin $\alpha v \beta 3$ Targeting	463
<i>Weibo Cai, Xianzhong Zhang, Yun Wu and Xiaoyuan Chen</i>	
Rigid Cyclic Tetrapeptides as Probes and Mimics of Reverse Turns	465
<i>Sage Berg-Cross and Garland Marshall</i>	
Solid-Phase Synthesis and Structure Characterization of N'-Biphenyl-N-2-Ethylbutyl-Demethylvancomycin	467
<i>Nian-Huan Yao, James R. Carlson, Gang Liu and Kit S. Lam</i>	
Stereo-controlled Synthesis of [L-Arg, L/D-3-(2-Naphthyl)alanine]-type (E)-Alkene Dipeptide Isosteres and its Application to the Preparation and Biological Evaluation of Peptidomimetic Analogs of the CXCR4 Antagonist FC131	469
<i>Hirokazu Tamamura, Kenichi Hiramatsu, Satoshi Ueda, Zixuan Wang, John O. Trent, Stephen C. Peiper, Naoki Yamamoto, Hideki Nakashima, Akira Otake and Nobutaka Fujii</i>	
Stoichiometric Inhibition of β -Amyloid Fibrillogenesis using C ^{α,α} -Disubstituted Amino Acid Containing Peptides	471
<i>Marcus A. Etienne, Cyrus Bett, Jed P. Aucoin, Tim J. Jensen, Robin L. McCarley, Ted Ajmo, Donna Herber, David Morgan and Robert P. Hammer</i>	
Structure Determination of the Human Angiotensin II Receptor Type 1 by the Methionine Proximity Assay	473
<i>Martin Clément, Stéphane S. Martin, Caroline Chamberland, Marie-Ève Beaulieu, Richard Leduc, Gaétan Guillemette and Emanuel Escher</i>	
Structure-Activity Relationship Studies of a Novel CXCR4 Chemokine Antagonist Reveal Unique Activity Profile	475
<i>Celia Amela-Cortés, Martha Rezende, Tatyana Yakovleva, Dan Papa, Elisabeth Perchellet, Jean-Pierre Perchellet and Sandra C. Vigil-Cruz</i>	
Studies on a Mutual Prodrug of Sulfamethoxazole and Nalidixic acid	477
<i>Asif Husain and M.S.Y. Khan</i>	
Studies on Interaction of CaM with CaM-Binding Peptides M13 and RS20 in the Presence of Al ³⁺ Ions	479
<i>Andrea Calderan, Paolo Ruzza, Alessio Osler, Andrea Guiotto, Barbara Biondi and Gianfranco Borin</i>	
Studies on the Peroxidase Mimetic Peptide	481
<i>Liping Wang, Xiaoming Zhao, Lili Guo, Roger W. Roeske and Wei Li</i>	
Use of Combinatorial Peptide Libraries and LC/MS/MS to Study TPP I Substrate Specificity	483
<i>Yu Tian, Istvan Sohar, John W. Taylor and Peter Lobel</i>	
Sunflower Derived Trypsin Inhibitors as Anti-Metastatics	485
<i>Peter P. Roller, Sheng Jiang, Peng Li, Ya-Qiu Long, Sheau-Ling Lee, Cheng-Yong Lin, Michael Johnson and Richard B. Dickson</i>	
Surface Plasmon Resonance- and Quartz Crystal Microbalance-based Methods for Detecting GRB2 SH2 / Peptide Interaction	487
<i>Feng-Di T. Lung, Wan Ching Li and Chien-Chung Liou</i>	
Synthesis and Biological Activity of Terlipressin and its Putative Metabolites	489
<i>Kazimierz Wisniewski, Sudar Alagarsamy, Hiroe Taki, Marcel Miampanba, Regent Laporte, Robert Galyean, Glenn Croston, Claudio Schteingart, Pierre Riviere and Jerzy Trojanar</i>	

Synthesis and Evaluation of Neuroprotective α,β -Unsaturated Aldehyde Scavenger Histidyl-containing Analogs of Carnosine <i>Andrea Guiotto, Andrea Calderan, Paolo Ruzza, Alessio Osler, Chiara Rubini, Dong-Gyu Jo, Sung-Chun Tang, Thiruma V. Arumugam, Mark P. Mattson and Gianfranco Borin</i>	491
Synthesis, Structural Characterization and Reactivity Study of Humanin, an Alzheimer's Disease Associated Peptide <i>Madalina Maftai, Heiko Moeller and Xiaodan Tian</i>	493
Synthesis of 4-amino-1,2,4,5-tetrahydro-2-benzazepine-3-ones and Study of their β -turn Inducing Properties <i>Isabelle Van den Eynde, Karolien Van Rompaey, Steven Ballet, Rien De Wachter, Kenno Vanommeslaeghe, Monique Biesemans, Rudolph Willem and Dirk Tourwé</i>	495
Synthesis of a RGD Peptide-PEG Hybrid for Carrying Adenovirus Vector into Cells <i>Shinya Kida, Mitsuko Maeda, Keiko Hojo, Yusuke Eto, Jian-Qing Gao, Shinnosuke Kurachi, Fumiko Sekiguchi, Hiroyuki Mizuguchi, Takao Hayakawa, Tadanori Mayumi, Shinsaku Nakagawa and Koichi Kawasaki</i>	497
Synthesis of Cyclic Imino Acids from α -Amino- ω -Bromoalkanoic Acids <i>Louis A. Watanabe, Mohammed P. I. Bhuiyan, Tamaki Kato and Norikazu Nishino</i>	499
Synthesis of Quantum Dots Labeled Short Peptides and their Application in Imaging the T Cell Surface Receptors <i>Lifeng Wang, Jie Chen, Liping Wang, Chunlei Wang and Wei Li</i>	501
Synthesis of Quantum Dot-Signal Peptides Bioconjugates and Targeting in Living Cells <i>Yaming Shan, Jiayue Hu, Liping Wang and Wei Li</i>	503
Synthesis of Symmetrical Dimeric Dicarboxylic Acid Linked Peptides on Solid Support <i>Sheng Jiang, Zaneta Nikolovska-Coleska, Shaomeng Wang and Peter P. Roller</i>	505
Systematic Study on the Structure-Activity Relationship of Pyrazinone Ring-Containing Bioactive Opioid Ligands <i>Kimitaka Shiotani, Anna Miyazaki, Tingyou Li, Yuko Tsuda, Toshio Yokoi, Akihiro Ambo, Yusuke Sasaki, Yunden Jinsmaa, Sharon D. Bryant, Lawrence H. Lazarus and Yoshio Okada</i>	507
Tetra and Pentapeptide Derivatives of Hemiassterlin. Synthesis and Activity Studies <i>Marcin Dyba, Nadya I. Tarasova, Teresa Kosakowska-Cholody, Ernest Hamel and Christopher J. Michejda</i>	509
The Chemo-enzymatic Synthesis of Oligosaccharide-linked Peptides Aimed at Improved Drug Delivery <i>Ken D. Johnstone, Manuela Dieckelmann, Michael P. Jennings, Joanne T. Blanchfield and Istvan Toth</i>	511
Neokytotorphin as Cell Protein Kinase Affector <i>Olga V. Sazonova, Elena Yu. Blishchenko, Anna G. Tolmazova, Dmitry P. Khachin, Andrei A. Karelin and Vadim T. Ivanov</i>	513
Towards Inhibition of Amyloid β -protein Oligomerization <i>Sean M. Spring, Summer L. Bernstein, Noel D. Lazo, Brigita Urbanc, H. Eugene Stanley, Michael T. Bowers, David B. Teplow and Gal Bitan</i>	515
Use of Betidamino Acids in Drug Design <i>Judit Erchevyi, Sandra Wenger, Beatrice Waser, Veronique Eltschinger, Renzo Cescato, Jean Claude Reubi, Steven C. Koerber, Christy R. R. Grace, Roland Riek and Jean E. Rivier</i>	517
Helical Peptide Analogs of gp41 to Develop an HIV Vaccine <i>Florence M. Brunel, Michael B. Zwick, Ian A. Wilson, Dennis R. Burton and</i>	519

<i>Philip E. Dawson</i>	
Structure-Activity Relationship Studies of a Novel AGRP-Melanocortin Chimeric Template	521
<i>Krista R. Wilson, Andrzej M. Wilczynski, Joseph W. Scott, Rayna M. Bauzo and Carrie Haskell-Luevano</i>	
Synthesis and Pharmacological Evaluation of a New Generation of TIPPP-Derived Dual-Labeled Ligands for Delta Opioid Receptors	523
<i>Xin Wang, Thomas F. Murray and Jane V. Aldrich</i>	
Synthesis and Pharmacological Evaluation of Dual Labeled Delta Opioid Receptor Peptides	525
<i>Angela M. Peck, Vivek Kumar, Thomas F. Murray and Jane V. Aldrich</i>	
Novel Retro-inverso Envelope Peptide Mimetic Fusion Inhibitors as a Potential Therapy for HTLV-1 Infected Individuals	527
<i>Marcus P. Lynch, Sharad V. Rawale, Ahmed A. Behery, William P. Hudleson, Norihiro Takenouchi, Karen Yao, Steven Jacobson and Pravin T. P. Kaumaya</i>	
Heteroclitc Analogs Derived from the HTLV-1 Gag Antigen Increase Cytolytic and IFN- γ Responses in HLA-A*0201 Transgenic Mice	529
<i>Marcus P. Lynch, Jacqueline C. Lieblein, Sharad V. Rawale, Danielle M. Carbin and Pravin T.P. Kaumaya</i>	
Development of a Monoclonal Antibody Therapeutic for the Prevention and Treatment of Pseudomonas aeruginosa Infection	531
<i>Daniel J. Kao and Robert S. Hodges</i>	
An Unexpected Side Reaction Involving the Deletion of an Acetylated N-Methyl-Amino Acid from the N-terminus of Peptides	533
<i>Wei-Jie Fang, Marco A. Bennett, Thomas F. Murray and Jane V. Aldrich</i>	
Synthesis and Biological Activities of Chimeric Bioactive Peptides Based on Amino Acids Coupled to 4-Anilino-N-Phenethyl-Piperidine	535
<i>Ravil R. Petrov, Ruben S. Vardanyan, Shou-wu Ma, Peg Davis, Yeon S. Lee, Minying Cai, Frank Porreca, Josephine Y. Lai and Victor J. Hruby</i>	
Discovery of Potent mMC1R Agonists with Prolonged Activity at Human Melanocytes	537
<i>Aleksandar Todorovic, Jerry R. Holder, Rayna M. Bauzo, Joseph W. Scott, Renny Kavanagh, Zalfa Abdel-Malek and Carrie Haskell-Luevano</i>	

Peptide and Protein Design

β -Hairpin Minimization and Optimization	541
<i>Niels H. Andersen, Katherine A. Olsen, R. Matthew Fesinmeyer and Lisa A. Eidenschink</i>	
Analogues of Interleukin 8 Containing non Proteinogenic Segments Show High Biological Activity	544
<i>Ralf David and Annette G. Beck-Sickinger</i>	
Optimization of the C-terminal Sequence in Glucagon to Maximize Receptor Affinity	547
<i>Jay J. Levy, Vasily M. Gelfanov and Richard D. DiMarchi</i>	
Design, Synthesis, and Evaluation of Piperazine-Based Small Molecule Peptide Mimetics Targeting the Melanocortin Receptors	550
<i>James P. Cain, Alexander V. Mayorov, Minying Cai, Yeon-Sun Lee, Jinfa Ying, and Victor J. Hruby</i>	
Structure-Based Design and Structure-Activity Relationships of D-Phe-Pro-D-Arg-P1'-CONH ₂ Tetrapeptides Inhibitors of Thrombin	553
<i>Cristina C. Clement and Manfred Philipp</i>	
A Gibberellin Mimetic Peptide Recognized by an Anti-gibberellin Monoclonal	555

Antibody	
<i>Hikaru Hemmi, Takashi Murata, Shugo Nakamura, Kentaro Shimizu, Yoshihito Suzuki and Isomaro Yamaguchi</i>	
Synthesis of the Spin-labelled β -Amino Acids <i>cis</i> - and <i>trans</i> - β -TOAC, and a Preliminary Conformational Study of <i>trans</i> β TOAC/ <i>trans</i> -ACHC Peptides	557
<i>Karen Wright, Matthieu Sarciaux, Michel Wakselman, Jean-Paul Mazaleyrat, Marco Crisma, Fernando Formaggio, Cristina Peggion, Antonio Toffoletti, Carlo Corvaja and Claudio Toniolo</i>	
High Affinity Grb2 SH2 Domain-Binding Macrocycles Derived from Ring-Closing Methathesis of Alkenylglycine Residues with β -Vinyl Phosphotyrosyl Mimetics	559
<i>Fa Liu, Shinya Oishi, Rajeshri Karki, Zhen-Dan Shi, Karen M. Worthy, Lakshman K. Bindu, Melissa Maderia, Marc Nicklaus, Joseph J. Barchi, Jr., Robert J. Fisher and Terrence R. Burke, Jr.</i>	
Towards Photo-Controlled Collagens	561
<i>Ulrike Kusebauch, Sergio A. Cadamuro, Luis Moroder and Christian Renner</i>	
Template-Assembled Peptide Models of the N-Peptide Helix Bundle from HIV-1 gp41	563
<i>Weiming Xu and John W. Taylor</i>	
Alignment of Three Nitroxide Radicals on the Same Face of a Helical Peptide Scaffold	565
<i>Marco Crisma, Simona Oancea, Fernando Formaggio, Elena Sartori, Carlo Corvaja and Claudio Toniolo</i>	
Design, Synthesis, and Preferred Conformation of Peptides Based on a Highly Constrained, β,β' -Diphenyl Substituted Cyclopropane α -Amino Acid	567
<i>Soledad Royo, Wim M. De Borggraeve, Cristina Peggion, Marco Crisma, Ana I. Jiménez, Carlos Cativiela and Claudio Toniolo</i>	
Identification of a Novel HIV-1 Neutralizing Antibody Using Synthetic Peptides that Mimic a GP41 Fusion Intermediate	569
<i>Elisabetta Bianchi, Michael D. Miller, Romas Geleziunas, Gaetano Barbato, Paolo Ingallinella, Marco Finotto, Renee Hrin, Meiqing Lu, Simon Lennard, David Lowe, Gennaro Ciliberto, Daria Hazuda, Riccardo Cortese, John Shiver and Antonello Pessi</i>	
Covalent Trimeric Coiled Coils of the HIV gp41 HR1 Region are Extremely Potent and Broadly Neutralizing Inhibitors of Viral Infection	571
<i>Elisabetta Bianchi, Marco Finotto, Paolo Ingallinella, Renee Hrin, Michael D. Miller, Romas Geleziunas and Antonello Pessi</i>	
Selective Agonists for the Human Vasopressin V1b Receptor are Potent Antidiuretic Agonists in the Rat	573
<i>Stoytcho B. Stoev, LingLing Cheng, Maurice Manning, Nga C. Wo, Hazel H. Szeto, Ana Pena, Brigitte Murat, Sylvain Derick, Miguel Trueba, Maria A. Ventura and Gilles Guillon</i>	
Prion Protein Misfolding: Conformational Stability of the α 2-Helix	575
<i>Pasquale Palladino, Luisa Ronga, Barbara Tizzano, Filomena Rossi, Raffaele Ragone, Teodorico Tancredi, Gabriella Saviano, Angelo Facchiano, Susan Costantini, Menotti Ruvo and Ettore Benedetti</i>	
Modeling Flexible Loops in the Dark-Adapted and Activated States of Rhodopsin, a Prototypical G-protein-Coupled Receptor	577
<i>Gregory V. Nikiforovich and Garland R. Marshall</i>	
Deducing 3D Models of the Activated States for TM Regions of GPCRs by Modeling Constitutively Active Mutants: The Test Case of Opsin	579
<i>Gregory V. Nikiforovich and Garland R. Marshall</i>	
Identification of a Unique Stability Propagation Site that Controls Protein Stability of α -Tropomyosin: a Two-Stranded α -Helical Coiled-coil	581

<i>Janine B. Mills, Stanley C. Kwok, Lawrence B. Smillie and Robert S. Hodges</i> The Introduction of Uncharged α -Hydroxymethyl Amino Acid Residues in Substrate Specificity P1 Position of Trypsin Inhibitor SFTI-1 from Sunflower Seeds Retains its Activity	583
<i>Ewa Zablotna, Agnieszka Kret, Anna Jaśkiewicz, Aleksandra Olma, Mirosław T. Leplawy and Krzysztof Rolka</i> Molecular Simulation of an α/ϵ -Peptide Dendrimer	585
<i>Qitao Yu, Yuguang Mu, Lars Nordenskiöld and James P. Tam</i> A GHS-1a Receptor Agonist that is Highly Effective in Stimulating Body Weight Gain	587
<i>Jesse Z. Dong, John Eynon, Jundong Zhang, John E. Taylor, Heather A. Halem, Rakesh Datta and Michael D. Culler</i> A Non-Competitive Peptide Agonist of GHSR1a Receptor Stimulates Growth Hormone Secretion and Food Intake	589
<i>Abdelkrim Habi, Patric Delhanty, Daniel Abran, Aart Jan van der Lely and Krishna G. Peri</i> Development of μ Opioid Receptor Selective 4-Anilindopiperidine Analogs	591
<i>Yeon Sun Lee, Joel Nyberg, Sharif Moye, Richard Agnes, Adriano Mollica, Peg Davis, Shou-Wu Ma, Josephin Lai, Frank Porreca, Ruben Vardanyan and Victor J. Hruby</i> A Whole-Cell Binding Assay for Testing the Targeting Potential of Cyclic Peptide Ligands	593
<i>Sonya Cressman, Ning Fang, David D. Y. Chen and Pieter R. Cullis</i> Synthesis and Evaluation of Chiral and Achiral α,α -Disubstituted Amino Acids as β -Sheet Stabilizing Factors	595
<i>Jia Wang and Robert P. Hammer</i> Evaluation of Malarial Protease Plasmeprin Inhibitors Containing Hydroxymethylcarbonyl Isostere	597
<i>Koushi Hidaka, Tooru Kimura, Yumi Tsuchiya, Aiko Kiso, Yoshio Hayashi, Azin Nezami, Ernesto Freire and Yoshiaki Kiso</i> Design and Synthesis of β -Secretase Inhibitors: Optimization at the P4 and P1' Positions	599
<i>Yoshio Hamada, Daisuke Shuto, Naoto Igawa, Soko Kasai, Ping Liu, Koushi Hidaka, Tooru Kimura, Yoshio Hayashi, Shoichi Ishiura and Yoshiaki Kiso</i> Synthesis of Non-linear Potential Vaccines for HSV-1	601
<i>Rosalba Mansi, Stefania Galdiero, Diego Tesauro, Ettore Benedetti, Giancarlo Morelli and Massiliano Galdiero</i> Intramolecular Triplet Quenching by Nitroxide Radicals as a Tool for Determining Peptide Secondary Structure in Solution	603
<i>Lorenzo Stella, Gianfranco Bocchinfuso, Emanuela Gatto, Antonio Palleschi, Mariano Venanzi, Daniela Zavallone, Andrea Bettio, Fernando Formaggio, Claudio Toniolo and Bilio Pispisa</i> A Time-Resolved Spectroscopic Study on Peptide Folding	605
<i>Bilio Pispisa, Emanuela Gatto, Gianfranco Bocchinfuso, Antonio Palleschi, Lorenzo Stella, Mariano Venanzi, Fernando Formaggio and Claudio Toniolo</i> Ion Channel Activities and Mechanisms of Ion Conduction about Cyclic Hexapeptides	607
<i>Junichi Taira, Ryo Hayashi, Satoshi Osada, Tsuguhisa Ehara and Hiroaki Kodama</i> Synthesis and Biological Activities of Proline Rich Cyclic Heptapeptide Hymenamide B Analogs	609
<i>Yasuhiro Shiki, Junichi Taira, Aya Nakamura, Satoshi Osada and Hiroaki Kodama</i>	

Synthesis and Biomaterials Application of Polymers Containing Pentapeptide and/or Hexapeptide Sequences Derived from Elastin <i>Kouji Okamoto, Shuichiroh Uehara, Kayoko Matsui, Maria Portia P. Briones, Iori Maeda and Masakazu Furuta</i>	611
Synthesis and Biological Activities of fMLP Analogs Containing 2,3-Cyclopropane Amino Acid Derivatives <i>Daisuke Sugiyama, Ryo Hayashi, Hiroshi Kawasaki, Hiroaki Kodama, Satoshi Osada, Masafumi Zaitu and Ichiro Fujita</i>	613
<i>pI</i> -shifted Basal Insulin Analogs with High Selectivity for Insulin vs IGF-1 Receptor <i>Wayne D. Kohn, Radmila Micanovic, Sharon L. Myers, Andrew M. Vick, Steven Kahl, Lianshan Zhang, Beth Striffler, Shun Li, Jing Shang, John M. Beals, John P. Mayer and Richard D. DiMarchi</i>	615
N-Backbone Methylations of Parathyroid Hormone (PTH) C-Terminal Region: Bioactivities and Implications for PTH-Receptor Complex <i>Zhanna Potetinova, Jean-René Barbier, Thomas J. Gardella, Thomas Dean, James F. Whitfield and Gordon E. Willick</i>	617
N-Backbone Methylations of Parathyroid Hormone (PTH) C-Terminal Region: Effects on Structure <i>Zhanna Potetinova, Feng Ni and Gordon E. Willick</i>	619
C-Terminal Modified Parathyroid Hormone: Effects on Structure and Activity <i>Zhanna Potetinova, Jean-Rene Barbier, Thomas Dean, Thomas J. Gardella and Gordon E. Willick</i>	621
Spectroscopic Characterization of PEG-Amylin Derivatives <i>Giuseppe Impellizzeri, Diego La Mendola, Antonio Magri, Giuseppe Maccarrone, Giuseppe Pappalardo and Enrico Rizzarelli</i>	623
Conformational Properties and Functional Role of VDAC N-Terminal Peptide <i>Vito De Pinto, Angela Messina, Rita Aiello, Flora Tomasello, Diego La Mendola, Antonio Magri, Danilo Milardi and Giuseppe Pappalardo</i>	625
Design of Membrane Active Peptides with Regularly Repeating Glycine or D-amino Acid Residues <i>Jyothi Thundimadathil, Roger W. Roeske and Lili Guo</i>	627
Design and Synthesis of Novel α -MSH Peptide Analogs Highly Selective for the hMC4R <i>Victor J. Hruby, Jinfa Ying, Xuyuan Gu, Minying Cai, Josef Vagner, Dev B. Trivedi and Katalin E. Kövér</i>	629
Design, Synthesis and Characterization of Conformational Peptides at the Interface of HER-2 Dimerization and Pertuzumab Binding <i>Joan T. Steele, Sharad Rawale and Pravin T. P. Kaumaya</i>	631
Synthesis of a Phosphino Triple Helical Collagen Mimic <i>John K. Whitehead, Shunzi Li, LaKeisha N. Myles, Robert P. Hammer and Gregg B. Fields</i>	633
Steric Hindrance of the HER-2/neu Dimerization Loop by Peptide Mimic Antibodies <i>Stephanie D. Allen, Sharad Rawale and Pravin T. P. Kaumaya</i>	635
Hydrogen/Deuterium Exchange Studies on Helical Peptides in a DMSO/MeOD Solvent System <i>Erin Daly, Adam Blom and Matt Kubasik</i>	637
Octapeptide Analogs of Somatostatin Containing α,α -Dialkylated Amino Acids with Potent Anticancer Activity <i>Sudhanand Prasad, Archana Mathur, Neena Gupta, Manu Jaggi, Anu T. Singh and Rama Mukherjee</i>	639
Backbone Cyclization Improves the Enzymatic Stability of χ -Conotoxin, MrIA,	641

whilst Maintaining its Structure and NET-Modulating Activity <i>Erica S. Lovelace, Christopher J. Armishaw, Michelle L. Colgrave, Paul F. Alewood, Norelle L. Daly and David J. Craik</i>	
<i>De novo</i> Design of Peptide Folds of Stereochemically Rationalized Molecular Architecture <i>Soumendra Rana, Bijoy Kundu and Susheel Durani</i>	643
Restructuring Artificial Peptide Networks by External Triggering <i>Gonen Ashkenasy and M. Reza Ghadiri</i>	645
Development of a Stilbene-type Photoswitchable β -Hairpin Mimetic <i>Máté Erdélyi and Adolf Gogoll</i>	647
The Guanidinium Group: A Key Player in Molecular Recognition <i>Ernest Giralt, Susana Gordo, Ignasi Belda, Silvia Pujals, Marc Martinell, Xavier Salvatella and Jimena Fernández-Carneado</i>	649
Novel and Highly Selective Antagonist Scaffold for Human Melanocortin 3 Receptor: Computer-Aided Design and Biological Evaluation <i>Alexander V. Mayorov, Minying Cai, Kevin B. Chandler, Ravil R. Petrov, April R. Van Scoy, Zerui Yu, Dustin K. Tanaka, Dev Trivedi and Victor J. Hruby</i>	651
Transmembrane Peptide Segments of the Uncoupling Protein-1: Chemical Synthesis and Biophysical Properties <i>Masoud Jelokhani-Niaraki and Marina Ivanova</i>	653
Discovery and Optimization of β -MSH Derived Melanocortin-4 Selective Agonists <i>John P. Mayer, Hansen M. Hsiung, David B. Flora, Patrick Edwards, Dennis P. Smith, Xing-Yue Zhang, Robert A. Gadski, Mark L. Heiman, JeAnne L. Hertel, Paul J. Emmerson, Saba Husain, Thomas P. O'Brien, Steven D. Kahl, David L. Smiley, Lianshan Zhang, Richard D. DiMarchi and Liang Zeng Yan</i>	655
Molecular Mechanisms of Constitutive Activity: Mutations at Position 111 of the Angiotensin AT1 Receptor <i>Gregory V. Nikiforovich, Balász Mihalik, Kevin J. Catt and Garland R. Marshall</i>	657
A Surprise End to 20 Year Search for Selective Agonists for Rat Vasopressin V _{1b} Receptor <i>Maurice Manning, LingLing Cheng, Stoytcho B. Stoev, Nga C. Wo, Hazel H. Szeto, Ana Pena, Brigitte Murat, Miguel Trueba, Maria A. Ventura and Gilles Guillon</i>	659
Furanoid Sugar Amino Acids in Design of Analogs of VIP Receptor Binding Inhibitor <i>Sudhanand Prasad, Archana Mathur, Manu Jaggi, Rajan Sharma, Neena Gupta, Rama Mukherjee, Ajit C. Kunwar and Tushar K. Chakraborty</i>	661
Two Residues at the Extracellular Face of TM5 and TM6 Interact in the Active State of a G Protein-coupled Receptor <i>Yong-Hun Lee, Fred Naider and Jeffrey M. Becker</i>	663
Molecular Probes for Visualizing Angiogenesis <i>Alan Cuthbertson, Grete Mørk Kindberg, Bård Indrevoll, Joseph Arukwe, Hege Karlsen, Alex Gibson, Julie Davis, Marivi Mendizabal, Matthew Morrison and Matthias Glaser</i>	665
The Two Cysteine-rich Head Domains of Minicollagen from <i>Hydra</i> Nematocysts Differ in their Cystine Framework and Overall Fold despite an Identical Cysteine Sequence Pattern <i>Alexander G. Milbradt, Cyril Boulegue, Luis Moroder and Christian Renner</i>	667
Polypeptide Ligands Containing Switchable Flexible Linkers as Retractable Inhibitors of Protein-Protein Interactions <i>Dmitri Tolkatchev, Anna Vinogradova, Rana Filfil and Feng Ni</i>	669
Helix Formation in α/β -, α/γ - and β/γ -Hybrid Peptides	671

<i>Carsten Baldauf, Robert Günther and Hans-Jörg Hofmann</i>	
Nanometer-Scale Amino Acids for Biomolecular Nanotechnology	673
<i>James S. Nowick, Chris M. Gothard, Sang-Woo Kang and Santanu Maitra</i>	
Design and Synthesis of Target-specific Contrast Agents	675
<i>Anouk Dirksen, Sander Langereis, Bas F.M. de Waal, Marcel H.P. van Genderen, E.W. Meijer, Wencke Adriaens and Tilman M. Hackeng</i>	
Design and Synthesis of Novel Chromone Based Peptidomimetics	677
<i>Kristian Dahlén, Morten Grøtli and Kristina Luthman</i>	
Determination of Intrinsic Hydrophilicity/Hydrophobicity Coefficients of Amino Acid Side-Chains using Synthetic Model Peptides	679
<i>James M. Kovacs, Colin T. Mant and Robert S. Hodges</i>	

Peptide Structures in Material Science and Disease

Peptide Reptation as a Mechanism for Rearrangements within a β -Sheet Aggregate	683
<i>Sarah A. Petty and Sean M. Decatur</i>	
The HIV-1 Fusion Peptide has Amyloid Properties	686
<i>Patrick Mobley, Alex Nisthal, Jeff Julius, Jonathan Kelber, Albert Gonzales, Sepehr Eskandari, Alan Waring and Larry Gordon</i>	
Self-Assembly of Collagen Mimetic Peptides	688
<i>Frank W. Kotch and Ronald T. Raines</i>	
Engineered Synthetic Peptide Epitopes from the Extracellular Domain of HER-2/neu are Recognized by Trastuzumab	690
<i>Joan T. Steele, Stephanie D. Allen, Sharad Rawale and Pravin T. P. Kaumaya</i>	
Mapping Protective Epitopes for Anthrax and Plague Vaccine Antigens by LC-MS/MS	692
<i>Bradford S. Powell, Jeffrey T. Enama, Stephen F. Little, Sylvia Trevino and Tran C. Chanh</i>	
Co-assembling Peptide based Biomaterials	694
<i>Sivakumar Ramachandran, Yiider Tseng, Peter Flynn and Yihua B. Yu</i>	
Three-Dimensional Solution Structure of the PAS1 Domain of Phytochrome A from Rice	696
<i>Toshimasa Yamazaki, Rintaro Suzuki, Paul Reay, Nobuya Sakai, Etsuko Katoh and Makoto Takano</i>	
Membrane Initiated Gelsolin Amyloid Formation	698
<i>Inta Liepina, Paul A. Janmey, Cezary Czaplewski and Adam Liwo</i>	
Cooperative Formation, Transformation, and Collapse of Hydrogen-Bonds in Polypeptides	700
<i>Akihiro Abe, Yosuke Imada, Toshihiro Hiejima and Hidemine Furuya</i>	
Reversible Insulin Self-Assembly under Carbohydrate Control	702
<i>Thomas Hoeg-Jensen, Svend Havelund and Jan Markussen</i>	
Influence of the Nucleophilic and Electrophilic Properties of Solvents for Peptide Solubilization: CD Monitoring and the Special Effect of the Water Molecule	704
<i>Luciana Malavolta and Clóvis R. Nakaie</i>	
VCD Spectroscopic Analysis of the Exendin-4 Truncated Analog TC5b	706
<i>Jeffrey Copps, Richard F. Murphy and Sándor Lovas</i>	
Type II β -Turn Formation in Tetrapeptides Evidenced by Vibrational Circular Dichroism Spectroscopy	708
<i>Attila Borics, Richard F. Murphy and Sándor Lovas</i>	
The Conformational Preference of C ^{α} -Centered Protein Radicals	710
<i>Michael Owen, Richard F. Murphy and Sándor Lovas</i>	
Impact of a Single α,α -Disubstituted Amino Acid on β -Hairpin Folding	712
<i>Larry R. Masterson, Marcus A. Etienne, George Barany, Gianluigi Veglia and</i>	

<i>Robert P. Hammer</i>	
RGD-Cy7 Conjugates as Near-Infrared Fluorescence Probes to Image $\alpha_v\beta_3$ Integrin Expression in Brain Tumor Xenografts	714
<i>Yun Wu and Xiaoyuan Chen</i>	
Parameters Influencing Helix Stability of Oligoureia Foldamers	716
<i>Aude Violette, Marie-Christine Averlant-Petit, Didier Rognan, Henri Monteil, Jean-Paul Briand and Gilles Guichard</i>	
The Tertiary Structure of A β 1-40 Determined by Scanning Tunnelling Microscopy	718
<i>Dusan Losic, Lisandra L. Martin, Adam Mechler, David H. Small and Marie-Isabel Aguilar</i>	
Validation of Active-Site Mapping of Enzymes	720
<i>Daniel J. Kuster and Garland R. Marshall</i>	

Peptide and Protein Arrays

Protein Arrays as Tools for Detection of Protein-Protein Interactions by Mass Spectrometry	725
<i>Christian F. W. Becker, Ron Wacker, Werner Bouschen, Ralf P. Seidel, Branko Kolaric, Pascal Lang, Hendrik Schroeder, Christof Niemeyer, Bernhard Spengler, Roger S. Goody and Martin Engelhard</i>	
New Tools for the Site-Specific Attachment of Proteins to Surface	728
<i>Youngeun Kwon, Matthew A. Coleman and Julio A. Camarero</i>	
Designed Peptide Microarrays for Protein Detection and Characterization	731
<i>Kenji Usui, Kin-ya Tomizaki, Kiyoshi Nokihara and Hisakazu Mihara</i>	
Luminescent Cd Te Quantum Dots/Albumin Conjugates: Preparation, Fluorescence, Characterization and Labeling of C. Elegans	734
<i>Huilian Ma, Hanzhi Liu, Liping Wang, Shukun Xu and Wei Li</i>	
SC ² : A Novel Process for Manufacturing of High Density Multi-Purpose Chemical Micro-Arrays	736
<i>Antonius J. Dikmans, Ulrike Beutling, Sabine Thiele and Ronald Frank</i>	
High Throughput Preparation of Peptide Arrays Containing Two Fluorescent Dyes Focusing on Practical Protein Detection Systems	738
<i>Kiyoshi Nokihara, Takafumi Ohyama, Koichi Yonemura, Yasuo Oka, Kenji Usui and Hisakazu Mihara</i>	
Identification of Antioxidant Peptides using SPOT Synthesis	740
<i>Marloes Schurink, Willem J. H. van Berkel, Harry J. Wichers and Carmen G. Boeriu</i>	
Water Channel (Aquaporin 3) Gene Activation Correlates with Substance P in ARDS	742
<i>Simon S. Wong, Nina N. Sun and Mark L. Witten</i>	

Proteomics and Emerging Technologies

RDC as a New NMR-Parameter for Peptides	747
<i>Horst Kessler, Burkhard Luy, Kyril Kobzar, J. Christoph Freudenberger, Sebastian Knör, Dominik Heckmann and Jochen Klages</i>	
Examination of the Role of Lipid Rafts in GPCR Signal Transduction Using Plasmon Waveguide Resonance (PWR) Spectroscopy	750
<i>Victor J. Hruby, Isabel D. Alves, Savitha Devanathan, Zdzislaw Salamon and Gordon Tollin</i>	
Switchable Inteins: New Tools to Control Protein Function by using Regulated Protein Splicing	754
<i>Steffen Brenzel, Christina Ludwig and Henning D. Mootz</i>	

Pin1: Inhibitors and Mechanism	759
<i>Felicia A. Etzkorn, Joseph P. Noel, Yan Zhang and Xiaodong J. Wang</i>	
Discovery and Structural Optimization of High Affinity Co-Agonists at the Glucagon and GLP-1 Receptors	763
<i>Vasily M. Gelfanov, David L. Smiley, Wesleyne Whittaker and Richard D. DiMarchi</i>	
Development of a Lanthanide-based Assay for δ -Opioid Receptor	765
<i>Josef Vagner, Rajesh Sankaranarayanan, Heather Handl, Victor J. Hruby and Robert J. Gillies</i>	
Interaction between a Minimum Hevein Domain and Chitooligosaccharides Studied by NMR and a Novel Surface Plasmon Resonance Method	767
<i>Miquel Vila-Perelló, Nuria Aboitiz, Ricardo Gutierrez Gallego, Francisco J. Cañada, Jesús Jiménez-Barbero and David Andreu</i>	
Cross-Reactivity Studies of rMOGED with Synthetic Putative Autoantigens CSF114(Glc) and [N31(Glc)]hMOG(30-50) in Multiple Sclerosis Patients' Sera	769
<i>Barbara Mulinacci, Constanze Breithaupt, Prajna P. Pal, Nedijlko Budisa, Marta Pazzagli, Benedetta Mazzanti, Paolo Rovero, Luis Moroder and Anna M. Papini</i>	
Thiohydantoins – A Technique for Labeling Peptides and Proteins	771
<i>Carole Brückler and Mark Bradley</i>	
Photodimerization in Substituted di- and Oligopeptides by UV-light for Optical Data Storage	773
<i>Brian Lohse, P. S. Ramanujam, Søren Hvilsted and Rolf H. Berg</i>	
Does an Aberrant Glucosylation Trigger Autoimmunity in Multiple Sclerosis?	775
<i>Francesca Nuti, Ilaria Paolini, Elisa Peroni, Feliciano Real-Fernández, Marta Pazzagli, Maria C. Pozo-Carrero, Francesco Lolli, Mario Chelli, Paolo Rovero and Anna M. Papini</i>	
Phosphopeptide Proteomics with On-Bead Chemical Synthesis and Display on PEGA Support	777
<i>Malene Brandt, Jens Chr. Madsen, Steen Gammeltoft and Knud J. Jensen</i>	
Optimization of Multiple Sclerosis Antigenic Probes by a Combinatorial Approach	779
<i>Maria C. Alcaro, Francesca Barbetti, Francesca Nuti, Feliciano Real-Fernández, Benedetta Mazzanti, Mario Chelli, Paolo Rovero and Anna M. Papini</i>	
Antiproliferative Effect of Lamprey Gonadotropin-releasing Hormone III on Cancer Cells from Non-reproductive Organs	781
<i>Krisztina Herédi-Szabó, Richard F. Murphy and Sándor Lovas</i>	
New Cyclotide Precursor Sequences	783
<i>Lillian Sando, Rekha Bharathi and David J. Craik</i>	
Development of an Efficient Multiple Sclerosis Diagnostic Technology Based on an Optical Glycopeptide Immunosensor	785
<i>Emily S. Bulukin, Elisa Peroni, Maria Minunni, Marta Pazzagli, Paolo Rovero, Marco Mascini and Anna M. Papini</i>	
Author Index	789
Subject Index	803

Merrifield Award Lecture

Dr. Richard A. Houghten

From Tens to Trillions - Advances in Synthetic Combinatorial Chemistry of Peptides, Peptidomimetics and Heterocyclic Compounds Derived from Peptides

Richard A. Houghten Ph.D.

Torrey Pines Institute for Molecular Studies, 3550 General Atomics Court, San Diego, CA 92121, USA

Introduction

An important shortcoming in contemporary biomedical research has been the lack of substantive progress in reducing the cost and time, while ultimately increasing the success rate of drug discovery. In spite of the many advances in technology and basic understanding over the past decade, surprisingly little increase has occurred in the number of new drugs available. This problem has resulted in the longstanding and continuing reality in the pharmaceutical industry that new drugs coming into the marketplace are often mere modifications of existing chemical entities (“me too drugs”), rather than truly novel compounds that are actually optimal or unique to the target of interest.

The revolutionary advances in combinatorial chemistry over the past 20 years now enable extremely large numbers of individual compounds to be synthesized. This has fostered a simple volume-driven approach not greatly different from that utilized for the past 50 years, but which in turn has several of its own challenges. The first involves the extremely large number, manner and format of compounds to be prepared and screened. The second involves the type(s) of assays with which these compounds can or should be used, and how the compounds should be tested in such assays. Both of these factors typically hamper academic and non-profit research organizations.

It started with peptides! Over the course of the past 20 years, our group has been consistently working toward the development of new techniques to discover simple solutions or approaches to complicated concepts or methodologies. To this end, we have directed our efforts toward the conception and development of novel approaches that permit the simplification of synthetic and screening processes of value to the drug discovery process. These efforts have resulted in the development of five key technologies: (1) the “tea bag” method for solid phase synthesis [1]; (2) the use of “mixture-based” combinatorial libraries to identify highly active individual compounds from literally millions of others [2]; (3) the use of “positional scanning” approaches for the rapid identification of individual compounds from highly diverse mixture-based combinatorial libraries [3]; (4) the “libraries from libraries” method for the generation of very large acyclic and heterocyclic combinatorial mixture-based libraries [4]; and (5) the solid phase synthesis on “volatilizable” solid supports and linkers that can be completely removed by their ultimate decomposition and ultimate “volatilization” during the final cleavage step of the synthetic process [5].

Tea bag technology

Early on, we realized that a significant factor in virtually every screening assay was the simple reality that the number of compounds that could be synthesized per chemist per year was extremely limited, typically 20-50 per year. In 1984, we

recognized that for the synthesis of every peptide ever prepared by manual and automated solid phase approaches, each of the dozens of repetitive wash, deprotection and neutralization steps were identical. In fact, only the addition of the desired successive amino acids in the growing peptide chain required an individualized step. We reasoned that if the resin for each separate peptide desired could be compartmentalized in separate polypropylene mesh packets (the “tea bag”

approach) (Fig. 1), then this simple expedient would enable peptides (and later all other compound types that could be synthesized on a solid support) to be synthesized more quickly and at a much lower cost per compound. The first successful use of this approach in our laboratory revealed that the method was not only feasible, but far exceeded even our most optimistic expectations. Thus, in our laboratory, in which we were fortunate at the time to have four automated synthesizers, we could prepare approximately 500

peptides per year. With the tea bag approach we were now able to synthesize between 5,000 and 10,000 individual different peptides using the same quantity of reagents, time, cost, laboratory space and personnel. The tea bag concept, and illustrations of its practical application, was published in 1985 in PNAS, followed by a U.S. patent in 1986 [1]. The apparatus

for cleavage of multiple compound resins with hydrogen fluoride (HF) illustrated in Figure 2 is described in detail elsewhere [6]. To cleave compounds from their resins, one can use free resin, or more conveniently a single resin packet is placed into each HF reaction vessel. A Teflon coated magnetic stir bar and an amount of anisole or other carbonium ion scavenger equaling 10% of the expected volume of HF are also added to each reaction vessel. After cooling in a dry ice/acetone solution, the vessels are purged with nitrogen, and HF is uniformly condensed, via the radial manifold, into all of the reaction chambers. When the desired amount of HF has been condensed, the dry ice/acetone bath is replaced with an ice/water bath and the reaction solutions stirred for 1 hr at 4°C. After 1 hr the HF

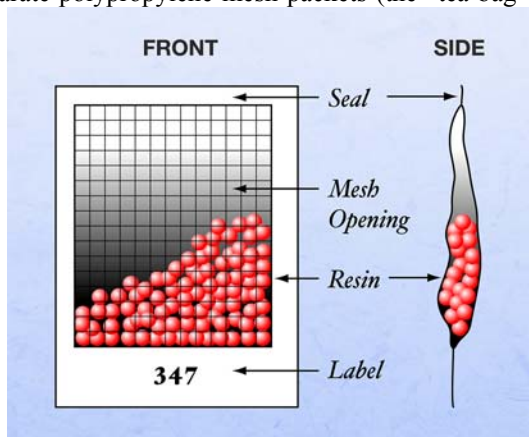


Fig. 1. Tea bag illustration.

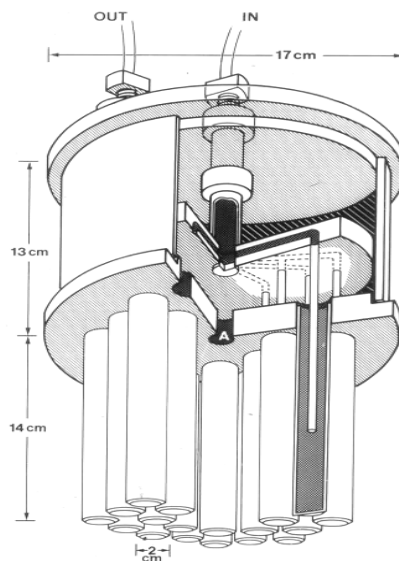


Fig. 2. HF cleavage apparatus.

is rapidly removed by nitrogen flow or with an aspirator vacuum. Residual HF is then removed under 1-2 mm vacuum for 15 min. After complete evaporation, the individual vessels are removed from the apparatus and placed in an extraction rack, which allows for simultaneous extraction of the resin in all vessels. The resins are extracted three times with ether or ethyl acetate to remove residual anisole. The crude products are then extracted from the spent resin or resin packet with three volumes of 5-15% acetic acid/water. The resulting pooled aqueous acetic acid extraction solutions are frozen and lyophilized to yield the desired crude products. This immediately allowed a number of studies in our laboratory, and in collaboration with other laboratories, that previously had not been possible.

The tea bag approach resulted in a substantial decrease in cost and delivery time for custom synthesized peptides. This prompted me to found Multiple Peptide Systems (now NeoMPS Inc.) to make synthetic peptides available more quickly and less expensively than previously possible. At the time, the cost for a typical custom synthesis of a single peptide, 10 residues in length, was approximately \$1,000. Using the tea bag method, the same peptide could be produced for approximately \$25, while not only passing the cost benefits on to the scientific community, but also maintaining a robust commercial business. This resulted in an enormous economic and scientific benefit to the scientific community.

Mixture-based combinatorial libraries

The success of MPS, lead me to found the Torrey Pines Institute for Molecular Studies (TPIMS), a non-profit research institute. The idea of mixture-based approaches to library synthesis and screening was prompted by the realization that, even with the large increase in synthetic capabilities enabled by the tea bag method, the number of compounds desired still far exceeded the numbers that could be synthesized. We recognized that if we could synthesize mixtures of compounds in a systematic and reproducible manner that could be utilized directly in assays without modification of existing protocols, then we would be able to identify highly-active individual compounds in a much shorter time frame than if the same numbers of compounds were prepared and screened individually. In short, existing assay systems would not have to be changed in order to use mixture-based libraries. Mixture-based synthetic combinatorial libraries (SCLs) can be closely likened to the screening of natural product extracts. Such extracts virtually always involve the screening of mixtures; however, natural product extracts not only are made up of a highly diverse range and type of compounds, but also the compounds in these extracts vary by orders of magnitude in their individual concentrations. The advantage of synthetic mixtures as compared to natural product extracts is that since these are inherently synthetic, one has an immediate synthetic process in hand, which in turn means that one also already knows the structure of the compounds being screened. Further, by the methods utilized to prepare the mixtures, the concentrations of the compounds in the mixtures are close to equal, which is certainly not the case for natural product extracts.

Our laboratory has used both the “split and mix” [2] method as well as the ratios of incoming building block reagent method [9] to ensure equal -- or close to equal -- molar concentrations of each compound making up the mixtures of interest. These methods have been successfully utilized in various formats in a wide variety of assays over the past 12 years and led to the founding of Houghten Pharmaceuticals in 1992 (later named Trega Biosciences). Published first in Nature in 1991 [2; reviewed in 7,8] (with 10 U.S. patents awarded over the period 1992-1997), the initial approach involved an iterative deconvolution strategy as the means to identify individual compounds from the mixtures making up the library. This approach, while steady and powerful, was ultimately determined to be synthetically slow, and the iterated mixtures, as well as the ultimate individual compounds, were rarely found to be of value in other assays. Figure 3 illustrates a highly simplified example of the iterative deconvolution process. In this example a hypothetical tetrapeptide mixture-based library totaling 256 tetrapeptides is shown (4 amino acids at each position, $4^4=256$). Using the one letter codes for alanine, arginine, serine and threonine (A, R, S and T), the four mixtures making up the starting library OXXX are AXXX, RXXX, SXXX and TXXX (64 tetrapeptides in each mixture $4 \times 4 \times 4$). If one assumes that one and only one tetrapeptide is active and if that one active peptide is RATS, then upon screening, the only mixture having activity would clearly be RXXX (since it is the only one that could contain RATS). The iterative process then entails making four new mixtures with their second position fixed (RAXX, RRXS, RSXX and RTXX—each now have 16 tetrapeptides per mixture). As before, only one mixture, RAXX, would be active. This process is repeated twice more to define the remaining two positions and will result in the identification of the only active tetrapeptide, RATS, from the 256 starting tetrapeptides. This

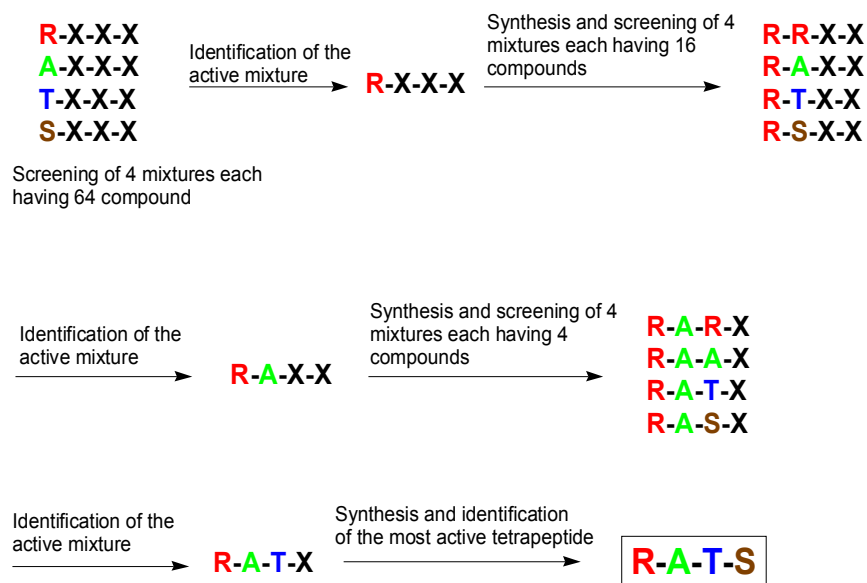


Fig. 3. Iterative deconvolution process.

iterative process has been utilized for libraries ranging in number from 6.25 million tetrapeptides to 64 million L- or D-amino acid hexapeptides and can be utilized for any mixture and compound type accessible by currently available synthetic methods. As anticipated, and found experimentally, for libraries made up of large numbers of compounds, more than one mixture will be typically found to be active at each iterative position. To reduce the number of individual compounds to be synthesized from the screening results, selection of the building blocks to be incorporated in the synthesis of individual compounds is based first on the overall activity of the mixture and then on differences in the chemical character of the building blocks identified.

Positional scanning libraries

This led to a third important advance from our laboratory, namely positional scanning deconvolution. This important and novel concept, which can be used in virtually any assay system, enables information regarding active functionalities to be determined at every position in a given template of compounds in a single screening. First published in 1992 [3] the opposition to these methods was often fierce!

The positional scanning (PS) approach involves the synthesis and screening of separate, single defined position SCLs to individually identify the most important functionalities at each position of diversity within a library. Therefore, each positional sub-library, while addressing a single position of the compound of interest, represents identical collection of compounds. For example, a complete PS-SCL having three positions of diversity consists of three single defined position SCLs (designated OXX, XOX, and XXO), each of which have a single defined

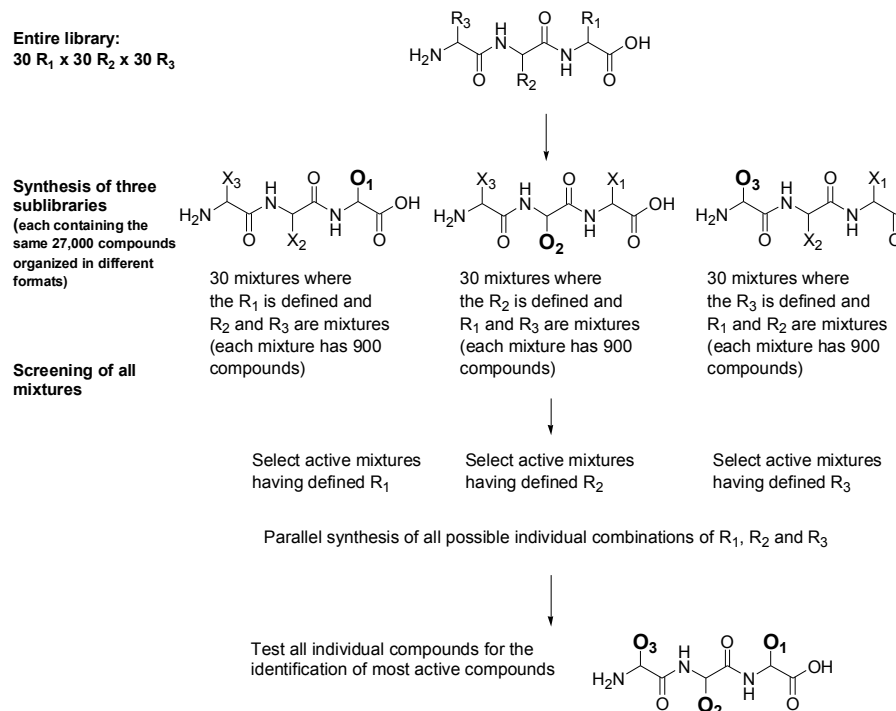


Fig. 4. Positional scanning deconvolution process.

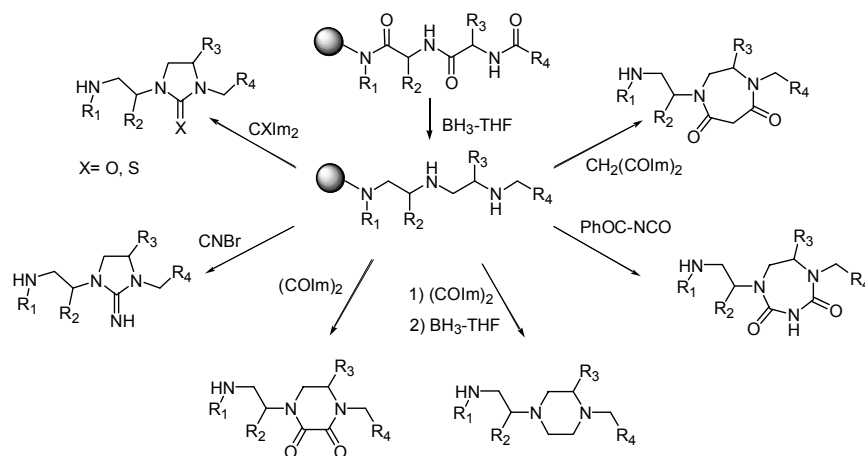
functionality at one position (O) and a mixture of functionalities at each of the other two positions (X) (Fig. 4). If such a library contains 27,000 compounds in total (30x30x30), the pooling of each sub-library containing thirty sets of the same 27,000 compounds (3 mixtures of 900 compounds) would vary based on the functionality at the defined position of that single defined position SCL. When used in concert, the data derived from each positional sub-set yields information about which are the most active functionalities at each of these positions. Information about possible active individual compounds can be determined in a single assay (i.e., in as little as 24 hrs).

The PS-SCL approach relies on the connectivity between the functionalities defining the most active mixtures at each position being addressed. If the functionalities defining the most active mixtures from each of the single positional SCL are indeed found to be connected to each other (i.e., represent the same active compound(s) present in the corresponding mixtures), then combinations of these functionalities will lead to active individual compounds. Thus, individual compounds that represent all possible combinations of the selected functionalities at each position will then be synthesized in order to confirm the screening data and determine their relative activities. This positional scanning process has been successfully used for the identification of a wide range of potent opioid agonists and antagonists that have little or no resemblance to the natural endorphins and affinities comparable to or greater than the native ligand [10]. In other examples, non-carbohydrate ligands having 10-fold greater activities than known carbohydrate inhibitors have been identified as inhibitors of glucosidase, as well as novel antimicrobial compounds that act selectively against gram-positive bacteria [7].

Mixture-based library approaches will continue to find favor with researchers who have limited resources, have limited knowledge of their biological target, and/or have assays that are not amenable to classic high throughput. Mixture-based libraries offer a powerful advantage in that very large diversities can be synthesized and screened in a rapid and cost efficient manner. Mixtures also enable large numbers of compounds to be tested in “low-throughput” assays (e.g., tissue and/or *in vivo* systems) and in those systems in which target reagents are limited by availability or cost.

Libraries from libraries

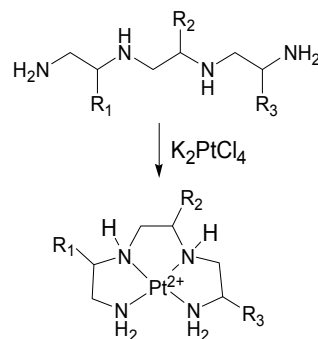
Peptides have often been (and still are) considered poor therapeutic candidates, despite the fact that a number of peptides are successful therapeutics. We recognized that in order to continue to progress in the field of drug design, we would have to generate low molecular weight acyclic and heterocyclic compounds of the type that were desired by medicinal chemists and the pharmaceutical industry. This led to yet another, my fourth, fundamental accomplishment: “libraries from libraries”. Realizing that we could use our existing peptide and peptidomimetic libraries as starting materials, we systematically transformed such libraries into a wide range of low molecular weight compounds (having dramatically differing physical and chemical properties from the starting peptide and peptidomimetic libraries) in exactly the same format and mixture size as the starting combinatorial libraries (Scheme 1) [4]. First published in 1994 (and patented in various forms from 1998 to the present), there now exists, as prepared by my research group over the past 10 years, more than 50 different low molecular weight acyclic and heterocyclic mixture-based combinatorial libraries that total more than 8,000,000 compounds. These combinatorial libraries can and have been screened in a wide



Scheme 1.

range of in vitro assays [7]. A recent notable accomplishment is the identification of a series of compounds that have clear and exciting anticancer activity [11].

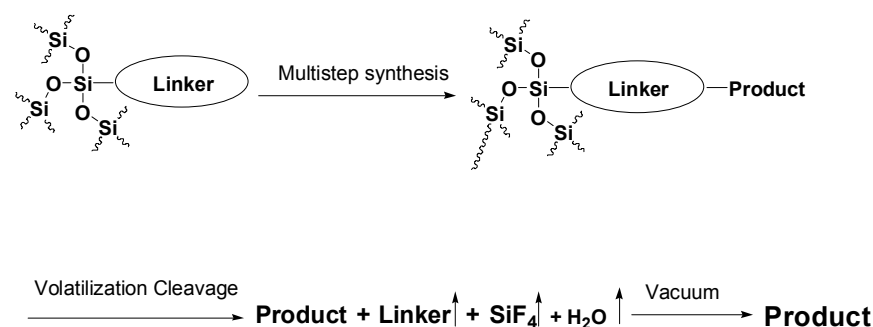
In order to expand the “libraries from libraries” concept, we have combined solid phase and solution phase syntheses for the synthesis of unique chemical libraries such as nitroso amines and platinum tetraamine coordination complexes (Scheme 2).



Scheme 2.

The concepts and use of “volatilizable” solid supports

Such supports, which are completely removed following volatilizing decomposition, improve the efficiency of the solid phase synthesis of low molecular weight acyclic and heterocyclic compounds as well as peptides, peptidomimetics, and protected peptide fragments. The “volatilizable” silica based solid supports and linkers used to illustrate this concept were found to be



Scheme 3.

completely removed by their decomposition and ultimate “volatilization” during the final cleavage step of synthetic process to yield solely the desired synthetic products in the final reaction vessel (Scheme 3) [5].

Future directions

The inception and growth of combinatorial chemistry over the past 20 years has quantitatively changed compound screening. As mentioned above, these libraries have been successfully utilized in a wide range of *in vitro* assays for the identification of highly active individual compounds. Of these approaches, many of the most practical and widely used were invented, pioneered and discovered in our laboratory, and have universally changed compound synthesis and screening by greatly increasing the quantity of compounds that are now possible to synthesize and, therefore, screen for activity. It is true that numbers per se, as is often pointed out, have not increased the number of approved drugs thus far. This is the result of many factors: often this is simply due to the fact that highly active and specific compounds identified at the initial targeted *in vitro* screening level have failed in animal models for reasons of bioavailability, toxicity, clearance time etc. New approaches are clearly needed to circumvent these typical failure-prone processes. For example, a more judicious use of animal models is required for the direct screening of more highly organized and thoughtfully selected mixture-based combinatorial libraries. Such an approach will inherently generate higher quality “hits”. It is of note that we have successfully used this approach in three separate *in vivo* systems: the determination of the increase or decrease of blood pressure or heart rate in rats [12]; the mouse allergic encephalitis mouse model for multiple sclerosis [13]; and two long-standing mouse pain models (tail flick and writhing) [14]. In each case, these pilot studies have yielded rapid, clear and immediately useful results. More importantly, when active mixtures are first identified, and active individual compounds later identified from the active mixtures, these compounds inherently have the desired biological activity, since this is the activity being measured. Furthermore, the compounds identified will cross the blood brain barrier (if that is a desired characteristic), will lack acute toxicity, and will have acceptable pharmacokinetic properties.

To the Young Scientists who read this article

I have been fortunate to have invented a number of useful and widely used scientific approaches and to have founded and run several successful companies (one becoming a public company in 1996). For young scientists at the beginning of their careers, I have found that success usually comes following what perhaps seem (in hindsight) obvious reasons. First, you must know your scientific field and know what its current condition is, what its current limitations are and, very importantly, what would be of value to advance your field. Second, know yourself and your limitations (do you have the necessary passion for your work that will enable you to put in the staggeringly large number of hours that are required to succeed, can you self police your own work honestly and objectively). Third, do you want to, and can you work with the highly intelligent and ambitious colleagues you will need as collaborators. Fourth, understand that your colleagues will not necessarily welcome your success (scientists are just as prone to envy and disappointment as anyone else!). Fifth, try to be patient with the “system” and your scientific colleagues as you will learn as you get older that change is in fact challenging for everyone. Finally,

never forget that luck, good fortune or whatever equivalent term you would like to use is an essential component in every endeavor, so do what you do every day for the love of scientific discovery. I find that scientific research is a never ending and exciting path and can imagine no better more continually exciting and constantly renewing occupation.

Acknowledgements

I am extremely moved and honored to be the recipient of the “Merrifield” award. The research described in this article would not have been possible without Bruce Merrifield’s initial solid phase approaches, as well as, the intellectual capabilities and efforts of my long time scientific and administrative colleagues and friends. These individuals are John Ostresh, Clemencia Pinilla, Jon Appel, Michal Lebl, Sylvie Blondelle, Jeanick Pascal, Colette Dooley, Adel Nefzi, Marc Giulianotti, Yong Ping Yu, Peggy Totzke and Karen Garitta. (See photos below.) While the award is affixed with only my name, the above mentioned people should be equally recognized for their very real and continuing contributions to this award. I have also been blessed with mentors who have been essential to my direction and successes over the past 30 years. George B. Kauffman from California State University, Fresno, who has had the patience and wisdom to help me both personally and professionally since I was 20 years old. Professor Henry Rapoport, University of California, Berkeley was my graduate advisor in synthetic organic chemistry and taught me not only how to carry out careful laboratory synthetic studies, but also the essential need to understand the variables important in all scientific studies. My post doctoral advisor, Professor Choh Hao Li, of the University of California, San Francisco, was always generous with his advice and patient as I learned to connect synthetic chemistry with biological systems. Richard A. Lerner, M.D. of The Scripps Research Institute has served as an admirable long time example of someone able to expand science to the larger community outside the laboratory. Rao Rapaka, Ph.D. from NIH had the foresight to understand very early the power and benefit of many of the approaches we have developed over the years and also helped me to better understand the entire NIH system. Garland Marshall, Ph. D. Saint Louis University, was able to give his generous advice and guidance at a critical time in my career. Finally, Murray Goodman, University of California, San Diego was always a man who I could look to as an admirable scientist when I was younger and a much appreciated friend and mentor over the past 10 years. I thank all of these individuals. Finally, it is also essential to acknowledge the long term support of the National Institutes of Drug Abuse (NIDA) Grant No. 5 RO1 DA09410 (Houghten), the National Cancer Institute Grant No. CA78040 (Houghten), and the Pain Management Research Institute of America (Dooley).

References

1. Houghten, R. A. *Proc. Natl. Acad. Sci. USA* **82**, 5131-5135 (1985); US Patent# 4,631,211.
2. Houghten, R. A., Pinilla, C., Blondelle, S. E., Appel, J. R., Dooley, C. T. and Cuervo, J. H. *Nature* **354**, 84-86 (1991).
3. Pinilla, C., Appel, J. R., Blanc, P. and Houghten, R. A. *Biotechniques*. **13**, 901-905 (1992); US Patent# 5,556,762.
4. Ostresh, J. M., Husar, G. M., Blondelle, S. E., Dörner, B., Weber, P. A., Houghten, R. A. *Proc. Natl. Acad. Sci. USA* **91**, 11138-11142 (1994).
5. Houghten, R. A. and Yu, Y. P. *J. Am. Chem. Soc.*, **127**, 8582-8583 (2005). U.S. Patent # 6,476,191.

6. Houghten, R.A., Bray, M.K., DeGraw, S.T., and Kirby, C.J. *Int. J. Pept. Prot. Res.* **27**, 673-678 (1986).
7. Houghten, R. A., Pinilla, C., Appel, J. R., Blondelle, S. E., Dooley, C. T., Eichler, J., Nefzi, A. and Ostresh, J. M. *J. Med. Chem.* **42**, 3743-3778 (1999).
8. Nefzi, A., Ostresh, J. M., Yu, Y. P. and Houghten, R. A. *J. Org. Chem.* **69**, 3603-3609 (2004).
9. Ostresh, J. M., Winkle, J. H., Hamashin, V. T. and Houghten, R. A. *Biopolymers* **34**, 1681-1689 (1994).
10. Dooley, C. T. and Houghten, R. A. *Biopolymers* **51**, 379-390 (2000).
11. Schimmer, A. D., Welsh, K., Pinilla, C., Wang, Z., Krajewska, M., Bonneau, M.-J., Pedersen, I. M., Kitada, S., Scott, F. L., Bailly-Maitre, B., Glinsky, G., Scudiero, D., Sausville, E., Salvesen, G., Nefzi, A., Ostresh, J. M., Houghten, R. A. and Reed, J. *Cancer Cell* **5**, 25-35 (2004).
12. Houghten, R. A. *Methods: A Companion to Meth.Enzymol.* **6**, 354-360 (1994).
13. Shukaliak, Q. J., Borrás, E., Prat, E., Gelderblom, H., Houghten, R. A., Kashani, A., Pinilla, C., Stuerzebecher, C. S. and Martin, R. *Mol. Immunol.* **40**, 1075-1087 (2004).
14. Houghten, R. A., Dooley, C. T. and Appel, J. R. *Pharm. Res.*, in press (2006).

Long Term Colleagues and Friends



John Ostresh
1981



Clemencia Pinilla
1987



Jon Appel
1987



Michal Lebl
1987



Sylvie Blondelle
1988



Jeanick Pascal
1989 – MPS

Long Term Colleagues and Friends



Peggy Totzke
1989



Colette Dooley
1990



Adel Nefzi
1995



Marc Giulianotti
1995



Karen Garitta
1997



Yongping Yu
2000

Goodman Memorial

Peptides in the Days of Photonics

Christian Renner and Luis Moroder

¹Max-Planck-Institute of Biochemistry, Martinsried, D-82152, Germany

Introduction

Light represents an ideal primary energy source for manipulating systems of either microscopic or macroscopic size since photons can be applied in well-controlled and clean manner and with extreme spatial and temporal resolution to induce reversible or irreversible photochemical reactions. While irreversible reactions have been applied towards the photocleavage of protecting groups as well as in photocaging and photoaffinity methodology, reversible photoreactions generate interconvertible distinct structures upon the external light stimuli that perfectly suit for molecular light-switches. Among the known photochromic compounds azobenzene, spiropyran, filgides, and diarylethene derivatives have found widespread application in light-switching of optical, chemical and mechanical properties of small molecules, macromolecules, and biopolymers [1-4]. In this context azobenzene proved to be particularly well suited because of the pronounced changes in geometry and polarity upon the light-triggered *cis-trans* isomerization, but foremost because of the high (photo)stability, the high isomerization and quantum yields [5]. The pioneering work of Murray Goodman [6,7] with azobenzene for photomodulation of conformational states in poly- α -amino acids has stimulated extensive studies in the field [8]. Because of the inherent drawbacks of using multiple photochromic units in molecular architectures, increasing attention has been paid more recently to the design of simple peptide systems with single light-switches appropriately positioned to constrain and relax the conformational space of the peptide backbone in reversible manner. By this approach the extremely fast and fully reversible isomerization process [9] was exploited to monitor folding/unfolding processes at femto- to picosecond time scales with ultrafast UV [10,11] and IR spectroscopy [12,13]. Model systems were used which were head-to-tail [14] and side chain-to-side chain [13] crossbridged with appropriate azobenzene derivatives. The most recent advances in the field obtained in our laboratory with azobenzene as a photoswitch are summarized below.

Results and Discussion

Photomodulation of conformational states: In our first studies (4-aminophenyl)-azobenzoic acid (APB) was used as backbone constituent of cyclic peptides for maximal transduction of changes in geometry of the photochromic unit onto the peptide backbone [14]. Indeed well defined conformational transitions were observed in the thiol-protected *c*[APB-ACATCDGF] peptide containing the active-site bis-cysteiny-motif of thioredoxin reductase. Ultrafast UV measurements clearly revealed overlapping kinetic components resulting from the photoisomerization of the chromophore itself and rearrangement of the peptide backbone which could also be simulated by MD calculations [10]. In order to decouple azobenzene isomerization at the time scale of 1 ps from the peptide backbone dynamics in conformational transitions, (4-aminomethyl)phenylazobenzoic acid (AMPB) [15] was used, which introduces additional degrees of rotational freedom. In the cyclic peptides *c*[AMPB-KCATCDKK] [16] and *c*[AMPB-KCGHCDKK] [17], related to the active-site bis-cysteiny-motif of thioredoxin reductase and protein disulfide

isomerase (PDI), respectively, indeed ultrafast UV [17] experiments clearly revealed such decoupling of the two processes and for the latter peptide in the oxidized bicyclic form well defined conformational preferences in both the *trans*- and *cis*-isomer. Although reduction of the disulfide bond relaxes the conformational constraints leading to more variable structural ensembles, these differ again significantly for the two isomeric states. The usefulness of such softer light-switches has been well documented even in light-driven unfolding of an α -helical model peptide as monitored by IR spectroscopy [13].

While the small cyclic azobenzene-peptides were useful tools for gaining elementary knowledge about dynamics of peptide backbones, in terms of protein folding events the photocontrol of secondary/tertiary structure elements is certainly more instructive. In this context, using 3-(3-aminomethylphenyl)azophenylacetic acid to replace the Asn-Gly dipeptide in the type 1 β -turn of the Trp-zipper hairpin [18], a light-switchable hairpin structure was obtained where the IR difference spectra between the two isomeric states are highly promising in terms of time-resolved photocontrol of related folding/unfolding processes [19]. The ultimate goal, however, remains the photocontrol of model tertiary structures, and for this purpose the design and synthetic approaches toward light-switchable collagen triple helices are in progress [20].

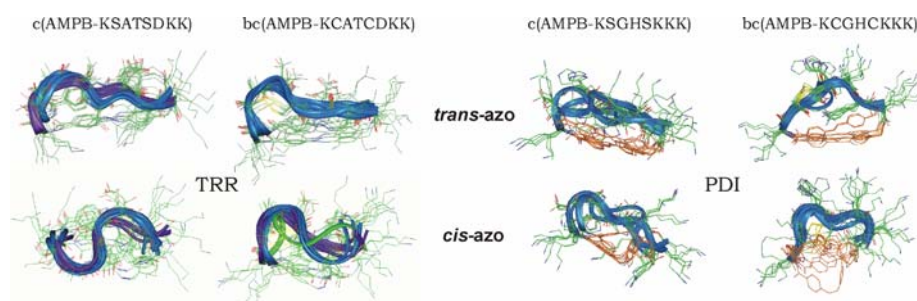


Fig. 1. NMR-derived structural ensembles of the azobenzene-peptides *c*[AMPB-KCATCDKK] (left) and *c*[KCGHCDKK] (right) in water; top: *trans*- and bottom: *cis*- isomers.

Photomodulation of biophysical properties: The redox potentials of thiol protein oxidoreductases are known to strongly depend upon the sequence composition of the active site CXYC motif and the structural constraints imposed on this small protein portion by the overall fold [21]. This was fully confirmed by comparing the redox potentials of linear and cyclic active-site bis-cysteinyl-fragments of these enzymes [22]. Correspondingly, the significant changes in conformational preferences induced by the *trans*→*cis* isomerization of the water-soluble *c*[AMPB-KCATCDKK] peptide in both the reduced and oxidized form (Fig. 1) lead to distinct redox potentials with values of -200 mV for the *trans*- and -146 mV for the *cis*-isomer, the latter being surprisingly similar to that of PDI (-110 mV [23]). Even more pronounced differences in redox potentials were expected for the *cis*- and *trans*-isomers of *c*[AMPB-KCGHCDKK] containing the active-site motif of PDI, since in the oxidized form the two isomers exhibit well defined, but distinct conformational states (Fig. 1). Indeed for the *trans*-isomer a redox potential of -167 mV was determined using GSH/GSSG ($E'_0 = -240$ mV [24]) as a reference redox system. However, for the *cis*-isomer an unexpected fast relaxation into the *trans*-

state was observed with concomitant reduction of the diazene to hydrazine at large extents by the excess GSH required in the experiments. Even replacing GSH/GSSG by the less reducing cysteine/cystine ($E'_0 = -223$ mV [25]) the diazene is rapidly reduced, a fact that might only be explained by a conformation-dependent shift of the redox potential of the azobenzene moiety to significantly higher values than those determined by voltametry for azobenzene itself (-480 mV for the *trans*- and -435 mV for the *cis*-isomer [26]). In fact, in the synthesis of the azobenzene-peptides reduction of the diazene was observed when exposing related compounds to strongly reducing agents such as phosphines or DTT [27], but precautions were also required with the use of 1,2-ethanedithiol or silanes as scavengers [17].

The efficient oxidative folding of proteins with the help of PDI has been attributed to its strongly oxidizing redox potential, but also to chaperone-like activities that enable preferred interactions with the substrate [28]. Although small bis-cysteiny-peptide systems cannot exert chaperone-like activities, the differing redox properties of the *cis*- and *trans*-azo-isomers of *c*[AMPB-KCGHCDKK] were expected to affect catalytic efficiencies in oxidative folding of proteins. As shown in Figure 2, a visible difference in kinetics of oxidative refolding of RNase A was observed using the AMPB-peptide in the *trans*- and *cis*-state as a catalyst [29], thus confirming our working concept.

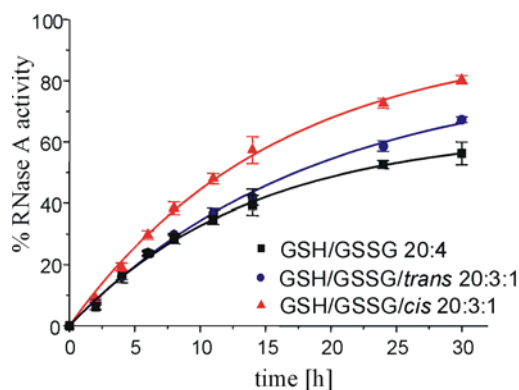


Fig. 2. RNase A refolding (pH 7.4, 30 °C) with 1 equiv. oxidized *c*(AMPB-KCATCDKK) as *cis*- and *trans*-azo-isomer in the presence of GSSG/GSH.

Toward light-driven nanomachines: Nature very elegantly demonstrates that devices can be constructed at a molecular level, which are close structural analogs of macroscopic motors. Nonetheless, the design of artificial molecular motors is only beginning to be explored [30,31]. Particular attention has so far been paid to interlocked molecules such as rotaxanes, catenanes or cyclodextrins [32,33]. Since azobenzene possesses the ability to convert excitation energy into molecular motion, we have selected photoresponsive azobenzene-polymers to attempt the construction of light-driven molecular machines [34,35]. For this purpose the basic principle had to be examined whether the contour length of an azo-containing polymer can be shortened against an external force by simple irradiation to demonstrate a photomechanical energy conversion in an individual molecule (Fig. 3). A photo-responsive polymer was synthesized, which fulfilled the experimental requirements: i) maximum chain-length change upon irradiation, ii) suitably functionalized to

allow the attachment of single polymer chains both to an AFM gold tip and to an amino-functionalized glass slide, iii) adequately long chains for the given experimental setup, and iv) sufficient mechanical stability of the polymer in the two different azobenzene conformations for operating an optomechanical cycle. The sequential poly-pseudotriptide H-[Lys(Adoc)-AMPB-Gly]_n-OH was synthesized with n values of ca 30 and 60 after size exclusion chromatography, depending upon the preparation.

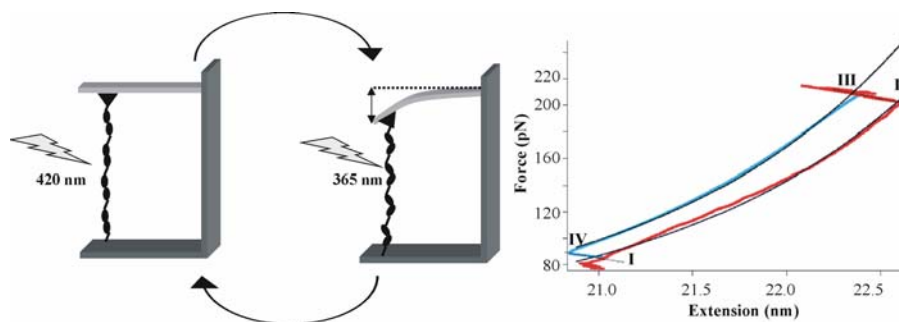


Fig. 3. The left panel outlines the working principle and the right panel the experimental optomechanical cycle.

As shown in Figure 3, starting from the mainly *trans*-azo-polymer the chain was stretched under a mechanical force of 200 pN (I→II). In this stretched state irradiation at 365 nm leads to *trans*→*cis* photoisomerization, which shortens the molecule against the external force applied by the cantilever and thus generates mechanical work by the optical contraction (II→III). Upon release of the mechanical stress, the polymer relaxes (III→IV) and irradiation at 420 nm induces again the *trans*-azo conformation (IV→I), thus closing the optomechanical cycle. Despite the low efficiency of our set-up, the experiments clearly demonstrate the basic feasibility of a single-molecule nano-machine that operates an optomechanical cycle and performs work at the molecular level.

Acknowledgments

The work was supported by the Deutsche Forschungsgemeinschaft (SFB 533, grant A8).

References

1. Willner, I. *Acc. Chem. Res.* **30**, 347-356 (1997).
2. Feringa, B. L., van Delden, R. A., Koumura, N. and Geertsema, E. M. *Chem. Rev.* **100**, 1789-1816 (2000).
3. Irie, M. *Chem. Rev.* **100**, 1685-1716 (2000).
4. Yokoyama, Y. *Chem. Rev.* **100**, 1717-1739 (2000).
5. Rau, H. In: *Studies in Organic Chemistry: Photochromism, Molecules and Systems*, vol. 40 (Dürr, H. and Bonas-Laurent, H., eds.) Elsevier, Amsterdam, pp-165-192 (1990).
6. Goodman, M. and Kossey, A. *J. Am. Chem. Soc.* **88**, 5010-5015 (1966).
7. Goodman, M. and Falxa, M.L., *J. Am. Chem. Soc.* **89**, 3863-3867 (1967).
8. Pieroni, O., Fissi, A., Angelini, N. and Lenci, F. *Acc. Chem. Res.* **34**, 9-17 (2001).
9. Nägele, R., Hoche, R., Zinth, W. and Wachtveitl, J. *Chem. Phys. Lett.* **272**, 489-495 (1997).

10. Spörlein, S., Carstens, H., Satzger, H., Renner, C., Behrendt, R., Moroder, L., Tavan, P., Zinth, W. and Wachtveitl, J. *Proc. Natl. Acad. Sci. USA* **99**, 7998-8002 (2002).
11. Wachtveitl, J., Spörlein, S., Satzger, H., Fonrobert, B., Renner, C., Behrendt, R., Oesterheld, D., Moroder, L. and Zinth, W. *Biophys. J.* **86**, 2350-2362 (2004).
12. Bredenbeck, J., Helbing, J., Sieg, A., Schrader, T., Zinth, W., Renner, C., Behrendt, R., Moroder, L., Wachtveitl, J. and Hamm, P. *Proc. Natl. Acad. Sci. USA* **100**, 6452-6457 (2003).
13. Bredenbeck, J., Helbing, J., Kumita, J. R., Wolley, G. A. and Hamm, P. *Proc. Natl. Acad. Sci. USA* **102**, 2379-2384 (2005).
14. Behrendt, R., Renner, C., Schenk, M., Wang, F., Wachtveitl, J., Oesterheld, D. and Moroder, L. *Angew. Chem. Int. Ed. Engl.* **38**, 2771-2774 (1999).
15. Ulysse, L., Cubillos, J. and Chmielewski, J. *J. Am. Chem. Soc.* **117**, 8466-8467 (1995).
16. Renner, C., Behrendt, R., Heim, N. and Moroder, L. *Biopolymers* **63**, 382-393 (2002).
17. Löweneck, M., Milbradt, A. G., Satzger, H., Root, C., Moroder, L., Zinth, W. and Renner, C., submitted (2005).
18. Cochran, A. G., Skelton, N. J. and Starovasnik, M. A. *Proc. Natl. Acad. Sci. USA* **98**, 5578-5583 (2001).
19. Dong, S. -L., Löweneck, M., Schrader, T. E., Schreier, W. J., Zinth, W., Moroder, L. and Renner, C. In *Understanding Biology Using Peptides, Proceedings of the 19th American Peptide Symposium*, this volume, pp. 36-37 (2006).
20. Kusebauch, U., Cadamuro, S., Moroder, L. and Renner, C. In *Understanding Biology Using Peptides, Proceedings of the 19th American Peptide Symposium*, this volume, pp. 561-563 (2006).
21. Huber-Wunderlich, M. and Glockshuber, R. *Folding Design* **3**, 161-171 (1998).
22. Cabrele, C., Fiori, S., Pegoraro, S. and Moroder, L. *Chem. Biol.* **9**, 731-740 (2002).
23. Darby, N. J. and Creighton, T. E. *Biochemistry* **34**, 16770-16780 (1995).
24. Rost, J. and Rapoport, S. *Nature* **201**, 185-187 (1964).
25. Millis, K. K., Weaver, K. H. and Rabenstein, D. L. *J. Org. Chem.* **58**, 4144-4146 (1993).
26. Gupta, P. N. and Raina, A. *J. Indian Chem. Soc.* **55**, 495-497 (1988).
27. Behrendt, R., Schenk, M., Musiol, H. -J. and Moroder, L. *J. Peptide Sci.* **5**, 519-529 (1999).
28. Freedman, R. B., Hirst, T. R. and Tuite, M.F. *Trends Biochem. Sci.* **19**, 331-336 (1994).
29. Cattani-Scholz, A., Renner, C., Cabrele, C., Behrendt, R., Oesterheld, D. and Moroder, L. *Angew. Chem. Int. Ed.* **41**, 289-292 (2002).
30. Balzani, V., Credi, A., Raymo, F. M. and Stoddart, J. F. *Angew. Chem. Int. Ed.* **39**, 3348-3391 (2000).
31. Yamaguchi, H., Kamachi, M. and Harada, A. *Angew. Chem. Int. Ed.* **39**, 3629-3831 (2000).
32. Schally, C. A., Beizai, K. and Vögtle, F. *Acc. Chem. Res.* **34**, 465-476 (2001).
33. Harada, A. *Acc. Chem. Res.* **34**, 456-464 (2001).
34. Hugel, T., Holland, N. B., Cattani, A., Moroder, L., Seitz, M. and Gaub, H. E. *Science* **296**, 1103-1106 (2002).
35. Holland, N. B., Hugel, T., Neuert, G., Cattani-Scholz, A., Renner, C., Oesterheld, D., Moroder, L., Seitz, M. and Gaub, H. E. *Macromolecules* **36**, 2015-2023 (2003).

It All Started in Brooklyn, NY, Forty-five Years Ago!

Claudio Toniolo

Department of Chemistry, University of Padova, 35131 Padova, Italy

In the mid 1950's the generally shared view of chemists investigating polypeptide conformations was that all known *synthetic* materials (the so-called *poly- α -amino acids*, prepared by polymerizing amino acid N-carboxy anhydrides) used as models were highly heterogeneous in regards to molecular weight [1]. As a consequence of this unfavorable property, the serious difficulties encountered in establishing a state of true conformational equilibrium for this type of compounds were not unexpected. Therefore, a series of detailed 3D-structural investigations of peptide molecules monodisperse with respect to molecular weight was considered of enormous potential usefulness.

In addition, from the nature of the α -helical and β -pleated sheet structures predicted by Pauling and coworkers [2,3], it was apparent that these conformations would not be attained by materials having very low molecular weights and that at least three types of main-chain length dependent conformational transitions would possibly take place (other relevant parameters in these processes being amino acid side-chain characteristics, solvent polarity, and peptide concentration) [1]:

random coil \rightarrow β -sheet \rightarrow α -helix
random coil \rightarrow β -sheet
random coil \rightarrow α -helix

Today we know that an additional conformation, the 3_{10} -helix, may play a role during the peptide folding pathway [4,5]. In other words, it was recognized that the occurrence of the so-called *end-group effects*, related to the different degree of exposure of the terminal residues to the solvent as compared to the internal residues, would have implied that the onset of each ordered peptide secondary structure is characterized by a peculiar *critical main-chain length* [1].

This was all the available information on these issues when in 1958 Murray Goodman began to study peptide conformation at the then celebrated Department of Chemistry, Polytechnic Institute of Brooklyn, NY. He immediately realized the importance of exploiting *complete* series of chemically and optically pure, strictly monodisperse oligomers (from the dimer to approximately the decamer level) as models for an in-depth investigation of the fundamental peptide 3D-structural preferences, stabilities and parameters in solution. Such a *bottom-up approach* turned out to be successful as had been the similar approach adopted by Pauling (who decided to begin solving the X-ray diffraction structures of simple amides, lactams, and peptides as short as dipeptides), which brought him to propose the α -helical structure as the most stable conformation for polypeptides [2].

The Goodman and Schmitt communication [6], published forty-five years ago (October 20, 1959), opened an avenue to the extremely productive field of conformational analysis of linear peptides, not restricted to model compounds, but, from the early 1970's, extended to bioactive molecules as well. In this pioneering work, fully protected [Glu(OMe)]_n homo-oligomers were examined using optical rotation as a function of a variety of parameters, such as nature of solvent, peptide concentration, and temperature. Unordered conformations and ordered secondary structures (α -helix and β -pleated sheet) were all discussed in that paper. The onset of the helical structure in that series was clearly demonstrated at the level of the

penta-/hexamer in the structure-supporting solvent 1,4-dioxane (first illustration of the *Goodman plot*; Fig. 1). Conversely, no indication for the onset of an ordered conformation was found in the structure-disrupting solvent dichloroacetic acid.

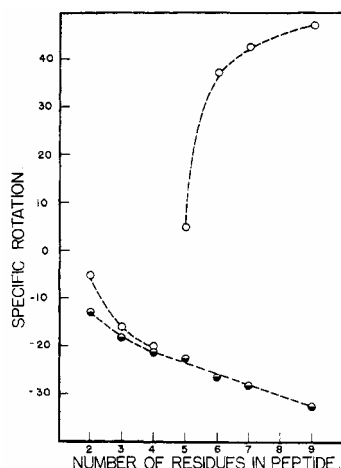


Fig. 1. The original Goodman plot. Specific optical rotations of the Z-L-Glu(OMe)-[L-Glu(OMe)]_n-L-Glu(OEt)-OEt peptide series as a function of the number of residues in the main chain: --o-- are rotations in 1,4-dioxane and —●— are rotations in dichloroacetic acid. Adapted from ref [6].

Intuitively, Murray also recognized the importance of investigating the conformation of peptide molecules by use of a combination of all available physico-chemical techniques to reduce the risk of data misinterpretation. Indeed, later on the list of physico-chemical techniques used by Murray and his coworkers was expanded to ultracentrifuge, IR and UV absorptions, ORD, CD, and NMR to put on more sound bases to the original conformational assignments. Interestingly, Murray's personal contacts and those of his Institution with the most advanced laboratories on polymer chemistry (*e.g.*, those at Du Pont, Wilmington, DL) also allowed him to extend the use of solvents for spectroscopic studies to a series of fluoroalcohols (including the now widely employed 2,2,2-trifluoroethanol [7]) with different capabilities to support ordered peptide conformations. When still at Brooklyn Poly, Murray's project on conformational analysis of model Glu(OEt), Ala, Val, Ile, and Met homo-oligopeptides was carried on by a collaborative effort of Fred Naider, currently at the Department of Chemistry, College of Staten Island, City University of New York, NY, and the author of papers [8,9] that culminated in a joint review article presented at the Rehovot Symposium in 1974 [10]. The 3D-structure type, conformational stability, and critical main-chain length for helix and β -sheet formation were all unambiguously elucidated.

Murray was able to follow the *bottom-up approach* because of his experience, unique among structural biochemists, in highly qualified laboratories of organic and peptide syntheses. During his postdoctoral work with Prof. J. C. Sheehan at the Massachusetts Institute of Technology, Boston, MA, he was introduced into the problems related to the activation of the α -amino acid α -carboxylic functionality in peptide coupling reactions, particularly to the use of the carbodiimide method [11]

developed by Sheehan and coworkers [12] for the semi-synthesis of penicillin. A subsequent postdoctoral stay in England (Lord A. Todd, University of Cambridge) allowed him to interact with Prof. G. T. Young (Oxford University), the first chemist carrying out systematic investigations on the problem of racemization in peptide synthesis [13], and with Prof. G. W. Kenner (University of Cambridge) with whom he wrote the monumental review-article "The Synthesis of Peptides" in 1957 [14].

Few years after his return to USA (Brooklyn Poly), in parallel with his ongoing research on peptide preferred conformations, he expanded his interest to the chemistry of α -amino acid and peptide 5(4*H*)-oxazolones which allowed him to perform detailed mechanistic studies of the racemization reaction in peptide synthesis. *Inter alia*, Goodman and McGahren described the synthesis and characterization of the L-enantiomer (and the racemate as well) of the 5(4*H*)-oxazolone from Z-Aib-Phe-OH [15-17]. Because of its extremely high optical rotation, despite the presence of the achiral Aib residue in the dipeptide sequence, the *Goodman oxazolone* proved to be extremely useful for kinetics studies of racemization (incidentally, Murray learned directly from Kenner and from the milestone papers of his group [18,19] of the peculiar synthetic methods and properties of peptides based on the C $^{\alpha}$ -tetrasubstituted α -amino acid Aib). Many years later (1995), our group published the X-ray diffraction structures of both the L-enantiomeric and racemic forms of the *Goodman oxazolone* (Fig. 2) [20]. This was the first structural analysis of a crystalline peptide oxazolone with a chiral C $^{\alpha}$ -trisubstituted (protein) amino acid in the heterocyclic moiety.

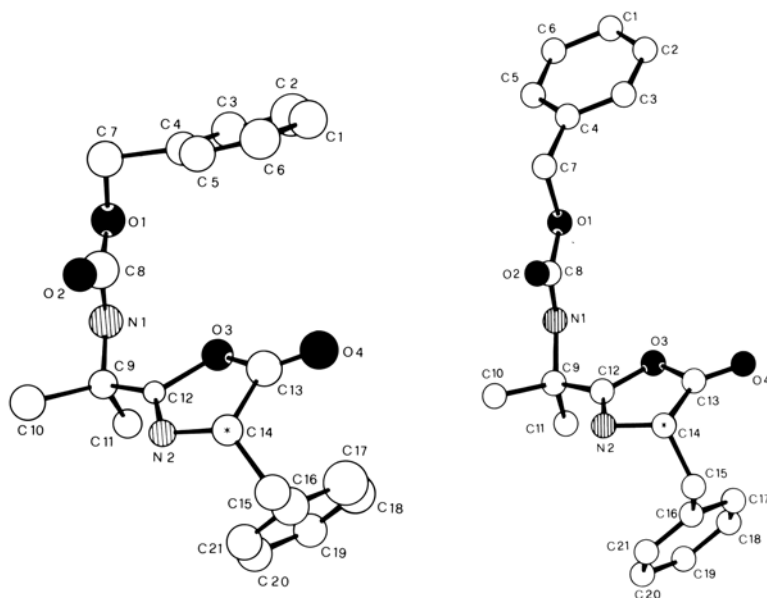


Fig. 2. X-Ray diffraction structures of the L-enantiomeric form (left) and the racemic form (right) of the oxazol-5(4*H*)-one from Z-Aib-Phe-OH (the *Goodman oxazolone*) with numberings of the atoms. Of the racemic form only the L-enantiomer is shown. In each molecule the chiral carbon atom is starred. Adapted from ref [20].

Murray's interest in peptides containing conformationally restricted C^α-tetrasubstituted α-amino acids continued over the years. He was among the first peptide chemists who took advantage of the emerging field of backbone modified peptides for drug design. His work at Brooklyn Poly on the Aib-based oxazolones was one of the stimulating factors which convinced me to enter the extremely rewarding field of conformational analysis of peptides rich in C^α-tetrasubstituted α-amino acids, the prototype of which is indeed Aib. My first publication (1982) on the 3D-structure of a complete set of (Aib)_n homo-oligomers [21] was part of an extremely productive collaboration with the crystallographic group at the University of Naples headed by E. (Bibi) Benedetti with whom I shared my postdoctoral stay at Brooklyn Poly. My coworkers and I have recently summarized the results of our (and others') conformational work on peptides based on C^α-tetrasubstituted α-amino acids in a review article [22].

I am deeply grateful to Murray for his inspiration on various areas of peptide research over the years and for his constant encouragement to follow his approach to find a well defined niche in our always evolving field.

References

1. *Poly-α-Amino Acids, Polypeptides, and Proteins*, Stahmann, M. A., Ed., The University of Wisconsin Press, Madison, WI, 1962.
2. Pauling, L., Corey, R. B. and Branson, H. R. *Proc. Natl. Acad. Sci. USA* **37**, 205-211 (1951).
3. Pauling, L. and Corey, R. B. *Proc. Natl. Acad. Sci. USA* **37**, 729-740 (1951).
4. Toniolo, C. and Benedetti, E. *Trends Biochem. Sci.* **16**, 350-353 (1991).
5. Millhauser, G. L. *Biochemistry* **34**, 3873-3877 (1995).
6. Goodman, M. and Schmitt, E. E. *J. Am. Chem. Soc.* **81**, 5507-5508 (1959).
7. Goodman, M. and Listowski, I. *J. Am. Chem. Soc.* **84**, 3770-3771 (1962).
8. Goodman, M., Verdini, A. S., Toniolo, C., Phillips, W. D. and Bovey, F. A. *Proc. Natl. Acad. Sci. USA* **64**, 444-450 (1969).
9. Goodman, M., Naider, F. and Toniolo, C. *Biopolymers* **10**, 1719-1730 (1971).
10. Goodman, M., Toniolo, C. and Naider, F. In *Peptides, Polypeptides and Proteins* (Blout, E. R., Bovey F. A., Goodman M. and Lotan N., eds.) Wiley, New York, NY, pp. 308-319 (1974).
11. Sheehan, J. C., Goodman, M. and Hess, G. P. *J. Am. Chem. Soc.* **78**, 1367-1369 (1956).
12. Sheehan, J. C. and Hess, G. P. *J. Am. Chem. Soc.* **77**, 1067-1068 (1955).
13. Young, G. T. In *Proc. Symposium on Methods of Peptide Synthesis*, Prague, 1958, *Coll. Czech. Chem. Commun.* **24**, 39-45 (1959).
14. Goodman, M. and Kenner G. W. *Adv. Protein Chem.* **12**, 465-638 (1957).
15. Goodman, M. and Mc Gahren, W. J. *J. Am. Chem. Soc.* **87**, 3028-3029 (1965).
16. Mc Gahren, W. J. and Goodman, M. *Tetrahedron* **23**, 2017-2030 (1967).
17. Goodman, M. and Mc Gahren, W. J. *Tetrahedron* **23**, 2031-2050 (1967).
18. Leplawy, M. T., Jones, D. S., Kenner, G. W. and Sheppard, R. C. *Tetrahedron* **11**, 39-51 (1960).
19. Jones, D. S., Kenner, G. W., Preston, J. and Sheppard, R. C. *J. Chem. Soc.* 6227-6239 (1965).
20. Crisma, M., Valle, G., Moretto, V., Formaggio, F. and Toniolo, C., *Peptide Res.* **8**, 187-190 (1995).
21. Benedetti, E., Bavoso, A., Di Blasio, B., Pavone, V., Pedone, C., Crisma, M., Bonora, G. M. and Toniolo, C. *J. Am. Chem. Soc.* **104**, 2437-2444 (1982).
22. Toniolo, C., Crisma, M., Formaggio, F. and Peggion, C. *Biopolymers (Peptide Sci.)* **60**, 396-419 (2001).

Short Transmembrane Peptide Sequences as Nucleation Sites for Globular Protein Folding

Arianna Rath, Linda Lee, Rachel M. Johnson and Charles M. Deber

Structural Biology and Biochemistry, Research Institute, Hospital for Sick Children, Toronto M5G 1X8; and Department of Biochemistry, University of Toronto, Toronto M5S 1A8, Ontario, Canada

Introduction

Two different classes of proteins are encoded in genetic sequences: those that are soluble in aqueous solvent (globular proteins) and those that are not (membrane proteins). Depending on whether a given amino acid sequence represents a globular or membrane protein, its *in vitro* folding can be divided into two general outcomes, based on the hydrophobic effect. Globular protein structure can be defined in terms of a hydrophobic interior and a hydrophilic exterior; during folding, globular protein segments driven from water by the hydrophobic effect can become the core residues in the final folded structure. During membrane protein folding, transmembrane (TM) segments (18-25 residues) escape water by membrane insertion [1,2]. Hydrophobic peptides used as TM segment mimics spontaneously transfer from water to a membrane phase only when their average non-polar character is well above that of a poly-alanine strand [3,4]. This requirement, termed “threshold hydrophobicity”, was found to be satisfied by >96% of over 5000 TM segments [5]. The purpose of the work described herein is to determine if the phenomenon of ‘threshold hydrophobicity’ operates in the folding of soluble proteins. Amino acid sequences of above-threshold hydrophobicity exist in soluble proteins [6]. If these segments do not long enough span the membrane, sequestration by membrane transfer is not possible. We hypothesized that a ‘hydrophobic collapse threshold’ may exist such that the ‘short transmembrane segments’ of above-threshold hydrophobicity in soluble proteins (termed STMs) specifically transfer spontaneously from water to nucleate the core. To address this question, a model protein system containing STMs and amenable to *in vitro* protein folding studies was selected from the structural database and the structural properties of peptides containing its STM segments were characterized by CD spectroscopy.

Results and Discussion

Several features of a good protein model for the study of the nucleating effect of STMs in globular proteins were considered: (i) the model must contain segments with above threshold hydrophobicity/helicity for membrane insertion; (ii) these segments should be in α -helix conformation in the folded protein structure; (iii) the protein should be easy to express and purify if necessary; and (iv) it should be amenable to protein folding studies, with a literature available to compare and evaluate the results of experiments on the STM peptides. To find a protein model that fit these criteria, the SwissProt database release 34 was searched as described [6] to obtain protein sequences with fewer than 210 residues that had a solved crystal structure available in the Protein Data Bank (found at <http://www.rcsb.org/pdb/>). STMs were identified in these proteins using the TM segment-predicting program *TM Finder* [5] (found at <http://www.ccb.sickkids.ca/tools/tmfinder/html/login.html>). The primary sequence of each protein was submitted to *TM Finder* with default parameters with the exception of N-terminal and C-terminal windows, which were

set at three instead of five; and segment length, which was set at five instead of ten. Importantly, *TM Finder* identified at least one STM in approximately 50% of the 2204 globular proteins investigated, and about 30% of the database had two or more STMs. The list of potential model systems was narrowed to those that were monomeric, α -helical, and had proven amenable to protein folding studies by literature searching in PubMed (<http://www.ncbi.nlm.nih.gov/entrez/query.fcgi>). Several potential protein model systems were identified in this manner, including: apomyoglobin, lysozyme, barstar, chymotrypsin inhibitor 2, ribonuclease H, and colicin immunity protein E7.

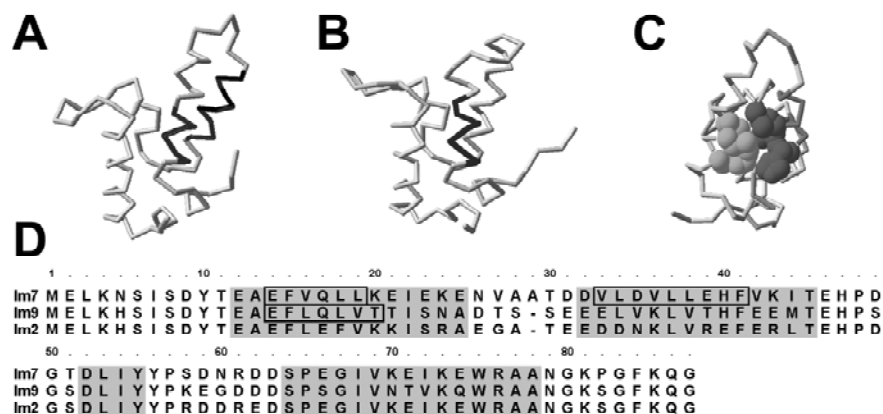


Fig. 1. (A) Ribbon diagram of the Im7 and (B) and Im9 structures [7,8] with the STMs found in helix 1 and helix 2 shaded black. (C) van der Waals contacts between the residues in the helix 1 and helix 2 STM segments of Im7. Images produced with Swiss PDB Viewer [9]. (D) Colicin immunity protein sequences. The residues that correspond to the STM segments in helix 1 and/or helix 2 of each protein are boxed. The residues that are found in α -helix conformation in the Im7 and Im9 structures are shaded, as are the corresponding regions of Im2. The Im7-1, Im9-1 and Im2-1 peptide sequences encompass positions 8-29 of Im7, Im9 and Im2, respectively; the Im7-2, Im9-2 and Im2-2 peptide sequences positions 30-49, respectively; and Im7-1/2, Im9-1/2 and Im2-1/2 positions 8-49, respectively.

The colicin immunity protein (Im) family was selected as a model system for characterization of the properties of STMs because it has three family members (Im7, Im9 and Im2) whose folding has been characterized [10-12]. Two of the three family members, Im7 and Im9, have STMs, while the third, Im2 does not, and can act as negative control for protein segments that lack STM sequences. The structures of Im7 and Im9, illustrated in Figure 1, are four-helix bundle proteins of approximately 90 residues [7,8]. Im7 has two STM segments located in its first (EFVQLLEHFK) and second (VLDVLLLEHFK) helices, respectively (Fig. 1A), and the hydrophobic residues of each contact one another in the protein tertiary structure (Fig. 1C). The lone STM in Im9 (EFLQLVT) is contained within the first helix of its sequence (Fig. 1B).

Previous studies have shown that the two STM-containing helices of Im7 form early (within 2.5 ms) in the folding pathway [10], consistent with a nucleating role for the STMs. We therefore hypothesized that STMs might nucleate structure

formation by adopting native-like structure in solution. To see if this was the case, peptides corresponding to the entire length of helix 1 (positions 8-29) and helix 2 (positions 30-49) from Im7 (denoted Im7-1 and Im7-2) and helix 1 of Im9 (positions 8-29, denoted Im9-1) (sequences given in Fig. 1D) were synthesized. The non-STM-containing sequences of Im9 helix 2 (positions 30-49, Im9-2) and Im2 helix 1 and helix 2 (positions 8-29, Im2-1 and positions 30-49, Im2-2) were also synthesized (sequences given in Fig. 1D) to serve as negative controls for secondary structure formation. The ability of each peptide to adopt an α -helical structure in solution was assessed by CD spectroscopy (Fig. 2).

The CD spectra of the single STM-containing peptides were predominantly random-coil, indicating that none adopted significant amounts of helical structure in solution (Fig. 2). The implication of this result is that the presence of a single STM sequence is not sufficient to nucleate helix structure formation. This conclusion is supported by similarity in the amount of helical structure observed in the STM and non-STM containing peptides from Im7 and Im9 (Table 1). The only peptide with significant amounts of helix was the non-STM peptide Im2-1 (Fig. 2), which has greater than 40% helical content (Table 1). Analysis of helical propensities of the peptide sequences (Table 1) does not provide an immediate rationale for the high helicity of the Im2-1 system.

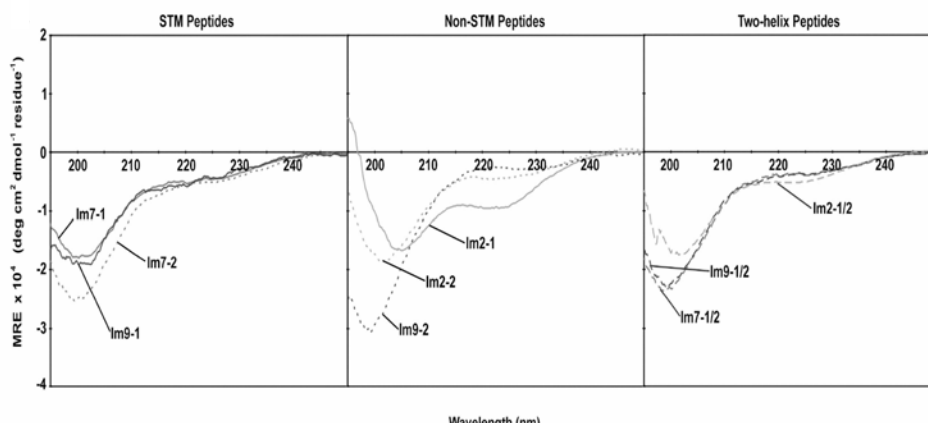


Fig. 2. CD spectra of Im peptides in 20 mM Tris, pH 8.

Since none of the single STM-containing peptides seemed to adopt a secondary structure in isolation, we inquired if the presence of more than one STM was necessary to allow formation of a structure that could nucleate folding. To determine if contact between two STMs was needed for structure formation, a two-helix peptide containing both Im7 helix 1 and helix 2 (positions 8-49, denoted Im7-1/2) was synthesized (sequence given in Fig. 1D). Corresponding peptides based on the Im9 (positions 8-49, Im9-1/2) sequence (containing a single STM) and on the Im2 (positions 8-49, Im2-1/2) sequence (containing no STMs) were also synthesized (sequences given in Fig. 1D) and their secondary structures determined. The CD spectra of the Im7-1/2, Im9-1/2 and Im2-1/2 peptides were predominantly random coil (Fig. 2). Each of the three peptides also had the same helix content within

Table 1. Helicity of immunity protein peptides. P_α and P_β values were calculated using the Chou-Fasman propensity scales in [13]. Percent helix values in buffer were obtained by fits to the CD spectra using CDFit [14]. Fitting errors are given.

Peptide	# STMs	P_α	P_β	%Helix
Im7-1	1	1.18	0.92	27 ± 5
Im7-2	1	1.13	1.02	23 ± 6
Im7-1/2	2	1.16	0.97	22 ± 5
Im9-1	1	1.05	1.01	20 ± 6
Im9-2	0	1.19	0.84	20 ± 6
Im9-1/2	1	1.12	0.93	22 ± 5
Im2-1	0	1.12	0.93	45 ± 6
Im2-2	0	1.12	0.80	29 ± 9
Im2-1/2	0	1.12	0.87	29 ± 5

experimental error (Table 1), indicating that the presence of two STM sequences in the case of Im7-1/2 was not sufficient to nucleate structure formation.

Although STM segments are highly hydrophobic and exist in globular protein sequences, their inability to adopt secondary structure in solution in the colicin immunity protein family - particularly in the case of the Im7-1/2 peptide that has two helical STM segments in contact in the native protein structure - implies that they do not appear to nucleate folding in this case. It remains to be determined if STMs have a role in the folding of other protein models that contain these sequences.

Acknowledgments

This work was supported, in part, by a grant to C.M.D. from the Natural Sciences and Engineering Research Council of Canada (NSERC). A.R. holds a post-doctoral award from the Canadian Institutes of Health Research (CIHR) Training Program in "Protein Folding: Principles and Diseases". R.M.J. is the recipient of an Ontario Graduate Scholarship (OGS) award. L.L. is an undergraduate participant in the Samuel P. Lunenfeld Summer Student Research Program at the Hospital for Sick Children.

References

1. Popot, J. L. and Engelman, D. M. *Annu. Rev. Biochem.* **69**, 881-922 (2000).
2. Popot, J. L. and Engelman, D. M. *Biochem.* **29**, 4031-4037 (1990).
3. Liu, L. P. and Deber, C. M. *Biopolymers* **47**, 41-62 (1998).
4. Liu, L. P., Li, S. C., Goto, N. K. and Deber, C. M. *Biopolymers* **39**, 465-470 (1996).
5. Deber, C. M., Wang, C., Liu, L. P., Prior, A. S., Agrawal, S., Muskat, B. L. and Cuticchia, A. *J. Protein Sci.* **10**, 212-219 (2001).
6. Wang, C., Liu, L. P. and Deber, C. M. *Proc. Am. Pep. Symp.* **16**, 367-368 (2000).
7. Chak, K. F., Safo, M. K., Ku, W. Y., Hsieh, S. Y. and Yuan, H. S. *Proc. Natl. Acad. Sci. USA* **93**, 6437-6442 (1996).

8. Osborne, M. J., Breeze, A. L., Lian, L. Y., Reilly, A., James, R., Kleanthous, C. and Moore, G. R. *Biochemistry* **35**, 9505-9512 (1996).
9. Guex, N. and Peitsch, M. C. *Electrophoresis* **18**, 2714-2723 (1997).
10. Capaldi, A. P., Kleanthous, C. and Radford, S. E. *Nat. Struct. Biol.* **9**, 209-216 (2002).
11. Ferguson, N., Capaldi, A. P., James, R., Kleanthous, C. and Radford, S. E. *J. Mol. Biol.* **286**, 1597-1608 (1999).
12. Ferguson, N., Li, W., Capaldi, A. P., Kleanthous, C. and Radford, S. E. *J. Mol. Biol.* **307**, 393-405 (2001).
13. Chou, P. Y. and Fasman, G. D. *Biochemistry*. **13**, 211-222 (1974).
14. Rupp, B.; Lawrence Livermore National Laboratory (LLNL). Available at <http://www-structure.llnl.gov/cd/cdtutorial.htm>.

Synthesis and In Vitro Opioid Activity Profiles of Novel Cyclic Enkephalin Analogs

Peter W. Schiller, Grazyna Weltrowska, Irena Berezowska, Carole Lemieux, Nga N. Chung and Brian C. Wilkes

Laboratory of Chemical Biology and Peptide Research, Clinical Research Institute of Montreal, 110 Pine Avenue West, Montreal, Quebec, Canada H2W 1R7

Introduction

Twenty-five years ago, the first cyclic enkephalin analog, H-Tyr-c[-D-A₂bu-Gly-Phe-Leu-] was reported [1]. This side chain-to-end group cyclized peptide turned out to be a μ receptor-selective opioid agonist. It rapidly became a popular parent compound for further structural modifications using novel principles of peptide analog design. Murray Goodman's group prepared one of the most interesting analogs, H-Tyr-c[-Glu-Gly-gPhe-D-Leu-] (gPhe denotes the *gem* diamino equivalent of Phe), which contains two reversed peptide bonds in the ring structure [2]. This partial retro-inverso modified analog showed about the same μ agonist potency as the cyclic parent peptide but was three times more μ -selective. Potent, cyclic enkephalin analogs containing a cystine bridge, H-Tyr-c[D-Cys-Gly-Phe-D(or L)-Cys]X, were synthesized independently by Sarantakis [3] and by Schiller et al. [4]. Analogs of this type with a C-terminal carboxamide function (X = NH₂) were essentially non-selective, whereas the corresponding free acids (X = OH) showed some preference for δ receptors over μ receptors. A lanthionine analog of these cyclic disulfide-bridged structures, H-Tyr-c[D-Val_L-Gly-Phe-D-Ala_L]OH, recently prepared by Murray Goodman and his colleagues, turned out to be a potent and very selective δ agonist [5]. Remarkably, this compound was as active as morphine in producing centrally-mediated analgesia when given intraperitoneally to rats [6].

In the present paper, we describe analogs of H-Tyr-c[D-Cys-Gly-Phe-D(or L)-Cys]NH₂ that are characterized by structural modifications, either in the peptide ring structure or at the exocyclic tyrosine residue. In one series of compounds, the metabolically less stable disulfide bridge was replaced with a -CH=CH- or -CH₂-CH₂- moiety. Replacement of the Tyr¹ residue with various novel des-amino analogs of tyrosine resulted in another series of compounds with opioid antagonist properties or with a novel mixed agonist/antagonist profile.

Results and Discussion

Dicarba analogs of H-Tyr-c[D-Cys-Gly-Phe-D(or L)-Cys]NH₂: The replacement of the disulfide bridge in cystine-containing biologically active peptides with two methylene groups is of considerable interest because the resulting dicarba analogs are metabolically more stable. In the past, this structural modification was synthetically demanding, as it required the replacement of cystine with diaminosuberic acid in a cumbersome multi-step synthesis [7]. Recently, the use of ring-closing metathesis (RCM) has been shown to be a relatively straightforward procedure for the preparation of a dicarba analogue of oxytocin [8]. Here, we describe the syntheses of dicarba analogs of H-Tyr-c[D-Cys-Gly-Phe-D(or L)-Cys]NH₂ (Fig. 1) by RCM between allylglycines (Allylgly) substituted

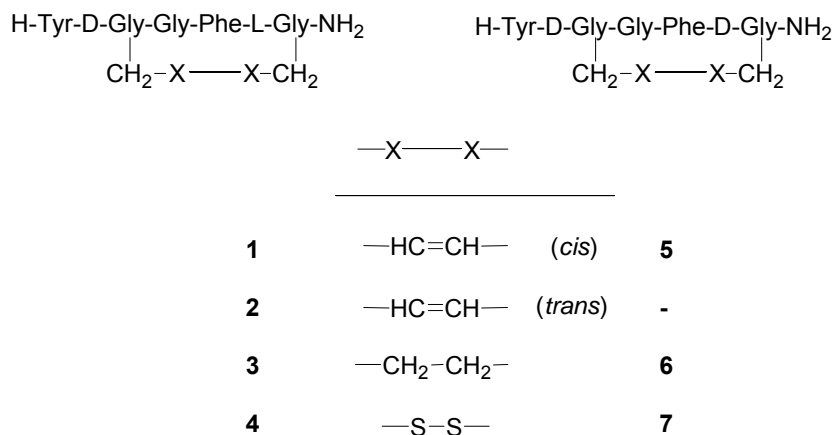


Fig. 1. Dicarba analogs of H-Tyr-c[D-Cys-Gly-Phe-D(or L)-Cys]NH₂.

for the Cys residues. RCM using the second generation Grubbs catalyst benzylidene[1,3-bis(2,4,6-trimethylphenyl)-2-imidazolidinylidene]dichloro(tricyclohexylphosphine)ruthenium afforded the cyclic, olefinic peptides in good yield (66% yield for the D,L-peptide and 68% yield for the D,D peptide). In the case of the peptide with a L-configuration in the 5-position a 56:44 mixture of *cis* and *trans* isomers was obtained, whereas the *cis* isomer only was formed with the peptide having the D-configuration. Catalytic hydrogenation yielding the saturated -CH₂-CH₂- bridged peptides was straightforward.

In comparison with the H-Tyr-c[D-Cys-Gly-Phe-L-Cys]NH₂ parent peptide (**4**), the *cis* isomer of the olefinic peptide, with a L configuration in position 5 (**1**) showed 2-3 fold higher μ - and δ agonist potencies in the guinea pig ileum (GPI) and mouse vas deferens (MVD) assays (Table 1). In agreement with these results, 2-3-fold higher μ and δ receptor affinities were determined for **1** in the receptor binding assays, whereas the κ receptor affinity was about the same for the two peptides. The *trans* isomer of the olefinic peptide (**2**) displayed about the same μ and δ agonist potencies as the parent peptide, similar μ receptor binding affinity and 4-5-fold lower δ and κ receptor affinity. The corresponding bis-methylene analog (**3**) showed about the same μ agonist potency and μ receptor binding affinity as the disulfide-bridged parent, but was a 5-fold less potent δ agonist and had 8-fold lower κ receptor binding affinity. The *cis* isomer of the olefinic peptide with a D-configuration in position 5 (**5**) showed similar or slightly lower μ and δ agonist potencies and binding affinities at all three receptors, as compared to the D-Cys²,D-Cys⁵-parent peptide (**7**), whereas the corresponding saturated analog (**6**) was 2-8-fold less potent in the bioassays and receptor binding assays. These results indicate that, in comparison with their respective disulfide bridged parent peptides, some of the dicarba analogs display similar or even higher μ and δ opioid agonist potencies. In contrast, replacement of the disulfide bridge in oxytocin [7,8] or in a somatostatin analog [9] with a bis-methylene moiety had resulted in very significant potency drops.

A theoretical conformational analysis based on molecular mechanics calculations performed with compounds **1**, **2**, **3**, and **4** resulted in 21, 11, 39 and 41 low energy conformers of their “bare” ring structures (within 3 kcal/mol of the lowest energy structure), respectively. This result indicates that among these four peptides the

Table 1. In vitro opioid activity profiles of cyclic enkephalin analogs

Compound	GPI	MVD	Receptor binding ^a		
	IC ₅₀ , nM	IC ₅₀ , nM	K _i ^μ , nM	K _i ^δ , nM	K _i ^κ , nM
1	0.898	0.275	0.616	1.25	57.6
2	1.81	0.469	2.40	6.55	200
3	1.02	3.19	2.34	5.87	309
4	1.65	0.603	1.74	1.61	40.1
5	4.26	0.671	0.593	2.19	86.0
6	11.2	3.64	1.17	3.34	71.5
7	1.30	0.562	0.550	0.822	44.9

^aDisplacement of [³H]DAMGO (μ-selective) and [³H]DSLET (δ-selective) from rat brain membrane binding sites; displacement of [³H]U69,593 (κ-selective) from guinea pig brain membrane binding sites.

trans isomer of the olefinic peptide (**2**) had the most rigid ring structure, whereas the ring structures of the bis-methylene analog (**3**) and of the disulfide-bridged parent peptide (**4**) were more flexible. Interestingly, the lowest-energy conformers of **1** and **4** have quite different ring structures, but show a very similar spatial disposition of the N-terminal amino group and of the aromatic rings of Tyr and Phe, which represent the crucial pharmacophoric moieties in the interaction with opioid receptors (Fig. 2). This may explain why peptides **1** and **4** have a similar opioid activity profile despite the pronounced difference in their ring structures.

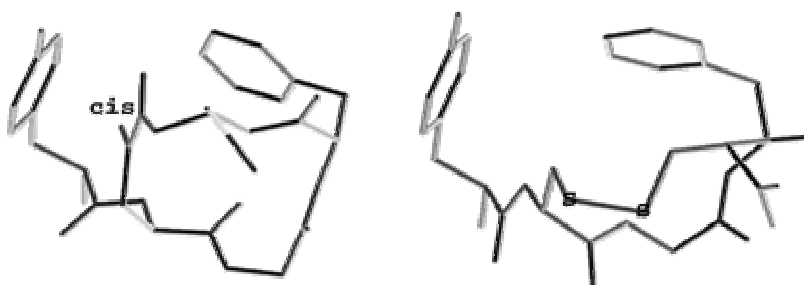


Fig. 2. Lowest-energy conformers of compounds **1** (left) and **4** (right)

Opioid peptides containing β-substituted Dhp analogs in place of Tyr¹: 2',6'-Dimethyl substitution of the Tyr¹ residue of opioid agonist peptides and deletion of the positively charged N-terminal amino group have been shown to represent a general structural modification to convert opioid peptide agonists into

antagonists [11]. This conversion required the syntheses of opioid peptide analogs containing 3-(2,6-dimethyl-4-hydroxyphenyl)propanoic acid (Dhp) in place of Tyr¹. The cyclic enkephalin analogue Dhp-c[D-Cys-Gly-Phe(*p*NO₂)-D-Cys]NH₂ turned out to be a potent μ opioid antagonist and a somewhat less potent δ and κ antagonist [12] (Table 2). An analog of this cyclic peptide containing β -methylated Dhp, (3*S*)-3-methyl-3-(2,6-dimethyl-4-hydroxyphenyl)propanoic acid [(3*S*)-Mdp] in place of Dhp showed increased antagonist activity at all three receptors, whereas the (3*R*)-Mdp¹-analog displayed weak antagonist activity [12].

Here we report the effect of introducing larger substituents at the β -position of Dhp¹ in opioid peptides on the activity profile (Fig. 3). Stereoselective syntheses of (3*S*)-3-ethyl-3-(2,6-dimethyl-4-hydroxyphenyl)propanoic acid [(3*S*)-Edp], (3*R*)-3-isopropyl-3-(2,6-dimethyl-4-hydroxyphenyl)propanoic acid [(3*R*)-Idp], (3*R*)-3-cyclopropyl-3-(2,6-dimethyl-4-hydroxyphenyl)propanoic acid [(3*R*)-cPdp] and (3*R*)-3-cyclohexyl-3-(2,6-dimethyl-4-hydroxyphenyl)propanoic acid [(3*R*)-Cdp] were carried out using a synthetic scheme [12] which was based on a published approach to the synthesis of chiral β -branched carboxylic acids [13].

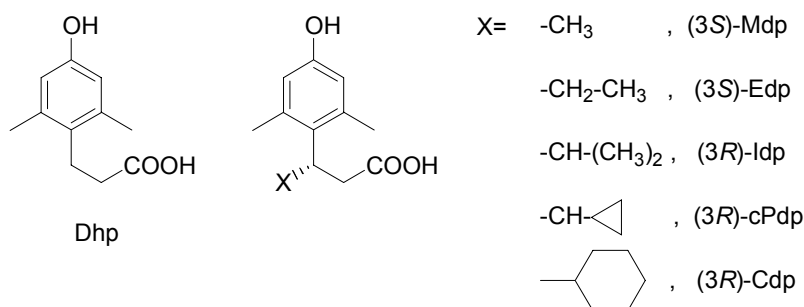


Fig. 3. Structural formulas of Dhp and β -alkylated Dhp analogs.

Table 2. GPI and MVD assay of opioid peptides containing β -substituted Dhp analogs in place of Tyr¹

Compound	GPI			MVD
	IC ₅₀ ^κ , nM	K _e ^κ , nM ^a	K _e ^μ , nM ^b	K _e ^δ , nM ^c
Dhp-c[cGF(<i>p</i> NO ₂)c]NH ₂	-	22.6	3.68	63.3
(3 <i>S</i>)-Mdp-c[cGF(<i>p</i> NO ₂)c]NH ₂	-	5.81	1.40	55.0
(3 <i>S</i>)-Edp-c[cGF(<i>p</i> NO ₂)c]NH ₂	9.65	-	85.7	78.0
(3 <i>R</i>)-Idp-c[cGF(<i>p</i> NO ₂)c]NH ₂	8.66	-	61.0	725
(3 <i>R</i>)IdpΨ[CH ₂ NH]c[cGF(<i>p</i> NO ₂)c]NH ₂	P.A. ^d	-	32.9	39.6
[(3 <i>R</i>)-Idp ¹]Dyn A(1-11)-NH ₂	-	47.9	-	9260
(3 <i>R</i>)-cPdp-c[cGF(<i>p</i> NO ₂)c]NH ₂	46.5	-	44.3	515
(3 <i>R</i>)-Cdp-c[cGF(<i>p</i> NO ₂)c]NH ₂	309 ^e	-	-	-

^aDetermined against U69,593; ^bDetermined against TAPP (H-Tyr-D-Ala-Phe-Phe-NH₂);

^cDetermined against DPDPE; ^dPartial agonist (*e* = 0.32); ^ePartial agonist (value represents IC₃₅).

Unexpectedly, the (3*S*)-Edp¹-analog of Dhp-c[D-Cys-Gly-Phe(*p*NO₂)-D-Cys]NH₂ turned out to be a κ -opioid agonist and a μ - and δ -antagonist (Table 2). Substitution of an isopropyl group in the β -position resulted in a compound with high κ agonist

potency ($IC_{50}^{\kappa} = 8.66 \text{ nM}$), significant μ antagonist activity ($K_e^{\mu} = 61 \text{ nM}$) and weak δ antagonist activity ($K_e^{\delta} = 725 \text{ nM}$). Thus, this peptide essentially showed a mixed κ agonist/ μ antagonist profile. There is evidence to indicate that mixed κ agonist/ μ antagonists have potential for treatment of cocaine abuse [14].

Interestingly, the cyclic analog with a reduced amide bond between the (3*R*)-Idp and the D-Cys² residues turned out to be a partial κ agonist and the (3*R*)-Idp¹ analog of dynorphin A(1-11)-NH₂ [Dyn A(1-11)-NH₂] was a κ antagonist. These results suggest that the κ agonist behavior of (3*R*)-Idp-c[D-Cys-Gly-Phe(*p*NO₂)-^d-Cys]NH₂ results from a specific interaction with the peptide ring structure. The analog with a cyclopropyl group in the β -position was a somewhat weaker κ agonist and the cyclohexyl- β -substituted analog was a weak partial κ agonist.

Acknowledgments

This work was funded by the CIHR (MOP-5655) and the NIH (DA-04443).

References

1. Di Maio, J. and Schiller, P. W. *Proc. Natl. Acad. Sci. USA* **77**, 7162-7166 (1980).
2. Berman, J. M., Goodman, M., Nguyen, T. M. -D. and Schiller, P. W. *Biochem. Biophys. Res. Commun.* **115**, 864-870 (1983).
3. Sarantakis, D. U.S. Patent 4148786 (1979).
4. Schiller, P. W., Eggimann, B., DiMaio, J., Lemieux, C. and Nguyen, T. M. D. *Biochem. Biophys. Res. Commun.* **101**, 337-343 (1981).
5. Rew, Y., Malkmus, S., Svensson, C., Yaksh, T. L., Chung, N. N., Schiller, P. W., Cassel, J. A., DeHaven, R. N. and Goodman, M. *J. Med. Chem.* **45**, 3746-3754 (2002).
6. Svensson, C. I., Rew, Y., Malkmus, S., Schiller, P. W., Taulane, J. P., Goodman, M. and Yaksh, T. J. *Pharmacol. Exp. Ther.* **304**, 827-832 (2003).
7. Keller, O. and Rudinger, J. *Helv. Chim. Acta.* **57**, 1253-1259 (1974).
8. Stymiest, J. L., Mitchell, B. F., Wong, S. and Vederas, J.C. *Org. Lett.* **5**, 47-49 (2003).
9. Nutt, R. F., Veber, D. F. and Saperstein, R. *J. Am. Chem. Soc.* **102**, 6539-6545 (1980).
10. Schiller, P.W. *Biochem. Biophys. Res. Commun.* **114**, 268-274 (1983).
11. Lu, Y., Nguyen, T. M. -D., Weltrowska, G., Berezowska, I., Wilkes, B. C., Nguyen, T. M. -D., Chung, N. N. and Schiller, P. W. *J. Med. Chem.* **44**, 3048-3053 (2001).
12. Weltrowska, G., Lu, Y., Lemieux, C., Chung, N. N. and Schiller, P. W. *Bioorg. Med. Chem. Lett.* **14**, 4731-4733 (2004).
13. Nicolás, E., Russell, K. C. and Hruby, V. J. *J. Org. Chem.* **58**, 766-770 (1993).
14. Bowen, C. A., Negus, S. S., Zong, R., Neumeyer, J. L., Bidlack, J. M. and Mello, N. K. *Neuropsychopharmacology* **28**, 1125-1139 (2003).

A Photo-Controlled β -Hairpin

Markus Löweneck¹, Shou-Liang Dong^{1,2}, Tobias E. Schrader³, Wolfgang J. Schreier³, Wolfgang Zinth³, Luis Moroder¹ and Christian Renner¹

¹Department of Bioorganic Chemistry, Max-Planck-Institute of Biochemistry, Martinsried 82152, Germany; ²School of life science, Lanzhou University, 222 Tianshui South Road, Lanzhou 730000, China; ³Institute of Biomolecular Optics, Ludwig-Maximilians-University, Munich 80538, Germany

Introduction

Light offers many advantages as means for manipulating systems of either microscopic or macroscopic size: Photons can be applied with extreme spatial and temporal resolution with modern laser techniques; they are perfectly clean in that photons leave no remaining waste and, in contrast to matter, the photons of light do not interact with each other (at moderate intensities) allowing for multiplexing. For these reasons molecular assemblies with optical triggers are ideal systems for the investigation of molecular processes as well as for the construction of molecular machines.

Our group and others have focused on combining light-switches based on azobenzene chromophores with peptide sequences for investigating protein folding and function in a time resolved manner after excitation with light of an appropriate wavelength [1]. Backbone cyclization of octapeptides via (4-amino)phenylazobenzoic acid (APB) or (4-aminomethyl)phenylazobenzoic acid (AMPB) yielded cyclic photoresponsive peptides with pronounced changes in conformation upon isomerization. The extremely fast isomerization process of the chromophore itself makes these peptides ideal model systems for the study of fast events in protein folding. To improve our models beyond local conformational dynamics we sought to combine a regular structural element such as a β -hairpin with an ultrafast light switch.

Results and Discussion

We have been able to design, synthesize and characterize a hairpin based on the tryptophan zipper motif [2] that incorporates an azobenzene-based photo-switch allowing for time-resolved folding studies of β -structures with unprecedented temporal resolution (Fig. 1). At room temperature the *trans*-azo isomer exhibits a largely disordered structure, but light-induced isomerization to the *cis*-azo form leads to formation of a β -hairpin, where the two peptide parts are linked by the novel photo-switch [3-(3-aminomethyl-phenylazo)-phenyl]-acetic acid (AMPP).

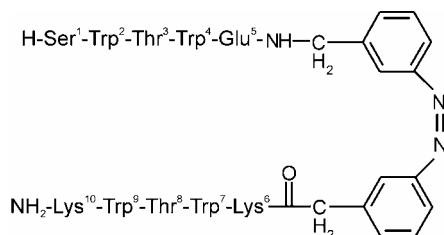


Fig. 1. Photoresponsive β -hairpin based on the very stable tryptophan zipper motif.

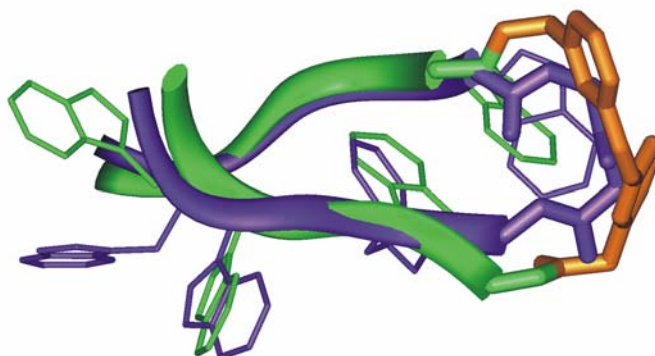


Fig. 2. Comparison of the NMR-structures of our Azo-hairpin (light colors) and the published tryptophan zipper hairpin [2] (dark color).

While in the original sequence the dipeptide Asn-Gly nucleates the type I' β -turn that connects the two strands of the hairpin, this role is taken in our photoresponsive β -hairpin by the AMPP chromophore that apparently can act as a β I'-turn mimetic. The β -hairpin structure was confirmed and determined by NMR spectroscopy (Fig. 2), but folding can be monitored by pronounced changes in the CD, IR and fluorescence spectra.

Parallel to our work a similar azobenzene containing hairpin peptide was synthesized by the group of Hilvert [3]. Both hairpins share the identical chromophore, but differ in the amino acid sequence of the extended strands. In our case the tryptophan zipper motif resulted in good solubility of both azo isomers allowing for structural characterization of the *cis*-azo and the *trans*-azo species, whereas the amino acid sequence chosen by Hilvert and colleagues lead to insolubility of the *trans*-azo isomer possibly compromising its use in folding studies. An additional advantage of the tryptophan zipper motif is that the characteristic band in the circular dichroism at 280 nm allows quantification of the folded fraction under given conditions.

Acknowledgments

The work was funded by the Deutsche Forschungsgemeinschaft (SFB 533, grant A8).

References

1. Renner, C., Kusebauch, U., Löweneck, M., Milbradt, A. G. and Moroder, L., *J. Peptide Res.* **65**, 4-14 (2005).
2. Cochran, A. G., Skelton, N. J. and Starovasnik, M. A., *Proc. Natl. Acad. Sci. USA* **98**, 5578-5583 (2001).
3. Aemissegger, A., Kräutler, V., von Gunsteren, W. F. and Hilvert, D. *J. Am. Chem. Soc.* **127**, 2929-2936 (2005).

Structure-Function Relationship Studies of Analogs of PTH(1-11) Fragment Containing Combinations of Aib and (α Me)Nle

Andrea Caporale¹, Nereo Fiori¹, Elisabetta Schievano¹, Michael Chorev², Stefano Mammi¹ and Evaristo Peggion¹

¹*Department of Chemical Sciences, University of Padova, Institute of Biomolecular Chemistry, CNR, via Marzolo 1, 35131 Padova, Italy;* ²*Laboratory for Translational Research, Harvard Medical School, 1 Kendall Square, Bldg 600, Cambridge, MA 02129, USA*

Introduction

Parathyroid hormone (PTH) is an 84 amino acid peptide hormone. Produced in the parathyroid glands, it acts primarily on bone and kidney to maintain extracellular calcium levels within normal limits. It has been shown that the N-terminal 1-34-fragment of PTH is sufficient for binding to and activation of the PTH type I receptor (PTH1R). The study of reduced-size PTH agonist and antagonist analogs has been the subject of extensive research [1], aiming at developing safer and non-parenteral bone anabolic drugs. Recent studies showed that certain modifications (e.g., Ser³ \rightarrow Ala³, Asn¹⁰ \rightarrow Gln¹⁰, Leu¹¹ \rightarrow Arg¹¹) can increase binding affinity and efficacy of peptides as short as 11 amino acids derived from the otherwise extremely weak PTH(1-11).

This work represents our ongoing effort to investigate the role of α -helicity in the interaction of short PTH fragments with PTH1R. We synthesized and conformationally characterized a series of PTH(1-11) analogs containing sterically hindered and helix-promoting C $^{\alpha}$ -tetrasubstituted amino acids. It has been demonstrated that the position and composition of C $^{\alpha}$ -tetrasubstituted amino acids within the 1-4 sequence plays a significant role in PTH action [2]. Therefore, in this series we limited the Aib residues to positions 1 and 3. Moreover, we inserted α (Me)Nle at position 8. It is known that in PTH(1-34) replacement of Met⁸ with Nle is well tolerated, maintaining binding affinity and efficacy. The hydrophobic side chain of Nle⁸ appears to be critical for the interaction with the receptor, and in the computer-based models for the PTH/PTH1R complex residue 8 is found in a deep hydrophobic cleft.

The following peptides were studied:

- I** [Aib¹, Ala³, (α Me)Nle⁸, Gln¹⁰, Arg¹¹]-hPTH(1-11)NH₂
- II** [Aib¹, Ala³, D-(α Me)Nle⁸, Gln¹⁰, Arg¹¹]-hPTH(1-11)NH₂
- III** [Ala¹, Aib³, (α Me)Nle⁸, Gln¹⁰, Arg¹¹]-hPTH(1-11)NH₂
- IV** [Ala¹, Aib³, D-(α Me)Nle⁸, Gln¹⁰, Arg¹¹]-hPTH(1-11)NH₂
- V** [Aib^{1,3}, (α Me)Nle⁸, Gln¹⁰, Arg¹¹]-hPTH(1-11)NH₂
- VI** [Aib^{1,3}, D-(α Me)Nle⁸, Gln¹⁰, Arg¹¹]-hPTH(1-11)NH₂

Results and Discussion

The peptides were synthesized by SPPS employing Fmoc-protected amino acids. Fmoc- α (Me)Nle-OH was prepared following Strecher's Synthesis and protected using Fmoc-Cl/TMS-Cl/DiPEA. We combined the HBTU/HOBt/DIPEA and the acyl fluoride coupling methods [3]. The latter was used to incorporate the C $^{\alpha}$ -tetrasubstituted amino acids.

The CD spectra of the six analogs in aqueous solution containing 20% TFE (v/v) show the typical CD pattern of the α -helical conformation, with a helix content in the range of 35-55% (calculated according to [4]). The helix contents were always higher than that of the native sequence. NMR spectra were recorded at 298 K in a 1 mM solution containing 20% TFE (v/v). In general, the chemical shift differences of the α CH protons with respect to the corresponding random coil values confirm the higher tendency toward the helical ordered structure relative to PTH(1-11). Moreover, there is an increasing tendency to stabilize the helical segment, especially for residues 2 and 4, going from analog **I** to analog **VI** indicating the presence of ordered structure even in the very first segment (Fig. 1).

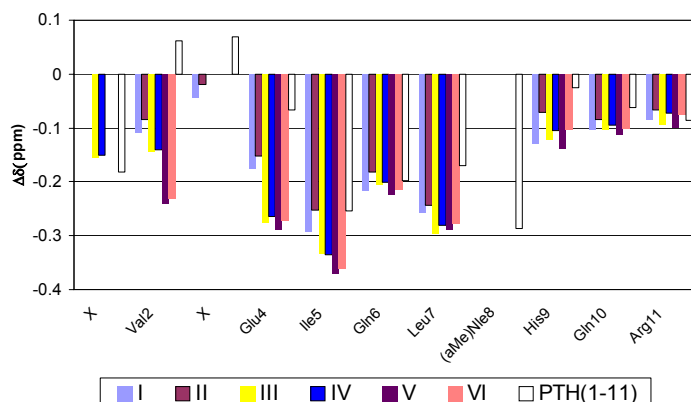


Fig. 1. Chemical Shift differences of the α H protons of PTH(1-11) and analogs **I-VI** with respect to the random coil value ($\Delta\delta = \delta_{\text{measured}} - \delta_{\text{random coil}}$).

In the ROESY spectra, a number of α H(i)-NH(i+3), α H(i)- β H(i+3) and α H(i)-NH(i+4) connectivities typical of the α -helix were observed in all analogs. According to the ROE tables, analogs that differ only in the configuration of residue 8 adopt the same structure.

Superimposition of the ensembles of the low energy structures resulting from distance geometry and molecular dynamics calculations clearly indicated a high convergence towards the helical structure for all analogs, and the atomic RMSD of the backbone atoms confirms an increasing convergence going from analog **I** to analog **VI**.

The results of biological tests, that are underway, will correlate these structural results with bioactivity.

References

1. Shimizu, N., Guo, J. and Gardella, T. J. *J. Biol. Chem.* **276**, 49003-49012 (2001); Barazza, A., Wittelsberger, A., Fiori, N., Schievano, E., Mammi, S., Toniolo, C., Alexander, J. M., Rosenblatt, M., Peggion, E. and Chorev, M. *J. Peptide Res.* **65**, 23-35 (2005).
2. Tsomaia, N., Pellegrini, M., Hyde, K., Gardella, T. J. and Mierke, D. F. *Biochemistry* **43**, 690-699 (2004).
3. Carpino, L. A., Beyermann, M., Wenschuh, H. and Bienert, M. *Acc. Chem. Res.* **29**, 268-274 (1996).
- 4 Yang, J. T., Wu, C. S. and Martinez, H. M. *Methods Enzymol.* **130**, 208-269 (1986).

Membrane Associated Structure of a Ghrelin Agonist as Determined by NMR

Dale F. Mierke^{1,2}, Andrea Piserchio¹, John Eynon³, Jundong Zhang³,
 John E. Taylor³, Heather Halem³, Michael D. Culler³ and Jesse Z. Dong³

¹Department of Molecular Pharmacology, Physiology, & Biotechnology, Division of Biology and Medicine, Brown University, Providence, RI 02912, USA; ²Department of Chemistry, Brown University, Providence, RI 02912, USA; ³IPSEN Group, 27 Maple Street, Milford, MA 01757, USA

Introduction

We have undertaken the structural characterization of a ghrelin inverse agonist, sequentially related to substance P, using high-resolution NMR methods. Given the evidence of a membrane associated pathway to interaction with the receptor, we carried out structural studies in the presence of a membrane mimetic. Based on the structural results we hope to understand the structural requirements for agonists versus antagonism.

Results and Discussion

To mimic the membrane associated structure, the study was carried out in the presence of zwitterionic micelles made of dodecylphosphocholine. The undecapeptide readily associates with the micelles and a number of negative NOEs were detected (Fig. 1). At least two β -turn-like conformations have been localized in position D⁵Phe⁶-Gln⁶, and D⁹Trp⁹-Leu¹⁰, respectively (Fig. 2). Altogether the backbone is well defined for the two fragments encompassing residues Pro²-Gln⁶ and D⁹Trp⁹-Leu¹¹. The aromatic and alkyl moieties located in the C-terminus generate a hydrophobic core. The NMR structure of this molecule indicates that Leu¹¹ occupies a central position in the C-terminal hydrophobic core. This suggests that the clustering of the hydrophobic residues in the compound provides the driving force for the peptide absorption on the membrane, adopting the proper structure for receptor interaction leading to inverse agonist activity (Fig. 3).

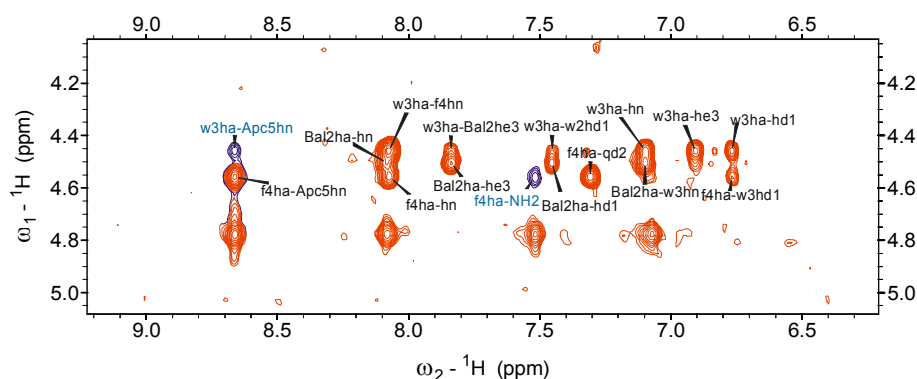


Fig. 1. Fingerprint region of a 1H-1H NOESY spectrum.



Fig. 2. Superposition of the resulting structures from the DG calculations.

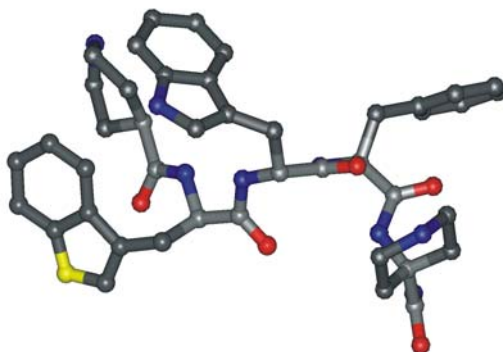


Fig. 3. One representative structure of the ghrelin inverse agonist while associated with the membrane environment as determined by NMR.

The structural results presented here provide insight into the structural features required for biological action of this important peptide system.

Scaffold, Dendritic and Metal-Assisted Assembly of Collagen-Like Biomaterials

Weibo Cai^{1,2}, Sen Wai Kwok², Joseph P. Taulane² and Murray Goodman²

¹Molecular Imaging Program at Stanford (MIPS), Stanford University School of Medicine, CA 94305, USA; ²Department of Chemistry & Biochemistry, University of California at San Diego, CA 92093, USA

Introduction

Collagen is the most abundant extracellular protein in vertebrates. Because of its low immunogenicity and high tensile strength, collagen has been widely used as biomaterials. Synthetic collagen structures incorporating unnatural amino acid residues offer an alternative to natural collagens and have better enzymatic stability [1]. We have incorporated the TRIS scaffold into our collagen mimetic research for scaffold and dendritic assembly of triple helical structures (Fig. 1) [2].

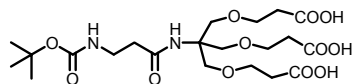


Fig. 1. The Boc- β -Ala-TRIS-[OH]₃ (TRIS) scaffold for collagen mimetic assembly.

Results and Discussion

We have synthesized single chain compound Boc-(Gly-Nleu-Pro)₆-OMe, TRIS assembled structure Boc- β -Ala-TRIS-[(Gly-Nleu-Pro)₆-OMe]₃ and the 165 AA dendrimer TMA[β -Ala-TRIS-[(Gly-Nleu-Pro)₆-OMe]₃]₃ where Nleu denotes N-isobutyl glycine and TMA denotes the trimesic acid core (Fig. 2 a) [2].

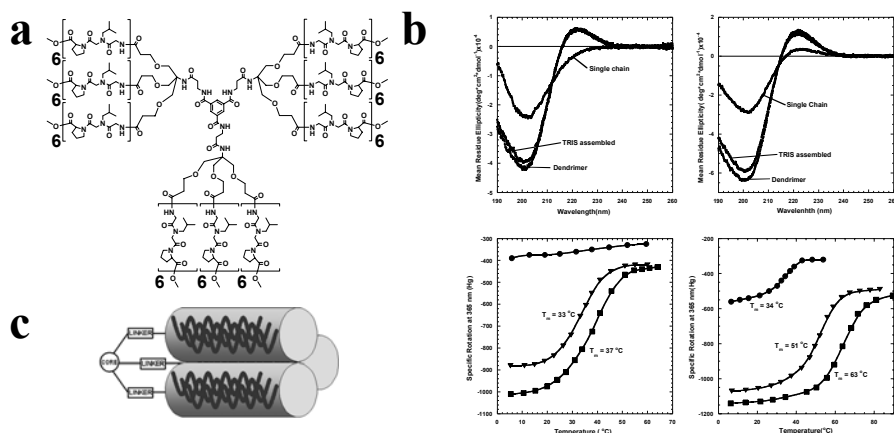


Fig. 2. **a**: Structure of the 165 residue dendrimer. **b**: The CD spectra and thermal denaturation curves at 0.2 mg/mL in H₂O (left) & 2:1 EG/H₂O (right): Single chain (●), TRIS assembled (▼), and Dendrimer (■). **c**: Schematic structure of the dendrimer.

It is clear from Figure 2 **b** that the dendritic structure forms more thermally stable triple helix than the corresponding TRIS-assembled structure, the melting

temperature (T_m) of the dendrimer is 4 °C (in H₂O) and 12 °C (in 2:1 EG/H₂O) higher. Since no change in the T_m value was observed over a concentration range from 0.05 to 2.0 mg/mL for the dendrimer, we believe that the stabilizing effect arises from an intramolecular clustering of the triple helical arrays about the core structure (Fig. 2 c). This cluster excludes solvent from the interior portion of the array which leads to stabilization of the triple helix bundle.

Recently, we have synthesized catechol-containing structures for metal-assisted assembly of the triple helices (Fig. 3 a) [3]. Molecules **A** and **B** have the same peptide sequence and chain length. The UV spectra of both compounds clearly suggest octahedral coordination of Fe³⁺. The CD spectra (data not shown) and thermal melting experiments shown in Figure 3 b indicate that compound **A** does not form a triple helix when Fe³⁺ is absent. However, when 1/3 equivalence of Fe³⁺ was added, it became triple helical with a T_m of 28 °C. When one equivalence of Fe³⁺ is added, T_m of molecule **B** increased from 36 °C to 58 °C. The formation of a Fe³⁺-catechol complex increased the T_m by a remarkable 22 °C. Based on our previous data, this can only be explained by an intramolecular complex where Fe³⁺ is coordinated by three catechol groups from the same molecule **B**. The complex acts as an additional scaffold which confers extra stability. A schematic of this discaffold-assembled triple helical collagen mimetic structure is shown in Figure 3 c.

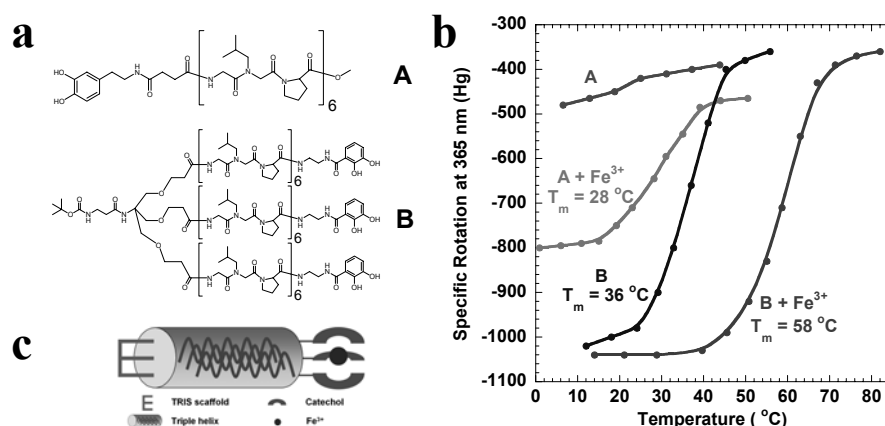


Fig. 3. **a**: Structure of two catechol-containing peptides; **b**: Thermal melting curves and **c**: Schematic structure of molecule **B** with Fe³⁺.

In conclusion, collagen-like peptides were synthesized through scaffold, dendritic and metal-assisted assembly. TRIS is an efficient scaffold at triple helical assembly while dendrimers exhibit enhanced thermal stability over TRIS-assembled structures. Metal-assisted assembly increased the T_m even more dramatically.

Acknowledgments

This project was supported by the NSF biomaterial division, DMR0111617.

References

1. Goodman, M., Melacini, G. and Feng, Y. *J. Am. Chem. Soc.* **118**, 10928-10929 (1996).
2. Kinberger, G. A., Cai, W. and Goodman, M. *J. Am. Chem. Soc.* **124**, 15162-15163 (2002).
3. Cai, W., *et al.* *J. Am. Chem. Soc.* **126**, 15030-15031 (2004).

Peptide and Protein Synthesis Strategies

Positional Scanning for Peptide Secondary Structure by Solid Phase Synthesis with Aza-Amino Acids and Freidinger Lactams

**Damien R. Boeglin, Mandar S. Bodas, Fabrice Galaud and
William D. Lubell**

*Département de chimie; Université de Montréal, C.P. 6128, Succursale Centre-Ville,
Montréal, Québec H3C 3J7, Canada*

Introduction

Positional scanning for the importance of structure for activity is fundamental for advancing peptide science. For example, the structural biology of a peptide may be ascertained using Ala, Pro and D-amino acid scans to provide information on the importance of side-chains, conformation and configuration for activity. Two new methods for positional scanning are being developed in our laboratory. “Aza-scanning” and “lactam-scanning” employ respectively, aza-amino acids and Freidinger lactams to study the importance of turns for peptide activity.

Results and Discussion

Aza-peptides are peptide analogs in which the α -carbon of one or more of the amino acid residues has been replaced with a nitrogen atom. Incorporation of a single aza-amino acid into model peptides has been shown to favor type I, II and VI β -turn geometry possessing the aza-residue at the $i+1$ or $i+2$ position contingent on the aza-residue structure and peptide sequence. Previously, three strategies have been devised for introducing aza-amino acids into peptides on solid-support. Activation of the N-terminal amino group of the growing peptide as an active carbamate or isocyanate followed by reaction with a suitable N'-alkyl fluoren-9-ylmethyl carbazate [1] is plagued by hydantoin formation from intramolecular amide acylation. Configurationally stable aza-tri or dipeptide building blocks have been coupled to the N-terminus of the resin-bound peptide [2-4] to circumvent hydantoin formation; however, their preparation required multiple synthetic steps in solution. Activated Fmoc-aza-amino acid building blocks [5] offered interesting potential for the assembly of aza-peptide on solid support.

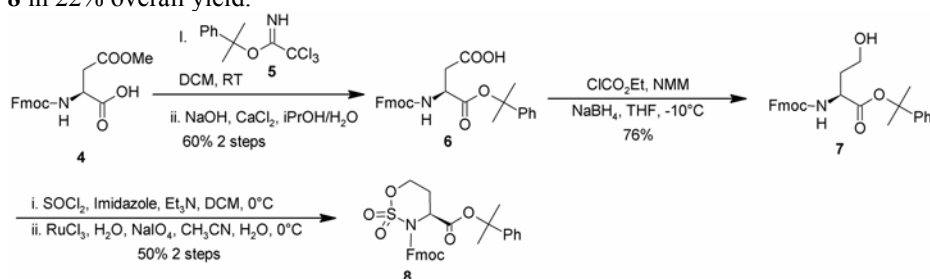
Aza-scanning required the synthesis of N'-alkyl fluoren-9-ylmethyl carbazate by reductive aminations with alkyl aldehydes and ketones using hydride reagents and aromatic aldehydes by hydrogenation with a Pd-catalyst [6]. Conversion to Fmoc-aza-amino acid chloride was achieved by reaction of the carbazate in DCM with excess phosgene in toluene for 15 min at room temperature. Unreacted phosgene was removed with the volatiles under vacuum and the crude Fmoc-aza-amino acid chloride was redissolved in DCM with DIEA as base and allowed to react with the free amine of the growing resin-bound peptide for 6h. The Fmoc protecting group of the aza-residue was removed by treating the resin with a DMF/piperidine solution and the resulting free aza-amino acid residue was acylated using an excess of Fmoc-amino acid chloride generated *in situ* with BTC and 2,4,6-collidine in THF. Peptide synthesis was pursued using standard Fmoc/*t*Bu protocols [7]. The final aza-peptides were cleaved using a TFA/TIS/H₂O (95/2.5/2.5, v/v/v) solution, isolated by precipitation from Et₂O and lyophilized from CH₃CN/H₂O (1/1, v/v solution). Characterization of the crude aza-peptides by LC/MS demonstrated their purity to be typically of 56-95% purity; for comparison the parent peptide was synthesized and

isolated in 84-93% purity. Aza-scans were performed on three biologically active peptides: potent tetrapeptide melanocortin receptor agonist **1**, growth hormone secretagogue **2** and human calcitonin gene-related peptide antagonist **3** (Fig 1).

Ac-His-D-Phe-Arg-Trp-NH ₂ , 1	His-D-Trp-Ala-Trp-D-Phe-Lys-NH ₂ , 2	PTDVGPF A F-NH ₂ , 3
Ac-His- aza Phe-Arg-Trp-NH ₂	His- aza Tyr-Ala-Trp-D-Phe-Lys-NH ₂	PT aza DVGPF A F-NH ₂
Ac-His-D-Phe- aza Arg-Trp-NH ₂	His-D-Trp- aza Ala-Trp-D-Phe-Lys-NH ₂	PTDV aza GP A F-NH ₂
Ac-His-D-Phe- aza Lys-Trp-NH ₂	His-D-Trp- aza Leu-Trp-D-Phe-Lys-NH ₂	PTDVG aza PF A F-NH ₂
Ac-His-D-Phe- aza Orn-Trp-NH ₂	His-D-Trp- aza Gly-Trp-D-Phe-Lys-NH ₂	PTDVG aza PF A F-NH ₂
Ac-His-D-Phe-Arg- aza Nal-1-NH ₂	His-D-Trp-Ala- aza Tyr-D-Phe-Lys-NH ₂	PTDVGPF aza AF-NH ₂
Ac-His-D-Phe-Arg- aza Nal-2-NH ₂	His-D-Trp-Ala-Trp- aza Phe-Lys-NH ₂	
Ac-His-D-Phe-Arg- aza Bip-NH ₂	His-D-Trp-Ala-Trp-D-Phe- aza Lys-NH ₂	

Fig. 1. Aza-amino acid scan of biologically active peptides.

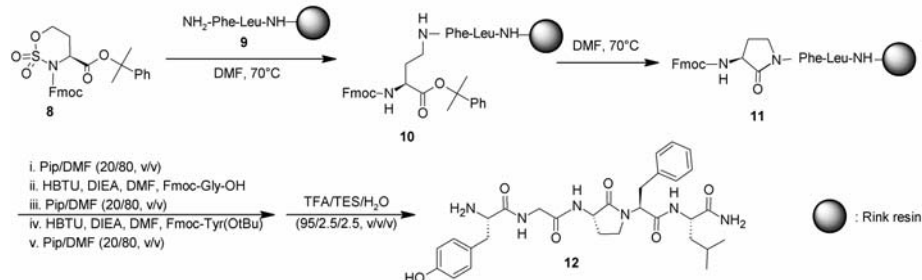
The placement of an α -amino lactam ("Freidinger lactam") moiety into a peptide constrains conformational liberty and as a consequence may improve potency and efficacy [8,9]. Since pioneering research on lactam analogs of peptides such as LH-RH [8] and enkephalin [10], a variety of synthetic methods have been developed to synthesize Freidinger lactams [11-14]. A new, general method for synthesizing enantiomerically pure α -amino γ -lactam bridged peptidomimetics is being pursued that employs homoserine-derived cyclic sulfamidates to sequentially alkylate and acylate the N-terminal of a resin-bound peptide. Homoserine-derived cyclic sulfamidate cumyl ester **8** was synthesized from β -methyl-Fmoc-aspartate **4** by esterification with 2-phenyl-2-propyl trichloroacetimidate **5** in DCM, β -methyl ester hydrolysis, activation as a mixed anhydride and reduction with NaBH₄ to yield homoserine **7** (Scheme 1). Treatment of homoserine **7** with SOCl₂, imidazole, and Et₃N in DCM gave a 4:1 mixture of diastereomeric sulfamidites which was oxidized with catalytic RuCl₃·H₂O and NaIO₄ in CH₃CN and H₂O at 0°C to afford sulfamidate **8** in 22% overall yield.



Scheme 1. Synthesis of cyclic sulfamidate.

Solid-phase Freidinger lactam synthesis and the potential for lactam-scanning were demonstrated by the synthesis of Leu-enkephalin lactam analog **12** (Scheme 2). Alkylation of a suspension of phenylalaninyl leucinamide bound to Rink resin in DMF was performed using cyclic sulfamidate **8** (200 ml%) at 70°C to provide a 4:3:3 mixture composed of starting material, *N*-alkylated peptide and the lactam, apparently from displacement of the cumyl ester, as assessed by cleavage of the resin with TFA:DCM (95:5) and LC-MS analysis. Conditions to improve conversion are being explored; however, heating the resin in DMF at 70°C caused further conversion of the alkylated peptide to the lactam without necessity of solvolysis of the cumyl ester and carboxylate activation. At this point, the resin was capped with 10% Ac₂O in DCM. Deprotection with 20% piperidine in DMF and couplings with

Gly and Tyr(*O*-*t*Bu) using HBTU and DIEA in DMF provided the final peptide lactam which was cleaved with TFA:TES:H₂O (95:2.5:2.5), and isolated by reverse phase HPLC (20-40% CH₃CN-H₂O, 0.1% TFA); *m/z* = 581 (*M*+1), 603 (*M*+Na).



Scheme 2. Solid-Phase synthesis of Freidinger lactam.

Two new positional scanning techniques are being developed using respectively activated aza-amino acid and homoserine-derived cyclic sulfamidate building blocks to construct aza- and lactam-peptide analogs. These approaches use complimentary electronic and structural constraints for inducing turn conformations within a peptide. Experiments are now in progress to test the combined use of aza- and lactam-scanning for identifying turn secondary structures responsible for peptide activity.

Acknowledgments

This work was supported by grants from FQRNT and VRQ (Québec), and CRSNG (Canada).

References

1. Zega, A. and Urleb, U. *Acta Chim. Slov.* **49**, 649-662 (2002).
2. Quibell, M., Turnell, W. G and Johnson, T. *J. Chem. Soc. Perkin Trans I*, 2843-2849 (1993).
3. Gray, C. J., Quibell, M., Bagget, N. and Hammerle, T. *Int. J. Peptide Prot. Res.* **40**, 351-362 (1992).
4. André, F., Marraud, M., Tsouloufis, T., Tzartos, S. J. and Boussard, G. *J. Peptide Res.* **3**, 429 (1997).
5. Melendez, R. E. and Lubell, W. D. *J. Am. Chem. Soc.* **126**, 6759 (2004).
6. Gilbson, C., Goodman S. L., Hahn, D., Hölzemann, G. and Kessler, H. *J. Org. Chem.* **64**, 7388-7394 (1999).
7. Chang, C. D. and Meienhofer, J. *Int. J. Peptide Prot. Res.* **11**, 246 (1978).
8. Aubé, J. In *Advances in Amino Acid Mimetics and Peptidomimetics*, Vol **1**, JAI Press: Greenwich, CT, pp 193-223 (1997).
9. Freidinger, R. M. *J. Med. Chem.* **46**, 5553-5566 (2003).
10. Freidinger, R. M. In *Peptides: Synthesis, Structure, Functions* (Rich, D. H. and Gross, E., eds.) Pierce Chemical Co., Rockford, IL, pp 673-683 (1981).
11. Freidinger, R. M., Veber, D. F., Perlow, D. S., Brooks, J. R. and Saperstein, R. *Science* **210**, 656-658 (1980).
12. Yu, K.-L., Rajakumar, G., Srivasgtava, L. K., Mishra, R. K. and Johnson, R. L. *J. Med. Chem.* **31**, 1430-1436 (1998).
13. Wolf, J.-P. and Rapoport, H. *J. Org. Chem.* **54**, 3164-3173 (1989).
14. Scott, W. L., Alsina, J., Kennedy, J. H. and O' Donnel, M. J. *Org. Lett.* **6**, 1629-1632 (2004).

Synthesis of Cyclic Peptides via Transition Metal Catalyzed C-C Bond Formation

Dirk T. S. Rijkers, Hefziba T. ten Brink, Nourdin Ghalit, Jan Tois and
Rob M. J. Liskamp

Department of Medicinal Chemistry, Utrecht Institute for Pharmaceutical Sciences, Faculty of
Pharmaceutical Sciences, Utrecht University, PO Box 80082, 3508 TB Utrecht,
The Netherlands

Introduction

The correct three-dimensional structure of a peptide is essential for its biological activity. Nature has found many elegant ways to reduce the flexibility of peptides and proteins in order to control their folding and shape to increase affinity as well as selectivity for receptor interaction. Disulfide bridges, thioether (sulfide) bridges and the even more sophisticated multiple chain knotting, are well known ways to control the three dimensional shape. Outstanding examples in this respect are the glycopeptide antibiotic vancomycin and the lantibiotic nisin Z containing a crossed bithioether ring system (Fig. 1).

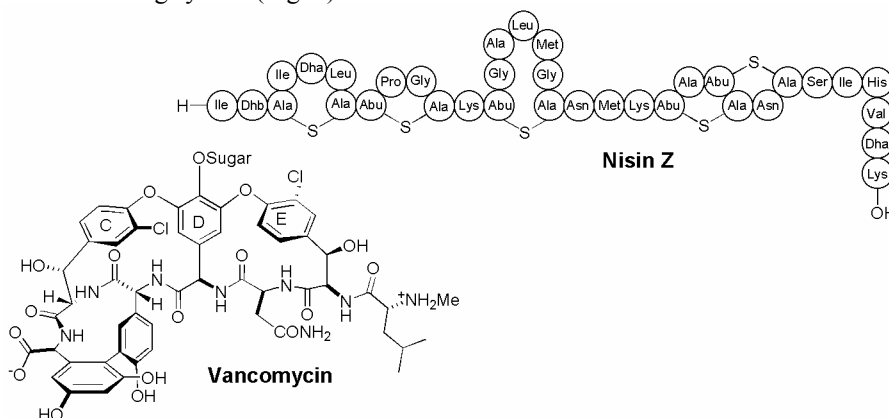


Fig. 1. Structures of vancomycin and nisin Z.

In order to investigate whether the repertoire of Nature involving such conformational constraints can be extended, we are interested in using among others alkene/alkyne bridges as alternative constraints for bioactive molecules [1]. These novel covalent constraints were introduced by ring-closing alkene metathesis (RCM) and ring-closing alkyne metathesis (RCAM) or using Sonogashira-, Heck- and Stille-based palladium-catalyzed C-C bond formation reactions.

Results and Discussion

Based on vancomycin's peptidic core-structure, we designed three different scaffolds for the synthesis of constrained cyclic tripeptides (Fig. 2). Tripeptide scaffold **1** was synthesized by means of RCM using Grubbs' Ru catalyst. Via this approach constrained cyclic tripeptides with 13 to 19 atoms in the ring were synthesized in yields ranging from 10 to 92%. Since RCM did not allow control of the *E/Z* configuration of the newly formed C-C double bond, a second approach was

followed. This approach was based on a Sonogashira reaction in order to obtain tripeptide scaffold **2** in which an alkyne moiety is part of the cyclic constraint. Two synthesis routes were explored. The first route comprised an *intramolecular* Sonogashira reaction as the cyclization step. As an alternative, the second route was based on an *intermolecular* Sonogashira coupling followed by an *intramolecular* amide bond forming reaction (macrolactamization). The latter route was the most efficient since the yields significantly increased from 6-27% (*intramolecular* Sonogashira reaction) to 54-61% (macrolactamization). Stereoselective reduction of the triple bond will enable control the *E/Z* configuration of the resulting alkene.

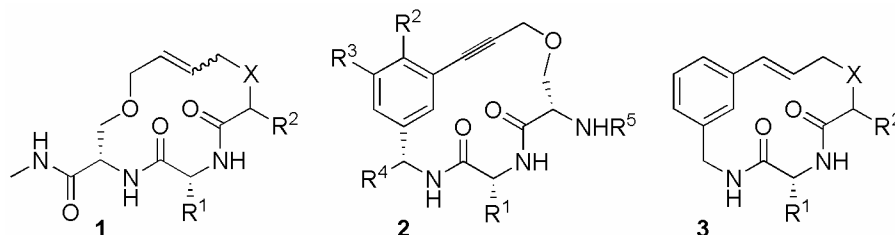


Fig. 2. Scaffolds for the synthesis of cyclic peptides as inspired by vancomycin.

A different method to control the stereochemistry of the newly formed double bond is by using the Heck reaction involving a Pd-catalyzed coupling of an arylhalide with a terminal alkene to yield predominantly an *E*-alkene. Coupling of Boc-Ala-(3-iodo)benzylamide with *tert*-butyl 6-heptenoate proceeded smoothly with 60% yield with an *E:Z* ratio of 98:2. However, attempted cyclization of the precursors into scaffold **3** mainly resulted into the formation of dimers.

For the synthesis of bicyclic pentapeptide **5** as a mimic of vancomycin, a Stille coupling followed by a tandem ring-closing metathesis reaction was explored (Fig. 3) [2]. An important design consideration in the synthesis of **5** was the right choice of the central phenylglycine derivative. After bromination on both the 3- and 5-positions, a Stille coupling with allyltributylstannane was performed in reasonable yield without affecting the chiral integrity of the phenylglycine moiety. Treatment of the linear metathesis precursor **4** with Grubbs' Ru-catalyst resulted in the formation of a bicyclic pentapeptide **5** with the correct side chain to side chain connectivity pattern as is present in vancomycin: $i - 2 \rightarrow i$, $i \rightarrow i + 2$.

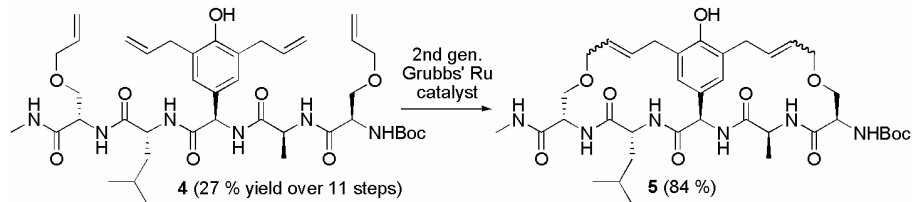


Fig. 3. Bicyclic pentapeptide **5** as a vancomycin mimic.

Nisin Z contains five consecutive thioether bridges (Fig. 1) that play an important role in the dual mode of action of nisin as a bactericide [3]. Nisin binds via its N-terminus, comprising the ABC-ring system, to lipid II, which is an essential precursor for cell wall biosynthesis. As a result, the C-terminus, comprising the knotted DE-ring, can form pores in the phospholipid membrane. This ultimately leads to cell leakage and causes a collapse of the vital ion gradients across the

membrane. We have synthesized several analogs of the A-, B-, C-, and DE-ring systems of nisin featuring both ring-closing *alkene*- and ring-closing *alkyne* metathesis (Fig. 4) [4, 5]. These analogs will be used to assemble a complete nisin mimic in which all thioether bridges have been replaced by alkene/alkyne bridges to investigate their binding potency of lipid II.

Alkyne bridged cyclic pentapeptide **6**, corresponding to the sequence of the A-ring in nisin, was synthesized from its linear precursor in a yield of 42% in the presence of the tungsten-alkylidyne complex $(t\text{BuO})_3\text{W}\equiv\text{C}^t\text{Bu}$ as a catalyst. The synthesis of **6** is the first example of RCAM of a peptide without any preorganization of the peptide backbone by e.g. the presence of a proline residue [4].

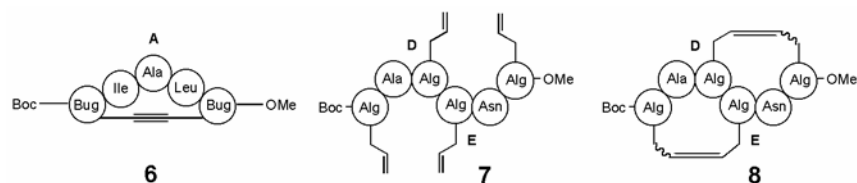


Fig. 4. Alkyne/alkene bridged mimics of nisin ring system.

In the DE-ring system of nisin the amino acid side chains cross each other. Therefore, the synthesis of an alkene mimic of this ring system is particularly challenging. However, treatment of peptide **7** with Grubbs' Ru-catalyst resulted in a defined mixture of monocyclic intermediates and bicyclic hexapeptide **8** was obtained in 72% in a single reaction step involving a double ring-closing metathesis reaction. Preferred formation of the intermediate monocyclic mimic, resulting in formation of the desired bicyclic mimic, may be due to a considerable degree of preorganization of the linear peptide RCM-precursor [5].

In conclusion, several synthetic approaches have been designed to introduce novel carbon-carbon conformational constraints in order to expand the repertoire of Nature. The assembly of the individual C-C bond containing partial mimics toward the complete mimic as well as the biochemical analyses to evaluate binding activity to natural targets (i.e., D-Ala-D-Ala/D-Ala-D-lactate or lipid II) are currently investigated.

Acknowledgments

Support by the council for Chemical Sciences of The Netherlands-Organization for Scientific Research (CW-NWO) is gratefully acknowledged. We thank C. Versluis and Dr. J. Kemmink for performing the mass- and NMR analyses, respectively. Prof. Dr. A. Fürstner is acknowledged for his collaboration in the nisin RCAM project. J.T. thanks TEKES and the Helsinki University of Technology for financial support.

References

1. Miller, S. J., Blackwell, H. E. Grubbs, R. H. *J. Am. Chem. Soc.* **118**, 9606-9614 (1996).
2. ten Brink, H. T., Rijkers, D. T. S., Kemmink, J., Hilbers, H. W. and Liskamp, R. M. *J. Org. Biomol. Chem.* **2**, 2658-2663 (2004).
3. Chatterjee, C., Paul, M., Xie, L. and van der Donk, W. A. *Chem. Rev.* **105**, 633-684 (2005).
4. Ghalit, N., Poot, A. J., Fürstner, A., Rijkers, D. T. S. and Liskamp, R. M. *J. Org. Lett.* **7**, 2961-2964 (2005).
5. Ghalit, N., Rijkers, D. T. S., Kemmink, J., Versluis, C. and Liskamp, R. M. *J. Chem. Commun.* 192-194 (2005).

Solid Phase Synthesis of Phosphorylated *Cis* and *Trans* 3-Peptidyl-4-(4'-hydroxyphenyl)- β -Lactams

David R. Coleman IV^{1,2}, Kumar K. Kaluarachchi² and John S.
McMurray²

¹The University of Texas Graduate School of Biomedical Sciences; ²The University of Texas
M. D. Anderson Cancer Center Department of Neuro-Oncology, Box 316, 1515 Holcombe
Blvd., Houston, TX 77030

Introduction

Phosphorylation and dephosphorylation of proteins on tyrosine residues is a major mechanism of signal transduction in the cell. New tyrosine mimics would be useful for the development of peptide-based inhibitors of the tyrosine kinases and tyrosine phosphatases that carry out these reactions. The 4-(4'-hydroxyphenyl)-3-amino β -lactam scaffold would serve this purpose. The hydroxyphenyl group mimics the side chain of tyrosine and the 3-amino groups afford a point on which to attach amino acid sequences that could impart specificity for a particular kinase or phosphatase.

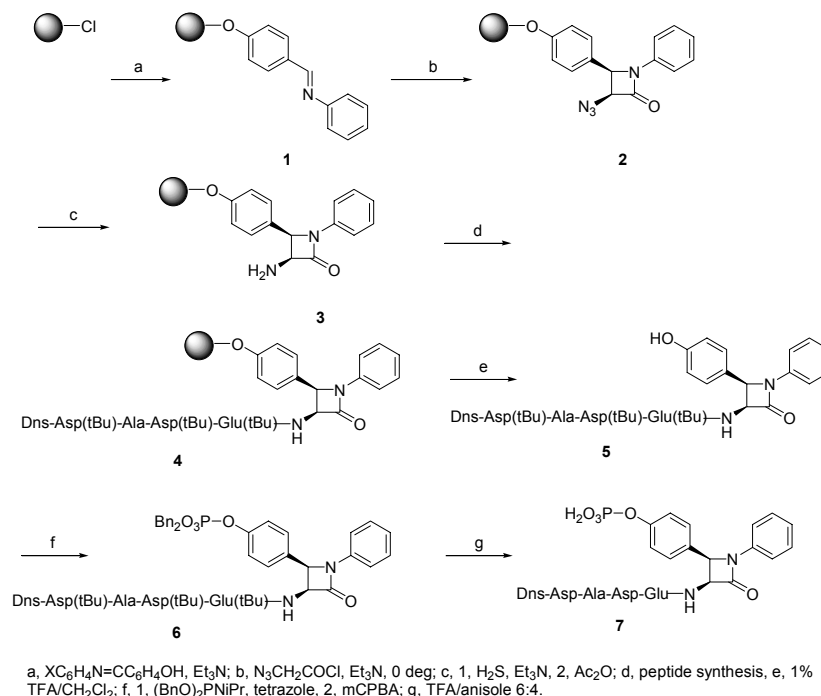
We envisioned that phosphorylated 4-(4'-hydroxyphenyl)-3-amino β -lactams could potentially be suicide inhibitors of tyrosine phosphatases. On dephosphorylation, electron transfer through the aryl ring to the amide nitrogen would result in 1,4 ring opening reaction with concomitant quinone methide formation similar to the base labile reaction described by us [1]. The quinone methide could alkylate the protein in a 1,6 conjugate addition reaction. We report here the synthesis of 3-(Dansyl-Asp-Ala-Asp-Glu)amino-4-(4'-phosphoryloxyphenyl)-1-phenyl-azetidine-2-ones. Solid phase synthesis of the β -lactam was carried out followed by assembly of the amino acid chain on the support. Phosphorylation was accomplished in solution. Both *cis* and *trans* β -lactams were used as starting materials. Ruhland et al. [2] were the first to report the solid phase synthesis of β -lactams and others followed.

Results and Discussion

4-(4'-Hydroxyphenyl)-3-amino β -lactams was prepared using [2+2] cycloadditions of ketenes to resin-supported imines. 2-Chlorotrityl chloride resin was used as the support. The starting imine, *N*-4-hydroxybenzylidene aniline, was prepared separately and was attached to the support as phenyl ethers in DCM in the presence of Et₃N (**1**, Scheme 1). Overnight couplings using 5 equivalents of imine and 6 equivalents of base were found to give the highest loading. This resin and linkage system was designed to produce 4-(4'-hydroxyphenyl) azetidine-2-ones on cleavage with 1% TFA in DCM.

The *cis* α -amino β -lactam (**2**) was prepared using the Bose reaction, i.e., the cycloaddition of azidoketene with the resin-bound imine (Scheme 1) (Caution: the preparation and use of azidoacetyl chloride poses a potential explosion risk). Thus, 5 equivalents of azidoacetyl chloride were dropped into a suspension of the resin in DCM containing 6 equivalents of Et₃N at 0°. Yields ranged from 50 - 100% and were difficult to control. This solid-supported reaction is diastereospecific and produced only *cis* diastereomers ($J_{H3,H4}$ = 5.6 Hz). Note that the β -lactams in Scheme 1 are actually mixtures of two *cis* diastereomers. To produce the 3-amino group, the azido group was reduced by bubbling H₂S into a suspension of the β -

lactam-resin in CH_2Cl_2 and Et_3N for 30 minutes to give **3** [3]. Dansyl-Asp(tBu)-Ala-Asp(tBu)-Glu(tBu) was then assembled on the amino group using manual SPPS with Fmoc-protection and PyBOP/HOBt/DIPEA coupling. Side chain protected peptide **5** was obtained by cleavage with 1% TFA in DCM.



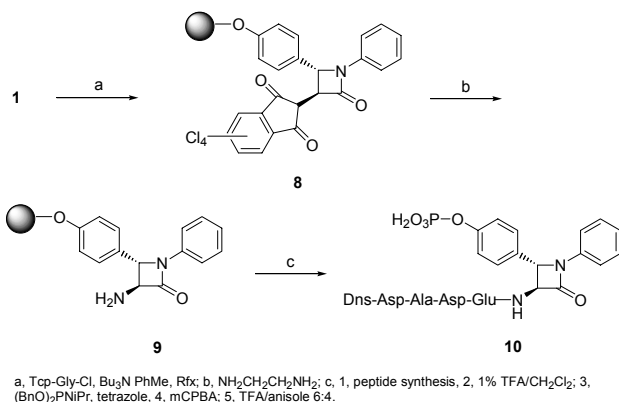
Scheme 1.

Global phosphorylation of **5** with *N,N*-diisopropyl-dibenzyl phosphoramidite followed by mCPBA oxidation gave protected intermediate **6**. This reaction was not complete as about 30% non-phosphorylated peptide was obtained. TFA treatment gave a mixture of two *cis* diastereomers, **7**.

For the synthesis of *trans* peptidyl β -lactams, excellent yields could be achieved by adding 5 equivalents of tetrachlorophthaloyl glycyl chloride [4] to resin-bound imines in refluxing in toluene containing 6 equivalents of Bu_3N to give **8** (Scheme 2) [5]. Cycloadditions were complete in 10 min. These conditions were diastereoselective and gave $\geq 90\%$ *trans* β -lactams ($J_{\text{H}3,\text{H}4} = 2.2$ Hz). Tetrachlorophthalimidoacetyl chloride was previously used in solution phase syntheses of α -amino- β -lactams under microwave heating by Bose et al. [4]. The Tcp group was removed by treating the resin 5 \times with a solution of 10% ethylenediamine and 20% EtOH in DMF for 10 min each at room temperature. Assembly of the peptide was carried out with automated protocols. Cleavage, phosphorylation and deprotection were accomplished as in Scheme 1. Phosphorylation was only 80% complete in this case.

HPLC elution systems containing gradients of ACN on 0.1%TFA were not effective in separating the diastereomers. However, gradients of MeOH in 0.01M NH_4OAc resulted in noticeable separation and that of the *trans* phosphopeptides was

much greater than the *cis* (Fig. 1). The individual diastereomers of **10** could be obtained by preparative HPLC but those of **7** could not.



Scheme 2.

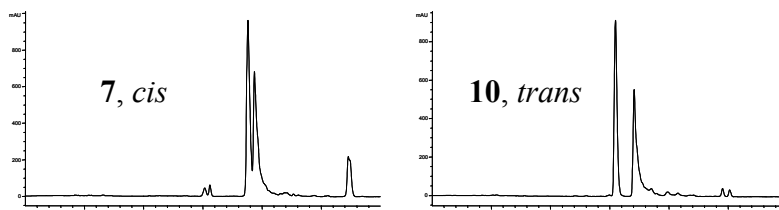


Fig. 1. HPLC chromatograms of *cis* and *trans* diastereomers of **7**, left panel and **10**, right panel. Gradient: 10 – 50% MeOH/30 min in 0.01M NH_4OAc .

Acknowledgments

This work was funded by Texas Higher Education Coordinating Board, #15-073 and the National Cancer Institute CA53617. We also acknowledge the NCI Cancer Center Support Grant CA16672 for the support of our NMR and mass spectrometry facilities.

References

1. Cabell, L. A., Hedrich, L. W. and McMurray, J. S. *Tetrahedron Lett.* **42**, 8409-8413 (2001).
2. Ruhland, B., Bhandari, A., Gordon, E. M. and Gallop, M. A. *J. Am. Chem. Soc.* **118**, 253-254 (1996).
3. Wagle, D. R., Garai, C., Chiang, J., Monteleonw, M. G., Kurys, B. E., Strohmeyer, T. W., Hegde, V. R., Manhas, M. S. and Bose, A. K. *J. Org. Chem.* **53**, 4227-4236 (1988).
4. Bose, A. K., Jayaraman, M., Okawa, A., Bari, S. S., Robb, E. W. and Manhas, M. S. *Tetrahedron Lett.* **37**, 6989-6992, (1996).
5. Brown, M., Burnett, D. A., Caplen, M. A., Chen, L. -Y., Clader, J. W., Domalski, M., Dugar, S., Pushpavanam, P., Sher, R., Vaccaro, W., Viziano, M. and Zhao, H. *Tetrahedron Lett.* **36**, 2555-2558 (1995).

Switch on Amyloid β Peptide Self-Assembly by Enzyme-Triggered Acyl Migration

Sonia Dos Santos, Arunan Chandravarkar, Bhubaneswar Mandal,
 Richard Mimna, Karine Murat, Lydiane Saucède, Marie-Stephanie
 Camus, Gabriele Tuchscherer and Manfred Mutter

*Institute of Chemical Sciences and Engineering, Ecole Polytechnique Fédérale de Lausanne
 (EPFL), CH-1015 Lausanne, Switzerland*

Introduction

Conformational transitions as origin of peptide aggregation are considered as a fundamental molecular event in early processes of degenerative diseases [1-3]. A detailed investigation of these processes is hampered by intrinsic problems such as high tendency of the involved peptides for β -sheet formation and spontaneous aggregation limiting their experimental accessibility [4,5]. We have recently developed a new generation of switch-peptides (S-peptides) for the controlled induction of conformational transitions at physiologic pH using $O \rightarrow N$ acyl migrations in situ [6]. Here, we explore the sequential triggering of $O \rightarrow N$ acyl migrations in amyloid β derived switch-peptides as a general tool to study the onset and inhibition of polypeptide folding, self-assembly and aggregation (Fig. 1) [7].

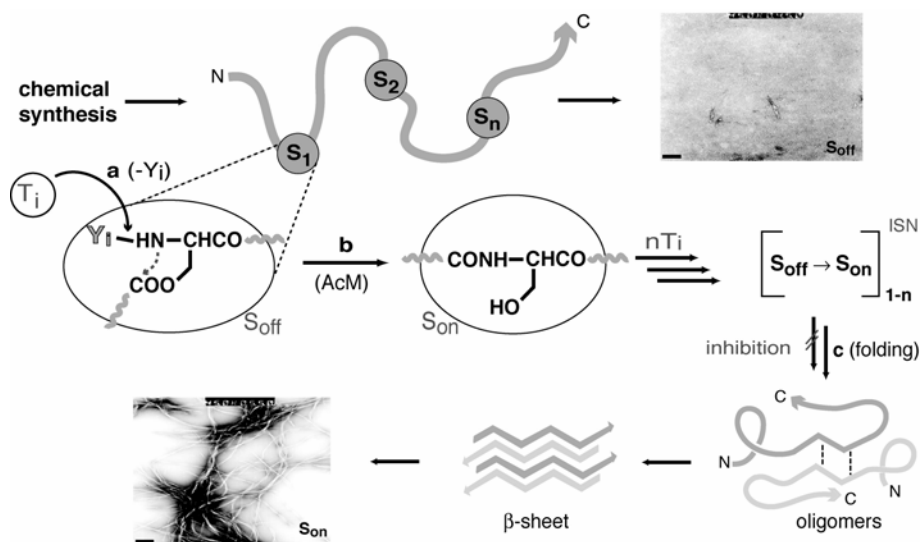


Fig. 1. The concept of switch-peptides (S_{off}): consecutive triggering of O, N -acyl migrations for the onset (S_{on}) and inhibition of peptide folding and self-assembly *in statu nascendi*.

Results and Discussion

The design and chemical synthesis of a $A\beta(1-42)$ S-peptide containing two orthogonal switch (S)-elements (Fig. 2) allows for the selective removal of Y by trigger systems T, i.e., exopeptidases with 'nonnative' specificities such as pyroglutamate aminopeptidase and D-amino acid peptidases or with unique cleavage

sites such as dipeptidyl amino peptidase IV (DPPIV), specific for N-terminal Axx-Pro.

Solid-phase synthesis of the S-peptide was achieved applying Fmoc/tBu-based chemistry. Most notably, the presence of one or multiple S-elements results in highly soluble compounds facilitating HPLC purification and structural characterization. As shown by CD, the conformational decoupling of the S-spaced peptide blocks results in flexible random-coil conformations. Even after 24 hrs at physiologic pH, no changes in the HPLC or CD spectra are observed for the Soff-state of the S-peptide, pointing to a high chemical and conformational stability.

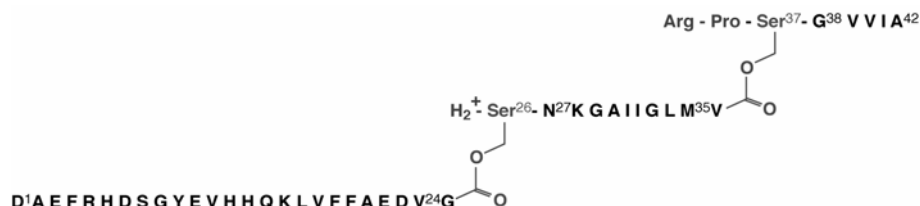


Fig. 2. Design of the A β (1-42) S-peptide containing an enzyme (DPPIV / Y = Arg-Pro; S2) and pH (Y = H⁺; S1) inducible switch (S)-element.

In contrast, the controlled removal of Y in the individual S-elements provokes spontaneous intramolecular O, N-acyl migration, resulting in dramatic changes of the conformational and physical properties (Son-state). Most notably, the consecutive switching on of S-elements according to Figure 1 provides an experimental tool for evaluating the impact of individual peptide segments upon folding.

For example, the consecutive switching on of peptide segments in [Ser³⁷]A β (1-42) containing a chemical (S1) and enzymatic (S2) cleaving site (see Fig. 2) is depicted in Figure 3 showing the acyl transfer reactions as monitored by HPLC. The pH-induced acyl migration at S1 (Fig. 3, left) proceeds very fast ($t_{1/2}$ = 5 min) restoring native A β (1-36). Interestingly, by the subsequent enzymatic switching on, i.e. cleavage of the ArgPro-dipeptide by DPPIV of the C-terminal segment (37-42), the characteristic phenomena observed for native A β (1-42), i.e., β -sheet and fibril formation are initiated, accompanied by self-association and aggregation. This is demonstrated by the evolution and subsequent degradation of the Son peak pointing

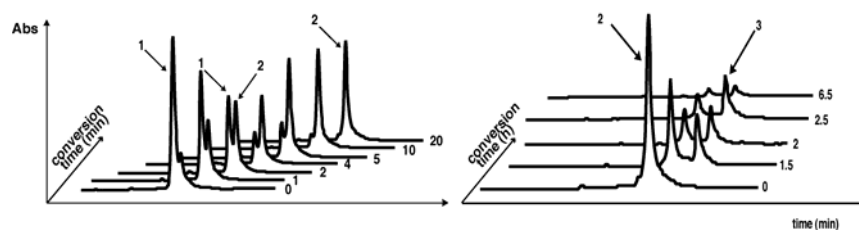


Fig. 3. HPLC monitoring of the pH- induced (left) and subsequent DPPIV-triggered (right) acyl migrations in [Ser³⁷]A β (1-42); switch-peptide in the Soff- (1), S1on, S2off (2)- and Son (3)-state.

to fast aggregation and precipitation originating from coil to β -sheet transitions (Fig. 3, right).

The pH-induced acyl migration at S1 does not result in a significant effect upon the CD spectra (Fig. 4, left) still representing predominantly a random-coil structure. Upon DPPIV-triggered acyl migration at S2, the CD curves are characteristic of β -sheet structures indicating the central impact of the hydrophobic C-terminus of A β (1-42) upon folding and oligomerization (Fig. 4, left).

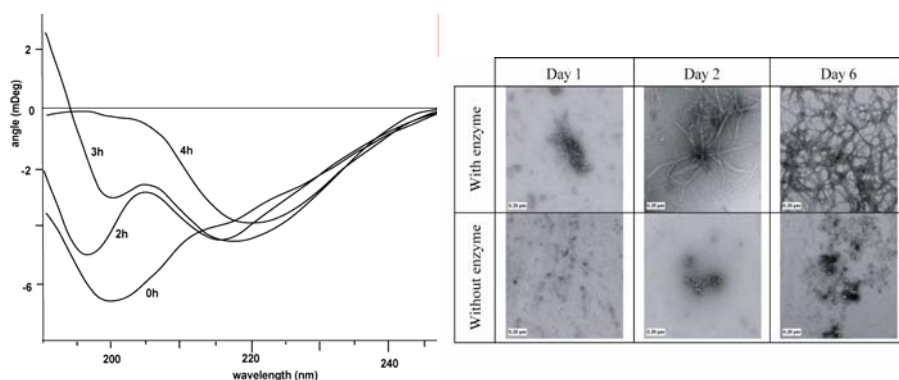


Fig. 4. CD spectra of the conformational transition from random-coil to β -sheet (left) and the onset of fibril formation upon consecutive pH- and DPPIV-triggered acyl migration (right).

Similarly, TEM studies (Fig. 4, right) show that pH-induced restoring of the N-terminal region of [Ser³⁷]A β (1-42) does not result in significant fibril formation, whereas fibrillization is observed upon DPPIV-triggered acyl migration.

In summary, the novel concept of switch-peptides for the controlled, sequential onset of peptide assembly *in vitro* offers a general tool for the study of early steps in polypeptide self-assembly and inhibition as key process in degenerative diseases.

Acknowledgments

This work was supported by the Swiss National Science Foundation.

References

1. Selkoe, D. J. *Physiol. Rev.* **81**, 741-766 (2001).
2. Bernstein, S. L., Wyttenbach, T., Baumketner, A., Shea, J. -A., Bitan, G., Treplow, D. B. and Bowers, M. T. *J. Am. Chem. Soc.* **127**, 2075-2084 (2005).
3. Soto, C. *Nature Rev. Neurosci.* **4**, 49-60 (2003).
4. Gorman, P. M. and Chakrabarty, A. *Biopolymers (Peptide Sci.)* **60**, 381-394 (2001).
5. Toniolo, C., Bonora, G. M. and Mutter, M. *J. Am. Chem. Soc.* **101**, 450-454 (1979).
6. Mutter, M., Chandravarkar, A., Boyat, C., Lopez, J., Dos Santos, S., Mandal, B., Mimna, R., Murat, K., Patiny, L., Saucède, L. and Tuchscherer, G. *Angew. Chem. Int. Ed.*, **43**, 4172-4178 (2004).
7. Dos Santos, S., Chandravarkar, A., Mandal, B., Mimna, R., Murat, K., Saucède, L., Camus, M.-S., Tuchscherer, G. and Mutter, M. *J. Am. Chem. Soc.* **127**, 11888-11889 (2005).

ROMP of Norbornyl Oligopeptides: A Versatile Synthetic Method for Exploring Receptor Topology

Younjoo Lee¹, Keith Baessler² and Nicole S. Sampson¹

¹Department of Chemistry; ²Graduate Program in Biochemistry and Structural Biology Stony Brook University, Stony Brook, NY 11794-3400, USA

Introduction

Ring-opening metathesis (ROMP) has gained wide popularity for making functional polymers because the ruthenium catalysts are very functional group tolerant [1]. Furthermore, recently developed catalysts rapidly initiate polymerization at room temperature. When initiation is faster than propagation, polymers of narrow molecular weight dispersity may be prepared (Fig. 1). In addition, if the polymerization is living, block polymers may be synthesized. The combination of block polymerization with functionalized monomers allows the rapid preparation of a series of multivalent ligands with which one can investigate receptor topology in biology.

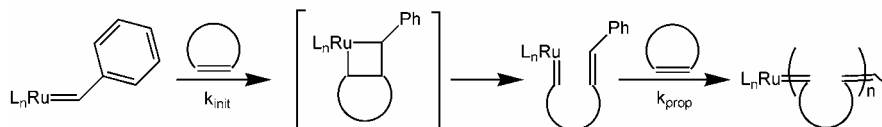


Fig. 1. Schematic of ring-opening polymerization reaction.

We are interested in identifying the receptor complex engaged by the sperm ligand protein fertilin β in mammalian fertilization [2]. The disintegrin domain of fertilin β is responsible for adhesion to the egg. The tripeptide glutamate-cysteine-aspartate (ECD) is the minimal recognition element of fertilin β . Linear peptides containing this sequence inhibit *in vitro* fertilization in many species including mouse, guinea pig, monkey, and human. However, these peptides are all of low potency, typically 500 μ M peptide is required for 50% inhibition. Previously, we have demonstrated that multivalent presentation of the ECD ligands improves potency \sim 100-fold. We have used both liposomes [3] and polymer [4] to present the ECD peptide in multivalent fashion. We are interested in understanding the fertilin β receptor topology on the egg and synthesized a series of polymers for evaluating the optimal topology for inhibition.

ROMP methodology that allows the synthesis of long (\sim 80 monomers) polymers fully substituted with peptide ligands has been developed [5]. Fully protected peptide monomers are utilized in order that ROMP can be performed under homogeneous catalytic conditions. The key to synthesizing these polymers is the inclusion of LiCl to solvate the growing polymer chain. The polymer backbone can serve as a template for β -sheet aggregation. LiCl disrupts the aggregation by coordination of the amides [6].

Results and Discussion

Using two building blocks (Fig. 2), a series of polymers was synthesized that range from 10 to 80-mers (Fig. 3). The first building block is monomer **1** containing the ECD ligand. The second building block is monomer **2** containing an ESA peptide that serves as both negative control and spacer. Thus, high density and low density ECD polymers were prepared by varying the ratio of **1** and **2**. In addition, block copolymers that alternate ECD ligand and ESA spacer were prepared.

After quenching and deprotection, the water soluble polymers are obtained in high yields ranging from 74-90%. The correct incorporation of monomer is confirmed by NMR integration of the end group against monomer signal, e.g., the methyl esters. Further analysis of the polymers is performed by gel permeation chromatography (GPC). GPC demonstrated that the molecular weight distribution is monomodal and of narrow dispersity.

The polymers synthesized were tested as inhibitors in a mouse *in vitro* fertilization assay. The inhibition results indicate that two ECD ligands separated by 4-5 nm make the optimal polymer for inhibition.

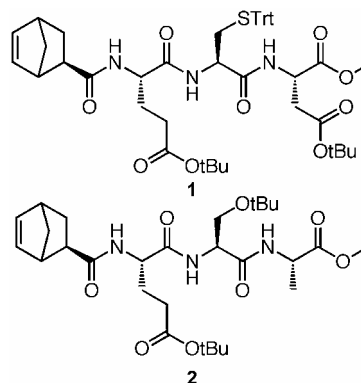


Fig. 2. ROMP monomer building blocks.

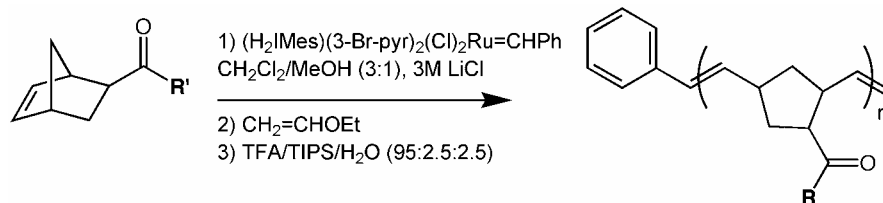


Fig. 3. Preparation of ROMP polymers.

Acknowledgments

This work was supported by funding from NIH (R01HD38519, N.S.), NSF (REU CHE0139256, N. F.; CRIF CHE0131146, NMR), and an ACS Cope Scholar Award (N.S.).

References

1. Trnka, T. M. and Grubbs, R. H. *Accounts Chem. Res.* **34**, 18-29 (2001).
2. Primakoff, P. and Myles, D. G. *Trends Genet.* **16**, 83-87 (2000).
3. Konkar, S., Gupta, S. and Sampson, N. S. *Bioorg. Med. Chem. Lett.* **14**, 1381-1384 (2004).
4. Roberts, S. K., Konkar, S. and Sampson, N. S. *ChemBioChem* **4**, 1229-1231 (2003).
5. Roberts, K. S. and Sampson, N. S. *J. Org. Chem.* **68**, 2020-2023 (2003).
6. Seebach, D., Thales, A. and Beck, A. K. *Helv. Chim. Acta* **72**, 857-867 (1989).

Native Chemical Ligation at Aromatic Residues

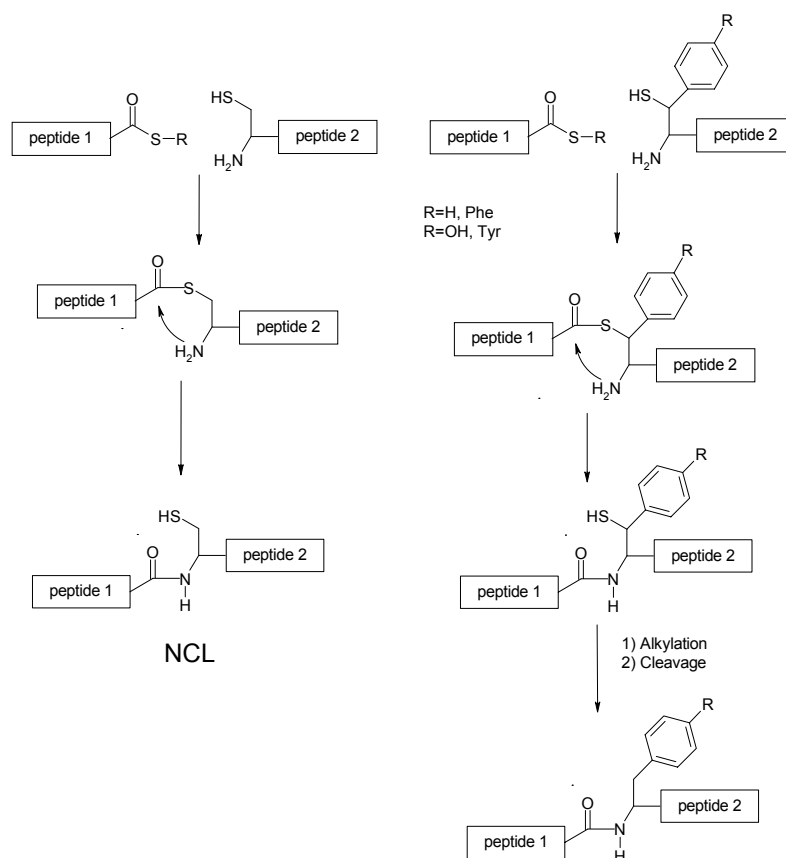
Sylvie Tchertchian¹, Fred Opligger¹, Marianne Paolini¹, Sonia Manganiello¹, Sylvain Raimondi¹, Benoît Depresle¹, Nicolas Dafflon¹,
 Hubert Gaertner¹ and Paolo Botti^{1,2}

¹Geneprot Inc. 2, Pré-de-la-Fontaine 1217 Meyrin/Geneva Switzerland;

²DBSB Department, University of Geneva, 1, rue Michel Servet, 1211 Geneva, Switzerland.

Introduction

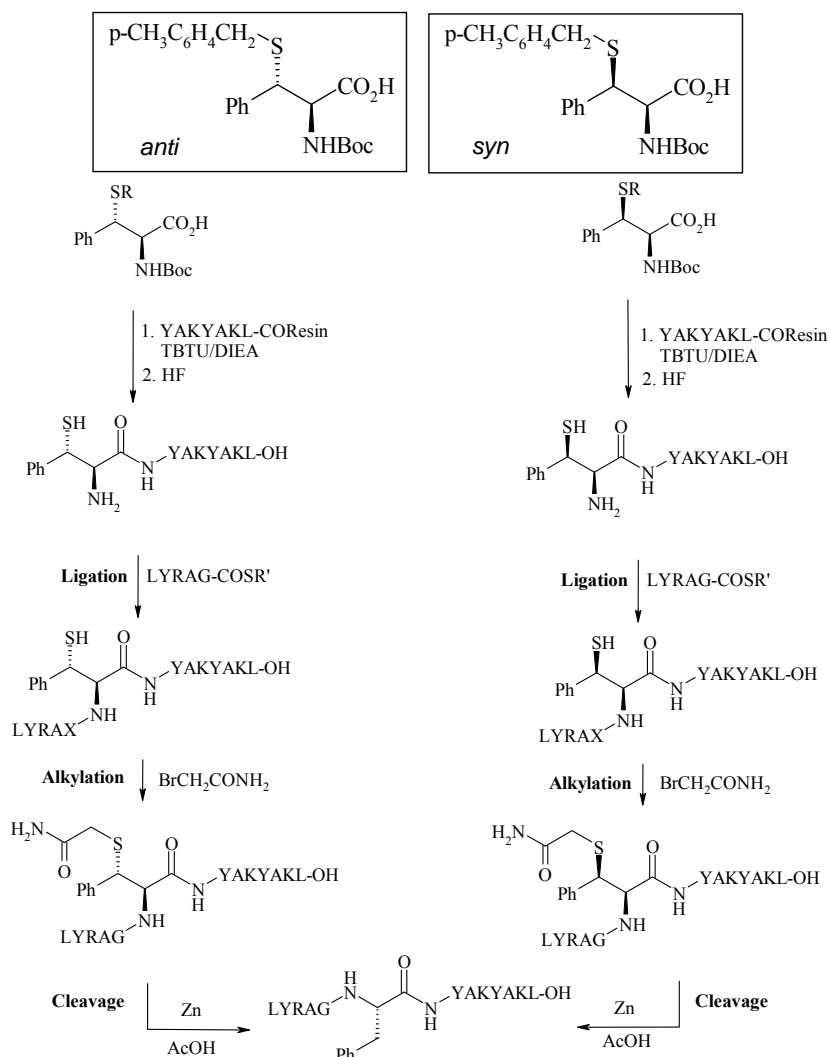
The last decade has provided extensive demonstration of the key role played by Native Chemical Ligation (NCL) for the preparation of small and medium size proteins [1]. Yet the requirement for cysteine at the site of ligation in standard NCL has limited its flexibility. Recently, different types of auxiliary groups [2-4] have been developed to extend the application of NCL to other ligation sites. However, the slower ligation rates especially with large fragments and the additional step required to cleave the auxiliary post-ligation have reduced their utility.



Scheme 1. NCL at aromatic residues (Phe, Tyr and Trp).

Results and Discussion

Our strategy does not make use of N-alkyl auxiliary groups [2,4], instead originally exploits the feature of particular side chain functionalities to generate a removable 2-mercapto amino group to mimic NCL. Our scheme takes advantage of the benzylic site of the aromatic residues to release a mercaptan under specific conditions. We use phenylcysteine [5] to exploit ligation with thioester fragments and the alkylation post-ligation is designed to produce a benzylic thioether suitable for cleavage. Benzyl groups are commonly employed in peptide synthesis to protect side chain functionalities *via* ether (Ser and Thr) and thioether (Cys) bonds. Thus, after ligation, alkylation of the free mercaptan generates a benzylic thioether suitable for cleavage.



Scheme 2. NCL using phenylcysteine derivatives.

Both N and S protected *anti* and *syn* phenylcysteine derivatives are coupled to a model peptide resin of sequence YAKYAKL. After HF cleavage and purification each peptide is exploited in ligation with thioester model peptides of sequence LYRAX-CO-SR, where X is alternatively Gly, Ala or Ile. As control, we also ligate CYAKYAKL standard with thioester fragments respectively with X = Ala and Ile.

Table 1.

Thioester Fragment	C-Terminal Fragment		
	Ligation with Z-YAKYAKL after 1h ^a		
	^{HS} F-YAKYAKL	^{HS} F-YAKYAKL	C-YAKYAKL
	<i>anti</i>	<i>syn</i>	
LYRAG-CO-SR	> 95%	> 95%	-
LYRAA-CO-SR	90%	> 95%	> 95%
LYRAI-CO-SR	20%	~ 50%	40%

^aLigation yield based on HPLC measured at λ 214nm.

Ligation crudes of both reactions using N-terminal *anti* and *syn* ^{HS}F-YAKYAKL peptides with LYRAG-CO-SR fragment are treated with excess of bromoacetamide at ~ pH 8 followed by ether extractions. Then approximately 20%v/v of acetic acid is added to each mixture with subsequent final addition of 30-fold excess of Zn dust. In both cases the reduction is completed in 1hr at r.t., generating a major identical product, which has mass and HPLC retention time identical to the native standard reference peptide (LYRAGFYAKYAKL) synthesized *via* SPPS.

In conclusion, we developed a new method to ligate peptide fragments at non-Cys residue. Ligation rates are high, and in the case of the *syn* phenylcysteine fully comparable with the ligation at cysteine. The overall process is “one pot” and the reductive cleavage post alkylation is easy and efficient. No racemization is detected by comparing both final products with reference standard peptides (LYRAGFYAKYAKL) assembled *via* SPPS with either L or D-Phe.

References

1. Dawson, P. E., Muir, T. W., Clark-Lewis, I. and Kent, S. B., *Science* **266**, 776-779 (1994).
2. Canne, L. E., Bark S. J. and Kent S. B. *J. Am. Chem. Soc.* **118** 5891-5896 (1996).
3. Offer, J. and Dawson, P. E. *Org. Lett.*, **2**, 23-26 (2000).
4. Botti, P., Carrasco, M. R. and Kent, S. B. H. *Tetrahedron Lett.* **42**, 1831-1833 (2001).
5. Xiong, C., Wang W. and Hruby, V. J. *J. Org. Chem.* **67**, 3514-3517 (2002).

Robotic Synthesis of Soluble Peptide Arrays

Wen Lin and James G. Boyd

*Department Exploratory Medicinal Sciences, Pfizer Global Research and Development,
Discovery Research, Groton, CT, 06340, USA*

Introduction

Peptide arrays are efficient tools for the identification of binding epitopes, and are useful sources of ligands for known and orphan receptors. For an array to be of maximal utility, we believe it should exist in a soluble form, arrayed in microtitre plates, and in sufficient quantity for hit follow-up experiments. Also, the sequence of the hit should be known or easily identified. The SPOT [1] synthesis and pin [2] synthesis techniques are suitable for the generation of soluble peptide arrays but are cumbersome if one desires >1000 peptides. Hence, we designed and built an economical robot driven peptide array synthesis system.

Results and Discussion

At the outset, we identified two major challenges that needed to be solved in order for this system to work. First, we required very efficient vacuum filtration of solvents and soluble reagents at each step. Second, we needed to have reliable peptide couplings without the luxury of active resin mixing.

We choose as our synthesis platform a Gilson Quad Z multiprobe robotic liquid handler equipped with a custom deck that accommodates four 96-well filterplate blocks (Fig. 1). The blocks are connected via vacuum tubing to a single line that runs through a computer-controlled solenoid valve. The tubing continues from the solenoid to a large waste vessel, which is continually evacuated using our house aspirator vacuum (~50 Torr). The vacuum rush provided by the large ballast pulls all four 96-well plates tightly against the vacuum block gaskets and all 384 wells are pulled dry in less than five seconds. In contrast, we found filtration by an in-line, computer-controlled vacuum (i.e., switched on/off) to be wholly unreliable.

Solid phase peptide synthesis is carried out at the bottom of polypropylene filterplate wells (on the filter) at 2mmol scale (~4mg resin/well). Amino acid couplings are performed using predissolved Fmoc-Xxx-OPfp esters, which are pipetted onto the static resin cakes and allowed to soak for 30 min. Five-fold excess of Pfp ester at 0.2 M concentration gives reliable peptide couplings without resin agitation. Chemistries and stoichiometries have been optimized such that the cost of goods is less than \$0.30 per cycle (\$3.00 per decapeptide). Reagent use is also very efficient. A synthesis of a 384-decapeptide library requires less than 3 L DMF and 0.25 L piperidine. Cycle times are about 90 minutes. Volatile tBu-based protecting groups are used except for Arg(Pmc). Peptides are cleaved and deprotected by treatment with TFA/water/TIS and filtered into 96-well receiving blocks. The volatiles are evaporated and the crude residues dissolved in DMSO for direct use in assays. At maximum efficiency, four 384-peptide synthesis runs can be carried out in a week (1,500 peptides / wk).

A prototype library of 2500 random decapeptides was produced. Random checks by LC-MS indicated that > 90% of syntheses provided the correct product in $\geq 60\%$ purity (Fig. 2). Deletion peptides were observed for Arg(Pmc), Asn, Trp(Boc), and at double beta-branched sequences (i.e. Ile-Val). These problems were minimized

by using 0.3M Pfp ester stock solutions and by frontloading delivery of these amino acids for longer coupling times (45-60min.)

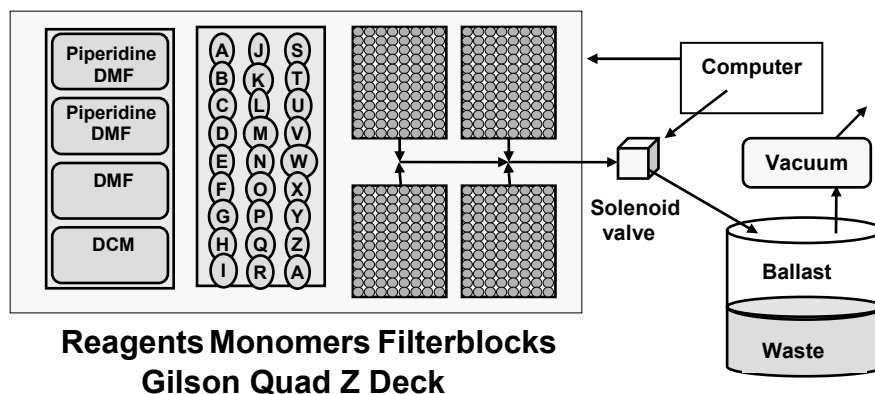


Fig. 1. Schematic layout of the robotic synthesis instrument.

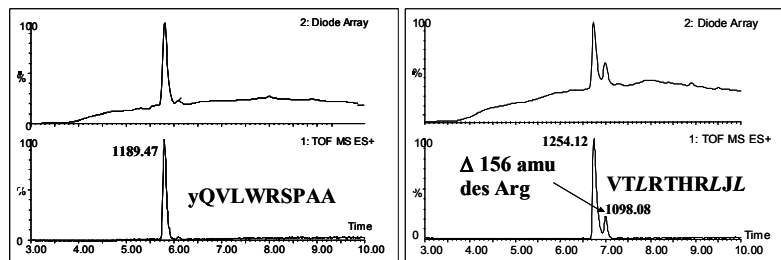


Fig. 2. Sample LCMS chromatograms of a crude peptide that was >90% pure (left) and a crude peptide containing an arginine deletion (right).

Acknowledgments

Technical assistance from Russ Constantineau and Norbert Wadke of Gilson Instruments is greatly appreciated.

References

1. Frank, R. J. *Immunol. Methods* **267**, 13-26 (2002).
2. Geysen, H. M., et al. *Proc. Natl. Acad. Sci. USA* **81**, 3998-4002 (1984).

Covalent Capture: Application to Peptides Possessing Auxiliary Groups for Extended Chemical Ligation

Nikolett Mihala and Keith Rose

Department of Structural Biology and Bioinformatics, University Medical Center (CMU)
 University of Geneva, Switzerland

Introduction

Covalent capture purification involves immobilization of N-terminal Cys- or Thr- polypeptides on an aldehyde support followed by washing peptides and finally release [1].

Here we show that this technique is suited for the purification of polypeptides used in native and extended chemical ligation. Among the removable auxiliaries known in the literature 2-mercapto-4,5-dimethoxybenzyl (Dmmb) [2] and N^α-(1-phenyl-2-mercaptoethyl) [3] were chosen and their H-G(aux)YAKYAKL-OH model peptides were synthesized and used in covalent capture experiments.

The covalent capture technique was also exploited in preliminary experiments for solid phase native chemical ligation (Fig. 1) [4].

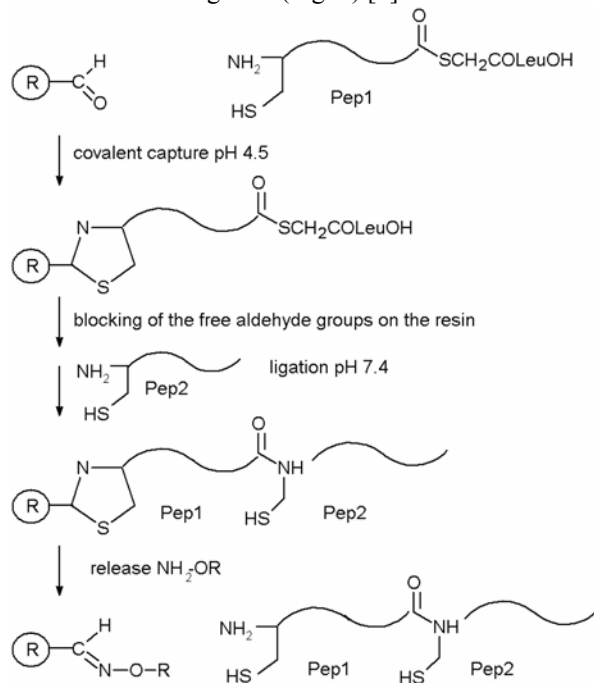


Fig. 1. Scheme showing the steps involved in Native Chemical Ligation to a captured peptide thioester.

Results and Discussion

Covalent capture was successfully applied to purify peptides possessing auxiliary groups used for chemical ligation. For Dmmb, release was accomplished with both O-methyl hydroxylamine and the cheaper hydroxylamine. With both Dmmb group and in general Cys peptides, the release with hydroxylamine was slower than with O-methyl hydroxylamine but was complete within 24 hrs. Under the release conditions (0.5M $\text{NH}_2\text{-OR}\cdot\text{HCl}$, 10mM TCEP in acetonitrile-water 1:1), neither hydroxylamine nor O-methyl hydroxylamine caused damage to peptides even those possessing an Asn-Gly motif. For the peptide with N^α -(1-phenyl-2-mercaptoethyl) group, release was more difficult. Using various aminooxy compounds the relative rates of release were $\text{NH}_2\text{-OH} < \text{NH}_2\text{-OCH}_3 < \text{NH}_2\text{-O-CH}_2\text{-COOH}$.

Under acidic conditions, capture of Cys peptide thioester could occur although some loss of peptide through cyclization was observed. The captured Cys peptide thioester could be released undamaged using standard release conditions (Fig. 2). Preliminary chemical ligation experiments with heptapeptides demonstrated that the captured Cys peptide thioester can undergo a ligation reaction.

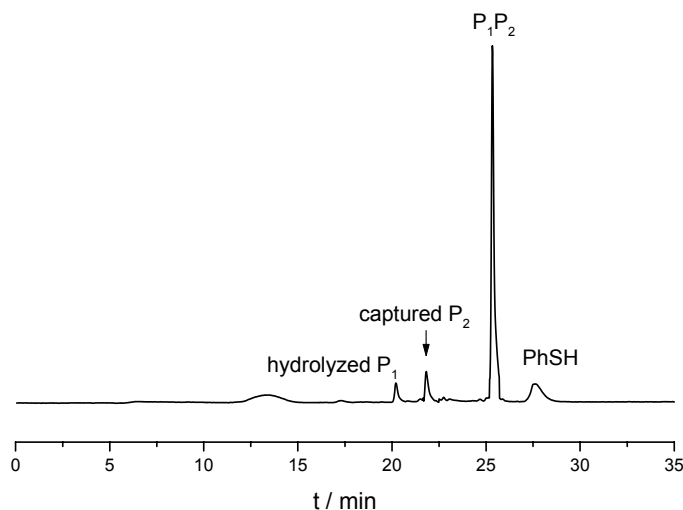


Fig. 2. Chromatogram of the ligation reaction mixture after elution from the capture column.

Acknowledgments

We thank the University of Geneva and the Swiss National Science Foundation for financial support. We thank Mrs Brigitte Dufour for expert technical assistance.

References

1. Villan, M., Vizzavona, J. and Rose, K. *Chem. Biol.* **8**, 673-679 (2001).
2. Vizzavona, J., Dick, F. and Vorherr, T. *Bioorg. Med. Chem. Lett.* **12**, 1963-1965 (2002).
3. Botti, P., Carrasco, M. R. and Kent, S. B. H. *Tetrahedron Lett.* **42**, 1831-1833 (2001).
4. Dawson, P. E., *et al.* *Science* **266**, 776-779 (1994).

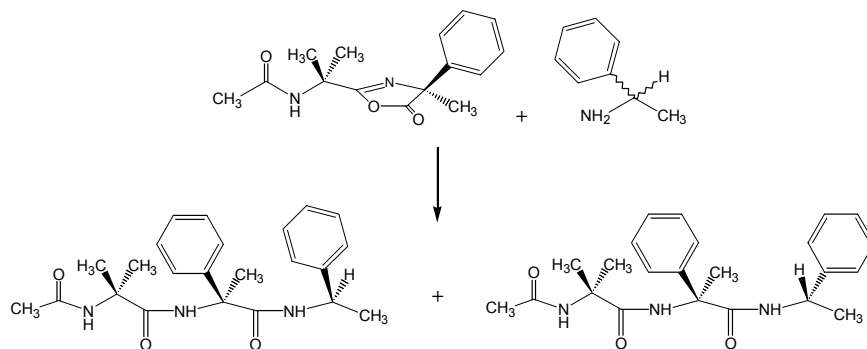
Asymmetric Induction on a Racemic Amine by Chiral Dipeptide 5(4*H*)-Oxazolones from C^α-Methyl Phenylglycine

Alessandro Moretto¹, Cristina Peggion¹, Fernando Formaggio¹, Marco Crisma¹, Bernard Kaptein², Quirinus B. Broxterman² and Claudio Toniolo¹

¹*Institute of Biomolecular Chemistry, CNR, Department of Chemistry, University of Padova, 35131 Padova, Italy;* ²*DSM Research, Life Sciences, Advanced Synthesis and Catalysis, P.O. Box 18, 6160 MD Geleen, The Netherlands*

Introduction

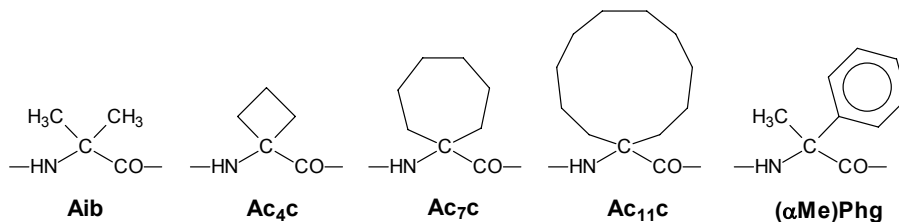
Only remarkably complex, chiral, acylating reagents have been so far developed and tested for stereoselective acylation of racemic amines. In contrast, in this work we exploited a set of simple, chirally stable, N^α-acetylated, C^α-methyl phenylglycine [(αMe)Phg]-based dipeptide 5(4*H*)-oxazolones to check to which extent they might be able to differentiate between the two enantiomers of a primary amine (α-phenylethylamine) during amide bond formation. A typical example of the test system developed for this study is shown in Scheme 1.



Scheme 1. Stereochemical course of the reaction between the 5(4*H*)-oxazolone from Ac-Aib-L-(αMe)Phg-OH and DL-α-phenylethylamine.

Results and Discussion

The reactions of the α-phenylethylamine racemate with the L-(αMe)Phg oxazolones, of general formula Ac-Xxx-L-(αMe)Phg-OXL, where Xxx is either Aib or Ac₄c, Ac₇c, Ac₁₁c, L-(αMe)Phg, D-(αMe)Phg, proceed diastereoselectively to give predominantly dipeptide alkylamides comprising the D-amine.



In general, the extent of diastereoselectivity is remarkable. Diastereoselectivity is sensitive to solvent polarity and reaction temperature. However, as shown in Figure 1, it is not significantly dependent on the nature of the C^α-tetrasubstituted α -amino acid at position 1 of the dipeptide.

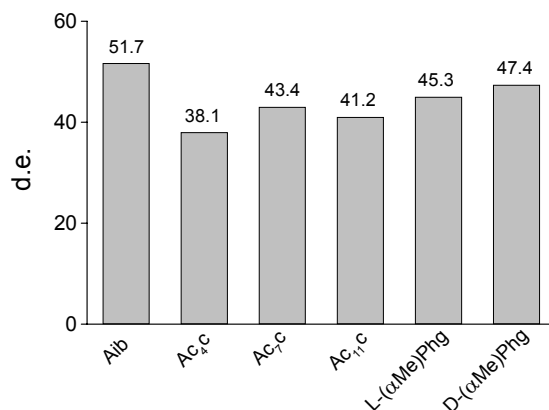


Fig.1. Histogram showing the d.e. values obtained in the reaction of the 5(4H)-oxazolone from Ac-Xxx-L-(α Me)Phg-OH, where Xxx is Aib, Ac₄c, Ac₇c, Ac₁₁c, L-(α Me)Phg or D-(α Me)Phg, with D,L- α -phenylethylamine in CHCl₃ solution at -10 °C. D.e. values are given as % D- α -phenylethylamide dipeptide diastereomer - % L- α -phenylethylamide diastereomer.

The β -turn 3D-structure of the aminolysis products was established in CDCl₃ solution (by FT-IR absorption) and for Ac-Aib-L-(α Me)Phg-D- α -phenylethylamide in the crystal state (by X-ray diffraction) as well (Fig. 2).

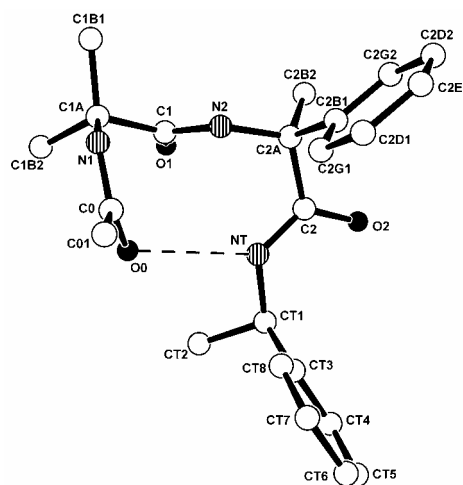


Fig. 2. X-Ray diffraction structure of Ac-Aib-L-(α Me)Phg-D- α -phenylethylamide with atom numbering. The C=O \cdots H-N intramolecular H-bond is represented by a dashed line.

Poly(ethylene glycol) (PEG) Modifications and Conformational Analysis of Thymosin α 1

Keliang Liu, Jiankun Qie, Jinbo Ma, Liangyou Wang, Wenxia Zhou, Chunhui Qi, Xiunan Zhao, Jianquan Zheng and Sijian Dong

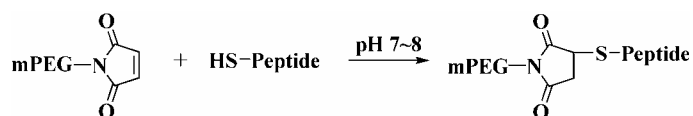
Beijing Institute of Pharmacology and Toxicology, Beijing 100850, P. R. China

Introduction

Thymosin alpha 1 (T α 1) is an N-terminal acylated peptide with 28 residues. Its synthetic product, Zadaxin, has been used as immunoenhancer to treat chronic viral HBV. PEG modifications of T α 1, also called as PEGylation, at different sites in different regions were carried out in this project. The influences of PEGylation on T α 1 conformation are discussed systematically.

Results and Discussion

According to the SAR results [1], the conjugating sites of T α 1 with PEG were chosen at the N-terminus, C-terminus, α -helix, β -turn, and the random coil regions. Referring to the method reported by Vanwetsswinkel *et al* [2,3], [Cys^x]T α 1 analogs (x: the chosen site) were synthesized firstly for conveniently introducing the covalent attachment mPEG-MAL into the chosen sites, and then the PEG conjugations were prepared as follows (Scheme 1).



Scheme 1. Conjugating reaction between mPEG-MAL and [Cys^x]T α 1.

Nine [Cys^x]T α 1 peptides and their corresponding PEGylated products, [Cys^x(mPEG-MAL)]T α 1, were synthesized, purified by RP-HPLC, and confirmed by ESI-MS or MALDI-TOF-MS (Fig. 1).

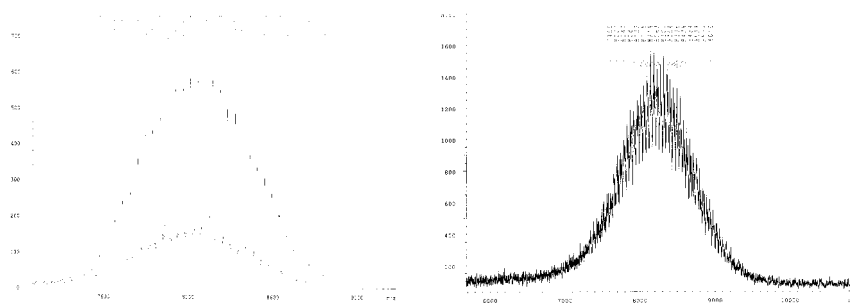


Fig. 1. MALDI-TOF-MS spectra of the PEGylated products, BMJB016 (Left) and BMJB017(Right).

The immunoactivities of both the $[\text{Cys}^x]\text{T}\alpha 1$ analogs and their PEGylated products were tested *in vitro* by measuring IFN- γ production and proliferation of mouse splenocytes induced by Con A. Most of the PEGylated products exhibited immunoenhancing activities, which indicates that the PEG modification does not significantly affect the peptide activities.

The circular dichroism spectra of the above compounds were assayed under different conditions. $\text{T}\alpha 1$ and its $[\text{Cys}^x]\text{T}\alpha 1$ analogs do not assume a preferred conformation in water solution, whereas in the presence of 2,2,2-trifluoroethanol, they form an α -helix (Fig. 2). Although PEG modification reduced the α -helical content, it was greatly influenced by the modification sites. This may be due to the high flexibility of the backbone chain and the binding to water of the PEG molecules, which affect the peptide conformation at the different sites.

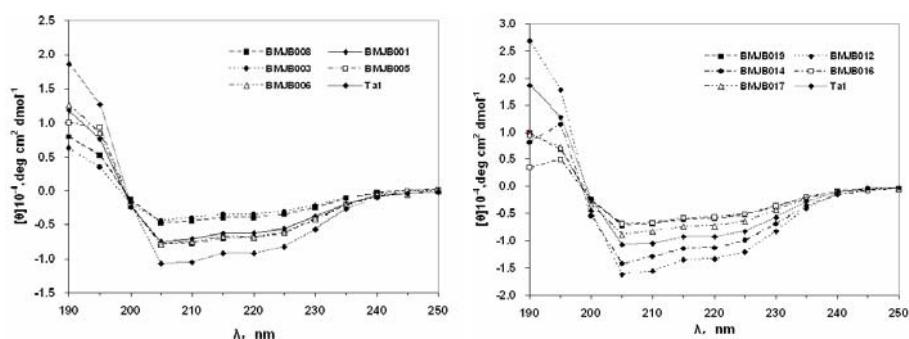


Fig.2. CD spectra of $[\text{Cys}^x]\text{T}\alpha 1$ (Left) and $[\text{Cys}^x(\text{mPEG-MAL})]\text{T}\alpha 1$ (Right).

In conclusion, the site-specific PEGylation was fulfilled by the way of cysteine-linked PEG reagent. Most of the PEGylated products exhibited immunoenhancing activities. The CD spectra revealed that the site chosen to conjugate with PEG is one of the key factors influencing the induction into a specific peptide conformation.

Acknowledgments

We would like to thank the National Natural Science Foundation of China for financial support (30300436). The National Center of Biomedical Analysis and the Institute of Biophysics Chinese Academy of Sciences are also acknowledged for the measurements of MALDI-TOF-MS and the CD spectra, respectively.

References

1. Grottesi, A., Sette, M., Palamara, T., Rotilio, G., Garaci, E. and Paci, M. *Peptides*, **19**, 1731-1738 (1998).
2. Vanwetsswinkel, S., Plaisance, S., Zhang, Z., Banlinthout, I., Brepoels, K., Lasters, I., Collen, D. and Jespers, L. *Blood*, **95**, 936-942 (2000).
3. Romani, S., *et al.* In *Chemistry of Peptides and Proteins* (W. Voelter, *et al.*, eds.), Walter de Gruyter, Berlin, vol 2, p29 (1984).

Suppression of Side Reactions Associated with Use of the Benzyloxymethyl Group on Histidine

Kumiko Yoshizawa-Kumagaye, Takehiro Ishizu, Shuji Isaka, Masaji Tamura, Rumi Okihara, Yuji Nishiuchi and Terutoshi Kimura

Peptide Institute, Inc., Protein Research Foundation, Minoh-shi, Osaka 562-8686, Japan

Introduction

His derivatives are known to be extremely prone to epimerization in activating and coupling steps involving the π -nitrogen of the imidazole moiety [1]. Therefore, regiospecific protection of the π -nitrogen should help suppress the epimerization, although the protecting groups conventionally used on the His residue with Boc chemistry are introduced at the τ -nitrogen such as the tosyl (Tos) and 2,4-dinitrophenyl (Dnp) groups, except for the benzyloxymethyl (Bom) group that is attached to the π -nitrogen. The epimerization of His(Tos) and His(Dnp) derivatives is not normally a problem since these electron-withdrawing protecting groups at the τ -nitrogen can attenuate the electron density of the π -nitrogen to reduce the rate of epimerization. During the chain assembly, however, the Tos and Dnp groups are susceptible to HOBT/ N^α -amino groups [2] and nucleophiles including N^α -amino groups [3], respectively. In contrast, His(Bom) possesses both the chemical and optical stability which have made this derivative a popular choice in peptide synthesis [4].

When treating the His(Bom)-containing peptide with HF, however, formaldehyde is generated from the Bom group. This can lead to methylated modification of the α - and ϵ -amino groups as well as the imidazole moiety of the His residue. In particular, when a Cys residue is located at the *N*-terminus of the peptide, formaldehyde can react almost quantitatively with it to produce a thiazolidyl (Thz)-peptide [5,6]. In the present study, we further examined the modifications associated with use of the Bom group and found that the reaction of formaldehyde with the *N*-terminal Trp and the *N*-methylanthranyl (Nma) group produces tetrahydro- β -carboline and dihydro-quinazoline derivatives, respectively, upon isolation from HF mixtures.

Results and Discussion

In order to examine the modification arising from the generation of formaldehyde, model peptides having several amino acids [*i.e.* Cys, Lys(Nma), Ser, Trp], which are suspected to react with formaldehyde, at the *N*-terminus of angiotensin II (Ang II: Asp-Arg-Val-Tyr-Ile-His-Pro-Phe) were treated with HF. The Nma group is frequently employed to prepare fluorescence resonance energy transfer substrates combined with the Dnp group. The resulting peptides were extracted with 0.1% TFA and analyzed by RP-HPLC to assess the extent of their modification with the *N*-terminal amino acid (Table 1). The conversion of a Trp- and a Lys(Nma)-peptide to a tetrahydro- β -carboline and dihydroquinazoline derivative, respectively, was observed at a significant rate, while the *N*-terminal Ser residue was not converted to an oxazoline derivative in an aqueous medium. Although the reaction of the Trp residue with aldehyde in the presence of an acidic catalyst is well known as the Pictet-Spengler reaction producing a tetrahydro- β -carboline derivative [7], this is the

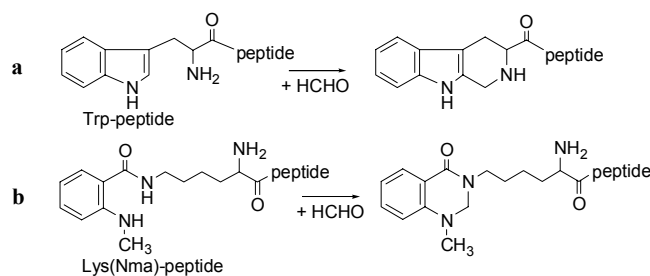


Fig. 1. Formation of (a) tetrahydro-β-carboline- and (b) dihydroquinazoline- peptides.

first report of the conversion of a Trp-peptide associated with use of the Bom group. The respective cyclic structures of modification with a Trp and a Lys(Nma)-peptides were confirmed by ESI MS and NMR analyses (Fig. 1).

The side reactions involved with formaldehyde were essentially suppressed by performing the HF reaction in the presence of cysteine hydrochloride (Cys·HCl) as a scavenger (Table 1). These events did not occur during the HF reaction but after removal of HF because addition of Cys·HCl to the reaction mixture immediately after removal of excess HF could suppress the modification with the *N*-terminal Trp residue and the Nma group. As has been observed previously [5], a reactive formaldehyde, remaining in the HF reaction mixture probably in a hydroxymethylated form on the imidazole moiety of the His residue, could be liberated and then similarly initiate the conversion of Trp- and Lys(Nma)-Ang II to tetrahydro-β-carboline- and dihydroquinazoline-containing peptides, respectively, as in the case of conversion of the Cys-Ang II peptide to a Thz-peptide.

Table 1. Effect of scavengers on the synthesis of the model peptide by HF method^a

Peptide	Additive	Ratio of the desired peptide to the modified one
Ser-Ang II	None	100 : 0
Trp-Ang II	None	83 : 17
	Cys·HCl (10 eq)	99 : 1
Lys(Nma)-Ang II	None	54 : 46
	Cys·HCl (30 eq)	99 : 1
Cys-Ang II	None	30 : 70
	Cys·HCl (10 eq)	95 : 5
	Cys-NH ₂ ·HCl (10 eq)	98 : 2

^aThe peptide resins were treated with HF/*p*-cresol (8/2, v/v) in the presence or absence of Cys·HCl or Cys-NH₂·HCl at -2° to -5°C for 1 hr.

References

1. Jones, J. H., Ramage, W. I. and Witty, M. J. *Int. J. Peptide Prot. Res.* **15**, 301-303 (1980).
2. Fujii, T., Kimura, T. and Sakakibara, S. *Bull. Chem. Soc. Jpn.* **49**, 1595-1601 (1976).
3. Siepmann, E. and Zahn, H. *Biochim. Biophys. Acta* **82**, 412-415 (1964).
4. Brown, T., *et al.* *J. Chem. Soc. Perkin Trans. 1* 1553-1561 (1982).
5. Kumagaye, K. Y., Inui, T., Kimura, T. and Sakakibara, S. *Peptide Res.* **4**, 84-87 (1991).
6. Mitchell, M. A., *et al.* *Int. J. Peptide Prot. Res.* **36**, 350-355 (1990).
7. Grigg, R., *et al.* *J. Chem. Soc. Perkin Trans. 1* 185-187 (1983).

Peptide Synthesis in Water: 2-(4-Sulfophenyl-sulfonyl)ethoxycarbonyl Group and Coupling Reagents

Keiko Hojo, Mitsuko Maeda and Koichi Kawasaki

*Faculty of Pharmaceutical Sciences, Kobe Gakuin University, Nishi-ku,
Kobe 651-2180, Japan*

Introduction

Solid phase peptide synthesis requires large amounts of organic solvents, whose safe disposal is an important environmental issue. Peptide synthesis, if performed in water and using less or nontoxic reagents, circumvents the disposal problem.

We have successfully used the water-soluble *N*-protecting groups, 2-[phenyl(methyl)sulfonio]ethoxycarbonyl (Pms) [1] and 2-(4-sulfophenylsulfonyl)ethoxycarbonyl (Sps) [2], for the SPPS of Leu-enkephalin amide in water. To perform SPPS in water, the coupling reagent must be water-soluble and maintain its reactivity in water. For this report, we tested the efficacy of the water-soluble coupling reagents, 2-(5-norbornene-2,3-dicarboximido)-1,1,3,3-tetramethyluronium tetrafluoroborate (TNTU) [3] and 4-(4,6-dimethoxy-1,3,5-triazin-2-yl)-4-methylmorpholinium chloride (DMT-MM) [4], towards SPPS in water. We successfully synthesized Leu-enkephalin amide on a solid support in aqueous 50% EtOH using DMT-MM and Sps-Lamino acids.

Results and Discussion

We studied the identification of novel coupling reagents that are suitable for SPPS in water. To do synthesis in water, a water-soluble coupling reagent must be not only water-soluble, but also stable in water, and highly reactivity as a coupling reagent. Previously we used the water-soluble carbodiimide [(WSCD), 1-ethyl-3-(3-dimethylaminopropyl)carbodiimide] [5], as the coupling reagent in conjunction with the additive, *N*-hydroxy-5-norbornene-2,3-dicarboximide (HONB) during SPPS in water [1,2]. Recently, two *in situ* activating reagents, TNTU [3] and DMT-MM [4] were reported to be efficient coupling reagents in non-aqueous media. Since these reagents are also water-soluble, we tested their potentials to act as coupling reagents during SPPS in water.

TNTU, an uronium salt and an *in situ* activating reagent, converts protected amino acids to the corresponding protected amino acid HONB esters in the presence of a tertiary base and now is widely used during SPPS performed in organic solvents. The other water-soluble *in situ* activating reagent, DMT-MM, is stable in water and alcohol. We first examined the aqueous coupling of Sps-Phe-OH to Leu-Rink amide-TentaGel resin mediated by TNTU or DMT-MM.

For SPPS in water, the resin must swell significantly when mixed with water. Therefore, TentaGel resin [poly(ethylene glycol)-grafted polystyrene resin], which swells well in various solvents, including water, was used. An aqueous 2.0% Triton X10 solution was used as the solvent because it increases the swelling ability of the resin and the solubilities of the reactants. After coupling Sps-Phe-OH to the H-Leu-Rink amide-TentaGel resin, the Sps group was removed by treatment with aqueous 0.025 M NaOH in aqueous 50% EtOH and the resin was hydrolyzed with 6 N HCl. The Phe and Leu content of the acid hydrolysate was determined and the coupling yield calculated using Phe to Leu ratio. The yield of the coupling reaction with TNTU was not satisfactory even when the reaction time was extended to 24 hrs. The

results of the coupling reactions using DMT-MM in the presence of *N*-methylmorpholine (NMM) in water was also not satisfactory. Kunishima *et al.* reported that condensation reactions using DMT-MM when dissolved in various alcohols, including EtOH and MeOH, gave satisfactory results (~99% yield) [4a]. Therefore, we tried the coupling reaction in aqueous EtOH. The reaction in aqueous 50% EtOH for 3 hrs proceeded smoothly and resulted in a quantitative coupling yield.

To evaluate our synthetic strategy, which uses Sps-amino acids, DMT-MM, and a solid support suspended in aqueous 50% EtOH, we attempted the synthesis of Leu-enkephalin amide. Synthetic Sps-Tyr(*t*Bu)-Gly-Gly-Phe-Leu-Rink amide-TentaGel resin was treated with 0.025 M NaOH in aqueous 50% EtOH and then treated with trifluoroacetic acid to cleave the peptide from the resin. The resulting crude Leu-enkephalin amide, H-Tyr-Gly-Gly-Phe-Leu-NH₂, was purified by HPLC. The yield of purified Leu-enkephalin amide, which was calculated using the amino group content of the starting resin is 58%.

We successfully synthesized Leu-enkephalin amide in aqueous 50% EtOH using DMT-MM. Our method is efficient and “environment-friendly” when compared with the usual solid phase methods performed in organic solvents.

References

1. (a) Hojo, K., Maeda, M. and Kawasaki, K. *J. Peptide Sci.* **7**, 615-618 (2001). (b) Hojo, K., Maeda, M., Takahara, Y., Yamamoto, S. and Kawasaki, K. *Tetrahedron Lett.* **44**, 2849-2851 (2003). (c) Hojo, K., Maeda, M. and Kawasaki, K. *Tetrahedron* **60**, 1875-1866 (2004).
2. Hojo, K., Maeda, M. and Kawasaki, K. *Tetrahedron Lett.* **45**, 9293-9295 (2004).
3. (a) Knorr, R., Trzeciak, A., Bannwarth, W. and Gillessen, D. *Tetrahedron Lett.* **30**, 1927-1930 (1989). (b) Bannwarth, W. and Knorr, R. *Tetrahedron Lett.* **32**, 1157-1160 (1991). (c) Bannwarth, W., Schmidt, D., Stallard, B., Hornung, C., Knorr, R. and Müller, F. *Helv. Chim. Acta*. **8**, 2085-2099 (1988).
4. (a) Kunishima, M., Kawachi, C., Morita, J., Terao, K., Iwasaki, F. and Tani, S. *Tetrahedron* **55**, 13159-13179 (1999). (b) Kunishima, M., Kawachi, C., Iwasaki, F., Terao, K. and Tani, S. *Tetrahedron Lett.* **40**, 5327-5330 (1999). (c) Kaminski, Z. J., Paneth, P. and Rudzinski, J. *J. Org. Chem.* **63**, 4248-4225 (1998). (d) Kaminski, Z. J. *Synthesis* 917-910 (1987). (e) Kaminski, Z. J. *Tetrahedron Lett.* **26**, 2901-2904 (1985).
5. (a) Sheehan, J. C. and Hlavka, J. *J. Org. Chem.* **21**, 439-441 (1956). (b) Sheehan, J. C., Cruickshank, P. A. and Boshart, G. L. *J. Org. Chem.* **26**, 2525-2528 (1961).

Efficient Synthesis in Solid-Phase of Freidinger-like Lactams by Microwave Irradiation

Teresa Lama, Pietro Campiglia, Luigia Auriemma, Isabel Gomez-Monterrey, Alfonso Carotenuto, Ettore Novellino and Paolo Grieco

Dip. Chimica Farmaceutica e Toss., University of Naples Federico II, Naples, Italy

Introduction

Among the numerous strategies toward the conformational restriction of peptides, incorporating the backbone into a “Freidinger” lactam structure has proven useful in the design of a variety of medicinally relevant targets, especially peptidase/protease inhibitors [1]. Such cyclization of the peptide backbone fixes the amide bond in the trans rotameric form, places severe limitations on ψ_1 rotation, and would be expected to bias neighboring ϕ_1 and ϕ_2 torsional angles. Several different synthetic strategies have been developed toward Freidinger lactams, including some stereoselective methods that allow control over the C-3 center (amino substituent) or the glycyl side chain (R_1 in Fig. 1) [2]. However, no one method has proved completely facile for the stereoselective synthesis of Freidinger lactams of various ring sizes containing a spectrum of C-terminal amino acid residues.

Here we report a new synthetic methodology to perform Freidinger lactams, developed under microwave irradiation. The structures were synthesized starting from iodine derivative of Asp opportunely protected that was reacted with an amino acid linked on Wang resin (Fig. 2). The iodine derivative of Asp was prepared as previously reported in literature. In this preliminary study, Gly, Phe, Lys, and Asp were used as amino acids loaded on Wang resin.

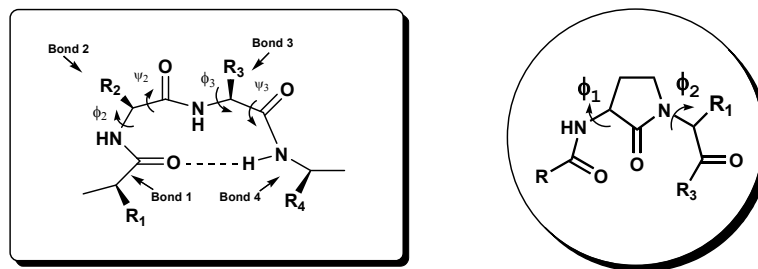


Fig. 1. General structure of a β -turn and a Freidinger β -turn mimetic

Results and Discussion

The compounds were synthesized by solid phase peptide synthesis method using Fmoc chemistry. The reaction of N-Boc protected β -Iodoamine of Aps with the respective amino acid loaded on Wang resin was performed under microwave irradiation in DMF/NMP, using 2 eq of Cs_2CO_3 as base. The complete procedure was performed using a Milestone CombChem Microwave Synthesizer that allows on-line control of irradiation time, temperature, and power. In these conditions, the intermediate of reaction was obtained in 90 min with good purity and yield. The final cyclization step was performed using HBTU/HOBt as activating agent for 3 hrs. Subsequently, the resin was washed and subjected to final cleavage. The crude product was precipitated using anhydrous diethyl ether and recovered by filtration.

Table 1. Reaction Conditions and Results

Amino Acid	Temp °C	Time (min)	Yield
Gly	70	90	60
Asp	70	90	48
Lys	70	90	60
Phe	70	90	46

All final products were purified by semipreparative RP-HPLC using a C-18 Vydac column. The physicochemical properties and purities of the final compounds were assessed by TLC, LC-MS, analytical RP-HPLC and ¹H-NMR.

This approach makes possible to generate these compounds in good yields, free or orthogonally protected, starting from inexpensive materials (Table 1). Also, by this methodology it is possible to generate Freidinger lactam structures with variable size starting from different iodine derivatives of appropriate amino acids (for ex. Glu).

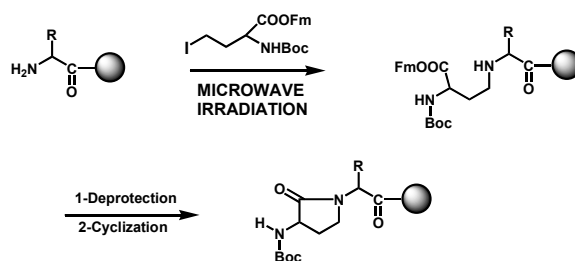


Fig. 2. Solid phase synthesis under microwave irradiation.

Acknowledgments

The LC-MS and ¹H NMR spectral data were provided by Centro di Ricerca Interdipartimentale di Analisi Strumentale Università degli Studi di Napoli Federico II. The assistance of the staff is gratefully appreciated.

References

- Freidinger, R. M. *J. Org. Chem.* **50**, 3631-3633 (1985).
- (a) Schuster, M. and Blechert, S. *Angew. Chem., Int. Ed.* **36**, 2036-2056 (1997); *Angew. Chem.* **109**, 2124-2139 (1997); (b) Furstner, A. *Angew. Chem., Int. Ed.* **39**, 3012-3043 (2000); *Angew. Chem.* **112**, 3140-3172 (2000); (c) Armstrong, S. K. *J. Chem. Soc., Perkin Trans. I* 371-388 (1998).
- Campiglia, P., Gomez-Monterrey, I., Longobardo, L., Lama, T., Novellino, E. and Grieco, P. *Tetrahedron Lett.* **45**, 1453-1456 (2004).

Synthesis of Monocyte Chemoattractant Protein 1 (MCP-1) Analogs via Native Chemical Ligation

**Tami L. Raguse, Nicole Stowell, Reannon Holland, Thomas Bodenshteyn,
Steven C. Pomerantz, Jennifer F. Nemeth, Anuk Das, Marian
Kruszynski and George A. Heavner**

Discovery Research, Centocor, Inc., Radnor, PA 19087, USA

Introduction

Human Monocyte Chemoattractant Protein 1 (MCP-1) is a 76-residue protein that has been implicated in a variety of conditions including atherosclerosis, rheumatoid arthritis, and cancer. A biotinylated analog of MCP-1 has been synthesized previously by stepwise solid phase peptide synthesis (SPPS) [1] and used to pan phage display libraries for anti-MCP-1 antibodies. The stepwise SPPS of MCP-1 and MCP-1 analogs has yielded material with full biological activity [2]. However, the use of affinity chromatography (in addition to reversed-phase high-performance liquid chromatography (RP-HPLC)) was sometimes necessary for the purification of these 76-residue proteins [2].

Results and Discussion

Here, we report the use of native chemical ligation [3] in the synthesis of MCP-1, MCP-1 [Ile⁴¹] (the valine residue at position 41 of MCP-1 is replaced with isoleucine), and MCP-1 [Ile⁴¹, Lys(Biotin-PEG₄)⁷⁵] (PEG₄ is a hydrophilic spacer containing four ethyleneoxy units). The polypeptide chain of each analog was synthesized by ligation of a 35-residue thioester peptide with a 41-residue peptide containing an N-terminal cysteine (demonstrated in Fig. 1 for the synthesis of MCP-1 [Ile⁴¹, Lys(Biotin-PEG₄)⁷⁵]).

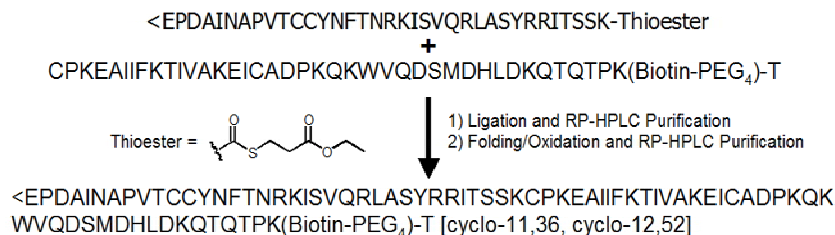


Fig. 1. Strategy for the synthesis of MCP-1 [Ile⁴¹, Lys(Biotin-PEG₄)⁷⁵] (“<E”= pyro-Glu).

Each 35- or 41-residue peptide was synthesized on an ABI 431A peptide synthesizer using standard Fmoc/*t*Bu chemistry and DCC/HOBt activation. The thioester peptide was synthesized on H-Lys(Boc)-sulfamylbutyryl NovaSyn TG resin. Activation with (trimethylsilyl)diazomethane and displacement with ethyl-3-mercaptopropionate [4] produced the side-chain protected thioester. We found that the use of pseudoproline dipeptide building blocks [5] in the synthesis of the thioester peptide enhanced the purity of the crude cleaved and side-chain-deprotected product. Therefore, pseudoproline dipeptide building blocks were used subsequently in the synthesis of all peptides.

Ligation of the two RP-HPLC-purified peptides was performed in pH 7.8 phosphate buffer containing 6 M GdnHCl and 1% thiophenol. The ligation reaction was followed by analytical RP-HPLC and/or capillary electrophoresis, and the linear products were purified by RP-HPLC. Oxidation using a glutathione redox system produced 26 mg MCP-1, 8.4 mg MCP-1 [Ile⁴¹], and 4.4 mg MCP-1 [Ile⁴¹, Lys(Biotin-PEG₄)⁷⁵] after RP-HPLC purification.

Results from disulfide bond analysis, binding assays, and calcium mobilization assays suggest that our synthetic analogs adopt the correct three-dimensional structure. Mass spectrometry data indicated that each protein contains the expected disulfide bond pattern. Furthermore, our three synthetic proteins each have similar ability to that of recombinant MCP-1 to bind to (Fig. 2, A-C) and activate (Fig. 2, D-E) CCR2. It is known that MCP-1 acts as a CCR2 agonist *in vivo*.

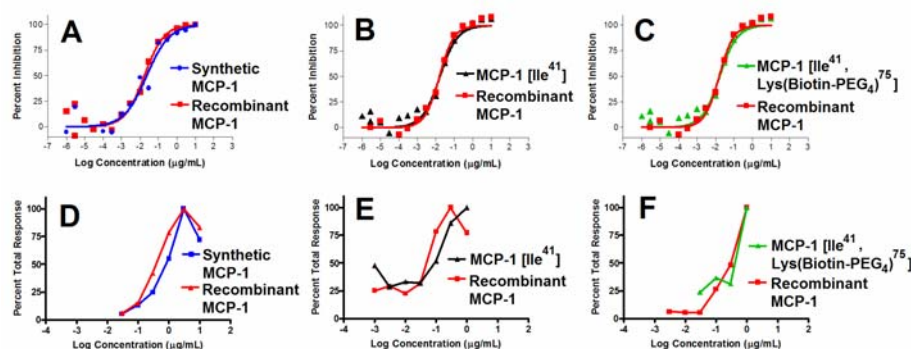


Fig. 2. Results from binding (A-C) and calcium mobilization (D-F) assays. THP-1 cells expressing the CCR2 receptor were incubated with 1 ng/mL ¹²⁵I-MCP-1 and various concentrations of recombinant or synthetic protein. The amount of unbound ¹²⁵I-MCP-1 was used to calculate the percent inhibition (A-C). The calcium mobilization assay measures calcium flux, which is induced by activation of the CCR2 receptor of THP-1 cells by MCP-1 or MCP-1 analogs (D-E).

We have applied native chemical ligation to the synthesis of MCP-1, MCP-1 [Ile⁴¹], and MCP-1 [Ile⁴¹, Lys(Biotin-PEG₄)⁷⁵]. The RP-HPLC-purified proteins have activity similar to that of recombinant MCP-1 in binding and calcium mobilization assays.

References

1. Kruszynski, M., Luo, J., Tsui, P., Stowell, N., Das, A., Nemeth, J. F., Sweet, R. and Heavner, G. A., manuscript in preparation.
2. Kruszynski, M., Stowell, N., Das, A., Seideman, J., Tsui, P., Brigham-Burke, M., Nemeth, J. F., Sweet, R. and Heavner, G. A. *J. Peptide Sci.* **12**, 25-32 (2006).
3. Dawson, P. E., Muir, T. W., Clark-Lewis, I. and Kent, S. B. H. *Science* **266**, 776-779 (1994).
4. Ingenito, R., Bianchi, E., Fattori, D. and Pessi, A. *J. Am. Chem. Soc.* **121**, 11369-11374 (1999).
5. Mutter, M., Nefzi, A., Sato, T., Sun, X., Wahl, F. and Wöhr, T. *Peptide Res.* **8**, 145-153 (1995).

NMR Analysis of a Multi-domain Peptide of the *Saccharomyces cerevisiae* Alpha Factor Receptor

Racha Estephan¹, Jacqueline Englander¹, Boris Arshava¹, Jeffrey M. Becker² and Fred Naider¹

¹Department of Chemistry, College of Staten Island, City University of New York, New York, NY 10016; ²Department of Microbiology, University of Tennessee, Knoxville, TN 37996, USA

Introduction

Biophysical studies on GPCRs are hampered by difficulty in crystallizing these molecules and conducting NMR on the intact receptor in the presence of vesicles. We have examined the biophysical properties of peptides representing fragments of Ste2p, a GPCR for α -factor, a tridecapeptide from the yeast *Saccharomyces cerevisiae*. To gain high resolution structural evidence supporting the interaction of the sixth and seventh transmembrane domains of Ste2p [1,2], milligram quantities of multidomain peptides are required for spectroscopic investigation. Receptor fragments were prepared as isotopically labeled fusion proteins by biosynthetic approaches. The ¹⁵N-labeled fusion protein was expressed and purified by HPLC. ¹⁵N-labeled E3-M7-24-T40 fusion protein (¹⁵N-M7FP) was cleaved with cyanogen bromide (CNBr) to remove the Trp Δ LE. The cleaved ¹⁵N-E3-M7-24-T40 was isolated by HPLC, characterized by mass spectrometry and its secondary and tertiary structure was obtained using circular dichroism and nuclear magnetic resonance spectroscopy, respectively.

Results and Discussion

Previously, a multidomain fragment (Ste2p 267-339) containing the third extracellular loop, the seventh transmembrane domain and the cytosolic tail of Ste2p (E3-M7-24-T40) was biosynthesized as a fusion protein using histidine-tagged Trp Δ LE as the N-terminus, and yielded high levels of expression [3]. Using this approach the fusion protein (MW=21,510 Da) was expressed in ¹⁵NH₄Cl minimal medium, purified to near homogeneity as judged by HPLC and its molecular weight verified by mass spectrophotometry. The 73-residue peptide was released from the fusion protein by CNBr and purified by HPLC. ¹⁵N-labeled forms of this multidomain peptide were isolated in ~10 mg quantities enabling high-resolution NMR analyses of the 73-residue region of Ste2p.

NMR experiments were performed in TFE/H₂O (1:1) and CDCl₃:CD₃OH:H₂O (4:4:1) to obtain a high resolution structure of the 73-residue multiple domain peptide. Chemical shift indices (CSI) suggested that in both aqueous-organic media helical subdomains existed in both the transmembrane region and cytoplasmic tail of the multi-domain peptide (Fig. 1). This conclusion was supported by NOE connectivities and coupling constant analyses. Preliminary structural modeling based on NOESY data of the ¹⁵N-labeled E3-M7-24-T40 peptide in both of the above aqueous-organic media revealed a peptide with three helical parts interrupted by three proline residues (data not shown). This cytosolic tail participates in down-regulation of Ste2p [4] and these helical regions of the protein may play a role in protein-protein interactions leading to endocytosis.

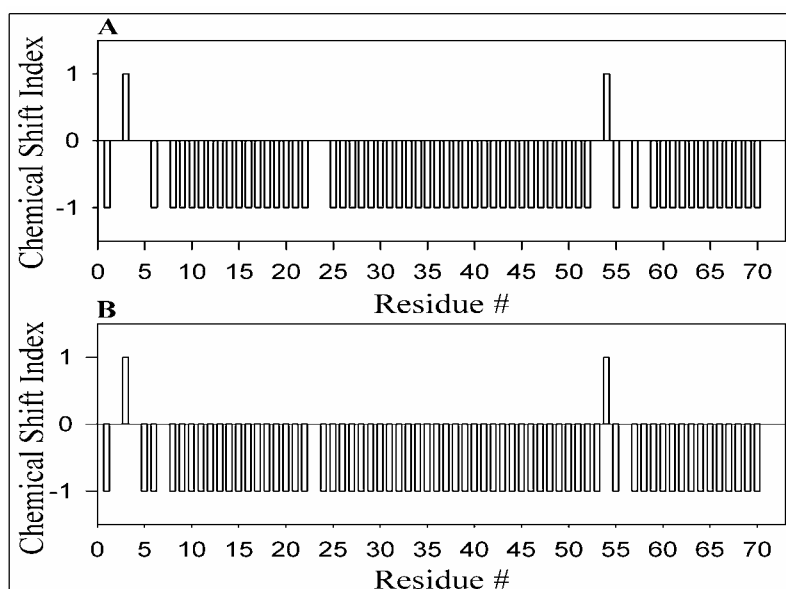


Fig. 1. Comparison of CSI values for the E3-M7-24-T40 peptide at 25°C in both TFE/H₂O [1:1] and CDCl₃:CD₃OH:H₂O [4:4:1]. The CSI values of the peptide in (A) TFE/H₂O [1:1] and (B) CDCl₃:CD₃OH:H₂O [4:4:1] are based on the $\delta\text{CH}\alpha$ values where a $\delta\text{CH}\alpha$ value of ≥ 0.1 is given a CSI value of 1.0, a $\delta\text{CH}\alpha$ value of ≤ -0.1 is given a CSI value of -1.0, and a $\delta\text{CH}\alpha$ value between 0.1 and -0.1 is given a CSI value of 0. CSI values of +1, -1, and 0 indicate β sheet, α -helical, and random structures, respectively. The $\delta\text{CH}\alpha$ values are the difference between the experimental CH α chemical shifts and the random coil values as per Wishart & Sykes [5].

Acknowledgments

The work was funded by grants GM22086, GM22087, and GM22086-27S1 from the National Institutes of Health and by the New York City Louis Strokes Alliance for Minority Participation (NYC LS-AMP) in Research from the National Science Foundation.

References

1. Dube, P. and Konopka, J. B. *Mol. Cell Biol.* **18**, 7205-7215 (1998).
2. Parrish, W., Eilers, M., Ying, W. and Konopka, J. B. *Genetics* **160**, 429-443 (2002).
3. Naider, F., Estephan, R., Englander, J., Suresh babu, V. V., Arevalo, E., Samples, K. and Becker, J. M. *Biopolymes* **76**, 119-128 (2004).
4. Rohrer, J., Benedetti, H., Zanolari, B. and Riezman, H. *Mol. Biol. Cell* **4**, 511-521 (1993).
5. Wishart, D. S. and Sykes, B. D. *Methods Enzymol.* **239**, 363-392 (1994).

Further Studies on an Alternative Approach to Prepare Esterified Protected Peptides under Mild Conditions

Patrícia B. Proti¹, Pedro V. de Oliveira² and M. Terêsa M. Miranda¹

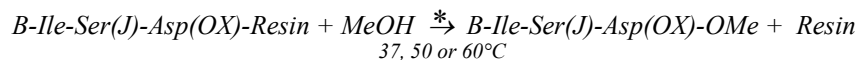
¹Department of Biochemistry; ²Department of Fundamental Chemistry, Institute of Chemistry, University of São Paulo, 05508-900, São Paulo, Brazil

Introduction

Methyl esters of protected peptides (*X-protected peptide-OMe*) are synthetic precursors of enzyme substrates and inhibitors, as well as of acyl donors employed in chemical and enzymatic fragment condensations [1]. In this context, the search for more efficient approaches to produce these compounds is quite relevant.

X-protected peptide-OMe can be obtained by the following routine: *Step 1*) stepwise peptide synthesis on polymer resin; *Step 2*) methanolysis of the peptide-resin linkage to generate the esterified fully side-chain protected peptide; *Step 3*) purification of the crude product; and *Step 4*) chemical characterization of the purified material. As *Step 2* is currently conducted through acid or base catalysis, it may lead to a mixture of products.

Here we present the results found in the study of an alternative approach to perform *Step 2*. Such approach is based on our observations that Ca^{+2} mediates the methanolyses of the peptide-resin linkages of peptidyl-Merrifield resin and peptidyl-Kaiser resin (KOR) [2]. Since these reactions were very slow (around 48 hrs), this work aimed to: 1) optimize methanolysis of oxime ester bond of peptidyl-KOR by varying the solvent systems and temperatures; 2) verify whether other metal ions would assist such reaction; 3) evaluate the metal contents in the resulting *X-protected peptide-OMe*; and 4) apply this new approach to other resins used in Boc and Fmoc strategies. Above all, we wanted to compare the efficiency of the metal ion assistance [2] with that of the base catalysis [3]. Thus, the model peptide Ile-Ser-Asp (fragment 22-24 of cholecystokinin 33) was built-up on four different polymer resins and the methanolysis reactions were conducted in several experimental conditions:



B: Ac, Boc or Fmoc; *J*: Bzl or *t*Bu; *X*: Bzl, *c*Hx or *t*Bu;

Resin: KOR or PAM (Boc strategy), HMBA or Wang (Fmoc strategy);

* bases, metal ions, or no additive.

Results and Discussion

The peptidyl-resins were synthesized using customized protocols [4]. Their characterization by amino acid analysis allowed calculating the substitution degrees (SD). The methanolysis reactions were monitored by RP-HPLC. The products were characterized by LC/ESI-MS. Determination of SD of the remaining peptidyl-resins allowed the determination of the yields of peptide detachment from the resins.

Initially, the conventional approaches were employed to perform the methanolysis of Ac-Ile-Ser(Bzl)-Asp(OBzl)-KOR (**I**). Among the bases employed, TEA was the most efficient followed by DIPEA (incubations of the peptide-resin for 3 hrs with these bases resulted in Ac-Ile-Ser(Bzl)-Asp(OBzl)-OMe (**II**) with high yields). DBU was the worst catalyst (peptide detachment from resin was high, but

the main product formed was Ac-Ile-Ser(Bzl)-Asp(OMe)-OMe. The best condition for Ca^{+2} -mediated reaction was 80% DMSO/MeOH at 60°C for 2 hrs, since it led to a quantitative peptide detachment from the resin without side-reactions. It was verified that the metal ions Zn^{+2} , Co^{+2} , and Cu^{+2} were also able to assist the desired methanolysis, although with different efficiencies. The best reaction condition found for the mediation by these transition metal ions was 80% DMF/MeOH at 50°C for 4 hrs (Zn^{+2} : peptide detachment from resin of 94%), 10 hrs (Co^{+2} : 84%), or 5 hrs (Cu^{+2} : 100%). In all cases the desired product was the only one detected in the reaction media. Therefore, the results of the qualitative screening showed that the metal ions assistance is: i) as efficient as the catalysis by TEA and DIPEA, and ii) more effective than DBU catalysis.

Since the metals mediated the methanolysis of **I** probably through coordination [2], it was relevant to determine whether the fully protected peptide ester kept the metal ions coordinated after its desalting by RP-HPLC. Analyses by atomic absorption spectrometry of desalted **II** resulting from methanolysis mediated by Ca^{+2} , Zn^{+2} , Co^{+2} , or Cu^{+2} revealed insignificant amounts of metal.

Our alternative approach was also applicable to other peptidyl-resins such as HMBA, Wang, or PAM resins (the two last resins are not used to generate C-terminal modified peptides). Interestingly, the Zn^{+2} -mediated methanolyses were even more effective than the conventional approaches. In fact, they yield the desired *X-protected peptide-OMe* faster and with higher quality.

Crude **II** resulting from Ca^{+2} -mediated methanolysis of the corresponding peptidyl-KOR was treated with HF/anisole to give the desired Ac-Ile-Ser-Asp-OMe (**III**). With the aim to check the suitability of our approach to generate substrates to be recognized by lipases and thus act as acyl donors in segment condensations catalyzed by these esterases, **III** was incubated with crude porcine pancreatic lipase (cPPL), an enzymatic preparation successfully used by us to catalyze peptide bond formation [5]. As expected, cPPL recognized the ester and catalyzed its hydrolysis.

In summary, our results reveal that the alternative approach reported here to produce *X-protected peptide-OMe* was quite effective and competitive.

Acknowledgments

We would like to thank to FAPESP for the grant to MTMM and the postgraduate scholarship to PBP and to Dr. Cleber W. Liria for the amino acids analyses.

References

1. Songster, M. F. and Barany, G. *Method Enzymol.* **289**, 126-174 (1997); Bordusa, F. *Chem. Rev.* **102**, 4817-4867 (2002).
2. Miranda, M. T. M., *et al.* *Int. J. Peptide. Prot. Res.* **37**, 451-456 (1991); Moraes, C. M., *et al.* *J. Peptide Res.* **55**, 279-288 (2000); Moraes, C. M., *et al.* In *Proceedings of the 26th European Peptide Symposium* (Martinez, J. and Fehrentz, J. -A., eds.), EDK, Paris, pp.255-256 (2001).
3. Mellor, S., *et al.* In *Fmoc solid phase peptide synthesis: A practical approach* (Chan, W. C. and White, P. D., eds.) Oxford University Press, Oxford, pp.147-148 (2000); Stewart, J. M. and Young, J. D. *Solid phase peptide synthesis, 2nd edition*, Pierce Chemical Company, Rockford, p.91 (1984); Pichette, A., *et al.* *Tetrahedron Lett.* **38**, 1279-1282 (1997).
4. Varanda, L. and Miranda, M. T. M. *J. Peptide Res.* **50**, 102-108 (1997).
5. Liria, C. W., *et al.* In *Peptides 2002, Proceedings of the 27th European Peptide Symposium* (Benedetti, E. and Pedone, C., eds.), Edizioni Ziino, Napoli, pp. 222-223 (2002).

A Long Range S,N-Acyl Migration by Silver Ion Assistance in Thioester Ligation

Yi-An Lu¹ and James P. Tam^{1,2}

¹Department of Biomedical Sciences, Scripps Florida, Jupiter, FL 33458, USA; ²School of Biological Sciences, Nanyang Technological University, Singapore

Introduction

Cysteine or native ligation is a robust method to couple unprotected peptides and proteins in an aqueous solution without coupling reagents [1-3]. For this ligation to occur, the amino-terminal Cys is obligatory and not always compatible with all synthetic objectives. Here we report a C-terminal Cys-mimetic approach for non-cysteine peptide ligation using silver ion-assisted long range S,N-acyl migration (Fig. 1). This method provides an alternative in choosing ligation sites. It also permits tandem ligation of multiple segments without a protecting group scheme.

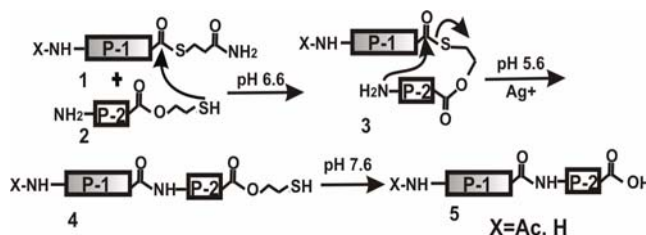


Fig. 1. General scheme of C-terminal Cys mimetic ligation using 2-mercaptoethylester-thioester peptides in aqueous solution.

Results and Discussion

The proposed ligation scheme is a two-step reaction, forming a peptide bond between peptide 1 and 2 (Fig. 1). First, the nucleophilic thiol from peptide mercaptoethylester 2 as a C-terminal Cys-mimetic undergoes a thiol-thioester exchange reaction with peptide thioester 1 to form a covalently-linked thioester intermediate 3. This diester intermediate was stable under HPLC conditions for isolation and characterization. Activation by AgTfa, the purified diester 3 then undergoes an S,N-acyl migration to form a peptide bond and concurrently regenerates the C-terminal mercaptoethylester in peptide 4 as a C-terminal Cys-mimetic.

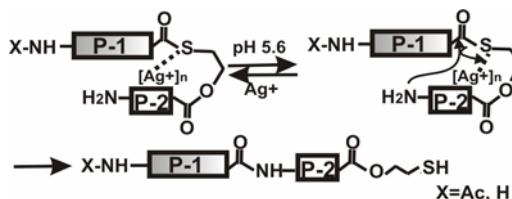


Fig. 2. Proposed mechanism of silver ion assisted S,N-acyl migration.

The regenerated mercaptoethylester could be used for another cycle of ligation with a new peptide thioester in tandem or removed to afford peptide **5** with a C-terminal carboxylic acid by a mild hydrolysis at near neutral pH. Hydrolysis of β -mercaptoethylester was facile due to the α -effect of a terminal thiol. To minimize premature hydrolysis of the β -mercaptoethylester handle, ligation reactions were performed in aqueous acidic conditions at pH 5.6. Table 1 shows a series of peptides prepared by this approach.

Table 1. Synthetic peptides prepared by C-terminal Cys-mimetic ligation

Peptide Sequences
Ac-GASLRRSFGG ^a -AEVSYG ^b -OH
Ac-GASLRRSFGG ^a -SAEVSYG ^b -OH
Ac-GASLRRSFGG ^a -GYGGFLG ^b
FTQGVGNPVG ^a -GYGGFLG ^b -OH
FTQGVGNPVG ^a -GYGGLG ^c
SFGG ^a -AEVSYG ^b

^a thioester segment (peptide-SCH₂CH₂CONH₂). ^b mercaptoethylester segment (peptide-OCH₂CH₂SH). ^c mercaptopropylester segment.

Since long-range S,N-acyl migration is unfavorable, the key to effect such a migration depends on a dual role played by silver ion [4,5] (Fig. 2). Entropic activation of an Ag⁺ ion-complex in bridging the N^α-amine and diester linker could favor an intramolecular acylation to form a peptide bond as we observed that there was selectivity for N-terminal amino acids. Sterically hindered amino acids on peptide thioester **1** and small α -amine amino acids on mercaptoethylester peptide **2** were favored for S,N-acyl migration. Enthalpic activation of thioester rather than O-ester of the diester linkage by Ag⁺ ion enabled selective ligation reaction at the thioester site.

In conclusion, a C-terminal Cys-mimetic bearing a removable mercaptoethylester for capture of peptide thioester and then activation by silver ion permits a long-range S,N-acyl migration to occur for ligation of unprotected peptide segments.

Acknowledgments

This work was funded in part by NIH EB 001986

References

1. Tam, J. P., Lu, Y. -A., Liu, C. -F. and Shao, J. *Proc. Natl. Acad. Sci. USA* **92**, 12485-12489 (2001).
2. Tam, J. P., Yu, Q. and Yang, J. -L. *J. Am. Chem. Soc.* **123**, 2487-2494 (2001).
3. Dawson, P. E., Muir, T. W., Clark-Lewis, I. and Kent, S. B. H. *Science* **266**, 776-779 (1994).
4. Zhang, L. and Tam, J. P. *J. Am. Chem. Soc.* **121**, 3311-3320 (1999).
5. Hojo, H. and Aimoto, S. *Bull. Chem. Soc. Jan.* **64**, 111-117 (1991).

The C-Terminal Fragment of Acanthoscurrin is a Difficult Sequence

César Remuzgo¹, Gustavo F. S. Andrade², Maria L. A. Temperini², Sirlei Daffre³ and M. Terêsa M. Miranda¹

Departments of ¹Biochemistry and ²Fundamental Chemistry, Institute of Chemistry, Av. Prof. Lineu Prestes, 748, 05508-900, University of São Paulo, São Paulo, Brazil; ³Department of Parasitology, Institute of Biomedical Sciences, Av. Prof. Lineu Prestes, 1374, 05508-900, University of São Paulo, São Paulo, Brazil

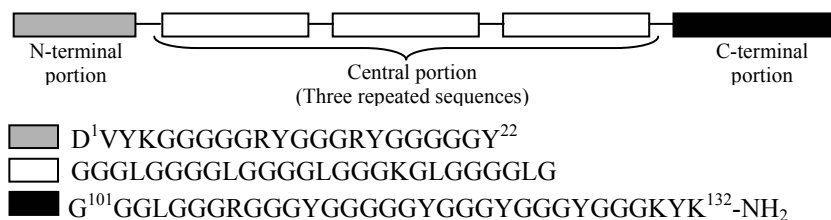
Introduction

Glycine-rich proteins (GRPs) with a variety of functions have been found in different organisms. Some of them have been described as components of the cell walls of plants [1]. Other distinct types have functions and structures similar to animal cytokeratins or present a domain with RNA-binding motifs [2].

Actually, very little is known about the structures of these proteins. Among the few data available are those found in the study of cast films of poly(Gly), poly(Tyr-Gly-Gly), poly(Gln-Gly-Gly), poly(Ala-Gly-Gly) by Raman and Infrared spectroscopies which revealed that these polypeptides present β -sheet conformation [3,4]. Likewise, theoretical predictions suggested that GRP domains are able to form β -pleated sheets [5].

Acanthoscurrin is a linear cationic antimicrobial GRP recently isolated from the hemocytes of the Brazilian spider *Acanthoscurria gomesiana*. This peptide is characterized by an over representation of glycine (73%), an amidated C-terminal residue, three repeated sequences of 26 amino acids (*Scheme 1*), and net charge of +8 in physiological pH. When tested against microorganisms it displayed activity against the Gram-negative bacteria *E. coli* (minimal inhibitory concentration, MIC, of 2.3-5.6 mM) and against the fungus *Candida albicans* (MIC of 1.15-2.3 mM) [6].

Isolation followed by purification furnishes acanthoscurrin with extremely low yields. Thus, attempts to produce the recombinant protein have been done. Our current involvement with antimicrobial peptides [7] also prompted us to study this GRP by using synthetic peptides. Here, we report the attempts to synthesize fragment 101-132 (*Scheme 1*).



Scheme 1. Amino acid sequence of acanthoscurrin.

Results and Discussion

At first, the synthesis of the desired fragment was approached with a stepwise solid-phase strategy at 60°C using customized protocols [8]. Peptide assembly on MBHA resin was characterized by repetitive incomplete aminoacylations after the

incorporation of the 7th residue. Changes of the solvent system and of the coupling reagent or addition of chaotropic salts to the reaction mixtures led to limited coupling improvements. Similar difficulties were encountered after the incorporation of the 8th residue on Rink amide resin. Overall, these characteristics suggested the occurrence of intramolecular aggregation [9]. As expected, the NIR-FT-Raman spectra of peptide-MBHA containing 8, 9, and 10 residues (*fragments 125-132, 124-132 and 123-132*) and of the nonapeptide-Rink amide resin (*corresponding to fragment 124-132*) presented a band in the amide I region with a maximum around 1673 cm⁻¹. This band can be assigned to β -sheet secondary structures.

The CLEAR amide resin is known to promote rapid reaction rates and avoid peptide aggregation. The use of this polymeric resin allowed the synthesis of fragment 113-132 straightforward up to the 18th residue. However, the incorporation of the 19th residue was difficult to accomplish and that of 20th residue was incomplete. NIR-FT-Raman spectra of the peptide-resins corresponding to fragments 126-132, 119-132, and 113-132 presented bands in the amide I and amide III regions with maxima around 1673 and 1236 cm⁻¹, respectively, indicative of β -sheet secondary structures.

In such context, the peptide-CLEAR amide resins corresponding to fragments 101-110, 111-120, and 121-132 were synthesized with the aim to prepare the C-terminal fragment of acanthoscurrin by convergent solid-phase method, which may overcome aggregation. All syntheses using the CLEAR amide resin were straightforward. The peptide detachments to produce the fully protected fragments 101-110 and 111-120 were easily accomplished. Unfortunately, the preliminary attempts to couple the protected fragment 111-120 to the peptide-resin corresponding to fragment 121-132 using TBTU as activating reagent was not successful even at 60°C. New attempts using other coupling reagents and solvents are in progress.

Finally, the free forms of fragments 125-132, 119-132, and 113-132 were purified and analyzed by circular dichroism (CD) in phosphate buffer pH 5.8, 50%TFE/buffer and 200mM SDS/buffer. The positive bands around 230 nm in the CD spectra collected may be related to the tendency of the tyrosines side chain to acquire a preferential orientation.

Acknowledgments

To FAPESP for the grant to MTMM, CNPq for the doctoral fellowship to CR, C.W. Liria for the amino acid analyses and A. Faljoni-Alário for her assistance in the obtainment of the CD spectra.

References

1. Sachetto-Martins, G. *Biochem. Biophys. Acta* **1492**, 1-14 (2000).
2. Mouravi, A. and Hotta, Y. *Appl. Biochem. Biotechnol.* **120**, 169-174 (2005).
3. Fukushima, Y. *Polym.Bul.* **45**, 237-244 (2000).
4. Small, E. W., *et al. J. Chem. Phys.* **52**, 4369-4379 (1970).
5. Condit, C. M. and Meaguer, R. B. *Nature* **323**, 178-181 (1986).
6. Lorenzini, D. M., *et al. Dev. Comp. Immunol.* **27**, 781-791 (2003).

A Novel Approach to Resin-based Cysteine Alkylation

Bin Yang and Richard D. DiMarchi

Department of Chemistry, Indiana University, Bloomington, IN 47405, USA

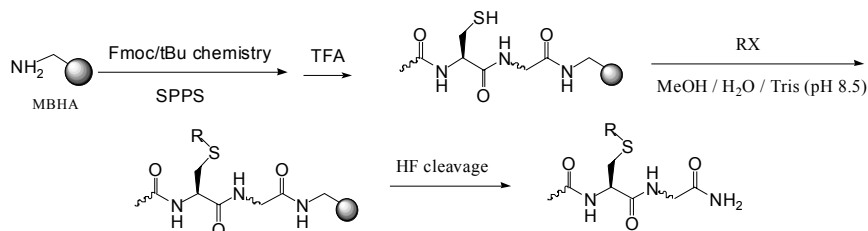
Introduction

Cysteine S-alkylation with structurally diverse alkylating agents has been used for the purpose of protein identification, assessment of protein folding, and localization of ligand binding sites. It also provides a rapid means to optimization of side chain structure within a biologically active peptide. This approach minimizes individual total syntheses with the corresponding amino acids. Direct alkylation of a free thiol in the presence of more nucleophilic amino acid side chains is typically achieved through pH control, or orthogonal protection [1]. We report here a novel on-resin cysteine alkylation method for unprotected peptides in aqueous methanol or DMF in the presence of Tris base. S-alkylation was obtained in yields as high as 90% with a variety of commonly used and a few novel reagents.

Results and Discussion

Scheme 1 describes the general details of this on-resin peptide cysteine alkylation procedure. Peptides were assembled on 4-methylbenzhyrlyamine resin using traditional Fmoc/tBu chemistry. All the side chain protection groups of the peptides were removed by TFA treatment to yield the unprotected peptide resin. Selective S-alkylation was performed with a 2-5 molar excess of a specific reagent in methanol or DMF, buffered with 50% aqueous Tris (pH 8.5). The peptides were cleaved from the resin with anhydrous HF and assessed by MS and HPLC (Table 1).

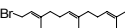
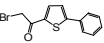
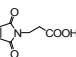
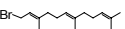
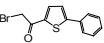
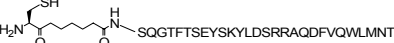
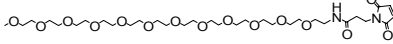
BrCH_2COOH was highly effective in alkylation of glucagon and the model peptide. $\text{ICH}_2\text{CH}_2\text{COOH}$ was slightly less reactive than BrCH_2COOH but still provided high yield and selectivity. $\text{I}(\text{CH}_2)_3\text{COOH}$ was not effective in this procedure. Polyethylene glycol maleimidopropionylimide proved to be quite reactive using similar conditions to those employed with the halo-acids. Modification of cysteine by addition of a farnesyl group was slow and required additional time, but eventually yielded ~ 50% of the desired product. 2-Bromo-1-(5-phenyl-2-thienyl)-ethanone is a selective and strong alkylating agent. We observed it to alkylate the thiol to high degree that also resulted in a dehydration product when alkylation occurred at the N-terminal cysteine. Clearly, 2-bromo-1-(5-phenyl-2-thienyl)-



Scheme 1. Synthesis of cysteine S-alkylated peptide by on-resin alkylation.

ethanone can function as a novel, highly effective S-alkylating agent.

Table 1. On-resin alkylation condition and yield with various agents and template peptides

Template peptide	Nucleophilic agents (RX)	Solvent and time	Yield (%)	Molecular Weight Calculated/MS	
GCSWARKHT	BrCH ₂ COOH	MeOH/H ₂ O/Tris (pH8.5), 4h	55	1102.1	1102.0
GCSWARKHT	ICH ₂ CH ₂ COOH	MeOH/H ₂ O/Tris (pH8.5), 4h	40	1116.1	1116.0
GCSWARKHT		DMF/H ₂ O/Tris (pH8.5), 16h	50	1248.1	1248.0
GCSWARKHT		DMF/H ₂ O/Tris (pH8.5), 4h	85	1245.1	1244.8
[Cys ⁹]Glucagon	BrCH ₂ COOH	MeOH/H ₂ O/Tris (pH8.5), 4h	90	3527.8	3528.0
[desHis ¹ , Cys ⁹]Glucagon	BrCH ₂ COOH	MeOH/H ₂ O/Tris (pH8.5), 4h	90	3390.7	3391.4
[Cys ⁹]Glucagon	ICH ₂ CH ₂ COOH	MeOH/H ₂ O/Tris (pH8.5), 4h	55	3541.8	3542.0
[desHis ¹ , Cys ⁹]Glucagon	ICH ₂ CH ₂ COOH	MeOH/H ₂ O/Tris (pH8.5), 4h	65	3404.7	3404.0
[desHis ¹ , Cys ⁹]Glucagon	I(CH ₂) ₃ COOH	MeOH/H ₂ O/Tris (pH8.5), 16h	0	3555.8	3332.8
[desHis ¹ , Cys ⁹]Glucagon		MeOH/H ₂ O/Tris (pH8.5), 4h	95	3501.7	3500.0
[Cys ⁹]Glucagon	m-dPEG ₁₂ MAL	MeOH/H ₂ O/Tris (pH8.5), 4h	80	4180.6	4180.3
[desHis ¹ , Cys ⁹]Glucagon	m-dPEG ₁₂ MAL	MeOH/H ₂ O/Tris (pH8.5), 4h	75	4043.5	4043.2
[Cys ⁰ , Ahx ¹ , Glu ⁹]Glucagon	m-dPEG ₁₂ MAL	MeOH/H ₂ O/Tris (pH8.5), 4h	85	4285.6	4285.0
[Cys ⁰ , Ahx ¹ , Glu ⁹]Glucagon		DMF/H ₂ O/Tris (pH8.5), 16h	55	3780.1	3780.0
[Cys ⁰ , Ahx ¹ , Glu ⁹]Glucagon		DMF/H ₂ O/Tris (pH8.5), 4h	90	3775.8	3774.0
Glucagon	HSQGTFTSDYSKYLSRRAQDFVQWLMNT				
[Cys ⁰ , Ahx ¹ , Glu ⁹]Glucagon					
m-dPEG ₁₂ TM -MAL					

References

1. Perrey, D. A. and Uckun, F. M. *Tetrahedron Lett.* **42**, 1859-1861 (2001).
2. Yang, C. C., Marlowe, C. K. and Kania, R. J. *Am. Chem. Soc.* **113**, 3176-3177 (1991).

Deprotection of the *p*-Methoxybenzyl Group of Selenocysteine by Neighboring Group Participation

Katharine M. Harris and Robert J. Hondal

*Department of Biochemistry, University of Vermont, College of Medicine, 89 Beaumont Ave,
Burlington, VT 05405 USA*

Introduction

Selenocysteine (Sec) is now recognized as the 21st amino acid in the universal genetic code and the discovery of 25 human proteins containing selenocysteine has generated renewed interest in synthetic peptides containing this rare amino acid [1]. The weakness of the carbon-selenium bond renders trityl-type protecting groups ineffective during peptide synthesis, thus benzyl (Bzl) and *p*-methoxybenzyl (Mob) groups have been used to protect the selenol side-chain [2,3]. While the Mob group is more acid labile than a benzyl group, very strong Lewis acids such as TMSBr and TMSOTf are still required for its removal. This is problematic because these reagents are not very soluble in ether, which makes work up of the peptide difficult. Thus, an alternative method of removal of the Mob group is needed.

Our group has been working on methods for making the biologically important peptide Cys-Sec-Gly, which corresponds to the C-terminus of mammalian thioredoxin reductase. A major difficulty in making this peptide is in the deprotection of the Mob group from the Sec residue. In order to address this problem, we started to explore other deprotection methods that did not include silyl reagents. One of our early attempts at removing the Mob group involved oxidative deprotection with I₂. As van der Donk had noted, deprotection of the Mob group from Sec using I₂ in the presence of a peptide disulfide bond resulted in oxidative deprotection of Sec(Mob) with concomitant formation of a selenylsulfide bond [4]. We found the use of I₂ as a reagent for the removal of Mob groups challenging, as many side products resulted that were unidentifiable by us. During the course of this investigation, we noticed spontaneous deprotection of the Mob group of Sec when the neighboring Cys residue was protected with a *S*-*t*-butyl group. However, very little deprotection was observed when the adjacent Cys residue was protected with a trityl group. When we further activated the neighboring Cys residue with a 5-Npys group [5], 100% deprotection of the Mob group of Sec was achieved in the presence of TFA, thioanisole, and phenol. This led us to use 2,2' dithiobis (5-nitropyridine) (DTNP) as a reagent for deprotecting Mob groups from Sec residues in peptides where no other Cys residue was present in the sequence.

Results and Discussion

Peptide CUG-amide (U is the one letter abbreviation for Sec) was synthesized using a method developed by Barany, which suppresses racemization of Cys residues [6]. The Cys residue was either protected with trityl (Trt), *S*-*t*-butyl, or 5-Npys groups. In order to place a 5-Npys group on the Cys residue, the peptide was first synthesized with a *S*-*t*-butyl group on the Cys residue. The *S*-*t*-butyl group was removed on resin with addition of a 20% βME solution, followed by addition of DTNP. The removal of the Mob group from these peptides is summarized in Table 1. The results in Table 1 clearly point to a neighboring group effect in deprotecting the Mob group of Sec. This effect is dependent upon the presence of an adjacent and reactive disulfide bond. A mechanism for this phenomenon is shown in Figure 1.

Table 1: Effect on Deprotection of a Sec(Mob) group by a Neighboring Cys Residue.

Peptide	% Deprotected and Cyclized Peptide
C(Trt)U(Mob)G-NH ₂	5 ^a
C(<i>S</i> - <i>t</i> -butyl)U(Mob)G-NH ₂	38 ^b
C(5-Npys)U(Mob)G-NH ₂	100 ^a

^aCleavage cocktail: TFA/thioanisole/phenol (90/2.5/7.5). ^bCleavage cocktail : TFA/H₂O (95/5).

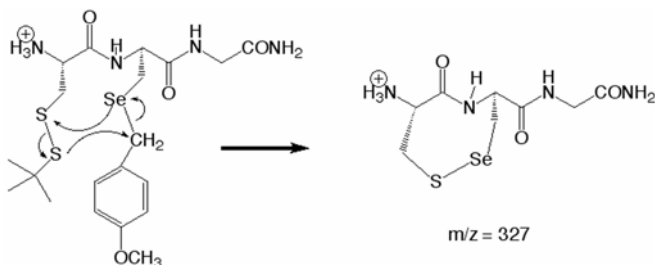


Fig. 1. Mechanism of deprotection and cyclization of a Sec(Mob) residue involving a neighboring Cys residue protected via a disulfide bond.

This reaction is dependent upon the high nucleophilicity of selenium since a peptide of sequence C(*S*-*t*-butyl)C(Mob)G-NH₂ did not show significant deprotection of the Mob group under the same conditions. Deprotection could be driven to completion if the neighboring disulfide was made a better electrophile by placing a 5-Npys group on the neighboring cysteine residue. This method of deprotection can be extended as a general method for deprotecting Sec(Mob) residues by adding DTNP to a cleavage cocktail of TFA/thioanisole/phenol. A postulated mechanism for this reaction is shown in Figure 2.

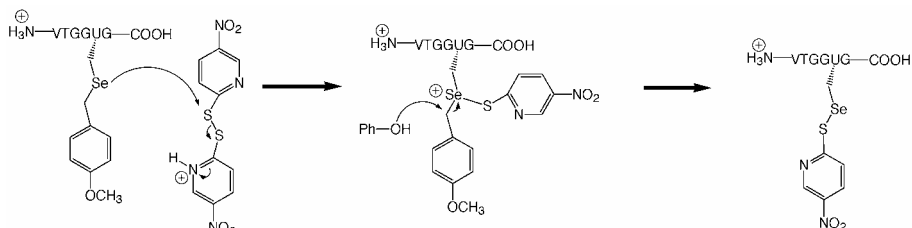


Fig. 2. A possible mechanism for deprotection of Sec(Mob) using DTNP as an additive. The 5-Npys group can then be easily removed by reducing agents such as DTT.

Acknowledgments

The work was funded by a NIH grant (GM070742) to R.J.H.

References

1. Kryukov, G. V., *et al. Science* **300**, 1439-1443 (2003).
2. Theodoroulos, D., Shuwartz, I. L. and Walter, R. *Biochemistry* **6**, 3927-3932 (1967).
3. Koide, T., *et al. Chem. Pharm. Bull.* **41**, 502-506 (1993).
4. Gieselman, M. D., Xie, L. and van der Donk, W. A. *Org. Lett.* **3**, 1331-1334 (2001).
5. Galande, A. K., *et al. J. Comb. Chem.* **7**, 174-177. (2005).
6. Han, Y., Albericio, F. and Barany, G. *J. Org. Chem.* **62**, 4307-4312 (1997).

Overcoming Challenges in Automated Long Peptide Synthesis – A Multi-pronged Approach

Yingwei He, Guodi Lu, John Mountzouris and Chun Wu

ABGENT, 6310 Nancy Ridge Drive, #106, San Diego, CA 92121, USA

Introduction

Over the past 20 years peptides have been identified as a promising source for novel pharmaceutical drug candidates, most recently evidenced by approval of Fuzeon® for treatment of HIV [1]. However, delivery and manufacturing challenges have impeded widespread development of peptide related therapeutics. Historically, the synthesis of longer peptides has been prohibited by synthetic inefficiencies associated with peptide aggregation. New strategies have tempered the resources required to achieve economically viable preparation of longer and “difficult” peptides. Recently, Abgent has substantially increased the success for synthesis of long and difficult peptides, working in conjunction with EMD Biosciences and Protein Technology Inc. to apply pseudoproline dipeptides in automated synthesis.

Pseudoproline dipeptides consist of ψ P-X, where X is any amino acid and ψ P is a serine or threonine modified via reversible linkage of amino and side chain hydroxy groups to form an oxazolidine ring [2,3]. Structural perturbation from pseudoproline dipeptides incorporated into protein or peptide structures disrupts adoption of α -helices and β -sheets, and this function has been successfully exploited to efficiently inhibit aggregation of hydrophobic peptides in solid-phase peptide synthesis (SPPS). Mild TFA cleavage post-synthesis lead to full recovery of the native serine or threonine amino acid structure. Pseudoproline dipeptides have proven indispensable to markedly improved yield, solubility and ease of HPLC purification., thereby rendering accessible to SPPS many previously infeasible long or difficult peptide sequences of biological value [4-7].

Results and Discussion

In the past year, we have synthesized 140 peptides with lengths from 30 mer to 96 mer. All peptides were synthesized on machines; no monitoring of coupling completion was engaged. Non-stop synthesis was done without any manual intervention. As shown in Table 1, average days for completion of synthesis is 3-5 times faster than for manual synthesis, and purity and yield is equivalent to or higher than that achieved by manual synthesis.

Table 1. Summary of synthesis of long peptides

Peptide Length	30-50	50-70	70-90	>90
Average synthesis days	1-2	2-3	3-4	5
Number of peptides	70	42	20	8
Average crude purity	80	50	40	40
Success rate	85	70	80	80

Chemical synthesis of full-length active chemokines is quite challenging [8]. RANTES is a member of the C-C chemokine subfamily including other monocyte chemoattractants such as MIP-1 α and β as well as MCPs. The active form of

RANTES is a 68mer polypeptide, traditionally prepared using an inefficient ligation strategy to couple two peptide sequences [9].

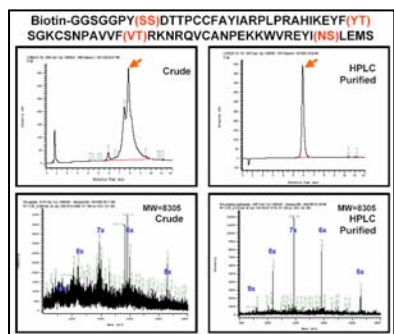


Fig. 1. The full-length active RANTES peptide was prepared directly on a resin utilizing the addition of four pseudoproline dipeptides (gray colored SS, YT, VT, and NS in the sequence). This method provided an efficient synthesis of the RANTES peptide.

Length, amino acid composition, purity, and amount required are most often used as a measure of potential difficulty in peptide synthesis. We have completed a number of peptide epitope mapping projects, providing a rich set of data demonstrating the specific combinations of amino acids and their positions in the sequence that significantly affect synthetic efficiency. We have combined this knowledge with the application of strategies used in long peptide synthesis (insertion of pseudoproline dipeptides, modulation of resin substitution ratios, improved coupling protocols) to significantly improve purity and yield of peptides otherwise infeasible to produce.

We have shown that both long peptides (up to 95 residues) and difficult peptides can be synthesized with high purity and good yield by using: (1) Specially prepared building blocks, such as reducing the substitution ratio using a combination of Fmoc-AA and Boc-AA; (2) Strategic incorporation of pseudoproline dipeptides; (3) Optimized coupling procedures for individual sequences; and (4) Optimized coupling temperatures.

Acknowledgments

We would like to thank Dr. Dave Duncan for scientific advice.

References

1. McGee, P. *Drug Disc. Dev.* **8**, 16 (2005).
2. Haack, T. and Mutter, M. *Tetrahedron Lett.* **33**, 1589-1592 (1992).
3. Mutter, M., *et al.* *Peptide Res.* **8**, 145-153 (1995).
4. White, P., *et al.* *J. Peptide Res.* **10**, 18-26 (2004).
5. von Eggelkraut-Gottanka, R., *et al.* *ChemBioChem* **4**, 425-433 (2003).
6. Schmiedeberg, N. and Kessler, H. *Org. Lett.* **4**, 59-62 (2002).
7. Wittelsberger, A., *et al.* *Angew. Chem. Int. Ed.* **39**, 1111-1115 (2000).
8. Thierry, A., *et al.* *Biologicals* **29**, 259 (2001).
9. Boykins, R., *et al.* *Cytokine* **11**, 8-15 (1999).

Synthesis and Biological Evaluation of Antagonist Analogs of the Peptide Hormone Oxytocin

Jake L. Stymiest¹, Bryan F. Mitchell², Susan Wong² and John C. Vederas¹

¹Department of Chemistry; ²Department of Obstetrics and Gynecology; University of Alberta, Edmonton, Alberta T6G 2G2, Canada

Introduction

Oxytocin (OT) is a mammalian nonapeptide hormone synthesized by the magnocellular neurons of the hypothalamus [1]. Among other functions, OT is responsible for the contraction of uterine smooth muscle at the onset of childbirth [2]. Antagonists of OT, such as atosiban **1** [3a] and peptide **2** [3b] (Fig. 1) are of interest as tocolytic agents that inhibit preterm labor and delay premature birth. There are an estimated 13 million premature births worldwide per annum [4a,b] that account for 66% of all neonatal mortality and contribute to serious complications and infant morbidity [4c]. Unfortunately peptides like **1** have relatively short metabolic half-lives are usually administered intravenously due to lack of metabolic stability [3b]. We have recently shown that analogs of OT, in which the disulfide bridge is replaced with an unsaturated ethylene linker with a *cis* conformation yields an analog with potent agonistic activity ($EC_{50} = 38$ nM) [5a]. Using a similar approach, we wanted to explore the synthesis and biological spectrum of a variety of 1,6-dicarba analogs of **2** and **3**.

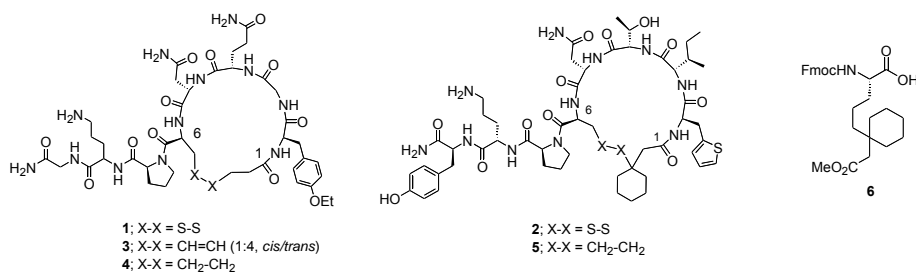
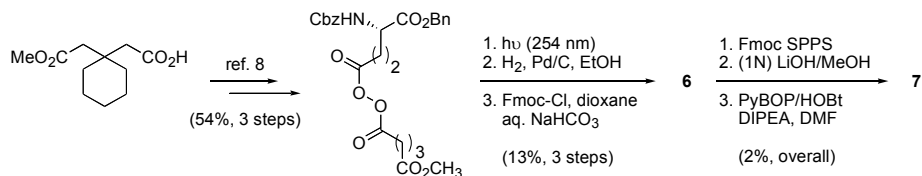


Fig. 1. Structures of peptides **1-5** and DAS analog **6**.

Results and Discussion

Linear precursors to peptides **1**, **3** and **4** were synthesized using standard Fmoc SPPS chemistry on Rink amide resin (0.62 mmol/g, 0.40 mmol). Incorporation of 4-pentenoic acid and L-allylglycine at positions 1 and 6 respectively followed by an on-resin Grubbs ring-closing metathesis (RCM) reaction yielded peptide mixture **3** in 21% overall yield after TFA cleavage and purification using RP-HPLC (Waters C₁₈ μ BondpakTM) with a gradient of 10-90% MeCN in aq. 0.1% TFA [8]. Standard hydrogenation of **3** with Pd/C in EtOH under H₂ gives saturated analog **4** [5b]. Unfortunately, 1,6-dicarba analogs of **2** were not attainable by RCM. Instead the orthogonally protected, diaminosuberic acid (DAS) analog **6** (Fig. 1) was prepared [8] and incorporated in to the peptide during Fmoc SPPS (Scheme 1) on Sieber amide resin (0.60 mmol/g, 0.2 mmol). Cleavage (1% TFA) followed by ester

hydrolysis of the partially protected peptide and PyBOP/HOBt/DIEA mediated intramolecular cyclization yielded peptide **5** (Fig. 1) after TFA deprotection.



Scheme 1. Synthesis of **6** and incorporation via Fmoc-SPPS to give **7**.

Peptides **1-5** were tested for *in vitro* OT antagonism using fresh rat uterine muscle, and their pA_2 values were compared (Table 1) [5b]. Both peptides **3** and **4** were shown to be potent antagonists ($pA_2 = 7.8$ and 8.0 respectively) versus their parent peptide **1** ($pA_2 = 9.9$) (Table 1). Unfortunately analog **5** ($pA_2 = 6.1$) was somewhat less active than parent peptide **3** ($pA_2 = 8.8$) (Table 1). Placental tissue stability tests were done on peptides **1** and **4** (Table 1). Replacement of sulfur in **1** with carbon markedly increases the half-life in rat placental tissue (Table 1). This observation provides a basis for the design of new oxytocin antagonists with increased potency and metabolic stability for use as possible therapeutics in the treatment of pre-term labor.

Table 1. Biological results for peptides **1-5**.

Peptide	IC ₅₀ (nM)	pA_2	$t_{1/2}$ (min)
1	0.2 ± 0.1	9.9 ± 0.3	132 ± 24
2	3.0 ± 1.0	8.8 ± 0.5	-
3	17.0 ± 6.0	7.8 ± 0.1	-
4	10.0 ± 1.0	8.0 ± 0.1	312 ± 6
5	750 ± 20	6.1 ± 0.1	-

^aMuscle baths were prepared using fresh uterine tissue from mature, virgin Sprague-Dawley rats (250g). Homogenates were made from placental tissue from pregnant Sprague-Dawley rats at day 19 of gestation.

Acknowledgments

The work was funded by the Natural Science and Engineering Council of Canada and the Canada Chair in Bioorganic and Medicinal Chemistry.

References

- Andersson, K. E., Forman, A. and Ulmsten, U. *Clin. Obstet. Gynecol.* **26**, 56-77 (1983).
- Nicholson, H. D., *Reviews of Reproduction*, **1**, 69-72 (1996).
- a) Melin, P., Trojnar, J., Johansson, B., Vilhardt, H. and Akerlund, M. *J. Endocrinol.* **111**, 125-131 (1986), b) Manning, M., Stoev, S., Cheng, L. L., Wo, N. C. and Chan, W. Y., *J. Peptide Sci.* **7**, 449-465 (2001).
- a) Havass, J., *et al. Peptides*, **23**, 1419-1425 (2002). b) Villar, J., Ezcurra, E. J., Gurtner de la Fuente, V. and Campodonico, L. *Res. Clin., Forums* **16**, 9-38 (1994), c) Goldenberg, R. L. and Rouse, D. J. *New Engl. J. Med.* **339**, 313-320 (1998).
- a) Stymiest, J. L., Mitchell, B. F., Wong, S. and Vederas, J. C. *Org. Lett.* **5**, 47-49 (2003). b) Stymiest, J. L., Mitchell, B. F., Wong, S. and Vederas, J. C. *J. Org. Chem.* **70**, 7799-809 (2005).

Development of Wang Resin Supported Evans-type Oxazolidinone for Asymmetric Reaction

Tomoya Kotake, Yoshio Hayashi, S. Rajesh, Tooru Kimura and
Yoshiaki Kiso

Department of Medicinal Chemistry, Center for Frontier Research in Medicinal Science,
21st Century COE Program, Kyoto Pharmaceutical University, Kyoto 607-8412, Japan

Introduction

Evans' oxazolidinone is one of the most versatile chiral auxiliaries. The previous application of this auxiliary in solid-phase chemistry resulted in a significant decrease in yield and stereoselectivity in asymmetric alkylation [1]. The maximum stereoselectivity reported was 90% ee in the case of benzylation using auxiliary resin **1** (Fig. 1A). This application was also inefficient in recycling the resin. We believe this is attributed to the anchoring strategy, in which the chirality discriminating benzyl moiety at the 4-position of the ring was used as an anchor. Namely, the chiral control ability is probably influenced by the polystyrene backbone of the resin, leading to low stereoselectivity. Hence, we proposed an alternative anchoring strategy, which leaves the crucial chiral discriminating moiety unmodified and utilizes the 5-position for the connection to the resin (Fig. 1B). Here, we describe the synthesis of a new Wang resin supported oxazolidinone **4**, anchored at the 5-position through the peptide bond with a piperidine-4-carboxylic acid linker and the ability of this resin as a chiral auxiliary in asymmetric alkylation reaction [1,2].

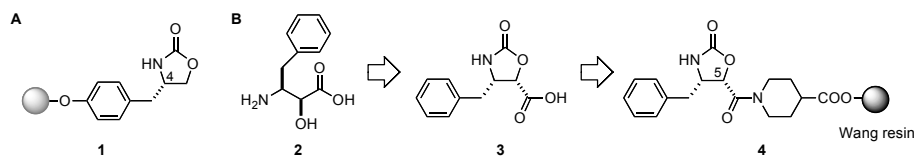
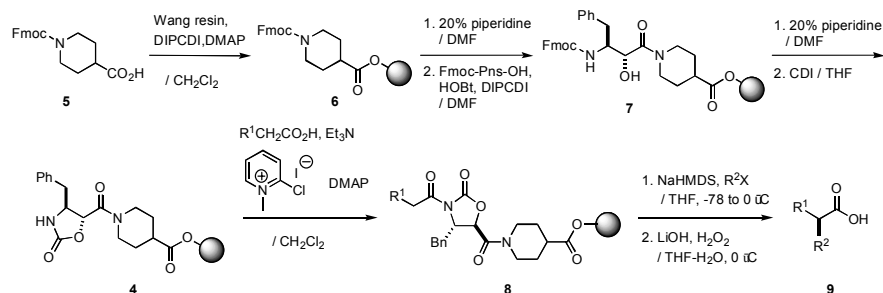


Fig. 1. Reported polymer-supported Evans' chiral auxiliary (A) and design of a new auxiliary anchored at the 5-position (B).

Results and Discussion

For preparing a new oxazolidinone, we focused our attention on α -hydroxy- β -amino acid, (2*R*,3*S*)-3-amino-2-hydroxy-4-phenylbutanoic acid (phenylnorstatine, Pns, **2**) (Fig. 1B) and developed a convenient synthetic route for **4** using a Fmoc-based solid-phase method as shown in Scheme 1. Each reaction proceeded smoothly in a few hours at room temperature with no epimerization, and gram-scale quantity of the oxazolidinone resin **4** with high loading yield could be synthesized in a day (95% yield for 6 steps determined by methanolysis).

We investigated the solid-phase asymmetric alkylation of several acylated carboximide resins **8** prepared by Mukaiyama method. The use of NaHMDS (3 equiv.) as a base and gradual increase of the reaction temperature up to 0°C was quite effective. After quenching the reaction with saturated NH₄Cl aq., the resin was recovered, washed, and subjected to the LiOOH-mediated hydrolysis. Resins **8** were reacted sufficiently with a series of electrophiles (R²X), not only highly reactive alkyl halides such as MeI and BnBr, but also less reactive EtI. Hydrolytic cleavage of the resultant resins afforded the corresponding chiral α -branched



Scheme 1. Solid-phase synthesis of Wang resin-supported oxazolidinone resin **4** and its application to asymmetric Evans' alkylation.

carboxylic acids in satisfying isolated yields (50-70%, over 3 steps) and enantiomeric excesses (84-97% ee). Especially in the case of benzylation, the obtained stereoselectivity was 97% ee, which is as high as in the corresponding solution-phase asymmetric alkylation utilizing the standard chiral 4-substituted oxazolidin-2-one. We assume that these successful results are attributed to our new polymer-anchoring strategy based on the connection at the 5-position of the oxazolidinone ring.

The ability to recycle the Wang resin-supported chiral auxiliary **4** was studied in the solid-phase asymmetric allylation of phenylpropionic acid. After the continuous second to fourth solid-phase asymmetric allylation, the desired product was obtained in high enantioselectivity (96% ee each), which was comparable to that of the first cycle, indicating that the product's stereoselectivity was maintained successfully. However, the chemical yield gradually decreased about 8% in each cycle. After the fourth cycle, the resin was cleaved by methanolysis to analyze the residual auxiliary. A 22% yield of the undesired *N*-allylated oxazolidinone derivative was obtained. This indicated that the substrate-loading site on the resin was partially blocked by the allyl group, suggesting a major reason for the reduced yield. This unfavorable side reaction is thought to be induced by the partial elimination of the *N*-acyl moiety during the enolate-alkylation steps. In fact, in a solution-phase model experiment, 6% of *N*-allylated byproduct was formed.

In conclusion, we have developed a new Wang resin-supported Evans' chiral auxiliary based on a novel polymer-anchoring strategy. Asymmetric Evans' alkylation and recycling of the new auxiliary resin were successfully achieved in high stereoselectivities. This is the first successful example of the Evans' asymmetric alkylation proceeding efficiently on solid-support. Further application to other solid-phase Evans' asymmetric reactions are now in progress.

Acknowledgments

This research was supported in part by grants, the "Academic Frontier" Project for Private Universities and the 21st Century COE Program from MEXT (Ministry of Education, Culture, Sports, Science and Technology).

References

1. Burgess, K. and Lim, D. *Chem. Commun.* 785-786 (1997).
2. Kotake, T., *et al. Tetrahedron Lett.* **45**, 3651-3654 (2004).
3. Kotake, T., Hayashi, Y., Rajesh, S., Mukai, Y., Takiguchi, Y., Kimura, T. and Kiso, Y. *Tetrahedron* **61**, 3819-3833 (2005).

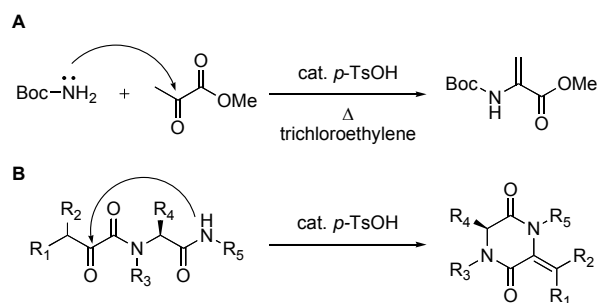
A Convenient Synthetic Method for Monodehydro-2,5-diketopiperazines

Yoshio Hayashi, Akiko Oda, Yuri Yamazaki, Yuka Okuno and Yoshiaki Kiso

Department of Medicinal Chemistry, Center for Frontier Research in Medicinal Science,
 21st Century COE Program, Kyoto Pharmaceutical University, Kyoto 607-8412, Japan

Introduction

2,5-Diketopiperazine (DKP) is a cyclic dipeptide and many naturally occurring derivatives of DKP possessing varied biological activity have been discovered. Phenylalhistin is one such naturally occurring monodehydrated DKP derivative, which is recognized as a new lead anticancer agent based on anti-microtubule depolymerization activity [1]. Development of potent synthetic derivatives would afford an important contribution in future cancer treatment. Additionally, monodehydroDKPs are useful templates for combinatorial chemistry. However, in the synthesis of monodehydroDKPs, racemization at the α -position is often observed during cyclization of the corresponding dipeptide unit, or during introduction of the dehydro-moiety onto the DKP ring having a chiral side chain [2]. In order to develop a new method that reduces such unfavorable racemization, we focused our work on Gladiali *et al.*'s report that the reaction of α -ketoester and Boc-NH₂ in the presence of a catalytic amount of *p*-TsOH resulted in the formation of dehydroamino acid as shown in Scheme 1A [3]. It was thought that, if this reaction was applied to an intramolecular reaction, monodehydroDKPs would be formed without any racemization (Scheme 1B). Here, we describe a new method based on an acid-catalysed cyclization of *N*- α -ketoacyl amino acid amides to facilitate the synthesis of monodehydroDKPs.



Scheme 1. Acid-catalyzed reaction of amide nitrogen with α -keto acid derivatives.

Results and Discussion

A series of α -ketoacyl-Phe-NH₂ was synthesized from H-Phe-NH₂ by EDC-HOBt method, followed by refluxing in toluene in the presence of a catalytic amount of *p*-TsOH (3-5 mol%). As shown in Table 1, the cyclization reaction of dioxopropyl- or β -aliphatic- α -keto acyl derivatives (Entry 1-3) gave the corresponding monodehydroDKPs in high chemical yields with no racemization. However, *N*-phenylpyruvoyl derivative (Entry 4) showed low reactivity and the obtained

Table 1. Synthesis of monodehydroDKP by acid catalyzed cyclization

entry	R1	R2	R3	yield (%) Step 1	<i>p</i> -TsOH	time (h)	yield (%) Step 2	E/Z ^a	ee (%) ^b
1	H	H	H	65	5	18	96	-	>99
2	Me	H	H	94	5	17	86	1/25	>99
3	Me	Me	H	74	5	18	94	-	>99
4	Ph	H	H	66	5	6	35	1/>99 ^c	73
5	H	H	Bn	30	3	24	53	-	>99
6	H	H	<i>i</i> -Pr	73	5	72	20	-	>99
7	H	H	<i>i</i> -Bu	57	3	72	43	-	>99
8	H	H	allyl	40	3	20	92	-	>99

^aE/Z ratio was determined by NMR. ^bEnantiomeric excess values were determined by chiral HPLC using CHIRALCEL OD column. ^cThe *E*-form was not detected.

monodehydroDKP was partly racemized. This was probably due to keto-enol tautomerism at the α-keto moiety, i.e., unfavorable enol form for cyclization was stabilized by conjugation with the phenyl ring. Even in this case, racemization was minimized by optimizing the reaction conditions (data not shown). Next, we examined the effect of an alkyl-substitution on amide nitrogen in **3** (Entry 5-8). In spite of the electron donating effect of these alkyl groups, the chemical yield of the corresponding monodehydroDKP was lower except for the allyl group (Entry 8), but no racemization was observed. Since the derivative with a bulky isopropyl group showed the lowest yield, it seems that steric factor is more important than electron donating effect in this cyclization reaction. In conclusion, this new method based on an acid-catalyzed cyclization of *N*-α-ketoacyl amino acid amides could be useful for the synthesis of monodehydroDKPs.

Acknowledgments

This research was supported in part by grants, the “Academic Frontier” Project for Private Universities and the 21st Century COE Program from MEXT (Ministry of Education, Culture, Sports, Science and Technology).

Reference

1. Kanoh, K., Kohno, S., Katada, J., Takahashi, J., Uno, I. and Hayashi, Y. *Bioorg. Med. Chem.* **7**, 1451-1457 (1999).
2. Hayashi, Y., Orikasa, S., Tanaka, K., Kanoh, K. and Kiso, Y. *J. Org. Chem.* **65**, 8402-8405 (2000).
3. Gladiali, S. and Pinna, G. *Tetrahedron: Asymmetry* **2**, 623-632 (1991).

Solid-Phase Synthesis of Azole-Based Peptides and Peptidomimetics

Eric Biron and Horst Kessler

Department Chemie, Lehrstuhl II für Organische Chemie, Technische Universität München,
Garching, D85747, Germany

Introduction

Oxazole- and thiazole-based heterocyclic amino acids are found in many bioactive natural products of peptide origin exhibiting interesting biological activities, including cytotoxicity, antibacterial and antiviral activities [1]. These substituted five-membered heterocycles are pharmacophore of many natural and synthetic bioactive compounds and therefore are very important intermediates for natural product synthesis. They can also be used as peptidomimetic structural templates [2,3], as macromolecular scaffolds [4], and as building blocks for combinatorial chemistry [5]. Oxazole-, thiazole- and imidazole-based amino acids are usually prepared in solution and then used on solid support. But in some cases, many steps and extensive purification are needed leading to overall low yields. To overcome this problem, our strategy was to prepare these five-membered heterocycles directly on solid support from natural amino acids and/or modified amino acids.

Results and Discussion

Wang resin-bound dipeptide **1**, composed of Phe and Thr(Trt) and bearing different N-terminal protecting group (Fmoc, Alloc and Cbz) were first prepared (Fig. 1). After removal of the trityl group with 1% TFA/DCM, oxidation was successfully achieved with the Dess-Martin periodinane (DMP). Amidoketone derivatives **2** were then submitted to different cyclodehydration procedures to form the corresponding oxazole- **3**, thiazole- **4** and imidazole-dipeptides **5**. The oxazole formation was achieved with Ph_3P , I_2 , and DIEA in very good yields. The thiazole module was formed with the Lawesson's reagent in good yields. These two procedures were compatible with all tested protecting groups. The amidoketone **2** was transformed into imidazole-based dipeptides **5** and **6** with the corresponding amine in the presence of acetic acid in refluxing xylenes with azeotropic removal of water. Imidazole formation could not be achieved with R larger than methyl.

The amidoketone approach is not suitable to prepare 2,4-substituted oxazole, thiazole and imidazole. To overcome this problem, cyclodehydration has to be

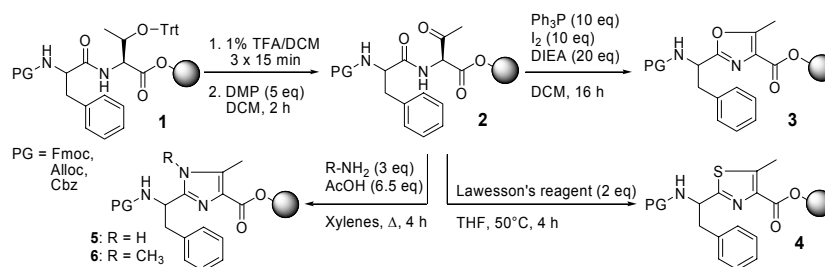


Fig. 1. Synthesis of 2,4,5-substituted oxazole-, thiazole- and imidazole-based dipeptides on solid support.

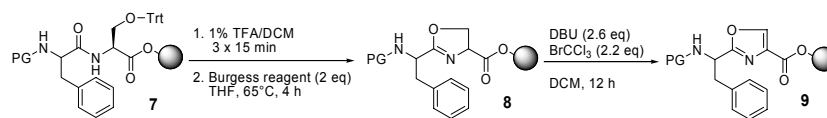


Fig. 2. Synthesis of oxazole-based peptide from serine.

performed before the oxidation step. To prepare oxazole-based dipeptide from serine, the Wang resin-bound dipeptide PG-Phe-Ser(Trt) **7** was first, after removal of the trityl group, subjected to cyclodehydration using the Burgess reagent to form the oxazoline derivative **8** (Fig. 2) [6]. This was followed by oxidation with BrCCl_3 in the presence of DBU to afford the oxazole-based dipeptide **9** [7]. This procedure can also be applied to dipeptide **1** to prepare 5-substituted oxazole-based dipeptide **3**.

Thiazoline and imidazoline have to be formed by nucleophilic attack of the corresponding side chain functional group and therefore the Burgess reagent cannot be used for the cyclodehydration step. You and Kelly recently described a very efficient procedure to form thiazole from cysteine and imidazole from diaminopropionic acid using bis(triphenyl)oxophosphonium triflate [8,9]. The procedure was applied to Wang resin-bound dipeptides PG-Phe-Cys(Trt) **10** and PG-Phe-Dap(Tos) **11** (Fig. 3). Azole-based dipeptides **12** and **13** were obtained in good yields after cyclodehydration of dipeptides **10** and **11** with triphenylphosphine oxide and triflic anhydride followed by oxidation with DBU and BrCCl_3 . The trityl group on the cysteine is removed during the cyclodehydration step.

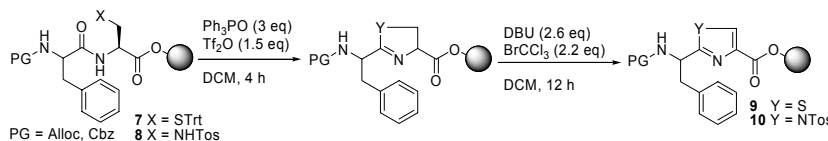


Fig. 3. Thiazole and imidazole via Bis(triphenyl)oxodiphosphonium triflate cyclodehydration.

The described procedures allow an efficient solid-phase synthesis of oxazole-, thiazole-, and imidazole-based peptides from natural amino acids and could be applied to the synthesis of macrolactam natural products on solid support.

Acknowledgments

E.B. thanks the Alexander von Humboldt Foundation for a Postdoctoral Fellowship.

References

- Roy, R. S., Gehring, A. M., Milne, J. C., *et al.* *Nat. Prod. Rep.* **16**, 249-263 (1999).
- Plant, A., Stieber, F., Scherkenbeck, J., Losel, P. and Dyker, H. *Org. Lett.* **3**, 3427-3430 (2001).
- Falorni, M., Giamocelli, G., Porcheddu, A., *et al.* *Eur. J. Org. Chem.* **18**, 3217-3222 (2000).
- Singh, Y., Stoermer, M. J., Lucke, A. J., *et al.* *Org. Lett.* **4**, 3367-3370 (2002).
- Grabowska, U., Rizzo, A. and Quibell, M. *J. Comb. Chem.* **2**, 475-490 (2000).
- Wipf, P. and Miller, C. P. *J. Am. Chem. Soc.* **114**, 10975-10997 (1992).
- Williams, D. R., Lowder, P. D., Yu-Gui, G., *et al.* *Tetrahedron Lett.* **38**, 331-334 (1997).
- You, S. -L. and Kelly, J. M. *Org. Lett.* **6**, 1681-1683 (2004); *Chem. Eur. J.* **10**, 71-75 (2004).
- You, S. -L., Razavi, R. and Kelly, J. W. *Angew. Chem. Int. Ed.* **42**, 83-85 (2003).

Efficient Synthesis of *N*-Methylamino Acids Compatible with Fmoc Solid-Phase Peptide Synthesis

Eric Biron, Jayanta Chatterjee and Horst Kessler

Department Chemie, Lehrstuhl II für Organische Chemie, Technische Universität München,
 Garching, D85747, Germany

Introduction

Incorporation of *N*-methylamino acids into biologically active peptides has been shown to improve useful pharmacological parameters such as lipophilicity, proteolytic stability and conformational rigidity [1]. It may also result in enhanced potency [2], new receptor subtype selectivity [3], and conversion of an agonist to an antagonist [4]. Therefore, *N^α*-methylamino acid containing peptides are increasingly recognized as potentially useful therapeutics. Unfortunately, their synthesis is hampered by the high price and unavailability of many *N^α*-methylamino acids. Various methods have been developed for the synthesis of optically active *N^α*-methylamino acids but most of these methods are limited to aliphatic amino acids or are characterized by harsh reaction conditions and are incompatible with Fmoc-SPPS protecting groups. To date, there has been no method describing the synthesis of *N*-methyl derivatives of the common 20 amino acids in high yields by a common general procedure. Therefore we were interested in developing an easy and highly efficient procedure to prepare side chain protected *N*-methylamino acids with the possibility to use them directly in Fmoc-SPPS.

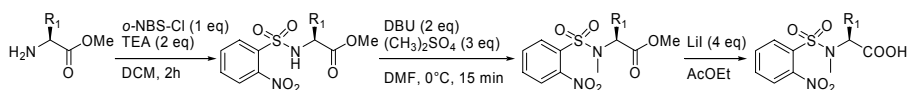


Fig. 1. Synthesis of *N^α*-methyl-*N^α*-*o*NBS-amino acids.

Results and Discussion

The *o*-nitrobenzenesulfonyl group (*o*NBS), first described by Fukuyama *et al.*, has been commonly used for selective *N*-alkylation and its compatibility with Fmoc-SPPS was also demonstrated. Our strategy was to transfer in solution the procedure, first described by Miller and Scanlan [5], for selective *N*-methylation of peptides on solid support. The described three-step procedure herein involves: 1) amine activation and protection of α -amino acid methyl esters with *o*NBS; 2) *N*-alkylation using the inexpensive DBU and dimethylsulfate or by Mitsunobu reaction [6] of the activated nitrogen, and 3) S_N2 -type saponification using LiI in boiling ethyl acetate to avoid racemization observed with LiOH hydrolysis (Fig. 1).

Table 1. Synthesis of *N^α*-methyl-*N^α*-*o*NBS amino acids (*o*NBS-MeXaa-OH)

Xaa	Yield ^a (%)	Xaa	Yield ^a (%)	Xaa	Yield ^a (%)
Phe	91	Lys(Boc)	88	Tyr(tBu)	82
Ile	79	Arg(Pbf)	91	Ser(tBu)	75
Glu(tBu)	80	Gln(Trt)	85	Thr(tBu)	81
Asp(tBu)	73	Asn(Trt)	89	His(Trt)	24
Met	75	Trp	92	Cys(Trt)	22

^a Overall yield of the three-step procedure.

Commonly used amino acids in Fmoc-SPPS were N-methylated using the described procedure and obtained in good yields (Table 1). The described procedure allows the preparation of *N*^α-methyl-*N*^α-*o*NBS α-amino acids in a very short period of time and without any extensive purification. These *N*-methylamino acids can be directly used in Fmoc-SPPS using TBTU/HOBt and collidine as coupling mixture.

We were also interested in optimizing every step of the procedure described by Miller and Scanlan for N-methylation on solid support with respect to time and economy. Indeed, the whole procedure is done in 3 hrs with solvent changes and can be time-consuming when peptide libraries are being synthesized. Therefore, every step of the three-step procedure described by Miller and Scanlan [5] was investigated on a trityl-resin-bound dipeptide (NH₂-Phe-Leu-TCP-resin) in different solvent versus time needed for complete conversion. Investigation of the first step revealed that complete *o*-NBS protection is achieved in 15 min in NMP with *o*NBS-Cl (4 eq) and collidine (10 eq). The N-methylation step was improved by using DBU (instead of the very expensive MTBD) followed by dimethylsulfate in NMP and was achieved in 10 min (2 x 5 min) (Fig. 2). N-Methylation under Mitsunobu conditions was also investigated and full conversion was observed after only 10 min. Finally, complete removal of the *o*NBS protecting group was achieved in 5 min with mercaptoethanol and DBU in NMP.

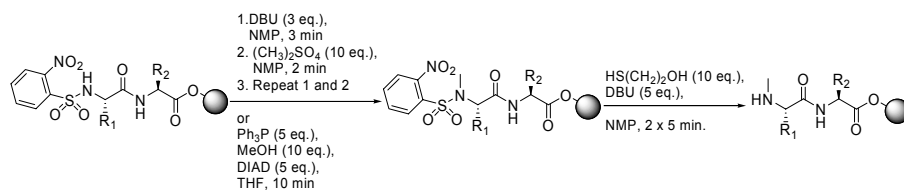


Fig. 2. Selective *N*-methylation of peptides on solid support.

To demonstrate its compatibility with commonly used amino acids in Fmoc-SPPS (Xaa in Table 1), the optimized procedure was applied to TCP resin-bound dipeptide (H-Xaa-Leu-TCP) containing these amino acids. Highly pure *N*-methylated dipeptides (H-MeXaa-Leu-OH) were obtained in every case when the optimized procedure was applied.

Both described procedures are compatible with Fmoc-SPPS conditions and protection groups and can be applied to commonly used amino acids. They allow a rapid synthesis of *N*-methyl peptides using Fmoc-SPPS.

Acknowledgments

E.B. thanks the Alexander von Humboldt Foundation for a Postdoctoral Fellowship.

References

1. Gilon, C., *et al.* In *Houben-Weyl Methods of Organic Chemistry, Synthesis of Peptides and Peptidomimetics*, Vol E22C, Georg Thieme Verlag, Stuttgart, Germany, pp. 215-271 (2002).
2. Dechansreiter, M. A., Planker, E., Mathä, B., *et al.* *J. Med. Chem.* **42**, 3033-3040 (1999).
3. Rajeswaran, W. J., Hocart S. J. and Murphy, W. A. *J. Med. Chem.*, **44**, 1305-1311 and 1416-1421 (2001).
4. Mazur, R. H., James, P.A., *et al.* *J. Med. Chem.* **23**, 758-763 (1980).
5. Miller, S. C. and Scanlan, T. S. *J. Am. Chem. Soc.* **119**, 2301-2302 (1997).
6. Yang, L. and Chiu, K. *Tetrahedron Lett.* **38**, 7307-7307 (1997).

The “*O*-Acyl Isopeptide Method” for the Synthesis of Alzheimer’s Disease-Related Amyloid β Peptide (A β) 1–42

Youhei Sohma, Maiko Kimura, Yousuke Chiyomori, Yoshio Hayashi, Atsuhiko Taniguchi, Masato Sasaki, Tooru Kimura and Yoshiaki Kiso

Department of Medicinal Chemistry, Center for Frontier Research in Medicinal Science, 21st Century COE Program, Kyoto Pharmaceutical University, Kyoto 607-8412, Japan

Introduction

Many studies using synthetic A β 1–42 have been carried out to clarify the involvement of A β 1–42 in Alzheimer’s disease (AD). However, the pathological self-assembly of A β 1–42 in amyloid plaque formation, a currently unexplained process, is very difficult to demonstrate *in vitro* due to its uncontrolled polymerization. For example, synthesized A β 1–42 already contains variable oligomeric forms [1], as A β 1–42 undergoes aggregation in an aqueous TFA–acetonitrile solution used in HPLC purification. Additionally, the A β 1–42 monomer easily forms an aggregate even in a standard storage solution such as dimethylsulfoxide (DMSO) [2]. The highly agglutinative property of A β 1–42 also results in synthetic difficulties with this peptide, a so-called “difficult sequence-containing peptide” [3].

To solve these problems, based on the “*O*-acyl isopeptide method” [4], we have developed a novel water-soluble isopeptide of wild-type A β 1–42, “26-*O*-acyl isoA β 1–42 (26-AIA β 42)” (Fig. 1) [5].

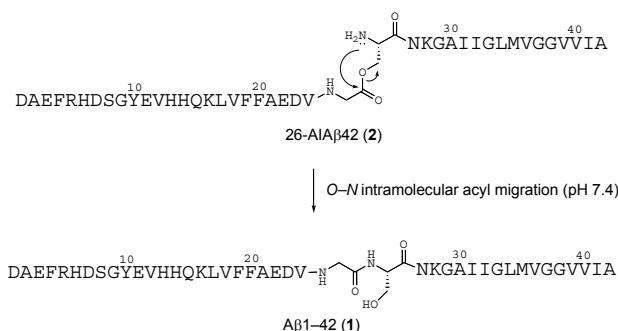
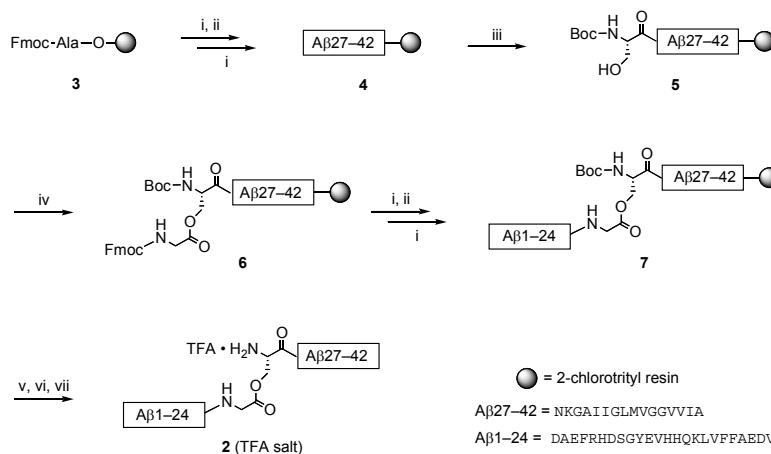


Fig. 1. “*O*-Acyl isopeptide method” for the efficient preparation of A β 1–42: The production of A β 1–42 (1) via *O*-N intramolecular acyl migration of 26-AIA β 42 (2).

Results and Discussion

The synthetic scheme of 26-AIA β 42 (2), based on the *O*-acyl isopeptide method, is depicted in Scheme 1. Protected 26-AIA β 42 peptide resin (7) was synthesized using 2-chlorotrityl chloride resin with minimum side reactions, and deprotected crude 26-AIA β 42 (2) was easily purified by HPLC due to its relatively good purity and narrow elution with reasonable water-solubility. In the use of NovaSyn[®]TGA resin, the ester bond between Gly²⁵ and Ser²⁶ was significantly cleaved by the treatment of TFA-containing cocktail in the final deprotection. On the other hand, we confirmed that the esterification of the β -hydroxy group of Ser²⁶ in 5 with Fmoc-Gly-OH



Scheme 1. Reagents and conditions: i, 20% piperidine/DMF, 20 min; ii, Fmoc-AA-OH (2.5 eq), DIPCDI (2.5 eq), HOBt (2.5 eq), DMF, 2 h; iii, Boc-Ser-OH (2.5 eq), DIPCDI (2.5 eq), HOBt (2.5 eq), DMF, 2 h; iv, Fmoc-Gly-OH (3.0 eq), DIPCDI (3.0 eq), DMAP (0.2 eq), CH_2Cl_2 , 16 h \times 2; v, TFA-*m*-cresol-thioanisole- H_2O (92.5:2.5:2.5:2.5), 90 min; vi, NH_4I (20 eq), dimethylsulfide (20 eq), TFA: H_2O (2:1), 60 min, 0°C ; vii, preparative HPLC (a linear gradient of CH_3CN in 0.1% aqueous TFA).

completed on the solid support, since the major product deprotected from peptide-resin **6** by TFA corresponds to *O*-acyl isoA β 25-42, and A β 26-42, which corresponds to the unreacted component, was not detected. In addition, another possible by-product with Fmoc-Gly-Gly sequence caused by elimination of the Fmoc group of **6** by DMAP during the reaction was not detected in the deprotected sample of peptide-resin **6**.

The isopeptide **2** exhibited 100-fold higher water solubility than A β 1-42. Interestingly, as a slight modification of the peptide chain by inserting one ester bond drastically increased the solubility of the insoluble original peptide with 42 residues, this suggests that *O*-acyl isopeptides totally destroy the secondary structures responsible for the insolubility of the original peptide. In addition, *O*-*N* intramolecular acyl migration reaction to the original A β 1-42 occurred quickly with no side reaction under physiological conditions (pH 7.4), while 26-AIA β 42 was stable under storage conditions. Thus, this isopeptide method would provide a novel biological evaluation system in AD research, in which 26-AIA β 42 can be stored in a solubilized form before use and rapidly produces intact A β 1-42 in situ during biological experiments.

References

1. Soto, C., *et al. Neurosci. Lett.* **200**, 105-108 (1995).
2. Stine, W. B. Jr, *et al. J. Biol. Chem.* **278**, 11612-11622 (2003).
3. Kim, Y. S., *et al. J. Org. Chem.* **69**, 7776-7778 (2004).
4. (a) Sohma, Y., *et al. In Peptide Revolution: Genomics, Proteomics & Therapeutics Proceedings of the 18th APS* (Chorev, M. and Sawyer, T. K., eds.), Kluwer Academic, Netherlands, pp. 67-68 (2003); (b) Sohma, Y., *et al. Chem. Commun.* 124-125 (2004).
5. (a) Sohma, Y., *et al. Tetrahedron Lett.* **45**, 5965-5968 (2004); (b) Sohma, Y., *et al. Biopolymers* **76**, 344-356 (2004); (c) Sohma, Y., *et al. J. Peptide Sci.* **11**, 441-451 (2005); (d) Sohma, Y., *et al. Bioorg. Med. Chem.* **13**, 6167-6174 (2005).

The “O-Acyl Isopeptide Method” for the Synthesis of Difficult Sequence-Containing Peptides: Application to the Synthesis of Alzheimer’s Disease-Related Amyloid β Peptide (Aβ) 1–42 Mutants

Yousuke Chiyomori, Youhei Sohma, Maiko Kimura, Yoshio Hayashi, Fukue Fukao, Atsuhiko Taniguchi, Tooru Kimura and Yoshiaki Kiso

Department of Medicinal Chemistry, Center for Frontier Research in Medicinal Science, 21st Century COE Program, Kyoto Pharmaceutical University, Kyoto 607-8412, Japan

Introduction

The pathological self-assembly of Aβ1–42 in amyloid plaque formation, a currently unexplained process in Alzheimer’s disease (AD), is very difficult to demonstrate *in vitro* due to its uncontrolled polymerization [1]. An *in situ* system that prepares an intact monomer Aβ1–42 under physiological experimental conditions while

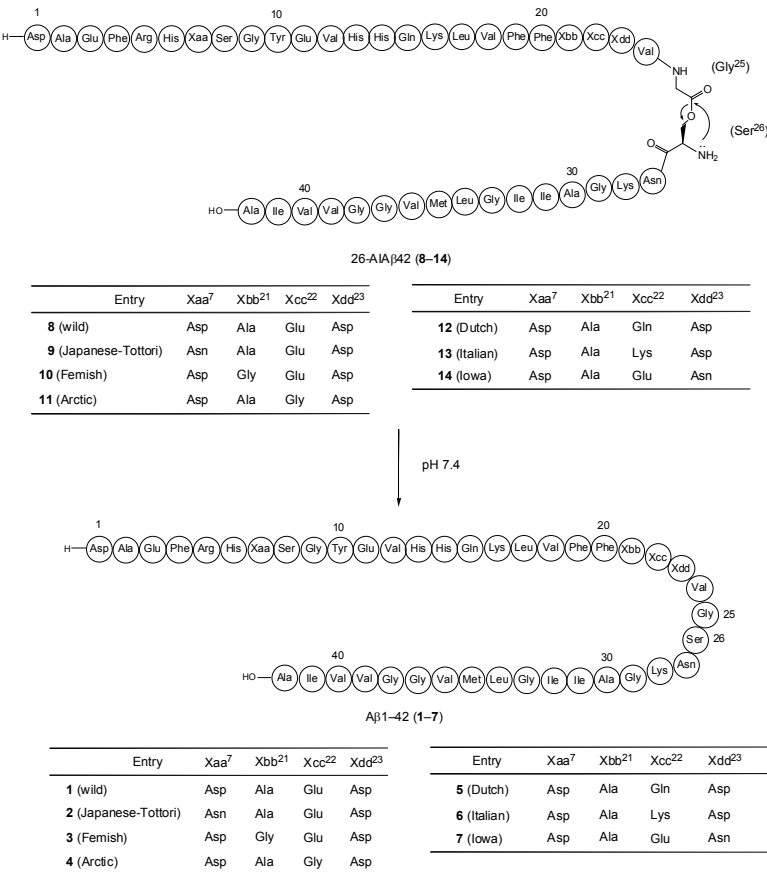


Fig. 1. “O-Acyl isopeptide method” for the efficient preparation of Aβ1–42 (1–7): The production of Aβ1–42 (1–7) via O–N intramolecular acyl migration of 26-AIAβ42 (8–14).

suppressing the spontaneous self-assembly of A β 1–42 under storage conditions would be advantageous in understanding the inherent pathological functions of agglutinative A β 1–42 in AD. For this purpose, based on the “*O*-acyl isopeptide method”, we developed a novel water-soluble isopeptide of wild-type A β 1–42, “26-*O*-acyl isoA β 1–42 (26-AIA β 42, **8**) [2]. Herein, we expand the “*O*-acyl isopeptide method” to the synthesis of novel water-soluble *O*-acyl isopeptides (**9**–**14**) of A β 1–42 mutants such as Japanese-Tottori-(D7N, **2**), Flemish-(A21G, **3**), Arctic- (E22G, **4**), Dutch-(E22Q, **5**), Italian-(E22K, **6**), and Iowa-type (D23N, **7**) (Fig. 1) [3].

Results and Discussion

The water solubility of synthesized mutant 26-AIA β 42s (TFA salt) was 15.0 (**8**), 4.4 (**9**), 18.3 (**10**), 5.1 (**11**), 14.5 (**12**), 16.2 (**13**) and 8.1 mg mL⁻¹ (**14**), higher than those in the corresponding mutant A β 1–42s (**1**: 0.14, **2**: 0.15, **3**: 0.95, **4**: 0.40, **5**: 0.93, **6**: 8.7, and **7**: 2.2 mg mL⁻¹). In addition, the HPLC analysis of isopeptides exhibited quite a sharp peak even in the slow gradient system (25–55% CH₃CN, 60 min), while the corresponding A β 1–42 was eluted as a broad peak under the same elution conditions as wild-type A β 1–42 **1**. These results indicate that the highly insoluble and agglutinative nature of A β 1–42 based on its secondary structure was suppressed by only one insertion of the isopeptide structure with a branched ester bond. On the other hand, Dutch-type 26-AIA β 42 **12** was quantitatively converted to the corresponding A β 1–42 **5** in phosphate-buffered saline (PBS, pH 7.4) at 37°C with a half-life of approximately 1 min with no side reaction such as hydrolysis of the ester bond, and migration was completed after 30 min (Fig. 2), while being stable under storage conditions. Other mutant isopeptides (**9**–**11**, **13** and **14**) were also quantitatively converted to each A β 1–42 mutant at pH 7.4 (37°C) with no significant difference in migration rate. These results suggest that this method provides a new system in AD-related research, in which 26-AIA β 42 can be stored in a solubilized form and rapidly produces intact A β 1–42 with no byproduct formation *in situ* during biological experiments, which is useful for investigating the biological function of A β 1–42 mutants.

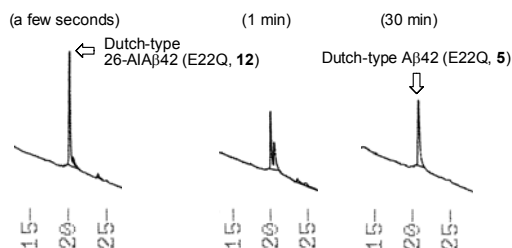


Fig. 2. Periodical HPLC profiles of the conversion of Dutch-type 26-AIA β 42 (**12**) to corresponding A β 1–42 (**5**) in PBS (pH 7.4) at 37°C.

References

1. (a) Soto, C., *et al. Neurosci. Lett.* **200**, 105–108 (1995); (b) Stine, W. B. Jr., *et al. J. Biol. Chem.* **278**, 11612–11622 (2003).
2. (a) Sohma, Y., *et al. In Peptide Revolution: Genomics, Proteomics & Therapeutics Proceedings of the 18th APS* (Chorev, M. and Sawyer, T. K., eds.), Kluwer Academic, Netherlands, pp. 67–68 (2003); (b) Sohma, Y., *et al. Chem. Commun.* 124–125 (2004); (c) Sohma, Y., *et al. Tetrahedron Lett.* **45**, 5965–5968 (2004); (d) Sohma, Y., *et al. Biopolymers* **76**, 344–356 (2004). (e) Sohma, Y., *et al. J. Peptide Sci.* **11**, 441–451 (2005).
3. Sohma, Y., *et al. Bioorg. Med. Chem.* **13**, 6167–6174 (2005).

Enhancing Atom Economy of SPS: Recoverable and Reusable Building Blocks for Depsipeptide Synthesis

Jan Spengler^{1,2}, Javier Ruíz-Rodríguez¹, Tommaso Cupido¹, Klaus Burger² and Fernando Albericio^{1,3}

¹Barcelona Biomedical Research Institute, Barcelona Science Park, University of Barcelona, 08028 Barcelona, Spain; ²University Leipzig, Department of Organic Chemistry, 04103 Leipzig, German; ³University of Barcelona, Department of Organic Chemistry, 08028-Barcelona, Spain

Introduction

Solid phase synthesis (SPS) is the strategy of choice for the preparation of small and medium size peptides because nearly every sequence can be assembled with standard reaction procedures. SPS reaction cycles are generally much faster than analogous solution syntheses. In order to drive each reaction to completion, a four- to ten-fold excess of reagents is typically added to the resin (Fig. 1). For laboratory scale runs, this excess material is normally non-recoverable and non-reusable. Consequently, SPS may be excluded for reactions involving very expensive monomers for purely economic reasons, regardless of its utility.

A potentially valuable approach to overcome this drawback may be the use of bidentate protecting/activating groups, that form with amino acids and other α -functionalized carboxylic acids storable, 1-carboxyl-activated and α -functionality protected derivatives. Because carboxyl-activation is an intrinsic property of such molecules, ideally no activation reagents and additives should be required for solid phase couplings. Added excess should be recoverable and reusable. We proofed this concept on hexafluoroacetone (HFA) - protected/activated α -amino, α -hydroxy and α -mercapto acids, which are easily obtained and remarkably stable, in order to evaluate their potential to enhance atom economy [1] of SPS.

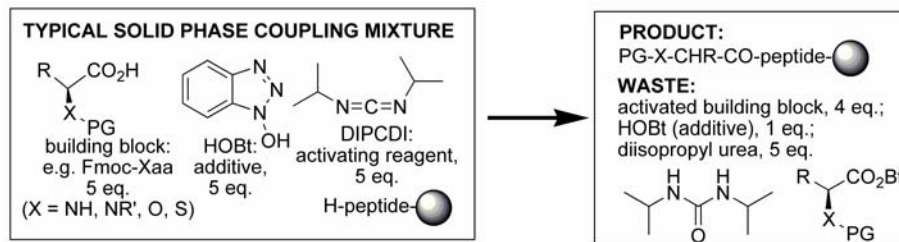


Fig. 1. Conventional solid phase protocols has a poor atom economy.

Results and Discussion

HFA has been demonstrated by our group [K. Burger et al.] to be a versatile bidentate protecting/activating reagent for α -amino, α -hydroxy, and α -mercapto acids. It was used for the stereoconservative synthesis of esters, amides, peptides, azapeptides and hydroxamic acids in solution.

HFA-hydroxy acids react with solid-phase anchored amino acids to yield the desired depsipeptides. Racemization can be suppressed by choice of suitable solvents, as demonstrated for the coupling of HFA-derivative of mandelic acid in

THF [2]. In case of citramalic acid as sterically hindered hydroxy acid (additional C^α-methyl group), the nucleophilic ring opening took place much slower (3 days), but also a HPLC-pure product was obtained. With HFA-amino acids, such clean reaction on solid phase was found only for HFA-Tic (HFA-tetrahydroisochinolinic acid), whereas HFA-Leu, HFA-Pro and HFA-Phe gave some amount of peptide in complex product mixtures [3]. Similar reaction behavior was found for HFA-2-mercaptosuccinic acid as member of α-mercapto acids. HFA-protected *N*-methyl amino acids do not react at all, even if the reaction was run in polar solvents such as DMSO and by addition of DMAP as acylating catalyst.

Once HFA-hydroxy acids were evaluated as suitable building blocks for solid phase couplings, it was demonstrated that the added excess can be recovered and reused conveniently. H-Tyr(OtBu)-Rink-MBHA-resin was treated with a 10-fold excess of HFA-D-phenyllactic acid in THF. After the reaction was complete (ninhydrin-test), the resin was filtered off; the filtrate was evaporated, re-dissolved and reused 4 more times. After the 5th coupling cycle, ¹⁹F NMR spectroscopy showed the signal of HFA-hydrate formed as by-product in each coupling turn. HFA-D-Phlac and HFA-hydrate appeared approximately with the same integration, indicating a consumption of ca. 50% of the HFA-compound in agreement with the theoretically estimated amount. The presence of HFA-hydrate did not show any negative influence on subsequent couplings. All 5 samples of product showed a HPLC purity of 98-99 % with amounts of the diastereomer H-L-Phlac-Tyr-NH₂ less than 1 %.

From these findings we conclude that the use of HFA-hydroxy acids is a valuable strategy for incorporation of precious and/or laborious α-hydroxy acids in depsipeptides on solid phase, applicable in laboratory scale or bulk production.

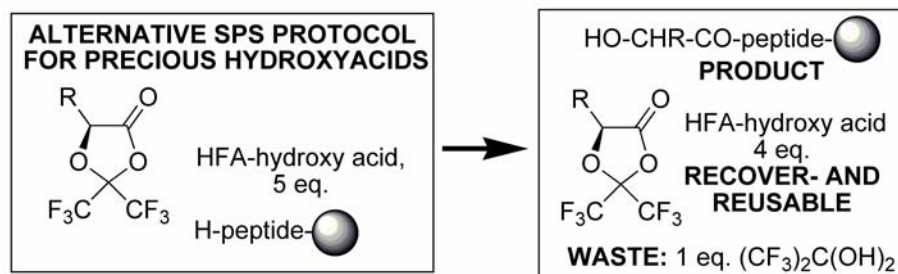


Fig. 2. Enhancement of atom economy by use of HFA-building blocks.

Acknowledgments

JS thanks the VW Foundation for providing a grant for this project. This work was partially supported by Generalitat de Catalunya [Grups Consolidats (2001 SGR 0047) and CERBA], Ministerio de Ciencia y Tecnología (BQU 2003-00089), Pharma Mar Ltd., and Barcelona Science Park.

References

1. Trost, B. M. *Science* **254**, 1471-1477 (1991).
2. Albericio, F., Burger, K., Ruíz-Rodríguez, J. and Spengler, J. *Org. Lett.* **7**, 597-600 (2005).
3. Albericio, F., Burger, K., Cupido, T., Ruíz-Rodríguez, J. and Spengler, J. *Arkivoc* **vi**, 191-199 (2005).

1-N-Methyl-Histidine as a Side-Product in Backbone N-Methylated PTH Analogs

Zhanna Potetinova and Gordon E. Willick

¹Institute for Biological Sciences, National Research Council, Ottawa, ON K1A 0R, Canada

Introduction

A backbone methylation scan is a useful tool for revealing peptide hormone interactions with a receptor [1] or providing subtle modifications that change receptor sub-type specificities [2]. N^α-methyl groups can be introduced into peptides either by incorporation of the suitably-protected N^α-methyl amino acid or by introduction during SPPS, e.g., by the method of Miller *et al* [3] for Fmoc-protocol SPPS. In this method, a temporary protecting group is introduced after removal of the α-Fmoc group and the secondary amine is then methylated. The group is then selectively removed and synthesis continued. In the course of preparing a set of N^α-Me PTH(1-14) analogs, we noticed the presence of a difficult to remove contaminant with MS +14 of the expected one. The contaminant was not present in analogs synthesized via coupling with a Fmoc-N^α-Me amino acid or where the point of methylation was to the C-terminus of the single His. Investigation of the contaminant by MS-MS and NMR revealed the presence of an unexpected methylation of the histidine ring.

Results and Discussion

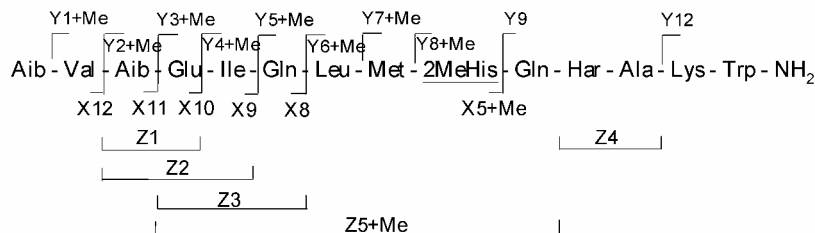
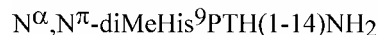
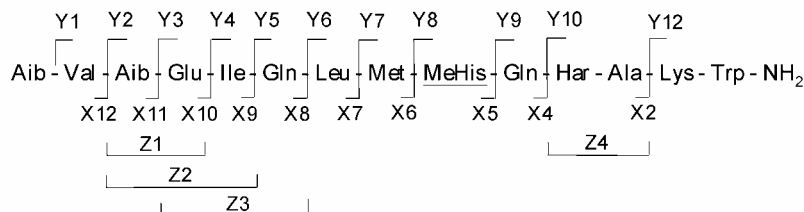


Fig. 1. MS-MS of expected single and side-product, double methylated PTH(1-14) [4].

A side-product with MS +14 was present as about 23% of the total product. The isolated double methylated product was subjected to MS-MS and compared to the expected methylated product (Fig. 1). The second methyl group was thus found to be on the His9 residue.

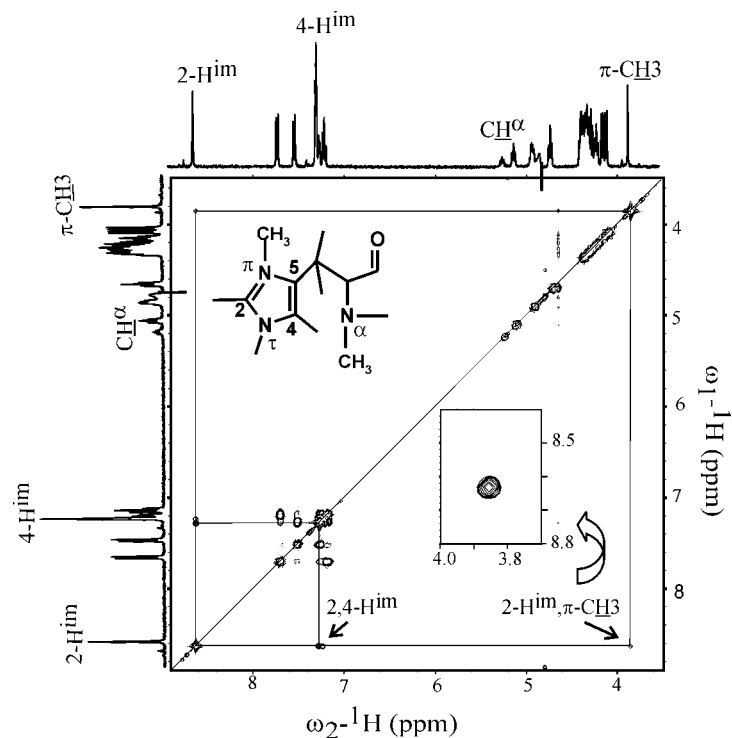


Fig. 2. 400 MHz ^1H COSY spectrum of double methylated $N^\alpha\text{-MeHis}^9\text{PTH}(1\text{-}14)\text{NH}_2$.

The experimental two-dimensional NMR data showed that the additional methylation was on the π -N position of the His ring (Fig. 2). A weak signal was detected at $\delta \approx (3.8, 8.6)$ and $\delta \approx (8.6, 3.8)$ on the COSY and NOESY spectra. These cross-peaks indicate an interaction between proton 2-CH and three protons 1-N-CH₃ of the His ring. For reasons of clarity only two squares have been drawn in, linking the signals of His ring. The second methyl group was apparently introduced as a result of displacement of the protecting trityl group. The formation of the double methylated side-product occurs only sometimes and can be avoided by using a preformed α -methyl His during SPPS or introduction of the remaining sequence by ligation of a fully protected peptide.

References

1. Barbier, J. R., *et al.* *J. Biol. Chem.* **280**, 23771-23777 (2005).
2. Erchegeyi, J., *et al.* *J. Med. Chem.* **48**, 507-514 (2005).
3. Miller, S. C. and Scanlan, T. S. *J. Am. Chem. Soc.* **119**, 2301-2302 (1997).
4. Shimizu, N., *et al.* *J. Bone Miner. Res.* **19**, 2078-2086 (2005).

Combinatorial Approach in the Synthesis of a Small Library of β -Turn Structures Based on Thiazolidine Moiety

Alfonso Carotenuto, Teresa Lama, Orazio Mazzoni, Pietro Campiglia,
 Ettore Novellino, Alessia Bertamino, Maria V. Diurno, Isabel Gomez-
 Monterrey, Luigia Auriemma and Paolo Grieco

Dip. Chimica Farmaceutica e Toss., University of Naples-Federico II-Italy

Introduction

β -Turns are known to be common structural motifs comprising up to 25% of all residues in folded proteins and peptides [1]. β -Turns also appear to play important roles in stabilizing tertiary structures, initiating folding and facilitating intramolecular recognition. Recently, as a part of our research work toward the synthesis of new small constrained mimetics of turn structure [2], we have described solution reactions to produce β -turn mimetics based on thiazolidine moiety (structure A, Fig. 1). In this communication we report the synthesis of two small libraries of β -turn mimetics in solid phase (A1 and A2) and the conformational analysis by molecular modeling of a model peptide.

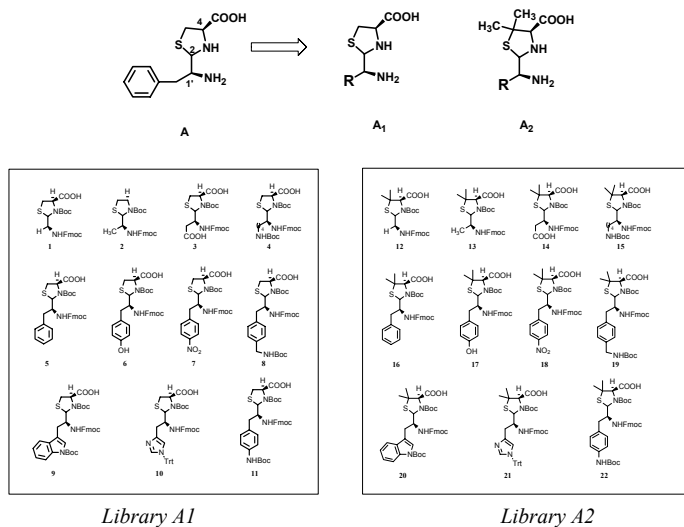
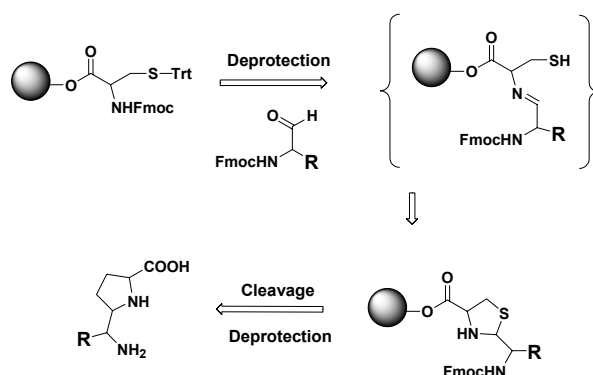


Fig. 1. β -turn mimetics based on thiazolidine moiety.

Results and Discussion

Chemistry: The dipeptide mimetics were synthesized in solid phase from the appropriate amino acid (Cys or Pen) loaded to Wang resin and different Fmoc-(Aa)-H [3], using Fmoc chemistry (Scheme 1). After cleavage, samples were analysed by LC/MS, which confirmed the mass of the expected materials with purity greater than 98%, and molecular weights were confirmed by HR-MS.



Scheme 1. Synthesis of thiazolidine mimetics.

Conformational Studies: The ability of the synthesized pseudopeptide analogs to adopt a β -turn-like conformation was evaluated by molecular modeling studies. Preliminary data obtained from the pseudotetrapeptide with two Ala residues in position 1 and 4, and the pseudodipeptide residue (6) in position 2 and 3, suggest that the absolute configuration of C-2 of the thiazolidine residue can affect the backbone conformation, which will ultimately influence the overall structure. In fact, only the (*R*) configuration at C-2 can induce a β -turn structure.

The products, obtained with good overall yields (55-60%), are somewhat flexible and the preliminary conformational analysis data indicate that the (*R*) configuration at C-2 atom of thiazolidine residue can induce a β -turn motif.

Acknowledgments

The LC-MS and ^1H NMR spectral data were provided by Centro di Ricerca Interdipartimentale di Analisi Strumentale Università degli Studi di Napoli Federico II. The assistance of the staff is gratefully appreciated.

References

1. Rose, G. D., Gerasch, I. M. and Smith, J. A. *Adv. Protein. Chem.* **37**, 1-109 (1985)
2. Grieco, P., Campiglia, P., Gomez-Monterrey I. and Novellino, E. *Tetrahedron Lett.* **43**, 1197-1199 (2002).
3. Meyer, J. P., Davis, P., Lee, K. B., Porreca, F., Yamamura, K. and Hruby, V. J. *J. Med. Chem.* **38**, 3462-3468 (1995).

Solid-Phase Peptide Synthesis Using ChemMatrix[®], a Polyethyleneglycol (PEG)-based Solid

Fernando Albericio¹, Nuria Bayo¹, Silvia A. Camperi², Osvaldo Cascone², Simon Côté³, Luis J. Cruz¹, Abdelhamid Errachid¹, Robert Furic³, Fayna García-Martín¹, Yesica García-Ramos¹, Nancy B. Iannucci², Mariela M. Marani², Mateu Pla-Roca¹, Martina Quintanar-Audelo¹, Josep Samitier¹ and Judit Tulla-Puche¹

¹Barcelona Science Park, University of Barcelona, Barcelona, Spain; ²UBA, Buenos Aires, Argentina; ³Matrix Innovation Inc., Montreal, Quebec, Canada

Introduction

Polystyrene (PS) and PEG-PS resins are currently the most widely used supports for SPS. Although large numbers of peptides and small molecules can be prepared using these supports, there is an ever-increasing need for resins that are suited to more universal applications. In this regard, amphiphilic matrices containing only PEG are very attractive. ChemMatrix[®] (Fig. 1), a novel 100% PEG-based resin, is herein introduced [1].

ChemMatrix[®] exhibits good loading and is a user friendly resin. It shows excellent performance for the preparation of hydrophobic peptides as well as for one-bead-one-peptide libraries. Nanotechnologic techniques like FIB (Focused Ion Beam) will be used for the bead-by-bead characterization of ChemMatrix[®].

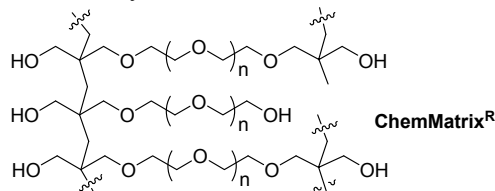


Fig. 1. The ChemMatrix[®] Resin.

Results and Discussion

PEG ChemMatrix[®] (Fig. 2) presents the following properties:

i) *Higher chemical stability.* ChemMatrix[®] is made exclusively from primary ether bonds which show high chemical stability. This matrix is therefore much more stable than other commercial amphiphilic resins.

ii) *Higher loadings.* The standard loadings of commercial amphiphilic resins are mainly from 0.2 up to 0.4 mmol/g. With an improved amphiphilicity, ChemMatrix[®] has loadings between 0.8 to 1.0 mmol/g, which is up to 3 times the loading of other PEG resins.

iii) *Purer crude products.* ChemMatrix[®] has been compared with several other types of resins for the synthesis of the *retroacyl carrier* (74-65), a 10-amino acid peptide, which, for decades, has been a difficult peptide sequence. While the crude purity varied between 9% and 63% with other commercial resins, ChemMatrix[®] generated a constant purity of 92%.

iv) *Free flowing.* ChemMatrix[®] is a user friendly resin because of its free flowing form once dried. The product is easily weighed and transferred with minimum

v) *Swelling*. ChemMatrix[®] allows the use of almost any kind of solvent, even water. The standard solvents used for polystyrene, such as dichloromethane and THF, are also highly compatible with this resin. Several amphiphilic resins show good swelling, but their loading and/or the mechanical stability are affected. Usually, these resins become tacky and hard to handle once solvated. ChemMatrix[®] is easily filtered and washed with almost any solvent.

ChemMatrix[®] resin is a superior support for the solid-phase synthesis of hydrophobic and highly structured peptides to polystyrene resins. In this respect, in contrast to the latter, complex poly-arginine sequences of 24 residues and an artificial decameric model peptide of repetitive sequence were successfully synthesized using this PEG. Furthermore, Bacuma, a synthetic vaccine of 38 residues, was synthesized using the ChemMatrix[®] whereas the peptide was not obtained using the polystyrene resin.

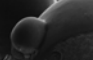


Figure 10 shows a spherical microcapsule with a textured surface, likely the polyurethane-coated microcapsule described in the text. The image is a secondary electron micrograph (SEM) showing the morphology of the microcapsule.

Acknowledgments

References

1. Côte, S. *PCT Int. Appl.* WO2005012277 A1 (2005).
2. Camperi, S. A., Marani, M. M., Ianucci, N. B., Côte, S., Albericio, F. and Cascone, O. *Tetrahedron Lett.* **46**, 1561-1564 (2005).

***p*-Nitrobenzyloxycarbonyl (*p*NZ) as an Alternative to Fmoc for the Protection of Amines in Solid-Phase Peptide Synthesis**

Albert Isidro-Llobet¹, Pilar E. López², Judit Guasch-Camell¹, Mercedes Álvarez^{1,3} and Fernando Albericio^{1,4}

¹Barcelona Biomedical Research Institute, Barcelona Scientific Park, University of Barcelona, Josep Samitier 1-5, 08028, Barcelona, Spain; ²Department of Organic Chemistry, University of Granada, Spain; ³Laboratory of Organic Chemistry, Faculty of Pharmacy, University of Barcelona, 08028 Barcelona, Spain; ⁴Department of Organic Chemistry, University of Barcelona, 08028 Barcelona, Spain

Introduction

The majority of peptides produced on solid phase are prepared using the fluorenylmethoxycarbonyl (Fmoc)-*tert*-butyl (*t*Bu) orthogonal protection strategy [1-3]. However, the synthesis of cyclic and branched peptides may require other protecting groups orthogonal to Fmoc and *t*Bu.

Furthermore, the conditions used to remove Fmoc are incompatible with several sequences. The main drawbacks of Fmoc chemistry are the basic and nucleophilic properties of both piperidine and the free amine obtained after Fmoc removal, often leading to side reactions such as diketopiperazine formation, aspartimide formation and the undesired removal of the α -Fmoc group during side chain deprotection of ornithine and lysine.

We report here the use of the *p*-nitrobenzyloxycarbonyl (*p*NZ) group (Fig. 1), which is removed with SnCl₂ in nearly neutral conditions, as an alternative to Fmoc for the temporary protection of amines [4].

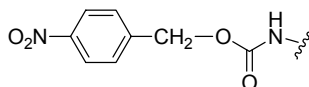


Fig. 1. *p*NZ group.

Results and Discussion

*p*NZ protected amino acids prepared using the azide method [5] were obtained as white solids in relatively high yields (71-94%) and purity, and characterized by HPLC, IR, ¹H/¹³C- NMR and HRMS.

*p*NZ removal is based on reduction of the nitro group, which gives the *p*-aminobenzyloxycarbonyl derivative, followed by spontaneous collapse *via* 1,6-electron pair shift to afford the quinonimine methide and the carbamic acid. Finally, the carbamic acid decomposes to the corresponding free amino acid [6]. *p*NZ removal conditions on solid phase were optimized using the model peptide *p*NZ-Phe-Gly-Gly-Leu-NH-Rink polystyrene resin. The best conditions obtained were: 6M SnCl₂, 1.6 mM HCl in DMF (2 x 30 min) at rt. or (2 x 10 min) at 50°C.

Use of pNZ to avoid side reactions typical to Fmoc chemistry: Aspartimide formation during Fmoc chemistry occurs after aspartic acid residues as a result of the repetitive piperidine treatments used for chain elongation [1,7]. The use of piperidine, and hence the side reaction, can be circumvented by using *p*NZ amino acids from the Asp residue to the *N*-terminus. This was demonstrated using the

sequence H-Ala-Orn(Boc)-Asp(tBu)-Gly-Tyr(tBu)-Ile-NH-Rink polystyrene resin, which is highly prone to aspartimide formation.

Diketopiperazine (DKP) formation is another common side reaction in Fmoc chemistry and stems from the nucleophilicity of the deprotonated α -amino group obtained after removal of the Fmoc group of the second amino acid of the peptide chain [1,8]. This side reaction is also sequence dependent (e.g., H-D-Val-L-Pro-OH gives 100% DKP). We have demonstrated that *p*NZ protection of the second amino acid of the peptide (in this case D-Val) does not lead to DKP formation, owing to the use of catalytic amounts of HCl during *p*NZ removal, which leaves the amino group protonated. Using catalytic HCl for *p*NZ side-chain deprotection of ornithine and lysine also prevents undesired removal of the α -Fmoc group. In both cases the next amino acid is coupled by *in situ* neutralization.

Use of pNZ in the orthogonal solid phase synthesis of complex peptides: Furthermore, the *p*NZ group can be used in strategies that require multiple orthogonal protecting groups. Thus, two derivatives of the anti-tumor cyclodepsipeptide Kahalalide F were synthesized using a tetraorthogonal protection scheme involving *p*NZ, Fmoc and Alloc protecting groups on a chlorotrityl resin.

Acknowledgments

This work was partially supported by CICYT (BQU 2003-00089), the Generalitat de Catalunya (Grup Consolidat and Centre de Referència en Biotecnologia), and the Barcelona Science Park. AI. thanks the Generalitat de Catalunya for a predoctoral fellowship.

References

1. Lloyd-Williams, P., Albericio, F. and Giralt, E. *Chemical Approaches to the Synthesis of Peptides and Proteins*. CRC: Boca Raton, FL (USA) (1997).
2. Chan, W. C. and White, P. D., eds. *Fmoc Solid Phase Peptide Synthesis*. Oxford University Press: Oxford (UK) (2000).
3. Barany, G. and Albericio, F. *J. Am. Chem. Soc.*, **107**, 4936 (1985).
4. (a) Carpenter, F. H. and Gish, D. T. *J. Am. Chem. Soc.* **74**, 3818-3821 (1952); (b) Gish, D. T. and Carpenter, F. H. *J. Am. Chem. Soc.*, **75**, 950-952 (1953).
5. Cruz, L. J., Beteta, N. G., Ewenson, A. and Albericio, F. *Org. Proc. Res. Develop.* **8**, 920 (2004).
6. (a) Loubinoux, B. and Gerardin, P. *Tetrahedron Lett.* **32**, 351-354 (1991); (b) Griffin, R. J., Evers, E., Davison, R., Gibson, A. E., Layton, D. and Irwin, W. J. *J. Chem. Soc., Perkin Trans. 1*, 1205-1212 (1996).
7. Nicolás, E., Pedroso, E. and Giralt, E. *Tetrahedron Lett.* **30**, 497-500 (1989).
8. Pedroso, E., Grandas, A., de las Heras, X., Eritja, R. and Giralt, E. *Tetrahedron Lett.* **27**, 743-746 (1986).

Synthesis and NMR Analysis of CCR5 and CXCR4 Peptides Containing Tyrosine Sulfate

Tatsuya Inui¹, Patricia Cano-Sanchez¹, Boris Arshava¹, Inbal
Ayzenshtat¹, Jacob Anglister² and Fred Naider¹

¹Dept. of Chemistry, College of Staten Island, C.U.N.Y., Staten Island, NY 10314, U.S.A. and

²Dept. of Structural Biology, The Weizmann Institute of Science, Rehovot 76100, Israel.

Introduction

Entry of human immunodeficiency virus type 1 (HIV-1) into target cells is mediated by specific interactions between viral envelope glycoprotein gp120, and two host cell membrane proteins, CD4 and chemokine co-receptors CCR5 or CXCR4 [1]. CCR5, which binds macrophage inflammatory proteins 1 α and 1 β (MIP-1 α and MIP-1 β) and RANTES, is used by HIV-1 viruses (designated R5 viruses) that infect macrophages, while CXCR4, which binds the stromal cell-derived factor-1 (SDF-1) as sole ligand, is used by HIV-1 strains that infect T-cells (designated X4 viruses). The N-termini of both of these GPCR co-receptors contain tyrosine sulfate residues that are required for viral uptake. Recent studies indicated that the N-terminal peptides could bind to the gp120/CD4 complex and inhibit interaction of the virus with target cells [2]. Therefore the N-terminal peptides of CCR5 and CXCR4 can be therapeutic agents against AIDS and allergic reactions. Determination of the 3D structure is important as a first step to understand molecular basis of the interaction of these receptors and their ligands. The CCR5 peptide contains tyrosine sulfate at positions 10 and 14 whereas the CXCR4 peptide contains tyrosine sulfate at position 21. These sulfate groups are essential to the binding activity [3]. In this study, we report the efficient synthesis of sulfated peptides of CCR5 (1-27) and CXCR4 (1-38), and discuss preliminary results on the 3D structure of sulfated and unsulfated CCR5 (1-27) (Fig. 1).

[Tyr^{10, 14} (SO₃H), Ala²⁰]-CCR5 (1-27)
MDYQVSSPIY(SO₃H)DINY(SO₃H)YTSEPAQKINVKQ

[Tyr²¹ (SO₃H), Ala²⁸]-CXCR4 (1-38)
MEGISIYTSNDNYTEEMGSGDY(SO₃H)DSMKEPAFREENANFNK

Fig. 1. Sequences of [Tyr^{10, 14} (SO₃H), Ala²⁰]-CCR5 (1-27) and [Tyr²¹ (SO₃H), Ala²⁸]-CXCR4 (1-38)

Results and Discussion

The peptides were synthesized on a preloaded C1Trt resin at 0.05 mmol scale using double coupling and acetyl capping protocol based on FastMoc chemistry. The building block Fmoc-Tyr(SO₃Na) was used for incorporation of Tyr(SO₃H). To suppress the hydrolysis of sulfate group on the tyrosine during acid treatment, the cleavage condition of TFA-H₂O-TIS (90:5:5) at 4°C [4,5] was employed. RP-HPLC using acetonitrile-ammonium acetate solvent system separated the di-, mono- and unsulfated peptides completely (Fig. 2). After purification by RP-HPLC using this solvent system, the CCR5 (1-27) and CXCR4 (1-38) peptides were obtained on the yield of 7.5% and 8.0% from their crude peptides, respectively. Molecular weights were confirmed by ESI/MS (negative scan mode) (Fig. 3).

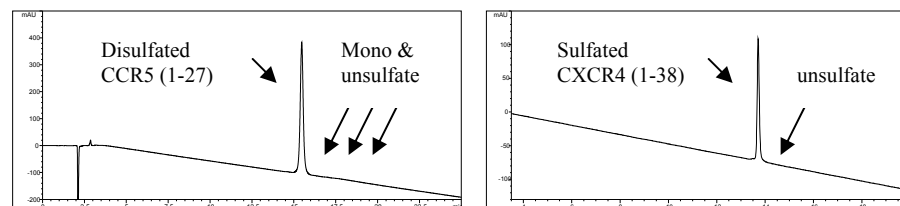


Fig. 2. HPLC profiles of the final products of CCR5 (1-27) (left) and CXCR4 (1-38) (right), Column: Zorbax extended C18 column, 4.5 x 250 mm, Elution: 10-40% acetonitrile in 0.1 M ammonium acetate (pH6.8) over 30 min at room temperature. Flow rate: 1ml/min, Detection: 220 nm.

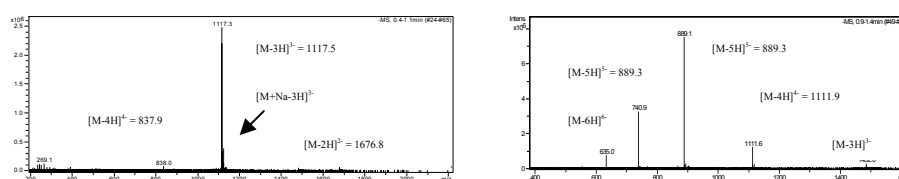


Fig. 3. Electron Spray Ionization Mass Spectra of CCR5 (1-27) (left) and CXCR4 (1-38) (right), CCR5 (1-27) and CXCR4 (1-38) gave the averaged mass of 3355.23 (Theoretical average mass is 3355.70) and 4451.76 (Theoretical average mass is 4451.77), respectively.

The 3D structure of disulfated and unsulfated forms of the CCR5 (1-27) is being determined using 2D NMR spectroscopy in water. Both CCR5 (1-27) peptides exhibited helical tendencies in the center of the peptides and this tendency was slightly increased upon tyrosine sulfation. A highly negative surface comprising two sulfated tyrosines (Y10, Y14) and two acidic amino acids (D11, E18) is formed in the sulfated peptide and may be crucial for its interaction with complementary domains on gp120 or CCR5 chemokines.

Acknowledgments

This work was supported by NIH grants GM 53329 and GM22086 and by a grant from the United States-Israel Binational Science Foundation.

References

1. Trkola, A., Dragic, T., Arthos, J., Binley, J. M., Olson, W. C., Allaway, G. P., Cheng-Mayer, C., Robinson, J., Maddon, P. J. and Moore, J. P. *Nature* **384**, 184-187 (1996).
2. Fazan, M., Vasileva, N., Schnitzler, C. E., Chung, S., Robinson, J., Gerard, N. P., Gerard, C., Choe, H. and Sodroski, J. *J. Biol. Chem.* **275**, 33516-33521 (2000).
3. Cormier, E. G., Persuh, M., Thompson, D. A., Lin, S. W., Sakmer, T. P., Plson, W. C. and Dragic, T. *Proc. Natl. Acad. Sci. USA* **97**, 5762-5767 (2000).
4. Yagami, T., Shiwa, S., Futaki, S. and Kitagawa, K. *Chem. Pharm. Bull. (Tokyo)* **41**, 376-380 (1993).
5. Kitagawa, K., Aida, C., Fujiwara, H., Yagami, T., Futaki, S., Kojire, M., Ida, J. and Inoue, K. *J. Org. Chem.* **66**, 1-10 (2001).

Steroid-Peptide Conjugates

Witold A. Neugebauer¹, Jérôme Côté¹, Audrey Fortier¹, Ghassan Bkaily², Levon Avedanian², Danielle Jaques² and Fernand Gobeil Jr.¹

¹Department of Pharmacology; ²Department of Anatomy and Cell Biology, Faculty of Medicine, Sherbrooke University, Sherbrooke, Québec, J1H 4N5 Canada

Introduction

The cholesterol molecule inserts itself in the membrane with the same orientation as the phospholipid molecules and has several functions in the membrane [1]. They immobilize the first few hydrocarbon groups of the phospholipid molecules, which makes the lipid bilayer less deformable and decreases its permeability to small water-soluble molecules. The steroid moiety conjugated to hormonal peptides at the site not responsible for its biological activity could become a delivering force to the molecule. Such conjugate could be driven by highly hydrophobic steroid moiety to its natural designation in the cell membrane. That might also cost internalization of a whole conjugate to cytosol site. We have chosen the cholesterol structure to charge hormonal peptides with steroid-lipid phase giving to the molecule side a very hydrophobic character. As a steroid-peptide model we have chosen cholesterol activated on the 3-hydroxy position as chloroformate. The coupling to the peptide *N*-terminal was performed on solid phase and the steroid-peptide cleaved from the resin using standard TFA procedure. The other orientation of steroid structure (cholic acid) attached to the *N*-terminal of the peptide via its carboxyl group to the peptide in solid phase. In both cases we used the kinin B₂ receptor antagonist HOE-140. We have evaluated the apparent antagonist potencies [2] as pA₂ (Table 1) of the synthesized compounds in relation to original peptide *HOE-140*. Fluorescein in form of isothiocyanate was coupled to the conjugate *N-134* in solution to evaluate the migration of this compound into cells by confocal microscopy. The structures of synthesized conjugates *N-133* and *N-134* are shown in Figure 1.

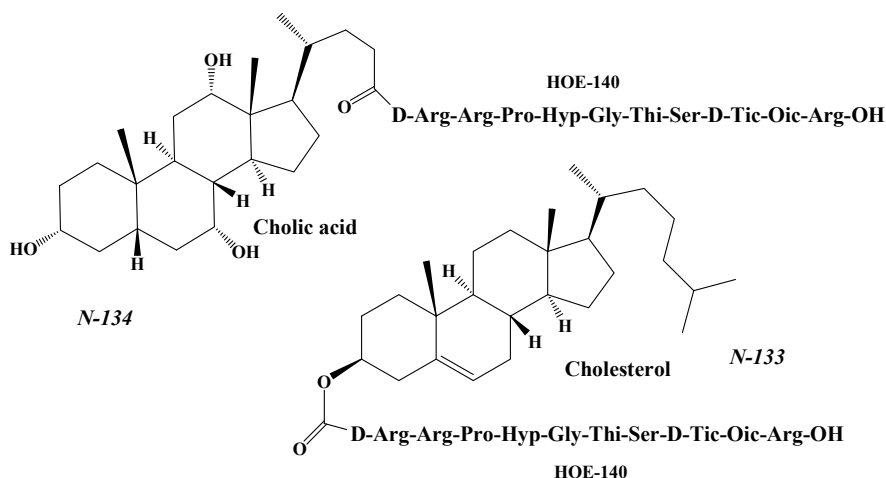


Fig. 1. Steroid-peptide conjugates [*N-133* and *N-134*] structures.

Table 1. Antagonist activity of peptides

Peptide	Human umbilical vein
	pA ₂
<i>N</i> -133	8.30 (mean of 4) tissue reversible in ~60 min
<i>N</i> -134	8.19 (mean of 2) tissue reversible in ~60 min
<i>HOE-140</i> (control) [4]	8.20 (standard control) tissue reversible in ~45 min

pA₂ is $-\log_{10}$ of the molar concentration of antagonist required to reduce the effect of a double concentration of agonist to that of a single concentration.

Results and Discussion

Synthetic peptide *HOE-140* was synthesized using Fmoc chemistry on Fmoc-Arg(Pbf)-NovaSyn TGA (0.2 mmol/g, 1g) resin in a Pioneer peptide synthesizer. The step by step coupling and final *N*-terminal acylation with cholic acid for *N*-134 was performed on solid phase with TBTU as coupling agent in DMF under regular conditions. Conjugation of cholesterol for *N*-133 onto *HOE-140* was performed with cholesterol chloroformate on solid phase in DCM and 2.5 fold excess of diisopropylethyl amine in Fmoc liberated the *N*-terminal side. Deprotection and cleavage of conjugates was performed with 97.5% TFA and 0.25% triisopropylsilane as scavenger. The crude peptide conjugates were precipitated in ether and lyophilized. Then the conjugates were purified on semi preparative C₁₈ column with a gradient of CH₃CN in aq. 0.1% TFA. Chromatographically pure fractions were selected and their purity verified by analytical HPLC chromatography on reverse phase C₁₈ column. The compounds *N*-133 and *N*-134 identities were confirmed by MALDI mass spectrometry giving respectively masses 1717 Daltons and 1695 Daltons. These compounds were tested against the contractile effect [3] induced by bradykinin on B₂ receptor bioassay with human umbilical vein. Their antagonistic activities (pA₂ 8.30 and 8.19 respectively) were compared with those of the *HOE-140* (8.2 [4]) [MS; 1304 Daltons] (Table 1). Steroid additive to the known B₂ antagonist did not significantly change its biological activity. At the same time steroidal moiety gave the chance to the molecule for association with membranes rich in peptide receptors and to permeable cell membrane. Confocal microscopy showed that fluorescein labeled *N*-134 crossed cell (human endocardial endothelial cell) membrane and concentrated in the cytosolic media. Steroid moiety on peptide hormone makes such compound cell permeable and should be considered as drug delivery vehicle.

References

1. Wolfe, S. L. *Molecular and Cellular Biology*, Wadsworth Publishing Company, 1993.
2. Gobeil, F., Neugebauer, W., Filteau, C., Jukic, D., Nsa Allogho, S., Pheng, L. H., Nguyen-Lee, X. K., Blouin, D. and Regoli, D. *Hypertension* **28**, 833-839 (1996).
3. Gobeil, F., Charland, S., Filteau, C., Perron, S. I., Neugebauer, W. and Regoli, D. *Hypertension* **33**, 829-829 (1999).
4. Marceau, F., Levesque, L., Drapeau, G., Rioux, F., Salvino, J. M., Wolfe, H. R., Seoane, P. R and Sawutz, D. G. *J. Pharmacol. Exp. Ther.* **269**, 1136-1143 (1994).

Influence of Natural Loop Residues or Oligolysines on the Biophysical Properties of Transmembrane Domains of a G Protein-Coupled Receptor

Patricia Cano-Sanchez¹, Tatsuya Inui¹, Beatrice Severino¹, V. V. Suresh Babu¹, Boris Arshava¹, Jeffrey M. Becker² and Fred Naider¹

¹Department of Chemistry, The College of Staten Island of the City University of New York, Staten Island, New York 10314; ²Department of Microbiology, University of Tennessee, Knoxville, Tennessee 37996, USA

Introduction

The α -factor pheromone receptor (Ste2p) that is required for mating in the yeast *Saccharomyces cerevisiae* is a member of the large family of G protein-coupled receptors (GPCRs) [1]. Comparison of Ste2p with other GPCRs shows that there is an overall structural similarity in that they are all composed of seven transmembrane domains (TMDs) connected by intracellular and extra cellular loops [2]. Biochemical studies indicated that ligand binding induces specific conformational changes in the TMDs [3], which play key roles in transducing the signal across the plasma membrane. Studies of the conformational and orientational states of regions of the Ste2p receptor in membranes are crucial to reveal the molecular mechanism of ligand-receptor interaction and signal transduction.

TMDs of GPCRs have very low water solubility and often aggregate during purification and biophysical investigations that makes them unsuitable for detailed structural analysis by techniques such as NMR spectroscopy. To circumvent this problem many laboratories add oligolysines to the N- and C-termini of peptides that correspond to the TMD. To systematically evaluate the effect of the oligolysines on the biophysical properties of a TMD we synthesized 21 peptides corresponding to either the 2nd or 6th TMD of Ste2p. Added to the termini of these peptides were either Lys_n (n=1,2,3) or the corresponding native loop residues (Table 1). Peptides were assembled using Fmoc/OtBu solid state methods and purified by reversed phase HPLC to near homogeneity. All peptides were verified by MS.

Table 1. Sequences of TMD of Ste2p

Peptide	Sequence	Peptide	Sequence
M6-33	QFDS ²⁴³ FHILLIMSSQSLVPSIIFILAYSLK ²⁶⁹ PNQ	KKKM6KKK	KKKS ²⁴³ FHILLIMSSQSLVPSIIFILAYSLK ²⁶⁹ KKK
M6-32	FDS ²⁴³ FHILLIMSSQSLVPSIIFILAYSLK ²⁶⁹ PNQ	KKM6KKK	KKKS ²⁴³ FHILLIMSSQSLVPSIIFILAYSLK ²⁶⁹ KKK
M6-31	DS ²⁴³ FHILLIMSSQSLVPSIIFILAYSLK ²⁶⁹ PNQ	KM6KKK	KS ²⁴³ FHILLIMSSQSLVPSIIFILAYSLK ²⁶⁹ KKK
M6-30	S ²⁴³ FHILLIMSSQSLVPSIIFILAYSLK ²⁶⁹ PNQ	M6KKK	S ²⁴³ FHILLIMSSQSLVPSIIFILAYSLK ²⁶⁹ KKK
M6-29	FHILLIMSSQSLVPSIIFILAYSLK ²⁶⁹ PNQ	M2 peptides	
M6-28(H)	HILLIMSSQSLVPSIIFILAYSLK ²⁶⁹ PNQ	M2-30	SRKT ⁷⁸ PIFIINQVSLFLIILHSALYFKY ¹⁰¹ LLS
M6-28(Q)	QFDS ²⁴³ FHILLIMSSQSLVPSIIFILAYS	M2-28	RKT ⁷⁸ PIFIINQVSLFLIILHSALYFKY ¹⁰¹ LL
KKKM6KK	KKKS ²⁴³ FHILLIMSSQSLVPSIIFILAYSLK ²⁶⁹ KK	M2-26	KT ⁷⁸ PIFIINQVSLFLIILHSALYFKY ¹⁰¹ L
KKM6KK	KKKS ²⁴³ FHILLIMSSQSLVPSIIFILAYSLK ²⁶⁹ KK	KKKM2KKK	KKKT ⁷⁸ PIFIINQVSLFLIILHSALYFKY ¹⁰¹ KKK
KM6KK	KS ²⁴³ FHILLIMSSQSLVPSIIFILAYSLK ²⁶⁹ KK	KKM2KK	KKKT ⁷⁸ PIFIINQVSLFLIILHSALYFKY ¹⁰¹ KK
M6KK	S ²⁴³ FHILLIMSSQSLVPSIIFILAYSLK ²⁶⁹ KK	KM2K	KT ⁷⁸ PIFIINQVSLFLIILHSALYFKY ¹⁰¹ K

Results and Discussion

The purification of the peptides corresponding to the 2nd and 6th TMD of Ste2p, proved to be very difficult because the low solubility of these peptides caused

frequent precipitation during HPLC purification. Purification was appreciably easier with the peptides containing non-native Lys residues at the termini as compared with the native loop residues. The peptides derived from the M2 domain gave better results both in terms of yield of the synthesis and the ease of purification. The final peptides all had the calculated MW as determined by ESI-MS and were highly homogeneous.

CD analyses showed that M6 peptides containing only native residues were highly helical in both TFE/water (95:5) and (50:50) mixtures. All peptides in this series showed a breakdown in the CD pattern in TFE/water (25:75) exhibiting broad minima centered near 215nm (Fig. 1a). This pattern is consistent with either a mixture of structures or the presence of peptide aggregates. M6 peptides with non-native lysine residues exhibited CD patterns typical of α -helices at all TFE/water ratios examined. Although some differences were observed for peptides containing different number of Lys residues at the termini we judged these as insignificant from a structural perspective.

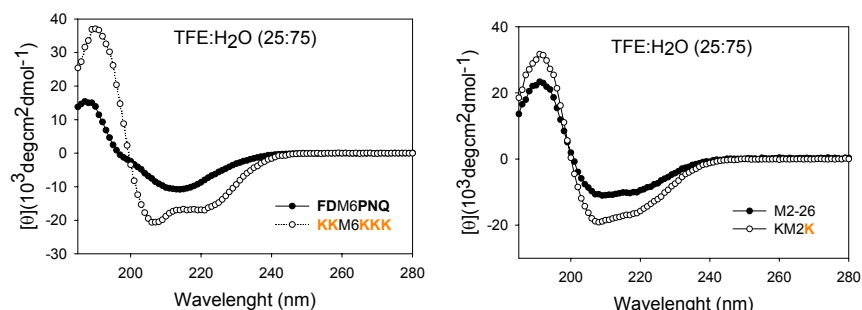


Fig. 1. Representative CD spectra of M6 and M2 peptides in TFE-water mixtures.

M2 peptides containing native residues and non-native Lys residues gave helical profiles in the CD analysis at all TFE/water ratios tested (Fig. 1b). M2 peptides with non-native Lys residues showed highly helical profiles for the peptide with three Lys residues at each termini and less helical profiles with the peptide having a Lys residue. The secondary structure of M2 peptides in micelles and lipid bilayers confirmed their highly helical tendencies since they all are helical both in 0.5% SDS and DMPC:DMPG bilayers. Once again, the number of non-native Lys residues was important to maintain the helical structure of these peptides. ATR-FTIR analysis of the M2 peptides are fully in concordance with the CD analyses in the presence of vesicles. We found differences in the tilt angle of the peptides, which seem to increase according to the number of residues at each end of the hydrophobic core. The possible influence of hydrophobic mismatch is still under investigation.

Acknowledgments

The work was funded by NIH grants GM22086 and GM22087.

References

1. Dohlman, H. G. and Thorner, J. W. *Annu. Rev. Biochem.* **70**, 703-754 (2001).
2. Okada, T., Ernest, O. P., Palczewski, K. and Hofmann, K. P. *Trends Biochem. Sci.* **26**, 318-324 (2001).
3. Dube, P. and Konopka, J. B. *Mol. Cell. Biol.* **18**, 7205-7215 (1998).

Design, Synthesis and Analysis of Constrained B-Cell Epitope from HER-2 Protein

Sharad V. Rawale¹ and Pravin T. P. Kaumaya^{1,2}

¹*Department of Obstetrics and Gynecology;* ²*Arthur G. James Cancer Hospital and The Comprehensive Cancer Center, The Ohio State University, Columbus, Ohio 43210 USA*

Introduction

Human Epidermal Growth factor Receptor (HER-2) is a tumor antigen in human cancers. The crystal structure of the extracellular domain and the Fab fragment of a monoclonal antibody Herceptin complex provide the molecular basis of understanding the role of HER-2 in signaling and cancer [1]. The extracellular domain contains multiple disulfide bonds. Recently, we showed that the conformational HER-2/neu B-cell epitope 626-649 with two disulfide bonds exhibits enhanced tumor cell binding and antitumor activity [2]. We have demonstrated that chimeric peptide vaccines incorporating B-cell epitopes of HER-2 and a 'promiscuous' T-cell epitope are able to elicit antibodies in an outbred population capable of controlling HER-2 associated cancers. We have developed several HER-2 peptide constructs as potential vaccine candidates, two of which are in a Phase 1 Clinical Trial in the James Cancer Hospital [3]. In order to develop more potent vaccine constructs, we designed epitope HER-2 563-598 with three disulfide bonds to mimic the three-dimensional structure of the extracellular domain of HER-2 protein that makes contact with Herceptin. We synthesized the B-cell epitope with controlled disulfide pairing and characterized the B-cell epitope using MS and CD spectroscopy.

The aim of this study is to design conformational antigenic epitope, which can lead to high affinity antibodies with potent antitumor activity. Disulfide bonds constrain the peptide and therefore the cyclic peptide can adopt a more defined conformation. We hypothesized that epitope HER-2 563-598 CYC could mimic the three-dimensional structure of HER-2 protein and able to elicit high affinity antibodies.

Results and Discussion

HER-2 563-598 CYC epitope was designed using chemoselective protecting groups Cys(Trt), Cys(Acm), Cys(tBu) for desired disulfide pairing [4]. The peptide was synthesized by Fmoc/t-butyl strategy on CLEAR acid resin and cleaved using reagent B (TFA:Water:TIS 95:5:5). The crude peptide was purified by RP-HPLC and characterized by ESI-MS. Selective disulfide bonding was achieved using I₂/H₂O and silyl-chloride method. Linear peptide HER-2 563-598 NC was generated using DTT reduction. Disulfide bond formation was analyzed using biotinylation agent (Maleimide-PEO₂), which binds free sulfhydryl groups and therefore could be used to determine the completion of disulfide pairing. Mass spectroscopy analysis indicated that the cyclic peptide did not display PEO addition, while the completely reduced peptide showed the addition of six PEO molecules, thereby confirming the cyclized product was obtained. Epitopes HER-2 563-598 CYC and NC were further analyzed by CD spectroscopy.

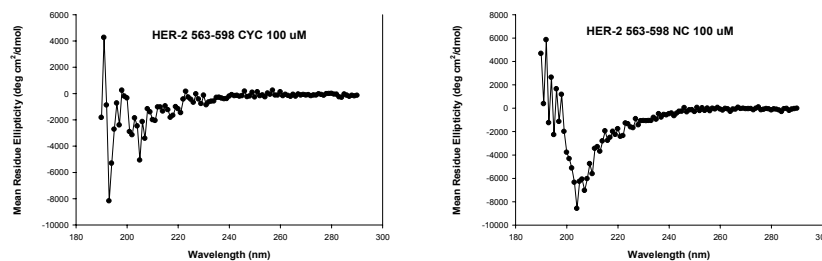


Fig. 1. CD measurements of HER-2 563-598 CYC and HER-2 563-598 NC in water.

Epitope HER-2 563-598 CYC, which is constrained with three disulfide bonds shows CD ellipticity minima at 193 nm, while epitope HER-2 563-598 NC, the free peptide shows CD ellipticity minima at 204 nm, which demonstrate significant differences in secondary structure (Fig. 1). The three disulfide bonds encompassing the B-cell epitope HER-2 563-598 CYC contributes to a structure that mimic Herceptin binding domain of HER-2 protein. The B-cell epitope 563-598 CYC in conjugation with T_H epitope MVF, measles virus fusion protein (amino acids 288-302), elicited potent immune response. The cyclized peptide recognized Herceptin with better binding characteristics than the non cyclized peptide.

Acknowledgments

This work was funded by the National Cancer Institute, # CA 84356-01A1 grant to P.T.P.K.

References

1. Hyun, -S. C., Karen, M., Kasra, X. R., Ann, M. S., Sandra, B. G., Dan, W. D. Jr and Daniel, J. L. *Nature* **421**, 756-760 (2003).
2. Dakappagari, N., Lute, K., Rawale, S., Steele, J., Allen, S., Phillips, G., Reilly, R. and Kaumaya, P. *J. Biol. Chem.* **280**, 54-63 (2005).
3. Dakappagari, N. K., Pyles, J., Parihar, R., Carson, W. E., Young, D. C. and Kaumaya, P.T. *P. J. Immunol.* **170**, 4242-4253 (2003).
3. Dakappagari, N. K., Douglas, D. B., Triozzi, P. L., Stevens, V. C. and Kaumaya P. T. P., *Cancer Res.* **60**, 3782-3789 (2000).
4. Kenichi, A., Kenji, F., Tadashi, T. and Yoshiaki K. *J. Am. Chem. Soc.* **115**, 11385-11392 (1993).

Synthesis of the Four Stereoisomers of N-Fmoc-O-*t*-Bu-4,4,4-trifluorothreonine

Zhong-Xing Jiang and Yihua Bruce Yu

Department of Pharmaceutics & Pharmaceutical Chemistry, University of Utah, Salt Lake City, UT 84112, USA

Introduction

Fluorination of peptide can lead to many benefits, such as increased stability, lipophilicity, and unique NMR signals. Hence, the synthesis of enantiomerically pure fluorinated amino acids in their protected forms ready for solid-phase peptide synthesis is of great value to engineering fluorinated peptides. In this regard, *N*-Fmoc-*O*-*t*-Bu-4,4,4-trifluorothreonine (tfT) poses a unique challenge as it has two chiral centers and hence four stereoisomers: (2*S*, 3*S*)-*N*-Fmoc-*O*-*t*-Bu-tfT **1**, (2*S*, 3*R*)-*N*-Fmoc-*O*-*t*-Bu-tfT **2**, (2*R*, 3*S*)-*N*-Fmoc-*O*-*t*-Bu-tfT **3**, (2*R*, 3*R*)-*N*-Fmoc-*O*-*t*-Bu-tfT **4** (Fig. 1). Although there are some reports on synthesis of tfT [1,2], those methods have great difficulties in introducing protective groups. Herein, we report some convenient methods for the stereoselective synthesis of all four isomers of tfT on 10g - 20g scale in high yield and good optical purity in 9-10 steps.

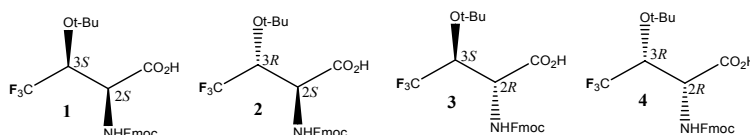


Fig. 1. Four isomers of *N*-Fmoc-*O*-*t*-Bu-4,4,4-trifluorothreonine (tfT).

Result and discussion

The synthesis started with Sharpless AD reaction on trifluoromethylated *trans*-disubstituted alkene **5**. The trifluoromethylated diols **6a/6b** were obtained with good yield and enantiomeric purity after recrystallization (Fig. 2).

The trifluoromethylated diol **6a** was first converted to cyclic sulfate **7**, and then the ring opening of cyclic sulfate **7** with NaN₃ occurred exclusively at C2 with clean inversion of chirality to provide the azide **8**. After protection of the hydroxy group in the azide **8** with iso-butene, the benzoyl group in compound **9** was removed by NaOH/MeOH to afford alcohol **10**. However, we found that racemization took place during removal of the benzoyl group. Then, Dibal-H was used to remove the benzoyl group to avoid the racemization. After hydrogenation, the azido group of

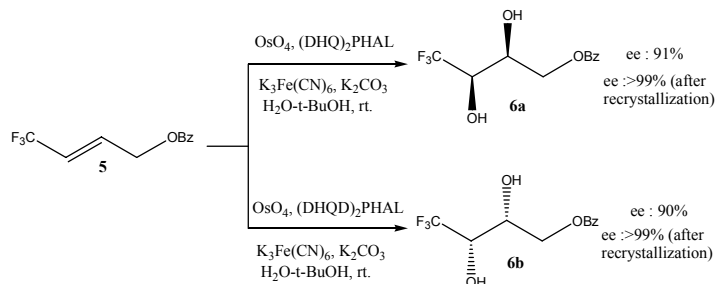


Fig. 2. Construction of chiral centers by Sharpless AD reaction.

compound **10**, protection of the newly formed amino group with Fmoc, and oxidation of the primary alcohol **12**, the (2*S*, 3*R*)-*N*-Fmoc-*O*-*t*-Bu-tfT **2** was prepared in good yield and 91% enantiomeric excess on 15g scale (Fig. 3). (2*R*, 3*S*)-*N*-Fmoc-*O*-*t*-Bu-tfT **3** was also prepared from trifluoromethylated diol **6b** on 10g scale in the same way.

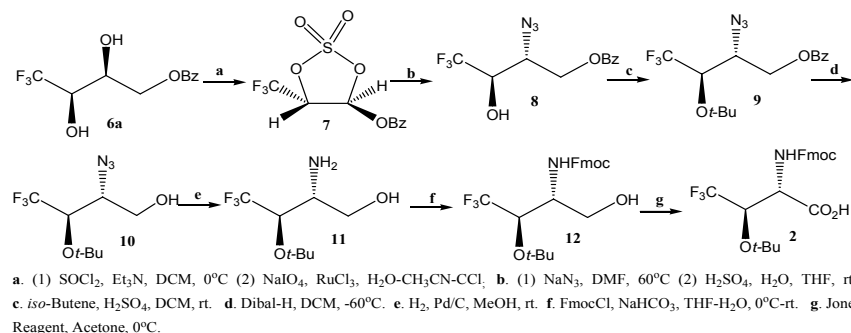


Fig. 3. Synthesis of (2*S*, 3*R*)-*N*-Fmoc-*O*-*t*-Bu-tfT.

In the synthesis of (2*R*, 3*R*)-*N*-Fmoc-*O*-*t*-Bu-tfT **4**, the ring opening of the trifluoromethylated cyclic sulfate **7** with LiBr lead to bromide **13** which then underwent nucleophilic substitution at C2. After twice inversion of the chirality of C2, the azide **14** was obtained in good yield and optical purity. (2*R*, 3*R*)-*N*-Fmoc-*O*-*t*-Bu-tfT **4** was synthesized from azide **14** in the similar fashion as (2*S*, 3*R*)-*N*-Fmoc-*O*-*t*-Bu-tfT **2** on 7g scale (Fig. 4).

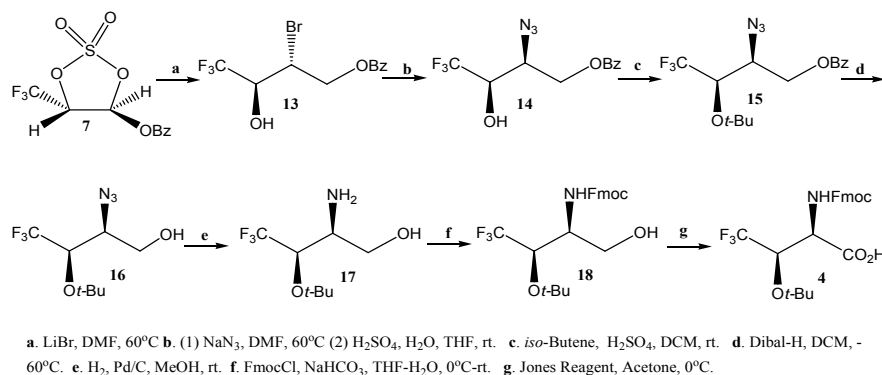


Fig. 4. Synthesis of (2*R*, 3*R*)-*N*-Fmoc-*O*-*t*-Bu-tfT.

Acknowledgement

We thank NIH (EB002880 and EB 004410) and Sidney Kimmel Foundation for Cancer Research for financial support.

Reference

1. Jiang, Z. -X., Qin, Y. -Y and Qing, F. -L. *J. Org. Chem.* **68**, 7455-7458 (2003).
2. Jiang, Z. -X. and Qing, F. -L. *J. Org. Chem.* **69**, 5486-5489 (2004).

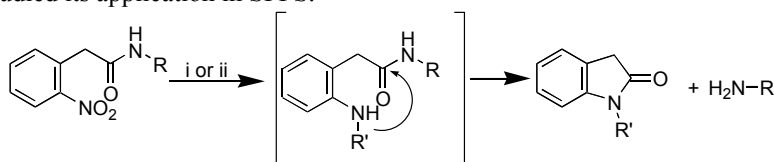
Synthesis of N^α -Fmoc- N^ϵ -[(2-nitrophenyl)acetyl]-lysine (Fmoc-Lys(Npa)-OH) and its Applications in Solid-Phase Peptide Synthesis

Aimin Song, Lucy Wu, Xiaobing Wang and Kit S. Lam

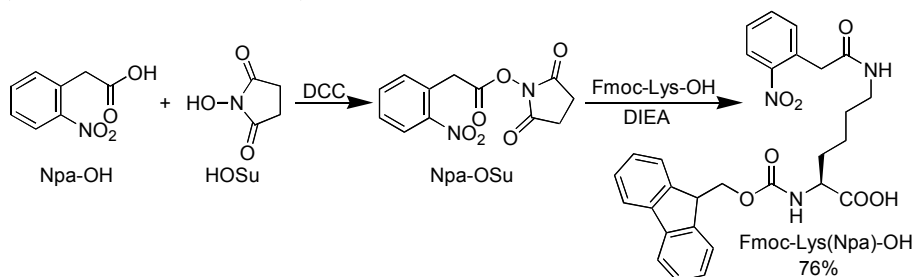
Division of Hematology and Oncology, Department of Internal Medicine, UC Davis Cancer Center, 4501 X Street, Sacramento, California 95817, USA

Introduction

Lysine derivatives with an orthogonal side-chain protecting group, e.g. Fmoc-Lys(Dde)-OH and Fmoc-Lys(Alloc)-OH, have found broad applications in solid-phase peptide synthesis. They are widely used for the synthesis of branched peptides and peptides with reporters. The 2-nitrophenylacetyl (Npa) group has been tentatively used as a protecting group for amines [1], but has not found much use because the structure of the amine has a significant effect on the rate of deprotection (Scheme 1). In addition, the deprotection of Npa usually requires heterogeneous catalysts or reagents and, therefore, is not suited for solid-phase peptide synthesis (SPPS). In 1990, Bartra *et al.* reported that aromatic nitro group can be selectively reduced to hydroxyamino group by treatment with a mixture of tin(II) chloride (SnCl_2), thiophenol (PhSH), and triethylamine (TEA) [2]. We envisioned that this reaction can be used for the deprotection of Npa group in solid phase as hydroxyamino group is much more nucleophilic than aromatic amino group. Thus, we synthesized N^α -Fmoc- N^ϵ -[(2-nitrophenyl)acetyl]-lysine (Fmoc-Lys(Npa)-OH) and studied its application in SPPS.



Scheme 1. Deprotection of Npa group in solution phase (i, H_2 , Pd/C, $\text{R}' = \text{H}$) and solid phase (ii, $\text{SnCl}_2/\text{PhSH}/\text{TEA}$, $\text{R}' = \text{OH}$).



Scheme 2. Synthesis of Fmoc-Lys(Npa)-OH.

Results and Discussion

The synthesis of Fmoc-Lys(Npa)-OH is illustrated in Scheme 2. The commercially available 2-nitrophenylacetic acid was condensed with *N*-hydroxysuccinimide in the presence of *N,N'*-dicyclohexylcarbodiimide (DCC) to form an active ester. The

resulting active ester was then reacted with Fmoc-Lys-OH without purification. Fmoc-Lys(Npa)-OH was obtained in an overall yield of 76%.

Deprotection of the Npa side chain protection group was studied in solid phase. A peptide with the sequence of Boc-Val-Lys(Npa)-Phe-Phe-Gly was synthesized on Wang resin. The resin-supported peptide was treated with a solution of SnCl_2 (5 equiv.), PhSH (20 equiv.), and TEA (25 equiv.) in dichloromethane (DCM) at room temperature. A portion of the resin beads was taken out at different time point and washed. The exposed amino groups were then blocked with acetic anhydride. The resulting peptide was released with 50% trifluoroacetic acid (TFA)/DCM, analyzed with HPLC and compared to the authentic sample. Complete deprotection was observed after 2 hrs of treatment with the SnCl_2 /PhSH/TEA complex.

The application potentials of Fmoc-Lys(Npa)-OH was demonstrated by the synthesis of FITC-labeled and biotinylated peptides. At the beginning of the synthesis, Fmoc-Lys(Npa)-OH was tethered to Rink amide resin. The Fmoc group was first removed by 20% piperidine/DMF and a linker was coupled to the α -amino group [3]. The peptide was then constructed on the linker using standard Fmoc chemistry and its N-terminus was blocked by Boc. The Npa side chain protecting group was removed by treatment with SnCl_2 /PhSH/TEA. The fluorescent probe or biotin was then attached to the ϵ -amino group of lysine, followed by TFA cleavage. As an example, a peptide ligand for anti- β -endorphin antibody, YGGFL, was labeled with FITC using this procedure. The HPLC and MS spectra of the crude product are shown in Figure 1.

In summary, we synthesized Fmoc-Lys(Npa)-OH as a useful building block in SPPS. The Npa group is stable to piperidine, TFA, and $\text{Pd}(\text{PPh}_3)_4$, but can be readily removed by treatment with SnCl_2 /PhSH/TEA. Biotinylated and fluorescent-labeled peptides were successfully synthesized in solid phase using Fmoc-Lys(Npa)-OH.

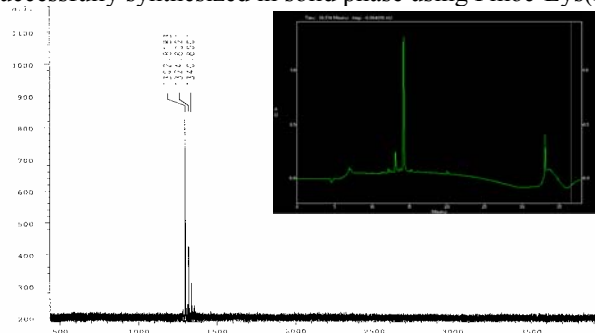


Fig. 1. MALDI-TOF MS and HPLC (insert) spectra of crude FITC labeled peptide YGGFL-linker-K(FITC)- NH_2 after TFA cleavage.

Acknowledgments

The work was funded by NIH and NSF.

References

1. Cuiban, F. *Rev. Roum. Chim.* **18**, 449-461 (1973).
2. Bartra, M., Romea, P., Urpi, F. and Vilarrasa, J. *Tetrahedron* **46**, 587-594 (1990).
3. Song, A., Wang, X., Zhang, J., Marik, J., Lebrilla, C. B. and Lam, K. S. *Bioorg. Med. Chem. Lett.* **14**, 161-165 (2004).

A MS-based Encoding Method for OBOC Combinatorial Branched Peptide Libraries

Xiaobing Wang and Kit S. Lam

Division of Hematology and Oncology, Department of Internal Medicine, UC-Davis Cancer Center, University of California Davis, Sacramento, CA 95817, USA

Introduction

Recently, we reported a novel PAD (Partial Alloc Deprotection) approach to encode OBOC combinatorial peptide libraries [1] to overcome the limitations of rapid MS-based sequencing approaches ("ladder-sequencing" [2] and "ladder-synthesis" [3]) [4]. This approach allows successive deprotection of alloc group on beads (starting from bead surface towards bead interior), controlled by the exposure time of water-swollen beads to palladium reagent (Fig. 1). In this report, we reported the application of the PAD approach to develop a novel MS-based encoding method for branched peptide libraries, which can result in a great degree of structural complexity and once encoded with fluorine tags by Ohlmeyer *et al*[6].

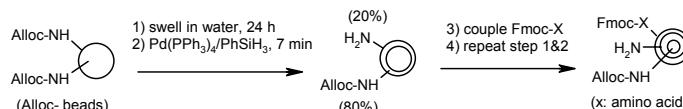


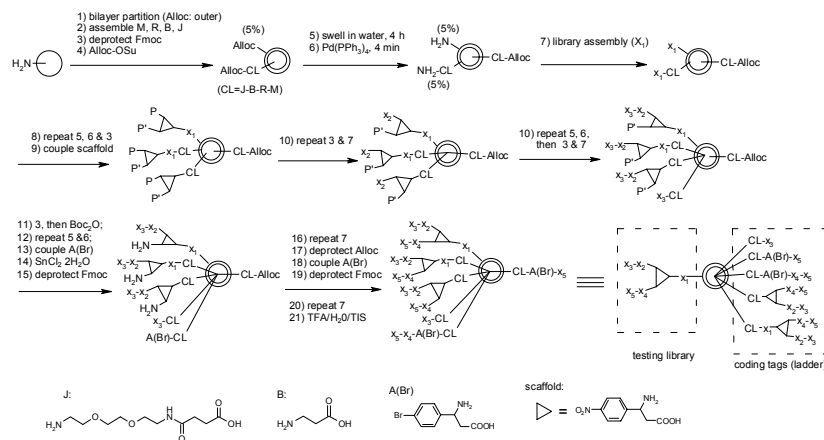
Fig. 1. Schematic representation of PAD approach.

Results and Discussion

The synthesis of a model OBOC branched peptide library was shown in Scheme 1. Before the library synthesis, a CNBr-cleavable linker consisting of Met, Arg, B (β -alanine) and J (2,2'-ethylenedioxy-bis(ethylamine) monosuccinamide) was assembled on the interior of bilayer TentaGel beads (outer layer: 5%, Alloc-protected). In this library, the bead surface only displays non-cleavable full length testing library compounds, and the bead interior carries a series of CNBr-cleavable coding tags.

Figure 2 illustrates the general decoding strategy for a hypothetical library bead. All coding tags after CNBr cleavage will produce a pseudo ladder of five mass members of which the second and the third tags (M_2 and M_3) have a doublet fingerprint because of bromine isotope. The library residues can be determined by the five mass peaks according to the following equations: $X_3 = M_1 - M_0$, $X_5 = M_2 - M_0'$, $X_4 = M_3 - M_2$, $X_2 = M_4 - (M_0 + M_5 + X_3 + X_4 + X_5)$, $X_1 = M_5 - M_4$; wherein, M_0 and M_5 represent the mass contributions of the cleavable linker and the scaffold precursor, respectively. M_0' represents the mass of the cleavage linker together with the bromine-containing β -amino acid. To demonstrate the feasibility and reliability of the synthetic encoding strategy for the library, fifty randomly picked library beads were sequenced by MALDI-TOF MS. 45 beads were unambiguously identified. The other five beads only generated four peaks. The first coding tag peak M_1 was lost in these beads. However, the four peaks still enabled us to identify the compound sequence because the pair of amino acids (X_2 and X_3) that summed together with the masses of identified X_4 and X_5 to the mass of M_4 could be easily calculated, although the order of the two residues could not be determined due to the loss of the peak M_1 .

Thus, the overall sequencing success rate of over 90% has demonstrated the reliability of the method.



Scheme 1. Synthetic route of a model tri-arm OBOC branched peptide library. In the library, X_i (i=1,2,3,4,5) denotes one of 15 L-amino acids (excluding Cys, Met, Ile, Gln).

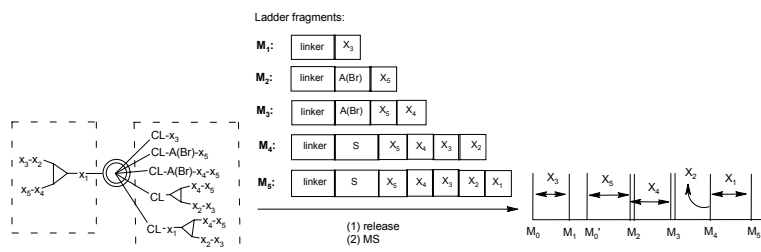


Fig. 2. Decoding strategy for the model branched library using MALDI-TOF MS.

In conclusion, we have developed a novel MS-based encoding method for OBOC branched peptide libraries. The method is efficient and reliable. The decoding is simple and rapid using mass spectrometry, and in principle, could be automated.

Acknowledgments

This work was supported by NIH R33CA-86364, NIH R33CA-99136 and NSF CHE-0302122.

References

1. Lam, K. S., et al. *Nature* **354**, 82-84 (1991).
2. Chait, B. T., et al. *Science* **262**, 89-92 (1993).
3. Youngquist, R. S., et al. *J. Am. Chem. Soc.* **117**, 3900-3906 (1995).
4. Wang, X., et al. *J. Comb. Chem.* **7**, 197-209 (2005).
5. Dong, D. L., et al. *Chem. Biol.* **6**, 133-141 (1999).
6. Ohlmeyer, M. H., et al. *Proc. Natl. Acad. Sci. USA* **90**, 10922-10926 (1993).

Sequential Chemical Ligation for Polypeptide Synthesis by the Combination of the Thioester Method and the Extended Chemical Ligation Using a Photoremovable Auxiliary

Toru Kawakami, Masahiro Tsuchiya, Ken'ichiro Nakamura and Saburo Aimoto

Institute for Protein Research, Osaka University, Suita, Osaka 565-0871, Japan

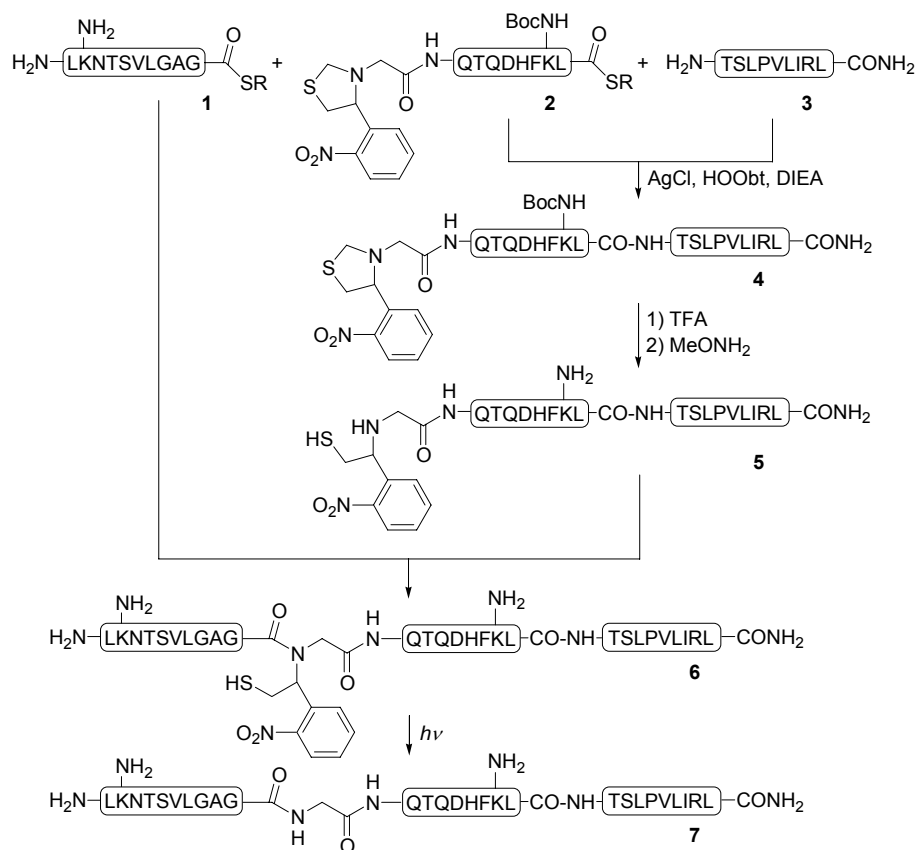
Introduction

Chemical ligation of peptide segments is widely used for polypeptide synthesis. Each ligation method, such as the thioester method [1,2] or native chemical ligation [3,4], has characteristic advantages and disadvantages. Thus, the thioester method can be performed at any ligation sites, while it requires some protecting groups, an activator such as silver salts, and organic solvents. On the other hand, the native chemical ligation can be carried out under neutral aqueous conditions without the need for protecting groups, although a cysteine residue is required at the condensation site. Several auxiliary groups have been introduced to permit the ligation to proceed without a cysteine residue [5-8], although it actually needs a glycine residue. As a result, a combination of these ligation methods offers a flexible choice of the condensation site in the multi-step polypeptide synthesis. Here we show the strategy that combines the thioester method and extended chemical ligation using the photoremovable auxiliary with sequential manner.

Results and Discussion

As a model peptide, Leu-Lys-Asn-Thr-Ser-Val-Leu-Gly-Ala-Gly-Gly-Gln-Thr-Gln-Asp-His-Phe-Lys-Leu-Thr-Ser-Leu-Pro-Val-Leu-Ile-Arg-Leu-NH₂ **7** was synthesized as shown in scheme 1. This peptide was divided into three segments, and ligated sequentially by the thioester method and extended chemical ligation. Thiazolidine ring was used for protection [9] of the photoremovable ligation auxiliary, *N*-2-mercapto-1-(2-nitrophenyl)ethyl (Mnpe) group, in the middle peptide thioester building block **2**. At first a peptide thioester **2** was condensed with a C-terminal peptide segment **3** in the presence of silver chloride, 3,4-dihydro-3-hydroxy-4-oxo-1,2,3-benzotriazine (HOOBt), and *N,N*-diisopropylethylamine (DIEA) in DMF for 48 hrs to give peptide **4**. After removal of Boc groups of Lys residues with TFA, the thiazolidine ring was opened with methoxylamine in sodium phosphate buffer to give the peptide **5** in 47% yield based on peptide **2**. Next, extended chemical ligation with peptide thioester **1**, in sodium phosphate buffer containing 6 M guanidine hydrochloride and 2% thiophenol for 24 hrs, gave peptide **6** in 77% yield, and finally the Mnpe group was removed by UV irradiation in sodium phosphate buffer for 1 hr, to give the peptide **7** in 56%.

In conclusion, the thioester method and extended chemical ligation can be combined with sequential manner by using over three building blocks for polypeptide synthesis. The thiazolidine ring can be used as a temporal protecting group for the ligation auxiliary. It would be also applied for the combination of the thioester method and native chemical ligation sequentially.



Scheme 1. A strategy for a sequential chemical ligation.

Acknowledgments

This research was supported, in part, by Grants-in-Aid for Scientific Research from the Ministry of Education, Culture, Sports, Science and Technology, Japan.

References

1. Hojo, H. and Aimoto, S. *Bull. Chem. Soc. Jpn.* **64**, 111–117 (1991).
2. Aimoto, S. *Biopolymers (Peptide Sci.)* **51**, 247–265 (1999).
3. (a) Dawson, P. E., Muir, T. W., Clark-Lewis, I. and Kent, S. B. H. *Science* **266**, 776–779 (1994); (b) Tam, J. P., Lu, C.-F. and Shao, J. *Proc. Natl. Acad. Sci. USA* **92**, 12485–12489 (1995).
4. Dawson, P. E. and Kent, S. B. H. *Annu. Rev. Biochem.* **69**, 923–960 (2000).
5. Canne, L. E., Bark, S. J. and Kent, S. B. H. *J. Am. Chem. Soc.* **118**, 5891–5896 (1996).
6. Botti, P., Carrasco, M. R. and Kent, S. B. H. *Tetrahedron Lett.* **42**, 1831–1833 (2001).
7. Kawakami, T., Akaji, K. and Aimoto, S. *Org. Lett.* **3**, 1403–1405 (2001).
8. Kawakami, T. and Aimoto, S. *Tetrahedron Lett.* **44**, 6059–6061 (2003).
9. (a) Villain, M., Vizzavona, J. and Gaertner, H. In *Peptides: The Wave of the Future*, 17th American Peptide Symposium (Houghten, R. A. and Lebl, M., eds.) Kluwer Academic, The Netherlands, pp 107–108 (2001); (b) Bang, D. and Kent, S. B. H. *Angew. Chem. Int. Ed.* **43**, 2534–2538 (2004).

Solid-Phase Synthesis of a Mucin Glycopeptide Segment from CD43 for NMR and Crystallization Studies

Mian Liu^{1,2}, George Barany¹ and David Live²

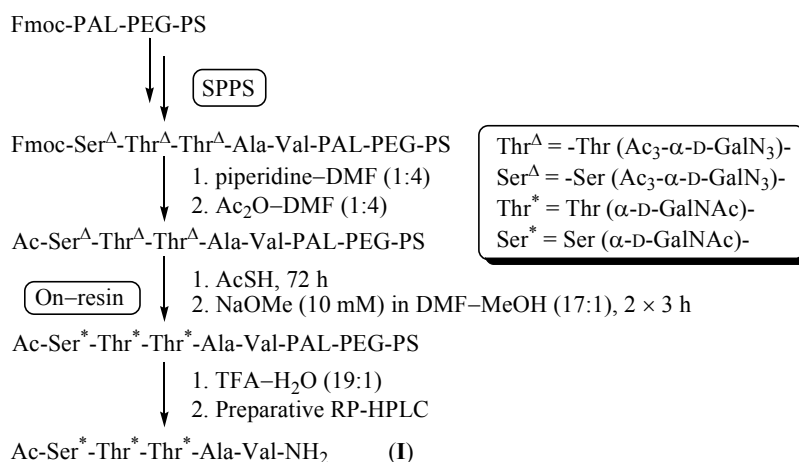
¹Department of Chemistry; ²Department of Biochemistry, Molecular Biology and Biophysics,
 University of Minnesota, Minneapolis, MN 55455, USA

Introduction

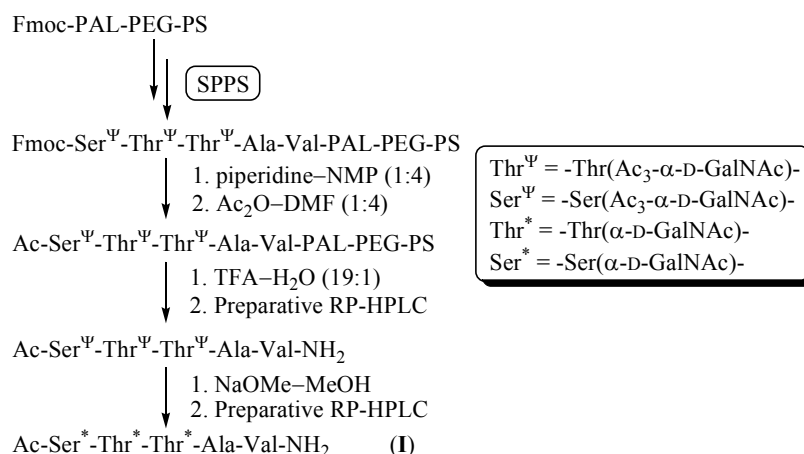
The extracellular domain of mucin glycoprotein CD43 is of interest due to its role in cell–cell recognition and signal transduction via conserved phosphorylation sites in its cytoplasmic domain [1]. Related to the recognition event, α -O-linked GalNAc glycosylation on a CD43 derived glycopeptide has been reported to induce a transition to a stable extended structure, arising from specific hydrogen-bonding interactions between the peptide and carbohydrate moieties [2]. We report here on the synthesis and characterization of a modified form of the CD43-derived segment, i.e., Ac-S^{*}T^{*}T^{*}AV-NH₂ (**I**), [^{*} = α -GalNAc]. 1D and 2D NMR data show that conversion of the carboxylate to carboxamide function does not perturb the structural characteristics. The unusual conformational stability for a glycopeptide segment of its size suggests that it is an attractive candidate for crystallization. Our ultimate goal is to carry out X-ray analysis and derive further high-resolution structural insights that help elucidate biological functions.

Results and Discussion

The title glycopeptide **I** has been synthesized by two different routes, which were then compared. In one route (Scheme 1), building blocks used were *N* ^{α} -(9-fluorenylmethoxycarbonyl)-*O*-(3,4,6-tri-*O*-acetyl-2-azido-2-deoxy- α -D-galactopyranosyl)-L-serine/L-threonine pentafluorophenyl esters [Fmoc-L-Ser/L-Thr(Ac₃- α -D-GalN₃)-OPfp] [3], while in the other route (Scheme 2), building blocks used were *N* ^{α} -(9-fluorenylmethoxycarbonyl)-*O*-(3,4,6-tri-*O*-acetyl-2-acetyl-2-deoxy- α -D-galactopyranosyl)-L-serine/L-threonine [Fmoc-L-Ser/L-Thr(Ac₃- α -D-GalNAc)-OH].



Scheme 1. Use of Fmoc-Ser/Thr(Ac₃- α -D-GalN₃)-OPfp as building blocks to prepare title glycopeptide.



Scheme 2. Use of Fmoc-Ser/Thr(Ac₃-α-D-GalNAc)-OH as building blocks to prepare title glycopeptide.

Both routes featured solid-phase chain assembly, and final *O*-deacetylation, but in the first route (Scheme 1), an extra chemical transformation, conversion of an azido group to acetamido, was required. Performing azide conversion and *O*-deacetylation on-resin was found to be more efficacious than carrying out one or both of these steps in solution. Ultimately, glycopeptides were cleaved from the support, and purified by RP-HPLC. The 1D ¹H NMR of the purified title glycopeptide is shown in Figure 1.

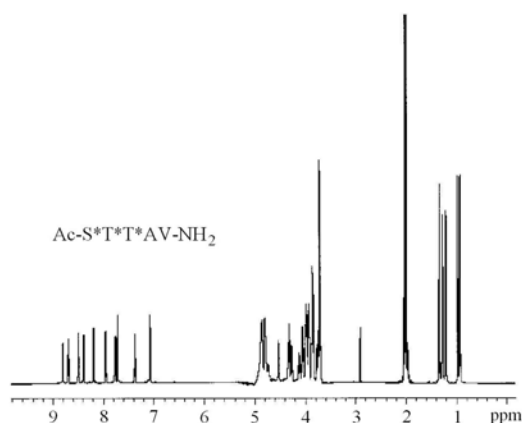


Fig 1. ¹H NMR spectra of glycopeptide I in water.

Attempts at crystallization of both *O*-protected and *O*-free glycopeptides are under way; if successful, they could further advance our knowledge of the structural properties of this glycopeptide, and be generalizable to other α-GalNAc *O*-linked mucin glycopeptides and proteins.

Acknowledgments

The work was funded by an NIH (GM 66148) grant.

References

1. Ostberg, J. R., Barth, R. K. and Frelinger, J. G. *Immunol. Today* **19**, 546-550 (1998).
2. Coltart, D. M., et al. *J. Am. Chem. Soc.* **124**, 9833-9844 (2004).
3. Liu, M., et al. *Carbohydr. Res.* **340**, 1273-1285 (2005).

SPPS of Bacterial Addressed Peptides and PNAs Overcoming the Resistance against Antibiotics

Rüdiger Pipkorn, Waldemar Waldeck and Klaus Braun

German Cancer Research Center, D-69120 Heidelberg INF 280, Germany

Introduction

Antibiotic Resistance: In the 40's soon after the start of penicillin-treatment the first resistance against antibiotics was documented. The abusiveness of antibiotics led to a rapid increase of the number of microbial strains resistant against antibiotics. Today the alarming problem is the increased inefficiency of the clinically used small glycoprotein Vancomycin. This situation seems to be one of the ultralarge current problems in the field of the antibiotic therapy. Recently great efforts in the pharmaceutical research resulted in the isolation of naturally occurring substances with antibiotic properties. In spite of all progress, due to the impetuous bacterial mutation rates, the time frame for successful antibacterial therapy is minimized. Due to the increasingly dramatic situation of therapy-resistant infections the 'Department of Health and Human Services' of the US 'Centers for Disease Control and Prevention' accentuates the need for new highly efficient antibiotics.

We could demonstrate that BioShuttle constructs are able to override the resistance of pathogens against antibiotics. The used BioShuttle consists of a circular peptide like human defensins as a transporter across bacterial membranes linked with PNA directed against bacterial resistance genes (Fig. 1). The results show a strong decrease of the growth of *E. coli* resistant against antibiotics after treatment with BioShuttle. It could be concluded that the reconstitution of 'Old fashioned' antibiotics like Penicillin and Kanamycin is possible.

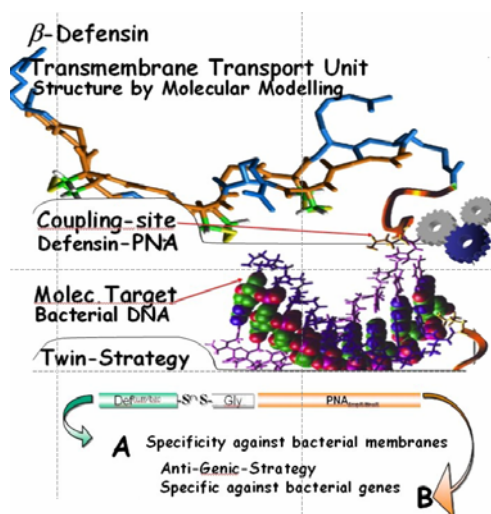


Fig. 1. The schematic structure of the BioShuttle-Defensin conjugate is displayed.

Chemical synthesis of Defensin: Fmoc-strategy was employed for solid phase synthesis of defensin in a fully automated synthesizer (ABI 431). The synthesis was

carried out on 0.05 mmol Fmoc-Arg(Pbf)-polystyrene resin (1% crosslinked). As coupling agent 2-(1H-Benzotriazole-1-yl)-1,1,3,3-tetramethyl uronium hexafluorophosphate (HBTU) was used. The following side chain protecting groups were used: Thr(But), Arg(Pbf). Three different selective cleavable protecting-groups were employed for Cys:



For Cys (3,16) we used t-butylthio, Cys (5,14) were blocked with acetamidomethyl, and Cys (7,12) were protected with a trityl group. In the first step we cleaved the t-Butylthio-protecting group with tris(2-carboxyethyl) phosphine (TCEP) and oxidized the sulfur bridge with 20% DMSO in water solution. In the second step we cleaved the acetamidomethyl protecting group and oxidized at the same time the second sulfur bridge with a 0.01mol iodine-solution. The protected peptidyl resin was treated with 20% piperidin in dimethylformamide for 12 min and then washed with dimethylformamide. Cleavage and deprotection of the peptide resin were affected by treatment with 90% trifluoroacetic acid, 5% ethanedithiol, 2.5% thioanisol, 2.5% phenol (v/v/v/v) for 2.5 hrs at room temperature. The products were precipitated in ether. The crude material was purified by preparative HPLC on an YMC-Pack ODS-AQ 120 Å,S-5u reverse phase column (20 x 150 mm) using an eluent of 0.1% trifluoroacetic acid in water (A) and 60% acetonitrile in water (B). The peptide was eluted with a successive linear gradient of 25% B to 60% B in 40 min at a flow rate of 20 ml/min. The fractions corresponding to the purified protein were lyophilized. As last step we performed the head to tail cyclization with propane phosphonic acid anhydride (T3P®) and repeated the purification procedure. The purified material was characterized with analytical HPLC and laser desorption mass spectrometry Vision 2000 (Finnigan MAT).

Results

Growth of *E. coli* blocked after BioShuttle Treatment: The application with 25 μM conjugate leads to a stop of growth of *E. coli*. The 2.5 μM BioShuttle-treated cultures show hardly bacterial growth (Fig. 2).

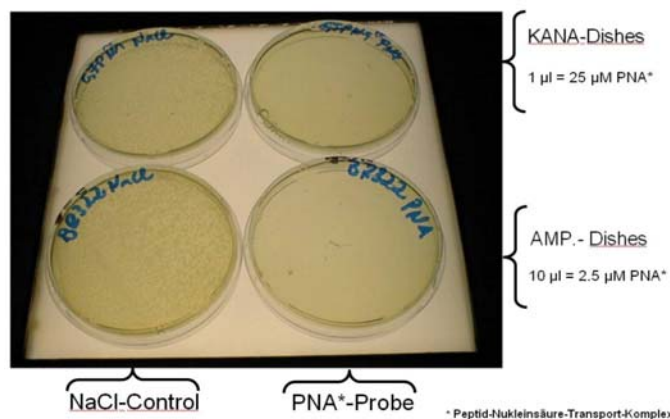


Fig. 2. *E. coli* treated without and with Defensin-transported PNAs complementary to sequences coding for Amp.-and Kan.-Resistance.

Convergent Synthesis of the Cysteine-rich Mdm2 RING Finger Domain

Zoe Vasileiou, Dimitrios Gatos and Kleomenis Barlos

Department of Chemistry, University of Patras, GR 26500 Patras, Greece

Introduction

The tumor suppressor protein p53 plays a pivotal role in DNA damage recognition, signal transduction, and initiation of mechanisms of apoptosis and repair. Mdm2 (murine double minute 2) interacts with p53, inhibits its function and promotes its degradation through ubiquitination (programmed protein degradation). In the ubiquitin pathway, Mdm2 plays the role of an E3 ubiquitin ligase. High levels of Mdm2 are responsible for cancer initiation and therefore it is characterized as oncogenic protein. It has been found that the RING domain of Mdm2 (Fig. 1) located at the C-terminus of the protein is necessary for E3 activity and therefore for the regulation of p53. For these reasons the RING domain of Mdm2 is an important target for studying its interaction with small anticancer drug candidates. Due to the presence of multiple cysteine residues, the synthesis of such small proteins is challenging and very difficult to be performed using recombinant techniques. Therefore, chemical syntheses are attractive and in two examples the ligation method was used [1,2]. As an alternative method, we studied the synthesis of the 48mer RING finger domain of Mdm2 (sequence 435-482) by the sequential condensation of protected fragments on 2-chlorotrityl resin.

H-IEPCVICQGRPKNGCIVHGKTGHLMACFTCAKKLKKRNKPCPVCRQPI-OH

Fig. 1. The RING finger domain of the oncoprotein Mdm2.

Results and Discussion

The protected fragments **1-6** (Fig. 2) corresponding to the RING domain 1-48 sequence were synthesized using 2-chlorotrityl resin and Fmoc/tBu-type amino acids. The seven cysteine residues were protected at their side chains with the very acid-labile 4-methoxytrityl (Mmt) group in order to achieve their quantitative deprotection. For the activation of the amino acids DIC/HOBt in DMF was used and for the Fmoc-removal 20% piperidine in DMF. The protected fragments were cleaved from the resin by treatment with trifluoroethanol (TFE)/dichloromethane (DCM) 30:70 mixture, analyzed by HPLC-MS and found to be of >92%. The main impurities detected were the des-trityl peptides in the case of the His-containing fragments **3** and **4** and the oxidized peptide in the case of the Met-containing fragment **4**. To avoid complication throughout the synthesis due to partial Met-oxidation, we also prepared and tested the fully oxidized 23-26 fragment **4a**. Oxidation was performed by treatment of the dipeptide Fmoc-Met-Ala-O-resin with 10% H₂O₂ in THF for 5 hrs. The resin-bound fragment **6** was of >95% purity and therefore its purification and reattachment onto the resin were not necessary.

The sequential condensation of fragments **1-6** was in all cases completed using 2.5 molar excess of fragments with the exception of **3**, where no completion was detected even after a double coupling. It is interesting that the condensation of the same fragment with the resin-bound peptide oxidized at the Met-residue proceeded much faster, revealing the high importance of the conformation of the fragments for

the condensation efficiency. In both cases the remaining unreacted amino functions were capped with excess acetic anhydride. However, the produced acetylated derivatives coeluted in HPLC with the required product. Therefore, instead of acetylating, we introduced the Boc-group using excess diboc-dicarbonate in NMP.

1. Fmoc-I¹-E(tBu)-P-C(Mmt)-V-I-C(Mmt)-Q(Trt)-G⁹-OH
2. Fmoc-R(Pbf)¹⁰-P-K(Boc)-N(Trt)-G¹⁴-OH
3. Fmoc-C(Mmt)¹⁵-I-V-H(Trt)-G-K(Boc)-T(tBu)-G²²-OH
4. Fmoc-H(Trt)²³-L-M-A²⁶-OH
- 4a. Fmoc-H(Trt)²³-L-M(O)-A²⁶-OH
5. Fmoc-C(Mmt)²⁷-F-T(tBu)-C(Mmt)-A-K(Boc)³²-OH
6. Fmoc-K(Boc)³³-L-K(Boc)-K(Boc)-R(Pbf)-N(Trt)-K(Boc)-P-C(Mmt)-P-V-C(Mmt)-R(Pbf)-Q(Trt)-P-I⁴⁸-O-2-chlorotrityl resin

Fig. 2. Protected fragments used.

After the assembly of the 1-48 sequence, the protected RING domain was cleaved from the resin by treatment with AcOH/TFE/DCM 1:2:7 and precipitated by the addition of ether. Side-chain deprotection was performed by testing various TFA/scavengers mixtures. Best results were achieved using the mixture TFA/EDT/TES (95:2.5:2.5) for 4 hrs at RT. The products were analyzed by LC-MS, after an 1 hr incubation with a reducing agent, such as DTT or TCEP to avoid Cys oxidations. As expected, the crude Met(O)²⁵-Fmoc-48mer peptide was obtained in higher purity than the corresponding non-oxidized peptide. The main impurity in both cases was the 23-48 truncated sequence. The final H-(1-48)-OH peptide was obtained in pure form and 10% yield after semipreparative HPLC and its correct structure confirmed by ES-MS (Fig. 3a, b).

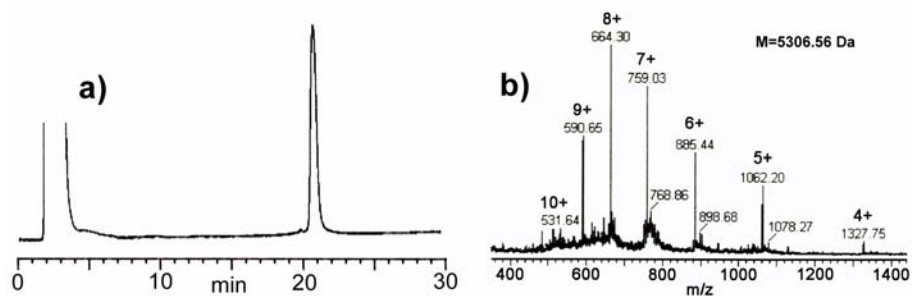


Fig. 3. HPLC-profile (a) and ES-MS (b) of purified RING domain.

Acknowledgments

The work was funded by CBL-Patras S.A.

References

1. Futaki, S., Tatsuto, K., Shiraishi, Y. and Sugiura, Y. *Biopolymers (Peptide Sci.)* **76**, 98-109 (2004).
2. Beligere, G. and Dawson, P. *Biopolymers (Peptide Sci.)* **51**, 363-369 (1999).

Evaluation of Polyamide-Polystyrene Block Polymers in Peptide Synthesis and Biochemistry

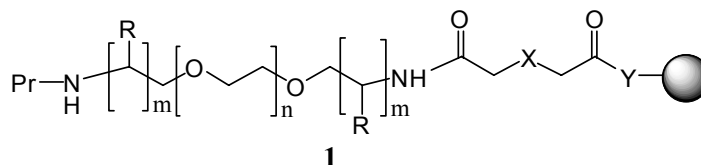
Spyros Markos, Antonios Saravanos, Michael Batistatos, Alexios Aletras, Dimitrios Gatos and Kleomenis Barlos

Department of Chemistry, University of Patras, Patras, Greece

Introduction

For the solid phase synthesis of peptides and other organic molecules, but also for applications in biochemistry, resins with good swelling in various solvents including water are required. Polyacrylamide resins or block polymers of polyethylene glycol (PEG) with polystyrene (PS), such as Tentagel, are the main hydrophilic resins used in synthesis.

We investigated now the application of resins of type **1** in SPPS and in biochemistry (Fig. 1).




Pr = Fmoc, Trt, Mmt, Boc; m = 1-2, n = 2-5;
 X = NR, O, S, (CH₂CH₂O)_n, or it is absent; Y = O, NR₂, R = H, alkyl
 = PS-resin, AM, MBHA, 2-Chlorotrityl, Trityl, Merrifield, etc.

Fig. 1.

Results and Discussion

The synthesis of the polyamide resins was performed either by the step by step method or by oligomerisation of a mixture of the Fmoc-derivative and the Mmt-derivatives. In Figure 2 is described the general strategy used for the preparation of the protected monomer amino acid units, on the example of the trioxa diamino derivative **2**. The loading of the resins vary with the loading of the starting resin, the polymerization degree of the amino acids and by introducing branches in the polyamide chain using lysine residues or other polyamino derivatives. As expected, resins **1** reveal a greatly increased hydrophilicity as compared to PS, but in addition, the swelling in methanol and other organic solvents was very satisfactory. In Table 1 the determined swelling results are summarized for aminomethyl resin loaded with PEG-oligomers

Resins **1** were tested in peptide synthesis. Very fast coupling rates (15-20 min) were determined during the synthesis of peptide amides and peptide acids with up to 40 amino acids in length.

To test the compatibility of the polyamide resins with biological systems we subjected resin-bound peptides to enzymatic degradation. For example, the Leu-Pro-Ser prothymosin α (84-101) derivative was synthesized using Fmoc/tBu amino acids

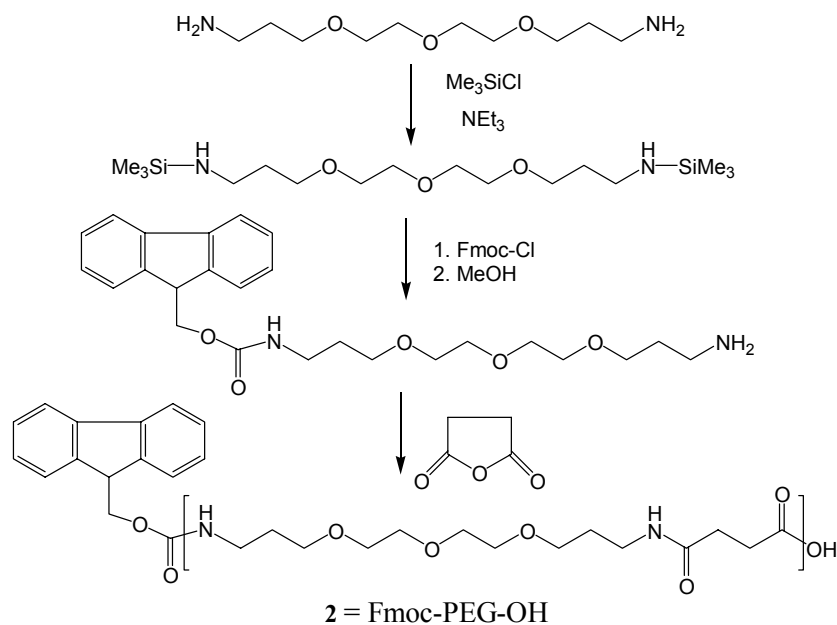


Fig. 2. Preparation of the protected monomer amino acid units.

and deprotected by 95% TFA, still remaining bound on the resin. During the trypsinolysis the expected tryptic fragments were released from the resin and identified by HPLC-MS. The same was observed also in the trypsinolysis of resin-bound DNP peptides like the DNP-hirudin(43-48) fragment, DNP-Glu-Gly-Thr-Pro-Lys-Pro-PEG₂-AM resin.

Table 1. Swelling of 1 g Fmoc-PEG_n-aminomethyl resin in various solvents

	n = 1	n = 2	n = 3	n = 4	n = 5
H ₂ O	3,5	4	4	4.5	4.5
DMF	6	7	6,5	6	6
DCM	6,5	7	6	6	6
MeOH	5	6	6	6	6
THF	5	4	5	5	5
AcN	5	4,5	4	4	4
NMP	7,5	7,5	7	7	7,5

The ability of H-ProTa(87-101)-PEG₂-AM Resin to react with rabbit polyclonal antibodies against to H-ProTa(87-101)-OH peptide (first antibodies) was tested, using goat anti-rabbit IgG, peroxidase conjugated, as second antibodies. It was found that the resin-bound H-ProTa(87-101)-resin was specifically recognized by antibodies.

Acknowledgments

The work was funded by CBL-Patras S.A.

New Nomenclature for Complex Cyclopeptides

**Jan Spengler^{1,2}, José-Carlos Jiménez^{1,3}, Klaus Burger², Ernest Giralt^{1,4}
and Fernando Albericio^{1,4}**

¹Barcelona Biomedical Research Institute, Barcelona Science Park, University of Barcelona, 08028 Barcelona, Spain; ²University Leipzig, Department of Organic Chemistry, 04103 Leipzig, Germany; ³Biogenidec Inc., 14 Cambridge Center, Cambridge, MA 02142, USA; ⁴University of Barcelona, Department of Organic Chemistry, 08028-Barcelona, Spain

Introduction

One-line text formulas for peptides are widely in use due to their convenience, although established nomenclature do not allow unequivocal representation for "side-chain to head (or tail)", "backbone to backbone", "side-chain to side-chain" cyclopeptides, "side-chain to side-chain" connected peptide strands, and branched peptides.

This new nomenclature offers an unambiguous and general nomenclature system that enables researchers to represent all cyclic and branched homo- and heterodetic peptides in a coherent manner in one-line text – as long as their constituents can be represented in (three) letter codes. Its application would overcome the existing difficulties and provide a way to express complex situations in the shortest way in order to highlight more clearly the salient points in a given scientific communication.

Results and Discussion

Symbolic representations use the hyphen ("-") as the symbol for a chemical bond and, since written text is one-dimensional, both binding partners have to be written side by side. This drawback creates a bottleneck in the established nomenclature system. The nomenclature system proposed here introduces "connection points". These points represent the sites where a chemical bond has been 'cut'. The symbol that represents the connecting point is "&" and is available on all computer keyboards. The appearance of "&" in a given position of the one-line formula represents the point at which one end of a chemical bond is located and the second "&" indicates the point to which this bond is attached. The symbol "&" has not been used to date in chemical formulae and so does not cause any problems in this respect.

As example is discussed here the melanocortin-AGRP chimeric peptide H-Tyr-c[β-Asp-His-DPhe-Arg-Trp-Asn-Ala-Phe-Dpr]-Tyr-NH₂ (I) [1]. Commonly, the term "c[β-Asp-His-DPhe-Arg-Trp-Asn-Ala-Phe-Dpr]" means that the cyclization site is located between the N-terminus of β-Asp and the C-terminus of Dpr (II). Instead, the formula refers to a lactam cyclization *via* the side chains of β-Asp and Dpr (III). Applying the proposed nomenclature makes this two cyclo-isomers clearly distinguishable: &β-Asp-His-DPhe-Arg-Trp-Asn-Ala-Phe-Dpr& (II) *versus* H-β-Asp(&)-His-DPhe-Arg-Trp-Asn-Ala-Phe-Dpr(&)-OH (III). Thus, writing H-Tyr-β-Asp(&)-His-DPhe-Arg-Trp-Asn-Ala-Phe-Dpr(&)-Tyr-NH₂ (I) avoids any misinterpretation.

The complexity of peptides with more than one cyclization sites prevented from one-line text expression. &¹Ala-Gly-Cys(&²)-Cys(&³)-Ser-Asp-Pro-Arg-Cys(&²)-Ala-Trp-Arg-Cys(&³)&¹ (IV) is a cysteine rich peptide belonging to the family of

conotoxins [2], and represents an application of the nomenclature on previously (in one-line text) inexpressible compounds.

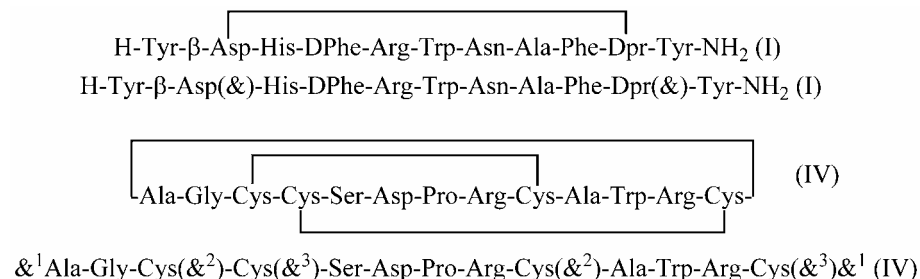


Fig. 1. Formula and corresponding one-line text representations of discussed examples.

In summary, the nomenclature system proposed here is based on the following rules:

1) "&" represents the start or the end of a chemical bond, which is 'cut' with the aim of visualizing a complex formula more easily. In this way, two "&" symbols represent one chemical bond.

2) If more than one bond is cut in a given system, a superscript number indicates the connecting points that belong together. Thus, &¹ binds with &¹, &² binds with &², etc.

3a) &Xaa- means the bond starts/ends at the N-terminus (only or first substituent); b) -Xaa& means the bond starts/ends at the C-terminus; c) -Xaa(&- means the bond starts/ends in the side chain; d) -(&)Xaa- means the bond starts/ends at the N-terminus as second substituent; e) -(&-)Xaa- means the bond starts/ends at the α -carbon of an amino acid Xaa.

4) If a molecule consists of two or more strands (or bridges), these strands (or bridges) are written separately in brackets as in mathematical terms or in a chemical formula: e.g. {[strand1][strand2][bridge]}. The longest strand is written first. Strands of equal length are given priority alphabetically.

5) Transcription of head to tail cyclopeptides begins with the building block of the highest alphabetical priority [3].

Acknowledgments

J. Spengler thanks the VW Foundation for providing a grant for this project. This work was partially supported by Generalitat de Catalunya [Grups Consolidats (2001 SGR 0047) and CERBA], Ministerio de Ciencia y Tecnología (BIO 2002-02301 and BQU 2003-00089), and Barcelona Science Park.

References

1. Wilczynski, A., Wilson, K. R., Scott, J.W., Edison, A.S. and Haskell-Luevano, C. *Biopolymers (Peptide Sci.)* **80**, 553 (2005).
2. Alewood, P. *Biopolymers (Peptide Sci.)* **80**, 497 (2005).
3. Spengler, J., Jiménez, J.-C., Burger, K., Giralt, E. and Albericio, F. *J. Peptide Res.* **65**, 550-555 (2005).

New Approaches for Native Chemical Ligation

Dana Baas, Daniel G. Mullen and George Barany

Department of Chemistry, University of Minnesota, Minneapolis, MN 55455-0431, USA

Introduction

Native chemical ligation (NCL) has become one of the preferred methods for producing small proteins of greater than 50 amino acids in length [1]. The rate-limiting step in NCL is the purification of the intermediate fragments and of the final product [2]. The C-terminal thioester intermediates are typically made by Boc-based methods, because thioesters are cleaved by the piperidine used in Fmoc-based chemistries.

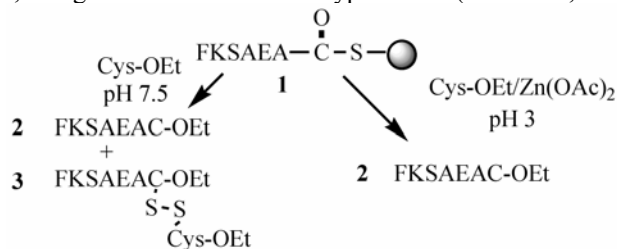
As part of a program to develop new NCL techniques, we have been exploring general methods to synthesize peptide thioesters compatible with Fmoc chemistry [3]. Peptides of about 25 amino acids in length can routinely be made in very high crude purity. The low levels of impurities that do occur generally result from the final acidic treatment, not from chain assembly steps. We reasoned that a method that would allow the capture of protected fragments from solution as resin-bound thioesters, followed by final acidic cleavage, would allow the synthesis of the desired NCL intermediates without purification.

Results and Discussion

Previous work has shown that peptide thioesters can be made in solution from protected fragments synthesized on 2-chlorotrityl resin with Fmoc chemistry [4]. We have extended this strategy by capturing protected fragments, synthesized with 2-chlorotrityl resin, from solution as resin-bound thioesters.

The polymer chosen for use in this work is CLEARTM resin [5], because it has excellent swelling properties in organic and aqueous solvents. Thiol-functionalized CLEARTM was synthesized by coupling CLEARTM-base resin with *S*-trityl-3-mercaptopropionic acid. After removal of the trityl group with reagent B, a thiol-CLEARTM resin resulted that gave a positive Ellman's test for sulfhydryl groups.

To test the validity of the thiol capture strategy, fully protected hexapeptide Fmoc-FK(Boc)S(tBu)AE(tBu)A was coupled to thiol-CLEARTM resin with the BOP reagent. Next, Fmoc removal with piperidine-DMF (1:4), followed by side-chain deprotection with reagent B gave CLEARTM thioester-linked peptide **1**. Treatment of **1** with Cys-OEt (10 eq.) in phosphate buffer resulted in the expected NCL product, heptapeptide **2**, along with mixed disulfide byproduct **3** (Scheme 1, left path).



Scheme 1. Model ligation experiments of a thiol captured hexapeptide reacted with Cys-OEt.

The critical chemical step in NCL is thioacylation of an *N*-terminal cysteine side-chain by a peptide C-terminal thioester. Facile rearrangement to the

thermodynamically more stable amide bond then occurs. However, when alkylating the thiol of cysteine-containing peptides, acidic conditions catalyzed by Zn^{2+} are optimal [6]. To test if the thiol of cysteine-containing peptides would be acylated by thioesters under these acidic conditions, **1** was treated with Cys-OEt (10 eq.) and $\text{Zn}(\text{OAc})_2$ (5 eq.). Only the desired product, **2**, was formed (Scheme 1, right path).

Next, experiments were run to optimize the yield of the thiol capture of peptides from solution. Three coupling protocols that have been routinely used to form thioesters were tested (Table 1). BOP was the most effective reagent for the capture step. However, low yields were found, even for the coupling of Fmoc-Lys(Boc)OH, where a maximum of 37% of the amino acid was captured from solution. When the hexapeptide of the model study or a fully protected 14-residue fragment of the nucleocapsid (NC) protein were tested, capture yields dropped to only about 10%. These yields are too low to make this procedure useful as a preparative NCL method.

Table 1. Optimization of capture from solution of protected peptides by thiol-CLEAR™ resin

Method ^a	Sequence	Actual Loading ^c	Theoretical Loading	Percent Capture
HBTU	Fmoc-Lys(Boc)OH	0.023	0.62	3.7
BOP	Fmoc-Lys(Boc)OH	0.23	0.62	37
DIPCDI/DMAP	Fmoc-Lys(Boc)OH	0.046	0.62	7.4
HBTU	Fmoc-FK(Boc)S(tBu)AE(tBu)A	0.020	0.45	4.4
BOP	Fmoc-FK(Boc)S(tBu)AE(tBu)A	0.060	0.45	13
DIPCDI/DMAP	Fmoc-FK(Boc)S(tBu)AE(tBu)A	0.019	0.45	4.2
BOP	Fmoc-NC 1-14 ^b	0.020	0.21	9.5

^aThe reagent, peptide, and thiol-CLEAR™ resin were coupled in equimolar ratios for 3 h.

^bSequence: Fmoc-IQ(Trt)K(Boc)GN(Trt)FR(Pbf)N(Trt)Q(Trt)R(Pbf)K(Boc)T(tBu)VK(Boc)

^cDetermined by Fmoc assay.

The low coupling yields may be due to hindered thiols on the resin. The Ellman's test on thiol-CLEAR™ continues to develop color over several hours, and cannot be used quantitatively for this reason. However, coupling peptides overnight does not increase capture yields. Possibly, the thiol-CLEAR™ resin needs to be in excess to successfully capture all the peptide from solution. Finally, the acidic ligation conditions may represent a useful alternative to the standard basic protocol. The scope and limitations of the acidic conditions applied to NCL are under study.

Reference

1. Dawson, P. E. and Kent, S. B. H. *Annu. Rev. Biochem.* **69**, 923-960 (2000).
2. Kent, S. J. *Peptide Sci.* **9**, 574-593 (2003).
3. Gross, C. M., Lelievre, D., Woodward, C. K. and Barany, G. *J. Peptide Res.* **65**, 395-410 (2005).
4. von Eggelkraut-Gottanka, R., Klose, A., Beck-Sickinger, A. G. and Beyermann, M. *Tetrahedron Lett.* **44**, 3551-3554 (2003).
5. Kempe, M. and Barany, G. *J. Am. Chem. Soc.* **118**, 7083-7093 (1996).
6. Naider, F. R. and Becker, J. M. *Biopolymers* **43**, 3-14 (1997).

Microwave-Assisted Solid-Phase Peptide Synthesis (MW-SPPS) on CLEAR Supports

Anne L. Carenbauer¹, Matthew R. Cecil¹, Andrzej Czerwinski¹,
Krzysztof Darlak¹, Mirosława Darlak¹, DeAnna Wiegandt Long¹,
Francisco Valenzuela¹ and George Barany²

¹Peptides International, Inc., 11621 Electron Drive, Louisville, KY 40299, USA; ²Department of Chemistry, University of Minnesota, Minneapolis, MN 55455, USA

Introduction

CLEAR (Cross-Linked Ethoxylate Acrylate Resin) polymers were introduced by Kempe and Barany [1] and further developed as a commercial product in 1997 [2]. From the outset, CLEAR has proven to be an excellent support for solid-phase peptide synthesis (SPPS), especially of challenging sequences. The entire cross-linked matrix of CLEAR is PEG-like in character and thus very hydrophilic. Therefore, CLEAR resins possess desirable solvation properties that aid disruption of secondary structure formation during synthesis. Also, CLEAR resins offer better swelling properties than polystyrene-based resins in a wider variety of solvents (i.e., DCM, THF, and highly polar solvents including lower alcohols and water), leading to better coupling efficiencies and improved yields and purities of SPPS products.

The application of microwave energy to chemistry has its roots in organic synthesis applications [3,4]. When compared to thermal heating, microwave-assisted chemistries have been reported to deliver products of higher purity at considerably reduced reaction times [5]. The present studies sought to evaluate the accelerated synthesis on CLEAR supports of Microwave-Assisted Solid-Phase Peptide Synthesis (MW-SPPS) [6].

Results and Discussion

Several short test sequences [H-YFLFRPRN-NH₂ (**1**), H-HwAWfK-NH₂ (**2**), H-RLLFT-NH₂ (**3**), H-HwkWfK-NH₂ (**4**), H-GSS(*n*-octanoyl)FL-NH₂ (**5**), H-GRGDSP-OH (**6**), H-rPKPfQwFwLL-NH₂ (**7**), Ac-YV-Nle-GHfRWDRFG-NH₂ (**8**), H-GSF-NH₂ (**9**), H-GsF-NH₂ (**10**), H-GDF-NH₂ (**11**), and H-GdF-NH₂ (**12**)] were prepared on CLEAR supports in controlled comparisons of MW-SPPS with traditional, automated SPPS protocols. MW-SPPS was performed on 0.5 – 1.0 mmol scales using the CEM Discover LabMate™ instrument with temperature feedback (CEM, Matthews, North Carolina). Fmoc deprotection was carried out with piperidine–DMF (1:4, v/v) using 5 cycles at 50 watts for 30 seconds each, and coupling reactions were performed with 6 cycles at 50 watts for 30 seconds each. Amino acids were single-coupled using 4-fold excess over resin (1 equiv), activated by BOP (4 equiv), HOBt (4 equiv), and NMM (6.8 equiv) in DMF. Between microwave cycles of deprotection or coupling, the sample tube containing the reaction mixture was chilled to approximately 4°C. Power and times of the cycles were determined empirically to maintain a sample temperature under 35°C for general synthesis. For synthesis of compound **5**, esterification of the hydroxyl group of serine with *n*-octanoic acid was achieved on-resin using the DIC/DMAP method [7], with substantial improvements in reaction rate and yield. In this case, microwave energy was also used to accelerate the esterification process (30 cycles) and the yield was quantitative. The same number of cycles for Fmoc deprotection (5

cycles) and the protected amino acid coupling (6 cycles) were used for all experiments and identical sequence-specific cleavage cocktails were used for each comparison. Cycles of 40 watts were used for 25 seconds to maintain the required maximum temperature (T_{\max} 30°C and T_{\max} 50°C) for 0.5 mmol scale. For all syntheses, only a short preactivation time of 30 seconds was used, with the goal to minimize potential racemization prior to coupling.

Racemization studies were conducted by assembling diastereomers of two model peptides, H-Gly-Xxx-Phe-NH₂, where Xxx = D or L, Ser or Asp (peptides **9-12**). There was no significant racemization (less than 1%) observed for **9**, **11**, or **12**, either by standard SPPS or MW-SPPS. In peptide **10**, the observed L-Ser diastereomer was slightly higher (1-2%) in all cases, which is most likely due to L contamination of the starting material, Fmoc-D-Ser(tBu)-OH.

In summary, fast manual synthesis of short peptides was achieved with CLEAR resins as the solid support. Microwave-assisted deprotections of the Fmoc group and couplings of the incoming protected amino acid components were complete within minutes. MW-SPPS was also found to be a fast method for loading C-terminal amino acids onto CLEAR-Amide Resin. However, microwave-assisted synthesis of C-terminal proline-containing peptide **6** was unsuccessful due to diketopiperazine formation leading to loss of all chains from the resin, while traditional SPPS gave a 30% yield of peptide **6**. While yields of crude products are comparable between classical SPPS and MW-SPPS, in the majority of cases, purities of crude peptides obtained with microwave radiation (MW-SPPS) were higher than those of traditional SPPS. Thus, those peptides obtained via MW-SPPS were easier to purify, and yields of the purified peptides were higher than with traditional SPPS. Racemization studies carried out with two model peptides did not indicate any substantial racemization from MW-SPPS in comparison to traditional SPPS, even at elevated temperatures of 50°C. Because our work shows that CLEAR supports are fully compatible with MW-SPPS, with reductions in synthesis times and improvements in purities and yields, practitioners in the field are encouraged to try this approach when more traditional methods are found wanting.

References

1. Kempe, M. and Barany, G. *J. Am. Chem. Soc.* **118**, 7083-7093 (1996).
2. CLEAR resins are produced exclusively by Peptides International and are protected under US Patents 5,656,707 and 5,910,554.
3. Kappe, C. O. and Stadler, A. In *Microwaves in Organic Synthesis* (Loupy, A., ed.) Wiley-VCH Verlag, Weinheim, pp. 405-433 (2002).
4. Blackwell, H. E. *Org. Biomol. Chem.* **1**, 1251-1255 (2003).
5. Mavandadi, F. and Lidstrom, P. *Current Topics in Medicinal Chemistry* **4**, 773-792 (2004).
6. Yu, H. M., Chen, S. T. and Wang, K. -T. *J. Org. Chem.* **57**, 4781-4784 (1992).
7. Hassner, A. and Alexanian V. *Tetrahedron Lett.* **46**, 4475-4478 (1978).

Microwave Assisted Peptide Synthesis – A Tool to Replace Classical SPPS?

Andreas Rybka and Hans-Georg Frank

AplaGen GmbH, Arnold-Sommerfeld-Ring 2, 52499 Baesweiler, Germany

Introduction

The solid phase approach is a well established method for synthesizing peptides since the work of Bruce Merrifield in the 1960s. Since the first serious experiments for synthesizing peptides with the help of microwaves in 1992, the method and the instruments have been optimized a lot. Nevertheless many peptide chemists around the world still think of "cooking peptides" when they hear of microwave assisted peptide synthesis and fear the enhancement of side-reactions. Some examples from our laboratory show that MAPS is definitely a valuable tool for synthesizing peptides and that there is no need to fear the side-reactions.

Example 1: Synthesis of EMP (20aa): The 20aa peptide is a well-known EPO mimetic we use as cheap internal standard for our own EPO mimetics. The manual synthesis without microwaves takes 10 days and leads - in spite of double deprotections and double couplings - to an impure crude peptide. The first synthesis in microwave at 70°C showed extensive racemization (3-5%). We were able to suppress racemization completely by using a cooling procedure and reducing the amount of base. The manual synthesis with the help of microwaves and external cooling with an ice bath takes about 4.5hrs total synthesis time (single deprotection and single coupling - Table 1) and leads to an excellent purity of the crude peptide (Fig. 1). After cyclization the EMP shows the expected biological activity (Fig. 2). Synthesis was carried out on the Discover-System (CEM) in a scale of 1.00mmol. Analysis of the crude peptide was carried out on a Nebula-LCMS system (Gilson).

Resin:	1mmol Fmoc-Gly-Wang 100-200mesh sr = 0.75 mmol/g
Deprotection:	3x30sec 100W ($T_{\max} = 40^{\circ}\text{C}$)
Coupling:	5x30sec 50W ($T_{\max} = 40^{\circ}\text{C}$) // 5eq aa, 5eq PYBOP, 7.5eq HOBT, 5eq DIEA
Cleavage:	60min Cocktail C (94% TFA, 1% TIS, 2.5% H_2O , 2.5% EDT)
Total Synthesis time:	4.5hrs
Yield:	342mg linear purified peptide (16%)
Cyclization:	10 mg peptide in 100ml 65% CH_3CN pH = 8.5 // 2eq $\text{K}_3[\text{Fe}(\text{CN})_6]$, 18h, 25%

Table 1. Optimized synthesis of EMP using microwaves.

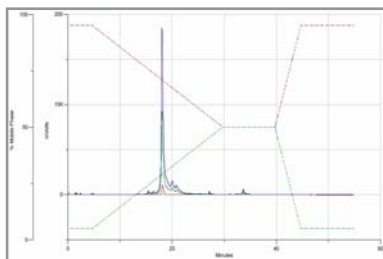


Fig. 1. Analytical LCMS of crude EMP.

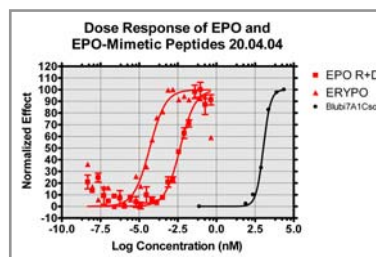


Fig 2. Biological activity of EMP.

Example 2: Improved synthesis of AGEM (41aa): The 41aa peptide is one of AplaGen's own EPO mimetics. With conventional methods using double couplings

the purity of the crude material was below 5%. The microwave assisted synthesis was carried out on the Liberty system (CEM) in a scale of 0.25mmol and gave a crude purity of about 40%. No cooling procedure was used and the bleeding effect was investigated further (use of different Rink-Amide resins from different suppliers). The highest yields could be achieved by the use of Tentagel R RAM (Resin no. 4) supplied by Rapp Polymere GmbH (Table 2). Purification of the crude peptide (Fig. 3) was carried out on a Nebula-LCMS system (Gilson). The peptide showed the expected biological activity (Fig. 4).

Resin:	0.25mmol Rapp Tentagel R-RAM, 100-200mesh, sr = 0.18mmol/g
Deprotection:	30sec 25W ($T_{\max} = 60^{\circ}\text{C}$), 180sec 35W ($T_{\max} = 70^{\circ}\text{C}$)
Coupling:	300sec 35W ($T_{\max} = 70^{\circ}\text{C}$) // 2x (4eq aa, 4eq PYBOP, 6eq HOBT, 4eq DIEA)
Cleavage:	180min Cocktail X (94% TFA, 1% TIS, 2.5% H_2O , 2.5% DODT)
Total Synthesis time:	31hrs
Yield:	126mg purified peptide (11%)

Table 2. Optimized synthesis of AGEM using microwaves.

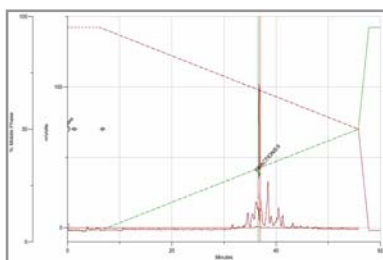


Fig. 3. Preparative LCMS of crude AGEM.

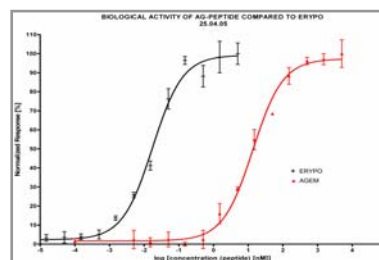


Fig 4. Biological activity of AGEM.

Results and discussion

Microwave assisted peptide synthesis enabled us to speed up the drug development process. An enhancement of racemization was seen in first experiments, but could be overcome by cooling and reduction of base excess. Side-reactions like aspartimide formation were observed in sensitive sequences, but could be overcome by standard means. Further research has to be done in fields of fragment condensations and optimization of coupling reagents.

Acknowledgments

We have to thank CEM for the excellent support.

Fast and Versatile Peptide Backbone Modifications Using Microwave Energy

Daniel Raichman and Gerardo Byk

Department of Chemistry, Laboratory of Peptidomimetics and Genetic Chemistry, Bar-Ilan University, 52900-Ramat Gan, ISRAEL

Introduction

The huge number of novel microwave-assisted organic procedures recently emerged, demonstrate that microwave energy will take, in the close future, a central place in the organic chemistry laboratories. Nevertheless, the use of microwave in the field of peptide and peptidomimetics syntheses is still very limited to date. The main application proposed recently in this field concerns amino acid coupling to solid supported growing peptides which is, in any case, a very efficient process under classical conditions [1], this application rather helps to propose a new kind of automation of the peptide synthesis process. Another attempt to use microwave was for the synthesis of peptoids on solid phase [2], in those works the efficiency of the process was similar to regular heating. Finally an interesting recent application is the production of reduced peptides in very short time as compared to classical methods [3]. In the context of our peptidomimetics program we started to study known “difficult organic reactions” performed on peptides, towards new faster and efficient synthetic procedures for renovating these difficult reactions. One of these reactions is the intramolecular Heck reaction in peptides. Larhed and others have recently demonstrated that the Heck reaction between two small molecules can be dramatically improved using a fast microwave-assisted intermolecular reaction [4-8]. In this work we have revisited the intramolecular Heck reaction

Results and Discussion

A model series of ring-varying peptides Acryloyl-[Gly]_n-Phe(4-I)NHR was synthesized on Rink resin as shown in Figure 1.

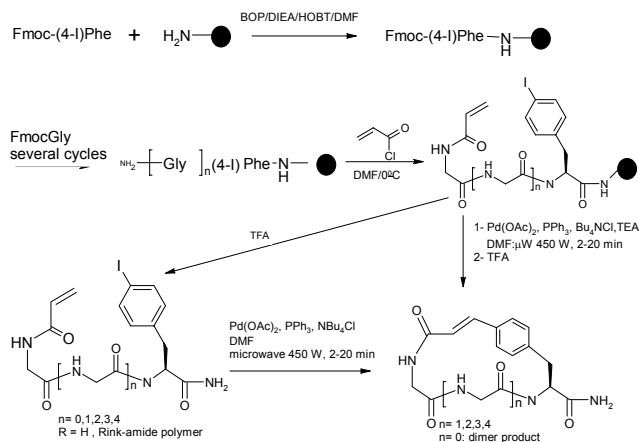
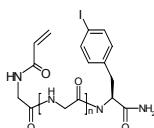
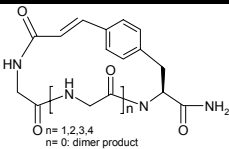


Fig. 1. Macrocyclization of model peptides using a microwave assisted Heck reaction.

The method was applied to solution and solid supported cyclizations. Results in Table 1 indicate that the intramolecular Heck reaction can be performed in peptides both in solution and solid support using a modified domestic microwave at 450 W energy level within 1 to 30 minutes in DMF (153°C) with moderated yields of the final purified products ranging from 15 to 25 % for a scale between 2-45 mg of linear precursors. Interestingly, when $n=0$, the product was exclusively a dimer composed of two units with a cycle of 26 atoms. This product was obtained first in solution and surprisingly also in solid phase reaction that implies a double Heck reaction on the solid support between two separate sites.

Table 1. Physical properties of macrocyclic products

						
n	MW Calc.	MW Obs.	MW Calc.	MW Obs.	Yield % Solid phase	Yield % Solution
0	401	401	273	546	13	20
1	458	458	330	330	17	24
2	515	515	387	387	13	20
3	572	572	444	444	15	24
4	629	629	501	501	15	15

One of the easily obtained macrocycles ($n=4$) was investigated under classical conditions, the cyclization needed 6 days at 90°C for total conversion unlike the microwave-assisted reaction that needed only 2 min. The reaction was tested also using Phe(4-Br) and Phe(4-Cl), only the former reacted significantly to give the cyclized peptide in 20% yield.

These results make the microwave-assisted Heck reaction an attractive renovated approach for peptidomimetics.

Acknowledgments

This work was financed by U.S.-Israel Bi-National Science Foundation [1998378] and by "The Marcus Center for Medicinal Chemistry". We thank Dr. Hugo Gottlieb, Dr. Vered Marks, Dr. Igor Ulanovsky and Dr. Rachel Persky from the Structural Analysis Dept. of Bar-Ilan University for NMR and MS analysis of products.

References

1. Yu, H. M., Chen, S. T. and Wang, K. T. *J. Org. Chem.* **57**, 4781-4784 (1992).
2. Olivos, H. J., Alluri, P., Reddy, M. M., Salony, D. and Kodadek, T. *Organic Lett.* **4**, 4057-4059 (2002).
3. Santagada, V., *et al.* *QSAR & Combinatorial Science* **23**, 899-901 (2004).
4. Nilsson, P., Larhed, M. and Hallberg, A. *J. Am. Chem. Soc.* **123**, 8217-8225 (2001).
5. Stadler, A., Yousefi, B. H., Dallinger, D., Walla, P., Van Der Eycken, E., Kaval, N. and Kappe, C. O. *Org. Process Res. Devel.* **7**, 707-716 (2003).
6. Noteberg, D., Schaal, W., Hamelink, E., Vrang, L. and Larhed, M. *J. Comb. Chem.* **5**, 456-464 (2003).
7. Tietze, L. F., Wiegand, J. M. and Vock, C. *J. Organometallic Chem.* **687**, 346-352 (2003).
8. Gracias, V., Moore, J. D. and Djuric, S. W. *Tetrahedron Lett.* **45**, 417-420 (2004).

Microwave-Assisted Synthesis of Multivalent Dendrimeric Peptides using Cycloaddition Reaction ('Click') Chemistry

Dirk T. S. Rijkers, G. Wilma van Esse, Remco Merkx, Arwin J. Brouwer, Hans J. F. Jacobs, Roland J. Pieters and Rob M. J. Liskamp

Department of Medicinal Chemistry, Utrecht Institute for Pharmaceutical Sciences, Faculty of Pharmaceutical Sciences, Utrecht University, PO Box 80082, 3508 TB Utrecht, The Netherlands

Introduction

Dendrimers are versatile constructs for the simultaneous presentation of especially biologically relevant ligands. These multivalent constructs are particularly interesting for enhancing the interaction of weakly interacting individual ligands e.g., carbohydrates [1]. We have successfully explored this in the design, synthesis, and biological evaluation of dendrimeric carbohydrates [2]. In addition, dendrimers might serve as promising molecular scaffolds for increasing effects merely by offering a number of ligands or by aligning these ligands [3].

A crucial issue is the complete and efficient attachment of ligands to dendrimers. In most cases peptides are attached to dendrimers by reaction of sulfhydryl groups of peptides with maleimide or iodoacetamide functionalities. However, new reactions with increased efficiency and chemoselectivity would be very welcome. The reaction between acetylenes with organic azides was recently reinvestigated independently by Meldal [4] and Sharpless [5] and seems particularly suitable for chemoselective bioconjugation reactions.

Here we show that (un)protected azidopeptides can be efficiently attached to a derivatized version of our earlier developed dendrimers [6] using a 1,3-dipolar cycloaddition ('click'-chemistry), which was conveniently assisted by microwave irradiation to ensure a complete modification of the alkyne endgroups.

Results and Discussion

In a first approach, peptide dendrimer **10** (Fig. 1) was synthesized by mixing azide **1** with the appropriate acetylene in the presence of CuSO₄/Na-ascorbate/Cu-wire in THF/H₂O (1:1 v/v). After 16 hrs at rt, **10** was isolated in a fair yield (56%). A tremendous improvement was achieved by running this reaction under microwave irradiation. After 10 min at 100°C in THF/H₂O in the presence of CuSO₄/Na-ascorbate **10** was isolated in 93% yield. Using these conditions, divalent peptide cycloadducts **14** – **17** were obtained in fair to good yields (48-72%). Analogously, tetravalent amino acid cycloadduct **11** and tetravalent dipeptide cycloadduct **18** were synthesized in 91 respectively 63% yield. Even more rewarding was the successful preparation of octavalent dipeptide **19** (69%) as well as octavalent and hexadecavalent systems **12** and **13** in 69 and 94% yield, respectively. The next challenge was the attachment of larger or bioactive peptides to these dendrimeric alkynes. Azidopeptide **6** (magainin I [12-23]), azido-Leu-enkephalin **7**, azide **8** (a fibronectin active fragment), and the *cyclo*-RGD azidopeptide **9** (an $\alpha_v\beta_3$ integrin binding peptide for tumor targeting [7]), were efficiently coupled to the 1st and 2nd generation dendrimers with alkyne endgroups (Fig. 1). In conclusion, we have developed an efficient chemoselective microwave-assisted cycloaddition reaction for the synthesis of di-, tetra-, octa- and hexadecavalent dendrimeric peptides.

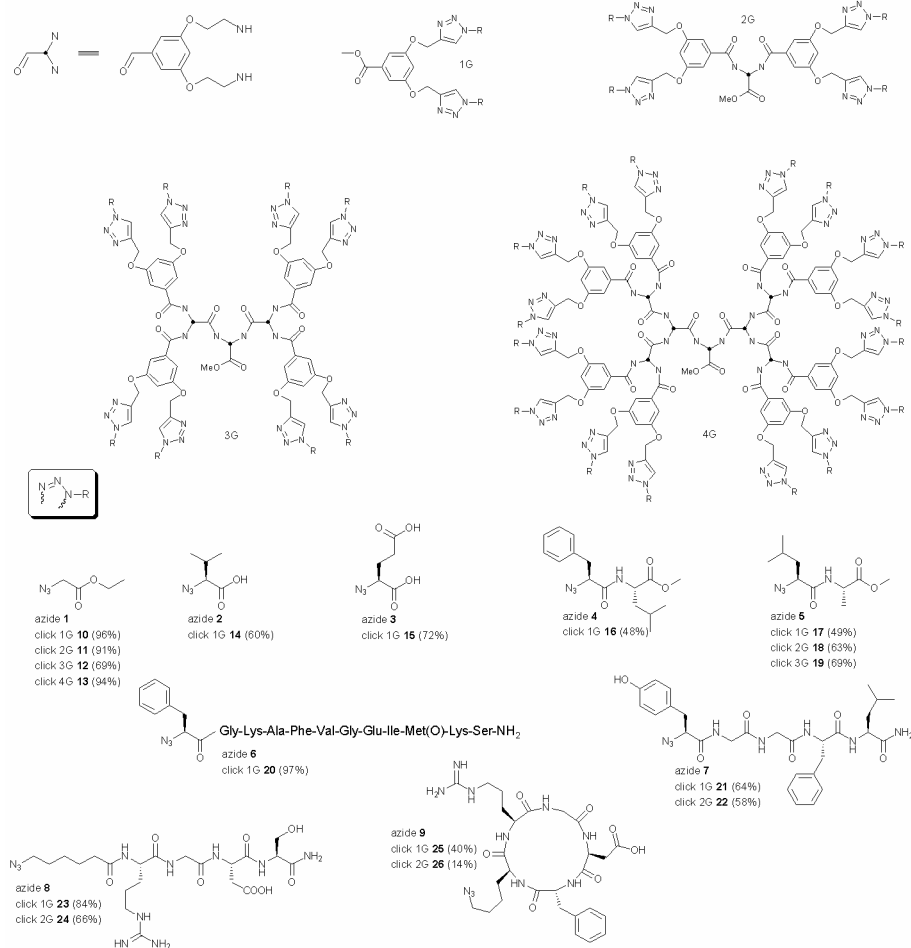


Fig. 1. Structures of the azides (1 – 9) and the corresponding peptide dendrimers: 1st generation: 10, 14 – 17, 20 – 21, 23 and 25; 2nd generation: 11, 18, 22, 24 and 26; 3rd generation: 12 and 19, and 4th generation: 13.

References

- Mammen, M., Choi, S. -K. and Whitesides, G. M. *Angew. Chem. Int. Ed.* **37**, 2754-2794 (1998).
- A representative example: Joosten, J. A. F., Loimaranta, V., Appeldoorn, C. C. M., Haataja, S., Ait El Maate, F., Liskamp, R. M. J. and Pieters, R. J. *J. Med. Chem.* **47**, 6499-6508 (2004).
- Newkome, G. R., Moorefield, C. N. and Vögtle, F. *Dendrimers, and Dendrons: Concepts, Synthesis, Applications*, Wiley, New York, (2001).
- Tornøe, C. W., Christensen, C. and Meldal, M. *J. Org. Chem.* **67**, 3057-3064 (2002).
- Rostovtsev, V. V., Green, L. G., Fokin, V. V. and Sharpless, K. B. *Angew. Chem. Int. Ed.* **41**, 2596-2599 (2002).
- For example: Brouwer, A. J. and Liskamp, R. M. J. *Eur. J. Org. Chem.* 487-495 (2005).
- Thumshirn, G., Hersel, U., Goodman, S. L. and Kessler, H. *Chem. Eur. J.* **9**, 2717-2725 (2003).

Efficient Synthesis of Disulfide Bridge Containing Peptides: Melanin Concentrating Hormone (MCH) and Brain Natriuretic Peptide (BNP)

Jianjun Jiang¹, Brian D. Dayton¹, Sevan J. Brodjian¹, Bryan C. Tieman²,
Susan E. Brophy² and Paul L. Richardson¹

¹Global Pharmaceutical Research and Development; ²Abbott Diagnostic Division, Abbott
Laboratories, Abbott Park, IL 60064, USA

Introduction

Melanin-concentrating hormone (MCH) DFDMLRC*MLGRVYRPC*WQV [1] is an endogenous neuropeptide expressed in the hypothalamus. The mammalian MCH receptor is an attractive target for treatment of obesity and obesity-associated pathologies. Brain natriuretic peptide (BNP) SPKMVQSGC*FGRKMDSRSSS-GLGC*KVLRRH [2] is a well-known cardiac hormone, which has several pharmacological activities including diuretic-natriuretic, hypotensive and vasorelaxant actions. Both MCH and BNP are disulfide cyclic peptides. We report the rapid, practical, high-yield synthesis of full-length MCH [3], full-length BNP and derivatives of each, using solid-phase assembly of the linear precursor followed by optimized solution-phase disulfide macrocyclization. (C*...C*, indicates disulfide bridge).

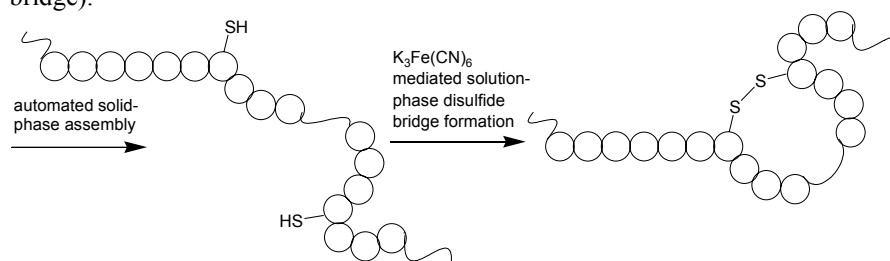


Fig. 1. General procedure for the synthesis of MCH and BNP.

Results and Discussion

Published methods for the synthesis of MCH generally involve the solid-phase synthesis of the linear peptide precursor followed by solution-phase disulfide macrocyclization. Published yields for MCH syntheses are generally modest, and as reported, produced less than 10 mg pure MCH. Mild oxidation conditions are required to prevent over-oxidation of the susceptible methionine, tryptophan and tyrosine residues. Air [4,5], $K_3Fe(CN)_6$ [5,6], and iodine [5,6] oxidations have all been described. In addition, the low solubility of the linear precursor results in aggregation and polymer formation, even under the high dilution conditions (0.25 - 1 mg/mL) typically employed for such macrocyclizations.

Our original synthesis of MCH via DMSO/air oxidation provided only 4.8 mg after using two RP-HPLC purifications from 362 mg crude peptide (1.3% yield). While this method provided material for early testing, it was not practical for the preparation of larger quantities of MCH as required for ongoing studies.

As the primary bottleneck to the original procedure, we decided to optimize the solution-phase oxidation. Crude linear peptide was used under three carefully

controlled conditions (Table 1) as monitored by RP-HPLC. In the first method, 20% acetonitrile was added to aqueous 100 mM NH_4HCO_3 buffer to improve the solubility of the peptide. This prevented the cloudiness that was observed in the absence of organic co-solvent, and resulted in improved yield (14 mg, 10.6%). Further dilution to 0.5 mg/mL and increasing the organic solvent to 40% acetonitrile did not result in improved yield, and the reaction did not go to completion even after 3 days of stirring (11.3 mg, 8.6%), likely due to a decrease in the pH of the solution (8.0 \rightarrow 3.0) over the course of the reaction. The final reaction employed both high dilution (0.5 mg/mL) and high organic co-solvent (40% acetonitrile), but with the addition of aqueous $\text{K}_3\text{Fe}(\text{CN})_6$ (0.05% w/v) batch wise until the yellow color of the $\text{K}_3\text{Fe}(\text{CN})_6$ persisted. The total time of reaction for the $\text{K}_3\text{Fe}(\text{CN})_6$ oxidation was two hours.

Table 1. Disulfide Cyclization Optimization

Conditions	Time	Yield
1 mg/mL 20% acetonitrile, air	2 days	14.0 mg (10.6%)
0.5 mg/mL, 40% acetonitrile, air	3 days ^a	11.3 mg (8.6%)
0.5 mg/mL, 40% acetonitrile, $\text{K}_3\text{Fe}(\text{CN})_6$	2 hours	22.4 mg (17.0%)

^aDid not go to completion.

To summarize, utilizing the optimized procedures, linear MCH (19 residues) and BNP (32 residues) derivatives were synthesized using Fmoc/tBu chemistry on Wang resin (MCH) or PEG-PS resin (BNP). Following deprotection and cleavage with reagent K [7] containing triisopropylsilane, the ether precipitated, and dried peptide was dissolved in DMSO (20 mg/mL) and diluted in the optimized disulfide formation buffer (3:2 100 mM aqueous NH_4HCO_3 :acetonitrile, final peptide concentration 0.5 mg/mL). Aqueous $\text{K}_3\text{Fe}(\text{CN})_6$ (0.05% w/v) was added batch wise until the yellow color persisted for at least 20 min, then the acetonitrile was evaporated with a stream of nitrogen gas prior to purification by RP-HPLC on a C18 column. The yield of MCH compounds was around 20% and of BNP and its derivatives 1.5 to 2.7% mainly due to the difficulties in preparing the linear BNP precursors. Improvements to the linear BNP synthesis are ongoing.

References

1. Kawauchi, H., *et al.* *Nature* **305**, 321-323 (1983).
2. Weber, T., Auer, J. and Eber, B. *Current Pharm. Design* **11**, 511-525 (2005).
3. Jiang, J. J., *et al.* In *8th Chinese International Peptide Symposium, Kunming, China*, July 3-6, O-22 and the meeting proceeding, in press (2006).
4. Okamoto, K., Yasumura, K., Fujitani, K., Kiso, Y., Kawauchi, H., Kawazoe, I. and Yajima, H. *Chem. Pharm. Bull.* **32**, 2963-2970 (1984).
5. Brown, D. W., *et al.* *Biopolymers* **29**, 609-622 (1990).
6. Matsunaga T. O., Castrucci, A. M., Hadley M. E. and Hruby, V. J. *Peptides* **10**, 349-354 (1989).
7. King, D. S., *et al.* *Int. J. Peptide Prot. Res.* **36**, 255-266 (1990).

Rapid Solution-phase Synthesis of a 20-mer Peptide According to the DioRaSSP[®] Method

Ivo F. Eggen¹, Frits T. Bakelaar¹, Paul B.W. Ten Kortenaar¹, Knut Adermann², Wolf-Georg Forssmann² and Axel Schulz²

¹Diosynth bv, P.O. Box 20, NL-5340 BH Oss, the Netherlands; ²IPF PharmaCeuticals GmbH, Feodor-Lynen-Strasse 31, D-30625 Hannover, Germany

Introduction

Two years ago Diosynth presented its newly developed method for the large-scale manufacturing of peptides in solution, called DioRaSSP – Diosynth Rapid Solution Synthesis of Peptides [1-3]. This method combines the advantages of the homogeneous character of classical solution-phase synthesis with the generic character and the amenability to automation inherent to the solid-phase approach. Processes according to this highly efficient synthesis method consist of repetitive cycles of coupling and deprotection in a permanent organic phase and are further characterized by the fact that intermediates are not isolated. The processes are easy to scale up and yield products of reproducible high purity, which is guaranteed by a new quenching method for residual activated compounds, applying an anion-forming amine such as a β -alanine ester. This ester should display a lability similar to that of the temporary amino-protecting function, allowing simultaneous deprotection of the growing peptide and the quenched compound. Subsequent basic aqueous (that is active) extractions assure the completely quantitative removal of deprotected quenched compounds before the coupling step of the next cycle of the synthesis, while the growing peptide remains anchored in the organic phase due to the presence of hydrophobic protecting functions, which are generally of the *tert*-butyl type.

DioRaSSP is essentially independent of the applied protecting scheme, allowing the application of relatively cheap, commercially available amino acid derivatives, and offering maximum flexibility with the applied (mild) chemistry, depending on the sequence of the actual peptide [4]. In Z-DioRaSSP, the benzyloxycarbonyl (Z) function is applied for temporary amino protection. This function is removed by hydrogenolysis in each cycle of the process, using formate as the preferred hydrogen donor. Several alternative amino-protecting functions have been applied in the DioRaSSP protocol, including Fmoc (9-fluorenylmethyloxycarbonyl), Msc (methylsulfonylethyloxycarbonyl) and Nsc (2-(4-nitrophenyl)sulfonylethyloxycarbonyl), thus enabling the incorporation of sulfur-containing residues. 1,8-Diazabicyclo[5.4.0]undec-7-ene (DBU) is used to effect fast cleavage of these protecting functions in ethyl acetate, while morpholine is added to scavenge the arising alkenes. Combined approaches (combi-DioRaSSP) are also encompassed by the scope of the DioRaSSP methodology and maximize its flexibility: the approach may be adapted to the actual sequence of the growing peptide at any stage of a synthesis.

Results and Discussion

Syntheses performed according to DioRaSSP proceed by a generic and fast protocol. In the last five years, a considerable number of protected peptides consisting of up to twelve residues have thus been synthesized. Purities are generally high, and average yields of more than 96% per chemical conversion are typically obtained in fast first-

trial syntheses. Several DioRaSSP processes have been directly scaled up after a preliminary feasibility study at the laboratory scale, achieving reproducible results in terms of both yield and purity [5]. Peptides manufactured according to the DioRaSSP method include Buserelin, Deslorelin, Goserelin, Histrelin, Leuprolide, Octreotide and Triptorelin. The scalability of DioRaSSP implies the same process and impurity profile throughout all stages of development, that is, from the first laboratory sample to production batches, combined with intrinsically short process times.

Based on the results obtained in the indicated syntheses, it was surmised that the use of appropriate protecting functions accounts for the fact that the actual length of a peptide (fragment) proved to be no limiting factor in terms of its solubility. The applicability of DioRaSSP in the synthesis of longer peptides was recently demonstrated with the preparation of a protected 20-mer precursor of VIR-576 [6]. This new therapeutic peptide is an analog of a naturally occurring fragment of human α 1-Antitrypsin called VIRIP (Virus Inhibitory Peptide), which was isolated from human hemofiltrate. It is a homodimer of the sequence LEAIPCSIPPEFLFGKPFVF connected via a disulfide bond. VIR-576 and closely related peptide analogs block infection with and replication of HIV-1 variants, including multi-resistant variants and patient-derived isolates. Since the inhibitory effects are independent of the host cell co-receptor, peptides of this type are considered a new type of entry inhibitors with the potential to block HIV-1 resistant against the currently available antiretroviral drugs. A first-trial synthesis on a 100-gram scale of the protected 20-mer sequence applying a combination of Z-DioRaSSP and Fmoc-DioRaSSP was completed successfully within a three weeks' period. Investigations of the synthesis steps towards the final product as well as the development of the DioRaSSP part of the synthesis to multi-kg scale are currently ongoing.

DioRaSSP has already proven its advantages in the preparation of relatively short peptides in terms of time-to-market, manufacturing efficiency, quality assurance and the environment. Based on the positive outcome of the topical synthesis of a 20-mer, it may be concluded that DioRaSSP is also the method of choice for the manufacturing of long peptides and peptide fragments.

References

1. Eggen, I. F., Ten Kortenaar, P. B. W. and Haasnoot, C. A. G. Patent Application No. US 2003/0018164 A1, 23 January 2003.
2. Eggen, I. F. and Ten Kortenaar, P. B. W. Patent No. US 6,864,357 B2, 8 March 2005.
3. Eggen, I. F., Bakelaar, F. T., Petersen, A. and Ten Kortenaar, P. B. W. In *Peptide Revolution: Genomics, Proteomics & Therapeutics* (Chorev, M. and Sawyer, T. K., eds.) American Peptide Society, San Diego, pp. 57-58 (2004).
4. Eggen, I. F., Bakelaar, F. T., Petersen, A., Ten Kortenaar, P. B. W., Ankone, N. H. S., Bijsterveld, H. E. J. M., Bours, G. H. L., El Bellaj, F., Hartsuiker, M. J., Kuiper, G. J. and ter Voert, E. J. M. *J. Peptide Sci.* **11**, 633-641 (2005).
5. Eggen, I. F., Bakelaar, F. T., Petersen, A. and Ten Kortenaar P. B. W. *Org. Process Res. Dev.* **9**, 98-101 (2005).
6. Münch, J., Ständker, L., Forssmann, W. G., Adermann, K. and Kirchhoff, F. Patent Application No. WO 01/34640 A2, 17 May 2001.

A New Efficient Post-Assembly Strategy for the Synthesis of Sulfated Peptides

John A. W. Kruijtz, Johan Kemmink and Rob M. J. Liskamp

*Department of Medicinal Chemistry, Faculty of Pharmaceutical Sciences, Utrecht Institute for
Pharmaceutical Sciences, Utrecht University, P.O. Box 80082, 3508 TB Utrecht,
The Netherlands*

Introduction

Tyrosine sulfation is an ubiquitous, reversible, post-translational modification found in many secreted and membrane-bound proteins [1]. Reversible covalent protein modifications represent general means for the physiological and pathophysiological regulation of essential cellular functions. Tyrosine-*O*-sulfate residues are often important for facilitating specific protein-protein interactions [2]. The negative charges of Tyr(SO₃H) residues might participate in intermolecular recognition and they may also affect protein folding by intramolecular interactions with cationic residues present in the protein. A prerequisite for investigating the biological functions of these modified peptides and proteins is the availability of an efficient synthesis for obtaining relatively large quantities. However, chemical synthesis of Tyr(SO₃H)-containing peptides is still challenging due to the intrinsic acid lability of the *O*-sulfate linkage [3].

We are interested in a reliable efficient synthesis of sulfated peptides, among others, for obtaining mimics of the N-terminus of the C5a-receptor in the development of C5aR antagonists [4].

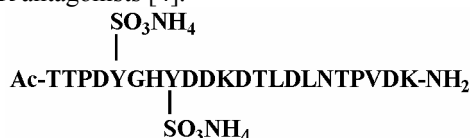


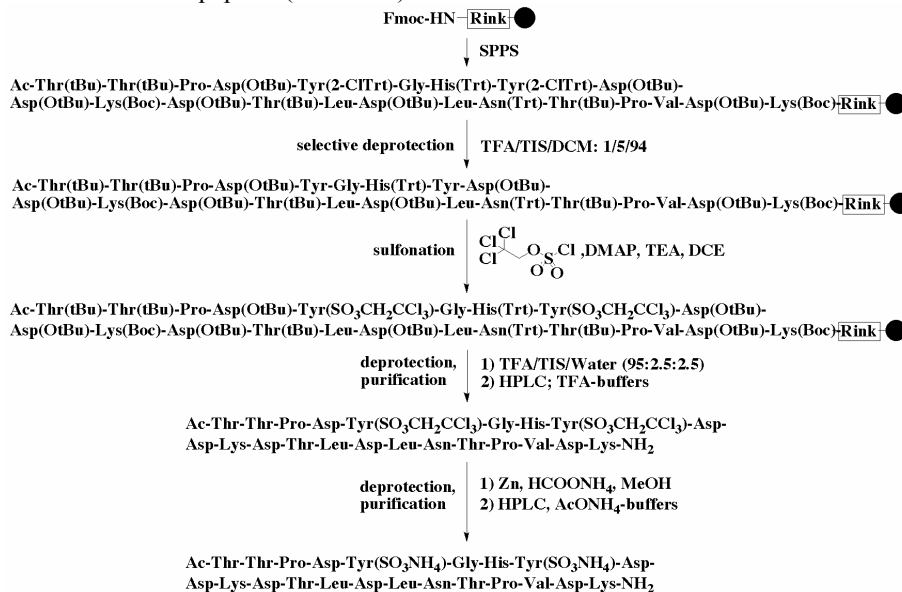
Fig. 1. Sequence of the sulfated C5aR(7-28) peptide.

C5a and its receptor (C5aR) play a pivotal role in many inflammatory diseases, including rheumatoid arthritis, systemic inflammatory response syndrome, ischemiareperfusion injury, acute respiratory distress syndrome, and multiple organ dysfunction syndrome. Hence, the C5aR constitutes a potential drug target for the treatment of inflammatory disorders. Here we report a new post-assembly sulfation strategy for the synthesis of sulfated peptides. Our approach involves Fmoc/tBu-based solid-phase peptide synthesis except for the incorporation of Tyr(2-ClTrt) residues at the position of the sulfated tyrosines. Selective deprotection of Tyr(2-ClTrt) residues followed by the introduction of the sulfate groups by reaction of the tyrosine phenolic hydroxyl groups with an ester of chlorosulfuric acid leading to the corresponding protected tyrosine sulfate esters which are stable to standard deprotection/cleavage conditions (95% TFA).

Results and Discussion

Immobilized C5aR(7-28) was synthesized using Fmoc/tBu-based solid-phase peptide chemistry on Fmoc-Rink ArgoGel resin in a ABI 433A peptide synthesizer (Fig. 1). At the position of the sulfated tyrosine residues, Fmoc-Tyr(2-ClTrt)-OH residues were incorporated. After assembly of the protected peptide on the resin the Tyr(2-

ClTrt)-residues were selectively deprotected on the resin by treatment with 1% TFA in DCM. Then, reaction of the free tyrosine phenolic hydroxyl groups with chlorosulfuric acid 2,2,2-trichloroethyl ester [5] in the presence of DMAP and TEA in 1,2-dichloroethane gave the protected sulfate esters on the resin bound peptide. These diesters are remarkably stable to acids such as TFA [5]. However, they are not stable to good nucleophiles or strong organic bases such as 20% piperidine in NMP. The thus obtained anchored protected sulfated peptide was cleaved from the resin and deprotected by treatment with TFA/H₂O/TIS (95/2.5/2.5) without desulfation of the peptide (Scheme 1).



Scheme 1. Synthetic route for the synthesis of sulfated C5aR(7-28) peptide.

The crude peptide was purified by preparative reversed-phase HPLC using a C₄ column with a gradient of 5-60% acetonitrile in aqueous 0.1% TFA. Subsequently, the 2,2,2-trichloroethyl ester protecting group of the tyrosine-*O*-sulfate ester residues were removed by catalytic transfer hydrogenolysis using Zn and ammonium formate in methanol/water (1/1) to yield the ammonium salts of the tyrosine-*O*-sulfate residues. Finally, the sulfated C5aR(7-28) peptide was purified by preparative reversed-phase HPLC using a C₄ column with a gradient of 5-60% acetonitrile in 10 mM ammonium acetate. In conclusion, we have developed a reliable and efficient solid-phase synthesis of Tyr(SO₃H) containing peptides as was exemplified by the synthesis of a disulfated 22-mer peptide representing a crucial part of the C5a-receptor.

References

1. Moore, K. L. *J. Biol. Chem.* **278**, 24243-24246 (2003).
2. Kehoe, J. W. and Bertozzi C. R. *Chem. Biol.* **7**, R57-R61 (2000).
3. Kitagawa, K., *et al.* *J. Org. Chem.* **66**, 1-10 (2001).
4. Postma, B., *et al.* *J. Biol. Chem.* **280**, 2020-2027 (2005).
5. Liu, Y., *et al.* *Org. Lett.* **6**, 209-212 (2004).

Auxiliary Group-Assisted Peptide Thioester Preparation Based on On-resin *N-S* Acyl Shift Triggered by TFA Treatment

Megumi Sumida¹, Ken'ichiroh Nakamura¹, Toru Kawakami¹, Thomas Vorherr² and Saburo Aimoto¹

¹Institute for Protein Research, Osaka University, Osaka 565-0871, Japan; ²BACHEM Folding AG, CH-4416 Bubendorf, Switzerland

Introduction

Peptide thioesters are key building blocks in contemporary ligation chemistry for polypeptide synthesis such as the thioester method [1,2] and native chemical ligation [3-5]. During the course of our studies related to new ligation methods, we developed the *N*-4,5-dimethoxy-2-mercaptopbenzyl (Dmmb) group as an auxiliary for extended chemical ligation [6]. After the ligation of the peptide segments, the Dmmb group can be removed by acidic treatment. However unexpected *N* to *S* acyl migration occurred, in part, was observed under the acidic conditions [7]. Similarly to protein splicing reactions, this *N-S* acyl shift reaction, which is mediated by the thiol auxiliary residue, must be utilized for the manufacture of peptide thioesters. In this scenario, thioester synthesis can be realized with no thioester bond present during peptide chain elongation

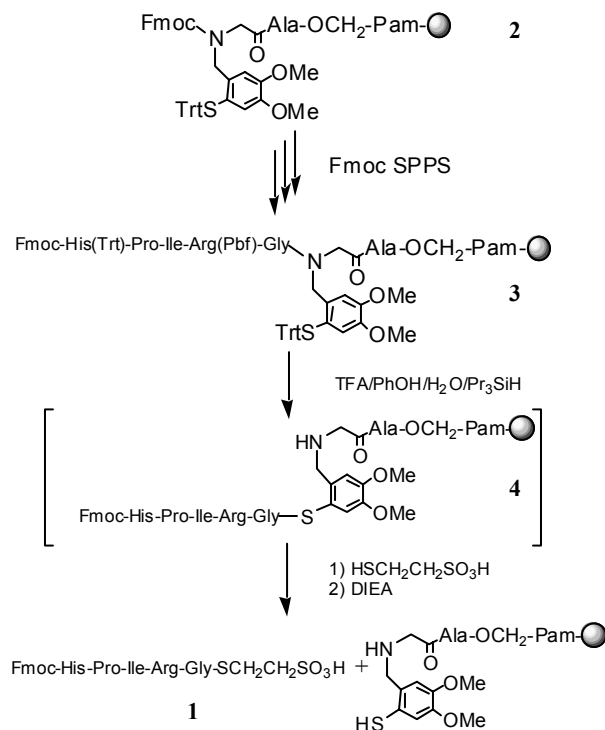
Results and Discussion

A model peptide thioester, Fmoc-His-Pro-Ile-Arg-Gly-SCH₂CH₂SO₃H (**1**), was synthesized according to scheme 1. The protected peptide, Fmoc-His(Trt)-Pro-Ile-Arg(Pbf)-Gly, was assembled by Fmoc-based solid-phase peptide synthesis (SPPS) starting from resin **2**, which contains a Dmmb auxiliary group attached to the Gly-Ala-OCH₂-Pam resin. The peptide resin **3** was treated with a reagent containing 88% TFA/ 5% water/ 5% phenol/ 2% triisopropylsilane (v/v) to remove the protecting groups as well as to initiate the *N-S* acyl shift, and to provide the resin-bound thioester intermediate **4**. After washing, the resin was treated with 0.1 M (final concentration) 2-mercaptoethanesulfonic acid in DMF, prepared *in situ* from sodium mercaptoethanesulfonate and 1 M hydrogen chloride in 1,4-dioxane, followed by 0.2 M (final concentration) *N,N*-diisopropylethylamine (DIEA) to release the peptide as peptide thioester **1**; MS (MALDI-TOF) found *m/z* 925.4 (MH⁺), calcd 925.4; amino acid analysis: Pro_{1.3}Gly₁Ile_{1.0}His_{0.9}Arg_{1.0}. The crude thioester was purified by reversed-phase HPLC in 8.2% yield, based on the Ala residue on the resin.

When the Dmmb auxiliary is attached to an alanine residue, *S-N* acyl migration is expected to proceed more slowly than in the case of a glycine residue. Therefore alanine was examined as the site of attachment for the Dmmb auxiliary, instead of glycine, to examine suppression of the *S-N* reverse acyl migration. In this case, from the protected peptide resin, peptide thioester **1** was obtained in a significant increased yield of 16%.

Acknowledgments

This research was supported, in part, by Grants-in-Aid for Scientific Research (15750143, 14380287, and 15083204) from the Ministry of Education, Culture, Sports, Science and Technology, Japan.



Scheme 1. Synthesis of peptide thioester **1** via an *N-S* acyl shift on a resin.

References

1. Hojo, H. and Aimoto, S. *Bull. Chem. Soc. Jpn.* **64**, 111–117 (1991).
2. Aimoto, S. *Biopolymers (Peptide Sci.)* **51**, 247–265 (1999).
3. Dawson, P. E., Muir, T. W., Clark-Lewis, I. and Kent, S. B. H. *Science* **266**, 776–779 (1994).
4. Tam, J. P., Lu, C. -F. and Shao, J. *Proc. Natl. Acad. Sci. USA* **92**, 12485–12489 (1995).
5. Dawson, P. E. and Kent, S. B. H. *Annu. Rev. Biochem.* **69**, 923–960 (2000).
6. Kawakami, T., Akaji, K. and Aimoto, S. *Org. Lett.* **3**, 1403–1405 (2001).
7. Vizzavona, J., Dick, F. and Vorherr, T. *Bioorg. Med. Chem. Lett.* **12**, 1963–1965 (2002).

Determination of an Optimal Solid Support for Use with Microwave-Assisted Solid-Phase Peptide Synthesis

Sandra C. Vigil-Cruz, Angela M. Peck and Jane V. Aldrich

Department of Medicinal Chemistry, University of Kansas, Lawrence, KS 66045, USA

Introduction

The success or failure of peptide synthesis is affected by many factors including the sequence of the peptide, complete removal of N-terminal amine protection, efficiency of coupling reactions and the solid support. The use of microwave energy to facilitate peptide synthesis, by accelerating coupling and deprotection reactions, was first reported over a decade ago using a conventional kitchen microwave oven [1]. Solvents play a key role in swelling the support during solid phase synthesis and also affect the transfer of microwave energy [2]. In order to explore how resins and solvents affect microwave-assisted peptide synthesis, three different types of resins, the polystyrene Wang resin, the polyethylene glycol-polystyrene PEG-PS resin and the non-polystyrene CLEAR resin were evaluated in microwave-assisted solid phase peptide synthesis (SPPS). These resins were examined under three different solvent conditions (*N,N*-dimethylformamide (DMF), dichloromethane (DCM)/DMF and *N*-methylpyrrolidone (NMP)) for coupling and washings. The acyl carrier protein (ACP) decapeptide was used as the model peptide to evaluate the resins and different solvent combinations (Fig. 1).

ACP-(65-74) Val-Gln-Ala-Ala-Ile-Asp-Tyr-Ile-Asn-GlyOH

Fig. 1. Structure of the acyl carrier protein (ACP) decapeptide.

Results and Discussion

The peptides were synthesized on the CEM Liberty™ Peptide Synthesizer using a 5-fold excess of Fmoc-amino acids relative to the resin. Couplings were achieved using PyBOP (amino acid/PyBOP/HOBt/*Ni*Pr₂Et = 1/0.9/0.9/1.8). The microwave conditions consisted of 5 cycles for 5 min total, with each cycle using 20 sec microwave power at 25W and 40 sec with the microwave power off, reaching a maximum temperature of 65°C. The deprotection reactions used 20% piperidine in DMF for a 1 min, and then a 2 min cycle; the microwave cycle involved 30 sec microwave power at 25W and then 30 sec off, reaching 75°C maximum.

The Fmoc-protected peptides were removed from the instrument, the final Fmoc deprotection was performed manually and the peptides were cleaved using Reagent B [3] for 2 hrs at RT. The crude peptides were analyzed by HPLC and the quantity of the desired peptide and various side products were estimated based on the area under the curve (AUC) of absorbance at 214 nm. The crude peptides were also analyzed by LC-MS for the desired product and impurity identification. The N-terminal Fmoc on the assembled resin-bound peptides was quantified by UV absorption after piperidine treatment.

The results in Table 1 indicate that all three resins could be used for microwave-assisted solid phase peptide synthesis. The peptide loading at the end of the synthesis as determined by quantitative Fmoc analysis were >80% of the expected values, except for the syntheses performed in NMP (data not shown), indicating that the peptidyl-resins were stable under the microwave conditions. Since NMP has a

high dielectric loss (8.86) that would allow for efficient transfer of microwave energy [2], this solvent was expected to be an optimal solvent for microwave-assisted SPPS. However, except for the synthesis on the Wang resin (75% AUC for the ACP decapeptide), the yield of the ACP decapeptide synthesized in NMP was low (20-45% AUC). Unexpectedly syntheses in the mixed solvent system resulted in products of the highest purity despite the low dielectric loss (0.38) of DCM [2].

Table 1. Analysis of ACP decapeptide synthesized under different conditions

Resin	Solvent	% ACP (AUC)	Major Side Products ^a (% AUC)
Wang	DMF	73	-Ile, -Val, -Asn (6-8%)
	DCM/DMF	83	-Val, -Asn (6-7%)
PEG-PS	DMF	53 ^b	-Ile (24%), -Val (7%), -Asn (3%)
	DCM/DMF	99	—
CLEAR	DMF	72	-Ile (6%), -Val (4%), -Asn (3%), Unknown (11%)
	DCM/DMF	77	-Val (3%), Unknown (11%)

^aGreater than 3%. ^bA separate synthesis performed entirely on the instrument (including microwave-assisted TFA cleavage) yielded pure (99% AUC) ACP; possible reasons for the differences in purity are under investigation.

The side products identified were similar for the syntheses performed on the Wang and PEG-PS resins and under different solvent conditions, with the quantities varying depending on the synthesis conditions (Table 1). Three deletion sequences lacking Asn and the β -branched residues Ile and Val were detected by LC-MS in varying amounts for all three resins. A unique side product with a molecular weight higher ($\Delta m/z + 72$) than the ACP decapeptide was detected following syntheses on the CLEAR resin; MS/MS analysis indicated that the modification was on the C-terminus of the peptide, suggesting that the side product arose from the Fmoc-Gly-OH CLEAR resin.

In conclusion, all three resins were compatible with microwave-assisted solid phase peptide synthesis. However, the purity of the ACP decapeptide varied substantially depending upon the solvent utilized. The mixed DCM/DMF solvent system resulted in the ACP decapeptide with the highest purity for all three resins.

Acknowledgments

We thank Dr. Tatyana Yakovleva for HPLC analysis and Jonathan Collins and Zachary Cox (CEM Corporation) for LC-MS analysis. The work was funded by NIH R01 DA010035 (JVA), an NIH COBRE Award 1P20 RR15563 with matching support from the State of Kansas and the University of Kansas (SVC), and an NIH IRACDA award 5K12 GM063651 (SVC).

References

1. Yu, H. -M., Chen, S. -T. and Wang, K. -T. *J. Org. Chem.* **57**, 4781-4784 (1992).
2. Hayes, B. L. *Microwave Synthesis: Chemistry at the Speed of Light*, CEM (2002).
3. Solé, N. A. and Barany, G. *J. Org. Chem.* **57**, 5399-5403 (1995).

Efficient Recombinant Production of the 16 Amino Acid Peptide AOD9604

**Allan W. Hey, Angelo Guidolin, Reza Zareie, Kathryn Smith, Ela
Knapik and Stan Bastiras**

BresaGen Limited, 8 Dalgleish Street, Thebarton, South Australia 5031, Australia

Introduction

Chemical synthesis is currently seen as the method of choice for production of therapeutic peptides. Production through recombinant bacteria is a viable alternative but is not often pursued due to perceived problems with efficiency and proteolysis. BresaGen has developed a “toolkit” approach for production of peptides as insoluble fusion proteins in *E. coli*. Segregation of peptides into insoluble inclusion bodies allows high expression rates and protects the peptides from proteolysis, while simplifying purification. A variety of fusion partners and cleavage mechanisms allow the system to be customized for the peptide in question, which is important in view of the widely-differing properties of different peptides with therapeutic potential. Certain post-translational modifications such as amidation at the carboxy terminal may also be incorporated.

Recently, BresaGen has applied this approach to production of AOD9604, a 16 residue peptide being developed by Metabolic Pharmaceuticals (Melbourne, Australia) as a potential anti-obesity drug (Fig. 1). A version of AOD9604 produced by chemical synthesis is presently in Phase II clinical trials. However, in view of the extremely large potential market for this product and the need to keep production costs as low as possible, BresaGen were commissioned to develop a recombinant method for production of this peptide.

Tyr Leu Arg Ile Val Gln Cys Arg Ser Val Asp Gly Ser Cys Gly Phe



Fig. 1. Structure of AOD9604.

We developed a simple, cost-effective and scalable method for production of recombinant AOD9604. By careful selection of purification parameters, final product which was greater than 98% pure by analytical HPLC could be produced using simple step gradients, without resorting to high pressure chromatographic techniques.

Results and Discussion

AOD9604 was expressed in *E. coli* with a 6.7kD N-terminal fusion partner, which directed expression of the protein into insoluble inclusion bodies. The inclusion bodies were dissolved under acid conditions, and the fusion partner cleaved using a chemical cleavage mechanism. 95% of the fusion partner and residual uncleaved fusion protein was removed by bulk precipitation, leaving almost all of the target peptide in solution (Fig. 2). Batch adsorption was then utilized to concentrate, desalt and further purify AOD9604.

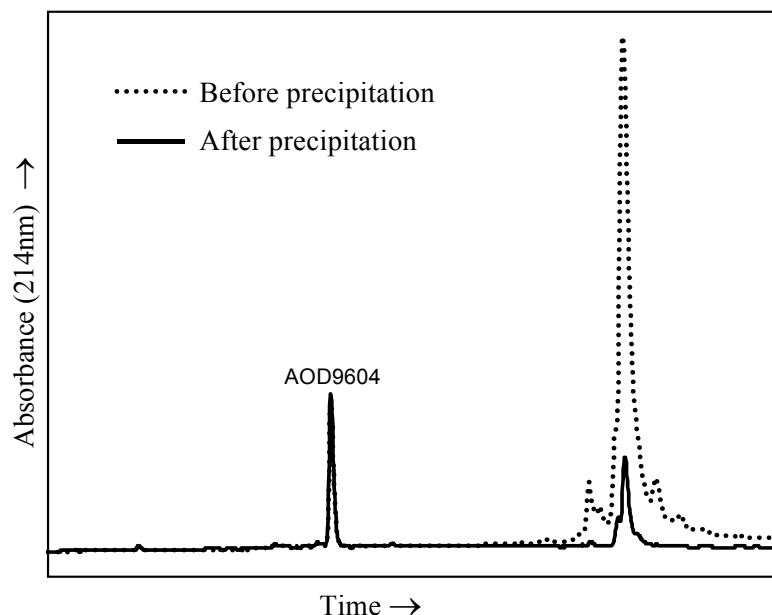


Fig. 2. Analytical HPLC showing precipitation of fusion protein-related contaminants from the AOD9604 preparation. Chromatography was performed at 0.3mL/min on a 2 x 250mm Phenomenex Jupiter C4 column, using a 5 - 50% acetonitrile gradient containing 0.1% TFA throughout.

Final purification was performed using low-pressure chromatography with a step gradient. By careful selection of elution conditions, final product greater than 98% pure by analytical HPLC was produced, without the use of high pressure chromatographic techniques and without resorting to gradient chromatography. The final product had the expected mass for AOD9604 (1815.9 Da) and showed the same elution time on analytical HPLC as synthetic AOD9604.

Recombinant production of peptides is considerably more expensive and time-consuming to develop than synthetic production, because the process must be worked out specifically for the individual peptide. However, once the process has been developed, considerable cost savings can be realized. These savings arise from two sources. Firstly, the raw materials for recombinant peptide production are simple sugar and salt solutions, which are much cheaper than the derivatized amino acids necessary for synthetic peptide production. Secondly, in contrast to synthetic peptides, most of the contaminants in crude recombinant peptide preparations are not structurally related to the target peptide, allowing purification using selective precipitation and relatively inexpensive low pressure chromatographic methods. Further savings can be achieved when a process is developed without any gradient purification steps, such as in the example given here, because this further simplifies the equipment necessary for peptide purification. Thus, consideration should be given to recombinant production when assessing the manufacturing options for peptides intended for therapeutic use.

Chemical Synthesis of the GstI Protein by a NCL Method on a X-Met Site

Daniela Marasco¹, Angela Saporito², Paolo Botti³, Eduardo Patriarca²,
Rossella Fasulo¹, Alessandro Spasiano⁴, Carlo Pedone^{1,4}, Ettore
Benedetti^{1,4} and Menotti Ruvo¹

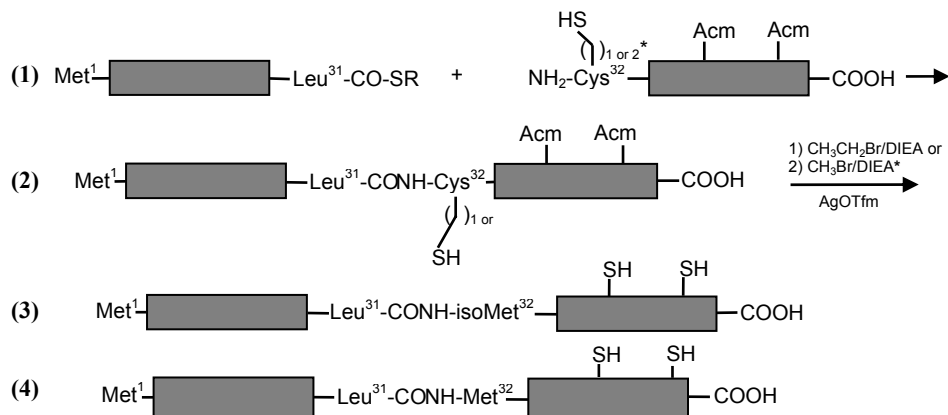
¹Istituto di Biostrutture e Bioimmagini del CNR, Sez. Biostrutture, via Mezzocannone 16, 80134 Napoli, Italy; ²Istituto di Genetica e Biofisica del CNR, via Pietro Castellino, 111, 80131, Napoli, Italy; ³University of Geneva I, rue Michel Servet, 1211, Geneva 4, Switzerland; ⁴Dipartimento delle Scienze Biologiche, Università Federico II, via Mezzocannone, 16, 80134, Napoli Italy

Introduction

The small GstI protein (63 amino acids) of *Rhizobium leguminosarum* inhibits the expression of *glnII* (glutamine synthetase II) gene, thus reducing the bacterial ability to assimilate nitrogen [1]. It was suggested that GstI mediates a block of translation and stabilization of *glnII* mRNA through direct binding to its 5' untranslated region but, due to the unavailability of adequate amounts of purified protein, this mechanism remains to be elucidated. Remarkably, when expressed in the heterologous background of *E. coli*, the protein appeared particularly sensitive to proteolytic degradation, mainly in the N-terminal region. Given the difficulties to obtain the full-length protein by recombinant methods we have undertaken the chemical synthesis of the protein by different approaches. In a first attempt, the stepwise synthesis was unsuccessful, with strong aggregation phenomena experienced after residue 44 from the C-terminus. In a second approach, we set up the conditions to carry out a native chemical ligation (NCL). Albeit the protein contains two cysteine residues, they are located in position 40 and 47. Therefore, to minimize the size of the N-terminal segment to be synthesized, we devised an alternative strategy of ligation on Met³², a residue essential for GstI inhibitory activity [2], utilizing Cys or homoCys as ligating moiety and then alkylating the resulting polypeptides with EtBr or MeBr [3,4]. The use of cysteine followed by ethylation results in an iso-methionine, while homoCys followed by methylation gives rise to a native methionine. Both polypeptides carried at the C-terminus a Gly residue introduced for synthetic facility. The intermediate GSTI[1-63]GlyAcm₂ and isoMet³²-GSTI[1-63]Gly-Acm₂ have been analyzed and identified by RP-HPLC/LC-MS and preliminarily characterized by CD spectroscopy.

Results and Discussion

The synthetic strategy (scheme 1, 1) foresees three main steps. In the first step, NCL is applied to ligate the following peptides: N-terminal GstI[1-31]COSR thioester moiety obtained by either Fmoc- or Boc-chemistry utilizing SPPS methodologies and GstI[32-63]Gly C-terminal domains carrying Cys³² (Cys³²-GstI[33-63]Acm₂Gly) or homoCys³² (hCys³²-GstI[33-63]Acm₂Gly) (scheme 1, 2). These two variants were used as precursors for the preparation of iso-Met³²GSTI[1-63] and GstI[1-63]Gly, respectively (scheme 1, 3-4). In a second step, iso-Met or Met residue were reconstructed by alkylation of the thiol group of Cys or hCys, by using the required alkyl bromide. In a final step, removal of Acm protecting groups on Cys⁴⁰ and Cys⁴⁷ must be carried out to achieve the final products.



Scheme 1. Synthetic strategy for the preparation of iso-Met³² GSTI[1-63]Gly and GSTI[1-63]Gly. * 1 refers to Cys and 2 to h-Cys.

NCL reactions were conducted in 0,2 M phosphate buffer, guanidine 6M, pH 7.8. After addition of 1% thiophenol, the pH was adjusted to ~7 and allowed to proceed overnight under stirring. The ligated products were isolated and characterized by ESI-MS. Ligated products were then alkylated using ethyl- or methylbromide and purified. CD spectra of iso-Met³²-GSTI[1-63]Gly(Acm)₂ and GSTI[1-63]Gly(Acm)₂ were acquired at pH=7.0. The overall spectral features indicate that both polypeptide chains do not assume canonical folds, although random-beta conformations are suggested by the presence of minima around 200-205 nm.

Conclusions

The GSTI[1-63]-Gly and its iso-Met³² variant (both Acm-protected on Cys⁴⁰ and Cys⁴⁷) have been produced by SPPS and NCL. The Leu³¹-Met³² peptide bond has been chosen as ligating site, using Cys³²- or hCys³²-polypeptides as precursors. Iso-Met or Met are then reconstructed by specific alkylation with ethylbromide (isomethionine) or methylbromide (native methionine) under different conditions. The Acm-protected derivatives so far obtained have been characterized by LC-MS and CD spectroscopy. Cysteine-free derivatives are being prepared and full structural and functional characterization will be carried out.

References

1. Spinosa, M., Riccio, A., Mandrich, L., Manco, G., Lamberti, A., Iaccarino, M., Merrick, M. and Patriarca, E. *J. Mol. Microbiol.* **37**, 443-452 (2000).
2. Napolitani, C., Mandrich, L., Riccio, A., Lamberti, A., Manco, G. And Patriarca, E. *FEBS Lett.* **558**, 45-51 (2004).
3. Pachamuthu, K. and Schmidt, R. R. *Synlett* **5**, 659-662 (2003).
4. Tam, J. P. and Yu, Q. *Biopolymers* **46**, 319-327 (1998).

N,O-Acyl Shifts: Unexpected Side-Reaction and Beneficial Tool in Fmoc-Chemistry

Louis A. Carpino¹, Calin D. Sferdean¹, Irene Coin², Sandra Tremmel²,
Eberhard Krause², Michael Bienert² and Michael Beyermann²

¹Department of Chemistry, Univ. Massachusetts, MA 01003, USA; ²Forschungsinstitut für
Molekulare Pharmakologie, D-13125 Berlin, Germany

Introduction

While inspecting the crude product from a “difficult” peptide synthesis, we observed a group of isomeric analogs that were subsequently identified as the corresponding N,O-shift isomers. Surprisingly, the extent of N→O shift depends on the peptide sequence and even TFA may give rise to large amounts of depsipeptide by-products [1]. Interestingly, the presence of the ester linkage helped dramatically to overcome synthesis problems as also reported by other groups [2-4]. We have now compared the novel approach with the well-known pseudo-proline method [5], applying both to the synthesis of FBP-28 WW domain peptides. FBP-28 WW domain is a 37 residue peptide that belongs to the family of WW domains showing triple stranded, anti-parallel β -sheet structure in aqueous solution. Standard Fmoc-SPPS of the FBP-28 WW domain failed, probably due to its tendency to associate during assembly as well as aspartimide formation. The N15D analog of the wild type is a good model of a “difficult” peptide GATAVSEWTEYKTANGKTYYYNNRTLES-TWEKPQELK.

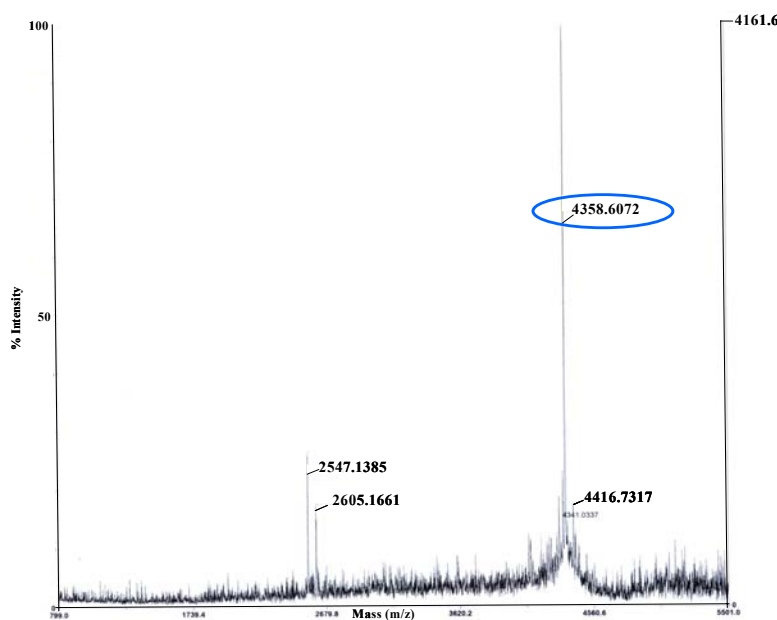


Fig. 1. Mass spectrum (MALDI-TOF) of crude FBP-28 WW domain synthesized via four depsipeptide units after re-shifting.

Results and Discussion

Using Fmoc-chemistry (0.25 M of solution Fmoc-aa/TBTU/2 DIEA) for SPPS of C-terminal FBP-28 WW(19-37) (including acetylation after double couplings), we did not find any significant amount of the desired peptide. On the other hand, incorporation of either a pseudo-proline or depsi-peptide unit at positions 27/28 led to crude products of high purity showing the correct mass.

Synthesis of the entire FBP-28 WW domain via either a single pseudoproline or depsi unit at 27/28 gave poor results, but incorporation of depsi units at four positions, 5/6, 12/13, 17/18, and 27/28, led to a smooth synthesis including the final re-shifting (O-to-N) in aqueous solution at pH 8.5 (Fig. 1).

Besides the advantageous application of depsi-peptides to overcome difficult syntheses, synthesis of difficult peptides via depsi-peptide intermediates may be extremely helpful in cases where the desired peptide shows strong association complicating its purification, as described in the case of amyloid peptides [4].

References

1. Carpino, L. A., *et al. Tetrahedron Lett.* **46**, 1361-1364 (2004).
2. Sohma, Y., *et al. Chem. Commun.* 124-125 (2004).
3. Mutter, M., *et al. Angew. Chem.-Int. Ed.* **43**, 4172-4178 (2004).
4. Carpino, L. A., *et al. Tetrahedron Lett.* **45**, 7519-7523 (2004).
5. Mutter, M., *et al. Peptide Res.* **8**, 145-153 (1995).

Magnetic CLEAR Beads for Solid-Phase Synthesis of Peptides and Affinity Ligands

Pottayil G. Sasikumar and Maria Kempe

*Unit for Biomedical Polymer Technology, Section for Cellular and Molecular Pharmacology,
Department of Experimental Medical Science, Biomedical Center, B12, Lund University, SE-
221 84 Lund, Sweden*

Introduction

The CLEAR supports were developed a decade ago to meet the need of versatile supports for solid-phase synthesis [1,2]. The resins are highly cross-linked and are compatible with a broad range of solvents; excellent swelling properties in both hydrophobic and hydrophilic solvents (including water) have been demonstrated [2]. The dynamic nature of the polymer network has made high-resolution magic-angle spinning (HR-MAS) NMR studies of resin-bound compounds possible [3]. Diffusion studies of N-protected amino acids within a number of solid-phase resins by pulsed-field-gradient spin-echo (PFGSE) NMR showed superiority of the CLEAR supports [4].

CLEAR supports have been used successfully for the synthesis of difficult peptide sequences such as ACP(65-74) [1,2], H-(Ala)₁₀-Val-NH₂ [1,2], human gastrin-I [1,2], APP(145-155) [5], sequences prone to aspartimide formation [6], cyclic peptides by solid-phase chemical ligation/cyclization [7], linear and cyclic olefin-containing peptides by the Horner-Emmons reaction [8], and β -secretase inhibitors [9]. CLEAR derivatized with Ellman's reagent has been demonstrated to be an efficient oxidizing agent for disulfide formation [10]. Wide-pore versions of CLEAR have been applied as the stationary phase in size-exclusion chromatography [11] and affinity chromatography [12]. The present work describes the preparation of magnetic CLEAR beads and their application as the support in solid-phase synthesis of peptides and small organic molecules.

Results and Discussion

Magnetic CLEAR composite beads were prepared by incorporating particles of paramagnetic magnetite into the CLEAR polymer network during the free-radical suspension polymerization of the beads. Comparative swelling studies of regular and magnetic CLEAR supports showed almost identical behavior in a broad range of solvents. The shape and texture of a magnetic CLEAR bead is shown in Figure 1.

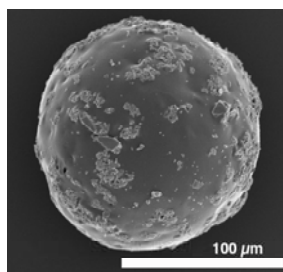


Fig. 1. Scanning electron micrograph of a magnetic CLEAR bead. Working magnification: 400 x; accelerating voltage: 10 kV.

The magnetic beads were applied as the support for the synthesis of several peptides, including Leu-enkephalin, substance P, and the difficult sequences ACP(65-74) and β -amyloid(34-42). Couplings, deprotections, and cleavages were carried out in regular test tubes. The beads were manipulated with a Dynal magnetic concentrator; reagents and solvents were easily removed by aspiration while the beads were retained in the tubes under the effect of the magnet.

The supports were also demonstrated as the solid phase in solid-phase synthesis of affinity ligands **1** and **2** based on the triazine scaffold (Fig. 2). These ligands have previously shown affinity to elastase [13] and glucose oxidase [14]. Coupling reactions were optimized and were carried out under various conditions; the temperature ranged from 0 to 120°C and the solvent from pure organic solvent to organic solvent–water mixtures. Products were obtained in high purity. Bead integrity and magnetic properties were maintained throughout the steps.

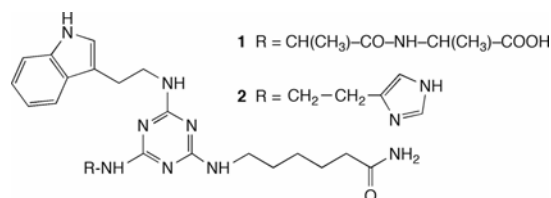


Fig. 2. Affinity ligands structures.

Acknowledgments

The work was funded by the Swedish Foundation for Strategic Research (Individual Grant for the Advancement of Research Leaders) and the Swedish Research Council.

References

1. Kempe, M. and Barany, G. In *Peptides: Chemistry, Structure & Biology, Proceedings of the Fourteenth American Peptide Symposium* (Kaumaya, P. T. P. and Hodges, R. S., eds.) Mayflower Scientific Ltd., Kingswinford, UK, pp. 865-866 (1996).
2. Kempe, M. and Barany, G. *J. Am. Chem. Soc.* **118**, 7083-7093 (1996).
3. Kempe, M., Keifer, P. A. and Barany, G. In *Peptides 1996, Proceedings of the Twenty-Fourth European Peptide Symposium* (Ramage, R. and Epton, R., eds.) Mayflower Scientific Ltd., Kingswinford, UK, pp. 533-534 (1998).
4. Yamane, Y., Matsui, M., Kimura, H., Kuroki, S. and Ando, I. *J. Appl. Polym. Sci.* **89**, 413-421 (2003).
5. Valensin, D., *et al.* *Dalton Trans.* 16-22 (2004).
6. Cebrián, J., Domingo, V. and Reig, F. *J. Peptide Res.* **62**, 238-244 (2003).
7. Tulla-Puche, J. and Barany, G. *J. Org. Chem.* **69**, 4101-4107 (2004).
8. Bang, J. K., Hasegawa, K., Kawakami, T., Aimoto, S. and Akaji, K. *Tetrahedron Lett.* **45**, 99-102 (2004).
9. Tamamura, H., Hori, T., Otake, A. and Fujii, N. *J. Chem. Soc., Perkin Trans. 1*, 577-580 (2002).
10. Darlak, K., *et al.* *J. Peptide Res.* **63**, 303-312 (2004).
11. Cederfur, J. and Kempe, M. *Polymer Bull.* **46**, 381-387 (2001).
12. Castro Franco, A. M. and Kempe, M. In *Innovation and Perspectives in Solid Phase Synthesis & Combinatorial Libraries* (Epton, R., ed.) Mayflower Scientific Ltd., Kingswinford, UK, pp. 205-208 (2004).
13. Filippusson, H., Erlendsson, L. and Lowe, C. R. *J. Mol. Recogn.* **13**, 370-381 (2000).
14. Palanisamy, U. D., Hussain, A., Iqbal, S., Sproule, K. and Lowe, C. R. *J. Mol. Recogn.* **12**, 57-66 (1999).

An Efficient and Facile Synthesis of Tyrosine-Sulfate-Containing Peptides: Synthesis of the N-Terminal Peptide of CCR5 and Its Analog

Hasmik Sargsyan¹, Boris Arshava¹, Patricia Cano¹, Tatsuya Inui¹, Jacob Anglister² and Fred Naider¹

¹*Department of Chemistry, The College of Staten Island/CUNY, Staten Island, NY 10314, USA;* ²*Department of Structural Biology, The Weizmann Institute of Science, Rehovot 76100, Israel*

Introduction

Sulfation of a tyrosine residue is a ubiquitous postranslational modification. Tyrosine sulfation occurs on an estimated 7% of mammalian proteins. To date 62 tyrosine-sulfated proteins have been identified. For the majority of these, a role for sulfation in the function of the protein has not been described. The chemokine receptor CCR5, contains four Tyr(SO₃H) residues in its N-terminus and belongs to the G-protein coupled (GPCR) receptor family [1,2]. The CCR5 chemokine receptor is the coreceptor for macrophage-tropic (M-tropic, R5) HIV-1 strains and appears to be the major coreceptor in the first stages of HIV-1 infection. Therefore CCR5 could play an important role as a therapeutic target in early phases of the disease. Synthesis of the CCR5 N-terminus may also allow the study of the mechanism of the interaction of CCR5 with the viral surface envelope glycoprotein gp120 and design new therapies to control HIV-1 cell entry.

Due to recent advances in the Fmoc-based solid-phase peptide synthesis (Fmoc-SPPS), tyrosine O-sulfate peptide chains can be directly constructed using Fmoc-Tyr(SO₃Na)-OH as a building block. However, a crucial problem that must be eliminated is the destruction of Tyr(SO₃H) during the final chain cleavage/deprotection step. At present the synthesis of Tyr(SO₃H) containing peptides has been limited to the synthesis of relatively small peptides and a total solid-phase synthesis of larger peptides containing O-sulfated tyrosine remains a challenge. The desulfation rate of the Tyr(SO₃H) during the synthesis of human big gastrin-II and cholecystokinin (CCK)-39 was shown to be strongly temperature dependent [3]. In contrast, the Sn¹-type cleavage and deprotection were less temperature-dependent and successful deprotection was achieved using aqueous TFA under cold conditions (0°C) [3]. We have applied this approach with some modifications to the synthesis of the N-terminal part of CCR5, containing two Tyr^{10,14}(SO₃H) residues and its [G²¹] analogs: [Tyr^{10,14}(SO₃H),Ala²⁰]-CCR5-27(1) and [Tyr^{10,14}(SO₃H),Ala²⁰,Gly²¹]-CCR5-27(2) (Fig. 1).

M D Y Q V S S P I Y¹⁰ (SO₃H) D I N Y¹⁴ (SO₃H) Y T S E P A²⁰ Q K I N V K Q (1)
M D Y Q V S S P I Y¹⁰ (SO₃H) D I N Y¹⁴ (SO₃H) Y T S E P A²⁰ G²¹ K I N V K Q (2)

Fig.1. Sequences of the N-terminal peptides of chemokine receptor CCR5-27(1,2).

Results and Discussion

Peptides (1,2) were synthesized using an automated peptide synthesizer (Applied Biosystems Model 433A) on 0.1 mmol of Fmoc-Gln(Trt)-Wang resin. Fmoc-Tyr(SO₃Na)-OH was used as a building block to incorporate the Tyr(SO₃H) residue.

Double coupling was carried out for each residue using HBTU/HOBt activation, and capping was accomplished with acetic anhydride in the presence of DIEA. The peptidyl resin's weight gain after completing the synthesis was quantitative (97%), confirming the successful assembly of the peptide chain including the two Tyr(SO₃H) residues. Cleavage and deprotection from the resin were achieved using 90% aqueous TFA, containing triisopropylsilane (TIS) at 0°C for 5-9 hrs. The kinetics of cleavage and deprotection for both peptides was monitored by analytical RP-HPLC. ESI-MS data of crude peptides did not show any detectable amounts of desulfated derivatives. Crude sulfated peptides were purified in one step by RP-HPLC on a Delta Pak C18 column, elution was carried out in conditions excluding acid in a gradient of CH₃CN in 0.1 M AcONH₄, pH 6.8. Final pure sulfated peptides were obtained with a yield of 35-38%. ESI-MS data (negative ion mode) gave the expected MW for both peptides: [Tyr^{10,14}(SO₃H),Ala²⁰]-CCR5-27(1): MW calculated: 3355.70, found: 3355.80; [Tyr^{10,14}(SO₃H), Ala²⁰,Gly²¹]-CCR5-27(2): MW calculated: 3284.8, found: 3284.7.

In summary an efficient method for the synthesis of two 27 residue peptides corresponding to the N-terminal domain of chemokine receptor CCR5-27, [Tyr^{10,14}(SO₃H), Ala²⁰]-CCR5-27(1) and [Tyr^{10,14}(SO₃H), Ala²⁰,Gly²¹]-CCR5-27(2) has been described. The following optimal conditions may be useful for synthesis of other Tyr sulfated peptides:

1. Quantitative yield (97%) in the stage of peptide assembly on the resin due to the use of Fmoc-Gln(Trt)-Wang resin and Fmoc-Tyr(SO₃Na)-OH as a building block.
2. Total prevention of desulfation of Tyr(SO₃H) residues during the critical stage of cleavage and deprotection (0°C, 90 % aqueous TFA, containing TIS).
3. Simple and effective (35-38%) one step purification in non acidic conditions (gradient of CH₃CN in 0.1 M AcONH₄, pH 6.8).

Acknowledgments

The work was funded by NIH grants GM 22086 and GM 22087 and from the US-Israel Binational Science Foundation.

References

1. Farzan, M., Vasilieva, N., Schnitzler, C. E., Chung, S., Robinson, J., Gerard, N. P., Gerard, C., Choe, H. and Sodroski, J. *J. Biol. Chem.* **275**, 33516-33521 (2000).
2. Farzan, M., Mirzabekov, T., Kolchinsky, P., Wyatt, R., Cayabyab, M., Gerard, N. P., Gerard, C., Sodroski, J. and Choe, H. *Cell* **96**, 667-676 (1999).
3. Kitagawa, K., Aida, C., Fujiwara, H., Yagami, T., Futaki, S., Kogire, M., Ida, J. and Inoue, K. *J. Org. Chem.* **66**, 1-10 (2001).

Interaction of DPH with the Local Anesthetic Receptor Site in D1-S6 of the Na⁺ Channel by NMR and Molecular Modeling

Bih-Show Lou¹ and Ta-Hsien Lin²

¹Chemistry division, Center of Education, Chang Gung University, Tao-Yuan, Taiwan;

²Institute of Biochemistry, National Yang Ming University, Taipei, Taiwan

Introduction

Voltaged-gated Na⁺ channels are the primary targets of many important therapeutic drugs, including local anesthetics and anticonvulsants [1]. These therapeutic drugs are used to block the voltage-gated Na⁺ channels, stop the propagation of action potentials in neurons, decrease Na⁺ channel activity in syndromes of hyper excitability, and treat epilepsy and several types of neuropathic pain [2]. To understand the molecular mechanism of these therapeutic drugs and the interactions of these drugs with Na⁺ channel inactivation is of considerable physiological and pharmacological importance. Evidence from receptor mapping of neurotoxins and therapeutic drugs within the multiple S6 segments of Na⁺ channel [3], along with information regarding functional changes after the binding of the ligands, clearly indicate the important structural and functional roles of these S6 receptors. Therefore, the S6 segments will be fruitful targets for rational drug design, as they may govern proper Na⁺ channel functions *in vivo*. Here, NMR spectroscopy and molecular modeling have been performed to investigate the interaction between the synthetic peptide, BL-DIS6: Ace-Gly-Ser-Phe-Tyr-Leu-Ile-Asn-Leu-Ile-Leu-Ala-Val-NH₂, where its sequence corresponds to the S6 segment within domain I of rat brain type IIA Na⁺ channel, and the anticonvulsant diphenyl drug, phenytoin (DPH). Detailed examination of the complex conformation between BL-DIS6 and DPH may provide more information about the location and organization of Na⁺ channel receptor for therapeutic drugs. It may also be critical for recognition and signal transduction of an inactivated Na⁺ channel.

Results and Discussion

The values of the NMR chemical shifts ($\Delta\delta$) are critical functions of the position in the molecule and the formation of complexation. Our NMR spectra had shown that the addition of DPH leads to variable degree of changes in $\Delta\delta$ s of BL-DIS6. The total chemical shift effects for each residue of BL-DIS6 on DPH bound are summarized in Fig. 1. Major changes in the NH part (\blacklozenge), in response to DPH binding, come from residues of Ile-6, Asn-7, and Val1-2. Their $\Delta\delta_{\text{NH}}$ s are 0.55, 0.49, and -0.45 ppm, respectively. A smaller but distinguishable $\Delta\delta_{\text{NH}}$ is observed in residue Leu-8 with $\Delta\delta_{\text{NH}} \sim 0.26$ ppm. Such large NMR signal perturbations, caused by bound DPH, are observed, and they

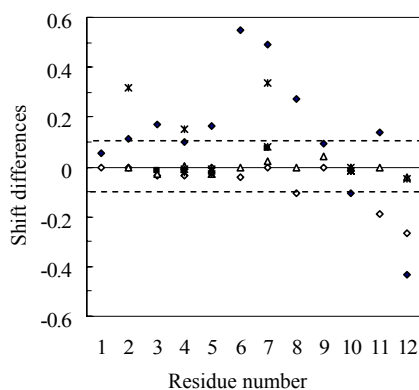


Fig. 1. Chemical shift changes on DPH binding to BL-DIS6. (\blacklozenge) for NH; (\diamond) for α H; (Δ) for β H, and ($*$) for side chain hydrogen.

indicate a substantial change in the environment around the amide protons of BL-DIS6, including the residues Ile-6, Asn-7, Leu-8, and Val-12. Furthermore, for most residues of BL-DIS6, their $\Delta\delta_{\text{NH}}$ s have shifted downfield, except the C-terminal residues Leu-10 and Val-12. In general, the shielding effect of aromatic rings is observed in shielding above the ring, and deshielding in the region in and near the plane of ring [4]. The unusual upfield shift of residues Leu-10 and Val-12 could be due to the influence of the ring current because of their NHs being held in position directly above the phenyl moiety of DPH to show such a shielding effect. On the other hand, NHs for residues Ile-6 to Leu-8 could be due to the perturbation induced a downfield shift by magnetic field of an aromatic π cloud when a phenyl plane of DPH is near by. Rather small $\Delta\delta_{\text{NH}}$ for the rest of residues indicates that they are not directly involved with DPH binding. The observations from NMR above are consistent with the photoaffinity labeling [5] and subsequent site-directed mutagenesis studies [3], that have revealed residues Ile-433, Asn-434, and Leu-437 in DI-S6 of Na⁺ channel that are probably involved in the BTX binding.

The conformation of BL-DIS6 was built (INSIGHT II environment) and modified with NOEs distance constraints that provide the inter-hydrogen distance information required for structure determination by solution NMR. This conformation was then taken as a starting structure for molecular dynamics (MD) simulations at 300 K. The 20 lowest restraint energy structures of BL-DIS6 from MD are illustrated in Figure 2. The orientations of side-chains in residues Asn-7, Leu-8, Ala-11, and Val-12 are shown in the top of Figure 2, towards the same surface (facing to the left side) that may function as a receptor for DPH binding. Affinity docking was performed to provide a possible complex conformation that the phenyl portion of DPH is accommodated in the proximity of the C-terminal residues Ala-11 and Val-12, and simultaneously the heterocyclic amine ring of DPH is perching at the residue Asn-7 periphery and stabilizing the phenyl portion deep insertion into the peptide (Fig. 3).

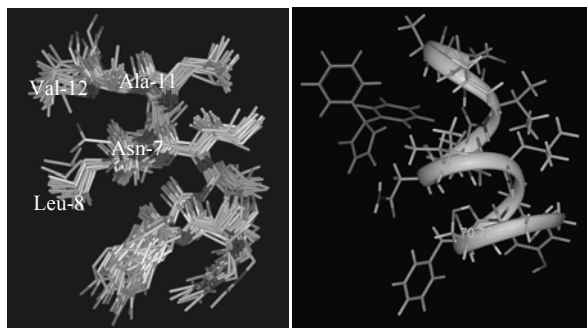


Fig.2. (in left) the 20 ensemble backbone structures with lowest restraint energy for BL-DIS6.

Fig.3. (in right) the possible complex conformation of BL-DIS6 and DPH.

Acknowledgments

The work was funded by an NSC93-2320-B-182-039 grant to B.-S. Lou.

References

1. Wang, S. Y. and Wang, G. K. *Cellular Signaling* **15**, 151-159 (2003).
2. Anger, T., Madge, D., Mulla, M. and Riddall, D. *J. Med. Chem.* **44**, 115-137 (2001).
3. Yarov-Yarovoy, V., et al. *J. Biol. Chem.* **20**, 35393-35401 (2002).
4. Bovey, E. A., et al. In *NMR Spectroscopy*, 2nd ed., Academic Press, Inc., pp. 87-145 (1988).
5. Trainer, V. L., Brown, G. B. and Catterall, W. A. *J. Biol. Chem.* **271**, 11261-11267 (1996).

The Structural Determinants of GPCR Binding and Activation: Insights from Mutagenesis and Molecular Modeling Studies of the Human Angiotensin II Type 1 (hAT1) Receptor

Marie-Eve Beaulieu, Pierre Lavigne and Emanuel Escher

Department of Pharmacology, Université de Sherbrooke, Sherbrooke, Quebec, Canada

Introduction

The G protein coupled receptors (GPCRs) are seven transmembrane domains (TMD) proteins involved in the mediation of environmental stimuli across the plasma membrane. Determination of the structural basis of GPCR ligand binding and activation is of primary importance in drug development. However, their structural analysis remains a considerable challenge and the only GPCR 3D structure experimentally determined to date is that of the bovine rhodopsin [1]. The mutation of an Asn residue in TMD 3, conserved in 29% of all family A GPCRs, has been reported to induce constitutive activation of several GPCRs, such as the PAF, B2, CXCR4, and hAT1 receptors. Rhodopsin-based homology models of the hAT1 receptor revealed an interaction between this residue (N111^{3.35}, Ballesteros numerotation in superscript) and a conserved Asp residue in TMD 2, D74^{2.50} (Fig. 1A). Interestingly, mutation of D74 impairs isomerization of the receptor toward an active form capable of activating the G_q protein. We hypothesized that the interaction between D74 and N111 is crucial for the stabilization of the inactive form of hAT1 in the absence of agonist and that this interaction maintains the ΔG_{iso} within a few kcal/mol in order to allow a small population of receptors to adopt the active form. We generated D74N and N111G mutant hAT1 receptors as controls, as well as two novel mutant receptors, D74N/N111D and D74N/N111G. After verifying the structural integrity of the mutant receptors by saturation and competition studies with angiotensin II (Ang II), their ability to activate G_q was assessed by IP production analysis (Fig. 1B).

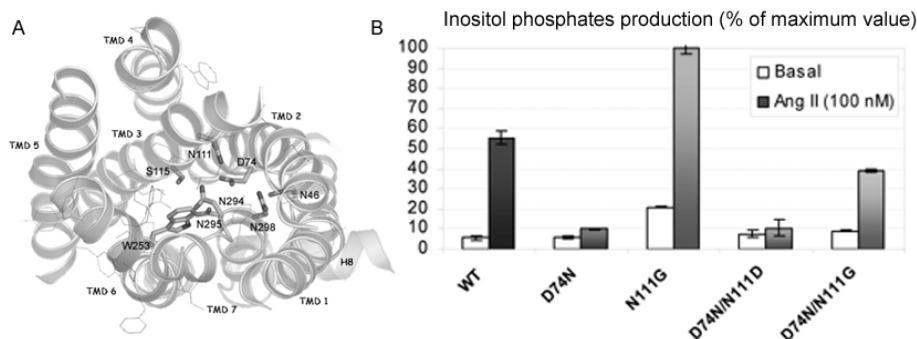


Fig. 1. A) Conserved residues involved in the hydrogen bonding network observed on the molecular model of hAT1. B) Inositol phosphates production of the WT and designed mutant hAT1 receptors.

Results and Discussion

The results show that, despite similar affinities towards Ang II, the ability of each mutant receptor to adopt an active form upon stimulation with the agonist is peculiarly altered. In the following discussion, we postulate that the binding free energy (ΔG_{bind}) leading to the activation of the receptor by an agonist is the sum of two components, i.e., the ΔG_{iso} (free energy of isomerization of the receptor) and the ΔG_{int} (free energy of stabilization through interactions between the agonist and the active form of the receptor). In accordance with the literature, the D74N mutant receptor showed no detectable IP production in absence or presence of a saturating concentration of Ang II. On the molecular model of hAT1, this mutation reduces the electrostatic potential at the level of an hydrogen bond network involving conserved residues, namely N46, D74, N111, S115, W253, N294, N295, and N298. We thus suggest that the free energy of the inactive state is lowered (larger ΔG_{iso}). In the presence of Ang II, a minute population of receptors adopts an active form because the ΔG_{int} (negative value) does not overcome the increased ΔG_{iso} (positive value), resulting in a positive ΔG_{bind} . Conversely and as reported before, the mutation N111G conferred higher basal and stimulated IP levels to the receptor, indicating its increased ability to isomerize into an active form due to a decreased ΔG_{iso} . Interestingly, the double mutant receptor D74N/N111G was still able to adopt an active form upon agonist binding, evidencing that residue 2.50 needs not to be charged to enable hAT1 isomerization into an active state. However, the activated population of mutant receptors is much less than for the WT receptor, emphasizing the role of the charged Asp side chain in bringing the ΔG_{iso} within a range where ΔG_{int} can tip up the receptor in its active form. The presence of a Gly residue in position 111, which cannot participate in polar interactions contrarily to the Asn residue, leads to a destabilization of the inactive state compared to the D74N. The potential involvement of D74 and N111 in Ang II binding was verified by interchanging both residues. The D74N/N111D mutant receptor had normal Ang II affinity but agonist binding did not induce activation of the receptor. A putative interaction in the active state of WT hAT1 between the carboxy-terminal group of Ang II and N111 would be replaced in the mutant by a repulsion between both carboxyl groups. However, ligand binding is normal, probably due to a stabilizing and counteracting interaction through the D74N mutation. Thus, Ang II may bind an inactive form of the D74N/N111D mutant receptor, but in a conformation that does not allow isomerization of the receptor into an active state. Mutational analysis of several conserved residues in spatial proximity to N111^{3,35} is now progressively defining an activation mechanism which appears to be common to all family A GPCRs. In this mechanism, residue D2.50, whereas not strictly essential to activation, confers an intrinsic instability to the receptor. This destabilization is counterbalanced by an interaction network comprising residue N3.35 to keep the receptor in an inactive state in the absence of agonist. In other GPCRs where N3.35 is not conserved, a similar hydrogen bonding interactions network is present to presumably stabilize the inactive state. A deeper analysis of these networks by generation of other specifically designed mutant receptors will precise the role of these network residues in the stabilization of the inactive state of family A GPCRs.

Reference

1. Palczewski, K., Kumasaka, T., Hori, T., Behnke, C. A., Motoshima, H., Fox, B. A., Le Trong, I., Teller, D. C., Okada, T., Stenkamp, R. E., Yamamoto, M. and Miyano, M. *Science* **289**, 739-745 (2000).

Protein Epitope Mimetics A New Approach to Target Protein-Protein Interactions

Frank Otto Gombert, Jan Willem Vrijbloed and Daniel Obrecht

Polyphor Ltd., Gewerbestrasse 14, Allschwil, CH 4123, Switzerland

Introduction

Protein-protein interactions play a key role in most biological processes, and offer attractive opportunities for therapeutic intervention. However, it is very difficult to develop small molecules able to selectively modulate protein-protein interactions. In collaboration with Prof. John Robinson at the University of Zurich, Polyphor has developed Protein Epitope Mimetics (PEM) Technology. PEM are medium-size, cyclic peptide-like molecules (MW 1-2kDa) mimicking beta-hairpin secondary structures of proteins. PEM are designed by variation of loop size, building blocks and templates (Fig. 1 right). The templates stabilize the β -hairpin conformation, facilitate the synthesis and add new pharmacological properties.

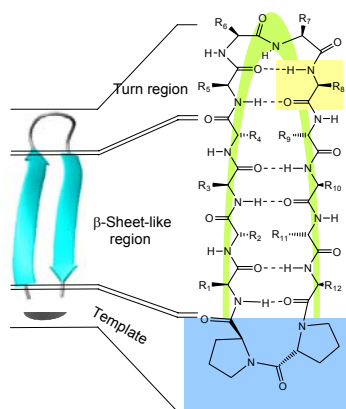
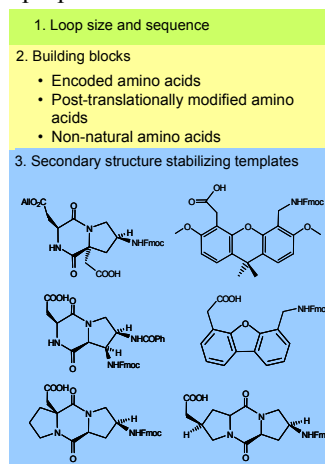


Fig. 1. Variables of the PEM design.



Results and Discussion

Chemokine receptor antagonists with improved potency, pharmacological properties and *in vivo* efficacy: The chemokine receptor CXCR4 is the co-receptor for T-tropic HIV entry into lymphocytes. In addition it is implicated in angiogenesis, metastasis and stem cell release by interfering with SDF-1, the natural ligand of CXCR4. T22 [1,2], which is a close analog of a naturally occurring β -hairpin peptide polyphemusin II, is an antagonists of the chemokine receptor CXCR4. Starting from T22 we applied PEM Technology and obtained after several iterative rounds of optimizing potency, selectivity and *in vitro* ADMET parameters POL3026 as a first lead. POL3026 shows high *in vitro* potency in a Ca^{2+} -flux assay ($\text{IC}_{50} = 1 \text{ nM}$, Fig. 2), potent inhibition of HIV cell fusion ($\text{IC}_{50} = 1.5 \text{ nM}$, data not shown, assay conditions in [3]) and a favorable, small-molecule-like PK profile in dog.

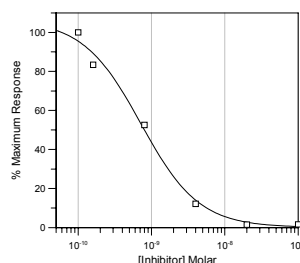


Fig. 2. Ca^{2+} flux assay. SDF-1 displacement in CXCR4 transfected cells.

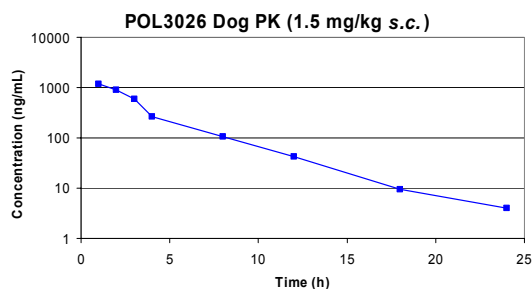


Fig. 3. Plasma levels of POL3026 after subcutaneous injection of 1.5 mg/kg in dog.

Potent and highly selective inhibitors of the serine proteases human cathepsin G, human neutrophil elastase and human trypsin: PEM design was based on Sunflower Trypsin Inhibitor (SFTI) [4]. Potent and selective Cathepsin G (K_i 33 nM, Fig. 4), Elastase (K_i 1 nM), or Trypsin (6 nM) inhibitors were developed. All inhibitors are competitive, fully reversible and have in most cases selectivity factors of 1:1000 (Fig. 4) towards 9 different serine proteases. The importance of substituents distant to the active site for modulating activity and selectivity was confirmed by NMR and x-ray co-crystallization studies. Good *in vitro* ADME properties encouraged us to perform rodent PK experiments. The oral bioavailability of POL3171 in rats was 3.6% (Fig. 5).

Inhibitor against	Cathepsin G		Elastase		Trypsase
	POL3171	POL4634	POL4480	POL5975	POL6111
Ki (nM)					
Cathepsin G	131	33			
Elastase			8	1	n.d.
Trypsase					6
Trypsin					
Chymotrypsin					n.d.
Plasmin					
Urokinase					n.d.
Chymase					n.d.
Thrombin					n.d.
Factor Xa					n.d.
selectivity	>1000	100-1000	10-100	<10	

Fig. 4. Inhibitory constants and selectivity in 10 serine proteases.

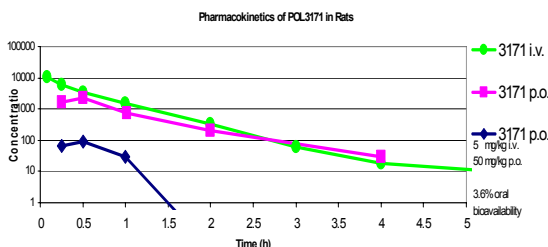


Fig. 5. Plasma levels of POL3171 after intravenous and oral application in rat.

In summary Polyphor conducted successfully several drug discovery programs to validate the PEM Technology. In all programs highly potent and selective lead compounds with excellent ADMET properties were obtained. In the protease project oral bioavailability of the Polyphor lead compound was demonstrated. Emphasis in further studies will be given to demonstrate efficacy in animal models.

References

1. Nakashima, H., Masuda, M., Murakami, T., Koyanagi, Y., Matsumoto, A., Fuji, N. and Yamamoto, N. *Antimicrob. Agents Chemother.* **36**, 1249-1255 (1992).
2. Tamamura, H., Omagari, A., Oishi, S., Kanamoto, T., Yamamoto, N., Peiper, S. C., Nakashima, H., Otake, A. and Fujii, N. *Bioorg. Med. Chem. Lett.* **10**, 2633 (2000).
3. Hamy, F., Felder, E. R., Heizmann, G., Lazdins, J., Aboul-ela, F., Varani, G., Karn, J. and Klimkait, T. *Proc. Natl. Acad. Sci. USA* **94**, 3548-3553 (1997).
4. Decours, A., Moehle, K., Renard, A. and Robinson, J. A. *ChemBioChem* **3**, 318-323 (2002).

Application of Phenylphosphate Mimetics to the Design and Synthesis of Olefin Metathesis-Derived Grb2 SH2 Domain-Binding Macrocycles

Sang-Uk Kang¹, Zhen-Dan Shi¹, Rajeshri Kariki¹, Jason Phan², Karen M. Worthy³, Lakshman K. Bindu³, Marc Nicklaus¹, David S. Waugh², Robert J. Fisher³ and Terrence R. Burke, Jr.¹

¹Laboratory of Medicinal Chemistry; ²Macromolecular Crystallography Laboratory, CCR, NCI, NIH, Frederick, MD 21702 USA; ³Protein Chemistry Laboratory, SAIC-Frederick, Frederick, MD 21702, USA

Introduction

The growth factor receptor bound protein 2 (Grb2) is an SH2 domain-containing component of signaling pathways associated with a variety of proliferative diseases. Grb2 SH2 domains preferentially recognize sequences of the form, “pTyr-Xxx-Asn”, with binding occurring in type-I β -bend conformations [1]. Significant research has been devoted to developing Grb2 SH2 domain-binding peptides and peptide mimetics as potential therapeutics. One aspect of these efforts has been directed toward overcoming bioavailability issues raised by the dianionic phenylphosphate moiety of pTyr. Using an open-chain display platform based on the peptide Ac-pTyr-Ac₆c-Asn-[3-(1-naphthyl)propylamide] reported by Novartis Corp [2], we had previously examined a number of monoanionic phosphoryl mimetics that exhibited micromolar to sub-micromolar Grb2 SH2 domain-binding affinities [3]. More recently, we reported macrocyclic variants of the Novartis peptide bearing dianionic phosphoryl replacements that provide low nanomolar to sub-nanomolar binding constants (analogs **1** [4] and **2** [5], X = a and b, Fig. 1). The focus of the current study was to examine phosphoryl mimicking groups bearing monoanionic charge (X = c,d,e and f) or no charge (X = g and h) within a macrocyclic platform (Fig. 1).

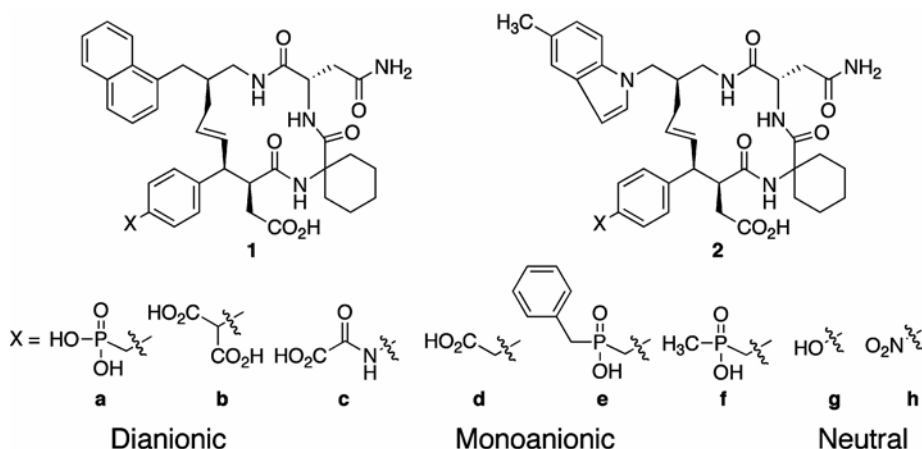


Fig. 1. Structures of Grb2 SH2 domain-binding macrocycles.

Results and Discussion

Final products **2a-h** were prepared as previously described [6]. Grb2 SH2 domain-binding affinities were determined using surface plasmon resonance assays that measured the direct binding of macrocyclic ligand to surface-bound protein (Table 1) [7].

Table 1. Grb2 SH2 domain-binding affinities

Dianionic		Monoanionic		Neutral	
No.	K _D (nM)	No.	K _D (nM)	No.	K _D (nM)
2a	1.47	2c	67	2g	>1000
2b	3.62	2d	33	2h	>1000
		2e	35		
		2f	16		

Macrocycles bearing monoanionic phenylphosphate mimetics provided K_D values of from 16 nM to 67 nM, while analogs having neutral mimetics showed no measurable affinity. The necessity of at least one anionic charge for good affinity is consistent with the known important role played by the ArgβB5 residue in binding thermodynamics. This residue is situated at the rear of the pTyr-binding pocket and provides a primary recognition element for open-chain pTyr-containing peptides. Results of the current study indicate that interaction of at least one anionic charge with the ArgβB5 residue may be essential for conformationally constrained peptides as well.

Acknowledgments

Appreciation is expressed to Drs. Christopher Lai and James Kelley of the LMC for mass spectral analyses.

References

1. Rahuel, J., Gay, B., Erdmann, D., Strauss, A., Garcia-Echeverria, C., Furet, P., Caravatti, G., Fretz, H., Schoepfer, J. and Gruetter, M. G. *Nature Struct. Biol.* **3**, 586-589 (1996).
2. Furet, P., Gay, B., Caravatti, G., Garcia-Echeverria, C., Rahuel, J., Schoepfer, J. and Fretz, H. *J. Med. Chem.* **41**, 3442-3449 (1998).
3. Burke, T. R., Jr., Luo, J., Yao, Z. -J., Gao, Y., Milne, G. W. A., Guo, R., Voigt, J. H., King, C. R. and Yang, D. *Bioorg. Med. Chem. Lett.* **9**, 347-352 (1999).
4. Shi, Z. -D., Wei, C. -Q., Lee, K., Liu, H., Zhang, M., Araki, T., Roberts, L. R., Worthy, K. M., Fisher, R. J., Neel, B. G., Kelley, J. A., Yang, D. and Burke, T. R., Jr. *J. Med. Chem.* **47**, 2166-2169 (2004).
5. Shi, Z. -D., Lee, K., Wei, C. -Q., Roberts, L. R., Worthy, K. M., Fisher, R. J. and Burke, T. R., Jr. *J. Med. Chem.* **47**, 788-791 (2004).
6. Kang, S. -U., Shi, Z. -D., Worthy, K. M., Bindu, L. K., Dharmawardana, P. G., Choyke, S. J., Bottaro, D. P., Fisher, R. J. and Burke, T. R., Jr. *J. Med. Chem.* **48**, 3945-3948 (2005).
7. Osihi, S., Karki, R. G., Shi, Z. -D., Worthy, K. M., Bindu, L., Chertov, O., Esposito, D., Frank, P., Gillette, W. K., Maderia, M. A., Hartley, J., Nicklaus, M. C., Barchi, J. J., Jr., Fisher, R. J. and Burke, T. R., Jr. *Bioorg. Med. Chem.* **13**, 2431-2438 (2005).

Radiolabeled Peptides as CXCR4 Ligands

Ettore Benedetti¹, Giancarlo Morelli¹, Raffaella Della Moglie¹, Stefania De Luca¹, Luigi Aloj^{1,2}, Andrea Ciarmiello², Secondo Lastoria², Claudio Arra², Amelia D'Alessio² and Laura Tarallo²

¹Department of Biological Science & CIRPeB, University "Federico II", I-80134 Napoli, Italy; ²National Institute of Tumors, "Fondazione Pascale" Napoli I-80127, Italy

Introduction

CXCR4 is a G-protein-coupled receptor that is widely expressed on the membranes of neutrophils, lymphocytes and monocytes, and less often on epithelial cells. It transduces cellular signals for stromal-derived cell growth factor 1 (SDF-1) [1]. The CXCR4 receptor is also known as major co-receptor for the CD4-dependent entry of target cells by T-tropic strains of HIV-1 that evolve during the course of HIV-1 infection. In addition, it results overexpressed on cell surface in particular types of human tumors such as breast cancer, and the expression of CXCR4 by mammary carcinoma results in the programming of metastatic spread to target organs that secrete SDF-1. Thus, CXCR4 represents a critical molecular target to disrupt the pathogenesis of HIV-1 infection, to block tumor metastasis, and to mobilize stem cells. Moreover, the individuation of the overexpression of the CXCR4 receptor could help in an early diagnosis of tumors such as breast cancer.

The 14-residues cyclic peptide named T140 [2] is reported as one of the more affine ligands for CXCR4 and act as inverse agonist: it binds CXCR4 in extracellular domains and in regions of the hydrophobic core proximal to the cell surface. We here report on the synthesis of a library of peptide conjugates based on the peptide sequence of T140 and carrying a chelating agent able to give stable complex with the radioactive ¹¹¹In isotope (Fig. 1). All peptide derivatives have been labeled with ¹¹¹In and studied *in vitro* by evaluating their binding specificity and affinity, cellular internalization and retention in cell cultures of CXCR4 overexpression to assess the best position to introduce the chelating agent, and the best peptide sequence to maintain high affinity and selectivity toward the CXCR4 receptor.

- # 1 (DTPAGlu)-Arg-Arg-Nal-Cys-Tyr-Arg-Lys-DLys-Pro-Tyr-Arg-Cit-Cys-Arg-NH₂
- # 2 (DTPAGlu)-βAla-Arg-Arg-Nal-Cys-Tyr-Arg-Lys-DLys-Pro-Tyr-Arg-Cit-Cys-Arg-NH₂
- # 3 H-Arg-Arg-Nal-Cys-Tyr-Arg-Lys-DLys(DTPAGlu)-Pro-Tyr-Arg-Cit-Cys-Arg-NH₂
- # 4 H-Arg-Arg-Nal-Cys-Tyr-Arg-Lys-DLys-Pro-Tyr-Arg-Cit-Cys-Arg-Lys(DTPAGlu)-NH₂
- # 5 Ac-Arg-Arg-Nal-Cys-Tyr-Cit-Leu-DLys(DTPAGlu)-Pro-Tyr-Arg-Cit-Cys-Arg-NH₂
- # 6 Ac-Arg-Arg-Nal-Cys-Tyr-Cit-Lys-DLys(DTPAGlu)-Pro-Tyr-Arg-Cit-Cys-Arg-NH₂
- # 7 Ac-Arg-Arg-Nal-Cys-Tyr-Cit-Glu-DLys(DTPAGlu)-Pro-Tyr-Arg-Cit-Cys-Arg-NH₂
- # 8 H-Arg-Arg-Nal-Cys-Tyr-Arg-Leu-DLys(DTPAGlu)-Pro-Tyr-Arg-Cit-Cys-Arg-NH₂
- # 9 H-Arg-Arg-Nal-Cys-Tyr-Cit-Leu-DLys(DTPAGlu)-Pro-Tyr-Arg-Cit-Cys-Arg-NH₂

Fig. 1. Amino acid sequences of the peptide conjugates labeled with ¹¹¹In through the chelating agent DTPAGlu. All peptides are cyclized through a disulfide bond between the two Cys residues.

Results and Discussion

All peptide conjugates were synthesized in solid-phase which provided high yields of the compounds, in the linear form, and high purity of the raw products. The

coupling of DTPAGlu as protected derivative, DTPA(OtBu)₅Glu, during the assembly of the peptide on the solid support, was very efficient while, the subsequent deprotection reactions required prolonged time to ensure complete removal of the tert-butyl protecting groups. The final Cys-Cys cyclization and the HPLC purification steps yielded well characterized compounds which corresponded to the desired molecules. We have evaluated the peptide conjugates for binding on native cells expressing CXCR4 (HeLa cells) and cells overexpressing the receptor by tranfection (A431 cells stable and transient transfectants) (Fig. 2).

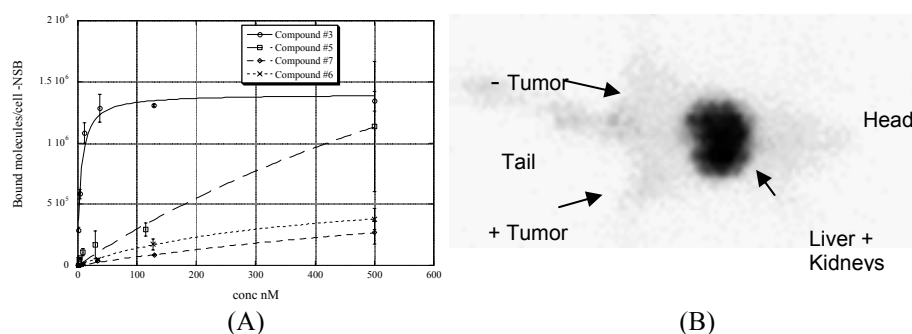


Fig. 2. (A) Binding properties of selected compounds to A431 transient transfectants. (B) γ -camera image obtained after 2 hrs after injection of compound # 3. Accumulation of the peptide is seen in tumor positive xenograft, less in the control tumor. Non specific binding to liver and kidneys is found.

In these models we have also assessed biodistribution experiments in xenograft bearing nude mice. We have identified one compound (compound #3) with the most promising binding properties (K_d and IC_{50} in the low nM range) whereas others have shown low or no affinity for the receptor. In particular, the compounds carrying the chelating agent on the N or C terminal end present negligible activity, thus confirming that the best position to introduce the chelating agent is the side-chain of D-Lys present in the central position of the peptide and far away from the receptor binding side.

Compound #3 and a low affinity peptide (compound #5) were utilized for the animal studies where specific targeting to the CXCR4 positive tumor was detected only with compound #3.

Notwithstanding the good efficiency of compound #3 in tumor imaging, the biodistribution data and the image indicate that improvement strategies need to be designed to decrease non-specific binding to liver and kidneys.

References

1. Takibana, K., Hirota, S., Iizasa, H., Yioshida, H., Kawabata, K., Kataoka, Y., Kitamura, Y., Matsushima, K., Yioshida, N., Nishikawa, S., Kishimoto, T. and Nagasawa, T. *Nature* **393**, 591-594 (1998).
2. Trent, J., Wang, Z., Murray, J., Shao, W., Tamamura, H., Fujii, N. and Peiper, S. *J. Biol. Chem.* **278**, 47136-47144 (2003).

Aza-peptides with Multiple Aza-amino Acids, Synthesis and Preliminary Conformational Analysis of Glu-azaAla-Ala-azaAla-Leu-azaAla-Lys-azaAla-NH₂

**Damien R. Boeglin, Mallem H.V. Ramana Rao, Jean-Philippe Demers
 and William D. Lubell**

*Département de chimie, Université de Montréal, C.P. 6128, Succursale Centre-Ville,
 Montréal, Québec H3C 3J7, Canada*

Introduction

Aza-peptides [1] are peptide analogs in which the α -carbon of one or more of the amino acid residues has been replaced with a nitrogen atom. In aza-peptides, replacement of the rotatable C α -C(O) bond by a rigid urea N α -C(O) and electronic repulsion between lone pairs of adjacent hydrazine nitrogens restrict motion about the dihedral angles ψ and ϕ respectively [2,3]. Spectroscopic, crystallographic and computational studies indicate that incorporation of a single aza-amino acid residue into model peptides induces β -turn type conformation [4]. Azatides, polymers composed only of aza-amino acids, have been synthesized [5], however, to the best of our knowledge, there are no reports concerning their conformational properties. The synthesis and conformational analysis of aza-peptides containing multiple aza-amino acid residues is now being explored by the synthesis and preliminary analysis of an aza-peptide possessing alternating aza and natural amino acids: Glu-azaAla-Ala-azaAla-Leu-azaAla-Lys-azaAla-NH₂ (**1**).

Results and Discussion

Aza-peptide **1** was synthesized on solid-support using Fmoc-aza-alanine acid chloride **4**. Fluoren-9-ylmethyl carbazate (**2**) was obtained in quantitative yield by acylation of excess of hydrazine with fluoren-9-ylmethyl chloroformate (Fig. 1), condensed with aqueous formaldehyde in ethanol at reflux to give an acyl hydrazone intermediate, then reduced with sodium cyanoborohydride in THF in the presence of AcOH. Decomplexation of the amino borane intermediate in ethanol at reflux gave N'methyl fluoren-9-yl-methyl carbazate (**3**) in 77% yield after purification. Carbazate **3** was dissolved in DCM and treated with a 2 fold excess solution of phosgene in toluene at room temperature. After 15 min, excess phosgene was removed with the other volatiles to provide Fmoc-aza-alanine acid chloride (**4**) which was employed without further purification in solid-phase peptide synthesis.

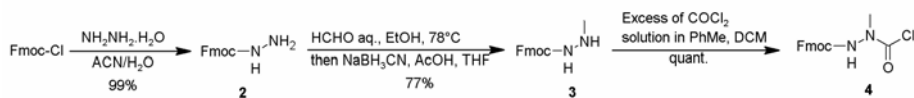


Fig. 1. Synthesis of Fmoc-aza-alanine chloride building block.

On Rink resin, the acid chloride **4** (500 mol%) was reacted on the peptide N-terminal in the presence of DIEA (500 mol%) in DCM. Natural amino acids were introduced as Fmoc-amino acid chlorides (500 mol%) generated *in situ* with BTC and 2,4,6-collidine as base (14000 mol%) in THF [6] (Fig. 2). For comparison, Glu-

Ala-Ala-Ala-Leu-Ala-Lys-Ala-NH₂ (**5**) was synthesized using standard Fmoc/tBu protocols on Rink resin [7].

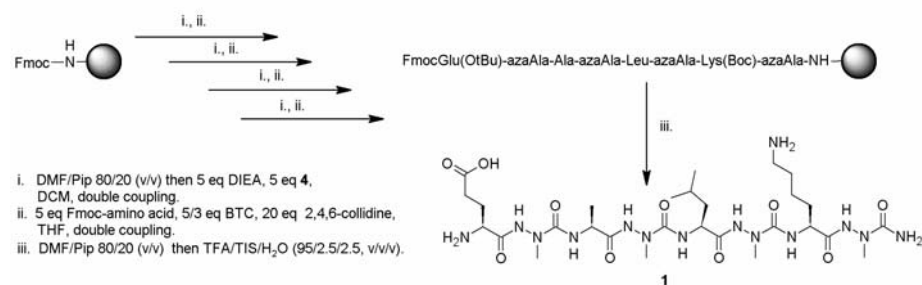


Fig. 2. Solid-phase synthesis of a tetra-aza-octa peptide **1**.

Preliminary conformational analyses of the purified peptides **1** and **5** were carried out by CD spectroscopy in MeOH, TFE and H₂O (20 mM phosphate buffer) and by NMR spectroscopy in a 9:1 mixture of H₂O and D₂O. The CD spectra of Aza-peptide **1** and peptide **5** exhibited distinctly different curves between 180-250 nm at 0.2 mM concentration. The CD spectrum of **5** exhibited negative maximum at 202 nm and positive maxima around 223 nm indicative of a random coil [8]. Aza-peptide **1** exhibited positive maxima at 195 nm and a negative maxima around 235 nm for which similar curve shapes were reported earlier in oligomers of β -amino acids adopting a right handed 10/12 helix [9] as well as for poly(Lys-Leu-Lys-Leu), which adopted a β pleated sheet conformation [10]. The NMR chemical shift dispersions for the amide protons in peptides **1** and **5** supported an organized structure. In the spectrum of **5**, $^3J_{\text{NH-}\alpha\text{H}}$ was < 5 Hz for all residues indicative of a helical conformation [11]. Similarly, in the spectrum of **1** the $^3J_{\text{NH-}\alpha\text{H}}$ was < 5Hz for Ala, Leu and Lys residues at 65 °C. At lower temperature, the amide proton signals broadened due to rapid conformational changes about the α -aza center.

In conclusion, a methodology for the synthesis of peptides containing multiple aza-residues has been developed and used to synthesize tetra-aza octapeptides. Detailed conformational analyses of such peptides are presently under investigation.

Acknowledgments

This work was supported by FQRNT and VRQ (Québec), and NSERC (Canada).

References

1. Zega, A. and Urleb, U. *Acta Chim. Slov.* **49**, 649-662 (2002).
2. Reynolds, C. H. and Hormann, R. E. *J. Am. Chem. Soc.* **118**, 9395-9401 (1996).
3. Lee, H. J., Lee, M. H., Choi, Y. S., Park, H. M. and Lee, K. B. *J. Mol. Struct. (Theochem)* **631**, 101-110 (2003).
4. Melendez, R. E. and Lubell, W. D. *J. Am. Chem. Soc.* **126**, 6759-6764 (2004).
5. Han, H. and Janda, K. D. *J. Am. Chem. Soc.* **118**, 2539-2544 (1996).
6. Falb, E., Yechezkel, T., Salitra, Y. and Gilon, C. *J. Peptide Res.* **53**, 507-517 (1999).
7. Chang, C. D. and Meienhofer, J. *Int. J. Peptide Prot. Res.* **11**, 246-249, (1978).
8. Johnson Jr, W. C. *Proteins: Struct. Funct. Genet.* **7**, 205-214 (1990).
9. Sharma, G. V. M., Reddy, K. R., Krishna, P. R., Sankar, A. R., Jayaprakash, P., Jagannadh, B. and Kunwar, A. C. *Angew. chem.* **43**, 3961-3965 (2004).
10. Brahms, S. and Brahms, J. *J. Mol. Biol.* **138**, 149-178 (1980).
11. Pardi, A., Billeter, M. and Wutrich, K. *J. Mol. Biol.* **180**, 741-751 (1984).

Design and Synthesis of Bicyclic Internal β -Turn Mimetics and their Applications toward Biologically Interesting Ligands

Byoung J. Min, Xuyuan Gu, Ravil R. Petrov, Yeon Sun Lee and
 Victor J. Hruby

Department of Chemistry, University of Arizona, Tucson, AZ 85721, USA

Introduction

The β -turn **1** is the simplest structure among the most common secondary structures found in peptides and proteins (Fig. 1) [1]. Although it only involves four consecutive amino acids, β -turns in biological active peptides or proteins often play important roles in their interactions with receptors, enzymes, or antibiotics [2]. In principle, such peptide-protein or protein-protein interactions can be mimicked by a constrained small molecule bearing similar local topographical features [3]. In order to achieve high affinity and selectivity to a specific receptor, many efforts have been devoted to the development of such a unique scaffold [4].

Recently, we have developed the parallel synthesis of external β -turn mimetics by the constrained bicyclic ring structures **2**, on solid supports [5]. As an expansion of this work, here we report the solution and solid phase syntheses of internal bicyclic β -turn mimetics **3**. During the process, an acetal was introduced at the N-terminal, which generates a desired bicyclic scaffold under acidic conditions. By doing so, we could not only generate different sizes of bicyclic rings, such as 6-6 and 7-6 membered rings, but also introduced different side chains at position *i* through *i*+3 with desired chiralities.

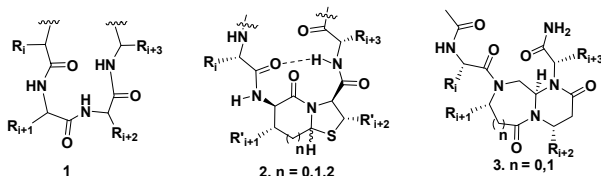
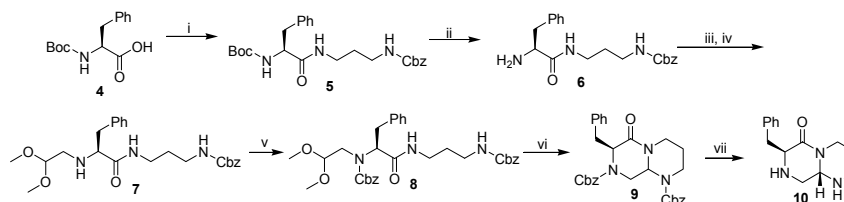


Fig. 1. β -turn structure(left) and its external(middle) and internal mimetics(right)

Results and Discussion

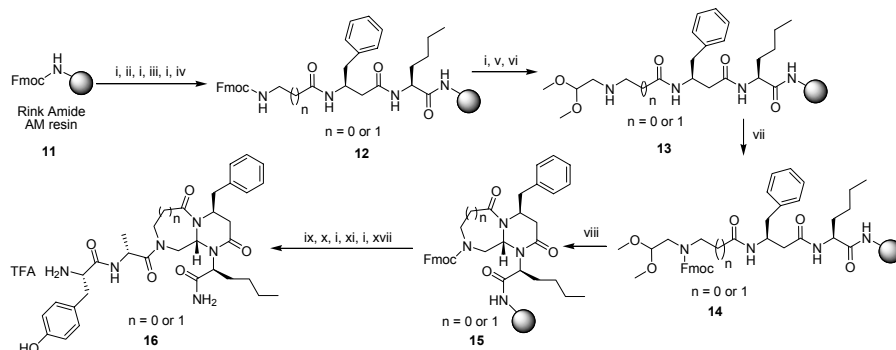
At the beginning of our investigation, the model bicyclic compound, (7*S*,9*aS*)-7-benzyl-octahydropyrazino[1,2-*a*]pyrimidin-6-one **10**, was designed (Scheme 1). Boc-Phe was coupled to Cbz protected 1,3-diaminopropane, followed by Boc group deprotection with 20% TFA in DCM. The corresponding free amine **6**, underwent to the reductive amination with glyoxal dimethyl acetal in the presence of NaBH(OAc)₃ to give exclusive mono alkylated product **7** [6]. After protection with a Cbz group, formic acid induced the intramolecular acyliminium ion cyclization to give the bicyclic product **9**. Unfortunately, this di-Cbz protected bicyclic compound was difficult to characterize due to the existence of rotamers in the NMR spectra. After removing its Cbz groups by hydrogenation, we were able to characterize this novel bicyclic compound **10** by HSQC, HMBC, TOCSY, nOe, etc. It was assigned as a single diastereomer with *S* configuration at the bridge head and the total yield of the 7 step synthesis was 30%. Based on this result, we confidently expanded our strategy to the synthesis of the opioid peptide ligand, Leu-enkephalin **16**, on a solid support (Scheme 2).

In summary, a novel methodology has been developed for the synthesis of internal bicyclic β -turn mimetics with different sizes. The conformational study and biological activity study of these internal bicyclic leu-enkephalin ligands will be reported in the future.



(i) Cbz-1,3-diaminopropane.HCl, BOP, HOBT, NMM in DMF; (ii) 20 % TFA in DCM; (iii) glyoxal dimethyl acetal in DCM; (iv) NaBH(OAc)₃, AcOH; (v) Cbz-Cl, DIEA in DCM; (vi) formic acid; (vii) H₂, Pd/C in MeOH

Scheme 1. The solution phase synthesis of (7S,9aS)-7-benzyl-octahydropyrazino-[1,2-a]pyrimidin-6-one.



(i) 25 % piperidine in DMF; (ii) Fmoc-Leu-OH, HBTU, HOBT, DIEA in DMF; (iii) Fmoc-D- β -homoPhe-OH, HBTU, HOBT, DIEA in DMF; (iv) Fmoc-Gly-OH or Fmoc- β -Ala-OH, HBTU, HOBT, DIEA in DMF; (v) (CH₃O)₂CHCHO in DCM; (vi) NaBH₃CN, AcOH in DCM; (vii) Fmoc-Cl, DIEA in DCM; (viii) formic acid; (ix) 50 % piperidine in DCM; (x) Fmoc-D-Ala-OH, DIC, HOAT in DMF; (xi) Fmoc-Tyr-OH, HBTU, HOBT, DIEA in DMF; (xii) 90 % TFA, 5% water, 5% triisopropylsilane

Scheme 2. The solid phase synthesis of different sizes of internal β -turn mimetics.

Acknowledgments

The work was supported by grants from the US Public Health Service and National Institute on Drug Abuse (DA 330720, DA 12394, DA 13449, and DK 17420).

References

- Smith, J. A. and Pease, L. G. *CRC Crit. Rev. Biochem.* **8**, 315-399 (1980).
- Rose, G. D., Gierasch, L. M. and Smith, J. A. *Adv. Protein. Chem.* **37**, 1-109 (1985).
- Eguchi, M., Lee, M. S., *et al.* *J. Am. Chem. Soc.* **121**, 12204-12205 (1999).
- Arnold, U., Hinderaker, M. P., *et al.* *J. Am. Chem. Soc.* **124**, 8522-8523 (2002).
- Gu, X., Ying, J., Min, B., Cain, J. P., *et al.* *Biopolymers* **80**, 151-163 (2005).
- Abdel-Magrid, A. F., Carson, K., *et al.* *J. Org. Chem.* **61**, 3849-3862 (1996).

Synthesis and Incorporation of Freidinger Lactam Analogs in GHRP-6

Fabrice Galaud¹, Annie Demers², Huy Ong² and William D. Lubell¹

¹Département de Chimie; ²Département de Pharmacie, Université de Montréal, C. P.6128, Succursale Centre Ville, Montréal, Qc, H3C 3J7, Canada

Introduction

Growth hormone-releasing peptides (GHRPs) are a class of synthetic peptides that stimulate GH release by way of a distinct pathway mediated through the G-protein-coupled receptor GHS-R 1a [1]. For example, the hexapeptide GHRP-6 [His-(D)Trp-Ala-(D)Phe-Lys-NH₂] was demonstrated to cause the release of GH from somatotrophs in a dose-dependant manner in several species including humans [2]. Molecular modeling studies of GHRP-6 have suggested that the active conformation of this peptide adopts a turn geometry [3]. α -Amino γ -lactam GHRP-6 analogs (*S*)-**1** and (*R*)-**1** have now been synthesized to study the importance of a turn conformation for biological activity.

Results and Discussion

Effective methodology for synthesizing enantiomerically pure α -amino γ -lactam-bridged dipeptides has been achieved by using homoserine-derived cyclic sulfamidates [4]. The first synthesis of *N*-(Fmoc)homoserine-derived cyclic sulfamidate was performed according to the sequence shown in Figure 1 which provided *tert*-butyl ester **7** from Asp in 31% overall yield.

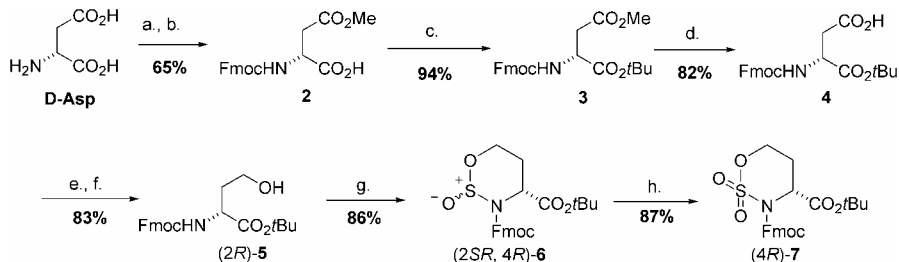


Fig. 1. Synthesis of sulfamidate (*4R*)-**6**: a. AcCl , MeOH ; b. FmocOSu , NaHCO_3 , $\text{Acetone}/\text{H}_2\text{O}$; c. $\text{tBuOC}(\text{NH})\text{CCl}_3$, CH_2Cl_2 ; d. CaCl_2 , NaOH , $i\text{PrOH}/\text{H}_2\text{O}$; e. ClCO_2Et , NMM , THF , -10°C ; f. NaBH_4 , MeOH , 0°C ; g. SOCl_2 , imidazole , Et_3N , CH_2Cl_2 ; h. $\text{RuCl}_3 \cdot x\text{H}_2\text{O}$, NaIO_4 , CH_3CN , H_2O , 0°C .

Freidinger lactams (*3S,2'S*)- and (*3R,2'S*)-**8** were respectively synthesized in 50% and 58% overall yields by ring opening of sulfamidates (*4S*)- and (*4R*)-**7** with L-Trp-OMe in acetonitrile at room temperature, *tert*-butyl ester solvolysis with a solution of TFA/DCM (1:1) containing Et_3SiH , lactam formation with TBTU and DIEA in DCM at room temperature, and methyl ester hydrolysis with CaCl_2 and NaOH in $i\text{PrOH}/\text{water}$ (9:1) (Fig. 2). Peptide lactam analogs (*S*)- and (*R*)-**1** were synthesized on Rink resin using a Fmoc protection strategy (Fig. 3). The crude peptide purity was analyzed by analytical HPLC and estimated to be around 78% for each peptide. Peptides were purified by RP-HPLC using a gradient of water/acetonitrile containing

0.1% TFA and their identity was confirmed by mass spectrometry (HRMS) and analytical HPLC.

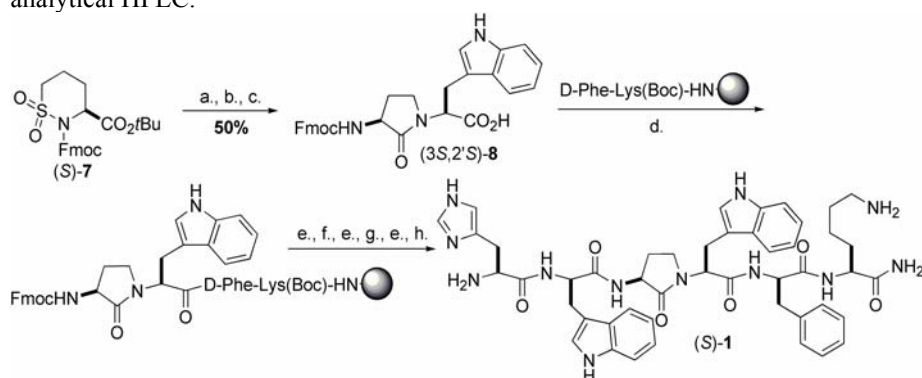


Fig. 2. Synthesis of GHRP-6 analog (S)-1: a. *L*-Trp-OMe, CH₃CN; b. TFA/DCM/Et₃SiH; c. TBTU, DIEA, DCM; d. HATU, HOAt, DIEA, DMF; e. DMF/piperidine; f. Fmoc-D-Trp(Boc)OH, TBTU, HOBT, DIEA, DMF; g. Fmoc-His(Trt)OH, TBTU, HOBT, DIEA, DMF; h. TFA/DCM/iPr₃SiH.

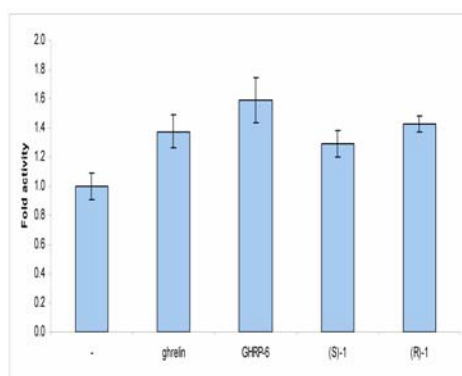


Fig. 3. GHS-r1a-mediated transactivation of PPAR_γ by analogs.

Although less than that of the parent peptide, GHRP-6, agonist activity was observed for both analogs (S)- and (R)-1 in a coupled-receptor bioluminescence assay (Fig. 3). In conclusion, Fmoc-protected cyclic sulfamidates have been used to synthesize two biologically active GHRP-6 analogs which indicate the importance of an active turn conformation.

Acknowledgments

This research was supported by NSERC (Canada), FQNRT (Québec) and Boehringer Ingelheim Canada Ltd.

References

1. Bowers, C. Y., Sartor, A. O., *et al.* *Endocrinology* **128**, 2027-2035 (1991).
2. Bowers, C. Y., Momany, F. A., *et al.* *Endocrinology* **114**, 1537-1545 (1984).
3. Momany, F. A. *Growth Hormone Secretagogues* Springer-Verlag: New-York (1996).
4. Galaud, F. and Lubell, W. D. *Biopolymers (Peptide Sci.)* **80**, 665-674 (2005).

Microwave-assisted Synthesis of *N*-glycosylated Building Blocks

Ilaria Paolini, Francesca Nuti, Giuseppina Sabatino, Mario Chelli
and Anna M. Papini

*Laboratory of Peptide & Protein Chemistry & Biology, Polo Scientifico, University of
Florence, I-50019 Sesto Fiorentino (FI), Italy*

Introduction

Although microwave-assisted reactions are widely applied in other domains of organic synthesis, their use in glycopeptide synthesis has been rather limited [1]. The microwave effect should mainly be related to heat effects, and many reports have focused on “improvement of reactions”. Generally speaking, the results show an enhanced reaction rates and higher product yields as compared to conventional approaches [2].

Considering that the most versatile methodology in chemical synthesis of *N*-glycopeptides is the building block approach, we focused our attention on the optimization of some key steps of synthetic pathways to glycosylated asparagine residues, via glycosylamines.

Results and Discussion

We decided to optimize by microwave approach some key steps to obtain glycosylated building blocks to be used in solid-phase peptide synthesis. In particular:

- 1) modification of the anomeric hydroxyl function in the amino one;
- 2) protection of hydroxyl functions of sugars;
- 3) coupling of glycosylamines with Fmoc-protected aspartic acid.

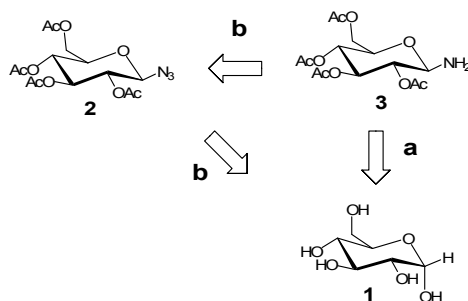


Fig. 1. Retrosynthesis of 2,3,4,6-tetraacetate β-D-glucopyranosylamine.

Two strategies can be followed to obtain glycosylamines (Fig. 1): a) conversion of the sugar, such as α-D-glucose (**1**) to β-D-glucosylamine, and then protection of hydroxyl functions (i.e., as acetate); b) reduction of the azide (**2**) obtained from the corresponding α-D-sugar. A CEM Discover® LabMate™ monomode microwave instrument was used for all the experiments.

Different reaction conditions and quantities of substrates and solvents were tested to develop simple and reproducible methodologies. Our interest was to optimize a large scale synthesis of glycosylated building blocks to obtain synthetic

Table 1. MW-assisted reactions

Reaction	Setting	Method	Yield %
Amination	α -D-glucose (1 g, 5.5 mmol)	300 W	78
	H ₂ O (5 mL)	1.5+0.5 min * 4 cycles	
	NH ₄ HCO ₃ (20%)	Tmax=60°C	
Acetylation	α -D-glucose (1 g, 5.5 mmol)	120 W	85
	Ac ₂ O (20 mL)	3 min	
	ZnCl ₂ (10%)	Tmax=85°C	
Coupling	2,3,4,6-tetraacetate β -D-glucopyranosylamine (100 mg, 0.3 mmol)	100 W	68
	FmocAspOtBu (1 eq)	1.5+3 min	
	coupling reagent (1 eq)	Tmax=60°C	
	NMM (1 eq)		
	MeCN (2.5 mL)		

glycopeptides [3]. Our best results are reported in Table 1. The best results were obtained using the triazine-based coupling reagents [4].

Further studies on a microwave-assisted synthesis of glycopeptides (CEM Liberty monomode instrument) using the above described building block are in progress.

Acknowledgments

We thank Fondazione Ente Cassa di Risparmio di Firenze, CEM Corporation, and the Travel Award Committee for the financial support to the participation of I. Paolini at 19th APS.

References

1. Iqbal, J., *et al. Tetrahedron Lett.* **44**, 4507–4509 (2003).
2. Shieh, W. C., *et al. Tetrahedron Lett.* **43**, 5607–5610 (2002).
3. Papini, A.M., *et al. Proc. Natl. Acad. Sci. USA* **102**, 10273–10278 (2005).
4. Patent Application (April 2004). Applicants: University of Lodz (Poland) & University of Florence (Italy). Inventors: Kaminski, Z.J., Papini, A.M., Kolesinska, B., Kolesinska, J., Jastrzabek, K.

Parallel Solid-Phase Synthesis of Mucin-Like Glycopeptides from an α -GalN₃ *O*-Linked Threonine Building Block

Mian Liu^{1,2}, David Live¹ and George Barany²

¹*Department of Biochemistry, Molecular Biology and Biophysics;* ²*Department of Chemistry, University of Minnesota, Minneapolis, MN 55455, USA*

Introduction

In pursuit of our goal to gain structural insights into mucin-like glycoproteins, particularly to understand the features that control their glycosylation as well as their ultimate molecular recognition events in cell-cell recognition and signal transduction events [1], we have prepared a series of glycopeptides based on the mucin 2 (MUC2) derived sequence, PTTTPLK. All possible glycopeptide permutations of partial α -GalNAc glycosylation of the Thr residues, and the control peptide without glycosylation, were synthesized and purified in amounts adequate for NMR studies. This sequence was chosen because of previously reported biochemical studies on its transformation by several GalNAc transferases [2]. To experimentally address conformational properties, well-defined homogeneous material is needed. This can be provided with considerable versatility through chemical synthesis of mucin-glycopeptides. Correlation of the structural characteristics with the biochemical data determined on synthetic glycopeptides should lead to an understanding of the role of structure in controlling the rates and positions of glycosylation, and thus the glycosylation patterns of mucins, an element of their diversity.

We have prepared the building blocks [3] with suitable protecting and activating groups for incorporation of glycosylated serine and threonine into the peptide chain by stepwise solid-phase synthesis. Chemical procedures were used that are based on 9-fluorenylmethoxycarbonyl (Fmoc) *N*^α-amino protection; the mild basic conditions for Fmoc removal are compatible with these building blocks. After chain assembly is complete, release of the glycopeptides from the resin is achieved by exposure to trifluoroacetic acid (TFA), in the range of 1–95%, depending on the precise resin and linkage. Acid-labile amino acid side-chain protecting groups are removed simultaneously at the higher TFA concentrations, with additional chemical steps needed for removal of protecting groups on the GalNAc to obtain the final desired mucin glycopeptides.

Results and Discussion

The glycopeptide Ac-Pro-Thr(α -D-GalNAc)-Thr(α -D-GalNAc)-Thr(α -D-GalNAc)-Pro-Leu-Lys-NH₂ (**1**), which features three consecutive *O*-glycosylated Thr residues and mimics a portion of mucin 2, has been prepared by solid-phase synthesis [4]. Seven related, partially glycosylated peptides (**2–8**) were synthesized as well (Fig. 1 and Table 1). *N*^α-(9-fluorenylmethoxycarbonyl)-*O*-(3,4,6-tri-*O*-acetyl-2-azido-2-deoxy- α -D-galactopyranosyl)-L-threonine pentafluorophenyl ester [Fmoc-L-Thr(Ac₃- α -D-GalN₃)-OPfp] [5] was used as a building block that coupled efficiently when used in a relatively low molar excess, i.e., ~1.5 equiv, with *N,N*-dimethylformamide (DMF) as the solvent. For conversion of the azido group to the *N*-acetyl function, direct treatment with thioacetic acid was preferred over a two-step procedure involving reduction with dithiothreitol (DTT) followed by *N*-acetylation. Effective *O*-deacetylation of **1–8**, in solution, was achieved by treatment with sodium

methoxide (10–15 mM; ~5 equiv) in methanol. On-resin deacetylation techniques were also examined, using sodium methoxide (6–10 mM) in DMF–methanol (17:3) (for **4**) or hydrazine (70 mM) in methanol (for **8**). The more convenient on-resin technique in DMF–methanol gave yields similar to solution conditions, and promises to be widely useful for solid-phase glycopeptide synthesis.

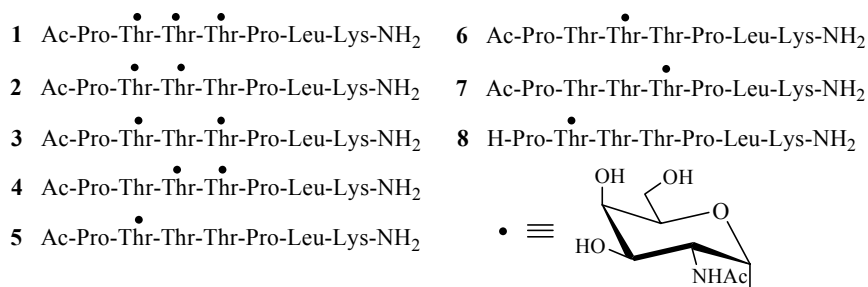


Fig. 1. Mucin-like glycopeptides **1–8**.

HPLC profiles showed that free glycopeptides elute earlier than the corresponding *O*-acetylated derivatives, and that retention times vary systematically with the number of sugar moieties. ¹H NMR studies carried out in water showed an increase in conformational organization of glycopeptides with increased density of glycosylation.

Table 1. Glycopeptides **1–8**

Glycopeptide	Molecular Formula	Sugar Number	t _R (min) ^a	Yield (%) ^b
1	C ₆₀ H ₁₀₂ N ₁₂ O ₂₆	3	14.0	7
2	C ₅₂ H ₈₉ N ₁₁ O ₂₁	2	15.8	25
3	C ₅₂ H ₈₉ N ₁₁ O ₂₁	2	16.5	19
4	C ₅₂ H ₈₉ N ₁₁ O ₂₁	2	15.4	32
5	C ₄₄ H ₇₆ N ₁₀ O ₁₆	1	17.0	30
6	C ₄₄ H ₇₆ N ₁₀ O ₁₆	1	18.4	25
7	C ₄₄ H ₇₆ N ₁₀ O ₁₆	1	17.8	29
8	C ₄₂ H ₇₄ N ₁₀ O ₁₅	1	14.4	36

^a0–40% 0.1% TFA in MeCN over 40 min. ^bIsolated yields based on initial substitution of resin.

Acknowledgments

The work was funded by NIH (GM 66148).

References

- Hollingsworth, M. A. and Swanson B. J. *J. Nature Rev. Cancer* **4**, 45–60 (2004).
- Takeuchi, H., *et al. Eur. J. Biochem.* **269**, 6173–6183 (2002).
- Liu, M., Live, D. and Barany, G. *Chimica Oggi* **22**, 30–34 (2004).
- Liu, M., Barany, G. and Live, D. *Carbohydr. Res.* **340**, 2111–2122 (2005).
- Liu, M., *et al. Carbohydr. Res.* **340**, 1273–1285 (2005).

Synthesis of Silyl Ether Linkers for Solid-Phase Peptide Synthesis

Cassidy M. Dobson¹, George Barany² and Rita S. Majerle¹

¹Hamline University, Department of Chemistry, 1536 Hewitt Ave, St Paul, MN 55104;

²University of Minnesota, Department of Chemistry, 207 Pleasant SE, Minneapolis, MN 55455, USA

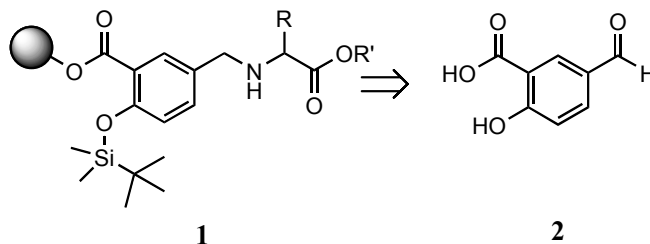
Introduction

This research describes the development of a silyl linker which allows for unique cleavage by the addition of fluoride. The initial target is a tri-functional spacer molecule (**1**) designed to allow attachment to the resin, protection of the elongated chain, and selective cleavage of a silyl ether functionality. To this end, 5-formylsalicylic acid (**2**) has been chosen as the starting material to create the desired spacer. *Tert*-butyldimethylsilylchloride (TBDMSCl), a common protecting group, is reacted with the phenolic OH to incorporate the silicon atom. The carboxylic acid moiety serves as the attachment point to the solid-phase synthesis resin and the formyl group serves to anchor an amine group using a reductive amination procedure.

The handle could be readily cleaved by the addition of fluoride which attacks the Si atom, followed by further electron rearrangement to force the cleavage of the newly synthesized target compound from the linker and resin support. The Si-F bond is one of the strongest bonds known, suggesting that the efficiency of cleavage of this method should be relatively high. Although previous research has shown effective development of a silane-containing linker molecule, this research seeks to develop a similar, more efficient synthesis [1].

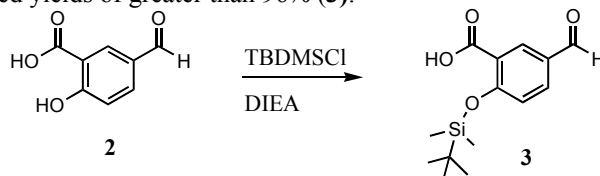
Results and Discussion

With 5-formylsalicylic acid (**2**) as the starting material for synthesis, three steps are required to obtain our linker molecule. These are, not necessarily in this order: addition of the silyl ether group to the phenol, reductive coupling to an amine from an amino acid, to the aldehyde functionality, and ester formation to the resin.

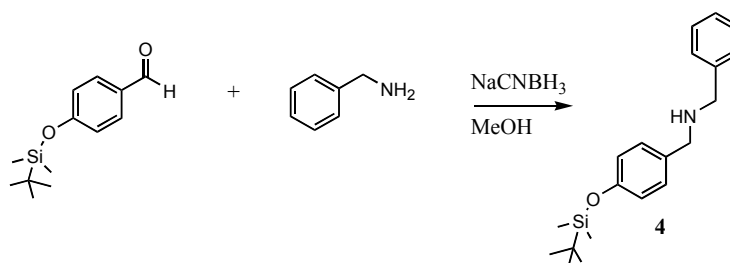


As the starting material **2** is approximately \$10 per gram, the reaction conditions were developed using a series of less expensive model compounds. Salicylic acid and *p*-formylphenol were chosen because of their ready availability. Among several procedures explored to attach the TBDMS protecting group to *p*-formylphenol, best results were obtained in the presence of *N,N*-diisopropylethylamine (DIEA) in DMF. Interestingly enough, although the product yields were quite disappointing with the

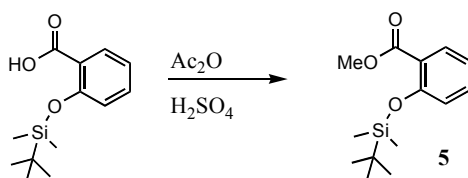
model compound (a modest 56-60%), the same procedure on the 5-formylsalicylic acid (2) produced yields of greater than 96% (3).



In order to simplify reaction monitoring, initial attachment of the amine to the linker molecule was conducted off-resin. Reductive amination conditions were developed using the TBDMS protected formylphenol with benzylamine.



It was found that mixing the reactants at 25°C with sodium cyanoborohydride in methanol for approximately 4-6 hrs produced 4 in quantitative yields. The reductive amination procedure on the TBDMS protected 5-formylsalicylic acid (3) was not as straightforward. The reaction proceeded sluggishly and it was speculated that the presence of the free carboxylic acid on 3 interfered with the Schiff base formation. Returning to the model system, an esterification procedure was developed. Esterification was readily accomplished using acetic anhydride in the presence of H₂SO₄ to produce (5) in quantitative yields. Currently we are applying this methodology to the 5-formylsalicylic acid (2) so that the procedures can be conducted successfully off resin.



Acknowledgments

This research was supported by the University of Minnesota Research Site for Educators in Chemistry (RSEC) which is funded in part through NSF-CHE-0113894.

References

1. Mullen, D. and Barany, G. *J. Org. Chem.* **53**, 5240-5248 (1988).

Synthetic Routes to, and Mechanistic Understanding of, Dithiasuccinoyl (Dts)-Amines and Chlorocarbonyl Carbamoyl Disulfanes

Michael J. Barany¹, Megan M. Corey¹, Michael C. Hanson¹, Rita S. Majerle^{1,2}, Robert P. Hammer³ and George Barany¹

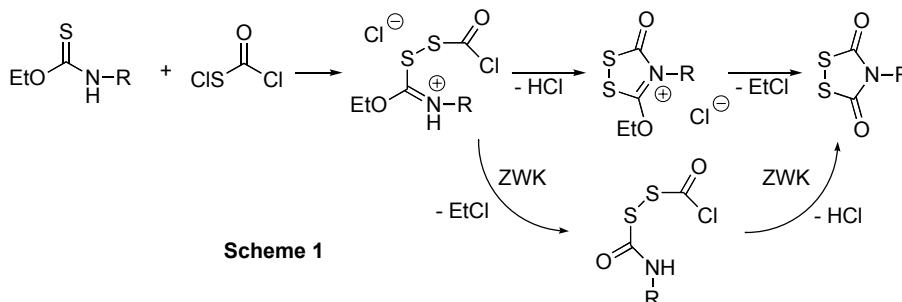
Departments of Chemistry of ¹University of Minnesota, Minneapolis, MN 55455; ²Hamline University, St. Paul, MN 55104; ³Louisiana State University, Baton Rouge, LA 70803, USA

Introduction

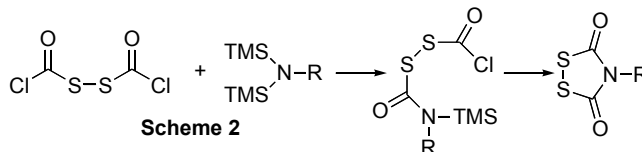
The dithiasuccinoyl (Dts) heterocycle had an inauspicious beginning in the German patent literature when Zumach, Weiss, and Kühle (ZWK) reported on their development of a simple pesticide. Little did they realize that their cursory mechanistic assumptions regarding the heterocycle [1] would later spark a long and fascinating tangent of investigations which would challenge the intuitions of scores of organosulfur chemists. We report here on a series of mechanistic studies stemming from early attempts to confirm the ZWK mechanism for Dts heterocyclization.

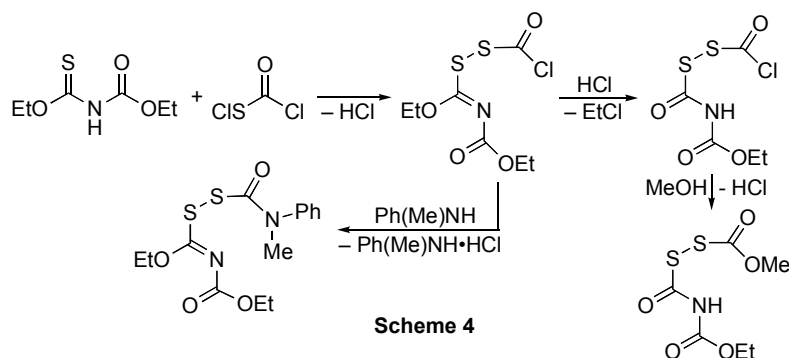
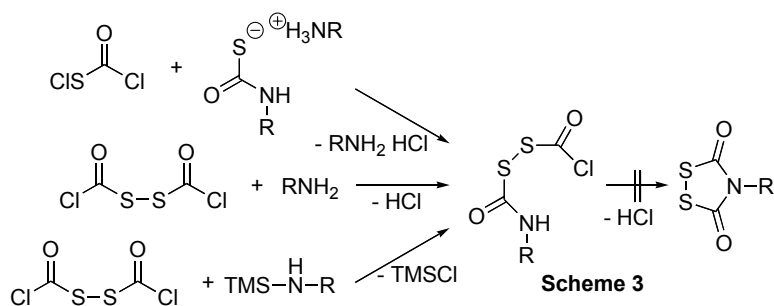
Results and Discussion

The proposed ZWK mechanism for the formation of the Dts heterocycle from ethoxythiocarbonyl amines and chlorocarbonylsulfenyl chloride, following



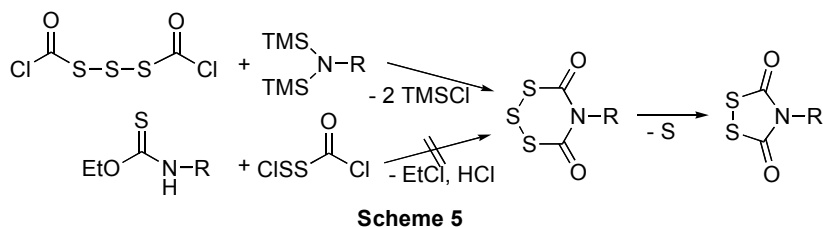
precedents of Harris, predicted a route involving chlorocarbonyl carbamoyl disulfane (Scheme 1: “ZWK”). We recently reported that bis(trimethylsilyl)amines (TMS_2NR) react with bis(chlorocarbonyl)disulfane to generate Dts-amines via a trimethylsilyl analog of such a chlorocarbonyl carbamoyl disulfane (Scheme 2) [2]. We have now generated a wide range of chlorocarbonyl carbamoyl disulfanes, by a variety of means (Scheme 3), and found that none of them further transform into the Dts heterocycle. From this, we conclude that the cyclization must occur *before* the loss of EtCl to form the chlorocarbonyl carbamoyl disulfanes. The title compounds are remarkably stable, and, in the case of $\text{R}=\text{CO}_2\text{Et}$ (Eoc), could even be crystallized





for x-ray structural analysis. The Eoc example reaction was also suitably slow to permit a series of traps (Scheme 4) to further ascertain intermediates.

A Dts version of the classical Gabriel synthesis permits facile alkylation, although the corresponding acylation, which could give rise to the putative Dts analog of the classical Nefkens reagent, remains unrealized. The curious incongruities in the silyl and ZWK syntheses of Dts-amines further befuddled us in our attempts to expand the syntheses to include a third sulfur in the backbone, preliminarily succeeding in only the silyl case (Scheme 5). In sum, these studies force a long-awaited re-examination of long-standing mechanistic assumptions.



References

1. Zumach, G. and Kühle, E. *Angew. Chem., Int. Ed. Engl.* **9**, 54-63 (1970).
2. Barany, M. J., Hammer, R. P., Merrifield, R. B. and Barany, G. *J. Am. Chem. Soc.* **127**, 508-509 (2005).
3. Barany, G. and Merrifield, R. B. *J. Am. Chem. Soc.* **99**, 7363-7365 (1977).

Peptide-Derived (Sulfonyl)Azides as Versatile Synthons in Chemoselective Bioconjugations

Remco Merkx, Dirk T. S. Rijkers, Arwin J. Brouwer, Johan Kemmink
and Rob M. J. Liskamp

Department of Medicinal Chemistry, Faculty of Pharmaceutical Sciences, Utrecht Institute for
Pharmaceutical Sciences, Utrecht University, PO Box 80082, 3508 TB Utrecht,
The Netherlands

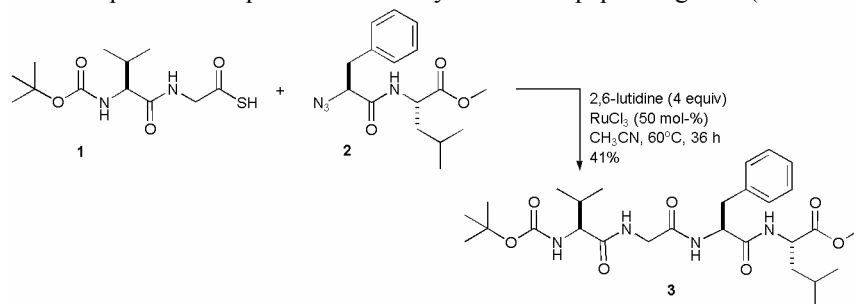
Introduction

Today, there is tremendous interest in the development of new chemoselective (bio)conjugation or ligation reactions for coupling large and complex biomolecules [1]. With respect to the assembly of peptides and the total synthesis of (mini)proteins, the reaction of a peptide thio ester with an N-terminal cysteinyl peptide (native chemical ligation [2]) and the reaction of a peptide triphenylphosphine (thio) ester with an N- α azido peptide (Staudinger ligation [3,4]) are well known amide bond formation reactions. The presence of an azide functionality allows the Staudinger ligation to be in principle independent of the nature of the side chain. However, we and others have found that sterical hindrance at the ligation site determines the efficiency of this reaction to a large extent [5].

The reaction of an azide with a thio acid has been described in the literature as a reliable amide bond formation reaction [6]. Recently, Williams et al. reinvestigated the reaction of thio acids with *aryl* (sulfonyl)azides, and found that thio acids reacted in a chemoselective manner with azides leading to amides without requirement of prior reduction of the azide to the amine [7]. We were triggered by this unconventional amide synthesis to explore its potential for chemoselective coupling of unprotected peptide thio acids and azido peptides in order to obtain an amide bond at the site of ligation.

Results and Discussion

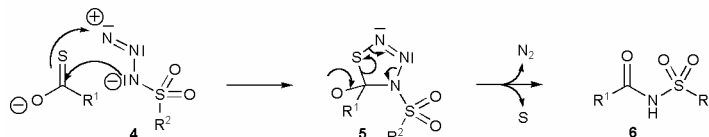
Our model system was the reaction between Boc-Val-Gly-SH **1** and N₃-Phe-Leu-OMe **2** to explore the scope of this amide synthesis as a peptide ligation (Scheme 1).



Scheme 1. Reaction of peptide thio acid **1** with azidopeptide **2** affording tetrapeptide **3**.

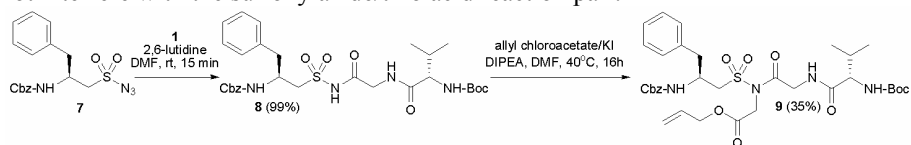
The optimal conditions consisted of performing this reaction at 0.15 M in CH₃CN with 2,6-lutidine as a base in the presence of RuCl₃ [8] at 60°C for 36h leading to tetrapeptide **3** in 41% yield. Although addition of RuCl₃ increased the efficiency of the reaction it was found to be detrimental to the chemoselectivity since other

nucleophiles than the azide (e.g. ϵ -NH₂ of lysine) reacted mainly with the thio acid. The yields of this amide formation reaction were significantly lower than those reported in the literature [7] even in the presence of RuCl₃. Formation of the proposed [7] thiatriazoline intermediate **5** (Scheme 2) via a concerted [2+3] cycloaddition reaction is probably favored when the azide bears an electron withdrawing functionality, e.g., a sulfonyl moiety **4** in order to increase its 1,3-dipolar character. However, the azidopeptides, which were used in this study, are more electron rich, thereby decreasing the reactivity of the azidopeptide.



Scheme 2. Proposed mechanism of amide formation from thio acids and sulfonylazides.

Furthermore, application of peptide-based thio acids and *amino acid*-derived sulfonylazides in this chemoselective coupling would provide access toward peptide mimics with densely functionalized acyl sulfonamides, like **6**. As an example [9], sulfonylazide Cbz-Phe-Ψ[CH₂SO₂]-N₃ **7** reacted smoothly with dipeptide thio acid **1** to give the orthogonally protected tripeptide mimic **8** in 99% yield (Scheme 3). Moreover, the addition of other nucleophiles (water, carboxylates and amines) did not interfere with the sulfonylazide/thio acid reaction pair.



Scheme 3. Synthesis of tripeptide mimic **8** and subsequent chemoselective N-alkylation to **9**.

The increased acidity of the sulfonamide NH allowed a chemoselective N-alkylation with suitable electrophiles, thus providing access to an orthogonally protected acyl sulfonamide scaffold to be used in bioconjugation and chemical ligation reactions.

References

1. Köhn, M. and Breinbauer, R. *Angew. Chem. Int. Ed.* **43**, 3106-3116 (2004).
2. Dawson, P. E., Muir, T. W., Clark-Lewis, I. and Kent, S. B. H. *Science* **266**, 776-779 (1994).
3. Saxon, E. and Bertozzi, C. R. *Science* **287**, 2007-2010 (2000).
4. Nilsson, B. L., Soellner, M. B. and Raines, R. T. *Annu. Rev. Biophys. Biomol. Struct.* **34**, 91-118 (2005).
5. Merckx, R., Rijkers, D. T. S., Kemmink, J. and Liskamp, R. M. J. *Tetrahedron Lett.* **44**, 4515-4518 (2003).
6. Rosen, T., Lico, I. M. and Chu, D. T. W. *J. Org. Chem.* **53**, 1580-1582 (1988).
7. Shangguan, N., Katukojvala, S., Greenberg, R. and Williams, L. J. *J. Am. Chem. Soc.* **125**, 7754-7755 (2003).
8. Fazio F. and Wong, C. -H. *Tetrahedron Lett.* **44**, 9083-9085 (2003).
9. Merckx, R., Brouwer, A. J., Rijkers, D. T. S. and Liskamp, R. M. J. *Org. Lett.* **7**, 1125-1128 (2005).

Chemically Synthesized Annexin-A5-Based Probes for Molecular Imaging

Cheng-Bin Yim¹, Anouk Dirksen², Chris P.M. Reutelingsperger¹ and
Tilman M. Hackeng¹

¹Cardiovascular Research Institute Maastricht, PO-Box 616, 6200 MD Maastricht, The Netherlands; ²Laboratory of Macromolecular and Organic Chemistry, Eindhoven University of Technology, PO-Box 513, 5600 MB Eindhoven, The Netherlands

Introduction

Apoptosis (programmed cell death) is a carefully regulated process of cell death that occurs as a normal part of development. Inappropriately regulated apoptosis is implicated in disease states, such as Alzheimer's disease and cancer.

In normal viable cells, phosphatidylserine (PS) is located on the cytoplasmic surface of the cell membrane. However, in apoptotic cells, PS is translocated from the inner to the outer leaflet of the plasma membrane. This PS exposure at the cellular surface, one of the earliest detectable molecular events in apoptosis, is detected by Annexin-A5 (AnV), a 35 kDa Ca²⁺-dependent phospholipid-binding protein that has a high affinity for PS [1].

AnV is widely used as a radiodiagnostic probe to visualize and localize apoptosis in patients in order to guide diagnosis and therapy decision-making. We aim to explore the potential of a labeled synthetic Ca²⁺-binding module of AnV as a target-specific contrast agent for MR and fluorescent imaging with increased affinity for apoptotic regions through multivalent binding.

The Ca²⁺-binding module of AnV (61 AA) was obtained through solid phase peptide synthesis (SPPS) and native chemical ligation [2] (Fig. 1). Multivalent structures were established through binding of biotinylated AnV-modules to avidin. Phospholipid binding analysis was performed with ellipsometry and cytometry.

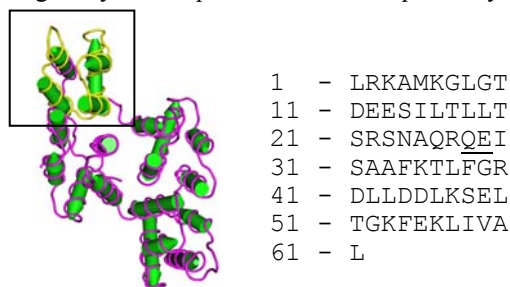


Fig. 1. 3D Model of Annexin-A5. The amino acid sequence of PS binding module, shown in box, is presented on the right. The Native Chemical Ligation site is underlined, the native residue glutamic acid at position 29 was replaced by cysteine.

Results

The biotinylated polypeptide was prepared into 2 segments, N-terminal thioester (residues 1-28) and C-terminal (Cys29-61-Lys-Biotin), by manual SPPS using the in situ neutralization/HBTU activation procedure for Boc chemistry on MBHA (0.94 mmol/g) resin, as described by Schnölzer et al. [3]

Following HF deprotection and cleavage, the crude peptides were analyzed and purified with reversed-phase HPLC. Subsequently, the two polypeptides were joined via native chemical ligation to form the full-length construct (Fig. 2).

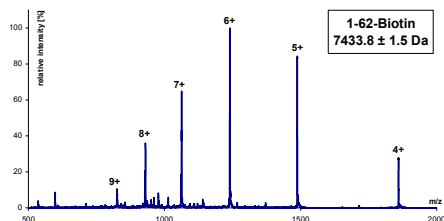


Fig. 2. ESI-MS spectrum of ligated 1-62-Biotin. This module has an alkylated cysteine-29 through treatment with bromoacetic acid, yielding an electronically and sterically similar residue to the glutamate residue found in native Annexin-A5.

Multivalent constructs were established through binding of biotinylated AnV-modules to avidin. The binding stoichiometry was determined with the HABA assay [4]. The ellipsometer was used to characterize the adsorption to phospholipid bilayers (Fig. 3) [5]. After addition of $\frac{1}{4}$ equivalent of Avidin to preincubated AnV-module the binding-affinity increased significantly.

In subsequent study we successfully bound AnV-modules to Qdot Streptavidin conjugates. The inner shells of Qdots contain an inherent fluorescent dye, which enables optical imaging. Using FACS-analysis we visualized apoptotic Jurkat cells [6] with Anv-module-Qdots. Apoptotic bodies are smaller cells with no morphology compared to viable cells. From the obtained data a clear distinction is observed between highly fluorescent small dead and low fluorescent large viable cells (Fig. 4).

In conclusion, we established chemical access to a phospholipid binding module from Annexin-A5. Multimerization by avidin contributes significantly to binding affinity through its multivalent nature. These promising results allow exploration of multivalent constructs of AnV-modules labeled with various imaging probes for the non-invasive detection of apoptosis.

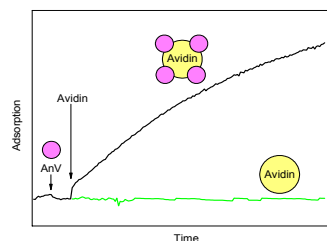


Fig. 3. Adsorption of AnV-module without and with Avidin to phosphatidylserine-coated silicon slides.

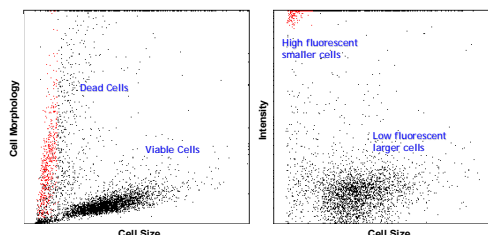


Fig. 4.

References

1. Reutelingsperger, C. P. M. and van Heerde, W. L. *Cell. Mol. Life Sci.* **53**, 527-532 (1997).
2. Dawson, P. E., Muir, T., Clark-Lewis, I. and Kent, S. B. H. *Science* **266**, 776-779 (1994).
3. Schnölzer, M. and Kent, S. B. H. *Science* **256**, 221-226 (1992).
4. Green, N. M. *Biochem. J.* **94**, 23c-24c (1965).
5. Andree, H. A. M., et al. *J. Biol. Chem.* **265**, 4923-4928 (1990).
6. Vermes, I. and Haanen, C., et al. *J. Immun. Meth.* **243**, 167-190 (2000).

Unequivocal Synthesis of (*Z*)-Alkene or (*E*)-Fluoroalkene Dipeptide Isosteres via DKP Mimetics to Probe Structural Requirements of Peptide Transporter

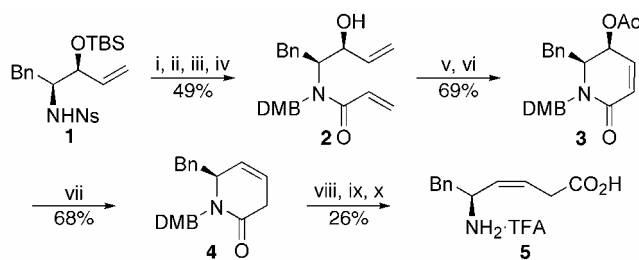
Ayumu Niida¹, Shinya Oishi¹, Makiko Mizumoto¹, Yoshikazu Sasaki¹,
 Kenji Tomita¹, Hirokazu Tamamura¹, Akira Otake¹, Tomohiro Terada²,
 Ken-ichi Inui² and Nobutaka Fujii¹

¹Graduate School of Pharmaceutical Sciences; ²Department of Pharmacy, Faculty of
 Medicine, Kyoto University, Kyoto, 606-8501, Japan

Introduction

Cis-/*trans* isomerization of peptide bond in several bioactive peptides plays an important role for their activities. (*Z*)-Alkene dipeptide isosteres represent potential *cis*-amide conformations and have structural similarity with a parent amide bond. Furthermore they do not isomerize to *trans*-conformations. (*E*)-Fluoroalkene dipeptide isosteres are electrostatically favorable *cis*-amide bond mimetics compared to simple alkene units. These dipeptide isosteres would be useful tools for conformational analysis of bioactive peptides and proteins. Recently we have engaged in the development of synthetic methodologies for (*E*)-alkene and (*Z*)-fluoroalkene dipeptide isosteres as *trans*-amide bond mimetics and applied them to bioactive peptides [1,2]. However, there are few reports concerning the efficient synthesis of (*Z*)-alkene or (*E*)-fluoroalkene dipeptide isosteres and their application to conformational studies. Herein, we described new synthetic routes for (*Z*)-alkene or (*E*)-fluoroalkene dipeptide isosteres via diketopiperazine mimetics [3] utilizing organocopper-mediated reduction. These isosteres proved to be successfully used to probe structural requirements for peptide transporter PEPT1.

Results and Discussion

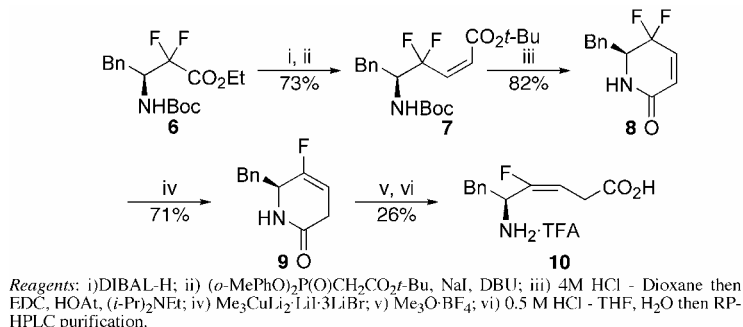


Reagents: i) DMB-OH, PPh₃, DEAD; ii) HSCH₂CO₂H, LiOH; iii) CH₂=CHCOCl, Et₃N; iv) TBAF; v) Grubbs' cat. 2nd generation; vi) Ac₂O, DMAP, pyridine; vii) Me₃CuLi₂·LiI·3LiBr; viii) TFA; ix) Me₃O·BF₄; x) 0.5 M HCl - THF, H₂O then RP-HPLC purification. Abbreviation: Ns = 2-nitrobenzenesulfonyl; TBS = *t*-butyldimethylsilyl; DMB = 2,4-dimethoxybenzyl.

Scheme 1. Synthesis of Phe-Gly type (*Z*)-alkene dipeptide isostere 5.

The synthesis of Phe-Gly type (*Z*)-alkene dipeptide isostere **5** was started from the sulfonamide **1** (Scheme 1). The γ -acetoxy- α,β -unsaturated- δ -lactam **3** was synthesized by a sequence of known reactions. Reaction of acetate **3** with Me₃CuLi₂·LiI·3LiBr proceeded smoothly at -78 °C to yield diketopiperazine mimetic **4** as a reduction product. After removal of a DMB group by TFA, the resulting

lactam was converted to a lactim ether with $\text{Me}_3\text{O}\cdot\text{BF}_4$ followed by hydrolyzation under mild acidic condition to yield Phe-Gly type (*Z*)-alkene dipeptide isostere **5**.



Scheme 2. Synthesis of Phe-Gly type (*E*)-fluoroalkene dipeptide isostere **10**.

The (*E*)-fluoroalkene dipeptide isostere **10** was synthesized from the chiral β -amino ester **6** prepared by a reported procedure (Scheme 2). After reduction of ester **6**, the resulting aldehyde was subjected to (*Z*)-selective Horner-Wadsworth-Emmons reaction followed by deprotection and cyclization to yield γ,γ -difluoro- α,β -unsaturated- δ -lactam **8**. Reduction of lactam **8** with Me₃CuLi₂·LiI·3LiBr gave γ -fluoro-diketopiperazine mimetic **9**, which was converted to (*E*)-fluoroalkene dipeptide isostere **10** by a procedure similar to the synthesis of isostere **5**. We also synthesized the corresponding Phe-Gly type (*E*)-alkene and (*Z*)-fluoroalkene dipeptide isosteres as *trans*-amide equivalents by reported procedures.

comp.	A	K _i (mM)
Phe-Gly	-CO-NH-	0.205
5	-ψ[(<i>Z</i>)-CH=CH]-	~10.0
10	-ψ[(<i>E</i>)-CF=CH]-	~10.0
11	-ψ[(<i>E</i>)-CH=CH]-	0.853
12	-ψ[(<i>Z</i>)-CF=CH]-	1.34

Fig. 1. Structures of synthetic Phe-Gly derivatives and their K_i values based on inhibition of [³H]-Gly-Sar uptake by PEPT1.

Next we evaluated affinities for human di/tripeptide transporter, PEPT1 of synthetic Phe-Gly derivatives (Fig. 1). The affinities for PEPT1 (Caco-2 cell) were evaluated by their ability to inhibit the transport of [³H]-Gly-Sar [4,5]. In these experiments, *trans*-amide equivalent isosteres **11** and **12** exhibited good affinities for PEPT1 corresponding to the parent dipeptide. On the other hand, affinities of *cis*-amide bond equivalents **5** and **10** were more than ten times lower than those of *trans*-isomers. These data suggested that PEPT1 predominantly recognizes *trans*-amide conformations of dipeptides.

References

- Oishi, S., Niida, A., Otaka, A. and Fujii, N., *et al. J. Org. Chem.* **67**, 6162-6173 (2002).
- Otaka, A., Fujii, N., *et al. J. Org. Chem.* **69**, 1634-1645 (2004).
- Niida, A., Fujii, N., Otaka, A., *et al. Tetrahedron Lett.* **46**, 4183-4186 (2005).
- Våbenø, J., Luthman, K., *et al. J. Med. Chem.* **47**, 1060-1069 (2004).
- Inoue, M., Terada, T., Okuda, M. and Inui, K. *Cancer Lett.* **230**, 72-80 (2005).

Development of New Photoremovable Amino Protecting Group and its Application toward Chemical Synthesis of 7TM-GPCR

Satoshi Ueda, Akira Otaka, Hirokazu Tamamura and Nobutaka Fujii

Graduate School of Pharmaceutical Sciences, Kyoto University, Sakyo-ku,
Kyoto 606-8501, Japan

Introduction

On the basis of our recent investigation into lipid bilayer-assisted chemical synthesis of 7-transmembrane G-protein coupled receptor (7TM-GPCR) [1], a new method for sequential native chemical ligation (NCL) using a peptide building block with both *N*-terminal Cys and *C*-terminal thioester [2] was strongly demanded for the synthesis of multi-pass membrane proteins. For this end, photoremovable protecting groups, which can be removed without adding any chemicals is thought to provide a promising avenue to establish the general strategy.

Among several photoremovable groups, *o*-nitrobenzyl-type protecting groups have been shown to be useful in peptide chemistry. However, photodeprotection of this type of protections on the *N*-terminal Cys residue proceeds in Norrish-type II mechanism to release the *N*/S-unprotected Cys and aldehyde which recombine to form thiazolidine moiety canceling any reactivity in the following NCL step. Photolabile phenacyl-type protections are potential alternative to *o*-nitrobenzyl group due to their photosolvolytic character. Phenacyl-type groups with methoxy or hydroxyl substituent have received attention as photosensitive group, where electron-donating substituents are responsible for the rapid release of parent molecules [3]. These precedents prompted us to examine the feasibility of the phenacyl-type groups with more electron-donating *p*-dimethylamino substituents for $-\text{CO}_2\text{H}$ or $-\text{NH}_2$ protection and the applicability to the one-pot sequential NCLs strategy.

Results and Discussion

First, we evaluated the reactivity of 4-dimethylaminophenacyl ester as the protected carboxylate using several kinds of Z-Gly-phenacyl esters **1** (Fig. 1). Photolysis of **1** were conducted in EtOH using a 100W high pressure Hg lamp ($h\nu > 300\text{ nm}$) at the concentration of 1 mM. Deprotection profiles of **1** are summarized in Table 1 (entries 1 - 4). Photolysis of novel 4-dimethylaminophenacyl ester **1c** proceeded efficiently to complete two times faster the release of Z-Gly-OH than that of 4-hydroxyphenacyl ester **1b**, which is the most photosensitive group in the reported phenacyl type protections. Next, we investigated the potential of 4-dimethylaminophenacyloxy-carbonyl (Mapoc) moiety for the protection of amino function using phenylalanine-derived carbamates **2**. Whereas the photolysis of **2b**

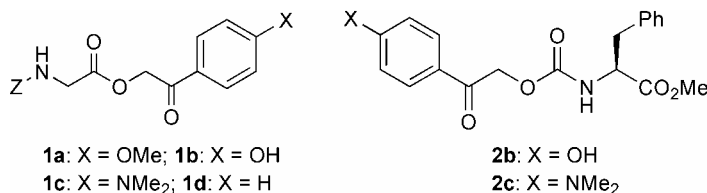


Fig. 1. Phenacyl-type protected compounds used in this study.

Table 1. Photoinduced-deprotection of protected amino acid derivatives (**1** and **2**)

Entry	Substrate (<i>p</i> -substituent)	Photolysis [t/min] ^[a]	Yield [%] ^[b]	t ^{1/2} /min ^[c]
1	1a (OMe)	90	22	n.d. ^[d]
2	1b (OH)	30	96	11
3	1c (NMe ₂)	7	97	5.3
4	1d (H)	90	11	n.d. ^[d]
5	2b (OH)	70	93	19
6	2c (NMe ₂)	20	95	7.5

[a] Determined by measurements of regenerated amino acid derivatives (Z-Gly-OH for **1** and H-Phe-OMe for **2** using reverse-phase HPLC analyses. [b] Determined by the disappearance of **1** or **2** using HPLC analyses. [c] not determined.

and **2c** proceeded slowly in comparison with the corresponding ester derivatives **1b** and **1c**, deprotected compound (H-Phe-OMe) was quantitatively regenerated (Table 1, entries 5 and 6). As seen in photolysis of the esters (**1b** vs **1c**), carbamate **2c** possessing dimethylamino substituent released the amine faster than **2b**.

As a practice toward the chemical synthesis of 7TM-GPCR, we applied this protecting group for the one-pot synthesis of human brain natriuretic peptide (hBNP-32) using three peptide fragments (Fig. 2). The first NCL in the presence of 0.3% (v/v) thiophenol in phosphate buffer (pH 7.6) at 37°C proceeded quantitatively to yield the ligated product. Without purifying the ligated product, photo-irradiation of the reaction mixture at 25°C for 30 min, followed by a second ligation for 1 hr in the presence of additional thiophenol (1% v/v), afforded the linear hBNP-32. The peptide solution was diluted three times with phosphate buffer, followed by the addition of DMSO (10% v/v) to yield the disulfide bridged hBNP-32. HPLC purification of the crude material afforded purified hBNP-32 in 57% yield calculated from peptide fragments employed in sequential NCLs.

Application of Mapoc protecting group for the chemical synthesis of 7TM-GPCR is now in progress.

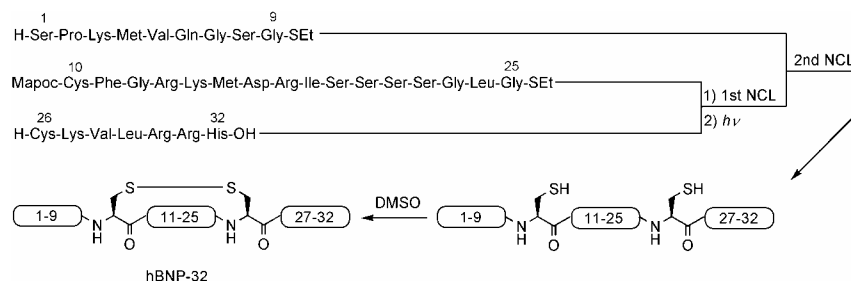


Fig. 2. Synthetic scheme for hBNP-32 utilizing the one-pot sequential NCLs followed by disulfide formation with DMSO.

References

1. Otaka, A., Ueda, S., Tmomita, K., Yano, Y., Tamamura, H., Matsuzaku, K. and Fujii, N. *Chem. Commun.* 1722-1723 (2004).
2. Bang, D. and Kent, S. B. H. *Angew.Chem. Int. Ed.* **43**, 2534-2538 (2004).
3. Givens, R. S., Weber, J. F. W., Conrad, P. G., Orosz, G., Donahue, S. A. and Thayer, S. A. *J. Am. Chem. Soc.* **122**, 2687-2697 (2000).

Multivalent Peptide Dendrimers: Native Chemical Ligation as a Synthetic Tool

Hinke Malda¹, Tilman M. Hackeng², Marcel H. P. van Genderen¹ and Egbert W. Meijer¹

¹Laboratory of Macromolecular and Organic Chemistry, Department of Biomedical Engineering, Eindhoven University of Technology, P.O.Box 513, 5600 MB Eindhoven, The Netherlands; ²Cardiovascular Research Institute Maastricht, Department of Biochemistry University Maastricht, P.O. Box 616, 6200 MD Maastricht, The Netherlands

Introduction

Today, dendrimers attract much attention due to their unique structure and properties that make them suitable candidates for biomedical applications [1]. They can be modified with a large number of end groups at the periphery of the dendrimer, either non-covalently or covalently. Therefore, dendrimers are considered as ideal multivalent scaffolds. Native Chemical Ligation is a commonly used synthetic method for the coupling of two peptide fragments [2]. If a C-terminal thioester peptide is combined with an N-terminal cysteine peptide under mild conditions (pH 7.5, buffered media, no protective groups), a chemical reaction takes place followed by a spontaneous rearrangement yielding a native peptide bond. The reaction is highly specific, the yields are quantitative and no racemization occurs. Here, we describe the modification of dendrimers with peptides via Native Chemical Ligation, the peptide dendrimers are currently tested in several biomedical applications.

Results and Discussion

Synthesis of first, second and third generation cysteine-dendrimers (G1-Cys₄, G2-Cys₈ and G3-Cys₁₆) succeeded in high purity. C-terminal thioester-peptides were synthesized by solid phase peptide synthesis using tBoc protocols (Fig. 1).

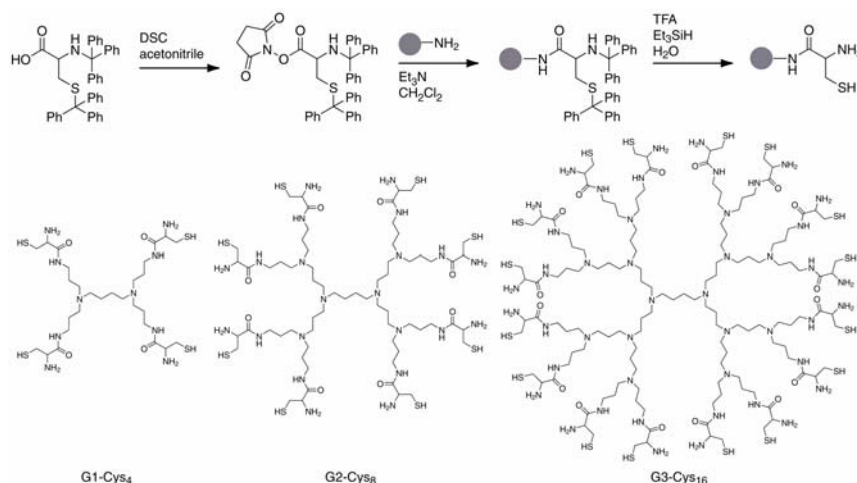


Fig. 1. Synthesis of first, second and third generation poly(propylene imine) dendrimers with cysteine residues at the periphery.

Ligation reactions of thioester-peptides with cysteine-dendrimers were performed in a 6 M guanidine Tris-buffer with the addition of thiols for thioester exchange. The peptide dendrimers were analyzed and purified by RP-HPLC coupled to ESI mass spectrometry. In this way, a large variety of peptides (hydrophobic and hydrophilic, large and small, linear and sterically hindered) was coupled to the first and the second generation dendrimer. ESI MS spectra of two examples of peptide dendrimers are shown in figure 2.

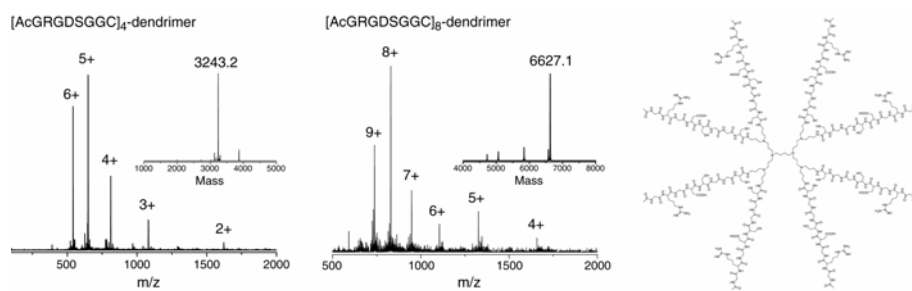


Fig. 2. ESI MS spectra and corresponding deconvoluted mass spectra of the ligation products of a first generation dendrimer with RGD-peptide ([AcGRGDSGGC]₄-dendrimer, left) and second generation dendrimer with RGD-peptide ([AcGRGDSGGC]₈-dendrimer, middle). The structure [AcGRGDSGGC]₈-dendrimer is shown at the right.

The multivalent peptide dendrimers are currently tested in biomedical applications *in vivo* as well as *in vitro*. Rabbits are vaccinated with peptide dendrimers to study their application as synthetic vaccines against malaria. In rats, peptide dendrimers are tested as inhibitors of testosterone production in prostate cancer. In addition, the aggregation of A β with and without peptide dendrimers is tested *in vitro*.

After ligation, the thiol group of cysteine reappears at the site of ligation and is subsequently reactive towards maleimide probes, such as Oregon Green 488 (OG488) maleimide (fluorescent probe) or DTPA-maleimide (probe for molecular imaging) [3]. For the first generation dendrimers, this resulted in a fluorescently labeled peptide dendrimer and a target-specific contrast agent based on a dendritic scaffold respectively. Also, both probes could be introduced at the same scaffold by reaction of DTPA maleimide with the cysteine-thiol and OG488 succinimidyl ester with the lysine ϵ -amine moiety in the peptide chain.

Acknowledgments

W. Adriaens (University Maastricht) is acknowledged for her help during peptide synthesis.

References

1. Bosman, A. W., Jansen, H. M. and Meijer E. W. *Chem. Rev.* **99**, 1665-1688 (1999).
2. Dawson, P. E., Muir, T. W., Clark-Lewis, I. and Kent, S. B. *Science* **266**, 776-779 (1994).
3. Dirksen, A., Langereis, S., de Waal, B. F. M., van Genderen, M. H. P., Meijer, E. W., de Lussanet Q. G. and Hackeng, T. M. *Org. Lett.* **6**, 4857-4860 (2004).

Synthesis and Use of C-terminally Biotinylated Peptidomimetics with High Grb2 SH2 Domain-binding Affinity

Zhen-Dan Shi¹, Benedetta Peruzzi², Pathirage G. Dharmawardana²,
 Tiffany Leech², Ettore Appella³, Karen M. Worthy⁴, Lakshman K.
 Bindu⁴, Robert J. Fisher⁴, Donald P. Bottaro² and Terrence R.
 Burke, Jr.¹

¹Laboratory of Medicinal Chemistry, CCR, NCI, NIH, Frederick, MD 21702 USA; ²Urologic Oncology Branch; ³Laboratory of Cell Biology, CCR, NCI, NIH, Bethesda, MD 20892 USA; ⁴Protein Chemistry Laboratory, SAIC-Frederick, Frederick, MD 21702 USA

Introduction

Compounds **1a** and **2a** bind to Grb2 SH2 domains with high affinity and exhibit interesting biochemical properties when given to whole cells in culture. In order to investigate cellular targets, biotinylated congeners were desired, however standard N-terminal biotinylation was not possible. Therefore, novel C-terminally biotinylated analogs **1b** and **2b** (Fig. 1) were prepared, which proved to exhibit remarkable Grb2 SH2 domain-binding affinity.

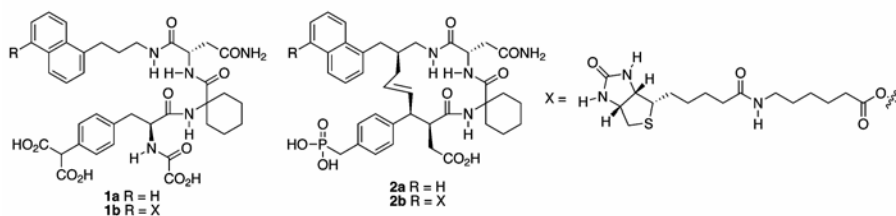


Fig. 1. Structures of analogs discussed in the text.

Results and Discussion

The biotinylated inhibitor **1b** was synthesized starting from 1,5-dihydroxy naphthalene **3** by first converting to the mono-triflate ester **4**. Subsequent Heck reaction gave the expected adduct **5** as well as its reduced product **6**. Reduction with LiAlH_4 provided primary amine **7** (Fig. 2). This was converted to intermediate **8** then to product **1b** following previously reported methods [1]. The synthesis of **2b** has been in literature [1].

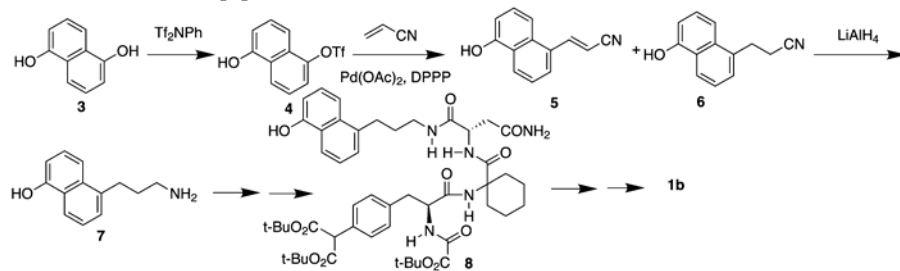


Fig. 2. Synthesis of **1b**.

The affinities of synthetic Grb2 SH2 ligands were determined using surface plasmon resonance (SPR). SPR data (k_a , k_d and K_D values) were measured for the binding of inhibitors in solution to sensor-bound Grb2 SH2 domain protein (Method a) or by binding of Grb2 SH2 domain protein in solution to sensor-bound inhibitor (Method b). As shown in Table 1, macrocyclic biotinylated inhibitor **2b** had K_D values in the low nanomolar range, while the K_D value of the open chain biotinylated inhibitor **1b** was an order of magnitude higher. The k_{on} values of both biotinylated inhibitors were similar, however the k_{off} value for the macrocyclic **2b** was approximately 20 times slower than for the open-chain **1b**.

Experiments were performed to identify cellular targets: Incubation of SK-LMS-1 cell lysates with **1b** captured on streptavidin-coated beads was followed by separation of bound proteins using SDS-PAGE. Immunoblot analysis revealed that (i) Grb2 was efficiently and specifically captured from cell lysates by **1b**; (ii) Known Grb2-associated signaling proteins, e.g., Gab1, Nck1 and 2, and Sos1, as well as β -catenin were also specifically captured by **1b**; (iii) c-Met was not captured, consistent with the ability of **1b** to antagonize Grb2/c-Met binding [2]. Work is in progress to differentiate proteins that bind directly to **1b** from those that are brought down by secondary association with direct binding proteins.

Table 1. SPR data of the ligands binding to Grb2 SH2 domain

Ligand	Assay Method	k_{on} ($M^{-1} \cdot sec^{-1}$)	k_{off} (sec^{-1})	K_D (nM)
2b	Biocore S51 ^a	2.24×10^6	1.78×10^{-2}	7.97
2b	Biocore S51 ^b	3.23×10^6	8.93×10^{-3}	2.77
1b	Biocore S51 ^a	1.66×10^6	2.57×10^{-1}	155

Method a: Binding of inhibitor in solution to sensor-bound Grb2 SH2 domain protein.

Method b: Binding of Grb2 SH2 domain protein in solution to sensor-bound inhibitor.

Acknowledgments

Appreciation is expressed to Drs. Christopher Lai and James Kelley of the LMC for mass spectral analysis.

References

- Shi, Z.-D., Liu, H., Zhang, M., Roberts, L. R., Worthy, K. M., Yang, D., Fisher, R. J. and Burke, T. R. Jr. *Bioorg. Med. Chem.* **13**, 4200-4208 (2005).
- Dharmawardana, P., Giubellino, A., Shi, Z. -D., Burke, T. R., Jr. and Bottaro, D. (Unpublished results).

Total Solid Phase Synthesis of a Marine Cyclodepsipeptide IB-01212

Luiz J. Cruz¹, Marta Martínez², Julia Pérez², Marta Trujillo², Librada M. Cañedo², Ricard Rodríguez¹, Ernest Giralt¹ and Fernando Albericio¹

¹Barcelona Science Park, University of Barcelona, 08028-Barcelona, Spain; ²Instituto Biomar S. A., 24231 Onzonilla, León, Spain

Introduction

A new cytotoxic cyclodepsipeptide IB-01212 was isolated from the mycelium extract of *Chlonostachys pitiroides* (Fig. 1) [1]. The novo cyclodepsipeptide is a symmetric cyclic peptide formed by the condensation of two chains of the tetrapeptide L-N,NMe₂Leu-L-Ser-L-NMeLeu-L-NMePhe. The absolute configuration was determined by our group and it was confirmed that all amino acids were in the L-configuration. Herein we describe several strategies of synthesis on solid phase such as i) dimerization of heterodetic fragment, ii) linear synthesis, and iii) convergent synthesis. All syntheses were performed using Fmoc/tBu chemistry and ester bond resin. A comparison of the yield and quality of the synthetic processes showed that the convergent synthesis that combines fragments synthesized on two different resins gave the best results. Thus, this strategy is particularly suitable for the large-scale synthesis of IB-01212 and other peptides containing the same motifs.

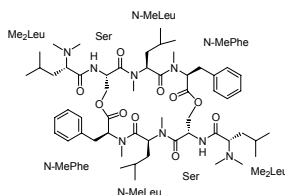


Fig. 1. Structure of the cyclodepsipeptide IB-01212.

Results and Discussion

Strategy 1: Dimerization of heterodetic fragment. Due to its symmetric character, the cyclodepsipeptide could be prepared by dimerization of heterodetic fragments. In this approach, the synthesis of the tetrapeptide was carried out using Fmoc/tBu chemistry and CTC-resin. Limited incorporation of Fmoc-NMePhe-OH on CTC-resin was performed using DIEA, while Fmoc-NMeLeu-OH, Fmoc-Ser(tBu)-OH, and N,NMe₂Leu-OH were introduced with PyBOP/HOAt. The protected peptide was cleaved from the resin with 1% TFA, and the tBu group was then removed with 95% TFA. The cyclization step (dimerization) of the tetrapeptide was performed at 5.6 mM using MSNT. The cyclodimer was purified by RP-HPLC to give the expected compound (2.3% yield) with a 98% purity. The low yield obtained for the cyclization reaction was due to the formation of cyclic monomer and trimer.

Strategy 2: Linear synthesis. For the linear synthesis approach the peptide chain elongation was performed on solid phase with controlled formation of each ester bond. The synthesis of the octapeptide was performed by Fmoc/tBu chemistry. Wang resin was used to allow the selective deprotection of the Trt group on Ser without cleaving the peptide from the resin. Fmoc-NMePhe-OH was anchored on Wang resin by esterification with MSNT. Fmoc-NMeLeu-OH, Fmoc-Ser(tBu)-OH,

and N,NMe₂Leu-OH were then introduced with PyBOP/HOAt. Trt group was removed selectively by treatment with 1.5% TFA and the esterification reaction of Fmoc-NMePhe-OH with the free hydroxyl group on Ser was performed with MSNT. Fmoc-NMeLeu-OH, Fmoc-Ser(tBu)-OH, and N,NMe₂Leu-OH were then coupled via asymmetric anhydride. The octapeptide was cleaved from the Wang resin with 95% TFA. The macrocyclization was carried out under diluted condition (1.05 mM) with MSNT. The crude product was purified by RP-HPLC to give IB-01212 (4% yield) with an excellent purity of 97.5%.

While the yield using this strategy was higher than using strategy 1, two main disadvantages were observed: 1) Diketopiperazine formation was detected by HPLC-MS after the third and seventh couplings despite the fact that this undesirable side reaction was minimized using asymmetric anhydride as coupling method and shorter treatments with piperidine and DBU for Fmoc group deprotection; 2) Low stability of the ester bonds between the Ser and NMePhe residues. These two factors are responsible for the overall low yield.

Strategy 3: Convergent synthesis. The preferred synthetic process for the IB-01212 formation was based on a convergent solid-phase (4 + 4) strategy. Synthesis of two tetrapeptides was carried out on two different resins. Thus, for peptide A, the ester bond on CTC-resin allowed the selective cleavage of the fully protected tetrapeptide, while, for peptide B, the ester bond on Wang resin was stable to the removal of highly acid labile side-chain protecting groups. Convergent synthesis was performed by incorporation of the protected tetrapeptide A onto the tetrapeptide B synthesized on Wang resin.

Peptide A synthesis was carried out by standard Fmoc/tBu chemistry on CTC-resin. The protected peptide was cleaved from the CTC-resin with 1% TFA.

Peptide B synthesis was also performed using standard Fmoc/tBu chemistry. Fmoc-NMePhe-OH was anchored on Wang resin by esterification with MSNT. For the third coupling Fmoc-Ser(tBu)-OH was replaced by Fmoc-Ser(Trt)-OH.

Esterification between the C-terminal carboxylic acid group of peptide A (N,NMe₂Leu-Ser(tBu)-NMeLeu-NMePhe-COOH) and the free hydroxyl group of Ser of peptide B (N,NMe₂Leu-Ser-NMeLeu-NMePhe-wang resin) was performed with MSNT for 24 hrs. The peptide was then cleaved from the Wang resin with 95% TFA. The final cyclization step was carried out with MSNT. The crude cyclic product was purified by RP-HPLC to give the target compound in 13.5% yield and 95.6% purity. According to these results, this strategy is suitable for large-scale preparation of IB-01212 and is also applicable to the synthesis of other analogs.

Acknowledgments

This work has been carried out at the Barcelona Science Park- Barcelona University. This work was supported by Pharma Mar, S.A., and Generalitat de Catalunya.

References

1- Trujillo, M., Luna, M. J., Fernandez, P., *et al.* Patent WO 2004012756, (2004).

Interference with Protein-Protein Interactions Involved in Protease Inhibitor Complex Formation

**Dirk-Jan van Zoelen¹, Maarten R. Egmond², Roland J. Pieters¹ and Rob
M. J. Liskamp¹**

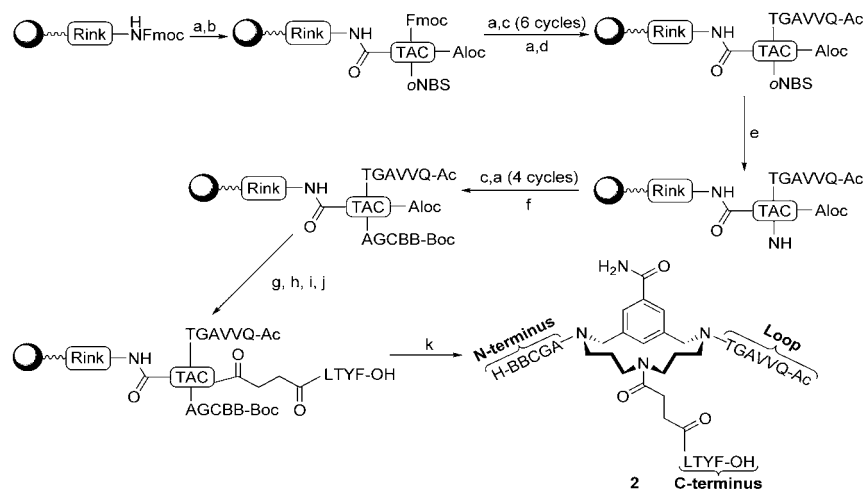
¹*Department of Medicinal Chemistry Utrecht Institute for Pharmaceutical Sciences Utrecht
University PO Box 80082, 3508 TB Utrecht, The Netherlands;* ²*Department of Membrane
Enzymology, Utrecht University, P.O. Box 80082, 3508 TB Utrecht, The Netherlands*

Introduction

Biological processes are regulated by protein-protein interactions. Outstanding examples include the immune response and signal transduction [1]. Defects in the regulation of these interactions are believed to be involved in several diseases. Therefore chemists have tried to develop general methods to modulate and interfere with protein-protein interactions. One of these methods is mimicry of the bioactive binding conformation by assembly of the binding sites or “epitopes” on scaffolds [2]. This method uses the information supplied by nature in order to obtain molecules that bind and function in the same manner as their parent biomolecules. Many biological targets possess discontinuous epitopes. A few years ago the TAC-scaffold was developed in our group [3]. In the triazacyclophane (“TAC”)-scaffold, three orthogonally protected secondary amines are present. As a result it can be used to subsequently introduce three different peptide chains and thus, can mimic discontinuous epitopes [4]. In our research the TAC-scaffold is used to modulate protein-protein interactions involved in the complex of papain and cystatin B (or human Stefin B). The complex consists of the protease papain and its natural inhibitor cystatin B. The inhibitor interacts through three epitopes *viz.* the N-terminus (Met6-Ala10), a β -hairpin loop (Gln53-Thr58), as well as the C-terminus (Leu122-Phe125) with papain. These three epitopes form a wedge capable of blocking the active site of papain, in which the N-terminus is located close to the catalytic triad [5]. By assembly of the three epitopes on the TAC-scaffold we wished to generate new tripodal inhibitors of papain. For synthetic reasons the β -hairpin loop mimic was synthesized on the Fmoc-position of the TAC-Scaffold, the N-terminus mimic on the *o*-NBS position and the C-terminus was assembled on the Alloc-position (Scheme 1).

Results and Discussion

The synthesis of the tripodal inhibitor started with loading of Rink amide resin with the TAC-scaffold (Scheme 1) by means of a BOP coupling. After determination of the loading (0.25 mmol.g⁻¹) and capping, the synthesis was continued by deprotection of the Fmoc-protecting group to liberate the secondary amine. Solid phase peptide synthesis (SPPS) was then performed to introduce the sequence which will serve as the mimic of the β -hairpin loop. In order to synthesize the N-terminus mimic the *o*-NBS group was removed. After deprotection, the second epitope was assembled. To circumvent oxidation, the methionine residues were replaced by norleucine residues. To create a correct mimic of the N-terminus, the final norleucine was introduced protected with a Boc-protecting group. This Boc group is cleaved in the final cleavage liberating the primary amine. Finally, the C-terminus was introduced by means of a reverse coupling of a tetrapeptide (**1**, H-LTYF-OH).



*Scheme 1. Synthesis of tripodal inhibitor of papain. a). 20 % Piperidine, NMP; b). TAC-scaffold, BOP, DiPEA, NMP; c). Fmoc-AA-OH, BOP, DiPEA; d). Ac₂O, DiPEA, HOBT; e). HSCH₂CH₂OH, DBU, DMF; f). Fmoc-B-Boc, BOP, DiPEA; g). Pd(PPh₃)₄, Phenylsilane, NMP; h). Succinic anhydride, DCM; i). BOP, NMP, N₂; j). peptide **1**, NMP; k). TFA/TIS/H₂O/EDT (94.5/1/2.5/2.5); overall yield 24%.*

This peptide was synthesized on Wang resin loaded with of Fmoc-Phe-OH [6] and standard Fmoc SPPS. For coupling of peptide **1** to the scaffold a C-terminus was synthesized, by first removing the alloc-protecting group [7] followed by reaction of the secondary amine with succinic anhydride. The resulting carboxylic acid was converted to the OBt-ester and reacted with peptide **1** to give the mimic of the C-terminus. Finally, the tripodal peptide construct was cleaved from the resin and molecular construct **2** was obtained. Compound **2** was tested for inhibitory activity resulting in a K_i of 12 nM. From this result, we conclude that the TAC-scaffold was capable of orienting the epitopes in the bioactive conformation and construct **2** was an excellent mimic of the natural inhibitor Cystatin B.

Acknowledgments

Dr J. Kemmink is acknowledged for 500 MHz NMR spectroscopy analysis. This research was funded by CW-NWO.

References

1. Dekker, F. J., de Mol, N. J., van Ameijde, J., Fischer, M. J. E., Ruijtenbeek, R., Redegeld, F. A. M. and Liskamp, R. M. J. *ChemBioChem* **3**, 238-242 (2002).
2. Franke, R., Doll, C., Wray, V. and Eichler, J. *Org. Biom. Chem.* **2**, 2847-2851 (2004).
3. Opatz, T. and Liskamp, R. M. J. *Org. Lett.* **3**, 3499-3502 (2001).
4. Chamorro, C., Hofman, J. -W. and Liskamp, R. M. J. *Tetrahedron* **60**, 8691-8697 (2004).
5. Stubbs, M. T., *et al.* *EMBO J.* **9**, 1939-1947 (1990).
6. Sieber, P. *Tetrahedron Lett.* **28**, 6147-6150 (1987).
7. Honda, M., Morita, H. and Nagakura, I. *J. Org. Chem.* **62**, 8932-8936 (1997).

Sequence-Enabled Reassembly (SEER) Peptides for the Detection of DNA Sequences

Aik T. Ooi¹, Cliff I. Stains², Jason R. Porter², Indraneel Ghosh² and David J. Segal¹

¹Department of Pharmacology and Toxicology; ²Department of Chemistry, University of Arizona, Tucson, AZ 85721, USA

Introduction

By combining custom zinc finger (ZF) DNA-binding technology [1,2] with protein fragment complementation [3], we have developed a technology, designated SEER (Sequence-Enabled Reassembly), that has the potential to “see” or detect genetic information within a living cell (Fig. 1). These agents consist of two inactive parts of signal-generating peptides that have the ability to recognize specific DNA sequences. The two parts bind near each other in the presence of a user-defined DNA target site and generate a fluorescent signal. Two prototype SEER systems have been constructed, based on the reassembly of green fluorescent protein (SEER-GFP) [4] and the enzyme β -lactamase (SEER-LAC). To our knowledge, these are the first examples of DNA-dependent reassembly of peptide fragments.

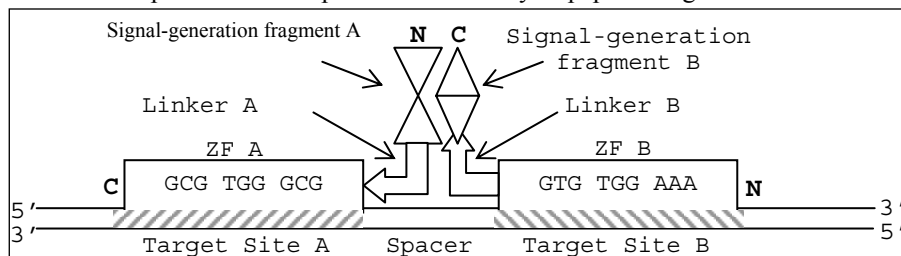


Fig. 1. Schematic representation of a SEER system for sequence-specific detection of dsDNA.

Results and Discussion

Custom DNA-binding proteins: Since biologically relevant target sites cannot be chosen until the optimal spacer and orientation parameters are established, initial experiments employ designed target sites that are recognized by existing, well-characterized, ZF. Zif268 is a naturally-occurring 3-finger ZF that has been extensively studied structurally and biochemically. It binds the 9bp sequence 5'-GCGTGGGCG-3'. PBSII is a designed 3-finger ZF assembled from predefined modified ZF domains [1,2], which recognizes the sequence 5'-GTGTGGAAA-3'. Together, the two proteins recognize 18bp of DNA, a target site sufficiently large to be unique in the human genome.

SEER-GFP: Peptide constructs were designed such that the C-terminus of GFP fragment (1-157) was fused to the N-terminus of ZF Zif268 by means of a 15-residue linker and the N-terminus of GFP fragment (158-236) was fused to the C-terminus of ZF PBSII (Fig. 2). Both proteins were separately purified under denaturing conditions. Equimolar mixtures (15 μ M each) were refolded in the presence or absence of the target oligonucleotide (4 μ M). Fluorescence (at 505 nm) was only observed for samples containing both halves of GFP-ZF fusions in the presence of target. No fluorescence was observed in the presence of the two half-

sites alone or non-specific herring sperm DNA, demonstrating the specificity of reassembly. A 4-fold excess of target DNA strongly inhibited GFP reassembly, confirming the expectation that a high molar ratio of DNA:proteins localizes the two proteins to different oligonucleotides.

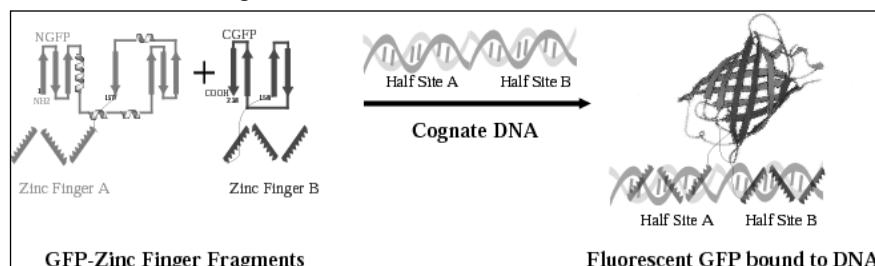


Fig. 2. A cartoon illustrating the SEER-GFP.

SEER-LAC: A different approach is to use an enzyme, such as β -lactamase, to produce the signal instead of a single GFP molecule. Having an enzyme convert a substrate into an easily detectable product would amplify the signal. Genetic constructs were generated by standard cloning methods to code for the following two peptides: “LacA”, an N-terminal zinc finger protein Zif268 linked by a 15aa (GlyGlyGlyGlySer)₃ linker to residues 26-196 of *E. coli* TEM-1 β -lactamase, and “LacB”, an N-terminal zinc finger protein PBSII linked by a 15aa linker to residues 198-290 of β -lactamase. LacA also contained a published M182T mutation in the β -lactamase domain for greater stability [5]. The constructs were cloned into the HindII/NotI sites of the bacterial expression vector pMAL (New England Biolabs), which expressed proteins as C-terminal fusions with maltose binding protein (MBP). The MBP domain improves protein solubility, and allows one-step purification over amylose resin. SDS-PAGE analysis confirmed proteins at >95% purity of approximately 72KD (LacA) and 65KD (LacB).

SEER should provide a sensitive yet inexpensive assay that may be useful as a clinical diagnostic agent. In addition to genomic rearrangements and telomere lengths, it could detect DNA accessibility, unusual structures and methylation, which are presently undetectable by similar methods. The most novel aspect of this method is its ability to recognize double-stranded DNA, presenting the possibility to report on genomic information within individual living cells, an ability not provided by any existing technology. The system could be reconfigured to kill cells through reactivation of a cytotoxic enzyme, producing sequence-dependent cell death. This research therefore impacts studies of disease detection and treatment.

Acknowledgments

This work was supported by the American Cancer Society (IRG7400125) and the NIH-NCI (SPORE in GI Cancer CA95060). C.I.S. received an NIH training grant.

References

1. Blancafort, P., Segal, D. J. and Barbas III, C. F. *Mol. Pharmacol.* **66**, 1361-1371 (2004).
2. Segal, D. J. *Methods* **26**, 76-83 (2002).
3. Ghosh, I., Hamilton, A. D. and Regan, L. *J. Am. Chem. Soc.* **122**, 5658-5659 (2000).
4. Stains, C. I., et al. *J. Am. Chem. Soc.* **127**, 10782-10783 (2005).
5. Galarneau, A., et al. *Nat. Biotechnol.* **20**, 619-622 (2002).

A Mild Acidic Method for the Selective Deprotection of *N*1-trityl-3*a*-hydroxypyrrolo[2,3-*b*]indole Derivatives

Jonathan P. May and David M. Perrin

Department of Chemistry, University of British Columbia, Vancouver, BC, V6T 1Z1, Canada

Introduction

3*a*-Hydroxy-pyrrolo[2,3-*b*]indole (Hpi) is an important structural motif found in many peptide containing natural products e.g. okaramines [1], phakellistatins [2], and himastatins [3]. There are a number of methods for the synthesis and incorporation of this moiety into peptides, but these are often multi-step procedures. Here we describe a convenient, efficient and mild deprotection of the acid labile trityl moiety for *N*1-trityl-3*a*-hydroxy-pyrrolo[2,3-*b*]indole derivatives using hexafluoroisopropanol (HFIP). This provides a suitable method for the deprotection of this moiety ready for incorporation into larger peptides, and in certain cases may obviate the need for successive deprotections and reprotections. This deprotection shows significant selectivity for the labile *N*1-trityl and is compatible with both solid and solution phase chemistry.

Reports of using HFIP mixtures for cleavage of the highly labile 2-chlorotrityl resin have been known for some time. Bollhagen *et al.* [4] reported such a method using a mixture of HFIP-dichloromethane (1:4 v/v), which successfully cleaved a range of short peptides from 2-chlorotrityl resin, yielding only fully protected peptides. Bollhagen *et al.* studied many different side-chain protecting groups, all of which were stable to the conditions except for the special cases of trityl-side chain protected Ser, Thr, and N^{im} of His, where minor amounts of deprotected peptides were also found.

We have since discovered that this method provides a convenient and highly selective method of deprotection for the extremely acid labile *N*1-trityl protection of Hpi-peptide derivatives. The nature of the HFIP/CH₂Cl₂ deprotection mixture provides good solubility, even for hydrophobic protected-peptides and evaporation *in vacuo* allows facile work up, avoiding the use of acetic acid which could interfere with further coupling steps if not removed.

Results and Discussion

An octapeptide **1** was synthesized by standard Fmoc solid-phase peptide synthesis methods on 2-chlorotrityl resin. The last two amino acids were added as a dipeptide (Tr-Hpi-Gly-OH) affording the fully protected peptide. This resin bound peptide was then treated with HFIP/ CH₂Cl₂ (1:4 v/v) at room temperature for 5 minutes (Fig. 1). The resin turned deep red initially, which lightened in colour over time. The mixture was then evaporated to dryness *in vacuo*, redissolved in dichloromethane and filtered to remove cleaved resin. Electrospray mass spectrometry was used to study the peptide, which corresponded to a loss of just one trityl moiety (*m/z*: 1359 (M+H)⁺).

A control hexapeptide of the same sequence, but omitting the Tr-Hpi-Gly-OH dipeptide was subjected to the same conditions, but on analysis with mass spectrometry, only fully protected peptide was obtained (*m/z*: 1100 (M+H)⁺). This suggests that the *N*1-trityl protection of the Hpi moiety can be selectively deprotected, even in the presence of other residues with trityl-protected side chains.

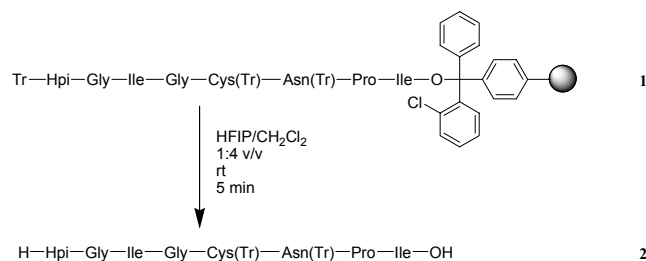
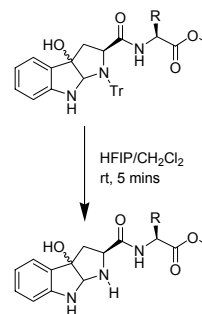


Fig. 1. Reaction scheme for the resin-bound cleavage and deprotection.

To investigate this selective deprotection further, a series of dipeptides Tr-Hpi-Xaa-OMe were studied. These were dissolved in HFIP/CH₂Cl₂ (1:4 v/v) and the mixtures were stirred at room temperature for 5 minutes. Consumption of starting material was observed by TLC (CH₂Cl₂/MeOH, 9:1) and on completion the mixture was evaporated to dryness *in vacuo*. Each mixture was then studied by mass spectrometry and the calculated and observed masses for deprotection of the trityl moiety are shown in Table 1. Selective deprotection of the *N*1-trityl on the Hpi was observed for each dipeptide with no trace of any side chain deprotection in each case.

Table 1. Mass spectrometry of HFIP deprotected dipeptides

Peptide	Mass <i>m/z</i> (M+H) ⁺	
	calculated	found
Tr-Hpi-Asn(Tr)-OMe	591.7	591.3
Tr-Hpi-Glu(^t Bu)-OMe	420.2	420.3
Tr-Hpi-Lys(Boc)-OMe	463.5	463.3
Tr-Hpi-Thr(^t Bu)-OMe	392.5	392.2



These results suggest that HFIP/CH₂Cl₂ mixtures are suitably mild for deprotecting the *N*1-trityl-3a-hydroxy-pyrrolo[2,3-*b*]indole moiety and in many cases can be used selectively, even with peptides containing acid labile protected side chains.

Acknowledgments

J.P.M. received a postdoctoral fellowship from the Royal Society, UK. This work was supported by UBC start-up funds and funding from the Michael Smith Foundation for Health Research, and PENCE Inc.

References

1. Roe, J. M., Webster, R. A. B. and Ganesan, A. *Org. Lett.* **5**, 2825-2827 (2003); Hewitt, P. R., Cleator, E. and Ley, S. V. *Org. Biomol. Chem.* **2**, 2415-2417 (2004).
2. Greenman, K. L., Hach, D. M. and Van Vranken, D. L. *Org. Lett.* **6**, 1713-1716 (2004).
3. Kamenecka, T. M. and Danishefsky, S. J. *Chem. Eur. J.* **7**, 41-63 (2001).
4. Bollhagen, R., Schmiedberger, M., Barlos and K., Grell, E. *J. Chem. Soc. Chem. Commun.* 2559-2560 (1994).

Enantiomerically Pure H-Arg(Z)₂-aldehyde Diethylacetal: A Useful Building Block in the Synthesis of Peptide Aldehydes

Fritz Dick¹, Juergen Gerhardt², Barbara Jakobi¹, Beat Sax¹, Joachim Schwindling¹ and Christian Stachelin¹

¹Bachem AG, Bubendorf, Switzerland; ²C.A.T. GmbH & Co, Tübingen, Germany

Introduction

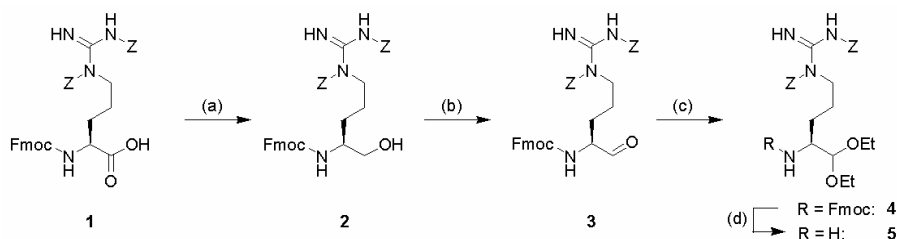
α -Amino and peptide aldehydes are useful synthetic intermediates [1,2], and some of them are potent inhibitors of proteases [3]. Their tendency to racemize during their synthesis, purification and acetalization is a widely known problem since the acidity of the α -proton facilitates the enolization of the aldehyde [4]. In the course of our work, we found only few examples that describe a suitable procedure of protected α -amino aldehydes in high enantiomeric purity [5,6].

Herein, we present a racemization free synthesis of H-Arg(Z)₂-aldehyde diethylacetal (**5**) starting from commercially available Fmoc-Arg(Z)₂-OH (**1**) [5], and detailed analytical procedures that confirm the high enantiomeric excess of **5**.

Synthesis

The synthesis started from **1** with the formation of the mixed anhydride, followed by sodium borohydride reduction to argininol **2** (Scheme 1). Subsequent Parikh-Doering oxidation [7] led to arginine aldehyde **3** whose acetalization under very mild conditions [6] provided Fmoc-Arg(Z)₂-aldehyde diethylacetal **4**. The Fmoc-cleavage was performed under standard conditions using piperidine in DMF to give **5**.

Determination of the Enantiomeric Purity



Scheme 1. Synthesis of H-Arg(Z)₂-aldehyde diethylacetal (**5**). Reagents and conditions: (a) (i) mixed anhydride, NMM, DME, (ii) NaBH₄, H₂O, 75%; (b) SO₃-pyridine, Et₃N, DMSO, THF, 85%; (c) triethyl orthoformate, THF, EtOH abs., *p*-TsOH, 65%; (d) piperidine, DMF, 70%.

Verification of the enantiomeric purity of **4** was obtained via two independent methods.

Direct determination of the enantiomeric excess at the stage of Fmoc-Arg(Z)₂-aldehyde diethylacetal was achieved in a chiral HPLC assay, in which less than 0.1% of the D-enantiomer (D-**4**) were found (Fig. 1).

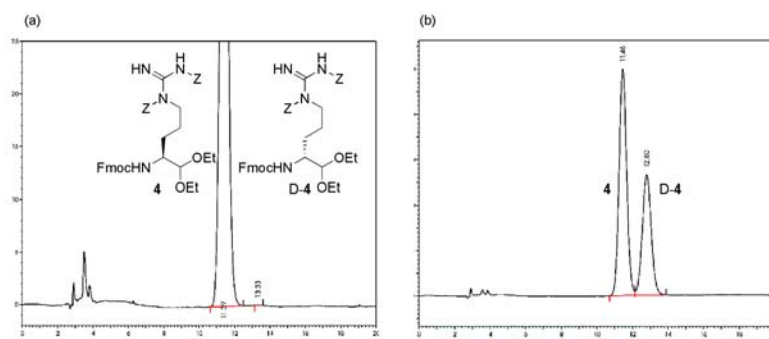


Fig. 1. Chiral HPLC of Fmoc-Arg(Z)₂-aldehyde diethylacetal (**4**). Chiral HPLC, Chiralpak AD 0.46x25cm, 30°C, flow 1.0 ml/min, Hexan/iso-Propanol 60:40, 0.01% TFA, detection 254 nm: (a) Chromatogram of synthesized **4** containing < 0.1% D-enantiomer D-**4**; (b) **4** spiked with D-enantiomer D-**4** (obtained by independent synthesis).

Alternatively, the result has been confirmed by an independent method in which **4** was Fmoc deprotected and coupled with Z-Leu-OH. HPLC analysis showed that the expected (L,L)-diastereomer was present in a large excess compared to the corresponding (L,D)-analog (*de*>98%).

Conclusion

The presented synthesis in Scheme 1 illustrates the easy access to enantiomeric pure H-Arg(Z)₂-aldehyde diethylacetal (**5**) that can be used as building block in the synthesis of peptide aldehydes. The enantiomeric purity was determined in two different ways. The analysis of the enantiomeric purity of diethylacetal **4** on a chiral HPLC column gave a similar result as the analytical experiment on the diastereomeric level.

The synthetic method described herein is very versatile and can be applied to a variety of different amino acids, thus representing a general approach for the preparation of amino and peptide aldehydes. In addition, mild reaction conditions and simple workup procedures in all the steps allow a scale-up towards an industrial scale.

Acknowledgments

Thanks to M. Obkircher for his helpful contributions to poster and manuscript.

References

1. Jurczak, J. and Golebiowski, A. *Chem. Reviews* **68**, 149-164 (1989).
2. Reetz, M. *Angew. Chemie* **12**, 1559-1573 (1991).
3. Chapman, K. *Bioorgan. Med. Chem. Lett.* **6**, 613-618 (1992).
4. Saino, T., Someno, T., Myazaki, H. and Ishii, S. -I. *J. Chem. Pharm. Bull.* **30**, 2319-2325 (1982).
5. Someno, T. and Ishii, S.-I. *Chem. Pharm. Bull.* **34**, 1748-1754 (1986).
6. Mindt, T., Michel, U. and Dick, F. *Helvetica Chimica Acta* **82**, 1960-1968 (1999).
7. Liu, C., Ng, J. S., Behling, J. R., Yen, C. H., Campbell, A. L., Fuzail, K. S., Yonan, E. E. and Mehrotra, D. V. *Org. Process Res. Develop.* **1**, 45-54 (1997).

Chlorotrityl Chloride (CTC) Resin as a Convenient Reusable Protecting Group

Fayna García-Martín¹, Nuria Bayo¹, Luis J. Cruz¹, James Bohling² and Fernando Albericio^{1,3}

¹Barcelona Science Park, University of Barcelona, Barcelona, Spain; ²Rohm and Haas Co., Philadelphia (PA), USA; ³Departament of Organic Chemistry, University of Barcelona, Barcelona, Spain

Introduction

CTC resin (Fig. 1) is perhaps one of the most useful resins for the SPS of C-terminal acid peptides. It can be used for the preparation of both protected and unprotected peptides. The main advantages of its use are:

- (i) it allows the release of the peptide in very mild acidic conditions (TFA-DCM (1:99) and HFIP or TFE in DCM);
 - (ii) it minimizes the formation of diketopiperazine;
 - (iii) it minimizes racemization during the incorporation of the first amino acid;
- and
- (iv) it allows the incorporation of several protected amino acids, through the free side-chain.

Here we discuss the use of CTC resin as a reusable mild protecting group of carboxylic acids.

Temporal protection of carboxylic acids in solution is not a straightforward. The preparation of tBu esters, which are probably the most common of this kind of protecting group, is a difficult process that involves the use of a gas and therefore of special equipment. Alternatively, the use of CTC resin is proposed. Furthermore, the regeneration of the resin after cleavage of the target compounds is discussed. Finally, capping studies were performed to establish the best method by which to block the remaining active Cl after the incorporation of the first amino acid.

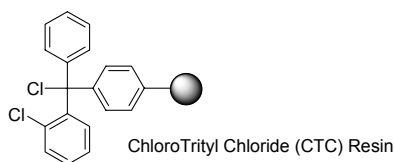


Fig. 1. The ChloroTrityl resin.

Results and Discussion

After the cleavage of a compound from the resin, three methods to recycle the resin were tested:

- i) 4N HCl in dioxane for 24 hours [1],
- ii) 0.35 mM SOCl₂ in DCM for 4 hours [2],
- iii) 10% AcCl in DCM for 3 hours.

The loadings obtained were 1.17, 1.13 and 1.07 mmol/g respectively.

The Thionyl Chloride method was chosen as the best one because it allowed higher loading in a shorter time.

Several Fmoc-amino acids were sequentially incorporated and cleaved to and from CTC resin, with intercalation of recycling processes. In all cases, HPLC analysis of the cleaved compounds showed excellent purity, with no contamination from the previous experiment.

Non-available amino acids from commercial Fmoc-aa-OH were synthesized using CTC resin (Fig. 2). Following the incorporation of a Fmoc-aa-OH and subsequent removal of the Fmoc group, a new protecting group was incorporated using conventional chloroformates or active carbonates. After cleavage from CTC resin, NMR studies showed excellent purity of the new derivatives. After a regeneration step, the resin can be used over and over again. Thus, pNZ-Val-OH [3], Alloc-Phe-OH, and Troc-Ala-OH were synthesized.

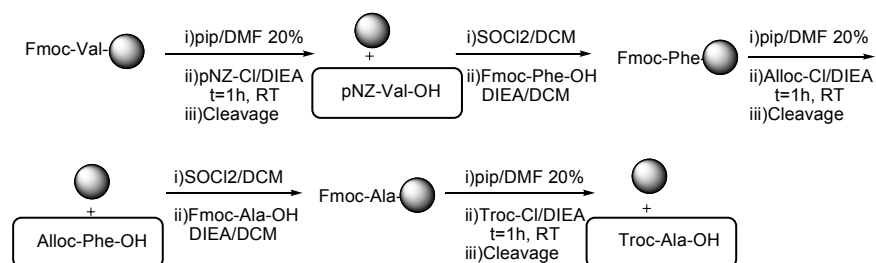


Fig. 2. ChloroTrityl Resin application.

Chlorotrityl capping studies were performed and the piperidine from the Fmoc removal capped the resin. Therefore, elimination of the capping step with methanol is being considered. New methods of capping will be optimized.

Acknowledgments

This work was partially supported by CICYT (BQU 2003-00089), the *Generalitat de Catalunya (Grup Consolidat and Centre de Referència en Biotecnologia)*, and the Barcelona Science Park. FGVG thanks the University of Barcelona for a predoctoral fellowship.

References

1. Barlos, K. *PCT Int. Appl.* WO 2004/056883 A2 (2004).
2. Bohling J. *Eur. Pat. Appl.* EP 1391447 (2004).
3. Isidro-Llobet, A., Guasch- Camell, J., Álvarez, M. and Albericio, F. *Eur. J. Org. Chem.* 3031-3039 (2005).

Synthesis and Purification of Multiphosphorylated Peptides

Vladimir V. Kalashnikov, Yongping Tang and Jeanick H. Pascal

NeoMPS, Inc. GROUPE SNPE, San Diego, CA 92126, USA

Introduction

The process of phosphorylation and dephosphorylation of proteins is frequently used in nature for activation/deactivation of enzymes, extracellular signal transduction or protein transportation, and synthetic phosphorylated peptides are widely used for the studying of these events.

The synthesis of peptides containing one or two phosphorylated amino acid residues is well developed and has become a routine procedure in many laboratories [1,2]. However, the production of multiphosphorylated peptides, especially in multi-gram quantities, still presents a serious challenge for peptide chemists.

Two major approaches can be considered for the synthesis of phosphorylated peptides:

- building block approach, where properly protected phosphoamino acids are directly incorporated into the growing peptide chain;
- global phosphorylation approach, where phosphate groups are introduced through selective phosphorylation of unprotected side chain hydroxyl groups of preassembled protected peptide.

Each method has its own advantages and disadvantages and a researcher's choice frequently depends on a particular peptide sequence. For large-scale syntheses the price of chemicals may also play a significant role in the final decision.

We have developed a reliable procedure for the synthesis and purification of peptides containing two or more phosphoamino acid residues, where phosphorylated residues may represent up to 50% of all amino acids in the sequences. Two of the peptide sequences under investigations are shown in Figure 1. All sequences have the same pattern: a stretch of adjacent phosphorylated residues separated one from another with a single nonphosphorylated residue.

1. $X_a(pSG)_bX_c$,
2. $X_cRDDSSESSDSGpSSpSEpSDGD$ [3]

Fig. 1. peptide sequences. $a=0-10$; $b=2-5$; $c=0-2$; pS is a phosphoserine residue; and X can be Gly, Ser, Ala, Ahx or biotin.

Results and discussion

All peptides were synthesized using standard Fmoc/tBu solid phase procedures [1] using a Symphony automatic peptide synthesizer for small scale, and by manual synthesis for both, small and large scale. The building block approach has first been performed for the syntheses of peptides type 1 and 2 using Fmoc-protected benzylphospho amino acid derivatives. In the case of type 1 peptides, the crude material showed a main peak with the correct mass, but the presence of large amount of side products prohibited the scale up of this process. Even more disappointing, no peaks with the correct molecular weight were observed with type 2 peptides. These poor results may have different explanations, including the possibility of side reaction of adjacent pS residues and formation of intramolecular pyrophosphate cycles, and the β -elimination of phosphate group to form a dehydroalanine residue

during repetitive piperidine-mediated removal of Fmoc-protection. Based on these results, and considering the high price of the building block itself, the building block approach was abandoned.

In the global phosphorylation approach, the amino acid residue to be phosphorylated is usually incorporated without side chain protection. An attempt to synthesize type **1** peptide precursors for global post-synthesis phosphorylation using unprotected Fmoc-Ser-OH (free hydroxyl group) was unsuccessful. LC-MS analysis of the product prior to phosphorylation showed the presence of branched peptides (through acylation of the side-chain of the serine residues) in substantial amount. The precursors for the type **1** peptides were finally successfully synthesized as completely protected molecules using Fmoc-Ser(Trt)-OH as a precursor for the phosphoserine residues and showed virtually no side products.

A test synthesis of type **2** peptide sequence using Fmoc-Ser(Trt)-OH as a precursor for the phosphoserine residues yielded peptide material with the correct structure but with ~20% of a side product having MW=M-18. This product was later shown to result from the intramolecular aspartimide formation between residues Asp¹⁷ and Gly¹⁸ as a result of repetitive piperidine-mediated removal of Fmoc-group (**R¹DDSSSESSDS¹⁰GpSSpSEpSDGD¹⁹**).

Several solutions can be used to avoid this side reaction [4]. For example, the N-(2-hydroxy-4-methoxybenzyl) (Hmb) peptide backbone protecting group is frequently used to suppress aspartimide formation [1,4]. Moreover, the Hmb-group has already been applied to the synthesis of phosphopeptides *via* global phosphorylation [5]. However, this route does not look very attractive for different reasons. Thus, two additional steps have to be performed to complete the synthesis of the peptide: reversible acylation of the hydroxyl of the Hmb-residue prior to peptide phosphorylation and specific removal of this particular protection before final peptide cleavage/deprotection from the resin. For these reasons, the N-(2,4,6-trimethoxybenzyl) group (Tmob) [6] was used to temporarily protect the nitrogen of the Asp¹⁷-Gly¹⁸ peptidic bond. In case of type **2** phosphopeptide synthesis the Tmob-protection is much more versatile than Hmb because Tmob does not need additional procedures prior to phosphorylation and peptide cleavage. Exploring this idea, Fmoc-(Tmob)Gly-OH was synthesized according to a published procedure [7] and used for the introduction of Gly¹⁸ residue during the preparation of the type **2** peptide precursors. Neither Fmoc-(Tmob)Gly-OH, nor the next residue, Fmoc-Asp(OtBu)-OH, showed any unusual behavior during standard coupling and Fmoc removal. Test cleaves of precursor peptides synthesized with (Tmob)Gly in position 18, and Ser(Trt) residues in positions 12, 14, and 16 showed real improvement in the quality of the material and no aspartimide side product was detected.

All the peptide type **1** and **2** precursors were globally phosphorylated following a three-step procedure [1]:

1. selective Trt removal using a mixture 2% TFA, 5% TIS in DCM;
2. phosphitylation using a mixture of dibenzyl-N,N-diisopropyl phosphoramidite and 4,5-dicyanoimidazole in DMF;
3. oxidation using tert-butylhydroperoxide solution in heptane/DMF.

Final cleavage of both types of peptides was performed using a mixture of trifluoroacetic acid/phenol/ triisopropylsilane/water (82.5:5.0:2.5:5.0, v/v) and lead to high quality crude products.

Both types of peptides are extremely hydrophilic and could not be analyzed or purified using traditional reversed-phase chromatography. All peptides were purified by ion-exchange chromatography with high yield and high purity.

References

1. White, P., Dörner, B. and Steinauer (Eds.) Synthesis Notes, in *NOVABIOCHEM Catalog* 2004/5.
2. McMurray, J. S., *et al.* *Biopolymers (Peptide Sci.)* **60**, 3-31 (2001).
3. Rowe, P. S. N., de Zoysa, P. Dong, R., *et al.* *Genomics* **67**, 54-68 (2000).
4. Cebrian, J., Domingo, V. and Reig, F. *J. Peptide Res.* **62**, 238-244 (2003).
5. Johnson, T., *et al.* *J. Chem. Soc., Perkin Trans.* **1**, 719-728 (1996).
6. Clausen, N., Goldammer, C., Jauch, K., Bayer, E., In *Peptides: Chemistry, Structure and Biology. 14th American Peptide Symposium* (Kaumaya, P.T.P. and Hodges, R.S., eds.) American Peptide Society, Columbus, Ohio, pp. 71-72 (2004).
7. Johnson, T., Quibell, M. and Sheppard, R. C. *J. Peptide Sci.* **1**, 11-25 (1995).

Dealing with the Aggregation Problem of Polyglutamine Peptides: Synthesis Strategies

**Myriam Létourneau¹, Martin Viau², Ariane Sirois², Yvan Boulanger²
and Alain Fournier¹**

¹*Laboratoire d'études moléculaires et pharmacologiques des peptides, INRS-Institut Armand-Frappier, Université du Québec, Pointe-Claire (Montréal), Canada;* ²*Hôpital Saint-Luc du CHUM, Montréal, Canada*

Introduction

Many neurodegenerative diseases, such as spinocerebellar ataxias and Huntington disease, share an abnormal expansion of a CAG trinucleotide that leads, upon gene expression, to an insertion of a glutamine homopolymer in the corresponding protein [1]. Proteins expressing this polyQ motif have a high propensity to associate themselves to form amyloid-like aggregates. This process appears to be the key element giving rise to neurodegeneration but the pathogenesis of these disease states is not yet understood. Therefore, suitable research tools are required, such as synthetic polyQ peptides. Unfortunately, their tendency to aggregate is the source of a tremendous challenge for peptide synthesis and purification methods. Polymerization processes have been used to generate polyQ peptides but this method involves a molecular weight dispersion [2]. Solid phase peptide synthesis (SPPS) can overcome this problem but the lack of solubility of the growing peptide chain can cause significant deletion amounts of the end product [3].

We studied various solid phase peptide synthesis and purification strategies to obtain polyQ peptides in good purity and yield. In light of our results, we describe a rather simple and straightforward method to generate polyQ peptides in the Q10-Q30 range. This protocol may also be useful to other studies involving highly aggregating peptides.

Results and Discussion

Two strategies were explored to obtain synthetic polyQ peptides: a standard stepwise SPPS and a pentameric fragment condensation approach. The latter involves the coupling of a N- α -protected peptide fragment of 5 residues to a N- α -deprotected peptide chain anchored to a solid support. For both strategies, Boc and Fmoc chemistry were employed. For Boc chemistry, Boc-Gln residues with a Merrifield resin were used and a Fmoc-Gln residue was incorporated at the peptide fragment terminus. As for Fmoc chemistry, Fmoc-Gln(Trt) were coupled to a Rink AM resin in SPPS, while the peptide fragment was anchored to a very acid-labile support, a 2-chlorotrityl chloride resin. Although the fragment condensation approach seems interesting due to its time saving advantage, no polyQ peptides were successfully obtained through this procedure. Indeed, peptide fragments synthesized using Boc chemistry were rather insoluble in all suitable coupling media while the bulkiness of the Trt protecting groups used in Fmoc chemistry probably hindered considerably any condensation reaction between the peptide chains. Stepwise SPPS strategy, using Boc chemistry, allowed the synthesis of polyQ peptides of up to 15 residues though the last five couplings were quite arduous. The use of unprotected side chain Gln residues in this approach can favor hydrogen bonds stabilizing a β -sheet like structure between growing peptide chains, thus creating aggregation related

problems. Through Fmoc chemistry SPPS, coupling reactions were carried out easily even after having incorporated 25 Gln residues. Moreover, from our MALDI-TOF MS analysis, no significant levels of deletion peptides were observed for the crude polyQ peptides in the Q10-Q30 range.

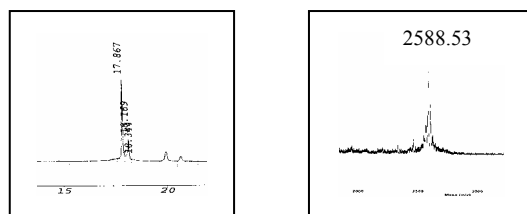


Fig. 1. Analysis of polyQ₂₀ by analytical HPLC (left) and MALDI-TOF MS (right).

Different organic solvents, such as dimethylsulfoxide, methanol, isopropanol, acetonitrile (ACN), dimethylformamide, dichloromethane, tetrahydrofuran, and dioxane were tested for their solubilization capability. Unfortunately, none of them was able to solubilize the crude polyQ peptides. However, trifluoroacetic acid (TFA) allowed to dissolve the peptides and maintain them in solution even after the addition of various solvents. Other organic solvents, such as glacial acetic acid and hexafluoroisopropanol (HFIP), were able to partially dissolve the crude polyQ peptides. Interestingly, partial dissolution in glacial acetic acid followed by lyophilization greatly improved the solubility of the crude peptides. Hence, about 200 mg of peptide were dissolved in 4 mL of 50%TFA/HFIP. Then, 10 mL of 0.06% TFA/H₂O were added dropwise and this peptide solution was diluted to 1L with distilled water.

Purification using RP-HPLC was not easy because the polarity of the glutamine-containing peptides considerably weakened the interaction with the bonded phase. Nevertheless, purification was achieved by injecting slowly the peptides dissolved in the abovementioned aqueous conditions onto a C₁₈ column, followed by a 2hr gradient from 0 to 10% ACN in 0.2% aq. TFA, with a flow rate increased to twice its initial value. During the purification step, we observed that N-terminal lactonization of polyQ peptides occurred. However, under our purification conditions, this side product was easily isolated. In fact, it can also be used in neurodegenerative disease studies because the N-pyroglutamate moiety is observed frequently in polyQ stretches and it was hypothesized that this N-terminal alteration could play a role in the pathogenesis of neurodegeneration [4].

Acknowledgments

The work was funded by the CIHR. A.F. is “*Chercheur National*” from the *Fonds de la recherche en santé du Québec*.

References

1. Temussi, P. A., Masino, L. and Pastore, A. *EMBO J.* **22**, 355-361 (2003).
2. Chu, B. C. and Orgel, L. E. *Biochem. Biophys. Res. Commun.* **283**, 351-355 (2001).
3. Perutz, M. F., Pope, B. J., Owen, D., Wanker, E. E. and Scherzinger, E. *Proc. Natl. Acad. Sci. USA* **99**, 5596-5600 (2002).
4. Russo, C., Violani, E., Salis, S., Venezia, V., Dolcini, V., Damonte, G., Benatti, U., D'Arrigo, C., Patrone, E., Carlo, P. and Schettini, G. *J. Neurochem.* **82**, 1480-1489 (2002).

Biosynthesis of Bioactive Peptides

Synthesis and Biological Assessment of Insulin-Like Analogs with Differential Activity at the Insulin and IGF-1 Receptors

**Richard D. DiMarchi¹, Jie Han¹, Amy Hoffman¹, Vasily M. Gelfanov¹,
Wayne Kohn², Radmila Micanovic² and John P. Mayer²**

¹*Department of Chemistry, Indiana University, Bloomington, IN 47405, USA*

²*Lilly Research Laboratories, Eli Lilly and Company, Indianapolis, IN, 46285, USA*

Introduction

Insulin is a physiological hormone of seminal importance to the utilization, storage and mobilization of glucose. Over the course of nearly a century millions of patients with diabetes have depended upon this medicine as a life-saving therapy. The advent of rDNA biosynthesis provided human insulin in virtually unlimited quantity and modest expense relative to most rDNA-derived medicines. More importantly, it provided a mechanism by which improved insulin analogs could be synthesized, evaluated and registered as new medicines. The development of biosynthetic insulin analogs has provided improved efficacy, safety and convenience to insulin-requiring diabetics [1]. In a broader manner these protein analogs represent the first step in elevating protein medicinal chemistry from an academic endeavor to a clinical reality. Chemical biotechnology (biosynthesis with unnatural amino acids) provides new opportunity for expanding the insulin structure-activity relationship and through it the development of protein analogs possessing superior pharmaceutical properties, at a scale and cost competitive with conventional biotechnology [2].

Insulin and insulin-like growth factors (IGF-I & II) are three highly homologous protein hormones of central importance to proper endocrine function [3]. Insulin is a two chain (A and B) peptide, while IGF-I and II are single chain hormones containing additional (C and D) regions. There is approximately 50% homology in the A and B chain sequences of insulin and each IGF [4]. These hormones function through three separate receptors of which two are highly homologous and constitute cell membrane-spanning glycoproteins with tyrosine kinase activity [3]. The selectivity within this set of hormonal ligands for their respective receptors exceeds more than 100-fold [4].

Our studies focus on the elucidation of the structural mechanisms by which these three hormones differentially interact with the insulin and IGF-1 receptors. The structural nature of the C-region was varied within the two-chain format and found to significantly modify receptor affinity and selectivity. Changes in the A and B chain amino acid sequences introduce an important and additional degree in receptor selectivity across a panel of insulin and IGF-like hormone analogs that were studied. Our observations build upon other structure-activity studies [5-10] to provide an explanation for the physiological design of these related hormones and form the basis for discovery of high affinity insulin-like agonists and antagonists.

Experimental Design

The multiple insulin/IGF-1 A and B chain analogs, extended with C and D regions as well as site specifically substituted with unnatural amino acids were successfully synthesized by solid phase peptide chemistry using predominately Boc-based technology. Peptides were cleaved from the support in strong anhydrous acid (HF) and purified under acidic conditions by preparative high performance reverse-phase

Table 1. Relative insulin and IGF-1 receptor affinity of insulin analogs

Peptide		Insulin Receptor Affinity IC ₅₀ (nM)	IGF-1 Receptor Affinity IC ₅₀ (nM)
Insulin		0.60 ± 0.21	194 ± 113
IGF-1		19.7 ± 7.83	0.57 ± 0.16
BC:AD	IGF-1	7.87 ± 1.34	0.65 ± 0.08
B:A	IGF-1	3.99 ± 0.46	8.73 ± 1.79
BC:AD	IGF-2	32.9 ± 4.11	2.95 ± 1.61
B:A	IGF-2	5.45 ± 3.93	28.9 ± 11.9

chromatography in the free sulfhydryl form. Each peptide was characterized by MALDI-MS and HPLC analysis to be at least 90% pure prior to chain combination.

The chain combination reaction was the most challenging part of each synthesis as the physical solubility of certain individual peptide chains proved challenging. The disulfide exchange reaction with each individual A or B-chain analog was achieved by mixing the synthetic peptide with a molar equivalent of the respective biosynthetic native A or B chain S-sulfonate, in a 50 mM glycine buffer, pH 10.5. A molar equivalent of DTT relative to each S-sulfonate was used to facilitate disulfide interchange. The reaction was conducted at 4°C, overnight. The product was purified by preparative high performance reverse phase chromatography in a slightly alkaline NH₄HCO₃ buffer with CH₃CN elution. The analogs were obtained in step yield that varied from 5-25%, and characterized by MALDI-MS and HPLC analysis to be greater than 95% pure.

The binding affinity of each analog for the insulin and the IGF-1 receptors was measured in a competition binding assay utilizing scintillation proximity assay technology. Serial 3-fold dilutions of the peptides were made in scintillation proximity assay buffer (0.05 M Tris-HCl, pH 7.5, 0.15 M NaCl, 0.1% w/v bovine serum albumin) in a 96 well plate (Corning Inc., Acton, MA) with 0.05 nM (3-[125I]-iodotyrosyl)insulin, or IGF-1. An aliquot of 1-6 micrograms of plasma membrane fragments prepared from cells over-expressing the human insulin or IGF-1 receptor and 1 mg/well polyethyleneimine-treated wheat germ agglutinin type A scintillation proximity assay beads (Amersham Biosciences, Piscataway, NJ) were added to each well. The plate was incubated for twelve hours at room temperature and measurements were made with MicroBeta1450 liquid scintillation counter (Perkin-Elmer, Wellesley, MA). Non-specifically bound (NSB) radioactivity was measured in the wells with fourfold greater concentration of “cold” native ligand than the highest concentration in test samples and total bound radioactivity was detected in the wells with no competitor. Percent specific binding was calculated as following: % Specific Binding = Bound-NSB / Total bound- NSB x 100. IC₅₀ values were determined by using Origin software (OriginLab, Northampton, MA).

Results

The total synthesis and purification of individual insulin and IGF-1 peptides were achieved in yields exceeding 25%. The conversion of these individual synthetic peptide analogs to the desired insulin or IGF-1 analogs was dependent on the nature of the specific peptides studied. The more cationic peptides proved to be of limited

solubility in the standard pH 10.5 disulfide-exchange reaction conditions. Various alternative approaches to minimizing the solubility limitations were explored. Changes in pH or temperature of the reaction were not successful. It was observed that low concentration of organic co-solvents had a constructive influence on the total yield and the apparent selectivity in formation of the correct disulfides.

The insulin and IGF-1 analogs were assessed for their affinity in displacement of the native hormone at each of the two receptors. Insulin and IGF-1 proved to be highly potent with IC_{50} values that typically ranged between 0.3-1 nM at their respective receptors (Table 1). For comparison purposes the results were normalized at both receptors, with insulin relative affinity set to unity. IGF-1 demonstrates nearly a thousand-fold greater potency for its receptor than for the insulin receptor, and yet its relative affinity for the insulin receptor is almost 2%. It certainly appears that insulin is more discriminating in its ability to specifically recognize the insulin receptor than IGF-1 is for these same two receptors.

The inversion of the native sequence at positions 28 and 29 of the B-chain (K^{B28} , p^{B29} insulin) yields a slight change in relative affinity at each of the two receptors [10]. The D^{B10} insulin is an analog where the natural histidine at position B10 is replaced with aspartic acid and it appears modestly enhanced in potency at both receptors. Introduction of cationic charge to the C-terminus of the B-chain (R^{B31} , R^{B32} insulin) provokes a tenfold increase in affinity at the IGF-1 receptor relative to that observed with native insulin. A simultaneous change at B10, in addition to the C-terminal di-Arg yielded D^{B10} , R^{B31} , R^{B32} insulin, an analog where the IGF-1 receptor affinity is intermediate to that of insulin and IGF-1. Interestingly, the IGF-1 receptor proved far more sensitive to amino acid substitutions in this region of insulin than the insulin receptor. We have observed that the addition of cationic amino acids to the N-terminus of the insulin A-chain serves the opposite effect at the IGF-1 receptor as that noted here at the C-terminus of the B-chain [11]. This observation has led to the discovery of insulin analogs that are relatively less active at the IGF-1 receptor than native insulin, and also to the attenuation of the sizably increased IGF-1 character of R^{B31} , R^{B32} -based insulin analogs.

To further our understanding of the molecular elements that define high binding affinity for the IGF-1 receptor we prepared a set of IGF-1 and IGF-2 analogs that resemble insulin in the fact that they are two-chain derivatives. The results of this study are provided in Table 2. The absolute binding affinities at each receptor for four unique analogs were found to largely reside in a range intermediate to that of the native hormones. Insulin and IGF-1 demonstrate similar sub-nanomolar affinity for their respective receptors and comparable selectivity at each other's receptor, as

Table 2. Relative insulin and IGF-1 receptor affinity of IGF-1 and IGF-2 analogs

Peptide	Insulin Receptor	IGF-1 Receptor
Insulin	1.0	1.0
K^{B28} , p^{B29} insulin	0.8	1.6
D^{B10} insulin	2.0	3.0
R^{B31} , R^{B32} insulin	1.5	10.2
D^{B10} , R^{B31} , R^{B32} insulin	4.7	28.1
IGF-1	0.016	700

shown in Table 1. High affinity binding to the IGF-1 receptor was highly dependent on the presence of the C and D regions. The removal of the respective peptides in the split IGF-1 and the split IGF-2 was observed to decrease the IGF-1 receptor binding affinity. It is not possible from these results to definitively assign the relative contribution of the C and D peptides to this observed change but prior studies have identified the C-region as the element predominantly possessing this property [8,9]. The binding affinity at the insulin receptor was relatively weak for all four of the split IGF analogs. The C and D peptides further diminish the potency of each split IGF. The shortened, split (B:A) IGF analogs were of comparable affinity (3.99 and 5.45 nM), but more than five-fold less potent than insulin (0.6 nM), the most homologous structural comparator. Clearly, amino acids unique to the A and B chains distinguish insulin such that it is able to recognize its receptor with higher affinity than these synthetic IGF-homologs.

We explored further the C-region as a basis for the differences identified in Table 2. A series of two chain C-terminally shortened IGF-1 analogs were prepared. In this instance the D-region was not included to provide an opportunity to assess the individual contribution that the C-peptide renders to the heterodimeric B:A IGF-1 construct. The results shown in Table 3 illustrate once again that the removal of the single peptide bond between the C-terminus of the C-region and the N-terminus of the A-region yields only a small change in IGF-1 binding affinity, but a nearly tenfold increase in insulin activity. These results are similar to those reported in Table 2 for IGF-1 BC:AD but demonstrate that the insulin and IGF-1 binding affinities are slightly increased in the absence of the D-region.

Successive trimming of the C-region by two amino acids yielded first an IGF-1 analog (des-C2) that possessed a surprising increase in IGF-1 and insulin receptor binding affinity. This single analog was nearly twice as potent at the insulin receptor as the full length but split IGF-1, and twice as potent at the IGF-1 receptor as native single chain IGF-1. An additional two amino acid removal from the C-terminus yielded the IGF-1 analog labeled des-C4. Its receptor profile was quite analogous to the des-C2 analog and shows that the last four amino acids are not necessary for high affinity interaction with the IGF-1 receptor, but serve to limit insulin affinity in this split IGF-1 format. An additional two amino acid removal (des-C6) yields a sizable decrease in IGF-1 binding affinity without significant change at the insulin receptor. While this one analog is clearly less potent at the IGF-1 receptor than the most potent analog studied, it remains approximately one-half the potency of the native

Table 3. Relative insulin & IGF-1 receptor affinity of (BC:A) IGF-1 shortened analogs

Analog	Amino Acid Sequence B-C-A (%)	Relative Affinity	
		IGF-1	Insulin
IGF-1	-T ^{B29} -G ^{C1} -Y-G-S-S-S-R-R-A-P-Q-T ^{C12} -G ^{A1} -	100	1.2
IGF-1(split)	-G ^{C1} -Y-G-S-S-S-R-R-A-P-Q-T ^{C12}	G ^{A1} - 127	9.8
IGF-1(des-C2)	-G ^{C1} -Y-G-S-S-S-R-R-A-P	G ^{A1} - 185	15.8
IGF-1(des-C4)	-G ^{C1} -Y-G-S-S-S-R-R	G ^{A1} - 141	16.4
IGF-1(des-C6)	-G ^{C1} -Y-G-S-S-S	G ^{A1} - 57	17.9
IGF-1(des-C12)	-T ^{B29}	G ^{A1} - 8	17.8

IGF-1 and sevenfold more potent than the shortened IGF-1 with the fully deleted C-peptide.

Discussion

We have focused our attention in this report on the determination of the molecular elements by which three highly homologous hormones differentially interact with the highly homologous insulin and IGF-1 receptors. The amino acid sequences of the hormone C-domains have proven to have a huge influence on the binding affinity of each peptide studied for the IGF-1 receptor [8,9]. The two-chain IGF-1 and IGF-2 analogs devoid of the respective C-regions were reduced in IGF-1 binding affinity by more than tenfold. Shortening of the IGF-1 C-peptide demonstrated that the N-terminal six amino acids were of far greater importance to IGF-1 receptor recognition than the remaining six, and that full potency was observed for an eight amino acid C-peptide extension to the B-chain. This result sheds important insight into the basis for high affinity interaction of IGF-2 with the IGF-1 receptor since the native IGF-2 C-peptide is shorter than that of IGF-1 by four amino acids.

The specific contribution that each amino acid renders to total binding affinity in this critical eight amino acid extension remains unknown, but it is striking that even a two amino acid di-arginine extension to the C-terminus of insulin yields a tenfold relative increase in insulin affinity for the IGF-1 receptor. Clearly, this C-domain is an important element in achieving high IGF-1 affinity and must be carefully designed to minimize introduction of excessive IGF-1 anabolic activity in insulin analogs used in diabetes care [1,10]. Future study will address the functional basis of the additional four amino acids in the C-domain of native IGF-1 relative to IGF-2.

Of equal importance to the characterization of the elements that define IGF-1 receptor interaction are those that similarly define high affinity insulin receptor recognition. The binding profile of the two IGF analogs most structurally similar to insulin (B:A) illustrate that the high sequence homology generates a common structural motif that is capable of high affinity insulin receptor interaction in all three peptides (Table 2). The difference in A and B-chain amino acid sequence renders the two IGF analogs considerably less potent than insulin for binding at the insulin receptor. Prior structure-activity studies suggest that the single inversion of aromaticity at the B16 and B17 residues of insulin with that of the IGFs is the predominant element that defines the reduction in activity [12]. The more subtle difference observed between the IGF-1 and IGF-2 B:A analogs are likely a result of the specific differences at amino acids analogous to 14 and 15 in the insulin A-chain [13].

Our observations support the belief that the single chain nature of the IGF hormones provides high affinity interaction with the IGF-1 receptor and attenuates binding at the insulin receptor. The most novel insight this work provides pertains to the fact that extensions to the B-chain of insulin or IGFs while acutely recognized by the IGF-1 receptor are not sensed at the insulin receptor to any where near the same magnitude. Given that these two receptors are highly homologous it is curious why there is such a striking difference in their respective recognition patterns. We surmise that analogous to the IGF-1 receptor there is likely to be an additional binding element in the insulin receptor for the C-region, the nature of which has yet to be identified. The binding affinity for the IGF-1 receptor of the each two-chain IGF analog with C-domains is increased logarithmically relative to those homologs without the C-domain. We believe it is possible to envision a similar increase in insulin activity at the insulin receptor if this additional hypothesized insulin receptor

binding element can be identified and optimized. Increases in binding affinity of this magnitude could constitute a vital element in the optimization of insulin for use in the treatment of insulin-requiring patients with diabetes.

References

1. Bolli, G. B., diMarchi, R. D., Park, G. D., Pramming, S. and Koivisto, V. A. *Diabetologia* **42**, 1151-1167 (1999).
2. Editorial Commentary *Science* **308**, 44-45 (2005).
3. DeMeyts, P. and Whittaker, J. *Nature: Drug Discovery* **1**, 769-83 (2002).
4. Denley, A., *et al.* *Mol. Endocrinol.* **18**, 2502-2512 (2004).
5. De Vroede, M. A., *et al.* *Diabetes* **35**, 355-361 (1986).
6. Schwartz, G. P., *et al.* *Collection Czechoslovak Chem. Commun.* **53**, 2920-2935 (1988).
7. Bayne, M. L., Applebaum, J., Chicchi, G. G., Hayes, N. S., Green, B. G. and Cascieri, M. A. *J. Biol. Chem.* **263**, 6233-6239 (1988).
8. Bayne, M. L., *et al.* *J. Biol. Chem.* **264**, 11004-11008 (1989).
9. Cara, J. F. and Tager, H. S. *J. Biol. Chem.* **265**, 17820-17825 (1990).
10. Sliker, L. J., *et al.* *Diabetologia* **40**, S54-S61 (1997).
11. Kohn, W., DiMarchi, R. D., *et al.* In *Understanding Biology Using Peptides, Proceedings of the 19th American Peptide Symposium*, this volume, pp. 615-616 (2006).
12. Kristensen, C. and Andersen, A. S. *J. Biol. Chem.* **272**, 12978-12983 (1997).
13. Cascieri, M. A., Chicchi, G. G., Applebaum, J., Green, B. G., Hayes, N. S. and Bayne, M. L. *J. Biol. Chem.* **264**, 2199-2202 (1989).

Biosynthesis of the Cyclotide Kalata B1 using Protein Splicing Tools

Richard Kimura¹, Krish Krishnan² and Julio A. Camarero¹

¹Chemical Biology and Nuclear Sciences Division; ²Biosciences Directorate, Lawrence Livermore National Laboratory, University of California, Livermore, CA 94550, USA

Introduction

Cyclotides are a new emerging family of large cyclic polypeptides (~30 residues long) that share a disulfide-stabilized core (3 disulfide bonds) with an unusual knotted structure (Fig. 1A) [1]. Cyclotides contrast with other circular polypeptides in that they have a highly defined three-dimensional structure, and despite their small size, can be considered miniproteins. Their unique circular backbone topology and knotted arrangement of three disulfide bonds makes them exceptionally stable to thermal and enzymatic degradation. Furthermore, their well defined structures have been associated with a range of biological activities, including uterotonic, inhibition of neurotension binding, hemolytic, anti-HIV, insecticidal as well as trypsin inhibitory activity. Altogether, these characteristics make cyclotides ideal candidates to be used as molecular scaffolds for the development of stable peptide drugs [2]. Access to biosynthetic cyclotides using recombinant DNA expression techniques would offer the exciting possibility of producing large combinatorial libraries of highly stable miniproteins using the tools of molecular biology. This would allow the generation of cell-based combinatorial libraries that could be screened inside living cells for their ability to regulate cellular processes. In the present work, we describe for the first time the biosynthesis of the cyclotide Kalata B1 in *E. coli*.

Results and Discussion

Our approach is based on the use of an intramolecular version of the native chemical ligation (NCL) combined with the use of a modified protein splicing unit [3]. In order to accomplish the cyclization of Kalata B1, the different linear precursors tested in this work (Fig. 1B) were fused to a Met residue at the N-terminus, and an engineered Sce VMA intein at the C-terminus (available in the pTYB expression vectors family from New England Biolabs). The Met residue was efficiently removed *in vivo* in *E. coli* by an endogenous Met amino peptidase. This *in vivo* proteolytic event unmasked the N-terminal Cys required for NCL. After affinity purification of the corresponding N-terminal Cys Kalata-Intein fusion protein, the cyclization was triggered by addition of 5% EtSH (Fig. 1C). Among the different linear precursors that were tested, KC3 and KC4 gave the best cyclization yields. The different linear precursors showed different propensities for *in vivo* cleavage of the corresponding Kalata-Intein fusion constructs. Thus, meanwhile the KC4 linear precursor gave only 30% *in vivo* cleavage and the KC6 precursor was almost completely cleaved *in vivo* (>90%). The resulting reduced circular Kalata B1 was oxidatively folded at pH 8.0 in the presence of reduced glutathione (GSH) and ¹Pr-OH (Fig. 1D). The folded recombinant Kalata B1 was characterized by ES-MS, HPLC and 2D-NMR, and it was shown to be identical to the natural product. Encouraged by this result we decided to explore the possibility of carrying out the cyclization and folding in a single-pot reaction. This was accomplished by treating the purified KC4-intein construct with different amounts and ratios of reduced to oxidized glutathione (GSH:GSSG). The best cleavage/cyclization of the KC4-intein

precursor was accomplished using 100 mM of GSH at pH 7.2. Under these conditions the cleavage of the linear KC4-intein precursor was almost quantitative in 18 hrs. Optimal conditions for the oxidative folding of reduced Kalata B1 were obtained using a buffer containing a GSH:GSSG ratio of 4:1 at pH 7.2 in 50% isopropanol. Hence, the purified KC4-intein linear precursor was treated first with 100 mM GSH at pH 7.2 overnight, then the crude reaction was complemented with isopropanol (50%) and 12 mM GSSG. After 20 hrs the reaction was checked by HPLC showing that the major component was the folded Kalata B1 (Fig. 1E). The recombinant folded cyclotide was obtained with a yield \approx 35% (based on linear KC4-intein precursor). Using this approach we also produced a small library based on the Kalata B1 scaffold (Fig. 1F).

In summary we report here the first biosynthesis of the cyclotide Kalata B1 in *E. coli*. We have also shown that our biosynthetic approach can be used to generate cyclotide-based libraries that could be screened *in vitro* or *in vivo*. Future work will focus in the biosynthesis of cyclotide-based libraries *in vivo*.

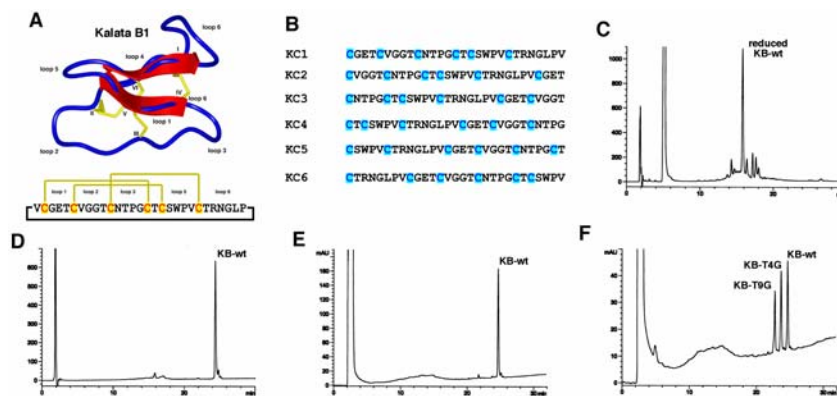


Fig. 1. A. Structure of Kalata B1. B. Sequences of the different linear precursors used in this study (KC1 through KC6). C. HPLC trace of the thiolytic cleavage of the KC4-intein precursor with EtSH. D. HPLC trace of the oxidative refolding of reduced Kalata B1. E. HPLC trace of the one-pot cyclization and folding reaction accomplished with GSH and GSSG in 50% $^1\text{Pr-OH}$. F. HPLC trace of the one-pot cyclization and folding of a 3 member set of Kalata-based peptides.

Acknowledgments

This work was performed under the auspices of the U.S. Department of Energy by University of California, Lawrence Livermore National Laboratory under Contract W-7405-Eng-48. We thank Dr. David Craik, University of Queensland, Australia, for kindly providing a sample of natural Kalata B1.

References

1. Daly, N. L., Love, S., Alewood, P. F. and Craik, D. J. *Biochemistry* **38**, 10606-10614 (1999).
2. Craik, D. J., Simonsen, S. and Daly, N. L. *Curr. Opin. Drug Discov. Devel.* **5**, 251-260 (2002).
3. Camarero, J. A. and Muir, T. W. *J. Am. Chem. Soc.* **121**, 5597-5598 (1999).

Exploration and Elaboration of Reported Insulin Superagonism through Site-Selective Replacement at TyrB26

David L. Smiley, Ma Boaquan, Vasily M. Gelfanov and Richard D. DiMarchi

Department of Chemistry, Indiana University, Bloomington, Indiana, 47405, USA

Introduction

Insulin has virtually the universal ability to lower blood glucose and is currently used in multiple forms by millions of patients in the treatment of diabetes. DNA technology has facilitated the biosynthesis of insulin and various related analogs in unlimited quantity. Nonetheless, the relatively low potency of insulin renders it a unique commercial challenge where yearly production is measured in tonnage. The low inherent potency of insulin is a significant obstacle in the development of non-invasive methods for insulin administration since low bioavailability is commonly reported.

A recent report [1] outlined replacements for TyrB26 in a C-terminally shortened insulin analog that yielded unprecedented increases in *in vitro* potency. Bioactivity constituted measurement of glucose transport in isolated primary rat adipocytes and insulin receptor binding in plasma membranes. N-methylHisB26, des(27-30) insulin prepared via semi-synthesis was reported to possess increased potency relative to native insulin, in excess of fifty-fold in receptor binding and tenfold in stimulating glucose uptake. We have explored this observation through synthesis of the same insulin analog by chain combination with totally synthetic A and B chains. Bioactivity was measured relative to insulin in engineered cells that over-express the human insulin receptor. Additionally, we have prepared a number of more acidic B26 insulin analogs to further elaborate the molecular basis for the superagonism.

Results and Discussion

B-chain analogs were prepared using either Boc or Fmoc solid phase synthesis. Most B26 amino acids were obtained commercially, while N-MeHis was generated via an on-resin N-methylation after conversion to the oNPS derivative [2]. On completion of the N-MeHis26 B-chain synthesis using an ABI 430A peptide synthesizer, an HF cleavage was conducted in the presence of m-cresol. The peptide was solubilized with aqueous acetic acid and purified by preparative Kromasil C18 chromatography in 0.1% TFA, with a linear acetonitrile gradient. The other des(27-30) B-chain analogs; Aad26, N-MeGlu26, and Phe(4-carboxy) were prepared using an Fmoc-based synthesis starting with Rink amide resin, and employing HOBt active esters. The His26(1-30) B-chain was also prepared using Fmoc chemistry starting from Fmoc-Thr(OtBu)Wang resin. These peptidyl-resins were cleaved using 90%TFA/5%TIS/ 5%MeOH and purified as described previously.

Each B-chain analog was used in a modified chain combination procedure to generate the respective insulin analog. A precise amount of B-chain in the free sulfhydryl form was added to a molar equivalent of native A-chain S-sulfonate (Eli Lilly) and a stoichiometric amount of DTT was added to reduce the remaining S-sulfonates. The disulfide exchange was conducted in 0.1M glycine buffer (pH 10.5) at 4°C for 22 hrs. The insulin analogs were purified by reverse-phase chromatography with a Zorbax C8 column in slightly alkaline 0.5M NH₄HCO₃ (pH

8.0) using a linear gradient of acetonitrile. The disulfide formation step yields for the isolated insulin analogs ranged between 10-20%. The nature and purity of the insulin analogs were confirmed by analytical HPLC and mass spectral analysis.

The binding affinity of the synthetic analogs for the insulin receptor was measured in a competition binding assay utilizing scintillation proximity technology. Membranes derived from engineered cells that over-express the human insulin receptor were prepared and utilized. IC₅₀ values were determined from displacement of ¹²⁵I-labelled insulin (Table 1). Percent specific binding was calculated as following: % Specific Binding = Bound-NSB / Total bound- NSB x 100. IC₅₀ values were determined by using Origin software (OriginLab, Northampton, MA)

Table 1. Insulin receptor binding

Peptide	IC ₅₀ (nM)	Number of measurements
Insulin	0.68±0.28	12
HisB26 insulin	1.33±0.58	2
N-MeHisB26 DTI	1.24±0.38	8
N-MeGluB26 DTI	0.71±0.81	4
AadB26 DTI	0.46±0.12	2
Phe(4-carboxy)B26 DTI	0.60±0.09	2

The N-methylHisB26,des(27-30) insulin analog exhibited an affinity for the insulin receptor that appeared similar to that observed with native insulin (Table 1). Multiple measurements were made and different incubation conditions were explored, but the results remained consistently similar among these two insulins. The additional B26-analogs studied appeared quite potent, but once again comparable to native human insulin. The basis for the difference in our observations and the superagonism of N-MeHisB26,des(27-30) previously reported is not immediately certain. We presume it to reside in the nature of the binding assay. We employed membranes from engineered cells that over-express the insulin receptor while the prior work utilized primary isolated rat hepatocytes [1]. Further work is necessary to reconcile the differences observed in binding affinity and to explore whether this inconsistency is maintained when measuring glucose transport.

Our observations illustrate that at B26 neither the aromatic character, nor an N-methylated amide bond exhibit differential influence on the receptor binding affinity. The IC₅₀ values of the AadB26 and N-MeGluB26 analogs were quite comparable to the other analogs studied and indicate that acidic moieties at B26 appear as near functional equivalents to the native TyrB26 residue.

References

1. Zakova, L., Barth, T., Jiracek, J., Barthova, J. and Zorad, S. *Biochemistry* **43**, 2323-2331 (2004).
2. Miller, S. C. and Scanlan, T. S. *J. Amer. Chem. Soc.* **119**, 2301-2302 (1997).

Synthesis of an RNase B 30-124 Glycoform by Native Chemical Ligation

Christian Piontek, Stefano Mezzato, Daniel Varon, Nelson Lombana, Manuela Schaffrath, Andreas Martin, Franz-Xaver Schmid and Carlo Unverzagt

Bioorganische Chemie, Gebaude NWI, Universitaet Bayreuth, 95440 Bayreuth, Germany

Introduction

Recent efforts to obtain functional glycoproteins as a single glycoform are an ongoing challenge for interdisciplinary chemical research [1]. We selected the native chemical ligation [2] of recombinant peptides [3] and synthetic glycopeptides [4] for the synthesis of uniform complex type N-glycoproteins. The target glycoprotein RNase B (124 AA) was disconnected into the non glycosylated segment 40-124 (**B**) accessible by intein mediated protein splicing of a recombinant fusion protein and the complex N-glycan glycopeptide thioester 1-39 (**A**) compound requiring extensive solid phase peptide synthesis.

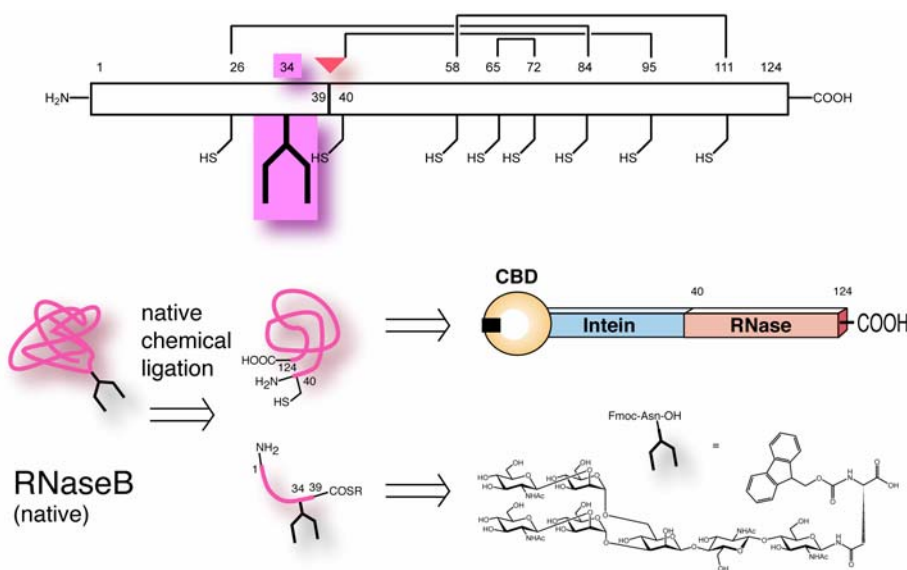


Fig. 1. Retrosynthesis of bovine pancreatic ribonuclease B bearing a complex type N-glycan.

Results and Discussion

The 35 kDa fusion protein consisting of a chitin binding domain, a monofunctional intein and the RNase 40-124 segment was constructed using the commercially available pTWIN vector and an synthetic gene fragment, which was amplified by PCR and subsequently ligated into the vector. Overexpression of the fusion protein in *E. coli* yielded non functional inclusion bodies, which were dissolved in strong denaturant and refolded. The splice reaction was shown to proceed nearly

quantitatively with the refolded intein liberating the desired RNase 40-124 fragment **B**, which was purified by HPLC.

To investigate the availability of the glycosylated thioester 1-39 **A**, a shorter model compound was evaluated first. The 30-39 thioester **A** was efficiently synthesized on a newly developed double linker resin [5], which allowed the LC-MS analysis of the safety-catch bound peptides and glycopeptides. Native chemical ligation of the segments **A** and **B** produced the desired glycosylated RNase B 30-124, which was deprotected in the oligosaccharide part. The ligation was confirmed by HPLC-MS of the crude reaction mixture and of the deprotected glycoprotein fragment.

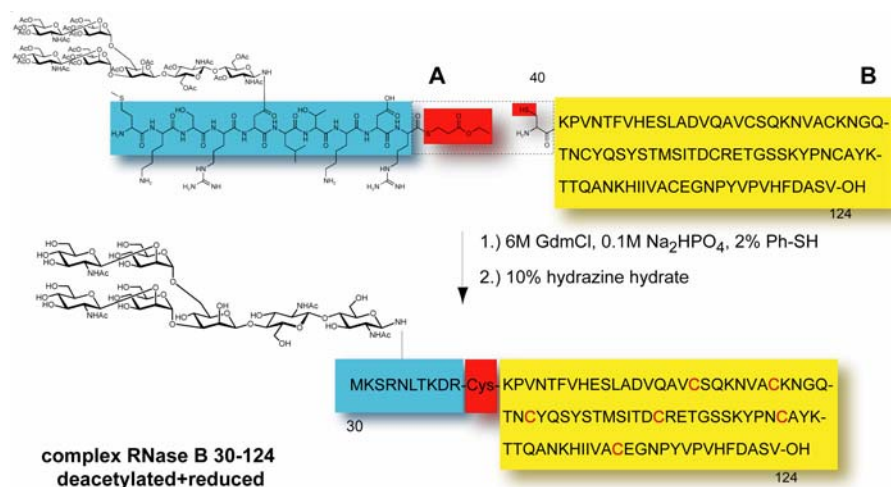


Fig. 2. Native chemical ligation of glycopeptide thioester **A** obtained by solid phase peptide synthesis and bovine pancreatic ribonuclease **B** fragment 40-124 **B** obtained by intein mediated protein splicing.

Acknowledgments

The work was funded by the Deutsche Forschungsgemeinschaft.

References

1. Review: Davis, B. G. *Chem. Rev.* **102**, 579-602 (2002).
2. Dawson, P. E., Muir, T. W., Clark-Lewis, I. and Kent, S. B. H. *Science* **266**, 776-779 (1994).
3. Muir, T. W. *Annu. Rev. Biochem.* **72**, 249-289, (2003).
4. a) Meinjohanns, E., Meldal, M., Paulsen, H., Dwek, R. A. and Bock, K. *J. Chem. Soc. Perkin. Trans. 1* 549-560 (1998); b) Warren, J. D., Miller, J. S. and Danishefsky, S. J. *J. Am. Chem. Soc.* **126**, 6576-6578 (2004); c) Yamamoto, N., Sasaki, K., Juneja, L. R. and Kajihara, Y. *Angew. Chem. Int. Ed.* **42**, 2537-2540 (2003); d) Hojo, H., Hagnoya, E., Matsumoto, Y., Nakahara, Y., Nabeshima, K., Toole, B. P. and Watanabe, Y. *Tetrahedron Lett.* **44**, 2961-2964 (2003); e) Macmillan, D. and Bertozzi, C. R. *Angew. Chem. Int. Ed.* **43**, 1355-1359 (2004).
5. Mezzato, S., Schaffrath, M. and Unverzagt C. *Angew. Chem. Int. Ed.* **44**, 1650-1654 (2005).

New Themes in Anti-Microbials and Quorum Sensing

Threaded Rings and Complex Topologies in Antimicrobial Peptides: Nature's Engineering Templates

David J. Craik, K. Johan Rosengren, Lillian Sando and Shane S. Simonsen

Institute for Molecular Bioscience and Australian Research Council Special Research Centre for Functional and Applied Genomics, University of Queensland, Brisbane, 4072, Australia

Introduction

Over recent years several families of naturally occurring antimicrobial peptides that contain a head-to-tail macrocyclic backbone have been discovered in bacteria, plants and animals [1]. Many of these peptides contain a unique additional topological constraint in the form of a covalent bond or peptide chain that threads through an embedded ring in the structure. The macrocyclic backbone and threaded structures make these peptides particularly stable and resistant to proteolysis, leading to suggestions of their use as stable peptide templates for drug design applications [2].

The largest family of such molecules is the cyclotides [3-4], currently estimated to comprise hundreds of members, each containing approximately 30-amino acids surrounding a cystine knot motif. They are present in plants as host defense molecules but have a range of potentially useful pharmacological activities, including anti-HIV activity [5]. Microcin J25 is another topologically complex antimicrobial molecule that has comparable stability to the cyclotides but lacks the disulfide bonding network [6]. Microcin J25 has attracted interest as a potential lead molecule for the design of novel antibacterial peptides because it has a unique mode of action that involves targeting bacterial RNA polymerase, and has an unusual threaded structure [7-9].

Figure 1 shows the generic structure of the prototypic cyclotide kalata B1 together with a schematic representation of the cyclic cystine knot (CCK) framework that defines the cyclotide family.

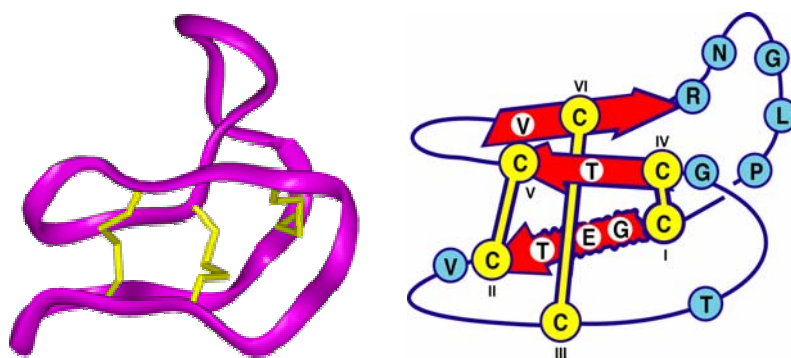


Fig. 1. A representative structure of the prototypic cyclotide kalata B1 (left) and the generic structure of the CCK framework seen in all cyclotides (right). The ribbon shows the peptide backbone with the disulfide bonds in stick form. The circled amino acids are highly conserved across all known members of the cyclotide family. The six conserved Cys residues that make up the cystine knot are numbered I-VI.

Results and Discussion

The aim of this study was to understand the factors that contribute to the antimicrobial activity of two types of threaded peptides, namely the cyclotides and microcin J25, the former an example of antiviral molecules and the later an example of an antibacterial. The cyclotides have also been reported to have relatively weak and salt-dependent antibacterial activity [10]. It was of particular interest to examine the remarkable stability of microcin J25, given its lack of disulfide bonds and small size of only 21 amino acids. This was done by determining the structure and molecular dynamics of recombinant expressed peptide, and comparing the threading arrangement with that of the cyclotides.

Figure 2 shows that a common feature of the cyclotides and microcin J25 is the presence of a threaded ring in the structures. In the case of the cyclotides the ring is formed by two of the disulfide bonds and their connecting backbone segments. The third disulfide bond threads through this ring, leading to the cystine knot motif, which plays an important role in the stability of the cyclotides. In the case of the microcin J25 the threading is through an 8-amino acid ring formed by the linkage of the side-chain of Glu8 to the N-terminus.

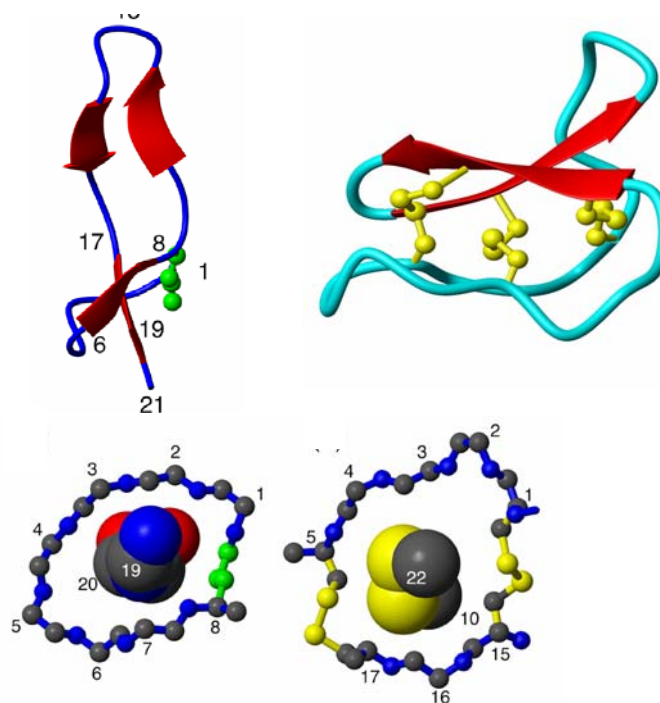


Fig. 2. Structures of microcin J25 (upper left) and kalata B1 (upper right) showing the comparable threading interactions in the two molecules. The two bottom views show that both involve threading through an 8-amino acid ring.

An analysis of the space-filling properties of the threading in the two molecules shows that there is a very tight packing of both the peptide chain and the disulfide bond through the embedded ring on a geometric level. The threading differs to the

extent that the penetrating chain in the case of microcin J25 has a terminus that is not further constrained by covalent linkage to another part of the molecule and so it was of interest to determine if this molecule was more flexible than the cyclotides.

To assess dynamic aspects of the threading a ^{15}N -labelled derivative of microcin J25 was expressed in *E. coli* and NMR relaxation measurement were made. These included T_1 , T_2 and the heteronuclear NOE at three magnetic field strengths (500, 600 and 750 MHz). Table 1 shows a selection of the relaxation data for selected sites in the molecule corresponding to the hairpin loop region (residues 9-16), the backbone-sidechain ring (residues 1-8) and the threaded tail (residues 17-21). Representative sites in these regions include G14 and F10 for the hairpin loop, V6 for the ring and S18 and Y20 for the embedded C-terminal tail.

Table 1. ^{15}N NMR relaxation data for microcin J25

	T_1 (sec)			NOE		
	500 MHz	600 MHz	750 MHz	500 MHz	600 MHz	750 MHz
G14	0.75	0.74	0.75	-0.99	-0.56	-0.10
F10	0.69	0.64	0.66	-0.76	-0.25	0.08
V6	0.64	0.58	0.62	-0.51	-0.16	0.23
S18	0.57	0.58	0.64	-0.55	-0.18	0.23
Y20	0.60	0.57	0.57	-0.72	-0.31	0.19

The data in Table 1 show that there is a steady decrease in T_1 values and a trend towards more positive NOE values in going from the hairpin loop to the ring and embedded tail, suggesting a decrease in mobility in this order. Although such a trend in mobility could not be predicted based on looking at the lowest energy structure alone, in hindsight it represents a logical trend. The NMR-derived ensemble of structures of microcin J25 has disorder in the turn near G14, at the apex of the hairpin, as shown in Figure 3 [8]. The relaxation data show that this is a reflection of mobility rather than simply being due to insufficient NOEs to define the structure. In combination with recent mutagenesis data [11-13] that are beginning to define the residues on RNA polymerase associated with interactions with microcin J25 the dynamics data will be valuable in understanding the mode of interaction of this peptide with the polymerase.

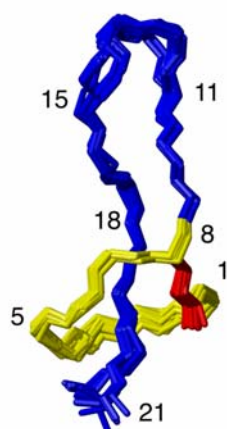


Fig. 3. Superposition of a family of 20 structures of microcin J25 reported by Rosengren et al [8]. Note the slight disorder in the turn between residues 11 and 15 at the end of the hairpin loop. The relaxation data reported here are consistent with this disorder being due to mobility rather than simply a lack of NOEs in this region of the structure. Similar structures have been independently reported by two other groups [9,10].

It is of interest that a thermolysin-cleaved derivative of microcin J25, in which one of the peptide bonds in the hairpin loop is broken, retains the ability to inhibit RNA polymerase in *in vitro* transcription assays [13]. A structure of this molecule shows that the cleaved hairpin region is highly disordered and is likely to be highly flexible [14]. Remarkably, the threaded chain remains associated with the 8-amino acid ring even though they are no longer covalently attached. In combination with other recent data [15] this result is consistent with the embedded ring and threaded C-terminal region being important for activity at the polymerase. On the other hand, the thermolysin-cleaved peptide is not active against *E. coli*, suggesting that the hairpin loop is important for crossing the bacterial membrane so as to reach the RNA polymerase target site [13].

Turning now to the cyclotides, it was of interest to see if there is a role for mobility in their antiviral activity. In previous studies we have shown that breaking the backbone of the cyclotides in any of loops 2, 3, 5 or 6 essentially does not disturb the three dimensional structures but does result in a loss of activity [5,16]. Table 2 shows the anti-HIV data for a range of representative cyclotides as well as for acyclic permutants of the prototypic cyclotide kalata B1 [5].

Table 2. Anti-HIV activity data for selected cyclotides

Peptide	EC ₅₀	IC ₅₀
Circulins A-F	40-275 nM	~500 nM
Cycloviolins A-D	~130 nM	~560 nM
Palicourein	100 nM	1500 nM
Kalata B1	~140 nM	>3500 nM
Acyclic permutants of B1	No activity	No activity

In this Table the EC₅₀ values represent the ability to inhibit viral replication while the IC₅₀ values are a baseline measure of toxicity against uninfected cells. Figure 4 shows schematic representations of two of the acyclic permutants, namely those with backbone breaks in loops 5 and 6, although examples with breaks in loops 2 and 3 were also studied.

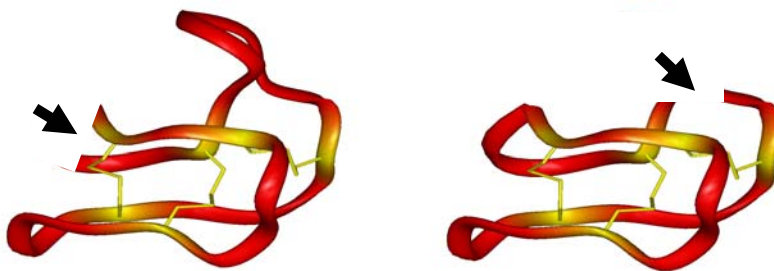


Fig. 4. Schematic illustration of acyclic permutants of kalata B1 with breaks in the backbone (arrowed) in loop 5 (left) and loop 6 (right) of the structure. NMR analysis shows that any of loops 2, 3, 5 or 6 may be broken and the molecules fold into the native three dimensional shape, yet have no activity.

The interesting finding from the study of the acyclic permutants is that it does not matter where in the backbone the chain is broken, the anti-HIV activity is lost. Since the backbone cleavages in the various permutants are in quite different parts of the molecules it appears likely that an intrinsic property of the cyclic backbone is important for activity. Data from amide exchange experiments [15] suggest that cyclization of the backbone produces an intrinsic tightening of the structure even though the global shape is not greatly affected. Thus, in both the cyclotides and in microcin J25 the threading/cyclization has resulted in a change to the dynamics of the molecules that is important for activity. In general, we believe that mobility will increasingly be recognized as an important facet of the activity of a range of antimicrobial molecules.

Acknowledgments

DJC thanks the Australian Research Council for a professorial fellowship. We thank Freda Jen for the recording of the ^{15}N relaxation data. Valuable discussions with Norelle Daly and Kirk Gustafson on previously published data are also gratefully acknowledged.

References

1. Trabi, M. and Craik, D. J. *Trends Biochem. Sci.* **27**, 132-138 (2002).
2. Craik, D. J., Simonsen S. and Daly N. L. *Curr. Opin. Drug Discov. Devel.* **5**, 251-260 (2002).
3. Craik, D. J., Daly, N. L., Bond, T. and Waine, C., *J. Mol. Biol.* **284**, 1327-1336 (1999).
4. Craik, D. J., Daly, N. L., Mulvenna, J., Plan. M. R. and Trabi, M., *Curr. Prot. Peptide Sci.* **5**, 297-315 (2004).
5. Daly, N. L., Gustafson, K. R. and Craik, D. J. *FEBS Lett.* **574**, 69-72, (2004)
6. Rebufatt, S., *et al. Curr. Prot. Peptide Sci.* **5**, 383-391 (2004).
7. Bayro, M. J., *et al. J. Am. Chem. Soc.* **125**, 12382-12383 (2003).
8. Rosengren, K. J., *et al. J. Am. Chem. Soc.* **125**, 12464-12474 (2003).
9. Wilson, K. A., *et al. J. Am. Chem. Soc.* **125**, 12475-12483 (2003).
10. Tam, J., *et al. Proc. Natl. Acad. Sci. USA* **96**, 8913-8918 (1999).
11. Mukhopadhyay, J., *et al. Mol. Cell* **124**, 739-751 (2004).
12. Aldeman, K., *et al. Mol. Cell* **124**, 753-762 (2004).
13. Semenova, E., *et al. J. Bacteriol.* **187**, 3859-3863 (2005).
14. Rosengren, K. J., *et al. Biochemistry* **43**, 4696-4702 (2004).
15. Vincent, P. A., *et al. Biochem. Biophys. Res. Comm.* **331**, 549-551 (2005).
15. Daly N. L. and Craik, D. J. *J. Biol. Chem.* **275**, 19068-19075 (2000).

A Minimalist Approach to Antimicrobial Proteins with Thionin as a Template

Miquel Vila-Perelló¹, Sabrina Tognon¹, Andrea Sánchez-Vallet²,
 Antonio Molina² and David Andreu¹

¹Department of Experimental and Health Sciences, Universitat Pompeu Fabra, 08003
 Barcelona, Spain; ² Department of Biotechnology, UPM-ETSIA, Madrid, Spain

Introduction

Thionins are small antimicrobial proteins, 45-47 residue-long and with four disulfide bonds, that are main constituents of the defense system of plants. Their 3D structure, consisting of one β -sheet and two antiparallel amphipathic α -helices, provides a very tight folding pattern, well preserved among plant species [1]. We have reported a structurally-guided dissection of the thionin from *Pyrularia pubera* (PpTH) [2] and demonstrated that its central twin helices are a key feature for activity. Peptides reproducing this motif [e.g., PpTH(7-32)] are fully active against a representative panel of pathogens, and circular dichroism, membrane permeation and surface plasmon resonance (SPR) experiments demonstrate that the mechanism of action remains unchanged [3] from the native protein.

Results and Discussion

This successful identification of a minimal thionin active motif contrasts with the fact that peptides separately reproducing each of the highly cationic and amphipathic α -helical regions [TH(7-19) and TH(24-32)] of the native structure lacked structural organization, had no antibiotic activity and did not bind model membranes.

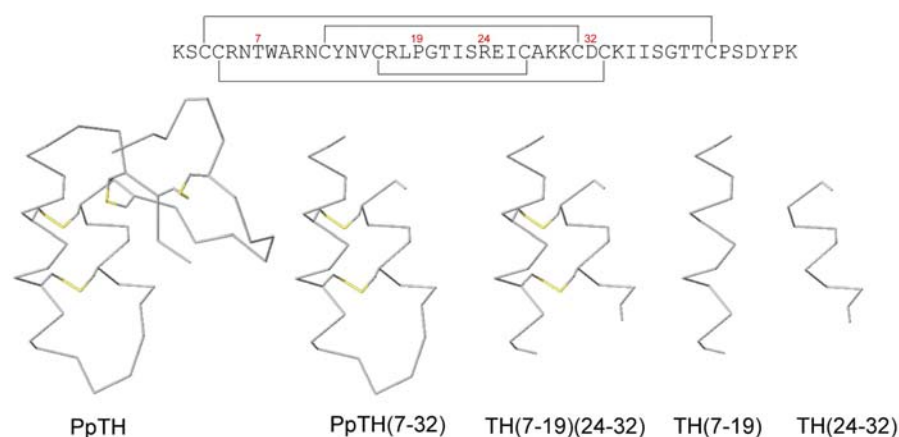


Fig. 1. Top: primary structure and disulfide bond pattern of the thionin from *Pyrularia pubera* (PpTH). Bottom: backbone of full-length PpTH, its minimal active motif [TH(7-32)], the chimeric heterodimer [TH(7-19)(24-32)] and the helical segments from which antimicrobially active peptides in this work are evolved.

We assumed this was due to the inability of the (7-19) and (24-32) segments to adopt the amphipathic helix conformation imposed by the thionin native context, and hypothesized that if these segments could be induced into native-like structure by appropriate structural restriction, membrane binding and thus antimicrobial potency might be regained.

An obvious step in the above direction was to show that the double helical motif of thionin could be replicated as a functional entity. To this end, we designed the chimeric TH(7-19)(24-32R) heterodimer (Fig. 1), in which the disulfide bonds linking the two core helices were preserved and an Arg-for-Asp replacement at residue 32, shown earlier to enhance activity [4], was introduced. This peptide, made by stepwise disulfide formation [5], showed remarkable antimicrobial activity, superior to full length PpTH, proving that thionin could be used as a template from which active, structurally simplified analogs could be evolved.

Having established a proof of principle, we decided to design even simpler peptides by restricting the (7-19) or (24-32) segments into amphipathic helices. Since the Cys residues in these PpTH helices are in a $i, i+4$ disposition, we decided to create an internal disulfide to favor an helical conformation. MD simulations (Fig. 2) showed that a D-Cysⁱ-L-Cysⁱ⁺⁴ but not a L-Cysⁱ-L-Cysⁱ⁺⁴ bridge was compatible with a helical structure, as shown earlier for $i, i+3$ disulfides [6]. Accordingly, an L-to-D Cys mutation was included in all new thionin analogs. To evaluate the contribution of the disulfide to the conformational restriction and activity of the cyclic peptides, analogs TH(7-19)Abu and TH(24-32R)Abu were made, with both Cys mutated to Abu, an isoster with no constraining effects. Finally, in order to explore the effect of the Cys side chain length on the disulfide-

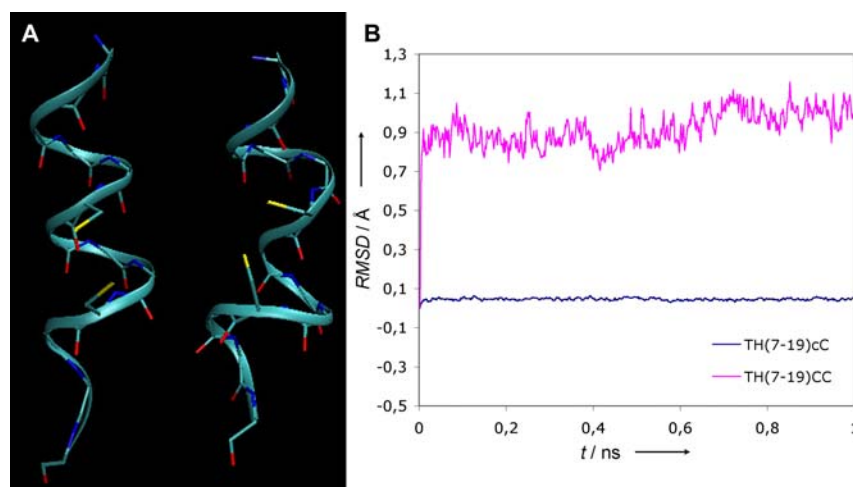


Fig. 2. A) Backbone structure of TH(7-19)cC (left) and TH(7-19)CC (right) after 1 ns of molecular dynamics simulation (c and C stand for D- and L-Cys, respectively). The helical structure for TH(7-19)cC is almost preserved while that of TH(7-19)CC is highly distorted and the preferred geometry of the disulfide bond is not fully achieved. B) Plot of backbone RMSD values vs time clearly shows that TH(7-19)CC quickly deviates from the original helical structure forced by the disulfide, while for TH(7-19)cC the D-Cys-L-Cys disulfide is compatible with the preservation of the initial structure.

Table 1. Antimicrobial activity of *P. pubera* thionin and minimalist analogs

Peptide	EC ₅₀ (μM) ^a			
	Gram positive	Gram negative		Fungus
	<i>C. michiganensis</i>	<i>R. meliloti</i>	<i>X. campestris</i>	<i>B. cinerea</i>
Native thionin	0.30±0.04	>20±0	3.65±0.58	0.32±0.19
TH(7-32R ^b)	0.80±0.04	4±0	4.60±0.37	0.80±0.19
TH(7-19)(24-32R ^b)	0.03±0.00	2.07±1.2	1.03±0.04	0.08±0.00
TH(7-19) ^{b,c}	>50±0.00	>20±0	>50±0.00	5.50±0.00
TH(7-19)Abu	3.27±1.25	>50±0	>50±0.00	1.60±0.00
TH(7-19)cC ^d	0.51±0.12	>50±0	29.33±5.73	0.20±0.00
TH(7-19)cH ^d	0.74±0.14	>50±0	18.33±0.47	0.19±0.01
TH(24-32R ^b)	21±2.55	>50±0	>50±0.00	3.50±0.35
TH(24-32R ^b)Abu	5.13±0.11	>50±0	>50±0.00	4.10±0.25
TH(24-32R ^b)cC ^d	0.90±0.00	>50±0	>50±0.00	0.55±0.24
TH(24-32R ^b)cH ^d	0.90±0.00	>50±0	>50±0.00	0.40±0.07

^aEC₅₀ is the peptide conc. able to inhibit microbial growth to 50% at 24 hrs.

^bThese peptides include the Arg-for-Asp replacement at residue 32 (see ref. 3).

^cThe two native Cys residues at 12 and 16 mutated to Ser.

^dC and c refer to L- and D-Cys, respectively; H to homocysteine.

stabilized helices, two peptides with Hcy replacement [TH(7-19)cH and TH(24-32R)cH] were also investigated.

An antimicrobial assay of the peptides against a panel of representative plant pathogens (three bacteria and one fungus, Table 1) confirmed to a satisfactory extent our hypothesis, i.e., all disulfide-containing peptides evolved from PpTH (7-19) and (24-32) fragments had significant antimicrobial activity. Thus, the conformationally constrained, cyclic disulfide TH(7-19)cC (Table 1, entry 6) was equipotent to PpTH against *C. michiganensis*, a typical Gram-positive, as well as against *B. cinerea*, a representative fungus, despite the drastic (>70%) reduction in size vs. the parent PpTH. The inactivity of this peptide against Gram-negative *R. meliloti* and *X. campestris* was not unexpected and parallels that of native PpTH.

The equally restricted analog, TH(24-32R)cC (Table 1, entry 10), with a >80% size reduction over the parent structure, exhibited similar potency and spectrum. Likewise, the presence of an additional CH₂ in the disulfide ring preserved the enhanced activity of the two Hcy-containing analogs (Table 1, entries 7 & 11). It also induced a comparable tendency to become structured in the presence of artificial membranes, though with quite different CD profiles than the all-Cys analogues (see below).

Secondary structure analysis of TH(7-19)cC by CD (Fig. 3) revealed a clear tendency to adopt substantial levels of helicity upon binding to negatively charged model membranes, suggesting that the internal cyclization restricts the conformational repertoire to a narrow set of membrane-active (i.e., amphipathic), native-like populations. For the other cyclic analog, TH(24-32)cC, correlation between activity and an helical CD signature was less obvious, probably because at 9 residues it is not large enough to promote sizeable levels of structure. In any event, the decisive influence of the cyclic restriction on activity is substantiated by the average 10-fold drop in antimicrobial potency of both Abu-containing analogs (Table 1, entries 5 & 9) relative to their disulfide counterparts, despite the similar

levels of helicity achieved upon binding to DMPG liposomes (Fig. 3). A plausible interpretation of this different behavior could be that, while both peptides are able to adopt helical structures, the limited conformational freedom of the disulfide-restricted peptides results in energetically favorable access to bioactive membrane-binding structures, with the ensuing killing effects.

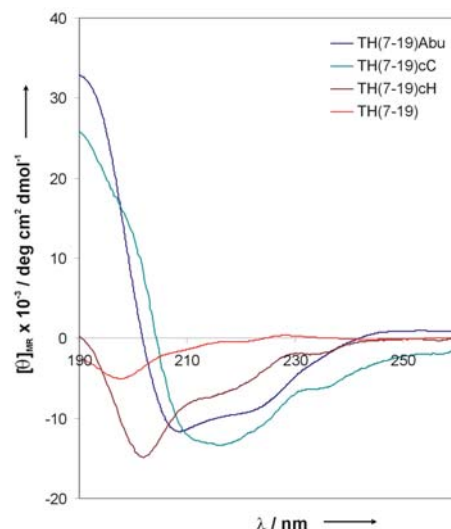


Fig. 3. CD spectra of TH(7-19), TH(7-19)Abu, TH(7-19)cC and TH(7-19)cH at 30 μ M in 25 mM phosphate, pH 6.0 in the presence of DMPG liposomes (peptide/lipid ratio 1:100). Disulfide- and Abu-containing peptides display characteristic helical signatures while the linear TH(7-19) (Cys residues mutated to Ser) is completely random coil.

In conclusion, internal $i,i+4$ disulfide restriction is a powerful tool to stabilize membrane-active helical conformations and, in our particular case, a successful route to the smallest, highly active antimicrobial peptides thus far derived from a complex, highly folded natural peptide. This approach should be of general applicability and its relevance to other AMP structures is currently under study.

References

1. García-Olmedo, F., Molina, A., Alamillo, J. M. and Rodríguez-Palenzuela, P. *Biopolymers* **47**, 479-491 (1998).
2. Fernandez de Caley, R., Gonzalez-Pascual, B., García-Olmedo, F. and Carbonero, P. *Appl. Microbiol.* **23**, 998-1000 (1972).
3. Vila-Perelló, M., Sánchez-Vallet, A., Molina, A., García-Olmedo, F. and Andreu, D. *J. Biol. Chem.* **280**, 1661-1668 (2005).
4. Vila-Perelló, M., Sánchez-Vallet, A., Molina, A., García-Olmedo, F. and Andreu, D. *FEBS Lett.* **536**, 215-219 (2003).
5. Andreu, D., Albericio, F., Solé, N. A., Munson, M. C., Ferrer, M. and Barany, G. In *Meth. Mol. Biol.* vol. 35: Peptide Synthesis Protocols (Pennington, M. W. and Dunn, B. M., eds.) Humana Press, Totowa, NJ, pp. 91-169 (1994).

Discovering Additional Chemical and Biological Functions for 3-Oxo-*N*-Acylhomoserine Lactones

Gunnar F. Kaufmann, Rafaella Sartorio, Sang-Hyeup Lee, Claude J. Rogers, Michael M. Meijler, Jason A. Moss, Bruce Clapham, Andrew P. Brogan, Tobin J. Dickerson and Kim D. Janda

The Skaggs Institute for Chemical Biology and Departments of Chemistry and Immunology,
The Scripps Research Institute 10550 North Torrey Pines Road La Jolla, CA 92037

Introduction

The term quorum sensing has been coined to describe the ability of a population of unicellular bacteria to act as a multicellular organism in a cell-density-dependent manner, that is, a way to sense “how many are out there” [1]. Bacteria use small diffusible molecules to exchange information amongst themselves. An important class of autoinducers is the family of *N*-acylhomoserine lactones (AHLs) used by Gram negative bacteria. Variation in *N*-acyl chain length and oxidation state of AHLs provide for bacterial strain specificity in the signaling process and subsequent synchronization of gene expression. Upon reaching a critical threshold concentration, they bind to their cognate receptor proteins, triggering the expression of target genes.

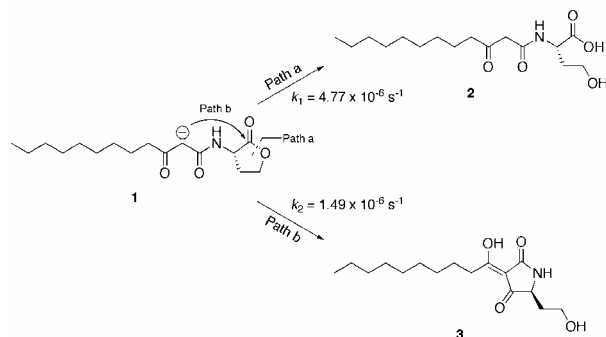
Pseudomonas aeruginosa is a common environmental microorganism that has acquired the ability to take advantage of weaknesses in the host immune system to become an opportunistic pathogen in humans [2]. Over the last ten years, significant progress has been made in elucidating the molecular mechanisms underlying *P. aeruginosa* pathogenicity. Two different AHLs, *N*-(3-oxododecanoyl) homoserine lactone **1** and *N*-butyrylhomoserine lactone, have been identified as the main quorum sensing signaling molecules in *P. aeruginosa* [3]. Importantly, genes regulated by this mechanism control the expression of virulence factors as well as the formation of structures known as biofilms [4]. Recently, we have assigned new roles for these compounds through the demonstration that **1** performs a previously unrecognized role; the autoinducer itself and a corresponding degradation product derived from an unusual Claisen-like condensation reaction function as innate bactericidal agents [5].

Results and Discussion

Our studies were initiated in an effort to study the lifetime of AHL **1** in an aqueous environment. Incubation of **1** *in aqua* produced an undocumented compound in addition to the expected hydrolysis product **2**. Extensive NMR characterization of this anomalous molecule revealed it to be 3-(1-hydroxydecylidene)-5-(2-hydroxyethyl)pyrrolidine-2,4-dione **3**, a compound belonging to a class of antibacterial compounds known as tetramic acids [6]; the mechanism of formation is a Claisen-like intramolecular alkylation of the β -ketoamide moiety (Scheme 1). Tetramic acid **3** was found to be very stable, with no decomposition or detectable reversion to **1**; most importantly, **3** was also detected in *P. aeruginosa* culture.

Given that *P. aeruginosa* employs AHL **1** as the principal autoinducer and the known bactericidal activity of tetramic acids, we hypothesized that **3** could function in the context of bacterial viability. Indeed, significant antibacterial activity was observed against all tested Gram positive bacterial strains in the presence of **3** after overnight incubation, while no toxicity was observed against *P. aeruginosa* or other tested Gram negative bacteria. The effective concentration of **3** is biologically

relevant, as high concentrations of **1** (>600 μM) have been previously detected in *P. aeruginosa* biofilms [7]. Furthermore, **3** has comparable activity to other known antibacterial compounds.



Scheme 1. Formation of tetramic acids from 3-oxo-*N*-acylhomoserine lactone autoinducers.

Similar to previously described tetramic acids and related analogs, sensitivity to **3** was only apparent in Gram positive cells with little variation present in EC_{50} values across different species and genera. Notably, **1** also displayed cytotoxicity suggesting a dual role for **1** in *P. aeruginosa* communities as both quorum-sensing molecules and as an interference mechanism against bacterial competitors. Although significant cell death was observed after overnight incubation with AHL **1**, the bacteria recovered after additional incubation, suggesting that although AHL **1** is bactericidal, upon hydrolysis, the resulting compound **2** is tolerated by bacteria. Interestingly, resistant *B. cereus* strains known to express a penicillinase or cephalosporinase in conjunction with a penicillinase (ATCC 13061 and 27348, respectively) were not affected by exposure to **1**, yet displayed comparable sensitivity to **3** as other tested *B. cereus* strains. We acknowledge that the observed antibacterial activity of **3** is relatively modest in comparison to other known more potent bactericidal agents; however, the fact that this compound is nonenzymatically produced from a molecule designed to play a role in cell-cell signaling is significant. Furthermore, even in the instance that only a small percentage of the competitor population is killed by **3**, this should provide a competitive advantage for *P. aeruginosa*.

The identification of AHL-hydrolyzing enzymes, or lactonases, in *B. cereus* 240B1 led to the hypothesis that certain bacteria have evolved quorum sensing signaling interference strategies [8]. The hydrolysis of AHL does not only prevent cell density-dependent signaling events from occurring, but also presumably could mitigate the cytotoxic effect of AHLs and furthermore prevent the formation of **3**. Indeed, *B. cereus* ATCC 14579 cells, previously shown to express lactonase [9] do not show sensitivity to **1**, yet are still affected by **3**. This advocates two distinct implications; the first, as previously hypothesized, lactonases may have evolved in certain Gram positive bacteria to interrupt quorum sensing signaling. However, our findings also suggest that these enzymes have a previously unrecognized function; to abrogate the toxic effects of **1** and prevent the formation **3**. Secondly, this finding raises the enticing evolutionary prospect that 3-oxo-AHLs and their corresponding tetramic acids were selected for as a result of their fortuitous cytotoxic abilities and resistance to lactonase degradation, respectively.

Iron plays an essential role in physiological processes and the pathogenesis of bacteria [10]. Many bacteria are known to produce siderophores in order to sequester iron, an element that although essential for their growth, has poor solubility under physiological conditions. *P. aeruginosa* synthesizes two siderophores, pyoverdine and pyochelin, and it has been shown that it is also able to use a variety of heterologous siderophores of microbial origin. The 3-acetylpyrrolidine-2,4-dione heterocycle found in **3** and in many other naturally occurring tetramic acids has been shown to efficiently chelate a variety of metal cations including iron. The role of metal binding in the bactericidal activity of tetramic acids is unclear, with some tetramic acids displaying increased toxicity as a metal complex, while in others, the toxicity is attenuated by metal ion chelation [11]. Given this disparity, we investigated the ability of **3** to complex metals in order to evaluate the potential bioactivity of these complexes. Bearing in mind the crucial role that iron plays in bacterial physiology and the demonstrated potential of tetramic acids to bind this metal, we focused our investigations on the chelation of iron by **3**.

Analysis of mixtures of **3** and Fe^{3+} by ESI-MS revealed the presence of a 3:1 **3**- Fe^{3+} complex. Using a previously described protocol based on the competition between tetramic acid **3** and EDTA for iron and the facile detection of **4**- Fe^{3+} complexes by their characteristic absorption, dissociation constants were also measured. Using the known affinity of EDTA for Fe^{3+} , we were able to determine the relative affinity ($K_{d,\text{app}}$) of **3** for Fe^{3+} to be $1.6 \times 10^{-29} \text{ M}^3$. In total, the compilation of this data suggests that **3** could compete for available iron in solution and providing an additional method for iron solubilization.

In summary, we propose that *P. aeruginosa* utilizes **3** as an interference strategy to preclude encroachment by competing bacteria. Although the complexation of iron may play a role in this process, further study is required into the mechanism and scope of the bactericidal activity and the potential of **3** to act as a primordial siderophore. The compilation of our data recommends that other autoinducers be reevaluated for the potential to perform additional biological functions.

Acknowledgments

We thank Professor Barbara Iglewski, Malcolm Wood and Theresa Fassel for expert assistance. This work was supported by NIH AI055781 (K.D.J.) and The Skaggs Institute for Chemical Biology.

References

1. Miller, M. B. and Bassler, B. L. *Annu. Rev. Microbiol.* **55**, 65-99 (2001).
2. Lyczak, J. B., Cannon, C. L. and Pier, G. B. *Microbes and Infection* **2**, 1051-1060 (2000).
3. Pearson, J. P., Passador, L., Iglewski, B. H. and Greenberg, E. P. *Proc. Natl. Acad. Sci. USA* **92**, 1490-1494 (1995).
4. Smith, R. S. and Iglewski, B. H. *J. Clin. Invest.* **112**, 1460-1465 (2003).
5. Kaufmann, G. F., *et al.* *Proc. Natl. Acad. Sci. USA* **102** 309-314 (2005).
6. Ghisalberti, E. L. *Studies in Natural Products Chemistry* **28**, 109-163 (2003).
7. Charlton, T. S., *et al.* *Environ. Microbiol.* **2**, 530-541 (2000).
8. Dong, Y. H., *et al.* *Nature* **411**, 813-817 (2001).
9. Dong, Y. H., *et al.* *Appl. Environ. Microbiol.* **68**, 1754-1759 (2001).
10. Gensberg, K., Hughes, K. and Smith, A. W. *J. Gen. Microbiol.* **138**, 2381-2387 (1992).
11. Gandhi, N. M., *et al.* *J. Antibiot.* **26**, 797-798 (1973).

Comparing Antimicrobial and Membrane Permeabilizing Activity of Peptides Derived from Human Cationic Proteins

Susana Sánchez-Gómez¹, Guillermo Martínez de Tejada¹, José Leiva-Leon¹, Ignacio Moriyón¹, Dagmar Zweytick², Karl Lohner² and Sylvie E. Blondelle³

¹Medical School of the University of Navarra, Spain; ²Institute for Biophysics and X-ray Structure Research, Austrian Academy of Sciences, Graz, Austria; ³Torrey Pines Institute for Molecular Studies, San Diego, CA, USA

Introduction

The increasing occurrence of pathogenic bacteria that are resistant to commercially available antibiotics has led to a growing interest in the development of peptides as a novel class of antibacterial drugs. Since bacteria have evolved to present multiple resistances to a large number of existing antibiotics, a new class of compounds is more likely to minimize the rapid emergence of bacterial resistance. Nature has taught us that effector molecules of mammalian innate immunity can provide a first line of defense against a substantial array of pathogenic microorganisms. In particular, host-defense peptides are considered to be multifunctional effector molecules and represent novel sources for the development of therapeutic agents with which to overcome antimicrobial resistance. Today, several hundred host defense peptides have been isolated from natural sources and their functions characterized [reviewed in 1-3]. These peptides are important components of innate defenses, since they not only have the ability to kill bacteria, but are also able to modulate inflammatory responses. While many conventional antibiotics damage or kill bacteria over a period of days, most antimicrobial peptides affect the bacterial membrane and kill almost instantaneously, i.e., within minutes. Therefore, a permeabilizing peptide may be able to counteract mechanisms of antibiotic resistance relying on an efficient membrane permeability barrier and be of great value in a combination therapy against drug-resistant bacterial strains.

In the aim to test whether antimicrobial peptides may be used as permeabilizing agents that render bacteria more vulnerable to conventional antibiotics, we compared the antimicrobial and permeabilizing activities of a panel of 70 peptides (7-11 amino acid) rich in positively charged residues derived from a human lactoferrin fragment (LF11, FQWQRNIRKVR-NH₂ [4]).

Results and Discussion

Analogues of LF11 including amino acid omissions, substitutions, and insertions were synthesized by standard solid-phase methods in the aim to modify the peptides overall charge, hydrophobic core, and/or amphipathicity. The peptides antimicrobial activities against a large panel of bacteria were assessed using both conventional tests (MIC, MBC) and non-conventional assays (MIC quantified by an automated turbidimetry-based system and MBC measured on resting cells suspended in low-ionic strength medium—"survival assay"). Both conventional and non-conventional tests lead to similar MIC results. On the other hand, absence of cations in the non-conventional "survival test" resulted in MBC values dramatically lower than those determined by the conventional test (up to >512 fold decrease in MBC value). Furthermore, addition of cations to the survival test medium for *P. aeruginosa* and

Table 1. Relationship between antimicrobial and permeabilizing activity against *P. aeruginosa* CUN 4158-02

Fold-decrease in novobiocin MIC ^b	Peptide MIC (μg/ml) ^a					
	16	32	64	128	256	>256
>512		5 ^c	3	1		
128-256			1	1	2	1
32-64				2		4
4-16			1	3	8	21
<4	1	1	2	2	16	30

^aThe MIC of 70 peptides was determined using conventional microdilution method. ^bThe decrease in novobiocin MIC in the presence of peptide was determined using a checker-board microdilution assay. ^cNumber of peptide analogs that has the respective listed MIC and lead to the respective listed fold-decrease in novobiocin MIC.

B. bronchiseptica restored the susceptibility to the peptide in most of the cases. These differences correlate with the differential role played by cations in the stabilizations of the outer membrane of these bacterial species and also reflect a competitive binding to the negatively charged lipids between the cationic peptides and cations.

The outer membrane of Gram negative bacteria acts as a permeability barrier against hydrophobic compounds. The permeabilizing activity of peptides was evaluated by the ability of hydrophobic substance to reach their inner target. Thus, two separate methods were used: 1) a fluorimetric assay that measures the ability of N-phenyl-naphthylamine (NPN) to access the lipid bilayer resulting in an increased fluorescence, and 2) a checker-board microdilution assay that determines the ability of novobiocin to reach DNA gyrase resulting in an increased antimicrobial activity (i.e., decrease in novobiocin MIC value). Tests were performed on *P. aeruginosa* 4158-02 (CUN), because of the intrinsic low permeability of this bacterial strain. A good correlation was observed between the two assays, i.e., peptides showing high decreases in novobiocin MIC also lead to high increases in NPN uptake.

Interestingly, the most potent permeabilizers did not always correspond with the peptides exhibiting the highest antimicrobial activity thus indicating that these two activities have different structural bases. For example as summarized in Table 1, five peptides having a great effect on novobiocin MIC (128-256 or 32-64 fold-decrease) had no or little antimicrobial activity (MIC value greater than 256 μg/ml). In a similar but reversed observation, two peptides having MIC of 16 or 32 μg/ml had little effect on the MIC of novobiocin (<4 fold-decrease).

Calorimetric experiments were carried out to evaluate the potential differences in mechanism of perturbation of cell membranes between antimicrobial and permeabilizing peptides using dipalmitoyl-phosphatidylglycerol (DPPG) model membranes. Thus, the effect of the most potent permeabilizing peptide (p48, Q2 omission/Q4 substitution analog) on negatively charged DPPG model membranes was determined and compared to an inactive analog (p4, core deletion analog) as well as to a strong antimicrobial analog (p31, tryptophan-rich analog) (Fig. 1). The permeabilizing analog only affected the so-called pretransition (shift to lower temperature and decrease in enthalpy) with no effect on the main transition

suggesting binding of the peptide to the lipid with no major insertion of the peptide into the bilayer. In contrast, as expected from previous studies [5,6] both abolition of the pretransition and significant decrease in the main transition temperature and cooperativity of DPPG were observed for the strong antimicrobial peptide indicating a strong perturbation of the membrane bilayer structure. No significant effect on the phase behavior of DPPG was detected in the presence of the inactive peptide.

In preliminary studies, the ability of the permeabilizing analog p48 to reverse the bacterial resistance to conventional antibiotics was assessed using a clinical strain of *P. aeruginosa* (PAO1) having known intrinsic resistance to ampicillin, fosfomycin and erythromycin. Synergistic effects were observed at peptide concentrations as low as 1.6, 50 and 25 $\mu\text{g/ml}$ with ampicillin, fosfomycin and erythromycin, respectively. These results demonstrate that the resistance mechanisms due to a decrease in drug accumulation involving low permeability and/or efflux pump expression/ overexpression can be reversed by permeabilizing peptides.

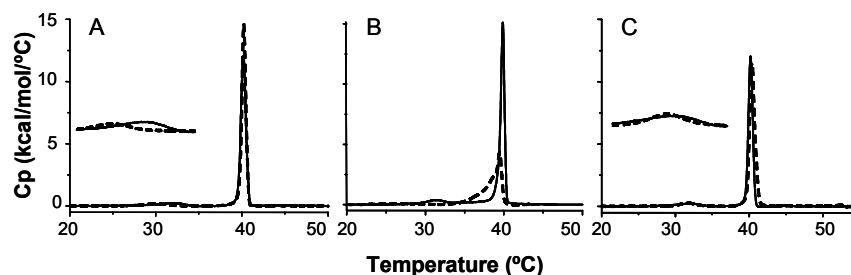


Fig. 1. Excess heat capacity as a function of DPPG liposomes in the absence (solid line) or presence (dotted line) of (A) p48, (B) p31 and (C) p4; pretransition enlarged in (A,C).

Acknowledgments

The work was funded in part by the Commission of the European Communities grant QLK2-CT-2002-01001, "Antimicrobial endotoxin neutralizing peptides to combat infectious diseases", and by the Alzheimer and Aging Research Center.

References

1. Hancock, R. E. and Lehrer, R. *Trends Biotechnol.* **16**, 82-88 (1998).
2. Otvos, L., Jr. *J. Peptide Sci.* **6**, 497-511 (2000).
3. Nissen-Meyer, J. and Nes, I. F. *Arch. Microbiol.* **167**, 67-77 (1997).
4. Andr , J., Lohner, K., Blondelle, S. E., Jerala, R., Moriyon, I., Koch, M. H. J., Garidel, P., Brandenburg, K. *Biochem. J.* **385**, 135-143 (2005).
5. Lohner, K., Latal, A., Lehrer, R. I. and Ganz, T. *Biochemistry* **36**, 1525-1531 (1997).
6. Abuja, P. M., Zenz, A., Trabi, M., Craik, D. J. and Lohner, K. *FEBS Lett.* **566**, 301-306 (2004).

Preliminary NMR Analysis of ProP440-500 the C-Terminal Cytoplasmic Domain of Bacterial Osmosensory Protein ProP

David L. Zoetewey¹, David N. M. Jones², Janet M. Wood³ and Robert S. Hodges¹

¹Department of Biochemistry and Molecular Genetics and ²Department of Pharmacology; University of Colorado at Denver and Health Sciences Center, Aurora, CO 80045, USA;

³Department of Microbiology, University of Guelph, Guelph, ON N1G2W1, Canada

Introduction

Bacteria sense and respond to the osmolarity of their media through a variety of different proteins that can import and/or export inorganic ions or organic zwitterions to help adjust cellular osmolarity. One such protein used by *Escherichia coli* is ProP, which imports proline and glycine betaine [1]. A member of the major facilitator superfamily (MFS), one key distinguishing feature of ProP in many but not all bacterial species is the presence of a sequence which forms a homodimeric antiparallel coiled-coil at the C-terminus. This coiled-coil has been shown to increase sensitivity to changes in osmolarity and be necessary for prolonged activity [2]. We have previously solved the structure of the minimal coiled-coil domain by NMR spectroscopy and hypothesize that the unique topology may account for the ability of a coiled-coil to sense changes in osmotic pressure [3]. Here we attempt to solve the structure of the entire soluble cytoplasmic extension of ProP from amino acid 440-500.

Results and Discussion

Our preliminary NMR data shows that ProP 440-500 is folded and lends itself to structural determination by NMR spectroscopy using standard triple resonance

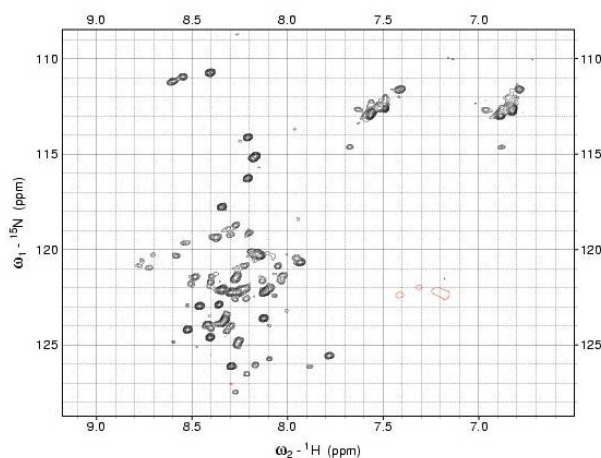


Fig. 1. ^1H ^{15}N HSQC shows correlation of amide proton and nitrogen in ProP 440-500. Overall, while there is some central spectral crowding and overlap, nearly all residues are resolved indicating that this peptide is folded and can be solved using standard 3D NMR techniques.

experiments. There is also preliminary evidence that ProP 440-500 interacts with bacterial membranes with a K_D of approximately 3 μM [4]. Thus once we have the initial chemical shifts tabulated we will be able to compare possible structures of ProP 440-500 interacting with a membrane mimicking micelle or as a homodimer. An important first step in structural determination is to make sure that the protein or peptide of interest is folded and structured. Each amide in the protein backbone corresponds to one peak in the ^1H ^{15}N HSQC spectrum (Fig. 1). Once the protein is fully sequenced each spot can be tracked to show chemical shift changes induced by binding to a ligand.

Thus far over 40 of the 74 amino acids including the His₆ tag have been identified and sequenced. Once the sequencing is complete we will run additional triple resonance experiments and finally NOE experiments to measure distance restraints and calculate an ensemble of structures which we will compare to the previously solved minimal coiled-coil domain ProP 468-497. We anticipate that the portion of the minimal coiled-coil will remain the same, and look forward to finding out what structure is present in the region of 440-467 as well as which part of ProP

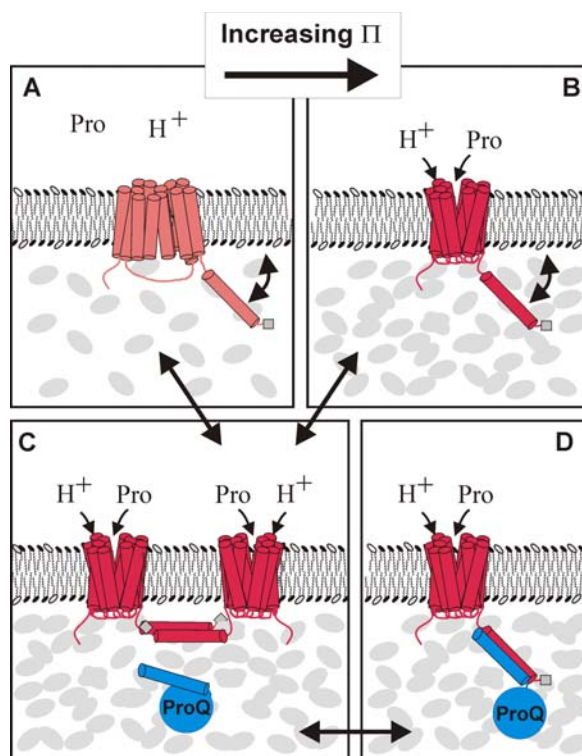


Fig. 2. Proposed mechanism of ProP activation. A) ProP inactive, monomeric helix interacts with the membrane. B) Cytoplasmic crowding leads to dissociation of monomeric helix and initial activation. C) Homodimeric coiled-coil formation helps stabilize active configuration of ProP. D) Activated ProP is further stabilized through heterodimeric coiled-coil formation with partner protein ProQ.

440-500 interacts with membrane mimicking micelles. The comparison of the structure of ProP 440-500 as a homodimeric antiparallel coiled-coil and the potential structure of ProP interacting with membrane mimicking micelles will be critical in the initial evaluation of our model shown in Figure 2. The model for activation is that the cytoplasmic C-terminal domain is associated with the membrane as a monomeric helix and as the cytoplasm starts to get crowded because of an increase in osmolality, the monomeric helix dissociates from the membrane and forms either a homodimeric coiled-coil with another ProP or a heterodimeric coiled-coil with the partner protein ProQ.

Acknowledgments

This work was funded by the NIH-RO1GM61855 and PO1AI059576 grants to R. S. Hodges and the John Stewart Chair in Peptide Chemistry.

References

1. Wood, J. M., Bremer, E., Csonka, L. N., Kraemer, R., Poolman, B., van der Heide, T. and Smith, L. T. *Comp. Biochem. Physiol. A Mol. Integr. Physiol.* **130**, 437-460 (2001).
2. Culham, D. E., Henderson, J., Crane, R. A. and Wood, J. M. *Biochemistry* **42**, 410-420 (2003).
3. Zoetewey, D. L., Tripet, B. P., Kutateladze, T. G., Overduin, M. J., Wood, J. M. and Hodges, R. S. *J. Mol. Biol.* **334**, 1063-1076 (2003).
4. Becker, D. F., Personal Communication Unpublished Results.

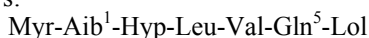
Synthesis and Conformation of Analogs of the Antiviral Peptide Halovir A

Andrea Dalla Bona¹, Cristina Peggion¹, Fernando Formaggio¹, Bernard Kaptein², Quirinus B. Broxterman² and Claudio Toniolo¹

¹Department of Chemistry, University of Padova, 35131 Padova, Italy; ²DSM Research, Life Sciences, Advanced Synthesis and Catalysis, P.O. Box 18, 6160 MD Geleen, The Netherlands

Introduction

Recently, the isolation, amino acid sequence and antiviral activity of halovir A, a terminally-blocked pentapeptide extracted from a marine-derived fungus of the genus *Scytalidium* have been reported [1,2]. The primary structure of this lipopeptaibol is as follows:



where Myr is the fatty acyl moiety myristoyl (C₁₄) and Lol is the 1,2-aminoalcohol leucinol.

Results and Discussion

In addition to the naturally occurring peptide and its [Leu⁶-OMe] analog, we have synthesized by solution-phase methods and studied the two C^α-tetrasubstituted α -amino acid-based analogs [(α Me)Leu³, Leu⁶-OMe] and [(α Me)Val⁴, Leu⁶-OMe] of halovir A with potentially reinforced helicity. The preferred conformations of the three analogs in solution, as compared to that of halovir A, have been determined by a combination of FT-IR absorption, 2D-NMR, and CD techniques.

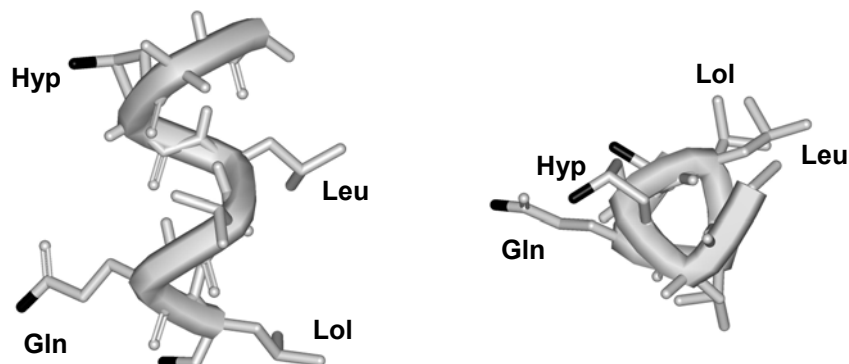


Fig. 1. Representation of halovir A in the 3_{10} -helical conformation (left: side view; right: top view). The amphiphilicity of the 3D-structure stands out clearly (the hydrophilic moieties are black-coloured). The N-terminal myristoyl chain has been omitted for clarity.

Our conformational analysis has established that in polar solvents halovir A and its analogs studied herein are predominantly folded in the right-handed 3_{10} -helix. This 3D-structural preference results in a marked amphiphilicity for these peptides (Fig. 1). Surprisingly, the membrane activities of the two analogs incorporating a

second C^α-tetrasubstituted α-amino acid (either at position 3 or 4) are quite low (Fig. 2). We hypothesize that the helical forms of these two peptides would be too rigidified to allow formation of the (usually self-associated) species responsible for membrane permeabilization.

Antiviral activity assays are currently in progress.

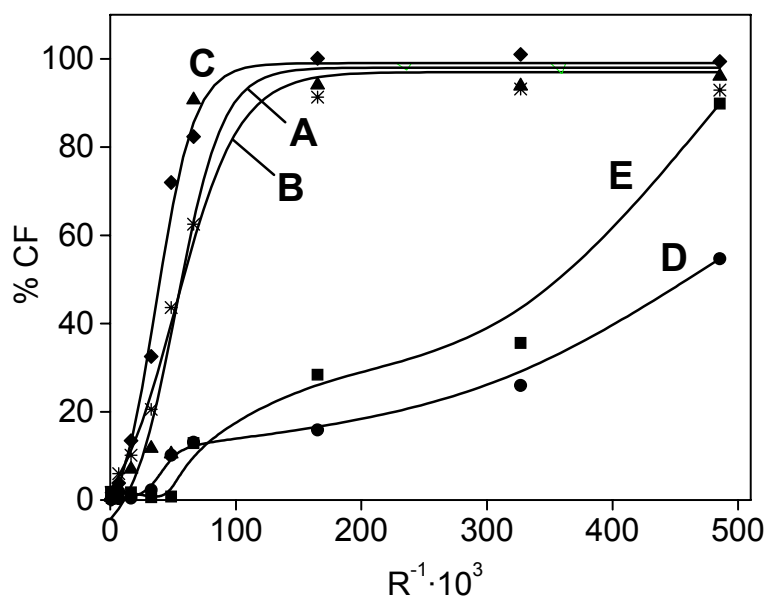


Fig. 2. Peptide-induced carboxyfluorescein (CF) leakage at 20 min for different ratios $R^{-1} = [\text{peptide}]/[\text{lipid}]$ from egg phosphatidylcholine/cholesterol (70:30) unilamellar vesicles: (A) natural halovir A sequence; (B) [Leu⁶-OMe] synthetic precursor; (C) trichogin GA IV (our standard lipopeptaibol antibiotic); (D) [(αMe)Leu³, Leu⁶-OMe] analog; and (E) [(αMe)Val⁴, Leu⁶-OMe] analog.

References

1. Rowley, D. C., Kelly, S., Kauffman, C. A., Jensen, P. R. and Fenical, W. *Bioorg. Med. Chem.* **11**, 4263-4274 (2003).
2. Rowley, D. C., Kelly, S., Jensen, P. R. and Fenical, W. *Bioorg. Med. Chem.* **12**, 4929-4936 (2004).

Total Synthesis in Solution and Preliminary Conformational Analysis of TOAC-Labeled Alamethicin F50/5 Analogs

Micha Jost, Cristina Peggion, Fernando Formaggio and Claudio Toniolo

Department of Chemistry, University of Padova, 35131 Padova, Italy

Introduction

Alamethicin, the most extensively investigated long peptaibol, is known to generate voltage-dependent pores in the biomembranes. Numerous details of its mechanism of membrane permeability are still under debate and several, more or less convincing, models have been postulated. The primary structure of one of the most important members of the *neutral* class of alamethicins (F50/5) is shown in the first line below:

1	5	10	15	19
Ac-Aib-Pro-Aib-Ala-Aib-Ala-Gln-Aib-Val-Aib-Gly-Leu-Aib-Pro-Val-Aib-Aib-Gln-Gln-Fol				
Ac- TOAC -Pro-Aib-Ala-Aib-Ala-Glu(OMe)-Aib-Val-Aib-Gly-Leu-Aib-Pro-Val-Aib-Aib-Glu(OMe)-Glu(OMe)-Fol				
Ac-Aib-Pro-Aib-Ala-Aib-Ala-Glu(OMe)- TOAC -Val-Aib-Gly-Leu-Aib-Pro-Val-Aib-Aib-Glu(OMe)-Glu(OMe)-Fol				
Ac-Aib-Pro-Aib-Ala-Aib-Ala-Glu(OMe)-Aib-Val-Aib-Gly-Leu-Aib-Pro-Val- TOAC -Aib-Glu(OMe)-Glu(OMe)-Fol				
Ac- TOAC -Pro-Aib-Ala-Aib-Ala-Glu(OMe)-Aib-Val-Aib-Gly-Leu-Aib-Pro-Val- TOAC -Aib-Glu(OMe)-Glu(OMe)-Fol				

(TOAC is 2,2,6,6-tetramethylpiperidin-1-oxyl-4-amino-4-carboxylic acid; Fol is the 1,2-aminoalcohol phenylalaninol).

While it is easy to covalently label the chromatographically purified, naturally occurring, alamethicin F50/5 at the C-terminus (on the primary alcoholic function), any N-terminal or C-terminal modification of the sequence requires the total synthesis of the peptaibol.

Results and Discussion

We have recently reported the total syntheses in solution of this terminally blocked, 19-mer peptaibol and its [Glu(OMe)^{7,18,19}] analog by an easy tunable segment condensation approach [1]. In this work we have extended our research to the syntheses of four analogs, three mono-labeled with the stable free radical TOAC residue at either position 1, 8 or 16, and one bis-labeled at positions 1 and 16 (the corresponding four amino acid sequences are shown above).

A preliminary conformational analysis, performed by FT-IR absorption and CD (Fig. 1) techniques indicates that replacement of the Aib residues with TOAC, another member of the class of C^α-tetrasubstituted α-amino acids, does not affect the overall alamethicin helical structure.

In addition, replacement of the Aib residues with TOAC may even be beneficial to the alamethicin ability to modify the permeability of lipid double layers (Fig. 2).

An EPR investigation of the TOAC-containing alamethicin analogs in a membrane environment is currently under way.

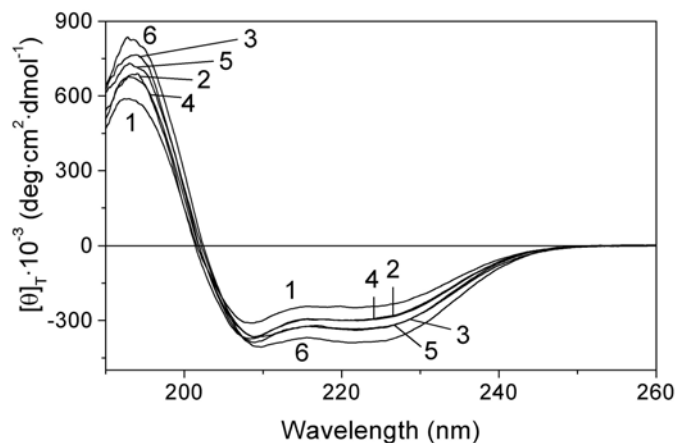


Fig.1. Far-UV CD spectra of alamethicin F50/5 (1), the $[Glu(OMe)^{7,8,19}]$ analog (2), the $[TOAC^I, Glu(OMe)^{7,8,19}]$ analog (3), the $[TOAC^8, Glu(OMe)^{7,8,19}]$ analog (4), the $[TOAC^{I6}, Glu(OMe)^{7,8,19}]$ analog (5), and the $[TOAC^{I,16}, Glu(OMe)^{7,8,19}]$ analog (6) in MeOH solution. Peptide concentration: 5×10^{-4} M.

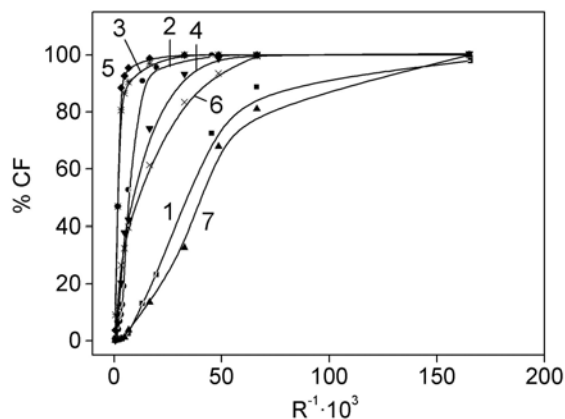


Fig. 2. Peptide-induced carboxyfluorescein (CF) leakage at 20 min for different ratios $R^{-1} = [\text{peptide}]/[\text{lipid}]$ from egg phosphatidylcholine/cholesterol (70:30) unilamellar vesicles: (1) alamethicin F50/5, (2) $[Glu(OMe)^{7,8,19}]$ analog, (3) $[TOAC^I, Glu(OMe)^{7,8,19}]$ analog, (4) $[TOAC^8, Glu(OMe)^{7,8,19}]$ analog, (5) $[TOAC^{I6}, Glu(OMe)^{7,8,19}]$ analog, (6) $[TOAC^{I,16}, Glu(OMe)^{7,8,19}]$ analog, and (7) trichogin GA IV (our standard lipopeptaibol antibiotic).

Acknowledgments

The financial support of MIUR (Italy) through a PRIN 2003 grant is gratefully acknowledged.

References

1. Peggion, C., Coin, I. and Toniolo, C. *Biopolymers (Peptide Sci.)* **76**, 485-493 (2004).

A Lipid Monolayer Made Permeable to Tl(I) Ions by the Lipopeptaibol Trichogin GA IV

Chiara Baldini¹, Cristina Peggion¹, Ester Falletta², Maria Rosa Moncelli², Rolando Guidelli² and Claudio Toniolo¹

¹Department of Chemistry, University of Padova, 35131 Padova, Italy; ²Department of Chemistry, University of Firenze, 50019 Sesto Fiorentino, Italy

Introduction

Trichogin GA IV [1], isolated from the soil fungus *Trichoderma longibrachiatum*, is one of the members of the family of peptaibols (antibiotic peptides containing Aib residues and with a C-terminal 1,2-amino alcohol) [2]. Its amino acid sequence is as follows:

n-Oct-Aib¹-Gly-Leu-Aib-Gly-Gly-Leu-Aib-Gly-Ile¹⁰-Lol
(*n*-Oct, *n*-octanoyl; Lol, leucinol)

Trichogin displays a number of characteristics that are unique with respect to the other members of its family. It is one of the peptaibols with the shortest sequence (10 amino acid residues) and does not contain any Pro or any clearly hydrophilic residue. In addition, it is blocked at the N-terminus by a fatty acyl (*n*-octanoyl) group. For the latter reason trichogin is classified as the prototype of a new sub-family of peptaibols, termed lipopeptaibols [3].

All peptaibols, the 3D-structures of which are highly helical (due to the significantly large presence of the helicogenic Aib) and somewhat amphiphilic, exhibit membrane-modifying properties. In particular, the long-sequence members, such as alamethicin (30 ~Å), are known to produce voltage-gated channels in planar membranes through which water molecules and ions may easily pass according to a "barrel-stave" mechanism. Surprisingly, despite its short main-chain length (~16 Å), trichogin GA IV too exhibits membrane modifying properties on liposomes. Clearly, trichogin is too short to fully span the membrane and its mechanism of action must be different, at least in part, from that displayed by the long peptaibols.

Results and Discussion

Since the thickness of a lipid monolayer (~20 Å) matches the main-chain length of trichogin, we planned to study this peptaibol in a dioleoylphosphatidylcholine (DOPC) monolayer self-assembled on a hanging mercury drop electrode. This simple membrane model has been well characterized [4-6]. Incorporating trichogin in DOPC-coated mercury electrode from its methanol solution in aqueous 0.1M KCl increases the capacity of the monolayer throughout the potential range of stability of the film, while leaving its resistance practically unaltered. This result indicates that inorganic ions can move back and forth within the monolayer made permeable by this peptaibol, but cannot be accommodated on its metal side. A broad hump in the *i*/A vs. *E*/V curve at about -0.900 V vs. Ag/AgCl (0.1 M KCl) (Fig. 1) denotes a conformational change of trichogin. The lipid monolayer, which is not permeable to Tl(I) ions in the absence of trichogin, gives rise to a well-defined cyclic voltammogram due to the Tl(I) ⇌ Tl(Hg) couple in its presence, thus confirming the membrane modifying properties of this lipopeptaibol (Fig. 2).

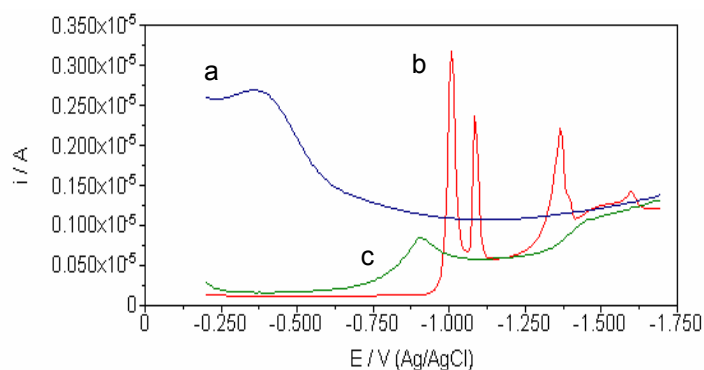


Fig. 1. AC voltammograms of bare (a) and DOPC-coated (b) mercury in contact with a 0.1M KCl aqueous solution. Curve (c) differs from curve (b) by the presence of the peptaibol trichogin incorporated in the DOPC monolayer.

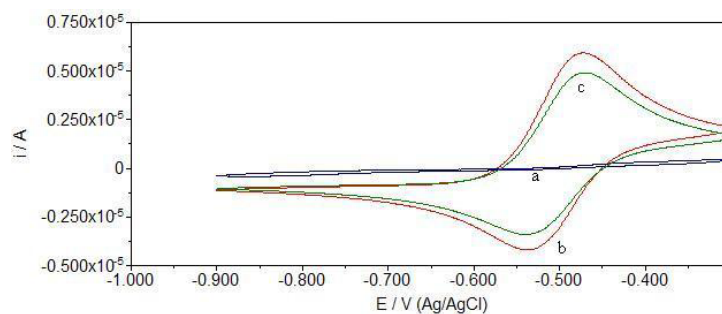


Fig. 2. Cyclic voltammogram of a mercury-supported DOPC monolayer in contact with an aqueous solution of $4 \times 10^{-4} M$ Tl^+ , both in the absence (a) and in the presence (c) of the peptaibol trichogin incorporated in the monolayer. Curve (b) is the cyclic voltammogram of Tl^+ ion on a bare mercury electrode.

Acknowledgments

The financial support of Cassa di Risparmio di Firenze through the PROMELAB Project and of MIUR (Italy) through the PRIN 2002 and PRIN 2003 grants are gratefully acknowledged.

References

1. Peggion, C., Formaggio, F., Crisma, M., Epand, R. F., Epand, R. M. and Toniolo, C. *J. Peptide Sci.* **9**, 679-689 (2003).
2. Benedetti, E., Bavoso, A., Di Blasio, B., Pavone, V., Pedone, C., Toniolo, C. and Bonora, G. M. *Proc. Natl. Acad. Sci. USA* **79**, 7951-7954 (1982).
3. Toniolo, C., Crisma, M., Formaggio, F., Peggion, C., Epand, R. F. and Epand, R. M. *Cell. Mol. Life Sci.* **58**, 1179-1188 (2001).
4. Moncelli, M. R., Becucci, L. and Guidelli, R. *Biophys. J.* **66**, 1969-1980 (1994).
5. Moncelli, M. R. and Becucci, L. *J. Electroanal. Chem.* **433**, 91-96 (1997).
6. Whitehouse, C., O'Flanagan, R., Lindholm-Sethson, B., Movaghar, B. and Nelson, A. *Langmuir* **20**, 136-144 (2004).

A Universal Influenza B Peptide Vaccine

Paolo Ingallinella¹, Elisabetta Bianchi¹, Xiaoping Liang², Marco Finotto¹, Michael Chastain², Jiang Fan², Tong-Ming Fu², Hong Chang Song², Melanie Horton², Daniel Freed², Walter Manger², Emily Wen², Li Shi², Roxana Ionescu², Colleen Price², Marc Wenger², Emilio Emini², Riccardo Cortese¹, Gennaro Ciliberto¹, John Shiver² and Antonello Pessi¹

¹IRBM P. Angeletti, Pomezia (Rome), Italy; ²Merck Research Laboratories, West Point, PA, USA

Introduction

The conventional, inactivated influenza vaccines currently in use contain an influenza A virus H1N1, an influenza A virus H3N2, and an influenza B virus strain [1]. The immunological targets of the vaccine are the envelope proteins, hemagglutinin (HA) and neuraminidase (NA). Because HA and NA constantly undergo point mutations to evade the immune system (antigenic drift), the vaccine formulation needs to be updated each year, and the efficacy of the vaccine depends on the degree of antigenic “match” between the strains used for vaccine preparation and those circulating, at a later time, in the population. The development of a universal vaccine providing broadly cross-reactive protection, without requiring yearly update, would therefore solve a major medical need. Here we describe the design and validation in an animal model of a universal subunit peptide vaccine for influenza B.

Results and Discussion

Our vaccine candidate is a peptide, corresponding to the consensus sequence of the maturational cleavage site of the hemagglutinin precursor, HA₀. The cleavage site is highly solvent exposed, and is conserved in all the available sequences of influenza B virus, as well as within each subtype of influenza A virus (Table 1).

Table 1. Solvent-exposed region of the influenza A and B maturational cleavage site

Virus/subtype	Strain	Peptide sequence ^a
A/H3/HA ₀	Consensus	NVPEKQTR↓GIFGAIAGFIE
A/H1/HA ₀	Consensus	NIPSIQSR↓GLFGAIAGFIE
B/HA ₀	Consensus ^b	PAKLLKER↓GFFGAIAGFLE

^acleavage occurs at positions indicated by arrow. ^bVictoria and Yamagata lineages.

Importantly, the sequence is conserved for both influenza B lineages, Victoria and Yamagata, which co-circulate but are not immunologically cross-reactive.

The chosen peptide epitope was conjugated to the Outer Membrane Protein Complex (OMPC) of *Neisseria meningitidis*, a carrier widely used in human vaccines. For this purpose, an N-terminal bromoacetyl-precursor of the peptide B/HA₀ was synthesized by standard Fmoc-SPPS, while OMPC was derivatized with N-acetyl homocysteine thiolactone to introduce a bromoacetyl-reactive thiol group.

Chemoselective ligation between the bromoacetyl-peptide precursor and thiolated-OMPC produced the B/HA₀-OMPC conjugate with an excellent loading of 6500 mol peptide/mol OMPC.

Vaccination of mice with the B/HA₀-OMPC conjugate showed that the vaccine was highly immunogenic, with 1 µg of antigen producing ELISA titers of 10⁶. Upon challenge with LD₉₀ of mouse-adapted influenza B/Ann Arbor/4/55 virus all the vaccinated mice survived, compared with the expected 10% of the control group (Fig. 1a). In addition, significantly lower weight loss was observed in the vaccinated mice, indicating that the vaccine also provided some protection from morbidity (Fig. 1b). The same protection was observed for the other influenza B lineages [2].

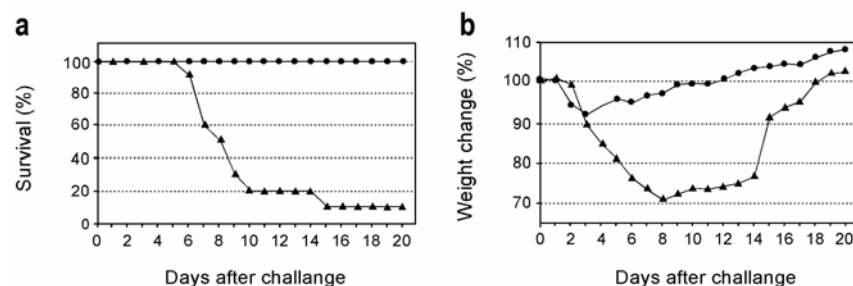


Fig. 1. Protection of B/HA₀-OMPC vaccinated mice against lethal challenge with mouse-adapted influenza B virus. (●) vaccinated group; (▲) control (OMPC vaccinated) group.

Passive transfer of immune serum or mAbs against B/HA₀ was able to protect mice against viral challenge, showing that protection was mediated by antibodies.

When we mapped the epitope of the protective anti-B/HA₀ mAbs, using a panel of terminally truncated peptides and alanine-scanning mutants, we found that they recognized a common, immunodominant epitope. The epitope was localized across the cleavage site, with only three critical residues: R8 at the P1 position of the scissile bond, and F11, F17 in the fusion peptide moiety.

Since this region of the cleavage site is also conserved in both subtypes of influenza A (Table 1) we tried the same approach for this virus. Vaccination was indeed effective in reducing mortality, and to a lower extent morbidity, but the protection was much less robust than for influenza B [2], although still an improvement over the original observations with unconjugated A/HA₀ peptides [3].

In conclusion, we have shown that a peptide conjugate vaccine based on the maturational cleavage site of the viral hemagglutinin can confer broadly cross-reactive protection against influenza B virus. In addition, we presented preliminary evidence that this approach can be extended to the influenza A virus. We believe that this is a promising step towards the development of a universal influenza vaccine, effective against all circulating strains of both influenza A and B viruses and not requiring continuous manufacturing update.

References

1. Palese, P., *et al. J. Clin. Invest.* **110**, 9-13 (2002).
2. Bianchi, E., *et al. J. Virol.* **79**, 7380-7388 (2005).
3. Horvath, A., *et al. Immunol. Lett.* **60**, 127-136 (1998).

Design, Synthesis and Analysis of a Cysteine-Deleted Analog of the Antimicrobial Peptide Tachyplesin-I

Deborah L. Heyl¹, Kiran Kumar Gottipati¹, Sreeja Sreekumar¹, Sathan Thennarasu² and Ayyalusamy Ramamoorthy²

¹*Department of Chemistry, Eastern Michigan University, Ypsilanti, MI 48197;* ²*Department of Chemistry, The University of Michigan, Ann Arbor, MI 48108 USA*

Introduction

Tachyplesin I (KWCFRVCYRGICYRRCR-NH₂) is a cyclic broad-spectrum antimicrobial peptide forming a rigid, antiparallel β -sheet structure because of two intramolecular disulfide linkages [1,2]. It is believed to act through a detergent-like mechanism due to amphipathic properties, permeabilizing bacterial membranes. The positive charge of the arginine and lysine residues confer specificity for bacterial membranes, as they are attracted to negatively charged phosphatidyl esters (mammalian membranes contain more positively charged or zwitterionic phospholipids). The hydrophobic part allows for penetration of the lipid membrane, disrupting membrane structure by creating holes and leading to cell death. Bacteria should not develop resistance to drugs that work through this mechanism.

To better understand the role of Cys residues in Tachyplesin I and to search for potent analogs having improved antimicrobial activity and lower cytotoxicity, we synthesized an analog of Tachyplesin I, CDT-I, in which all four cysteines were deleted (KWFRVYRGIIYRRR-NH₂). We investigated the antimicrobial activity of CDT-I, and its ability to permeabilize the outer membrane of Gram-negative and positive bacteria and to interact with model membranes. To obtain information on the lipid specificity, we measured the binding energy and the binding affinity using fluorimetry experiments. CD studies provided information on secondary structure.

Results and Discussion

CDT-I shows antimicrobial activity against a variety of bacteria (Table 1) and permeabilizes outer membrane at micromolar concentrations. Since CDT-I is rich in basic amino acids, the antibacterial activity is likely to stem from the peptide's affinity for negatively charged cell surface components such as lipopolysaccharides (LPS) on the outer membrane of Gram-negative bacteria and lipoteichoic acids in Gram-positive bacteria [3]. Our results also indicate that *in vitro* antimicrobial activity correlates with the binding enthalpy and affinity for anionic phospholipids.

CDT-I binds to both neutral and acidic liposomes but with varying affinities, showing much higher affinity for acidic membranes. The partition coefficients derived for different acidic liposomes suggest that CDT-I binding to liposomes is modulated by the lipid composition.

Circular dichroism measurements (Fig. 1) indicate that CDT-I adopts a largely unordered conformation upon binding to neutral membranes. In the presence of neutral POPC/CHL (7:3) liposomes, the CD spectrum of CDT-I showed no characteristic features attributable to any defined peptide secondary structure, which might suggest that the peptide binds weakly to the membrane and that the membrane induces structural disorder upon binding. However, in the presence of anionic POPC/LPS (7:3) liposomes, CDT-I gave a sharp negative band at ~ 204 nm and a weak broad band with a minimum at ~ 215 - 219 nm. These features clearly indicate

Table 1. Antibacterial activity of CDT-I against different microbes ($OD_{600} = 0.002$)

Minimum Inhibitory Concentration ($\mu\text{g/mL}$)				
<i>E. coli</i>	<i>B. subtilis</i>	<i>P. aeruginosa</i>	<i>P. gingivalis</i>	<i>L. monocytogenes</i>
6.25	>200	12.5	3.13	12.5

conformational changes in CDT-I upon partitioning into POPC/LPS (7:3) liposomes and the induction of a more ordered structure, perhaps a combination of extended and β -structures. The CD profiles of CDT-I also showed changes in the backbone conformation of the peptide upon binding to anionic POPC/POPG (7:3) and POPE/POPG (7:3) liposomes.

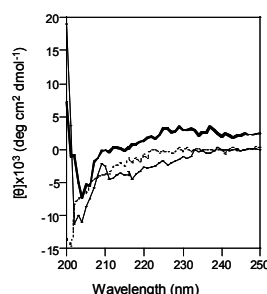


Fig. 1. CD spectra of CDT-I ($34.5 \mu\text{M}$) in buffer and in the presence of lipid vesicles ($400 \mu\text{M}$). Spectra were recorded in 10 mM HEPES, 150 mM NaCl, 2 mM EDTA, pH 7.4 (top) and in the presence of 7:3 POPC/CHL (middle) or 7:3 POPC/LPS (bottom).

Previous studies have confirmed that a definite secondary structure may not be crucial for antimicrobial activity, but that hydrophobicity, net charge, and distribution pattern of amino acids along the peptide chain are more important determinants [4,5]. Our results suggest that the cysteine residues of Tachyplesin-I do not have any functional role and that the β -sheet conformation is not required for antimicrobial activity.

Acknowledgments

The work was funded by an NSF grant to A Ramamoorthy and a Graduate Research Support Fund and Seller's Fund grant to D. Heyl.

References

1. Nakamura, T., Furunaka, H., Miyata, T., Tokunaga, F., Muta, T., Iwanaga, S., Niwa, M., Takao, T. and Shimonishi, Y. *J. Biol. Chem.* **263**, 16709-16713 (1988).
2. Miyata, T., Tokunaga, F., Yoneya, T., Yoshikawa, K., Iwanaga, S., Niwa, M., Takao, T. and Shimonishi, Y. *J. Biochem. (Tokyo)* **106**, 663-668 (1989).
3. Scott, M. G., Gold, M. R. and Hancock, R. E. W. *Infect. Immun.* **67**, 6445-6453 (1999).
4. Tachi, T., Epand, R. F., Epand, R. M. and Matsuzaki, K. *Biochemistry* **41**, 10723-10731 (2002).
5. Lee, K. H. *Curr. Pharm. Design* **8**, 795-813 (2002).

Progress toward Total Solid-Phase Synthesis of Cyclic Lipodepsipeptide Antibiotic Fusaricidin A

**Rekha Rawat, Ralph T. Martello, Pierre Y. Jean-Charles and Predrag
Cudic**

*Department of Chemistry and Biochemistry, Charles E. Schmidt College of Science, Florida
Atlantic University, Boca Raton, FL 33431-0991, USA*

Introduction

Cyclic depsipeptides have been found in many natural organisms such as fungi, bacteria and marine organisms. It is very well known that these natural products and their derivatives exhibit a variety of biological activities, including insecticidal, antiviral, antimicrobial, anti-tumor, tumor-promotive, anti-inflammatory, and immunosuppressive actions [1]. Occurrence of multidrug-resistant pathogens and urgent demands for new and more potent antimicrobials place this class of natural products in the center of the attention for the development of new antibacterial agents. Some of those compounds, such as cyclic lipodepsipeptides daptomycin (Cubist Pharmaceuticals, Inc.) and ramoplanin (Genome Therapeutics Corporation), are among the agents in advanced stages of clinical development for eradication of vancomycin-resistant *Enterococcus faecium* (VRE) and methicillin-resistant *Staphylococcus aureus* (MRSA). Other promising candidate for reverting multi-drug resistant bacteria is naturally occurring cyclic depsipeptide antibiotic fusaricidin A. Fusaricidin A was isolated in 1996 by Y. Kajimura *et al.* from *Bacillus polymyxa* strain KT-8 [2]. Its simple peptide sequence (L-Thr¹-D-Val²-L-Val³-D-allo-Thr⁴-D-Asn⁵-D-Ala⁶) has strong activity against various kinds of fungi and Gram-positive bacteria including *S. aureus*, and indications that it may be active against MRSA make this natural product particularly interesting as a lead compound for development of new antimicrobial agents. The total solid-phase syntheses of fusaricidin A represents the first step toward a complete exploitation of fusaricidin A's antibacterial potentials.

Results and Discussion

Our strategy for the solid-phase synthesis of lipodepsipeptide antibiotic fusaricidin A involves side-chain attachment and on-resin head-to-tail cyclization. To prove this concept we have synthesized cyclic fusaricidin A's analog **1** (Fig. 1). Peptide analog **1** differs from the natural compound only in the lipid tail part. Since in fusaricidin A 15-guanidino-3-hydroxypentadecanoic acid is attached *via* an amide bond to the *N*-terminal L-Thr α -amino group we decided to couple the closest analog to this acid, 12-aminododecanoic acid, and convert it on the solid support into a more desired guanidinium form. In order to use on-resin head-to-tail cyclization strategy, Fmoc-D-Asp-OAllyl was attached *via* its side chain to Rink MBHA amide resins (substitution level 0.6 mmol/mg) using DIC/DMAP procedure. Standard Fmoc-chemistry was used throughout. The last amino acid in the linear peptide sequence, Fmoc-D-Ala⁸, was coupled *via* an ester bond to the hydroxyl group of Trt-L-Thr³ residue using DIC/DMAP coupling methodology previously developed by R. Rugiera *et al.* [3]. The efficiency of this coupling was monitored by MALDI-TOF MS analysis. After selective removal of Fmoc and Allyl protective groups, the linear peptide was cyclized between D-Ala⁸ and D-Asn⁷ residues with an excess of PyBOP/HOBt/DIEA mixture.

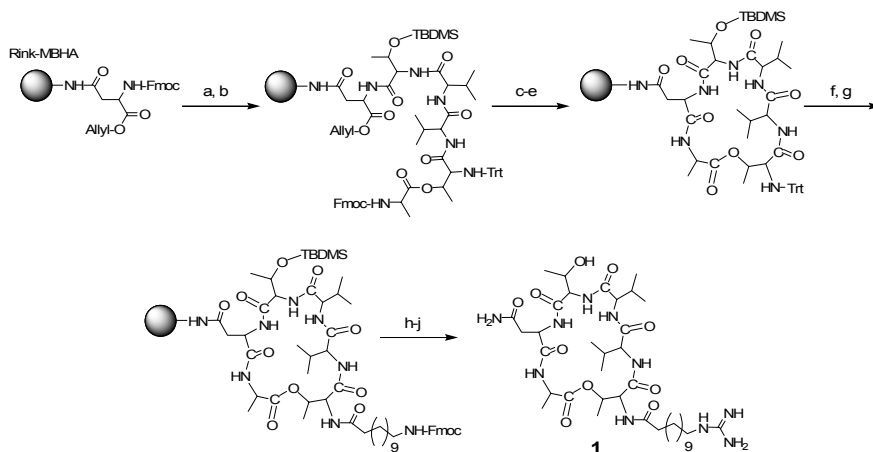


Fig. 1. Solid-phase synthesis of fusaricidin A analog.

a) Standard Fmoc-SPPS, b) DIC/DMAP, c) $\text{Pd}(\text{PPh}_3)_4/\text{PhSiH}_3/\text{CH}_2\text{Cl}_2$, d) 20% piperidine/DMF, e) PyBOP/HOBt/DIEA, f) 0.2% TFA/ CH_2Cl_2 , g) PyBOP/HOBt/DIEA, h) 20% piperidine/DMF, i) 1H-pyrazole-1-carboxamide/DIEA, j) 95% TFA/thioanisole/water.

Trityl (Trt) protecting group was then selectively removed from N^α -L-Thr³ residue with 0.2% TFA in CH_2Cl_2 in the presence of TBDMS group used for the protection of D-allo-Thr⁶ side-chain hydroxyl group. Fmoc-protected 12-aminododecanoic acid was attached using standard PyBOP/HOBt coupling protocol. Conversion of lipid tail's amino into desired guanidinium group was achieved by removal of Fmoc-protective group using standard piperidine deprotection protocol followed by treatment of the peptidyl-resin with 1H-pyrazole-1-carboxamide/DIEA/DMF mixture [4]. Final deprotection and cleavage of the cyclic lipodepsipeptide **1** from the resins was carried out with TFA/ H_2O /thioanisole (95:2.5:2.5) mixture. The final product was analyzed by HPLC and MALDI-TOF MS [5]. With the synthesis of fusaricidin A's analog **6** we demonstrated feasibility of our synthetic approach that includes resin attachment of the first amino acid *via* side chain, successful use of combination of four quasi-orthogonal removable protecting groups, stepwise solid-phase synthesis of linear peptide analog, and on-resin head-to-tail cyclization. The total solid-phase synthesis of naturally occurring lipodepsipeptide antibiotic fusaricidin A is in progress and will be reported elsewhere.

Acknowledgments

The work was funded by NIH SCORE grant to P. Cudic.

References

1. Sarabia, F., *et al.* *Curr. Med. Chem.* **11**, 1309-1332 (2004).
2. Kajimura, Y. and Kaneda, M. *J. Antibiot.* **49**, 129-135 (1996).
3. Kuisle, O., Quinoa, E. and Riguera, R. *J. Org. Chem.* **64**, 8063-8075 (1999).
4. Bertranovic, M. S., Wu, Y. and Matsueda, G. R. *J. Org. Chem.* **57**, 2497-2502 (1992).
5. $M/z=826.0074$; $t_R=9.446$ min., analytical HPLC, Vydac C4 (4.5 mm x 150 mm), mobile phase A: $\text{H}_2\text{O}/\text{TFA}$ (99.9/0.1, v/v), mobile phase B: $\text{CH}_3\text{CN}/\text{TFA}$ (99.9/0.1, v/v).

Biological and Structural Characterization of a New Linear Gomesin Analog

Marcos A. Fázio¹, Laurence Jouvensal², Françoise Vovelle², Philippe Bulet³, M. Terêsa M. Miranda⁴, Sirlei Daffre⁵ and Antonio Miranda¹

¹Dept. of Biophysics, Federal University of São Paulo, 04044-020, São Paulo, Brazil; ²Centre de Biophysique Moléculaire, 45071 Orléans cedex 2, France; ³Atheris Laboratories, CH-1233 Bernex, Geneva, Switzerland; ⁴Dept. of Biochemistry, IQ-USP, 05509-800, São Paulo, Brazil; ⁵Dept. of Parasitology, ICB-USP, 05509-800, São Paulo, Brazil

Introduction

Gomesin (*Gm*) is a potent antimicrobial peptide isolated from the hemocytes of the Brazilian tarantula spider *Acanthoscurria gomesiana*. This peptide contains four cysteines involved in two intramolecular disulfide bridges Cys^{2,15} and Cys^{6,11}, a pyroglutamic acid (Z) as N-terminal residue, and an amidated C-terminal carboxyl group [1] as shown in Figure 1. The intramolecular disulfide bridges help the molecule to fold in a β -hairpin structure [2] that results in a high stability in human plasma. In this work, we described the properties, biological activities, and the NMR data obtained with the new linear gomesin analog [D-Thr^{2,6,11,15}, Pro⁹]-D-*Gm*. This peptide revealed similar antimicrobial activities and equipotent resistance to proteolysis, while it was less hemolytic than *Gm*. Furthermore, it showed to be easier to synthesize.



Fig. 1. Sequences of gomesin and of the synthetic linear analog. Lower case letters mean D amino acid residue.

Results and Discussion

The D-linear *Gm* analog was designed by replacing the four cysteine residues by threonines. To mimic the turn presented in the middle of the *Gm* molecule, we also replaced Gln⁹ by a proline residue. Peptides were synthesized by SPPS using the *t*-Boc strategy on a MBHA-resin. They were purified by RP-HPLC and characterized by AAA, LC/ESI-MS and CE. Antimicrobial activities were evaluated by liquid growth inhibition assays against *Staphylococcus aureus* (Gram positive bacteria), *Escherichia coli* SBS 363 (Gram negative bacteria), and the yeast *Candida albicans* MDM 8. The minimal inhibitory concentrations (MICs) are expressed as the [a]-[b] interval of concentrations, where [a] is the highest concentration tested at which the microorganisms are growing, and [b] is the lowest concentration that causes 100% growth inhibition. As summarized in Table 1, the linear analog was four-fold less active against bacteria strains and ten-fold less hemolytic than the wild-type *Gm*. Proteolytic assays in the presence of human plasma at 37°C revealed that both peptides showed the same resistance to the plasmatic proteolytic enzymes (around 85% intact after 24hrs incubation). CD studies were carried out in different environments, showing that in 50% TFE and in SDS micelles, the analog [D-Thr^{2,6,11,15}, Pro⁹]-D-*Gm* displayed α -helix-like spectra with low intensities and blue-shifted bands that suggest a β -turn structure [3] (data not shown). ¹H-NMR

Table 1. Antimicrobial and hemolytic activities of the peptides

Peptide	Minimum Inhibitory Concentration (μM)			Hemolysis (%) ^c
	<i>S. aureus</i> ^a	<i>E. coli</i> ^a	<i>C. albicans</i> ^b	
Gomesin (<i>Gm</i>)	1.28-2.56	0.32-0.64	0.32-0.64	27.5 \pm 2.1
[D-Thr ^{2,6,11,15} ,Pro ⁹]-D- <i>Gm</i>	5.12-10.25	1.28-2.56	0.32-0.64	2.7 \pm 1.2

^aPB (217 mOsM; 1.0 g Peptone + 86 mM NaCl in 100 mL of H₂O).

^bPDB (79 mOsM; 1.2 g potato dextrose in 100 mL of H₂O).

^cDetermined at a peptide concentration of 10 μM in fresh washed human erythrocytes.

spectra (NOESY, clean-TOCSY, DQF-COSY) were recorded at 600 MHz on a 1.4 mM [D-Thr^{2,6,11,15}, Pro⁹]-D-*Gm* sample dissolved in 200 mM SDS micelles at pH 4.6, temperature 293°K. Dihedral angles and distance restraints obtained from measured NMR parameters were used in structural calculations within ARIA 1.1 to determine the conformation of the peptide. An ensemble of 20 models were selected to represent the structure of [D-Thr^{2,6,11,15}, Pro⁹]-D-*Gm* in SDS micelles. As native *Gm*, the peptide folds in a slightly twisted hairpin (Fig. 2). The secondary structure elements are well defined, either the β -sheet or the turn. The former is a little shorter than in *Gm*, due to the absence of the extremity-maintaining Cys^{2,15} disulfide bridge. The amino acid side chains positions are different (e.g., both tyrosine rings), most likely due to the interaction with the micelles. Whereas both peptides exhibit comparable hydrophobic potentials at their surfaces, the packing of the charged residues appears stronger in [D-Thr^{2,6,11,15}, Pro⁹]-D-*Gm*, which probably allows a better interaction with the polar heads of SDS, and leads to a slightly more positive electrostatic potential at the surface (302 vs. 263 kcal.mol⁻¹; data not shown).

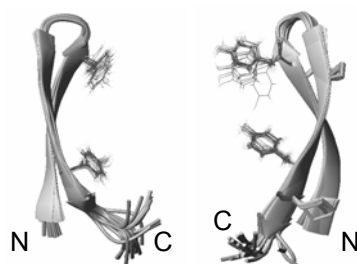


Fig. 2. Superposition of ribbon representations of the 20 models representing the structures of [D-Thr^{2,6,11,15}, Pro⁹]-D-*Gm* in SDS micelles (left) and of the wild-type *Gm* in water (right).

Acknowledgments

This work was supported by grants and fellowships from CNPq and FAPESP.

References

1. Silva Jr., P. I., Daffre, S. and Bulet, P. *J. Biol. Chem.* **275**, 33464-33470 (2000).
2. Mandard, N., Bulet, P., Caille, A., Daffre, S. and Vovelle, F. *Eur. J. Biochem.* **269**, 1190-1198 (2002).
3. Hollóssi, M., Kovér, M., Holly, S. and Fasman, G. D. *Biopolymers* **26**, 1527- 1553 (1987).

Monomeric Analogs of Halocidin

Xavier Doisy

Department of Chemistry Department, The Royal Veterinary and Agricultural University, DK-1871 Frederiksberg C, Copenhagen, Denmark. Present address: PolyPeptide Laboratories A/S, Herredsvejen 2, 3400 Hillerød, Denmark

Introduction

Resistance in bacteria is becoming a dramatic problem both in community and in hospital environment and there is a great need for new antibiotics with a new mode of action. Antimicrobial peptides belong to such a class, acting by disrupting the bacterial membrane, and are promising candidates.

Halocidin is a heterodimeric antimicrobial peptide isolated from a tunicate, *Halocynthia aurantium*, and is contained in the haemocytes, phagocytic cells considered to be the functional counterparts of the mammalian leukocytes in protochordates. We used as lead structure the most active of the two monomers composing halocidin, an 18 residue amidated peptide **1** with the following sequence: WLNAL⁵LHHGL¹⁰NCAKG¹⁵VLA-NH₂, and determined the role of each amino acid with alanine scanning. The results obtained led to the synthesis of a first generation of analogs with antimicrobial activity. The selectivity of these peptides towards bacterial versus mammalian cells has been explored, as well as the specificity for gram positive (*Staphylococcus aureus* ATCC 25923) versus gram negative bacteria (*Escherichia coli* ATCC 25922). The hydrophobic moment was used to analyze the results.

Results and Discussion

The Ala-scan of peptide **1** gave several indications about the structural requirements for optimal activity: a) an aromatic side chain in position 1; b) a bulky side chain in position 2, 4, 5, and 17; c) a positive charge in position 7 and 14; d) a small aliphatic side chain in position 8; and e) a hydrophilic side chain in position 3 and 11. Finally, the other amino acids should be conserved as their replacement did not yield any substantial gain in activity.

The hydrophobic moment μ_H calculated with the normalized Eisenberg consensus [1], which reflects the amphiphilicity of an α -helical peptide, varied in the same direction, albeit not in the same intensity, as the HPLC retention time for all peptides.

Using the results from the Ala-scan, we synthesized 8 new peptides (**2** to **9**) in which one or several (7) amino acids were replaced (Table 1). The data obtained can be distributed among four groups of two peptides each. The first group includes peptides **2** and **3** displaying a worse MIC and being as or more hemolytic than our reference peptide **1**. In the second group, peptides **5** and **9** had worse MIC values but were less hemolytic than our reference 18-mer **1**. The third group contained two hemolytic peptides, **4** and **6**, with nearly identical or lower MIC values than our reference peptide **1**. The fourth and last group encompasses the most interesting peptides, **7** and **8**. Both are less hemolytic than our reference **1**. The selectivity of peptide **7** for gram positive and gram negative bacteria is the reverse of the parent peptide **1** whereas peptide **8** has better MIC values than our reference **1**.

The hydrophobic moment μ_H and the HPLC retention time for peptides **2**, **3**, and **6** varied in the same direction, albeit not in the same intensity, whereas for peptides

Table 1. Antibacterial and hemolytic activity of the first generation analogs of peptide 1

Peptide	Modification	<i>S. aureus</i> ^a	<i>E. coli</i> ^a	Hemolysis ^b	μH ^c
1		14.7	29.4	5.5%	6.44
2	G ⁹ → L	75.5	>75.5	6.6%	7.02
3	N ³ → L	>81.3	>81.3	43.5%	8.28
4	H ⁷ → K	10.1	10.1	43.6%	5.34
5	H ⁸ → K	36.8	36.8	3.8%	5.34
6	N ¹¹ → K	19.4	19.4	39.8%	5.72
7	H ^{7,8} , N ¹¹ → K	32.0	16.0	2.2%	3.52
8	W ¹ → 2-Nal	10.4	10.4	0%	ND
9	C ¹² → C ^{Acm}	>92.2	>92.2	0%	ND

^aMIC in μg/ml. ^bHemolysis in % for a concentration of 230 μg peptide/ml. ^cHydrophobic moment

4, 5, and 7 the variation was in opposite direction with no correlation with the intensity. These results complement our analysis of the same peptides with GRAVY (Grand Average of Hydropathicity) [2].

Overall, the results obtained from these analogs confirmed the results from the Ala-scan with some additional information. Glycine and cysteine should be conserved in position 9 and 12, respectively, despite a higher hemolytic activity with a hydrophilic side chain in position 12. A hydrophilic amino acid is preferred in position 3 and 11. The side chain should be small in position 11, suggesting serine as a promising candidate. More details were obtained for position 8: a small aliphatic side chain was more active on gram positive bacteria whereas a positively charged side chain was more active on gram negative bacteria. A positive charge in position 7, 8, and 11 was beneficial. Although lysine in position 7 gave good MIC values, the hemolytic activity increased. This is probably correlated with the hydrophobic character of the methylene groups of the side chain. A hydrophilic amino acid is preferred to lysine in position 11. Finally, an aromatic side chain is necessary in position 1 as shown in peptide 8 which displays an overall improvement for both the MIC values and the hemolytic activity due to the incorporation of a non natural aromatic amino acid in position 1: 3-(2-naphthyl)-alanine. We were also able to identify specific positions with an impact on the MIC value of gram positive and/or gram negative bacteria, with or without concomitant influence on the hemolytic activity. The prediction of the additivity of these properties being impossible, we are currently investigating the homo and heterodimerisation of these peptides.

Acknowledgments

Support from the Danish Research Council (grant 9900234) and the Augustinus Foundation are gratefully acknowledged.

References

1. Eisenberg, D. and McLachlan, A. D. *Nature* **319**, 199-203 (1986).
2. Doisy, X., et al. *Org. Biomol. Chem.* **2**, 2757-2762 (2004).

Fragment of Human Lysozyme Conjugated on the N-terminus and Displaying Antibacterial Properties

Xavier Doisy

Chemistry Department, The Royal Veterinary and Agricultural University, DK-1871
Frederiksberg C, Copenhagen, Denmark. Present address: PolyPeptide Laboratories A/S,
Herredsvejen 2, 3400 Hillerød, Denmark

Introduction

Resistance in bacteria is becoming a dramatic problem both in community and in hospital environment and there is a great need for new antibiotics with a new mode of action. Antimicrobial peptides belong to such a class, acting by disrupting the bacterial membrane, and are promising candidates.

Lysozyme is a small sized enzyme (14.4 KDa, 129 amino acids) widely distributed in living organisms and implicated in many biological processes amongst which antimicrobial activity. This activity is due to two different mechanisms: an enzymatic antimicrobial activity targeting gram positive bacteria, and an antimicrobial activity against gram positive and negative bacteria due to a domain located in the loop structure at the upper lip of the enzymatic site. This active helix-loop-helix motif has been obtained by clostripain digestion of lysozyme [1]. The resulting C-terminus nonamer **1** RAWVAWRNR-NH₂ is more active than the N-terminus fragment and displays a higher activity on gram positive bacteria than on gram negative bacteria [2].

Continuing previous studies using this sequence **1** and its reverse sequence **2** RNRWAVWAR-NH₂ as lead structure [3], we have conjugated fatty acids on the N-terminus of these peptides. Their antibacterial activity on gram positive (*S. aureus* ATCC 25923) and gram negative bacteria (*E. coli* ATCC 25922) has been studied.

Results and Discussion

Peptides were manually synthesized by standard SPPS methods using Fmoc chemistry. The resin used was Tentagel S RAM (50 mg, loading 0.24 mmol/g), which upon cleavage yielded the corresponding amidated peptides. The following coupling conditions were used: Fmoc-AA-OH/TBTU/HOBt/DIPEA (3:3:3:4.5) in NMP with double coupling. Cleavage of the peptides from the resin was achieved using TFA/TES/H₂O (95:2.5:2.5) for 2 hrs. The peptides were then precipitated, washed with cold diethyl ether, centrifuged, and the resulting white pellets were lyophilized. The peptides were purified by RP-HPLC, their mass confirmed with MALDI-TOF and LC-MS, and their sequence with amino acid analysis.

The MIC was determined with the broth microdilution assay on *E. coli* and *S. aureus* with ampicillin as internal standard. Triplicate serial twofold dilutions of the peptides were made, ranging from 64 to 2 µg/ml, and assayed on an average bacterial concentration of 4x10⁶ cfu/ml. The MIC values obtained were then corrected with the results from amino acid analysis.

Fatty acid acylation is a common post-translational modification for a wide variety of peptides. One of the major roles of peptide or protein acylation is to increase membrane association. Surprisingly, fatty acid acylation of antimicrobial peptides is quite rare (polymyxins) but it has been shown that synthetic conjugates display improved antimicrobial activity [4,5]. Using **1** and **2** as lead structures, we

Table 1. Antibacterial activity of peptides

Peptide	Sequence	<i>S. aureus</i> ^a	<i>E. coli</i> ^a
1	RAWVAWRNR-NH ₂	>67.8	>67.8
1-deca	deca-RAWVAWRNR-NH ₂	3.0	11.8
1-laur	laur-RAWVAWRNR-NH ₂	4.5	18.1
1-myr	myr-RAWVAWRNR-NH ₂	23.0	11.5
1-palm	palm-RAWVAWRNR-NH ₂	60.2	30.1
1-stea	stea-RAWVAWRNR-NH ₂	21.1	10.6
2	RNRWAVWAR-NH ₂	>83.8	>83.8
2-deca	deca-RNRWAVWAR-NH ₂	4.2	16.6
2-laur	laur-RNRWAVWAR-NH ₂	16.6	8.3
2-myr	myr-RNRWAVWAR-NH ₂	2.8	5.5
2-palm	palm-RNRWAVWAR-NH ₂	26.7	53.4
2-stea	stea-RNRWAVWAR-NH ₂	>40.3	>40.3

^aMIC in µg/ml corrected with amino acid analysis results

conjugated their N-terminus with various fatty acids: decanoic (C10), lauric (C12), myristic (C14), palmitic (C16), and stearic (C18) acid, and the resulting acylated peptides displayed an inverse positive charges distribution (Table 1).

Overall, fatty acids with a short chain produced better MIC values than their superior homologues. This might be the result of their anchoring capacity of the antimicrobial peptide into the bacterial membrane that then forces the peptide to adopt an α -helical structure. The hydrophobic contribution of the shorter fatty acids is therefore better assimilated within the antimicrobial peptide. Longer fatty acids upset too much the amphiphilic properties of these peptides, resulting in poor MIC values. Surprisingly, both gram positive and gram negative bacteria are equally susceptible to fatty acids with short chains. The drastic differences in the structure of their membranes would have suggested otherwise. Further experiments are required to elucidate the details of this improved antibacterial activity. Particular attention will be paid to the self-assembly of these peptides. Other analogs are being synthesized and tested and their activity will be reported in due time.

Acknowledgments

Support from the Danish Research Council (grant 9900234) and the Augustinus Foundation is gratefully acknowledged.

References

1. Ibrahim, H. R., *et al.* *J. Agric. Food Chem.* **44**, 1416-1423 (1996).
2. Ibrahim, H. R., Thomas, U. and Pellegrini, A. *J. Biol. Chem.* **276**, 43767-43774 (2001).
3. Doisy, X., *et al.* In *Peptide Revolution: Genomics, Proteomics and Therapeutics, Proceedings of the 18th APS* (Chorev, M. and Sawyer, T. K., eds.), Springer, Boston, pp 888-889 (2003).
4. Chu-Kung, A. F., *et al.* *Bioconjugate Chem.* **15**, 530-535 (2004).
5. Avrahani, D. and Shai, Y. *J. Biol. Chem.* **279**, 12277-12285 (2004).

Synthesis and Raman Spectroscopy Studies of the Antimicrobial Peptide Cecropin B2

Susanne Ladefoged Nielsen^{1,2} and Xavier Doisy^{2,3}

¹Department of Chemistry, University of Copenhagen, 2100 Copenhagen, Denmark;

²Department of Natural Sciences, Royal Veterinary and Agricultural University, 1871 Frederiksberg, Denmark; ³Present address; PolyPeptide Laboratories A/S, Herredsejvej 2, 3400 Hillerød, Denmark

Introduction

The widespread use of antibiotics for treatment and prevention of bacterial infections has resulted in an alarming increase in multi-resistant pathogenic bacteria. In recent years, much research in this area has focused on naturally occurring antimicrobial peptides, which rapidly kill a wide range of pathogenic microorganisms.

Cecropin B2 (CecB2), an antimicrobial peptide originally isolated from the silkworm *Bombyx mori* [1,2] was synthesized manually using Fmoc chemistry. Raman spectroscopy was used to monitor the secondary structure of the resin bound peptide at every other step of the synthesis. Furthermore, the secondary structure of CecB2 was investigated in solid state, aqueous solution, and 50% aqueous TFE.

The antibacterial activity of CecB2 towards *Staphylococcus aureus* (ATCC 25923) and *Escherichia coli* (ATCC 25922) was determined.

Finally, Raman spectroscopy was used to study the differences between the aforementioned bacterial strains and for probing the interaction of CecB2 with *E. coli* at different concentrations.

Results and Discussion

The peptide was manually synthesized by standard solid phase peptide synthetic methods using Fmoc chemistry. The following protective groups were used on the amino acid side chains: Boc for Trp and Lys, Pbf for Arg, Trt for Asn and His. The resin used was Tentagel S RAM (100 mg, loading 0.24 mmol/g), which upon cleavage yielded the corresponding peptide amidated on the C-terminus. The coupling conditions used were: Fmoc-AA-OH/HOBt/TBTU/DIPEA (3:3:2.9:4.5) in NMP with double coupling. Cleavage of the peptide from the resin was achieved by using TFA/TES/H₂O/Thioanisole (95:2:1.5:1.5).

The MIC was determined with the broth microdilution assay on *S. aureus* (ATCC 25923) and *E. coli* (ATCC 25922) with ampicillin as internal standard. Triplicate serial twofold dilutions of the peptides were made, ranging from 64 µg/ml to 2 µg/ml, and assayed on an average bacterial concentration of 2 x 10⁷ cfu/ml. The Raman spectra were obtained on a Near Infra-Red (NIR) Fourier Transform (FT) Raman spectrometer, Bruker IFS 66, equipped with a FRA 106 Raman module. The light source was a Nd:YAG laser with a wavelength at 1064 nm with a maximum output of 280 mW.

The continuous growth of the peptide during the synthesis was followed by Raman spectroscopy. The formation of the amide I and III bands reflected the secondary structure of CecB2. The bands around 1667 cm⁻¹ and those around 1235 cm⁻¹ gradually increased with the number of amino acids coupled on the resin and were assigned to the amide I band and the amide III band, respectively of random coil conformation. This was confirmed by the amide I band at 1667 cm⁻¹ and the

amide III band at 1244 cm^{-1} of a solid state sample and of a 10% aqueous solution of CecB2. The secondary structure of peptides can be affected by TFE [5]. The influence of TFE on CecB2 in an aqueous solution was spectroscopically studied and the amide I and III bands clearly indicated the change in secondary structure from random coil to α -helix.

Many of the natural antimicrobial peptides isolated from mammalian and insect origin, like CecB2, assume a unique amphiphilic secondary structure upon interaction with the outer phospholipid bilayer of the bacteria.

CecB2 was studied interacting with the bacterial membrane of both Gram-positive (*S. aureus*) and Gram-negative (*E. coli*). *S. aureus* showed a lack of susceptibility toward CecB2, whereas the peptide was found to be highly active against *E. coli* as indicated by the MIC value of $2\text{ }\mu\text{g/ml}$.

The two bacteria strains were successfully examined by Raman spectroscopy and showed each their unique details and characteristics. By comparing the spectra of the two intact strains differences were identified as expected because of the major dissimilarities between their membranes.

The main interspectral variance between the Gram-positive and the Gram-negative bacteria was found to be located in those spectral regions where the various C-H stretching ($3000\text{--}2800\text{ cm}^{-1}$) and bending ($1500\text{--}1400\text{ cm}^{-1}$), and vibrations of the CH_2 groups of the fatty acids were observed.

The band at 1735 cm^{-1} from C=O stretching from the ester groups of the phospholipids appeared as a low intensity band but is of major importance in the understanding of the acting mode of CecB2.

To illustrate the interaction between *E. coli* and CecB2 three different concentrations of this combination, *E. coli*/CecB2 at the MIC value, and two concentrations below, one at 75% of the MIC and one at 50% of the MIC value, were studied by Raman spectroscopy. The spectra of the two interacting species *E.coli*/CecB2 showed interesting variations between the different concentrations. Moreover, to clarify the changes in the spectrum of the bacterial membrane affected by the peptide, the spectrum of the *E. coli* was compared to the one of *E. coli*/CecB2. As expected markedly changes were observed especially in the band of the CH_2 deformation.

The spectrum of *E. coli*/CecB2 at the MIC value consist of separated bands whereas the bands in the spectrum of the two concentrations below the MIC value seemed to merge and shift toward lower wavenumbers, suggesting a deformation of the bacterial membrane at the MIC value.

References

1. Brey, P. T., *et al. Proc. Natl. Acad. Sci. USA* **90**, 6275-6279 (1993).
2. Lee, W. J. and Brey, P. T. *Anal. Biochem.* **217**, 231-235 (1984).
3. Hultmark, D., *et al. Eur. J. Biochem.* **106**, 7-16 (1980).
4. Fink, J., *et al. Int. J. Peptide Prot. Res.* **33**, 412-421 (1989).
5. Fioroni, M., *et al. J. Am. Chem. Soc.* **124**, 7737-7744 (2002).

Alamethicin Interaction with Lipid Membranes: A Spectroscopic Study on Synthetic Analogs

Lorenzo Stella¹, Marcello Burattini¹, Claudia Mazzuca¹, Antonio Palleschi¹, Mariano Venanzi¹, Cristina Peggion² and Claudio Toniolo²

¹Dipartimento di Scienze e Tecnologie Chimiche, Università di Roma Tor Vergata, 00133 Roma, Italy; ²Dipartimento di Chimica, Università di Padova, 35131 Padova, Italy

Introduction

Alamethicin is one of the most extensively studied membrane-active antibiotic peptides. However, several aspects of its mechanism of action are still debated. To investigate the effect of peptide hydrophobicity on its membrane-perturbing activity and to determine the peptide position and orientation inside the lipid bilayer, we have employed synthetic analogs of alamethicin F50/5 (Fig. 1).

Ala-N (F50/5)	Ac-UPUAUAQUVUGLUPVUUQQFol
Ala-S	Ac-UPUAUAQUVUGLUPVUUE(OMe)E(OMe)Fol
Ala-P	Ac-UPUAUA E(OMe)UVUGLUPVUUE(OMe)E(OMe)Fol
F-Ala	Fmc-UPUAUA E(OMe)UVUGLUPVUU E(OMe) E(OMe)Fol
Ala-F	Ac-UPUAUA E(OMe)UVUGLUPVUU E(OMe) E(OMe)Fol-Fmc

Fig. 1. Primary structure of alamethicin F50/5 and the synthetic analogs investigated. Ac is acetyl, U is α -aminoisobutyric acid, E(OMe) is γ -methyl glutamic acid, Fol is phenylalaninol, and Fmc is fluorenyl-9-methylcarbonyl.

Results and Discussion

CD spectra show that the synthetic analogs have the same helical conformation as that of the natural peptide in MeOH solution. However, experiments of peptide-induced leakage in liposomes demonstrate that the membrane perturbing activity of the analogs Ala-S and Ala-P is significantly higher than that of the natural peptide (Table 1). Water-membrane partition experiments show that this difference is mainly due to a higher affinity of Ala-S and Ala-P for the membrane phase, as compared to Ala-N, in agreement with their higher hydrophobicity. Furthermore, the small modifications introduced in the alamethicin sequence have a profound effect on the aggregation behavior in water: Ala-N remains monomeric up to a concentration of 100 μ M, while Ala-S and Ala-P tend to form aggregates, even at 10 μ M. Finally, all peptides display a selectivity for cholesterol-free membranes (Table 1), an important finding in view of potential antibacterial applications.

The two fluorescent analogs (F-Ala and Ala-F), labeled at the N- or at the C-terminus, respectively, have a comparable membrane-lytic activity. However, the fluorescence of F-Ala is significantly affected by membrane binding and can be quenched by doxyl-labeled lipids (Fig. 2), while the emission properties of Ala-F are the same when the peptide is associated to liposomes or when it is in bulk water. This result suggests that, in the absence of a transmembrane potential, alamethicin inserts its N-terminus into the membrane, while the C-terminus remains exposed to the aqueous phase. Furthermore, depth-dependent quenching experiments show that the quenching efficiency of F-Ala fluorescence by liposomes characterized by lipids labeled with a doxyl moiety is almost independent of the position of the quencher along the acyl chain of the lipid (Fig. 2). This finding, together with the results of

polarized ATR-FTIR measurements performed on planar and oriented lipid bilayers, indicates that the peptide orientation with respect to the membrane normal is heterogeneous. Finally, a fluorescence assay based on Förster energy transfer, recently developed by us [1], shows that the peptide binds only to the outer leaflet of the bilayer and that no translocation to the inner leaflet takes place.

Table 1. Membrane perturbing activity of alamethicin analogs

Peptide	50% release concentration (μM) ^a	
	<i>ePC</i> /cholesterol (1:1 mol/mol) liposomes	<i>ePC</i> liposomes
Ala-N	9.3	0.21
Ala-S	1.6	0.033
Ala-P	0.90	0.091

^aPeptide concentration inducing leakage of 50% of the vesicle content in a suspension of liposomes (lipid concentration, 20 μM), 20 minutes after peptide addition. The error is estimated to be 10%. *ePC* is egg yolk phosphatidylcholine.

The observed asymmetry of insertion into the membrane and distribution into the lipid bilayer provide a structural basis for the voltage dependence of the conductance of alamethicin channels. Our findings support the hypothesis that a transmembrane electric field, acting on the dipole moment of the peptide helix, induces its reorientation and a deeper insertion into the bilayer, thus favoring the formation of transmembrane channels.

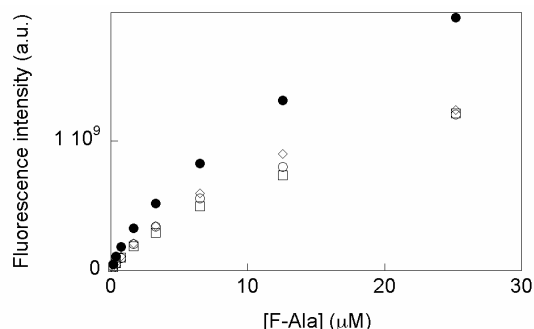


Fig. 2. Quenching of *F*-Ala fluorescence after binding to liposomes containing doxyl-labeled lipids. Results obtained with lipids labeled at positions 5, 10 and 14 along the acyl chain are reported as empty circles, squares and diamonds, respectively. The fluorescence intensity measured with unlabeled liposomes is represented by full circles. *ePC* liposomes, 200 μM .

Acknowledgments

The work was funded by MIUR of Italy through the grant PRIN 2003.

References

1. Mazzuca, C., Stella, L., Venanzi, M., Formaggio, F., Toniolo, C. and Pispisa, B. *Biophys. J.* **88**, 3411-3421 (2005).

Design of Bactericidal Self-Assembling Cyclic D,L- α -Glycopeptides

Shai Rahimipour, Leila Motiei and Reza M. Ghadiri

Departments of Chemistry and Molecular Biology and the Skaggs Institute for Chemical
Biology, The Scripps Research Institute, La Jolla, California 92037, USA

Introduction

The increased prevalence of antibiotic resistance of bacterial pathogens requires development of novel antibacterial agents. Much attention in recent years has focused on the discovery, design, and characterization of glycopeptides as potential antibacterial agents [1]. The glycosyl residue can play a crucial role in the glycopeptide activity and this opens a large area for developing new biologically active structures. Glycosylation of peptide structures has the advantages of increasing the hydrophilicity of the molecule, often enhancing oral bioavailability, and conferring resistance to proteolytic cleavage of the peptide backbone. Recently our laboratory has developed a general class of antimicrobial agents based on the self-assembling D,L- α -cyclic peptide nanotube supramolecular structures that are highly effective against gram-positive and gram negative bacterial membranes [2]. Here we describe how glycosylation of specific residues in cyclic D,L- α -peptide sequences can improve their physical properties and ameliorate their biological activity.

Results and Discussion

Cyclic glycopeptides **2-8** were designed based on non-glycosylated analog **1** that showed previously high *in vitro* antibacterial activity (Table 1 [2]). We probed the role of glycosyl residue in the biological activity by varying the type of carbohydrate moiety as well as its position. In particular, each peptide was constructed to bear one glycosyl moiety in which the lysine residue in analog **1** was replaced by the positively charged serine(β GlcN) and the serine residues were either substituted by serine(β Gal) or serine(α Man). The synthetic strategy involved incorporation of a glycosylated serine residue (Fig. 1) into solid phase peptide synthesis. The *O*-acetylated building blocks **1b**, **2b**, and **3b** were prepared according to published methods [3]. The linear peptide chain synthesis was carried out according to standard Fmoc synthesis protocols under base-free HOBt/DIC coupling conditions. Following the deprotection of N-terminal Fmoc and removal of the C-terminal allyl ester, the linear peptides were cyclized on the solid support (Fig. 1). The *O*-acetyl groups were then removed with 20% hydrazine hydrate in MeOH while on the solid phase. Cleavage of the cyclic glycopeptides from resin and concomitant deprotection of the side chains was then carried out with TFA/water/TIS. The crude peptides were purified to homogeneity by RP-HPLC and characterized by mass spectroscopy. Table 1 compares the *in vitro* antibacterial activity of cyclic glycopeptides **2-8** to that of cyclic peptide **1**. In general, the MIC values of glycopeptides **2-8** were similar to that of **1** indicating that glycosylation and the resulting increase in peptide hydrophilicity did not adversely influenced cell membrane uptake and activity. Furthermore, glycosylation also did not diminish the bactericidal activity as indicated by the rapid killing (< 2 hrs) action observed with glycopeptides **3**, **5**, and **7** against MRSA. Moreover, hemolytic activity studies showed that depending on the position and the type of glycosyl residue employed, glycosylation could significantly attenuate the reactivity toward erythrocyte

Table 1. *In vitro* antibacterial activity of cyclic D,L α -glycopeptides

Cyclic peptide ^a	MIC (μ M) ^b				MBC ^c (μ M)	HD ₅₀ ^d
	MRSA	B. cereus	VRE	E. coli	MRSA	(μ M)
1 (WLWKSKSK)	2.5	2.5	5	25	5	120
2 (WLWKSKSX)	5	10	10	>40		85
3 (WLWKSKSK)	5	10	10	>40	10	140
4 (WLWKSXSK)	5	15	10	>40		150
5 (WLWKSKZK)	5	10	15	>40	10	260
6 (WLWKZKSK)	5	5	10	>40		190
7 (WLWKSKUK)	5	10	10	>40	5	120
8 (WLWKUKSK)	2.5	5	5	>40		105

^a The brackets indicate cyclic structure and underlining represents D-amino-acid residues. The bold letters depict O-glycosylserine residues with **X** = Ser(β GlcN), **Z** = Ser(β Gal), **U** = Ser(α Man). ^b Minimal inhibitory concentration. ^c Minimal bactericidal concentration. ^d Hemolytic activity (human red blood cells).

membranes (Table 1). Glycopeptides **5** and **6** with the β -Gal side chain modifications were the most selective sequences displaying low *in vitro* toxicity. The attenuated total reflectance (ATR) FT-IR study of cyclic glycopeptides **3**, **5** and **7** in dimyristoyl phosphatidylcholine multi-bilayers indicate formation of β -sheet-like hydrogen bonded tubular assemblies that are oriented roughly parallel ($70 \pm 5^\circ$ tilt angle) to the plane of the lipid membrane. Peptides also induced membrane permeation that was evidenced by the facile release of entrapped fluorescent dye from large unilamellar lipid vesicles.

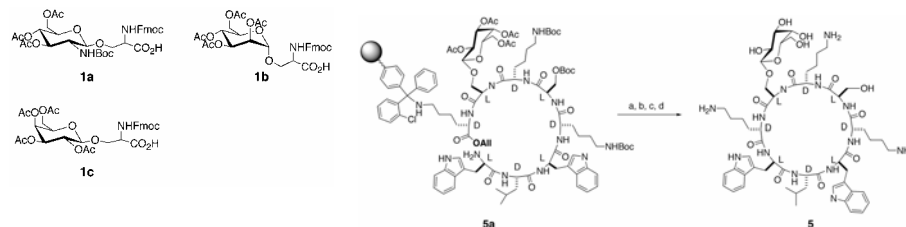


Fig. 1. (a) $\text{Pd}(\text{PPh}_3)_4$, PhSiH_3 , CH_2Cl_2 ; (b) PyAOP, HOAT, DIEA; (c) N_2H_4 , MeOH; (d) TFA/water/TIS (95/2.5/2.5).

References

1. Fu, X., Albermann, C., Jiang, J., Liao, J., Zhang, C. and Thorson, J. *Nature Biotech.* **21**, 1467-1469 (2003).
2. Fernandez-Lopez, S., Kim, H. S., Choi, E. C., Delgado, M., Granja, J. R., Khasanov, A., Kraehenbuehl, K., Long, G., Weinberger, D. A., Wilcoxon, K. M. and Ghadiri, M. R. *Nature* **412**, 452-456 (2001).
3. Salvador, L. A., Elofsson, M. and Kihlberg, J. *Tetrahedron* **51**, 5643-5656 (1995).

HB-50: A Pre-Clinical Study of a Prophylactic for Wound Infection

Scott M. Harris¹, Lijuan Zhang¹, Jody Parente¹, George T. Rodeheaver²
and Timothy J. Falla¹

¹Helix BioMedix, Inc. 22122 20th Ave. SE. Bothell WA 98021; ²University of Virginia Plastic Surgery Research, Charlottesville, VA 22908, USA

Introduction

Topical antibiotics are used to control acute wound infection such as in post-surgery, burn and chronic wounds. Lack of effective bacterial control can lead to systemic infection and significant morbidity and mortality particularly in the immuno-compromised patient. In the hospital environment such infections are often caused by pathogens such as *Staphylococcus aureus*, *Pseudomonas aeruginosa*, and *Candida albicans* which are resistant to multiple antibiotics. Conventional topical antibiotic options consist of narrow spectrum agents such as mupirocin (BactrobanTM) or combinations of anti-gram-negative, gram-positive and fungal agents. However resistance has become a significant challenge to virtually all antimicrobials currently in use to treat infectious diseases. The aim of this work was to identify a broad-spectrum agent active against gram-positive and gram-negative bacteria, as well as yeast, lacking cross-resistance with traditional therapeutics and demonstrating efficacy in vivo.

Antimicrobial peptides are essential components of innate defense. They are expressed in high concentrations in neutrophils, epithelial cells, and are constitutively expressed on mucosal surfaces of humans exposed to microbial infections. These peptides have attracted an increasing amount of interest in the development of antimicrobials due to their broad spectrum of activity against gram-positive and gram-negative bacteria, fungi, enveloped viruses, and parasites. Although there is still a debate as to how these peptides combat microorganisms, they are likely to interact with multiple targets on and within microorganisms resulting in a fast killing action with low risk of resistance development. In this study, we took advantage of our extensive peptide library and screened for candidates with broad spectrum antimicrobial coverage. As a result we identified HB-50 as a potential topical antimicrobial with application to wound and skin infections.

HB-50 H-VAKKLAKLAKKLAKLAL-NH₂

Results and Discussion

HB-50 exhibits significant activity against mupirocin resistant *S. aureus* in an abraded skin model in the rat compared to BactrobanTM. HB-50 is effective against a broad range of pathogens. The peptide is effective in preventing *S. aureus* wound infection when used prophylactically. *In vivo* activity extends to *S. pyogenes* and *P. aeruginosa* (data not shown). The activity of HB-50 can be enhanced by using non-ionic carrier formulations and additional formulation development should aid in helping to deliver the peptide to the pathogens. HB-50 does not dramatically affect the process of wound healing with treated and non-treated wounds healing in 12 and 11 days respectively. HB-50 proves to be effective in a simple topical wound

infection model compared to the currently accepted therapy and provides a broader spectrum of activity. It is effective against mupirocin resistant organisms and exhibits no toxicity.

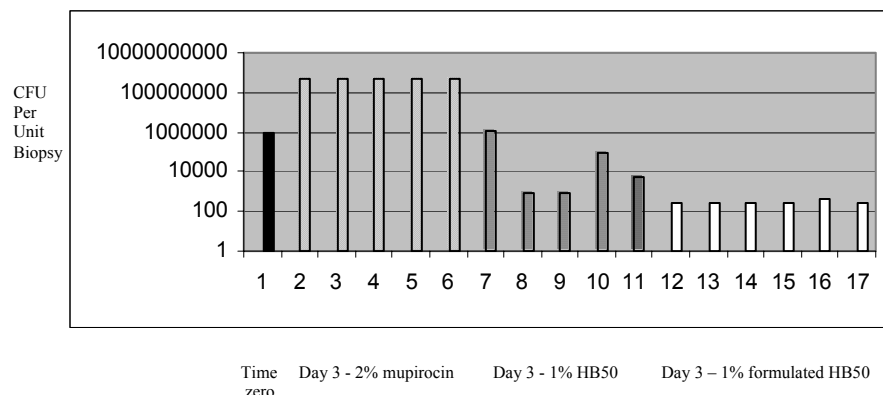


Fig. 1. Wound infection results from the rat incision model.

Table 1. Broad spectrum antibacterial activity of peptide HB50

Minimum Inhibitory Concentration (µg/mL)*			
Gram Positive Organisms	<i>S. aureus</i> MuRSA	<i>P. acnes</i>	<i>S. pyogenes</i>
	8	4	4
Gram Negative Organisms	<i>E. coli</i>	<i>S. typhimurium</i>	<i>P.aeruginosa</i>
	1	2	2
Yeast	<i>C. albicans</i>	<i>C. tropicalis</i>	<i>C. glabrata</i>
	16	2	8

* MIC determined by NCCLS microbroth dilution assay

The sequence of HB-50 has been tailored to be more cost effective to manufacture. The sequence has 4 tri-peptide repeat units (K-L-A) which helps to make it more economical to produce via standard solution phase methodologies. It is also comprised of simple inexpensive natural amino acids (valine, alanine, lysine, and leucine). This sequence is covered under allowed claims by the USPTO and held by Helix BioMedix Inc. HB-50 continues to be developed by Helix BioMedix Inc.

References

1. Gisby, J., *et al. Antimicrob. Agents Chemother.* **44**, 255-260 (2000).
2. Gear, J. L., *et al. Burns* **23**, 387-391 (1997).
3. Kokai-Kun, J. F., *et al. Antimicrob. Agents Chemother.* **47**, 1589-1597 (2003).

Designer Multifunctional Antimicrobial Peptides Kill Fluoroquinolone-Resistant Clinical Isolates

Laszlo Otvos^{1,2}, John D. Wade³, Feng Lin³, Barry A. Condie², Christine Snyder², Jorg Hanrieder⁴ and Ralf Hoffmann⁴

¹OLPE, LLC, Audubon, PA 19403, USA; ²The Wistar Institute, Philadelphia, PA 19104, USA;

³Howard Florey Institute, Parkville 3010, Victoria, Australia; ⁴Department of Chemistry,
University of Leipzig, Leipzig D-04103, Germany

Introduction

Approximately 10-25% of *Escherichia coli* and *Klebsiella pneumoniae* strains, bacteria responsible for most urinary tract infections (UTI), are resistant to fluoroquinolones, the currently preferred UTI treatment. Native antibacterial peptides destroying the membrane structure are potentially toxic and peptides with intracellular targets are usually not potent enough when the *in vitro* assays are run in microbiology-approved media. To overcome these limitations, we designed proline-rich antibacterial peptides that maintain their DnaK-binding ability to inhibit protein folding in bacteria and low toxicity in eukaryotes, but enter bacterial cells much more avidly than any earlier derivative (Fig. 1) [1]. The antibacterial efficacies were compared with native pyrrolicin, drosocin, apidaecin, as well as with earlier designer dimers.

Results and Discussion

The basis of the design process was a multiple alignment of all known proline-rich sequences and sequence optimization as a second step. The resulting chimeric and combinatorial analogs exhibited 8-16 µg/ml minimal inhibitory concentration (MIC) efficacies in full-strength Muller-Hinton broth against a series of UTI pathogens, collected from various locations all over the world [2]. Significantly, the best peptide, A3-APO, resisted serum degradation and retained full activity in the presence of mouse serum. Across a set of 8 fluoroquinolone-resistant clinical isolates, the A3-APO peptide was 4 times more potent than ciprofloxacin and 20-fold more active than the best single peptide-based analog, the Pip-pyrr-MeArg dimer [3]. In a 24 hr proliferation assay, the A3-APO derivative was not toxic to the monkey kidney-originated COS cells up to 1.5 mg/ml peptide concentration.

LO2C: (Chex-Lys-Val-Asp-Lys-Gly-Ser-Tyr-Leu-Pro-Arg-Pro-Arg-Pro-Pro-His-Pro-Arg)₂-Dab

WI-517: (Chex-Asp-Lys-Pro-Arg-Pro-Tyr-Leu-Pro-Arg-Pro-Thr-Arg-Pro-Pro-His-Pro-Ile-Arg)₂-Dab

A2-APC: (Chex-Arg-Val-Asp-Lys-Pro-Ser-Pro-Tyr-Leu-Pro-Lys-Pro-Thr-Pro-Pro-Pro-Arg-Pro-Val-Tyr-Asn-Arg)₂-Dab

A3-APO: (Chex-Arg-Pro-Asp-Lys-Pro-Arg-Pro-Tyr-Leu-Pro-Arg-Pro-Arg-Pro-Pro-Arg-Pro-Val-Arg)₂-Dab

Fig. 1. Sequences of newly designed chimeric and combinatorial peptides.

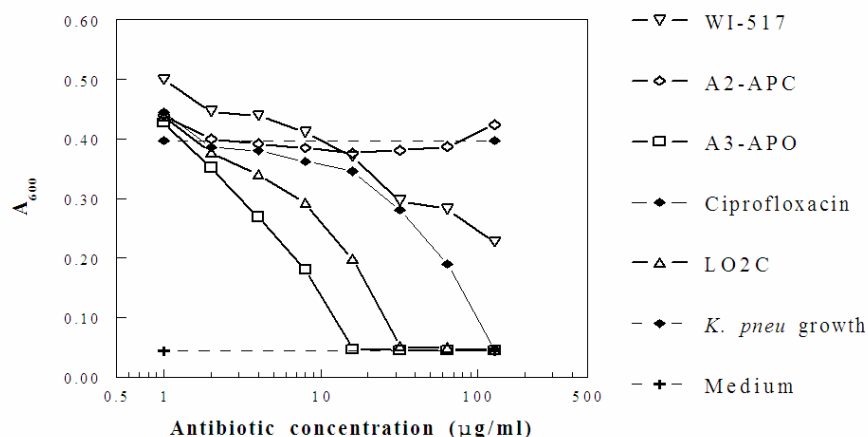


Fig. 2. Liquid broth dilution antimicrobial assay of the designer proline-rich peptides. The test strain, *Klebsiella pneumoniae* 012-3132 was isolated from a USA patient with catheter-induced urinary tract infection, and deposited to the collection of the SENTRY Antimicrobial Surveillance program.

For the A3-APO peptide, similar *in vitro* antimicrobial efficacies were observed in 1% tryptic soy broth medium. The microbiology literature generally recommends using a therapeutic dose of 130% of the MIC (measured in full-strength media) for protecting animals in a bacteremia model [4]. With the designer A3-APO peptide we managed to develop an antibacterial peptide derivative that kills bacteria in various full-strength media. Calculating with 16 $\mu\text{g/ml}$ MIC, our dose would be 21 $\mu\text{g/ml}$, or 36 μg peptide per mouse, or 2 mg/kg. This dose range is comparable with that of non-peptide antibiotics on the market [5]. Preliminary pharmacokinetic studies of WI-105 indicate that a 2 hr period exists, enough to kill bacteria, when 40% of subcutaneously injected peptide (or a chromatographically co-eluting active metabolite) is present in mouse blood. Partial decomposition of the combinatorial proline-rich peptides *in vivo* will push the dose up to 5 mg/kg for systemic applications, although as peptide drugs are concentrated in the urinary tract, the dose will be lower against UTI.

References

1. Otvos, L., Jr., et al. *Int. J. Peptide Res. Ther.* **11**, 29-42 (2005).
2. Otvos, L., Jr., et al. *J. Med. Chem.* **48**, 5349-5359 (2005).
3. Cudic, M., et al. *Peptides* **24**, 807-820 (2003).
4. Bush, K., Macielag, M. and Weidner-Wells, M. *Curr. Opin. Microbiol.* **7**, 466-476 (2004).
5. Hvidberg, H., et al. *Antimicrob. Agents Chemother.* **44**, 156-163 (2000).

Solution Structures of Stomoxyn and Spinigerin, Two Antimicrobial Peptides from Insects

Celine Landon¹, Herve Meudal¹, Nathalie Boulanger², Philippe Bulet³,
Reto Stöcklin³ and Françoise Vovelle¹

¹Centre de Biophysique Moléculaire, CNRS UPR 4301, 45071 Orléans Cedex 2, France;

²EA3432, Faculté de Pharmacie, Université Louis Pasteur, 67401 Illkirch Cedex, France;

³Atheris Laboratories, CH-1233 Bernex, Geneva, Switzerland

Introduction

Recently, we have isolated two novel linear cysteine-free insect antimicrobial peptides (AMPs). The first one, stomoxyn, constitutively expressed in the gut of the blood-sucking insect *Stomoxys calcitrans* [1], is a 42-residue C-terminally amidated peptide with no significant sequence similarity to known AMPs. Stomoxyn is highly effective against Gram-positive (MICs < 10 μ M), Gram-negative (MICs < 5 μ M) bacteria and filamentous fungi (MICs < 5 μ M), and slightly less active on yeast cells (MICs < 50 μ M). In addition, stomoxyn shows some activity on trypomastigote forms of *Trypanosoma brucei rhodesiense*, which is responsible for African sleeping sickness. The second AMP, spinigerin [2], is a 25-residue peptide, constitutively expressed in the hemocytes of the termite *Pseudacanthotermes spiniger*. Spinigerin is effective on filamentous fungi and yeast cells (MICs < 5 μ M) and also affects the growth of Gram-negative bacteria such as *Escherichia coli* (MIC < 5 μ M) but has a lower efficacy (MICs < 100 μ M) on *Pseudomonas aeruginosa*, an opportunistic pathogen for humans. Spinigerin has a limited action on Gram-positive bacteria [2].

To better understand the features responsible for the activity of stomoxyn and spinigerin, we have determined the 3D structures of both peptides in 50% trifluoroethanol (TFE) by NMR spectroscopy and molecular modelling. These structures were compared to those obtained in membrane mimetic solvents for other α -helical peptides such as cecropin [3] (α -helical AMPs from insects) and magainin [4] (α -helical AMPs from frogs). To gain insight into the folding pathway of these molecules in membrane mimetic solvent, the circular dichroism (CD) spectra were recorded at different concentrations of TFE and the 3D structure of spinigerin was also determined in the presence of 10 % TFE.

Results and Discussion

Stomoxyn and spinigerin adopt a flexible random coil structure in water while both assume a stable helical structure in the presence of TFE. Stomoxyn remains unstructured below 20% TFE and shows subsequently a gradual increase in helicity when increasing the TFE concentration to 80 % (figure 1A). In 50% TFE, the structure of stomoxyn is typical of cecropins (figure 1B), including an amphipathic helix at the N-terminus and a hydrophobic C-terminus with helical features. The position of the hinge region separating the two helices is not related to the presence of a Gly-Pro or Gly-Xaa-Gly sequence as in cecropins. With such structural similarities, we may expect for stomoxyn and spinigerin a similar mode of action on the bacterial membrane including an initial binding to the polar heads through electrostatic interactions, favoring the helical conformation. The hydrophobic C-terminal tail further strengthens the interaction with the membrane leading to membrane lyses.

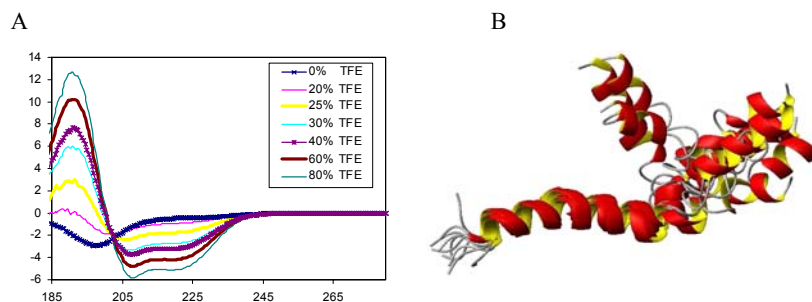


Fig. 1. **A** CD spectra of stomoxyn at different TFE concentrations. **B** Superposition of 10 NMR structures of stomoxyn in 50% TFE.

In contrast to stomoxyn, spinigerin acquires very rapidly a helical conformation (Fig. 2A). In 10% TFE the helix is highly bent and the structure poorly defined (data not shown). But, at a concentration in TFE higher than 20%, the CD spectra evidence a rapid structuring of the peptide. In 50% TFE, the helical structure is well defined all along its sequence, and the slightly bent α -helix displays an amphiphilic character, as observed for magainin 2 (Fig. 2B). Despite the lack of sequence similarities both structures share an amphiphilic character, with the hydrophobic residues on the concave side of the helix. This is presumably indicative of a similar

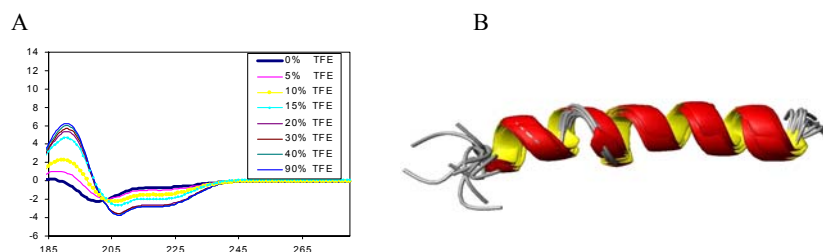


Fig. 2. **A** CD spectra of spinigerin at different TFE concentrations. **B** Superposition of 10 NMR structures of spinigerin in 50 % TFE.

mode of action though the formation of toroidal pores leading to the membrane lyses.

The comparison of the structures in 10% and 50% TFE confirms that TFE induces helix formation and propagation for amino acids showing helical propensity in water but also enhances the helix propagation propensity of non-polar β -branched residues.

References

1. Boulanger, N., *et al. J. Biol. Chem.* **277**, 49921-49926 (2002).
2. Lamberty, M., *et al. J. Biol. Chem.* **276**, 4085-4092 (2001).
3. Holak, T. A., *et al. Biochemistry* **27**, 7620-7629 (1988).
4. Gesell, J., Zasloff, M. and Opella, S. J. *J. Biomol. NMR* **9**, 127-135 (1997).

Rational Design of α -Helical Antimicrobial Peptides

Yuxin Chen¹, Michael Guarnieri¹, Michael Vasil² and Robert S. Hodges¹

¹*Department of Biochemistry and Molecular Genetics; ²Department of Microbiology,
University of Colorado at Denver and Health Sciences Center, Aurora, CO 80045, USA*

Introduction

We believe that a synthetic peptide rational design approach of small incremental changes in hydrophobicity/hydrophilicity, amphipathicity, helicity and stability of cationic antimicrobial peptides will enable rapid progress in development of new potential peptide antibiotics. Utilizing this approach, we modified an existing antimicrobial peptide (V₆₈₁) with excellent antimicrobial activity and strong hemolytic activity (a poor therapeutic index) by substituting single D- or L-amino acid residues in the center of the non-polar and polar face. We were able to optimize the specificity of the parent peptide V₆₈₁ with significantly increased therapeutic indices for V13K_L of 89-fold and 17-fold against Gram-negative and Gram-positive bacteria, respectively, and for V13A_D of 42-fold and 23-fold against Gram-negative and Gram-positive organisms, respectively [1].

Results and Discussion

In this study using our lead component V13K_L, we addressed the question of whether we could increase hydrophobicity by Ala to Leu substitutions in the non-polar face without having any significant effect on dimerization or helicity in benign medium and obtain the advantage of increased hydrophobicity which should enhance antimicrobial activity and have little effect on hemolytic activity. As shown in the helical net representation of Figure 1, we made three single Ala to Leu substitutions at positions 12, 23 and 20. With the Ala to Leu substitution at position 23, the Leu cannot form any *i* to *i*+3 or *i* to *i*+4 hydrophobic interactions along the helix and was expected to be a favorable substitution. Ala at position 12 is next to the critical Lys 13 and was expected to be a favorable substitution even with an increased number of hydrophobic interactions. Ala at position 20 not only increases hydrophobicity similar to the other Leu to Ala substitutions but also increases the number of hydrophobic interactions to 9 and creates a hydrophobic cluster or patch which could have dramatic effects on biological activities. The double and triple substitution analogs were made as positive controls where the overall hydrophobicity was expected to be too high to generate the desired biological activities.

In Table 1, we can see that 1) as hydrophobicity on the non-polar face increases (as measured by retention time at 25°C), the ability of the peptide to dimerize also increases, as expected; 2) as hydrophobicity of the non-polar face increases, there is a systematic increase in hemolytic activity as much as 62-fold for that of the triple Leu analog compared to V13K_L; 3) there is also an excellent correlation between increasing dimerization and hemolytic activity; and 4) as hydrophobicity of the non-polar face increases for the single Leu substitution analogs, the antimicrobial activity increased, as expected (A20L was the most active peptide with a 3.6-fold increase compared to V13K_L). What was unexpected was the dramatic loss of antimicrobial activity with increasing hydrophobicity from the single Leu analog (A20L) to the triple Leu analog which was 18-fold less active than A20L, likely due to the increase in dimerization.

In conclusion, the advantage of increasing antimicrobial activity with increasing peptide hydrophobicity can be easily overridden by the increase in toxicity. The clustering of large hydrophobes on the non-polar face dramatically increases dimerization. Interestingly, the most hydrophobic analog (triple Leu analog) showed the strongest dimerization ability but had essentially no antimicrobial activity and was extremely hemolytic. This demonstrates that dimerization does not prevent toxicity (hemolysis) of eukaryotic cells but can prevent antimicrobial activity in prokaryotic cells. Thus, it is important to reduce dimerization for the desired antimicrobial activity against prokaryotic organisms.

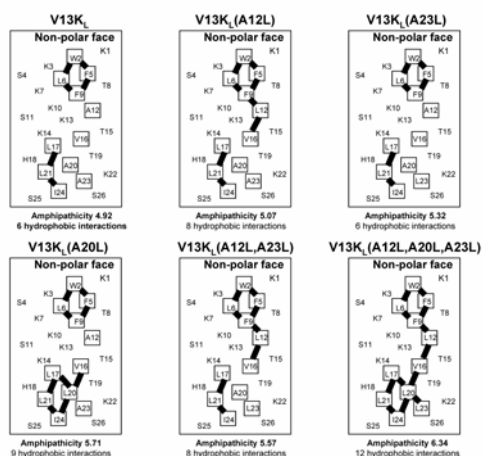


Fig. 1. Helical net representations of analogs to investigate the role of increased hydrophobicity, hydrophobic interactions and hydrophobic clusters on the non-polar faces of V13K_L. The *i* to *i*+3 and *i* to *i*+4 interactions are indicated by the solid bar between residues.

Table 1. Biological/biophysical studies

Peptide	Hydrophobicity as measured by RP-HPLC retention time (min)	Dimerization ability as measured by temperature profiling in RP-HPLC ¹	Hemolytic activity (μg/ml) ²	Fold ³	Antimicrobial activity (MIC) normalized to V13K _L (fold improvement) ⁴
V13KL	42.1	3.0	250.0	1.0	1.0
V13KL (A23L)	45.7	4.5	62.5	4.0	1.0
V13KL (A12L)	46.3	5.5	31.3	8.0	2.0
V13KL (A20L)	47.1	5.4	31.3	8.0	3.6
V13KL (A12L,A23L)	50.3	7.0	15.6	16.0	2.2
V13KL (A12L,A23L,A20L)	55.1	11.3	4.0	62.5	0.2

¹Gradient rate was 0.5% acetonitrile/min; for additional discussion of this novel method to determine dimerization, see references [2,3]. ²Hemolytic activity was determined after 18 hrs. ³Fold denotes the fold increase in toxicity. ⁴Geometric mean of 6 resistant strains of *Pseudomonas aeruginosa*.

Acknowledgments

This work was supported by National Institutes of Health Grants RO1GM61855 and RO1AI48717 to R.S.H. and the John Stewart Chair in Peptide Chemistry to R.S.H.

References

1. Chen, Y., Mant, C. T., Farmer, S. W., Hancock, R. E., Vasil, M. L. and Hodges, R. S. *J. Biol. Chem.* **280**, 12316-29 (2005).
2. Mant, C. T., Chen, Y. and Hodges, R. S. *J. Chromatogr. A* **1009**, 29-43 (2003).
3. Lee, D. L., Mant, C. T. and Hodges, R. S. *J. Biol. Chem.* **278**, 22918-22927 (2003).

Dimer Formation of Novel Cationic Antimicrobial Peptides in Membrane Environments

Evgenia Glukhov and Charles M. Deber

Department of Structural Biology & Biochemistry, Research Institute, Hospital for Sick Children, Toronto, Ontario M5G 1X8; and Department of Biochemistry, University of Toronto, Toronto, Ontario M5S 1A8, Canada

Introduction

Novel cationic antimicrobial peptides typified by structures such as KKKKKKAAXAAWAXAA-NH₂, with hydrophobic core sequence of 11 residues where X=F/W, and several of their analogs, display high activity against a variety of bacteria, including well-known antibiotic resistant species, but generally exhibit no hemolytic activity even at high dose levels in mammalian erythrocytes [1]. We have been examining their mechanism of action and source of selectivity for bacterial vs. mammalian membranes. Studies where the peptides were challenged with micelles and lipid vesicles of varying lipid composition including ones resembling the compositions of natural bacterial (anionic) and mammalian outer leaflet (zwitterionic) membranes have indicated that membrane selectivity is governed primarily by (anionic) charge of the lipid head groups at the bacterial surface, and only slightly by the presence/absence of cholesterol, the latter common to mammalian membranes [3].

However, sequences in transmembrane segments of proteins that consist of “small residue-xxx-small residue” motifs (such as GxxxG) – which place the two small residues on the same helical face - are known to enhance packing by facilitating the close approach of helices [2]. Peptides under investigation in this work similarly have in common multiple AxxxA sequence motifs, which would therefore be expected to promote their dimerization in membrane environments. We felt that dimerization could produce larger, more “destructive” particles, which may represent an additional factor in the high antimicrobial activity displayed by this peptide series.

Results and Discussion

Two peptides selected for study here - kkkkkkaafaawaafaa-NH₂ (termed All D-F17-6K) and kkkkkkaafaawaafll-NH₂ (termed All D-F17-6K-(2L)) (lower case letters = D-enantiomers) ran as dimers in SDS-PAGE gel analysis even at very low (silver staining) concentrations [3]. In the present work, this dimerization is confirmed by fluorescence energy transfer (FRET) experiments using N-terminal dansyl/dabcyl-tagged All D-F17-6K and All D-F17-6K-(2L) peptides in the membrane-mimetic environment of SDS micelles. In FRET experiments, dimerization is signaled when the fluorescence of the dansyl-tagged peptide (donor) is linearly decreased in the presence of increasing mole fractions of the dabcyl-tagged derivative of the same peptide (acceptor) [4]. As shown in Figure 1, both peptides display clear dimer formation in SDS micelles. By comparing slopes of the two lines, we may further conclude that at the same concentration and peptide length, the population of the dimer of the peptide with three AxxxA motifs (All D-F17-6K) is greater than that of the peptide with two of these motifs (All D-F17-6K-(2L)).

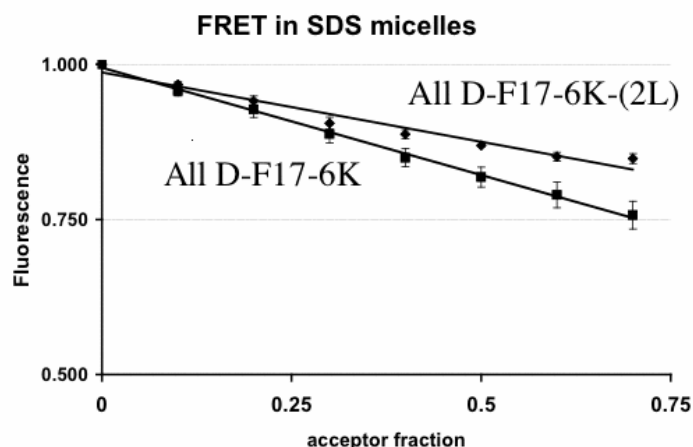


Fig. 1 FRET efficiencies in experiments using dansyl-labeled donor peptides All D-F17-6K and All D-F17-6K-(2L) at 1 μ M in 25 mM SDS micelles, in the presence of increasing mole fractions of the corresponding dabcy-labeled acceptor peptides. Total peptide concentrations are 5 μ M in SDS. Aqueous buffer is 10 mM Tris-HCl, 10 mM NaCl, pH = 7.0. Emission spectra were collected at 450-650 nm at room temperature. Values shown are the average of three repetitions of each measurement.

The overall results, in conjunction with molecular modeling, support a mechanism involving an initial electrostatic interaction step, in which bacterial membranes – but not mammalian membranes – attract and bind the peptide dimers into their surface region, followed by insertion of the peptide hydrophobic core substantively into the bacterial membrane [1,3]. The high selectivity of these peptides for bacterial-like membranes, combined with their activity toward a wide spectrum of gram-negative and gram-positive bacteria - while retaining water solubility - represent significant advantages of this class of peptides.

Acknowledgments

Supported, in, part, by a grant to C.M.D. from the Canadian Institutes for Health Research (CIHR). E.G. is a post-doctoral trainee of the CIHR Program in Structure of Membrane Proteins Linked to Disease.

References

1. Stark, M., Liu, L. P. and Deber, C. M. *Antimicrob. Agents Chemother.* **46**, 3585-3590, (2002).
2. Lear, J. D., Stouffer, A. L., Gratkowski, H., Nanda, V. and Degrado, W. F. *Biophys. J.* **87**, 3421-3429, (2004).
3. Glukhov, E., Stark, M., Burrows, L. L. and Deber, C. M., *submitted for publication* (2005).
4. Melnyk, R. A., Partridge, A. W. and Deber, C. M. *J. Mol. Biol.* **315**, 63-72 (2002).

Post-Translational Modifications of Peptides and Proteins

Enzymatic Incorporation of Prenyl Azides into Peptides and Proteins: Tools for Selective Protein Labeling

Juhua Xu, Stepan Lenevich, Jason Boggs, Daniel G. Mullen, George Barany and Mark D. Distefano

Department of Chemistry, University of Minnesota, Minneapolis, MN 55455, USA

Introduction

Protein prenylation consists of the attachment of 15 (farnesyl) or 20 (geranylgeranyl) carbon isoprenoids to proteins via a thioether linkage. The prenyl groups originate from the corresponding allylic diphosphates and are attached to their cognate target proteins by a class of enzymes called prenyltransferases (Fig. 1). This post-translational modification has received considerable attention in recent years due to the fact that many proteins involved in signal transduction pathways including Ras are prenylated. Inhibition of protein prenylation can negate the effects of transforming mutations in Ras. This has resulted in significant interest in the prenyltransferase class of enzymes as potential targets for anticancer therapy [1].

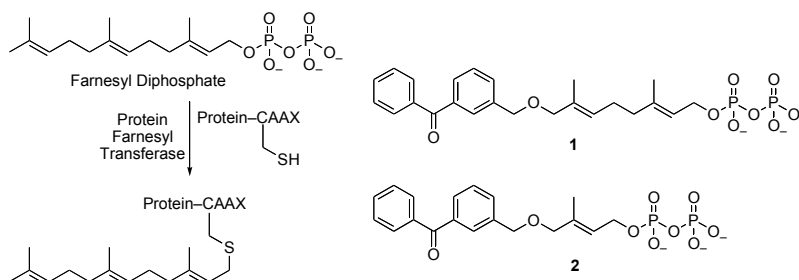


Fig. 1. Reaction catalyzed by protein farnesyltransferase and benzophenone-containing analogues of farnesyl diphosphate

Early work in our group focused on the development of photoactive analogs of farnesyl (FPP) and geranylgeranyl diphosphate (GGPP) that could be used to identify the active sites of the prenylating enzymes. Compound 1 (Fig. 1) was shown to be a competitive inhibitor with respect to FPP of protein farnesyl transferase (PFTase) and was shown to label the β -subunit upon photolysis. However, 1 was not a substrate for the enzyme. Subsequent X-ray crystallographic analysis revealed that while 1 bound within the isoprenoid binding site, closely mimicking the natural substrate FPP, part of the benzophenone group projected into the adjacent peptide/protein binding site making it impossible for the target peptide to be oriented in a manner suitable for efficient prenyl group transfer [2]. These results made it clear that there was an upper limit to the size of isoprenoid analogs that could be processed by the enzyme. Concurrent work with a smaller benzophenone-containing analog 2 (Fig. 1) gave significantly different results. Incubation of 2 and a peptide substrate, *N*-dansyl-GCVIA, with PFTase led to the production of the thioether-linked prenylated peptide. While 2 is not incorporated by PFTase at the same rate as FPP is, the reaction can be driven to completion using excess analog and greater amounts of enzyme. Analysis by X-ray crystallography of

the structure of **2** bound to PFTase showed that this smaller analog does not interfere with the binding of the peptide substrate in the manner observed with **1** [3]. Taken together, this early work provided compelling evidence that PFTase was capable of accepting alternative substrates that incorporate non-natural functionalities while at the same time illustrated that some size restrictions do exist in terms of what can be tolerated by the enzyme.

As noted above, prenyltransferases catalyze the attachment of isoprenoids to proteins. The primary sequence recognized by these enzymes is the tetrapeptide CAAX where C is cysteine, A is an aliphatic residue and X can be a variety of possibilities; the identity of X determines the nature of the isoprenyl group incorporated. Since virtually any protein can be converted into a substrate for PFTase by adding on this CAAX box sequence at the C-terminus, we were interested in developing this approach for use as a tool for protein labeling. The concept was that bio-orthogonal functional groups such as azides [4] could be incorporated into isoprenoids which would in turn be transferred to proteins using PFTase. Following enzymatic prenylation, the azide could be functionalized using a broad range of reagents for applications ranging from fluorescence detection to protein immobilization. Here we describe several analogs of FPP that have been used to incorporate azides into peptides and report on their subsequent reaction in Staudinger ligation reactions.

Results and Discussion

To examine the ability of PFTase to incorporate azide containing substrates, we initially focused on the synthesis of compounds **3** and **4** [5]. For **3**, the molecule was synthesized by allylic oxidation of THP-protected geraniol with SeO_2 followed by reaction of the resulting alcohol with $(\text{PhO})_2\text{PON}_3$. The prenyl azide was then deprotected and the resulting allylic alcohol was converted to the corresponding bromide followed by pyrophosphorylation to yield **3**; a similar route was used to prepare **4**. It should be noted that **3** and **4** are actually isomeric mixtures since they equilibrate via a 1,3 rearrangement with the corresponding secondary azides at C-6 and C-10, respectively. To avoid this isomeric complication, the dihydro analogs **5** and **6** were prepared. To obtain compound **5**, THP-protected geraniol was subjected to allylic oxidation to yield an α,β -unsaturated aldehyde. Sequential reduction of the C-6 alkene followed by reduction of the C-8 aldehyde afforded the C-8 alcohol which was subsequently converted to the corresponding C-8 azide. The desired diphosphate **5**, was obtained using the deprotection, bromination, pyrophosphorylation sequence used for the preparation of **3**; a similar route was used to prepare **6**.

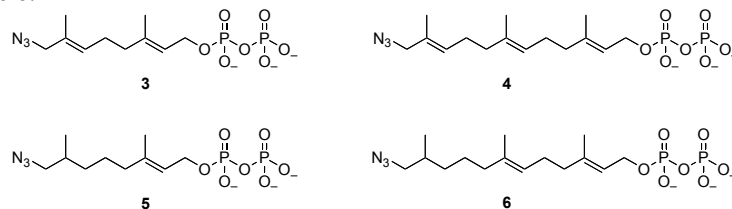


Fig. 2. Analogs of geranyl and farnesyl diphosphate incorporating azide functional groups.

To examine whether **3** was a substrate for PFTase, the compound was incubated with *N*-dansyl-GCVIA in the presence of the enzyme (Fig. 3). The reaction was

monitored by following the dansyl group fluorescence with time; in the case of FPP, it is known that farnesylation of the peptide causes a ca. 10-fold increase in fluorescence and can hence be used to measure the rate of reaction. Analog **3** produced a time dependant increase in fluorescence suggesting that this molecule was a substrate for the enzyme. Isolation of the reaction product and purification by reversed-phase HPLC followed by analysis by ESI-MS-MS confirmed that the desired product **7** (Fig. 3) had been formed. Reaction of the resulting azide-functionalized peptide with Staudinger reagent **8** in CH₃CN containing 30% H₂O gave a new product that was purified by reversed-phase HPLC. Interestingly, ESI MS-MS analysis indicated that the new product was not the normal amide-linked Staudinger product. Instead, the product appears to be an alkoxyimide whose structure is shown in Figure 3 as **9**. Such products are observed in Staudinger reactions with aryl azides as opposed to the amides that are formed with alkyl azides. Analogs **4**, **5**, and **6** were also examined for their ability to be used as alternative substrates for PFTase and subsequent Staudinger reactions. In all cases, the compounds could be enzymatically processed and reacted with **8** to give alkoxyimide products similar to **9**. This suggests that the unusual reactivity of these compounds in the Staudinger reaction is not due to the allylic azide functionality and may instead be a consequence of the β -branched nature of the azides used in these experiments. In summary, the work reported here demonstrates that prenyl azides can be incorporated into peptides using PFTase and that the resulting enzymatically modified peptides can be further elaborated by chemical methods targeted to the azide functionality. Given the small size of the sequence (a tetrapeptide) that is necessary to convert a protein into a PFTase substrate, the approach described here may prove to be a useful method for selective protein labeling [6].

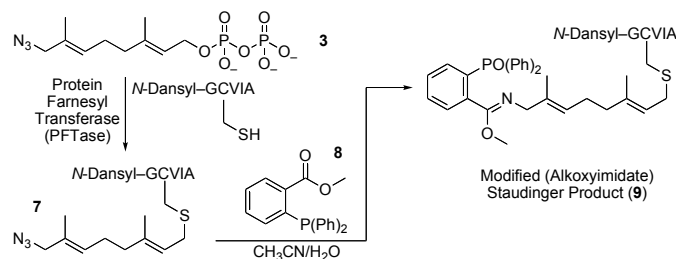


Fig. 3. Incorporation of a prenyl azide into a peptide using PFTase and subsequent product modification via Staudinger reaction.

Acknowledgments

The work was funded by a grant from NIH (GM 58442) to MDD.

References

1. Haab, B. B. *Curr. Opin. Drug Discovery Dev.* **4**, 116-123 (2001).
2. Turek-Etienne, T., Strickland, C. and Distefano, M. *Biochemistry* **42**, 3716-3724 (2003).
3. Turek, T., Gaon, I., Distefano, M. and Strickland, C. *J. Org. Chem.* **66**, 3253-3264 (2001).
4. Saxon, E. and Bertozzi, C. R. *Science* **287**, 2007-2010 (2000).
5. Rose, M. W., Xu, J., Kale, T. A., O'Doherty, G., Barany, G. and Distefano, M. *Biopolymers* **80**, 164-171 (2005).
6. Kho, Y., *et al. Proc. Natl. Acad. Sci. USA* **101**, 12479-12484 (2004).

***N*-Alkylaminooxy Amino Acids as Versatile Derivatives for "Post-Translational" Modifications of Synthetic Peptides**

Michael R. Carrasco

Department of Chemistry, Santa Clara University, Santa Clara, CA, 95053-0270, USA

Introduction

Post-translational modifications of peptides and proteins are responsible for many critical biological changes in structure and function. My research group has been interested in developing synthetic methods for chemoselective reactions of peptides that emulate common post-translational modifications, particularly glycosylation and lipidation. The key for such methods is determining and utilizing organic functional groups that are uniquely reactive in the presence of those moieties found in coded amino acids. With an original focus on glycosylation, we looked for organic functionality that met two criteria: (1) selective reaction with native, unprotected carbohydrates and (2) adoption of cyclic sugar conformations by the carbohydrate after attachment to the peptide. From the work of Peri, Dumy, and Mutter [1], we realized that *N*-alkylaminooxy groups would meet those criteria.

To explore the use of *N*-alkylaminooxy groups for post-synthetic peptide modifications, we developed syntheses of several protected amino acids with *N*-alkylaminooxy side chains [2-4]. The derivatives that proved successful for subsequent glycosylations are shown in Figure 1. Each can be synthesized in > 50% overall yield from commercially-available starting materials and incorporated into peptides using standard Boc-chemistry based protocols [5]. We have also synthesized **Z**₁ and **Z**₃ in protected forms appropriate for Fmoc-chemistry based protocols [3].

Each amino acid places the reactive aminoxy nitrogen at a different distance from the α carbon, which corresponds to allowing attachment of other molecules at various distances relative to the peptide backbone. We have previously demonstrated the chemoselective glycosylation of peptides containing the **Z** amino acids [2,4]. Here we highlight preliminary results on the chemoselective alkylation and acylation of *N*-alkylaminooxy side chains in peptides. We also demonstrate the pseudo-orthogonality of *N*-alkylaminooxy groups and their ordinary aminoxy counterparts.

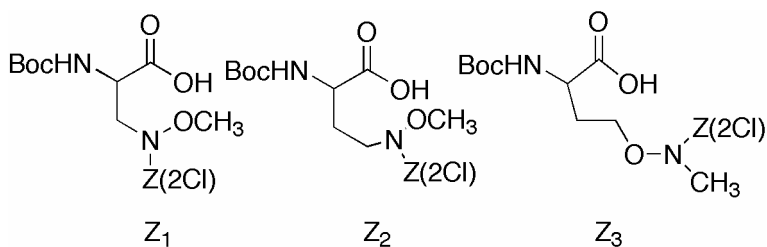


*Fig. 1. Available *N*-alkylaminooxy amino acids.*

Results and Discussion

Alkylation and acylation reactions were attempted with peptides based on three model sequences: H-LAZSK-NH₂, H-ELFHSIZEKAR-NH₂, and H-FAZRLEGFCSK-NH₂. Substrates containing variations at the Z amino acid site (Z₁, Z₂, Z₃, and des-Z as a control) were synthesized using *in situ* neutralization Boc chemistry [5] on MBHA resin by manual synthesis. HF deprotection and cleavage with *m*-cresol as a scavenger afforded crude peptides that were purified by RP-HPLC and analyzed by ESI-MS.

For the alkylation reactions, peptides were reacted with a variety of alkyl bromides. Typical conditions were ~ 1 mM peptide, 500 mol% of the bromide, 0.1 M NaOAc, pH 4.0, and 37 °C. We found no reaction with ordinary primary and secondary bromides, but α -keto bromides, benzyl bromide, and allyl bromide reacted successfully. These alkylations were chemoselective for the *N*-alkylaminoxy groups in the presence of all of the side chains except the thiol of cysteine. In successful cases, the starting *N*-alkylaminoxy peptides typically underwent 80-90 % conversion to their mono-alkylated counterparts in 24-48 hrs.

For the acylation reactions, peptides were reacted with a variety of acyl electrophiles. Typical conditions were ~ 1 mM peptide, 200 mol% of the electrophile, 0.1 M phosphate, pH 3.2, and 25 °C. With these conditions, we found no reaction with phenolic or thioesters, but succinimidyl and pentafluorophenyl esters reacted with good yields and chemoselectivity for the *N*-alkylaminoxy groups in the presence of all of the side chains except the thiol of cysteine. More reactive derivatives, such as anhydrides, showed a general lack of chemoselectivity, and multiple additions were observed. For successful reactions, the starting *N*-alkylaminoxy peptides typically underwent 80-90 % conversion to their mono-acylated counterparts in < 24 hrs.

In addition to their chemoselective glycosylation, alkylation, and acylation, *N*-alkylaminoxy groups offer the advantage of a complete *lack* of reactivity with ordinary aldehydes and ketones. This feature simplifies the handling of *N*-alkylaminoxy peptides because rigorous exclusion of common laboratory solvents like acetone is not required. By contrast, ordinary aminoxy groups react extremely rapidly with ordinary aldehydes and ketones, such as acetone, to form oxime products. This differing reactivity can be used to effect sequential chemoselective modification reactions with peptides. An example reaction sequence with the corresponding HPLC chromatograms is shown in Figure 2. A peptide, **1**, derivatized with both an aminoxy group at the N-terminus and an *N*-alkylaminoxy group on a side chain (top trace), was reacted with an excess of isobutyraldehyde in 0.1 M NaOAc, pH 4.0. Complete conversion to the oxime product was observed in less than 1 hr (middle trace). Without any intermediate purification, an excess of D-glucose was added. Although the *N*-alkylaminoxy group did not react with the isobutyraldehyde, it could still be chemoselectively glycosylated. Peptide **2** was seen to undergo > 60 % conversion to the glycosylated peptide **3** within 4 d (bottom trace). Importantly, no other byproducts were seen.

Overall, we have established ready access to *N*-alkylaminoxy-containing peptides, and the *N*-alkylaminoxy side chains can be chemoselectively glycosylated, alkylated, and acylated to give a range of neoglyco- and neolipopeptides. Quick access to many "post-translationally" modified substrates will enable studies of the biologically-relevant effects that these modifications have on peptide structure and function.

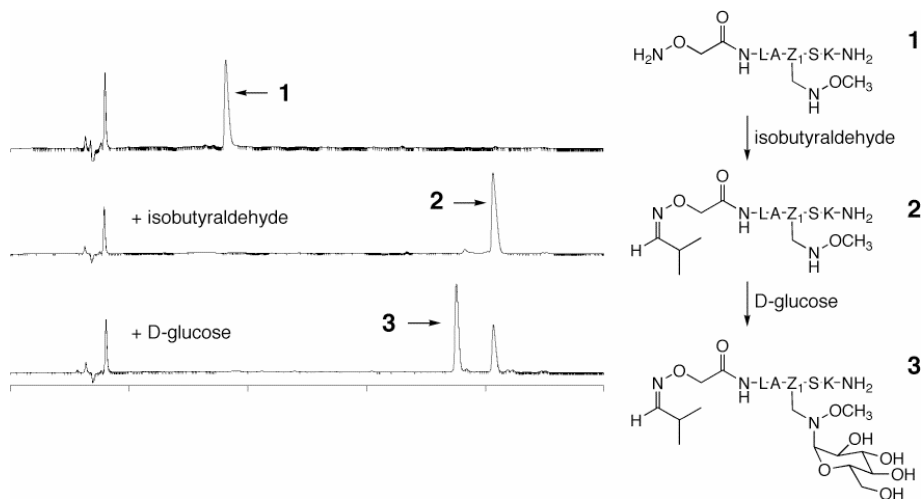


Fig. 2. Sequential chemoselective reactions of an aminooxy and a *N*-alkylaminooxy group. The side chain of Z_1 is shown for emphasis.

Acknowledgments

I gratefully acknowledge the contributions of all the talented undergraduates who have developed the chemistry described. I also acknowledge financial support from the Camille and Henry Dreyfus Faculty Start-up Grant Program for Undergraduate Institutions, the National Science Foundation (NSF-REU grant CHE01-39527 and NSF-CAREER grant CHE01-34818), the Donors of The Petroleum Research Fund, administered by the American Chemical Society, and an award to Santa Clara University under the Undergraduate Biological Sciences Education Program of the Howard Hughes Medical Institute.

References

1. Peri, F., Dumy, P. and Mutter, M. *Tetrahedron* **54**, 12269-12278 (1998).
2. Carrasco, M. R., Nguyen, M. J., Burnell, D. R., MacLaren, M. D. and Hengel, S. M., *Tetrahedron Lett.* **43**, 5727-5729 (2002).
3. Carrasco, M. R., Brown, R. T., Serafimova, I. M. and Silva, O. *J. Org. Chem.* **68**, 195-197 (2003).
4. Carrasco, M. R. and Brown, R. T. *J. Org. Chem.* **68**, 8853-8858 (2003).
5. Schnölzer, M., Alewood, P., Jones, A., Alewood, D. and Kent, S. B. H. *Int. J. Peptide Prot. Res.* **40**, 180-193 (1992).

Improved Synthesis of 5-hydroxylysine (Hyl) Derivatives

Mare Cudic, Janelle L. Lauer-Fields and Gregg B. Fields

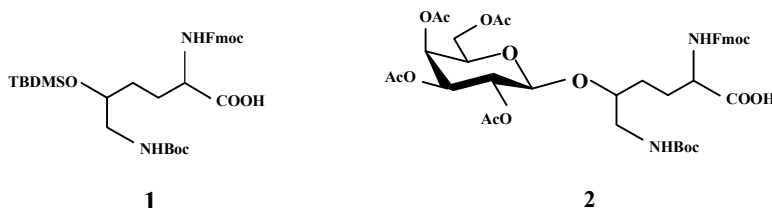
*Department of Chemistry and Biochemistry, Florida Atlantic University,
Boca Raton, FL 33431, USA*

Introduction

Hydroxylysine is the mayor glycosylation site within collagens, a diverse group of proteins made up of at least 25 members. The initial step in collagen glycosylation is hydroxylation of Lys residues in the 5-position. This posttranslational modification is performed by lysyl hydroxylases (LH1, LH2 and LH3). The second step is addition of galactose (β -D-galactopyranosyl). The third step is the addition of glucose [α -D-glucopyranosyl-(1 \rightarrow 2)- β -D-galactopyranosyl]. The roles of collagen glycosylation are multifaceted, and include regulation of cell-surface receptor interactions with collagen and collagen fibril assembly. Receptors whose recognition of collagen can be modulated by glycosylation include the DDR receptor tyrosine kinase family and CD44 proteoglycan [1,2]. T-cells have also been shown to specifically recognize a glycosylated sequence within type II collagen [3]. Research on the enzymology of Lys hydroxylation and subsequent glycosylation, as well as the role of glycosylated Hyl in receptor recognition would be greatly aided by convenient synthetic methods for the preparation of Hyl-containing peptides.

Results and Discussion

The goals of this work were two-fold: first, develop a convenient method for the synthesis of *O*-protected Fmoc-Hyl; second, evaluate the efficiency of methods for the synthesis of *O*-glycosylated Fmoc-Hyl. To achieve the first goal, *tert*-butyldimethylsilyl (TBDMS) protection of the Hyl 5-hydroxyl group was examined. The TBDMS group is base stable and acid labile, and can be introduced easily to secondary alcohols. Initial attempts to introduce TBDMS group using TBDMS-Cl under basic catalysis by imidazole in *N,N*-dimethylformamide failed, at least partially due to disruption of copper complexed Hyl. Recently, silylation of the hydroxyl group had been successfully performed using TBDMS trifluoromethanesulfonate and 2,6-lutidine as base in dichloromethane (CH₂Cl₂) [3]. Due to the low solubility of complex in CH₂Cl₂, different solvent systems and base catalysts were examined. The TBDMS Fmoc-Hyl derivative was conveniently prepared by the addition of TBDMS trifluoromethanesulfonate to copper-complexed Hyl[ϵ -*tert*-butyloxycarbonyl (Boc)] in the presence of 4-dimethylaminopyridine (DMAP) in pyridine as solvent [4]. Silylation of the hydroxyl group of copper complexed Hyl resulted in reduced solubility of the complex. We thus applied the original method for copper removal described by Barral and Savrda [5], using a pyridine:H₂O mixture and Na⁺ Chelex resin. The Fmoc group was added to the α -amino group and the resulting residue purified by flash chromatography to provide Fmoc-Hyl(ϵ -Boc,*O*-TBDMS) **1** in 67% overall yield. NMR and mass spectra confirmed the purity and composition of Fmoc-Hyl(ϵ -Boc,*O*-TBDMS) **1**.



Many different glycosylation procedures have been established and are constantly being improved and further developed. However, formation of β -D-glucosides of secondary alcohols with acceptable yields remains a challenge. In the present study we compared the efficiency of the thioglycoside, trichloroacetimidate, and Koenigs-Knorr methods for glycosylation of Hyl [4]. Recently, weakly acidic conditions for the classical glycosidation method of Koenigs-Knorr have been used in the synthesis of β -D-glucosides of hindered alcohols [6]. The described method represents compromises between orthoester formation and acidity of the reaction mixture. AgOTf in the presence of the very hindered base 2,6-di-*tert*-butyl-4-methylpyridine and TfOH scavenger were required in order to obtain good yields. Weakly acidic conditions proved to be beneficial in the synthesis of glycosylated Hyl as well. The most efficient method was found to be the Koenigs-Knorr, performed under inverse conditions. Fmoc-Hyl(ϵ -Boc)-OBzl and peracetylated galactosyl bromide were added to silver trifluoromethane sulfonate in 1,2-dichloroethane at -15°C and allowed to react for 15 min in acidic conditions before adding the base, resulting in 45% isolated yield. Catalytic hydrogenation of fully protected glycosylated Hyl at room temperature in EtOAc resulted in Fmoc-Hyl[ϵ -Boc, *O*-(2,3,4,6-tetra-*O*-acetyl- β -D-galactopyranosyl)] **2** in 61% yield. The Koenigs-Knorr inverse procedure presented here allows for the straightforward and efficient synthesis of the monoglycosylated Fmoc-Hyl[ϵ -Boc, *O*-(2,3,4,6-tetra-*O*-acetyl- β -D-galactopyranosyl)] derivative. The incorporation of hydroxyl-protected and glycosylated Hyl into peptides will allow for the further study of enzymes involved in collagen post-translational modification and the effects of glycosylation on cell recognition and signaling and collagen fibril formation.

Acknowledgments

This work was supported by the National Institutes of Health CA77402 and CA98799 (to G.B.F.), the National Science Foundation (NSF-0311369), and the FAU Center of Excellence in Biomedical and Marine Biotechnology.

References

1. Vogel, W., Gish, G. D., Alves, F. and Pawson, T. *Mol. Cell* **1**, 13-23 (1997).
2. Lauer-Fields, J. L., Malkar, N. B., Richet, G., Drauz, K. and Fields, G. B. *J. Biol. Chem.* **278**, 14321-14330 (2003).
3. Brodfalk, J., Backlund, J., Almqvist, F., Johansson, M., Holmdahl, R. and Kihlberg, J. *J. Am. Chem. Soc.* **120**, 7676-7683 (1998).
4. Cudic, M., Lauer-Fields, J. L. and Fields, G. B. *J. Peptide Res.* **65**, 272-283 (2005).
5. Barral, I. and Savrda, J. *Synthesis* 795-796 (1973).
6. Desmares, G., Lefebvre, D., Renevret, G. and Le Drian, C. *Helv. Chim. Acta* **84**, 880-889 (2001).

Synthesis and Biological Assessment of Sulfonic Acid-Based Glucagon Antagonists

Bin Yang, Vasily M. Gelfanov and Richard D. DiMarchi

Department of Chemistry, Indiana University, Bloomington, IN 47405, USA

Introduction

The structure-activity relationship of glucagon has been studied with a particular emphasis on the identification and refinement for selective receptor antagonism. Replacement of Asp⁹ with Glu⁹, in addition to the deletion of His¹ yields a potent antagonist [desHis¹, Glu⁹]glucagon amide, which is purported to retain weak partial agonist activity [1]. Sulfonic acid-based amino acids are structurally and electronically homologous to the more native carboxylic acid containing amino acids [2]. The dramatic biological significance exhibited by the subtle replacement of Asp⁹ with Glu⁹ attracted our attention to explore the suitability of a set of sulfonic acid-based glucagon homologs for Asp and Glu.

Results and Discussion

Peptides were synthesized with Rink resin by Fmoc/tBu chemistry. Sulfonic acid modified peptides devoid of Trp and Met were obtained by oxidation of the corresponding cysteine and homocysteine peptides in CH₃COOH/HCOOH/H₂O₂. Homocysteic acid substitution for Glu⁹ was tested in a set of peptides (peptide 4, 7, and 8) related to previously reported glucagon antagonists, and yielded fully efficacious and highly potent peptide ligands (Table 1). These analogs demonstrated a variable level of cAMP release that varied between 9-85% of the maximal level. The differences were clearly a function of the additional N-terminal modifications, such as des-Phe⁶ (peptide 7) and Leu⁴ (peptide 8). Substitution of Glu⁹ in peptide 2 with cysteic acid (homologous to Asp) yielded a full agonist (peptide 3, Fig. 1) without any apparent antagonist property.

Phe²⁵ and Leu²⁷ glucagon substitutions for Trp²⁵ and Met²⁷ were previously reported to increase the potency of the hormone [3]. Consequently, all the cysteic acid-based peptides were prepared with Phe²⁵ and Leu²⁷ to facilitate peptide synthesis without formation of oxidative by-products. Our results demonstrate an increase in the binding potency and cAMP bioactivity of the Phe²⁵ and Leu²⁷ analog.

Des-Phe⁶ as an additional modification to the standard antagonist (peptide 1) yielded a weak agonist analog devoid of any apparent antagonistic properties (peptide 5, Fig.1). This result is inconsistent with the previous report [4] and warrants additional study. Interestingly, the substitution of Glu⁹ with homocysteic acid in peptide 5 yielded a relatively pure antagonist (peptide 7, Fig. 2) with higher receptor binding than the Glu⁹-based peptide 5. Peptide 7 was identified to have the lowest level of cAMP stimulation and blocked glucagon-induced cAMP release to the fullest extent of any peptide studied (less than 10% of maximal) at a concentration of 50 μ M (Fig. 2).

Leu⁴ was reported to increase the antagonistic potency of peptide 1 and our results confirm this observation [5]. Surprisingly, the substitution of Glu⁹ with homocysteic acid in peptide 6 yielded a weak mixed agonist-antagonist with lower receptor binding activity, peptide 8.

In summary, the single deletion of the N-terminal histidine was insufficient to render the Glu⁹ glucagon-based analogs pure antagonists. We found that

homocysteic acid can function as a substitute for Glu⁹ in glucagon structure-function relationships, although the correlation is not simple with a number of unexpected findings. Substitution of Glu⁹ with homocysteic acid in peptides 2 and peptide 6 failed to produce significant antagonist properties. This same modification converted peptide 5 from an agonist to a specific antagonist with only modest agonist activity.

Table 1 Receptor binding, cAMP stimulation and inhibition of glucagon-induced cAMP release

#	Glucagon T ²⁹ -amide	Receptor Binding	cAMP Stimulation	cAMP Inhibition ^a	
		IC ₅₀ (nM)	EC ₅₀ (nM)	Max %	IC ₅₀ (nM)
	Native Glucagon Standard	1.75±0.31	0.21±0.11	100	N/A
1	[desH ¹ , E ⁹]	36.90±0.32	65±37	38.5	1862±1234
2	[desH ¹ , E ⁹ , F ²⁵ , L ²⁷]	12.59±0.41	81±23	81.5	N/A*
3	[dH ¹ , C ⁹ (SO ₃ ⁻), F ²⁵ , L ²⁷]	74.82±0.38	312±31	100	N/A*
4	[dH ¹ , hC ⁹ (SO ₃ ⁻), F ²⁵ , L ²⁷]	13.90±0.37	430±45	85.2	N/A*
5	[dH ¹ , dF ⁶ , E ⁹]	128.47±7.53	1178±105	88.2	N/A*
6	[dH ¹ , L ⁴ , E ⁹]	36.88±0.03	318±112	54.7	102±52
7	[dH ¹ , dF ⁶ , hC ⁹ (SO ₃ ⁻), F ²⁵ , L ²⁷]	37.08±0.30	3212±368	9.3	9217±3176
8	[dH ¹ , L ⁴ , hC ⁹ (SO ₃ ⁻), F ²⁵ , L ²⁷]	170.0±47.50	1614±1132	27.2	4456±1469

N/A* not antagonist; ^a 0.25 nM glucagon in each sample to stimulate cAMP production.

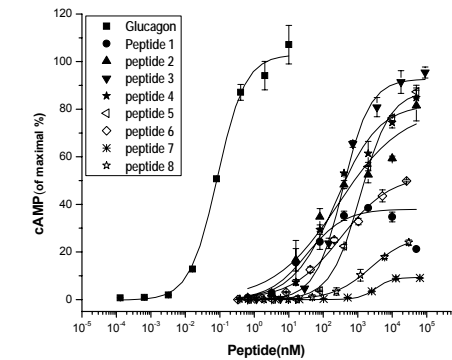


Fig. 1. Stimulation of cAMP synthesis in cells over-expressing glucagon receptor.

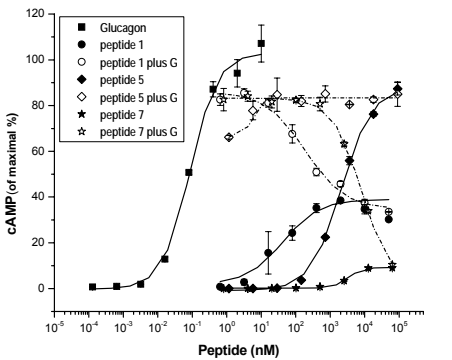


Fig. 2. Stimulation (solid) and inhibition (dashed) of cAMP production (dashed).

References

1. Unson, C. G., Gurzenda, E. M. and Merrifield, R. B. *Peptides* **10**, 1171-1177 (1989).
2. Arendt, A., *et al.* *Prot. Peptide Lett.* **7**, 359-364 (2000).
3. Murphy, W. A., Coy, D. H. and Lance, V. A. *Peptides* **7**, 69-74 (1986).
4. Azizeh, B. Y. *et al.* *Peptides* **18**, 633-641 (1997).
5. Ahn, J. M. *et al.* *J. Peptide Res.* **58**, 151-158 (2001).

Thioester Bond Liability: Study on Natural Influenza and Model Acylpeptides

Marina V. Serebryakova¹, Larisa V. Kordyukova², Boris V. Vaskovsky³
and Ludmila A. Baratova²

¹Orekhovich Institute of Biomedical Chemistry RAMS, Moscow 119121, Russia; ²Belozersky Institute of Physico-Chemical Biology MSU, Moscow 119992, Russia; ³Shemyakin-Ovchinnikov Institute of Bioorganic Chemistry RAS, Moscow 117997, Russia

Introduction

Influenza A hemagglutinin (HA) is a major envelope glycoprotein having attachment and fusion functions to deliver viral nucleoprotein into the host cell. It is a spike homotrimer; each monomer consists of two disulfide-linked chains (HA₁ and HA₂) and is anchored in the membrane by the light HA₂ chain C-terminal segment. Three conservative cysteine residues of the segment were shown to be palmitoylated via thioester bond [1] (Fig.1). Probably, fatty acids may serve to orient the TMD in the lipid bilayer and influence membrane fusion processes.

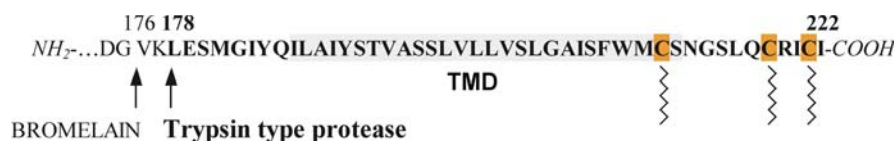


Fig. 1. Sequence of C-terminal region of Influenza HA₂ chain (strain A/Puerto Rico/8/34). Identified after bromelain digestion of viruses, bromelain- and some trypsin type protease-cleaved peptides (176-222 HA₂ and 178-222 HA₂, respectively) included transmembrane domains (TMD, light gray box) and three acylated Cys residues (dark gray boxes).

Previously, we have observed by MALDI-TOF MS that the C-terminal anchoring peptides, isolated from the bromelain-digested influenza viruses, are acylated heterogeneously (by palmitic and/or stearic acids) and to different degrees [2]. The latter could occur during isolation procedure or might reflect the natural state of the influenza A HA C-terminal region. Since digestion by bromelain was usually performed in the presence of 50 mM 2-mercaptoethanol (ME) [3] at 37°C for 18 hrs, we have now studied thioester bond sensitivity to thiol reagent both for influenza HA acylpeptides and for several Cys-modified model peptides.

Results and Discussion

Influenza viruses (strain A/Puerto Rico/8/34; PR8) were subjected to bromelain digestion in the presence or absence of 50 mM ME to obtain (+ME) or (-ME) subviral particles, respectively. The subviral particles were extracted by a chloroform-methanol (CM) (2:1) mixture and the organic phase was analyzed by MALDI-TOF MS using Ultraflex instrument (Bruker Daltonic, Germany). The HA₂ C-terminal peptides isolated from the (-ME) subviral particles predominantly possessed three palmitic/stearic acid residues, which were partly removed if the peptides were isolated from (+ME) particles (Fig. 2).

We have performed quantitative deacylation analysis by incubating the sample of triply acylated 178-222 HA₂ peptides with dithiotreitol (DTT, 10 mM) at 50°C and getting mass spectra in several time periods. As shown in Fig. 3A, full removing of palmitate and stearate residues from the peptide proceeded in 100 min incubation.

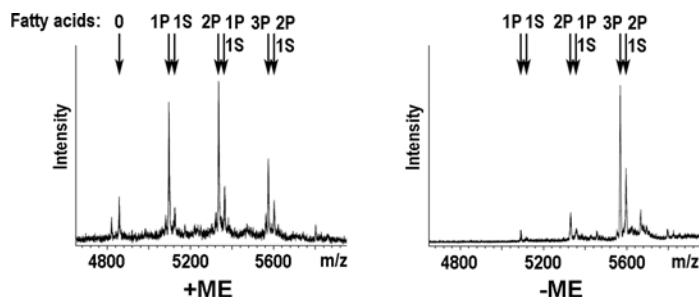


Fig. 2. MALDI-TOF MS analysis of the organic phase obtained by CM extraction of PR8 (+ME) or (-ME) subviral particles. Peaks of 178-222 HA₂ peptides bearing palmitate (P) and/or stearate (S) residues are designated.

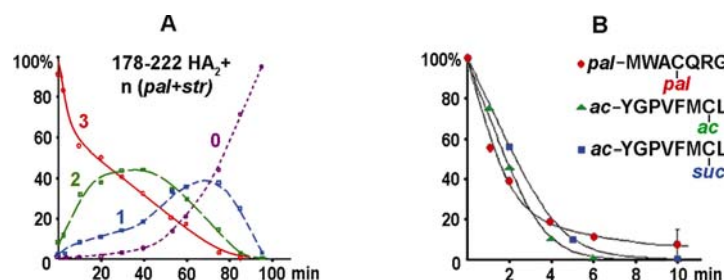


Fig. 3. Quantitative analysis of Cys-modifying groups removal by 10 mM DTT from Influenza PR8 acylpeptide 178-222 HA₂ (A); model peptides (B). Curves for triply (3), dually (2), mono- (1) and de- (0) acylated peptides are represented in (A); detaching of thioester-linked palmitic (pal), acetic (ac) or succinic (suc) residues is shown in (B).

The high liability of the thioester bond in the extracted HA acylpeptides became a surprise for us since the thioester-linked fatty acids was reported to detach from viral acylproteins by 1,4 M ME or 0,1 M DTT for 5 min of boiling in the presence of SDS [4]. We conducted a series of experiments on model S-palmitoylated peptide MWACQRG analogous to the influenza 207-213 HA₂ fragment (strain A/X-31) and have found that 10 mM DTT removed Cys-bound palmitic acid for 10 min at 20°C (Fig. 3B). Similar kinetics was found for model Cys-acetylated or Cys-succinylated peptide YGPVFMCL. To our mind, the rate of the deacylation process may represent the accessibility of the bond to the reducing reagent.

Acknowledgments

We thank Zhmak M.N. and Chikin L.D. (Shemyakin-Ovchinnikov IBCh RAS) for presenting YGPVFMCL and palmitoylated MWACQRG peptides, respectively. The work was supported by #2816p ISTC/BTEP grant.

References

1. Naeve, C. W. and Williams, D. *EMBO J.* **9**, 3857-3866 (1990).
2. Kordyukova, L. V., Serebryakova, M. V., Ovchinnikova, T. V., Ivanova, V. T. and Baratova, L. A. In *Peptides 2004, Proc. 3rd IPS and 28th EPS* (Flegel, M., Fridkin, M., Gilon, C. and Slaninova, J., eds.) in press (2006).
3. Brand, C. M. and Skehel, J. J. *Nat. New Biol.* **238**, 145-147 (1972).
4. Schmidt, M., Schmidt, M. F. and Rott, R. *J. Biol. Chem.* **263**, 18635-18639 (1988).

Chemical Synthesis of MUC2 Tandem Repeat Model Carrying Multiple *O*-GalNAc Moieties

Hironobu Hojo¹, Yoshiyuki Matsumoto¹, Yoshiaki Nakahara¹, Yusuke Suzuki², Minoru Suzuki² and Akemi Suzuki²

¹*Department of Applied Biochemistry, Tokai University, Kanagawa 259-1292, Japan;*

²*Sphingolipid Expression Laboratory, RIKEN Frontier, Saitama 351-0198, Japan*

Introduction

Mucins constitute the major component of mucus gels that cover the epithelial surfaces of various organs. They are heavily *O*-glycosylated within their tandem repeat region, where unit sequence carrying multiple *O*-glycosylation sites is repeated consecutively. The carbohydrate portion has a highly heterogeneous structure, except that the reducing end is α -GalNAc. The major role of mucins is the protection of the epithelial surfaces. However, recent studies show that they are also engaged in other important roles, such as growth, fetal development, epithelial differentiation, and carcinogenesis. However, due to the heterogenic nature at the sugar chain, further structural and functional studies would be difficult using natural mucins. We have established a facile method of glycoprotein synthesis based on the thioester method [1] combining the benzyl-protection strategy at the carbohydrate portion. Here, we report the extension of this procedure for the preparation of MUC2 basal structure carrying multiple *O*-GalNAc moieties.

Results and Discussion

To achieve the efficient synthesis of the tandem repeat structure, glycosylated peptide thioester of the repeating unit was prepared by solid-phase method and then repeatedly condensed by the thioester method. The sequence of MUC2 unit is PTTTPITTTTPTPTPTGTQT. To avoid the epimerization of the C-terminal amino acid residue during the segment coupling, the original sequence was designed to shift three residues so that the carboxyl terminal of this sequence is made to be glycine as shown in Figure 1. Among fourteen potential *O*-glycosylation sites within this sequence, we selected seven sites and introduced Tn-antigen for this initial study. The consecutive five Thr residues were included for the glycosylation site to mimic the dense cluster of carbohydrates of mucins. The synthetic route for this glycosylated peptide thioester **2** is shown in Figure 1. Starting from Fmoc-Gly-SCH₂CH₂CO-CLEAR amide resin, the peptide chain was elongated by Li's method, which uses Fmoc deblocking reagent compatible with peptide thioester synthesis [2]. For the introduction of the second and third amino acid, the combination of triisopropylsilyloxy (Tsoc)-protected amino acid and Fmoc-amino acid fluoride was used to suppress the formation of diketopiperazine [3]. GalNAc moiety was introduced using Fmoc-Thr carrying benzyl protected GalNAc **3** by HBTU-HOBt-DIEA. After the complete assembly of the peptide chain, the protected peptide resin was treated with Reagent K followed by Low-TfOH treatment [3,4] to remove the benzyl groups. In spite of the introduction of five consecutive GalNAc moieties and of the presence of multiple benzyl groups, the desired peptide thioester carrying seven GalNAcs was obtained in good purity as shown in Figure 2. The yield of peptide **2** was 6% based on the amino groups on the initial resin.

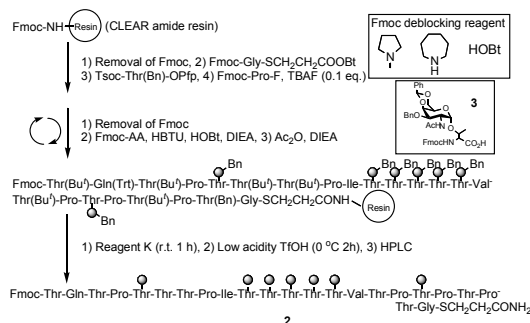


Fig. 1. Synthetic route for the repeating unit of MUC2 carrying 7 GalNAcs **2**.

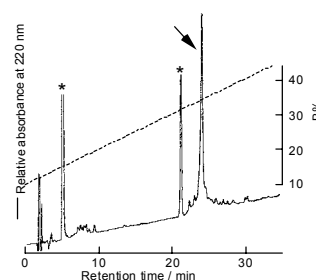


Fig. 2. HPLC profile of the crude glycopeptide thioester **2**.

Then the glycosylated peptide thioester **2** was repetitively condensed by the thioester method as shown in Figure 3. Each coupling reaction proceeded without serious side reactions within six hours. Even in the case of the 6th coupling reaction, which yielded a glycoprotein of over 20kDa, the efficiency of the coupling was maintained high. The yield of the coupling reactions was about 70% on average. The final product **1** was well characterized by the amino acid analysis (Thr_{80.70}Glu_{7.07}Pro_{29.09}Gly₆Val_{5.75}Ile_{5.98}) and ESI mass (Fig. 4). These results demonstrate this method to be highly efficient in the synthesis of tandem repeat structures. The method is also useful for the preparation of tandem repeats carrying various heterogeneous carbohydrates at the predetermined positions, which will simulate real mucin surfaces. Together with homogeneous models, these heterogeneous models will contribute to the functional and structural studies of mucins.

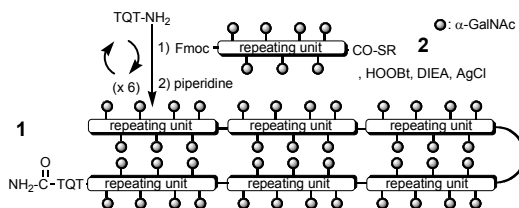


Fig. 3. Synthetic route for the tandem repeat glycoprotein **1**.

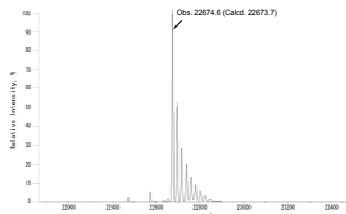


Fig. 4. ESI mass spectrum of glycoprotein **1**.

Acknowledgments

We acknowledge Tokai University for a grant-in-aid for high-technology research.

References

1. Aimoto, S. *Biopolymers*, **51**, 247-265 (1999).
2. Li, X., Kawakami, T. and Aimoto, S. *Tetrahedron Lett.* **39**, 8669-8672 (1998).
3. Hojo, H., *et al.* *Tetrahedron Lett.* **44**, 2961-2964 (2003).
4. Takano, Y., *et al.* *Tetrahedron Lett.* **43**, 8395-8399 (2002).

Site Specific Introduction of Unnatural Amino Acids at Sites Critical to Insulin Receptor Recognition and Biological Activity

Beili Quan, David L. Smiley, Vasily M. Gelfanov and Richard D. DiMarchi

Department of Chemistry, Indiana University, Bloomington, IN 47405, USA

Introduction

Insulin constitutes a hormone of central importance in physiology and a vital element in glucose management. Its use in diabetes care has been of seminal significance for nearly a century. The advent of rDNA biosynthesis provided human insulin in virtually unlimited quantity. The advent of chemical biotechnology (biosynthesis with unnatural amino acids) provides a new venue for optimizing insulin pharmacology through the use of chemistry that otherwise would be prohibitively expensive. Our work has focused on two amino acids in the C-terminus of the B-chain that are central to insulin activity, specifically positions B24 and B25.

Experimental Design

Insulin B chain analogs with unnatural amino acids at B24 and B25 were successfully synthesized by solid phase methodology using Fmoc/tBu chemistry. Peptides were removed from the support in strong anhydrous acid and purified under acidic conditions by preparative high performance reverse-phase chromatography in the free sulfhydryl form. Each peptide was characterized by MALDI-MS and HPLC analysis to be at least 90% pure prior to chain combination. B-chain analogs were mixed with a molar equivalent of native A-chain S-sulfonate in a 0.05 M glycine buffer, pH 10.5. A molar equivalent of DTT relative to each S-sulfonate was used to facilitate disulfide interchange. The reaction was conducted at 4°C, overnight. The product was purified by preparative HPLC in a slightly alkaline NH_4HCO_3 buffer with CH_3CN elution. The insulin analogs were obtained in step yield that varied from 5-30%, and characterized by MS and HPLC analysis to be >95% pure.

The binding affinity of each insulin analog for the insulin receptor was measured in a competition scintillation proximity assay, with 3- ^{125}I ,TyrA¹⁴. Plasma membrane fragments prepared from cells over-expressing the human insulin receptor were the source of insulin receptor. Non-specifically bound radioactivity was measured with fourfold greater concentration of “cold” native ligand than the highest concentration in test samples and total bound radioactivity was detected in the wells with no competitor. IC_{50} values were determined by using Origin software (OriginLab, Northampton, MA).

Results and Conclusion

Nineteen different amino acids (17 non-natural) were substituted for the native insulin phenylalanine residues at positions B24 and B25. The analogs were successfully prepared from individual A and B chains in total yields that varied between 1-10%. The relative binding affinity of this group of insulin analogs for the insulin receptor was determined to differ by more than a thousand-fold from the most potent to the least potent peptide studied (Table 1). Consistent with previous observations predominantly employing native amino acids, we observed that insulin

activity was dependent upon aromatic character at both residues [1]. Position B24 was extremely restrictive to structural change while B25 was extremely permissive.

Each of the B25 insulin analogs were of high affinity while only one of the B24 analogs did not exhibit a sizable reduction in binding affinity. The highly homologous B24 Phe(4-F) analog is a rare example of an L-amino acid with comparable potency to the native hormone, and represents an opportunity for structural study in the receptor recognition site with F¹⁹ isotopically enriched amino acid. Further study at B24 illustrated that even a single methyl group added to the phenyl ring is deactivating and most notably when ortho to the ring. Phenylalanine heterocycle-based mimetics were studied. An appreciable difference was observed among two commonly used derivatives. The 5-membered thiophene ring provided nearly native insulin affinity but the more alkaline 6-membered pyridine ring was sizably reduced in potency.

Additional study at position B25 demonstrated that movement of the phenyl ring closer or further from the peptide backbone had a significant deactivating impact upon binding affinity [2]. Modifications that introduced negative charge (4-COOH) and size (4-Br) were largely without effect on insulin binding affinity. In contrast, the alkaline amino-methyl substitution (4-CH₂NH₂) reduced binding affinity to a significant degree. This observation is consistent with the more subtle reduction noted for the less alkaline 4-NH₂ modification.

In summary, B24 has proven highly restrictive to modification, and yet for the first time we have identified two L-amino acids of near-native affinity. In comparison, position B25 is quite accommodating to sizable changes in side-chain structure, but highly demanding in that the phenyl ring must be positioned at the beta-carbon. These collective observations establish a foundation for application of unnatural amino acids as a route to insulin pharmacology that may not be obtainable with natural amino acids alone.

Table 1. Binding affinity of insulin analog

B24	IC ₅₀ , nM	B25	IC ₅₀ , nM
Phe	0.67±0.18	Phe	0.67±0.18
Phe(4-F)	0.51±0.18	Phe(4-F)	0.91±0.16
(4-NH ₂)	3.55±1.80	(4-NH ₂)	1.03±0.25
(4-OH)	6.79±1.53	(4-OH)	0.72±0.21
(4-CF ₃)	16.58±3.37	(4-CF ₃)	0.49±0.10
2-Me	18.25±4.58	hPhe	13.15±0.73
3-Me	6.78±1.91	Phg	>1000
4-Me	5.25±0.88	4-Me	0.67±0.11
4-Pyridyl	22.54±1.17	4-COOH	0.83±0.37
Thienyl	0.63±0.04	4-Br	0.54±0.16
		4-CH ₂ NH ₂	3.15±0.12

References

1. Mirmira, R. G., Nakagawa S. H. and Tager, H. S. *J. Biol. Chem.* **266**, 1428-1436 (1999).
2. Nakagawa, S. H. and Tager, H. S. *J. Biol. Chem.* **261**, 7332-7341 (1986).

Towards Peptides as Potential Therapeutics

Target-Based Proteolytic Profiling for Characterizing Cancer Progression

**Janelle L. Lauer-Fields¹, Dmitriy Minond¹, Diane Baronas-Lowell¹,
Michael J. Chalmers², Scott A. Busby², Patrick R. Griffin², Hideaki
Nagase³ and Gregg B. Fields^{1,2}**

¹Department of Chemistry & Biochemistry, Florida Atlantic University, Boca Raton, FL 33431, USA; ²Drug Discovery, Scripps Florida, Jupiter, FL 33458 USA; ³Kennedy Institute of Rheumatology Division, Imperial College London, Hammersmith W6 8LH, UK

Introduction

Proteases play fundamentally important roles in normal physiology and disease pathology. Methods for detection of active proteolysis may greatly aid in the diagnosis of disease progression, and suggest modes of therapeutic intervention. Current proteolytic profiling can be organized into two categories: (1) activity-based protein profiling (ABPP) (also known as mechanism-based profiling) using an enzyme active site-directed chemical probe to assess the proteolytic activity of a class of enzymes in a complex sample; and (2) target-based profiling using targets based either on (a) a given proteinase or (b) a given substrate in a complex sample.

The hydrolysis of collagen (collagenolysis) is one of the committed steps in basement membrane turnover [1], and it has long been demonstrated that tumor extracts can possess collagenolytic activity [2]. The triple-helical structure of collagen renders it resistant to most proteases. In vertebrates, the enzymes that cleave triple-helical structure include cathepsin K and collagenolytic matrix metalloproteinase (MMP) family members (MMP-1, -2, -8, -13, -14, and -18). Other members of the MMP family, such as MMP-3, share similar primary and three-dimensional structures and substrate sequence specificities with collagenolytic MMPs, but do not cleave triple-helical structures [3-5]. Triple-helical structure itself provides favorable interactions with several MMPs (i.e., MMP-1 and MMP-8 hydrolyze a triple-helical substrate more efficiently than an analogous single-stranded one), while the activities of other MMPs are inhibited by triple-helical structure (i.e., MMP-3) [5,6].

The roles that MMPs play in the metastatic process are diverse and include involvement in primary and metastatic tumor growth, angiogenesis, and degradation of basement membrane barriers (such as collagen) during tumor cell invasion [2]. Multiple studies have correlated MMP production and melanoma metastasis. Melanoma cells have been found to express MMPs with collagenolytic activity, including MMP-1, MMP-2, MMP-9, MMP-13, and MMP-14 [7].

Melanoma cell interactions within the microenvironment (which includes extracellular matrix proteins such as collagen) are mediated by various receptors, including integrins and proteoglycans. The $\alpha 1\beta 1$, $\alpha 2\beta 1$, and $\alpha 3\beta 1$ integrins and CD44/chondroitin sulfate proteoglycan (CSPG) are present on melanoma cells and bind to collagen [8]. The $\alpha 1\beta 1$ and $\alpha 2\beta 1$ integrins and CD44/CSPG are upregulated in metastatic melanoma, while the $\alpha 3\beta 1$ integrin is upregulated in both primary and metastatic melanoma [8]. Melanoma cell $\alpha 2\beta 1$ integrin and CD44/CSPG receptors bind type IV collagen at $\alpha 1(\text{IV})382\text{-}393$ and $\alpha 1(\text{IV})1263\text{-}1277$, respectively, and triple-helical peptide (THP) models of these sites have been constructed (Fig. 1) [5,8,9].

The interactions of collagen with various melanoma cell surface receptors trigger signaling pathways that result in the release of proteinases, cell surface receptor shedding, and growth factor and cytokine activation, and ultimately promote tumor cell progression. The present study has focused on the induction of MMP collagenolytic activity by the melanoma microenvironment.

$\alpha 1(\text{IV})1263\text{--}1277$ THP: $\text{C}_{16}\text{--}(\text{GPP}^*)_4\text{GVKGDKGNGWPGAP}(\text{GPP}^*)_4\text{--NH}_2$
 $\alpha 1(\text{IV})382\text{--}393$ THP: $\text{C}_{16}\text{--}(\text{GPP}^*)_4\text{GAP*GFP*GERGEK}(\text{GPP}^*)_4\text{--NH}_2$
fTHP-4: $\text{H--}(\text{GPP}^*)_5\text{GPK[Mca]GPQGLRGQK[Dnp]GVR}(\text{GPP}^*)_5\text{--NH}_2$
fTHP-9: $\text{H--}(\text{GPP}^*)_5\text{GPK[Mca]GPQGC[Mob]RGQK[Dnp]GVR}(\text{GPP}^*)_5\text{--NH}_2$
 $\alpha 1(\text{V})436\text{--}447$ THP: $\text{H--}(\text{GPP}^*)_5\text{GPK[Mca]GPPGVVGEK[Dnp]GEQ}(\text{GPP}^*)_5\text{--NH}_2$
fTHP-10: $\text{H--}(\text{GPP}^*)_5\text{GPK[Mca]GPOGLRGQK[Dnp]GVR}(\text{GPP}^*)_5\text{--NH}_2$
fTHP-11: $\text{H--}(\text{GPP}^*)_5\text{GPK[Mca]GPOGC[Mob]RGQK[Dnp]GVR}(\text{GPP}^*)_5\text{--NH}_2$

Fig. 1. Sequences of THP ligands and substrates. P = Hyp, O = Orn, Mca = (7-methoxycoumarin-4-yl)acetyl, Dnp = 2,4-dinitrophenyl, Mob = 4-methoxybenzyl.*

Results and Discussion

Collagenous barriers are often compromised during invasion; thus, assays utilizing THP collagen models as “targets” have been developed and applied to study constitutive and induced MMP activity in human melanoma. For MMP-1, active enzyme was quantified by solid-phase mAb immobilization of the enzyme followed by reaction with the fluorogenic substrate fTHP-4 (Fig. 1) [10]. The solid-phase assay showed more activity induced by the $\alpha 2\beta 1$ integrin than by CD44 (Table 1), and treatment of samples with an activator of proMMPs (4-aminophenylmercuric acetate) resulted in a further increase in MMP-1 activity [10], indicative of the production of both MMP-1 and proMMP-1 by engagement of either the $\alpha 2\beta 1$ integrin or CD44.

General triple-helical peptidase activity was evaluated using fTHP-4 in solution. Engagement of either the $\alpha 2\beta 1$ integrin or CD44 resulted in significant triple-helical peptidase activity detected in melanoma cell conditioned media, with greater activity found in response to CD44 [8]. This activity was completely inhibited by EDTA, suggesting metalloproteinase activity [5]. The MMP-14 selective substrate C_{10} -fTHP-9 (Fig. 1) [11] was used for comparison to general triple-helical peptidase activity. Soluble MMP-14 activity, which can be generated by non-autocatalytic shedding of MMP-14 [12,13], was significant at early time points and then decreased over 8 hrs in response to the $\alpha 2\beta 1$ integrin and CD44 ligands [8]. The MMP-14 activity profiles correlate well with the mRNA expression profiles, in that MMP-14 is induced at early time points (Table 1). The subsequent decrease in MMP-14 activity may be due to degradation of MMP-14. Other MMP activity profiles do not decrease at later time points, and exogenous MMP activity is not significantly affected over a 24 hr period by melanoma conditioned media. These results suggest that degradation of MMP-14 is specific, which is not surprising considering the multitude of MMP-14 shedding processes [13].

Gelatinase activity was initially evaluated using the MMP-2/MMP-9 selective substrate $\alpha 1(\text{V})436\text{--}447$ fTHP (Fig. 1) [5]. Gelatinase activity showed virtually identical increases in response to the $\alpha 2\beta 1$ integrin and CD44 ligands (Table 1) [8]. Since the MMP-2/MMP-9 selective substrate does not differentiate between the two gelatinases, additional activity assays were performed using gelatin zymography. Zymography indicated that the $\alpha 2\beta 1$ integrin and CD44 ligands produced

predominantly MMP-2 [8]. Treatment with 1,10-phenanthroline (a zinc metalloenzyme inhibitor) resulted in complete loss of gelatinolysis [8], indicative of metalloproteinase activity.

Table 1. Relative induction of target genes by the $\alpha 2\beta 1$ integrin and CD44/CSPG triple-helical ligands^a

Target	Receptor Engaged	mRNA	Protein	Active Enzyme
MMP-1	$\alpha 2\beta 1$ integrin	++	+	++
“	CD44/CSPG	+	+	+
MMP-2	$\alpha 2\beta 1$ integrin	$\sim \rightarrow ++$	ND	++
“	CD44/CSPG	$\sim \rightarrow +$	ND	++
MMP-3	$\alpha 2\beta 1$ integrin	+	$++ \rightarrow \sim$	ND
“	CD44/CSPG	NM	+	ND
MMP-8	$\alpha 2\beta 1$ integrin	NM	-	ND
“	CD44/CSPG	$+++ \rightarrow \sim$	++	ND
MMP-13	$\alpha 2\beta 1$ integrin	+++	+++	ND
“	CD44/CSPG	+	++	ND
MMP-14	$\alpha 2\beta 1$ integrin	$+ \rightarrow \sim$	ND	$+ \rightarrow \sim$
“	CD44/CSPG	$+ \rightarrow \sim$	ND	$+ \rightarrow \sim$

^aNM = negligible modulation; ND = not determined; “+” indicates relative upregulation; “ \sim ” indicates relative down regulation; “ $+ \rightarrow \sim$ ” indicates upregulation followed by down regulation; “ $\sim \rightarrow +$ ” indicates down regulation followed by upregulation.

Ligands to the $\alpha 2\beta 1$ integrin or CD44 were found to induce different proteolytic profiles (Table 1), suggesting that the microenvironment can modulate melanoma invasion. These initial studies have prompted our (1) further investigation of the interactive role of CD44 and MMP-14 in melanoma progression and (2) comparison between surface-bound and soluble active MMP-14 levels utilizing MMP-14 discriminatory substrates. Analysis of surface-bound MMP-14 will be especially valuable, as prior methods cannot quantify MMP-14 levels in cellular environments.

As the roles of individual MMPs in cancer progression are better understood, it would be beneficial to use this information to design selective MMP inhibitors. A typical collagenolytic MMP consists of a catalytic domain, a proline-rich linker region, and a C-terminal hemopexin-like (Hpx) domain (Fig. 2). Collagenolytic activity is only expressed by the full-length enzyme containing the linker and Hpx domain. Elucidation of the three-dimensional structure of MMP-1 indicated that the enzyme active site is too narrow to accommodate a collagen triple-helix [14]. We have recently demonstrated that MMP-1 unwinds the triple-helical structure prior to hydrolysis of the peptide bond [14]. This unwinding activity requires both the catalytic and Hpx domains [11,14]. The detailed interactions between an inactive mutant of MMP-1 [MMP-1(E200A)] and collagen model peptides during binding and unwinding of triple-helical structure was investigated using hydrogen/deuterium exchange mass spectrometry (HDX MS) [15]. The triple-helix was found to

significantly slow exchange at several MMP-1 regions outside of the active site, including residues 141-148 and 198-207 (solvent-exposed loops in the catalytic domain), 258-276 (the solvent exposed linker between the catalytic and Hpx domains), and 285-296 (the first two β -sheets of the Hpx domain). Identification of these regions will direct future studies of site-directed mutants of MMP-1, to precisely determine the MMP residues participating in triple-helix binding and unwinding.

Mapping of MMP/THP interactions led to the identification of MMP regions distant from the active site that participate in collagenolysis. These “exosites” represent unique opportunities for design of inhibitors with enhanced specificities. Exploration of THP sequence specificity may also allow for unique inhibitor design. The THP sequence specificity of collagenolytic MMPs was examined by substitution of Orn in the P_2 subsite of fTHP-4 (creating fTHP-10; Fig. 1) and fTHP-9 (creating fTHP-11; Fig. 1). The hydrolysis of fTHP-4, fTHP-9, fTHP-10, and fTHP-11 was compared for MMP-8, MMP-13, and MMP-14 (Table 2). Substitution of the P_1' subsite Leu by Cys(Mob) (fTHP-4 versus fTHP-9) was favored by all three MMPs. Substitution of the P_2 subsite Gln by Orn (fTHP-4 versus fTHP-10) was greatly preferred by MMP-13, detrimental to MMP-14 activity, and had little effect on MMP-8. Analysis of the double substitution of Orn for Gln in the P_2 subsite and Cys(Mob) for Leu in the P_1' subsite (fTHP-11) suggested non-additive effects on MMP activity. Compared to fTHP-9, substitution of Orn in the P_2 subsite resulted in both MMP-13 and MMP-14 activity decreasing by ~50%, while MMP-8 activity was considerably worse. However, the earlier comparison of fTHP-4 and fTHP-10 activities (which differ only by Orn in the P_2 subsite) showed little effect on MMP-8 activity and *increased* activity for MMP-13. This indicates non-independence of the interaction of substrate subsites with MMPs, which was previously observed using single-stranded substrates [3]. While difficult to quantify, this non-independence could be correlated to individual MMP structural features and used to further the development of selective substrates and inhibitors. Overall, the use of collagen-based proteolytic profiling has lead to quantitative monitoring of proteolysis regulation in cellular systems and insight into novel inhibitor design.

Acknowledgments

The work was funded by NIH CA 98799 and the FAU Center of Excellence in Biomedical and Marine Biotechnology. Scripps Florida is funded by the State of Florida.

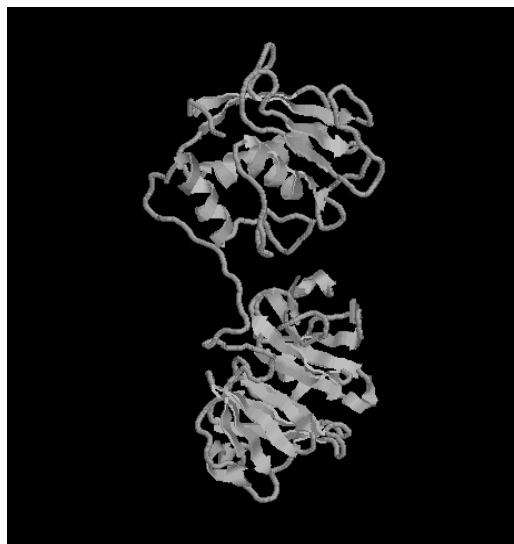


Fig. 2. Structure of MMP-1. The catalytic domain is shown on top, and the hemopexin-like domain below.

Table 2. Hydrolysis of THP substrates by MMP-8, -13, and -14

Substrate	MMP	k_{cat}/K_M (sec ⁻¹ M ⁻¹)
fTHP-4 (P ₁ ' = Leu)	8	4,490
“	13	1,570
“	14	59,600
fTHP-9 [P ₁ ' = Cys(Mob)]	8	175,480
“	13	25,000
“	14	169,000
fTHP-10 (P ₂ = Orn; P ₁ ' = Leu)	8	4,260
“	13	18,950
“	14	25,125
fTHP-11 [P ₂ = Orn; P ₁ ' = Cys(Mob)]	8	19,400
“	13	13,150
“	14	78,500

References

1. Chang, C. and Werb, Z. *Trends Cell Biol.* **11**, S37-S43 (2001).
2. Nelson, A. R., Fingleton, B., Rothenberg, M. L. and Matrisian, L. M. *J. Clin. Oncol.* **18**, 1135-1149 (2000).
3. Nagase, H. and Fields, G. B. *Biopolymers* **40**, 399-416 (1996).
4. Chung, L., Shimokawa, K., Dinakarpandian, D., Grams, F., Fields, G. B. and Nagase, H. *J. Biol. Chem.* **275**, 29610-29617 (2000).
5. Lauer-Fields, J. L., Sritharan, T., Stack, M. S., Nagase, H. and Fields, G. B. *J. Biol. Chem.* **278**, 18140-18145 (2003).
6. Ottl, J., Gabriel, D., Murphy, G., Knäuper, V., Tominaga, Y., Nagase, H., Kröger, M., Tschesche, H., Bode, W. and Moroder, L. *Chem. Biol.* **7**, 119-132 (2000).
7. Hofmann, U. B., Westphal, J. R., van Muijen, G. N. P. and Ruiter, D. J. *J. Invest. Dermatol.* **115**, 337-344 (2000).
8. Baronas-Lowell, D., Lauer-Fields, J. L., Borgia, J. A., Sferrazza, G. F., Al-Ghoul, M., Minond, D. and Fields, G. B. *J. Biol. Chem.* **279**, 43503-43513 (2004).
9. Lauer-Fields, J. L., Malkar, N. B., Richet, G., Drauz, K. and Fields, G. B. *J. Biol. Chem.* **278**, 14321-14330 (2003).
10. Lauer-Fields, J. L., Nagase, H. and Fields, G. B. *J. Biomol. Tech.* **15**, 305-316 (2004).
11. Minond, D., Lauer-Fields, J. L., Nagase, H. and Fields, G. B. *Biochemistry* **43**, 11474-11481 (2004).
12. Toth, M., Hernandez-Barrantes, S., Osenkowski, P., Bernardo, M. M., Gervasi, D. C., Shimura, Y., Meroueh, O., Kotra, L. P., Galvez, B. G., Arroyo, A. G., Mobashery, S. and Fridman, R. *J. Biol. Chem.* **277**, 26340-26350 (2002).
13. Osenkowski, P., Toth, M. and Fridman, R. *J. Cell. Physiol.* **200**, 2-10 (2004).
14. Chung, L., Dinakarpandian, D., Yoshida, N., Lauer-Fields, J. L., Fields, G. B., Visse, R. and Nagase, H. *EMBO J.* **23**, 3020-3030 (2004).
15. Hamuro, Y., Coales, S. J., Southern, M. R., Nemeth-Cawley, J. F., Stranz, D. D. and Griffin, P. R. *J. Biomol. Tech.* **14**, 171-182 (2003).

From Simple Consensus Peptides to High Affinity Ligands: A Stepwise Diversity Oriented Strategy for the Acquisition of Potent Signaling Inhibitors

David S. Lawrence

Department of Biochemistry, The Albert Einstein College of Medicine, Bronx, NY 10461

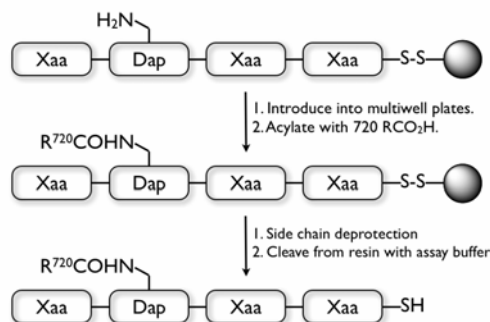
Introduction

Cells recognize and respond to environmental changes via signal transduction, biochemical pathways mediated by protein-protein interactions. There is a great deal of interest in acquiring agents that disrupt the ability of signaling proteins to associate with their binding partners. These inhibitors have not only proven useful as reagents for correlating protein action with cellular behavior, but ultimately may find utility as therapeutics.

Peptides containing consensus sequences recognized by signaling proteins can block protein-protein interactions. However, peptides containing conventional amino acid residues are limited in a number of ways. First, most signaling proteins engaged in protein recognition will bind consensus sequence-containing peptides, but the thermodynamic stability of these complexes is generally modest ($K_d \sim$ low μ M). Consequently, inhibitory potency represents a key unmet challenge. Second, individual protein recognition domains (e.g., SH2, SH3, PDZ, etc.) exist as subfamilies containing a number of highly homologous members. Indeed, simple consensus peptides are generally unable to discriminate between related protein recognition domains. Third, interactions between proteins typically transpire over a large surface area. For conventional peptides, potential high affinity interactions with surface functionality are inaccessible to standard amino acid residues. Finally, unlike conformationally well-defined active sites, protein surfaces are structurally flexible and therefore the design of a ligand that targets the surface can be quite difficult. We have developed a stepwise library-based strategy that addresses these issues and thereby allows us to convert consensus sequence peptides into high affinity ligands.

Results and Discussion

The general strategy outlined in Scheme 1 begins with a consensus peptide that is attached to a resin via a chemically engineered disulfide bridge [1,2]. (L)-2,3-diaminopropionic acid (Dap) is inserted into the consensus sequence at specific positions along the peptide chain based on the 3-dimensional structure of the target protein (or at random positions in the absence of structural information). The peptide resin is subsequently introduced into individual wells of a multiwell synthesis plate. Each well contains a unique carboxylic acid moiety. The libraries described in this study are derived from 720 commercially available, structurally diverse, carboxylic acids. Following Dap side chain acylation, any protecting groups on the peptide are removed, the peptide cleaved from the resin with assay buffer (which contains dithiothreitol), and the liberated peptide filtered into a receiving plate in an assay ready form. The advantages of this approach are several-fold. First, the diversity at the Dap site (720) is dramatically greater than what is available with conventional genetically encoded amino acid residues (20). Second, the spatially focused nature of the Scheme 1 strategy allows one to target specific



Scheme 1. General library strategy for the construction of peptide-substituent hybrids.

subsites of the protein surface. Third, the process can be iteratively applied, with additional Dap residues (and therefore additional molecular diversity) introduced at other positions along the peptide chain. Finally, the overall process can be easily automated, a significant advantage given the hundreds, if not thousands, of potentially interesting protein interaction domains.

Our initial studies applied the Scheme 1 approach to SH2 domains, protein interaction domains that recognize and bind to phosphotyrosine-containing peptides [3,4]. The Lck SH2 domain exhibits a K_D of 1.3 μ M for the conventional peptide, Ac-pTyr-Glu-Glu-Ile **1**. The N-terminal acetyl moiety (oriented toward subsite A) and the glutamic acid side chains (oriented toward subsites B and C), only weakly interact with the protein surface (Fig. 1) [5]. We introduced molecular diversity at these three sites in a stepwise fashion to ultimately produce the lead ligand **2**, which exhibits

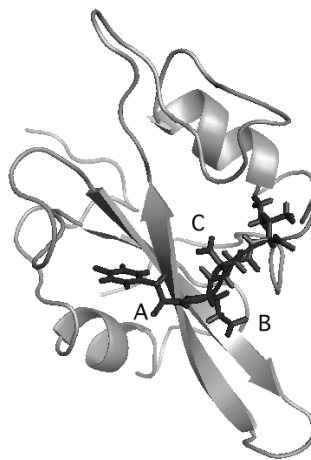
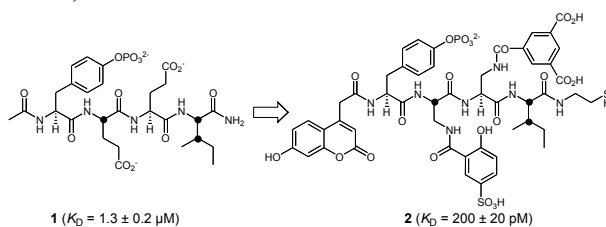


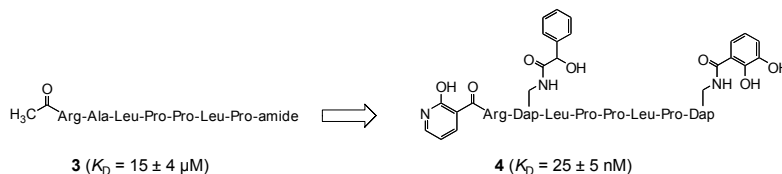
Fig. 1. The 3-dimensional structure of Ac-pTyr-Glu-Glu-Ile bound to the Lck SH2 domain. The acetyl moiety is oriented into subsite A and the glutamic acid side chains are positioned toward subsites B and C.



Scheme 2

nearly four orders of magnitude enhanced affinity for the Lck SH2 domain relative to the parent peptide (Scheme 2) [1,2].

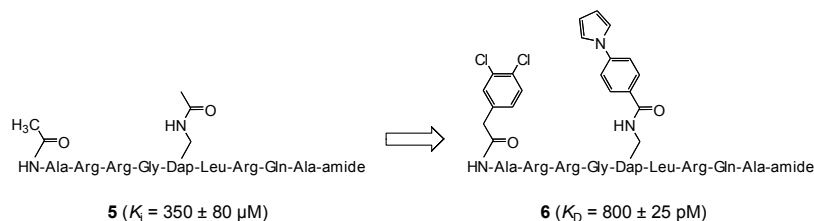
We have also investigated the acquisition of ligands for the SH3 domain from Fyn, a member of the Src kinase subfamily of protein tyrosine kinases. SH3 domains are small (~60 amino acid residues) motifs that recognize proline-rich sequences [6]. We were not only interested in identifying inhibitors that could bind with a reasonable affinity relative to conventional peptides, but we also wished to acquire a selective reagent that displays a special affinity for the Fyn SH3 domain versus the other SH3 domains from the Src kinase family. We felt that this would be a good test of the Scheme 1 strategy given the high sequence identity (80%) and small size of these protein interaction domains. The starting consensus sequence parent peptide, Ac-Arg-Ala-Leu-Pro-Pro-Leu-Pro **3**, exhibits a moderate affinity for the Fyn SH3 domain. Subsequent transformation into the triply derivatized peptide **4** furnished a high affinity ligand with a 10-fold selectivity for the Fyn domain relative to the other Src kinase SH3 domains (Scheme 3) [7].



Scheme 3

The protein kinase C (PKC) subfamily of enzymes is comprised of a dozen highly homologous members (up to 80% active site sequence identity) [8]. We were especially interested in acquiring a potent and selective inhibitor for PKC α , an enzyme whose overexpression and/or unregulated activity has been implicated in enhanced cellular motility and metastasis [9]. In the absence of a 3-dimensional structure, we chose three random sites on the consensus sequence peptide to introduce molecular diversity. Two of these sites furnished useful derivatives, which ultimately lead to the identification of compound **6** (Scheme 4). The latter is nearly six orders of magnitude more potent than the starting parent peptide **5** [10]. Furthermore, the doubly derivatized peptide exhibits impressive selectivity against the PKC isoform family that ranges from 385-fold (versus PKC β) up to more than 2700-fold (versus PKC δ) [10].

PTP1B is a negative regulator of the insulin and leptin signaling pathways [11]. The enzyme catalyzes the hydrolysis of phosphotyrosine to tyrosine in peptide and protein substrates, including the β chain of the insulin receptor and various insulin receptor substrates. Knock-out mice lacking this protein are resistant to diet induced



Scheme 4

diabetes and obesity, suggesting that PTP1B inhibitors could be useful for the treatment of these disorders. In collaboration with my colleagues Zhong-Yin Zhang and Steve Almo, we demonstrated that PTP1B simultaneously binds two molecules of phosphotyrosine: at the active site and at a nearly peripheral site (Fig. 2) [12]. Although the active site region is highly conserved among members of the protein tyrosine phosphatase family, the residues that constitute the peripheral site are not.

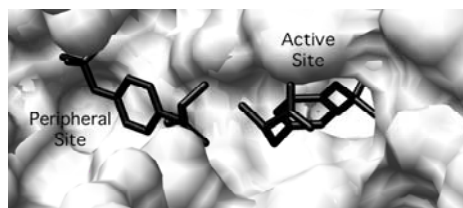


Fig. 2. The 3-dimensional structure of PTP1B with two simultaneously bound phosphotyrosine moieties.

Consequently, it occurred to us that a single molecule, which occupies both sites, could exhibit high potency and selectivity for PTP1B. My laboratory, in collaboration with the Zhang group, prepared a small library of 184 compounds [13]. These derivatives contained an active site-directed phosphotyrosine moiety, a tether residue designed to link the substituents embedded within the

active and peripheral sites, and a proximal site-directed aryl acid terminal element (Fig. 3). Since the library members possessed hydrolyzable phosphates, the screen employed an inactive PTP1B mutant that is catalytically inactive but still capable of binding active site-directed compounds with the same affinity as the wild type enzyme. Based on the identified lead derivative **7**, we prepared the non-hydrolyzable bis-difluorophosphonate **8** (Scheme 5). The latter is a powerful PTP1B inhibitor that exhibits impressive selectivity against a broad range of protein tyrosine phosphatases. We also prepared several membrane permeable analogs of **8**, including the fatty acid derivatized species **9** [14]. As we anticipated, cells treated with compound **9** enhance insulin-induced phosphorylation levels of the insulin receptor as well as one of the insulin receptor's substrate, IRS-1. Furthermore, downstream signaling proteins, such as Akt, also exhibit enhanced levels of activation. Finally, inhibitor-treated cells display a significantly increased insulin-induced glucose uptake. In short, the PTP1B inhibitor **9** serves as an insulin sensitizer. However, much to our surprise, we discovered that an analogous biochemical response was observed with inhibitor-treated cells even in the absence of insulin. The latter was unanticipated, but clearly demonstrates that compound **9** also behaves as an insulin mimetic.

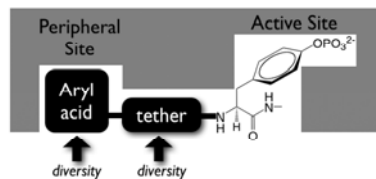
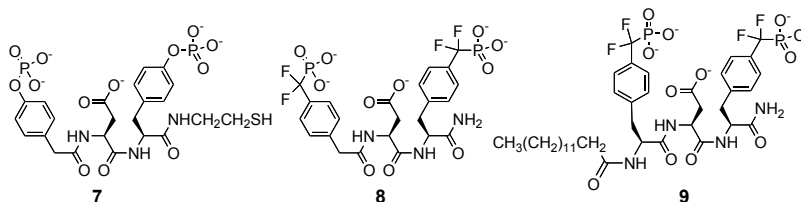


Fig. 3. Library-based strategy for the acquisition of PTP1B inhibitors.



Scheme 5

Acknowledgments

The work was funded by the National Institutes of Health.

References

1. Lee, T. R. and Lawrence, D. S. *J. Med. Chem.* **42**, 784-787 (1999).
2. Yeh, R. H., Lee, T. R. and Lawrence, D. S. *J. Biol. Chem.* **276**, 12235-12240 (2001).
3. Machida, K. and Mayer, B. J. *Biochim. Biophys. Acta* **1747**, 1-25 (2005).
4. Schlessinger, J. and Lemmon, M. A. *Sci. STKE* **2003**, RE12 (2003).
5. Tong, L., Warren, T. C., King, J., Betageri, R., Rose, J. and Jakes, S. *J. Mol. Biol.* **256**, 601-610 (1996).
6. Dalgarno, D. C., Botfield, M. C. and Rickles, R. J. *Biopolymers* **43**, 383-400 (1997).
7. Li, H. and Lawrence, D. S. *Chem. Biol.* **12**, 905-912 (2005).
8. Mackay, H. J. and Twelves, C. J. *Endocr. Relat. Cancer* **10**, 389-396 (2003).
9. Nakashima, S. *J. Biochem. (Tokyo)* **132**, 669-675 (2002).
10. Lee, J. H., Nandy, S. K. and Lawrence, D. S. *J. Am. Chem. Soc.* **126**, 3394-3395 (2004).
11. Zhang, Z. Y. and Lee, S. Y. *Expert. Opin. Investig. Drugs* **12**, 223-233 (2003).
12. Puius, Y. A., Zhao, Y., Sullivan, M., Lawrence, D. S., Almo, S. C. and Zhang, Z. Y. *Proc. Natl. Acad. Sci. USA* **94**, 13420-13425 (1997).
13. Shen, K., Keng, Y. F., Wu, L., Guo, X. L., Lawrence, D. S. and Zhang, Z. Y. *J. Biol. Chem.* **276**, 47311-47319 (2001).
14. Xie, L., Lee, S. Y., Andersen, J. N., Waters, S., Shen, K., Guo, X. L., Moller, N. P., Olefsky, J. M., Lawrence, D. S. and Zhang, Z. Y. *Biochemistry* **42**, 12792-12804 (2003).

Cyclic Modular β -Sheets

James S. Nowick, Justin O. Brower, Omid Khakshoor, Wade A. Russu
and R. Jeremy Woods

Department of Chemistry, University of California Irvine, Irvine, CA 92697-2025, USA

Introduction

Our research laboratory has embarked on a program to mimic, understand, and control the type of edge-to-edge interactions that occur widely between β -sheets in protein quaternary structures, protein-protein interactions, and protein aggregation [1-3]. Our approach involves creating families of well-behaved macrocyclic peptides that adopt preorganized β -sheet structures in aqueous solution. Unlike the widely studied β -hairpin peptides, our systems achieve these structures largely without regard to the sequence of amino acids that they comprise. We call these structures *cyclic modular β -sheets*.

Here we briefly describe two families of cyclic modular β -sheets, which contain the unnatural amino acids δ -linked ornithine, which functions as a turn unit, and *Hao*, which functions as a β -strand mimic and template that blocks one edge of the β -sheet [4-6]. Cyclic modular β -sheets **1** consist of a 42-membered ring and present a pentapeptide in a β -strand conformation, while cyclic modular β -sheets **2** consist of a 54-membered ring and present a heptapeptide in a β -strand conformation (Fig. 1).

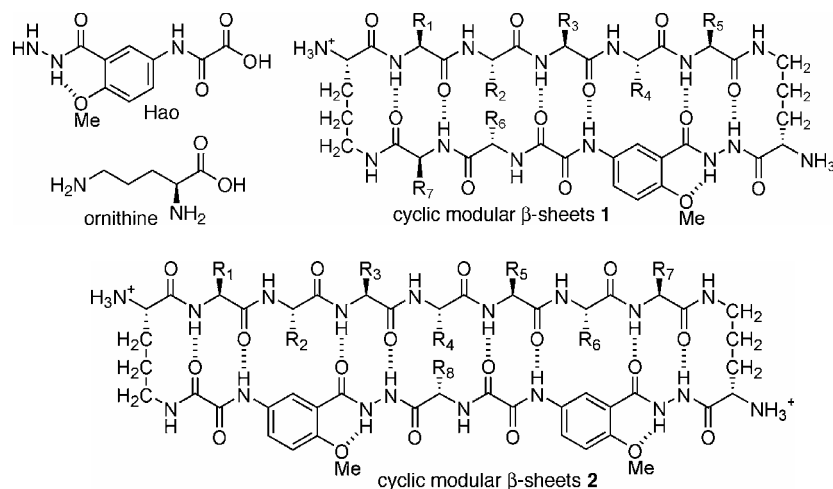


Fig. 1.

Results and Discussion

Cyclic modular β -sheets **1** and **2** are readily synthesized by macrocyclization of the corresponding protected linear peptides, which are prepared by Fmoc-based solid-phase peptide synthesis on trityl resin. An appealing aspect of the syntheses is that the macrocyclization step does not involve risk of epimerization, because the δ -linked ornithine that must be activated is an amino acid α -carbamate, rather than an amino acid α -amide. Figure 2 outlines the syntheses of cyclic modular β -sheets **1**;

cyclic modular β -sheets **2** are prepared in a similar fashion. Another appealing aspect of the syntheses is that linked cyclic modular β -sheets, such as those shown in Figure 3, can be prepared by using Boc-Orn(Fmoc)-OH for one turn unit and Cbz-Orn(Fmoc)-OH for the other turn unit. Selective deprotection by hydrogenolysis after macrocyclization, followed by coupling with a dicarboxylic acid and complete deprotection, generates the linked cyclic modular β -sheets. By these methods we have prepared roughly two dozen variants of cyclic modular β -sheets **1** and **2**.

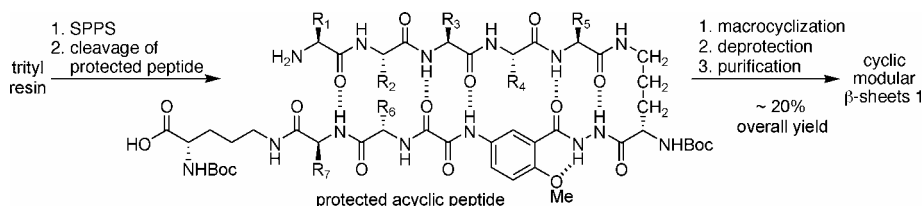


Fig. 2. Synthesis of cyclic modular β -sheets **1**.

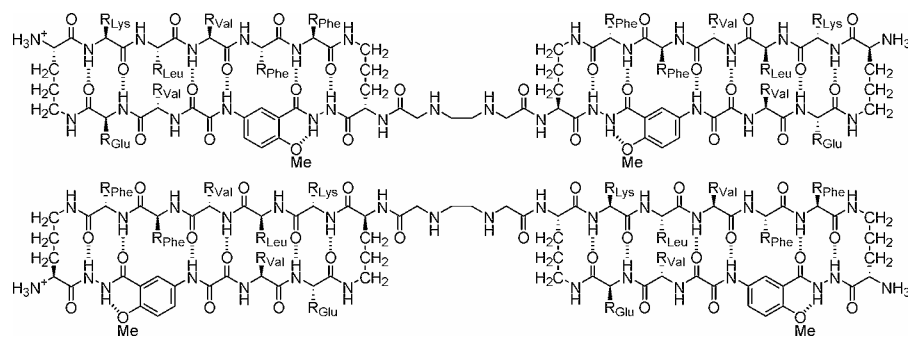


Fig. 3. Two of the linked cyclic modular β -sheets that we have prepared.

^1H NMR studies show that most of the macrocycles **1** and **2** that we have prepared fold into well-defined β -sheet structures in aqueous solution. Key evidence for the β -sheet structure of macrocycles **1** consists of strong interstrand NOEs and magnetic anisotropies of the ornithine δ -protons. Figure 4 summarizes the most important of these data for cyclic modular β -sheet **1a**. Cyclic modular β -sheets **2** form edge-to-edge β -sheet dimers that further self-assemble through face-to-face interactions to form tetramers (dimers of dimers). Evidence for folding and dimer formation consists of strong interstrand and intersheet NOEs, magnetic anisotropies of the ornithine δ -protons, and dramatic downfield shifting of the amino acid α -protons. Figure 5 summarizes the most important of these data for cyclic modular β -sheet **2a**; Figure 6 illustrates the structure of the putative tetramer. Evidence for tetramer formation comes from its cooperative formation at millimolar concentrations from the monomer, which is not folded, upfield shifting of the phenylalanine and tyrosine aromatic resonances, which appear to participate in hydrophobic cluster formation, and PFG-NMR diffusion experiments, which show the tetramer to be about four times the size of the monomer.

These studies establish that cyclic modular β -sheets are robust and versatile units with which to mimic β -sheet structure and interactions. Ongoing efforts to use these structures to bind proteins through β -sheet interactions appear promising.

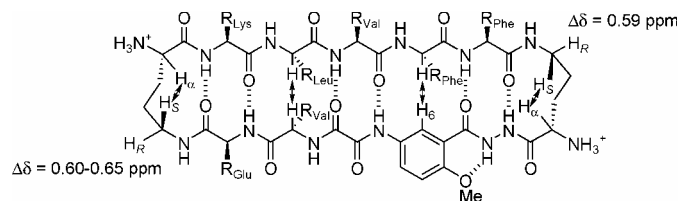


Fig. 4. Key NOEs (arrows) and magnetic anisotropies ($\Delta\delta$) of the ornithine δ -protons in representative cyclic modular β -sheet **1a** (amino acids 1-7 = KLVFFVE).

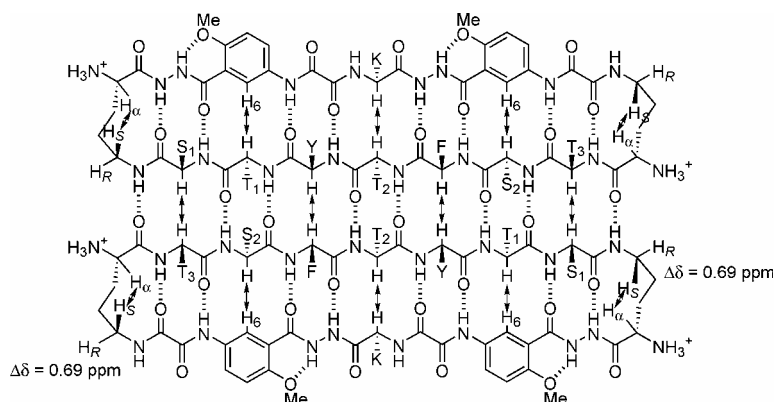
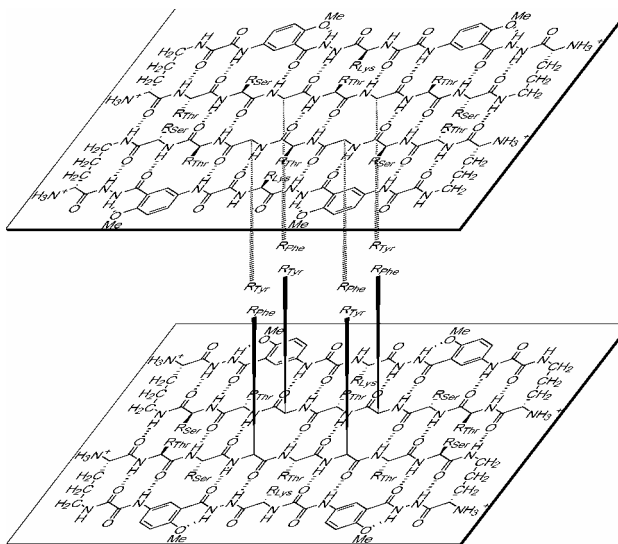


Fig. 5. Key NOEs (arrows) and magnetic anisotropies ($\Delta\delta$) of the ornithine δ -protons in representative cyclic modular β -sheet **2a** (shown as the dimer, amino acids 1-8 = TSFTYTSK).

Fig. 6. Representation of the putative structure of the tetramer of cyclic modular β -sheet **2a**. The tetramer consists of a dimer of dimers. Edge-to-edge interactions between the cyclic modular β -sheets help stabilize a four-stranded β -sheet dimer, while face-to-face interactions between these dimers, mediated by aromatic and hydrophobic interactions between the Phe and Tyr groups, help stabilize the tetramer.



Acknowledgments

We thank the NIH for grant support (GM-49076).

References

1. Maitra, S. and Nowick, J. S. In: *The Amide Linkage: Structural Significance in Chemistry, Biochemistry, and Materials Science*, Chapter 15 (Greenberg, A., Breneman C. M. and Liebman, J. F., eds.) Wiley, New York (2000).
2. Dou, Y., Baisnée, P. -F., Pollastri, G., Pécout, Y., Nowick, J. and Baldi, P. *Bioinformatics* **20**, 2767-2777 (2004).
3. The ICBS Database (<http://www.igb.uci.edu/servers/icbs>).
4. Nowick, J. S., Chung, D. M., Maitra, K., Maitra, S., Stigers, K. D. and Sun, Y. *J. Am. Chem. Soc.* **122**, 7654-7661 (2000).
5. Nowick, J. S., Lam, K. S., Khasanova, T. V., Kemnitzer, W. E., Maitra, S., Mee, H. T. and Liu, R. *J. Am. Chem. Soc.* **124**, 4972-4973 (2002).
6. Nowick, J. S. and Brower, J. O. *J. Am. Chem. Soc.* **125**, 876-877 (2003).

Apolipoprotein A-I Mimetic Peptides

G. M. Anantharamaiah¹, Mohamad Navab², Sreenivas T. Reddy², Susan Hama², Greg Hough², Mayakonda N. Palgunachari¹, Manjula Chaddha¹, Geeta Datta¹, David W. Garber¹ and Alan M. Fogelman²

¹UAB Medical Center, Birmingham, AL 35294; ²David Geffen School of Medicine at Los Angeles, CA-900095

Introduction

Over the years human apolipoprotein A-I (apo A-I), the major protein component of high density lipoproteins (HDL), has been intensely studied to understand the mechanism by which it protects atherosclerosis. Recent observations that administration of apo A-I_{Milano}:phospholipid complexes causes regression in humans have given further stimulus to understanding the structure and function of apo A-I [1]. Our approach over the years has been to study the nature of amphipathic helical motifs, the lipid associating domains present in this and other plasma apolipoproteins responsible for not only associating with phospholipids but also exerting antiatherogenic properties.

Results and Discussion

The first question we asked was whether there is any sequence requirement for lipid association. This led us to design an 18 residue peptide 18A with the sequence Asp-Trp-Leu-Lys-Ala-Phe-Tyr-Asp-Lys-Val-Ala-Glu-Lys-Leu-Lys-Glu-Ala-Phe. This peptide has no sequence homology to any of the naturally occurring proteins. However, when folded as an α -helix, it produces an amphipathic helix with the polar and non polar face segregated. The helical wheel diagram showed positively charged residues at the polar-nonpolar interface and negatively charged residues at the center of the polar face. It solubilized multilamellar vesicles of dimyristoyl phosphatidylcholine (DMPC) as effectively as apo A-I and formed discoidal particles, which upon examination with negative stain electron microscopy were similar in size to those formed by apo A-I:DMPC interaction. These observations for the first time led to the idea of "Synthetic HDL". This peptide and its complexes with lipid mimicked several properties human apo A-I [2].

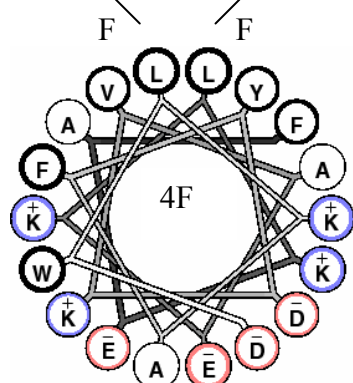


Fig. 1 Antiatherogenic peptide 4F was obtained by substituting the two Leu residues at the center of the nonpolar face of the baseline peptide 2F.

That the presence of positive charges at the polar-nonpolar interface is important for lipid affinity of class A amphipathic helical peptides was determined by reversing the charged residue positions. In the peptide 18R, Asp and Glu residues were positioned at the polar-nonpolar interface and positively charged Lys residues at the center of the polar face. The peptide 18R was less effective than 18A in associating with phospholipids. This led to the hypothesis that positively charged Lys residues at the interface

"snorkel" such that the long side-chain of Lys at the polar-nonpolar interface of 18A

contributes to the hydrophobicity of the nonpolar face while the NH₂ group is involved in interaction with the choline head group of phospholipids. It was then shown that protecting the end groups of 18A with Ac (for the amino end) and -NH₂ (for the carboxyl end) increased helicity and lipid affinity of the resulting Ac-18A-NH₂ [3].

Next we investigated the nature of hydrophobic face that may be responsible for increased lipid affinity and increased biological properties of class A peptides. We substituted the existing hydrophobic residues with Phe. Thus we produced 2F (Ac-18A-NH₂) to 7F (a peptide with all of the nonpolar residues was substituted with Phe). The peptide 4F had maximum solubility and lowest retention in HPLC. In the helical wheel of 2F there are two Leu residues which are replaced by Phe to produce 4F (Fig. 1). Examination of the helical wheel of 4F indicated the presence of aromatic amino acids at the center of the nonpolar face. If one Leu is replaced by Phe, the nonpolar face contains 3 Phe residues and thus we synthesized 3F³ and 3F¹⁴ (3rd and 14th Leu residues are replaced by Phe – Table 1). All of the peptides synthesized possessed similar physico-chemical properties. These studies did not distinguish these peptides.

A coculture assay developed by us was used to study the ability of these peptides to inhibit low density lipoprotein (LDL)-induced monocyte chemotaxis [4]. This assay consists of a layer of endothelial cells layered on a layer of monocytes. This represented artificial arteries. When LDL enters into arteries, LDL gets further oxidized to produce more lipid hydroperoxides on the LDL surface. This modified LDL enhances monocyte chemotaxis. Monocytes take up oxidized LDL and become macrophages and then foam cells. However, HDL can take up lipid

Table 1

Peptide	Sequence
3F-1	Ac-DKLKAFYDKVFEWAKEAF-NH ₂
3F-2	Ac-DKWKA VYDKFAEAFKEFL-NH ₂
3F ³	Ac-DWFKAFYDKVAEKLKEAF-NH ₂
3F ¹⁴	Ac-DWLKAFYDKVAEKFKEAF-NH ₂

hydroperoxides from the LDL surface. The resulting LDL does not enhance monocyte chemotaxis. The apo A-I mimetic peptides were tested for their ability to inhibit LDL-induced monocyte chemotaxis. 3F analogs did not inhibit LDL-induced monocyte chemotaxis. 4F was the best peptide in inhibiting LDL-induced monocyte chemotaxis. Administration of a peptide containing D amino acids (D-4F) into mice showed that the peptide circulated in the plasma as intact peptide whereas the L-4F was hydrolyzed resulting in free trichloroacetic acid–nonprecipitable iodine. Thus, D-4F was used for further studies and it was shown that oral administration of D-4F inhibited lesion formation in several dyslipidemic mouse models [5].

To understand why 4F but not 3F peptides inhibited LDL-induced monocyte chemotaxis, two more 3F analogs were synthesized. The four 3F analogs are shown in Table 1. The new 3F analogs had their aromatic groups clustered at the center (3F-2) or at the interface (3F-1). Unlike 3F³ and 3F¹⁴, the new 3F analogs 3F-1 and 3F-2 were able to inhibit LDL-induced monocyte chemotaxis. To further understand the possible reason for the differences in properties of 3F analogs, we used a fluorescent lipid (2-[3-(diphenylhexamethyl)propionyl]-1-hexadecanoyl-*sn*-glycero-3-phosphocholine) mixed with vesicles of POPC and studied the fluorescent

properties. Presence of water quenches the fluorescence of these peptides whereas hydrophobic milieu increases fluorescence. In the presence of 4F the fluorescence was quenched maximally. The new 3F analogs 3F-1 and 3F-2 also quenched fluorescence of the fluorescent lipid indicating that water molecules penetrate into the hydrophobic milieu. Based on these observations and molecular modeling we proposed that the active peptides possess a cylindrical cross-sectional shape which is capable of perturbing lipid acyl chains to the maximum extent to allow water and lipid hydroperoxide into the hydrophobic milieu. The inactive peptides possessed a wedge cross-sectional shape, due to the presence of clustered π electron containing aromatic residues; the hydrophobic residues strongly interacted with the lipid acyl chains to inhibit entrance of water molecules and lipid hydroperoxides. 4F, which also has the cylindrical cross-sectional shape, when administered to animals is able to form HDL-like particles which recruit apo A-I and paraoxanase, an enzyme that is capable of reducing lipid hydroperoxides [6]. This in turn is able to scavenge lipid hydroperoxides from LDL and inflammatory HDL and destroys them or eliminates from circulation [7]. Thus 4F *in vivo* is able to convert atherogenic lipoproteins into nonatherogenic lipoproteins and thus inhibits atherosclerosis and recently it has been shown that 4F is able to inhibit other inflammatory diseases [5]. Peptides to ameliorate atherosclerosis and other inflammatory diseases can be designed using this strategy.

References

1. Nissen, S.E., Tsunoda, T., Tuzcu, E.M., Schoenhagen, P., Cooper, C.J., Yasin, M., Eaton, G.M., Lauer, M.A., Sheldon, W.S., Grines, C.L., Halpern, S., Crowe, T., Blankenship, J.C. and Kerensky, R. *JAMA* **290**, 2292-300 (2003).
2. Segrest, J.P., Jones, M.K., De Loof, H., Brouillette, C.G., Venkatachalapathi, Y.V. and Anantharamaiah, G.M. *J. Lipid Res.* **33**, 141-66, (1992).
3. Venkatachalapathi, Y.V., Phillips, M.C., Epand, R.M., Epand, R.F., Tytler, E.M., Segrest, J.P. and Anantharamaiah, G.M. *Proteins* **15**, 349-59 (1993).
4. Datta, G., Chaddha, M., Hama, S., Navab, M., Fogelman, A. M., Garber, D. W., Mishra, V. K., Epand, R. M., Epand, R. F., Lund-Katz, S., Phillips, M. C., Segrest, J. P. and Anantharamaiah, G. M. *J. Lipid Res.* **42**, 1096-1104 (2001).
5. Navab, M., Anantharamaiah, G. M., Reddy, S. T., Van Lenten, B. J., Datta, G., Garber, D. and Fogelman, A. M. *Curr. Opin. Lipidol.* **15**, 645-649 (2004).
6. Navab, M., Anantharamaiah, G. M., Reddy, S. T., Hama, S., Hough, G., Grijalva, V. R., Wagner, A. C., Frank, J. S., Datta, G., Garber, D. and Fogelman, A. M. *Circulation* **109**, 3215-3220 (2004.)
7. Datta, G., Epand, R. F., Epand, R. M., Chaddha, M., Kirksey, M. A., Garber, D. W., Lund-Katz, S., Phillips, M. C., Hama, S., Navab, M., Fogelman, A. M., Palgunachari, M. N., Segrest, J. P. and Anantharamaiah, G. M. *J. Biol. Chem.* **279**, 26509-26517 (2004).

Understanding BBB Transport using Glycosylated Enkephalins and Endorphins

Dhana Muthu¹, Isabel Alves¹, Charles M. Keyari¹, Larisa Yeomans¹,
 Richard D. Eggleton², Jean M. Bidlack³, Henry I. Yamamura², Victor J.
 Hruby¹, Edward J. Bilsky⁴ and Robin Polt¹

¹Carl S. Marvel Laboratories — Department of Chemistry; ²Department of Pharmacology;
 The University of Arizona, Tucson, AZ 85721 USA; ³Department of Pharmacology, University
 of Rochester Medical Center, Rochester, NY 14642, USA; ⁴Department of Pharmacology,
 University of New England College of Medicine, Biddeford, ME 04005, USA

Introduction

A series of glycopeptides based on the Leu-enkephalin analog YtGFS*-CONH₂, **MMP-2200**, led to greatly enhanced stability *in vivo* and effective penetration of the BBB [1]. Glycosylated enkephalins display potent analgesic effects in mice following *i.v.* or *s.c.* injection. Glycosylated enkephalins with mixed δ/μ agonist properties lack virtually all of the dopaminergic (DA) and norepi-nephrenergic (NE) mediated side effects that are common to μ -opioid agonists (e.g., morphine) [2]. The best cases (mixed δ/μ agonists) are 2—3X the potency of morphine, and show greatly reduced locomotor activity, relative to morphine (Table 1).

Results and Discussion

Highly μ -selective agonists are >10X the potency of morphine, but show greatly increased locomotor activity. The μ -selective glycopeptide **LYM-147** shows extreme levels of analgesia in mice, but also shows extreme levels of locomotor activity in mice, and significant negative effects upon withdrawal (data not shown).

Transport through the BBB hinges on the biousian nature of the glycopeptides - the glycopeptides have two conflicting conformational manifolds, a H₂O soluble state, and an amphipathic state at H₂O-membrane phase boundaries [3]. Multiple lines of evidence suggest that the BBB transport is mediated by absorptive endocytosis [4]. The design was extended to glycopeptides related to β -endorphin,

Table 1. Binding and analgesic activity of glycopeptides

Glycopeptide	Binding		Antinociception ^a	
	μ	δ	<i>i.c.v.</i>	<i>i.v.</i>
Morphine	55 nM ^b	258 nM ^b	2.7 nmol	6.3 μ mol/Kg
MMP-2200	35 nM ^b	5.7 nM ^b	0.020 nmol	3.2 μ mol/Kg
LYM-147	0.66 nM ^c	1600 nM ^c	0.003 nmol	1.0 μ mol/Kg
MD-100H	91 nM ^b	6.2 nM ^b	0.030 nmol	n.d.

^aMouse 55°C tail flick A₅₀ values. ^b Binding = IC₅₀ values from GPI/MVD functional assays.

^c Binding = Ki values from CHO cells w/human receptors.

MMP-2200 H-YtGFLS**-NH₂ S* = β -D-Glc-O-Serine
LYM-147 H-YaG[N-Me-F]S**-NH₂ S* = β -Lactosyl-O-Serine
MD-100H H-YtGFLPNLBKALKS*L-NH₂ B = α -aminoisobutyric acid

which also penetrated the BBB and produced antinociception in mice [5]. Plasmon waveguide resonance (PWR) studies showed that the amphipathic helices bound to membrane bilayers with μM to low nM K_D 's. The presence of diverse endogenous neuropeptide transmitters and neuromodulators in the human brain is potentially applicable to the treatment of a wide range of behavioral disorders.

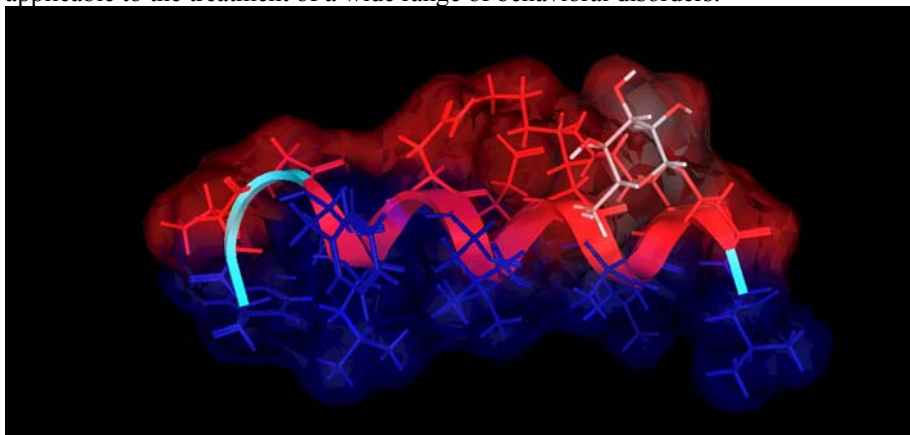


Fig. 1. Lowest energy structure of **MD-100H** in the presence of bicelles with a Connolly surface illustrating the hydrophobic (blue) and hydrophilic (red) faces of the amphipathic helix. This structure is believed to represent a “Class A” amphipathic helix [5].

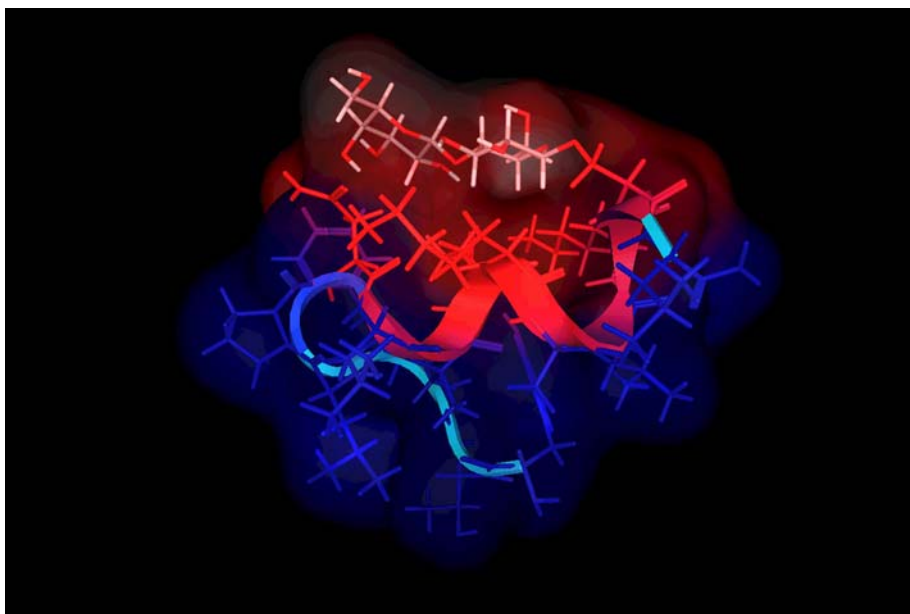


Fig. 2. Higher energy structure of **MD-120H** (lactoside analog of **MD-100H**) in the presence of bicelles with a Connolly surface illustrating the hydrophobic (blue) and hydrophilic (red) faces of the amphipathic helix. This structure is believed to represent a “Class L” structure.

Several amphipathic helices (e.g., **MD-100H**, Fig. 1) have now been examined by CD in H₂O, H₂O–CF₃CH₂OH mixtures, and by 600 MHz NMR in the presence of micelles. All of the compounds showed disordered structures in H₂O, as indicated by ¹H-NMR (NOE distances, J₃ dihedral angles and by C^α chemical shift index). The interconversion between a H₂O-soluble, random coil conformational ensemble and a helical amphipathic ensemble (biousian behavior) is postulated to be responsible for efficient penetration of the BBB *via* transcytosis, and to allow for “membrane hopping” on either side of the endothelial barrier [5].

Minor amounts of lytic or “Class L” amphipathic structures [6] (Fig. 2) may be responsible for membrane destabilization, which is postulated to result in the glycopeptide being delivered to the cytoplasmic face of the endothelial layer, an irreversible event which can result in reduced BBB penetration. Thus, replacement of Pro⁶ with β-Alanine reduces transport, and replacement with Gly⁶-Gly⁷ prevents BBB transport altogether [7]. Coupled plasmon waveguide resonance (CPWR) [5] suggest that adsorption of the glycopeptide to the membrane is critical for transport. Thus, **MD-100H** has a K_D of 7.3 nM, and transports well, whereas the Gly⁶-Gly⁷ analog binds much more weakly and does not penetrate the BBB.

Further studies of both the biophysics of the glycopeptide-membrane interactions, BBB transport and receptor binding are in progress. We are also seeking to address the practical aspects of drug development for **MD-2200** as a replacement for morphine in severe trauma cases (i.e., combat casualty care). Larger quantities of cGMP material have been manufactured and testing in larger species (e.g., rhesus) has begun.

Acknowledgments

The work was funded by an ONR grant (#N00014-02-1-0471) to R. Polt. We wish to thank Protein Technologies, Inc., of Tucson, AZ for the loan of a PS-3 synthesizer.

References

1. Polt, R., *et al.* *Proc. Natl. Acad. Sci. U.S.A.* **91**, 7114-7118 (1994).
2. Bilsky, E. J., *et al.* *J. Med. Chem.* **43**, 2486-2590 (2000).
3. Egelton, R. D., *et al.* *J. Pharm. Exp. Therap.* **299**, 967-972 (2001).
4. Palian, M. M., *et al.* *J. Am. Chem. Soc.* **125**, 5823-5831 (2003).
5. Muthu, D., *et al.* *J. Am. Chem. Soc.* **127**, 5435-5448 (2005).
6. Segrest, J. P., *et al.* *Protein Struct. Funct. Genetics* **8**, 103-117 (1990).
7. Egleton, R. D., *et al.* *Tetrahedron Asymm.* **16**, 65-75 (2005).

Design and Study of Novel Peptide Inhibitors against the SARS-Coronavirus Spike Protein

Zhe Yan, Brian Tripet and Robert S. Hodges

Department of Biochemistry and Molecular Genetics. University of Colorado at Denver and Health Sciences Center, Aurora, CO, 80045, USA

Introduction

Severe Acute Respiratory Syndrome (SARS) is an acute respiratory illness caused by infection with a novel coronavirus (SARS-CoV). Infection by SARS coronaviruses requires fusion of the viral and cellular membranes, which is mediated by the viral envelope Spike (S) glycoprotein and receptors on the target cell. The S protein contains two hydrophobic repeat regions, denoted HRN and HRC, which oligomerize the S glycoprotein into a trimer in the native state, and when activated collapse into a six-helix bundle structure driving fusion of the host and viral membranes. We and others have previously reported that the HR regions of SARS-CoV S protein can associate to form a very stable helical six-stranded structure and residues 902–950 in HRN and 1151–1185 in HRC were identified to be crucial for their interaction [1-4].

Due to the severity and mortality (10%) witnessed in the fall of 2003 during the spread of the SARS-CoV pandemic, and the current lack of effective agents for the antiviral therapy of SARS-CoV infection, it has become imperative to learn as much as possible about this virus and the ability to prevent future infection. As successfully used in fusion inhibitor design for HIV [5], peptides derived from HRC can bind to the transiently exposed HRN coiled-coil trimer and block the formation of the six-helical bundle (Fig. 1), which ultimately leads to a loss of membrane-fusion activity. In this study, HRN (902-950) peptide of SARS-CoV S protein was chosen as the target for testing the interaction of HRC analogs.

The 36-residue HRC peptide (1150-1185) was chosen as the region to design a series of HRC analogs, in order to increase their stability and binding affinity with HRN. These substitutions /modifications involved: (1) increasing helical propensity (HRC2 and HRC4); (2) increasing hydrophobicity in the hydrophobic core (HRC1 and HRC3); and (3) introducing a lactam bridge (HRC5). The sequences of these peptides are shown in Figure 2.

Results and Discussion

To examine the helical structure changes of the HRC analogs, we analyzed each peptide by circular dichroism spectroscopy (CD). Under physiological conditions, these analogs are well folded, soluble, have higher α -helical content and are more stable than native HRC as expected (in Fig. 3A and Table 1).

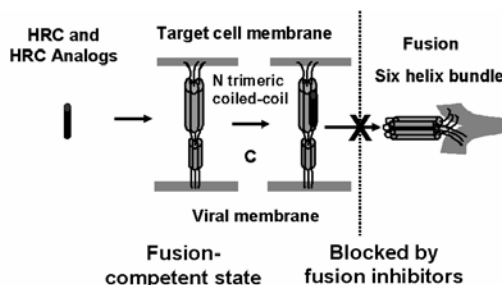


Fig. 1. Schematic model illustrating the action of SARS-CoV fusion inhibitors that target HRN.

native PAGE. The results are shown in Figure 4 and Table 1. HRC or HRC analogs alone showed a band in the lower part of the gel. With the exception of HRC4, the mixture of HRC analogs and HRN showed two bands: the lower one had the same position as isolated HRC analog, and the upper band is higher order oligomeric complex formed by HRN and HRC analog. HRN alone showed no band because it carries a net positive charge under the native electrophoresis conditions, and consequently does not enter the gel.

Table 1. Summary of HRC analogs and interaction with HRN

Peptide Name	[θ] ₂₂₂ ^a		% α helix ^b		T _m ^c (°C)	Complex with HRN		Complex formation tested by Native PAGE
	Benign	50%TFE	Benign	50%TFE		T _m (°C)	Δ T _m (°C)	
HRC	-21370	-29720	61	85	37	85	0	+
HRC 1	-32060	-31510	92	90	57	74	-11	+
HRC 2	-27060	-29740	77	85	48	86	+1	+
HRC 3	-30900	-31450	88	90	66	75	-10	+
HRC 4	-28560	-30990	82	89	74	59	-26	-
HRC 5	-27770	-32320	80	92	41	88	+3	+

a. [θ]₂₂₂ is the mean residue molar ellipticity (deg cm² dmol⁻¹) measured at 222 nm in a 100 mM PBS, pH 7.0, in the absence (benign) or presence of 50% TFE (v/v). Concentration of peptides was 70 μ M. b. % α helix was calculated from [θ]₂₂₂ based on an ellipticity value for 100% α -helical content derived from the equation, $XH_n = XH_\infty (1 - k/n)$, where XH_∞ is -37,400, the wavelength dependent constant, k, is 2.5, and n is the number of residues in the helix. c. T_m is the temperature at which there is a 50% decrease in fraction folded compared to the fully folded coiled-coil as determined by CD at 5 °C.

Conclusions

1. The substitutions/modifications have increased the HRC α -helical structure and stability. As shown in Table 1, the results from CD and native PAGE suggested HRC2 and HRC5 have increased binding affinity with HRN.
2. The two analogs, HRC2 and HRC5, will now be tested as peptide fusion inhibitors in an antiviral activity assay.

Acknowledgments

This work was supported by NIH grants to R.S.H. (PO1AI059576) and the John Stewart Chair in Peptide Chemistry. We thank Dziuleta Cepeniene for help with peptide synthesis.

References

1. Tripet B., et al. *J. Biol. Chem.* **279**, 20836-20849 (2004).
2. Xu Y., et al. *J. Biol. Chem.* **279**, 49414-49419 (2004).
3. Bosch, B.J., et al. *Proc. Natl. Acad. Sci. USA* **101**, 8455-8460 (2004).
4. Chan, D.C. and Kim, P.S. *Cell* **93**, 681-684 (1998).
5. Ingallinella, P., et al. *Proc. Natl. Acad. Sci. USA* **101**, 8709-8714 (2004).

Screening Biosynthetic Peptide Libraries for Antimicrobial Activity

Lisa O. Nilsson, Mostafa Louassini and Ernesto Abel-Santos

Department of Biochemistry, the Albert Einstein College of Medicine, Bronx, NY 10461 USA

Introduction

We have recently demonstrated the feasibility of utilizing the ligase activity of inteins for the *in vivo* backbone cyclization of peptidic chains [1]. This procedure - called SICLOPPS for Split Intein Circular Ligation Of Peptides and ProteinS - provides a biosynthetic pathway for peptides that are metabolically stable and can be produced with spatial and temporal control. To screen for bacteriotoxic peptides, a SICLOPPS library was introduced into an *Escherichia coli* population, such that each bacterium encodes a different peptide sequence. SICLOPPS library over-expression afforded six distinct bacteriostatic peptides that reduce cell growth. One of these peptides (LN05) also caused cell aggregation. An *E. coli* genomic library was introduced into cells encoding LN05. Co-expression of the genomic library and LN05 peptide rescues growth only in cells expressing genomic fragments able to counteract peptide toxicity. Genomic library and LN05 co-expression resulted in enrichment of a single genomic construct, a fragment of the NarZ gene. NarZ is part of a nitrate reductase complex and has a role in tuberculosis persistence.

Results and Discussion

a. Identification of individual toxic peptides: A SICLOPPS peptide library was plated in non-inducing plates and replica plated onto plates containing 1 mM IPTG. Approximately 200 colonies unable to grow upon peptide induction were picked from the non-inducing plate and grown on LB media with different IPTG concentrations. Six peptides were selected that stopped cell growth at the lowest IPTG concentration.

Table 1. Bacteriostatic /

Bactericidal peptide sequences

Name	Peptide sequence
LN01	c[SGYHSVVGPL]
LN05	c[SGWRMWVYPL]
LN06	c[SGMFLWEVPL]
ML04	c[SGSIHVGGPL]
ML07	c[SGLWVLSSPL]
ML11	c[SGPGESWLPL]

The six peptides identified have a hydrophobic character but share no sequence homology (Table 1). All of them, however, are able to stop cell growth upon induction. Furthermore, cells expressing these peptides show no propidium iodide uptake. Thus, these peptides do not target cellular membranes and may stop cell growth by inhibiting different essential enzymatic pathways. One of these constructs, LN05, not only inhibited cell growth, but caused extensive bacterial aggregation when grown in

liquid media. Similar phenotypes have been obtained when cell structural proteins have been deleted from the bacterial genome [2].

b. Transient expression of SICLOPPS peptides is sufficient for bacteriostatic effect: ML04, ML07, and ML11 peptides were induced for four, six or twenty hours and then plated on non-inducing plates. After four hours induction, viability of cells expressing ML07 is reduced more than 90% (Fig. 1). Cells expressing ML04 show a

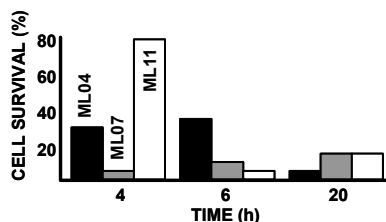


Fig. 1. SICLOPPS peptides show different cell survival kinetics after transient induction of peptide production.

c. Functional complementation identify genomic constructs that counteract LN05 peptide effect:

A genomic library was created by ligating 1.5-3.0 Kb *E. coli* genomic fragments in the pPROTet vector. The resulting genomic library was transformed in cells encoding LN05. Co-expression of LN05 peptide (with IPTG) and the genomic library (with anhydrotetracycline, aTc) resulted in growth of approximately 100 colonies. DNA sequencing of 10 colonies showed different genomic constructs in each one. However, two of the constructs sequenced corresponded to fragments of the NarZ and NarG genes. These two genes encode for the same physiological function, namely, both take part in the reduction of nitrates to nitrites. Ten constructs sequenced from a control plate showed totally different genomic sequences. The cells from the LN05 plate were harvested; the DNA was extracted, and used to transform fresh *E. coli* cells. The resulting transformed cells were selected as above. Three out of ten clones from the second

four fold decrease in CFU, while cells expressing ML11 remain basically unaffected. On the other hand, after six hours of induction, ML11 cell survival has decreased to the same level as ML07, while ML04 remains the same. Thus, although ML04 have a faster effect on cell viability, the toxicity is not as pronounced as in cells expressing ML07 and ML11. After 20 hours induction, cells expressing ML07 and ML11 show a slight increase in CFU, probably due to the appearance of resistant clones. ML04 on the other hand, show a continuous decrease in cell viability.

selection corresponded to the NarZ gene previously detected. Under these conditions, the probability of randomly picking out the same genomic construct three times out of ten is 10^{-6} .

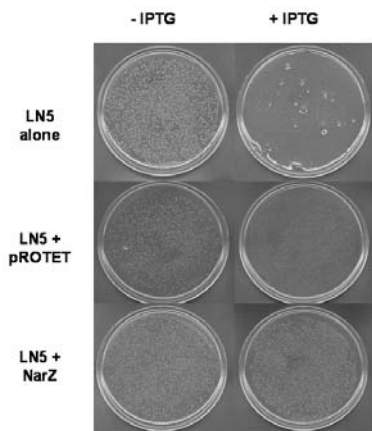


Fig. 2. LN05 peptide induction eliminates colony formation (Top panels). Co-expression with pPROTET vector partially ameliorates LN05 action (middle panels). NarZ and LN05 co-expression completely eliminated LN05 toxicity.

Cells expressing LN05 peptide alone, LN05 peptide together with the empty pPROTet vector, and LN05 peptide together with the NarZ fragment were individually plated onto LB agar supplemented with 0.1 μ g/ml aTc and 0 or 1 mM IPTG. As before, LN05 peptide production prevented colony formation when expressed alone (Fig. 2, top panels). Co-expression of the pPROTet vector partially ameliorates the bacteriostatic properties of the LN05 peptide (Fig. 2, middle panels). Colonies from co-expressed cells grow slightly better than colonies expressing cyclic peptide alone, indicating that the expression level of the cyclic peptide is at the minimal inhibitory concentration. SDS-PAGE analysis of expression shows that co-expression of LN05 peptide with pPROTet vector lowered the expression level of the

cyclic peptide slightly (data not shown). When the NarZ fragment was co-expressed with the LN05 peptide, CFU number and colony growth rate was similar for the IPTG induced and non-induced plates (Fig. 2, bottom panels). Co-expression of genomic constructs other than NarZ or NarG failed to rescue cell viability (data not shown).

There are three nitrate reductases in *E. coli*, one periplasmic, Nap (encoded by the napFDAGHBC operon), and two membrane bound, nitrate reductase A (NRA, encoded by the narGHJI operon) and nitrate reductase Z (NRZ, encoded by the narZYWV operon). One double knockout mutant has been made where both membrane bound nitrate reductases are compromised and one triple knockout. These knockout clones grow under aerobic conditions, suggesting that nitrate reductases are not essential under aerobic conditions [3]. Since two apparently redundant nitrate reductase enzymes are maintained, the membrane bound reductases may have different physiological functions. These nitrate reductases seem to have evolved by gene duplication because the transcription unit is homologous with 73% identity [4]. Interestingly they are regulated very differently: Nitrate Reductase A (narGHJI) is regulated by oxygen and nitrate levels and therefore expressed only during anaerobic conditions. Nitrate Reductase Z (narZYWV) is constitutively expressed at low levels during exponential growth, and induced by RpoS during stationary phase under aerobic conditions [5].

The fact that NarZ is not essential under aerobic conditions is consistent with our results. The LN05 peptide slows down bacterial growth rate, but does not cause bacterial death. Furthermore, immediately after plating, cells will be in the exponential phase where expression of the NarZ operon is at its lowest levels. If the LN05 peptide inhibits NarZ, cell growth would be slowed dramatically (as seen in our results). Thus, no colony formation would be detected. Over time, plated cells would enter into stationary phase with concomitant increased expression of NarZ operon. The increased NarZ concentration would reduce the inhibitory effect of LN05, allowing the formation of visible colonies. This is, again, consistent with our observations that pin-point colony formation can be seen at very high plate density (where there is strong competition for available IPTG) or after long incubation times (where most cells will have entered into stationary phase).

Acknowledgments

This work was supported by the National Institute of Allergy and Infectious Diseases through NIH Grant Number 5R01AI053212-03 to Ernesto Abel-Santos.

References

1. Abel-Santos, E., Scott, C. P., Wall, M., Wahnnon, D. C. and Benkovic, S. J. *Proc. Natl. Acad. Sci. USA*. **96**, 13638-13643 (1999).
2. Vilcheze, C., Morbidoni, H. R., Weisbrod, T. R., Iwamoto, H., Kuo, M., Sacchettini, J. C. and Jacobs, W. R. Jr. *J. Bacteriol.* **182**, 4059-4067 (2000).
3. Potter, L., Millington, P., Griffiths, L. and Cole, J. *Int. J. Food Microbiol.* **55**, 11-18 (2000).
4. Blasco, F., Iobbi, C., Ratouchniak, J., Bonnefoy, V. and Chippaux, M. *Mol. Gen. Genet.* **222**, 104-111 (1990).
5. Chang, L., Wei, L. I., Audia, J. P., Morton, R. A. and Schellhorn, H. E. *Mol. Microbiol.* **34**, 756-766 (1999).

Cellular Delivery and Design of Proprotein Convertase Inhibitors

Ajoy Basak, Xiaolei Hao, Ying Feng, Dayani Mohottalage, Farzaneh Lotfipour and Sarmistha Basak

*Ottawa Health Research Institute, University of Ottawa, Regional Protein Chemistry Center,
Ottawa, ON K1Y 4E9, Canada*

Introduction

Proprotein Convertases (PCs) are Ca^{+2} dependent cellular endoproteases that cleave inactive protein precursors to generate bioactive peptides. There are 7 PCs including furin which cleave precursor proteins at the C-terminus to basic amino acids **R/H/K-X-K/R/X-R**. Because of implications in cancer, bacterial and viral infections, PCs are therapeutic targets [1]. Consequently interest has grown for development of specific PC-inhibitors that can block proprotein maturation. Owing to proteolytic and metabolic stabilities and oral viability, small molecule inhibitors are more attractive and useful compared to macromolecule inhibitors. However such compounds suffer from poor cell permeability. To overcome this, we conjugated inhibitors with cell penetrating peptides poly-d (dextro) arginines, HIV-Tat, or Pep-21 [2,3] and showed that such conjugates cross membrane and block PC-processing. We also studied delivery efficacy of Pep-21 and its various domains. Moreover we developed new strategy for design of PC-inhibitors using reactive site loop of α 1-PDX & radical generating Ene-diyne amino acid (Eda).

Results and Discussion

Pep-21 and **poly-dArg** peptides were shown to cross cell membranes [2-4]. Cellular uptake of Pep-21 and its various domains were studied using fluorescent tags EDANS or fluorescein (Table 1). Peptides were synthesized as terminal amides using HATU/DIEA Fmoc chemistry [2,3] and purified on C_{18} column with a gradient of 10-70% CH_3CN in aq. 0.1% TFA. Pep-6, 9, and 21 peptides were tested for their cell translocation ability in 3T3-L1 adipose cells at 1-50 μM concentrations following 5min-6hr transfection. Cells were examined in fluorescence mode and after staining with DAPI (4',6-Diamidino-2-phenylindole) that allows nuclei to be visible [5]. Neither Pep-6 nor Pep-9 was able to cross cell membrane. However, Pep-21 internalizes efficiently even with 5 min incubation at 1 μM (Fig. 1) suggesting that the N-terminal Trp-rich hydrophobic domain of Pep-21 is crucial for its cell permeability. CD spectra showed that only Pep-21 possesses an helical structure unlike Pep-6 and Pep-9. dR₈-EDANS penetrates membrane with less efficiency. The presence of both R₈ and Pep-21 as in R₈-EDANS-pep-21 allows the most efficient cell permeability.

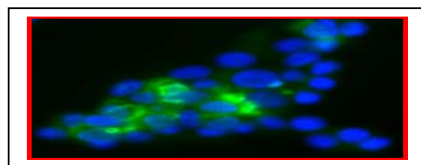


Fig. 1. Microscopic picture of 3T3 L1 cells treated with Flu-Pep-21 (25 μM , 6h) stained with DAPI and examined with fluorescence and DAPI filters.

These delivery tools were utilized for the design of cell permeable furin inhibitors. In one approach peptides with dArg_{8/6} which inhibit furin [7], were attached to Pep-21 containing a fluorescent tag and a linker. Both analogs inhibit furin in low μM range while control EDANS-pep-21 inhibits only weakly (Table 1). Inhibition

was tested using the intramolecular quench substrate Q-VEGF-C (Abz-²²⁰QVHSIIRR↓S LP²³⁰Tyx-A-NH₂) [6]. In a second approach, S-S bridge cyclo-miniPDX peptide mimicking PDX-reactive site loop structure was designed. It inhibits furin in sub μM range. A model structure (Fig. 2) indicated that it is stabilized by intramolecular H-bonds. Alternatively, Eda (8) was inserted at P1-P1' position of pro-hfurin⁹⁸⁻¹¹² which efficiently inhibited furin activity (K_i 40nM) against Boc-RVRR-MCA. When tested in CHO cells, both cell permeant inhibitors, R₈-EDANS-pep-21 and R₆-EDANS-pep-21 blocked furin cleavage of pro-PDGF-A into its mature form at 1 μM concentration, while cyclo mini-PDX did not, possibly because of its poor cell permeability. Thus, covalent conjugation of furin inhibitor to Pep-21 enhances cellular delivery and blockade of furin cleavage.

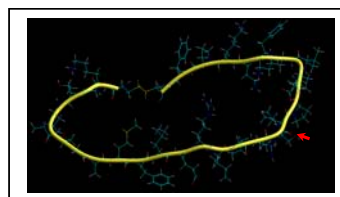


Fig. 2. 3D model structure of cyclo mini-PDX peptide.

Table 1. Cell penetrating peptides and cell permeant furin inhibitors and their bioactivities

Peptide	Sequence	Cell penetration	Furin inhibition (K_i), μM
Flu-pep-6	Flu-(Ahx) ₂ -KKKRKV	None	ND
Flu-pep-9	Flu-(Ahx) ₂ -SQP-KKKRKV	None	ND
Flu-pep-21	Flu-(Ahx) ₂ -KETWWETWWTEW-SQP-KKKRKV	Efficient	ND
EDANS-pep21	Cys-Glu(EDANS)-(Ahx) ₂ -KETWWETWWTEW-SQP-KKKRKV-Cys	Efficient	> 50
R ₈ -EDANS-pep-21	dR ₈ -Glu(EDANS)-(Ahx) ₂ -KETWWETWWTEW-SQP-KKKRKV-Cys	Efficient	2.2
R ₆ -EDANS-pep-21	dR ₆ -Glu(EDANS)-(Ahx) ₂ -KETWWETWWTEW-SQP-KKKRKV-Cys	Moderate	4.1
R ₈ -EDANS	Cys-Glu(EDANS)-(Ahx) ₂ -dR ₈	Moderate	1.2
Cyclo-mini-PDX	[Cys-K ³⁶⁷ GTEAAGAMFLERL ³⁸⁰ PR ³⁸⁰ SIPPE KFNKPF ³⁹⁴ -Cys]*	ND	0.57
Eda-peptide	⁹⁸ QQVAKRRTKR-Eda-DVYQE ¹¹² *	ND	0.04

Flu=Fluoresceyl 5-carboxyl, EDANS=5-[(2'-amino ethyl)-amino] naphthalene 1-sulfonyl, dR =dextro Arg, * =Number refers to sequence of α 1-PDX or furin, ND= not determined.

Acknowledgments

We thank Drs. A. Basak & SS Bag, IIT, India for Eda and NSERC & CFI for funds.

References

- Seidah, N. G. and Chrétien, M. *Brain Res.* **848**, 45-62 (1999).
- Basak, A., et al. *Peptides, 18th American Peptide Symposium* (Chorev, M. and Sawyer, T. K., eds.) Kluwer Academic Publishers, the Netherlands, pp. 343-345 (2004).

3. Basak, A., *et al. Peptides*, 17th American Peptide Symposium (Lebl, M. and Houghten, R. A., eds.) Kluwer Academic Publishers, the Netherlands, pp. 558-560 (2001).
4. Deshayes, S., *et al. Biochemistry* **43**, 1449-1457 (2004).
5. Du, H., *et al. Photochemistry and Photobiology* **68**, 141-142 (1998).
6. Siegfried, G., *et al. J. Clin. Investigative* **111**, 1723-1731 (2003).
7. Apletalina, E., *et al. J. Biol. Chem.* **273**, 26589-26595 (1998).
8. Basak, A., *et al. Bioorg. Med. Chem.* **13**, 4096-4102 (2005).

Mechanism of Interaction between the (17-31) Binding Domain of PTH and the PTH Receptor

**Thomas Dean¹, Ashok Khatri¹, Zhanna Potetinova², Gordon Willick²
and Thomas J. Gardella¹**

¹*Endocrine Unit, Massachusetts General Hospital and Harvard Medical School, Boston, MA 02114;* ²*Institute for Biological Sciences, National Research Council, Ottawa, ON, K1A 0R6*

Introduction

Parathyroid hormone (PTH) plays a critical role in bone and calcium metabolism and does so by interacting with its receptor, the PTHR, which is a class 2 G protein-coupled receptor. The interaction of PTH with the PTHR is thought to occur via a multi-step mechanism that involves an initial docking of the ligand, via an amphiphilic α -helix (AAH) within the PTH(17-31) region, to the amino-terminal extracellular (N) domain of the receptor, and a subsequent engagement of the N-terminal pharmacophoric region of the ligand with the extracellular loop/heptahelical core, or juxtamembrane (J) domain of the PTHR, resulting in activation. Most of the specifics of the interaction, however, are unknown. For example, while it is clear that the (17-31) AAH domain is critical for binding to the PTHR, as shown by the failure of N-terminal PTH fragments lacking this domain to bind to the receptor, it is not known how the (17-31) domain interacts with the PTHR N domain, and whether or not the (17-31) region contributes to the J domain interaction. Recent backbone methylation studies performed on PTH(1-31) [1], and cross-linking studies performed with photo-reactive PTH(1-34) analogs [2], in fact, suggest that the (17-31) domain can interact with the PTHR J domain. To explore further the PTH/PTHR interaction mechanism, and specifically the role of the AAH domain, we performed an alanine-scan analysis of the (17-31) region of PTH(1-31). We tested the peptides for binding affinity and cAMP-stimulating potency in HKRK-B7 cells, which stably express the cloned human PTHR, and in COS-7 cells transiently transfected with a mutant PTHR construct, PTHR-delNt, that lacks most of the N domain. We also assessed peptide structure by CD spectroscopy.

Results and Discussion

CD analysis indicated that none of the substitutions caused major changes in peptide helical content. On the intact PTHR, alanine substitutions at Arg20, Trp23 and Leu24 caused the strongest reductions in binding affinity (5- to 10-fold, relative to parent PTH(1-31), Fig. 1). Ala substitutions at Val21, Arg25 and Val31 caused three- to five-fold reductions in affinity; Ala substitutions at Lys26 and Leu28 caused ~two-fold reductions, and Ala substitutions at Glu19 and Glu22 caused a ~two-fold enhancement in affinity. The remaining substitutions were neutral. These data suggest that the binding energy provided by the PTH(17-31) domain is derived from a dispersed receptor-contact surface, with Arg20, Trp23 and Leu24 contributing, directly or indirectly, most importantly to this binding interaction. The same three residues were identified as key PTHR-binding determinants in previous PTH structure-activity relationship studies [3,4].

In cAMP signaling assays performed in HKRK-B7 cells, only the Ala substitution at Arg20 reduced potency by more than three-fold, but this effect did not reach significance ($P = 0.09$). The lack of correlation between effects observed on

binding affinity and those observed on cAMP signaling potency, as seen, for example, with Ala23 and Leu24, may be due, in part, to the amplified nature of the cAMP response that occurs in cells expressing high levels of the PTHR in the presence of phosphodiesterase inhibitor (IBMX), as this would likely render the response resilient to modest changes in affinity. In any case, the findings are consistent with the principal N-terminal signaling pharmacophore of the substituted analogs being intact.

With PTHR-delNt, conventional competition binding assays performed with ^{125}I -PTH(1-34) were not possible due to the expected poor binding of the tracer. We could, however, monitor the interactions of the analogs with PTHR-delNt by assessing cAMP responses, as the cAMP response elicited by the control PTH(1-31) on PTHR-delNt, although considerably weaker than that seen on the intact PTHR ($\text{EC}_{50}\text{s} = 2\text{ }\mu\text{M}$ versus 4 nM), was easily measurable. None of the alanine mutations reduced cAMP activity on PTHR-delNt, with the exception of the Ala25 mutation, which reduced potency by three-fold. We conclude, therefore, that the surface in the PTH(17-31) domain that involves Arg20, Trp23, and Leu24 and plays a critical role in binding to the intact PTHR, does not form critical interactions with the PTHR J domain. This conclusion is consistent with the hypothesis that the principal ligand interactions to the PTHR J domain are mediated by the N-terminal residues of PTH. On the other hand, the data with Arg25 are consistent with the notion that some residues in the (17-31) domain can contribute to the J domain interaction, as suggested by the prior backbone methylation studies, which revealed the importance of amide NH groups at positions 17, 23 and 26 for the J domain interaction [1], as well as by the cross-linking of residue 27 of PTH(1-34) to the receptor's first extracellular loop [2].

Interestingly, increases in cAMP potency of four- to six-fold were observed on PTHR-delNt for the Ala19,22 and Arg19,Ala22 double mutants, and the Arg19 single mutant PTH(1-31) analogs. Prior studies showed that the Arg19 substitution in PTH(1-34) and PTH(1-20) analogs enhances potency on PTHR-delNt [5], possibly by altering interaction with the extracellular end of transmembrane domain 2 [6] and/or stabilizing the local helical structure [7]. Our current CD analyses indeed revealed a modest increase in peptide helicity for the [Ala19,Ala22]-PTH(1-31) analog.

The overall results suggest that multiple side chains in the 17-31 helical domain of PTH form a molecular surface that contacts a complementary surface in the PTHR N domain, and that this broad contact surface contributes importantly to the overall binding energy of the complex; Arg20, Trp23 and Leu24 are key players in this interaction. The data also suggest that certain side-chains in the (17-31) domain, e.g. Glu19, Glu22 and Arg25, can modulate, directly or indirectly, interactions with the PTHR J domain. The results provide new clues for understanding the biomolecular PTH/PTHR complex, and potentially for developing new therapeutic ligands for this medically important G protein-coupled receptor.

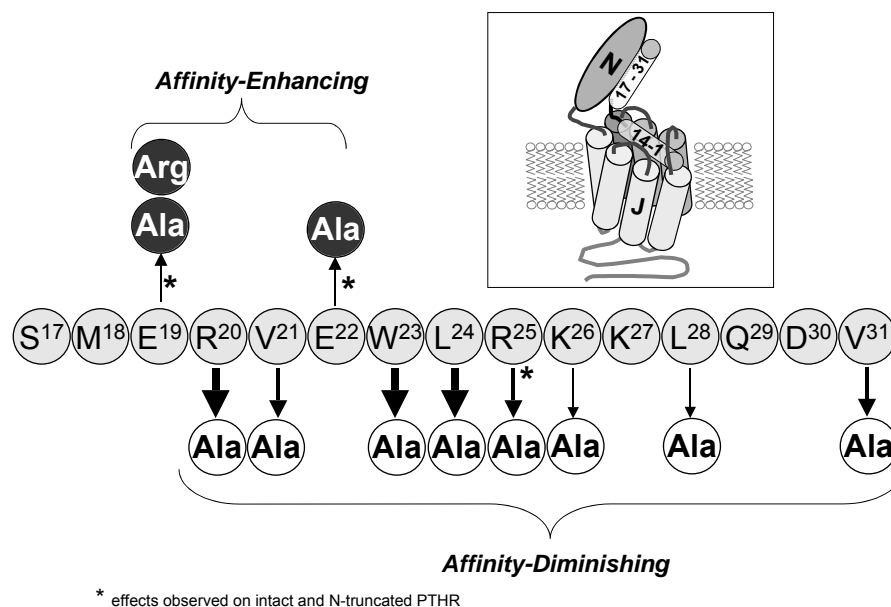


Fig. 1. Sequence of the PTH(17-31) domain, summary of results, and schematic of the PTH/PTH receptor complex.

References

1. Barbier, J. R., Gardella, T. G., Dean, T., Maclean, S., Potetinova, Z., Whitfield, J. F. and Willick, G. E. *J. Biol. Chem.* **280**, 23771-23777 (2005).
2. Greenberg, Z., Bisello, A., Mierke, D., Rosenblatt, M. and Chorev, M. *Biochemistry* **39**, 8142-8152 (2000).
3. Barbier, J., MacLean, S., Whitfield, J., Morley, P. and Willick, G. *Biochemistry* **40**, 8955-8961 (2001).
4. Gardella, T. J., Wilson, A. K., Keutmann, H. T., Oberstein, R., Potts, J. T., Jr, Kronenberg, H. M. and Nussbaum, S. R. *Endocrinology* **132**, 2024-2030 (1993).
5. Shimizu, M., Shimizu, N., Tsang, J., Petroni, B., Khatri, A., Potts, J. J. and Gardella, T. *Biochemistry* **41**, 13224-13233 (2002).
6. Gensure, R. C., Shimizu, N., Tsang, J. and Gardella, T. *J. Mol. Endocrinol.* **17**, 2647-2658 (2003).
7. Piserchio, A., Shimizu, N., Gardella, T. and Mierke, D. *Biochemistry* **41**, 13217-13223 (2002).

[3,3]-Sigmatropic Rearrangements, and Chiral Aziridines for the Asymmetric Synthesis of Novel Amino Acids

Hongchang Qu, Lu Liu, Xuyuan Gu and Victor J. Hruby

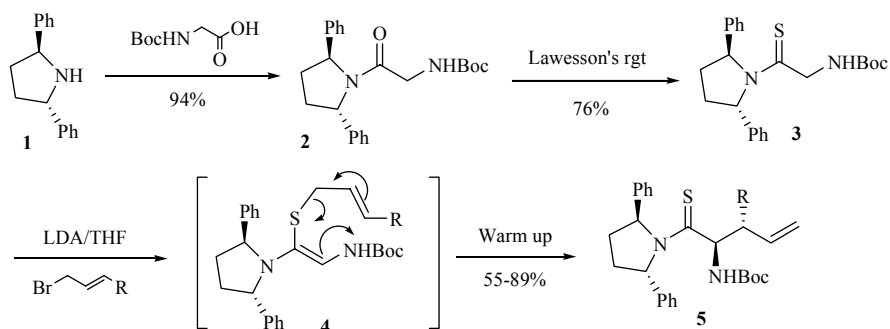
Department of Chemistry, University of Arizona, Tucson, AZ 85721, USA

Introduction

ω -Unsaturated amino acids are important synthetic building blocks in organic synthesis and peptidomimetics. The introduction of a β -substituent to such chiral amino acids can retain the stereostructural properties of the original amino acid that are important for the bioactivities of the ligand, and at the same time provide an unsaturated site necessary for further synthesis [1]. One of the most effective ways to synthesize γ,δ -unsaturated amino acids is by a [3,3]-sigmatropic rearrangement. While most of these reported rearrangements take advantage of allyl esters or chelated allyl ester intermediates [2], Meerwein Eschenmoser or thio-Claisen rearrangements have not been reported. Enlightened by work done in related areas [3], we decided to apply these strategies to novel amino acid synthesis. In addition, the great potential value of chiral aziridines led us to explore their conversion to α - or β -thio-amino acids using mercaptan nucleophiles under various conditions.

Results and Discussion

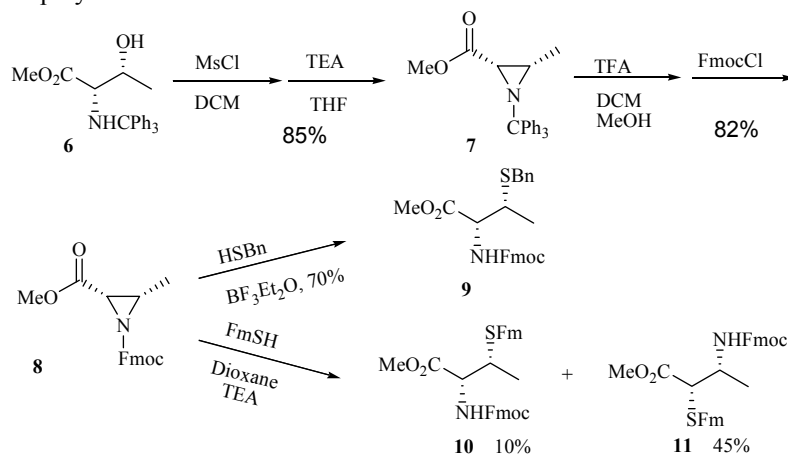
The Meerwein Eschenmoser rearrangement started from the tertiary amide of a glycine derivative. Racemic anti- β -substituted γ,δ -unsaturated α -amino acids have been synthesized via Meerwein salts as intermediates. Free amino acids and other derivatives were obtained after reductive hydrolysis of the rearranged amide. In order to have enantiopure amino acids, chiral auxiliary **1** was synthesized using modified literature procedures [4]. This C_2 symmetric amine was used in a [3,3]-sigmatropic thio-Claisen rearrangement (Scheme 1). In practice, excellent diastereoselectivity was observed due to not only the preferred formation of a *Z*-thioenolate, but also the low energy chair like transition state [5]. The reactions were clean under mild conditions. The final product **5** was obtained in good yield and diastereoselectivity, with the anti diastereomer as the major product. Different R groups have been introduced to mimic different side chain functionalities.



Scheme 1. Thio-Claisen rearrangement.

The synthesis of chiral aziridines and their application have been a hot topic in organic chemistry. Chiral aziridine **7** was synthesized as a model compound

following a reported method (Scheme 2 [6]). Traditional ring-open reaction with the help of a Lewis acid afforded α -amino- β -thio product **9** [7]. However, in the presence of base, α -thio- β -amino acid **11** was obtained as the major product in moderate yield. To the best of our knowledge, this is the first report that enantiopure α -thio- β -amino acids can be synthesized from a chiral aziridine. Various mercaptans were employed under both conditions.



Scheme 2. The reactions of chiral aziridine.

In conclusion, Meewein Eschenmoser and thio-Claisen rearrangements have been successfully explored for the synthesis of γ,δ -unsaturated amino acids. The conversion of chiral aziridines to α - and/or β -thio-amino acids using mercaptan nucleophiles were also investigated. Asymmetric synthesis of novel amino acids via the above mentioned methods and their application to peptidomimetics are under investigation.

Acknowledgments

This work was supported by US Public Health Service grants (DK 17420) and the National Institute of Drug Abuse (DA 06284, DA 13449).

References

1. Rutjes, T. P. J. T., Larissa, L. B. and Schoemaker, H. E. *J. Chem. Soc., Perkin Trans. 1* **24**, 4197-4212 (2000).
2. Kazmaier, U. *Angew. Chem., Int. Ed. Engl.* **33**, 998-999 (1994).
3. (a). Welch, J. T. and Eswarakrishnan, S. *J. Am. Chem. Soc.* **109**, 6716-6719 (1987). (b). He, S., Kozmin, S. A. and Rawal, V. H. *J. Am. Chem. Soc.* **122**, 190-191 (2000).
4. Aldous, D. J., Dutton, W. M. and Steel, P. G. *Tetrahedron: Asymmetry* **11**, 2455-2462 (2000).
5. Wipf, P. In *Comprehensive Organic Synthesis*, Vol. 5 (Trost, B. M. and Fleming, I., eds.) Pergamon, Oxford, p. 827 (1991) and references therein.
6. Wakamiya, T., Shimbo, K., Shiba, T., Nakajima, K., et al. *Bull. Chem. Soc. Jpn.* **55**, 3878-3881 (1982).
7. Zhou, H. and van der Donk, W. A. *Org. Lett.* **6**, 1335-1338 (2002).

A Library of Cysteine-Biotin Derivatives Useful for Pretargeting Avidin-Biotin Radioimmunosciintigraphy

Cristina Bolzati¹, Andrea Caporale², Davide Carta³, Liliana Cofano³, Elisabetta Schievano², Francesco Tisato¹, Fiorenzo Refosco¹, Evaristo Peggion² and Giuliano Bandoli³

¹ICIS-CNR-Padua, Italy; ²Department of Chemistry; ³ Department of Pharmaceutical Science, University of Padua, Padua, Italy

Introduction

The use of anticancer monoclonal antibody (mAb) to deliver radionuclide for detection (radioimmunosciintigraphy, RIS) and/or therapy (radioimmunoteraphy, RIT) of tumor has been impaired by the inability to achieve a high tumor/non-tumor ratio in a time compatible with that of many radionuclides of clinical interest. This problem may be overcome using the 'so-called' pretargeting technique which requires the separate administration, at different times, of the mAb and of the radionuclide targeting. To this purpose, the avidin-biotin system is the most studied strategy. The attractiveness of this system lies in the very high affinity of avidin for biotin ($K_d = 10^{-15}$ M).

^{99m}Tc ($t_{1/2} = 6.02$ h; $\gamma = 142$ keV) and ^{186/188}Re ($t_{1/2} = 17.3$ h; $\beta^- = 2.01$ MeV; $t_{1/2} = 3.8$ d; $\beta^- = 1.07$ MeV) are considered ideal radionuclides for RIS and RIT, respectively. Here, we explore the applicability of the $[\text{Tc}(\text{N})(\text{PNP})]^{2+}$ metal fragment approach (PNP = diphosphine) [1], in the preparation of a new class of Tc-based agents useful in pretargeting avidin-biotin RIS. According to this strategy, the strong electrophilic $[\text{Tc}(\text{N})(\text{PNP})]^{2+}$ moiety efficiently reacts with bifunctional ligands (L) carrying π -donors as coordinating atoms to afford dissymmetrical nitride hetero-complexes of the type $[\text{Tc}(\text{N})(\text{L})(\text{PNP})]^{0/+}$. In particular, it was found that N-functionalized cysteine[O, S] ligands react with $[\text{Tc}(\text{N})(\text{PNP})]^{2+}$ to yield the final complex in very high specific activity (180 GBq/ μmol). This demonstrates that cysteine can be

used as an efficient bifunctional chelating system to include a bioactive molecule in a Tc(N) complex [2]. Hence, a small library of N-functionalized cysteine-biotin derivatives were synthesized (Fig. 1). To study the steric and the electronic influence of the Tc-carrying complex on the biotin-avidin receptor interaction, the effect of the length and flexibility of the spacer was evaluated.

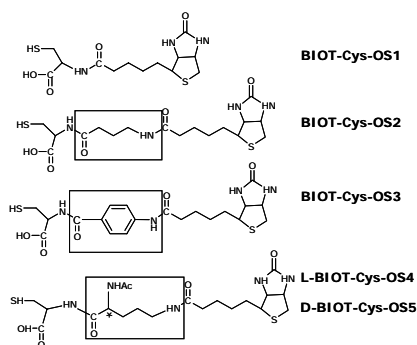


Fig. 1. N-functionalized cysteine-biotin ligands.

Results and Discussion

The nitrido-Tc(V) $[\text{Tc}(\text{N})(\text{Biot-Cys-OS}_n)(\text{PNP}_3)]$ complexes were prepared in high yields (> 95%), at nanomolar level, through a two-step procedure which

requires the simultaneous addition of PNP3 and the biotinylated ligand to a mixture of ^{99m}Tc -nitrido precursors. TLC and HPLC analyses revealed a mixture of isomeric forms, *syn* and *anti* (15:85 ratio), which depends on the orientation of the N-substituted cysteine pendant group with respect to the terminal $[\text{Tc}\equiv\text{N}]$ group. The *anti* form is the thermodynamically favored species. The chemical identity of ^{99m}Tc -complexes was established by comparison of their chromatographic properties with those of the corresponding fully characterized ^{99}Tc -compounds obtained at millimolar level.

The affinity of all ^{99m}Tc -complexes to avidin was evaluated *in vitro* at 1 and 24 hr, at 37 °C, following the procedure reported in literature [3]. In general, binding saturation curves revealed a good affinity toward the concentrator for *anti* isomers (>60%/1µg avidin) depending on the nature of the spacer. On the contrary, *syn* isomers exhibited lower affinity (<40%/1µg avidin), the only exception being *syn*- $^{99m}\text{Tc}(\text{N})(\text{Biot-OS2})(\text{PNP3})$ (79,3%/1µg of avidin).

Complexes (Biot-Cys-OS2,4,5) containing a bifunctional ligand with an aliphatic spacer (sequence of 6 atoms, mimicking the lysine chain) retained the best affinity for avidin, since the biotin was kept away from the $[\text{Tc}(\text{N})(\text{PNP3})]^{2+}$ moiety and could not interact with the metal fragment. On the contrary, a partial loss of the receptor affinity was observed for *anti*- $^{99m}\text{Tc}(\text{N})(\text{Biot-Cys-OS1,3})(\text{PNP3})$ complexes. In *anti*- $^{99m}\text{Tc}(\text{N})(\text{Biot-Cys-OS1})(\text{PNP3})$, the absence of the spacer could cause undesired interactions between biotin and the $[\text{Tc}(\text{N})(\text{PNP3})]^{2+}$ moiety making possible, thereby lowering the affinity. In *anti*- $^{99m}\text{Tc}(\text{N})(\text{Biot-Cys-OS3})(\text{PNP3})$, the presence of a rigid aromatic ring in the bifunctional ligand prevented the correct molecule rearrangement for avidin binding.

For the best agents, the stability of the avidin-radiolabeled biotinylated complex was evaluated by incubation at 37 °C for 24 hrs. These data established that approximately 40-50% of bound activity of *syn*- $^{99m}\text{Tc}(\text{N})(\text{Biot-Cys-OS2})(\text{PNP3})$ and *anti*- $^{99m}\text{Tc}(\text{N})(\text{Biot-Cys-OS4,5})(\text{PNP3})$ derivatives was released from the avidin complex, indicating an aspecific interaction, while such interaction in the case of *anti*- $^{99m}\text{Tc}(\text{N})(\text{Biot-Cys-OS2})(\text{PNP3})$ was almost irreversible.

The complexes were found to be stable in aqueous solution and in phosphate buffer. *In vitro* challenge experiments with an excess of GSH and cysteine indicated that no trans-chelation reaction occurred.

A new class of technetium complexes incorporating biotin has been successfully obtained in high yields through the application of the labelling procedure based on the metal fragment $^{99m}\text{Tc}(\text{N})(\text{PNP})^{2+}$ technology. *In vitro* affinity studies of the complex *anti*- $^{99m}\text{Tc}(\text{N})(\text{Biot-Cys-OS2})(\text{PNP3})$, evaluated at 1 and 24 hr at 37 °C, indicated that the binding occurred rapidly and was almost irreversible despite the presence of the bulky $^{99m}\text{Tc}(\text{N})(\text{PNP3})^{2+}$ molecular fragment. Studies are currently in progress aiming at the investigation of the applicability of this class of nitrido-Tc complexes in the RIS of malignant tumors using pretargeting techniques.

References

1. Bolzati, C., Boschi, A., Tisato, F., *et al.* *J. Am. Chem. Soc.*, **124**, 11468-11479 (2002).
2. Boschi, A., Bolzati, C., Duatti, A., *et al.* *Bioconjugate Chem.* **12**, 1035-1042 (2001).
3. Foulon, C. F., Alston, K. L. and Zalutsky, M. R. *Bioconjugate Chem.* **8**, 179-186 (1997).

A Methionine Scan of Region [168-176] of the Parathyroid Hormone Receptor 1 – The “Magnet Effect”

Angela Wittelsberger¹, Beena E. Thomas¹, Dale F. Mierke² and Michael Rosenblatt¹

¹Department of Physiology, Tufts University School of Medicine, Boston, MA 02111;

²Departments of Chemistry and Molecular Pharmacology, Brown University, Providence, RI 02912, USA

Introduction

Parathyroid hormone receptor 1 (PTHr1) is a member of the class II G protein-coupled receptor family and is fully activated by the first 34 amino acids of parathyroid hormone (PTH). The system plays a role in regulating calcium levels in blood [1]. With the goal to elucidate the three-dimensional structure of this ligand-receptor complex, photoaffinity crosslinking followed by digestive mapping was used to identify single contacts between specific residues in the ligand and a region/residue in the receptor. Recently, the C-terminal region of the N-terminal extracellular domain (N-ECD) of PTHr1 has emerged as an important site of interaction with the mid-region of PTH(1-34). For example, a photoreactive group in position 13 of PTH(1-34) was shown to crosslink to Arg186 of the receptor [2], and position 15 crosslinked to receptor region [183-189], close to the start of trans-membrane helix 1 (TM-1). Both ends of the mid-region, residues 11 and 21 of PTH, were found to photo-crosslink to receptor region [165-176], also in the N-ECD. This region includes helix [169-176], expected to lie on the surface of the membrane [3]. We now present a “methionine (Met) scan” of receptor region [168-176].

Results and Discussion

The two ligands containing the photoreactive group *p*-benzoylphenylalanine (Bpa) in position 11 or 21, [Bpa¹¹]-PTH and [Bpa²¹]-PTH, were crosslinked to the mutant receptors [S168M]-, [E169M]-, [V171M]-, [K172M]-, [F173M]-, [L174M]-, and [N176M]PTHr1, transiently expressed on Cos-7 cells. The ligand-receptor conjugates were isolated, digested with endoglycosidase F (Endo-F) and cyanogen bromide (CNBr), and analyzed by SDS-PAGE.

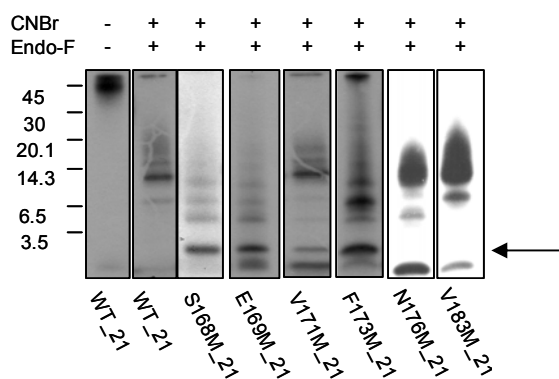


Fig. 1. SDS-PAGE analysis of the wildtype and mutant [Bpa²¹]-PTH-receptor conjugates digested with CNBr and Endo-F. Similar results were obtained for [Bpa¹¹]-PTH (not shown).

A band similar in size to free ligand was obtained for the whole range of mutants when crosslinked to Bpa¹¹-PTH, and for [S168M]- up to mutant [L174M]PTHr1 when crosslinked to Bpa²¹-PTH (Fig. 1). Such a band is generated if photoinsertion occurred at the methyl group of Met, and it represents the thiocyanomethyl-derivatized ligand (ligand + CH₃SCN) [4].

The reactivity of Bpa to Met was known to be favored over other amino acids, and Escher and coworkers recently took advantage of this property to introduce the Methionine Proximity Assay [5]. Our results show that Bpa in both position 11 and 21 crosslinks to Met over a range of 8 or 9 amino acids. As a general result, this means that crosslinking contact points can be shifted by the presence of Met in a receptor domain. This needs to be taken into account when Met is reported as site of ligand contact based on benzophenone-based cross-linking experiments. We call this the “Magnet Effect” of Met. Outside the above-mentioned range, i.e., with receptor mutant [V183M], we do not observe the characteristic band with either Bpa¹¹-PTH or Bpa²¹-PTH.

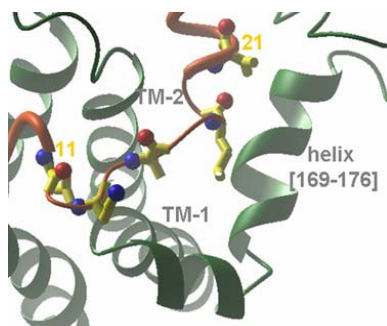


Fig. 2. Zoom into the model of the PTH ligand-receptor complex.

For our recently proposed PTH ligand–receptor model (Fig. 2), this result characterizes the interaction of the mid-region with the N-ECD as a highly dynamic process, allowing side chains throughout region [168-176] to interact with Bpa. This indicates conformational changes taking place at that stage, and adds emphasis to our recently proposed second step in the ligand–receptor interaction: mid-region contacts directing the N-terminus of PTH into the right position to enter the helical bundle for receptor activation involving a conformational change of helix [169-176].

Acknowledgments

The work was funded by grant DK-47940 to M.R.

References

1. Hock, J. M., Fitzpatrick, L. A. and Bilezikian, J. P., in *Principles of Bone Biology* (Bilezikian, J. P., Raisz, L. G. and Rodan, G. A., eds.) Academic Press, San Diego, pp. 463 (2002).
2. Adams, A. E., Bisello, A., Chorev, M., Rosenblatt, M. and Suva, L. J. *Molecular Endocrinology* **12**, 1673-1683 (1998).
3. Pellegrini, M., Bisello, A., Rosenblatt, M., Chorev, M. and Mierke, D. F. *Biochemistry* **37**, 12737-12743 (1998).
4. Kage, R., Leeman, S. E., Krause, J. E., Costello, C. E. and Boyd, N. D. *J. Biol. Chem.* **271**, 25797-25800 (1996).
5. Clement, M., et al. *J. Biol. Chem.* **280**, 27121-27129 (2005).

A New Approach to the Synthesis of Polycyclic Dipeptide Derivatives as Potential Antitumoral Agents

Teresa Lama, Orazio Mazzoni, Pietro Campiglia, Alessia Bertamino, Ettore Novellino, Maria V. Diurno, Isabel Gomez-Monterrey, Antonio Mazzella di Bosco and Paolo Grieco

Dip. Chimica Farmaceutica e Toss., University of Naples-Federico II -Naples-ITALY

Introduction

The tetrahydro- β -carboline scaffolds appear in a diverse array of biologically active compounds of natural and synthetic origin. The reported effects of this class of compounds comprise anticonvulsive, anxiolytic, sedative, anti-HIV, DNA intercalation as well as topoisomerase inhibition [1]. In the present work, we report the synthesis and cytotoxicity evaluation of novel tetrahydro- β -carboline derivatives starting from our previous results [2]. The structures synthesized are reported in Figure 1.

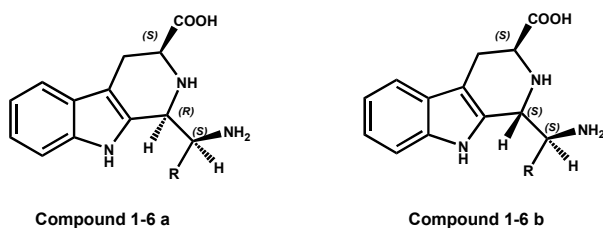
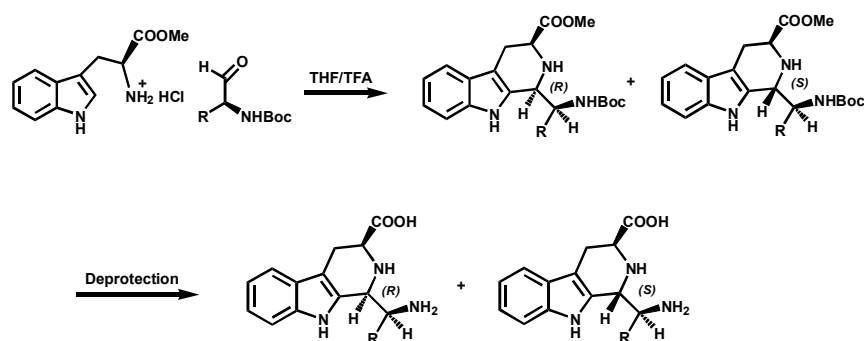


Fig. 1. Structures of tetrahydro- β -carboline derivatives synthesized.

Results and Discussion

The tetrahydro- β -carboline derivatives were prepared via Pictet-Spengler reaction utilizing L-tryptophan methyl ester hydrochloride and the appropriate aldehyde Boc-L-Aaa-H as shown in Scheme 1 [2]. The compounds 1-6 were obtained as epimeric mixture and resolved by flash chromatography to the corresponding diastereoisomers



Scheme 1. Synthesis of tetrahydro- β -carboline derivatives.

1-6a (35-25%) and **1-6b** (29-15%). The determination of the configuration at the new asymmetric center C-1 was deduced from the NOESY experiments.

All new synthesized compounds were tested for their cytotoxic activities *in vitro* against a human tumor MCF7 cell line. The preliminary data show that a number of these compounds displayed medium cytotoxic activities (Table 1). Further biological evaluation, which are required to confirm these results, are in progress.

Table 1. Cytotoxic activity of synthesized compounds

Compound	R	Yield %	IC ₅₀ μ M
1a	H	35	50
1b	H	20	45
2a	CH ₃	30	-
2b	CH ₃	15	-
3a	CH ₂ OH	25	97
3b	CH ₂ OH	20	90
4a	CH ₂ Ph	35	-
4b	CH ₂ Ph	18	-
5a	CH ₂ Ph(4-OH)	36	45
5b	CH ₂ Ph(4-OH)	18	40
6a-b	cycle(CH ₂) ₃	55	-

Here, we have reported a simple route to synthesize β -carboline derivatives that may be used in drug development of new pharmaceutical compounds. The synthesized compounds showed an interesting cytotoxic activity in preliminary assays. To acquire more information about the structural requirements for the possible improvement of the cytotoxic properties, syntheses of additional new β -carboline derivatives are in progress in our laboratory.

References

1. Scott, J. D. and Williams, R. M. *Chem. Rev.* **1002**, 1669-1730 (2002).
2. Campiglia, P., Gomez-Monterrey, I., Lama, T., Novellino, E. and Grieco, P. *Molecular Diversity* **8**, 427-430 (2004).

A Purification Strategy for Synthetic Peptides that Utilizes pH to Optimize Selectivity

Andrew F. Coffey¹, Linda L. Lloyd¹, Keeley J. Mapp¹, Louise E. Rochell¹ and Alasdair MacDonald²

¹*Polymer Laboratories Ltd, Essex Road, Church Stretton, Shropshire, SY6 6AX, UK;* ²*Polymer Laboratories Inc, 160 Old Farm Road, Amherst, MA 1002, USA*

Introduction

For economic analysis and purification of synthetic peptides an exceptionally robust HPLC column/media is required. The diversity in nature/modification of the peptides means that not all separations can be achieved using the conventional 0.1% TFA, the resolution may be poor or the peptide/peptide conjugate may have limited solubility/stability. An RP-HPLC material is needed that can operate under acidic, neutral and basic conditions. A range of particle sizes is also needed; high performance small particles for screening and early stage method development, and larger particle sizes for scale up to preparative and process purifications.

The PLRP-S materials described in this report are rigid polymeric reversed phase materials optimized for peptide/protein analysis and purification. They form part of a larger family of rigid macroporous materials developed for biomolecule analysis and purification [1]. For synthetic peptide work there are two pore sizes, the 100Å and 300Å and six particle sizes ranging from 3µm to 15-20µm. The 100Å material is ideal for small peptides and the 300Å for peptides that have a larger molecular size in solution, defined structure, or associate under the conditions of the purification. The chromatographic characteristics of these materials for large scale purification of synthetic peptides have been reported in a previous paper [2] so this report will focus on the strategy used for method development using the 10µm prep particles in analytical column format.

Results and Discussion

Unlike the silica based RP-HPLC materials PLRP-S particles are inherently hydrophobic and do not have an alkyl ligand to impart hydrophobicity. However, for reversed phase separations of synthetic peptides the retention characteristics fall within the range of silica-RP materials. There are some differences in selectivity due to the possibility of additional pi-pi interactions with aromatic amino acids and the aromatic polymer. Figure 1 compares the separation of a crude synthetic peptide using three commercially available silica based columns and the PLRP-S 100Å and 300Å media with the same screening conditions, gradient of 5-38% CH₃CN in aq. 0.1% TFA over 30 minutes at a flow rate of 1.0ml/min. The overall retention characteristics and profile are similar for all the columns but there are differences in selectivity which appears to correlate with pore size. The 300Å materials have better resolution of the earlier eluting peaks and the 100Å the later eluting peak. Not only does pore size influence the loading – and hence the economics of a purification but can also have a significant effect on resolution as in this example.

There are many successful purification schemes that utilize acidic eluents but many peptides have better solubility at neutral or alkaline pH. With the PLRP-S columns there is no restriction on the solvent used to dissolve the peptide, other than miscibility with the HPLC eluent, and it provides a single column approach to

screening separations at acidic/neutral and basic pH. The approach taken when developing a purification method is to first check solubility/stability using acidic, neutral and alkaline eluents and then to do HPLC screens to explore the preferred pH. The chromatogram in Figure 2 shows the screening gradients, acidic and alkaline of a crude synthetic 15mer peptide. By optimization of the gradient it would have been possible to resolve the by-product peak seen under acidic conditions however, when alkaline pH is used not only is an additional by-product peak seen but the impurities elute prior to the product peak. It is clear that there is a difference in selectivity at acid and alkaline pH which can be utilized for the purification. By working at high pH it may be possible to use a self displacement technique or even SMB which would give a significant improvement in the process economics. By using the stability of the PLRP-S material it may now be possible to develop more economical purification processes for synthetic peptides.

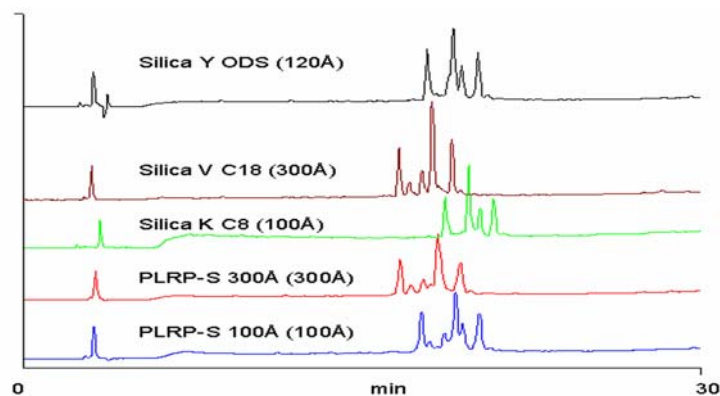


Fig. 1. Separation of a crude synthetic 14mer peptide on 10µm 250x4.6mm ID columns.

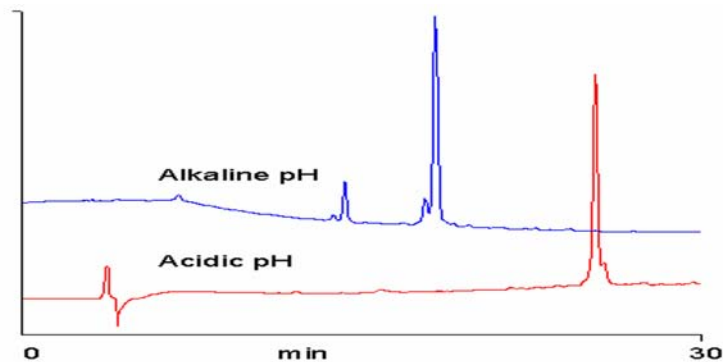


Fig. 2. Separation of a crude synthetic 15mer peptide at acidic and basic pH.

References

1. Lloyd, L. L. *J. Chromatogr.* **544**, 201-217 (1991).
2. Lloyd, L. L., et al. *J. Chromatogr. A* **944**, 169-177 (2002).

Agonist Activation of the Angiotensin II Type 1 Receptor Alters the Spatial Proximity of Transmembrane Domain 7 to the Ligand Binding Pocket

Dany Fillion, Gaétan Guillemette, Richard Leduc and Emanuel Escher

Department of Pharmacology, Faculty of Medicine, Université de Sherbrooke,
 Sherbrooke, Québec, Canada, J1H 5N4

Introduction

Activation of seven-transmembrane domains (TMDs) G protein-coupled receptors (GPCRs) involves important movements of TMDs following binding of an agonist. The underlying molecular mechanism by which GPCR activation takes place is largely unknown and may be inferred by the photoaffinity labeling (PAL) method. PAL allows gaining insight into dynamic systems under physiological conditions through the possibility to directly map the ligand-receptor interaction by covalent bonding of the photoprobe ligand within its cognate receptor. This information may then be used, in conjunction with computational molecular modeling procedures based on the X-ray crystal structure of bovine rhodopsin [1], to build and validate homology molecular models of liganded receptors. We have combined PAL with an X→Methionine (Met) mutagenesis strategy followed by Met-specific CNBr cleavage to study the implication of the C-terminal position of angiotensin II (AngII) in the activation of the AngII type I receptor (AT₁), since the C-terminal position of AngII is the so called ‘‘aromatic agonist switch’’ [2]. AT₁ is a typical class-A, rhodopsin-like GPCR, which mediates virtually all of the known physiological action of AngII, it is responsible for cardiovascular and electrolyte homeostasis.

Results and Discussion

We compared the photolabeling of a partially agonistic photoprobe, ¹²⁵I[Sar¹,Tdf⁸]AngII (Tdf: p-[3-(trifluoromethyl)-3H-diazirin-3-yl]-L-phenylalanine), with a neutral antagonist photoprobe, ¹²⁵I[Sar¹,Bpa⁸]AngII (Bpa: p-benzoyl-L-phenylalanine), on the hAT₁ receptor (Fig. 1). Both AngII photoprobes showed specific high affinity binding, similar to AngII, both on X→Met mutated hAT₁-WT receptors as well as the X→Met series of constitutively active hAT₁-N111G receptors.

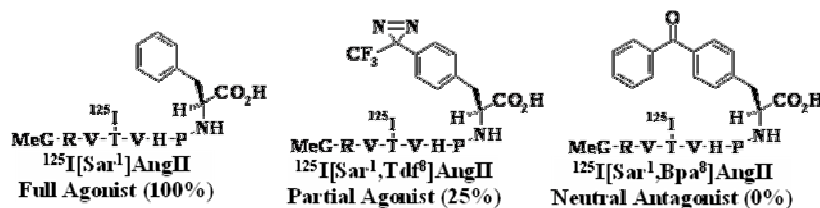


Fig. 1. AngII photoprobe structures.

Photolabeling followed by CNBr cleavage on the Met mutated receptors allowed the identification, by characteristic new fragments, of receptor domains that were covalently photolabeled (Fig. 2). The results taken together indicate that on hAT₁-WT receptors, as well as on hAT₁-N111G mutant receptor, agonist

$^{125}\text{I}[\text{Sar}^1, \text{Tdf}^8]\text{AngII}$ was shown to incorporate into TMD III and TMD VI only, whereas antagonist $^{125}\text{I}[\text{Sar}^1, \text{Bpa}^8]\text{AngII}$ was shown to incorporate into TMD III, VI and VII in the Methionine Proximity Assay (MPA) [3].

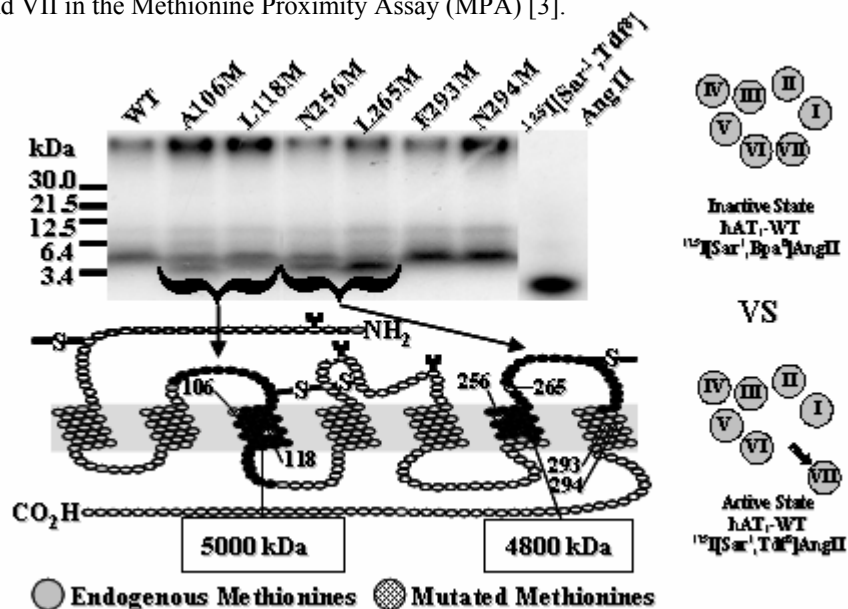


Fig. 2. Left upper panel: SDS-PAGE autoradiography of $^{125}\text{I}[\text{Sar}^1, \text{Tdf}^8]\text{AngII}$ photolabeled followed by CNBr cleaved AT_1 -mutants. Left lower panel: Schematic AT_1 presentation with labeled fragments in black closed circle. Right panel: Proposed activation molecular mechanism for the AT_1 receptor.

Our data suggest that upon activation, TMD VII of the AT_1 receptor is moving outward from the binding pocket as we have previously shown using the SCAM approach [4]. The present study adds to the accumulating evidence that this outward movement of TMD 7 is part of the molecular mechanism of AT_1 activation and seems to be a common feature found in numerous class A, rhodopsin-like, GPCRs.

Acknowledgments

This work was funded by the Canadian Institutes of Health and the Quebec chapter of the Canadian Heart and Stroke Foundation to G. Guillemette, R. Leduc and E. Escher.

References

1. Palczewski, K., *et al. Science* **289**, 739-745 (2000).
2. Miura, S., *et al. J. Biol. Chem.* **274**, 7103-7110 (1999).
3. Clément, M., *et al. J. Biol. Chem.* **280**, 27121-27129 (2005).
4. Boucard, A. A., *et al. J. Biol. Chem.* **278**, 36628-36636 (2003).

An Asymmetric Synthesis of (*R*)- and (*S*)-*o*-cyano-phenylalanine Leading to Chiral Constrained Phenylalanine Dipeptide Mimetics

Karolien Van Rompaey, Isabelle Van den Eynde, Steven Ballet and Dirk Tourwé

Organic Chemistry Department, Vrije Universiteit Brussel, Pleinlaan 2, B-1050 Brussels, Belgium

Introduction

Conformationally constrained amino acids can be used in peptides to improve the enzymatic stability, to enhance binding affinity, to alter receptor selectivity, to change agonists into antagonists, to provide enzyme inhibitors, and to examine binding models. The rotational freedom of a Phe residue around the C $_{\alpha}$ -C $_{\beta}$ bond results in three staggered low energy conformations: g(+), t and g(-). By introducing a methylene bridge between the aromatic ring of Phe and the nitrogen of an adjacent amino acid in the peptide sequence, the rotational freedom around the C $_{\alpha}$ -C $_{\beta}$ bond is limited to g(+) and t. This operation equals the replacement of a Phe-Xxx dipeptide by the aminobenzazepinone Aba-Xxx (Fig. 1).

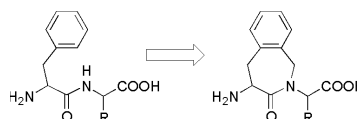


Fig. 1. Dipeptide Phe-Xxx and its constrained analog Aba-Xxx.

Results and Discussion

(*R*)- and (*S*)-*o*-CN-Phe are required as starting materials for the benzazepinones. An attractive strategy to obtain these compounds is the asymmetric phase transfer catalyzed alkylation of a prochiral Gly derivative with *o*-cyano-benzyl bromide (Fig. 2). Third generation Cinchona derived catalysts were chosen as phase transfer catalysts [1].

The Cinchonidine catalyst – providing the (*S*)-enantiomer – was commercially available; the Cinchonine catalyst – providing the (*R*)-enantiomer – was prepared in two steps from Cinchonine by N-quaternisation and O-allylation [1]. Several

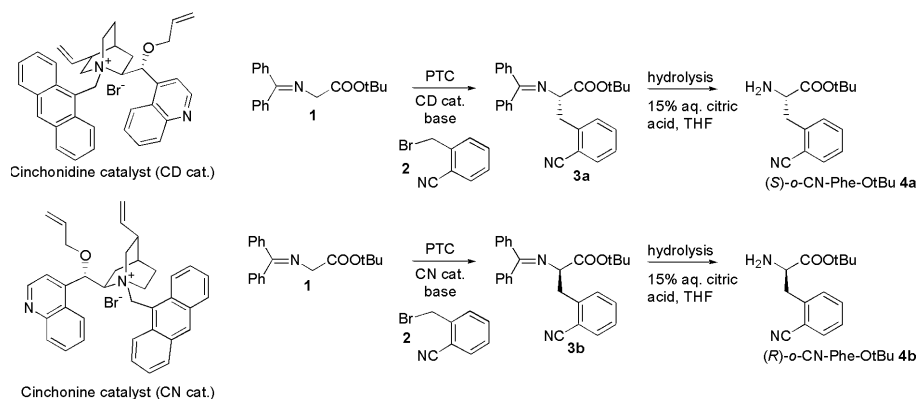


Fig. 2. Phase transfer alkylation using Cinchona derived catalysts.

Table 1. Evaluation of reaction conditions for the asymmetric phase transfer alkylation.

	conditions	yield (%)	%S	%ee
1	300 mg scale, 50% KOH, toluene, r.t., 1.2 eq. <i>o</i> -CN-BnBr, 0.1 eq. CD cat.	75	81	62
2	600 mg scale, 10 eq. CsOH.H ₂ O (dried 130°C, vacuum), CH ₂ Cl ₂ , Ar atm., -78°C, 5 eq. <i>o</i> -CN-BnBr, 0.1 eq. CD cat.	73	97	94
3	600 mg scale, 10 eq. CsOH.H ₂ O (dried 130°C, vacuum), CH ₂ Cl ₂ , Ar atm., -78°C, 2 eq. <i>o</i> -CN-BnBr, 0.1 eq. CD cat.	70	97	94
4	6 g scale, 10 eq. CsOH.H ₂ O (dried 130°C, vacuum), CH ₂ Cl ₂ , Ar atm., -78°C, 2 eq. <i>o</i> -CN-BnBr, 0.1 eq. CD cat.	90	98.2	96.4
5	600 mg scale, 1.5 eq. BEMP, CH ₂ Cl ₂ , Ar atm., -78°C, 5 eq. <i>o</i> -CN-BnBr, 0.1 eq. CD cat.	83	93	86
6	600 mg scale, 10 eq. CsOH.H ₂ O (dried 130°C, vacuum), CH ₂ Cl ₂ , Ar atm., -78°C, 2 eq. <i>o</i> -CN-BnBr, 0.1 eq. CN cat.	68	3	94
7	600 mg scale, 1.5 eq. BEMP, CH ₂ Cl ₂ , Ar atm., -78°C, 5 eq. <i>o</i> -CN-BnBr, 0.1 eq. CN cat.	84	6	88

reaction conditions were examined for the phase transfer alkylation (Table 1). At first a liquid/liquid PTC at room temperature was evaluated, resulting in a poor stereinduction [2]. Solid/liquid PTC at -78°C using CsOH led to good yields (90 %) and excellent enantiomeric excess (96% ee) [1]. In order to facilitate the experimental conditions, also a homogeneous alkylation using the phophazene base BEMP was evaluated [3]. The stereinduction was however lower.

Compounds **4a** and **4b** could then be used for the synthesis of benzazepinones **8** as depicted in figure 3 [4]. In this way Phth-(*R*)-Aba-Gly-OBn (44%), Phth-(*R*)-Aba-(*S*)-Ala-OBn (49%), Phth-(*S*)-Aba-(*R*)-Ala-OBn (39%), and Phth-(*S*)-Aba-(*R*)-Phe-OBn (44%) could be prepared (yields calcd. from **7**).

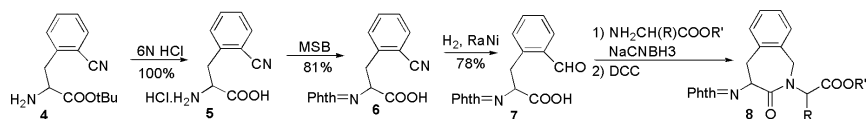


Fig. 3. Synthesis of benzazepinones starting from *o*-CN-Phe.

Acknowledgments

This research was financed by the FWO-Vlaanderen and the IWT.

References

1. Corey, E. J., Xu, F. and Noe, M. C. *J. Am. Chem. Soc.* **119**, 12414-12415 (1997).
2. Lygo, B. and Wainwright, P. G. *Tetrahedron Lett.* **38**, 8595-8598 (1997).
3. O'Donnell, M. J., Delgado, F., et al. *Tetrahedron Lett.* **39**, 8775-8778 (1998).
4. Van Rompaey, K., Van den Eynde, I., De Kimpe, N. and Tourwé, D. *Tetrahedron* **59**, 4421-4432 (2003).

Analogs of Multifunctional Ligands for Opioid and CCK Receptors

**Ekaphol Wooden¹, Vinod Kulkarni¹, Yeon S. Lee¹, Richard S. Agnes¹,
Christine Salibay¹, Peg Davis¹, Shou-Wu Ma², Josephine Lai², Frank
Porreca² and Victor J. Hruby¹**

¹Department of Chemistry; ²Department of Pharmacology, University of Arizona, Tucson,
AZ 85721, USA

Introduction

Recently, our group introduced a new paradigm in drug design for the treatment of pain in the disease state [1]. Biologically, many disease states lead to changes in expressed proteins, therefore, “system changes” that occur must be considered in any treatment for the disease. This new approach to drug design and discovery would be particularly applicable to the diseases that involve adaptive changes in the central nervous system, such as neuropathic pain. There is growing evidence that drugs behave differently in pathological states than in normal states, thus preventing their effectiveness in pathological disease states. Therefore, a new paradigm for drug design is needed.

In this new approach, single peptide molecules are designed to interact with opioid receptors as an agonist, and as an antagonist at the CCK receptors. For the treatment of pain, a series of linear and cyclic peptides [2] based on the overlapping pharmacophores of opioid and CCK ligands of SNF-9007 [3] were prepared. CCK is known to have an anti-opioid effect and this can be used to alleviate pain. The opioid/CCK analogs were synthesized and evaluated for their biological activities. Several of the opioid/CCK analogs were found to simultaneously interact with opioid receptors as agonists and CCK receptors as antagonists. As a promising peptide in the treatment of neuropathic pain, the lead compound RSA402 (Fig. 1) was modified.

RSA402: Tyr-c[**D-Lys-Gly-Trp-Glu**]-Asp-Phe-NH₂

HW2030: Tyr-c[**D-Lys-Gly-Phe(p-Cl)-Glu**]-Asp-Phe-NH₂

HW2044: Tyr-c[**D-Glu-Gly-Phe(p-Cl)-Lys**]-Asp-Phe-NH₂

Fig. 1. Cyclic analogs of opioid-CCK.

In recent years, the melanocortin receptor-4 (MC4R) found in the spinal cord and CNS has received growing attention as a therapeutic target. Researchers have shown that an antagonist of the MC4R can produce an anti-allodynic effect [4]. Linear and cyclic analogs of α -melanocyte stimulating hormone (MSH) have been used as lead molecules for targeting MC4R. Our approach here is to combine the three core units of opioid, CCK and MSH, and investigate their effect on MC4R and subsequently pain. The opioid pharmacophore is bridged through a linker to the N-terminus of the MC-CCK pharmacophores based peptide, which share a Trp residue.

Results and Discussion

As a lead compound, RSA402, which was highly potent at opioid receptors was modified. Para-substituted phenylalanine analogs of [L-Ala³]DPDPE are highly

selective for δ opioid receptors [5]. Therefore, Trp⁴ residue was modified to Phe(*p*-Cl)⁴ in the sequence and evaluated. The positions of D-Lys² and Glu⁵ in the lactam bridge also were reversed. The modification of Trp⁴ residue to Phe(*p*-Cl)⁴ had no effect on binding affinity to δ opioid receptor. The binding affinity of HW2030 to μ opioid receptor increased approximately 5-fold. While the GTP binding for both HW2030 and HW2040 increased 25-fold and 8-fold respectively for δ opioid and 10-fold and 7-fold respectively for μ opioid receptor. Thus, HW2030 has shown agonist property to MVD/GPI at nM range and antagonist property to unstimulated GPI/LMMP. The reverse of D-Lys² and Glu⁵ residues in the lactam bridge did not affect the results although HW2044 was more δ opioid receptor selective in binding affinity.

Multifunctional ligands of opioid, MSH and CCK like **1** (Fig. 2) has shown considerable biological activity towards the MC4R. Designing other related scaffold based ligands is in progress with various types of linkers attached to improve biological activity.

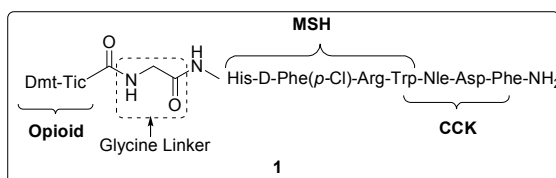


Fig. 2. Multifunctional ligand of opioid, MSH and CCK.

Acknowledgments

Grants supported by USPHS and NIDA.

References

1. Hruby, V. J., *et al.* In *Peptides: The Wave of the Future* (Lebl, M. and Houghten, R. A., Eds) American Peptide Society, San Diego, pp 969-970 (2001).
2. Agnes, R. S. *Ph.D. Dissertation*, University of Arizona, (2003).
3. Slaninova, J., *et al.* *Eur. J. Pharmacol.* **200**, 195-198, (1991).
4. Chaki, S. *Drugs of the future*, **299**, 1065-1074 (2004).
5. Haseeth, R. C., Zalewska, T., Davis, P., Yamamura, H. I., Porreca, F. and Hruby, V. J. *J. Peptide Res.* **50**, 171-177 (1997).

Antigen Effects of Peptide Nucleic Acids on HIF-1 α Expression

Zhanna Zhilina, Amy Ziemba, Lenka Stankova, Stacey Wood, Meghan Boros and Scot Ebbinghaus

Cancer Center, University of Arizona, Tucson, AZ, 85724, USA

Introduction

Peptide nucleic acids (PNAs) are DNA mimics with pseudopeptide backbone [1]. PNAs have a high affinity and specificity for complementary DNA and RNA sequences, and high resistance to enzymatic degradation. These properties make PNAs leading agents for antigene and antisense applications. In this study we designed several PNAs to downregulate expression of hypoxia inducible factor 1 α (HIF-1 α). HIF-1 α is overexpressed in many human cancers and overexpression is associated with treatment failure and increased mortality [2]. We selected polypurine/polypyrimidine tract (PPT) in the HIF-1 α untranslated region (5'UTR) for targeting by antigene PNAs to prevent the binding of activating transcription factors and to present a roadblock to RNA polymerase.

Results and Discussion

Mono- and bis-PNAs were designed to target 9 base pairs purine/pyrimidine tract (-83 to -93) in the 5'UTR of HIF-1 α (Fig. 1.). The PNAs were synthesized by Biosynthesis, Inc using Fmoc chemistry and were given to us on solid support for further modifications (Table 1).

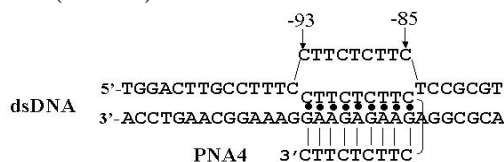


Fig. 1. Schematic representation of the HIF-1 α 5'UTR target sequence and bis-PNA forming a strand invasion complex. Dots represent Watson-Crick bonds, vertical lines represent Hoogsteen bonds.

In order to evaluate the cellular uptake of PNAs in cancer cells, the PNAs were modified with fluorescein by conjugation between the free amino group of the PNA N-terminal and 6-carboxyfluorescein succinimidyl ester. In order to improve the cellular uptake of PNAs, we modified mono-PNA with a lipophilic molecule, cholesterol, by reaction between terminal amino group and cholesteryl chloroformate. The PNAs were cleaved from the resin with 20% m-cresol in TFA and analyzed by C₁₈ RP-HPLC with a gradient 0-80% CH₃CN in aq. 0.1% TFA. All the PNAs were characterized with MALDI-TOF analysis.

Binding affinities (C₅₀) of the PNAs were analyzed by EMSAs at different pH. PNAs were incubated with the radio-labeled HIF-1 α duplex target sequence for 18 hrs and then separated on 12% nondenaturing polyacrilamide gel. Conjugation with fluorescein or cholesterol did not significantly affect PNAs binding. In future experiments, the cholesterol effect on cellular uptake will be studied.

Table 1. PNA sequences and characteristics

Name	Description	Sequences	MH ⁺	t _R , min	C ₅₀ , μM, pH 6.5	C ₅₀ , μM, pH 7.0
PNA1	mono-PNA	CTTCTCTTC-O-K-O	2772	17.6	0.3	0.8
PNA2	mono-PNA- Cholesterol	Chol- CTTCTCTTC-O- K-O	3145.9	21.18	0.3	8.0
PNA3	mono-PNA- Fluorescein	FAM-CTTCTCTTC-O- K-O	3129.8	21.09	0.25	7.0
PNA4	bis-PNA	CTTCTCTTC-OOO-K- CTTCTCTTC	5253.0	15.44	0.008	0.5
PNA5	bis-PNA(J)	O-KK-O-TTCTCTTC- OOO-JTTJTJTJ-O-KK	6296.5	17.39	0.045	5.0
PNA6	bis-PNA(J)- Fluorescein	FAM-O-KK-O- CTTCTCTTC-OOO- JTTJTJTJ-O-KK	6654.3	25.63	0.7	7.0

C-Cytosine, T-Thymine, J-Pseudoisocytosine, O – 2-amino-ethoxy-2 ethoxyacetic acid (linker)

The ability of the PNAs to downregulate HIF-1 α transcription was evaluated by transient transfection assays with a HIF-1 α promoter-luciferase reporter plasmid [3]. The pGL3/HIF plasmid containing the HIF-1 α 5'UTR region was incubated with 10 μ M PNAs for 18 hrs and then transfected into HeLa cells. Transfection was accomplished with Lipofectamine 2000 and included an internal control plasmid (pRL/SV40). Data are presented as a percentage of luciferase activity from plasmid without PNA treatment (Fig. 2).

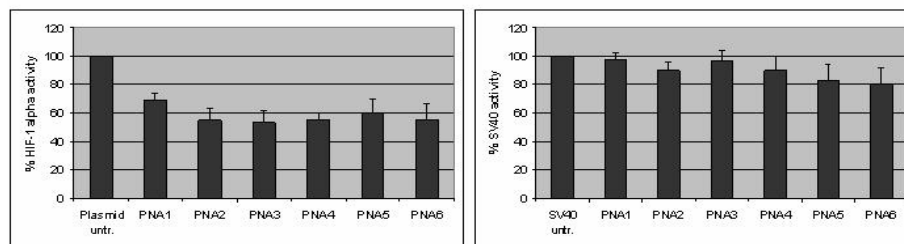


Fig. 2. Transient transfection analysis.

The PNAs demonstrated up to 50% downregulation of HIF-1 α in HeLa cells while not affecting control plasmid SV40. In summary, these data demonstrate the facile synthesis of PNAs conjugated to either fluorescein or cholesterol. Binding to duplex DNA and inhibition of transcription are not significantly altered by the conjugation.

References

1. Hyrup, B. and Nielsen, P. E. *Bioorg. Med. Chem.* **4**, 5-23 (1996).
2. Semenza, G. L. *Physiology (Bethesda)* **19**, 176-82 (2004).
3. Ziemba, A. J., Zhilina, Z. V., Krotova-Khan, Y., Stankova, L. and Ebbinghaus, S. W. *Oligonucleotides* **15**, 36-50 (2005).

Novel Glyco-lipid-arsenicals (III) with Anti-proliferative Effects on MCF-7 Human Breast Cancer Cells

Norbert Wimmer¹, Jodie A. Robinson², Nagaraj Gopisetty-Venkatta², Sarah J. Roberts-Thomson², Gregory R. Monteith² and Istvan Toth¹

¹School of Molecular and Microbial Sciences; ²School of Pharmacy, The University of Queensland, Brisbane, Queensland 4072, Australia

Introduction

Today there is a renewed interest by researchers in parasitic and anti-tumor activity of arsenicals (III) as drugs for the future, particularly because these drugs are fairly cheap and are therefore also suitable as therapeutics for developing countries.

Arsenic trioxide appears to be effective in the treatment of pro-myelocytic leukaemia. It is assumed that the electronically soft species RAS_2^+ and R_2As^+ (R = alkyl, aryl, substituted aryl) block biological closely spaced sulphhydryl groups, however, the inhibition of thiol-enzymes by As (III), although widely quoted, is poorly understood [1]. Closely spaced sulphhydryl groups occur in several intracellular proteins [2]. In this study we chemically modified *p*-amino-phenylarsen(III)oxide (PAO) by attaching a lipoaminoacid (Laa) and a sugar (Fig. 1). The Laa increases a compound's biological stability and passive diffusion by increasing its lipophilicity [3]. Additionally Laa modification on the *p*-amino function of compound **2** may have a favorable effect on toxicity.

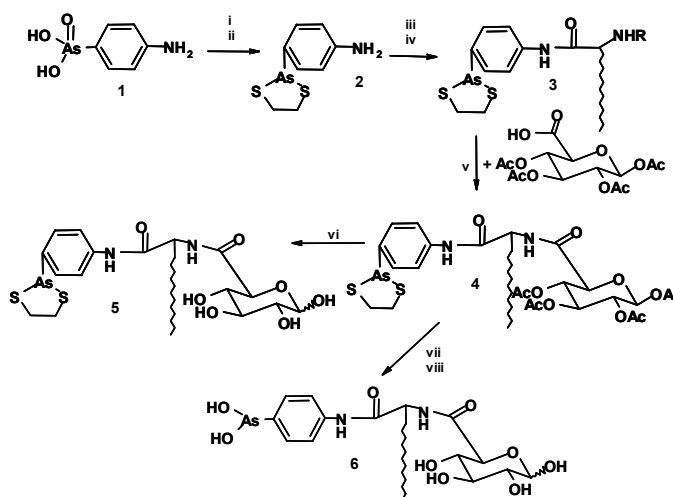


Fig. 1. Synthesis of sugar-lipoaminoacid linked arsenicals (III) **5** and **6**.

Reagents and conditions: (i) phenylhydrazine, methanol, reflux, 1 hr; (ii) ethanedithiol, ethanol, reflux, 10 min; (iii) HBTU, DIEA, DMF/THF, $\text{BocC}_{12}\text{Laa}$ o/n; (iv) TFA/ DCM (30 %), 45 min; (v) HBTU, DIEA, DMF/THF, 16 hrs; (vi) NaOMe/MeOH (0.1 M), 3 hrs, Dowex 50-AG WX8 (H^+); (vii) $\text{Hg}(\text{ClO}_4)_2$ in methanol, K_2CO_3 , 10 min; (viii) NaOMe/MeOH (0.1 M), 4 hrs, Dowex 50-AG WX8 (H^+).

The arsenicals are a class of therapeutics, which are receiving increasing attention as possible cost-effective anticancer agents. Structural modifications of arsenicals may confer improved bioavailability, selectivity and potency. Our goal was to characterise both compounds **5** and **6** for their ability to initiate cell death in MCF-7 cells and HT-29 colon cancer cells, and additionally to determine the mode of cell death. The apoptosis pathway is often targeted for therapeutic design because of the controlled mechanism of removal of cellular components and a lack of release of intracellular contents which could affect surrounding normal cells.

Results and Discussion

A significant decrease in MCF-7 cell proliferation was observed using 1 μ M and 10 μ M of compound **6** and 10 μ M of compound **5**. Treatment with compound **6** triggered apoptosis (analyzed using a TUNEL assay) of MFC-7 cells while compound **5** induced inhibition of cellular proliferation was not via rapid induction of apoptosis and more likely reflected necrosis and/or alterations in the cell cycle. Differences in the anti-proliferative potency of the two compounds indicate that structural modifications influence effectiveness. An increase in lipophilicity did not correlate with increased anti-proliferative effects. Most likely the reduced potency observed for compound **5** is related to the requirement for cleavage of the five-membered dithiarsolane ring to the arsenoxide group. Our observation that inhibition of proliferation was mediated via apoptosis only for compound **6** demonstrates that structural alterations to the arsenoxide group may yield compounds which inhibit proliferation via mechanisms other than non-rapid (< 24 hrs) apoptosis, thus reducing their favorable properties as anti-cancer agents. The altered mechanism initiated by compound **5** may be related to its enhanced lipophilicity allowing greater access to more intracellular targets, the consequence of which is uncontrolled cell death and/or alterations in the cell cycle [4]. The toxicity of compound **5** and **6** at concentrations that were used in *in vitro* assays (10 nM-100 μ M) was negligible (analyzed by hemolysis assay). There were no effects of compounds **5** and **6** on the proliferation of HT-29 colon cancer cells indicating the high cell selectivity of arsenicals [5,6].

The high micromolar concentrations required to significantly inhibit MCF-7 proliferation suggest that these compounds are not potential therapies for the treatment of breast cancer. However, the ability of these novel glyco-lipid arsenicals (III) to induce cell death may indicate that further studies of other novel arsenical derivatives are warranted. Future work will be based on modifying the lipid-chain, the sugar entity and more importantly using less stable As-protective groups in order to liberate the arsenoxide functionality *in vivo* more effectively.

References

1. Ni Dhubhghaill, O. M. and Sadler, P. J. *Struct. Bonding (Berlin)* **78**, 129-190 (1991).
2. Don, A., Kisker, O., Dilda, P., Donoghue, N., Zhao, X., Decollogne, S., Creighton, B., Flynn, E., Folkman, J. and Hogg, P. J. *Cancer Cell* **3**, 497-509 (2003).
3. Toth, I., Flinn, N., Hillery, A. M., Gibbons, W. A. and Artursson, P. *Int. J. Pharm.* **105**, 241-247 (1994).
4. Okada, H. and Mak, T. W. *Nature Reviews Cancer* **4**, 592-603 (2004).
5. Akay, C. and Gazitt, Y. *Cell Cycle* **2**, 358-368 (2003).
6. Hogg, P. J. *PCT Int. Appl.* WO 2003039564 (2003).

Antisense PNA and PNA-peptide Conjugates for the Modulation of β -globin Gene Splicing

Alessandra Romanelli¹, Soccorsa Pensato¹, Erminia Di Niola², Giordana Feriotto³, Francesca Salvatori³, Giulia Breveglieri³, Laura Zaccaro², Michele Saviano², Roberto Gambari³, Carlo Pedone¹ and Ettore Benedetti¹

¹University of Naples and; ²Institute of Biostructure and Bioimaging, via Mezzocannone 16-80134 Naples, Italy; ³University of Ferrara, via L. Borsari 46-44100 Ferrara, Italy

Introduction

Peptide Nucleic Acids (PNA) are oligonucleotide analogs widely used as antisense and antigene molecules thanks to their stability and affinity towards DNA and RNA targets. Since antisense PNAs, unlike oligonucleotides, do not recruit RNaseH upon binding to mRNA [1], they can be used to interfere in splicing events, and any time the RNase support is not required. There are several examples of aberrant splicing induced diseases, one of which is β -thalassemia [2], a very common genetic disease due to mutations causing defective β globin gene expression, leading to a deficiency in haemoglobin A production. More than 100 thalassemic mutations have been identified so far, the most common being those causing aberrant splicing [3]. These mutations are found in intron 1 and intron 2 of the β globin gene. In this work we investigated the effect of a 14-mer PNA (PNA110) targeting the IVS-110 region of the β globin gene intron 1, where a G to A mutation is found. Furthermore, the 14-mer PNA was conjugated to the SV40 NLS peptide (PNA110/NLS) to enhance the PNA concentration in cells.

PNA110 H- AATAGACTAATAGG-NH₂

PNA110/NLS H- AATAGACTAATAGG- KPKKKRKV-NH₂

Results and Discussion

The 14-mer PNA complementary to a mutated region of the IVS I-110 β globin gene (PNA110) and the conjugate PNA-peptide (PNA110/NLS) were synthesized on solid phase by Fmoc chemistry on a PALPEG-PS resin and purified by HPLC. Cleavage and deprotection were carried out by treatment with a TFA/m-cresol solution for PNA110 and with TFA/m-cresol/TIS for PNA110/NLS. Purified compounds were characterized by MALDI ToF. Affinity of the PNA based molecules for their target was measured by Surface Plasmon Resonance (SPR) based biospecific interaction analysis (BIA). The results obtained (Fig. 1) demonstrate that both PNA110 and PNA110/NLS hybridize efficiently with target DNA sequences, while the peptide does not bind to the DNA as expected.

In vitro experiments with HeLa Cell Nuclear Extracts were carried out to monitor the effect of PNAs on splicing reactions [4]. Splicing of pre-mRNAs was carried out for 4 hr at 30°C in the presence or absence of PNA110, PNA110/NLS and NLS peptide. The splicing products were then retrotranscribed and the obtained cDNAs were amplified by PCR. These experiments showed that splicing of mutated transcript was always less efficient than the splicing of wt transcript. The data obtained (Fig. 2) demonstrated that, as it was found for RNA-based oligonucleotides recognizing this region [5], splicing of both mutated and wt transcripts was inhibited by PNA110 and PNA110/NLS.

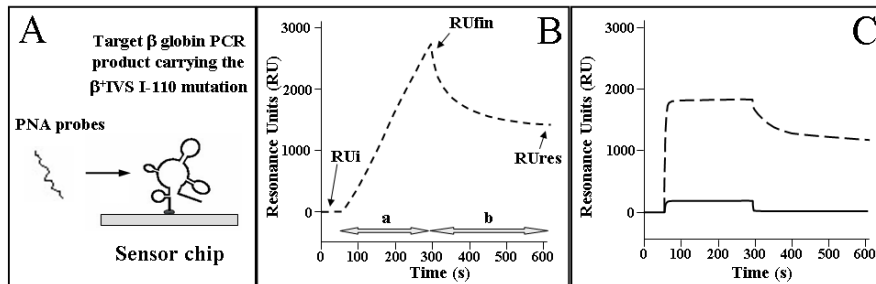
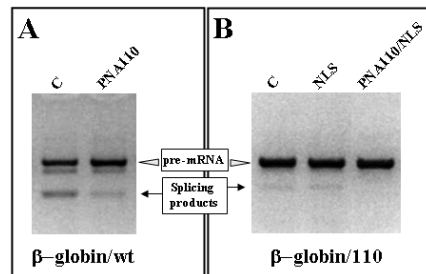


Fig. 1. **A**, Experimental strategy for SPR-based BIA. A biotinylated PCR product carrying the β +IVS I-110 mutation was immobilized on a Streptavidin-coated flow cell and PNA probes were injected. **B,C**, Sensograms obtained after injection of PNA110 (**B**), PNA110/NLS (**C**, dotted line) or NLS peptide (**C**, solid line) on the flow cell carrying the β +IVS I-110 PCR product. **a** = Injection of 0.3 nmol of each probe dissolved in HBS-EP buffer; **b** = injection of 15 μ l of HBS-EP buffer. **RU_i** = initial resonance units; **RU_{fin}** = final resonance units; **RU_{res}** = residual resonance units.

Fig. 2. Effects of 5 μ M PNA110 and PNA110/NLS on *in vitro* splicing of the wild type (**A**) and mutant IVS I-110 (**B**) β -globin pre-mRNA.



RT-PCR products of the splicing reactions were analyzed by 3% agarose gel electrophoresis. **C**: control reaction without PNAs; **NLS**: pre-mRNA incubated with 5 μ M NLS peptide. Pre-mRNAs were transcribed, using the MAXIscript T7 In Vitro Transcription Kit (Ambion), from PCR products containing wild type and mutant IVS I-110 β -globin sequences.

Splicing of pre-mRNAs was carried out in HeLa Cell Nuclear Extract (Jena Bioscience) for 4 hr at 30°C. PNA110, PNA110/NLS and NLS peptide were added together with the other components of the splicing reaction. The splicing products were retrotranscribed, using random primers, and the obtained cDNAs amplified by PCR using the 5'-AGT TGG TGG TGA GGC CCT G-3' (forward) and the 5'-CCA CTC CTG ATG CTG TTA TGG G-5' (reverse) primers.

In conclusion, two PNA-based molecules (PNA110 and PNA110/NLS) targeting the IVS I-110 region of the human β globin gene were synthesized and demonstrated to efficiently hybridize with target DNA sequences and to inhibit *in vitro* splicing of β globin primary transcripts. Experiments on cellular systems will clarify whether these molecules maintain the effects we found *in vitro*. Furthermore, PNA-based molecules targeting the branchpoint site will be employed for correction of the IVS I-110 mutation [5].

References

1. Nielsen, P. E., Egholm, M., Berg, R. H. and Buchardt, O. *Science* **254**, 1497-1500 (1991).
2. Olivieri, N. F. *N. Engl. J. Med.* **341**, 99-109 (1999).
3. Huisman, T. H. *Br. J. Haematol.* **75**, 454-457 (1990).
4. Scamborova, P., Wong, A. and Steitz, J. A. *Mol. Cell. Biol.* **24**, 1855-1869 (2004).
5. Dominski, Z. and Kole, R. *Proc. Natl. Acad. Sci. USA* **90**, 8673-8677 (1993).

β -Amino Acid Analogs of an Insect Neuropeptide

Pawel Zubrzak¹, Howard J. Williams², Geoffrey M. Coast³, Gloria Reyes-Rangel⁴, Eusebio Juaristi⁴, Janusz Zabrocki⁵, Allison Strey¹ and Ronald J. Nachman¹

¹Areawide Pest Management Research Unit, Southern Plains Agricultural Research Center, US Department of Agriculture, 2881 F/B Road, College Station, TX, U.S.A.; ²Department of Chemistry, Texas A&M University, College Station, TX 77843, USA; ³School of Biological and Chemical Sciences, Birkbeck College, London, WC1E 7HX, U.K.; ⁴Departamento de Quimica, CIEA del IPN, Mexico D.F.; ⁵Technical University of Lodz, 90-924 Lodz, Poland

Introduction

Insect neuropeptides of the insect kinin class share a common C-terminal pentapeptide sequence Phe¹-Xaa²-Xaa³-Trp⁴-Gly⁵-NH₂ (Xaa¹ = His, Asn, Phe, Ser or Tyr; Xaa² = Pro, Ser or Ala) and have been isolated from various insects [1,2]. It has been reported that this peptide family can regulate such critical physiological processes as water and ion balance, hindgut motility and digestive enzyme release in insects [3].

The C-terminal pentapeptide sequence is all that is required to elicit a physiological response in cockroach *Leucophaea maderae* hindgut myotropic [1] and cricket *Acheta domesticus* Malpighian tubule secretion [1] assays. The active core sequence Phe¹-Tyr²-Pro³-Trp⁴-Gly⁵-NH₂ is equipotent with the parent nonapeptide in these two assays. However, in the house fly *Musca domestica* Malpighian tubule secretion assay, longer sequences are required to elicit a full physiological response. Within the active core sequence, the aromatic residues Phe¹ and Trp⁴ are crucial for activity in both bioassay systems, whereas position 2 tolerates wide variations of side chain character [4,5].

Unfortunately, insect kinin peptides are unsuitable as pest control agents and/or research tools for insect neuroendocrinologists due, in large measure, to susceptibility to both exo- and endopeptidases in the hemolymph and gut of the insect. Two susceptible hydrolysis sites in the insect kinins [6] have been reported. The primary site is between the Pro³ and the Trp⁴ residues and the secondary site is the peptide bond N-terminal to the Phe¹ residue in natural, extended peptides.

Incorporation of β -amino acids in these peptides can enhance both resistance to peptidase attack and biological activity [7]. This strategy has not been previously applied to insect neuropeptides.

Results and Discussion

Synthesis and diuretic activity (stimulation of fluid secretion on the isolated Malpighian tubules of the cricket) was performed as described previously [4].

The analog **1460** demonstrated diuretic activity equipotent with the natural insect kinins, with an EC₅₀ value of 30 pM. The analog **1457** was 5 times less active in this assay, with an EC₅₀ value of 270 pM. Analogs **1458** and **1459** demonstrated lower stimulation of fluid secretion with EC₅₀ values of 22,500 and 20,000 pM, respectively (Table 1).

All analogs produce a maximal diuretic response that is not significantly different from that obtained with the endogenous achetakinin peptides. The natural

Achetakinins elicit cricket Malpighian tubule fluid secretion at EC₅₀ values ranging from about 18 to 325 pM [4].

Table 1. The cricket diuretic activity of insect kinin analogs containing β -amino acids

		Malpighian Tubule Fluid Secretion	
	Peptide Analog	EC ₅₀ (pM)	Maximum Response (%)
AK I	SGAD-Phe-Tyr-Pro-Trp-Gly-NH ₂	78	100
1460	Ac-Arg-Phe-Phe- β^3 Pro-Trp-Gly-NH ₂	30	110
1457	Ac-Arg- β^3 Phe-Phe-Pro-Trp-Gly-NH ₂	270	100
1459	Ac-Arg-Phe-Phe-Pro- β^3 Trp-Gly-NH ₂	20,000	100
1458	Ac-Arg- β^2 homoPhe-Phe-Pro-Trp-Gly-NH ₂	22,500	95

The two analogs **1460** and **1457** are therefore as potent as naturally occurring achetakinin peptides. More important, they have been modified at the two known susceptible hydrolysis peptide bond sites, which make these peptides potentially resistant to ACE and NEP endopeptidase hydrolysis.

Incorporation of β -amino acid residues into insect kinins can produce potent analogs which are more flexible and may therefore better interact with the receptor. In addition, this modification can lead to analogs which are more resistant to enzyme hydrolysis. These results open additional possibilities for the design of potent agonist/antagonist analogs, which could provide the basis for selective, environmentally friendly pest arthropod control strategies based on insect kinin neuropeptides.

Acknowledgments

We wish to thank Nan Pryor (USDA, College Station) and Alan Tyler (Birkbeck College, London) for technical assistance. We also acknowledge financial assistance from the North Atlantic Treaty Organization (NATO) (RJN, GMC, JZ) Collaborative Research Grant (#LST.CLG.979226), the Texas Advanced Technology/Advanced Research Program (#000517-0103-2001)(HJW, RJN) and the USDA/DOD DWFP Initiative (#0500-32000-001-01R) (RJN, PZ).

References

1. Holman, G. M., Cook, B. J., Nachman, R. J. *Comp. Biochem. Physiol. (C)* **88**, 31–34 (1987).
2. Coast, G. M. In *Recent advances in arthropod endocrinology* (Coast, G. M. and Webster, S. G., eds) Cambridge University Press, Cambridge, UK, pp. 189–209 (1998).
3. Nachman, R. J., Strey, A., Isaac, E., Pryor, N., Lopez, J. D., Deng, J. G. and Coast, G. M. *Peptides* **23**, 735–745 (2002).
4. Coast, G. M., Holman, G. M. and Nachman, R. J. *J. Insect Physiol.* **36**, 481–488 (1990).
5. Nachman, R. J. and Holman, G. M. In *Insect neuropeptides: Chemistry, biology, and action*. (Menn, J. J. and Masler, E. P., eds.) American Chemical Society, Washington, DC, pp. 194–214 (1991).
6. Roberts V. A., Nachman R. J., Coast G. M., Hariharan M., Chung J. S., Holman G. M., Williams H. and Tainer J. A. *Chem. Biol.* **4**, 105–117 (1997).
7. Cheng, R. P., Gellman, S. H. and DeGrado, W. F. *Chem. Rev.* **101**, 3219–3232 (2001).

Branched Neurotensin for Tumor Targeting

Chiara Falciani, Monica Fabbrini, Barbara Lelli, Luisa Lozzi,
Alessandro Pini and Luisa Bracci

Department of Molecular Biology, University of Siena, Via Fiorentina 1, Siena, Italy

Introduction

One of the major problems in classic chemotherapy is the non-specific toxicity of most anticancer agents against normal cells. The specific targeting of tumors has been the main challenge in research on cancer therapy and diagnosis. Presently, innovative tumor-specific therapies address tumor cells via tumor associated antigens, specifically expressed or over expressed on tumor cells, and deliver cytotoxic moieties directly producing tumor cell death. The observation that receptors for different endogenous regulatory peptides are expressed in a number of primary human cancers opened new perspectives on the use of synthetic peptides for tumor-selective targeting [1]. In fact, anticancer drugs or radiotracers have been coupled to analogs of many regulatory peptides. Nonetheless, the use of peptides *in vivo* has largely been limited by their short half-life.

In a previous study we reported that the synthesis of bioactive peptides in dendrimeric MAP form can result in increased half-life, due to acquired resistance to protease and peptidase activity [2]. Our results indicated that synthesis in dendrimeric form may be a general method to increase *in vivo* stability of bioactive peptides.

Currently, analogs of neurotensin (NT) and particularly of its short active fragment NT(8-13) are under investigation to target a variety of neuroendocrine human tumors (prostate, pancreatic, and small cell lung cancer) over-expressing NT receptors [1,3]. Nonetheless, chemical modifications of NT sequence aimed to increase its half-life, significantly decrease peptide receptor affinity. We demonstrated that the binding activity of branched NT and NT(8-13) is fully retained or enhanced. Moreover tetrabrached peptides become much more resistant to proteolysis. These results bring new perspectives to the use of NT as a carrier for tumor targeting tracers or therapeutics.

Results and Discussion

We synthesized several tetrabrached MAP NT(8-13) conjugated to different functional units for tumor therapy or diagnosis (Fig. 1). Tetrabrached NT(8-13) was synthesized in a coupled form with chlorine e6 (NT4-Chlo), methotrexate (NT4-MTX), biotin (NT4-Bio and NT4-PEG-Biotin), tetramethyl rhodamine (NT4-TMR),

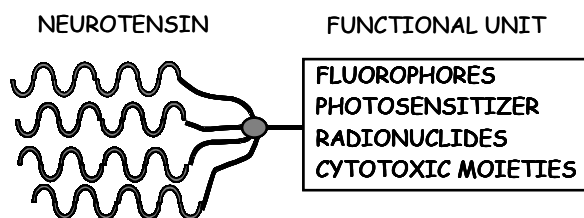


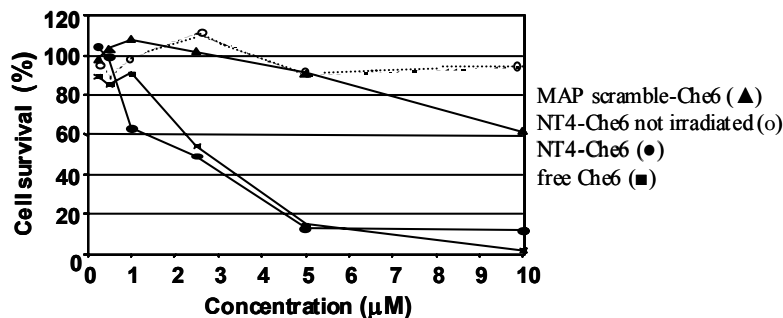
Fig. 1. Schematic representation of branched neurotensin derivatives.

fluoresceine (NT4-Fluo), and DTPA (NT4-DTPA). The binding of these new molecules to NT receptors was assayed by testing the inhibition of ^{125}I -NT specific binding to membranes prepared from the human colon

adenocarcinoma cell line HT29. The binding activity of all MAPs was always retained, whereas a tetrabranch peptide with a scrambled sequence of NT(8-13) showed no binding ability.

MAP NT(8-13)-tetramethyl rhodamine (NT4-TMR) was used to perform cell internalization and localization assays. HT29 cells were incubated with NT4-TMR at different time intervals, then washed, fixed in paraformaldehyde, and observed with a confocal laser microscope. The plasma membrane was stained with concavalinA-biotin and avidin-FITC and the lysosomes with Lysotracker green in different experiments. The peptide was completely internalized in 4 hrs and localized in the lysosomes.

Cytotoxicity of MAP NT(8-13)-chlorine e6 (NT4-Che6) was measured in HT29 cells, incubated with different concentrations of NT4-Che6, scramble NT4-Che6, or free chlorine e6. The cells were then washed, irradiated for 5' (except the dark controls), and the phototoxicity was monitored with an MTT assay 24 hrs later (Fig. 2). The results showed that, as known, free Che6 is toxic to cells, whereas conjugated Che6 is toxic only when coupled to active NT. In fact, NT4-Che6 is as toxic as free Che6, whereas scramble NT4-Che6 is not.



Ex vivo immunofluorescence assays were performed on HT29 tumor removed from transplanted nude mice. Frozen tissue was sectioned with a cryostat and incubated first with NT4-Biotin and then with Cy3-Streptavidin. Confocal images showed remarkable staining of the tumor tissue.

MAP NT(8-13) carrying different functional moieties is therefore a promising new tool for the specific therapy and *in vivo* imaging of NTR-expressing tumors. Moreover, our results indicate that the use of regulatory peptides synthesized in MAP form may open new perspective in the specific targeting of many different types of cancer. Moreover, it may allow combined therapy with different peptides and different cytotoxic moieties.

Acknowledgments

The work was funded by AIRC.

References

1. Reubi, J. C. *Endocr. Rev.* **4**, 389-427 (2003).
2. Bracci, L., Falciani, C., Lelli, B., Lozzi, L., Runci, Y., Pini, A., De Montis, M. G., Tagliamonte, A. and Neri, P. *J. Biol. Chem.* **278**, 46590-46595 (2003).
3. Dal Farra, C., Sarret, P., Navarro, V., Botto, J. M., Mazella, J. and Vincent, J. P. *Int. J. Cancer* **92**, 503-509 (2001).

CCK/MSH Analogs and Derivatives for Imaging and Incorporation in Multimeric Ligands

Rajesh Sankaranarayanan¹, Fang Gao¹, Jatinder S. Josan¹, Heather Handl², Josef Vagner¹, Robert J. Gillies² and Victor J. Hruby¹

¹Department of Chemistry, University of Arizona, Tucson AZ 85721; ²Arizona Cancer Center, Tucson AZ 85724, USA

Introduction

The simultaneous binding of multiple ligands to multiple receptors occurs with an increased affinity as compared to a single receptor-ligand binding event. There have been several efforts in the past to exploit such interactions for potential therapeutic use [1]. We, on our part, are interested in using these multimeric interactions for cancer imaging and therapy. Thus, these multimeric ligands will target specific combinations of cell surface receptors presented by the cancer cells, but not by the normal cells. Here-in, we discuss our recent synthesis of heterodimers of MSH, a peptide hormone that binds human melanocortin receptor (hMC4R), and CCK, a neurotransmitter that binds to the CCK receptor.

Results and Discussion

We have previously synthesized homodimers of the pharmacophoric fragments of α -MSH and found that these dimers bound with higher affinity and co-operativity than their constituent monomers [2]. In the current work, we have synthesized heterodimers consisting of the N-terminal heptapeptide fragment of NDP- α -MSH and the C-terminal hexapeptide fragment of CCK with various linker lengths. The linkers consisted of Pro-Gly dipeptide repeats with or without a flexible 20-atom long PEGO sub-linker, and the linker length ranged from 20 to 148 atoms (Table 1).

Table 1 List of the heterodimers of MSH-CCK synthesized

Ac-SXEH/RW-Linker-XGWXDF-NH ₂ ^a	Linker length	<i>t_R</i> ^c
-[Pro-Gly] ₃ -	18	20.3 ^d
-[Pro-Gly] ₆ -	36	19.2 ^d
-[Pro-Gly] ₉ -	54	18.3 ^d
-[Pro-Gly] ₁₂ -	72	18.0 ^d
-[Pro-Gly] ₁₅ -	90	17.7 ^d
-PEGO- ^b	20	21.7 ^d
-PEGO-PEGO- ^b	40	21.2 ^d
-PEGO-[Pro-Gly] ₃ -PEGO- ^b	58	20.0 ^d
-PEGO-[Pro-Gly] ₆ -PEGO- ^b	76	26.1 ^e
-PEGO-[Pro-Gly] ₁₂ -PEGO- ^b	112	25.4 ^e
-PEGO-[Pro-Gly] ₁₈ -PEGO- ^b	148	24.7 ^e

^a *f* = D-Phe; *X* = Nle; ^b PEGO = -HN(CH₂)₃-(OCH₂CH₂)₃-NHCOCH₂OCH₂CO-; ^c HPLC eluents (*A* = 0.1% TFA in water; *B* = CH₃CN); ^d 20-60% *B* in 50 min; ^e 10-40% *B* in 50 min.

The synthesis was carried out using Rink amide AM resin and was done in a stepwise fashion. Each coupling was monitored either through an “on-resin” Bromophenol blue or a Kaiser test. After the synthesis, the peptides were cleaved off the resin using a cocktail of TFA:TIS:H₂O (92:4:4). The resin was then filtered off and the filtrate concentrated with a gentle nitrogen flow. Peptides were then precipitated with cold diethyl ether. The ether layer was decanted off and the precipitate was dried and redissolved in 10% acetic acid and purified by size exclusion chromatography and preparative HPLC. The final product was characterized by mass spectroscopic methods (MALDI-TOF).

Among the compounds assayed, the 148-atom linker showed a 14-fold increase in affinity at the hMC4R and a 2-fold increase at the CCK-BR. These initial results suggest a simultaneous binding of these heterodimers to the hMC4R and CCK-BR. If statistically validated, this would be the first demonstration of heteromeric binding involving two different cell surface receptors.

We have also considered the other orientation of the ligand in the dimer, where CCK would be presented at the N-terminal. As the C-terminal amide of CCK is very important for its activity, we chose its N-terminal as the anchoring point for the MSH ligand. As a model study, we derivatized the N-terminus of CCK with various carboxylic acids and also further functionalized these –CO₂H groups with primary amines such as benzylamine and compared their activities in an assay against CCK-B receptors. It was found that among the carboxylic acids, the compound N-terminally capped with malonic acid was the most potent and the corresponding benzyl amides showed almost equal activity as their parent carboxylic acids (Table 2).

Table 2 Model Study for the synthesis of differently oriented heterodimers (CCK-linker-MSH)

Ligand	EC ₅₀ (nM)
HO ₂ CCH ₂ CO-Trp-MeNle-Asp-Phe-NH ₂	2.44
HO ₂ CCH ₂ OCH ₂ CO-Trp-MeNle-Asp-Phe-NH ₂	9.74
HO ₂ C(CH ₂ OCH ₂) ₂ CO-Trp-MeNle-Asp-Phe-NH ₂	3.23
PhCH ₂ NHOCCH ₂ CO-Trp-MeNle-Asp-Phe-NH ₂	0.65
PhCH ₂ NHOCCH ₂ OCH ₂ CO-Trp-MeNle-Asp-Phe-NH ₂	13.85

In conclusion, we have synthesized heterodimers of MSH and CCK and the preliminary data show a 9-fold increase in activity at hMC4 receptor and 3-fold increase at the CCK receptor. We have also synthesized several derivatives of CCK(6) and found that the malonic acid derived compound was the most potent compound and also found that further functionalization of the –CO₂H group did not lead to any loss in activity. The latter strategy can be employed to synthesize heterodimers where the position of MSH and CCK ligands has been flipped.

Acknowledgments

The work was supported by grants from USPHS and NCI.

References

1. Macdonald, S. J. F., *et al. Antimicrob. Agents Chemother.* **48**, 4542-4549 (2004).
2. Vagner, J., Handl, H. L., Gillies, R. J. and Hruby, V. J. *Bioorg. Med. Chem. Lett.* **14**, 211-215 (2004).

Cellular Uptake of Pyrrolidine-Based Oxy-Peptide Nucleic Acid

Mizuki Kitamatsu, Rino Matsuzaki and Masahiko Sisido

Department of Bioscience and Biotechnology, Okayama University, Okayama, 700-8530,
 Japan

Introduction

Pyrrolidine-based oxy-peptide nucleic acid (POPNA) is a PNA surrogate that contains ether linkage and pyrrolidine rings in the main and side chain [1-4]. The POPNA can hybridize with complementary DNA and RNA. The melting curves are very sharp. Therefore, POPNA may attract as antisense drugs and biological molecular tools. The two chiral centers on the pyrrolidine ring allow four stereoisomers that are named as *trans*-L-POPNA, *cis*-L-POPNA, *trans*-D-POPNA and *cis*-D-POPNA, after the corresponding stereoisomers of 4-hydroxyprolines that are used as the starting materials. In the four POPNA stereoisomers, *trans*-L-POPNA can form most stable hybrid with RNA.

Our goal was to develop the *trans*-L-POPNA as a biological molecular tool for targeting RNA inside cells. In this work, we investigate the cellular uptake of *trans*-L-POPNA inside cells. To uptake the *trans*-L-POPNA inside cells, the *trans*-L-POPNA was conjugated to Arg₇ known as a cell penetrating peptide [5].

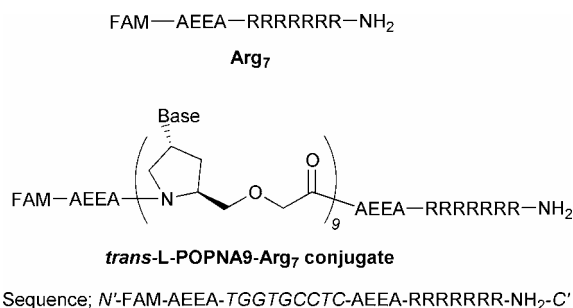


Fig. 1. Chemical structures and sequences of FAM-labeled Arg₇ and FAM-labeled *trans*-L-POPNA-Arg₇ conjugate. The italic indicates the sequence of POPNA. 8-amino-3,6-dioxaoctanoic acid designated as AEEA.

Results and Discussion

The *trans*-L-POPNA-Arg₇ conjugate and Arg₇ were manually synthesized on SAL-PEG resin and labeled at the N-terminus with 5-(and-6)-carboxyfluorescein (FAM) by standard Fmoc chemistry. The sequence of the *trans*-L-POPNA-Arg₇ conjugate is shown in Figure 1. Crude peptides were purified by reverse-phase HPLC over a C₁₈ preparatory column. A Niesen-type PNA-Arg₇ conjugate that is labeled at the N-terminus with FAM was also synthesized to compare with the *trans*-L-POPNA-Arg₇ conjugate. The identity of all compounds was confirmed by MALDI-TOF mass spectroscopy.

CHO cells were cultured in Dulbecco's modified Eagle's medium (DMEM). The medium was supplemented with penicillin/streptomycin (10 µg/ml) and 10% fetal bovine serum (FBS). The cells were incubated at 37°C in 5% CO₂ to give ~70% confluence. The subculture was performed on 35 mm glass-based dishes that coated

with poly(L-lysine) and incubated at 37°C in 5% CO₂ to give 40~60% confluence at the time of cellular uptake. Before the cellular uptake, the culture medium was exchanged. The cells were incubated at 37°C for 2 hrs with the fresh medium containing FAM-labeled *trans*-L-POPNA-Arg₇ conjugate, FAM-labeled Nielsen-type PNA-Arg₇ conjugate or FAM-labeled Arg₇. The final concentration of each peptide in the medium was adjusted at 1.0 µM. The cells were washed three times with PBS. Cells were examined by confocal laser-scanning microscopy without any fixation.

The fluorescence image of the CHO cells with the FAM-labeled *trans*-L-POPNA-Arg₇ conjugate shows in Figure 2. The conjugate was taken up within 2 hrs. The intracellular localization of the FAM-labeled *trans*-L-POPNA-Arg₇ conjugate was almost exclusively confined to vesicular compartments in the cytosol. We also observed uptake of a FAM-labeled Nielsen-type PNA-Arg₇ conjugate inside CHO cells as vesicular compartment at the same condition. This result was reported elsewhere previously [6]. No uptake was observed with the FAM-labeled Arg₇ or the unmodified FAM-labeled *trans*-L-POPNA at the same conditions. These results may be shown that it is important to control the valance of hydrophobicity of the peptide [7]. We are progress in transferring the conjugate into cytosol.

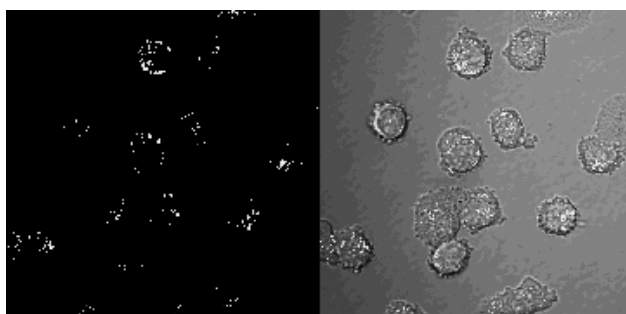


Fig. 2. CHO cells were incubated for 2 hrs with the FAM-labeled *trans*-L-POPNA-Arg₇ conjugate (1.0 µM), washed three times with PBS, and then observed by confocal fluorescence microscopy without any fixation. A left panel shows a fluorescence image and a right panel shows a merger of fluorescence and DIC image.

References

1. Shigeyasu, M., Kuwahara, M., Sisido, M. and Ishikawa, T. *Chem. Lett.* 634-635 (2001).
2. Kitamatsu, M., Shigeyasu, M., Okada, T. and Sisido, M. *Chem. Commun.* 1208-1209 (2004).
3. Kitamatsu, M., *et al.* In *Peptides 2002, Proceedings of the 27th European Peptide Symposium* (Benedetti, E. and Pedone, C., eds.) Edizioni Ziino, Napoli, pp. 532-533 (2003).
4. Kitamatsu, M., *et al.* In *Peptides-Peptide Revolution: Genomics, Proteomics & Therapeutics, Proceedings of the 18th American Peptide Symposium* (Chorev, M. and Sawyer, T. K., eds.) American Peptide Society, Boston, pp. 538-539 (2004).
5. Futaki, S., Suzuki, T., Ohashi, W., Yagami, T., Tanaka, S., Ueda, K. and Sugiura, Y. *J. Biol. Chem.* **276**, 5836-5840 (2001).
6. Koppelhus, U., Awasthi, S. K., Zachar, V., Holst, H. U., Ebbesen, P. and Nielsen, P. E. *Antisense and Nucleic Acid Drug Development* **12**, 51-63 (2002).
7. Fernandez-Carneado, J., Van Gool, M., Martos, V., Castel, S., Prados, P., de Mendoza, J. and Giralt, E. *J. Am. Chem. Soc.* **127**, 869-874 (2005).

Chemical Biology and Biomedical Application of Synthetic Molecules Targeted to Apoptosis Regulated by the Bcl-2 Family

Jun Wang^{1,2}, Dongxiang Liu^{1,2}, Krishna Kumar², Aihua Nie^{1,2}, Yohichi Kumaki³, Pak-Nei Hon³, R. Wayne Fritzsche³, Jing An^{1,2,3}, John C. Reed² and Ziwei Huang^{1,2}

¹Departments of Biochemistry and Chemistry, University of Illinois at Urbana-Champaign, Urbana, IL 61801, USA; ²The Burnham Institute, La Jolla, CA 92037, USA; ³Raylight Chemokine Pharmaceutical Inc., La Jolla, CA 92037, USA

Introduction

Protein-protein or protein-ligand interaction plays a crucial role in a variety of biological processes. Apoptosis is generally regulated by the fine balance and interplay among the members of Bcl-2 family proteins [1] and considered to start from the formation of heterodimerization of anti-apoptotic and pro-apoptotic members [2]. In the 3-D structure of a complex between an anti-apoptotic member Bcl-X_L and the death-promoting region of the Bcl-2 related protein Bak, the Bak peptide is shown to adopt a α helical structure [2]. Based on this structure, we try to modulate the interaction with the target proteins through several different routes.

Results and Discussion

Since helix structure was found in the complex of Bcl-X_L with Bak derived peptide, the first idea that came to our mind was to stabilize this secondary structure unit. To achieve this goal, one intuitive way was to link the side chains of two spatially adjacent residues within a helix through a covalent bond bridge such as lactam [3]. As shown in Table 1, we replaced some positions of original sequence of BakBH3 moiety with Lys and Glu or Asp, resulting in four analogs. As we expected, these Bak BH3 analogs exhibited higher content of helical structure. However, none of them could give high binding affinity to Bcl-X_L (data not shown). This indicates that in addition to the helix structure, there are some other factors that contribute the high affinity of Bak peptide, such as some key residues involved in the hydrophobic and electrostatic interactions.

Another way we tried to improve the binding affinity was to introduce another external moiety, which was previously known to be capable of increasing the affinity. We chose two units from mouse Bad BH3 (140-144, **NLWAA**) and (161-165, **SFKGL**) as AEM (**A**ffinity **E**nhancing **M**otifs). The data listed in Tables 2 and 3 demonstrate the binding activities to Bcl-2 of these core structures were dramatically increased to about 100 times when AEMs were introduced at both N and C termini.

Table 1. Modified peptides derived from Bak BH3 domain with lactam bridges

Peptides	Sequences*	% Helix (in PBS)
Bak BH3	GQVGRQLAIIGDDINR	14
LB1	GQVGRQLA K IGDDINR	35
LB2	GQVGRQL K IIGDDINR	41
LB3	GQVG K QLA E IGDDINR	78
LB4	GQVGRQLAIIGDDIN K	56

*Lactam bridges form between two highlighted residues in each modified peptide.

Table 2. mBad AEMs significantly enhance Bak BH3 peptide binding to Bcl-2 protein

BH3 domain peptides	Sequences	IC ₅₀ (μ M)
Bak BH3 (72-87)	GQVGRQLAIIGDDINR	50.0
N-AEM-Bak BH3-C-AEM	NLWAA GQVGRQLAIIGDDINR SFKGL	0.58
Bak BH3 (67-92)	PSSTMGQVGRQLAIIGDDINRRYDSE	14.95

Table 3. mBad AEMs significantly enhance Bid BH3 peptide binding to Bcl-2 protein

BH3 domain peptides	Sequences	IC ₅₀ (μ M)
Bid BH3 (84-99)	RNIARHLAQVGDSMDR	158.0
N-AEM-Bid BH3-C-AEM	NLWAA RNIARHLAQVGDSMDR SFKGL	1.24
Bid BH3 (79-104)	QEDIIRNIARHLAQVGDSMDRSIPPG	14.08

In addition to investigating various peptide analogs in regulation of Bcl-2 family proteins, traditionally many researchers [4] including us [5] have been doing *de novo* design or screening of small molecules based on computer modeling. Along this direction, we come up with a potent small molecule lead compound HA14-1, which on further studies in vitro is shown to be very effective on cancer cells (shown in Fig. 1), especially when combined with radiotherapy, as shown in Figure 2.

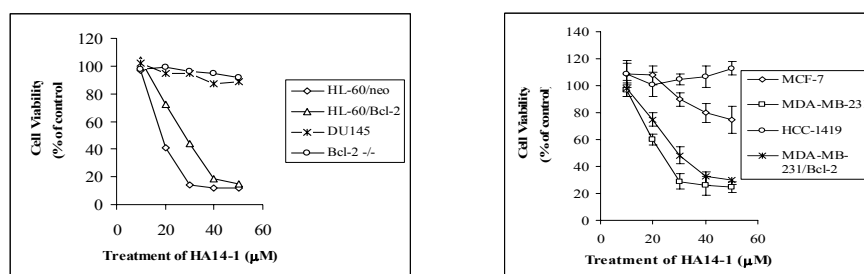


Fig. 1. HA14-1 selectively induces apoptosis of leukemia (left) and breast cancer cells (right) that express Bcl-2.

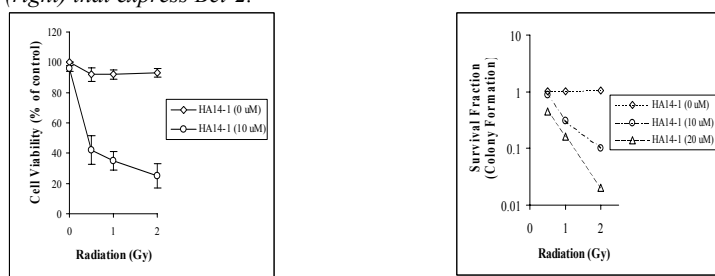


Fig. 2. When used in combination with radiotherapy, HA14-1 shows high potency against prostate cancer cells.

References

1. Cory, S. and Adams, J. M. *Nat. Rev. Cancer* **2**, 647-656 (2002).
2. Sattler, M., Liang, H., Nettesheim, D., *et al. Science* **275**, 983-986 (1997).
3. Yang, B., Liu, D. and Huang, Z. *Bioorg. Med. Chem. Lett.* **14**, 1403-1406 (2004).
4. Oltschdorf, T., Elmore, S. W., Shoemaker, A. R., *et al. Nature* **435**, 677-681 (2005).
5. Wang, J., Liu, D., Zhang, Z., *et al. Proc. Natl. Acad. Sci. USA* **97**, 7124-7129 (2000).

Comparative Immunogenicity of Common and Rare HIV Mutant Peptides

Sylvie E. Blondelle, Rosa Moya, Kim Schroder and Darcy B. Wilson

Torrey Pines Institute for Molecular Studies, San Diego, CA 92121, USA; Mixture Sciences Inc., San Diego CA 92121, USA

Introduction

Immunogenicity studies of human immunodeficiency virus (HIV) have revealed that cytotoxic T-lymphocyte (CTL) responses are directed primarily to the conserved regions of various HIV proteins [1]. However, sequencing studies, summarized in various public databases, reveal that numerous viral mutations are found in these conserved regions. These CTL epitope sequence mutations can be grouped in two categories: a) a few common mutations found in a high percentage of viral isolates and b) numerous different rare mutations found only in single or very few individuals. One way to interpret these two facts is that the common mutants represent immunogenically weaker sequence variations that have most successfully eluded the selective pressure of CTL recognition, and that the rare mutants are more immunogenic.

Results and Discussion

The ability of HIV to escape CTL responses, thereby reducing the number of effectively recognized epitopes, is a major challenge for the development of an epitope-based vaccine. CTL escape mutations typically occur at critical sites within HLA-restricted CTL epitopes where an amino acid substitution may abrogate epitope-HLA binding, reduce T cell receptor recognition, or generate antagonistic CTL responses [2]. Interestingly, while 30-40% HIV isolates that have been sequenced have mutation(s) at a number of CTL epitopes, the majority of these mutations, i.e., "common mutants", represent a few subsets of epitope variants. In contrast, a large number of CTL epitope variants are only observed in isolates from a single or few individuals, i.e., "rare mutants". As exemplified in Table 1 for Gag-derived epitopes, the predominance of the common mutants is independent of the frequency of mutation of an epitope.

Table 1. Frequency of HIV Gag-derived CTL epitope mutations

CTL Epitope	HLA restriction	Frequency of mutants ^a (%)	No. different mutant sequences ^b		Frequency among mutants ^c (%)	
			Common	Rare	Common	Rare
p17 77-85	A2	70	7	46	70	30
p24 19-27	A2	53	2	10	91	9
p24 230-7	A2	71	7	31	83	17
p24 16-24	B7	7	2	10	46	54
p24 131-140	B27	14	4	16	60	40

^aPercent of isolates in the Los Alamos Database HIV Molecular Immunology Database [<http://www.hiv-lanl.gov> - 3] with a mutated CTL epitope sequence. ^bVariants that have five or more entries in the Los Alamos Database are considered as common mutation. ^cPercent of isolates among the mutated sequences corresponding to common or rare variant sequences.

Since Gag CTL epitopes are highly conserved among HIV clades, HIV Gag protein appears to be an excellent target for vaccine design. In particular, about 70% of HIV-infected, HLA-A2⁺ individuals have circulating T-cells that recognize the late-escaping Gag p17 77-85 epitope SLYNTVATL (SL9). In a first study, a common mutant and 18 rare mutants of SL9 were synthesized and assayed using a standard ⁵¹Cr release assay against four SL9-specific CTL clones established from two HIV infected individual (subjects 161j and 115i) [4]. Clonal cross-recognition was observed for the common mutant (peptide 83) and 10 rare mutants. The four most active mutants listed in Fig. 1A were also recognized by PBMC from more than a third of a panel of 19 HIV⁺ HLA-A*0201⁺ patients as determined by ELISpot supporting the cross-recognition of both common and rare mutants.

To investigate if the SL9 variants could induce a greater SL9 specific immune responses in HLA-A2⁺ transgenic mice, mice were immunized with the four variants and the original SL9 peptide and assessed for *ex vivo* SL9 reactivity. The two rare mutant peptides 34 and 107 were more potent in inducing a CTL response than the cognate, original SL9 sequence (Fig. 1B, left panel). The CTLs generated by immunization with peptide 107 also significantly responded to SL9 *in vitro* (Fig. 1B, right panel). These results further suggest that rare variants such as peptide 107 may have high potential as vaccine candidate.

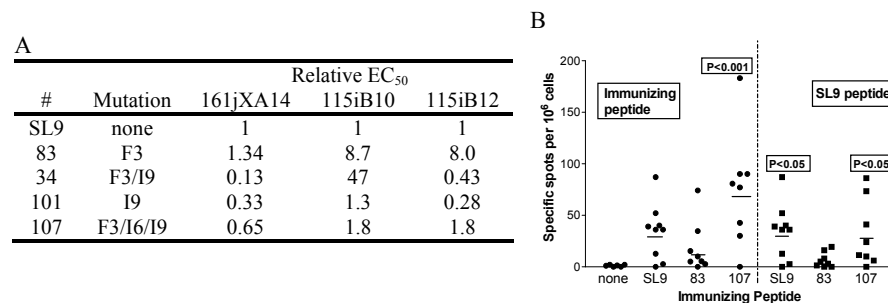


Fig. 1. A. Clonal cross-recognition of SL9 mutants. B. Assessment of *in vivo* peptide immunogenicity. Each data point represents the average ELISpot response above background (i.e., no peptide challenge) for a single animal and the horizontal bar represents the average response for all animals. Control mice immunized solely with the hepatitis B virus core helper peptide are shown as “none”.

Acknowledgments

The work was funded by the NIH (AI 49086 to S.E.B. and DA 015212 to D.B.W.).

References

1. Yusim, K., Kesmir, C., Gaschen, B., Addo, M. M., Altfeld, M., Brunak, S., Chigaev, A., Detours, V., Korber, B. T. J. *J. Virol.* **76**, 8757-8768 (2002).
2. McMichael, A. J. and Rowland-Jones, S. L. *Nature* **410**, 980-987 (2001).
3. Korber, B., Walker, B., Brander, C., Koup, R., Moore, J., Haynes, B., Meyers, G. *HIV Molecular Immunology Database. Los Alamos National Laboratory: Theoretical Biology and Biophysics*, Los Alamos, NM (1996).
4. Boggiano, C., Moya, R., Pinilla, C., Bihl, F., Brander, C., Sidney, J., Sette, A., Blondelle, S. E. *Eur. J. Immunol.* **35**, 1428-1437(2005).

Conformational Studies of Agouti-Related Protein (AGRP)- Melanocortin Chimeric Peptides

**Andrzej Wilczynski¹, Krista R. Wilson¹, Joseph W. Scott¹, Arthur S.
Edison² and Carrie Haskell-Luevano¹**

¹*Department of Medicinal Chemistry; ²Department of Biochemistry and Molecular Biology
University of Florida, Gainesville, FL 32610, USA*

Introduction

The melanocortin system consists of five G-protein coupled receptors (MC1R-MC5R), endogenous agonists (α -, β -, γ -melanocyte stimulating hormones) and endogenous antagonists – agouti protein and agouti-related protein (AGRP). Melanocortin agonists contain a core His-Phe-Arg-Trp tetrapeptide sequence that has been hypothesized to be important for melanocortin receptor molecular recognition and stimulation. The endogenous melanocortin receptor antagonist AGRP has a core Arg-Phe-Phe tripeptide sequence that has been demonstrated to be important for AGRP to bind and antagonize melanocortin receptors. It has been postulated that the antagonist AGRP Arg-Phe-Phe amino acids may be mimicking the agonist Phe-Arg-Trp residues.

Our previous studies identified a melanocortin-AGRP chimeric peptide Tyr-c[β -Asp-His-DPhe-Arg-Trp-Asn-Ala-Phe-Dpr]-Tyr possessing subnanomolar agonist activity at MC1 and MC3-5 receptors [1]. Herein we present the structure-activity relationship of this novel template that was characterized using amino acids previously reported in other melanocortin agonist templates. Six peptides were selected for ¹H NMR and computer assisted molecular modeling structural analysis (Fig. 1).

- 1.) Tyr-c[β -Asp-His-DPhe-Arg-Trp-Asn-Ala-Phe-Dpr]-Tyr-NH₂
- 2.) Tyr-c[β -Asp-Ala-DPhe-Arg-Trp-Asn-Ala-Phe-Dpr]-Tyr-NH₂
- 3.) Tyr-c[β -Asp-Pro-DPhe-Arg-Trp-Asn-Ala-Phe-Dpr]-Tyr-NH₂
- 4.) Tyr-c[β -Asp-Phe-DPhe-Arg-Trp-Asn-Ala-Phe-Dpr]-Tyr-NH₂
- 5.) Tyr-c[β -Asp-His-DNal(2')-Arg-Trp-Asn-Ala-Phe-Dpr]-Tyr-NH₂
- 6.) Tyr-c[β -Asp-His-DNal(1')-Arg-Trp-Asn-Ala-Phe-Dpr]-Tyr-NH₂

Fig. 1. Sequences of peptides used in this study (Dpr-diaminopropionic acid).

Results and Discussion

In attempts to correlate the melanocortin receptor functional studies with peptide structure, we performed 2D ¹H NMR and CAMM experiments. For all the peptides examined by NMR in this study, a reverse turn conformation within the putative His-DPhe-Arg-Trp message sequence was found. Our results are consistent with previous studies that identified the presence of a reverse turn in this His-DPhe-Arg-Trp domain of various melanocortin agonist ligands [2,3].

Agonist peptides examined in these studies are generally characterized to possess a β -turn involving the Trp and Asn residues (Fig. 2). Decreased potency of peptide 2 at the MC1R and MC3R may suggest that stacking interactions between side chains of His and DPhe observed in peptide 1 may be important for the agonist potency at these receptors.

Table 1. Functional activity of the AGRP-melanocortin chimeric peptides (PA – partial agonist)

Peptide	EC ₅₀ (nM)			
	MC1R	MC3R	MC4R	MC5R
1	0.22±0.14	0.97±0.49	0.13±0.04	0.37±0.26
2	7.20±2.89	29.0±7.5	0.36±0.07	0.46±0.18
3	22.1±18	PA, pA ₂ = 7.2±0.2	0.63±0.20	7.16±0.22
4	6.04±1.36	PA, pA ₂ = 7.2±0.6	0.64±0.17	3.15±1.38
5	5.56±3.40	pA ₂ =8.2±0.2	PA, pA ₂ =9.1±0.1	22.3±10.6
6	9.20±0.97	320±250	0.57±0.08	3.13±1.89

Another interesting structural feature of peptide 1 is the positioning of the side chain of the Arg residue which is directed in an opposite orientation from the D₁Phe and Trp residues (Fig. 2A). This side chain orientation may suggest that peptide 1 possesses the amphiphilic characteristic similar to structures observed in other melanocortin ligands.

The common feature of peptides possessing partial agonist or antagonist melanocortin receptor pharmacology is a reverse turn including the Arg and Trp residues (Fig. 2B). Additionally, these peptides are generally more flexible, as compared with the full agonist peptides discussed above.

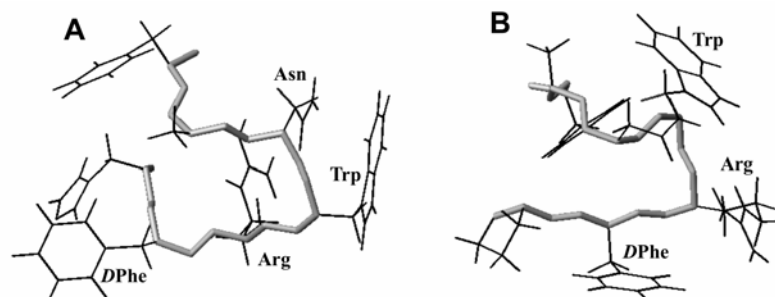


Fig. 2. Representative structures of peptide 1 (A) and peptide 3 (B). Both Tyr residues, Asp and Dpr are omitted.

Acknowledgments

The work was funded by NIH Grants DK57080 and DK64250 and American Heart Association Postdoctoral Fellowship (AW).

References

1. Wilczynski, A., *et al.* *J. Med. Chem.* **47**, 2194-2207 (2004).
2. Silva Elipse, V. M., *et al.* *Biopolymers* **68**, 512-527 (2003).
3. Ying, J., *et al.* *Biopolymers* **71**, 696-716 (2003).

C-Terminal Ether Analogs of NN703

Kjeld Madsen, Peter Andersen, Michael Ankersen, Bernd Peschke,
 Birgit Sehested and Jan Soerensen

Novo Nordisk A/S, DK-2760 Maaloev, Denmark

Introduction

Starting with the Growth Hormone Secretagogue **NN703**, we wanted to explore the *N*- and *C*-terminal region of this type of compounds. A comparison of **NN703** [1] and Ipamorelin [2] suggested that an extension of the amide group at the *C*-terminus could be beneficial for the efficacy of the compounds (Fig. 1). On the other hand, we did not want to increase the polarity of the compounds in order to maintain the good pharmacokinetic properties we had found with **NN703**. Therefore, we decided to incorporate either an ether or an alcohol as amide-mimetic at the *C*-terminus of our analogs.

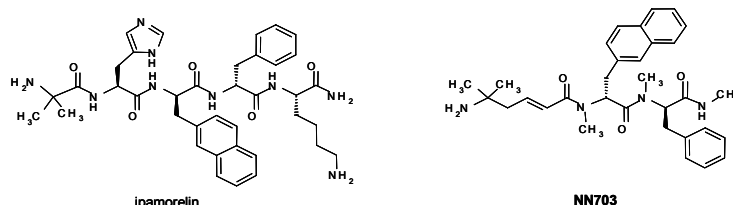


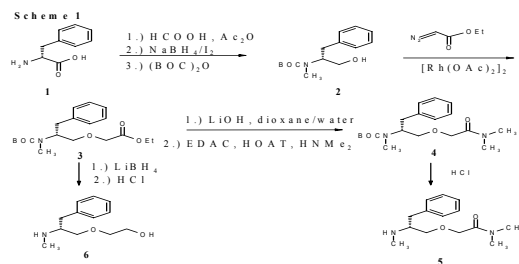
Fig. 1.

Chemistry

The ether-analogs were prepared from *N*-methylphenylalaninol [3], which was easily synthesized from phenylalanine by simultaneous alkylation and reduction, employing first a mixture of acetic acid anhydride and formic acid, followed by a reduction with sodium borohydride/iodine [4]. This alcohol was reacted with ethyl diazoacetate under the catalysis of rhodium acetate [5]. After protection of the amine-functionality, the ester was further elaborated to the dimethyl amide and the alcohol by standard chemistry. Both dimethyl amide and alcohol were chosen in order to keep the polarity of the compound as low as possible. The building blocks were used for the synthesis of the final Growth Hormone secretagogues together

with the appropriate amino acids [1] and applying HOAT [6] as coupling reagents. The BOC-protective groups were removed with HCl.

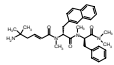
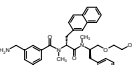
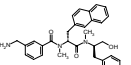
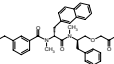
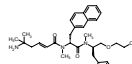
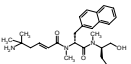
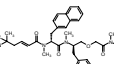
Pituitary cells were isolated from wista rats (150g) and grown for 3 days before stimulating with the compounds of interest. Compounds in different concentrations were added to



Scheme 1

the cells and after 15 min the supernatant was removed and the content of growth hormone was determined using an ELISA.

Table 1

EC ₅₀ E _{max} *		EC ₅₀ E _{max} *		EC ₅₀ E _{max} *	
Entry	(nM)	Entry	(nM)	Entry	(nM)
Ipamorelin	1.3 85	NN703	2.5 110		
7 	7 100	10 	100 105	12 	265 75
8 	55 80	11 	16 105	13 	36 120
9 	16 115				

* % of GHRP-6

Results and Discussion

As it can be seen from Table 1, the order of potency of the test compounds in the rat pituitary cell assay is dependent on the nature of the C-terminus. The dimethylamide **7** showed almost the same potency as the lead-compound NN703. However, when the alcohols **12** and **13** were tested, only very modest potency was observed. On the other hand, upon extension by an ether linker the dimethylamides **8** and **9** had only slightly changed potency relative to the alcohols **10** and **11**. The potency of none of the extended compounds **8**, **9**, **10**, and **11** matched the potency found for either ipamorelin or NN703. Therefore, the initial hypothesis that extending the C-terminal amide by a length of one amino acid could be beneficial for the potency was not supported. This indicates that both the secondary amide and the lysine side-chain in ipamorelin could not be mimicked by an ether bond and placement of the C-terminus amide in a corresponding position.

In conclusion, an extension of the C-terminus of analogs of NN703 by an ether linkage did not improve but rather decreased the potency in the rat pituitary cell assay slightly. However, in contrast to the effect on potency of the moieties introduced in compounds **7**, **12**, and **13**, hydroxy moieties can surprisingly mimic a dimethylamide group in the C-terminus of extended analogs.

References

1. Hansen, T. K., Ankersen, M., Hansen, B. S., Raun, K., Nielsen, K. K., Lau, J., Peschke, B., Lundt, B. F., Thøgersen, H., Johansen, N. L., Madsen, K. and Andersen, P. H. *J. Med. Chem.* **41**, 3705-3714 (1998).
2. Raun, K., Hansen, B. S., Johansen, N. L., Thøgersen, H., Madsen, K., Ankersen, M. and Andersen, P. H. *Eur. J. Endocrinol.* **139**, 552-561 (1998).
3. Karim, A., Mortreux, A., Petit, F., Buono, G., Peiffer, G. and Siv, C. *J. Organomet. Chem.* **317**, 93-107 (1986).
4. McKennon, M. J., Meyers, A. I., Drauz, K. and Schwarm, M. *J. Org. Chem.* **58**, 3568-3571 (1993).
5. Hlaváček, J. and Kral, V. *Collect. Czech. Chem. Commun.* **57**, 525-530 (1992).
6. Carpino, L. A. *J. Am. Chem.* **115**, 4397-4398 (1993).

Cyclic Statine-based Peptides as Inhibitors of β -Secretase

Alessandra Barazza¹, Marion Götz¹, Christian Renner¹,
Michael Willem² and Luis Moroder¹

¹Max-Planck-Institut für Biochemie, 82152 Martinsried; ²Adolf-Butenandt-Institut,
Ludwig-Maximilians Universität, 80336 München, Germany

Introduction

Extracellular amyloid β -peptide (A β) deposition into plaques is one of the characteristic histopathological lesions found in brains of Alzheimer's disease patients. The 40- to 42 amino acid peptide A β is generated by the successive proteolysis of the integral membrane protein APP, the amyloid precursor protein, by γ - and β -secretase (BACE) [1]. The 1.9Å crystal structure of the catalytic domain of BACE complexed with the inhibitor OM99-2 revealed the characteristic architecture of the active-site cleft of aspartic proteases of the pepsin family [2].

Statine and phenylstatine have been used as a transition-state dipeptide isostere to develop β -secretase, renin, cathepsin D, and other aspartic protease inhibitors. We used them here as a core to explore β -secretase structure-activity relationships.

Results and Discussion

In order to determine the minimum structure having inhibitory activity toward β -secretase, statine-containing peptide ladders were designed by the removal of amino acids from the fully active octapeptide (data not shown). On the C-terminus, peptides lacking the P3 position showed no inhibitory activity, while removal of P3' residue had mild influence on the activity. These experiments indicated that the minimal sequence retaining activity is P3-P2' and that interactions at the C-terminus were more significant than those at the N-terminus. Moreover, it demonstrated that the lateral chain of the Asp in position P3' could be effectively used for the construction of macrocycles in which the side chain of this Asp was covalently linked to a second Asp at position P2 through a linear aliphatic or aromatic linker.

Computer modeling based on crystal structures of the enzyme-peptide inhibitor complexes suggested that the enzyme can accommodate cyclized tri-, tetra- and pentapeptides analogs corresponding to the minimized linear sequences of peptidomimetic inhibitors. Inhibitors following this design have the advantage of being restrained in a β -extended conformation (Fig. 1) and therefore preorganized for binding to the protease with reduced entropic cost.

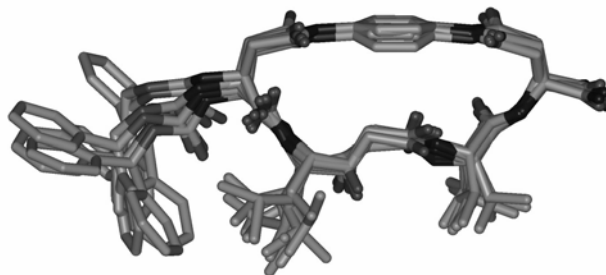


Fig. 1. Superimposition of the 10 lowest-energy structures of compound 5 from molecular modelling experiments.

Replacement of the amino acid in position P3 with different hydrophobic lateral chains, mimicking the Ile moiety, resulted in complete loss of inhibitory activity (data not shown), indicating the necessity of a stereochemical orientation of the residue. Nevertheless, comparison between compounds **1** and **4** with the corresponding cyclic compound **5** (Table 1) demonstrated the potentials of a macrocyclic ring closure.

Table 1. Inhibitory activities, expressed as K_i (μM)

	R^2	$R^1\text{-Asp-X-Val-Asp-NH}_2$ R^2	$R^1\text{-Asp-X-Val-Asp-NH}_2$ $\text{---}R^2\text{---}$
X : Sta R ¹ : Z	H	>1000	(1) -
		>1000	(2) >1000 (3)
		>1000	(4) 44 ± 16 (5)
X : (Phe)Sta R ¹ : Ac-Ile	H	5.4 ± 1.1	(6) -
		135 ± 12	(7) 10.5 ± 1.5 (8)
		71 ± 8	(9) 12.5 ± 1.7 (10)
		16 ± 1.4	(11) 10.2 ± 1.6 (12)
		5.9 ± 0.6	(13) 2.8 ± 0.6 (14)
		7.5 ± 0.8	(15) not soluble (16)

To confirm these findings and in order to improve inhibition, the preferred Ile in position P3 was reintroduced and cyclization reactions were performed with aromatic and aliphatic linkers, as reported in Table 1. Although activities of the open chain compounds **7**, **9**, and **11** were not improved with respect to the pentapeptide **6** by the linker, their cyclization resulted in macrocyclic peptides with a 13-, 5.6-, and 1.5-fold increase in inhibition, respectively (peptides **8**, **10**, and **12**). The use of an aromatic, flexible linker to partially constrain peptide **6** resulted in a 2-fold increase in inhibitory activity (peptide **14**). Unfortunately the cyclic peptide **16**, incorporating the N-terminal Ile and the extended conformation frozen in a rigid structure, was insoluble in the assay buffer. Nevertheless, these findings confirm the validity of the concept and suggest that an improvement in solubility of compound **16** could lead to submicromolar inhibitors. These constrained macrocycle templates are further used to independently optimize inhibitor components.

References

- Haass, C. *EMBO J.* **23**, 483-488 (2004).
- Hong, L., Koelsch, G., Lin, X. L., Wu, S. L., Terzyan, S., Ghosh, A. Z., Zhang, X. C. and Tang, J. *Science* **290**, 150-153 (2000).

Design and Structure Determination of a Selenium Labeled Antimicrobial Peptide

Xiaomei Zhou^{1,2}, Phat L. Tran^{2,3}, Joe Fralick³ and Ted W. Reid^{1,2,3}

¹Department of Chemistry and Biochemistry, Texas Tech University, Lubbock, TX 79401;

²Department of Ophthalmology and visual sciences, ³Department of Microbiology and Immunology, Texas Tech University Health Science, TX 79430, USA

Introduction

Molecular interactions between pathogens and host-cells are necessary for infection [1]. The capsular F1 antigen from *Yersinia pestis* plays the role of targeting the site of infection on a human cell [2]. To design a compound that can selectively bind to the F1 antigen and then kill the bacteria is a feasible way to protect human cells from infection. In our laboratory we used phage expression libraries to successfully screen for a peptide that can specifically bind to the F1 antigen of *Y. pestis*. Selenocyanate coupled to the peptide (1) was able to kill nearly 90% *Escherichia coli*, which expressed the F1 antigen, in 15 minutes at micromolar concentrations, by the selenium catalyzed production of superoxide radicals on the bacterial cell surface. However, the peptide did not kill *E. coli* that did not express the F1 antigen. In order to elucidate the structure of this peptide, a conformation study using NMR was carried out.

Ser-Ser-Leu-Thr-Leu-Ala-Pro-Phe-Ser-Trp-Ser-Leu-NH₂ (1)

Results and Discussion

Sparky was obtained from UCSF; CYANA from L.A.SYSTEMS Inc.; and Chimera from <http://www.cgl.ucsf.edu/chimera>. The *Y. pestis* F1 antigen expressed pYPR-1b *E. coli* strain was grown in LB medium (10 g/L Bacto-Tryptone, 5 g/L yeast extract, 5 g/L NaCl) supplemented with carbenicillin (100µg/ml). All spectra were recorded at 500MHz on a Varian spectrometer at room temperature. Water Suppression was achieved by Water suppression Enhanced through T1 effects (WET). The Peak assignments were achieved using Sparky. The peak volumes determined using

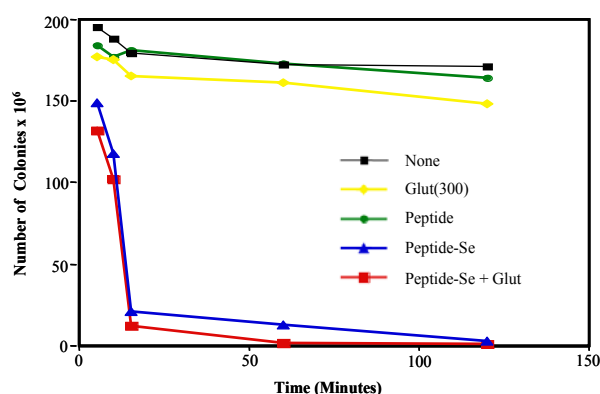
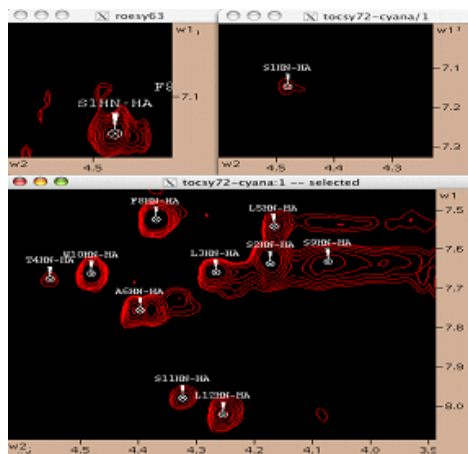


Fig. 1. Survival of *E. coli* expressing the F1 antigen in the presence and absence of 10µM peptide 8 +/- Se.



SPARKY were converted into distance constraints using macro CALIBA from CYANA. Then, on the basis of these distance constraints and $^3\text{JHN-C}_\alpha\text{H}$ coupling constants from 1-D proton NMR, the systematic analysis of the local conformation around the C_α atom of each residue was performed by the macro GRIDSEARCH. Finally, the structures were calculated by the macro ANNEAL using torsion angle dynamics to obtain a PDB file. To visualize the PDB file, the program Chimera was used.

Peptide (1) coupled with seleno-cyanate was able to kill nearly 90% *E. coli* (Fig. 1), which expressed the F1 antigen. The fingerprint region (7.0-8.5 vs. 4.0-5.0 ppm) of 2-D NMR was assigned (Fig. 2) using Sparky. Based on the NMR spectra, peptide (1) has restricted structures rather than a random coil. After structure annealing and energy minimization, 40 conformers were obtained. Twenty conformers were

found to have strong aromatic interactions. Figure 3 shows a simulation of one structure.

The F1 antigen is a membrane protein, which contains lots of hydrophobic components. Therefore, when the peptide containing Phe-X-Trp cage binds to F1 antigen, it results in a decrease in entropy (ΔS). Thus, the Phe-X-Trp cage probably is important for peptide recognition of the membrane protein F1 Antigen [3,4].

References

1. Thanassi, D. G., Säulino, E. T. and Hultgren, S. J. *Curr. Opin. Microbiol.* **1**, 223-231 (1998).
2. Zavialov, V. A., Berglund, J., Pudney, F. A., *et al.* *Cell* **113**, 587-596 (2003).
3. Hunter, C. A., Lawson, K. R., Perkins, J., *et al.* *J. Chem. Soc-Perkin Trans.* **2**, 651-669 (2001).
4. Meyer, E. A., Castellano, R. K. and Diederich, F. *Angew. Chem. Int. Ed.* **42**, 1210-1250 (2003).

Design and Synthesis of Encoded One-bead One-compound Peptidomimetic Libraries for Identification of $\alpha_4\beta_1$ Integrin Ligands

Ruiwu Liu, Li Peng, Jan Marik and Kit S. Lam

Division of Hematology/Oncology, Department of Internal Medicine, UC Davis Cancer Center, University of California Davis, 4501 X Street, Sacramento, California 95817, USA

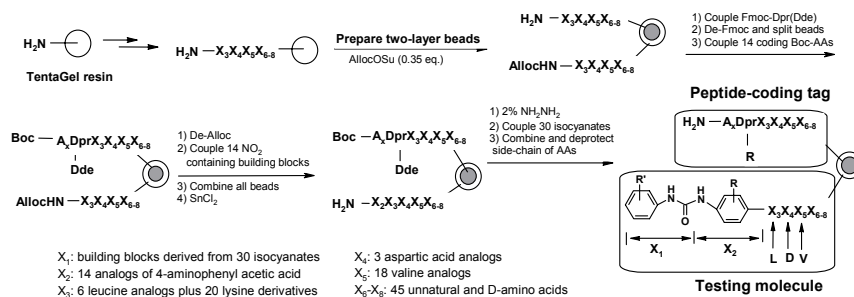
Introduction

$\alpha_4\beta_1$ integrin is a leukocyte cell surface receptor that participates in a wide variety of both cell-cell and cell-matrix adhesive interactions. $\alpha_4\beta_1$ integrin is implicated in metastasis, regulates leukocyte trafficking, and plays a critical role in inflammation and autoimmune diseases. $\alpha_4\beta_1$ integrin is an excellent therapeutic and imaging target for lymphoid cancer [1]. Potent and specific ligands can be developed into useful radiolabeled agents for treatment and/or diagnosis of lymphoid cancer. Fibronectin (FN) is a natural ligand for $\alpha_4\beta_1$ integrin. $\alpha_4\beta_1$ integrin recognizes the sequence ILDV in FN. In the past, we have identified LDI [1] and Nle-DI/V/Nle (Nle: norleucine) [2] as binding motifs of $\alpha_4\beta_1$ integrin through one-bead one-compound (OBOC) combinatorial peptide library method [3]. BIO-1211 is a known potent peptidomimetic ligand with a 4-((N'-2-methylphenyl)ureido)-phenylacetyl *N*-terminal cap on LDVP sequence [4]. Using all the structure-activity information and combining rational drug design strategy with a combinatorial OBOC approach, we have designed various peptide-encoded OBOC peptidomimetic libraries containing many unnatural amino acids to elucidate $\alpha_4\beta_1$ integrin ligands with increased affinity, specificity, and proteolysis stability.

Results and Discussion

To save time for the synthesis and screening of OBOC library but get maximal SAR information, the initial encoded OBOC library L-1 is designed to consist of three sub-libraries: 6mer, 7mer and 8mer with billions permutations (Scheme 1).

The library L-1 is screened with Jurkat cell (expresses $\alpha_4\beta_1$ integrin) using on-bead cell binding assay. A newly developed competition method is used to eliminate ligands with lower affinity by incorporating BIO-1211 as a competitive ligand in solution. The positive beads with a fully covered monolayer live cells are decoded with microsequencing [5]. The sequence results show that 4-[N-(2-(methylphenyl)ureido)] group is the optimal building block for X_1 , X_2 positions



Scheme 1. Synthetic approach of the peptide-encoded OBOC peptidomimetic library L-1.

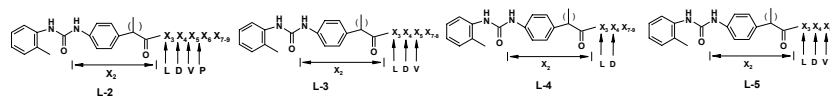


Fig.1 Chemical structure of four focused OBOC peptidomimetic libraries.

could be either 4-aminophenyl acetic acid or 2-methyl-4-aminophenyl acetic acid. Interestingly, two ligands have the lysine derivative K_{38} [the ϵ -amine of lysine side chain is acylated with trans-3-(3-pyridyl)acrylic acid] at X_3 position (L in BIO-1211), and 14 out of 23 ligands had Aad (α -amino hexanedioic acid) at X_4 position (D in BIO-1211). The other positions in the C terminal do not show significant preference. Since it is impossible and impractical to screen beads to cover all the permutations in library L-1, a focused library approach was employed to eliminate the non-ligands and/or low binding ligands. Based upon the common motif/building blocks of the hits from the initial library results, four focused OBOC peptidomimetic libraries (Fig. 1) have been designed by fixing or limiting the number of amino acids required in the essential position.

The focused libraries have been screened under a higher stringency to identify ligands that have much higher affinity than those identified from the primary screening. Some of the identified ligands are shown in Table 1. All ligands prefer Aad at position X_4 , and 8 out of 10 ligands require K_{38} at position X_3 , which are different from BIO-1211. Among them, 2A is the most potent ligand ($IC_{50}=2$ pM) which is about 150-fold potent than BIO-1211, and specifically binds to only $\alpha_4\beta_1$ integrin expressed cancer cell lines. These ligands are particularly useful for imaging a tumor and for treating cancer, inflammatory diseases, and autoimmune diseases.

Table 1. Selected ligands identified from the focused libraries

No.	X_3	X_4	X_5	X_6	IC_{50} (nM)
1A	K_{38}	Aad	D-Phe		0.022
2A	K_{38}	Aad	Ach		0.002
3A	K_{38}	Aad	Acpc	D-Asp	0.5
4A	K_{38}	Aad	D-Phe	D-Asp	0.4
6A	HoPhe	Aad	D-Nal-2	D-Glu	9.4
7A	K_{38}	Aad	D-Phe	D-3-Pal	4.0
8A	Nle	Aad	Cha	D-Glu	0.75
14A	K_{38}	Aad	Phe		0.2
15A	K_{38}	Aad	Val		0.2
16A	K_{38}	Aad	D-Val		0.2
BIO-1211					0.3

HoPhe, homophenylalanine; Ach, 1-amino-1-cyclohexane carboxylic acid; Acpc, 1-amino cyclopropane-1-carboxylic acid; D-Nal-2, D-3-(2-Naphthyl)alanine; D-3-Pal, D-3-(3-pyridyl) alanine.

Acknowledgments

The work was funded by NIH R33CA-86364 and NIH R33CA-99136.

References

1. Park, S. I., et al., *Lett. Peptide. Sci.* **8**, 171-178 (2002).
2. Mikawa, M., et al. *Mol. Cancer Ther.* **3**, 1329-1334 (2004).
3. Lam, K. S., et al. *Nature* **354**, 82-84 (1991).
4. Lin, K., et al. *J. Med. Chem.* **42**, 920-934 (1999).
5. Liu, R., Marik, J. and Lam, K. S. *J. Am. Chem. Soc.* **124**, 7678-7680 (2002).

Design and Synthesis of Histone Deacetylase Inhibitors by Side Chain Modification of 2-Amino-(n-1)-alkenoic Acids

Mohammed P. I. Bhuiyan, Tamaki Kato and Norikazu Nishino

Graduate School of Life Science and Systems Engineering, Kyushu Institute of Technology,
 Kitakyushu 808-0196, Japan

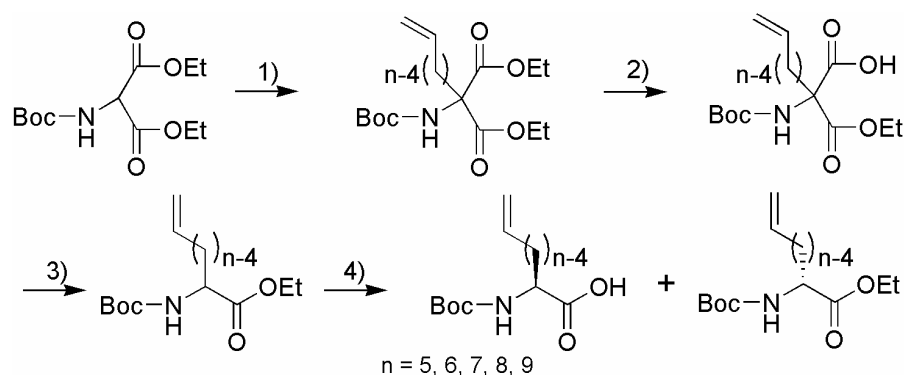
Introduction

Enantiomerically pure aliphatic amino acids having easily modifiable functional groups at the end of the side chain on α -carbon atom are highly interesting synthetic targets as the terminal functional groups can be changed to the required groups which provide a series of non-potentiogenic amino acids [1]. As the double bond is a masked functional group and is stable to most acidic and basic reaction conditions, the classical reactivity of alkenes towards addition, oxidation, etc., can be used for the side chain modification. So it is worthy to synthesize α -amino acids containing side chains with a terminal double bond, 2-amino-(n-1)-alkenoic acids (Aens). As a precursor, it can be easily converted to various amino acids having different side chain functionality. In fact several methods are available for the synthesis of specific ω -unsaturated α -amino acids [2,3]. Here we report a convenient method, for the synthesis of Boc-2-amino-(n-1)-alkenoic acids (Boc-Aen-OH, $n = 5-9$) from commercially available reagents, diethyl Boc-aminomalonate and ω -bromoalkenes.

We also explored the possibility of their use in the synthesis of some new zinc ligands for chlamydocin type cyclic tetrapeptide scaffold in order to develop histone deacetylase inhibitors as anti-cancer agents with optimized pharmacokinetic properties.

Results and Discussion

The synthetic strategy for the preparation of Aens starting from diethyl Boc-aminomalonate with ω -bromoalkenes is illustrated in Figure 1.



Reagents and conditions: (1) (i) Na, Anhy EtOH, reflux, 30 min; (ii) $\text{Br}(\text{CH}_2)_{n-4}\text{-CH=CH}_2$, reflux, 4 h, 85-90%; (2) NaOH aq, EtOH, 0°C, 4 h, 80-85%; (3) toluene, reflux, 4 h, >96%; (4) subtilisin Carlsberg, $\text{H}_2\text{O}/\text{DMF}$ (3/1), >90%.

Fig. 1. Synthesis of 2-amino-(n-1)-alkenoic acid.

The generality of this method lies in the fact that Aens can easily be synthesized with side chain lengths ranging from three to seven carbon atoms starting from *N*-protected diethyl Boc-aminomalonate. One equivalent of an ω -bromoalkene was coupled with diethyl Boc-aminomalonate preceded by the treatment of sodium ethoxide in ethanol. One of the ethyl ester groups of the adduct is hydrolyzed by one equivalent of 1 M sodium hydroxide at low temperature (0-5°C). The oily monoacid monoester after work-up is then subjected to the decarboxylation by refluxing in toluene. After evaporation of toluene the resulting oily Boc-DL-Aen-OEt was purified by silica gel column chromatography. Finally Boc-DL-Aen-OEt was subjected to the action of subtilisin Carlsberg from *Bacillus licheniformis* (Sigma) in a mixture of dimethylformamide and water (1/3, v/v). Boc-L-Aen-OH was isolated as colorless oil.

The fully protected amino alkenoic acids were converted into diols by treatment with MC OsO₄. The olefin was also conveniently changed to the epoxide by reacting with *m*CPBA. As a demonstration of the usefulness of this method of Aen synthesis, the 2-amino-9, 10-epoxy-8-oxodecanoic acid (Aoe) of chlamydocin [4] was replaced by Aen and the terminal double bond of the side chain was equipped with diol and epoxide. They were examined and found to have weak inhibitory activity towards histone deacetylases (Fig. 2).

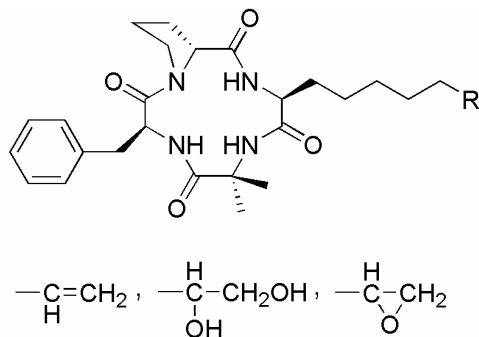


Fig. 2. Chlamydocin analog as HDAC inhibitors.

References

1. Watanabe, L. A., *et al. Tetrahedron Lett.* **45**, 491-494 (2004).
2. Gu, X., *et al. Tetrahedron* **60**, 8233-8243 (2004).
3. Douat, C., *et al. Tetrahedron Lett.* **42**, 3319-3321 (2001).
4. Closse, A and Huguenin, R. *Helv. Chim. Acta* **57**, 533-545(1974) .

Design of a Library of Histone Deacetylase Inhibitors Based on Chlamydocin

Norikazu Nishino¹, Mohammed P. I. Bhuiyan¹, Yoshinori Hirashima¹,
Louis A. Watanabe¹, Priti Soni¹, Tamaki Kato¹, Tomonori Nishino² and
Minoru Yoshida²

¹Graduate School of Life Science and Systems Engineering, Kyushu Institute of Technology,
Kitakyushu, 808-0196, Japan; ²RIKEN, Wako, 351-0198, Japan

Introduction

Post-translational modification of proteins by acetylation and deacetylation of ϵ -amino groups of lysine residues by histone acetyl transferase (HAT) and histone deacetylase (HDAC) enzymes is involved in chromatin remodeling and plays a crucial role in gene expression. Modification of the level of histone acetylation and its consequences have received enormous interest in recent years and increasing evidence supports their importance for basic cellular functions such as DNA replication, transcription, and apoptosis. Deregulation of HAT and HDAC has been implicated in the formation and development of certain human cancers by changing the expression pattern of various genes. A number of natural and synthetic HDAC inhibitors have been reported, and in recent years the importance of HDAC inhibitors has increased due to their decay against many malignant diseases [1].

Chlamydocin was originally isolated from the fungus *D. chlamydosporia*, and has been shown to exhibit potent anticancer activity *in vitro*. Chlamydocin belongs to a small family of hydrophobic cyclic tetrapeptides containing the unusual amino acid, 2-amino-8-oxo-9,10-epoxy decanoic acid (Aoe), which is essential for their biological activity [2]. In this work, based on Chlamydocin cyclic tetrapeptide framework, we designed and synthesized a focused library to find out specific inhibitors toward HDAC, which may relate to various diseases.

Results and Discussion

Our aim is to synthesize potent inhibitors of HDACs based on the natural product chlamydocin. For this, we synthesized some cyclic tetrapeptides containing zinc ligands in the side chain as HDAC inhibitor (Fig. 1). For this deprotected tripeptide, H-Aib-L-Phe-D-Pro-OrBu was coupled with Boc-L-Axx-OH (Axx: Asu (2-amino suberic acid), Ab7 (2-amino-7-bromoheptanoic acid), Ae9 (2-amino-9-alkenoic acid)) to give Boc-L-Axx-Aib-L-Phe-D-Pro-OrBu.

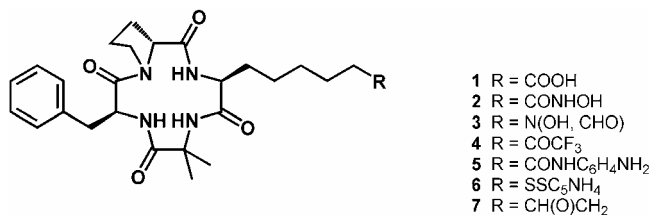


Fig. 1. Structures of the synthesized HDAC inhibitors.

The C-terminal and N-terminal protections of the tetrapeptide were removed by treatment with trifluoroacetic acid (TFA) and the resulted linear peptide was cyclized in DMF under high dilution condition using HATU as a coupling reagent to give *cyclo*(-L-Axx-Aib-L-Phe-D-Pro-). Next, the side chain of each cyclic tetrapeptides was modified.

The results of HDAC inhibitory activity and p21 promoter assay of the compounds are shown in Table 1. The inhibitory activity *in vitro* of compound **6** was very weak. But, after reduction of the disulfide bond using dithiothreitol, the HDAC inhibitory activity showed excellent activity (data not shown). On the other hand, compound **2** and **3** have high inhibitory activity. However, the inhibitory activity of compound **3** is lower than compound **2**. In an early report on retrohydroxamate inhibitor for thermolysin, the inhibitory activity was also reduced about one tenth of the corresponding hydroxamic acid [3]. The results indicate that these cyclic tetrapeptides can lead to potent inhibitors of HDAC and anticancer agents.

Table 1. HDAC inhibitory activity ^a

Compound	IC ₅₀ (μM)			p21 promoter assay
	HDAC 1	HDAC 4	HDAC 6	EC ₁₀₀₀ (μM)
1	5.15	3.30	>100	34.0
2	8.73×10 ⁻²	2.00×10 ⁻²	16.3×10 ⁻²	1.42×10 ⁻²
3	13.9×10 ⁻²	3.30×10 ⁻²	38.8×10 ⁻²	2.72×10 ⁻²
4	3.52	2.59	>100	30.1
5	6.85	39.6	>100	11.3
6	>100	>100	>100	4.49×10 ⁻²
7	4.69	4.05	>100	22.7

^a HDAC inhibitory activity was evaluated using HDACs prepared from 293T cells.

References

1. Yoshida, M., Matsuayama, A., Komatsu, Y. and Nishino, N. *Curr. Med. Chem.* **10**, 2351-2358 (2003).
2. Furumai, R., Komatsu, Y., Nishino, N., Kochbin, S., Yoshida, M. and Horinouchi, S. *Proc. Natl. Acad. Sci. USA* **98**, 87-92 (2001).
3. Nishino, N. and Powers, J. C. *Biochemistry* **18**, 4340-4347 (1979).

Design of an Antibody for Early Detection of Ovarian Cancer

**Danielle Carbin¹, Sharad Rawale¹, Carl Morrison³, Jeffrey Fowler¹,
Larry Maxwell⁴ and Pravin T. P. Kaumaya^{1,2}**

¹*Department of Obstetrics and Gynecology, Division of Vaccine Research,* ²*Arthur G. James Comprehensive Cancer Center,* ³*Department of Pathology, The Ohio State University, Columbus, OH 43210, USA,* ⁴*Walter Reed Army Medical, Division of Gynecologic Oncology, Washington DC 20307, USA*

Introduction

Phosphoserine phosphatase (PSP), a catalytic enzyme that dephosphorylates proteins within a cell, is over-expressed in ovarian cancer tissues. The aim of this project was to design a set of antibodies that could be used for the early detection of ovarian cancer. Algorithms for sequence prediction were used to predict antigenic sites located on PSP that are surface exposed. The sequence we identified is amino acids 135-157 of the PSP protein. The peptide was synthesized as a chimeric construct with the promiscuous T-cell epitope MVF, and pairs of rabbits were immunized using this construct. High titers of antibodies produced by the rabbits have been purified and tested against a variety of ovarian cancer tissue and cell lines. The results of these experiments are presented along with preliminary data from investigations into the use of these antibodies as a possible marker for ovarian cancer diagnosis.

Results and Discussion

Outbred New Zealand white rabbits were immunized with MVF PSP 135-157 and boosted three weeks post immunization (denoted 2Y). Results show that very high titers of antibodies were obtained after the boost which was maintained for 18 weeks without further immunization (2y+11) (Fig. 1A). The relative affinities of the purified antibodies (2y+1) against the immunogen (MVF PSP 135-157) and B-cell epitope (PSP 135-157) were analyzed by competitive ELISA. High affinity of antibodies against the immunogen was obtained (Fig. 1B).

To determine the efficacy of the antibodies for use as a diagnostic tool, tissue microarrays (TMA) were done using the purified antibodies. Patients included in the TMA were diagnosed and treated for uterine malignancy between 1980 and 2003 at the Arthur James Cancer Hospital. Tissue cores from formalin-fixed paraffin embedded donor blocks were arrayed into a new recipient paraffin block and four cores from each block were used to create a TMA of 0.6mm cores. The endometrial cancer TMA was constructed from over 500 tumor specimens. Normal tissue controls were from 10 different organs. Chi square analysis was used for comparison of surgical-pathologic variables and PSP protein expression, as well as univariate and multivariate logistic regression analysis. PSP antigen retrieval was performed by a heat method where specimens were stained using the PSP antibodies purified from the immunized rabbits (1:400 dilution) and detected using enzyme conjugated streptavidin and substrate chromogen. A case was considered negative on TMA if all four cores scored negative. Results with strong cytoplasmic staining in >50% of the cells were scored as 3+. Weak cytoplasmic staining in >50% of the cells was considered 2+, and strong or weak staining in <10% of cells or no staining

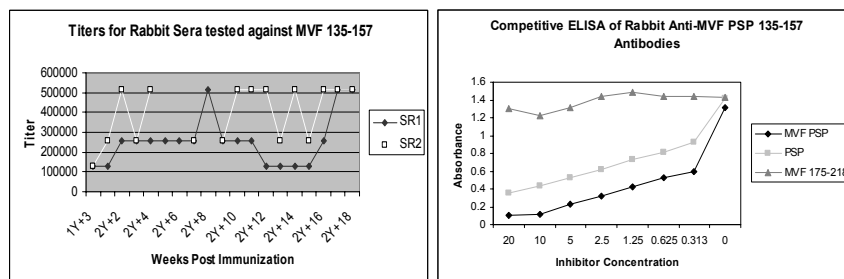


Fig. 1. A. Direct ELISA titers for rabbit sera tested against the immunogen. B. Competitive ELISA results for 2y+11 purified sera tested against the immunogen and inhibited using MVF PSP, PSP, and a control peptide. The purified antibody was used at a dilution of 1:128,000.

was considered 1+ or 0. Scores of 3+ or 2+ are positive and 1+ and 0 scores are negative.

It was found that the antibodies effectively identified PSP in cancerous tissues and not in normal tissues. 96%-100% of normal tissues tested negative while the varying types and stages of cancerous tissues ranged between 13%-48% of samples identified as positive (Table 1).

Table 1. Results from immunohistochemistry staining using biotin conjugated purified anti-MVF PSP 135-157 antibodies against ovarian cancer and normal tissue samples.

				PSP IHC		Positive		PSP IHC		Negative	
				No.	%	No.	%	No.	%	No.	%
Histological Subtypes	Endometrioid G1	176	38%	51	29%	125	71%				
	Endometrioid G2	111	24%	41	37%	70	63%				
	Endometrioid G3	62	13%	22	35%	40	65%				
	Mixed Epithelial	27	8%	11	41%	16	59%				
	MMT	25	18%	12	48%	13	52%				
	Serous	56	12%	27	48%	29	52%				
Normal Endometrium	Clear Cell	8	5%	1	13%	7	88%				
	Proliferative	51	50%	2	4%	49	96%				
	Secretory	49	50%	0	0%	49	100%				

The first two columns are the number and percent of patients for each category and the remaining columns are the number and percentage of positive or negative tissue microarrays for each category.

Acknowledgements

This work was supported by a GYN Cancer Center Grant.

References

1. Kaumaya, P. T. P., Kobs-Conrad, S., DeGeorge, A. M. and Stevens, V. C. *Peptides: Design, Synthesis, and Biological Activity* 133-161 (1994).
2. Barford, D., Das, A. K. and Egloff, M. P. *Annu. Rev. Biophys. Struct.* **27**, 133-164 (1998).

G_i3 α ³⁴⁶⁻³⁵⁵ construct translocated into RBL-2H3 cells with first order, saturable kinetics with a half-life of 3 minutes at a concentration of 3 μ M [4].

Table 1 summaries the biological activities of a range of mimetic peptide cargoes effectively delivered to the intracellular compartment of RBL-2H3 or U373MG astrocytoma cells as TP10 chimera.

Table 1. Biological activities of peptide cargoes

Peptide Cargo		Biological Activity	
		Secretion	Map Kinase Stimulation
Cys ⁰ PKC ²³⁸⁻²⁴⁹	CRRLSVEIWDWDL	Active	Inactive
CB ₁ ⁴⁰¹⁻⁴¹⁷	RSKDLRHAFRSMFPSCE	Active	Inactive
Cys ⁰ [Ser ⁴¹⁶]CB ₁ ⁴⁰¹⁻⁴¹⁷	CRSKDLRHAFRSMFPSSE	Inactive	Not determined
Cys ⁰ Rab3A ⁴⁷⁻⁶¹	CTPAFVSTVGIDFKVK	Inactive	Not determined
G _i 3 α ³⁴⁶⁻³⁵⁵	KNNLKECGLY	Inactive	Active

Data are taken from references [3] and [4]. Secretion assays measured the exocytotic release of β -hexoseaminidase from RBL-2H3 cells. Map kinase assays assessed the dual phosphorylation of p42/p44 MAP kinase in the U373MG astrocytoma line. All cargoes were synthesized as peptide amides in an effort to improve intracellular stability.

Our data indicate that TP10-mediated translocation is an effective methodology to deliver concentrations of bioactive cargoes that modulate intracellular signal transducing proteins. Clearly, as indicated in Table 1, translocated cargoes display sequence-dependent biological activities. Comparison of the secretory properties of CB₁⁴⁰¹⁻⁴¹⁷ and Cys⁰[Ser⁴¹⁶]CB₁⁴⁰¹⁻⁴¹⁷ indicates that even minor changes to primary sequence can dramatically influence the biological properties of the delivered cargo. Related investigations have indicated that is possible to activate and inhibit the same enzymatic activity using rationally designed mimetic peptide cargoes. Our studies have also confirmed that, at concentrations of 3 μ M, TP10 has no significant influence on cellular viability. Moreover, despite containing mastoparan (MP) as a C-terminal sequence, TP10 is suitable for applications even in cells such as RBL-2H3 that are responsive to MP and its analogs. Our current investigations are designed to identify the intracellular protein targets that bind bioactive peptide cargoes using a combination of affinity purification and biological mass spectrometry.

Acknowledgments

The work was supported by the Wellcome Trust.

References

1. Langel, Ü. *Cell-penetrating peptides, processes and applications*. CRC Press, Boca Raton.
2. Soomets, U., et al. *Biochim. Biophys. Acta* **1467**, 165-176 (2000).
3. Howl, J., Jones, S. and Farquhar, M. J. *ChemBioChem* **4**, 1312-1316 (2003).
4. Jones, S., et al. *Biochim. Biophys. Acta* **1745**, 207-214 (2005).

Novel MTII/AGRP Hybrid Analogs that Lead to Selective Ligands for the Human Melanocortin Receptors

Minying Cai, Alexander Mayorov, Kevin Chandler, Christopher Cabello, Dustin Tanaka, Dev Trivedi and Victor J. Hruby

Department of Chemistry, University of Arizona, Tucson, AZ 85721, USA

Introduction

Agouti-related protein (AGRP) is an endogenous antagonist for melanocortin receptors (MCRs). In the hypothalamus melanotropin peptide agonists act as satiety-inducing factors that mediate their action through the melanocortin-4 receptor (MC4R), whereas AGRP is an opposing orexigenic agent. AGRP has a cysteine-rich COOH-terminal domain and nuclear magnetic resonance studies (PDB: 1HYK) demonstrated that the cysteine residues in AGRP adopts a structural motif known as an inhibitor cysteine knot [1]. This knot has been shown *in vitro* to be an inverse agonist with a potential *in vivo* to regulate the various MCRs, even in the absence of melanocortins [1]. MTII is a super potent agonist, and it has been implicated in the treatment of sexual dysfunction and obesity, and recently, the 3D NMR structure of MTII has been reported by Ying *et al.* [2]. The superimposed NMR structure of the AGRP knot c[Cys¹¹¹-Arg-Phe-Phe-Asn-Ala-Phe-Cys¹¹⁸] and NMR based molecular modeling derived structure of the hybrid analogs of MTII were compared. Though the primary sequence of AGRP (110-117) is totally different from that of MTII, the 3D topological structures of both pharmacophores are similar and their structures fit quite well when observed either from the α -carbon or from their backbone structure.

To further study the 3D topographical structure of agonist and antagonist, a group of MTII/AGRP hybrid analogs have been designed and synthesized based on the MTII template and the pharmacophore of AGRP (110-117), and the AGRP cysteine knot template and MTII pharmacophore. Their biological activities were determined to further examine the selectivity.

Results and Discussion

A few of the hybrid structures are given below and Table 1 summarizes the biological data for the MTII/AGRP hybrid analogs which were designed based on the NMR structure of AGRP the (110-117) knot and the NMR based molecular modeling derived structure of the hybrids (Fig. 1). Generally, it was observed that the analogs in this series were agonist at the hMC1R and had very weak binding affinity for the hMC5R. On the contrary, these analogs were antagonist at the hMC3R and hMC4R that coincides with the natural AGRP which was not a surprise. We did observe selectivity between the hMC3R and hMC4R, though analog MC11 was found to be 30 fold more selective antagonist for the hMC4R when compared to the hMC3R. Interestingly, analog MC15 exhibited selective agonist activity for the hMC1R. Superimposing the MTII/AGRP core sequence derived from NMR and the core sequence of MC15 derived from LLMOD (Figs.1 and 2) [3] demonstrate that the structure of MC15 is in close proximity to the structure of AGRP which results in

MC11. Ac-Nle-c[Asp-Phe-Phe-Arg-Phe-Lys]-NH₂
MC15. Ac-Nle-c[Asp-Phe-Nal(2')-Arg-Phe-Lys]-NH₂
MC17. Ac-Nle-c[Asp-Nal(2')-Phe-Arg-Phe-Lys]-NH₂

Table 1. Competition binding assay and cAMP assay of MTII/AGRP hybrid at hMCRs

	hMC1R			hMC3R			hMC4R			hMC5R		
	IC ₅₀ (nM)	EC ₅₀ (nM)	% Act	IC ₅₀ (nM)	EC ₅₀ (nM)	% Act	IC ₅₀ (nM)	EC ₅₀ (nM)	% Act	IC ₅₀ (nM)	EC ₅₀ (nM)	% Act
MC11	3537	NA	/	1975	NA	/	72	NA	/	6055	NA	/
MC15	17	1.5	100	>10,000	NA	/	1735	NA	/	146	NA	/
MC17	26	6	100	671	1681	100	1791	NA	/	2728	NA	/

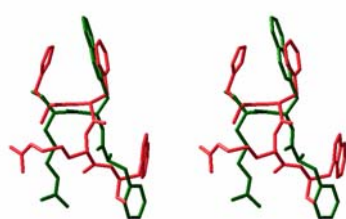


Fig. 1. Superimposed NMR structure of MTII core sequence (His-D-Phe-Arg-Trp) and MC15 core sequence (Phe-Nal(2')-Arg-Phe) LLMOD derived structure (blue: AGRP, green: MC15) (red: MTII, green: MC15).

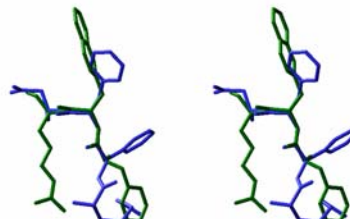


Fig. 2 Superimposed NMR structure of AGRP core sequence (Arg-Phe-Phe-Asn-Ala-Phe) and MC15 core sequence (Phe-Nal(2')-Arg-Phe) LLMOD derived structure (blue: AGRP, green: MC15).

selective agonist activity toward the hMC1R. Analog MC11, a selective hMC4R antagonist, and MC15, a selective hMC1R agonist, could be further evaluated in *in vivo* animal models.

Acknowledgments

Supported by Grants from the USPHS, DK17420, and DA06284.

Reference

1. McNulty, J. C., Thompson, D. A., Bolin, K A., Wilken, J., Barsh, G. S. and Millhauser, G. *Biochemistry* **40**, 15520-15527 (2001).
2. Ying, J., Koeber, K. E., Gu, X., Han, G., Trivedi, D., Kavarana, M. J. and Hruby, V. J. *Biopolymers* **71**, 696-716 (2003).
3. Cai, M., Cai, C., Mayorov, A.V., Xiong, C., Cabello, C. M., Soloshonok, V. A., Trivedi, D. and Hruby, V. J., *J. Peptide Res.* **63**, 116-131 (2004).

Design, Synthesis, and Evaluation of Gluten Peptide Analogs as Selective Inhibitors of Human TG2

Olga Fierro², Stefania Albrizio¹, Alfonso Carotenuto¹, Gabriella Caliendo¹, Daniela Guarino², Paolo Grieco¹, Pietro Campiglia¹, Teresa Lama¹ and Ettore Novellino¹

¹Dip. Chimica Farmaceutica e Toss., University of Naples- Federico II; ²Istituto di Scienze dell'Alimentazione CNR, Avellino, Italy

Introduction

Celiac Sprue is an inflammatory disease of the small intestine that causes the destruction of the intestinal villi with severe consequences for the growth and the health of the organism. The pathogenesis of this disease is initiated by the ingestion of the gluten held in different cereals. At present the only therapy is a gluten-free diet. Therefore, to find a pharmacological alternative is an important and urgent objective.

Recent studies have indicated a crucial role for tissue transglutaminase (TG2) in the pathogenesis of Celiac Sprue. This enzyme has a particular affinity for the glutamine-rich proteins of gluten. Actually, several immunodominant gluten peptides have been identified as substrates of TG2 [1]. All these gluten epitopes show the common characteristic to be very rich in proline and glutamine residues (Fig. 1).

Starting from a short peptide of sequence PQPQLPY, known to be a good substrate of human TG2 and remarkably resistant toward proteolysis, we designed new analogs by replacing Pro3 with constrained amino acids (Fig. 2) to develop specific inhibitors of TG2 [2]. In fact, the proline residues present in the gluten epitopes were reported to have a key role in determining the immunogenicity of the epitopes and an important influence on TG2 specificity [3].

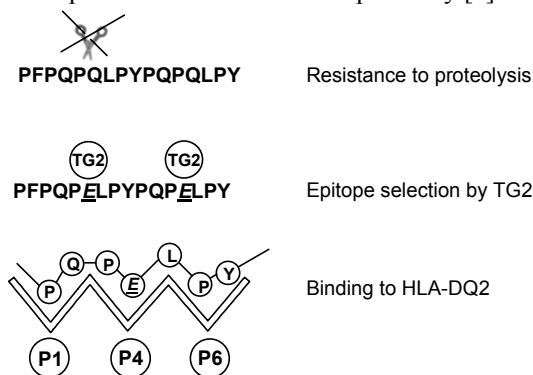


Fig. 1. T-cell epitopes cluster in regions of gliadins with high proline residues.

Results and Discussion

The new analogs were obtained using solid phase peptide synthesis based on Fmoc chemistry. Batch syntheses were carried out on 0.1 mmol scale starting from a PAL support for peptide amides. The incorporation of constrained amino acids in peptides has been optimized using HATU and DIPEA as activating agents in DMF.

Before cleavage, each product was acetylated at the N-terminus. The crude peptides were purified by semipreparative RP-HPLC. Their identity was confirmed by HR-MS. HPLC analyses showed that the synthetic compounds were between 97-99% pure.

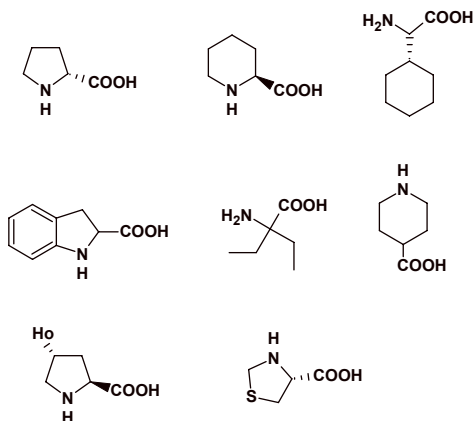


Fig. 2. Residues of constrained amino acids replaced in position 3 of PQPQLPV peptide.

To evaluate the activity of the synthetic compounds, we used the GDH-linked continuous spectrophotometric assay [2,4]. In this assay, the activity of TG2 is monitored indirectly by measuring the reduction of the absorbance of NADH when it is transformed in NAD⁺. The preliminar biological results showed that some compounds in which Pro³ has been replaced with constrained residues such as D-Pro, Hyp, Inp, and Pip had similar biological effect compared to the native substrate while compounds containing Chg, Ind, Thz, and Deg are currently under investigation.

Additional biological tests and structural studies on the compounds synthesized will help to clarify the role of the proline residues in the interaction of the gluten epitopes with TG2 and, consequently, to gain new insight in the molecular mechanism of celiac disease.

References

1. Koning, F. and Vader, W. *Science* **299**, 513-515 (2003).
2. Hausch, F., Halttunen, T. Maki, M. and Khosla, C. *Chem. Biol.* **10**, 225-231 (2003).
3. Sollid, L. M. *Nature Reviews* **2**, 647-655 (2002).
4. Day, N. and Keillor, J. W. *Anal. Biochemistry* **274**, 141-144 (1999).

Novel Blue- and Red-Shifted Internally Quenched Fluorogenic Substrates for Continuous Monitoring of SARS-CoV 3CL^{pro}

Pamela Hamill¹, Martin Richer¹, Derek Hudson², Hongyan Xu³ and
François Jean¹

¹Department of Microbiology and Immunology, University of British Columbia, Vancouver, BC, V6T 1Z3, Canada; ²Biosearch Technologies Inc., Novato, CA, 94949-5750, USA;

³GL Biochem Ltd., Shanghai, 201203, China

Introduction

The SARS coronavirus (SARS-CoV)-encoded main protease, 3CL^{pro} or M^{pro}, plays an essential role in the viral life cycle and is currently the main focus for the development of anti-coronaviral therapies. The genome of SARS-CoV is translated in the cytoplasm of infected cells to generate several large polyproteins. For viral replication to occur, these polyproteins must be proteolytically processed into individual proteins, a process that is mediated by two viral proteases; PL2^{pro} and 3CL^{pro} [1]. 3CL^{pro} is considered the main viral protease as it releases the key replicative proteins of the virus, including the viral RNA polymerase and helicase proteins. Since the emergence of SARS-CoV in late 2002, the development of sensitive assays to detect recombinant 3CL^{pro} activity in formats amenable to high-throughput screening (HTS) has been a priority for the generation of novel 3CL^{pro} inhibitors as anti-viral therapies. Here, we report our success in developing blue- and red-shifted internally quenched fluorogenic substrates (IQFSs) based on resonance energy transfer between the donor and acceptor pairs Abz/Tyr(3-NO₂) [IQFS-1], and CAL Fluor Red 610 (CalRed 610)/Black Hole Quencher-2 (BHQ-2) [IQFS-2], using a decapeptide sequence corresponding to that of the cleavage site between the non-structural protein (nsp)4/nsp5 in the SARS-CoV polyprotein pp1ab.

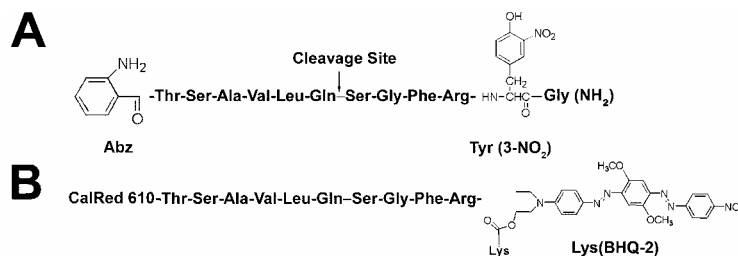


Fig. 1. Amino acid sequences of SARS-CoV 3CL^{pro} IQFSs (A) IQFS-1 and (B) IQFS-2. The chemical structures of the donor group *o*-aminobenzoyl (Abz) and acceptor groups 3-nitrotyrosine (3-NO₂) [2-4] and Black Hole Quencher-2 (BHQ-2) are shown.

Results and Discussion

SARS-CoV 3CL^{pro} quenched fluorescent substrate IQFS-1 (Fig. 1) was synthesized using Fmoc solid phase peptide chemistry [2-4]. The synthesis protocol for IQFS-2 will be presented elsewhere (Hamill P. *et al.*, manuscript in preparation). In both cases, peptide purity and composition were demonstrated by RP-HPLC, mass spectrometry and amino acid analysis. Following expression in *E. coli*, His-tagged SARS-CoV 3CL^{pro} was purified to > 90% homogeneity by nickel chromatography.

The ability of purified SARS-CoV 3CL^{pro} to cleave both IQFSs was then tested by using a continuous protease assay (Fig. 2A) and RP-HPLC assay (Fig. 2B and 2C).

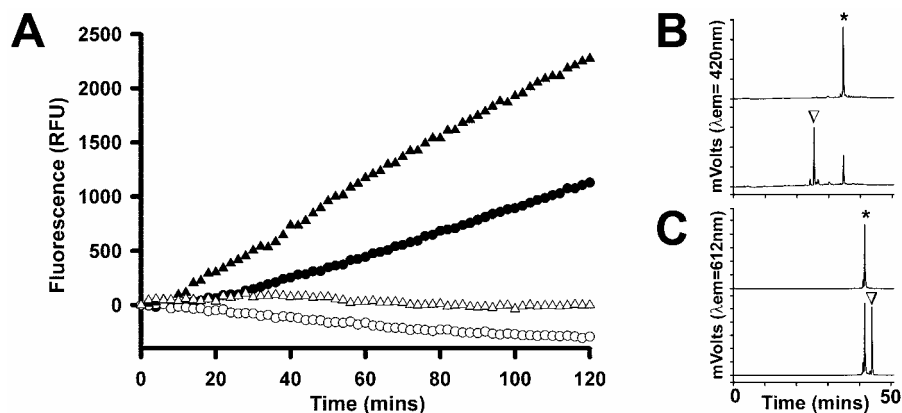


Fig. 2. Processing of blue- and red-shifted quenched fluorescent peptidyl substrates by recombinant SARS-CoV 3CL^{pro} (A) Continuous protease assay using a fluorescence plate reader [3-4]. IQFS-1 and IQFS-2 were added at concentrations of 36 μ M or 18 μ M, respectively, to assay reactions containing 500 nM of 3CL^{pro} in reaction buffer (50 mM Hepes, 100 mM NaCl, [pH 7.3], 10 mM DTT and 10 μ g/well of BSA) at 30°C. The fluorescence emitted from reactions in the presence (closed symbols) or absence (open symbols) of 3CL^{pro} was measured using $\lambda_{ex}/\lambda_{em}$ of 320/420 nm or 584/612 nm for IQFS-1 (circles) and IQFS-2, (triangles) respectively. RP-HPLC analysis [4] of fluorescent peptide products present in reactions containing (B) IQFS-1 and (C) IQFS-2 in the absence (top panel) or presence (lower panel) of 3CL^{pro}. Intact IQFS (*) and N-terminal cleavage products (∇) are indicated.

Our results show that both the blue- and red-shifted IQFSs are sensitive substrates that are efficiently processed at low micromolar concentration by recombinant SARS-CoV 3CL^{pro} in our continuous assay. In addition, we demonstrate that both are cleaved in one position only following the glutamine residue, consistent with the known proteolytic specificity of SARS-CoV 3CL^{pro}. Our novel *in vitro* continuous assay system utilizing both blue- and red-shifted IQFS is advantageous since both the efficacy and mode of inhibition of putative 3CL^{pro} inhibitors can be determined. Moreover, our dual-substrate continuous 3CL^{pro} assay may offer advantages for HTS of small molecule natural-colored compounds, since the number of false positives resulting from non-specific interference with the fluorophore group may be reduced.

Acknowledgments

Supported by NCE/PENCE and CIHR (F. Jean). F. Jean is a CIHR Scholar.

References

1. Ziebuhr, J. *Curr. Opin. In. Micro.* **7**, 412-19 (2004).
2. Jean, F., Basak, A., DiMaio, J., Seidah, N. G. and Lazure, C. *Biochem. J.* **307**, 689-695 (1995).
3. Richer, M., Juliano, L., Hashimoto, C. and Jean, F. *J. Biol. Chem.* **279**, 10222-10227 (2004).
4. Hamill, P. and Jean, F. *Biochemistry* **44**, 6586-6596 (2005).

Discovery and Optimization of a TRAIL R2 Agonist for Cancer Therapy

Yvonne M. Angell, Ashok Bhandari, Anjan Chakrabarti, M. Nuria De Francisco, Amy N. Duguay, Brian T. Frederick, Karen Leu, Kerstin Leuther, Xianfeng Li, Kalyani Penta, Sunila Piplani, Reuben Sana, Erik A. Whitehorn, Pete J. Schatz, Kevin Yin and Christopher P. Holmes

Affymax, Inc., 4001 Miranda Avenue, Palo Alto, CA 94304, USA

Introduction

TRAIL is a cytokine that induces apoptosis in a wide variety of tumor cells but rarely in normal cells. The TRAIL R2 ligand triggers tumor cell apoptosis independently of the p53 tumor-suppressor gene [1-5]; thus, peptide agonists may offer a complementary approach to conventional cancer therapy. Ligands belonging to the TNF family are expected to function as a homotrimer as suggested by the crystal structures of a subset of the family (TNF α , TNF β , CD40L, and TRAIL). The TNFR family members are transmembrane proteins. The extracellular domain of the receptors is characterized by the concatenated cysteine-rich domains (CRDs) [6] that are responsible for ligand binding. TRAIL R2 is a single transmembrane receptor arranged as a homo-trimeric complex on the cell membrane, and TRAIL ligand is a Zn-coordinated trimer [7]. Formation of a complex between TRAIL and its signaling receptors, DR4 and DR5, triggers apoptosis by inducing the oligomerization of intracellular death domains.

A novel peptide sequence identified through recombinant peptide screening was found to bind the TRAIL R2 receptor with 120 nM binding affinity. The sequence of this peptide is unrelated to that of native or recombinant TRAIL yet the sequence was found to compete with TRAIL for binding the TRAIL R2 receptor. Hit to lead optimization strategies included both sequence optimization as well as architecture optimization. Truncation analysis of the hit sequence enhanced the binding affinity and identified a 15-mer as the minimal sequence necessary to maintain good binding ($IC_{50} = 1$ nM). Alanine scanning identified three critical residues for binding affinity including an *N*-terminal tryptophan and two residues within the disulfide loop whereas the C-terminus was found to be critical for functional activity. Specific architectural modifications of the peptide structure, including dimerization, enhanced the binding affinity from 1000 to 10,000-fold depending on the architecture. In addition, the point of multimerization significantly affected functional activity in whole cell assays, resulting in peptides with potencies ranging from no functional activity to low micromolar apoptotic activity. Figure 1 illustrates how architecture influences both binding activity and functional activity. It is interesting to note there is not a direct correlation between binding affinity and functional activity.

Results and Discussion

Synthetic peptides were prepared using Fmoc chemistry on TentaGel R RAM (0.18 mmol/g, 0.4 g) resins using standard DIC/HOBt batchwise solid-phase synthesis protocols on a PTI Symphony peptide synthesizer. The N-terminal Fmoc-group was removed with 20% piperidine in DMF. Following resin and side-chain cleavage with 85% TFA/10% triisopropylsilane/2.5% H₂O/2.5% thioanisole, the crude peptides were precipitated with cold diethyl ether and washed twice with ether;

Development of Peptide Vaccines against HPV-16 Associated Cervical Cancer and Group A Streptococci

Peter M. Moyle¹, Aniko Horváth¹, Levente Karpáti¹, Colleen Olive²,
 Nadia Barozzi¹, Norbert Wimmer¹, Michael Good² and Istvan Toth¹

¹School of Molecular and Microbial Biosciences and School of Pharmacy, the University of Queensland, St Lucia, QLD 4072, Australia; ²Queensland Institute of Medical Research, Herston, QLD 4006, Australia

Introduction

Vaccination has proven to be one of the most successful and cost-effective public health interventions. While vaccines exist to prevent many diseases, opportunities still exist for development of new vaccines or to further improve existing vaccines. An area of recent interest is mucosal vaccine delivery. This entails the administration of vaccines to mucosal membranes, resulting in induction of both mucosal and systemic immune responses. Many advantages are offered by this technique, including ease of administration and improved patient compliance. One technique examined for mucosal immunization is peptide lipidation. A system of interest to our group is the Lipid Core Peptide (LCP) system [1]. This system incorporates peptide antigens, a poly-lysine multiple antigen peptide (MAP) system [2], and synthetic lipidic amino acids into a single molecular entity. Our group has investigated this system for the synthesis of novel vaccines against many diseases. Of recent interest is the utilization of this system for the production of therapeutic and prophylactic vaccines against Human Papillomavirus Type-16 (HPV-16) associated cervical cancer (Fig. 1), and prophylactic vaccines against Group A Streptococcal (GAS) strains common to the Australian aboriginal populations of Northern Queensland and the Northern Territory [3]. Of particular interest to our group is the utilization of peptide ligation and fragment condensation to synthesize highly pure LCP analogs (Fig. 2) [3]. It is the aim of our research to produce a highly pure, well characterized analog of the LCP system using these techniques.

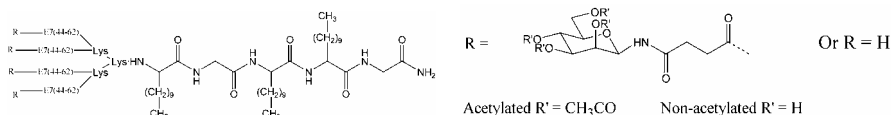


Fig. 1. HPV-16 E7(44-62) containing LCP systems.

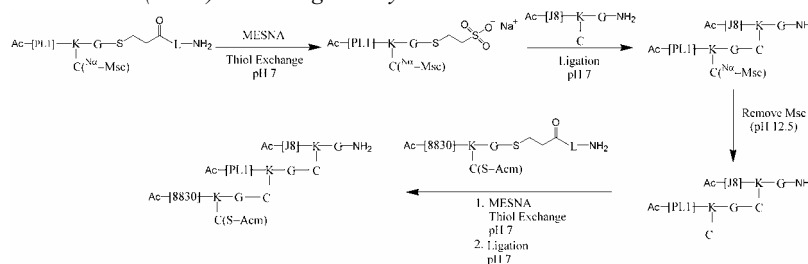


Fig. 2. Synthesis of highly pure tri-epitope GAS vaccine using native chemical ligation (PL1: EVLTR RQSQD PKYVT QRIS, J8: QAEDK VKQSR EAKKQ VEKAL KQLED KVQ, 8830: DNGKA IYERA RERAL QELGP).

Results and Discussion

All peptides were synthesized on *p*-MBHA resin using in situ neutralization Boc-chemistry [4]. Peptides were removed from the resin using anhydrous HF with *p*-cresol (5% v/v). *p*-thiocresol (5% v/v) was also used during cleavage of HPV LCP systems. All peptides were purified by preparative HPLC, with LCP systems also purified by size exclusion on sephadex LH-20. Peptides were characterized by HPLC and ES-MS (where possible), and the LCP systems were also characterized by SDS-PAGE.

HPV LCP systems containing four copies of the HPV-16 E7(44-62) peptide (QAEPDRAHYNIVTFCKCD) were synthesized as per previously published methods [3]. The peptide LCP system was also coupled to four copies of an acetylated mannose derivative (4-(2,3,4,6-tetra-O-acetyl- β -D-mannopyranosyl amino)-4-oxobutanoic acid) using HBTU/DIPEA activation. A portion of this resin was treated with 12.5% (v/v) hydrazine hydrate in MeOH to remove O-Ac protection of mannose residues. C57BL/6 mice were immunized subcutaneously with the HPV LCP-systems without additional adjuvant, as well as control peptides. Mice were then challenged one week after the last boost with approximately 7×10^5 TC-1 tumor cells, with tumors resected 15 days post-challenge and weighed. Preliminary results demonstrated that LCP immunized mice had significantly reduced tumor masses compared to mice immunized with controls without adjuvant. Most significantly, 9 of 10 mice immunized with the deacetylated mannose containing LCP vaccine had no tumors at resection. As such, the results suggest that mannosylation of the vaccine has improved the immune response against the LCP vaccine. This may be caused by targeting of mannose receptors on antigen presenting cells.

The highly pure tri-epitopic peptide vaccine [3] was synthesized using native chemical ligation (Fig. 2). The vaccine was administered subcutaneously to B10.BR mice using an homologous prime-boost regimen [3] with and without additional adjuvant (Complete Freund's Adjuvant). Serum IgG levels induced by vaccine administration were measured by ELISA. Results indicated the vaccine was not immunogenic without the addition of an adjuvant. In comparison, an LCP vaccine synthesized to contain the same peptide epitopes induced high IgG antibody titres against each epitope without need for additional adjuvant. As such, research is now focused on synthesis of highly pure LCP based vaccines with a built in lipidic adjuvant.

Acknowledgments

This work was funded by an Australian National Health and Medical Research Council (NMHRC) Program Grant, the National Heart Foundation of Australia, and the Prince Charles Hospital Foundation. The author would like to acknowledge the Queensland Government for their financial support through the awarding of a Growing the Smart State PhD funding grant.

References

1. Toth, I., Danton, M., Flinn, N. and Gibbons, W. A. *Tetrahedron Lett.* **34**, 3925-3928 (1993).
2. Tam, J. P. *Proc. Natl. Acad. Sci. USA* **85**, 5409-5413 (1988).
3. Horváth, A., *et al.* *J. Med. Chem.* **47**, 4100-4104 (2004).
4. Schnolzer, M., Alewood, P., Jones, A. and Alewood, D. *Int. J. Peptide Prot. Res.* **40**, 180-193 (1992).

Disulfide as a Constraint to Build Super Potent and Selective Melanocortin-4 Receptor (MC4R) Agonists

Liang Zeng Yan, David Flora, Patrick Edwards, David L. Smiley, Paul J. Emmerson, Hansen M. Hsiung, Robert Gadski, JeAnne Hertel, Mark L. Heiman, Saba Husain, Thomas P. O'Brien, Steven D. Kahl, Lianshan Zhang, Richard D. DiMarchi and John P. Mayer

Lilly Research Laboratories, A Division of Eli Lilly & Company, Lilly Corporate Center, Indianapolis, IN, 46285, USA

Introduction

The melanocortin peptides are tissue-specific, posttranslationally processed products of the proopiomelanocortin (POMC) prohormone. Those peptide hormones, including ACTH, α -MSH, β -MSH, and γ -MSH, are unified by the fact that they contain the sequence His-Phe-Arg-Trp, which is the key pharmacophore necessary for their biological activity. Those peptide ligands enact various biological functions, such as pigmentation, inflammation, energy homeostasis, etc., through binding to their specific G protein-coupled receptors, MC1R through MC5R [1]. Work reported by Huszar and others highlighted MC4R as a validated target for the intervention of the fast growing pathological obesity and metabolic syndrome [2]. Our goal was to develop potent and selective MC4R agonists that may be potentially applied to therapeutic obesity management.

Results and Discussion

Early work on non-natural melanocortin agonists by Hruby and co-workers have resulted in a highly potent, non-selective cyclic lactam (**1**) with D-Phe in the core sequence [3]. Our efforts in this field have generated a disulfide constrained peptide agonist **2**. The cyclic peptide showed a good potency towards MC4R (Ki 2.10 nM) and a selectivity over MC5R (~90 fold) and MC1R (~5 fold). This initial result encouraged us to perform a more extensive SAR around this disulfide scaffold.

MC4R binding potency was enhanced more than 5 fold when the 22-membered ring (**2**) was modified to a 21-membered ring (**3**) by replacing the second homoCys with Cys. The selectivity over MC1R remained the same. Removal of the N-terminal Tyr from **3** afforded **4** with an improved MC4R potency (Ki 0.08 nM) and a 50 fold selectivity over MC1R. Further deletion of N-terminal Arg resulted in **5**. This 6-mer cyclic peptide showed a 340 fold selectivity over MC5R, while the selectivity over MC1R was maintained at 50 fold. From compound **2** to **5**, the size of the molecule was reduced by a quarter, while both the potency towards the target MC4R receptor and the selectivity over MC1R were increased by ten fold.

Both compounds **5** and **6** have a 21-membered ring and the only difference was switching the positions of Cys and homoCys. This subtle change significantly reduced the binding towards MC4R (Ki 0.27 and 9.37 nM for **5** and **6**, respectively). This suggested that the ring size is not the single parameter that effected the ligand-receptor interactions, even though a proper ring size is critical for high receptor affinity as we observed in compounds **7** and **8**. Expanding the ring size to 22-member or contracting the ring size to 20, both afforded a much less potent peptide (Ki 2.25 nM for **7** and 127.80 nM for **8**).

Table 1. Peptide structure and in vitro assay data [4]

No.	Structure	MC1R Ki(nM)	MC3R Ki(nM)	MC5R Ki(nM)	MC4R Ki(nM)	MC4R EC50(nM)	MC4R rel. eff.(%)
1	Ac-Nle-c[Asp-His-D-Phe-Arg-Trp-Lys]-NH ₂	0.61	15.75	8.42	0.68	0.16	113.23
2	Ac-Tyr-Arg-c[hCys-His-D-Phe-Arg-Trp-hCys]-NH ₂	10.46	85.08	186.4	2.10	0.04	107.80
3	Ac-Tyr-Arg-c[hCys-His-D-Phe-Arg-Trp-Cys]-NH ₂	2.96	9.04	14.31	0.38	0.05	103.45
4	Ac-Arg-c[hCys-His-D-Phe-Arg-Trp-Cys]-NH ₂	4.02	1.91	4.42	0.08	0.05	107.60
5	Ac-c[hCys-His-D-Phe-Arg-Trp-Cys]-NH ₂	13.82	10.34	92.35	0.27	0.11	103.20
6	Ac-c[Cys-His-D-Phe-Arg-Trp-hCys]-NH ₂	>500	360.3	>500	9.37	0.55	89.70
7	Ac-c[hCys-His-D-Phe-Arg-Trp-hCys]-NH ₂	65.03	80.96	> 500	2.25	0.26	92.78
8	Ac-c[Cys-His-D-Phe-Arg-Trp-Cys]-NH ₂	> 500	> 500	> 500	127.8	4.88	91.75
9	Ac-c[hCys-His-(p-Cl-D-Phe)-Arg-Trp-Cys]-NH ₂	25.63	1.87	7.67	0.20	0.23	56.35
10	Ac-c[hCys-His-(p-F-D-Phe)-Arg-Trp-Cys]-NH ₂	20.42	7.98	37.17	0.28	0.16	101.50
11	Ac-c[hCys-His-(p-Cl-D-Phe)-Arg-Trp-Pen]-NH ₂	56.10	1.29	11.39	0.04	0.60	66.40
12	Ac-Nle-c[hCys-His-D-Phe-Arg-Trp-Cys]-NH ₂	0.06	0.36	0.27	0.05	0.10	95.28

It was interesting to observe that, even though **2** has two extra residues outside of the cyclic core, it showed a comparable affinity towards MC4R (2.10 nM) as that of **7** (2.25 nM). This suggests that the two residues (Tyr-Arg) located outside of core structure were not involved in any critical interactions with this target receptor MC4R. However, the two residues may play a role in binding towards other receptor subtypes, since the smaller peptide **7** showed a much higher selectivity over MC1R and MC5R. A second pair of compounds, **3** and **5**, showed a similar activity and selectivity pattern (Table 1).

Bulky substitutes on the side chain of D-Phe appear to transform the molecule from an agonist to an antagonist. While p-Cl-D-Phe generated a relatively weaker agonist (**9**, relative efficacy 56%), p-F-D-Phe afforded a full agonist (**10**, relative efficacy 101%). Furthermore, adding two methyl groups to the β -carbon of Cys (penicillamine) markedly boosts the selectivity over both MC1R and MC5R. Peptide **11** showed a MC4R Ki 0.04 nM and a 1400 fold selectivity over MC1R.

These observations demonstrated that the disulfide ring offers an important alternative scaffold to build constrained peptide ligands. Replacement of the lactam ring system (**1**, MC4R Ki 0.68 nM) with our disulfide bond ring system afforded peptide **12** (MC4R Ki 0.05 nM). This compound, while as nonselective as the lactam, showed a more than 10 fold increase in affinity toward all receptor subtypes. We speculated that the disulfide bond ring system might offer a more specific and fine tuned conformation for optimal interactions with the corresponding receptor. On the other hand, the enhanced potency might be also due to the different hydrophobic/hydrophilic properties of the side chain lactam ring and the disulfide bond. These data further suggest that the amide bond of the lactam ring linkage is not involved in any critical interactions with melanocortin receptors.

To summarize, we have demonstrated that disulfide bond ring system is an excellent alternative scaffold of lactam to develop both potent and selective MC4R agonists. Further development of these potent and selective melanocortin agonists may translate into therapeutic applications.

References

1. Gantz, I. and Fong T. M. *Am J. Physiol. Endocrinol. Metab.* **284**, E468-474 (2003).
2. Huszar, D., *et al.* *Cell* **88**, 131-141 (1997).
3. Al-Obeidi, F., *et al.* *J. Med. Chem.* **32**, 2555-2561 (1989).
4. For detailed procedure, see Mayer, J. P., *et al.* *J. Med. Chem.* **48**, 3095-3098 (2005)

Effect of Dimerization and Tetramerization on the Potency of HIV-1 Integrase Inhibitory Peptides

Krzysztof Krajewski¹, Christophe Marchand², Yves Pommier² and Peter P. Roller¹

¹Laboratory of Medicinal Chemistry, NCI, NIH, Frederick MD 21702, USA; ²Laboratory of Molecular Pharmacology, NCI, NIH, Bethesda, MD 20892, USA

Introduction

HIV-1 integrase (IN) is essential for the HIV virus replication cycle. Furthermore, it is a key enzyme for the ability of HIV to infect non-dividing cells [1]. The mechanism of IN enzymatic activity involves two steps: 3'-processing and strand transfer. In addition to reverse transcriptase and protease, IN is an attractive target for HIV antiviral chemotherapy. It has no counterpart in mammalian cells, therefore selective IN inhibitors should not produce any side effects. Many IN inhibitors have been reported to date, and some promising compounds are in clinical trials [2]. However, no clinically useful drugs have yet been approved. Here we present results of our studies on the effect of dimerization and tetramerization (Fig. 1) on the IN inhibitory potency of peptides. For these studies, we used IN inhibitory peptide sequences discovered by us or published by others [3-6]. These results may be helpful in the process of designing new IN inhibitory drugs.

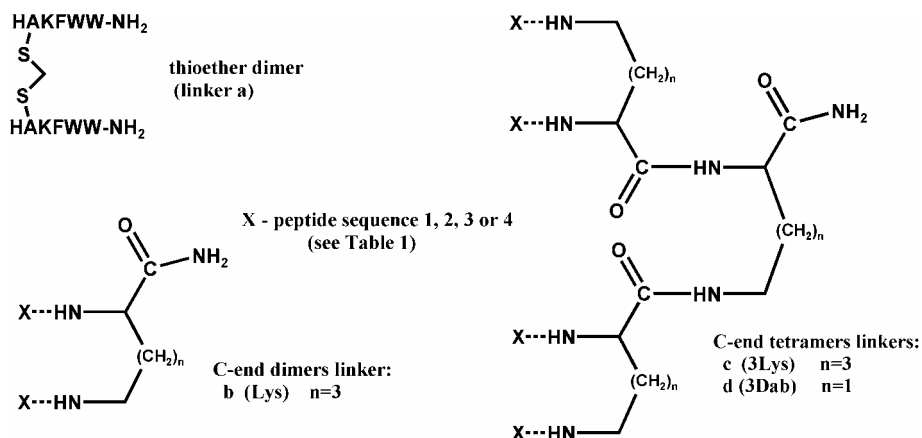


Fig. 1. Methods of dimerization and tetramerization of HIV-1 integrase inhibitory peptides.

Results and Discussion

Peptides were synthesized using Fmoc chemistry on a Rink amide resin or a Sieber resin (thioether dimer, see [7]). Following deprotection and cleavage with TFA and scavengers (TIS/EDT/H₂O), the crude peptides were precipitated with cold Et₂O, washed 5 times with Et₂O, dried, dissolved in a water/acetonitrile mixture, and lyophilized, then dissolved again in a water/acetonitrile mixture and purified by RP-HPLC (Vydac C₁₈, C₈, or C₄ preparative columns). The purity of peptides (90-95%) was confirmed by RP-HPLC (Agilent C₁₈ and CN columns) and MALDI-TOF-MS.

Table 1. Results of wild type HIV-1 integrase *in vitro* inhibitory assays

Peptide	IC ₅₀ (μM)			
	3'-processing		strand transfer	
	Mg ²⁺	Mn ²⁺	Mg ²⁺	Mn ²⁺
Monomer: HCKFWW-NH₂ (1) [3]	-	102	-	97
Thioether dimer (linker a) of sequence 1	85	5	85	7
C-end dimer (Lys, linker b) of sequence 1	13	15	7	6
C-end tetramer (3Lys, linker c) of sequence 1	0.7	0.5	0.5	0.4
C-end tetramer (3Dab, linker d) of sequence 1	0.8	1.4	0.2	1.2
Monomer: ILPWKWPWWPWP-NH₂ (2) [4]	21	16	19	13
C-end dimer (Lys, linker b) of sequence 2	3	3	2	5
C-end tetramer (3Lys, linker c) of sequence 2	0.7	0.6	0.4	0.6
Monomer: WRWYCR-NH₂ (3) [5]	>100	>100	>100	>100
C-end dimer (Lys, linker b) of sequence 3	6	10	8	10
C-end tetramer (3Lys, linker c) of sequence 3	4	5	0.3	0.6
Monomer: YQLLIRMIY-NH₂ (4) [6]	21	16	19	13
C-end dimer (Lys, linker b) of sequence 4	5	6	7	0.5

The peptides were tested *in vitro* for IN 3'-processing and strand transfer inhibitory potency (Table 1, assay conditions described in [9]). The assays were performed with wild type HIV-1 integrase, in the presence of Mg²⁺ or Mn²⁺ ions. For all tested sequences, the dimeric peptides were more potent inhibitors than monomeric peptides, and tetrameric peptides were the most potent inhibitors of both 3'-end processing and strand transfer (up to 200 times more potent than the monomers). The results suggests that one molecule of dimeric or tetrameric peptide may interact with multiple (2 or 4) active centers (may be with more than one IN unit within a multimeric complex of IN). This is consistent with research results suggesting that at least octameric complex of integrase is required to accomplish the integration process [9].

References

1. Vodicka, M. A. *Somat. Cell. Mol. Genet.* **26**, 35-49 (2001).
2. Pommier, Y., Johnson, A. A. and Marchand, C. *Nat. Rev. Drug Discov.* **4**, 236-248 (2005).
3. Lutzke, R. A. P., *et al. Proc. Natl. Acad. Sci. USA* **92**, 11456-11460 (1995).
4. Krajewski, K., Long, Y. Q., Marchand, C., Pommier, Y. and Roller, P. P. *Biol. Med. Chem. Lett.* **14**, 5595-5598 (2004).
5. Boldt, J. L., Pinilla, C. and Segall, A. M. *J. Biol. Chem.* **279**, 3472-3483 (2004).
6. de Soultrait, V., *et al. J. Mol. Biol.* **318**, 45-58 (2002).
7. Krajewski, K., Long, Y. Q., Marchand, C., Pommier, Y. and Roller, P. P. *Biol. Med. Chem. Lett.*, **13**, 3203-3205 (2003).
8. Marchand, C., Neamati, N. and Pommier, Y. *Methods Enzymol.* **340**, 624-633 (1999).
9. Cherepanov, P., *et al. J. Biol. Chem.* **278**, 372-381 (2003).

The Effects of Stable Bradykinin Receptor 2 Agonist B9972 on Pulmonary Vasculature *in vitro* and *in vivo*

Laimute Taraseviciene-Stewart¹, John M. Stewart², Lajos Gera², Nana Burns¹, Robertas Scerbavicius¹ and Norbert F. Voelkel¹

¹Pulmonary Hypertension Center; ²Department of Biochemistry, University of Colorado Health Sciences Center, Denver, CO 80262, USA

Introduction

The nine-amino-acid vasoactive peptide bradykinin (BK) has a twofold action profile by exerting pathophysiological as well as pronounced beneficial physiological effects. Bradykinin plays a powerful role in angiogenesis [1] and cardioprotection [2-5]. Since bradykinin itself has a very short lifetime, we synthesized a novel stable B2-receptor agonist B9972 [6] to study the effects of this compound on human pulmonary microvascular endothelial (HPMVEC) cells *in vitro* and in our animal model of severe pulmonary hypertension [7] *in vivo*. Since bradykinin is known to stimulate angiogenesis, we used two inhibitors of angiogenesis: SU5416 that inhibits VEGFR1-3 and a broad spectrum tyrosine kinase inhibitor SU6668 that inhibits PDGFR, and to a lesser extent VEGFR-2 [8].

Results and Discussion

In HPMVEC, B9972 caused the induction of MAPK synthesis, while it did not induced phosphorylation of MAPK as did VEGF or bradykinin antagonist B9430 (Fig. 1). Treatment of HPMVEC with vascular endothelial factor receptor inhibitor SU5416 resulted in inhibition of MAPK activity that was partially restored by B9972, but not VEGF or B9430 treatment. While protein kinase B (PKB/Akt) activation (phosphorylation) was induced by bradykinin antagonist B9430, B9972 attenuated this effect (Fig. 1). B9972 induced eNOS (endothelial nitric oxide synthase) activation suggesting a protective effect of bradykinin agonist on

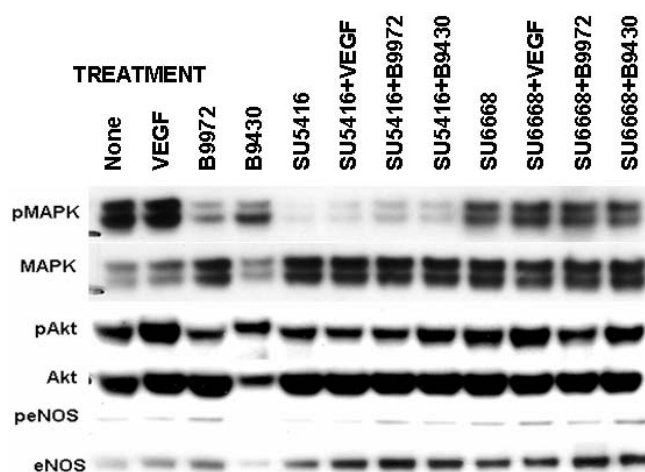


Fig. 1. HPMVEC were pre-treated with 10 μ M SU5416 or SU6668 for 30 min and then treated with 100 nM of B9972 or B9430 for 15 min.

Table 1. Pulmonary artery pressures (PAP) and right ventricle over left ventricle plus septum weight ration (Rv/Lv+S)

Treatment	PAP	Rv/Lv+S
Hx 3wk	34±2.7	0.4±0.02
Hx 3wk+DA 4wk	23±1.2	0.3±0.02
Hx SU6668 3wk	39±3.1	0.4±0.03
Hx SU5416 3wk	56±3.3	0.5±0.02
Hx SU5416 3wk+ DA 4wk	68±2.8	0.73±0.03
Hx SU5416 3wk + B9972 DA 4wk	51±2.0	0.55±0.02

endothelial cells against SU5416 inhibitory signaling in endothelial cells. Neither B9972, VEGF, nor B9430 had an effect on SU6668-treated HPMVEC, suggesting that PDGF has no signaling capacity on these cells.

In vivo SU5416 in combination with chronic hypoxia caused severe pulmonary hypertension and the formation of vascular lesions in rats [7], while SU6668 did not. Treatment with B9972 caused a reversal of pulmonary vascular remodeling as well as a reduction in the number of plexiform lesions in the lungs.

Our data suggest that stable bradykinin B2 receptor agonist B9972 has a protective effect on HPMVEC *in vitro* and that it can repair vascular remodeling and reopen obliterated vessels in animals with severe pulmonary hypertension *in vivo*.

Acknowledgments

The authors thank K. Morris for measurement of pulmonary artery pressures. This work was supported by NIH grant 1PO1 HL66254.

References

1. Miura, S., Matsuo, Y. and Saku, K. *Hypertension* **41**, 1118-1123 (2003).
2. Heitsch, H. *Expert. Opin. Investig. Drugs* **12**, 759-770 (2003).
3. Groves, P., Kurz, S., Just, H. and Drexler, H. *Circulation* **92**, 3424-3430 (1995).
4. Veeravalli, K. K. and Akula, A. *Pharmacol. Res.* **49**, 23-29 (2004).
5. Emanuelli, C. and Madeddu, P. *Trends Pharmacol. Sci.* **22**, 478-484 (2001).
6. Taraseviciene-Stewart, L., Scerbavicius, R., Stewart, J. M., Gera, L., Demura, Y., Cool, C., Kasper, M. and Voelkel, N. F. *Peptides* **26**, 1292-1300 (2005).
7. Taraseviciene-Stewart, L., Kasahara, Y., Alger, L., Hirth, P., Mc, M. G., Waltenberger, J., Voelkel, N. F. and Tuder, R. M. *FASEB J.* **15**, 427-438 (2001).
8. Laird A. D., Christensen, J. G., Li, G., Carver, J., Smith, K., Xin, X., Moss, K. G., Louie, S. G., Mendel, D. B. and Cherrington, J. M. *FASEB J.* **16**, 681-690 (2002).

Etk/Bmx Tyrosine Kinase Peptide Substrates and Inhibitors Derived from the Autophosphorylation Site of the Enzyme

Ching-Yi Hsieh^{1,2}, Jan Marik², Jenny Kung¹, Coleen Sweeney¹, Kit S.
Lam² and Hsing-Jien Kung¹

¹Department of Biological Chemistry and Cancer Center; ²Department of Internal Medicine,
University of California at Davis, School of Medicine, 4645 2nd Avenue, Sacramento, CA
95817, USA

Introduction

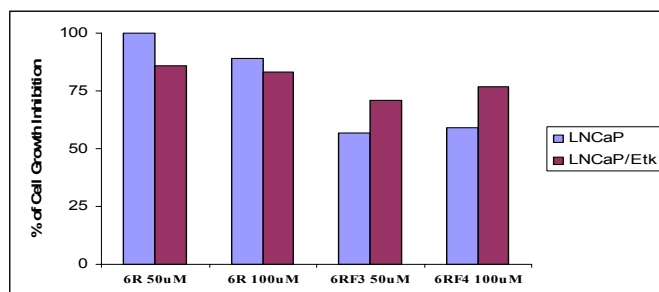
Etk (also called Bmx) is a member of the Btk nonreceptor tyrosine kinase family. This family of kinases is characterized by a modular structure, including an N-terminal pleckstrin homology (PH) domain, a Tec homology domain, Src homology 2 (SH2) and SH3 domains, and a C-terminal kinase domain [1]. Many members of the Btk family are predominantly expressed in cells of hematopoietic origin. In contrast to these family members, Etk is expressed in a variety of tissues and cell types including hematopoietic, epithelial, and endothelial cells as well as several prostate cancer cell lines and tissues [2]. Little is known about the biological function of Etk and the signaling pathways in which Etk is involved. So far, Etk is known to be required for IL-6-induced differentiation of prostate cancer cells, STAT3 is the downstream effector of this pathway [3], and Gal2/13-induced activation of serum response factor in fibroblasts. Etk/Bmx has been shown to play a pivotal role in the regulation of various cellular processes including differentiation, apoptosis, tumorigenesis, and cell motility. And the interaction proteins of Etk/BMX have been found such as, Src (interacts with Etk Y566), Fak (interacts with Etk Y40, E42), STAT3, RhoA, Pak1, PTPD1, RUFY1, and Jak1. All of above evidences indicated that Etk/BMX could be the potential cancer therapeutic target. But, none of peptide substrates and good inhibitor candidates have been reported nowadays. Therefore, the finding of short peptide inhibitors of Etk/BMX could provide an alternative treatment of Etk kinase involved cancers.

Results and Discussion

We identified Etk/Bmx peptide substrates: 1. 25 amino acid, VKFYGVCSKEYP IY₄₈₆ IVTEYISNGSL; 2. 10 amino acid, YPIYIVTEYI; 3. short peptide substrates, IYIVT, IYIVTE, IYIVT, IYIV, and IYI. The core sequence is as short as IYI. The sequence from human Etk Y486 is also confirmed by the autophosphorylated GST-Etkc kinase which was analyzed by ESI-nanosplit LC-MS as a potential Etk autophosphorylation site (unpublished data by Dr. Jenny Kung and Dr. Ching-Yi Hsieh). We also identified Etk/Bmx short peptide inhibitors: rRRRRR-IFIVTEF (6RF3) and rRRRRR-IFIVT (6RF4). 6RF3, 6RF4 is able to penetrate into prostate cancer cells and kill cells, and 6RF3 is a better Etk/Bmx inhibitor *in vivo*. IC₅₀ of 6RF3 is ~5 μ M, IC₅₀ of 6RF4 is ~25 μ M (Fig. 1A). Overexpress Etk/Bmx in prostate cancer cells can rescue inhibitor caused cell death. The Etk/Bmx inhibitor peptides are specific and competitive to inhibit the Etk/Bmx tyrosine kinase activity. The results of the inhibition effect of 6RF3 and 6RF4 in Etk-Stat3 induced the cis-acting response elements stimulating the transcription of the luciferase reporter gene expression showed in Figure 1B. The IC₅₀ of 6RF3 to inhibit the Etk/Bmx kinase

activity is around 1 to 10 μM , and the IC_{50} of 6RF4 to inhibit the Etk/Bmx kinase activity is around 50 μM . 6RF3 is a better Etk/Bmx kinase inhibitor *in vivo*.

A



B

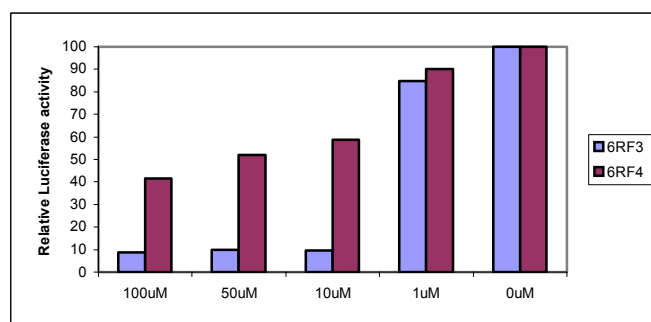


Fig. 1. A. Membrane-permeant form of the Etk/Bmx inhibitory peptides inhibits Etk/Bmx in prostate cancer cells. The synthesis peptides, rRRRRR-IFIVTEF (6RF3) and rRRRRR-IFIVT (6RF4) as the Etk/Bmx inhibitor peptides. B. The inhibition effect of 6RF3 and 6RF4 in Etk-Stat3 induced the cis-acting response elements stimulating the transcription of the luciferase reporter gene expression.

Acknowledgments

We would like to thank Dr. Yi-Mi Wu, Dr. Yoshihiro Izumiya, Dr. Dan P. Robison and Dr. David L. Boucher for the technical assistance and valuable discussion.

References

1. Qiu, Y. and Kung, H. J. *Oncogene* **19**, 5651-5661 (2000).
2. Jiang, T., Guo, Z., Dai, B., Kang, M., Ann, D. K., Kung, H. J. and Qiu, Y. *J. Biol. Chem.* **279**, 50181-50189 (2004).
3. Tsai, Y. T., Su, Y. H., Fang, S. S., Huang, T. N., Qiu, Y., Jou, Y. S., Shih, H. M., Kung, H. J. and Chen, R. H. *Mol. Cell Biol.* **20**, 2043-2054 (2000).

Fluorescence Resonance Energy Transfer Substrates for Determining Cathepsin B pH Specificity

Paolo Ruzza¹, Luigi Quintieri², Alessio Osler¹, Andrea Calderan¹, Barbara Biondi¹, Maura Floreani², Andrea Guiotto¹ and Gianfranco Borin¹

¹Institute of Biomolecular Chemistry of CNR, Padova Unit; ²Department of Pharmacology and Anesthesiology, University of Padova, 35131 Padova, Italy

Introduction

Cathepsin B is a cysteine proteinase of the papain family that in malignant tumors is present both in lysosomes and in the pericellular space. At the acidic pH of lysosomes (4.5-5.5), it has mainly peptidyl-dipeptidase and carboxy-peptidase activity, its active site being partially occluded by a flexible loop [1]; above pH 5.5 this loop is displaced and the enzyme behaves mainly as an endopeptidase having a pH optimum around 7.4 [2-4].

In the present study, we describe the preparation and the use of fluorescence resonance energy transfer (FRET) peptides to search for substrates selectively cleaved by cathepsin B at different pHs. Each peptide contained a highly fluorescent 2-(N-methylamino)benzoyl (Nma) group linked to the amino group of the N-terminal Orn residue (Fig. 1). This group is efficiently quenched by a 2,4-dinitrophenyl (Dnp) group linked to the side-chain of a Lys residue. The development of substrates cleaved by the enzyme at neutral pH can provide useful information for the design of peptide pro-drugs releasing anticancer drugs in the pericellular space of tumor cells.

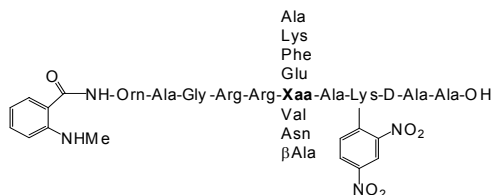


Fig. 1. General structure of the studied FRET peptides.

Results and Discussion

Quenching efficiency $[(F_0-F)/F_0]$ reflecting the flexibility of designed substrates was calculated from the fluorescence intensity of the donor (Nma) in the absence (F_0) and in the presence (F) of the acceptor (Dnp). Results show that only the β Ala⁶ peptide was characterized by a relatively low quenching efficiency ($\sim 83\%$) compared to the high values showed by other peptides ($\sim 96\%$), suggesting that the introduction of this residue into the peptide chain decreases the flexibility of the substrate with subsequent increase of the average distance between Nma and Dnp groups.

Peptide hydrolysis by cathepsin B was monitored by measuring the increase of fluorescence at 440 nm following excitation of solutions of each substrate at 340 nm. Time courses of the enzyme-mediated hydrolysis of the FRET peptides at 37°C at two different pHs are shown in Figure 2; the corresponding kinetic parameters are summarized in Table 1. Data show as Ala and Phe residues in the Xaa position yield preferred substrates for cathepsin B at both tested pH values. By contrast, substrates

with a negatively charged amino acid (Glu), a polar uncharged amino acid (Asn) or a positively charged amino acid (Lys) at the same position were poorly hydrolyzed by cathepsin B at pH 5.0 due to either reduced k_{cat} or increased K_m , or both. Similarly, the Val⁶ peptide was poorly hydrolyzed by the enzyme at pH 5. At neutral pH all of the tested peptides (Glu⁶, Asn⁶, Lys⁶ and Val⁶) were poor substrates for cathepsin B. The introduction at the Xaa position of the β Ala residue was detrimental for the enzyme activity at both pH values.

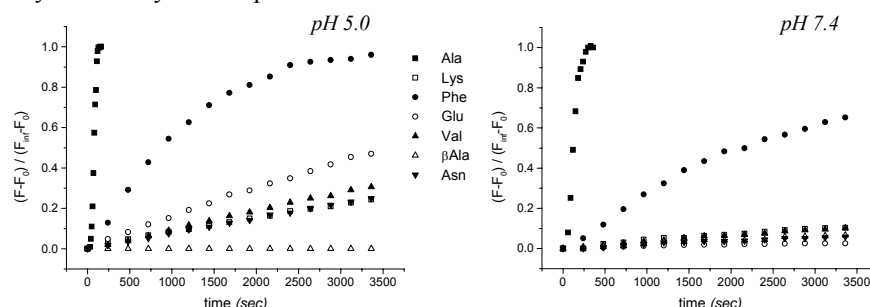


Fig. 2. Time-courses of FRET peptides hydrolysis by bovine cathepsin B at different pHs.

The cleavage sites were then determined by HPLC analysis after incubation of each peptide with cathepsin B at 37°C for 1 hr in the two tested buffers. All chromatograms, with the exception of those related to the Phe⁶ peptide, contained only two new peaks in addition to that of the remaining substrate. ESI-MS analysis showed that the cleavage site was at the **Xaa-Ala** bond. The Phe⁶ peptide was also cleaved at the Arg-Xaa bond, even if it was preferentially hydrolyzed at the Xaa-Ala bond. This double cleavage is likely due to the longer reaction time as confirmed by further HPLC analysis.

Table 1. Kinetic parameters of peptides hydrolysis by bovine cathepsin B at different pHs.

Peptide	pH 5.0			pH 7.4		
	K_m (μM)	k_{cat} (sec^{-1})	k_{cat}/K_m ($mM \cdot sec^{-1}$)	K_m (μM)	k_{cat} (sec^{-1})	k_{cat}/K_m ($mM \cdot sec^{-1}$)
Ala ⁶	16.2	10.3	635.8	4.4	1.44	327.2
Lys ⁶	3.3	$9.0 \cdot 10^{-3}$	2.7	n.d.	n.d.	n.d.
Phe ⁶	30.0	0.26	8.7	48.0	0.36	7.5
Glu ⁶	20.7	$4.0 \cdot 10^{-2}$	1.9	n.d.	n.d.	n.d.
Val ⁶	7.1	$1.3 \cdot 10^{-2}$	1.8	n.d.	n.d.	n.d.
Asn ⁶	14.3	$1.4 \cdot 10^{-2}$	0.9	n.d.	n.d.	n.d.
β -Ala ⁶	n.d.	n.d.	n.d.	n.d.	n.d.	n.d.

References

1. Aronson, N. N. and Barrett, A. J. *Biochem. J.* **171**, 759-765 (1978).
2. Illy, C., et al. *J. Biol. Chem.* **272**, 1197-1202 (1997).
3. Musil, D., et al. *Embo J.* **10**, 2321-2330 (1991).
4. Nagler, D. K., et al. *Biochemistry* **36**, 12608-12615 (1997).

Ghrelin Attenuates Burn-induced Cachexia

**Ambikaipakan Balasubramaniam, Rashika Joshi, Chunhua Su, Lou
Ann Friend and James H. James**

*Department of Surgery, University of Cincinnati Medical Center and Shriners Hospital for
Children, Cincinnati, OH 45267, USA*

Introduction

Major burn injury, the most severe form of trauma, results in increased production of catabolic hormones and inflammatory cytokines, and lower levels of anabolic hormones, causing prolonged hypermetabolism, loss of lean body mass, and muscle wasting. Treatments to date to reduce this debilitating body protein loss have employed anabolic hormones, such as insulin, growth hormone, IGF-I or anabolic steroids [1]. Recently, a 28-residue octanoylated peptide, ghrelin [2], was isolated from stomach. After peripheral administration, ghrelin stimulates appetite via upregulating the synthesis and release of the hypothalamic orexigenic hormones NPY and AGRP, and also causes release of growth hormone, thus increasing IGF-I production. Daily injection of ghrelin increases body mass in normal rodents [3,4] and it has been suggested that treatment with ghrelin may be of value in patients with cachectic conditions [5]. Our initial studies in rats 7–10 days after a 30% surface area burn injury revealed that ghrelin expression in stomach was significantly reduced compared to controls. In other studies, we treated burn-injured rats overnight using implanted osmotic pumps with either saline, or ghrelin at two different doses (2.4 mg/kg or 24 mg/kg); EDL muscles were isolated to measure protein breakdown rates *in vitro* [6]. Compared to saline, ghrelin at either dose significantly inhibited protein breakdown to a comparable degree. We therefore hypothesized that treatment with exogenous ghrelin might reduce burn-induced tissue wasting by beneficially altering either metabolism, feeding, or both.

Results and Discussion

To test this hypothesis, we measured food intake, body-weight and -composition in mice subjected either to a 20% surface area dorsal burn or to a sham procedure, and treated daily either with ghrelin (2.5 μ mol/kg/day, *sc.*) or saline-vehicle for 7 days (Burn-Ghrelin, Burn-Saline, Sham-Ghrelin and Sham-Saline, *n* = 10–12 per group – Fig. 1). Ghrelin significantly increased both the body weight and the food intake over 7 days in both sham and burn groups compared to respective controls. When ghrelin injections were suspended on days 7, 8 and 9 after burn, the Burn-Ghrelin animals lost all the weight gained on days 1–7, but regained weight after ghrelin injections resumed on days 10 to 15. In contrast, during the 3 day non-treatment period, the Sham-Ghrelin group lost only part (< 50%) of the weight previously gained, and regained the lost weight again when injections resumed. Although Burn-Saline mice lost body weight over 14 days (*p* < 0.02), ghrelin treatment prevented this loss. Ghrelin caused significantly greater weight gain in sham-burned mice compared to burned mice (*p* < 0.05), suggesting that ghrelin was able to partially counteract the anorexigenic and catabolic signals after burn injury. Ghrelin-treated mice had greater fat stores than saline-treated controls. These observations suggest that exogenous ghrelin is a powerful “on-off switch” to alter body mass and composition after burn injury in rodents. These observations also

suggest that ghrelin retains its ability to favorably alter both the peripheral anabolic signals and the central energy homeostasis system after thermal injury. It may be feasible therefore to develop novel therapies based on ghrelin to combat cachexia caused burn injury and possibly by other conditions such as cancer, AIDS and sepsis.

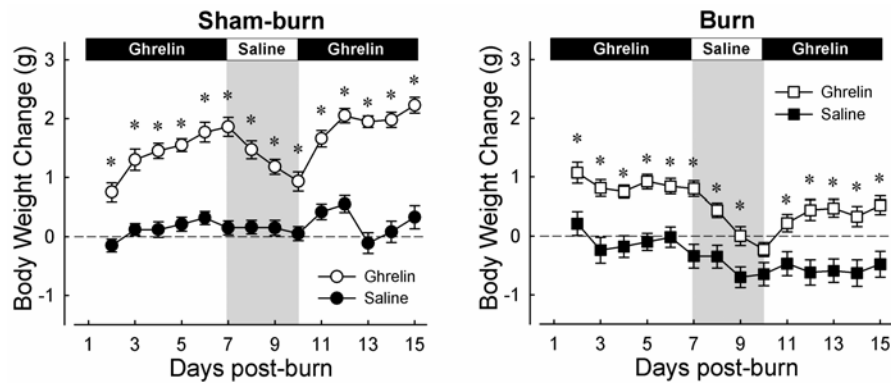


Fig. 1. Ghrelin ($2.5 \mu\text{mol/kg/day,sc}$) significantly enhanced the body weight in both Sham (Left) and Burn (Right) groups during the first seven days, with the Sham group exhibiting a greater increase than the Burn group. On stopping ghrelin treatment during days 7, 8 and 9, Sham group lost only 50% of the gained weight, whereas the Burn group lost all the gained weight. Both groups regained the lost weight on restarting ghrelin treatment during days 10 to 15. The Burn-Saline group continued to lose body weight throughout the study compared to Sham-Saline group.

Acknowledgments

The work was supported in part by a grant from Shriners Hospital for Children.

References

1. Herndon, D. N. and Tompkins, R. G. *Lancet* **363**, 1895-1902 (2004).
2. Korbonits, M., Goldstone, A. P., Gueorguiev, M. and Grossman, A. B. *Front Neuroendocrinol.* **25**, 27-68 (2004).
3. Tschöp, M., Smiley, D. L. and Heiman, M. L. *Nature (Lond.)* **407**, 908-913 (2000).
4. Wren, A. M., et al. *Diabetes* **50**, 2540-2547 (2001).
5. Inui, A. *Nat. Rev. Neurosci.* **2**, 551-560 (2001).
6. Fang, C. H., Li, B. G., Wang, J. J., Fischer, J. E. and Hasselgren, P. O. *Am. J. Physiol.* **275**, R1091-R1098 (1998).

High Affinity High Specificity $\alpha 4\beta 1$ Integrin Targeting Peptidomimetics for Lymphoid Cancers

**Li Peng¹, Ruiwu Liu¹, Xiaobing Wang¹, Jan Marik¹, Yoshikazu Takada²
and Kit S. Lam¹**

¹*Department of Internal Medicine; ²Department of Dermatology; UC Davis Cancer Center,
University of California Davis, 4501 X Street, Sacramento, California 95817, USA*

Introduction

Peptides have attracted wide interest as cancer targeting agents because of their favorable pharmacokinetics and rapid tumor uptake. Peptides are chemically stable, easy to derivatize, and proteolytically stable if D-amino acids are used [1]. The combinatorial peptide libraries are important sources of novel cancer specific peptides. The one-bead one-compound (OBOC) combinatorial library method offers a powerful technique to identify and optimize cancer-specific ligands [2]. OBOC libraries can incorporate D-amino acids, unnatural amino acids, and small molecule moieties, making the final ligands proteolytically more stable and with favorable pharmacokinetics.

$\alpha 4\beta 1$ integrin is involved in inflammation, cancer development, and metastasis. It prevented malignant B-CLL (chronic lymphocytic leukemia) cell apoptosis by binding to fibronectin [3]. $\alpha 4\beta 1$ integrin on lymphoma cells promoted dissemination in distal organs and facilitated tumor cells extravasation [4]. Therefore, $\alpha 4\beta 1$ integrin may represent an excellent target for imaging and treatment of lymphoid malignancies.

Here we report on the identification of high-affinity ligands of $\alpha 4\beta 1$ integrin from a focused OBOC peptidomimetic combinatorial library using a high stringency cell-based screening method, and the application in imaging of $\alpha 4\beta 1$ -positive lymphoid cancers.

Results and Discussion

A 1568-membered focused OBOC peptidomimetic library based on the LDV binding motif (Fig. 1) was synthesized on TentaGel S NH₂ resin using a bilayer-bead approach [5], in which only testing compounds were displayed on bead surface. An increasing amount of known $\alpha 4\beta 1$ antagonist was included into screening solution to compete with the interaction between the immobilized library compounds on beads, until the top candidates were distinguished in the library. We screened approximately 75,000 beads with Jurkat cells ($\alpha 4\beta 1$ integrin-positive) (3×10^5 /ml) in complete RPMI medium containing 500 μ M BIO-1211, which is one of the best $\alpha 4\beta 1$ antagonists reported in the literature [6]. Twelve positive beads were selected and submitted for structure sequencing. Six beads contained identical sequences named 2A, and the rest were another sequence called 1A (Fig. 1). This was not surprising because a large excess of beads were screened in this rather small highly-focused library. Binding affinities (IC₅₀s) of the ligands were studied in a Jurkat cell adhesion assay by inhibiting the $\alpha 4\beta 1$ -mediated cell adhesion to CS-1 peptides, which is the binding motif of fibronectin to $\alpha 4\beta 1$. The IC₅₀ of BIO-1211 was determined to be 0.3 ± 0.1 (SD) nM, similar to that reported in the literature [5], whereas the IC₅₀s of ligand 2A and 1A were found to be 2.0 ± 1.4 (SD) and 22 ± 18 pM. The binding affinity was greatly improved with ϵ -6-[(2E)-1-oxo-3-(3-

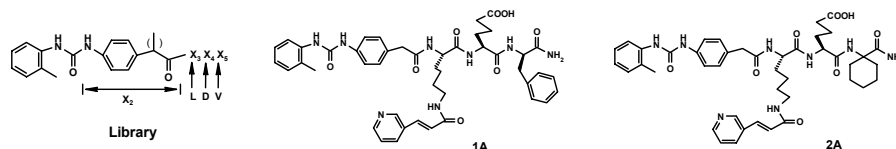


Fig. 1. Structures of the focused OBOC library for $\alpha 4\beta 1$ targeting and ligands, 1A, and 2A.

pyridinyl-2-propenyl)-L-Lysine at L position, α -aminohexanedioic acid at D position, and 1-amino-1-cyclohexane carboxylic acid or D-Phe at V position.

The tumor targeting potential of 2A ligand was first evaluated for binding to $\alpha 4\beta 1$ -positive tumor cell lines. Fluorescent microscopies confirmed strong and specific binding to these cells. *In vivo* optical imaging studies of mouse xenografts bearing bilateral Molt-4 T-leukemia ($\alpha 4\beta 1$ -positive) and A549 non-small cell lung cancer ($\alpha 4\beta 1$ -negative) tumors were used to investigate the lymphoma targeting efficiency of the 2A ligand in live animals. The near infrared imaging probe was prepared by pre-incubating biotinylated 2A with streptavidin-Alexa680, which was *i.v.* injected into nude mice. Whole-body *in vivo* scanning demonstrated a high-intensity near-infrared signal from the Molt-4 tumor, whereas no signal was observed from the negative control A549 tumor (Fig. 2). Control experiment using an unrelated linear peptide (TPNNEIDSFVKSGDF) showed no uptake in either tumor.

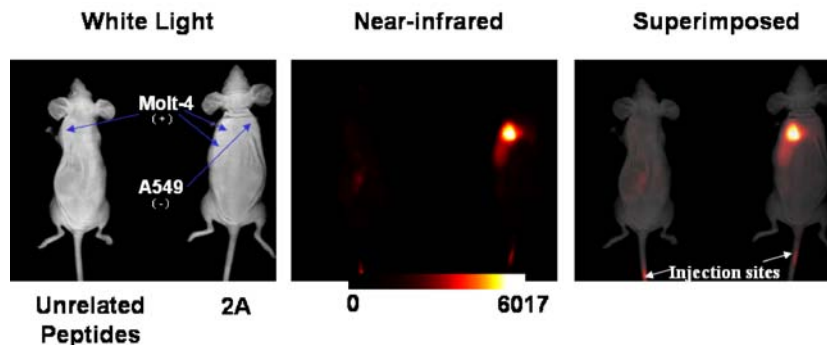


Fig. 2. *In vivo* optical imaging of Molt-4 lymphoma with 2A.

Acknowledgments

This work was supported by NIH R33CA-86364 and NIH R33CA-99136.

References

- Okarvi, S. M. *Med. Res. Rev.* **24**, 357-397 (2004).
- Lam, K. S., *et al.* *Nature* **354**, 82-84 (1991).
- de la Fuente, M. T., *et al.* *Leukemia* **13**, 266-274 (1999).
- Holzmann, B., Gossler, U. and Bittner, M. *Curr. Top. Microbiol. Immunol.* **231**, 125-141 (1998).
- Liu, R., Marik, J. and Lam, K. S. *J. Am. Chem. Soc.* **124**, 7678-7680 (2002).
- Lin, K., *et al.* *J. Med. Chem.* **42**, 920-934 (1999).

Highly *N*-Methylated Somatostatin Analogs: Synthesis, Biological Activity and Structure-Activity Relationship Studies

Eric Biron¹, Daniel Langenegger², Daniel Hoyer² and Horst Kessler¹

¹Department Chemie, Lehrstuhl II für Organische Chemie, Technische Universität München, Garching, D85747, Germany; ²Novartis Institutes for Biomedical Research, Novartis Pharma AG, CH-4002 Basel, Switzerland

Introduction

Somatostatin, a cyclic tetradecapeptide (NH₂-AG-c[CKNFFWKTFSC]-OH), is a major endocrine hormone with multiple physiological actions which are modulated by one or more of the five known G-protein-coupled receptor subtypes: sst1-sst5 [1]. The biological role as well as the cellular distribution of each receptor subtypes is far from being completely understood. Therefore, the search for synthetic analogs which exhibit selective affinities for the five receptors subtypes is of considerable basic and therapeutic interest. In the past, conformational restriction of the side chains and the peptide backbone has yielded the most interesting results. On the other hand, *N*-methylamino acids are known to increase pharmacologically useful parameters such as membrane permeability and proteolytic stability [2]. Therefore, we were interested in the potential effects of one or many *N*-methylation of peptide bond NH groups on the binding affinity of some somatostatin analogs.

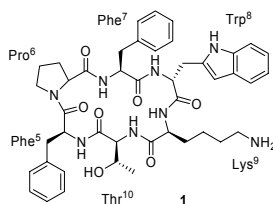


Fig. 1. *Veber* peptide, L-301-306 [3].

Results and Discussion

The somatostatin cyclopeptidic analog *Veber* peptide (c[Phe⁵-Pro⁶-Phe⁷-DTrp⁸-Lys⁹-Thr¹⁰]) [3] was chosen to study the effects of one or many *N*-methylation on the structure and binding affinity of bioactive cyclic peptides since its structure, activity and selectivity are very well known and many test systems already exist. Full *N*^α-methyl scanning of the *Veber* peptide was aided by the introduction of *N*^α-methyl group during regular solid-phase peptide synthesis using an optimized Miller and Scanlan procedure [4]. Peptide synthesis was carried out on TCP-resin following standard Fmoc-SPPS. Coupling on resin-bound free *N*-methylamine was achieved with triphosgene [5]. Following cyclization, deprotection and purification by HPLC, a new series of 30 *N*-methylated *Veber* peptide analogs has been synthesized.

The binding affinity of all somatostatin analogs was screened by concentration-dependent displacement of [¹²⁵I]-Tyr³ Octreotide in rat cerebral cortex. These preliminary results showed that *N*-methylation on Phe⁷ is fatal for binding while it does not affect the affinity (pIC₅₀ >9) on Lys⁹ or Thr¹⁰. Lower affinity was observed with *N*-methylation on DTrp⁸, Phe⁵, Lys⁹ and Phe⁵ or DTrp⁸ and Lys⁹.

Table 1. Binding affinities of *N*-methylated analogs for cloned human *sst1* and *sst5* receptors

#	<i>N</i> ^α -Methylation	$K_d \pm \text{SEM (nm)}$		hSST-5/hSST-2
		hSST-2	hSST-5	
0	none	9.77 ± 0.05	15.14 ± 1.5	1.5
1	Thr ¹⁰	2.75 ± 0.09	8.13 ± 0.03	3.0
2	Lys ⁹	2.51 ± 0.11	6.46 ± 0.02	2.6
3	Phe ⁵	11.75 ± 0.04	5.25 ± 0.04	0.4
4	Trp ⁸	24.55 ± 0.02	45.71 ± 0.04	1.9
5	Lys ⁹ and Phe ⁵	10.96 ± 0.04	13.49 ± 0.04	1.2
6	Trp ⁸ and Lys ⁹	25.12 ± 0.13	40.74 ± 0.02	1.6
7	Trp ⁸ and Phe ⁵	54.95 ± 0.03	33.88 ± 0.01	0.6
8	Trp ⁸ , Lys ⁹ and Phe ⁵	61.66 ± 0.02	60.25 ± 0.04	1.0

The most active analogs were tested *in vitro* for their specific binding to the five human somatostatin receptors expressed in CHO cell lines. *N*-Methylated analogs **1-8** displayed high affinity for type 2 receptor but lower affinity for the other receptor types. *N*-Methylation of Lys⁹ in the critical DTrp-Lys motif yielded interesting results since almost every active analogs ($\text{pIC}_{50} > 7$) in the library are *N*-methylated at this position. The plane of the peptide bond between DTrp⁸ and Lys⁹ is roughly normal to the plane of the backbone ring. Therefore, *N*-methylation of Lys⁹ may be accommodated sterically without major disruptions to the conformation. *N*-Methylation of the peptide bond constrains the conformational space of the amino acid and eliminates the possibility of donor hydrogen bond formation from the amide linkage. A hydrogen bond between Phe⁷ and Thr¹⁰ is normally observed next to the β -bend conformation around DTrp⁸-Lys⁹. Surprisingly, *N*-methylation of Thr¹⁰ does not affect the active conformation and the affinity demonstrating that the hydrogen bond is not essential to stabilize the β -bend.

In summary, a new series of highly *N*-methylated Veber peptide analogs has been successfully synthesized using selective *N*-methylation on solid support during Fmoc-SPPS. No new receptor subtype selectivity has been observed but bioactivity was maintained in many cases. Bioavailability and proteolytic stability studies are underway to demonstrate that *N*-Methylation could be an interesting approach to improve pharmacological properties with retention of bioactivity. Studies to determine the effects of many *N*-methylation on the structure are also underway.

Acknowledgments

E.B. thanks the Alexander von Humboldt Foundation for a Postdoctoral Fellowship.

References

1. Patel, Y. C. *Front. Neuroendocrinol.* **20**, 157-198 (1999).
2. Fairlie, D. P., Abbenante, G. and March, D. R. *Curr. Med. Chem.* **2**, 654-686 (1995).
3. Veber, D. F., Freidlinger, R. M., Perlow, D. S., *et al.* *Nature* **292**, 55-58 (1982).
4. Miller, S. C. and Scanlan, T. S. *J. Am. Chem. Soc.* **119**, 2301-2302 (1997).
5. Falb, E., Yechezkel, J., Salitra, Y. and Gilon, C. *J. Peptide Res.* **53**, 507-517 (1999).

Highly Sensitivity FRET Substrate for Assay of HCV Protease

Xiaohu Tong, Ling Sheng, Xiaofen Zhong, Yi Tang, Junge Lu, Zhenjun Diwu and Anita Hong

AnaSpec Inc., 2149 O'Toole Ave., San Jose, CA 95131, USA

Introduction

The alarming spread of hepatitis C viral (HCV) infections and the consequences associated with chronic hepatitis C have resulted in a world-wide medical problem affecting 170 million patients [1]. The inhibition of HCV protease activity serves as an important method for preventing HCV infection caused by multiplication of the HCV virus. Although a fluorescence resonance energy transfer (FRET) depsipeptide, Ac-DED(Edans)EE- α Abu ψ [COO]ASK(DabcyI)-NH₂ (substrate **I**) is widely used for detecting HCV NS3/4A serine protease activity [2], its low sensitivity and short detection wavelength limit its use for high throughput screening.

We have recently developed a sensitive FRET HCV protease substrate for high throughput screening of HCV protease inhibitors. This new FRET substrate, Ac-DE-Dap(QXLTM520)EE- α Abu ψ [COO]ASC(5-FAMsp*)-NH₂ (substrate **II**), incorporates 5-FAM (donor) and QXLTM520 (quencher). QXLTM520 is proven to be the most effective quencher for fluoresceins such as FAM and FITC. In comparison to substrate **I**, this new FRET peptide offers several advantages.

Results and Discussion

Substrate **II** was synthesized by a combination of Fmoc solid phase and solution phase synthesis methods. The resin used was Rink amide MBHA resin. All couplings, including Dap(Mtt), were performed with fourfold excess of activated amino acids over the resin-free amino groups, using the ratio of Fmoc-amino acid:HBTU:HOBt:DIEA (1:1:1:2). L-(+)-lactic acid was activated using DIC:HOBt (1:1). Esterification of Abu to the free hydroxyl of lactic acid was performed using Fmoc-Abu-F in the presence of a catalytic amount of DMAP. At the end of the assembly, the peptide-resin was treated with 1% TFA and 3% TIPS in DCM to remove the Mtt group. QXLTM520-OH was coupled to β -amino group of Dap with DIC:HOBt. Complete deprotection of the peptide was performed with TFA: water:TIPS (93:4:3) for 2 h to obtain crude Ac-DE-Dap(QXLTM520)EE- α Abu ψ [COO]ASC-NH₂ (**III**). Peptide **III** was incubated with 5-FAMsp to obtain crude substrate **II**. The crude peptide was purified by RP-HPLC using as eluents (A) 50 mM ammonium acetate (pH 6.5), and (B) acetonitrile.

Substrate **II** peptide was derived from the sequence of the NS4A/ NS4B cleavage site (DEMEECASHL). In comparison with the sequence of substrate **I** peptide, Ac-Asp-Glu-Asp(Edans)-Glu-Glu- α Abu ψ [COO]-Ala-Ser-Lys(DabcyI)-NH₂, we have changed the Asp(Edans) to Dap(QXLTM520) and Lys(DabcyI) to Cys(5-FAMsp).

Compared to Edans, the extinction coefficient of 5-FAM is 13-fold higher and its fluorescence receives less interference from the short wave-length auto-fluorescence of drug candidates. Additionally, 5-FAM is much brighter and less sensitive to the environment than Edans. These characteristics of 5-FAM prompted us to design a more sensitive 5-FAM FRET peptide substrate for HCV NS3/4A protease. We developed the QXLTM520 to serve as a quencher for the 5-FAM. Its absorption spectrum perfectly overlaps with the emission spectrum of 5-FAM (Fig. 1).

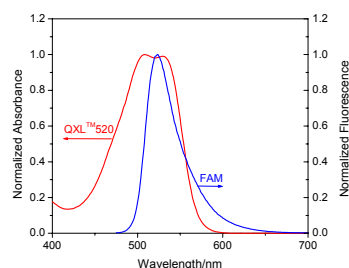


Fig. 1. Absorption of QXL™520 and 5-FAM.

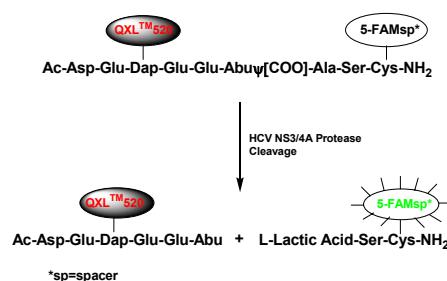


Fig. 2. Scheme of the proteolytic cleavage of substrate **II** by HCV NS3/4A protease.

Additionally, QXL™520 is a hydrophilic compound unlike Dabcyl which is hydrophobic. This property of QXL™520 increases the solubility of the peptide substrate. The problem caused by the hydrophobic nature of many fluorescent donors and quenchers is thus alleviated.

In the intact substrate **II** FRET peptide, the fluorescence of 5-FAM is quenched by QXL™520 (Fig. 2). Upon cleavage, the fluorescence of 5-FAM is recovered and can be continuously monitored at Excitation/ Emission = 490 nm/520 nm over time.

The substrate **II** peptide showed significantly less inner filter effect than substrate **I** peptide. The new 5-FAM/QXL™520-based substrate **II** has inner filter effect < 5% when the peptide concentration is <50 μM . The inner filter effect is the phenomenon in which light emitted by the fluorophore is absorbed by nearby quencher on intact substrates or cleaved products, so that only a fraction of its fluorescent signal can be detected by a fluorometer. When the substrate **I** peptide concentration reaches 20 μM , 50% of Edans's fluorescence is quenched. The inner filter effect significantly reduces the accuracy of enzymatic kinetic parameters (K_m and K_{cat}).

The enzyme detection dynamic range of substrate **II** is from 8.27 to 0.064 pmole, while that of substrate **I** is from 8.27 to 0.52 pmole. These results demonstrate substrate **II** is eight times more sensitive than substrate **I**.

Substrate **II** has smaller K_m and higher K_{cat}/K_m value compared to substrate **I** (Table 1). Individual kinetic parameters (K_m and K_{cat}) are determined over a substrate concentration range of 0-100 μM and calculated by double reciprocal plots.

Table 1. The comparison of kinetic parameters of two FRET substrates ^a

	$K_m(\mu\text{M})$	$K_{cat}(\text{min}^{-1})$	$K_{cat}/K_m(\text{M}^{-1}\text{s}^{-1})$
Substrate II	3.2	2.7	14127.3
Substrate I	69.4	16.5	3961.0

^a HCV NS3/4A protease is incubated with the substrates in 50 mM Tris, pH 7.5, 30 mM DTT, 1% Chaps, 15% glycerol at room temperature.

References

- Wesley, A. and Alter, M.J. *Semin. Liver Dis.* **20**, 1-16 (2000).
- Taliani, M., et al. *Anal. Biochem.* **240**, 60-67 (1996).

Identification and Characterization of Synthetic Peptide Substrates and Small Molecule Inhibitors of Non Receptor Tyrosine Kinase Etk

Lauren Lee^{1,3}, Ruiwu Liu^{1,3}, Nianhuan Yao^{1,3}, Jan Marik^{1,3}, Ching-Yi Hsieh^{1,2,3}, Hsing-Jien Kung^{2,3} and Kit Lam^{1,3}

¹Division of Hematology and Oncology, Department of Internal Medicine; ²Department of Biological Chemistry; ³UC Davis Cancer Center, University of California Davis, 4501 X Street, Sacramento, CA 95817, USA

Introduction

Etk is a member of the Btk family of tyrosine kinases that has a modular structure consisting of N-terminal PH domain, SH3, SH2, and C-terminal catalytic domain [1]. First identified in LNCaP prostate cancer cells, Etk is widely expressed in hematopoietic, epithelial, and endothelial cells [2]. Previous studies show that Etk is involved in several networks of signaling cascades through its PH domain. So far Etk is considered to be a downstream effector of phosphatidylinositol 3'-kinase (PI3-kinase) during interleukin 6 (IL-6) induced neuroendocrine differentiation, PI3 kinase and upstream signaling molecule of Pak1 (p21 activator kinase) in cell proliferation and anchorage dependent growth pathway [1]. In other studies, Etk has been demonstrated to function as a link between Src and STAT3 [3]. Taken together, Etk is involved in a network of complicated signaling pathways with possible overlapping upstream and downstream effectors.

In this study, a random peptide library was screened to identify synthetic peptide substrates of Etk [4]. Further, several peptidomimetic compound libraries were also screened for ligands that bind to Etk [5]. Using the short peptides as substrate, Etk binding peptidomimetic ligands were tested for Etk kinase inhibition activity. These Etk substrates and inhibitors will serve as essential reagents in elucidating the effect of Etk kinase activity in cellular processes including cancer development. Moreover, Etk inhibitors may serve as potential lead compounds in the development of therapeutic agents for prostate cancer.

Results and Discussion

Peptide substrate identification: 17 peptide substrates for tyrosine kinase Etk were identified from screening random peptide libraries using an on-bead ³³P-phosphorylation assay [4]. From these sequences (Table 1), XXI/VYXXK, XXI/YXXY, and SSI motifs were found. The kinetic parameters of two of the best substrates, TSFYGRH and WKVYEKH, were determined and were found to have a Km of 119 and 151 µM and Vmax of 0.39 and 0.907 nmol/min/mg, respectively.

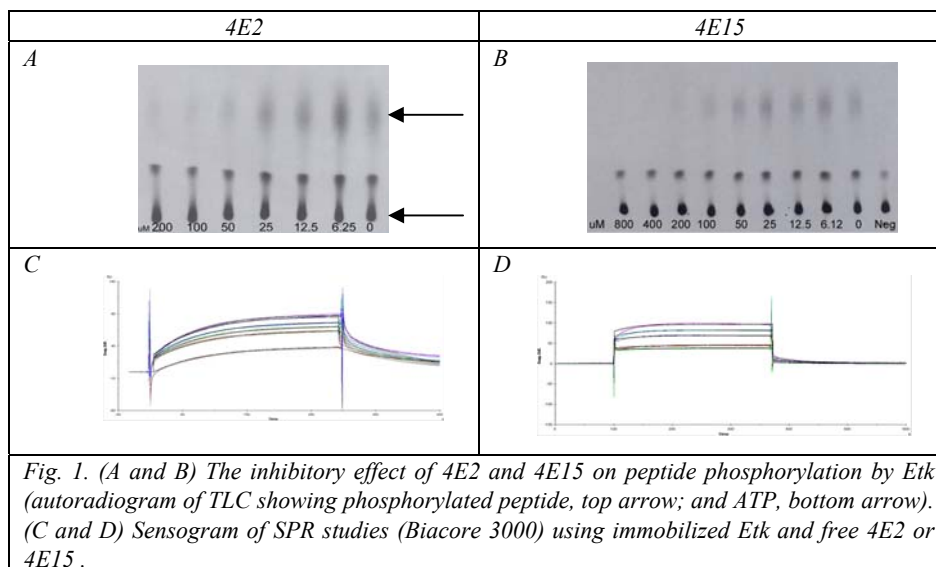
Table 1. Peptide substrates for Etk identified from OBOC peptide libraries

SSLYWHK	DSWYKYY	KHLYYEK	TSFYGRH	VGIYTRH
YKVYSSI	DNAYYYF	AQIYTMR	KHLYATK	
YAEYAYY	GSHYRWD	RAFYDVF	DMMYYVK	
WSVYMYM	NRAYYRL	RFHYQWL	WKVYEKH	

Peptidomimetic ligands and inhibitors: Several peptidomimetic and small molecule libraries were screened for Etk binding ligands. The binding motif showed strong

consensus towards the presence of hydrophobic amino acid residue with a thiophene or benzene group. Some of these Etk ligands were evaluated for Etk kinase inhibition activity. Two of the ligands, 4E2 and 4E15, representing each of the consensus motifs, exhibited some Etk kinase inhibition activity (Fig. 1A and B).

The IC₅₀ of the two compounds was estimated to be at the 25 μ M and 50 μ M range. Surface plasmon resonance (SPR, Biacore) studies were also performed using immobilized Etk. The study revealed a K_D of 40.5 μ M and 14.4 μ M for 4E2 and 4E15, respectively (Fig. 1C and D).



Acknowledgment

The work is funded by NIH grant CA098116.

References

1. Bagheri-Yarmand, R., Mandal, M., Taludker, A. H., Wang, R., Vadlamudi, R. K., Kung, H.-J. and Jumar, R. *J. Biol. Chem.* **276**, 29403-29409 (2001).
2. Qui, Y., Robinson, D., Pretlow, T. and Kung, S. -J. *Proc. Natl. Acad. Sci. USA* **95**, 3644-3649 (1998).
3. Tsai, Y. -T., Su, Y., Fang, S., Huang, T., Qui, Y., Jou, Y., Shih, H., Kung, S. -J. and Chen, R. -H. *Mol. Cell. Biol.* **20**, 2043-2054 (2000).
4. Wu, J., Ma, Q. N. and Lam, K. S. *Biochem.* **33**, 14825-14833 (1994).
5. Lam, K. S., Salmon, S. E., Hersch, E. M., Hruby, V. J., Kazmiersku, W. M. and Knapp, R. J. *Nature* **354**, 82-84 (1991).

Identification of High Affinity Anti-MCP-1 Antibodies using Synthetic Proteins

Marian Kruszynski¹, Ping Tsui¹, Jinquan Luo¹, Anuk Das¹, Nicole Stowell¹, Michael Brigham-Burke¹, Jennifer F. Nemeth¹, Li Yan¹, Heena Beck¹, Jil Carton¹, Raymond Sweet¹, George A. Heavner¹, Michael Bardroff², Daniela D. Ducata², Ute Jager² and Robert Rauchenberger²

¹Centocor, Inc., Radnor, PA 19087, USA; ²MorphoSys AG, D-82152 Martinsried, Germany

Introduction

Human Monocyte Chemoattractant Protein 1 (MCP-1, CCL2), a 8.6 kDa protein, is implicated in a number of diseases including atherosclerosis, rheumatoid arthritis, chronic obstructive pulmonary disease, and cancer. To develop a therapeutic antagonist against MCP-1, we synthesized a biotinylated human MCP-1 analogs, hMCP-1[Ile⁴¹], for isolation and affinity maturation of human Fabs using MorphoSys antibody phage display technology, HuCAL GOLD[®] [1]. In contrast to chemical biotinylation of synthetic hMCP-1[Ile⁴¹] [2] the site-specific, synthetic, MCP-1[Ile⁴¹] analogs were homogeneous and retained full activity. The site-specific biotinylated MCP-1 analogs facilitated selection, maturation and characterization of potent neutralizing antibodies by phage display.

Results and Discussion

The nine lysine residues present in MCP-1 were considered as sites for biotinylation. Figure 1 shows the side chains of MCP-1 residues that are important for function and the exposed Lys⁶⁹ that is not required for activity.

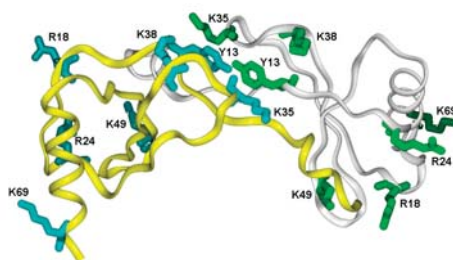


Fig. 1. Ribbons representation of hMCP-1 dimer based upon IDOL.PDB.

Lys⁷⁵ is disordered in the crystal structure and not shown. The lysines, Lys³⁵, Lys³⁸, and Lys⁴⁹ were excluded from modification because of their biological importance. The lysines, Lys¹⁹, Lys⁴⁴, Lys⁵⁶, and Lys⁵⁸ are in the vicinity of the active surface and were also excluded to minimize potential disruption of MCP-1 function. Lysines, Lys⁶⁹ and Lys⁷⁵ were chosen for biotinylation. A hydrophilic spacer of four ethyleneoxy units (PEG4) was inserted between the biotin and the ε-amino group of lysine residue. The analogs were synthesized using standard Fmoc chemistry of SPPS then oxidized and purified as described previously [2]. Reversed phase HPLC and a monomeric avidin affinity column were used for purification. These synthetic analogs were similar in activity to recombinantly produced human

MCP-1. Their ability to induce Ca^{2+} mobilization from internal stores as a result of CCR2 activation on THP-1 cells is compared in Figure 2A, and their competition with ^{125}I -rhMCP-1 binding to the CCR2 receptors on THP-1 cells is shown in Figure 2B:

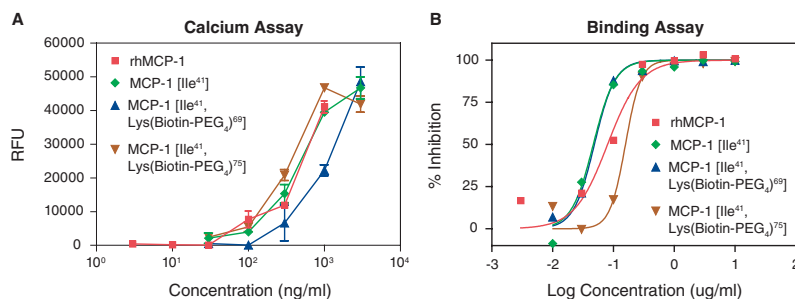


Fig. 2. Calcium mobilization assay (A); Competitive radio-ligand binding (B).

The MorphoSys HuCAL GOLD[®] library [1] was used to generate highly potent MCP-1 neutralizing antibodies. Antibodies selected from the primary library were further engineered by CDR cassette diversification to improve affinity and activity. The synthetic, biotinylated MCP-1 was used for all phage selections and for Fab characterization. Fabs with activities in the low pM range were isolated by this process. Figure 3 shows the over 2 log improvement for inhibition of receptor binding for an affinity matured Fab relative to the parental Fab from the primary library.

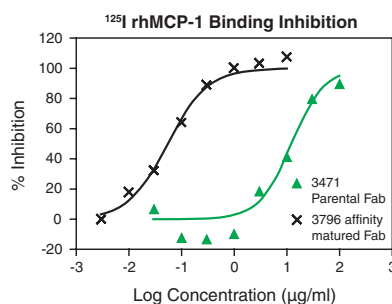


Fig. 3. Inhibition of rhMCP-1 binding by parental and affinity matured Fab.

In conclusion, two site-specific biotinylated MCP-1 analogs, [Ile⁴¹, Lys(Biotin-PEG₄)⁶⁹] and [Ile⁴¹, Lys(Biotin-PEG₄)⁷⁵], were synthesized and found to have comparable activities to rhMCP-1. Synthetic analogs of MCP-1 were used to identify highly potent and selective anti-MCP-1 antibodies using phage display. This study demonstrates the utility of chemical synthesis for production of small proteins with site-specific modifications that cannot be achieved by recombinant expression systems.

References

1. Kretzschmar, T. and von Ruden, T. *Curr. Opin. Biotech.* **13**, 598-602 (2002).
2. Kruszynski, M., et al. *J. Peptide Sci.* **12**, 25-32 (2006).

Mapping Cell Binding using Collagen III “Toolkit”

Nicolas F. Raynal, Tony Peachey and Richard W. Farndale

*Department of Biochemistry, University of Cambridge, Downing Site, Cambridge CB2 1QW,
UK*

Introduction

The triple-helical domains of the collagens interact with both cell-surface receptors and extracellular matrix proteins. Work over the past 20 years has produced indications that these interactions are specific, relying upon the sequence of collagen as well as on its triple-helical three-dimensional structure. The triple-helical structure of collagen can be exploited in short collagen-like peptides by inserting a stretch of Gly-Pro-Hyp or Gly-Pro-Pro triplets before and after a specific collagen binding sequence; this is referred to as the “host-guest” strategy. Collagen-related peptides (CRPs) and GFOGER peptides [1] have been shown to induce platelet activation through GpVI [2] and to act as antagonists of platelet recognition of collagen through $\alpha 2\beta 1$ [3], respectively.

Results and Discussion

We have prepared a synthetic “toolkit” to allow us first to map and then define the collagen III motifs responsible for recognition of receptors and other proteins which bind collagen, and to probe for unknown collagen receptors. We have cut the 163-1196 collagen III sequence into 27-AA sequences with a 9-AA overlap which gives us 57 peptides. To ensure a triple helical structure, we use the “host-guest” strategy adding on each extremity the GPC-(GPP)₅- unit. We obtain in this way, GPC-(GPP)₅-(GXX')₉-(GPP)₅-GPC-NH₂ peptides of 63 AA. The peptides were synthesized by Fmoc chemistry on solid phase supports, purified by HPLC, and characterized by MALDI-TOF. Triple-helical peptides support several classes of cell adhesion, easily separated into divalent cation (Mg²⁺)-dependent and -independent components. Based on the known properties of GER and GPO motifs in supporting integrin $\alpha 2\beta 1$ and GpVI recognition, provisional assignment of receptor-specificity can be made for several of the sequences of interest (Table 1). We have found that GROGER is the best motif in Col III for recognition of $\alpha 2\beta 1$ integrins. Col III contains also GAOGER, GMOGER, and GLSGER as GER sequences but with a weaker binding. Regarding the GpVI recognition, our studies have shown that the motif GPOGPO (peptides 3, 9, 10, 31 and 57) is not sufficient to bind GpVI and the best combination in Col III is GPOxxxxxxxxGPOGPO (peptide 30). We have also seen that sequences without any GPO can strongly bind and might contain a new binding site. The total platelet adhesion has shown that new sequences present interest. These can be probed with receptor specific antibodies, to further identify the platelet receptors involved, and may form the basis for the identification of novel collagen receptors on platelets. These data cast further doubt on the authenticity of the sequence proposed to bind a new collagen receptor, TIII Collagen-Binding Protein since no adhesion was observed to its reported motif, KOGEOPK, found in peptides 27 and 28 [4].

This study demonstrates the utility of the Collagen III Toolkit for the identification of receptor and protein-binding sites within the collagens.

Table 1. Sequences of interest of Col III “Toolkit” and biological targets

Col III	Sequences	Targets
1	GPC (GPP) ₅ -GLAGYOGFAGPOGPOGTSGHOGSO- (GPP) ₅ GPC-NH ₂	GpVI
4	GPC (GPP) ₅ -GPSGPAGKDGESGRO GROGER GLOGPO- (GPP) ₅ GPC-NH ₂	$\alpha 2\beta 1$
5	GPC (GPP) ₅ -GERGLOGPOGIKGPAGIOGFOGMKGHR- (GPP) ₅ GPC-NH ₂	??
8	GPC (GPP) ₅ -GAOGPMGPR GAOGER GROGLOGAAGAR- (GPP) ₅ GPC-NH ₂	$\alpha 2\beta 1$
9	GPC (GPP) ₅ -GLOGAAGARGNDGARGSDQOGPOGPO- (GPP) ₅ GPC-NH ₂	?GpVI
13	GPC (GPP) ₅ -GPOGINGSOGGKGEMGPAGIOGAOGLM- (GPP) ₅ GPC-NH ₂	??
30	GPC (GPP) ₅ -GAOGLRGGAGPOGPEGGKGAAGPOGPO- (GPP) ₅ GPC-NH ₂	GpVI
31	GPC (GPP) ₅ -GAAGPOGPOGAAGTOGLQ GMOGER GGL- (GPP) ₅ GPC-NH ₂	GpVI + $\alpha 2\beta 1$
32	GPC (GPP) ₅ - GMOGER GGLGSOGPKGDKGEOGGOGAD- (GPP) ₅ GPC-NH ₂	$\alpha 2\beta 1$
38	GPC (GPP) ₅ -GEGGPQGVAGPOGGSGPAGPQGPQGVK- (GPP) ₅ GPC-NH ₂	?GpVI
39	GPC (GPP) ₅ -GPOGPQGVKGERGSOGGOGAAGFOGAR- (GPP) ₅ GPC-NH ₂	??
40	GPC (GPP) ₅ -GAAGFOGARGLOGPOGSNGNOGPOGPS- (GPP) ₅ GPC-NH ₂	?GpVI
43	GPC (GPP) ₅ -GDAGQOGKEKSGOGAQQGPOGAOGPLGIA- (GPP) ₅ GPC-NH ₂	??
50	GPC (GPP) ₅ -GPOGPVGPAGKSGDRGESGPAGPAGAO- (GPP) ₅ GPC-NH ₂	??

We propose that the Toolkit will find wider application in several different cellular and extracellular contexts.

Acknowledgments

We thank the Wellcome Trust, the Medical Research Council and the British Heart Foundation for the financial support.

References

1. Knight, C. G., Morton, L. F., Peachey, A. R., Tuckwell, D. S., Farndale, R. W. and Barnes, M. J. *J. Biol. Chem.* **275**, 35-40 (2000).
2. Emsley, J., Knight, C. G., Farndale, R. W., Barnes, M. J. and Liddington, R. C. *Cell* **100**, 47-56 (2000).
3. Knight, C. G., Morton, L. F., Onley, D. J., Peachey, A. R., Ichinohe, T., Okuma, M., Farndale, R. W. and Barnes, M. J. *Cardiovasc. Res.* **41**, 450-457 (1999).
4. Monnet, E., Depraetere, H., Legrand, C., Deckmyn, H. and Fauvel-Lafeve, F. *Thromb. Haemost.* **86**, 694-701(2001).

Modeling of α_1 Adrenergic Receptors: the Application in the Design of Selective α_{1B} -Adrenergic Antagonists

Slavica Erić¹, Tomaž Šolmajer^{2,3}, Marko Oblak², Miha Kotnik³ and Danica Agbaba¹

¹Faculty of Pharmacy, Department of Pharmaceutical Chemistry and Drug Analysis, Vojvode Stepe 450, 11000 Belgrade, Serbia and Montenegro; ²National Institute of Chemistry, Hajdrihova 19, 1000 Ljubljana, Slovenia; ³Lek Pharmaceuticals, d.d., Drug Discovery, Verovškova 57, 1526 Ljubljana, Slovenia

Introduction

Structure based drug design attempts to use the structure of proteins as a basis for designing new ligands by applying the principles of molecular recognition phenomenon.

When the drug design target is a receptor for which there is no experimentally determined three-dimensional structure, the different molecular modeling tools can be applied to construct models of the receptor site.

In this work, molecular modeling of α_{1b} -receptor has been performed in order to estimate the binding energies of α_1 adrenergic antagonists- α_{1b} adrenergic receptor interactions and to investigate the application of scoring functions in the design and QSAR studies of these drugs.

Results and Discussion

Molecular modeling of α_{1b} -receptor has been performed based on the multiple sequence alignment of bovine rhodopsin using Insight II software (Fig. 1) [1]. Docking simulations have been used to estimate the binding energies of complexes α_1 -adrenergic antagonists- α_{1b} -adrenergic receptor (Sybil software – Fig. 2 [2]).

The scoring functions obtained (Table 1) were correlated with the selectivity of the compounds investigated. The following correlations have been obtained:

For selectivity $\alpha_{1a/1b}$ ($S_{1a/1b}$): $S_{1a/1b} = -0.0932 +$

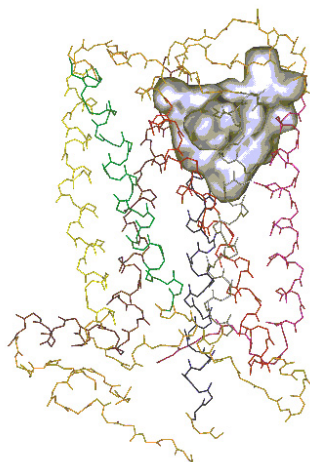


Fig. 1. View of the minimized average structure of α_{1b} AR.

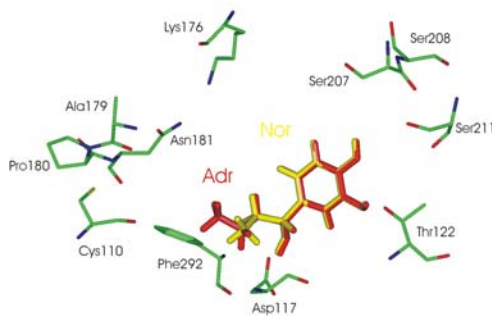


Fig. 2. View of the minimized complexes adrenaline-noradrenaline/ α_{1b} .

Table 1. Relative PMF scoring functions of adrenaline-noradrenaline/ α_{1b} adrenoreceptor complex and selectivities of data set [3]

Compound	PMF	$-\log Ki_{\alpha_{1a/1b}}$	$-\log Ki_{\alpha_{1b/1d}}$
Cyclazosine	-1.0769	-1.9652	1.3872
Abanoquile	1.5565	0.301	-0.301
REC-15/2615	1.7525	-0.8014	0.9393
AH-11110A	-1.2717	-1.5171	1.5528
Spiperon	0.4497	0.0633	1.4202

0.5255PMF ($R=0.7632$) (eq. 1).

For selectivity $\alpha_{1b/1d}$ ($S_{1b/1d}$): $S_{1b/1d} = 1.1066 - 0.3792PMF$ ($R=0.7061$) (eq. 2).

Potentially selective α_{1b} -adrenergic antagonists have been designed based on the cyclazosine as a lead compound. The correlation presented in equation 1 has been used for the prediction of selectivity $\alpha_{1a/1b}$ of proposed ligands (Fig. 3).

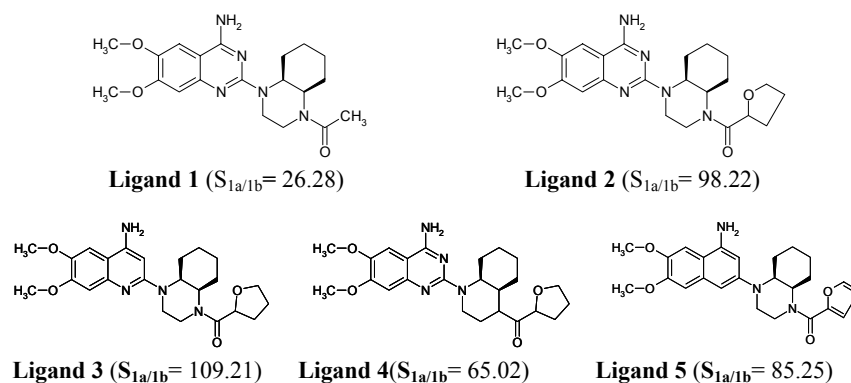


Fig. 3. The chemical structures of proposed ligands and predicted values of selectivity $\alpha_{1a/1b}$.

Acknowledgments

The work was funded by Ministry of Science and Environment Protection of Republic Serbia and Ministry of Education, Science and Sport of Republic Slovenia.

References

1. Insight II, Version 2000, Accelrys Inc., Cambridge, UK
2. TRIPOS Associates, Inc. St. Louis, Missouri, USA (1994). SYBIL Molecular Modeling Software Version 6.X.
3. Bremner, J., Coban, B., Griffith, R., Groenwoud, K. and Yates, B. *Bioorg. Med. Chem.* **8**, 201-209 (2000).

Characterization of the Interaction of HIP Analog Peptide with Heparin

Jing Wang and Dallas Rabenstein

Department of Chemistry, University of California, Riverside, CA 92507, USA

Introduction

Heparin has been used clinically as an anticoagulant for more than 70 years. The anticoagulant activity of heparin has been widely used in cardiopulmonary bypass surgeries. The protein protamine is administered as a heparin antidote after the surgery to halt substantial bleeding. However, side effects such as hypotension and thrombocytopenia are associated with protamine. Heparin interacting protein (HIP) and a peptide derived from HIP (HIP peptide) have been shown to recognize the same binding domain of heparin as antithrombin, indicating that they might have potential for neutralization of the anticoagulant activity of heparin [1]. In this paper, an analog of HIP peptide (Ac-SRGKARVRKVKDQTK-NH₂) was synthesized and its interaction with heparin was characterized in detail. The information gained from these studies will contribute to the design of new peptides to neutralize the anticoagulant activity of heparin, and provide insight to the interaction of peptides and proteins with heparin.

Results and Discussion

Synthetic peptides were synthesized using Fmoc methodology on a Millipore 9050 Plus peptide synthesizer. The C-terminus of the peptide was amidated and the N-terminus of the peptide was acetylated. The peptides were cleaved from the resin using the cleavage cocktail Reagent B (88% trifluoroacetic acid, 5.8% phenol, 2% triisopropylsilane and 4.2% water). After cleavage, the crude peptides were purified by RP-HPLC and identified by Mass Spectrometry. TOCSY, ROESY, BASHD-TOCSY and BASHD-ROESY proton NMR spectra were measured on a Varian INOVA 500 MHz spectrometer equipped with a triple-axis pulsed field gradient probe. TOCSY and BASHD-TOCSY experiments [2] were used to assign resonances to the type of amino acid by through-bond correlations; ROESY and BASHD-ROESY experiments were used to establish the sequence of the amino acids in the peptide by through space correlations. The resonances of free peptide and heparin bound peptide were completely assigned. The NH proton chemical shifts in the absence and presence of heparin, and the chemical shift differences for NH proton in the absence and presence of heparin are listed in Table 1. As shown in this table, the chemical shifts of three arginines and four lysines change more upon binding to heparin than other amino acids present in this peptide. Since lysine and arginine are the basic residues in the peptide, and heparin is a negatively charged polymer, chemical shift results indicate that the interaction of peptide with heparin is primarily by electrostatic interaction [3].

The composite chemical shift-pH titration curves for the C_εH₂ protons of the lysine residues of free peptide and heparin bound peptide are shown in Figure 1. The chemical shift titration curve reflects titration of the lysine ammonium groups. As shown in Figure 1, the chemical shift-pH titration curve is shifted to higher pH upon binding to heparin. Electrostatic interaction between the positive charges of

Table 1. Comparison of the chemical shifts of backbone amide NH resonances of peptide and heparin bound peptide

Residue	δ (Free Peptide)	δ (With Heparin)	$\Delta\delta^a$
Ser-1	8.346	8.321	-0.025
Arg-2	8.505	8.43	-0.075
Gly-3	8.385	8.358	-0.027
Lys-4	8.157	8.099	-0.058
Ala-5	8.283	8.274	-0.009
Arg-6	8.365	8.138	-0.227
Val-7	8.177	8.17	-0.007
Arg-8	8.466	8.289	-0.177
Ala-9	8.317	8.238	-0.079
Lys-10	8.379	8.159	-0.22
Val-11	8.159	8.127	-0.032
Lys-12	8.42	8.331	-0.089
Asp-13	8.331	8.32	-0.011
Gln-14	8.532	8.455	-0.077
Thr-15	8.317	8.307	-0.01
Lys-16	8.252	8.099	-0.153

$$\Delta\delta^a = \delta (\text{With Heparin}) - \delta (\text{Free Peptide})$$

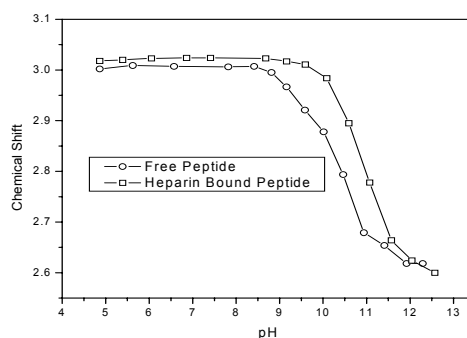


Fig. 1. Composite chemical shift-pH titration curves for the lysine $C_\epsilon H_2$ protons of peptide.

the lysine residues and the negative charges of the sulfate groups of heparin, results in the shift in the dissociation of the lysine ammonium groups shifting to higher pH.

Acknowledgments

The work was funded by an NIH grant HL56588

References

1. Liu, S., Zhou, F., Höök, M. and Carson, D. D. *Proc. Natl. Acad. Sci. USA* **94**, 1739-1744 (1997).
2. Kaerner, A. and Rabenstein, D. L. *Magn. Reson. Chem.* **36**, 601-607 (1998).
3. Hari, S. P., McAllister, H., Chuang, W., Christ, M. D. and Rabenstein, D. L. *Biochemistry* **39**, 3763-3773 (2000).

New Urotensin-II Analogs Modified at Position 4

Paolo Grieco¹, Pietro Campiglia¹, Alfonso Carotenuto¹, Teresa Lama¹,
 Ettore Novellino¹, Paolo Rovero² and Guido Iaccariono³

¹Department of Cell and Molecular Biology; ²Department of Biomedical Sciences; ³Graduate School of Oceanography; ⁴Department of Fisheries, Animal and Veterinary Sciences, University of Rhode Island, Kingston, RI 02881, USA

Introduction

Urotensin II (U-II), a potent vasoconstrictor, is found in diverse species, including human. U-II C-terminal cyclic heptapeptide portion (CFWKYCV), which is essential for the biological activity, has been highly conserved in evolution from fish to mammals. Several biological studies indicate that hU-II is the most potent mammalian peptide vasoconstrictor reported to date, and it appears to be involved in the regulation of cardiovascular homeostasis and pathology.

Recently, we have reported a superagonist (P5U) and a full antagonist (Urantide) at rat UT receptor with a partial activity at human receptor [1,2]. With the aim to shed light on the most important substructural features responsible for agonist/antagonist activity of these important peptides we decided to explore the position 4 replacing the Asp residue with several amino acids with different physiochemical properties (Fig. 1).

P5U	H-Asp-c[Pen-Phe-Trp-Lys-Tyr-Cys-]-Val-OH
Urantide	H-Asp-c[Pen-Phe-DTrp-Orn-Tyr-Cys-]-Val-OH
1	H-Cpa-c[Pen-Phe-Trp-Lys-Tyr-Cys-]-Val-OH
2	H-Cpa-c[Pen-Phe-DTrp-Orn-Tyr-Cys-]-Val-OH
3	H-Phe-c[Pen-Phe-Trp-Lys-Tyr-Cys-]-Val-OH
4	H-Nal-c[Pen-Phe-Trp-Lys-Tyr-Cys-]-Val-OH
5	H-Phe(NO ₂)-c[Pen-Phe-Trp-Lys-Tyr-Cys-]-Val-OH
6	H-Tic-c[Pen-Phe-Trp-Lys-Tyr-Cys-]-Val-OH

Fig. 1. Sequences of Urotensin-II analogs.

Results and Discussion

The compounds were synthesized by solid phase peptide synthesis method using Fmoc chemistry. Disulfide bridge was obtained by potassium ferricyanide oxidation, using the syringe pump method. All final products were purified by semipreparative RP-HPLC. Analytical HPLC indicated a purity greater than 98%, and molecular weights were confirmed by HRMS.

The peptides were tested for their ability to induce efficacious contractions in the rat isolated thoracic aorta. As reference compounds we used P5U and Urantide. Table 1 shows the biological activity of the hU-II-(4-11) analogs tested in this study.

Table 1. Biological activity of synthesized peptides

Compounds	pEC ₅₀	E _{max} (% hU-II)
P5U	9.6±0.07	97
Urantide	-	-
1	8.86	96
2	Antag.	-
3	9.23	96
4	8.91	94
5	8.2	81
6	9.8	98

We have highlighted that position 4 may be important to modulate the potency of peptides P5U and Urantide. The experiments currently in progress will evaluate additional compounds to define structural requirements at position 4.

Acknowledgments

The LC-MS and ¹H NMR spectral data were provided by Centro di Ricerca Interdipartimentale di Analisi Strumentale Università degli Studi di Napoli Federico II. The assistance of the staff is gratefully appreciated.

References

1. Grieco, P., Carotenuto, A., Campiglia, P., Zampelli, E., Patacchini, R., Maggi, C. A., Novellino, E. and Rovero, P. *J. Med. Chem.* **45**, 4391-4394 (2002).
2. Patacchini, R., Santicioli, P., Grieco, P., Rovero, P., Novellino, E. and Maggi, C. A. *British J. Pharmacol.* **140**, 1155-1158 (2003).

New Urotensin-II Analogs with a Constrained Trp-7 Side Chain

Alfonso Carotenuto¹, Paolo Grieco¹, Pietro Campiglia¹, Teresa Lama¹,
Ettore Novellino¹, Paolo Rovero² and Guido Iaccarino³

¹Dept. Chimica Farmaceutica e Toss., University of Naples-Federico II; ²Dept. Scienze Farmaceutiche, University of Florence; ³Dept. Medicina Clinica Scienze Cardiovascolari ed Immunologiche, University of Naples - Federico II, Italy

Introduction

Urotensin II (U-II), a potent vasoconstrictor, is found in diverse species, including human. U-II C-terminal cyclic heptapeptide portion (CFWKYCV), which is essential for the biological activity, has been highly conserved in evolution from fish to mammals. Several biological studies indicate that U-II is the most potent mammalian peptide vasoconstrictor reported to date, and it appears to be involved in the regulation of cardiovascular homeostasis and pathology.

Recently, we have reported the first superagonist (P5U) and full antagonist (Urantide) at UT receptor [1,2], and we have elucidated the structural bases of the agonist activity [3] and the agonist/antagonist functional switching of these ligands [4]. We found that a type II' β -hairpin structure was a common feature found in all the active peptides, regardless their agonist or antagonist activity. Furthermore, the side chain orientation of the Trp-7 was crucial for the agonist/antagonist switching. In particular, P5U and other UT receptor peptide agonists show a *trans* orientation at this side chain. In contrast, Trp-7 side chain is more flexible in Urantide, with increased amount of the *gauche*⁺ population. Hence, we designed and synthesized new compounds (Fig. 1), in which the Trp-7 side chain is constrained in a *gauche*⁺ conformation with a tetrahydro- β -carboline (Tbc) moiety. Furthermore, the Tbc moiety was substituted in position 8 with different groups.

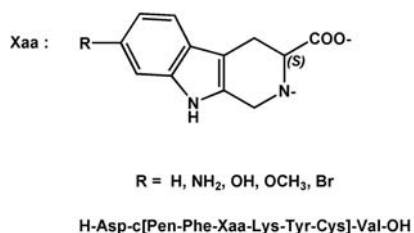


Fig. 1. Structures of the synthesized peptido-mimetics.

Results and Discussion

The new compounds were synthesized by solid phase peptide synthesis method using Fmoc chemistry. Unnatural amino acids with a tetrahydrocarboline moiety were synthesized as previously reported [5]. The disulfide bridge was obtained by potassium ferricyanide oxidation, using the syringe pump method. All final products were purified by semipreparative RP-HPLC. Analytical HPLC indicated a purity greater than 98%, and molecular weights were confirmed by HR-MS.

The dynamic behavior of the unsubstituted Tbc derivative (R = H) was investigated in detail by molecular dynamics simulations *in vacuum*. To this end, we

performed a 300ps unrestrained MD simulations, at 300K. The Discover algorithm (Accelrys) and the CVFF force field, were employed. The NMR structure of P5U, in which the Trp-7 residue was replaced by Tbc, was chosen as starting conformation. The stability of the β -II'-turn structure was followed monitoring the ϕ and ψ dihedral angle values of residues Tbc-7 and Orn-8. The ϕ and ψ dihedral angles defining the type II' β -turn are quite stable along all the simulation time, indicating that the β -II'-turn represents a local minimum, also for the new designed analogs. Furthermore, the spatial position of the Tbc indole ring was similar to that observed in the Urantide (Fig. 2).

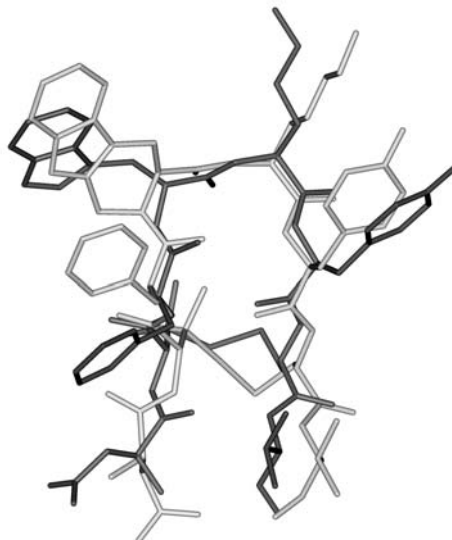


Fig. 2. A representative structure of the Tbc-7 derivative (grey) superimposed to a NMR representative structure of Urantide (black).

In conclusion, we have designed, synthesized, and analyzed by molecular dynamic simulation new peptido-mimetics that should possess the suitable pharmacophoric features to behave as a Urotensin-II receptor antagonist. Biological evaluations are currently in progress.

References

1. Grieco, P., Carotenuto, A., Campiglia, P., Zampelli, E., Patacchini, R., Maggi, C.A., Novellino, E. and Rovero, P. *J. Med. Chem.* **45**, 4391-4394 (2002).
2. Patacchini, R., Santicoli, P., Grieco, P., Rovero, P., Novellino, E. and Maggi, C.A. *British J. Pharmacol.* **140**, 1155-1158 (2003).
3. Carotenuto, A., Grieco, P., Campiglia, P., Novellino, E. and Rovero, P. *J. Med. Chem.* **47**, 1652-1661 (2004).
4. Carotenuto, A., Grieco, P., Campiglia, P., Marinelli L., Novellino, E. and Rovero, P. *European Peptide Symposium* P387 (2004).
5. Grieco, P., Campiglia, P., Gomez-Monterrey, I. and Novellino, E. *Tetrahedron Lett.* **43**, 6297-6299 (2002).

Novel GnRH Antagonists Derived from Degarelix: Exploration of the GnRH Antagonist Pharmacophore

Manoj P. Samant¹, Doley J. Hong², Glenn Croston², Catherine Rivier¹
and Jean Rivier¹

¹The Salk Institute, La Jolla, California 92037, USA; ²Ferring Research Institute Inc., San Diego, California 92121, USA

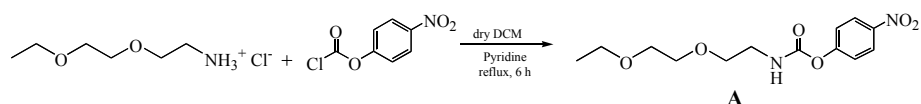
Introduction

Degarelix [1] (**1**, FE2000486) is a potent and very long acting antagonist of gonadotropin-releasing hormone (GnRH) after subcutaneous (sc) administration and is currently in phase II clinical development for the treatment of prostate cancer. We synthesized a series of degarelix analogs (Table 1) with novel substitutions at positions 3, 5, 6, 7, 8, and the *N*-terminus. These substitutions were designed to influence solubility and bioavailability of the analogs and to explore the spatial limitations of the pharmacophore.

Results and Discussion

Analogues were synthesized by SPPS using the Boc strategy and tested in an *in vitro* human GnRH reporter gene assay and *in vivo* for inhibition of LH release in castrated male rats (duration of action) [2].

Reductive monoalkylation on D-Dap/D-Dab generated a variety of amino acids at position 3 of degarelix. Increase in the length of the side chain from D-Dap (**2**, **4**, and **6**) to D-Dab (**3**, **5**, and **7**) resulted in a decrease in antagonist potency. We acylated the ω -amino function of 4Aph⁵ with various carboxylic acids to increase the number of hydrophobic aromatic groups (**8-11**) and the propensity for the formation of inter or intra molecular hydrogen bonds (**12-13**). These analogs were potent *in vitro* but shorter acting than degarelix. The pegylated ureido group was introduced by the reaction of the free amino function of the resin-bound peptide with the PEG urea donor (**A**, Scheme 1) in presence of *N,N*-diisopropylethylamine in DMF. All of the pegylated analogs (**14-17**) were readily soluble in 5% mannitol and potent *in vitro*.



Scheme 1. Synthesis of PEG urea donor.

The diverse functional groups such as imidazole (**18**), phenol (**19**) and a triple bond (**20**) substituted in degarelix at positions 7 yielded analogs that were potent *in vitro* (with the exception of **18**) and shorter acting *in vivo*. Analogs substituted at position 8 were equipotent with degarelix *in vitro*, however their duration of action extended from intermediate (**24**) to long (**22** and **25**) and long* (**21** and **23**). From the observation that the modifications of the optimized substitution found in degarelix results in little changes in antagonist potency and significant changes in duration of action, we conclude that other parameters than those intrinsically associated to receptor recognition and binding may play a critical role in providing

the physicochemical properties for optimal bioavailability and extended duration of action.

Table 1. *In vitro* and *in vivo* biological activities of degarelix analogs

#	Compound	IC ₅₀ ^a (nM)	Duration of action ^c
1	[Ac-D-2Nal ¹ ,D-4Cpa ² ,D-3Pal ³ ,4Aph(L-Hor) ⁵ ,D-4Aph(Cbm) ⁶ ,Lys(iPr) ⁸ ,D-Ala ¹⁰]GnRH (degarelix)	1.64	very long
2	[N ^β -(2-pyridyl-methyl)D-Dap ³]degarelix	2.71	short
3	[N ^γ -(2-pyridyl-methyl)D-Dab ³]degarelix	3.79	short
4	[N ^β -(2-quinolyl-methyl)D-Dap ³]degarelix	4.25	short
5	[N ^γ -(2-quinolyl-methyl)D-Dab ³]degarelix	5.52	short
6	[N ^β -(2-imidazolyl-methyl)D-Dap ³]degarelix	5.52	short
7	[N ^γ -(2-imidazolyl-methyl)D-Dab ³]degarelix	3.50	intermediate
8	[4Aph(Hva) ⁵]degarelix	1.54	short
9	[4Aph(Hvn) ⁵]degarelix	1.47	long*
10	[4Aph(2,5-dmpa) ⁵]degarelix	1.58	short
11	[4Aph(3,5-dmpa) ⁵]degarelix	1.66	short
12	[4Aph(L-pGlu) ⁵]degarelix	1.85	long
13	[4Aph(thymine-1-acetyl) ⁵]degarelix	2.46	short
14	[4Aph(CO-NH-(CH ₂ CH ₂ O) ₂ -C ₂ H ₅) ⁵]degarelix	3.16 ^b	long*
15	[D-4Aph(CO-NH-(CH ₂ CH ₂ O) ₂ -C ₂ H ₅) ⁶]degarelix	0.88 ^b	short
16	[4Aph(CO-NH-(CH ₂ CH ₂ O) ₂ -C ₂ H ₅) ⁵ ,D-4Aph(CO-NH-(CH ₂ CH ₂ O) ₂ -C ₂ H ₅) ⁶]degarelix	2.04 ^b	short
17	des-Ac-[Aph(CO-NH-(CH ₂ CH ₂ O) ₂ -C ₂ H ₅) ⁵ ,D-4Aph(CO-NH-(CH ₂ CH ₂ O) ₂ -C ₂ H ₅) ⁶]-C ₂ H ₅ -(OCH ₂ CH ₂) ₂ -NH-CO-degarelix	2.55 ^b	short
18	[His ⁷]degarelix	10.64	short
19	[Tyr ⁷]degarelix	2.85	intermediate
20	[Pra ⁷]degarelix	2.11	short
21	[Orn(iPr) ⁸]degarelix	1.72	long*
22	[N ^ε -cyclohexyl-Lys ⁸]degarelix	1.50	long
23	[N ^γ -(Gly(iPr))Dab ⁸]degarelix	1.56	long*
24	[N ^β -(Gly(iPr))Dap ⁸]degarelix	1.54	intermediate
25	[N ^β -(βAla(iPr))Dap ⁸]degarelix	1.98	long

Abbreviations: 4Aph = 4-aminophenylalanine; Cbm = carbamoyl; 2,5-dmpa = 2,5-dimethoxyphenylacetyl; 3,5-dmpa = 3,5-dimethoxyphenylacetyl; Hor = hydroorotyl; Hva = homoveratryl; Hvn = homovanillyl; Pra = propargylglycine.

^ahGnRH reporter gene assay; ^banalogs **14-17** were tested in a separate experiment, where for degarelix IC₅₀ = 0.58 nM; ^c*In vivo* castrated male rat assay. Duration of action: very long = over 80% inhibition of LH release for more than 120 hrs; long* = over 80% inhibition of LH release at 96 hrs but not at 120 hrs; long = over 80% inhibition of LH release at 72 hrs but not at 96 hrs; intermediate = partial inhibition of LH release at 72 hrs; short = over 80% inhibition of LH release at 3 hrs but not at 72 hrs.

Acknowledgments

This work was supported by NIH grant HD-39899. We thank R. Kaiser, W. Low and C. Miller for technical assistance and D. Doan for manuscript preparation.

References

- Jiang, G., Stalewski, J., Galyean, R., *et al.* *J. Med. Chem.* **44**, 453-467 (2001).
- Samant, M. P., Gulyas, J., Hong, D. J., *et al.* *J. Med. Chem.* **48**, 4851-4860 (2005).

Novel Neuroprotective Neurotrophic NAP Analogs Targeting Iron Toxicity and Oxidative Stress in Neurodegenerative Diseases

Hailin Zheng¹, Dan Blat¹, Moussa B.H. Youdim², Lev M. Weiner¹, Dudy Dangoor^{1,3}, Ilana Gozes³ and Mati Fridkin¹

¹Department of Organic Chemistry, The Weizmann Institute of Science, Rehovot 76100, Israel; ²Eve Topf and US National Parkinson Foundation Centers of Excellence for Neurodegenerative Diseases, Department of Pharmacology, Technion-Faculty of Medicine, Haifa 31096, Israel; ³Department of Clinical Biochemistry, Sackler Faculty of Medicine, Tel Aviv University, Tel Aviv 69978, Israel

Introduction

Several factors, among them metal ion ($\text{Fe}^{3+/2+}$, Cu^{2+} , Zn^{2+}) dyshomeostasis, inflammatory processes, reduced expression of neurotrophic factors, and oxidative stress, have all been implicated in the neurodegeneration in Alzheimer's disease (AD) and Parkinson's disease (PD). Iron and iron-related oxidative stress are thought to play a pivotal role in the pathogenesis of these disorders [1]. Accordingly, multifunctional compounds combining metal chelating and antioxidative activity hold a great promise as potential drugs for treating AD and PD. The 8-amino acid peptide NAP (NAPVSIPQ), derived from Activity-Dependent Neuroprotective Protein (ADNP), has been shown to possess potent neuroprotective action [2]. However, NAP has no significant iron chelating capabilities *in vitro* or *in vivo*. In this study, two novel NAP analogs, one with a hydroxamate moiety (M98) and the other with an 8-hydroxyquinoline moiety (M99), were designed and investigated in the aim to improve the poor metal chelating and antioxidative activity of their parent peptide NAP.

Results and Discussion

NAP (NAPVSIPQ) and $[\text{Cys}^4]\text{NAP}$ (NAPCSIPQ) were synthesized via the Fmoc strategy by an automatic multiple solid-phase peptide synthesizer. Synthesis of M98 was performed by initial attachment of Fmoc-Glu(ODmab)-OH to 2-chlorotrityl chloride resin, followed by coupling of the corresponding amino acids. The Dmab protecting group was removed by treating the peptide-resin with 2% hydrazine- H_2O . This was followed by conjugation of O-tertbutyl hydroxylamine hydrochloride to the free carboxyl group via DCC/HOBT activation. M99 was synthesized by adding 5-chloromethyl-8-hydroxyquinoline hydrochloride to a solution of $[\text{Cys}^4]\text{NAP}$ and NMM in DMF.

The metal binding ability, antioxidative activity and *in vitro* neuroprotective effects of the two novel NAP analogs were investigated and compared with those of the parent NAP peptide. UV-vis spectroscopy was employed to study the formation of metal ion ($\text{Fe}^{3+/2+}$, Cu^{2+} , Zn^{2+}) complexes. Our experiments suggested that both M98 and M99 formed stable complexes with the above metal ions in water at RT, as indicated by shift and/or disappearance of bands and appearance of new ones in the absorption spectrum (data not shown). On the other hand, the parent NAP peptide showed complex formation only with Fe^{3+} . The iron-binding capacities of NAP and M99 were further investigated using the ferrozine method, in which drugs are assessed for their ability to compete with ferrozine for Fe^{2+} ions, resulting in decreased absorbance at 562 nm [3]. As expected, desferal [DFO], a very strong

iron chelator [4], showed very high iron-binding capacity (Fig. 1). The parent NAP did not exhibit any significant iron-binding capacity, while its analog M99 displayed strong iron-binding capacity with an IC_{50} of 0.1 mM (Fig. 1).

In lipid peroxidation (LPO) assays, M98 and M99 exhibited significant inhibition of Fe^{2+} -induced LPO in rat brain homogenates at concentrations of $\geq 30\mu M$ (not shown). In contrast, the parent NAP failed to show any similar effect at the range of 1-100 μM .

Finally, the MTT assay was employed to investigate the neuroprotective action of M98 and M99 against 6-hydroxydopamine (6-OHDA)-induced neurotoxicity. This test is based on the conversion of MTT to blue formazan crystals by viable cells, followed by determination of absorption at 570/650nm. As demonstrated in Figure 2, exposure of SH-SY5Y cells to 25 μM 6-OHDA resulted in cell death by about 25%. Treatment of the cells with NAP, M98, M99, or DFO (all at 1 μM) 30 min prior to the addition of 6-OHDA increased the cell viability to approximately control levels. In these experiments, the two novel NAP analogs (M98 and M99) showed similar effects to their parent peptide NAP and DFO in protecting the cells against 6-OHDA toxicity. In addition, treatment with only NAP, M98, M99, or DFO (all at 1 μM) did not affect significantly cell death (Fig. 2), suggesting that NAP, M98, M99, or DFO were not toxic to SH-SY5Y cells at the tested concentration.

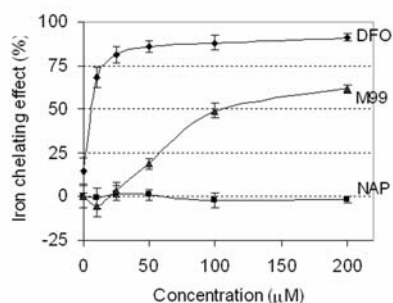


Fig. 1. Effects of M99, NAP and DFO on $Fe(II)$ -ferrozine formation, expressed by iron-binding capacity (%).

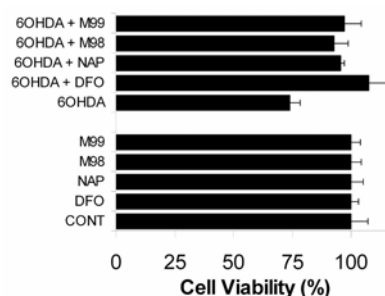


Fig. 2. Protection against 6-OHDA-induced toxicity in SH-SY5Y cells by NAP, M98, M99 and DFO at 1 μM .

In conclusion, we have designed and synthesized two novel NAP analogs, both possessing good metal ion chelating properties, as opposed to the poor metal chelating properties of their parent peptide NAP. M98 and M99 exhibited significant inhibition of iron-induced lipid peroxidation in rat brain homogenates at concentrations of $\geq 30\mu M$, while NAP did not show any inhibition even at 100 μM . In cell cultures, M98 and M99 showed potent protection against 6-OHDA toxicity, comparable to NAP and DFO. These results suggest that M98 and M99 deserve further investigation as potential drug candidates for neuroprotection.

References

1. Mandel, S., *et al. CNS Drugs.* **17**, 729-762 (2003).
2. Bassan, M., *et al. J. Neurochem.* **72**, 1283-1293 (1999).
3. Carter, P., *et al. Anal. Biochem.* **40**, 450-458 (1971).
4. Anderegg, G. *et al. Helvetica Chimica Acta.* **46**, 1400-1408 (1963).

One-bead One-compound: Different Type of Screening Assays for Anti-bacterial Adhesion

Yanlei Liu¹, Li Peng², Xiaobing Wang², Kit S. Lam² and Joseph W. Leung¹

¹Division of Gastroenterology; ²Division of Hematology/ Oncology; Department of Internal Medicine, University of California Davis Medical Center, Sacramento CA 95817, USA

Introduction

The adhesion of bacteria to host tissues is one of the initial stages of the infectious process [1]. In addition, the alarming increase in drug-resistant bacteria makes a search for novel means of fighting bacterial infections imperative. An attractive approach is the use of agents that interfere with the ability of the bacteria to adhere to tissues of the host. Since anti-adherent agents are not bactericidal, the propagation and spread of resistant strains is much less likely to occur than as a result of exposure to bactericidal agents. The major drawback of anti-adhesion therapy is that most pathogens possess genes encoding more than one type of adhesin [2].

The concept of combinatorial chemistry has truly revolutionized the drug discovery process. The “one-bead one-compound” (OBOC) combinatorial library makes it convenient to identify a single agent against multiple adhesins and adhesion factors by screening thousands of compounds with many bacterial strains in parallel. In this method, the library is prepared by a “split-mix synthesis” approach using polystyrene beads as a solid support. As a result, each bead displays only one chemical entity but there are approximately 10^{13} copies of the same chemical compound on and within one single bead [3]. In this study, OBOC library approach was employed to identify anti-bacterial adhesion compounds.

Fluorescent labeled assay: bacteria were labeled with fluorescent probe kit consisting of SYTO 9 for *Escherichia coli* at a concentration of 0.004 ml/ml (V/V) and hexidium iodide for *Enterococcus faecalis* at a concentration of 0.0035 ml/ml and then incubated with OBOC library for 48 hrs. Anti-adhesion beads were isolated and sequenced (Fig. 1).

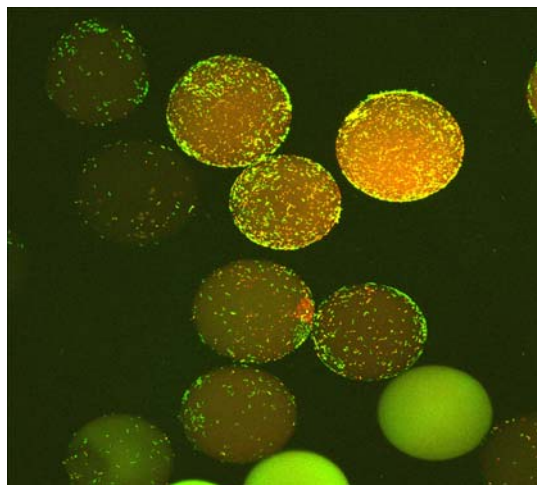


Fig. 1. CLSM detailed the appearances of OBOC library challenged with *E. coli* and *E. faecalis* for 2 days. Negative beads have no bacteria identified on the surfaces.

Cell culturing assay: OBOC library was incubated with *E. coli* and *E. faecalis* for 48 hrs and transferred into LMP BHI agar for culturing. Negative beads were isolated and sequenced (Fig. 2).

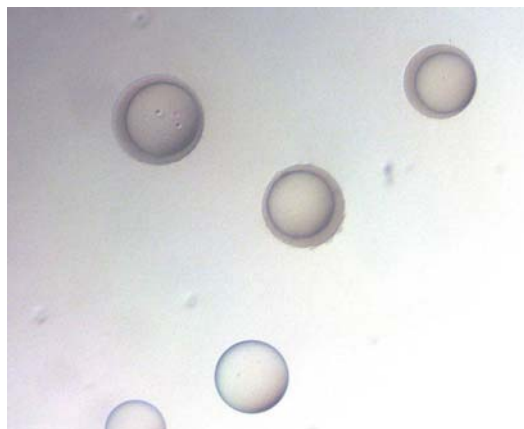


Fig. 2. Photomicrography of OBOC library challenged with *E. coli* and *E. faecalis* for 48 hrs shows positive and negative beads. Bacteria attached compound-beads appeared as an amorphous layer covering the surface of positive beads. No amorphous layers are seen on surfaces of the negative beads.

Results and Discussion

Through on-bead screening of the one-bead one-compound library with *E. coli* and *E. faecalis*, a few of anti-adhesion compounds have been identified. The structure elucidation was achieved by decoding the anti-adhesion beads with Procise 494 Protein sequencer. Our experiment indicated that “one-bead one-compound” library approach is a powerful and reliable approach to detect anti-adhesion agents. By using the methods and results from this work, specific anti-pathogen adhesion compounds may be developed in the future.

Staining the bacteria prior to adhesion provides a better

way to visualize bacterial attachment. We have successfully applied this novel assay to select anti-adhesion peptide beads. Since TentaGel beads have intrinsically fluorescent property, it is difficult to visualize the bacterial attachment if the bead library is stained after incubation with bacteria. Staining bacteria prior to incubation minimizes dye staining on the beads and gives an overall lighter background for the detection of bacterial attachment. In order to delay the fluorescent decay in the bacteria, the incubation process and washing were done in a dark room. With this preparation, the fluorescent bacteria on the beads can be easily recognized with the use of fluorescent microscope.

Cell culturing assay can be applied for the long-term screening for anti-adhesion compounds. However, the false negative rate is very high, because the beads have to be heavily rinsed before transferred into LMP BHI agar.

Acknowledgments

The work was funded by an NIH grant to J. Leung.

References

1. Costerton, J. W. *Int. J. Antimicrob. Agents* **11**, 2217-2221(1999).
2. Ofek, I., Hasty, D. L. and Sharon, N. *FEMS Immunol. Med. Microbiol.* **38**, 181-191 (2003).
3. Lam, K. S., Salmon, S. E. and Hersh, E. M. *Nature* **354**, 82-84 (1991).

Peptide - Mediated Delivery of siRNA via Noncovalent Complexes and Covalent Conjugates

Renata T. Witkowska, Mohammad Ahmadian, James W. Dattilo, Lafe J. Purvis, Sasha J. Mayer, Lishan Chen, Yuching Chen, Kunyuan Cui, Ken W. Farber, Sharin E. Roth, Michael E. Houston, Paul H. Johnson and Steven C. Quay

Nastech Pharmaceutical Co. Inc., 3450 Monte Villa Parkway, Bothell, WA 98021, USA

Introduction

Improving the intracellular delivery of synthetic oligonucleotides and their analogs is an important goal in the development of small interfering RNA (siRNA) therapeutics for affecting gene expression in cell culture and *in vivo*. One of the major challenges to the effective use of therapeutic siRNAs is their relatively inefficient uptake by cells. siRNAs are polyanions and their *in vitro* and *in vivo* activity is improved substantially by covalent attachment or complex formation with natural peptide sequences that possess the ability to translocate across the cell membrane [1-3]. We have performed a systematic analysis of the ability of different structural classes of peptides to translocate across cell membranes and deliver siRNA into cells. Over 100 peptides were screened by mixing with siRNA to generate a noncovalent complex; the top 20 candidates with the best uptake properties were covalently conjugated to the 5'- or 3'- end of the siRNA sense strands via a thioether bond. The uptake efficiency of siRNA was evaluated by flow cytometry using fluorescently labeled siRNAs (FAM or Cy5) in both established and primary human and mouse cells (Fig. 1). The localization of siRNA within the cells was visualized by fluorescence microscopy. Finally, the ability of complexed or conjugated siRNA to mediate knockdown of TNF- α mRNA was measured in activated human monocytes.

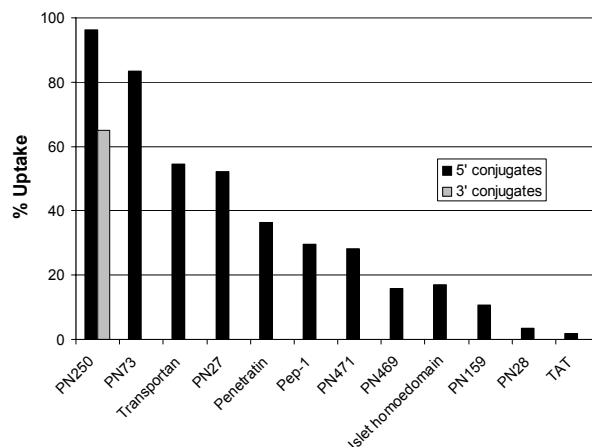


Fig. 1. Delivery by siRNA-peptide conjugates. Fluorescently labeled siRNA-peptide conjugates were tested for uptake in mouse tail fibroblast cells. Chart summarizes the highest percent uptake obtained for conjugates tested at a maximum concentration of 4 μ M. In all cases, cytotoxicity was less than 10%.

Results and Discussion

Peptides were synthesized by the solid phase method on CLEAR-amide resin using standard Fmoc chemistry. Oligoribonucleotides were synthesized using standard 2'-TBDMS phosphoramidite chemistry. For conjugation, the N-termini of the peptides were functionalized with 3-maleimidopropionic acid while the 5' or 3' end of the siRNA sense strands were modified with a 1-O-dimethoxytrityl-hexyl-disulfide linker and propyl-disulfide linker, respectively. Peptides were conjugated to the 5' or 3' end of the siRNA sense strand via a thioether bond or mixed with siRNA to generate a noncovalent complex. The thiol was liberated by reduction of the disulfide bond of the 5'-linker of the oligonucleotide using aqueous TCEP hydrochloride and reacted with the maleimide groups attached to the N-termini of the peptides. Conjugates were synthesized under high denaturing conditions (50% formamide) to prevent aggregation and precipitation [4] and were purified by ion exchange chromatography (IEX).

Synthesis of peptide-siRNA conjugates and their purification (ion exchange chromatography) was improved with the emphasis on maintaining solubility through use of highly denaturing conditions. New method for analysis of peptide-siRNA conjugates by electrospray ionization mass spectrometry was developed. Several peptides capable of delivering siRNA into cells in either complex or conjugated forms were identified. Peptide-assisted delivery achieved higher transfection efficiency and more uniform siRNA distribution in the cells than Lipofectamine. The intracellular location of siRNA mixed with or conjugated to the peptide was visualized by Fluorescence Microscopy: peptides PN73 and PN278 delivered siRNA to cytoplasm. Both peptide-siRNA complexes and conjugates effectively knockdown TNF- α mRNA in activated human monocytes at low nM concentration. The knockdown activity of the siRNA N145-PN73 complex and conjugate was comparable; for siRNA N104 the knockdown activity was better for the corresponding conjugate (Fig. 2). Ability of complexed and conjugated siRNAs to knockdown human TNF- α in a rheumatoid arthritis (RA) transgenic mouse model is in progress.

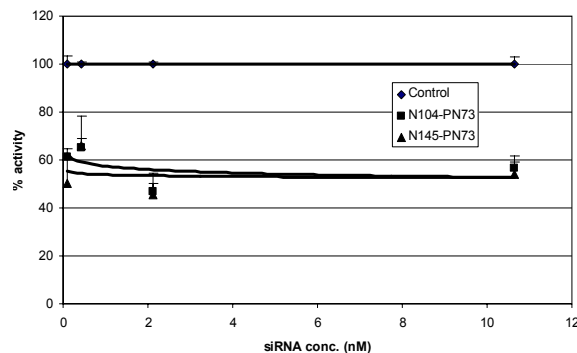


Fig. 2. PN73-siRNA conjugates activity on activated human monocytes.

References

1. Lindgren, M., Hällbrink, M., Prochiantz, A. and Langel, Ü. *Trends Pharmacol. Sci.* **21**, 99-103(2000).
- 2) Hawiger, J. *Curr. Opin. Neurobiol.* **6**, 629-634 (1997).
- 3) Tung, C. H. and Stein, S. *Bioconj. Chem.* **11**, 605-618 (2000).
- 4) Turner, J. J., Arzumanow, A. A. and Gait, J. *Nucleic Acids Res.* **33**, 27-42 (2005).

Peptides Reproducing the ApoA-I 141-164 Region: Studies on Hpt Recognition

Luca D. D'Andrea¹, MariaStefania Spagnuolo², Angela De Stefano¹,
 Marianna Morra¹, Alessandro Carlucci², Annarita Del Gatto²,
 Pasqualina Caso², Carlo Pedone¹, Paolo Abrescia² and Ettore Benedetti²

¹Istituto di Biostrutture e Bioimmagini, CNR, Napoli, 80134, Italy, ²Dipartimento delle Scienze Biologiche, Università degli Studi di Napoli "Federico II", Napoli, 80134, Italy

Introduction

Apolipoprotein A-I (Apo A-I) is the major component of the high density lipoproteins (HDL) which are involved in the reverse cholesterol transport. In particular, Apo A-I stimulates the efflux of cholesterol from cell toward HDL and the enzyme lecithin-cholesterol acyltransferase (LCAT) to convert, on the HDL surface, cell-derived cholesterol into cholesteryl ester, which is then placed into the lipoprotein core and transported through circulation to liver for catabolism and bile production [1]. It has been demonstrated that the protein haptoglobin (Hpt) binds to Apo A-I [2] and inhibits the Apo A-I-dependent activity of LCAT [3]. Hpt is long far known to capture and transport to the liver free hemoglobin (Hb) in the pathway of iron recycling for erythropoiesis. Hpt is one of the most abundant proteins in the plasma and its level increases during inflammation processes.

Hpt-dependent masking of the Apo A-I site involved in the LCAT stimulation was suggested to be responsible for decreased LCAT activity [3,4]. Thus, high Hpt levels, as present in the acute phase of inflammation, might impair cholesterol removal from peripheral cells, including vascular cells, and play an important role in worsening vascular endothelial dysfunction and accelerating atherosclerosis.

To get more information about the biochemical mechanism(s) underlying the negative control of Hpt on the reverse cholesterol transport, we are investigating the molecular bases of the Hpt-Apo A-I recognition.

Results and Discussion

Recently, we have mapped the Hpt-binding site of Apo A-I to the sequence 141-164 and demonstrated that peptides reproducing this site compete with Apo A-I for

LSPLGEEMRDRARAHVDALRTHLA	Apo 141-164
LSPLGAEMRDRARAHVDALRTHLA	146Glu
LSPLGEAMRDRARAHVDALRTHLA	147Glu
LSPLGEEMADRARAHVDALRTHLA	149Arg
LSPLGEEMRARARAHVDALRTHLA	150Asp
LSPLGEEMRDAARAHVDALRTHLA	151Arg
LSPLGEEMRDRAAAHVDALRTHLA	153Arg
LSPLGEEMRDRARAAVDALRTHLA	155His
LSPLGEEMRDRARAHVAALRTHLA	157Asp
LSPLGEEMRDRARAHVDALATHLA	160Arg
LSPLGEEMRDRARAHVDALRTALA	162His

Fig. 1. Peptide sequences of the Apo A-I 141-164 analogs. In bold are highlighted the charged residues and the corresponding replacing alanine.

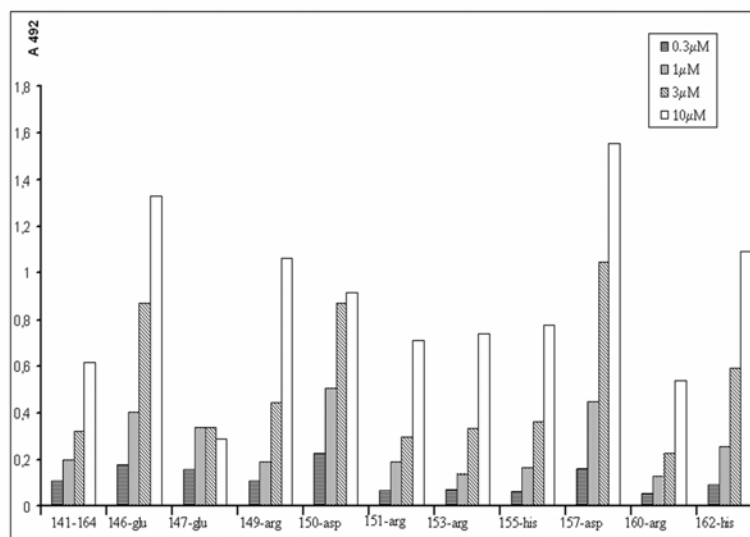


Fig. 2. Biotinylated peptides were incubated at different concentration in Hpt coated wells. Bound peptides were revealed with Avidin-HRP.

binding to Hpt, prevent the Hpt binding to HDL, and restore the LCAT activity in the presence of Hpt [5]. The Hpt-binding site of Apo A-I contains ten charged residues, which are strictly conserved between species. We singularly mutate to alanine each of these residues in order to evaluate their contribution to the binding to Hpt. The sequences of the synthesized peptides are reported in Figure 1.

Peptides were synthesized by standard Fmoc SPPS using the PAL-PEG PS resin. All peptides were amidated at the C-terminus and biotinylated or acetylated at the N-terminus. The Hpt binding studies are reported in Figure 2 and were performed using the biotinylated peptides.

These data suggest that the charged residues are not involved in the Hpt-Apo A-I recognition and in some cases the removal of the charge improve the binding to Hpt.

References

1. Sorci-Thomas M. G. and Thomas M. J. *Trends Cardiovasc. Med.* **12**, 121-128 (2002).
2. Kunitake, S. T., Carilli, C. T., Lau, K., Protter, A. A., Naya-Vigne, J. and Kane, J. P. *Biochemistry* **33**, 1988-1993 (1994).
3. Balestrieri, M., Cigliano, L., De Simone, M. L., Dale, B. and Abrescia, P. *Mol. Reprod. Dev.* **59**, 186-191 (2001).
4. Spagnuolo, M. S., Cigliano, L. and Abrescia, P. *Biol. Chem.* **384**, 1593-1596 (2003).
5. Spagnuolo, M. S., Cigliano, L., D'Andrea, L. D., Pedone, C., Abrescia P. *J. Biol. Chem.* **280**, 1193-1198 (2005).

Peptidomimetic Inhibitors of Platelet Adhesion as Potential Novel Antiplatelet Agents

Vivienne Buckley¹, Elise Bernard¹, Edelmiro Moman¹, Lorraine Coleman², Dermot Kenny² and Marc Devocelle¹

¹Centre for Synthesis and Chemical Biology, Department of Pharmaceutical & Medicinal Chemistry; ²Department of Clinical Pharmacology, Royal College of Surgeons in Ireland, 123 St. Stephen's Green, Dublin 2, Ireland

Introduction

There is currently no agent in clinical use that prevents thrombosis by targeting its earliest upstream event, *i.e.* platelet adhesion [1]. This occurs through the interactions of the platelet-receptor, glycoprotein Ib α (GPIb α), with its immobilized ligand Willebrand factor (vWF) [2]. These interactions take place in response to vessel injury or are induced by shear stress in occluded arteries. The crystal structure of the GPIb α -vWF complex has been reported recently [3] and showed that the interaction surface encompasses two distinct areas and is extended, making this interface a difficult target for small ("drug-like") molecules. The two epitopes of GPIb, (Cys⁴-Cys¹⁷) and (Asp²³⁵-Ser²⁴¹), in contact with vWF, form a 14-residue and a 16-residue β -hairpin, respectively. We have therefore prepared β -hairpin peptidomimetics modeled on these surface portions of GPIb α , by cyclizing 12 to 16 residues from the protein sequence onto a β -turn stabilizing motif. The ability of these mimetics to disrupt GPIb α -vWF interactions was evaluated *in vitro*. The results obtained with the β -hairpin mimetics based on the epitope Asp²³⁵-Ser²⁴¹ are presented here.

Results and Discussion

The sequences were assembled by standard Solid Phase Peptide Synthesis on an automated synthesiser, according to the Fmoc-*t*Bu strategy. The sequences were elongated from a Fmoc-Asp-OAll residue attached on a NovaSyn TGA resin and the macrocyclisation was performed on the resin.

GPIb and vWF do not interact at a detectable level unless an exogenous modulator, such as ristocetin, is added or shear stress is applied. A platelet aggregation assay mediated by an agonist was used as a screening tool and peptides that demonstrated inhibition in these studies were then tested under more physiologically relevant conditions. Their effect on the translocation of platelets across a vWF coated matrix, under arterial shear conditions, was investigated using a modified parallel plate flow chamber assembly [4]. The velocity of rolling platelets, which is a measure of the GPIb-vWF interaction, was assayed. Inhibition of the interactions between GPIb and vWF enhances the velocity of platelets.

The most promising results, reconciling a minimum size for the cyclic peptide with a good inhibitory activity, were obtained with the peptidomimetic containing the sequence (W²³⁰-V²³⁹) of the GPIb *N*-terminus. This peptidomimetic consists of a 12-mer cyclic peptide containing a heterochiral diproline unit, which stabilises the β -hairpin conformation of the peptide loop. An internal disulphide bridge was also introduced in the macromolecule to further constrain the backbone conformation.

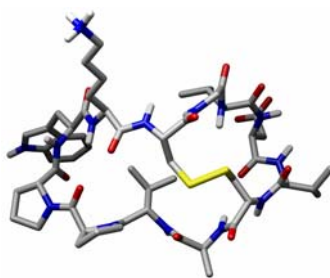


Fig. 1. Schematic representation of the β -hairpin mimetic DVCAVPpWKCGV.

In washed platelets, 100 μ M β -hairpin mimetic inhibited ristocetin-induced platelet aggregation by 44%. Some minimal reduction (16%) in low-dose thrombin-induced aggregation was also observed at working concentration of 100 μ M. Interestingly, with a larger 14-mer homologue (V²²⁹-T²⁴⁰), which extends the modeled region of GPIb toward the binding site of thrombin [5], the inhibition of low-dose thrombin-induced aggregation was increased to 81%. To verify that this activity was maintained even in presence of plasma proteins, the platelet aggregation assays were reproduced with platelet rich plasma (PRP). In PRP, 100 μ M β -hairpin mimetic inhibited ristocetin-induced platelet aggregation by 39%.

The peptide controls used in these studies were identical sequences, but lacking one or all the β -hairpin stabilizing motifs. Their evaluation confirmed that a stabilized secondary structure is required for the inhibitory activity. Indeed, the increasing conformational flexibility of these control peptides resulted in partial (heterodetic peptide) or total (linear peptide) loss of the activity of the mimetic. Subsequently, the effect of the β -hairpin mimetic and its controls on platelet translocation at physiologically relevant high shear were measured by platelet rolling velocity on vWF. We observed that platelets incubated with the β -hairpin mimetic prior to flow, showed an overall increase in translocation velocities relative to untreated platelets ($P < 0.001$). Again, the conformationally well-defined β -hairpin mimetic was the only active molecule. These preliminary results suggest that a β -hairpin peptidomimetic has an impact on platelet function in terms of rolling velocity and aggregation and is therefore a promising lead compound in antithrombotic therapy.

Acknowledgments

The work was funded by an Enterprise Ireland grant (IF/2002/042) and grants from the Health Research Board and Higher Education Authority Ireland.

References

1. Bhatt, D. L. and Topol, E. J. *Nature Rev. Drug Discov.* **2**, 15-28 (2003).
2. Jackson, S. P. and Schoenwaelder, S. M. *Nature Rev. Drug Discov.* **2**, 1-15 (2003).
3. Huizinga, E. G., *et al.* *Science* **297**, 1176-1179 (2002).
4. Lawrence, M. B., McIntire, L. V. and Eskin S. G. *Blood* **70**, 1284-1290 (1987).
5. Celikel, R., *et al.* *Science* **301**, 218-221 (2003); Dumas, J. J., *et al.* *Science* **301**, 222-226 (2003).

Peptidyl-based Delivery Systems as a Strategy for the Therapeutic Intervention of Human Astrocytoma and Medulloblastoma

Sarah Jones and John Howl

Research Institute in Healthcare Science, School of Applied Sciences, University of
 Wolverhampton, Wolverhampton, WV1 1SB, UK

Introduction

The cell-type specific targeting of cytotoxic agents and other functional moieties can be achieved using peptidyl *address* motifs that selectively bind protein targets expressed at high density at the cell membrane. Indeed, numerous studies have confirmed the utility of ligands for G protein-coupled receptors as components of heterofunctional peptide chimerae that are selective biological probes [1]. Our current efforts are directed towards the further development of chimeric peptidyl constructs that employ sequences derived from GPCR ligands or cell penetrant motifs to affect the selective delivery of cytotoxins and signal transduction modulators to human astrocytoma and medullablastoma. Moreover, over-expression of somatostatin receptor type 2 on medullablastoma [2] that avidly binds octreotide analogs and identification of a novel membrane binding site on U373MG astrocytic tumor cells are potential membrane targets for our peptidyl-based delivery systems.

We have designed and synthesized a range of hybrid constructs consisting of peptidyl cytotoxins covalently linked to an address peptide derived from the C-terminal of gastrin (G7; H-AYGWMDF-NH₂). The G7 *homing* motif targets a novel binding site expressed by U373MG astrocytic tumor cells that is distinct from classical CCK₁/CCK₂ receptors. Moreover, biological responses following activation of this novel membrane bound protein may offer additional therapeutic advantages. For example, G7 receptor activation is reported to inhibit the motility of malignant astrocytoma *in vitro* whilst avoiding the growth promoting effects of gastrin [3]. Thus, G7 was synthesized at the N-terminal of the G protein modulator and pore-forming tetradecapeptide MP (H-INLKALAALAKKIL-NH₂) and also attached via an aminohexanoic (AHX) linker to the pro-apoptotic peptide _D(KLAKLAK)₂ [1], to generate novel peptidyl chimerae.

Results and Discussion

We evaluated the cytotoxicity of our chimeric peptides by comparing changes in

Table 1. Comparative cytotoxicity of G7 chimeras and their composite parts

Peptide	Δ Cell Viability
G7	33.5
MP	24.5
G7:MP	40
_D (KLAKLAK) ₂	21.8
G7(AHX) _D (KLAKLAK) ₂	42.1

Changes in cell viability (Δ) were calculated as % reduction of viable cells compared to untreated cells (100%). Values were determined at a peptide concentration of 10 μM.

cellular viability using MTT conversion assays. Our data indicate that chimeric peptides dose-dependently and rapidly (<8hours) reduced the viability of U373MG cells (Fig. 1). Moreover, as an chimeric amino-terminal extension of MP and $D(KLAKLAK)$, the G7 address motif enhanced the cytotoxicity of each peptidyl cytotoxin tested (Table 1 and Fig. 1). Thus, preliminary data have demonstrated that our chimeric constructs provide a suitable strategy for the delivery of peptidyl cytotoxins to human astrocytoma.

In addition, we have demonstrated that in U373MG cells, MP specifically targets intracellular signaling proteins, besides that of heterotrimeric G proteins and that MP does not promote cell death of these cells by random pore formation, but initiates apoptosis as detected by *in situ* TUNEL staining. Thus, the authors anticipate further development of brain tumor-specific cytotoxic peptidyl chimerae and continue to resolve intracellular signaling mechanisms leading to astrocytic tumor cell death.

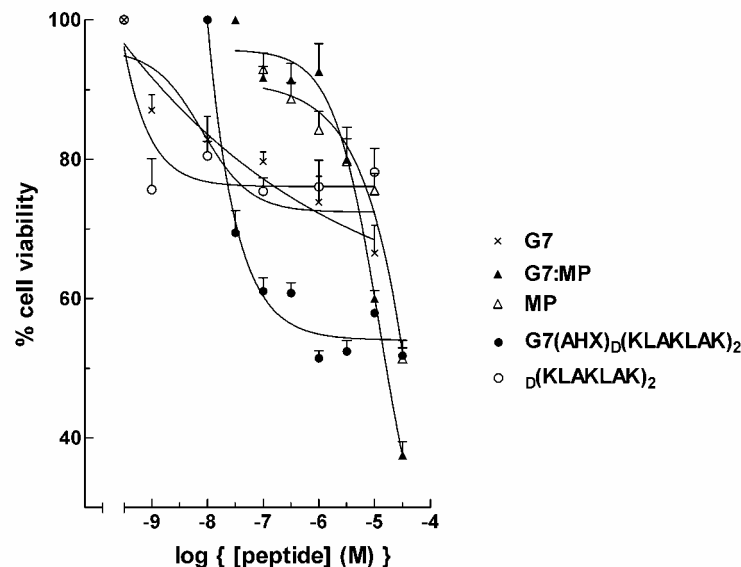


Fig. 1. Chimeric strategies for the delivery of cytotoxic peptides. U373MG cells were incubated with G7 and G7:MP peptides for 4 hrs and G7(AHX) $D(KLAKLAK)_2$ for 8 hrs. Data are expressed as mean \pm S.E.M. from 2 experiments performed in triplicate.

Acknowledgments

The work was supported by the Wellcome Trust.

References

1. Ellerby, H. M., *et al.* *Nat. Med.* **5**, 1032-1038 (1999).
2. Muller, H. L., *et al.* *J. Neurooncol.* **38**, 27-40 (1998).
3. Pannequin, J., *et al.* *J. Pharmacol. Exp. Ther.* **302**, 274-282 (2002).

Photolabeling with N-Terminal Urotensin II Photoprobes Identifies Methionine 288 of Rat Urotensin Receptor as a Contact Point

Brian J. Holleran, Christophe Proulx, Marie-Ève Beaulieu, Emanuel Escher and Richard Leduc

Department of Pharmacology, University de Sherbrooke, Sherbrooke, Qc, J1H 5N4, Canada

Introduction

Urotensin II (U-II) is a cyclic undecapeptide which has recently been shown to be the endogenous ligand of a G Protein Coupled Receptor (GPCR) termed UT [1]. U-II has potent vasoactivity in the peripheral vasculature and it may be implicated in the pathogenesis of cardiovascular diseases such as essential hypertension and heart failure. Our laboratory is interested in defining the spatial orientation of biological ligands within the binding pocket of peptidergic GPCRs. By introducing spatial constraints between distant residues of the receptor and homology modelling, the number of possible structures is narrowed down to a very few [2]. Spatial constraints can be experimentally determined by finding the points of contact between a peptide ligand and its receptor using multiple photoaffinity labeling e.g., with photoprobe radioligands incorporating *para*-benzoyl-*L*-phenylalanine (Bpa) at different positions within the peptide sequence. Using this approach, we have shown that the sixth residue of U-II is in close proximity to two adjacent Met residues within the fourth transmembrane domain of the rat UT (rUT) [3]. In order to determine ligand orientation and better define interactions within the binding pocket of UT, further contact points are needed. We have introduced Bpa into the N-terminal portion of U-II since this portion of the ligand is highly heterogeneous across species while still maintaining full biological properties.

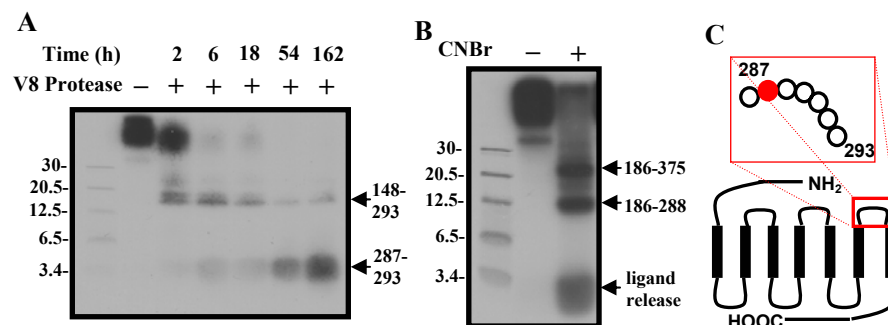


Fig. 1. Labeling contents of U-II in rUT. Autoradiography of SDS-Page from photoaffinity labeled rat UT from transiently transfected COS-7 cells **A**. V8 protease digestion time course of Bpa¹ photolabeled rUT complexes. **B**. CNBr digestion of Bpa³ photolabeled rUT complex. **C**. Schematic representation of the labeled fragment.

Results and Discussion

We have generated a series of ¹²⁵I radioiodinated photoprobes incorporating the Bpa moiety in the first ([Bpa¹]U-II), second ([Bpa²]U-II), and third ([Bpa³]U-II) positions of U-II. Following transfection of the rUT cDNA in COS-7 cells we determined that

all three analogs were agonists with binding affinities in the order of 1-3 nM similar to endogenous U-II and all three strongly photolabeled rUT in a specific manner. Each photolabeled complex was purified by SDS-PAGE, eluted from the gel and concentrated. Several biochemical analyses were carried out on each photolabeled complex in order to determine the region of contact between the Bpa moiety and the rUT receptor. Consensus of the labeling pattern obtained from BNPS-Skatole and Endo-Arg-C indicate a label portion between TMD6 and TMD7 which is limited by V8 protease to a small ECL3 fragment Ala²⁸⁷-Glu²⁹³ for all three labels (Fig. 1A). CNBr fragmentation however further limits label position to Met²⁸⁸ for all three ligands which is evidenced by discrete and characteristic ligand release (Fig. 1B). Two contact points, Met^{184/185} with position 6 [3] and Met²⁸⁸ with positions 1,2,3 in addition to the salt bridge at Asp¹³⁰ with position 8 (Lys) has allowed us to propose a bovine rhodopsin-based model of the rat UT receptor docked with U-II (Fig. 2).

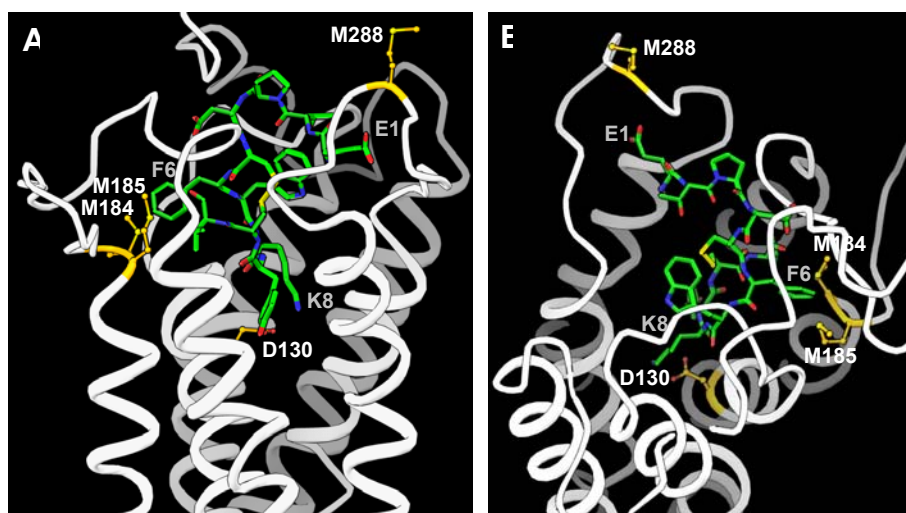


Fig. 2. Molecular modeling of rUT. Orientation of U-II in the rUT binding pocket. **A.** Side view **B.** Top down view.

Acknowledgments

The work was funded by grants from the CIHR and the HSFC.

References

1. Ames, R. S., *et al.* *Nature* **401**, 282-286 (1999).
2. Boucard, A. A., *et al.* *Biochemistry* **39**, 2662-2670 (2000).
3. Boucard, A. A., *et al.* *Biochem. J.* **362**, 829-238 (2002).
4. Rihakova, L., *et al.* *J. Recept. Signal Transduct.* **22**, 297-313 (2002).

Protein Kinase C Isoform (PKC) Peptide Activator/Inhibitors Exert Cardioprotective Effects in Polymorphonuclear Leukocyte (PMN)-induced Ischemia/Reperfusion (I/R) Injury

Lindon H. Young, Aisha Phillipson, Didi Omiyi, Norrell Atkinson,
 Manoj Jivani, Jovan Adams, Ellen E Peterman, Philip Taormina II,
 Richard J. Brue and Margaret Harvey

Department of Pathology/Microbiology/Immunology, Philadelphia College of Osteopathic
 Medicine, Philadelphia, PA 19131 USA

Introduction

Myocardial I/R injury is characterized by endothelial dysfunction, enhanced PMN infiltration into the myocardium, that results in sustained cardiac contractile dysfunction [1,2]. Enhancement of endothelial basal nitric oxide (NO) release or inhibition of PMN superoxide (SO) release reduces endothelial dysfunction and attenuates PMN/endothelial interaction. PKC is a key enzyme that regulates endothelial NO release and PMN SO release [1,2]. However, selective PKC isoforms mediating these responses are not well understood.

Myristoylated PKC isoform peptides (MW=1130 to 1928; Genemed Synthesis, Inc.) penetrate into cells by simple diffusion. The PKC beta II (β II) (N-Myr-SLNPEWNET) and delta (δ) isoform (N-Myr-HDAPIGYD) inhibitors bind to its receptor-activated C kinase region attenuating PKC translocation. By contrast, the PKC δ peptide activator (N-Myr-MRAAEDPM) augments translocation. The PKC zeta (ζ) peptide inhibitor (N-Myr-SIYRRGARRWRKL) binds to the pseudo-substrate domain, attenuating interaction with cell membrane substrates, eNOS and NADPH oxidase [1,2].

We hypothesized that selective PKC peptide isoforms would attenuate PMN-induced contractile dysfunction (i.e., left ventricular developed pressure; LVDP) after I/R when given separately or in combination (i.e., β II/ ζ) during reperfusion in the isolated perfused rat heart. We also wanted to determine the mechanism of action to account for any potential cardioprotective effects following I/R.

Results and Discussion

NO release was measured with a NO electrode connected to a NO meter (Table 1). Endothelial NO release was significantly increased from basal (n=46) values in PKC β II (n=8) or ζ , inhibitor (n=20) treated segments when tested separately and in combination (β II/ ζ) (n=8). It was also significantly increased with the PKC δ (-) inhibitor (n=22), whereas the δ (+) activator (n=13) did not significantly affect basal levels. Acetylcholine (Ach 500 nM; n=32) was used as a positive control.

The change of absorbance (Δ Abs.) was measured spectrophotometrically 360 sec after PMA (15 nM) addition (peak response) to rat PMNs (Table 2). SO release was significantly inhibited in the presence of PKC β II (n=22) or ζ (n=26) separately, but

Table 1. Measurement of NO release from rat aortic segments (pmol/mg).

Group	Basal	Ach	β II -	ζ -	β II/ ζ -	δ +	δ -
NO release	2.5 \pm 0.4	6.5 \pm 0.7	5.3 \pm 0.6	3.7 \pm 0.2	7.2 \pm 0.8	2.5 \pm 1.1	4.7 \pm 0.3
		**	**	**	**		**

(** p <0.01 from basal values expressed as mean \pm SEM)

Table 2. Measurement of SO release from rat PMNs (5×10^6).

Group	PMA	SOD	β II -	ζ -	β II/ ζ -	δ +	δ -
Δ Abs.	0.5 ± 0.05	0.02 ± 0.01	0.4 ± 0.04	0.3 ± 0.04	0.2 ± 0.02	0.3 ± 0.02	0.5 ± 0.1
		**	*	**	**	**	

(* $p < 0.05$, ** $p < 0.01$ from PMA ($n = 66$) values expressed as mean \pm SEM)

there was greater inhibition when used in combination (i.e., β II/ ζ ; $n = 7$). The PKC δ + ($n = 9$) significantly inhibited SO release, whereas the δ - ($n = 8$) did not. Superoxide dismutase (SOD 10 μ g/ml; $n = 36$) was used as a positive control.

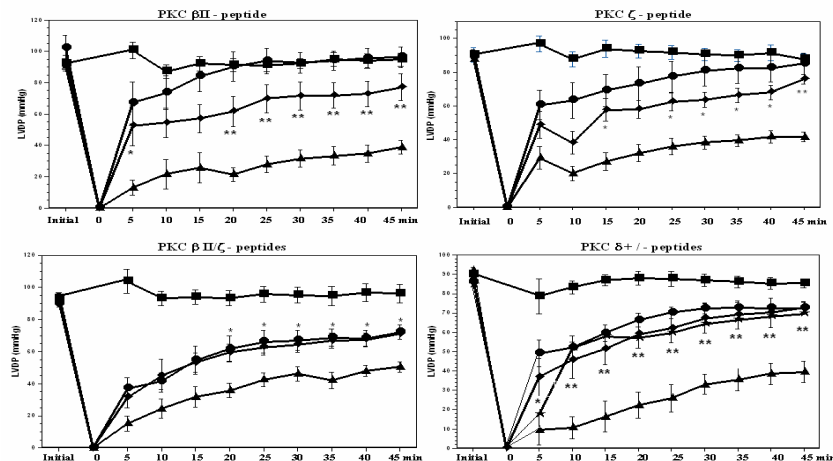


Fig. 1. Time course of LVDP in Sham (\blacksquare), I/R (\bullet), I/R+PMN (\blacktriangle) and I/R+PMN+PKC peptides (\blacklozenge) (5 or 10 μ M) perfused rat hearts ($n = 6$ to 10). LVDP data is shown at initial (baseline) and reperfusion from 0 to 45 min. following 20 min. ischemia. The sham group (not subjected to I/R) maintained the same LVDP throughout the 80 min. protocol. The PKC β II/ ζ peptide inhibitor combination completely eliminated the PMN-induced contractile dysfunction at every time point during post-reperfusion relative to the control I/R group. Interestingly, both PKC δ peptide inhibition (\clubsuit) and activation (\blacklozenge) were cardioprotective, but the δ activator restored LVDP faster (5 min. vs. 10 min.) during reperfusion. All values are expressed as mean \pm SEM. (* $p < 0.05$, ** $p < 0.01$ from final I/R+PMN values).

These results suggest that the PKC δ + restores LVDP via inhibition of PMN SO release, whereas the δ - does so via increased endothelial derived NO release, and the β II/ ζ inhibitors restore LVDP by both mechanisms.

Acknowledgments

This work was funded by NIH/NHLBI grant to L. H. Young, and the Center for Chronic Disorders of Aging at PCOM.

References

1. Phillipson, A., et al. *Am. J. Physiol.* **289**, H898-H907 (2005).
2. Omiyi, D., et al. *J. Pharmacol. Exp. Ther.* **314**, 542-551 (2005).

Rational Design of Small Molecules for a Novel Class of Anti-Cancer Drugs using a Phenylalanine Library

**Lajos Gera^{1,4}, Daniel C. Chan^{3,4}, Laimute Taraseviciene-Stewart²,
Vitalija Simkeviciene¹, Paul A. Bunn, Jr.^{3,4} and John M. Stewart^{1,2,4}**

¹Department of Biochemistry and Molecular Genetics; ²Pulmonary Hypertension Center, University of Colorado Health Sciences Center, Denver, CO 80262; ³Cancer Center, Aurora, CO 80010; ⁴Carcinex Inc., 7034 Indian Peaks Trail, Boulder, CO 80301, USA

Introduction

Lung cancer (LC) and prostate cancer (PC), the most common major cancers, have receptors for bradykinin (BK). The first-full-chain peptide BK antagonist with highly potent B1 and B2 receptor antagonist activity, B9430, developed by Gera in the Stewart laboratory a decade ago [1], had negligible anticancer activity. However, its N-terminal acylated analogs B10238, B10324, and its N-terminal dimer B9870 were highly active *in vivo* against small-cell lung cancer (SCLC) cells and PC3 cells in nude mouse xenografts. Our small-molecule peptide mimetic, M-570, also showed potent growth inhibition of lung and prostate cancers. Therefore, we designed newer analogs of M-570 and tested them against these cancer lines.

Results and Discussion

Peptides and mimetics were prepared using solution or solid phase methods, purified by HPLC and characterized by TLC, analytical HPLC, LDMS and amino acid analysis.

Our lead compound, M-570, is a simple acyl-tyrosine amide derivative with 91% anticancer activity against SCLC and with 65% activity against prostate cancer PC3 *in vivo*. In our earlier studies a tyrosine library was created based on M-570. In that study we gave preference to the incorporation of a variety of nonsteroidal anti-inflammatory drugs (NSAIDs: aspirin, diclofenac, ketorolac, naproxen, etc.) as the acylating group in position (A) of M-570 (Fig. 1). M-1394 (Ktlc-OC2Y-Atmp, Ktlc: ketorolac) showed high growth inhibition (70%) *in vivo* against NSCLC line A-549 and M-1376 gave an encouraging growth inhibition (44%) of PC3 [2]. Because tyrosine could be considered as a phenylalanine analog we extended our early tyrosine library to a phenylalanine library for structure-function relationship study. In each step a phenylalanine-derivative (B) was coupled to the 4-amino-piperidine-derivatives (C) by BOP or HATU in DMF to afford the amide derivatives. The Boc groups were cleaved by TFA in DCM and the primary amines (B-C) were acylated with the appropriate carboxylic acids (A) in the presence of BOP to give the M-570 analogs (Fig. 1). A simple extraction was used for the isolation and purification of each intermediate and final product. Our phenylalanine-library approach provided promising new agents (M-1764 and M-1846) and also revealed structure features that enhance the desired activity. Thus, the phenylalanine R2 group and the *N*-acyl R1 group need to be bulky and hydrophobic. In the amide group C basic moieties are tolerated and are useful as they increase solubility (Fig. 1.). Some of our compounds have higher growth inhibition *in vivo* against lung cancer and androgen-independent PC3 than standard anti-cancer drugs such as cisplatin and taxotere (39-60%) (Table1).

Table 1. Structures and Activities of selected BK Antagonists and Mimetics

Number	Structure	Biological Activity			
		GPI ^a	SCLC ^b	SHP-77 ^c	PC3 ^c
B9430	DR-R-P-Hyp-G-Igl-S-DIgl-Oic-R	8.2	120	15	0
B9870	SUIM-(B9430) ₂	8.4	0.15	65	78
B10238	F5c-DR-R-P-Hyp-G-Igl-S-DIgl-Oic-R	8.1	50	61	--
B10324	F5c-K-K-R-P-Hyp-G-CpG-S-DTic-CpG	--	--	86	43
M-570	F5c-OC2Y-Atmp	5.6	1.8	91	65
M-1108	F5c-D-OC2Y-Atmp	--	Dead	--	25
M-1376	Indo-OC2Y-Atmp	--	1.5	--	44
M-1586	Indo-D-OC2Y-Atmp	--	1.7	--	32
M-1764	Pcn-Bip-Atmp	--	1.2	--	--
M-1846	Nif-Bip-Atmp	--	1.4	--	--
	Cisplatin	--	--	60	39
	Taxotere	--	--	49	42

^a pA_2 for bradykinin antagonist activity on isolated guinea pig ileum. ^b ED_{50} (μM) for cytotoxicity by MTT test for SHP-77 SCLC in vitro. ^cPercent inhibition of growth of xenografts in nude mice. Compounds were injected i.p. at 5 mg/kg/day. Cisplatin was administered as 4 weekly injections of 10 mg/kg. Taxotere was injected 8 mg/kg/week, three times. Abbreviations: Atmp, 4-amino-2,2,6,6-tetramethylpiperidine; Bip, β -(4-biphenyl)alanine; CpG, α -cyclopentylglycine; F5c, 2,3,4,5,6-pentafluorocinnamoyl; Hyp, trans-4-hydroxyproline; Igl, α -(2-indanyl)glycine; Indo, indomethacin; OC2Y, O-(2,6-dichlorobenzyl)-tyrosine; Nif, niflumic acid; Oic, octahydroindole-2-carboxylic acid; Pcn, (E)- α -phenylcinnamoyl; SUIM, suberimidyl; Tic, tetrahydroisoquinoline-3-carboxylic acid.

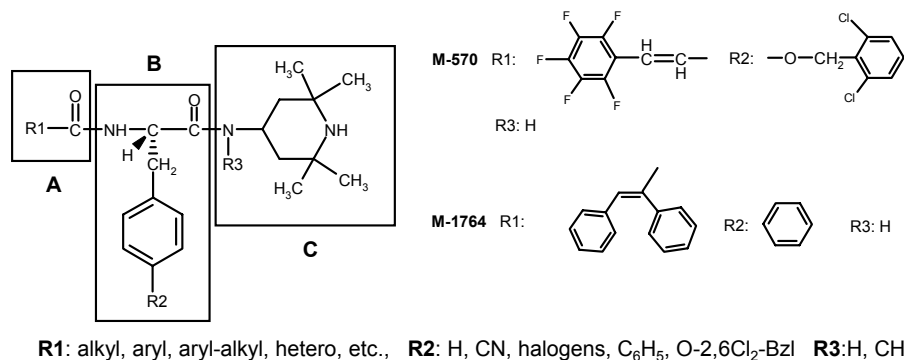


Fig. 1. Phenylalanine-library-designed structural analogs of BKM-570.

References

- Gera, L. and Stewart, J. M. *Immunopharmacol.* **33**, 174-177 (1996).
- Gera, L., Chan, D. C., York, E. Y., Simkeviciene, V., Bunn, P. A., Jr., Taraseviciene-Stewart, L. and Stewart, J. M. *J. Peptide Sci.* **10S**, 245 (2004).

Repair of Photodamaging Effects on Human Melanocytes by 4-Phenylbutyryl-His-D-Phe-Arg-Trp-NH₂. A Superpotent Analog of α -Melanocortin

James J. Knittel¹, Leonid N. Koikov¹, Pilgrim Jackson², Glenn Milhauser², Ana Luisa Kadekaro³, Renny J. Kavanagh³ and Zalfa Abdel-Malek³

¹Division of Pharmaceutical Sciences, University of Cincinnati, College of Pharmacy;

²Department of Chemistry and Biochemistry, University of California-Santa Cruz;

³Department of Dermatology, University of Cincinnati College of Medicine, Cincinnati, OH 45267-0592, USA

Introduction

The melanocortins α -, β -, γ -MSH and ACTH are a family of structurally-related peptides derived from the same precursor peptide proopiomelanocortin (POMC). The four melanocortins share a common four amino acid sequence, His-Phe-Arg-Trp, which is regarded as the core sequence that is essential for the melanogenic effect of α -MSH. Comparison of the effects of melanocortins on cultured human melanocytes revealed that α -MSH and ACTH are the most potent in stimulating melanogenesis, particularly eumelanogenesis, and proliferation. Recently, we discovered that α -MSH and ACTH promote human melanocyte survival after exposure to ultraviolet radiation (UVR) or treatment with hydrogen peroxide. The significance of α -MSH as a physiological regulator of pigmentation in many vertebrate species generated tremendous interest in synthesizing and biologically evaluating analogs of the physiological hormone. Many of these analogs have been used in structure-function studies, and some for diagnosis and therapeutic targeting of melanoma. Some potent agonists of α -MSH have been promoted as tanning agents that stimulate human cutaneous pigmentation in the absence of harmful sun exposure.

The 6-9 amino acid sequence of α -MSH (His-Phe-Arg-Trp) is the core sequence that is crucial for the pigmentary effect of the hormone. In an earlier report [1] we used this tetrapeptide as a lead for developing a series of fragment analogs of α -MSH in which the L-Phe⁷ is replaced by D-Phe and the N-terminus substituted with acids of varying chain length and functional groups. We hereby report on the effects of one of these analogs, 4-phenylbutyryl-His-D-Phe-Arg-Trp-NH₂, on tyrosinase activity, proliferation, and survival of cultured human melanocytes, as well as the induction and repair of UVR-induced cyclobutane pyrimidine dimers.

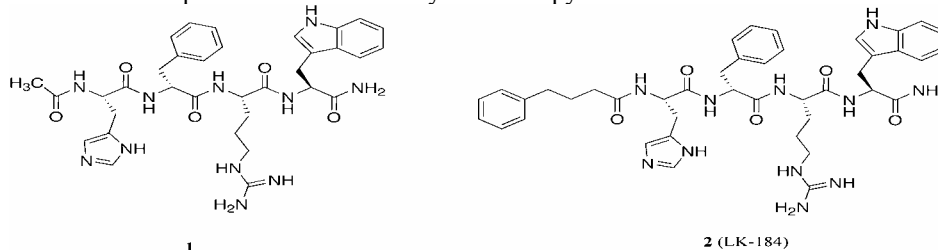


Fig. 1. Primary structures of the tetrapeptide template (**1**) and superpotent N-terminally modified analog (LK-184, **2**).

Results and Discussion

LK-184 was obtained on Rink amide resin using standard Fmoc methodology. The product was purified by HPLC on a C₁₈ column and characterized by ESI MS (purity >98%).

Both tetrapeptides **1** and **2** (Fig. 1) showed dose-dependent effects on cultured human melanocytes with respect to both melanocyte proliferation and tyrosinase activity. The EC₅₀ values for **1** and **2** are 3×10⁻⁹ and 5×10⁻¹² M, respectively, as determined by the dose-dependent effects on tyrosinase activity. Compound **2** also exhibited a residual effect on tyrosinase activity that markedly exceeds the residual effect of α-MSH and is comparable to that of the best-known α-MSH agonist NDP-α-MSH. Four days after wash off of compound, a statistically significant increase in tyrosinase activity was still apparent with analog **2** relative to α-MSH and NDP-α-MSH. UV-irradiated melanocytes (105 mJ/cm² UVBR) had a greater survival rate when pretreated with analog **2** than with α-MSH (concentration of 1 nM α-MSH or **2**). The MC1R was shown to mediate the effects of **2** as evidenced by abrogation of the stimulatory effect of this agonist on tyrosinase activity by an analog of human agouti signaling protein (ASP). Stimulation of tyrosinase activity by **2** (1 nM) was reduced to control levels in the presence of 50 nM ASP. In addition, human melanocytes with non-functional MC1R failed to respond to α-MSH or **2** with increased survival when exposed to 105 mJ/cm² UVBR.

The induction of cyclobutane pyrimidine dimers (CPDs) was reduced and their removal enhanced when human melanocytes were exposed to UVBR in the presence of analog **2** (Fig. 2). Treatment with **2** (1 nM) for 4 days prior to, and immediately after irradiation 21 mJ/cm² UVR (UVB + UVC) resulted significantly in reduced induction and enhanced repair as shown by Southwestern blot analysis using a monoclonal antibody that recognizes this form of DNA photoproducts.

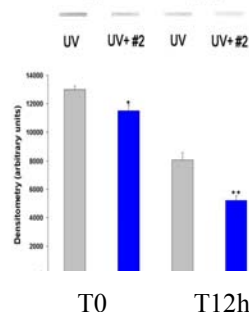


Fig. 2. Reduced induction and repair of cyclobutane pyrimidine dimers by analog **2**. * = significantly different from UV21 at T0; ** = significantly different from UV21 at T24h, as determined by ANOVA followed by SNK at $p < 0.05$.

In conclusion analog **2** may be a useful agent in the prevention of skin cancer, since it reduces the photodamaging effects of sun exposure and contributes to photoprotection by increasing cutaneous pigmentation.

Acknowledgments

Supported by the Skin Cancer Foundation Henry W. Menn Memorial Award to J.J. Knittel.

References

1. Koikov, L. N., Ebetino, F. H., Solinsky, M. G., Cross-Doersen, D. and Knittel, J. J. *Bioorg. Med. Chem. Lett.* **13**, 2647-2650 (2003).

RGD Peptide-Labeled Quantum Dots for Integrin $\alpha_v\beta_3$ Targeting

Weibo Cai, Xianzhong Zhang, Yun Wu and Xiaoyuan Chen

Molecular Imaging Program at Stanford (MIPS), Stanford University School of Medicine, CA 94305, USA

Introduction

Quantum dots (QDs) with size- and composition-tunable fluorescence emission have high quantum yields and photostability suitable for optical imaging and multiplexing [1]. Integrins are heterodimeric transmembrane cell adhesion molecules involved in tumor angiogenesis and metastasis. Integrin $\alpha_v\beta_3$, which binds to Arginine-Glycine-Aspartic acid (RGD)-containing components of the interstitial matrix such as vitronectin, fibronectin and thrombospondin, plays a key role in tumor angiogenesis and metastasis [2,3]. It is significantly upregulated on invasive tumor cells and tumor vasculature but not in quiescent endothelium. The ability to non-invasively visualize and quantify integrin $\alpha_v\beta_3$ expression level will provide new opportunities to document tumor (tumor cells and sprouting tumor vasculature) integrin expression, to more appropriately select patients for anti-integrin treatment and to monitor treatment efficacy in integrin-positive patients. Quantum dot-based probes, in particular, have great potential in imaging-guided surgery and therapy.

Results and Discussion

We have labeled quantum dot QD655 with c(RGDyK) (potent integrin $\alpha_v\beta_3$ antagonist) and the resulting conjugate QD655-RGD was tested for *in vitro* staining of cancer cell lines MDA-MB-435 (human breast cancer, high integrin $\alpha_v\beta_3$ expression) and C6 (rat glioma, low integrin $\alpha_v\beta_3$ expression) (Fig. 1). We successfully demonstrated the integrin targeting ability of QD655-RGD, as the QD655 stained cells showed no visible fluorescence signal while the cells were lit up by QD655-RGD and the fluorescence could be effectively blocked when unconjugated c(RGDyK) was added (Figs. 2 and 3).

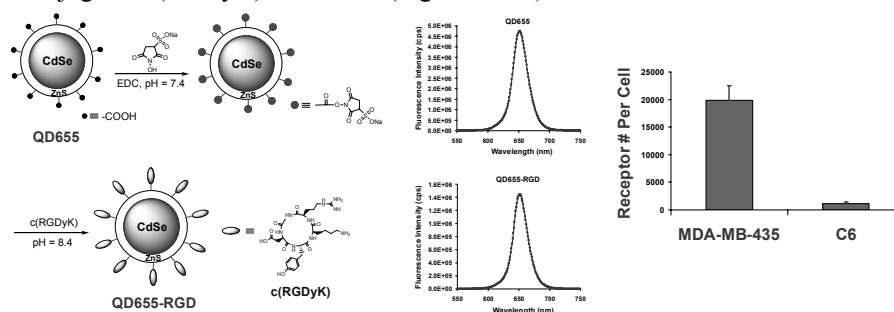


Fig. 1. Left: the synthesis of QD655-RGD conjugate. Middle: emission spectra of QD655 and QD655-RGD conjugate. Right: number of integrin $\alpha_v\beta_3$ per cell for MDA-MB-435 and C6.

In conclusion, we have successfully demonstrated the integrin $\alpha_v\beta_3$ targeting ability of QD655-RGD. *In vivo* optical imaging using quantum dot-based probes is currently under way. Based on the initial results shown here, a combinatorial approach which takes advantage of the multiplexing ability of the quantum dots,

high integrin targeting efficacy of the cyclic RGD peptides, and emission wavelength in the near infrared window (700 - 900 nm) will have great potential in cancer diagnosis, imaging-guided surgery and therapy.

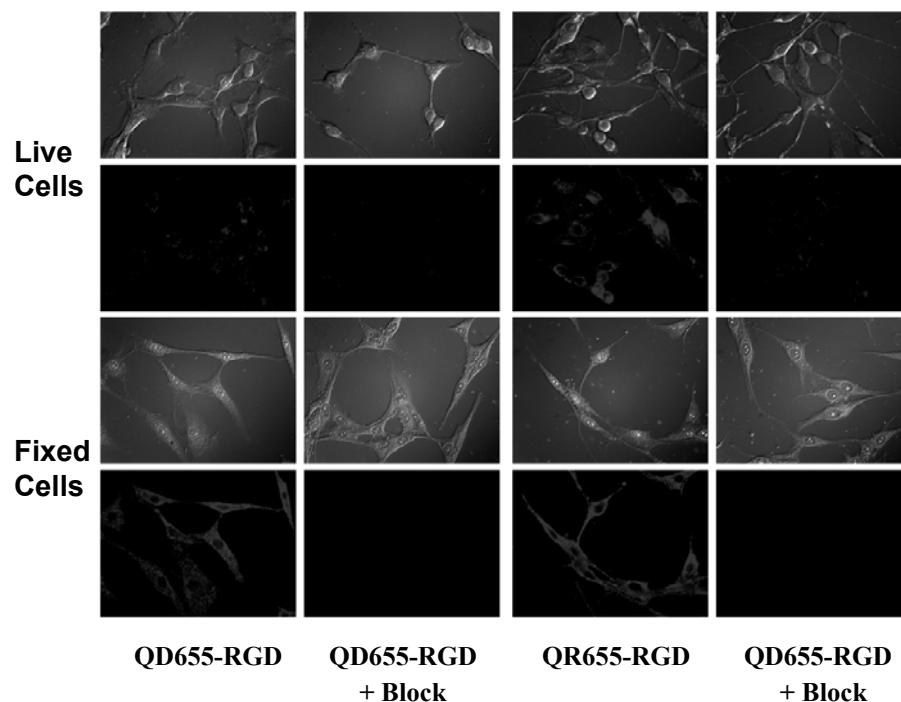


Fig. 2. Staining of C6 cells (left two columns) and MDA-MB-435 cells (right two columns) using 0.5 nM QD655-RGD with or without a blocking concentration of 2 μ M c(RGDyK). All fluorescence images were obtained under the same condition and displayed at the same scale for each cell line. Filter set: excitation: 420/40 nm; emission: 660/40 nm.

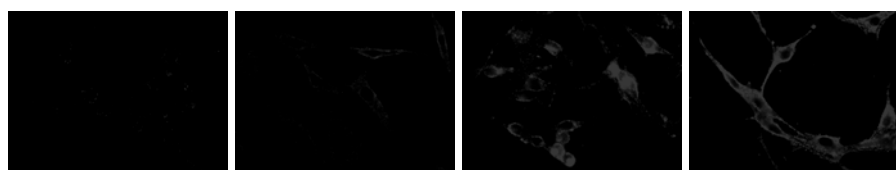


Fig. 3. Fluorescence images of QD655-RGD stained live and fixed C6 (left) and MDA-MB-435 cell (right) displayed under the same scale.

Acknowledgments

This project was funded in part by NIBIB Grant R21 EB001785, DOD BCRP Concept Award DAMD17-03-1-0752 and IDEA Award W81XWH-04-1-0697.

References

1. Michalet, X., *et al. Science* **307**, 538-544 (2005).
2. Hood, J. D. and Cheres, D. A. *Nat. Rev. Cancer* **2**, 91-100 (2002).
3. Xiong, J. P., *et al. Science* **296**, 151-155 (2002).

Rigid Cyclic Tetrapeptides as Probes and Mimics of Reverse Turns

Sage Berg-Cross and Garland Marshall

Department of Biochemistry, Washington University, St. Louis, MO 63110, USA

Introduction

Cyclic tetrapeptides, like β -turns, form $\sim 180^\circ$ turn between the first and fourth amino acid and therefore inherently possess bonds in close proximity to the $C\alpha$ - $C\beta$ bonds of a β -turn. We have found certain sequences of cyclic tetrapeptides that have both one unique conformation and bonds that overlap a significant portion of the $C\alpha$ - $C\beta$ bonds from β -turns found in the PDB [1,2]. Substitution off these bonds is the basis for β -turn mimetics that uniquely orient side chains. The use of proline or pipecolic acid adds rigidity, prevents internal hydrogen bonding, reinforces cis conformations, and provides extended rigid bonds distal that of $C\alpha$ - $C\beta$ (i.e., $C\beta$ - $C\gamma$, $C\gamma$ - $C\delta$). These compounds can be used to mimic known β -turns pharmacophores and probe unknown β -turn recognition motifs. The rigidity of these compounds should minimize the entropy of binding and enhance affinity by preorganization. Cyclic tetrapeptides were synthesized and analyzed by NMR and computational dynamics methods.

Results and Discussion

All four cyclic peptides c[pro-Pip-pro-Pro], c[pro-Pip-pro-Nma], c[pip-Pro-pip-Pro], and [Ala-Pro-pip-Pro] were synthesized by solid phase peptide synthesis (SPPS) methods; uppercase and lower case amino acids refer to L and D amino acids respectively (pip = pipecolic acid, Nma = N-methylalanine). The L-proline 2-chlorotrityl resin was used to prevent premature cleavage by DKP formation after addition of the second residue. Cyclizations were performed using HOBt and BOP or PyBop in DMF at 0.5mg/mL (~ 1.3 mM) concentrations. All cyclic compounds were HPLC purified and analyzed by H1, TOCSY, COSY, and NOESY NMR in both D_2O and $CDCl_3$. All compounds retained the same conformers in both solvents.

Of the four compounds, only c[pro-Pip-pro-Pro] appeared to have mixed conformers. The H1 NMR spectrum for c[pro-Pip-pro-Pro] showed 8 $C\alpha H$ peaks corresponding to two conformers. The two sets of four peaks have intensities with a ratio of 5:1. These conformers differ in their amide bond cis/trans conformations. It is noteworthy that in the major and minor conformations of c[pro-Pip-pro-Pro] there were two and one amide bonds which did not have NOE data to suggest either a cis or trans amide bond. By comparison, the H1 NMR spectrum for c[pro-Pip-Pro-Nma], c[pip-Pro-pip-Pro], and [Ala-Pro-pip-Pro] show only 4 $C\alpha H$ peaks indicating one conformer for each. The four peptides were cooled to minus $25^\circ C$ in chloroform and NMR performed to see if quickly exchanging conformers would become apparent. Aside from pro-Pip-pro-Pro the three other peptides displayed only one conformation. The conformations of the each peptide are outlined in Table 1.

Table 1. Omega torsions of cyclic tetrapeptides

Peptide	Torsion 1	Torsion 2	Torsion 3	Torsion 4
c[pro-Pip-pro-Pro] major conformation	trans	X	trans	x
c[pro-Pip-pro-Pro] minor conformation	trans	trans	x	trans
c[pro-Pro-pro-Nma]	trans	trans	trans	trans
c[pip-Pro-pip-Pro]	trans	Trans	cis	trans
c[Ala-Pro-pip-Pro]	trans	trans	cis	trans

Torsions for cis(0°) and trans(180°) were found to vary by as much as +/- 50° as determined by simulated annealing dynamics studies and still conform the NMR data. An "x" indicates that there was no NOE to indicate either a cis or trans conformation. Torsions 1 thru 4 refer to the sequence listed on the leftmost column with the fourth torsion being between the last and first residue.

Simulated annealing (SA) dynamic calculations are underway using the NOE NMR data as a constraint. All dynamic simulations were performed using the Tripos Sybyl 7.0 software. 1000 cycles of simulated annealing, heating to 1000°K for 1000fs and annealing to 200°K in 1000fs. The Kollman all-atom force field was used with Gasteiger-Huckel charges applied to the molecules. Spring constraints based on NOE data was applied during annealin steps. Low energy conformers of c[pro-Pro-pro-Nma] found below 300°K were analyzed. All omega angles were found to be constrained to the trans (180°) conformation. The two D-pro residues opposite each other are pointed downward in the same direction and perpendicular to the macrocycle. Likewise the L residues are pointed upward in the same direction and perpendicular to the macrocycle. Lastly the carbon-carbon and carbon-hydrogen of the all trans conformation of c[pro-Pro-pro-Nma] were screened by RMS fit for overlapping a set of vectors that represent the C α -C β bonds of β -turns[2]. Figure 1 shows the excellent overlap c[pro-Pro-pro-Nma] had with all four of the vectors (green) representing ~10% of the C α -C β bonds of β -turns in the PDB.

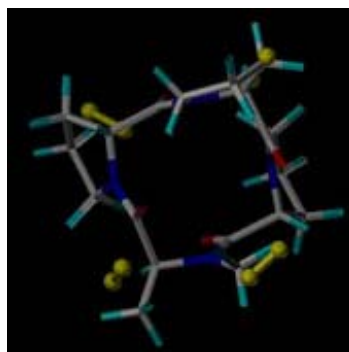


Fig. 1. C[pro-Pro-pro-Nma] overlapped with 4 C α -C β vectors from β -turns in the PDB, displayed in stick and ball and stick models respectively.

References

1. Berg-Cross, S., Zhang, W. and Marshall, G., unpublished.
2. Tran, T., Smythe, M., McKie, J., Meutermaans, W., Bourne, G. and Andrews, P., unpublished.

Solid-Phase Synthesis and Structure Characterization of *N'*-Biphenyl-*N*-2-Ethylbutyl-Demethylvancomycin

Nian-Huan Yao¹, James R. Carlson¹, Gang Liu² and Kit S. Lam¹

¹Division of Hematology & Oncology, Department of Internal Medicine, UC Davis Cancer Center, 4501 X Street, Sacramento, California 95817, USA; ²Chinese Academy of Medical Sciences & Peking Union Medical College, Institute of Materia Medica, 1 Xian Nong Tan Street, Beijing 100050, P. R. China

Introduction

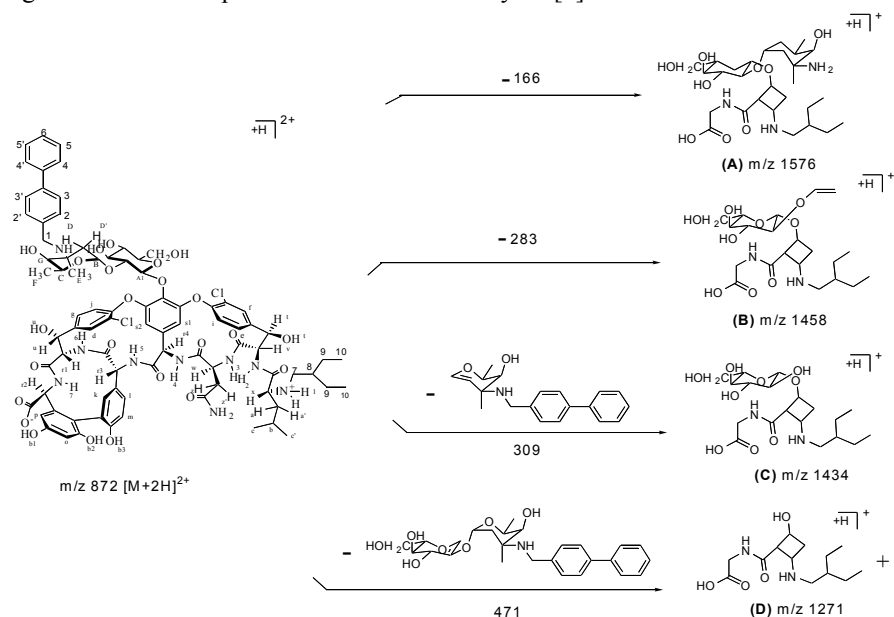
Vancomycin, a potent glycopeptide antibiotic, is the last resort against gram-positive pathogens such as methicillin-resistant *Staphylococcus aureus* [1]. Recent studies indicate that carbohydrate derivatives of vancomycin have excellent activity against vancomycin-resistant *enterococci* [2]. *N*-Demethylvancomycin, an analog of vancomycin that has been used clinically in China since 1967 differs from vancomycin at the *N*-terminus, where the *N*-methyl-leucine is replaced by leucine [3]. We report a new solid-phase synthesis strategy for *N*-demethylvancomycin derivatization, which involves chemoselective protection of amino groups by Fmoc at the *N*-terminus. *N'*-Biphenyl-*N*-2-ethylbutyl-demethylvancomycin was found to restore the activity against vancomycin-resistant *Enterococcus faecalis*. The structure of this vancomycin derivative was determined by 1D-NMR and 2D-NMR.

Results and Discussion

The *N*-terminal free amino group of *N*-demethylvancomycin was regioselectively derivatized with 9-fluorenylmethyl-*N*-succinimidyl carbonate (Fmoc-OSu), while pH was maintained at 7.0 with NaHCO₃. Fmoc-*N*-demethylvancomycin was then coupled onto solid support through its C-terminus, followed by selective reductive alkylation of the remaining amino group of the vancosamine with biphenyl-4-carboxyaldehyde. The *N*-terminal amino group then underwent reductive alkylation to form *N'*-Biphenyl-*N*-2-ethylbutyl-demethylvancomycin.

The structure of *N'*-Biphenyl-*N*-2-ethylbutyl-demethylvancomycin was determined by LC-MS/MS analysis. Its proposed fragmentation pathway is illustrated in Scheme 1. The full scan MS spectrum revealed a doubly charged ion [M+2H]²⁺ of the expected molecular weight. In the full scan MS/MS spectrum, the loss of biphenyl group (166Da) resulted in the generation of fragment **A** (m/z 1576). Fragment **B** (m/z 1458) produced by vancosamine ring cleavage and elimination of fragment moiety (283 Da) containing biphenyl substituent, indicated that the amino group of vancosamine was selectively alkylated by biphenyl aldehyde. This was further confirmed by the generation of fragment **C** (m/z 1434) through losing biphenylated vancosamine (309Da), and fragment **D** (m/z 1271) through elimination of biphenylated disaccharide (471Da). Furthermore, the fact that major fragments **A**, **B**, **C**, and **D** all contained an 2-ethylbutyl group demonstrated that the *N*-terminus of demethylvancomycin was selectively 2-ethylbutylated by 2-ethylbutylaldehyde. Together, the MS data confirms the chemical structure of demethylvancomycin on TentaGel resin.

^1H -NMR study of *N'*-Biphenyl-*N*-2-ethylbutyl-demethylvancomycin revealed new signals 7.38-7.72, and 0.83, 1.32, 1.49 and 2.71ppm, which were assigned to biphenyl and ethylbutyl groups respectively. The rest of the NMR signals were in agreement with the published data on vancomycin [4].



Scheme 1. Proposed fragmentation pathways of *N'*-Biphenyl-*N*-2-ethylbutyl-demethylvancomycin based on the ESI-MS/MS spectrum.

The antibacterial activity of *N'*-biphenyl-*N*-2-ethylbutyl-demethylvancomycin against *E. faecalis* (ATCC 29212), *S. aureus* (ATCC 29213), and methicillin resistant *S. aureus* (ATCC 43300) decreased 2, 8, and 4 folds, respectively. However, its antibacterial activity against vancomycin-resistant *E. faecalis* (ATCC 51299) was restored at a MIC of 10 $\mu\text{g/mL}$.

We have developed a solid-phase synthesis method with Fmoc protection strategy to prepare demethylvancomycin derivatives. This method allows us to efficiently and regioselectively reductive alkylate demethylvancomycin at both the vancosamine and *N*-terminal sites. The synthetic scheme outlined in this report is relatively simple and can be readily applied to large scale combinatorial synthesis, including substituting the glycine with many other natural and unnatural amino acids.

References

1. Leclercq, R. and Courvalin, R. *Clin. Infect. Dis.* **24**, 545-554 (1997).
2. Eggert, U. S., Ruiz, N., Falcone, B. L. V., Branstrom, A. A., Goldman, R. C., Silhavy, T. J. and Kahne, D. *Science* **294**, 361-364 (2001).
3. Ling, D. K., Yu, Z. and Su, C. *Acta Pharmaceutica Sinica* **21**, 208-212 (1986).
4. Kannan, R., Harris, C. M., Harris, T. M., Waltho, J. P., Skelton, N. J. and Williams, D. H. *J. Am. Chem. Soc.* **110**, 2946-2953 (1988).

Stereo-controlled Synthesis of [L-Arg, L/D-3-(2-Naphthyl)alanine]-type (*E*)-Alkene Dipeptide Isosteres and its Application to the Preparation and Biological Evaluation of Peptidomimetic Analogs of the CXCR4 Antagonist FC131

Hirokazu Tamamura^{1,2}, Kenichi Hiramatsu², Satoshi Ueda², Zixuan Wang³, John O. Trent⁴, Stephen C. Peiper³, Naoki Yamamoto⁵, Hideki Nakashima⁶, Akira Otaka² and Nobutaka Fujii²

¹Institute of Biomaterials and Bioengineering, Tokyo Medical and Dental University, Tokyo 101-0062, Japan; ²Graduate School of Pharmaceutical Sciences, Kyoto University, Kyoto 606-8501, Japan; ³Medical College of Georgia, Augusta, GA 30912, USA; ⁴James Graham Brown Cancer Center, University of Louisville, Louisville, KY 40202, USA; ⁵Tokyo Medical and Dental University, School of Medicine, Tokyo 113-8519, Japan; ⁶St. Marianna University, School of Medicine, Kawasaki 216-8511, Japan

Introduction

Backbone replacements of amide bonds in peptides by (*E*)-alkene dipeptide isosteres (EADIs) provide information on the contributions of the corresponding amide bonds on biological activity. We established a completely stereo-controlled synthetic process for both L,L- and L,D-type EADIs starting from L-amino acids. Treatment of *N*-aryl- γ,δ -*cis*- γ,δ -epimino (*E*)- α,β -enoates (*cis*-(*E*)-enoates) with methanesulfonic acid (MSA) gives γ -mesyloxy- α,β -enoates, which can be converted into L,D-type EADIs by organocopper-mediated α -alkylation *via anti*-S_N2' reactions, whereas organocopper-treatment of *cis*-(*E*)-enoates affords L,L-type EADIs [1,2]. However, this synthetic procedure has not yet been optimized, since it involves a potential limitation on the introduction of functional groups into the side chain at the α -position. In the present study, to demonstrate the utility of organozinc-copper reagents, a set of EADIs of L-Arg-L/D-3-(2-naphthyl)alanine (Nal) were synthesized as model compounds *via* the γ,δ -*cis*- γ,δ -epimino (*E*)- α,β -enoate by the combination of MSA-mediated aziridinyl ring-opening reactions and α -alkylation with organozinc-copper reagents, which were prepared from 2-naphthylmethylZnBr and CuCN. The dipeptide sequence, Arg-Nal, is part of the low molecular weight CXCR4 antagonist, FC131, which was recently developed based on a 14-mer peptide T140 (Fig. 1) [3]. Then, FC131 analogs, in which several isosteres including the above EADIs were introduced, were synthesized to identify the biological importance of these amide bonds.

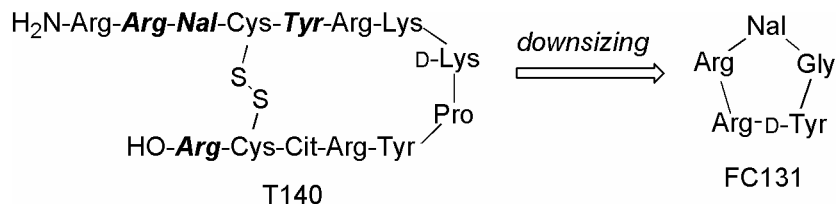
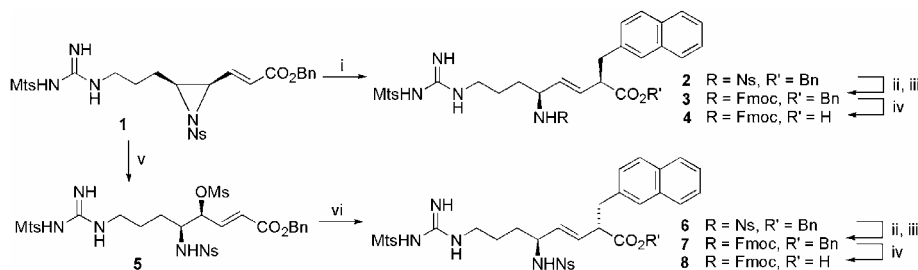


Fig. 1. Reduction of the molecular size of the CXCR4 antagonist T140 to the cyclic pentapeptide FC131. Bold/italic residues are the indispensable residues of T140 for the expression of strong CXCR4 antagonistic activity.

Results and Discussion

Synthesis of (L-Arg-L/D-Nal)-type EADIs: (L-Arg-L/D-Nal)-type EADIs were synthesized *via* the same key intermediate *N*-2-nitrobenzenesulfonyl (Ns)- γ,δ -*cis*- γ,δ -epimino (*E*)- α,β -enoate **1**, which was prepared by successive treatments of the corresponding allyl alcohol with the Mitsunobu reaction, ozonolysis and the modified Horner-Wadsworth-Emmons olefination (Scheme 1). *Anti*-S_N2' reaction of **1** with an organozinc-copper reagent, 2-naphthylmethylCu(CN)ZnBr·2LiCl, afforded an L,L-type EADI **2**, in which a (2*R*)-2-naphthylmethyl side chain was incorporated at the α -position, stereoselectively in 83% yield. *N* ^{α} -Fmoc substitution for the *N* ^{α} -Ns group of **2** followed by selective deprotection of the benzyl ester afforded a desired EADI, Fmoc-L-Arg(Mts)- $\psi[(E)\text{-CH=CH}]$ -L-Nal-OH, **4**. Alternatively, exposure of **1** to MSA afforded exclusively δ -aminated γ -mesyloxy- α,β -enoate **5** by regio- and stereo-selective S_N2 ring-opening reaction at the γ -carbon of **1**. Mesylate **5** was successively treated by an organozinc-copper reagent, 2-naphthylmethyl Cu(CN)ZnBr·BF₃, to afford an L,D-type EADI **6**, in which a (2*S*)-2-naphthylmethyl side chain was incorporated at the α -position, stereoselectively *via* an *anti*-S_N2' mechanism in 67% yield. **6** was similarly converted into another desired EADI, Fmoc-L-Arg(Mts)- $\psi[(E)\text{-CH=CH}]$ -D-Nal-OH, **8**.



Scheme 1. Reagents: (i) 2-naphthylmethylCu(CN)ZnBr·2LiCl; (ii) PhSH, K₂CO₃; (iii) Fmoc-OSu, Et₃N; (iv) thioanisole, TFA; (v) MsOH; (vi) 2-naphthylmethylCu(CN)ZnBr·BF₃.

Cyclic pseudopeptides: FC131 analogs, in which the above EADIs were introduced, were synthesized by Fmoc-based solid-phase synthesis and two steps of deprotection/cleavage system involving cyclization with the azide procedure [4]. For comparative studies, several FC131 analogs, which include other isosteres, were prepared and biologically evaluated. An (L-Arg-L-Nal)-type EADI containing FC131 analog showed moderate anti-HIV and CXCR4-antagonistic activities. NMR analysis showed that the parent peptide (FC131) and the EADI-introduced pseudopeptides have nearly equal distances between any two β -carbons in all of the side chains. It suggests from this study that these compounds maintain similar dispositions of pharmacophores, and that the biological differences between these compounds are derived from the (*E*)-alkene/amide bond units. Thus, EADIs become useful tools for investigation of biological contributions of amide bonds.

References

1. Tamamura, H., *et al.* *Chem. Commun.* 2327-2328 (1997).
2. Tamamura, H., *et al.* *J. Chem. Soc., Perkin Trans. 1* 2983-2996 (1999).
3. Tamamura, H. and Fujii N. *Curr. Drug Targets-Infectious Disorders* **4**, 103-110 (2004).
4. Tamamura, H., *et al.* *J. Med. Chem.* **48**, 380-391 (2005).

Stoichiometric Inhibition of β -Amyloid Fibrillogenesis using $C^{\alpha,\alpha}$ -Disubstituted Amino Acid Containing Peptides

Marcus A. Etienne¹, Cyrus Bett¹, Jed P. Aucoin¹, Tim J. Jensen¹, Robin L. McCarley¹, Ted Ajmo², Donna Herber², David Morgan² and Robert P. Hammer¹

¹*Department of Chemistry, Louisiana State University, Baton Rouge, LA 70803;* ²*Alzheimer Research Laboratory, Department of Pharmacology, University of South Florida, Tampa, FL 33612, USA*

Introduction

Alzheimer's Disease (AD) is the most common form of dementia. This degenerative disease is characterized by the presence of neurofibrillar structures, mostly consisting of the β amyloid protein ($A\beta$), that self assemble into senile plaques deposited on the brain [1]. Insoluble fibrils have been linked to the pathogenesis of AD, but recently, intermediates of this process (protofibrils) have been shown to have a cytotoxic effect in rat neuronal cells [2-4]. Research interests pertaining to the inhibition of $A\beta$ fibrillogenesis has increased; therefore, detailed knowledge of the $A\beta$ mechanistic pathway is necessary for the development of effective therapeutic targets.

Our design of inhibitors of $A\beta$ fibrillogenesis builds on the hypothesis that peptides that contain the hydrophobic core of $A\beta$ (KLVFF) can interact with the corresponding residues in $A\beta$ via self-recognition and disrupt the self-assembly of $A\beta$ into protofibrils and fibrils. In particular, we have utilized an alternating $\alpha\alpha AA/L$ -amino acid design to give a peptide that could interact with $A\beta$ by hydrogen bonding as well as by side-chain interactions, but has one hydrogen bonding edge blocked. It is known that $\alpha\alpha AAs$ with larger side-chain groups stabilize extended conformations in homo-oligomers [5] thus we hypothesize that peptides designed in this manner might have strong affinity for β -sheet assemblies of $A\beta$ and also preventing further aggregation by blocking one face of the assembly.

Results and Discussion

A protocol that renders monomeric $A\beta$ starting solutions which allows for reliable and reproducible results have been devised. We have studied the effects of AMY-1 (oligolysine unit on the C-terminus), AMY-2 (disrupting oligolysine unit on the N-terminus), and modified -AMY (Aib substitution) on the aggregation and fibrillization of $A\beta$. Spectroscopically, we find that AMY-1 greatly alters the progression of the β -sheet secondary structure associated with the $A\beta$ protein and also increases the rate of aggregation forming non-fibrillic assemblies. An alternate aggregation pathway yielding non-fibrillic assemblies have also been discovered. Cellular toxicity studies show that the novel inhibitor is capable of decreasing neurotoxicity against PC-12 cells and TEM results indicate the inhibition of fibrillic assemblies over prolong periods of time at both equimolar and submolar concentrations. AMY-1 (2 μ L, 500 mM, 1 nanomole) was injected into the hippocampus at the point marked * (Fig. 1). DG is the location of the dentate gyrus. CA3 is Cajal's area 3. LV is the lateral ventricle. Dark stained areas are diffuse $A\beta$ aggregates recognized by the anti- $A\beta$ antibody. Similar clearing results were seen for Congo Red staining, which is selective for fibrillar $A\beta$. The decrease of the ratio

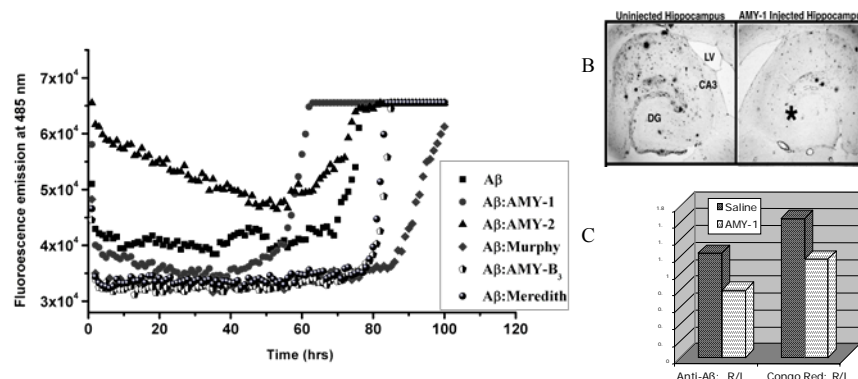


Fig. 1. (A) Thioflavin-T kinetic assay of A β in the presence of inhibitor compounds. Results indicate that AMY-1 increases A β aggregation rate as well as AMY-2 compared to other peptide-based inhibitor (50 μ M A β : 100 μ M inhibitor). (B) Anti-A β antibody staining of hippocampal region of untreated transgenic Tg2576 APP mouse (left) and AMY-1-treated APP mouse (right). (C) Anti-A β comparison with Congo Red staining of saline vs. AMY-1.

of right hemisphere to left hemisphere staining is a strong indicator of a specific effect of the AMY-1 injection on A β clearance as seen in prior work using A β specific antibodies [6]. Currently, detailed *in vitro* and *in vivo* studies along with fibril dissolution are in progress. Monomeric, oligomeric, and fibrillic species of A β are being tested to elucidate inhibitor efficiencies.

Acknowledgments

We thank the National Institute on Aging of the National Institutes of Health (AG 17983) for financial support of this research.

References

1. Hardy, J. and Selkoe, D. J. *Science* **297**, 353-356 (2002).
2. Walsh, D. M., Hartley, D. M., Kusumoto, Y., Fezoui, Y., Condron, M., Lomakin, A., Benedek, G. B., Selkoe, D. J. and Teplow, D. B. *J. Biol. Chem.* **274**, 25945-25952 (1999).
3. Kaye, R., Head, E., Thompson, J. L., McIntire, T. M., Milton, S. C., Cotman, C. W. and Glabe, C. G. *Science* **300**, 486-489 (2003).
4. Bucciantini, M., Giannoni, E., Chitti, F., Baroni, F., Formigli, L., Zurdo, J., Taddei, N., Ramponi, G., Dobson, C. M. and Stefani, M. *Natur*, **416**, 507-511 (2002).
5. Wyssong, C. L., Yokum, T. S., McLaughlin, M. L. and Hammer, R. P. *CHEMTECH* 26-33 (1997).
6. Wilcock, D. M., DiCarlo, G., et al. *J. Neurosci.* **23**, 3745-3751 (2003).

Structure Determination of the Human Angiotensin II Receptor Type 1 by the Methionine Proximity Assay

Martin Clément, Stéphane S. Martin, Caroline Chamberland, Marie-Ève Beaulieu, Richard Leduc, Gaétan Guillemette and Emanuel Escher

Department of Pharmacology, Faculty of Medicine, Sherbrooke University, Sherbrooke, Québec, J1H 5N4 Canada

Introduction

Labeling studies using benzophenone photoprobes have identified many ligand-receptor contact-points but with a surprisingly high ratio of methionine contacts [1-3]. Despite the fact that methionine represents a small proportion of the proteinogenic amino acids in most receptors, *p*-benzoyl-L-phenylalanine (Bpa) containing peptide labels have been shown to incorporate into Met residues at a disproportionate frequency [4]. Previous photochemical studies of the benzophenone radical have indicated that it exhibits strong selectivity for thioether groups due to the formation of an intermediate charge-transfer complex [5]. This selectivity would explain the high ratio of methionine insertion into target proteins through benzophenone photoaffinity labeling. This property can be exploited to introduce Met residues into target structures as 'bait' with the goal of identifying other receptor residues that are in close proximity to the ligand label. The immediate molecular environment of this ligand residue can thus be determined.

The C-terminal residue of angiotensin II (Ang II) interacts with the 7th transmembrane domain (TMD) of the Ang II receptor AT₁ [1] at non-Met contacts since no endogenous Met residue is in the immediate vicinity of the ligand binding pocket. We used the methionine proximity assay (MPA) to investigate the binding environment of the C-terminal residue of Ang II within this receptor with [Sar¹, Bpa⁸]AngII, a neutral antagonist [7]. We found 11 ligand contacts in TMD III, VI and VII with this approach. In the present study we applied the MPA approach also to the constitutively active hAT₁-mutant N111G-hAT₁ and compared the results with those obtained from wt-hAT₁. This would allow evidencing contact differences in the receptor and, eventually, structural changes related to receptor activation.

Results and Discussion

A further series of 54 transmembrane X→Met mutants of hAT₁ were constructed in all TMDs as double mutants on the N111G mutation (itself in TMD III and producing constitutive activity). The affinity of all double mutants was assessed, showing close to 1 nM affinity for [Sar¹, Bpa⁸]AngII for all, except S105M/N111G, where no binding was observed. Photolabeling of all receptor mutants was followed by isolation of the covalently labeled receptor complex, by CNBr digestion, and by SDS-PAGE. Labeling of wt-hAT₁ and N111G-hAT₁ produced a 7.2kDa fragment, corresponding to TMD VII and most of the intracellular C-terminal sequence (285-334) [1] (Fig. 1A). All mutant receptors in TMD I, II, IV, and V produced the same 7.2kDa fragment, indicating that labeling took place on TMD VII only. Mutants L112 and Y113 (TMD III), F249, W253, H256 (TMD VI), F293, N294, N295, C296, and L297 (TMD VII) produced new fragments, indicative of ligand contacts and are identical to those of the WT-hAT₁ MPA. The only exception is the T260M/N111G mutant who is no more MPA positive. Surprisingly, the double

mutants A104M/N111G and H263M/N111G recovered ligand affinity where the single mutants were inactive. These differences are highly significant in the context of the previous MPA and SCAM studies on AT₁. The two inactive mutants, A104M and H263M, are outside of the consensus binding area on the extracellular-membrane rim. A104C is also the most SCAM sensitive position, i.e., obstructive against ligand binding in the alkylated state [8] as well as H263C (to be published). In the MPA analysis [7] T260M was positive but definitely outside the consensus binding locus and all three residues are pointing inwards towards the presumed ligand access path during binding. These results are compatible with the reported outward movement of TMD VII in the N111G mutant [8], allowing for a slightly enlarged ligand access path.

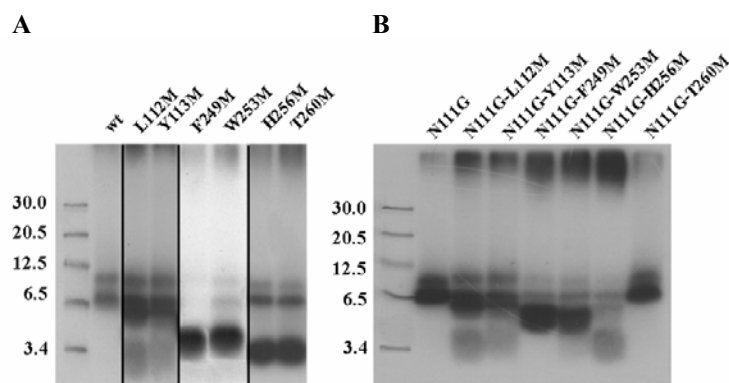


Fig. 1. CNBr (100 mg/ml) hydrolysis of partially purified ¹²⁵I-[Sar^I, Bpa⁸]Ang II-labeled mutant receptors before resolution by SDS-PAGE.

Conclusions

These results confirm the structural model of the AngII-hAT₁ interaction where the C-terminal residue of Ang II points deep into the transmembrane core towards TMD III, TMD VI, and TMD VII (Fig. 1B). The small but significant differences between WT receptor and N111G-receptor further support an outward movement of TMD VII in the receptor activation mechanism but with no other major structural change of the liganded receptor complex.

Acknowledgments

The work was supported by funds from CIHR and CHSF to E. Escher.

References

1. Perodin, J., *et al. Biochemistry* **48**, 14348-14356 (2002).
2. Rihakova, L., *et al. J. Recept. Signal Transduct. Res.* **22**, 297-313 (2002).
3. Palczewski, K., *et al. Science* **289**, 739-745 (2000).
4. Riggs, R. M., *et al. J. Med. Chem.* **30**, 1914-1918 (1987).
5. Horner, M. *Chem. Ber.* **85**, 520-530 (1952).
6. Ballesteros, J. A., Shi, L. and Javitch, J. A. *Mol. Pharmacol.* **60**, 1-19 (2001).
7. Clement, M. J., *et al. J. Biol. Chem.* **281**, 2317-2332 (2006).
8. Martin, S. S., *et al. J. Biol. Chem.* **279**, 51415-51423 (2004).

Structure-Activity Relationship Studies of a Novel CXCR4 Chemokine Antagonist Reveal Unique Activity Profile

Celia Amela-Cortés¹, Martha Rezende¹, Tatyana Yakovleva¹, Dan
Papa¹, Elisabeth Perchellet², Jean-Pierre Perchellet² and Sandra C.
Vigil-Cruz¹

¹Department of Medicinal Chemistry, University of Kansas, Lawrence, KS 66045, USA;

²Division of Biology, Kansas State University, Manhattan, KS 66506, USA

Introduction

Antagonists at the CXCR4 chemokine receptor represent an exciting potential to be inhibitors of breast cancer metastasis [1] and potentially other types of cancer metastasis [2]. Hence, our interest is in understanding how ligands interact at this receptor. Viral macrophage inflammatory protein-II (vMIP-II) is a viral chemokine encoded by Kaposi's sarcoma associated herpes virus-VIII and is an antagonist at both the CXCR4 and CCR5 chemokine receptors [3]. The fragment vMIP-II-(1-21)OH is a selective CXCR4 antagonist but has a 14-fold loss of CXCR4 receptor affinity compared to the parent protein [4]. vMIP-II-(1-21)NH₂ (virokine L) (Fig. 1), which was designed with an amidated C-terminus to increase metabolic stability, demonstrates substantial receptor affinity and antagonist potency [5]. In order to identify residues of virokine L required for ligand-receptor interaction, a systematic alanine scan was performed on the first eighteen amino acids of this peptide.

Virokine L H-LGASWHRPDKCCLGYQKRPLP-NH₂

Fig. 1. Structure of Virokine L (vMIP-II-(1-21)NH₂).

Results and Discussion

The peptides were prepared using Fmoc-amino acids and PyBOP-mediated couplings on a PAL-PEG-PS resin. They were deprotected and cleaved from the solid support using Reagent B (88% TFA, 5% phenol, 5% water and 2% TIPS) [6] and purified to >98% homogeneity using semi-preparative reverse-phase HPLC. Purity and identity were evaluated by HPLC and mass spectrometry, respectively.

Competition binding assays were performed on the pure peptides using the radioiodinated endogenous ligand [¹²⁵I]stromal cell-derived factor-1 (SDF-1) to evaluate CXCR4 receptor affinity. The results demonstrate that Leu in position 1 and His in position 6 are critical for receptor interaction as indicated by a loss of 6.5- and 13-fold in receptor affinity, respectively upon Ala substitution. The basic residues Arg⁷ and Lys¹⁰ also contribute to receptor binding, as Ala substitution resulted in a 3-fold loss of receptor affinity for both positions. Data for selected analogues are shown in Table 1.

The most unique finding is the significant enhancement (7.8-fold) in receptor affinity by Ala replacement for Leu in position 13, suggesting that the amino acid sequence for virokine L can be further optimized.

The high affinity [Ala¹³]virokine L analog was examined for antagonist activity in a GTPase assay. In this assay, the ability of the synthetic peptide to reverse SDF-1-induced GTPase hydrolysis in Sf9 insect cells engineered to contain CXCR4 and associated G-proteins was examined [5]. The IC₅₀ values determined were converted

Table 1. CXCR4 affinity of selected virokinine L analogs

Analog	CXCR4 Affinity ^a	
	IC ₅₀ (nM) ± SEM	Relative Affinity
[Ala ¹]virokinine L	805 ± 13	6.6
[Ala ⁶]virokinine L	1,580 ± 56	13
[Ala ⁷]virokinine L	412 ± 18	3.4
[Ala ¹⁰]virokinine L	419 ± 10	3.4
[Ala ¹³]virokinine L	15.8 ± 0.8	0.13
virokinine L	123 ± 3	1

^an = 3 independent experiments

to K_i using the Cheng and Prusoff equation [7]. [Ala¹³]virokinine L is potent antagonist in this assay (K_i = 36.0 ± 6.3 nM) with almost 2-fold enhanced antagonist potency over virokinine L (K_i = 61.2 ± 9.4 nM) and represents a new lead compound.

The high receptor affinity of the ligands (IC₅₀ = 16 - 123 nM) suggests there is some overlap in the binding site with that of SDF-1.

Acknowledgments

We would like to acknowledge Dr. Roland Seifert (University of Regensburg) for his collaboration on the design and implementation of the GTPase assays. The work was funded by an NIH COBRE Award 1P20RR15563, and matching support from the State of Kansas and the University of Kansas and an NIH IRACDA award 5K12GM063651 (SVC). Additional support provided by Howard Hughes Medical Institute (Biological Sciences Education Grant) and by Kansas State University (Terry C. Johnson Center for Basic Cancer Research) (JPP).

References

1. Tamamura, H., Hori, A., Kanzaki, N., Hiramatsu, K., Mizumoto, M., Nakashima, H., Yamamoto, N., Otake, A. and Fujii, N. *FEBS Lett.* **550**, 79-83 (2003).
2. Balkwill, F. *Semin. Cancer Biol.* **14**, 171-179 (2004).
3. Kledal, T. N., Rosenkilde, M. M., Coulin, F., Simmons, G., Johnsen, A. H., Alouani, S., Power, C. A., Lutichau, H. R., Gerstoft, J., Clapman, P. R., Clark-Lewis, I., Wells, T. N. and Schwartz, T. W. *Science* **277**, 1656-1659 (1997).
4. Zhou, N., Luo, Z., Luo, J., Hall, J. W. and Huang, Z. *Biochemistry* **39**, 3782-3787 (2000).
5. Amela-Cortés, C., Rezende, M., Wang, X., Papa, D., Perchellet, E., Perchellet, J. -P. and Vigil-Cruz, S. C. (Manuscript in Preparation).
6. Solé, N. A. and Barany, G. *J. Org. Chem.* **57**, 5399-5403 (1995).
7. Cheng, Y. -C. and Prusoff, W. H. *Biochem. Pharmacol.* **22**, 3099-3108 (1973).

Studies on a Mutual Prodrug of Sulfamethoxazole and Nalidixic acid

Asif Husain and M.S.Y. Khan

Department of Pharmaceutical Chemistry, Faculty of Pharmacy, Jamia Hamdard, New Delhi-110 062, India

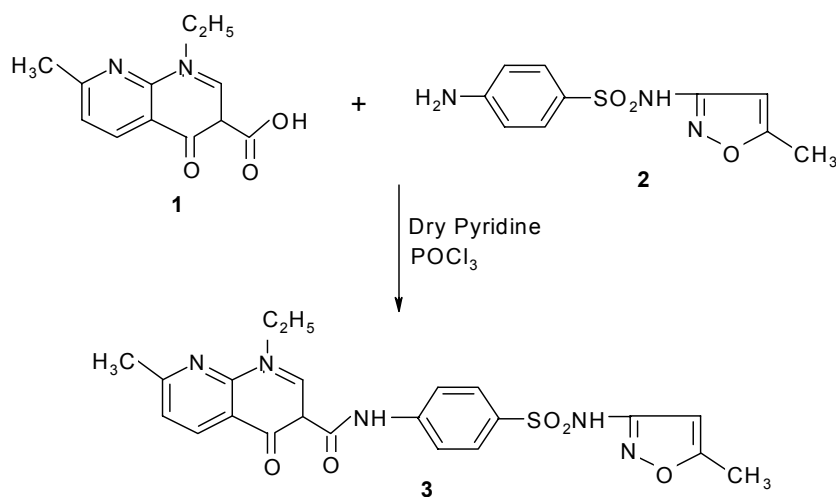
Introduction

The potential of microorganisms is tremendous with respect to their detrimental and perhaps outweighs the beneficial effects with respect to health of a human being. The search for new antibacterial agents is one of the most challenging tasks of the current medicinal chemistry. Nalidixic acid is highly effective against infections with Gram- bacteria, but it is ineffective against most Gram+ bacteria whereas sulfamethoxazole is a broad spectrum antibacterial agent having good action against infections caused by Gram+ bacteria as well [1-3]. In view of these facts it was considered worthwhile to synthesize a mutual prodrug of sulfamethoxazole and nalidixic acid. The aim of this study has been to synthesize a useful drug, which may act with effectiveness both on the Gram+ and Gram- bacteria.

Results and Discussion

Melting point was taken in open capillary tubes and is uncorrected. Analytical data of C, H, O, N and S were within 0.4% of the theoretical values. ¹H NMR spectrum was recorded on varian E-360 MHz with tetramethylsilane as internal standard in CDCl₃. Mass spectrum of the compound was recorded on a JEOL-DX 303 instrument. Dry solvent were used throughout. The mutual prodrug was synthesized according to scheme 1.

Sulfamethoxazole (0.02 mole) and Nalidixic acid (equimolar) were separately dissolved in dry pyridine (5 ml each). Both solutions were mixed together and stirred magnetically. Phosphorous oxychloride (0.9 ml) was added dropwise



Scheme 1

maintaining the temperature below 5°C while stirring. The contents were stirred for another half-hour and left overnight. It was poured into ice cold water and a solid mass, which separated out, was filtered, washed with water, dried, and crystallized from acetone followed by recrystallization from methanol to give dark brown small needles of the mutual prodrug [M.P. 226° C, Rf: 0.81 (Toluene: Ethylacetate: Formic acid, 5:4:1), Percentage Yield: 50.32%].

¹H NMR- δ 1.632 triplet and δ 4.9 quatret, methyl and methylene of ethyl moiety in nalidixic acid; δ 2.4 and δ 2.9 singlet each, 2x methyl group; δ 6.32 singlet, 1H, oxazole ring, δ 9.5 singlet, 1H nalidixic acid; δ 7.68 & δ 8.7 doublet each (ortho coupled), 2 x ortho coupled protons of the nalidixic acid system; δ 9.93 singlet, NH, sulfonamide moiety. Mass- m/z 467 (M⁺), 306 & 215.

Hydrolysis studies were carried out in aqueous buffer in order to study whether the prodrug hydrolyzes or not in aqueous medium and to what extent, suggesting the fate of the prodrug in such a system. Hydrolysis kinetics of the synthesized mutual prodrug were performed in acidic and basic buffer. The detection was done on HPLC in the mobile phase methanol: acetonitrile: potassium dihydrogen phosphate (0.015 M) [3:2:5 v/v/v]. The hydrolysis of the mutual prodrug to its components, sulfamethoxazole and nalidixic acid, was not observed either in acidic or basic buffer suggesting that the drug was highly stable. Hydrolysis studies in rats are under progress to ascertain its fate *in vivo*.

The antibacterial activity was assessed against *Staphylococcus aureus* (Gram+ bacteria) and *Escherichia coli* (Gram- bacteria). The test was carried out according to the turbidity method [4] and the minimum inhibitory concentration (MIC) was determined. Compound **3** showed very good activity against *S. aureus* (MIC=25 µg/ml) and good activity against *E. coli* (MIC=50 µg/ml).

In conclusion, an amide-based (-CONH-) mutual prodrug **3** has been successfully synthesized by condensing nalidixic acid **1** with sulfamethoxazole **2**. Its structure was established on the basis of elemental analysis, ¹H NMR, and Mass spectral data. The prodrug is resistant to hydrolysis in acidic and basic buffer system indicating its stability. The compound itself exhibited significant antibacterial activity, we expect that after hydrolysis *in vivo* by amidase the prodrug would break into its parent components which have established antibacterial activity. *In-vivo* studies are in progress to establish the suggested hypothesis. The compound exhibited very good *in-vitro* antibacterial activity against *S. aureus* and good activity against *E. coli*.

Acknowledgments

The work was funded by U.G.C. and H.N.F., New Delhi, India.

References

1. Northey, E. H. *American Chemical Society Monograph Series*, Reinhold, New York (1997).
2. Sabin, A. B. and Warren, J. J. *Biopolymers* **41**, 80-85 (2000).
3. Husain, A. *M.Pharm & Ph.D. Thesis*, Jamia Hamdard University, New Delhi, India (1996 & 2000).
4. Cruickshank, R., Dugid, J. P., Marmion, D. P. and Swain, R. H. A. *Medical Microbiology*, vol. 2, Churchill-Livingstone, Edinburg, London (1975).

Studies on Interaction of CaM with CaM-Binding Peptides M13 and RS20 in the Presence of Al³⁺ Ions

Andrea Calderan, Paolo Ruzza, Alessio Osler, Andrea Guiotto, Barbara Biondi and Gianfranco Borin

Institute of Biomolecular Chemistry of CNR, Padova Unit, 35131 Padova, Italy

Introduction

Ca-free CaM (apoCaM) contains two globular domains connected by a flexible central linker. Each domain contains two well-defined helix-loop-helix EF-motifs that are responsible for Ca²⁺ binding. Upon binding, the calcium ions organize and stabilize the four-domains structure inducing large conformational changes: in this active form CaM can bind to its numerous target regulatory proteins. Since most of them are large and multimeric proteins, the CaM-protein complexes are usually simulated with template peptides.

A neurotoxic factor that alters the intracellular Ca²⁺ regulatory system is Al³⁺. The alteration of Ca²⁺ homeostasis and the Al³⁺-induced CaM conformational changes may constitute the molecular basis of aluminum toxicity in Alzheimer's disease [1].

In the present work, fluorescence studies were aimed at the understanding of Al³⁺ role in CaM conformation and binding activity towards its physiological protein targets. To this purpose we studied, in the presence of Ca²⁺ and/or Al³⁺, the peptide fluorescence spectral changes induced by the formation of the complexes between CaM and two synthetic peptides: M13, corresponding to the sequence 577-602 of skMLCK [2], and RS20, corresponding to the sequence 796-815 of smMLCK [3].

M13	H-KRRWKKNFIAVSAANRFKKISSSGAL-OH
RS20	H-ARRKWQKTGHAVRAIGRLSS-OH

Results and Discussion

The changes of the fluorescence emission of the single Trp residues of M13 and RS20 were exploited to study the peptide conformational modifications induced by CaM in the presence of Ca²⁺ and/or Al³⁺. M13 spectrum (Fig. 1, spectrum 1) is significantly modified in the presence of Ca-CaM as a result of the formation of the well known M13/CaM complex (Fig. 1, spectrum 2). The addition of EDTA (10 eq. with respect to Ca²⁺) causes a conformational change in CaM which is no longer able to form the complex with M13 (Fig. 1, spectrum 3). Further addition of Al³⁺ (3 eq. with respect to EDTA) induces a significant decrease of the fluorescence intensity (Fig. 1, spectrum 4). Surprisingly, the spectrum is no longer modified by a new addition of Ca²⁺ (2 eq. with respect to Al³⁺) (Fig. 1, spectrum 5). Also RS 20 spectrum (Fig. 2, spectrum 1) undergoes a similar modification following the formation of the RS20/Ca-CaM complex (Fig. 2, spectrum 2) and the addition of EDTA, seizing Ca²⁺, causes the collapse of the complex (Fig. 2, spectrum 3). The situation changes when Al³⁺ is added: in this case RS20 spectrum is significantly modified and looks similar to that of the RS20/Ca-CaM complex but with a decrease of the fluorescence intensity (Fig. 2, spectrum 4). Further addition of EDTA causes the collapse of this situation (Fig. 2, spectrum 5). A new addition of Ca²⁺ ions seems to induce again the formation of the RS20/Ca-CaM complex (Fig. 2, spectrum 6).

Fluorescence measurements show that the conformational modifications, that cause the Trp fluorescence emission change when M13 forms the complex with Ca-CaM, seem to be impossible in the presence of Al^{3+} . On the contrary, the effect of Al^{3+} on RS20 fluorescence suggests that, in this case, the presence of ions different from Ca^{2+} doesn't prevent the complex formation. This behavior, surprisingly different for two peptides belonging to the same family of CaM targets (basic 1-8-14, according to the classification of "The Calmodulin Target Database", <http://calcium.uhnres.utoronto.ca/ctdb/flash.htm>), could arise from the same conformational peculiarity which is at the root of the capability of RS20 to bind not only Ca-CaM but also apoCaM [4]. Further NMR studies are in progress to better explain this situation.

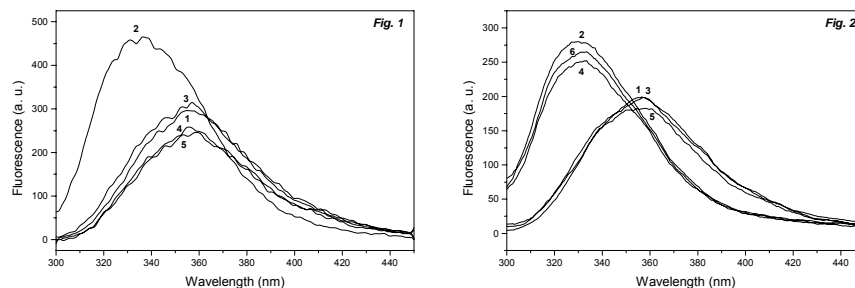


Fig. 1. M13 fluorescence spectra. The spectra were recorded at 25°C in 10 mM Tris/HCl, 0.1 M KCl, pH 8.0. Excitation wavelength: 290 nm. [M13]: 4.4×10^{-6} M. 1: M13; 2: M13 + Ca-CaM; 3: M13 + Ca-CaM + EDTA; 4: M13 + Ca-CaM + EDTA + Al^{3+} ; 5: M13 + Ca-CaM + EDTA + Al^{3+} + Ca^{2+} .

Fig. 2. RS20 fluorescence spectra. The spectra were recorded at 25°C in 10 mM Tris/HCl, 0.1 M KCl, pH 8.0. Excitation wavelength: 290 nm. [RS20]: 3.0×10^{-6} M. 1: RS20; 2: RS20 + Ca-CaM; 3: RS20 + Ca-CaM + EDTA; 4: RS20 + Ca-CaM + EDTA + Al^{3+} ; 5: RS20 + Ca-CaM + EDTA + Al^{3+} + EDTA; 6: RS20 + Ca-CaM + EDTA + Al^{3+} + EDTA + Ca^{2+} .

Acknowledgments

This work was supported by CNR/MIUR - Legge 449/97 - DM 30/10/2000.

References

1. Haug, A. and Vitorello V. *Coord. Chem. Rev.* **149**, 113-124 (1996).
2. Ikura, M., *et al.* *Science* **256**, 632-638 (1992).
3. Meador, W. E., Means, A. R. and Quiocho, F. A. *Science* **257**, 1251-1255 (1992).
4. Hill, T. J., *et al.* *Biochemistry* **39**, 7284-7290 (2000).

Studies on the Peroxidase Mimetic Peptide

Liping Wang¹, Xiaoming Zhao¹, Lili Guo², Roger W. Roeske² and Wei Li¹

¹College of Life Science, Jilin University, Changchun, 130023, P.R. China; ²Department of Biochemistry and Molecular Biology, Indiana University School of Medicine, Indianapolis, IN 46202, USA

Introduction

Cataract is a leading cause of blindness in the world. Cases of cataract-blindness are almost half of the total blindness population [1]. As our knowledge of the mechanism of oxidative damage in cataracts has evolved [2], anti-oxidants, especially peroxidase mimetic, have been used to develop agents to protect the eye and cure cataracts. In spite of the significance of peroxidases in the prevention and therapy of the diseases caused by free radicals, the limitations of using natural peroxidases make it necessary to design and synthesize effective enzyme mimics. According to the structure of the enzyme mimics, they could be classified as simple organic compounds, peptide mimics, and protein mimics. Compared to the simple organic compounds, peptide mimics have the advantages of low toxicity, high activity, and easy synthesis. In addition, peptide mimics have a low molecular weight and high stability compared with the protein enzyme mimics.

Results and Discussion

In order to find a peptide that can mimic the ascorbate peroxidase (APX) activity, we first screened a 7 amino acid peptide library using deuterohemin. After three rounds of screening, individual clones were isolated and sequenced, and a series of small peptide ligands specifically to the deuterohemin were obtained. One sequence with high occurrence frequency has the conserved domain His/Trp/Arg of natural APX. From the result of sequence alignment in the database, this small peptide sequence is homologous to many catalases. This indicates that the putative peptide mimic has the potential of becoming a new mimic of peroxidase. On the basis of the data and information obtained from the experiment, several deuterohemin-His-peptides were designed. In the mimics, the deuterohemin take the place of the hemin whose alkenyls are easily oxidized by the peroxide [3], which reduces its stability to the peroxide. Then one mimic of peroxidase, Dh- β -Ala -His-Trp-Lys-Pro-Tyr-Arg, was synthesized, and a relatively high enzyme activity was measured (Fig. 1).

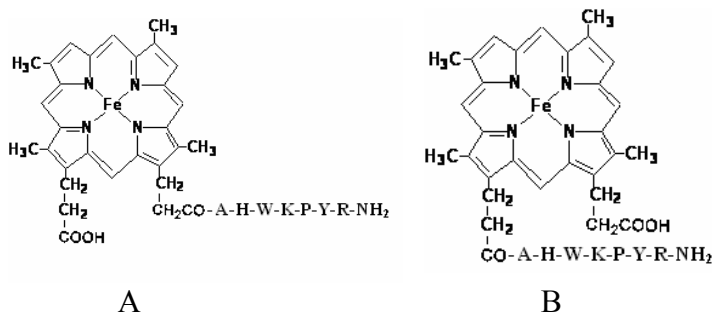


Fig. 1. Structure of peroxidase mimics, A and B are isomers of DhHP-7.

The APX activity of DhHP-7 was measured by degrading H_2O_2 in ascorbate-specific peroxidase test. The specific activity was 4.0×10^3 U/ μ mol with H_2O_2 as the substrate (1U DhHP-7 can catalyze 1 μ g ascorbate per minute). The steady state kinetic of the DhHP-7 was also studied. The enzyme activity of DhHP-7 increased with increasing DhHP-7 concentration and reached a maximum value, indicating that it obeys enzyme kinetics. In 0.5 mM of ascorbate in 50 mM PB, pH 7.0, the dependence of the reaction rate on H_2O_2 was hyperbolic with K_m of 9.8 μ M, which showed Michaelis-Menten kinetics. The value of K_{cat}/K_m was 1.64×10^7 .

To investigate the effects of DhHP-7 on galactose cataract, animal models of galactose cataract were induced in 6-week-old Sprague-Dawley (SD) rats by feeding them on a 50% galactose-rich diet. After the examination by reversed lamp microscope, 30 rats which two side lens do not have cataract were randomly allotted into three groups: the first group is normal control, the second group is cataract model group and the third group is DhHP-7 protecting group.

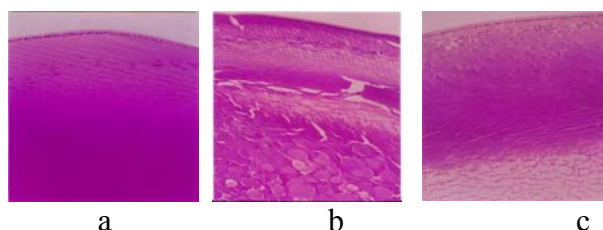


Fig. 2. The effects of DhHP-7 on galactose cataract were determined by immunohistochemistry. a: normal group; b: model group of galactose cataract; c: galactose cataract was treated by DhHP-7 as experimental group.

The lens with each of the above three groups were embedded with paraffin, sliced, dyed with HE, and the effects of DhHP-7 on cataract were further determined by immunohistochemistry. The results are showed in Figure 2. In the control group, the tissue structure was normal, with no visible pathological changes, and the cell structure was integrated, smooth and didn't have inflammation. In the cataract model group, the distinct cataract characters were observed, such as most of cells seemed to be squama-like, with serious turbidity, swelling, denaturation and necrosis. In the DhHP-7 treated group, the lens transparency was seen, the structure distributing of lens epithelium was very clear and only low-grade turbidity and denaturation were observed. These results showed that DhHP-7 can significantly prolong the occurrence of cataract and inhibit the development of cataract lens turbidity degree. Data obtained by our group have also shown DhHP-7 can effectively prevent and treat cataract by decreasing the lipid peroxide MDA and increasing the activity of anti-oxidase (SOD, GSH-Px) as well as the glutathione content.

References

1. Spector, A., Ma, W., Wang, R. -R. and Kleiman, N. J. *Exp. Eye Res.* **65**, 457-470 (1997).
2. Spector, A. *FASEB J.* **9**, 1173-1182 (1995).
3. Wang, L. -P., Liu, Y. -L. and Li, W. *Chem. J. Chi. U.* **25**, 2171-2173 (2004).
4. Qi, M., Huang, X. and Wang, Z. *Chin. Ophthal. Res.* **19**, 220-223(2001).

Use of Combinatorial Peptide Libraries and LC/MS/MS to Study TPP I Substrate Specificity

Yu Tian¹, Istvan Sohar¹, John W. Taylor² and Peter Lobel^{1,3}

¹Center for Advanced Biotechnology and Medicine; ²Department of Chemistry and Chemical Biology, Rutgers University, Piscataway, NJ 08854; ³Department of Pharmacology, University of Medicine and Dentistry of New Jersey, Piscataway, NJ 08854, USA

Introduction

Classical late-infantile neuronal ceroid lipofuscinosis (LINCL) is a fatal hereditary neurodegenerative disease caused by mutations in the CLN2 gene [1], which encodes a lysosomal protease with tripeptidyl-peptidase I (TPP I) activity [2]. While lysosomal storage is seen in LINCL, the natural substrates for TPP I and the pathophysiological processes associated with disease progression are not well understood. One approach that should provide useful insight is the detailed characterization of TPP I substrate specificity, which should also aid in the development of improved clinical and biochemical assays.

Several recent methodological developments facilitate our current study. First, the fluorogenic compound 7-amino-4-carbamoylmethylcoumarin (ACC) allows a fluorogenic molecule to be incorporated as the C-terminal residue of peptides using standard solid-phase synthetic methods [3]. Hydrolysis of the C-terminal amide bond results in release of free ACC and a ~900 fold increase in fluorescence, thus enabling the determination of kinetic parameters and the substrate specificity constant k_{cat}/K_M . Second, use of an “isokinetic mixture” of Fmoc-amino acids facilitates incorporation of multiple residues at a given position [4]. Third, recent advances in LC/MS/MS technologies allow quantification of relatively complex mixtures of peptides for studies of enzyme kinetics.

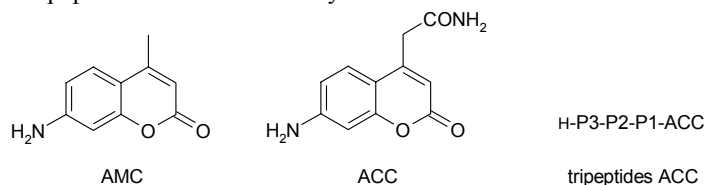


Fig. 1. Structure of AMC, ACC, and ACC substrates, P3, P2, P1 is according to the “Schechter & Berger” nomenclature, the cleavable bond is between P1 and P1' (ACC).

Results and Discussion

We have used combinatorial fluorogenic ACC-tripeptides as well as tetrapeptide and pentapeptide libraries for systematic evaluation of the substrate specificity of TPP I. We sequentially evaluated each P1, P2 and P3 position, using the results of the previous analysis to design subsequent libraries such that the residues surveyed in each consecutive round of peptide synthesis were restricted, thus decreasing the complexity of the library (Table 1). In addition, a LC/MS/MS-based assay allowed individual peptides in the P2 peptide pools to be studied and thus expand the scope of the analysis at the P3 position. Non-fluorogenic tetrapeptide and pentapeptide libraries were synthesized and analyzed by the LC/MS/MS assay to evaluate the P1' and P2' positions. This comprehensive substrate specificity information could benefit future investigation of the true biological substrates of TPP I.

Table 1. Summary of TPP-I substrate specificity studies

Positions of substrate	P3	P2	P1	P1'	P2'
Peptide or pools	Peptides ^a	Pools ^a	Pools ^a	Peptides ^b	Pools ^c
# pool × # peptide/pool	133 × 1	76 × 19	19 × 361	19 × 1	19 × 18
Method ^d	Fluoro & Mass	Fluoro	Fluoro	Mass	Mass
Optimum residues ^e	R>H>Y	n>P>A	L>n>F	F>W>Y	V>L>n

^aTripeptide-ACC as shown in Fig. 1; ^bTetrapeptide; ^cPentapeptide; ^dFluoro, fluorometric assay; Mass, LC/MS/MS assay; ^en, Nle.

Another goal of this study is to identify new substrates that may be used for research and clinical purposes. From the comprehensive survey, several substrates were identified that have significantly higher TPP I specificity compared to the widely used Ala-Ala-Phe-AMC (Table 2). More importantly, the new substrates show much less reactivity when measured in human lymphoblast extracts at neutral pH (Fig. 2). It is likely that this neutral activity contributes to the background signal under conditions used to measure TPP I activity (pH 4.5). The new substrates may prove to be superior reagents due to their enhanced sensitivity to and increased specificity for digestion by TPP I.

Table 2. Representative TPP-I substrates (measured using fluorometric assays)

substrate	k_{cat} (s ⁻¹)	K_M (μM)	k_{cat}/K_M (μM ⁻¹ s ⁻¹)
Ala-Ala-Phe-AMC	5.2	188	0.028
Ala-Ala-Phe-ACC	5.3	233	0.022
Arg-Nle-Leu-ACC	3.6	28	0.133
Arg-Nva-Nle-ACC	4.7	30	0.169
Arg-Pro-Phe-ACC	8.2	54	0.156

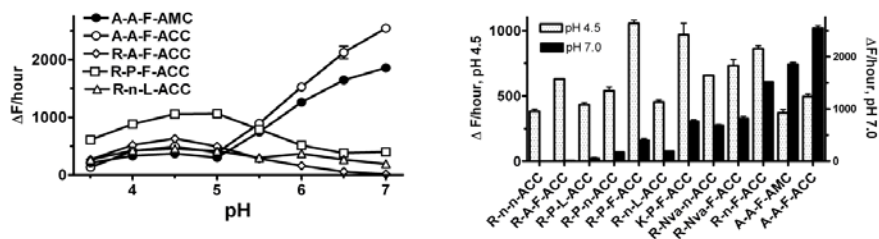


Fig. 2. pH profiles of different TPP I substrates determined in human lymphoblast.

Acknowledgments

This research was supported by NIH grant NS 37918 (PL) and a Batten Disease Support and Research Association fellowship (YT).

References

1. Sleat, D. E., Donnelly, R. J., Lackland, H., Liu, C. G., Sohar, I., Pullarkat, R. K. and Lobel, P. *Science* **277**, 1802-1805 (1997).
2. Rawlings, N. D. and Barrett, A. J. *Biochim. Biophys. Acta* **1429**, 496-500 (1999).
3. Maly, D. J., Leonetti, F., Backes, B. J., Dauber, D. S., Harris, J. L., Craik, C. S. and Ellman, J. A. *J. Org. Chem.* **67**, 910-915 (2002).
4. Ostresh, J. M., Winkle, J. H., Hamashin, V. T. and Houghten, R. A. *Biopolymers* **34**, 1681-1689 (1994).

Sunflower Derived Trypsin Inhibitors as Anti-Metastatics

**Peter P. Roller¹, Sheng Jiang¹, Peng Li¹, Ya-Qiu Long¹, Sheau-Ling Lee²,
Cheng-Yong Lin², Michael Johnson² and Richard B. Dickson²**

¹Laboratory of Medicinal Chemistry, National Cancer Institute, NIH, Bldg 376, Frederick,
MD 21702; ²Lombardi Cancer Center, Georgetown University Medical Center, 3970
Reservoir Road, Washington DC 20007, USA

Introduction

Matriptase is a large trans-membrane serine protease, originally isolated from the extracellular domain of human mammary epithelial cells [1]. Overexpression of this membrane bound protease on cancer cells functions in the degradation of basement membrane extracellular matrix. Matriptase is also known to activate hepatocyte growth factor by specific proteolytic cleavage of the inactive pre-pro/growth factor. Matriptase activates urokinase-type plasminogen activator, and the protease activated receptor (Par-2). Based on these biological functions of matriptase, developing inhibitors to matriptase may provide therapeutic applications for prevention of cancer invasion and metastasis.

Our aim in this project is to develop selective inhibitors to matriptase, as a way of inhibiting the metastatic and oncogenic cell proliferation. We discovered earlier that a bicyclic cage-like conformationally restricted and proteolytically stable cyclopeptide, termed SFTI-1, inhibited the matriptase enzyme, with an impressive K_i of 0.92 nM [2]. We carried out homology modeling with the catalytic core of the matriptase protein. Our target protein has a 34% amino acid identity and 53% similarity to thrombin.

Results and Discussion

The synthesis of SFTI analogs was carried out using Fmoc chemistry based protocols. The linear peptide was assembled on a Rink acid resin. Gly was attached as the first amino acid on the resin, in order to avoid racemization during the first step in the synthesis. The side-chain protected peptide was cleaved from the resin with 2% TFA, and the peptide was cyclized with HATU/HOAt/DIEA/DMF. The protective group was removed with TES-TFA-H₂O. The bicyclic peptide, SFTI-1, was generated by air oxidation of the two cysteines in weakly basic medium. This approach also provided us with a methodology to prepare a variety of analogs. Enzyme inhibitory assays were carried out with matriptase proteolysis assay using fluorescent substrate, N-t-Boc-Gln-Ala-Arg-AMC [2]. K_i values were determined using Dixon plots (Table 1).

A number of closely related analogs of the natural product, SFTI-1, were synthesized, in order to discover cyclic peptides that would offer more pharmacologically compatible properties. Particular attention was given to designing a bicyclic peptide that contains a stable bisecting bridge in the structure, such as for example the olefinic linkage in peptide SFTI-9, (K_i = 25 nM). This peptide is only moderately less active than the natural product, SFTI-1, whereas the absence of the bicyclic olefinic linkage, as shown in peptide SFTI-8, results in a large loss of potency (K_i = 1070 nM).

Table 1. Matriptase Inhibitory Properties of SFTI analogs

Peptide	Ki ^a (nM)
SFTI-1	1
SFTI-8	1070
SFTI-9	25

^aSerine protease inhibitory assay on matriptase, by Long et al [2].

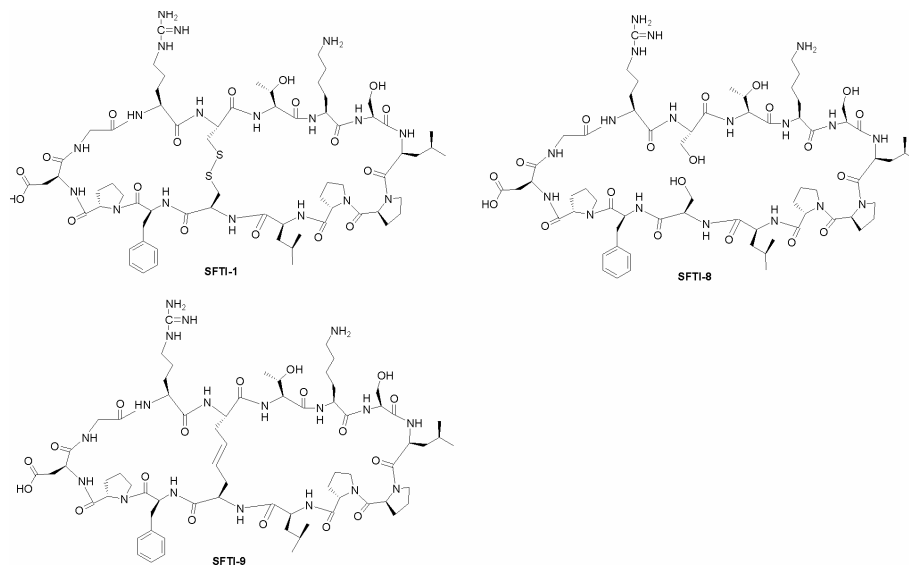


Fig. 1. Molecular structure of SFTI-1 and its two analogs.

References

1. Lin, C. -Y., Anders, J., Johnson, M., Sang, Q. -A. and Dickson, R. B. *J. Biol. Chem.* **274**, 18231-18236 (1999).
2. Long, C. -Y., Lee, S. -L., Lin, C. -Y., Enyedy, I. L., Wang, S., Li, P., Dickson, R. B. and Roller, P. P. *Bioorg. Med. Chem. Lett.* **11**, 2515-2519 (2001).

Surface Plasmon Resonance- and Quartz Crystal Microbalance-based Methods for Detecting GRB2 SH2 / Peptide Interaction

Feng-Di T. Lung¹, Wan Ching Li² and Chien-Chung Liou¹

¹*Department of Chemistry, Tunghai University;* ²*Department of Nutrition, China Medical University, Taichung 407, Taiwan*

Introduction

The growth factor receptor-binding protein (Grb2) is an adaptor protein with a domain structure of SH3-SH2-SH3 [1]. The Grb2 SH2 domain binds phosphotyrosyl peptides with the consensus sequence pYXNX (pY, phosphotyrosine) within several proteins, such as members of the erbB family, subsequently activates Ras, then trigger the kinase cascade, which is essential for cell growth and differentiation [2]. Therefore, Grb2 SH2 inhibitors show promise for targeted inhibition of this pathway.

Recently, we synthesized a few peptides and studied their inhibitory effects on Grb2 interactions by surface plasmon resonance (SPR) technology-based biosensor, BIAcore X instrument [3]. In this study, the inhibitory effects of our peptides on the Grb2 SH2 domain were evaluated by quartz crystal microbalance (QCM)- and SPR-based methods with modification on the experimental design of sensor chips.

Results and Discussion

Solid phase peptide synthesis: Peptides were synthesized manually using the standard Fmoc/tBu chemistry. The PAL resin, 5-(4-Fmoc-aminomethyl-3,5-dimethoxyphenoxy)-valeric acid-MBHA resin, was solvated in DMF for 10 min at room temperature, followed by the removal of the Fmoc protecting group on the resin solvated by treatment with 20% piperidine in DMF for 15 min, repeated twice. The N[□]-Fmoc, side-chain-protected amino acid, Fmoc-Asn(Trt)-OH, was activated by mixing with the coupling reagent, HOBt/HBTU/DIEA (1:1:2), for 3 min and then added to the reaction vessel for coupling with resin at room temperature for 1.5 hrs. Cycles of deprotection of Fmoc and coupling with the subsequent amino acids were repeated to synthesize the desired peptide bound-PAL resin. The peptide bound-PAL resin was treated with 95% TFA/5% H₂O for 1.5 hrs at room temperature to simultaneously remove their side chain protecting groups and cleave the peptide from the resin, and then filtered to separate the peptide from the PAL resin. TFA in the filtrate was evaporated with a gentle stream of N₂ gas to produce the crude peptide. After lyophilization, the peptide was purified by reverse-phase high-performance liquid chromatography (RP-HPLC) using a C18 column, eluted with H₂O containing 0.05 % TFA (solution A) and acetonitrile containing 0.05% TFA (solution B) with a solvent gradient from 10% to 90% B over 30 minutes, and detected at 220 nm. The lyophilized peptides, Fmoc-Glu-Tyr-Aib-Asn amide and H-Glu-Tyr-Aib-Asn amide, were characterized by FAB-MS spectrometer and their purity was characterized by analytical HPLC.

Analysis of peptide-protein interaction by SPR- and QCM-based methods: Anti-GST antibodies, the ligands, were covalently immobilized on the CM5 sensor chip or AM25 (Fig. 1). Followed by the injection of GST-Grb2 SH2 protein, various concentrations of synthetic peptides were injected onto the sensor surface to interact with the captured GST-Grb 2 SH2. The interaction between each peptide and captured GST-Grb2 SH2 were detected and analyzed. Equilibrium association and dissociation constants of each peptide were determined as summarized in Table1.

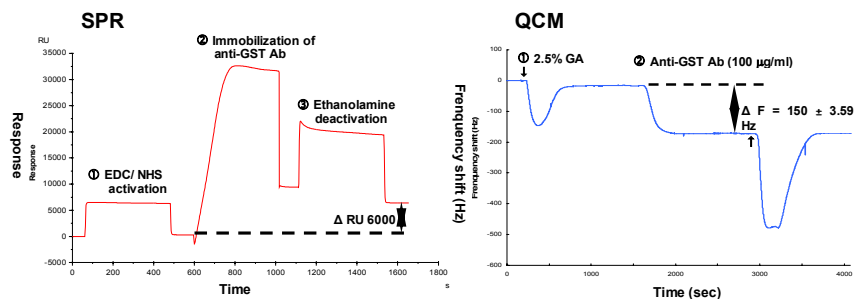


Fig. 1. Immobilization of anti-GST Abs on the surface of CM5 (SPR) and AM25 (QCM) chips.

Table1. Equilibrium constants of peptides 1 and 2 determined by SPR- and QCM-methods

Peptide	Method	K_A (1/M)	K_D (M)
1	SPR	1.14×10^8	8.79×10^{-9}
1	QCM	1.75×10^8	5.71×10^{-9}
2	SPR	3.24×10^4	3.09×10^{-5}
2	QCM	3.69×10^4	2.741×10^{-5}

Analytical results of SPR- and QCM-based methods are in good correlation, indicating their applicability for further development of biosensor-based *in vitro* bioassay for elucidating effects of peptides on the expression levels of apoptosis-related proteins, which can serve as high-throughput screening methods.

Acknowledgments

The work was funded by the National Science Council in Taiwan (NSC92-2320-B-039-023) grant to F.-D. T. Lung.

References

1. Maignan, S., Guilloteau, J. P., Fromage, N., Arnoux, B., Becquart, J. and Ducruix, A. *Science* **268**, 291–293 (1995).
2. Pawson, T. *Nature* **373**, 573–580 (1995).
3. Lung, F. -D. T., Long, Y. Q., King, C. R., Varady, J., Wu, X. -W., Wang, S. and Roller, P. P. *J. Peptide Res.* **57**, 447–454 (2001).

Synthesis and Biological Activity of Terlipressin and its Putative Metabolites

Kazimierz Wisniewski, Sudar Alagarsamy, Hiroe Taki, Marcel Miampamba, Regent Laporte, Robert Galyean, Glenn Croston, Claudio Schteingart, Pierre Riviere and Jerzy Trojnar

Ferring Research Institute, Inc., San Diego, CA 92121, USA

Introduction

Terlipressin (H-Gly₃-LVP, GLYPRESSIN[®] [1]), **1**, is a peptide drug approved in some European and Asian countries for the treatment of bleeding esophageal varices and in France for hepatorenal syndrome. It presumably acts on the vasopressin 1a receptor (V1a-R), whose endogenous ligand is arginine vasopressin (AVP), to increase peripheral vascular resistance leading to increase in arterial blood pressure (ABP). Although **1** and AVP have both been used clinically to correct syndromes of inappropriate vasodilatation, **1** has much longer onset and duration of action [2,3]. It is hypothesized that **1** acts as a pro-drug and that its onset and duration of action are due to successive cleavage of the glycine N-terminal moieties to ultimately produce lysine vasopressin (LVP, **4**). Each of the putative metabolites **2-4** would be biologically active. To determine the biological activity of the metabolites and further investigate the mechanism of action of **1**, the peptides **1-4** were synthesized and tested both *in vivo* and *in vitro*.

Results and Discussion

Peptides **1-4** (Fig. 1) were synthesized by SPPS using Boc strategy. All analogs were prepared on MBHA resin by assembling the LVP sequence, adding single Gly residues, and splitting the resin where appropriate. The peptides were purified by preparative HPLC and their structure and purity was confirmed by LCMS.



Fig. 1. Structures of terlipressin (**1**) and its putative metabolites (**2-4**)

Table 1. Activity of peptides at the hV1a receptor

Peptide	Number of Gly (see Fig. 1)	Functional (RGA) assay ^a		Binding (SPA) assay ^b	
		EC ₅₀ [nM]	Efficacy [%AVP]	IC ₅₀ [nM]	Max. displ. [%AVP]
Terlipressin, 1	3	148	60	n.c. ^c	31
2	2	181	54	n.c. ^c	0
3	1	37.5	80	64.3	72
LVP, 4	0	0.93	100	2.50	92

^aRGA – reporter gene assay; ^bSPA scintillation proximity (binding) assay; ^cn.c. - not calculated due to low max. displacement.

A rat model was developed to characterize these peptides *in vivo* (thiobutabarbital-anesthetized male Wistar pre-treated with dibenamine). Identical doses (\sim ED₈₀) of AVP and LVP were equieffective in raising ABP, had rapid response onset, $t_{max} \sim 1$ min, and rapid response decay with return to baseline in ~ 20 min. In contrast, a 100 times larger dose of **1** was necessary to be equieffective, and it had a much slower response onset, $t_{max} \sim 15$ min, and very slow response decay with return to baseline in ~ 70 -80 min. **2** and **3** had faster response onset than **1**, shorter t_{max} (~ 7 and 4 min, respectively), faster response decay, and the equieffective dose of **1** was lower (30 x AVP dose). *In vivo* conversion of **1** to more active metabolites is consistent with these responses, supporting the pro-drug hypothesis.

Recombinant systems were employed (HEK-293 cells co-transfected with recombinant human V1a-R expression vector and NFAT-luciferase reporter construct) to define the molecular targets and mechanisms of action of **1-4**. In a functional assay, **1** and **2** had similar potency and efficacy, while **3** had a higher potency, and **4** was the most potent (Table 1 and Fig. 2a). In a binding assay, **1** and **2** displayed minimal binding compared to **4** or AVP, while **3** or **4** were the most potent (Table 1 and Fig. 2b). Although the lack of significant binding of **1** and the direct correlation between potency and reduced number of Gly residues would be consistent with the pro-drug hypothesis, the activity of **1** in the functional assay appears inconsistent with these results. One possible explanation is that the cells and/or media used in the functional assay possess peptidase activity able to cleave **1** to more active metabolites, which would be revealed by the long incubation time required to measure responses in this assay (5 hrs). Future studies will examine the conversion of **1** to **2-4** *in vivo* and *in vitro*, and confirm the role of these metabolites in the vasopressor activity of **1**.

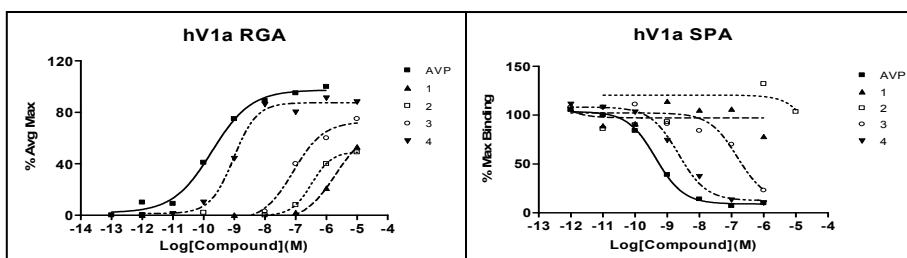


Fig. 2. Responses of **1** and its putative metabolites at the hV1a-R in functional (left panel) and binding (right panel) assays.

Acknowledgments

The authors would like to thank Marlene Brown, Kristina Cook, Michael Dunn, Joshua Heitzmann, Arash Kohan, Steve Qi, Steve Sheh, Erin Song, Dorain Thompson and Halina Wisniewska for their expertise and assistance in this study.

References

1. GLYPRESSIN® is the registered trademark of Ferring B.V. or one of its affiliates.
2. O'Brien, A., Clapp, L. and Singer, M. *Lancet* **359**, 1209-1210 (2002).
3. Landry, D. W., Levin, H. R., Gallant, E. M., Ashton, R. C. Jr., Seo, S., D'Alessandro, D., Oz, M. C. and Oliver, J. A. *Circulation* **95**, 1122-1125 (1997).

Synthesis and Evaluation of Neuroprotective α,β -Unsaturated Aldehyde Scavenger Histidyl-containing Analogs of Carnosine

Andrea Guiotto¹, Andrea Calderan¹, Paolo Ruzza¹, Alessio Osler¹,
Chiara Rubini¹, Dong-Gyu Jo², Sung-Chun Tang², Thiruma V.
Arumugam², Mark P. Mattson² and Gianfranco Borin¹

¹Institute of Biomolecular Chemistry of CNR, Padova Unit, 35131 Padova, Italy; ²Laboratory of Neurosciences, National Institute on Aging Intramural Research Program, Baltimore, MD 21224-6825, USA

Introduction

α,β -Unsaturated aldehydes formed upon oxidation of unsaturated lipids, like malondialdehyde (MDA, existing under physiological conditions as its unsaturated enol tautomer), 4-hydroxyalkenals, and 2-alkenals (e.g., acrolein and crotonaldehyde) are reactive species of particular interest for their direct or indirect influence in human pathologies [1,2]. Among these, acrolein and 4-hydroxy-trans-2,3-nonenal (HNE) have been extensively studied for their involvement in the pathogenesis of diseases such as atherosclerosis, diabetes, and neurodegenerative disorders [3,4].

Pharmacological efforts to attenuate oxidative injury in degenerative diseases have typically focused on drugs with antioxidant properties. Such approaches provide a “first line of defence” against free radicals, but do not target secondary products of oxidative stress. A complementary strategy involves the identification of low molecular weight drugs bearing nucleophilic centers (e.g., primary amine groups) that exhibit high reactivity toward endogenous aldehydes and, acting as “aldehyde scavengers”, spare cellular constituents and slow down the disease’s progression. Carnosine and carnosine-related peptides are promising candidates for this new therapeutic approach.

The aim of this research project is the synthesis and the neuroprotective activity studies on new histidyl-containing molecular entities that combine the imidazole ring and the L-stereochemistry of histidine with aldehyde-reactive moieties able to increase the scavenging efficiency against α,β -unsaturated aldehydes. In particular, we initially considered two nucleophilic moieties known to react promptly with carbonyl species, 1,2-diols and hydrazides [5].

Results and Discussion

To investigate the effect of modified carnosine analogs on α,β -unsaturated aldehydes we considered the series of molecules depicted in Figure 1. Compounds **2-5** were synthesized in our laboratories and bear, in addition to the imidazole ring of L-histidine, an 1,2-diol or hydrazide moiety as an aldehyde-reactive center. To test the ability of the synthesized compounds to bind to α,β -unsaturated aldehydes, each derivative was incubated in sealed vials with trans-2-nonenal (1:20 ratio) at 40°C in 5 mM phosphate buffer, pH 7.4 (Fig. 2). Compounds **2**, **4**, and **6** showed higher scavenging activity compared to carnosine, and were chosen for *in vivo* neural cells protection assays against HNE-induced death. Cultured SH-SY5Y cells and rat hippocampal neurons were pre-treated with analogs **2**, **4**, and **6**, and then exposed to HNE at concentrations of 10-20 μ M. In cultures exposed to HNE alone 60-80% of the SH-SY5Y cells and hippocampal neurons died during a 24 hr period of exposure.

Compounds **2** and **4** had no significant effect on the number of neurons killed by HNE. In contrast, there was a highly significant decrease in the death of SH-SY5Y cells and hippocampal neurons in cultures pre-treated with **6**. The cytoprotective effect of **6** was concentration-dependent in the range of 100-600 μ M with 400-600 μ M affording nearly complete protection against HNE-induced cell death. At equimolar concentrations (500 μ M) compound **6** significantly protected hippocampal neurons against death induced by HNE, whereas carnosine and homocarnosine had no significant effect (Fig. 3).

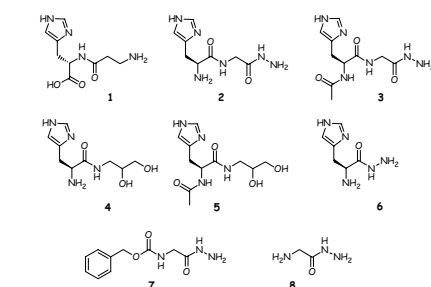


Fig. 1. Tested compounds.

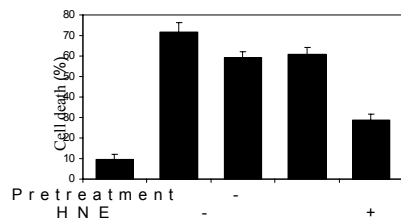


Fig. 3. Primary cultured rat hippocampal neurons were incubated with 500 μ M of compound **6**, L-carnosine (Carn) or homocarnosine (Hcarn) for 1 hr prior to a 24 hr exposure to 20 mM HNE.

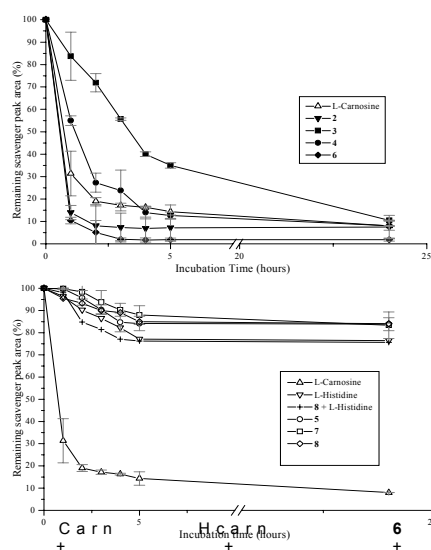


Fig. 2. Changes in peak area of carnosine and carnosine analogs during 24 hrs of incubation of scavenger (1.4 mM) with trans-2-nonenal (28 mM; scavenger / aldehyde ratio = 1:20) in 0.12 M KCl, 5 mM phosphate buffer (pH 7.4) at 40°C. Data represent means \pm SD of duplicate analyses.

References

1. Esterbauer, H., Schaur, R. J. and Zollner, H. *Free Radic. Biol. Med.* **11**, 81-128 (1991).
2. Halliwell, B. and Gutteridge, J. M. C. *Free radicals in biology and medicine*, third ed. Oxford University Press, Oxford, UK (1999).
3. Poli, G. and Schaur, R. J. *IUBMB Life* **50**, 315-321 (2000).
4. Romero, F. J., Bosch-Morell, F., Romero, M. J., Jareno, E. J., Romero, B., Marin, N. and Roma, J. *Environ. Health Perspect.* **106**, 1229-1234 (1998).
5. Guiotto, A., Calderan, A., Ruzza, P., Osler, A., Rubini, C., Jo, D-G., Mattson, M. P. and Borin, G. *unpublished results*.

Synthesis, Structural Characterization and Reactivity Study of Humanin, an Alzheimer's Disease Associated Peptide

Madalina Maftai, Heiko Moeller and Xiaodan Tian

Department of Chemistry, University of Konstanz, 78457 Konstanz, Germany

Introduction

Humanin (HN) is a novel 24 residue secretory peptide, detected in a normal region of human Alzheimer's disease (AD) brain and shown to abolish *in vitro* neurotoxicity by all types of familial Alzheimer's disease (FAD) mutants and by different β -amyloid (A β) species. Therefore, HN represents a neuroprotective factor with therapeutic potential in AD [1]. However, mechanisms behind the rescue effects of HN in neuronal cells are still unclear.

In this work, full-length HN was synthesized by solid phase peptide synthesis (SPPS) and the peptide homogeneity and amino acid sequence were confirmed by mass spectrometric measurements. HN secondary structure was characterized by circular dichroism spectroscopy (CD), NMR, and H/D exchange MS studies.

Interaction of HN with synthetic A β (1-40) peptide, highly involved in late-onset AD, was investigated using affinity chromatography in combination with high accuracy and resolution FTICR mass spectrometry. Preliminary results indicate a strong binding between HN and A β (1-40) and allow a first delimitation of the recognition sequences, providing a new insight into understanding the *in vivo* function of HN.

Humanin MAPRGF***SC***LLLLTSEIDL***LP***VKRRA
A β (1-40) DEAFRHDSGYEVHHQKL***VFF***AEDVGSNKGAIIGLMVGGVV

Fig. 1. Sequences of synthetic HN and A β (1-40). In italic are highlighted HN residues essential for its rescue function, as revealed by Ala-scan procedure [2]. In bold are pointed out the interacting regions of the two peptides.

Results and Discussion

HN and A β (1-40) (Fig. 1) were synthesized on NovaSyn TGR resins by a semi-automated peptide-synthesizer (ABIMED EPS-221), using Fmoc/tBu chemistry and PyBOP activation.

Purification was performed by RP-HPLC, applying linear gradients of 80% CH₃CN in 0.1% TFA and the final products were ascertained by MALDI-FTICR MS. HN was also measured in an ESI-Q-Trap MS/MS experiment and the fragments obtained covered the whole sequence, fully confirming HN primary structure.

CD spectra of HN indicated an unstructured, flexible conformation of the peptide in aqueous solution (MilliQ and 10mM NH₄HCO₃, pH=7.4), the same result was also obtained by NMR. On the other hand, long incubation of the peptide in MilliQ resulted in a conformation change towards an α -helical structure, which may be explained by extensive homodimerisation or Cys-oxidation of the peptide, both have been reported in literature [3]. The same structure modification was observed in the less polar environment of 50% organic modifier (MeOD) in D₂O, the same result was also obtained by our H/D exchange studies of the peptide (data not shown).

In order to evaluate the specificity and strength of HN interaction with A β (1-40), an affinity experiment using a NHS-activated Sepharose matrix immobilized with A β (1-40) peptide was performed. After 2hr incubation at RT, the unbound molecules were removed by washing with 60 ml PBS and the elution of the retained compounds was done with 500 μ l 0.1%TFA for 15 min. The MALDI-TOF mass spectrometric measurement showed the presence of HN exclusively in the elution fraction, pointing to a strong, specific interaction between HN and A β (1-40).

Furthermore, epitope extraction experiments were performed in order to identify HN binding region to A β (1-40). The experiments were carried out by applying the proteolytic fragments onto the A β (1-40) microcolumn after digestion of HN with different endopeptidases (Trypsin and Glu C). The enzymatic reaction was stopped in each case using an inhibitors cocktail composed of Leupeptin, Antipain, and Aprotinin. The resulting supernatant and elution fractions were analyzed by MALDI-FTICR mass spectrometry and the results indicated the HN(5-15) played an essential role in A β (1-40) recognition (Fig. 2). This conclusion was supported by another extraction experiment performed with α -Chymotrypsin, in which none of the obtained proteolytic fragments 13-24, 12-24, 11-24, 10-24 were retained on the A β (1-40) column.

Pro3 and Pro19, although revealed as essential for the rescue function of HN by Ala-scan method, seem not to be involved in HN-A β (1-40) interaction, suggesting a complex of mechanisms by which HN exerts its neuroprotective function.

In another experiment, HN was immobilized on NHS-activated Sepharose and a Trypsin extraction of A β (1-40) binding region to HN was performed. This first experiment indicated the sequence A β (17-28), located between α -secretase cleavage site and the membrane, was essential for the binding of HN to A β . Therefore, A β (1-40) might be the putative cell-surface receptor for HN revealed by radiolabelling methods [1].

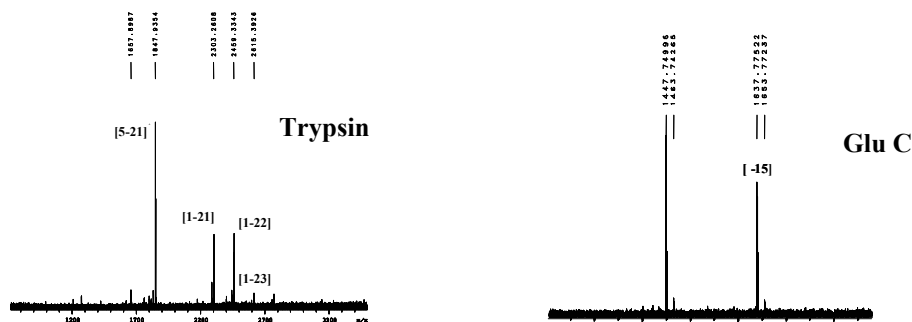


Fig. 2. MALDI-FTICR mass spectra of the elution fractions from a)HN extraction experiment with Trypsin b)HN extraction with Glu C .The A β 2-13 signal in this spectrum is due to incomplete efficacy of the used inhibitors against Glu C.

References

1. Hashimoto, Y., Niikura, T., Tajima, H., *et al.* *Proc. Natl. Acad. Sci. USA* **98**, 6336-6341 (2001).
2. Hashimoto, Y., Niikura, T., Ito, Y., *et al.* *J. Neurosci.* **21**, 9235-9245 (2001)
3. Terashita, K., Hashimoto, Y., Niikura, T., *et al.* *J. Neurochem.* **85**, 1521-1538 (2003).

Synthesis of 4-amino-1,2,4,5-tetrahydro-2-benzazepine-3-ones and Study of their β -turn Inducing Properties

Isabelle Van den Eynde¹, Karolien Van Rompaey¹, Steven Ballet¹, Rien De Wachter¹, Kenno Vanommeslaeghe¹, Monique Biesemans², Rudolph Willem² and Dirk Tourwé²

¹Organic Chemistry Department; ²HNMR Centre, Vrije Universiteit Brussel, Pleinlaan 2, B-1050 Brussels, Belgium

Introduction

Conformationally restricted peptides are the subject of increasing interest as potential new bioactive molecules. Peptide mimetics with constrained side chains can give valuable information on the bioactive conformation of the mimicked peptide. β -Turns are an important recognition element in proteins and peptides. Since Freidinger reported the use of a 5-membered lactam **1** (Fig. 1) in 1980, these β -turn mimics have attracted considerable interest [1].

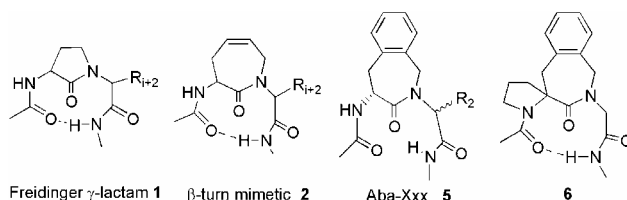


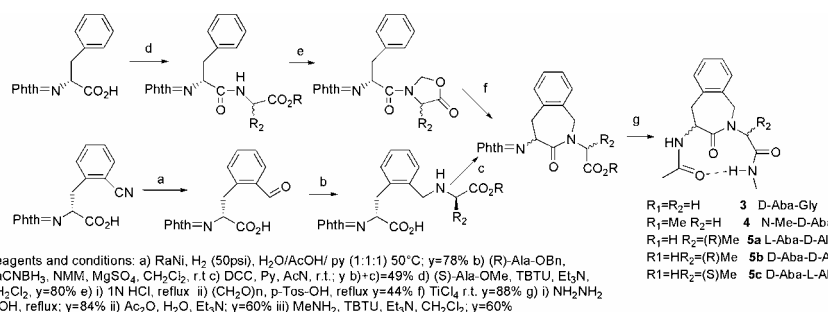
Fig. 1. Structures of β -turn mimics.

Piscopio *et al.* reported a combinatorial approach leading to compounds **2** [2]. These compounds were classified as part of the Freidinger lactam class of β -turn mimetics. Because of the striking structural resemblance with compound **2**, we have prepared 4-amino-1,2,4,5-tetrahydro-2-benzazepine-3-ones (Aba-Xxx) **3-5**, and we have investigated their conformation.

Results and Discussion

Chemistry: Two synthetic routes were used for the preparation of the Aba-Xxx derivatives (Scheme 1). One pathway involves the intramolecular lactam formation after reductive amination of an *o*-formylphenylalanine precursor [3]. This phthaloyl protected *o*-formylphenylalanine was prepared enantioselectively [4]. After reductive amination with alanine benzyl ester, the lactam was formed in good yield. In this way D-Aba-Gly **3**, N-Me-D-Aba-Gly **4** and L-Aba-D-Ala **5a** were synthesized. The other pathway starts from phthaloyl protected D-Phe and after coupling of alanine, an oxazolidinone is formed with paraformaldehyde. Acyliminium cyclization in presence of TiCl₄ proceeds in good yield [5]. This route was used to synthesize D-Aba-D-Ala **5b** and D-Aba-L-Ala **5c**. Deprotection was followed by incorporation in a minimal β -turn sequence.

Conformational study: We investigated the presence of an intramolecular hydrogen bond by determining the temperature dependence of the amide proton chemical shift and its solvent dependence. A temperature coefficient less negative than -4.6 ppb/K has been suggested as a criterion for identifying the solvent shielded



Scheme 1. Different pathways for the synthesis of Aba-Xxx.

amide protons due to hydrogen bonding [6]. The values in Table 1 show that Aba-Gly **3** and Aba-Ala **5a** analogs show no indication of turn structures. The N-methyl Aba-Gly **4** shows a larger temperature dependence, but still a small solvent dependence, indicating a possible equilibrium between hydrogen bonded and extended conformations.

Table 1. Temperature and solvent dependence of the amide protons chemical shifts

	$\Delta\delta/\Delta T$ (ppb/K)	δ CDCl ₃ (ppm)	δ DMSO (ppm)	$\Delta\delta$ (CDCl ₃ \leftrightarrow DMSO, ppm)
NH-CH ₃ 3	-6.6	6.32	7.83	-1.51
NH-CH ₃ 4	-5.7	7.51	7.75	-0.24
NH-CH ₃ 5a	-5.7	6.41	7.86	-1.45
NH-CH ₃ 6	-4.17	7.18	7.71	+0.1

Model 6 (Fig 1), previously reported by us [7], has the smallest temperature coefficient, combined with the smallest solvent dependence, supporting the hypothesis that this structure is an effective β -turn mimetic.

Acknowledgments

We thank the IWT (Instituut voor de Aanmoediging van Innovatie door Wetenschap en Technologie in Vlaanderen), the Fund for Scientific Research-Flanders (F.W.O.-Vlaanderen) and the VUB (R&D department) for the financial support and the APS and FWO for the travel grants.

References

- Freidiger, R. M., Veber, D. F., Perlow, D. S., Brooks, J. R. and Saperstein, R. *Science* **210**, 656-658 (1980).
- Piscopio, A. D., Miller, J. F. and Koch, K. *Tetrahedron* **55**, 8189-8198 (1999).
- Van Rompaey, K., Van den Eynde, I., De Kimpe, N. and Tourwé, D. *Tetrahedron* **59**, 4421-4432 (2003).
- Van Rompaey, K., *et al.* In *Understanding Biology Using Peptides, Proceedings of the 19th American Peptide Symposium*, this volume, pp. 359-360 (2006).
- Tourwé, D., *et al.* *Biopolymers*. **38**, 1-12 (1996).
- Cierpicki, T. and Otlewski, J. *Biomol. NMR* **21**, 249-261 (2002).
- Ballet, S., *et al.* In *Peptides 2004, Proceedings of the 28th European Peptide Symposium* (Flegel, M., Fridkin, M., Gilon, C. and Slaninova, J., eds.) Kenes International, Israel, pp. 698-699 (2005).

Synthesis of a RGD Peptide-PEG Hybrid for Carrying Adenovirus Vector into Cells

Shinya Kida¹, Mitsuko Maeda¹, Keiko Hojo¹, Yusuke Eto², Jian-Qing Gao², Shinnosuke Kurachi², Fumiko Sekiguchi², Hiroyuki Mizuguchi³, Takao Hayakawa⁴, Tadanori Mayumi¹, Shinsaku Nakagawa² and Koichi Kawasaki¹

¹Faculty of Pharmaceutical Sciences, Kobe Gakuin University, Nishi-ku, Kobe 651-2180, Japan; ²Graduate School of Pharmaceutical Sciences, Osaka University, Yamadaoka, Suita 565-0871, Japan; ³Division of Cellular and Gene Therapy Products, National Institute of Health Sciences, Setagaya-ku, Tokyo 158-8501, Japan; ⁴National Institute of Health Sciences, Setagaya-ku, Tokyo 158-8501, Japan

Introduction

PEGylation of bioactive proteins/peptides has been well documented for clinical therapeutics, since poly(ethylene) glycol (PEG) has low toxicity and long half-life. In gene therapy, PEGylation of adenovirus vector enhanced its circulation period and high antibody evasion ability, but reduced in gene expression [1]. Modification of adenovirus (Ad) with Arg-Gly-Asp (RGD) enhanced gene expression in many organs and melanoma cells via integrin [2-4]. We designed a PEG hybrid to RGD containing peptide YGGRGDTP [5], and the peptide-PEG hybrid conjugated to adenovirus using a hetero-functional cross-linking reagent 6-maleimido-hexanoic acid N-hydroxysuccinimide ester (MHS). We have prepared (Ac-YGGRGDTPβA)₂K-PEG-βAC amide and modified adenovirus by two steps, as shown in Figure 1.

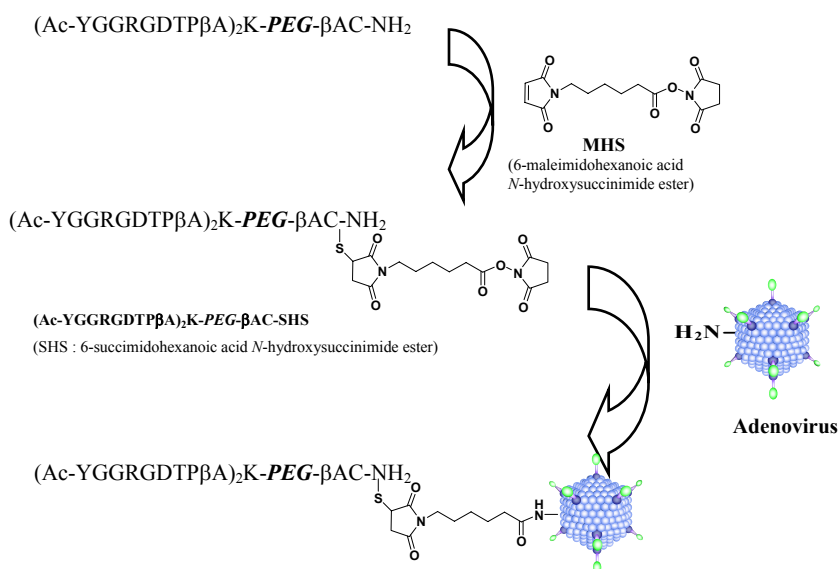


Fig. 1. Modification of adenovirus with RGD peptide-PEG hybrid.

Results and Discussion

(Ac-YGGRGDTP β A)₂K-PEG- β AC amide was synthesized manually by Fmoc-/Bu^t-solid-phase strategy on a Rink amide resin. Fmoc-Cys(Trt)-OH, Fmoc-Arg(Pbf)-OH, Fmoc-Lys(Fmoc)-OH and Fmoc-PEG-OSu (PEG:amino acid type poly(ethylene) glycol, OSu:N-hydroxysuccinimide ester, average of molecular weight was 3,400) were coupled by HBTU-HOBT-DIEA/DMF as coupling reagents and 20% piperidine/ DMF for N-terminus deblocking treatment. On the step of Fmoc-PEG coupling, adding HBTU-HOBT-DIEA was required, since active ester Fmoc-PEG-OSu did not react to β Ala-Cys(Trt)-Rink amide resin. After the PEG introduction to the protected peptide resin, all reaction periods were prolonged. Final cleavage was achieved by two successive treatments with TFA/TIPS/H₂O (95/2.5/2.5) for 2 hrs at room temperature, followed by HPLC purification. (Ac-YGGRGDTP β A)₂K-PEG- β AC was coupled with MHS and the resulting 6-[(Ac-YGGRGDTP β A)₂K-PEG- β AC-succinimido]-hexanoic acid N-hydroxysuccinimide ester ((Ac-YGGRGDTP β A)₂K-PEG- β AC-SHS) reacted with adenovirus in PBS (pH 7.4). The modified adenovirus vector with integrin targeting RGD peptide-PEG hybrid was examined the luciferase activity of cells after Ad infection. It exhibits high gene expression, even in coxsackie-adenovirus receptor (CAR) negative cell lines. We have developed an efficient peptide-PEG hybrid for carrying adenovirus vector into cells.

References

1. Eto, Y., Gao, J. -Q., Sekiguchi, F., Kurachi, S., Katayama, K., Mizuguchi, H., Hayakawa, T., Tsutsumi, Y., Mayumi, T. and Nakagawa, S. *Biol. Pharm. Bull.* **27**, 936-938 (2004).
2. Gao, J. -Q., Inoue, S., Tsukada, Y., Katayama, K., Eto, Y., Kurachi, S., Mizuguchi, H., Hayakawa, T., Tsutsumi, Y., Mayumi, T. and Nakagawa, S. *Pharmazie* **59**, 571-572 (2004).
3. Koizumi, N., Mizuguchi, H., Hosono, T., Ishii-Watanabe, A., Uchida, E., Utoguchi, N., Watanabe, Y. and Hayakawa, T. *Biochim. Biophys. Acta* **1568**, 13-20 (2001).
4. Reynolds, P., Dmitriev, I. and Curiel, D. *Gene Ther.* **6**, 1336-1339 (1999).
5. Erbacher, P., Remy, J. S. and Behr, J. P. *Gene Ther.* **6**, 138-145 (1999).

Synthesis of Cyclic Imino Acids from α -Amino- ω -Bromoalkanoic Acids

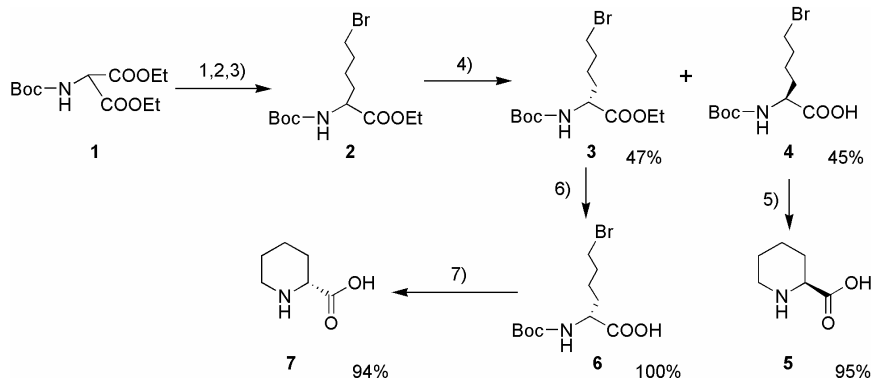
Louis A. Watanabe, Mohammed P. I. Bhuiyan, Tamaki Kato and
Norikazu Nishino

Graduate School of Life Science and Systems Engineering, Kyushu Institute of Technology,
Kitakyushu, 808-0196, Japan

Introduction

Pipecolic acid, a widespread natural nonproteinogenic amino acid, is an attractive synthetic target because it is a key constituent of many synthetic and natural bioactive molecules and useful building blocks for the preparation of peptides and peptidomimetics. Replacement of proteinogenic amino acids with cyclic imino acids has been carried out in structure-activity relationship studies and in search of new peptidomimetics that have improved pharmacological profiles. All these facts contributed to the growing interest in finding a convenient and efficient synthetic route to pipecolic acid and related imino acids with high enantiomeric purity.

However, most of these methods have some limitations, such as tedious procedures, low yields, unavailability of starting materials, etc. Therefore new and convenient method for the preparation of optically active pipecolic acid is still required. We have recently reported the synthesis of α -amino- ω -bromoalkanoic acid for side chain modifications [1]. During that course of work we explored a convenient route to L and D-pipecolic acids. Furthermore, hydroxypipecolic acid and hydroxyproline derivatives were also synthesized using same methodology.

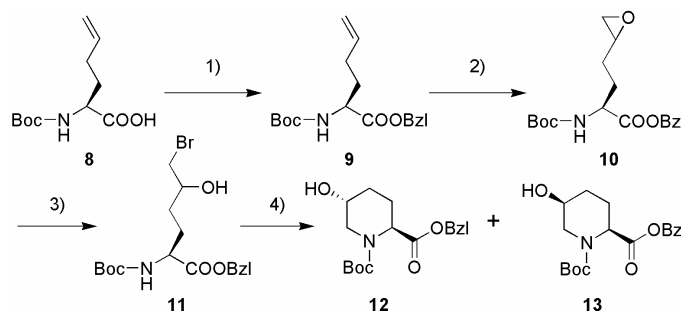


Scheme 1. Reagents and conditions: (1) (i) EtOH, sodium ethoxide, reflux, 30 min; (ii) 1,4-dibromobutane, reflux, 5 hrs, 92%; (2) NaOH aq, EtOH, 0°C, 3 hrs, 80%; (3) toluene, reflux, 3 hrs, 85%; (4) subtilisin, H₂O/DMF = 3/1, pH 8, 38°C, 3 hrs; (5) (i) 2 M HCl/dioxane, 0°C, 2 hrs; (ii) Et₃N, DMF, pH 8, 0°C, 5 hrs; (6) NaOH aq, EtOH, 0°C, 3 hrs; (7) (i) 2 M HCl/dioxane, 0°C, 2 hrs; (ii) Et₃N, DMF, pH 8, 0°C, 5 hrs.

Results and Discussion

The synthesis of pipecolic acid was started with commercially available diethyl Boc-aminomalonate **1** and dibromobutane (Scheme 1). Excess amount of dibromobutane was reacted with **1** in the presence of sodium ethoxide in absolute ethanol. One eq.

of 1 M NaOH was added at 0-5°C to the reaction mixture and obtained the corresponding monoacid monoester as an oil. It was then decarboxylated by refluxing in toluene. After refluxing in toluene, resulted Boc-DL-amino-6-bromohexanoic acid ethyl ester (Boc-DL-Ab6-OEt) **2** was resolved to Boc-L-2-amino-6-bromohexanoic acid **4** using subtilisin Carlsberg from *Bacillus licheniformis* (Sigma) in a mixture of water and DMF (3/1, v/v) at pH 8. The pH was maintained at 8 by the addition of 1 M ammonia and the reaction was completed in 3 hrs. Then the unreacted Boc-D-Ab6-OEt **3** was removed by ether extraction. **4** was extracted to ethyl acetate at pH 3 using citric acid. The Boc group of **4** was removed using 2 M HCl in dioxane to give the corresponding amino acid hydrochloride. It was then cyclized to L-pipecolic acid **5** in DMF by the addition of triethylamine. **3** recovered after resolution was hydrolyzed using dilute NaOH. It was then processed as mentioned above to yield D-pipecolic acid **7**. Thus, both enantiomers of pipecolic acid were prepared with high enantiomeric purity in high overall yield (27%) in five steps [2].



Scheme 2. Reagents and conditions: (1) benzyl bromide, Et_3N , DMF, 0°C , 6 hrs, 87%; (2) *m*-chloroperbenzoic acid, DCM, 0°C , 24 hrs, 90%; (3) LiBr, AcOH, THF, 5 hrs, 86%; (4) (i) TFA, 0°C , 1 hr; (ii) DIEA, DMF, pH 8, 0°C , 6 hrs; (iii) Boc₂O, Et_3N , DMF, 0°C , 6 hrs.

We attempted to synthesize hydroxypipecolic acid (Scheme 2) by a modification of the procedure in the literature [3]. Boc-L-2-amino-5-hexenoic acid **8** was synthesized starting from diethyl Boc-aminomalonate with 4-bromo-1-butene. The initial steps are the same as described earlier. The free carboxyl group of **8** was protected with benzyl group, then the side chain olefin was converted into epoxide by treatment with *m*-chloroperbenzoic acid in DCM. We opened the epoxide **10** with LiBr in THF under nitrogen, and compound **11** was obtained in high yield. The Boc group of **11** was removed using TFA to give the corresponding amino acid TFA salt. It was then cyclized to L-hydroxypipecolic acid derivative in DMF by the addition of DIEA. Finally, both diastereomeric L-hydroxypipecolic acid derivatives were treated with Boc₂O, and **12** and **13** could then be separated by column chromatography.

In conclusion, we have developed a convenient method for the synthesis of L- and D-pipecolic acid. The pipecolic acids can be obtained in very high enantiomeric purity and high yields. Furthermore, hydroxypipecolic acid derivatives were also successfully synthesized.

References

1. Watanabe, L. A., *et al. Tetrahedron Lett.* **45**, 491-494 (2004).
2. Watanabe, L. A., *et al. Tetrahedron: Asymmetry* **16**, 903- 908 (2005).
3. Hoarau, S., *et al. Tetrahedron: Asymmetry* **7**, 2585- 2593 (1996).

Synthesis of Quantum Dots Labeled Short Peptides and their Application in Imaging the T Cell Surface Receptors

Lifeng Wang, Jie Chen, Liping Wang, Chunlei Wang and Wei Li

College of Life Science, Jilin University, Changchun, 130023, P.R. China

Introduction

Quantum dots (QDs) are spherical semiconductor nanocrystals with a diameter of 1-10 nm. QDs are quite promising for bio-labeling. Comparing with organic dyes, QDs have superior absorption/emission properties, flexible form, and long lifetime. They can be attached to a variety of surface ligands, and also made to enter into a variety of organisms for imaging *in vivo*.

Since the successful coupling of QDs with biomolecules by Alivisatos [1], QDs have been coupled with many biomolecules such as proteins, peptides, nucleic acids, and small organic molecules. It remains, however, a challenge to couple QDs with short peptides. Several coupling methods regarding QDs and short peptides have been reported but all with some limitations. In this research, we propose a method to be appropriate to any short peptides and used it to couple QDs (CdTe) with two short immune peptides: thymopentin (TP5) and thymosin α 1 (T α 1). The QDs labeled immune peptides were applied to monitor their bindings with T- cell surface receptors *in vitro*.

Results and Discussion

The CdTe quantum dots were directly synthesized in water with mercaptopropionic acid as stabilizer [2]. The aqueous solution of QDs was first treated with a C₁₈ solid phase extracting column, washed by water to remove impurities, and then the QDs were released from the column by pure acetonitrile. The QDs were reacted with N-hydroxysuccinimide (NHS) in acetonitrile solution and DCC in acetonitrile solution was added for 20 min at room temperature. After that, aqueous solution of TP-5 or T α 1 was added, respectively, to the reaction mixture and the pH of the resultant solution was adjusted by N-methylmorpholine (NMM) to pH 8-9.

The whole reaction was performed at room temperature for 4 days, monitored by RP-HPLC every 24 hrs, and the products or QDs labeled peptides were also purified by RP-HPLC.

To confirm that TP-5 and T α 1 were coupled with QDs, we examined QDs-TP5, QDs-T α 1 by RP-HPLC and the results were shown in Figure 1. The QDs have weak fluorescence intensity and retention time of 10.7 min in RP-HPLC (Fig. 1A). The maximum fluorescence of QDs-TP5 and QDs-T α 1 were 21.2523 and 37.7362, respectively. The fluorescence intensities of QDs labeled peptides were at least 25 times stronger than that of QDs; their retention times in RP-HPLC were also substantially increased, indicating a coupling between QDs and TP-5 or T α 1. The results also show that the fluorescence intensity of the reaction products keeps increasing with reaction time up to 96 hrs.

QDs-TP5 has a HPLC retention time from 14.8 to 20.4 min (Fig. 1B) and QDs-T α 1 from 18.3 to 28.6 min (Fig. 1C). This shows that the reaction mixture was composed of multiple products. QDs were capped with mercaptopropionic acid, so the surfaces of QDs are covered by free carboxyl groups. As a result, QDs can form amide bond with free amino group of peptides.

TP5 and T α 1 are both immune peptides and can bind to specific T cell surface receptors. Due to the special fluorescent properties of QDs labeled peptides, QDs-TP5 and QDs-T α 1 can be potentially utilized to visualize and monitor their immune modulating activity.

In this study, T cells were treated with QDs (used as positive control), QDs-TP5, and QDs-T α 1, and observed under fluorescence microscope. The results are given in Figure 2. T cells were cultured with QDs IMDM medium. Some T cell nuclei produced yellow fluorescence, suggesting that QDs could enter T cell without coupling immune peptides (Fig. 2A and 2B). Fig. 2C and 2D show that the surface of the T cells treated with QDs-TP5 emits yellow fluorescence. Fig. 2E and 2F show that the surface of T cells treated with QDs-T α 1 emits brighter yellow fluorescence. Those results indicate that QDs-TP5 and QDs-T α 1 tend to aggregate on the surface of T cells. The results show that these QDs labeled peptides can be used to visualize and to study the immune modulating activity of TP-5 and T α 1 *in vivo*.

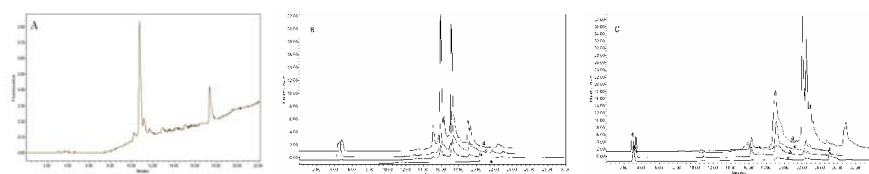


Fig. 1. HPLC chromatograms of QDs (A), QD-TP5 (B), QD-T α 1 (C). a, b, c and d denoted the fluorescence chromatograms after a reaction time of 24hrs, 48 hrs, 72hrs, and 96 hrs, respectively.

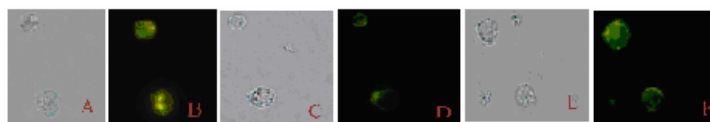


Fig. 2. Distribution of QDs (A, B), QD-TP5 (C, D) and QD-T α 1 (E, F) in T cells as observed by fluorescence microscope. A, C, and E were bright-field image.

References

1. Chan, W. C. W. and Nie, S. M. *Science* **281**, 2016-2018 (1998).
2. Zhang, H., Wang, L. P., Xiong, H. M., Hu, L. H., Yang, B. and Li, W. *Advanced Materials* **15**, 1712-1715 (2003).

Synthesis of Quantum Dot-Signal Peptides Bioconjugates and Targeting in Living Cells

Yaming Shan, Jiayue Hu, Liping Wang and Wei Li

College of Life Science, Jilin University, P.R.China 130021

Introduction

Quantum dots (QDs) are spherical semiconductor nanocrystals with a diameter of 2-8 nm that have shown promise for bio-labeling [1]. Specific binding of QDs to cell surfaces, insertion into cells, and binding to cell nuclei have been demonstrated following conjugation with the appropriate targeting protein. ZnS-capped CdSe QDs could also be coated with peptides by a thiol-exchange reaction. Despite these developments, aggregation always occurs when QDs are coupled to peptides and then results in the loss activities of coated protein or peptide. In this research, we used water-soluble 3-mercaptopropyl acid-stabilized CdTe nanoparticles to form acylamino-bond with nuclear targeting signal peptide (NTS) and the aggregation of the QDs-labeled peptide was successfully avoided. We showed that QDs coated with NTS accumulated selectively in nucleus of living cells. These results encourage the application of QDs-labeled biomolecules for targeted imaging in living cells.

Results and Discussion

The original sequence of NTS comes from the archetypal nuclear location sequence of the Simian Virus SV40 large tumor antigen (T-ag), which comprises a single short stretch of basic amino acids ($_{126}\text{PKKKRKV}_{132}$) [2].

The method of Fmoc solid phase was used to synthesize QDs-NTS-NH₂. However, aggregation always occurs when QDs are coupled to the peptide, and QDs are easily quenched in acidic environments when TFA was used to cleave peptides from resin. In order to overcome these problems, an alternative strategy was proposed that Fmoc-Lys(-Tfa)-OH was used to synthesize nuclear targeting signal (NTS(-Tfa)). The Fmoc group of the signal peptide was deprotected by pyridine in DMF, then the signal peptide was cleaved from resins by TFA, while the -Tfa group still remained to exclude the undesirable cross-linking of $\epsilon\text{-NH}_2$ and carboxyl groups. The -Tfa group was cleaved by pyridine in water after coupled to QDs.

The peptides quality were examined using the analytical HPLC to determine the purity while the molecular weight were determined using MS. The crude peptides were further purified using the reversed phase HPLC.

The QDs-NTS complex was incubated with Hep-2 cells for 2 hrs, then resuspended and plated on polylysine-coated cover slide. The cells were observed by Olympus fluorescent microscope (Fig. 1).

The results showed that the QDs-NTS complex was internalized by Hep-2 cell and specifically localized on the nuclei, while un-conjugated QDs have no such effect. Similar results were also observed in HELA cell lines (data not shown). Neither obvious toxicity nor any effect on cell behavior after labeled with QDs were observed. Currently, we are exploring direct linked QDs with other signal peptide in the study of cells or organs for their functions.

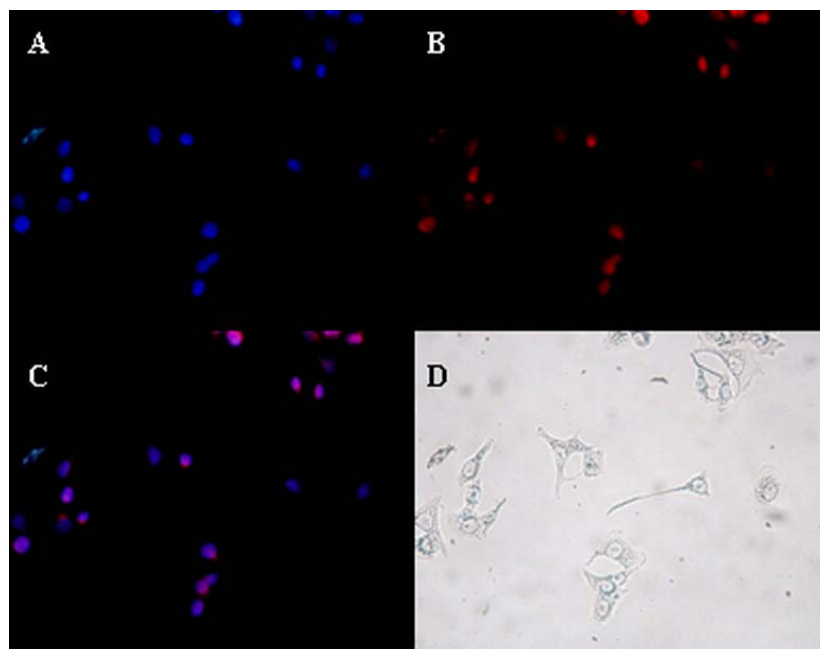


Fig. 1. Internalization and localization of fluorescent particles in the cytoplasmic compartment of Hep-2 cells. Hep-2 cells were incubated in the presence of Hoechst 33342 or QDs -NTS for 2 hrs, resuspended and plated on polylysine-coated cover slide. Images were acquired with an Olympus fluorescent microscope. (A) Nuclear staining with Hoechst 33342. (B) Nuclear imaging with QDs -NTS. (C) Overlay of (A) and (B). (D) Visible light field. All images were acquired with constant microscope settings (laser power, filters, detector gain, amplification gain, and amplification offset).

References

1. Bailey, R. E., Smith, A. M. and Nie, S. *Physica E* **25**, 1-12 (2004).
2. Marcos, R., Fontes, M., The, T. and Kobe. B. *J. Mol. Biol.* **297**, 1183-1194 (2000).

Synthesis of Symmetrical Dimeric Dicarboxylic Acid Linked Peptides on Solid Support

Sheng Jiang¹, Zaneta Nikolovska-Coleska², Shaomeng Wang² and Peter P. Roller¹

¹Laboratory of Medicinal Chemistry, CCR, NCI-Frederick, NIH, Frederick MD 21702, USA;

²University Michigan Cancer Center, 1500 E Medical Center Drive, Ann Arbor MI 48109-0934, USA

Introduction

Merrifield's invention of solid-phase peptide synthesis (SPPS) revolutionized the field of peptide chemistry [1]. Through 40 years development, a rich variety of molecular transformations have been discovered, including peptide cyclization [2], intramolecular thioetherification [3], and ring closing metathesis [4]. The emphasis of these reactions has been the intramolecular transformation, while intermolecular transformation on the solid support has been much less explored. In 2000, Conde-Frieboes *et al.* published the synthesis of symmetrical dimeric peptides on solid support by olefin metathesis [5]. Herein we report a facile dimerization of peptides on solid-phase supports using a series of dicarboxylic acids as linkers.

Results and Discussion

The 3-amino acid-long linear precursor **1** for the tetrapeptides was synthesized by an automated SPPS (ABI 433A Peptide Synthesizer), starting with Rink amide MBHA resin (0.78 mmol/g, 100-200 mesh) for establishing the C-terminal carboxamide, and using the chemical protocols based on Fmoc chemistry (coupling with HBTU/HOBt/DIPEA in NMP) (Fig. 1). After the construction of the 3-mer peptide **1**, Boc protected Alanine can be cleanly incorporated to produce **2**. After completion of peptide elongation, the Mtt protecting group on Lys was removed by treatment with 1% TFA in DCM to afford the resin bound peptide **3**. Subsequently, compound **3** was reacted with a series of dicarboxylic acids (n from 1 to 8) using the coupling reagent HATU with the addition of HOAt. Then, the peptide-bound resins were washed six times with NMP, DCM, and MeOH, then dried under reduced pressure overnight. The peptides were cleaved from the resin and fully deprotected by treatment with 2.5% TIS, 2.5% H₂O in TFA (10 mL/g resin). After 2 hrs the mixture was filtered into cold diethyl ether. After 30 min at -10 °C the precipitated peptides were separated by centrifugation, washed four times with diethyl ether, and dried under reduced pressure (1 hr over KOH). The dicarboxylic acid-linked dimeric tetrapeptides and the monomeric tetrapeptides with one carboxylate linker were separated by preparative RP HPLC (Vydac C₁₈ column). The purity of all peptides was between 95% and 99% as measured by RP HPLC on an analytical C₈ column. MALDI-TOF-MS spectra (Kratos Axima-CFR instrument, matrix: α -cyano-4-hydroxycinnamic acid) verified molecular masses of all peptides.

The product ratio of the dimeric tetrapeptides (**6**) to the monomeric tetrapeptides (**7**) was quantitated by HPLC. Results indicate that the ratio of dimer to monomer increases when the number of CH₂ units in the dicarboxylic acids (n) increases in the range of n = 1-6. For example, we cannot obtain the dimeric peptide but only the monomer using malonic acid (n = 1), while we obtain the dimer only using suberic acid (n = 6) with a high overall yield of 41%. When the distance between the two

carboxylic acid motifs is unduely long, as is the case with sebacic acid ($n = 8$), the selectivity of dimeric over monomeric product drops to a ratio of 1.4 to 1 percent.

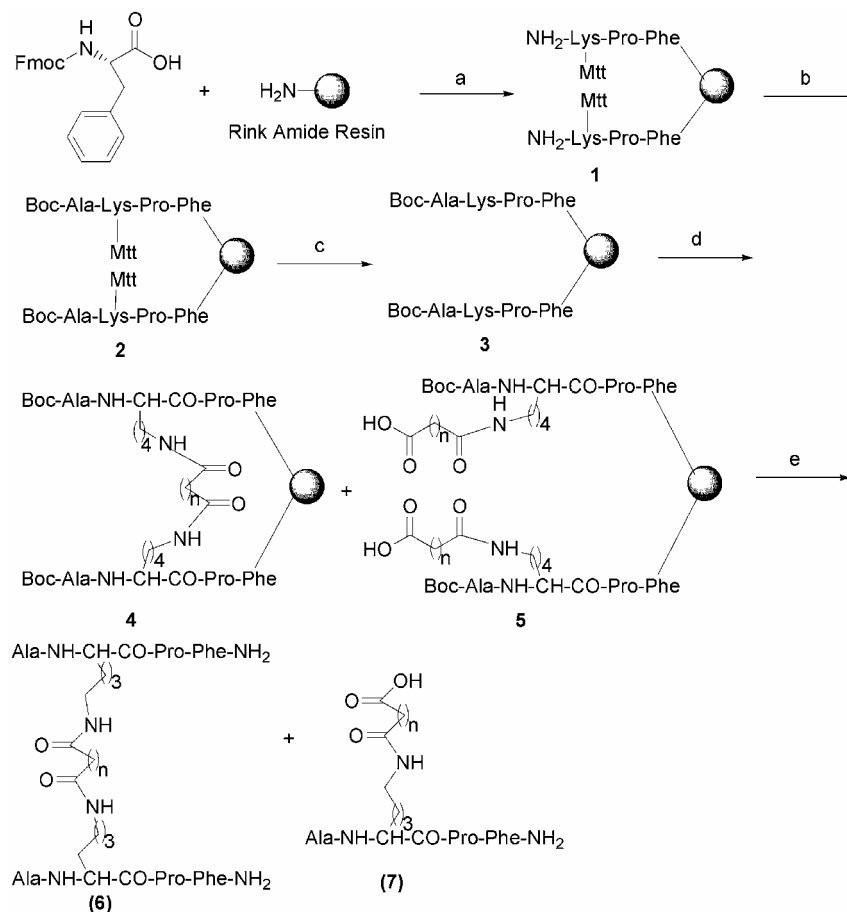


Fig. 1. Synthesis of peptides (6) and (7).

a) 1) HBTU, HOBt, DIPEA in NMP, 2) 20% piperidine in NMP, 3) 2 cycles of Fmoc SPPS with HBTU/HOBt/DIPEA coupling; b) Boc-alanine, TBTU/HOBt/DIPEA in DMF; c) 1% TFA in DCM, 10×2 mins; d) dicarboxylic acid, HATU/HOAT/DIPEA in DMF, overnight; e) 95% TFA, 2.5% TIS and 2.5% H₂O, 2hrs.

References

1. Merrifield, R. B. *J. Am. Chem. Soc.* **85**, 2149-2154 (1963).
2. Humphrey, J. M. and Chamberlin, A. R. *Chem. Rev.* **97**, 2243-2266 (1997).
3. Long, Y. -Q., Voigt, J. H., Lung, F. -D. T., King, C. R. and Roller, P. P. *Bioorg. Med. Chem. Lett.* **9**, 2267-2272 (1999).
4. Jaevo, E. R., Copeland, G. T., Papaioannou, N., Bonitatebus, Jr., P. J. and Miller, S. J. *J. Am. Chem. Soc.* **121**, 11638-11643 (1999).
5. Conde-Frieboes, K. and Andersinholt, J. *Tetrahedron Lett.* **41**, 9153-9156 (2000).

Systematic Study on the Structure-Activity Relationship of Pyrazinone Ring-Containing Bioactive Opioid Ligands

Kimitaka Shiotani¹, Anna Miyazaki², Tingyou Li¹, Yuko Tsuda^{1,2,3},
 Toshio Yokoi^{1,2,3}, Akihiro Ambo⁴, Yusuke Sasaki⁴, Yunden Jinsmaa⁵,
 Sharon D. Bryant⁵, Lawrence H. Lazarus⁵ and Yoshio Okada^{1,2,3}

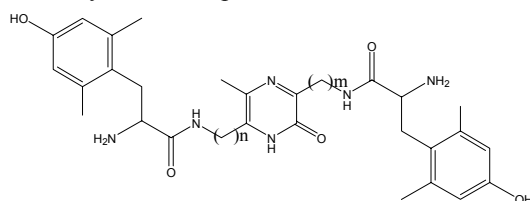
¹The Graduate School of Food and Medicinal Sciences; ²Faculty of Pharmaceutical Sciences;

³High Technology Research Center, Kobe Gakuin University, Kobe 651-2180, Japan;

⁴Tohoku Pharmaceutical University, Sendai 981-8558, Japan; ⁵Medicinal Chemistry Group,
 LCBRA, National Institute of Environmental Health Sciences, NC 27709, USA

Introduction

We previously reported the development of pyrazinone ring-containing analgesics, 3, 6-bis[Dmt-NH-(CH₂)_n]-5-methyl-2(1*H*)pyrazinones (n=1-4), which exhibited considerably potent antinociceptive activity after intracerebroventricular (i.c.v.), subcutaneous (s.c.) and oral (p.o.) administration in mice [1]. These compounds bound to mu-opioid receptors (MOR) with high affinity and high selectivity over delta-opioid receptor (DOR). A rapid and facile procedure of 2(1*H*)-pyrazinone derivatives from dipeptidyl chloromethyl ketones was developed in our laboratory [2,3]; the opioid ligands containing Dmt (2',6'-dimethyl-L-tyrosine) as the functional N-termini were prepared [4]. In this presentation, synthesis of the full set of 3-[Dmt-NH-(CH₂)_m]-6-[Dmt-NH-(CH₂)_n]-5-methyl-2(1*H*)-pyrazinones [Fig. 1 (m, n = 1-4)] and their structure-activity relationship are discussed.



(I) m=4, n=4	(V) m=3, n=4	(IX) m=2, n=4	(XIII) m=1, n=4
(II) m=4, n=3	(VI) m=3, n=3	(X) m=2, n=3	(XIV) m=1, n=3
(III) m=4, n=2	(VII) m=3, n=2	(XI) m=2, n=2	(XV) m=1, n=2
(IV) m=4, n=1	(VIII) m=3, n=1	(XII) m=2, n=1	(XVI) m=1, n=1

Fig. 1. Structure of pyrazinone ring-containing opioid mimetics (I-XVI).

Results and Discussion

Synthesis: Pyrazinone ring-containing opioid mimetics were prepared as described previously [3]. The final opioid mimetics were obtained as HCl salts with greater than 98% purity by analytical HPLC. The purified compounds were identified by MALDI-TOF MS, ¹H NMR spectra and elemental analyses.

Binding affinity: Relative to the DOR, compound IX (m=2, n=4) exhibited the highest affinity *K_i* value of 1.46 nM and for the MOR, compound II (m=4, n=3) exhibited an exceptional *K_i* value of 0.021 nM. Compound VIII (m=3, n=1) exhibited the best selectivity with 3,126 (*K_i*Δ/*K_i*μ). These data indicated that the

length of the alkyl chain at the positions 3 and 6 of pyrazinone affected receptor binding affinity, suggesting that structure of pocket in MORs might be different from that of DORs.

In vitro biological activity: Compounds **I** (m, n=4), **II** and **VI** (m, n=3) exhibited full agonistic activity in guinea pig ileum (GPI) assay with IC₅₀ values of 1.90, 1.76 and 1.33 nM, respectively. On the contrary, in mouse vas deferens (MVD) assay, compounds **I** and **II** exhibited moderate agonist activity with IC₅₀ values of 41.5 and 25.8 nM, respectively, and compound **XIII** (m=1, n=4) did not exhibit any detectable activity; on the other hand, compounds **XI** (m, n=2) and **XVI** (m, n=1) exerted weak δ opioid antagonism (pA_2 = 6.56 and 6.47, respectively).

In vivo biological activity: Tail-flick (TF) and hot-plate (HP) tests in mice were utilized to measure the effect after i.c.v., s.c., and p.o. administration of compounds **II**, **VI** and **X** (m=2, n=3) in comparison with morphine. The i.c.v. administration of compounds **II**, **VI**, and **X** manifested more potent antinociceptive activity than morphine in both tests, being 65, 50-63, and 10 fold, respectively, in TF test, but 71, 18-21, and 14 fold compared with morphine, respectively, in the HP test. The fact that **II**, **VI** exhibited antinociceptive activity after p.o. administration suggests that those compounds can transit through the intestinal tract and the blood-brain barrier (BBB) [5,6].

References

1. Jinsmaa, Y., Miyazaki, A., Fujita, Y., Fujisawa, Y., Shiotani, K., Li, T., Tsuda, Y., Yokoi, T., Ambo, A., Sasaki, Y., Bryant, S. D., Lazarus, L. H. and Okada, Y. *J. Med. Chem.* **47**, 2599-2610 (2004).
2. Taguchi, H., Yokoi, T., Tsukatani, M. and Okada, Y. *Tetrahedron* **51**, 7361-7372 (1995).
3. Okada, Y., Fukumizu, A., Takahashi, M., Yamasaki, J., Yokoi, T., Tsuda, Y., Bryant, S. D. and Lazarus, L. H. *Tetrahedron* **55**, 14391-14406 (1999).
4. Okada, Y., Fujita, Y., Motoyama, T., Tsuda, Y., Yokoi, T., Li, T., Sasaki, Y., Ambo, A., Jinsmaa, Y., Bryant, S. D. and Lazarus, L. H. *Bioorg. Med. Chem.* **11**, 1983-1994 (2003).
5. Jinsmaa, Y., Okada, Y., Tsuda, Y., Shiotani, K., Sasaki, Y., Ambo, A., Bryant, S. D. and Lazarus, L. H. *J. P. E. T.* **309**, 432-438 (2004).
6. Igarashi, K., Murabayashi, Y., Hotta, K., Kitamura, Y., Kasuya, F., Shiotani, K., Li, T., Miyazaki, A., Tsuda, Y., Okada, Y. and Fukushima, S. *J. Chromatography B* **806**, 53-57 (2004).

Tetra and Pentapeptide Derivatives of Hemiasterlin. Synthesis and Activity Studies

Marcin Dyba¹, Nadya I. Tarasova¹, Teresa Kosakowska-Cholody¹,
Ernest Hamel² and Christopher J. Michejda¹

¹Molecular Aspects of Drug Design Section, Structural Biophysics Laboratory; ²Screening Technologies Branch, National Cancer Institute at Frederick, Frederick, MD 21702-1201, USA

Introduction

Hemiasterlin **1** (Fig. 1) is a natural tripeptide toxin first isolated from the marine sponge *Hemiasterella minor* [1] and later from a number of other sponges. Hemiasterlin acts as an extremely potent inhibitor of tubulin polymerization and is active against leukemia, ovarian carcinoma, and breast cancer cells [2,3].

We investigated a very active hemiasterlin analog **2** (Fig. 1) [4] as a toxin in a receptor-mediated, enzyme-dependent, drug delivery approach. Since the lysosomal processing of a receptor-targeted peptide prodrug adds 1 or 2 amino acid residues to the C-terminus of the toxin, it was necessary to select residues that would lead to the most active final products.

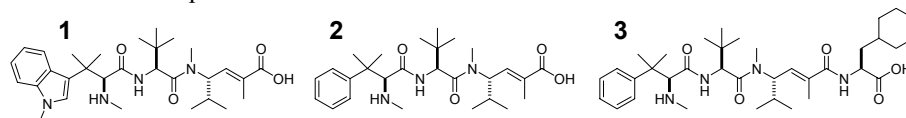


Fig. 1. Chemical structures of hemiasterlin (**1**), HTI-286 (**2**), and HTI-286 extended on the C-terminus by cyclohexylalanine (**3**).

Results and Discussion

We generated a small library of hemiasterlin tetra- and pentapeptide derivatives using both natural and unnatural amino acids in the fourth and fifth positions and determined their inhibitory activities in MTT cytotoxicity and tubulin polymerization assays.

Hemiasterlin analog **2** (HTI-286) was synthesized according to a slight modification of the method of Andersen *et al.* [4]. All tetra- and pentapeptide derivatives of **2** were synthesized on solid support by coupling Boc protected **2** to the appropriate amino acid or dipeptide attached to a resin.

Cytotoxicity was determined by the MTT assay [5] using NIH 3T3 cells. Inhibition of tubulin polymerization was determined as described earlier [6]. Purified tubulin from bovine brain tissue was used for this study.

All elongated hemiasterlin derivatives showed much lower activities than **2** in the MTT cytotoxicity assay. Even the most active tetrapeptide **3** (Fig. 1), $IC_{50} = 8$ nM, was three orders of magnitude less active than **2**, $IC_{50} = 3$ pM (Table 1). Surprisingly, no significant differences were observed between **2** and any of the tetra- or pentapeptides in their abilities to inhibit tubulin polymerization. All 25 compounds had IC_{50} 's between 1 and 3 μ M in the tubulin assay, as compared to the value of 1.4 μ M obtained for **2**. Results in the tubulin assay corresponded very well to previously reported values for different hemiasterlins and dolastatins [4].

The lack of correlation between cytotoxicities of the newly synthesized hemiasterlin derivatives and the activities of those compounds in the tubulin polymerization assay suggests that other factors must be critical for the extraordinary cell toxicity of the most potent hemiasterlin derivatives. One possibility could derive from differences in cell penetration of the various compounds or, once taken up by the cells, differences in intracellular drug distribution. However, other factors that are independent of the ability of the molecules to bind to tubulin may also be important determinants of toxicity.

Table 1. Activities of hemiasterlin derivatives in MTT and tubulin assays

Name	Residue	IC ₅₀ [μ M] MTT, 3T3	IC ₅₀ [μ M] Tubulin
HTI-286	—	0.000003	1.4 \pm 0.07
MD039	Gly	2.3	2.8 \pm 0.09
MD040	Asp	0.59	1.6 \pm 0.04
MD041	Lys	1.0	2.1 \pm 0.16
MD042	Phe	0.066	1.6 \pm 0.06
MD044	Ser	0.70	1.7 \pm 0.05
MD047	Trp	0.38	1.2 \pm 0.01
MD049	Bip	0.50	1.4 \pm 0.03
MD051	1-Nal	0.028	1.1 \pm 0.07
MD052	Hfe	0.078	1.2 \pm 0.09
MD053	Tic	0.39	1.1 \pm 0.05
MD054	Cha	0.008	1.8 \pm 0.13
MD055	2-Nal	0.052	1.2 \pm 0.04
MD056	Phe(4-F)	0.084	1.3 \pm 0.07
MD057	Chg	0.049	1.3 \pm 0.10
MD058	Phe(4-CN)	0.50	1.2 \pm 0.11
MD059	Tyr	0.60	1.2 \pm 0.10
MD046	Phe-Ala	1.1	1.2 \pm 0.07
MD091	Cha-Asp	0.45	1.7 \pm 0.08
MD092	Cha-Phe	0.45	1.4 \pm 0.07
MD093	Cha-Lys	0.10	1.5 \pm 0.13
MD094	Cha-Gly	2.3	1.3 \pm 0.07
MD095	Cha-Leu	0.42	1.4 \pm 0.02
MD096	Cha-Ser	2.9	1.3 \pm 0.01
MD097	Cha-Cha	0.079	1.6 \pm 0.21

References

1. Talpir, R., Benayahu, Y. and Kashman, Y. *Tetrahedron Lett.* **35**, 4453-4456 (1994).
2. Coleman, J. E., Desilva, E. D., Kong, F. M., Andersen, R. J. and Allen, T. M. *Tetrahedron* **51**, 10653-10662 (1995).
3. Anderson, H. J., Coleman, J. E., Andersen, R. J. and Roberge, M. *Cancer Chemother. Pharmacol.* **39**, 223-226 (1997).
4. Nieman, J. A., Coleman, J. E., Wallace, D. J., Piers, E., Lim, L. Y., Roberge, M. and Andersen, R. J. *J. Nat. Prod.* **66**, 183-199 (2003).
5. Woynarowski, J. M., Napier, C., Koester, S. K., Chen, S. F., Troyer, D., Chapman, W. and MacDonald, J. R. *Biochem. Pharmacol.* **54**, 1181-1193 (1997).
6. Hamel, E. *Cell Biochem. Biophys.* **38**, 1-22 (2003).

The Chemo-enzymatic Synthesis of Oligosaccharide-linked Peptides Aimed at Improved Drug Delivery

Ken D. Johnstone¹, Manuela Dieckelmann², Michael P. Jennings¹,
Joanne T. Blanchfield¹ and Istvan Toth¹

¹ School of Molecular and Microbial Sciences, University of Queensland, St. Lucia, Qld. 4072, Australia; ²School of Molecular and Microbial Biosciences, University of Sydney, Sydney, N.S.W. 2006, Australia

Introduction

Endomorphin-1 is an endogenous opioid peptide with high affinity for opioid receptors in the brain that has been investigated as a potential pain-relieving drug [1]. Our research group has demonstrated that chemically modifying short peptides with lipidic groups in combination with mono and disaccharides can dramatically improve the peptide's stability, membrane permeability and bioavailability [2]. Our aim was to extend this work to more complex carbohydrate-containing glycopeptides using glycosyltransferases [3].

To investigate the specificity and reactivity of the *N*-acetylglucosaminyltransferase LgtA, isolated from *Neisseria meningitidis*, a series of three carbohydrate-modified endomorphin-1 derivatives were synthesised, containing either an *N*-terminus-connected glucose **1**, galactose **2** or lactose **3** moiety (Fig. 1).

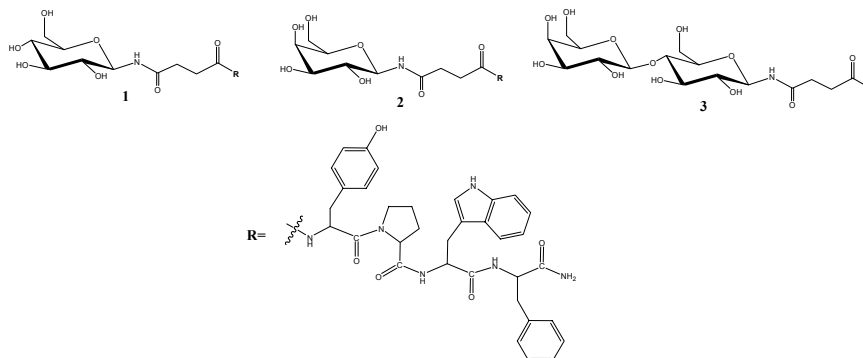
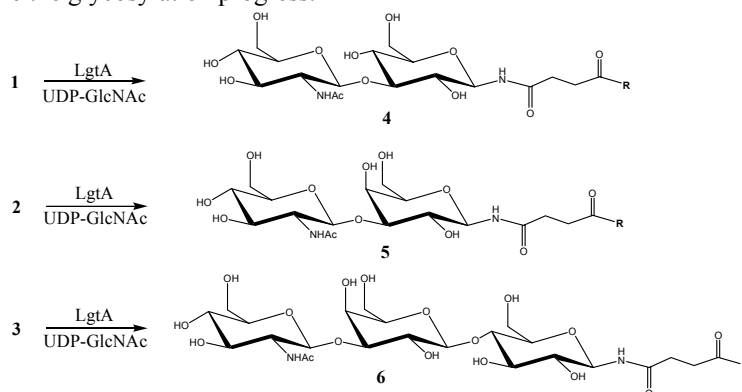


Fig. 1. Chemically synthesized *N*-terminus sugar-attached glycopeptides utilized in the glycosyl transferase experiment: glucose-linked endomorphin-1 **1**, galactose-linked endomorphin-1 **2** and lactose-linked endomorphin-1 **3**.

Results and Discussion

We were interested in testing the specificity of LgtA, by examining its ability to add *N*-acetyl glucosamine to the terminal glucose of glycopeptide **1**, and exploring the effects of varying the terminal sugar environment, by comparing the enzyme's ability to add *N*-acetyl glucosamine to the terminal galactose unit of **2** and **3** (Scheme 1). The three glycopeptides **1-3** were each mixed with one equivalent of the donor sugar nucleotide UDP-GlcNAc (uridine diphosphate *N*-acetyl glucosamine) and the glycosyltransferase enzyme LgtA in a buffer solution and left to incubate at 37 °C

for twenty-four hours. Electrospray mass spectrometry (ES-MS) was used to analyze the glycosylation progress.



Scheme 1. The theoretical products of enzymatic glycosylation of glycopeptides 1-3. The R substituent is the same as in Fig. 1.

ES-MS analysis of the glycosylations showed that LgtA added the *N*-acetylglucosamine unit to the lactose glycopeptide very effectively, but was much less effective with the galactose compound and no glycosylation product was observable for the glucose derivative. This result highlights the selectivity of the enzyme and suggests that future studies on this type of glycosyltransferase enzyme require disaccharide precursors. The lactose glycosylation progress could be followed using TLC and yielded **6** quantitatively after 13 days when a 3-fold excess of UDP-GlcNAc was used.

In summary, the LgtA glycosyltransferase enzyme is an extremely useful tool for the synthesis of oligosaccharide-modified peptide derivatives. In the future, we plan to utilize the chemo-enzymatic techniques described with a variety of different glycosyl transferase enzymes. This will enable large libraries of oligosaccharide-linked peptide drug candidates to be easily synthesized and subsequently screened for enzyme stability, receptor affinity and oral absorption. We also aim to use these techniques to design complex oligosaccharide-linked peptide drugs that mimic natural receptor-recognised oligosaccharides in the body to investigate its feasibility as a highly site-specific drug delivery strategy.

Acknowledgments

The work was funded by an Australian NHMRC grant.

References

1. Przewlocka, B., Mika, J., Labuz, D., Toth, G. and Przewlocki, R. *Eur. J. Pharmacol.* **367**, 189-196 (1999); Zadina, J., Hackler, L., Ge, L. -J. and Kastin, A. *Nature* **386**, 499-502 (1997).
2. Blanchfield, J. T., *et al.* *Lett. Peptide Sci.* **8**, 235-239 (2002); Blanchfield, J. T., *et al.* *J. Med. Chem.* **46**, 1266-1272 (2003); Kellam, B., Drouillat, B., Dekany, G., Starr, M. S. and Toth, I. *Int. J. Pharm.* **161**, 55-64 (1998).
3. Johnstone, K. D., Dieckelmann, M., Jennings, M. P., Toth, I. and Blanchfield, J. T. *Current Drug Delivery* **2**, 215-222 (2005).
4. Blixt, O., van Die, I., Norberg, T., van den Eijnden, D. *Glycobiology* **9**, 1061-1071 (1999).

Neokyotorphin as Cell Protein Kinase Affector

Olga V. Sazonova, Elena Yu. Blishchenko, Anna G. Tolmazova, Dmitry P. Khachin, Andrei A. Karelin and Vadim T. Ivanov

Group of Regulatory Peptides, Shemyakin-Ovchinnikov Institute of Bioorganic Chemistry, Moscow, 117997, Russia

Introduction

In the present study we report on the last results on the mechanism of action of neokyotorphin (TSKYR), α -hemoglobin fragment (137-141). This peptide was shown to be secreted by human erythrocytes [1] and to accumulate in human lung carcinoma tissue [2]. Its effect depends on the cell type [3]: it stimulates proliferation in normal cells (murine embryonic fibroblasts; spleen and bone marrow cells derived from adult mice) and some types of tumor cells (murine melanoma M3 and transformed fibroblasts L929); it is not active in murine transformed myelomonocytes WEHI-3 and decreases cell number in rat pheochromocytoma PC-12. The maximal proliferative activity of the peptide was observed in the case of growth factors deficiency and low initial cell density [4]. According to the literature data, neokyotorphin increases Ca influx through L-type channels [5]. Earlier we have shown that the proliferative effect of neokyotorphin is abolished by L-type channel blockers verapamil and nifedipine, and by intracellular Ca^{2+} chelator BABTA-AM [3]. Staurosporine (which inhibits several forms of PKC, Src, CaMKII, PKA) also abolished the peptide effect, indicating that protein kinases are involved in the realization of its activity. In the present work the concrete kinases involved in neokyotorphin effect realization were distinguished

Results and Discussion

The results PKA and PKC activation depend on cell type and can strongly vary, leading both to inhibition and stimulation of proliferation. The effects of phorbol-12-myristate 13-acetate (PMA, PKC activator), 8-Br-cAMP (PKA activator) were compared to neokyotorphin effect in 3 types of fibroblasts (Table 1). In all cell cultures, the effect of 8-Br-cAMP correlated with neokyotorphin effect, pointing at probable involvement of PKA in realization of the peptide activity.

Table 1. Compare of neokyotorphin effect with PKC and PKA activators

Cell line	0.1 μM PMA	50 μM 8-Br-cAMP	1 μM neokyotorphin
L929 transformed murine fibroblasts	50 \pm 15*	26 \pm 6*	25 \pm 5*
Spontaneously transformed murine Swiss embryonic fibroblasts	40 \pm 6*	5 \pm 7	2 \pm 7
CV-1 African green monkey fibroblasts	-48 \pm 4*	-16 \pm 10	-14 \pm 10

*the effect is reproducible with $CV < 30\%$.

After down-regulation of PKC in L929 cells by 24 hr pre-incubation with 5 μM PMA the activity of neokyotorphin did not change, as well as in the presence of PKC

inhibitor bis-indolylmaleimide XI (0.5, 1 and 2 μM). In the presence of 1-10 μM PKA inhibitor H-89 the activity of the peptide was abolished, confirming that PKA and not PKC is intracellular target of neokyotorphin. According to the literature, activation of L-type channel can lead to calmodulin-dependent or -independent activation of adenylylcyclase [6], resulting in PKA activation.

PKA-induced proliferation is reported to be mediated through activation of Rap1/B-Raf, activators of MAPK/Erk cascade [7]. MAPK/Erk cascade inhibitor PD 98059 in 20 μM concentration fully inhibited 1 μM neokyotorphin and 50 μM 8-Br-cAMP effect in L929 cells, while the effect of standard growth factors set (10% FBS) was inhibited by 50%. It indicates the involvement of PKA→MAPK/Erk pathway in neokyotorphin effect realization.

In the presence of 10 μM CaMKII inhibitor KN-62, inducing 50% suppression of 10% FBS effect in L929 cells, both 1 μM neokyotorphin and 50 μM 8-Br-cAMP were inactive. CaMKII, like PKA, can contribute in Erk activation [8]. It could be that both CaMKII and PKA are necessary for sufficient Erk activation. Neokyotorphin as L-type Ca^{2+} channel activator can also increase CaMKII activity.

Based on the results obtained, the mechanism of action of neokyotorphin is similar to that described for proliferative glucagons-like peptide-1 in pancreatic β -cells, which induces activation of Ca^{2+} L-channels leading to activation of PKA and CaMKII [9].

Acknowledgments

The work was funded by RAS Presidium programme “Molecular and Cell Biology”

References

1. Ivanov, V., Karelin, A. and Yatskin, O. *Biopolymers* **80**, 332-346 (2005).
2. Zhu, Y. X., Hsi, K. L., Chen, Z. G., Zhang, H. L., *et al.* *FEBS Lett.* **208**, 253-257 (1986).
3. Sazonova, O., Blishchenko, E., Tolmazova, A., *et al.* In *In Peptides 2004, Proceedings of the 28th European Peptide Symposium* (Flegel, M., Fridkin, M., Gilon, C. and Slaninova, J., eds.) Kenes International, Israel, pp. 563-564 (2005).
4. Sazonova, O., Blishchenko, E., Kalinina, O., *et al.* *Prot. Peptide Lett.* **4**, 386-395 (2003).
5. Kokoz, Y., Zenchenko, K. I., Alekseev, A. E., *et al.* *FEBS Lett.* **411**, 471-476 (1997).
6. Ferguson, G. D. and Storm, D. R. *Physiology (Bethesda)*, **19**, 271-276 (2004).
7. Takahashi, H., Honma, M., Miyauchi, Y., *et al.* *Arch. Dermatol. Res.* **296**, 74-82 (2004).
8. Dolmetsch, R. E., Pajvani, U., Fife, K., *et al.* *Science* **294**, 333-339 (2001).
9. Gomez, E., Pritchard, C. and Herbert, T. P. *J. Biol. Chem.* **277**, 48146-48151 (2002).

Towards Inhibition of Amyloid β -protein Oligomerization

**Sean M. Spring¹, Summer L. Bernstein², Noel D. Lazo¹, Brigita Urbanc³,
H. Eugene Stanley³, Michael T. Bowers², David B. Teplow¹ and Gal
Bitan¹**

¹*Department of Neurology, David Geffen School of Medicine at UCLA, Los Angeles, CA 90095;* ²*Department of Chemistry and Biochemistry, UC Santa Barbara, CA 93106;* ³*Department of Physics, Boston University, Boston, MA 02215, USA*

Introduction

Multiple lines of evidence indicate that amyloid β -protein ($A\beta$) oligomers are key effectors of neurotoxicity and a primary cause of Alzheimer's disease (AD). Therefore, inhibition of $A\beta$ oligomerization is an attractive strategy for preventing and treating AD. Two major forms of $A\beta$ are produced from the amyloid β -protein precursor (APP), $A\beta_{40}$ and $A\beta_{42}$. Despite the small structural difference between these two alloforms, the dipeptide Ile⁴¹-Ala⁴², their clinical, biological, and biophysical characteristics are distinct. $A\beta_{40}$ is ~10 times more abundant than $A\beta_{42}$, yet $A\beta_{42}$ is more neurotoxic and more strongly linked to AD. Structural studies of $A\beta$ oligomers are difficult because the oligomers are metastable and exist in dynamic mixtures comprising monomers and oligomers of various sizes. To study the composition of these dynamic mixtures, we applied Photo-Induced Cross-linking of Unmodified Proteins (PICUP) [1] to the characterization of $A\beta$ oligomer size distributions. PICUP allows taking "snapshots" of metastable oligomer mixtures and analyzing size distributions quantitatively [2]. Using PICUP, we demonstrated that $A\beta_{40}$ and $A\beta_{42}$ comprised distinct oligomer populations [3] and provided a plausible explanation for their distinct biological and clinical behavior. An intermediate comprising pentamer/hexamer units, which self associate to form larger assemblies formed exclusively by $A\beta_{42}$ and was termed "paranucleus" [3].

To study the tertiary structure of $A\beta$ oligomers, a combination of discrete molecular dynamics and a coarse-grain peptide model was used. This allowed simulation of $A\beta$ assemblies which cannot to be modeled by traditional modeling techniques in a reasonable time frame. The oligomer size distributions of $A\beta_{40}$ and $A\beta_{42}$ obtained were distinct and in good agreement with those observed using PICUP [4]. Analysis of intramolecular residue-residue contacts revealed a strong interaction between Val³⁶-Val³⁹. In $A\beta_{42}$, this results in the formation of a turn centered at Gly³⁷-Gly³⁸, which is stabilized by multiple weaker interactions. In $A\beta_{40}$, despite a strong interaction between Val³⁶-Val³⁹, a similar structure is scarcely populated due to insufficient stabilizing interactions [4]. These insights offer a likely explanation for the distinct oligomerization patterns of $A\beta_{40}$ and $A\beta_{42}$. Limited proteolysis experiments revealed a restricted conformation in the C-terminus of $A\beta_{42}$ but not in the C-terminus of $A\beta_{40}$ [5], consistent with the modeling data [4].

Results and Discussion

Based on the experimental and theoretical data described above, we hypothesized that peptides derived from the C-terminus of $A\beta_{42}$ could interact with paranuclei and disrupt them. To test this hypothesis, the C-terminal fragments (CTFs) $A\beta(11-42)$, $A\beta(20-42)$, and $A\beta(30-42)$, and the analog [Phe¹⁰] $A\beta_{40}$, were mixed with full-

length A β 42 and the mixtures were cross-linked and analyzed by SDS-PAGE. If the CTFs disrupt paranucleus formation, the observed oligomer size distribution of A β 42 would be expected to display a decrease in the abundance of pentamers/hexamers and an increase in the abundance of lower order oligomers. We found that in the presence of the CTFs, the abundance of A β 42 hexamers decreased, suggesting that the CTFs disrupted A β 42 paranuclei. In contrast, in the presence of [Phe¹⁰]A β 40 the oligomer size distribution of A β 42 remained essentially unchanged, suggesting that the C-terminal dipeptide Ile⁴¹-Ala⁴² is required for paranucleus disruption. To study the relationship between peptide length and inhibitory activity, we synthesized a series of A β (x-42) CTFs with x=28-39 and screened them for paranucleation inhibition. Each CTF was mixed with A β 42 at a 1:1 ratio (v/v), and the mixtures were cross-linked and analyzed by SDS-PAGE. The relative abundance of A β 42 hexamer was the most sensitive measure of the inhibitory effect of the CTFs. Hexamer abundances relative to each lane were quantified densitometrically (Fig. 1). Inhibition of hexamer formation was observed for peptides longer than A β (35-42). Peptides beginning at positions 32-34 caused a ~50% decrease of the relative hexamer abundance and peptides beginning at positions 30-31 inhibited 85-90% of hexamer abundance relative to uninhibited A β 42 (C). Control peptides comprising non-C-terminal sequences of A β , Ac-A β (16-22)-NH₂ and A β (21-30) had no effect on the oligomer size distribution of A β 42 (data not shown). The data demonstrate that A β 42 CTFs can attenuate paranucleus formation by A β 42 in a length-dependent manner and thus can serve as leads for rational design of A β 42 oligomerization inhibitors.

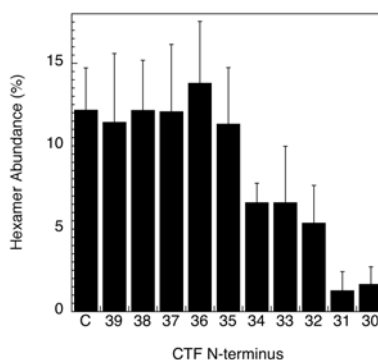


Fig. 1. Inhibition of A β 42 paranucleus formation shown as relative A β 42 hexamer abundance versus peptide length.

Acknowledgments

The work was supported by AFAR grant A04084 to G. Bitan and by NIH grant AG18921 to D. B. Teplow.

References

1. Fancy, D. A. and Kodadek, T. *Proc. Natl. Acad. Sci. USA* **96**, 6020-6024 (1999).
2. Bitan, G. and Teplow, D. B. *Acc. Chem. Res.* **37**, 357-364 (2004).
3. Bitan, G., et al. *Proc. Natl. Acad. Sci. USA* **100**, 330-335 (2003).
4. Urbanc, B., et al. *Proc. Natl. Acad. Sci. USA* **101**, 17345-17350 (2004).
5. Lazo, N. D., et al. *Prot. Sci.* **14**, 1581-1596 (2005).

Use of Betidamino Acids in Drug Design

Judit Erchehy¹, Sandra Wenger³, Beatrice Waser³, Veronique Eltschinger³, Renzo Cescato³, Jean Claude Reubi³, Steven C. Koerber¹, Christy R. R. Grace², Roland Riek² and Jean E. Rivier¹

¹The Clayton Foundation Laboratories for Peptide Biology; ²Structural Biology Laboratory, The Salk Institute, La Jolla, CA, 92037 USA; ³Division of Cell Biology and Experimental Cancer Research, Institute of Pathology, University of Berne, Berne, Switzerland

Introduction

Earlier, we successfully used betidamino acids (N^{β} -monoacylated, optionally N^{α} -mono-or N^{α},N^{β} -dialkylated, aminoglycine (Agl) derivatives) [1,2] in the design of bioactive GnRH antagonists [3]. Here, we present the introduction of Agl(N^{β} Me,benzoyl) and Agl(N^{β} Me,2-naphthoyl) in shortened sequences of somatostatin (SRIF) such as: CH-275 (2) [4], Octreotide (4) [5], and ODT-8 (9) [6]. Schematic illustration of the backbone structures is shown below:



Results and Discussion

Table 1 summarizes the binding affinity of the analogs (expressed as IC_{50}) at the five human SRIF receptor subtypes. The substitution of the betide homolog of β -methyl-D-2Nal, [D-Agl(N^{β} Me,2-naphthoyl)]⁸ for D-Trp⁸ in the CH-275 template resulted in a very potent and highly ss_{t1} -selective agonist (3). The introduction of the same betidamino acid in the Octreotide template also in position 8 (SRIF numbering) resulted in potent and ss_{t5} -selective ligands (5-8), which differ from all the previously published analogs in not binding to ss_{t2} at all. The [D-Agl(N^{β} Me,2-naphthoyl)]⁸ substitution in the ODT-8 template resulted in a potent and ss_{t3} -selective antagonist (10). The substitution of the carbamoyl moiety in 10 by DOTA (1,4,7,10-tetraazacyclotetradecane- N,N',N'',N''' -tetraacetic acid), which is a chelator used to radiolabel peptides with radiometals, yielded 11 with retention of high ss_{t3} selectivity (>200-fold over the other receptors) and binding affinity. Analog 11, with a Tyr in the sequence as well, can be radiolabeled with both radiohalogens and radiometals, therefore it can serve as a tracer for ss_{t3} binding or localization studies. The substitution of the betide homolog of β -methyl-Phe, [Agl(N^{β} Me,benzoyl)]⁷ for Phe⁷ also in the ODT-8 template resulted in potent and highly ss_{t4} -selective agonists (12, 13). The substitution of [Agl(N^{β} Me,benzoyl)]⁷ for Phe⁷ in the Octreotide template resulted in a potent and ss_{t2} -selective antagonist (14) with good binding affinity and selectivity mainly for ss_{t2} (>45-fold over ss_{t1} , ss_{t3} , ss_{t4} , and >25-fold over ss_{t5}). These results suggest that the methylated betide scaffold is versatile and will induce conformational constraints leading to potent and highly receptor-selective peptide ligands. We recommend the use of betidamino acid scans (and more particularly N^{β} -methyl betidamino acid scans) of biologically active peptides in addition to the alanine, D-amino acid and other scans routinely used in the SAR of peptides to identify potential receptor-selective agonists and antagonists.

Table 1. Binding affinities [IC_{50} , nM] at the five human SRIF receptors

	Compound	sst ₁	sst ₂	sst ₃	sst ₄	sst ₅
1	Somatostatin-28, SRIF-28	4.2	2.4	5.3	4	4.4
2	H-c[Cys-Lys-Phe-Phe-DTrp-IAMP-Thr-Phe-Thr-Ser-Cys]-OH (CH-275)	31	>10K	345	>1K	>10K
3	H-c[Cys-Lys-Phe-Phe-DAGl(N ⁶ Me,2-naphthoyl)-IAMP-Thr-Tyr-Thr-Ser-Cys]-OH	3.3	>1K	>1K	562	>1K
4	H-DPhe-c[Cys-Phe-DTrp-Lys-Thr-Cys]-Thr-NH ₂ Octreotide amide	908	2.5	59	>1K	3.3
5	H-DPhe-c[Cys-Phe-DAGl(N ⁶ Me,2-naphthoyl)-Lys-Thr-Cys]-Thr-NH ₂	191	>1K	495	66	11.6
6	H-DPhe-c[Cys-Tyr-DAGl(N ⁶ Me,2-naphthoyl)-Lys-Thr-Cys]-Thr-NH ₂	>1K	>1K	>1K	762	75
7	H-2Nal-c[Cys-3Pal-DAGl(N ⁶ Me,2-naphthoyl)-Lys-Val-Cys]-2Nal-NH ₂	>1K	>1K	171	335	27
8	H-D2Nal-c[Cys-3Pal-DAGl(N ⁶ Me,2-naphthoyl)-Lys-Val-Cys]-2Nal-NH ₂	>1K	>1K	610	103	24
9	H-[Cys-Phe-Phe-DTrp-Lys-Thr-Phe-Cys]-OH (ODT-8)	28	44	13	1.3	45
10	H ₂ N-CO-[DCys-Phe-Tyr-DAGl(N ⁶ Me,2-naphthoyl)-Lys-Thr-Phe-Cys]-OH	>10K	>10K	6.7	>10K	>10K
11	DOTA-[DCys-Phe-Tyr-DAGl(N ⁶ Me,2-naphthoyl)-Lys-Thr-Phe-Cys]-OH	>1K	>10K	4.7	>10K	>10K
12	H-[Cys-Phe-Agl(N ⁶ Me,benzoyl)-DTrp-Lys-Thr-Phe-Cys]-OH	>1K	460	447	5.2	768
13	H-[DCys-Phe-Agl(N ⁶ Me,benzoyl)-DTrp-Lys-Thr-Phe-Cys]-OH	>1K	533	382	3.4	460
14	H-Cpa-c[DCys-Agl(N ⁶ Me,benzoyl)-DTrp-Lys-Thr-Cys]-2Nal-NH ₂	>1K	17	727	872	442

The IC_{50} values are mean of two or more experiments.

Acknowledgments

This work was supported by NIH Grant RO1 DK 59953. We thank R. Kaiser, W. Low and C. Miller for technical assistance and D. Doan for manuscript preparation.

References

1. Qasmi, D., René, L. and Badet, B. *Tetrahedron Lett.* **34**, 3861-3862 (1993)
2. Jiang, G.-C., Simon, L. and Rivier, J. E. *Prot. Peptide Lett.* **3**, 219-224 (1996)
3. Rivier, J. E., Jiang, G. -C., Koerber S. C., Porter, J., Craig, A. G. and Hoeger, C. *Proc. Natl. Acad. Sci. USA* **93**, 2031-2036 (1996)
4. Liapakis, G., Hoeger, C., Rivier, J. and Reisine, T. *J. Pharmacol. Exper. Ther.* **276**, 1089-1094 (1996)
5. Bauer, W., Briner, U., Doepfner, W., Haller, R., Huguenin, R., Marbach, P., Petcher, T. and Pless, J. *Life Sci.* **31**, 1133-1140 (1982)
6. Rivier, J. E., Hoeger, C., Erchevyi, J., Gulyas, J., DeBoard, R., Craig, A. G., Koerber, S. C., Wenger, S., Waser, B., Schaer, J. -C. and Reubi, J. C. *J. Med. Chem.* **44**, 2238-2246 (2001)

Helical Peptide Analogs of gp41 to Develop an HIV Vaccine

Florence M. Brunel¹, Michael B. Zwick², Ian A. Wilson^{3,4}, Dennis R. Burton^{2,3} and Philip E. Dawson^{1,4}

¹*Department of Chemistry and Cell Biology;* ²*Department of Immunology;* ³*Department of Molecular Biology;* ⁴*Skaggs Institute for Chemical Biology, The Scripps Research Institute, La Jolla, CA, 92037, USA*

Introduction

A vaccine is considered by many as the best hope to control the AIDS epidemic. Poor immunogenicity and high mutation rate in HIV-1 have made the development of such a vaccine quite a challenge. However, few broadly neutralizing antibodies have been identified and they have proven to be effective to protect against infection in vaginal and intravenous challenges [1]. The most broadly neutralizing antibody, 4E10, recognizes a highly conserved region in the membrane-proximal external region (MPER) of the envelope glycoprotein gp41 [2]. Recently, a crystal structure has been solved of a 13-mer peptide bound to the 4E10 neutralizing antibody, and it showed that the peptide adopts a helical conformation [3]. One probable reason previous attempts to elicit 4E10-like antibodies failed is the inability of the antigens to adopt and maintain a configuration similar to the one adopted by the peptides when bound to the antibody. We decided to characterize the 4E10 epitope and to synthesize constrained analogs of the MPER to increase their helical content. This strategy represents initial steps towards the development of a HIV vaccine.

Results and Discussion

The epitope of the broadly neutralizing 4E10 antibody is found in the MPER of gp41 and contains WFDIT, however the importance of flanking residues has been suggested [2,3]. Based on the crystal structure and mutation experiments on the virus, the length of the epitope was studied from the starting peptide NWFDITNWLW. The binding to the antibody was assessed by a in-solution ELISA. Solubility appeared to be a major problem and a four-lysine tail was routinely added on the C-terminal end of the peptides. Truncation and elongation experiments performed on both ends allowed us to refine the epitope as NWFDITNWLWYIK. The importance of each amino acid within this newly defined epitope was assessed by Ala-scanning. The helicity of each mutant was studied by circular dichroism. Amino acids within the new epitope could then be ranked according to their importance, and, comparing the results from the crystal structure of a truncated version and our CD data, their role could be assigned to a direct contact with the antibody or structure stabilization. As expected, **NWFDIT**NWLWYIK were found to be crucial for the binding because they make direct contact with the antibody [3]. The important role of isoleucine was also confirmed, and the suggested importance of W680 was shown. Surprisingly, leucine also appeared to be playing a major role, and this had not been foreseen from the crystal structure where a glycine spacer replaced the leucine. N677, W678 and Y681 could be replaced with alanine without affecting the binding ability to the antibody: those three positions can be used for future modifications.

Table 1. Structure and IC₅₀ of some of our best derivatives and KGND

Name	Structure	IC ₅₀
KGND	KG-WNWF D ITNW-GK	>10,000
44-1	NWFDITNWLW-RR-NH ₂	150
84-1	NWFDITNWLW-KKKK-NH ₂	40
94-1	NWFDITNWLWYIK-KKK-NH ₂	10
102-1 ¹	NWFDITNWLW-KBKB-NH ₂	10
102-2 ¹	KKB-NWFDITNWLW-KBKB-NH ₂	10
119	NWFDITNWLWYIK-KKKK-NH ₂	10
104-1	NWFCITOWLW-KKKK-NH ₂	40
104-2 ²	NWFCITOWLW-KKKK-NH ₂	10

To confirm the binding to 4E10, the effect on neutralization of one of the derivatives was studied. The peptide blocked neutralization by 4E10 of different HIV-1 strains, but it did not block neutralization by other neutralizing antibodies. In addition, we have induced helicity into the C-terminal part of the peptide through the introduction of Aib residues as well as tethers. The introduction of a lactam bridge between the positions i and i+3, and i and i+4 is a known method to increase the helical character of a peptide. We developed an alternative where a thioether tether is being formed [4]. This method yields cleaner products with an enhanced helical character compared to the acyclic analog and sometimes even compared to the corresponding lactam. The same tight binding (10 nM) could be achieved with different constrained derivatives. The length of those constrained peptides could even be reduced compared to the newly defined epitope. The ability to reduce the peptide length is important in drug design because it removes potential immunogenic pieces that would have generated non-neutralizing antibodies.

Conclusion

We have characterized the peptide epitope of the neutralizing antibody 4E10 as NWFDITNWLWYIK. The importance of each amino acids has been assessed and permissive sites have been identified for future modifications. The helical character of the analogs has been enhanced by the introduction of Aib or some tethers. Several derivatives present a very tight binding (10 nM) to the antibody.

Acknowledgments

We acknowledge support from the American Foundation for AIDS Research (to F.M.B.), the Elizabeth Glaser Pediatrics AIDS Foundation (to M.B.Z.), the NIH, AI 058725 (to M.B.Z), AI 33292 (to D.R.B), GM46192 (for I.A.W.) and MH062261 (to P.E.D.), the Neutralizing Antibody Consortium of the International AIDS Vaccine Initiative, the Pendleton Trust and the Skaggs Institute for Chemical Biology.

References

1. Baba, T. W., *et al. Nat. Med.* **6**, 200-206 (2000).
2. Zwick, M. B., Jensen, R., Church, S., Wang, M., Stiegler, G., Kunert, R., Katinger, H. and Burton, D. R. *J. Virol.* **79**, 1252-1261 (2005).
3. Cardoso, R. M., Zwick, M. B., Stanfield, R. L., Kunert, R., Binley, J. M., Katinger, H.; Burton, D. R. and Wilson, I. A. *Immunity*, **22**, 163-173 (2005).
4. Brunel, F. M. and Dawson, P. E. *Chem. Comm.* **20**, 2552-2554 (2005).

Structure-Activity Relationship Studies of a Novel AGRP-Melanocortin Chimeric Template

Krista R. Wilson, Andrzej M. Wilczynski, Joseph W. Scott, Rayna M. Bauzo and Carrie Haskell-Luevano

*Department of Medicinal Chemistry, College of Pharmacy, University of Florida,
Gainesville, FL 32610, USA*

Introduction

The melanocortin system is made up of five receptors (MC1-5), which are members of the superfamily of seven transmembrane-spanning G-protein coupled receptors (GPCR). The melanocortin receptors are stimulated by the endogenous agonists α -, β -, and γ -MSH, and ACTH, and are antagonized by the only two known endogenous antagonists of GPCRs, agouti and agouti-related protein (AGRP) [1]. The MC3R and MC4R have been shown to be involved in energy and weight homeostasis, making agonists of these receptors important in the treatment of obesity and related diseases [2,3].

This study involves the creation of a 21-membered “focused” combinatorial library based on the AMW3-23 template [4], peptide **1** in Table 1. The AMW3-23 template is a chimeric peptide that was created by substituting the core sequence of α -MSH, His-DPhe-Arg-Trp, into the AGRP(109-118) sequence in place of the Arg-Phe-Phe core sequence of AGRP (Fig. 1). The disulfide bridge was also replaced with a lactam bridge. This ligand was shown to be a subnanomolar agonist that is more potent than α -MSH at the MC1, 3, 4, and 5 receptors [4]. In this library, each peptide contained a single amino acid substitution. Each amino acid of the His-DPhe-Arg-Trp tetrapeptide sequence was replaced by a series of natural and unnatural amino acids. The library was synthesized on solid phase using standard Boc methodology by a parallel synthesis approach, purified to homogeneity, and analytically and pharmacology characterized for agonist or antagonist activity at the MC1, MC3, MC4, and MC5 receptors [5].

α -MSH	Ac-SYSME-HFRW-GKPV-NH ₂
AGRP(109-118)	Y-c[C-RFF-NAFC]-Y-NH ₂
AMW3-23	Y-c[D-H- DF -RW-NAF-Dpr]-Y-NH ₂

Fig. 1. Aligned sequences of α -MSH, AGRP(109-118)[6], and AMW3-23[4]. Core amino acid sequences in bold.

Results and Discussion

This study resulted in the design of compounds with unique pharmacology at the melanocortin receptors. These data indicate that the template AMW3-23 is a novel template for the design of potent melanocortin ligands.

Substitution at the His position with Ala (peptide 2) resulted in a compound that was equipotent to the lead peptide 1 at the mMC4R (Table 1). Replacing His with Pro (peptide 3) or Phe (peptide 4) resulted in compounds that were subnanomolar agonists at the mMC4R and potent antagonists at the mMC3R. Substitution for DPhe with bulky aromatic groups (peptides 6, 7) resulted in potent antagonists at the mMC3R and mMC4R, while substitution with Ala resulted in a loss of activity at melanocortin receptors. Substitution for Arg resulted in compounds with decreased

activity (peptide 8), confirming the importance of this amino acid in ligand-receptor interactions. Substitution of the Trp with Ala (peptide 9) resulted in compounds with decreased agonist activity at the melanocortin receptors, though substitution with aromatic groups (peptide 10) resulted in compounds that were nanomolar agonists at all four receptors.

Table 1. Pharmacology of AGRP-Melanocortin chimeras at melanocortin receptors [5]

Peptide	mMC1R	mMC3R	mMC4R	mMC5R
Y-c[D-X ¹ -X ² -X ³ -X ⁴ -NAF-Dpr]-Y-NH ₂	EC ₅₀ (nM)	EC ₅₀ (nM)	EC ₅₀ (nM)	EC ₅₀ (nM)
α-MSH	0.50±0.11 ^a	0.57±0.08	1.93±0.39	0.32±0.09
1. -His-DPhe-Arg-Trp-	0.22±0.14	0.13±0.03	0.13±0.04	0.37±0.26
2. -Ala-DPhe-Arg-Trp-	7.20±2.9	29.0±7.5	0.36±0.07	0.46±0.18
3. -Pro-DPhe-Arg-Trp-	22.1±16	pA ₂ = 7.16±0.22	0.63±0.17	1.46±1.0
4. -Phe-DPhe-Arg-Trp-	6.0±1.4	pA ₂ = 7.22±0.57	0.85±0.25	3.2±1.4
5. -His-Ala-Arg-Trp-	>10000 ^b	>10000	>10000	620±120
6. -His-p(I)DPhe-Arg-Trp-	0.3±0.05	pA ₂ = 8.90±0.20	pA ₂ = 10.0±0.21	2.33±1.0
7. -His-DNal(2')-Arg-Trp-	7.06±4.3	pA ₂ = 8.30±0.18	pA ₂ = 9.33±0.04	16.9±9
8. -His-DPhe-Ala-Trp-	70±30	2700±1800	32.5±17	2.06±0.7
9. -His-DPhe-Arg-Ala-	350±150	>10000	700±170	50±10
10. -His-DPhe-Arg-DNal(2')-	0.20±0.05	13.2±7	0.65±0.35	0.95±0.40

^aStandard errors derived from at least three independent experiments.

^b>10000 indicates no agonist activity below 10μM agonist concentration.

Acknowledgments

This work was supported by NIH R01DK57080, and R01DK064250.

References

1. Ollman, M. M., *et al. Science* **278**, 135-138 (1997).
2. Fan, W., *et al. Nature* **385**, 165-168 (1997).
3. Huszar, D., *et al. Cell* **88**, 131-141 (1997).
4. Wilczynski, A., *et al. J. Med. Chem.* **47**, 2194-2207 (2004).
5. Wilczynski, A., *et al. J. Med. Chem.* **48**, 3060-3075 (2005).
6. Haskell-Luevano, C., *et al. Peptides* **21**, 683-689 (2000).

Synthesis and Pharmacological Evaluation of a New Generation of TIPP-Derived Dual-Labeled Ligands for Delta Opioid Receptors

Xin Wang¹, Thomas F. Murray² and Jane V. Aldrich¹

¹Department of Medicinal Chemistry, School of Pharmacy, University of Kansas, Lawrence, KS, 66045, USA; ²Department of Physiology and Pharmacology, College of Veterinary Medicine, University of Georgia, Athens, GA 30602, USA

Introduction

Understanding δ -opioid receptor structure and function will aid in the discovery of potential therapeutic agents targeting this receptor. We are interested in developing potent and selectively labeled opioid peptide ligands as pharmacological tools to study this receptor at the molecular level. TIPP, which contains a Tic (1,2,3,4-tetrahydroisoquinoline-3-carboxylic acid) residue at the 2-position, is a potent and selective δ -opioid receptor antagonist [1].

The affinity label [Phe(*p*-NCS)³]TIPP retains high δ -opioid receptor affinity (IC_{50} = 12.4 nM) and exhibits wash-resistant inhibition of the binding [2]. However attachment of a biotin derivative via a hydrophilic spacer to the C-terminus of [Phe(*p*-NCS)³]TIPP resulted in a drastic decrease in δ -opioid receptor affinity (IC_{50} = 1650 nM) [3]. Therefore, an alternative placement of an affinity label group at the meta position on the phenyl ring of Phe³ in the dual labeled TIPP derivatives was explored.

Results and Discussion

The dual-labeled TIPP derivatives were prepared using Fmoc solid phase peptide synthesis on a 4-(4-formyl)-3-methoxyphenoxy butyl resin (Fig. 1) [4]. The complete peptide was assembled using Fmoc-protected amino acids except for the N-terminal Tyr residue, which was protected as the Boc derivative; Fmoc-Phe(*m*-NO₂)-OH was incorporated in position 3 of the peptide. The *meta*-NO₂ group on Phe³ in the peptide was reduced to the primary amine on resin by SnCl₂•2H₂O [5], and the affinity label was then introduced [6].

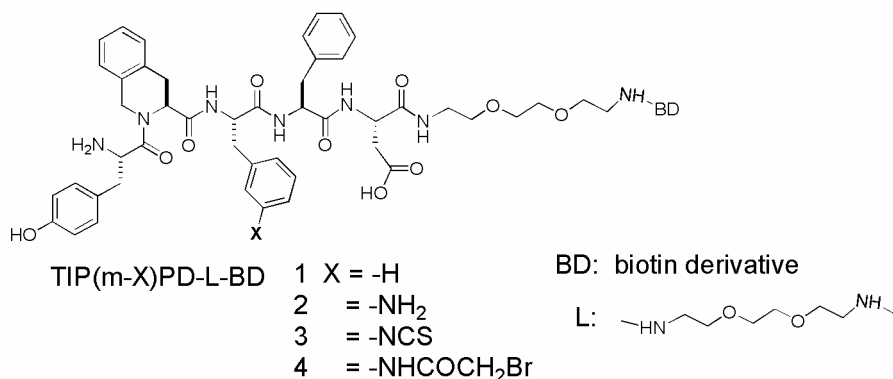


Fig. 1. TIPP-derived dual labeled affinity ligands.

The affinities of these ligands for δ - and μ -opioid receptors were determined using cloned receptors stably expressed on CHO cells by competitive inhibition of the binding of radioligands [^3H]DPDPE and [^3H]DAMGO, respectively. The results are summarized in Table 1. The *meta*-amino control compound **2** ($\text{IC}_{50} = 32$ nM) showed only a 2.4-fold decrease in δ -opioid receptor affinity compared to that of the unsubstituted compound **1** ($\text{IC}_{50} = 13$ nM). In contrast, the *para*-amine analog ($\text{IC}_{50} = 152$ nM) caused a 11-fold decrease in δ -opioid receptor affinity [3]. The isothiocyanate compound **3** exhibited very low affinity for the δ -opioid receptor ($\text{IC}_{50} = 1200$ nM) similar to the result from the *para*-substituted analog. However, affinity label compound **4** from the substituting Phe³ with a *meta*-bromoacetamide group resulted only a small decrease (6-fold, $\text{IC}_{50} = 79$ nM) in the δ -opioid receptor affinity. This *meta*-bromoacetamide derivative represents a promising lead compound to assist in the study of δ -opioid receptors.

Table 1. Delta opioid receptors affinities of the TIPP-derived affinity ligands

TIP(<i>m</i> -X)PD-NH-L-NH-BD	δ $\text{IC}_{50} \pm \text{SEM}$ (nM)
1	13.4 ± 2.3
2	32.5 ± 7.0
3	1200 ± 100
4	79.1 ± 23.3

The IC_{50} values of these ligands for μ -opioid receptors are all >10 μM .

Acknowledgments

The authors thank Marinda Thomas (University of Georgia) for performing the pharmacological assays. This research was founded by National Institute on Drug Abuse R01 DA10035.

References

- Schiller, P. W., Nguyen, T. M. D., Weltrowski, G., Wilkes, B. C., Marsden, B. J., Lemieux, C. and Chung, N. N. *Proc. Natl. Acad. Sci. USA* **89**, 11871-11875 (1992).
- Maeda, D. Y., Berman, F., Murray, T. F. and Aldrich, J. V. *J. Med. Chem.* **43**, 5044-5049 (2000).
- Wang, X. and Aldrich, J. V. Unpublished results.
- Kumar, V. and Aldrich, J. V. *Org. Lett.* **5**, 613-616 (2003).
- Makara, G., Ewing, W., Ma, Y. and Wintner, E. *J. Org. Chem.* **66**, 5783-5789 (2001).
- Kumar, V., Murray, T. F. and Aldrich, J. V. *J. Med. Chem.* **43**, 505-5054 (2000).

Synthesis and Pharmacological Evaluation of Dual Labeled Delta Opioid Receptor Peptides

Angela M. Peck¹, Vivek Kumar², Thomas F. Murray³ and Jane V. Aldrich¹

¹Department of Medicinal Chemistry, University of Kansas, Lawrence, KS 66025, USA; ²Department of Pharmaceutical Sciences, University of Maryland, Baltimore, Maryland 2120; ³Department of Physiology and Pharmacology, College of Veterinary Medicine, University of Georgia, Athens, GA 30602, USA

Introduction

Understanding receptor-ligand interactions is important in the design of novel ligands. G-Protein coupled receptors such as opioid receptors are difficult to study because they are membrane bound proteins that are expressed at very low levels. Affinity labels, ligands that bind to receptors via a covalent bond, have aided in the study and characterization of opioid receptors. By identifying the attachment point of affinity labels they can provide information about receptor-ligand interactions.

We prepared affinity labeled derivatives of TIPP (Tyr-Tic-Phe-Phe, Tic = 1,2,3,4-tetrahydroisoquinoline-3-carboxylic acid) which bind to the δ opioid receptor (DOR). TIPP, which consists of all aromatic residues, possesses high potency and selectivity for DOR [1]. Modified TIPP derivatives containing a reactive functionality on Phe⁴ exhibit high affinity and wash-resistant inhibition of binding to DOR [2,3]. Here we describe dual labeled TIPP derivatives that contain an affinity label on Phe⁴ and a His tag functionality, which will assist in receptor isolation. The His tag is attached to the C-terminus via a hydrophilic linker, and an acidic residue was incorporated to maintain selectivity for DOR over μ opioid receptors [4].

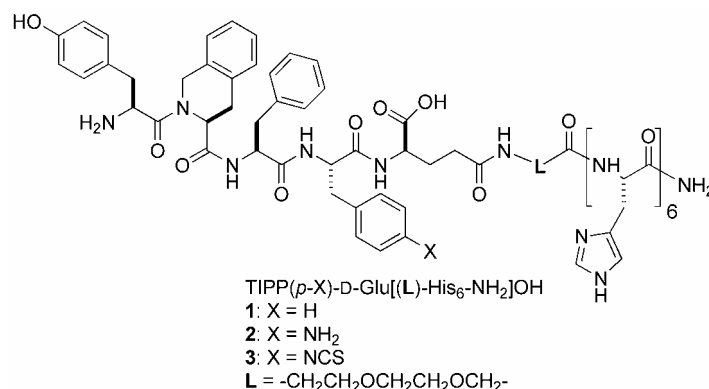


Fig. 1. His-tagged TIPP analogs.

Results and Discussion

The His-tagged TIPP peptide analogs were synthesized using a modified Fmoc solid phase synthesis protocol [5] on low-load PAL-PEG-PS resin (0.17-0.19 mmol/g). The protected peptide assembly began with the coupling of Fmoc-His(Trt) to the resin; Fmoc-Phe(*p*-NHAlloc) was incorporated in position 4 of the peptide, and Boc-Tyr(*t*Bu) was attached at the N-terminus [5]. Following complete assembly of the

Table 1. DOR binding affinity of TIPP and His-tagged analogs

Peptide	IC ₅₀ ± SEM (nM)
1	30.5 ± 1.9
2	9.8 ± 2.3
3	22.5 ± 1.2
TIPP	5.8 ± 1.2 ^a
[Phe(<i>p</i> -NH ₂) ⁴]-TIPP	11.8 ± 2.5 ^a
[Phe(<i>p</i> -NCS) ⁴]-TIPP	5.4 ± 1.3 ^a

^a ref. 3

peptide the Alloc group was deprotected using Pd(PPh₃)₄ and the reactive functionality introduced [5]. The final peptides were cleaved from the resin using TFA, H₂O, and TIPS (80:10:10). All peptides were purified using reversed-phase HPLC, characterized using analytical HPLC, and the mass confirmed using ESI-MS.

During the reaction of protected **2** on resin with bromoacetic acid and DIC, the molecular weight of the desired bromoacetamide analog was not observed in the ESI mass spectrum. Loss of neutral HBr was prominent, suggesting that intramolecular displacement of bromine had yielded a novel cyclic peptide. The nucleophilic imidazole π -nitrogen within histidine has been shown to be reactive towards alkyl bromides but not to alkyl chlorides [6,7]. A preliminary experiment indicated that the imidazole π -nitrogen of histidine is not reactive towards chloroacetic acid. The expected molecular weight for the unreacted His tag was present in the ESI mass spectrum, and no product corresponding to loss of HCl was observed upon treatment of the His tag with chloroacetic acid.

The DOR affinity of compounds **1-3** (Table 1) was determined in radioligand binding assays using cloned DOR expressed on CHO cells under standard conditions with [³H]DPDPE as the radioligand. Introduction of the His tag resulted in only a 4-fold decrease in DOR affinity for the dual labeled peptide **3**. These preliminary pharmacological data indicate that both the His tag and the Phe⁴ modification are well tolerated by DOR. These dual labeled peptides will be examined further in pharmacological assays and used to study the interactions of TIPP with DOR.

Acknowledgments

The authors thank Marinda Thomas (University of Georgia) for performing the pharmacological assays. Funding for this research was provided by NIDA grant R01 DA10035.

References

- Schiller, P. W., Nguyen, T. M. D., Weltrowska, G., Marsden, B. J., Lemieux, C. and Chung, N. N. *Proc. Natl. Acad. Sci. USA* **89**, 11871-11875 (1992).
- Kumar, V., Murray, T. F. and Aldrich, J. V. *J. Med. Chem.* **45**, 3820-3823 (2002).
- Maeda, D. Y., Berman, F., Murray, T. F. and Aldrich, J. V. *J. Med. Chem.* **43**, 5044-5049 (2000).
- Kumar, V., Murray, T. F. and Aldrich, J. V. *J. Med. Chem.* **43**, 5050-5054 (2000).
- Leelaswatanakij, L. and Aldrich, J. V. *J. Peptide Res.* **56**, 80-87 (2000).
- Wieghardt, T. and Goren, H. J. *Bioorg. Chem.* **4**, 30-40 (1975).
- Chivikas, C. J. and Hodges, J. C. J. *Org. Chem.* **52**, 3591-3594 (1987).

Novel Retro-inverso Envelope Peptide Mimetic Fusion Inhibitors as a Potential Therapy for HTLV-1 Infected Individuals

Marcus P. Lynch^{1,2}, Sharad V. Rawale², Ahmed A. Behery¹, William P. Hudleson¹, Norihiro Takenouchi³, Karen Yao³, Steven Jacobson³ and Pravin T. P. Kaumaya^{1,2,4}

¹Department of Microbiology; ²Department of Obstetrics and Gynecology; ³Viral Immunology Section, NINDS, National Institutes of Health, Bethesda, MD; ⁴Arthur G. James Comprehensive Cancer Center, The Ohio State University, Columbus, OH 43210, USA

Introduction

The clinical success of the viral fusion inhibitor T20 for the treatment of HIV-1 has spawned a new class of antiretroviral drugs. Peptide mimetics use only key residues of the binding region of a receptor or ligand, which are transferred to a smaller molecule with their binding properties intact. Retro-inverso (RI) peptides consist of D-amino acids in a reversed sequential order and are a mirror image of a mirror image with respect to sidechain orientation, resulting in a sidechain topology resembling the parent peptide. One drawback of T20 therapy is that it must be administered twice daily, resulting in astronomical cost. Retro-inverso peptide inhibitors are inherently protease resistant from the use of D-amino acids resulting in increased half-life *in vitro* and *in vivo* [1,2]. HTLV-1 infected individuals with lower proviral loads are less likely to develop inflammatory diseases such as HAM/TSP (HTLV-1 associated myelopathy/tropical spastic paraparesis). Therefore, therapeutic strategies that target viral dissemination and replication may have direct clinical application. It has been shown that peptides corresponding to HTLV-1 envelope glycoprotein (Env) residues 197-216 and 400-429 can reduce viral fusion [3,4]. The P400 region of HTLV-1 first described by Sagara *et al.* [3] and T20 derived from an analogous region of HIV-1 have been shown to be effective in inhibiting fusion. Here we report the neutralizing ability of a retro-inverso peptide inhibitor corresponding to residues 400-429 of HTLV-1 Env.

Results and Discussion

HTLV-1 Env peptide mimetic fusion inhibitors were synthesized using Fmoc/t-butyl strategy on CLEAR amide resin. N-termini were acetylated and the C-termini were amidated to promote rigidity and stability (Fig. 1). All peptides were purified by reverse phase HPLC and were >95% and characterized by mass spectroscopy. CD spectra of peptide fusion inhibitors P400 and RI P400 were measured at a concentration of 100 μ M in water and 50% TFE. Spectra characteristic of α -helices with minima at 208 nm and 222 nm and a maximum at 193 nm were shown by P400 (all L-amino acids) in water and 50% TFE. RI P400 (all D-amino acids) adopted an

P400 CH₃CO-(L)-CRFPNITNSHVPILQERPPLENRVLTGWGL-CONH₂
RI P400 CH₃CO-(D)-LGWGTLVARNELPPREQLIPVHSNTINPFRC-CONH₂
SCRC40 CH₃CO-(L)-PSEIVQRPIFGLWKSRLR-CONH₂

Fig. 1. Sequences of P400 RI P400 retro peptide mimetics derived from the HTLV-1 Env region. Peptide sequences are labeled with (L) or (D) to identify amino acid chirality. A scrambled sequence from CD40L was used as a control.

almost identical mirror image structural conformation when dissolved in water or in 50% TFE.

P400 and RI P400 were evaluated for their ability to inhibit syncytia using a three cell based fusion assay [5]. At 100 μ M both peptides demonstrated similar neutralizing capacities. At lower peptide concentrations P400 retained its neutralizing capacity better than RI P400 (Fig. 2). These results demonstrate that a retro-inverso peptide mimetic fusion inhibitor against HTLV-1 gp21 can inhibit virus-mediated fusion. The *in vivo* benefits of using this strategy have yet to be determined.

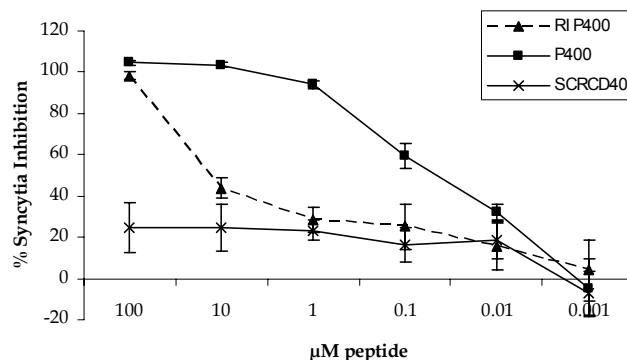


Fig. 2. To measure the neutralizing capacity of the P400 and RI P400 peptide fusion inhibitors a three cell line based fusion assay was used. 5×10^4 HTLV-1 infected and producing MT-2 cells were incubated for 2 hrs with various peptides prior to the addition of 5×10^4 CosZ28 (containing HIV-LTR-lacZ) and Hela-Tat (expressing HIV Tat). After a 20 hr incubation of all three cells, the reduction in β -galactosidase production from peptide-mediated fusion inhibition was determined by chemiluminescence.

References

1. Fletcher, M. D. and Campbell, M. M. *Chem. Rev.* **98**, 763-796 (1998).
2. Chorev, M. and Goodman, M. *Trends Biotechnol.* **13**, 438-445 (1995).
3. Sagara, Y., Inoue, Y., Shiraki, H., Jinno, A., Hoshino, H. and Maeda, Y. *J. Virol.* **70**, 1564-1569 (1996).
4. Pinon, J. D., Kelly, S. M., Price, N. C., Flanagan, J. U. and Brighty, D. W. *J. Virol.* **77**, 3281-3290 (2003).
5. Sundaram, R., Lynch, M. P., Rawale, S. V., Sun, Y., Kazanji, M. and Kaumaya, P. T. P. *J. Biol. Chem.* **279**, 24141-24151 (2004).

Heteroclitic Analogs Derived from the HTLV-1 Gag Antigen Increase Cytolytic and IFN- γ Responses in HLA-A*0201 Transgenic Mice

**Marcus P. Lynch^{1,2}, Jacqueline C. Lieblein¹, Sharad V. Rawale²,
Danielle M. Carbin² and Pravin T.P. Kaumaya^{1,2,3}**

¹Department of Microbiology; ²Department of Obstetrics and Gynecology; ³Arthur G. James Comprehensive Cancer Center, The Ohio State University, Columbus, OH 43210, USA

Introduction

The Human T-cell Leukemia Virus type-1 (HTLV-1) is the etiologic agent of Adult T-cell Leukemia (ATL); HTLV-1 associated myelopathy/tropical spastic paraparesis (HAM/TSP), and other inflammatory disorders. There is an increasing body of evidence demonstrating the value of CTL in controlling viral infection. HTLV-1 infected individuals with active cytolytic responses, and lowered provirus load are less likely to develop ATL or HAM/TSP. Therefore strategies aimed at improving the cytolytic properties of CTL generated in a prophylactic or therapeutic vaccine may be of value. Heteroclitic analogs (epitope enhanced peptides) with optimized MHC I anchor residues have been used to increase the immunogenicity of CTL epitopes for various viral and cancer antigens [1]. Recently it has been demonstrated that this strategy could be used to increase the immunogenicity of CTL directed against a highly conserved, low affinity epitope derived from HIV-1 reverse transcriptase [2]. Peptide immunogens with enhanced binding properties induce stronger MHC I-peptide-TCR interactions and therefore induce stronger activation signaling cascades, thereby increasing immunogenicity. The HTLV-1 Gag protein contains no optimal HLA-A*0201 restricted epitopes (an aromatic residue in position 1, Leu in the 2 position, and Val in the 9 position). Therefore, epitope enhancement is a feasible strategy to increase the immunogenicity of peptides against this antigen [3].

Results and Discussion

The use of predictive computer algorithms demonstrated the lack of strong HLA-A*0201 restricted CTL epitopes against the HTLV-1 Gag protein; although the possible application of epitope enhancement was demonstrated (Table 1). To evaluate the application of epitope enhancement, three groups of three HLA-A*0201 transgenic mice (HHD) were immunized twice with the 410, 410 9V, and 410 1Y9V immunogens. Ten days after the last immunization ELISPOT and ⁵¹Cr release assays were performed with harvested spleenocytes. Spleenocytes from mice immunized with 410 9V were able to generate a >3 fold increase in IFN- γ producing spleenocytes and >2 fold increase in cytotoxicity when compared to spleenocytes from 410 immunized mice in response to the wild type peptide (Table 2). Mice immunized with 1Y9V did not increase the frequency of IFN- γ producing cells in response to 410, but increased cytotoxic responses by ~50%. These results confirm previous reports that mutating a residue to tyrosine in the 1 position forfeit cross reactivity with the wild type peptide [2]. Here we demonstrate that epitope enhancement is an effective way to increase the immunogenicity of low to moderate affinity CTL epitopes in synthetic peptide vaccine preparations against HTLV-1.

Table 1. Sequences and predicted affinities of HLA-A*0201 restricted wild type (410) and epitope enhanced peptides (410 9V and 410 1Y9V) derived from residues 410-418 of the HTLV-1 Gag protein

Designation	Sequence	Predicted Affinity ^a
410	LLLDLPADI	269.05
410 9V	LLLDLPADV	1793.67
410 1Y9V	YLLDLPADV	4853.47
Tax 11-19 ^b	LLFGYPVYV	2406.15

^aComputer generated HLA binding predictions using algorithms based on Parker et al., [4].

^bPredicted affinity of the well defined Tax 11-19 epitope is shown above for reference.

Table 2. Frequency of peptide specific IFN- γ producing CD8⁺ splenocytes and cytolytic responses of splenocytes from HLA-A*0201 transgenic mice immunized with peptides derived from HTLV-1 Gag protein residues 410-418

Target cells pulsed with 10 μ M peptide	ELISPOT (Spot forming cells/10 ⁵ CD8 ⁺ splenocytes)			⁵¹ Cr Release (% Specific lysis)		
	410	410 9V	410 1Y9V	410	410 9V	410 1Y9V
410	64 \pm 10	200 \pm 20	46 \pm 16	22.9 \pm 6.2	54.9 \pm 1.9	33.3 \pm 9.0
410 9V	64 \pm 8	213 \pm 25	58 \pm 21	22.3 \pm 4.3	52.0 \pm 0.7	31.6 \pm 11.8
410 1Y9V	12 \pm 3	67 \pm 17	62 \pm 16	8.5 \pm 4.4	39.9 \pm 15.9	48.8 \pm 7.5
SVRD	6 \pm 3	7 \pm 4	5 \pm 1	0.5 \pm 0.2	0.7 \pm 1.2	0.1 \pm 0.5

References

1. Fikes, J. D. and Sette, A. *Expert Opin. Biol. Ther.* **3**, 985-993 (2003).
2. Okazaki, T., Pendleton, C. D., Lemonnier, F. and Berzofsky, J. A. *J. Immunol.* **171**, 2548-2555 (2003).
3. Chen, J. L., Stewart-Jones, G., Bossi, G., Lissin, N. M., Wooldridge, L., Choi, E. M., Held, G., Dunbar, P. R., Esnouf, R. M., Sami, M., Boulter, J. M., Rizkallah, P., Renner, C., Sewell, A., van der Merwe, P. A., Jakobsen, B. K., Griffiths, G., Jones, E. Y. and Cerundolo, V. *J. Exp. Med.* **201**, 1243-1255 (2005).
4. Parker, K. C., Bednarek, M. A. and Coligan, J. E. *J. Immunol.* **152**, 163-175 (1994).

Development of a Monoclonal Antibody Therapeutic for the Prevention and Treatment of *Pseudomonas aeruginosa* Infection

Daniel J. Kao and Robert S. Hodges

Department of Biochemistry and Molecular Genetics, University of Colorado at Denver and Health Sciences Center, Aurora, CO 80045, USA

Introduction

Unlike conventional vaccine formulations, peptide vaccines are able to target the immune system to specific neutralizing or otherwise protective epitopes. Despite this, there are no peptide vaccines approved for use in humans. In the development of a peptide vaccine, selection and design of the peptide immunogen is critical for generating antibodies that are cross-reactive with the cognate protein of interest.

Here we describe our approach in the development of a monoclonal antibody therapeutic for the prevention and treatment of *Pseudomonas aeruginosa* (*Pa*) infection. *Pa* is a Gram-negative bacillus that is an opportunistic pathogen. One of the key events in the initial pathogenesis of *Pa* infection is type IV pilus-mediated adhesion to host epithelial cells in the respiratory tract. This adhesion is mediated through a 17-residue C-terminal disulfide loop in the pilin protein monomer, which is the basic subunit of the pilus fiber. This region is considered the host receptor binding domain.

This C-terminal disulfide loop presented itself as an excellent candidate for development of a peptide vaccine which would also be used to develop a monoclonal antibody therapeutic. However, although the host receptor binding domain is functionally conserved among known strains of *Pa*, the amino acid sequences are only semi-conserved. One goal in the development of the vaccine and antibody therapeutic was to have cross-reactivity among the commonly occurring strains of *Pa*. We hypothesized that this was feasible because all strains bind the same host receptor. This led to the development of a consensus sequence immunogen that generates antibodies that are cross-reactive among *Pa* strains [1].

Structural studies of the PAK strain monomeric pilin protein (which has a truncation of residues 1-28 to prevent multimerization) and peptide analogs of the receptor binding domain suggest that the pilin protein and the peptide analogs present conformationally different epitopes to the immune system (Fig. 1A). The

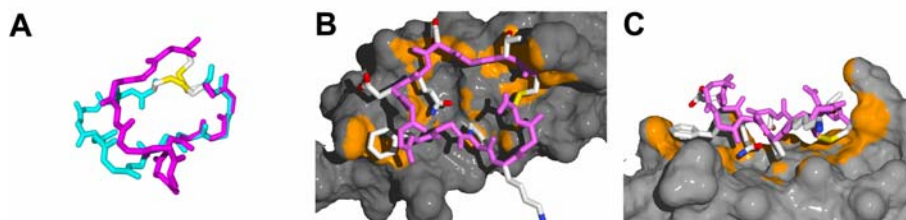


Fig. 1. A, Comparison of the conformation of the PAK receptor binding domain (128-144) as part of the pilin protein (dark chain) [2] and as a peptide analog (light chain) [3]. B and C, Crystal structure of PAK monomeric pilin (29-144) showing the receptor binding domain as a stick model and the remainder of the protein as a molecular surface. White patches on the surface represent contacts between the receptor binding domain and other regions of the protein.

receptor binding domain in the pilin monomer makes a number of intrachain contacts with other regions of the protein (Fig. 1B and 1C), which serve to define a specific conformation of the receptor binding domain and are expected to make the receptor binding domain more conformationally rigid in comparison to the peptide analog. Furthermore, the receptor binding domain in the peptide is completely accessible and only partially accessible in the pilin protein (Fig. 1C). A peptide immunogen could generate antibodies that are specific for the face of the receptor binding domain that is buried in the pilin protein, but we anticipate that these would not be as protective as antibodies that recognize the surface accessible face.

In the development of a monoclonal antibody therapeutic, it is critical to maximize its affinity for the epitope in the context in which the epitope is presented by the pathogen, in this case the pilin protein. As the structural data suggests, this is not necessarily the same as the epitope presented by a peptide immunogen. The goal of our experiments was first to determine whether there was a sacrifice in the affinity of antibodies raised against a peptide immunogen compared to a protein immunogen. We hypothesized that a peptide immunogen would generate antibodies of lower affinity for the pilin protein receptor binding domain because the immunogen has a different conformation and is more conformationally flexible. Our second objective was to determine whether there was a difference in cross-reactivity among *Pa* strains when using a peptide immunogen in comparison to using a protein immunogen. Here, we hypothesized that the peptide immunogen may generate more cross-reactive antibodies because the flexibility in the immunogen would allow for flexibility in the complementarity determining regions of the generated antibodies. Our findings will help us determine the best way to produce a monoclonal antibody with the desired properties of high affinity and cross-reactivity.

Results and Discussion

Two synthetic peptide immunogens and two recombinant pilin protein immunogens were used to generate polyclonal and monoclonal antibodies. The synthetic peptide immunogens were conjugated to keyhole limpet hemocyanin (KLH) to enhance immunogenicity. For each type of immunogen, one was based on the PAK strain sequence and the other was based on the consensus sequence. Antibody affinities were measured using a novel surface plasmon resonance technique using a heterodimeric coiled-coil affinity capture system [4].

Preliminary data from the polyclonal antibodies shows that the peptide and protein immunogens generate antibodies of comparable affinity for *Pa* antigens. The cross-reactivity of the peptide-specific antisera also appears to be greater than the antisera raised against the protein immunogens. Further analysis, including affinity purification of receptor binding domain specific antibodies from the polyclonal pools, is required to determine which immunogen generates antibodies of optimal affinity and cross-reactivity.

Acknowledgments

This work was funded by NIH grants to R.S..H. (RO1GM61855 and RO1AI48717).

References

1. Cachia, P. J. and Hodges, R. S. *Biopolymers* **71**, 141-168 (2003).
2. Hazes, B., *et al.* *J. Mol. Biol.* **299**, 1005-1017 (2000).
3. Campbell, A. P., *et al.* *Biochemistry* **34**, 16255-16268 (1995).
4. Cachia, P. J., Kao, D. J. and Hodges, R. S. *J. Mol. Recognit.* **17**, 540-557 (2004).

An Unexpected Side Reaction Involving the Deletion of an Acetylated N-Methyl-Amino Acid from the N-terminus of Peptides

Wei-Jie Fang¹, Marco A. Bennett², Thomas F. Murray³ and Jane V. Aldrich¹

¹Department of Medicinal Chemistry, University of Kansas, Lawrence, KS 66045, USA;

²Department of Pharmaceutical Sciences, University of Maryland, Baltimore, MD 21201, USA; ³Department of Physiology and Pharmacology, University of Georgia, Athens, GA 30602, USA

Introduction

Our research focuses on the development of potent and highly selective peptide antagonists for KOR (kappa opioid receptors) and examination of the structure-activity relationships (SAR) for antagonist activity at these receptors. Dynorphin A (Dyn A) is proposed to be an endogenous ligand for KOR [1]. It is a potent peptide, but is not very selective for KOR, demonstrating significant activity at the other opioid receptors.

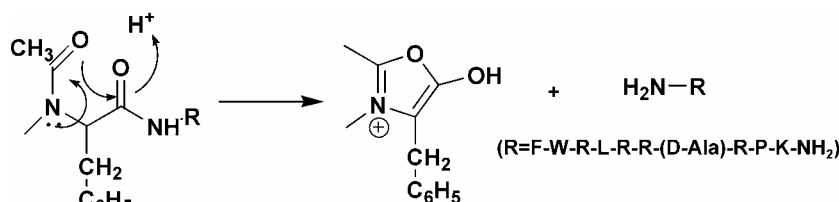
Arodyn (**1**, Fig. 1) is an acetylated Dyn A analog that is a potent and selective KOR antagonist [2], and its analog [NMePhe¹]arodyn shows even higher affinity and selectivity for KOR [3]. During the synthesis of [NMePhe¹]arodyn, this peptide underwent the unexpected deletion of Ac-NMePhe, apparently during the cleavage of the peptide from the resin. We examined the mechanism of this deletion and synthesized other stable analogs to study the SAR for antagonist activity at KOR. [NMePhe¹,Trp³]arodyn, **2** (Fig. 1) was chosen as the parent compound for these studies.

Dyn A-(1-11)NH₂ Tyr-Gly-Gly-Phe-Leu-Arg-Arg-Ile-Arg-Pro-Lys-NH₂
Arodyn, 1 Ac-Phe-Phe-Phe-Arg-Leu-Arg-Arg-D-Ala-Arg-Pro-Lys-NH₂
2 and 3 X-NMePhe-Phe-Trp-Arg-Leu-Arg-Arg-D-Ala-Arg-Pro-Lys-NH₂

Fig. 1. Structures of Dyn A-(1-11)NH₂, arodyn (**1**), [NMePhe¹,Trp³]arodyn (**2**, X = Ac) and analog **3** (X = CH₃OCO-).

Results and Discussion

All peptides were synthesized on the PAL-PEG-PS resin (0.16 mmol/g) by solid-phase peptide synthesis using Fmoc-protected amino acids according to standard procedures. All crude peptides were analyzed by analytical HPLC and ESI-MS. The percent HPLC peak area for the crude peptides was used to estimate the recovery of the desired peptides (R_t = 24.9 min for **2**) vs the deletion product (R_t = 15 min). We hypothesized that deletion of the Ac-NMePhe moiety occurred during the cleavage of the peptide from the resin under acidic conditions (Scheme 1). The degradation of pure **2** under standard cleavage conditions was observed. Different cleavage conditions were evaluated to maximize the yield of pure **2** and minimize the side reaction; the highest yield was obtained with pure TFA (without scavengers) at 4°C for 3 hrs. The desAc [NMePhe¹,Trp³]arodyn analog does not undergo the deletion reaction, indicating the important role of the acetyl group in the deletion process. When the first amino acid residue is Phe instead of NMePhe, no deletion product was detected, suggesting that the N-methyl group in **2** changes the backbone conformation to one that favors the cyclization. Different N-terminal groups were



Scheme 1. Proposed mechanism for the deletion of Ac-NMePhe from **2** under acidic conditions.

examined for their ability to prevent this side reaction. Groups that are strongly electron withdrawing such as methyl carbamate (compound **3**) can decrease the electron density on the carbonyl and thus make the oxygen less nucleophilic, preventing the side reaction. However, hindered acyl groups examined could not prevent the side reaction.

Four functionalities were identified that when substituted for the N-terminal acetyl group resulted in stable peptides. These stable analogs were purified and examined for their affinity for KOR and MOR (mu opioid receptors). Results suggested that the methyl carbamate group (compound **3**) can be substituted for the acetyl group in [NMePhe¹,Trp³]arodyn (**2**) without loss of KOR affinity and with high KOR selectivity (Table 1). This strategy is being applied to the synthesis of other [NMePhe¹]arodyn analogs.

Table 1. Opioid receptor affinities of arodyn (**1**), **2** and **3**

Compound	K _i ± S.E.M. (nM)		K _i ratio (KOR/MOR)
	KOR	MOR	
Arodyn, 1	10.0 ± 3.0	1740 ± 130	1/174
2	13.0 ± 2.6	ND ^a	-
3	9.69 ± 1.82	1280 ± 280	1/132

^aND = not determined

In conclusion, a side reaction involving the deletion of an acetylated N-methyl amino acid from the N-terminus of a peptide has been observed and a mechanism involving the formation of a 5-membered heterocyclic ring has been proposed. Substitution of the N-terminal acetyl group with an electron-withdrawing group was found to prevent the side reaction. Pharmacological evaluation showed that a methyl carbamate group can be substituted for the acetyl group in a [NMePhe¹]arodyn analog without loss of KOR affinity or selectivity.

Acknowledgments

The authors thank Miranda Thomas (University of Georgia) for performing the pharmacological assays. This research was supported by NIDA grants R01 DA05195 and R01 DA18832.

References

1. Chavkin, C. and Goldstein, A. *Proc. Natl. Acad. Sci. USA* **78**, 6543-6547 (1981).
2. Bennett, M. A., Murray, T. F. and Aldrich, J. V. *J. Med. Chem.* **45**, 5617-5619 (2002).
3. Bennett, M. A., Murray, T. F. and Aldrich, J. V. *J. Peptide Res.* **65**, 322-332 (2005).

Synthesis and Biological Activities of Chimeric Bioactive Peptides Based on Amino Acids Coupled to 4-Anilino-*N*-Phenethyl- Piperidine

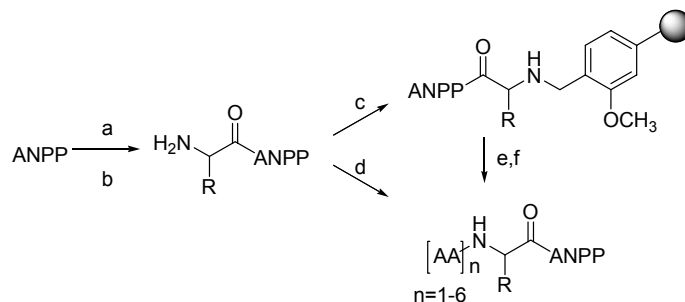
Ravil R. Petrov¹, Ruben S. Vardanyan¹, Shou-wu Ma², Peg Davis², Yeon
 S. Lee¹, Minying Cai¹, Frank Porreca², Josephine Y. Lai² and Victor J.
 Hruby¹

¹Department of Chemistry, University of Arizona; ²Department of Medical Pharmacology,
 University of Arizona, Tucson, AZ 85705, USA

Introduction

4-Anilidopiperidines represent the most powerful class of analgesics of the fentanyl family. These compounds are among the most potent drugs in modern medicine for relief of severe acute and chronic pain, but their use is highly limited due to serious side effects. In order to decrease the toxicity profile of this class of compounds we are replacing the propionyl moiety of fentanyl with nontoxic amino acids and peptide residues (Scheme 1). The key feature of our design is to utilize the concept of overlapping pharmacophores of i) nonpeptide and peptide opioid ligands, and ii) opioid and melanotropin ligands.

Although the synthesis and evaluation of 1- and 2-substituted fentanyl analogs go back to the early 1980 [1], these studies have been limited by the difficulty in preparing *N*-phenyl amino acid substituted analogs. We found that the desired compounds can be easily prepared by coupling of Fmoc [2] or phthaloyl [3] amino acid chlorides with 4-anilino-*N*-phenethyl-piperidine (ANPP).



Scheme 1. Reagents and conditions: (a) Fmoc amino acid chloride, 5% NaHCO₃, DCM or Pht (phthaloyl) amino acid chloride, DIPEA, DCM, 0°C; (b) 50% piperidine in DCM for Fmoc or ethanol amine in refluxing EtOH for Pht removal; (c) 4-(4-formyl-3-methoxyphenoxy)butyryl AM resin, NaBH(OAc)₃, DMF/DCM (1/3); (d) Boc-AA-OH, DCC, DIPEA, DCM or Boc-AA-OSu, DIPEA, DMF; (e) Fmoc-AA-OH, HOBt, HBTU, DIPEA in DMF; (f) TFA/*i*-PrSiH₃/H₂O (90/5/5).

Results and Discussion

X-ray diffraction data for PhtPheANPPHCl [5] demonstrated that attachment of a sterically demanding amino acid to 4-anilino-*N*-phenethyl-piperidine does not disturb the bioactive conformation characteristic of fentanyl. However, both phenylalanine and glycine derivatives had low affinity for both δ- and μ-opioid

Table 1. Functional analysis and affinity for opioid receptors

Drug	Competition		GTP Binding			
	<i>hDORNG108</i>	<i>rMORCHO</i>	<i>hDORNG108-10D</i>		<i>rMORCHO</i>	
	[³ H]DPDPE	[³ H]DAMGO	EC ₅₀ (nM)	E _{max} (%)	EC ₅₀ (nM)	E _{max} (%)
1. H-Tyr-D-Ala-Gly-Phe-Gly-Gly-ANPP	4.0±2.3	0.73±0.37	not determined		86	19
2. H-D-Phe-ANPP citrate	290±71	510	n.s. ^a		n.s. ^a	
3. H-Gly-ANPP	7700±3060	820±670	n.s. ^a		n.s. ^a	

^a Non-saturable at concentrations higher than 10⁻⁴nM.

receptors. This result can be explained according to the docking model proposed by Govindan S. *et al.* [4]: the propionyl moiety of fentanyl is located in a hydrophobic μ -receptor binding pocket which is unlikely to accommodate a positively charged nitrogen of an α -amino acid. Further attachment of an opioid peptide sequence, Tyr-D-Ala-Gly-Phe-Gly (entry 1), produced an analog with high δ - and μ -opioid receptor

Table 2. Functional analysis and affinity for melanocortin receptors

Drug	hMC1R		hMC3R		hMC4R		hMC5R	
	IC ₅₀ (nM)	B.E. ^a	IC ₅₀ (nM)	B.E. ^a	IC ₅₀ (nM)	B.E. ^a	IC ₅₀ (nM)	B.E. ^a
1. AcNle-His-D-Phe-Arg-Trp-OH	1800	100	860	100	>10 ⁴	/	N.B.	/
2. AcNle-His-D-Phe-Arg-Trp-Gly-Gly-ANPP	12	80	43	55	44	100	N.B.	/
MTII (control)	0.1	100	1.9	100	1.8	100	7	100

affinity but low potency in GPI (K_i=150±42nM), and MVD (K_i=360±170nM) bioassays. Attachment of the ANPP moiety to the melanotropin message sequence via a Gly-Gly tether produced an analog (entry 2, Table 2) with substantially increased binding affinity for all receptor subtypes except the hMC5R.

Acknowledgments

The work was supported by grants from USPHS and NIDA.

References

1. Essawi, M. Y. and Portoghese, P. S. *J. Med. Chem.* **26**, 348-352 (1983).
2. Oku, A., Yamaura, Y. and Harada, T. *J. Org. Chem.* **51**, 3732-3734 (1986).
3. Shouming, W., *et al.* *Bioorg. Med. Chem.* **12**, 2367-2370 (2002).
4. Govindan S., *et al.* *J. Med. Chem.* **43**, 381-391 (2000).
5. Petrov, R. R., Vartanyan, R. S., Carducci, M. D. and Hruby, V. J. *unpublished results* (2005).

Discovery of Potent mMC1R Agonists with Prolonged Activity at Human Melanocytes

Aleksandar Todorovic¹, Jerry R. Holder¹, Rayna M. Bauzo¹, Joseph W. Scott¹, Renny Kavanagh², Zalfa Abdel-Malek² and Carrie Haskell-Luevano¹

¹*Department of Medicinal Chemistry, University of Florida, Gainesville, FL 32610, USA;*

²*Department of Dermatology, University of Cincinnati, Cincinnati, OH 45267, USA*

Introduction

The melanocortin (MC) pathway consists of receptors, agonists, antagonists and putative ancillary proteins that regulate physiological roles linked with this system. Five isoforms of the melanocortin receptors have been identified to date, MC1R-MC5R. All naturally processed melanocortin agonists are derived by posttranslational modification of the pro-opiomelanocortin (POMC) prohormone and include α -melanocyte stimulating hormone (α -MSH), β -MSH, γ -MSH and adrenocorticotrophic hormone (ACTH). The MC system is also regulated by two naturally occurring antagonists, agouti (ASP/ASIP) and agouti related protein (AGRP). This is a unique physiological feature of MC pathway, because no other identified GPCR system is regulated by natural antagonists.

Positional scanning approach and truncations studies identified the tetrapeptide His-Phe-Arg-Trp as an important sequence in eliciting pharmacological response at the melanocortin receptors. Recently, we have performed extensive SAR studies at the N-terminus of His-DPhe-Arg-Trp-NH₂ tetrapeptide where we studied the importance of the capping group with regard to the MCR potency and/or selectivity [1]. It has been shown that the introduction of octanoyl residue at the N-terminus leads to the increase of potency at the MCR system. This study is undertaken to probe the importance of long-chain-fatty-acyl (LCFA) residues at the N-terminus of His-DPhe-Arg-Trp-NH₂ [2].

Results and Discussion

Peptides in this study were synthesized manually or on a semi automated synthesizer applying the Fmoc solid phase methodology. Peptides were cleaved in parallel, pelleted with cold anhydrous ethyl ether and purified using RP-HPLC chromatography (Shimadzu) on a C₁₈ bonded silica column. All peptides were more > 95% pure as estimated by HPLC in two diverse systems and 1D-NMR. Compounds were assayed at mouse MC1R, mMC3R-mMC5R (Table 1) and human melanocytes. Octanoyl derivative possessed increased potency at all MCR tested in this study. However, compounds with more than eleven C atoms in the LCFA region are equipotent to unacylated peptide **1** at the MC3R-MC5R. Every compound with eight or more carbon atoms in the acyl region is more potent at the mMC1R than the reference peptide **1**. This preference for the mMC1R has prompted us to investigate these analogs in the tyrosinase assay at human melanocytes. Tyrosinase is a key limiting step in the melanin synthesis. LCFA-tetrapeptides caused dose-dependant increase in tyrosinase activity. In addition, pentacanoyl derivative (**7**), possessed significant prolonged activity (residual tyrosinase activity after the ligand is removed from the assay media) that was superior to the NDP-MSH, which is characterized as a superpotent synthetic analog of α -MSH.

Table 1. Functional activity of LCFA-peptides at the mouse MCR

X-His-DPhe-Arg-Trp-NH ₂			mMC1R	mMC3R	mMC4R	mMC5R
PEPTIDE	(n ^a)		EC ₅₀ (nM)	EC ₅₀ (nM)	EC ₅₀ (nM)	EC ₅₀ (nM)
1. -NH ₂	(0)		67±15	250±57	18.5±5.35	2.78±0.34
2. -Octanoyl	(8)		0.33±0.07	9.29±0.84	2.52±0.35	0.57±0.22
3. -Decanoyl	(10)		3.34±0.88	44.8±10.2	14.4±2.38	4.83±0.54
4. -Undecanoyl	(11)		2.80±1.17	102±27	19.0±6.06	10.0±4.63
5. -Lauryl	(12)		3.07±1.12	167±58	23.4±4.18	6.30±2.09
6. -Myristoyl	(14)		0.58±0.17	220±80	10.5±4.67	3.39±0.85
7. -Pentadecanoyl	(15)		2.07±1.47	134±10	13.2±3.70	3.02±1.38
8. -Palmitoyl	(16)		0.99±0.59	154±31	26.6±2.61	2.99±1.05
9. -Stearyl	(18)		0.83±0.30	277±135	13.4±3.20	2.43±0.27

^an is the number of carbon atoms in the acyl region of the LCFA-His-DPhe-Arg-Trp-NH₂.

We have shown that LCFA modification of peptide **1** results in compounds with improved mMCR potency, selectivity and prolonged activity at human melanocytes.

Acknowledgments

The work was supported by NIH grants RO1-DK57080 (C.H.L.) and RO1-ES09110 (Z.A.M.). Aleksandar Todorovic is a recipient of an American Heart Association Predoctoral Fellowship.

References

1. Holder, J. R., *et al. Eur. J. Pharmacol.* **462**, 41-52 (2003).
2. Todorovic, A., *et al. J. Med. Chem.* **48** 3328-3336 (2005).

Peptide and Protein Design

β -Hairpin Minimization and Optimization

Niels H. Andersen, Katherine A. Olsen, R. Matthew Fesinmeyer and
 Lisa A. Eidenschink

Department of Chemistry, University of Washington, Seattle, WA 98195, USA

Introduction

Peptide models of β -sheet structures continue to be viewed as useful tools for understanding the factors that favor and accelerate hairpin formation and the possible nucleation of protein folding. We have extended our prior study of GB1 analogs [1], which afforded more stable species. This optimization utilized a stabilizing loop sequence (N/D-PATGK) bracketed by two Trp residues (Fig. 1). We now report that the W-loop-W motif (for 4-, 5- and 6-residue loops), first reported for Cochran's trpzip peptides (trpzip4 = GEWTWDDATKTWTWTE-NH₂, T_m = 70 °C) [2], can be used to generate stable folds for shorter peptides. We also have elucidated the specific features of the loop that promote chain direction reversal.

GB1	GEWTYDDATKTFTVTE	T _m = 6 °C
GB1m3	KKWTYNPATGKFTVQE	T _m = 61 °C
HP5W4	KKWTWNPATGKWTWQE	T _m = 85 °C
HP7	KTWNPATGKWTE	T _m = 67 °C
HP6V	KYVW-SNGK-WTVE	T _m = 58 °C
tr-HP6	AW-SNGK-WT	T _m = 25 °C

Fig. 1. Key sequences examined in this study and the melting temperatures (T_m's) observed.

Results and Discussion

Peptides were synthesized by standard fast Fmoc methods. The structures were confirmed by MS and 2D NMR studies; the latter also provided chemical-shift measures of structuring. The common feature in the CD spectra of trpzip4, HP5W4, HP7, and both the full-length and truncated versions of HP6 is an exciton couplet due to the interaction of the Trp side-chain aryl rings. The changes in the spectra of HP7 and tr-HP6 with temperature appear in Figure 2.

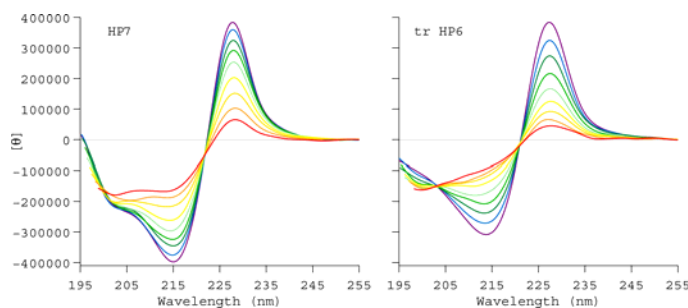
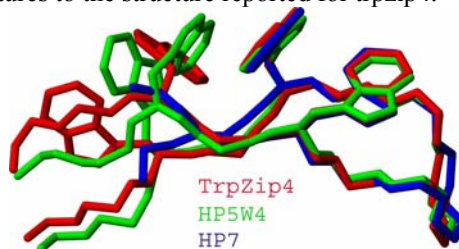


Fig. 2. Temperature dependence (5 – 85 °C) of the CD spectra of HP7 and tr-HP6.

The intensity of the CD maximum at 228 nm became one of the parameters that we employed to determine the T_m values for the listed peptides, single-site mutants, and truncated versions of these motifs.

Since peptides HP5W4 and HP7 were clearly well folded in water based on the CD melts, we used the NOEs observed to generate NMR structure ensembles. The restrained dynamics procedure employed only distances from NOE measurements; no dihedral or H-bond restraints were used. Nonetheless, the ensembles were well converged and in agreement (to within 0.59 Å backbone RMSD) over the common residues. Figure 3 compares these structures to the structure reported for trpzp4.

Fig. 3. A least squares overlay of representative structures from the NMR ensembles derived for trpzp4 (black), HP5W4, and HP7. The indole ring appearing nearest to the turn is Trp⁵ of trpzp4 and HP5W4, Trp³ of HP7.



The structural overlap within the W-loop-W motif was remarkable, showing the same edge-to-plane (“T”) W/W interaction geometry. This interaction explains both the CD exciton couplet and the extreme upfield ring-current shift (2.2 – 2.65 ppm) of Trp Hε3 at the turn’s N-terminus. The relative orientations of the more remote Trp rings of HP5W4 and trpzp4, however, differ significantly. The additional “T” interaction in trpzp4 is confirmed by the W14 Hε3 upfield shift (CSD = –2.4 ppm). This proton is only 0.86 ppm upfield of its random-coil value in HP5W4. For HP7, both NOEs and ring-current shifts establish the close proximity of the K1 and W10 side chains (a cation- π interaction). Mutational studies imply a 1.7 and 3.7 kJ/mol fold stabilization, respectively, for K1/W10 and R1/W10 interactions in the HP7 hairpin series. We posit that the corresponding interaction (K1/W14) in HP5W4, competing with W3/W14 alignment, is responsible for the aryl ring geometry differences between HP5W4 and trpzp4.

Based on these studies, we expected the W/W interaction in W-loop-W motifs to remain constant. Thus, stability changes associated with mutations should be available from melting curves based on both $[\theta]_{228}$ and the $\delta(\text{H}\epsilon 3)$. Representative melts are shown in Figure 4. Using the HP7 strands, we examined loop mutations and loop replacements. Through a series of mutants we found, and calibrated, a linear correlation of $\Delta\Delta G_F$ and ΔT_m . In most cases, ΔT_m can be readily measured and all of the $\Delta\Delta G_F$ -values (kJ/mol at 298K) quoted herein are based on this measure. The NPATGK loop ($T_m = 67^\circ\text{C}$) was replaced by two shorter loops: INGK ($T_m = 49^\circ\text{C}$, $\Delta\Delta G_F = 2.5$) and NPDGT ($\Delta\Delta G_F \geq 3.5$). All of the spectroscopic parameters associated with folding (including the diagnostic CSDs at all strand positions) were retained in the 4-residue loop analog. This was not the case with the 5-residue loop, which is favorable for [3:5]-hairpin formation [3]; although a modestly stable hairpin formed, the W/W interaction geometry is altered. In the six-residue loop series, N→D and P→A mutations had little effect ($\Delta\Delta G_F < 0.8$) on hairpin stability. Considerably more flexible loops also supported hairpin formation: NPATGK → NGGTGK, $T_m = 28^\circ\text{C}$, $\Delta\Delta G_F = 5.1$.

As these and related studies evolved, it became clear that the optimized 6-residue loop should be designated as N/D-XXTGX; the Pro unit does not enhance fold stability but is a useful addition since it prevents the formation of alternative turn types. The stability enhancements associated with each site were determined by single site mutations in an NPATGK context: T→A ($\Delta\Delta G_F = 1.0$), G→A ($\Delta\Delta G_F = 2.4$), and N→A ($\Delta\Delta G_F = 6.4$). The glycine preference can be attributed to the

positive ϕ/ψ values at this loop site. The very large effect of the Asx unit has been rationalized from the NMR structures: the side-chain function is involved in a dense web of H-bonds with other loop residues and one strand site.

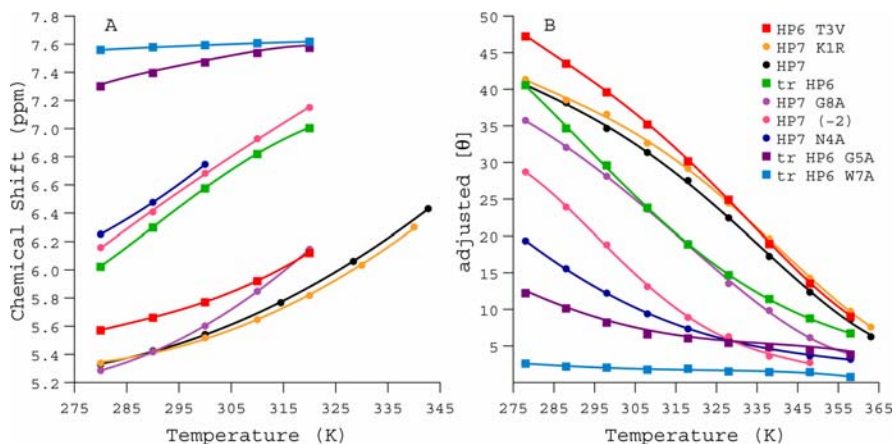


Fig. 4. **A**, $\delta(H\epsilon 3)$ versus T , and **B** amplitude of the 228 nm CD band (10^4 molar ellipticity, not residue-molar, units) for representative W-loop-W peptides and a control, (W7A)-tr-HP6.

We also determined the extent to which the termini of the hairpin could be truncated and still retain a stable fold. With HP7 each pairwise residue deletion resulted in some loss of stability, but Ac-WNPATGKW-NH₂ was still >65% folded at 7 °C. Likewise, the SNGK turn series could be truncated to AWSNGKWT (tr-HP6, shown in Fig. 4) and still retain both spectroscopic diagnostics of the stable W/W interaction (see Fig. 2 for the CD). This species also shows diagnostic backbone H α and H β CSDs in the turn. These (as well as the CD exciton couplet and ring-current effects) disappear upon a W7A mutation. Both (W7A)-tr-HP6 and Ac-NPATGK-NH₂ display less than 20% turn formation.

Conclusions

Peptide fold stability ($\Delta G_F^{290} < 0$) has now been achieved for 8 – 10 residue constructs. This stability is not due to extraordinary turn propensities; rather, specific chiral W/W interaction geometries in W-(X)_n-W loop motifs ($n = 4, 6$) are greatly preferred and provide *circa* 7 kJ/mol of fold stabilization. Turn propensity is still a factor even with this unusually favorable cross-strand hydrophobic cluster: in tr-HP6, a G→A mutation in the SNGK turn is destabilizing by 4.4 kJ/mol.

Acknowledgments

The work was funded by an NSF grant to N. H. Andersen.

References

1. Fesinmeyer, R. M., Hudson, F. M. and Andersen, N. H. *J. Am. Chem. Soc.* **126**, 7238-7243 (2004).
2. Cochran, A. G., Skelton, N. J. and Starovasnik, M. A. *Proc. Natl. Acad. Sci. USA* **98**, 5578-5583 (2001).
3. deAlba, E., Jimenez, M. A. and Rico, M. *J. Am. Chem. Soc.* **119**, 175-183 (1997).

Analog of Interleukin 8 Containing non Proteinogenic Segments Show High Biological Activity

Ralf David and Annette G. Beck-Sickinger

University of Leipzig; Institute of Biochemistry, Brüderstraße 34, 04317 Leipzig, Germany

Introduction

Human Interleukin 8 (hIL-8) [1] is a proinflammatory chemokine that acts predominantly at neutrophil granulocytes. Thus, it plays an important role in neutrophil driven diseases. Its action is mediated by two seven-transmembrane-helical receptors CXCR1 and CXCR2, which couple to an inhibitory G-protein. This leads to an inhibition of the adenylate-cyclase after activation and thus to a decrease of the cAMP-level in the cell.

The human IL-8 is mainly expressed by endothelial cells, macrophages and monocytes as a 72 amino acid form and as a 77 amino acid variant [2]. We are using the latter one in our studies. It contains four conserved cysteines that form two disulfide-bridges, which are necessary for structure and function. The first two cysteines are separated by another amino acid, and accordingly these chemokines, including hIL-8 belong to the so-called CXC-chemokine family. The N-terminal ELR-motive in this class is essential for receptor-binding and activation.

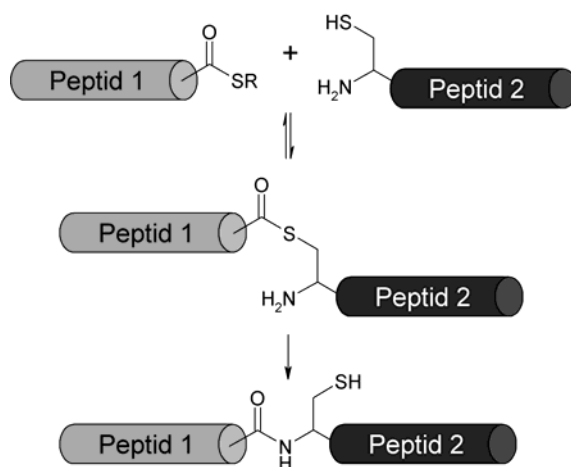


Fig. 1. Native Chemical Ligation: One peptide with an N-terminal cysteine reacts with another peptide bearing a C-terminal thioester. The first step is the nucleophilic attack of the cysteine thiol group at the C-terminal thioester followed by a trans-thioesterification. In the second step the thiol-function is replaced by the amino group of the N-terminal cysteine (S-N-acyl transfer) and a native peptide bond is formed between the two peptide fragments. Side chain protecting groups are not necessary.

To get a deeper insight into ligand-receptor interactions, the introduction of non canonical amino acids and biophysical probes like spin-labels or fluorescent dyes can be useful. Such modified peptide ligands can be easily made by solid phase peptide synthesis. Larger peptides beyond 60 amino acids can not easily be obtained in a one-step peptide synthesis, but the occurrence of cysteines in the sequence

enables the application of Native Chemical Ligation methodology (NCL, Fig. 1 [3]). An extension of this method is Expressed Protein Ligation (EPL [4,5]), in which one or both fragments are expressed in bacteria.

Results and Discussion

By using EPL methodology we have introduced different probes to the C-terminus of IL-8. The fourth cysteine in the 77 amino acid sequence (Cys 55) was chosen as ligation side. The segment 1-54 was expressed as a recombinant thioester by using the IMPACT-system (intein-mediated purification with an affinity chitin-binding tag). Expression in *E. coli* led to a fusion-protein with an MxeGyrA-intein and a C-terminal chitin-binding domain, which enables the purification at chitin-beads. The fusion-protein was expressed as insoluble inclusion body that required solubilization with 6 M urea. Prior to column-loading the solution was diluted to 1.5 M urea to enable chitin-binding. Thiol-induced cleavage led to the C-terminal thioester. The segment 55-77 was synthesized by solid phase peptide synthesis applying the Fmoc-strategy. By this method carboxy-fluoresceine (CF) was introduced at the side-chain of Lys 69. Ligation to IL-8 1-54-thioester led to a CF-labeled IL-8 variant, which was as active as the native IL-8 in the inhibition of forskolin-stimulated cAMP-production at HL60-cells (expressing both receptors CXCR1 and CXCR2). Furthermore, it was able to replace the native ligand from HL60 membranes containing both receptor subtypes [6]. Furthermore, we could use this ligand to study receptor-induced ligand-internalization (Fig. 2) and accumulation of the CF fluorescence in the cell. Thus, we could show that CF-labeled ligands could act as an indicator for receptor-mediated internalization and recycling pathways.

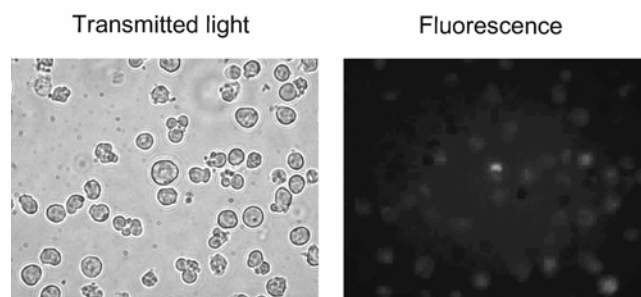


Fig. 2. Receptor-mediated ligand internalization. HL60 cells have been incubated with 20 nM CF-labeled IL-8 for 1 hr. Fluorescence was monitored with a fluorescence-microscope (excitation 470 nm, emission 525 nm).

Furthermore we introduced benzoyl-phenylalanine (Bpa) by expressed protein ligation instead of Glu 68 and Ala 74 (Fig. 3). Both variants showed biological activity at CXCR1- and CXCR2-expressing cells. Bpa can act as a photocrosslinker and crosslinking of both variants with the receptor-subtypes may give an insight in the orientation of the ligand during receptor binding. In addition, we replaced the C-terminal α -helix by a β -peptide using a similar expressed ligation methodology.

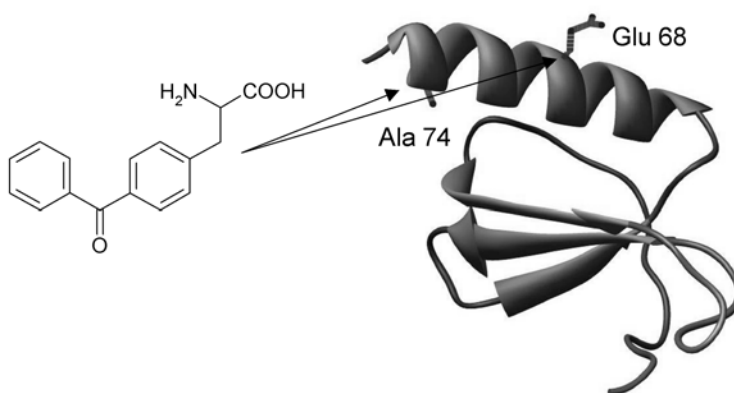


Fig. 3. Assembly of benzoyl-phenylalanine (left). Glu 68 and Ala 74 have been replaced by Bpa. Crosslinking of the receptor bound ligand may give insight into the orientation of the C-terminal helix in the receptor-ligand complex.

Acknowledgments

The work was funded by the German Research Foundation BE 1264-5/2.

References

1. Baggiolini, M., Dewald, B. and Moser, B. *Annu. Rev. Immunol.* **15**, 675-705 (1997).
2. Hebert, C. A., *et al. J. Immunol.* **145**, 3033-3040 (1990).
3. Dawson, P. E., Muir, T. W., Clark-Lewis, I. and Kent, S. B. *Science* **266**, 776-779 (1994).
4. Muir, T. W., Sondhi, D. and Cole, P. A. *Proc. Natl. Acad. Sci. USA* **95** 6705-6710 (1998).
5. David, R., Richter, M. P. O. and Beck-Sickinger, A. G. *Eur. J. Biochem.* **271** 663-677 (2004).
6. David, R., Machova, Z. and Beck-Sickinger, A. G. *Biol. Chem* **384** 1619-1630 (2003).

Optimization of the C-terminal Sequence in Glucagon to Maximize Receptor Affinity

Jay J. Levy, Vasily M. Gelfanov and Richard D. DiMarchi

Department of Chemistry, Indiana University, Bloomington, IN 47405, USA

Introduction

Glucagon is a linear peptide hormone of 29 amino acids of central importance in physiology. For more than half a century it has been used as a critical care medicine in the treatment of life-threatening insulin-induced hypoglycemia. The biophysical properties of natural sequence glucagon are not conducive to formulation in a patient-friendly formulation. The hormone is poorly soluble at physiologic pH and prone to physical aggregation to insoluble fibrils. Consequently, glucagon is commercially supplied as a lyophilized powder to be solubilized in dilute aqueous HCl immediately prior to administration. To a patient that is semi-conscious this represents an obstacle to proper administration and could constitute a fatal flaw.

We are exploring the structural modification of native glucagon with the intent of enhancing the physical properties, with minimal change to pharmacology. As a first step, we completed an alanine scan in the C-terminal region of the hormone (residues 20-28) to identify those residues that are central to biological function. Alanine scanning is a proven approach to initial segregation of those amino acids that contribute structurally to receptor signaling through peptide backbone conformational effect versus direct side chain interaction. In a similar study with the highly homologous peptide GLP-1 [1] it was demonstrated that *in vitro* bioactivity was extremely sensitive to substitution with alanine at the amino acids comparable to glucagon residues 22 and 23. Our study explores changes in potency at the glucagon receptor and specificity for *in vitro* action at the GLP-1 receptor.

Experimental Design

Each glucagon analog was synthesized on a solid support using Boc-based *in situ* neutralization chemistry as described by Kent, *et al.* [2]. Peptides were cleaved from the support using HF/p-cresol, 95:5, for 1 hr at 0°C. The peptides were solubilized in 10% HOAc and purified by RP-HPLC in 0.1% TFA with a linear gradient of CH₃CN. The identity and purity of each analog was confirmed by analytical HPLC and MALDI-MS analyses.

The ability of each analog to stimulate cAMP production was measured in a luciferase-based reporter assay. HEK293 cells co-transfected with either glucagon or GLP-1 receptor and luciferase gene linked to a cAMP responsive element were employed for bioassay. The cells were serum deprived by culturing 16 hrs in DMEM supplemented with 0.25% Bovine Growth Serum and then incubated with serial dilutions of either glucagon, GLP-1, or test analog for 5 hrs at 37°C. At the end of the incubation, 100 microliters of LucLite luminescence substrate reagent were added to each well for detection purposes. Effective 50% concentrations (EC₅₀) were calculated by using Origin software (OriginLab, Northampton, MA).

Results & Discussion

The synthesis and purification of the nine glucagon analogs was achieved with total yields in excess of 20%. None of the peptides proved any more problematic than

native glucagon in the physical handling and formulation for bioassay. The results of the bioassay at each of the receptors are shown in Table 1.

It is immediately obvious that glucagon has a number of amino acids in this C-terminal region of the peptide where the bioactivity at both receptors is extremely sensitive to substitution with alanine. As we anticipated from previously reported alanine scanning studies with GLP-1, residues 22 and 23 were extremely sensitive to alanine substitution [1]. Residues 25 and 26 were also significantly reduced in bioactivity with alanine substitution, but to a more modest degree. Most notably, the amino acids that border these four residues were relatively insensitive to substitution and support the belief that this region of glucagon is prone to alpha-helix formation [3]. The directional changes in bioactivity at the two receptors with each substitution studied were consistent and differed in magnitude only at positions 21 and 28 where in both instances the GLP-1 activity appeared to decrease to an appreciably larger extent.

Table 1. Bioactivity of glucagons alanine analogs

Peptide	Glucagon Receptor		GLP-1 Receptor	
	EC ₅₀ , nM	n	EC ₅₀ , nM	n
Glucagon	0.16±0.11	3	6.48±2.40	3
A-20	0.22±0.12	3	4.96±2.54	3
A-21	0.23±0.09	2	42.4±13.1	3
A-22	97.65±35.35	4	6150±294	3
A-23	18.96±10.49	4	534±9.97	3
A-24	0.09±0.03	2	10.8±5.92	3
A-25	2.22±1.07	3	134±70.2	3
A-26	6.44±0.19	2	312±119	3
A-27	0.66±0.19	2	72.0±37.6	3
A-28	0.21±0.04	2	31.6±10.0	3
GLP-1	2908.50±357.09	2	0.05±0.02	5

Comparing the helical nature of this region of glucagon with GLP-1, the change from glutamine at residues 20 and 24 to lysine and alanine, respectively, is notable. We believe that these two differences are the structural basis for the physical properties that render glucagon more prone to physical aggregation and formation of high molecular weight fibrils [4], since glutamine is much more supportive of secondary beta-structure than either alanine or lysine. These results in concert with prior glucagon structure-activity reports [5,6] form the basis for design of more potent and physically stable agonists.

References

1. Adelhorst, K., *et al. J. Biol. Chem.* 269, 6275-6278 (1993).

2. Schnolzer, M., Kent, S. B. H., *et al.* *Int. J. Peptide Prot. Res.* **40**, 180-193 (1992).
3. Ying, J., Hruby, V. J., *et al.* *Biochemistry* **42**, 2825-2835 (2003).
4. Onoue, S., *et al.* *Pharm. Res.* **21**, 1274-1283 (2004).
5. Hruby, V. J. and Ahn, J- M. *Curr. Med. Chem.–Imm., Endoc. Metab. Agents* **1**, 199-215 (2001).
6. Unson, C. G. and Merrifield, R. B. *Proc. Natl. Acad. Sci. USA* **91**, 454-458 (1994).

Design, Synthesis, and Evaluation of Piperazine-Based Small Molecule Peptide Mimetics Targeting the Melanocortin Receptors

**James P. Cain, Alexander V. Mayorov, Minying Cai, Yeon-Sun Lee,
Jinfa Ying, and Victor J. Hruby**

Department of Chemistry, University of Arizona, Tucson, AZ 85721, USA

Introduction

The functions of melanocortin receptors (MCRs) are critical to myriad biological activities, including pigmentation, steroidogenesis, energy homeostasis, erectile activity, glandular lipid secretion, and inflammatory response [1]. These G-Protein Coupled Receptors (GPCRs) have become a hot target for drug discovery, particularly in the area of obesity therapeutics [2]. In spite of the knowledge of endogenous agonists (α -, β -, and γ -MSH) and antagonists (agouti and agouti-related protein), relatively few potent and selective ligands for MCRs are available [3]. This problem is addressed with a pharmacophore-based rational design strategy, which compares designed small molecule structures to the NMR solution structure of the potent, nonselective agonist MT-II. Guided by these insights, a focused library of piperazine-based peptide mimetics has been synthesized. Analogs have been synthesized to examine the effect of variations in the stereochemistry, the distance between key pharmacophore elements, substituents on a crucial phenyl group, and lipophilic appendages to the core structure. Initial data from binding assays is presented.

Results and Discussion

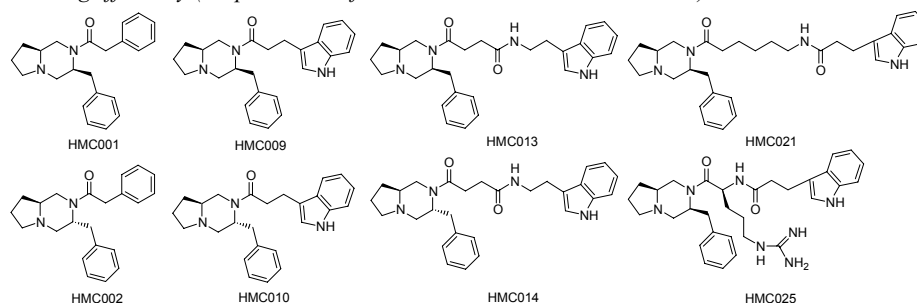
The synthesis of the core structure began with the coupling of D- or L-proline methyl ester and D- or L-Boc-phenylalanine using BOP/HOBt/DIEA. Deprotection with TFA was followed by cyclization under basic conditions. Reduction of the 2,5-diketopiperazine with LAH gave the bicyclic scaffold, which could then be functionalized in a number of ways. The simplest analogs, in which a phenyl group takes the place of indole, were produced by the direct reaction with phenylacetyl chloride in the presence of DIEA and a catalytic amount of DMAP. Only the catalytic base was necessary for the ring-opening reaction with succinic anhydride. Subsequent BOP-mediated coupling to tryptamine was performed in the same pot. This coupling protocol, used in the initial formation of dipeptide, seems to be a generally applicable method for amide bond formation between the piperazine and carboxylic acids as well. Indolepropionic acid, Boc-protected 6-aminohexanoic acid, and Boc-arginine coupled in high yield. Cleavage of the protecting group from the latter two products with TFA was followed by another coupling, with indolepropionic acid. The products were purified using RP-HPLC.

The preliminary biological data for these compounds is encouraging, as each structure tested thus far exhibits potent binding and most are selective for a particular MCR subtype (Table 1). **HMC001** is a potent MC1R-selective compound with greater than 150-fold selectivity over MC3R and no binding to MC4R or MC5R. There are also five compounds which may be some of the most potent and completely MC5R-selective ligands yet discovered. The fact that all compounds with linkers longer than three atoms are selective for the MC5R supports previous suggestions of a larger binding pocket for this subtype. A comparison of **HMC001**

Table 1. Binding of analogs at human melanocortin receptors

Ligand	hMC1R		hMC3R		hMC4R		hMC5R	
	IC ₅₀ (nM)	Eff. ^a	IC ₅₀ (nM)	Eff.	IC ₅₀ (nM)	Eff.	IC ₅₀ (nM)	Eff.
HMC001	2.2	80	347	70	NB	-	NB	-
HMC002	1.3	90	5	30	1.2	30	NB	-
HMC009	NB	-	NB	-	NB	-	0.8	50
HMC010	4.0	50	1.2	50	NB	-	NB	-
HMC013	NB	-	NB	-	NB	-	0.5	50
HMC014	NB	-	NB	-	NB	-	0.1	60
HMC021	NB	-	NB	-	NB	-	0.4	65
HMC025	NB	-	NB	-	NB	-	0.1	60

^aBinding efficiency (Displacement of ¹²⁵I-NDP- α -MSH relative to MT-II).



and **HMC002**, and particularly **HMC009** and **HMC010**, demonstrates that the stereochemistry of the phenylalanine-derived side chain can indeed be critical to activity, depending on the combination of ligand and receptor subtype. In the case of **HMC001** and **HMC002**, the binding to MC1R is quite similar, but the change in stereochemistry affects the affinity and efficiency of binding to MC3R, and the affinity for MC4R. **HMC009** only shows affinity for MC5R, while **HMC010** binds to MC1R and MC3R. The similarity of results between **HMC025** and compounds with linkers of similar length is consistent with previous findings that the presence of arginine is unnecessary for activity of small molecule ligands.

Further analogs incorporate substituents on the common phenyl group, starting for instance from *p*-chlorophenylalanine, or replace one or both hydrophobic groups with naphthalene. Other isosteric replacements are being explored. The appendage of a lipophilic side chain is easily accomplished using a hydroxyproline starting material. Each of these modifications may lead to improved selectivity or potency, or a change in the biological response to the ligand (i.e. conversion of an agonist to an antagonist). Ideally, systematic exploration will lead to full agonists, partial agonists, neutral antagonists, and inverse agonists selective for each receptor subtype.

Acknowledgments

Thanks to Dev Trivedi for assistance with data interpretation. This work was funded by the USPHS and NIDA.

References

1. Cone, R. D. *The Melanocortin Receptors*. New Jersey: The Humana Press, Inc. (2000).
2. Sebhat, I., *et al.* *Ann. Rep. Med. Chem.* **38**, 31-40 (2003).
3. Irani, B. G., *et al.* *Curr. Pharm. Des.* **10**, 3443-3479 (2004).
4. Ying, J., *et al.* *Biopolymers (Peptide Sci.)* **71**, 696-716 (2003).

Structure-Based Design and Structure-Activity Relationships of D-Phe-Pro-D-Arg-P1'-CONH₂ Tetrapeptides Inhibitors of Thrombin

Cristina C. Clement and Manfred Philipp

Chemistry Department, Lehman College & Biochemistry Ph.D. Program, Graduate Center, City
 University of New York, 250 Bedford Park BLVD, West Bronx, 10468, NY, USA

Introduction

Thrombosis is the most common singular cause of death in the developed countries. The American heart Association estimates that 54% of mortality in the US is due to cardiovascular diseases. An understanding of the biochemical and biophysical mechanisms of blood coagulation have helped in developing specific inhibitors of different enzymes involved in blood coagulation, especially thrombin, a serine protease involved in the conversion of soluble fibrinogen into soluble fibrin which is further cross-linked into fibrin fibers generating thrombus. Synthetic thrombin inhibitors are either irreversible, reversible covalent or reversible-non-covalent. They were mostly derived originally from the peptide chloromethyl ketone D-Phe-Pro-ArgCH₂Cl [1-2]. As a part of a research proposal aimed at studying structure activity relationship (SAR) of reversible non-covalent peptides inhibitors for thrombin, we performed structure-based design to obtain “*in silico*” libraries of compounds by docking peptides into active site of protein template 1ABJ.pdb. We selected the leads based on their predicted free energy of interaction with thrombin (below -50 kcal/mol). Two classes of sequences were used to generate new peptides candidate inhibitors: **1: D-Phe (P3)-Pro (P2)-Arg (P1)-D-Pro (P1')-P2'-CONH₂** and **2: D-Phe (P3)-Pro (P2)-D-Arg (P1) -P1'-CONH₂**. The use of D-Pro in the P1' position and the use of D-Arg instead of Arg in the P1 position were hypothesized to inhibit the hydrolysis of peptides, allowing these sequences to function as inhibitors for thrombin [3]. We varied the P1' position with D and L-amino acids and a SAR was performed using an *in vitro* assay for thrombin inhibition. Since the structural requirements for P1' had been determined through X-Ray using peptide inhibitors with L-Arg at P1 position [2] our original interest was to determine the amino acid specificity for the P1' position in the new designed sequence space: **2: D-Phe-Pro-D-**

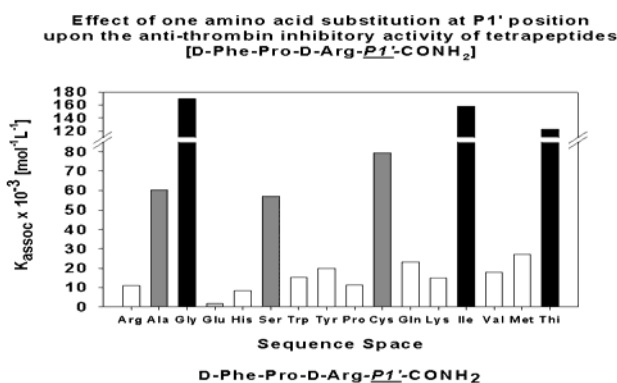


Fig. 1. SAR of D-Phe-Pro-D-Arg-P1'-CONH₂ tetrapeptides as determined from kinetics of *in vitro* thrombin inhibition.

Arg-P1'-CONH₂. This paper presents the first SAR results for the P1' position and show that structural requirements for P1' are close to those found for natural substrates of thrombin.

Results and Discussion

Fmoc chemistry was used for the synthesis of lead compounds screened "*in silico*" for their ability to interact with thrombin. Peptides were synthesized using the 432A Synergy Personal Peptide Synthesizer from Applied Biosystems or were manually synthesized as peptide libraries on Rink Amide resin using standard Fmoc chemistry. Kinetics experiments were performed in pseudo-first order conditions using S2238 (H-D-Phe-Pip-Arg-pNA). The absorption at 405 nm was monitored in real-time assuring that the hydrolysis of p-nitroanilide substrate was complete. Each kinetic trace was fitted to a first order reaction mathematical model ($A_t = A_0 \cdot e^{-kt}$ or $A_t = A_0 + a \cdot (1 - e^{-kt})$). The inhibitory constant (K_i) was determined from the equation $K_i = [I] / (k_{obs \text{ uninhibited}} / k_{obs \text{ inhibited}} - 1)$ ($[I]$ = the inhibitor concentration in μ M).

Figure 1 shows the SAR between amino acid sequences and inhibitory activity. This suggests that the amino acid at P1' in the sequences D-Phe-Pro-D-Arg-P1'- may induce significant changes in the conformation of the peptide inhibitor bound reversibly to the active site of thrombin, which can be responsible for the experimentally determined differences in their inhibitory activity [3]. Also, the significant differences between the K_i s of tetrapeptides from the series D-Phe-Pro-D-Arg-P1' (varying from 10 fold to 500 fold) suggest that the interaction between the amino acid at P1' position and the S1' pocket in thrombin is very specific. These results are partially consistent with the X-Ray data which where already shown that S1' pocket of thrombin is a small cavity lined by amino acids of the back side of the apolar S2 pocket (His57, Tyr60A & Trp60D) and the side chain of Lys60F. This S1' pocket can accommodate small polar or hydrophobic amino acid side chains as observed from P1' amino acids in a number of natural thrombin substrates (P1' in most physiological substrates is occupied by Gly, Ser, Thr, Ile, Leu & Val) [2]. In addition a new phenylalanine analog, L-thienylalanine (L-Thi) was discovered as being a promising new lead in this serie suggesting the presence of an independent small hydrophobic pocket adjacent to S1' as previously reported by others [2].

References

1. Sruvastava, S., Gosmani, L. N. and Dikshit, D. K. *Med. Res. Rev.* **25**, 66-92 (2005).
2. Qiu, X., Padmanabhan, K. P., Carperos, V. E., Tulinsky, A., Kline, T., Maraganore, J. M. and Fenton, J. W. II *Biochemistry* **31**, 11689-11697 (1992).
3. Clement, C. C. and Philipp, M. *Med. Chem. Poster presentation*, 228th National ACS Meeting, Philadelphia, August 22-26th (2004).

A Gibberellin Mimetic Peptide Recognized by an Anti-gibberellin Monoclonal Antibody

Hikaru Hemmi¹, Takashi Murata¹, Shugo Nakamura², Kentaro Shimizu², Yoshihito Suzuki³ and Isomaro Yamaguchi³

¹National Food Research Institute, Tsukuba, Ibaraki 305-8642, Japan; ²Department of Biotechnology; ³Department of Applied Biological Chemistry, Division of Agriculture and Agricultural Life Sciences, The University of Tokyo, Bunkyo-ku, Tokyo 113-8657, Japan

Introduction

Gibberellins (GAs) are a class of plant hormones and play important roles in various plant growth phenomena, including seed germination, stem elongation, and flower development. However, a receptor for GAs still remains unidentified. If a peptidyl mimotope of GA is available, it will provide useful probes for the study of GA receptor, because of easy modification such as biotinylation, photoaffinity labeling and radio isotope labeling. Two kind of homologous peptides, ACLPWS₄GPC (SD) and ACLPW₄GTGPC (GT), were recently screened as peptidyl mimotopes of GA₄ against monoclonal antibody (mAb) 4-B8(8)/E9 by phage display method [1]. Both peptides were cyclized by a disulfide cross-link between Cys² and Cys¹⁰. Unfortunately, synthetic peptides SD and GT showed neither promotive nor inhibitory effects on GA action in α -amylase induction in barley aleurone tissue or shoot elongation of dwarf rice seedlings [1]. In order to investigate the interaction between the GA mimetic peptide and the antibody, we first determined the solution structure of the peptide SD by two-dimensional (2D) NMR spectroscopy. The epitopes of the peptide to the antibody were assessed by saturation transfer difference (STD)-NMR experiments. Further, the computational docking simulation between the peptide and the antibody was performed to investigate the interaction between the peptide and the mAb.

Results and Discussion

Peptide SD was synthesized using Fmoc method and a disulfide bond between Cys² and Cys¹⁰ in the peptide was formed under an oxidized condition. The sequence-specific assignments of the proton resonance from the residue in the three conformers, one major conformer and two minor conformers, of peptide SD were performed using standard procedures from 2D ¹H-NMR spectra. The two minor conformers of peptide SD had concentrations too low to determine the solution structures by NMR. Three-dimensional structure of the major conformer of peptide SD was determined by 2D NMR spectroscopy and simulated annealing calculation. The results showed that the major conformer of peptide SD is comprised of a β -turn-like conformation (residues 3 – 5) (Fig. 1). It is well known that the β -turn motif has been observed in other antigenic peptides. Thus, we suggest that the β -turn like conformation of peptide SD is important for interacting with the antibody. Next, we performed STD-NMR experiments in order to analyze epitopes of peptide SD to the mAb 4-B8(8)/E9. The STD-NMR technique is a method of epitope mapping by NMR spectroscopy. The building block of the ligand having the strongest contact to the protein shows the most intense STD-NMR signals [2]. Strong STD enhancement of major conformer of peptide SD was observed only for residues, Leu³ – Trp⁵, constituting a β -turn-like structure, while C-terminal residues, Ser⁶ – Cys¹⁰, have

lower STD enhancement, suggesting that the region from Leu³ – Trp⁵ is important to interact with the surface of the mAb (Fig. 1). Finally, we performed the computational docking simulation between peptide SD and Fab fragment of mAb 4-B8(8)/E9. The structure of Fab fragment of mAb 4-B8(8)/E9 was obtained from the crystal structure of the complex of the Fab fragment and GA₄ determined in our previous work [3]. The best three complex structures showed that peptide SD interacted with the antigen binding site in mAb 4-B8(8)/E9. Residues of Pro⁴ and Trp⁵ of peptide SD showed hydrophobic interaction with mAb 4-B8(8)/E9 in the model structures. Further, we analyzed the interaction between peptide SD and mAb 4-B8(8)/E9 in detail. The result indicated that two hydrogen bonds exist between the antibody and the peptide. Comparison between the model structures obtained in this study with the crystal structure of mAb 4-B8(8)/E9 with GA₄ suggested that peptide SD in the model structures interacts with very important residues of the mAb for antigen recognition in the same manner as the interaction between the mAb and GA₄. Thus, we propose that peptide SD – mAb 4-B8(8)/E9 interaction is very similar to GA₄ – mAb 4-B8(8)/E9 interaction. Based on our present results, it may be possible to re-design better peptidyl mimics that can be bound to the mAb with higher affinity while holding the above important interactions by structure modeling and docking simulation.

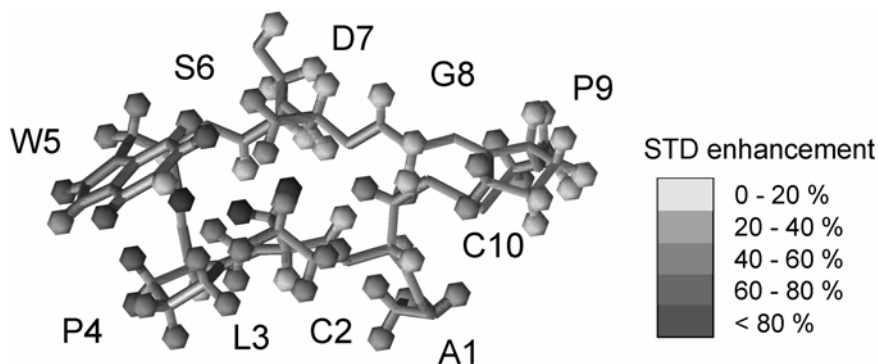


Fig. 1. The lowest energy structure of major conformer of peptide SD among all the calculated structures with STD enhancements of protons. This figure was generated by MOLMOL [4].

References

1. Sekimoto, H., Suzuki, Y. and Yamaguchi, I. *Biosci. Biotechnol. Biochem.* **68**, 2408-2410 (2004).
2. Mayer, M. and Meyer, M. *J. Am. Chem. Soc.* **123**, 6108-6117 (2001).
3. Murata, T., et al. *Biochem. Biophys. Res. Commun.* **293**, 489-496 (2002).
4. Koradi, R., Billeter, M. and Wüthrich, K. *J. Mol. Graph.* **14**, 51-55 (1996).

Synthesis of the Spin-labelled β -Amino Acids *cis*- and *trans*- β -TOAC, and a Preliminary Conformational Study of *trans*- β -TOAC/*trans*-ACHC Peptides

Karen Wright¹, Matthieu Sarciaux¹, Michel Wakselman¹, Jean-Paul Mazaleyra¹, Marco Crisma², Fernando Formaggio², Cristina Peggion², Antonio Toffoletti², Carlo Corvaja² and Claudio Toniolo²

¹SIRCOB, UMR CNRS 8086, Bât. Lavoisier, University of Versailles, F-78035 Versailles, France; ²Institute of Biomolecular Chemistry, CNR, Department of Chemistry, University of Padova, I-35131 Padova, Italy

Introduction

The nitroxide-bearing, achiral, cyclic, C ^{α} -tetrasubstituted α -amino acid residue TOAC has been widely used to label conformationally restricted α -peptides at *N*-terminal and/or internal positions for biological studies or 3D-structural investigations involving intramolecular spin-spin interactions (ESR) [1]. We have been interested in the spin-labelled, chiral, cyclic β -amino acids *cis*- β -TOAC [2] and *trans*- β -TOAC, that could be used for the structural investigation of helical β -peptides [3]. Herein, we report the synthesis of the *cis*-/*trans*- β -TOAC amino acids in an enantiomerically pure form, as well as the synthesis and a preliminary conformational study of terminally protected *trans*- β -TOAC/*trans*-ACHC (2-aminocyclohexane carboxylic acid) peptides.

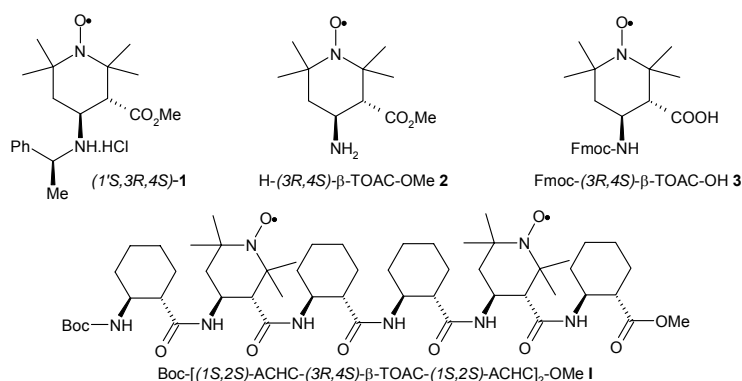


Fig. 1. Chemical structures of the *trans*- β -TOAC derivatives **1-3** and the hexapeptide Boc-[*(1S,2S)*-ACHC-(3*R*,4*S*)- β -TOAC-(*1S,2S*)-ACHC]₂-OMe **I**.

Results and Discussion

The synthesis of *cis*- and *trans*- β -TOAC was performed by condensation of 3-carboxymethyl-1-oxyl-2,2,6,6-tetramethyl-4-piperidone with either (*R*)- or (*S*)- α -methyl-benzylamine, followed by reduction of the corresponding enamines. While the use of NaBH₃CN/CH₃COOH gave predominantly a mixture of the two possible *cis*-**1** diastereomers [2], changing the reducing agent to NaBH₄/(CH₃)₂CHCOOH surprisingly resulted in a mixture of only one *cis*-**1** and only one *trans*-**1** diastereomer [represented in Fig. 1 is only the *trans*-(1*S*,3*R*,4*S*)-**1** isomer] in varying

proportions. Removal of the chiral auxiliary from the separated diastereomers **1** by hydrogenolysis (H_2 ; Pd/C; EtOH), and regeneration of the nitroxide radical [$\text{Cu}(\text{OAc})_2$; MeOH; air] gave the expected β -amino esters **2** [*trans*-(3*R*,4*S*)-**2** enantiomer in Fig. 1]. Saponification of the methyl ester (1N NaOH; MeOH) and protection of the amino function with the Fmoc-group (Fmoc-OSu; NaHCO_3) gave derivatives **3** [*trans*-(3*R*,4*S*)-**3** enantiomer in Fig. 1]. The Boc-/OMe *trans*-(3*R*,4*S*)- β -TOAC/*trans*-(1*S*,2*S*)-ACHC terminally protected peptides to the hexamer level (**I**) were synthesized in solution *via* the EDC/HOAt C-activation procedure.

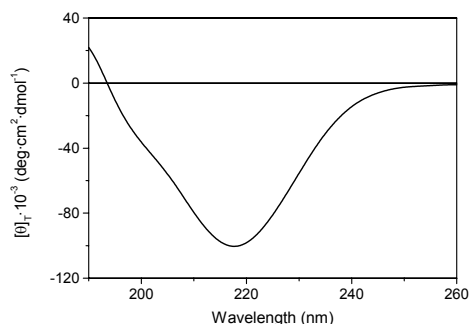


Fig. 2. Far-UV CD spectrum of the hexapeptide (**I**) in MeOH solution.

FT-IR absorption analysis in CDCl_3 solution showed intense N-H stretching bands typical of intramolecularly H-bonded -CONH- groups of helical peptides ($< 3400 \text{ cm}^{-1}$) which were first seen at the level of the terminally protected tetramer Boc-(1*S*,2*S*)-ACHC-(3*R*,4*S*)- β -TOAC-[(1*S*,2*S*)-ACHC]₂-OMe. The far-UV CD spectrum of the longest, terminally protected *trans*- β -TOAC/*trans*-ACHC peptide **I** in MeOH solution (Fig. 2) closely resembles that of the 3_{14} -helical homo- β -peptide based on (*S,S*)-*trans*-ACHC [4]. The ESR spectrum of the terminally protected dipeptide Boc-*trans*-(1*S*,2*S*)-ACHC-*trans*-(3*R*,4*S*)- β -TOAC-OMe in MeOH solution is that expected for a mono-labelled nitroxide-containing molecule, showing that the radical character of β -TOAC survived peptide synthesis and purification. A preliminary study indicated that an intramolecular spin...spin interaction between the nitroxide labels of the two (3*R*,4*S*)- β -TOAC residues at the *i* and *i*+3 relative positions of hexapeptide **I** does indeed take place. Details of the preferred conformation of this oligopeptide are under active investigation using this latter technique.

References

- Schreier, S., Barbosa, S. R., Casallanovo, F., de F. F. Vieira, R., Cilli, E. M., Paiva, A. C. M. and Nakaie, C. R. *Biopolymers* **74**, 389-402 (2004); Hanson, P., Millhauser, G., Formaggio, F., Crisma, M. and Toniolo, C. *J. Am. Chem. Soc.* **118**, 7618-7625 (1996).
- Wright, K., Crisma, M., Toniolo, C., Török, R., Péter, A., Wakselman, M. and Mazaleyrat, J. -P. *Tetrahedron Lett.* **44**, 3381-3384 (2003); Péter, A., Török, R., Wright, K., Wakselman, M. and Mazaleyrat, J. -P. *J. Chromatogr. A* **1021**, 1-10 (2003).
- Gellman, S. H. *Acc. Chem. Res.* **31**, 173-180 (1998); Seebach, D., Beck, A. K. and Bierbaum, B. J. *Chem. Biodiv.* **1**, 1111-1239 (2004).
- Appella, D. H., Christianson, L. A., Karle, I. L., Powell, D. R. and Gellman, S. H. *J. Am. Chem. Soc.* **121**, 6206-6212 (1999).

High Affinity Grb2 SH2 Domain-Binding Macrocycles Derived from Ring-Closing Metathesis of Alkenylglycine Residues with β -Vinyl Phosphotyrosyl Mimetics

Fa Liu¹, Shinya Oishi¹, Rajeshri Karki¹, Zhen-Dan Shi¹, Karen M. Worthy², Lakshman K. Bindu², Melissa Maderia¹, Marc Nicklaus¹, Joseph J. Barchi, Jr.¹, Robert J. Fisher² and Terrence R. Burke, Jr.¹

¹Laboratory of Medicinal Chemistry, CCR, NCI, NIH, Frederick, MD 21702, USA; ²Protein Chemistry Laboratory, SAIC-Frederick, Frederick, MD 21702, USA

Introduction

Growth factor receptor-bound 2 (Grb2) proteins are non-catalytic docking modules containing one SH2 domain and two SH3 domains that are involved with a variety of growth factor signaling pathways [1]. Binding antagonists of Grb2 SH2 and SH3 domains are being developed by several groups as potential antiproliferative agents. Peptide **1** (Fig. 1) represents a general signaling inhibitor directed against the Grb2 SH2 domain, whose structure is based on preferential binding of 'pTyr-Xxx-Asn-Yyy' sequences, wherein critical recognition features are provided by the pTyr phenylphosphate group and the Asn side chains. Because binding of peptide ligands to Grb2 SH2 domains occurs in β -bend conformations [2], macrocyclic congeners of open-chain peptides have been examined, including those such as **3a** that are derived by ring-closing metathesis (RCM) reactions involving allylglycine and substituted allylglycine residues in precursors such as **2a** [3]. The focus of the current work was to examine effects on binding potency resulting from alteration of the ring-closing alkenyl bridge.

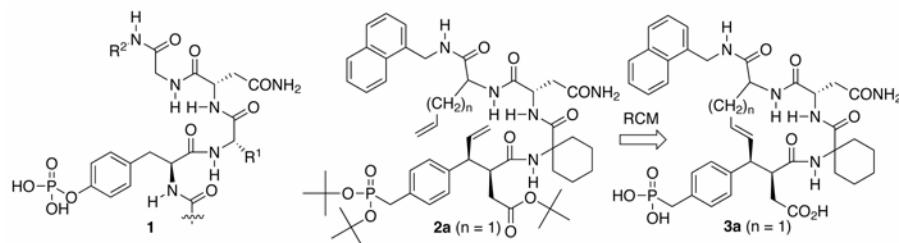


Fig. 1. Structures of analogs discussed in the text.

Results and Discussion

Fully protected open-chain RCM precursors **2** were prepared starting from an acid

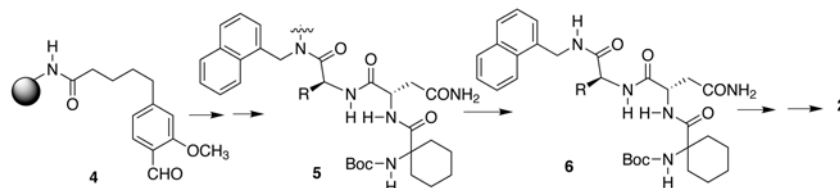


Fig. 2. Synthesis of fully protected open-chain precursors **2**.

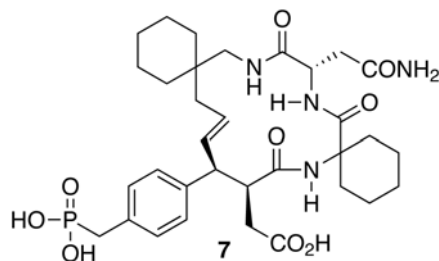


Fig. 3. Structure of macrocycle 7.

labile aldehyde resin **4**, through alkenylglycine derivative **5** (Fig. 2).

In addition to the alkenylglycine-derived analogs **3a** ($n = 1$) and **3b** ($n = 2$) (Fig. 1), compound **7** was also prepared as an example of a macrocycle that lacked chirality in the upper ring-forming segment. Grb2 SH2 domain-binding affinities were determined by surface plasmon resonance (SPR) (Table 1). For **3a**, stereochemistry at the alkenylglycine center had little effect on binding affinity. Complex kinetics were observed for **3b** and **7**, which could be fit to two component steady state systems exhibiting both low and high affinity binding constants in both cases [4]. The physical interpretation of this complex binding is unclear. Work is in progress to more fully explore structural aspects of this family of Grb2 SH2 domain-binding macrocycles.

Table 1. SPR data of the ligands binding to Grb2 SH2 domain

Affinity ^a	Compound 3a ^b	Compound 3a ^c	Compound 3b ^d	Compound 7 ^d
K _D (nM)	23	55	K _{D1} 10; K _{D2} 600	K _{D1} 9; K _{D2} 21,000

^aSteady state K_D values as determined in reference 4. ^b(S)-Configuration at the allylglycyl center. ^c(R)-Configuration at the allylglycyl center. ^dComplex binding kinetics as described in reference 4.

Acknowledgments

Appreciation is expressed to Drs. Christopher Lai and James Kelley of the LMC for mass spectral analysis.

References

- Lowenstein, E. J., Daly, R. J., Batzer, A. G., Li, W., Margolis, B., Lammer, R., Ullrich, A., Skolnik, E. Y., Barsagi, D. and Schlessinger, J. *Cell* **70**, 431-442 (1992).
- Rahuel, J., Gay, B., Erdmann, D., Strauss, A., Garcia-Echeverria, C., Furet, P., Caravatti, G., Fretz, H., Schoepfer, J. and Gruetter, M. G. *Nature Struct. Biol.* **3**, 586-589 (1996).
- Oishi, S., Shi, Z. -D., Worthy, K. M., Bindu, L. K., Fisher, R. J. and Burke, T. R., Jr. *ChemBioChem* **6**, 1-7 (2005).
- Oishi, S., Karki, R. G., Kang, S. -U., Wang, X., Worthy, K. M., Bindu, L. K., Nicklaus, M. C., Fisher, R. J. and Burke, T. R., Jr. *J. Med. Chem.* **48**, 764-772 (2005).

Towards Photo-Controlled Collagens

Ulrike Kusebauch, Sergio A. Cadamuro, Luis Moroder and Christian Renner

Department of Bioorganic Chemistry, Max-Planck-Institute of Biochemistry, 82152 Martinsried, Germany

Introduction

Collagen is the most abundant protein in mammals. In contrast to most other globular proteins collagens are not built from more or less independent structural motifs assembled in a variety of structural scaffolds for correct display of functional groups. Rather they consist of three polypeptide strands arranged in a triple helical super coil of variable stability (Fig. 1). The local stability and recognition sites for interaction with other proteins of the extracellular matrix are defined and highly fine-tuned by the amino acids in the X- and Y-positions of the repeating Gly-Xaa-Yaa triplets. The Gly-Pro-Hyp sequence is the most favorable tripeptide unit for stabilizing the triple helix motif. Despite the repetitive and regular primary, secondary, tertiary, and even quaternary structure of collagen, the rules for tuning the local conformation and plasticity are still not well understood due to a complex interplay of various contributions. As strands with different amino acid sequences can assemble to the super coil further complexities arise, our aim is to design and characterize well-defined model peptides that can increase our understanding of folding and stability of the collagen triple helix.

In a similar approach to our previous work where photomodulation of conformation, redox potential, binding properties and, most recently, of tertiary structure was achieved for peptide model systems [1], we try to combine azobenzene-containing chromophores with triple helical collagen peptides. The favorable optical properties of azobenzene together with the regular supramolecular structure of the collagen triple helix should result in valuable models for time-resolved studies on collagen folding and unfolding. Molecular modeling experiments suggest that crosslinking of two side chains in appropriate sequence positions via the chromophore should result in triple-helical peptides where the stability of the supra structure can be modulated by isomerization of the azobenzene moieties. At a suitable temperature folding and unfolding can, thus, be initiated by irradiation with light of the appropriate wavelength.

Results and Discussion

The structural properties of the designed peptide sequences are of equal importance as the chemical nature of the light switch. Analogously to the photo-switchable helical peptides of Woolley and coworkers [2] we introduced two cysteine residues into a regular (Gly-Pro-Hyp)_n sequence for crosslinking by the chromophore via a bis-iodide derivative.



Fig. 1. Schematic representation of the collagen triple helix consisting of three strands.

As a starting point we used the minimal number of five regular (Gly-Pro-Hyp)-repeats that by them can form a triple helix. N-terminal to the (Gly-Pro-Hyp)₅, three further triplets were positioned with the first and the third containing a cysteine in X- and Y-position, respectively. Stepwise elongation at the N-terminus leads to collagen peptides of increasing thermal stability suggesting that also the cysteine-containing triplets participate in the triple-helix formation.

In host-guest studies [3] of Ac-(Gly-Pro-Hyp)₃-(Gly-Xaa-Yaa)-(Gly-Pro-Hyp)₄-Gly-Gly-NH₂ the destabilizing effect of cysteine was found to be 11.2 °C for the Xaa position and 9.6 °C for the Yaa position. It would therefore be expected that in a Ac-(Gly-Pro-Hyp)₈-Gly-NH₂ collagen peptide ($T_m = 47.3$ °C in PBS [3]) placement of one cysteine in a Xaa position and a second one in a (distant) Yaa position would yield triple-helical peptides with a melting point of 47.3 °C $- 11.2$ °C $- 9.6$ °C = 26.5 °C. Experimentally, we found a markedly higher value of 37.8 °C in water at 1 mM peptide concentration. CD spectra and melting curves as well as NMR spectra, temperature shifts and translational diffusion measurements proved the presence of the triple-helix (Table 1). Upon deprotection of the cysteines the thiol groups were successfully cross-linked using our novel photo-switch 4,4'-azobenzene-dicarboxylic acid-(4-iodo-but-2-ynyl)-bis-amide (ACAB) albeit with poor yields (despite optimization of the reaction conditions). The attachment of the photo-switch did not qualitatively change the CD spectra or the CD melting curve of the first azo-collagen peptide and CD characteristics were indicative of a triple-helix of even slightly enhanced thermal stability (Table 1). However, NMR revealed that even at 4 °C no triple-helix is formed at all. The resulting question whether circular dichroism is a sufficiently reliable tool for identifying triple-helix formation is quite severe since almost all studies on thermal stability of collagens are based on measurements of the circular dichroism (or optical rotation in early studies) in the UV range (200-250 nm) and not in all of the published studies other techniques, such as ultracentrifugation or NMR spectroscopy, were used to verify the CD results.

Studies on azo-collagen peptides with increased numbers of stabilizing (Gly-Pro-Hyp)-triplets are in progress.

Table 1. CD parameters and NMR results for the collagen peptides

collagen peptide	λ_{\min}	θ_R^{\min}	λ_{\max}	θ_R^{\max}	Rpn	T_m (225nm)	NMR-results	
							Diffusion	triple helix
no azo	197.3	-35101	224.3	5044	0.144	37.8 °C	trimeric	yes
with azo	197.5	-23325	224.5	3050	0.130	39.5 °C	monomeric	no

Acknowledgments

The work was funded by the Deutsche Forschungsgemeinschaft (SFB 533, grant A8).

References

1. Renner, C., Kusebauch, U., Löweneck, M., Milbradt, A. G. and Moroder, L., *J. Peptide Res.* **65**, 4-14 (2005).
2. Kumita, J. R., Smart, O. S. and Woolley, G. A., *Proc. Natl. Acad. Sci. USA* **97**, 3803-3808 (2000).
3. Persikov, A. V., Ramshaw, J. A. M., Kirkpatrick, A. and Brodsky, B. *Biochemistry* **39**, 14960-14967 (2000).

Template-Assembled Peptide Models of the N-Peptide Helix Bundle from HIV-1 gp41

Weiming Xu and John W. Taylor

Department of Chemistry, Rutgers University, Piscataway, NJ 08854, USA

Introduction

Infection of target cells by HIV-1 is initiated by fusion of the viral and cell membranes, leading to release of viral genetic materials into the cell. The envelope glycoprotein, gp41, whose core structure in its post-fusion state comprises a helical trimer of N-peptides with three copies of helical C-peptide folded onto it [1], is directly responsible for the fusion process. Peptides or synthetic molecules that interfere with the folding of gp41 into its six-helix bundle state by binding to exposed regions of either the N- or C-terminal helices may either block or prematurely trigger folding of this structure, either of which would lead to the inhibition of fusion.

Template-assembly approaches have been applied extensively to the construction of peptide-model systems with helix-bundle structures [2-4]. The use of a template converts an intermolecular assembly into an intramolecular one and therefore reduces the entropy loss involved in the formation of a helical aggregate or bundle.

We would like to use template-assembled N-helix bundles to investigate the energetics of the gp41 core structure, either in terms of its component parts, or as a whole structure. In our approach, two three-fold symmetric molecules derived from M. Goodman's templates were designed and synthesized [5], and then three copies of peptide N29 (gp41 553-581) with an N-terminal Cys were connected to each template, giving the N-peptide three-helix bundle structures (Fig. 1).

Results and Discussion

TREN-Br and **KTA-Br** templates were synthesized from **TREN** and **KTA**, with overall yields of 63% and 58%, respectively. These templates were then coupled to the Cys thiol of the synthetic peptide Ac-Cys-[gp41 (553-581)]-amide in DMF/H₂O, pH 8.0, to produce **TREN-N29** and **KTA-N29**, respectively, with about 20% yield.

CD studies were then performed to evaluate the properties of each structure. At pH 2.5, both model structures were much more helical than the single peptide chain, based on fitting spectra to standard secondary structure data sets (Table 1 and Fig. 2a.).

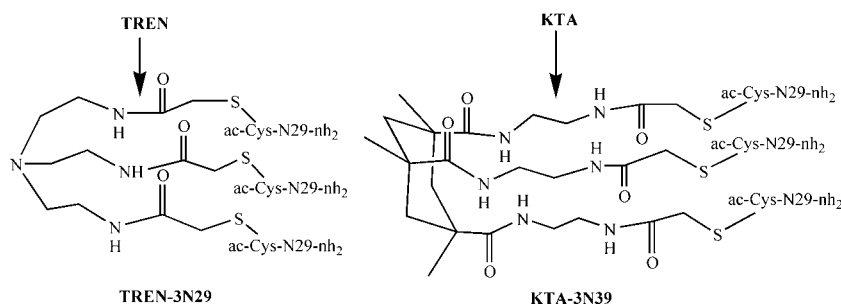


Fig. 1. Synthesis of N-peptide three-helix bundle structures, TREN-3N29 and KTA-3N29.

Table 1. CD analysis of Cys-N29 (blocked at thiol) and helix bundle structures

	Curve fitting of 20°C spectra			Curve fitting for melting curves ^a		
	% helix	% beta	% random	ΔH (kcal.mol ⁻¹)	ΔS (cal.mol ⁻¹ K ⁻¹)	t_m (°C)
Cys-N29	41	0	59			
TREN-3N29	90	0	10	-31	-88	83
KTA-3N29	93	0	7	-27	-78	78

^a Thermodynamic properties refer to the folding process.

Curve fitting analysis of the melting curves showed that: (a) At pH 2.5, both helix bundle structures underwent reversible thermal denaturation with high t_m values, near 80°C (Table 1 and Fig. 2b). The folding-unfolding processes fit a two-state model, although additional minor conformational changes may also occur at low temperature. (b) Folding of both structures was strongly enthalpy-driven. The **KTA-Br** template was better at minimizing entropy losses upon folding since it is preorganized; the **TREN-Br** template was better at maximizing the enthalpy changes upon folding, because of its flexibility. (c) t_m values of both structures varied very little over a 10-fold concentration range (Table 2), showing that most or all of the molecules were in the monomeric state at pH 2.5.

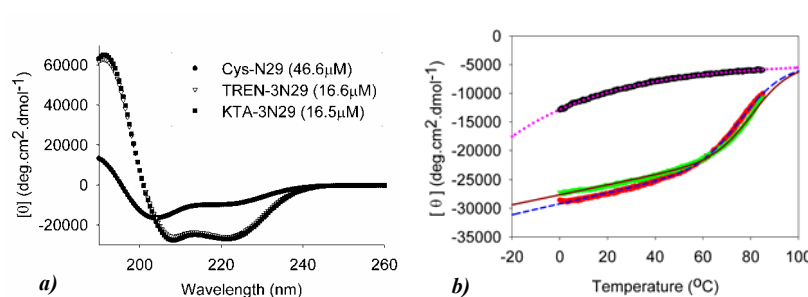


Fig. 2. CD analysis of model structures. **a)** Spectra at 20°C; **b)** Melting curves. Dotted, 46.6 μM Cys-N29 (blocked at thiol); Dash, 15.6 μM KTA-3N29; Solid, 16.3 μM TREN-3N29.

Table 2. T_m (°C) values from curve fitting of melting curves at different concentrations

Concentration (μM)	40.4	16.5	6.1	Concentration (μM)	40.8	16.3	7.0
t_m (KTA-3N29)(°C)	78	77	76	t_m (TREN-3N29)(°C)	82	82	81

Acknowledgments

This research was supported by a grant from the Charles and Johanna Bush Memorial Fund.

References

1. Chan, D. C., Fass, D., Berger, J. M. and Kim, P. S. *Cell* **89**, 263-273 (1997).
2. Eckert, D. M. and Kim, P. S. *Proc. Natl. Acad. Sci. USA* **98**, 11187-11192 (2001).
3. Louis, J. M., et al. *J. Biol. Chem.* **278**, 20278-20285 (2003).
4. Gochin, M., Kiplin Guy, R. and Case, M. A. *Angew. Chem. Int. Ed* **42**, 5325-5328 (2003).
5. Kwak, J., et al. *J. Am. Chem. Soc.* **124**, 14085-14091 (2002).

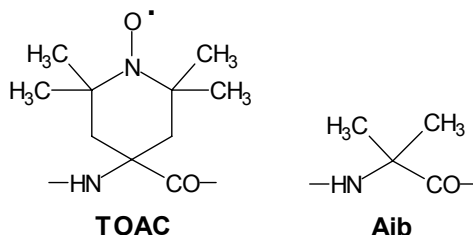
Alignment of Three Nitroxide Radicals on the Same Face of a Helical Peptide Scaffold

Marco Crisma¹, Simona Oancea¹, Fernando Formaggio^{1,2}, Elena Sartori²,
Carlo Corvaja² and Claudio Toniolo^{1,2}

¹Institute of Biomolecular Chemistry, CNR, 35131 Padova, Italy; ²Department of Chemistry,
University of Padova, 35131 Padova, Italy

Introduction

A few investigations have been performed dealing with stable *trinitroxide* radicals, examined by EPR, to obtain information on the dependence of the electron spin-spin exchange interaction between unpaired electrons on 3D-structural parameters, temperature, and solvent polarity. These studies are a prerequisite for our understanding of the molecular magnetic phenomena and the structure and dynamics of biological systems in which poly-radicals are introduced as spin probes.



Results and Discussion

In this Communication we present our data on a trinitroxide system in a *linear* configuration built on a 3_{10} -helical peptide template. To this end, we synthesized by solution-phase methods the terminally protected octapeptide Fmoc-TOAC-(Aib)₂-TOAC-(Aib)₂-TOAC-Aib-OMe, entirely based on C ^{α} -tetrasubstituted α -amino acids, with the three nitroxyl-bearing residues at positions 1, 4, and 7. This peptide is folded in a 3_{10} -helical structure in CDCl₃ and in the crystal state, as assessed by our IR absorption and X-ray diffraction analyses, respectively.

The three TOAC residues are aligned on the same face of the ternary helix (Fig. 1). The distances between the midpoints of the N-O bonds are: TOAC(1)⋯TOAC(4) 6.128(12) Å, TOAC(4)⋯TOAC(7) 6.796(13) Å, and TOAC(1)⋯TOAC(7) 12.645(13) Å, and the angles between the N-O bonds are: TOAC(1)⋯TOAC(4) 32.3(6)°, TOAC(4)⋯TOAC(7) 19.7(7)° and TOAC(1)⋯TOAC(7) 27.6(7)°. The piperidine ring system of all three TOAC residues adopts a conformation close to the ⁶T₂ (*twist*) disposition. In the packing mode of the octapeptide in the crystal no direct peptide⋯peptide intramolecular H-bond is observed. Rather, the unsatisfied N-H groups at the N-terminus and C=O groups at the C-terminus are involved in a complex network of intermolecular H-bonds with the four co-crystallized solvent (methanol) molecules.

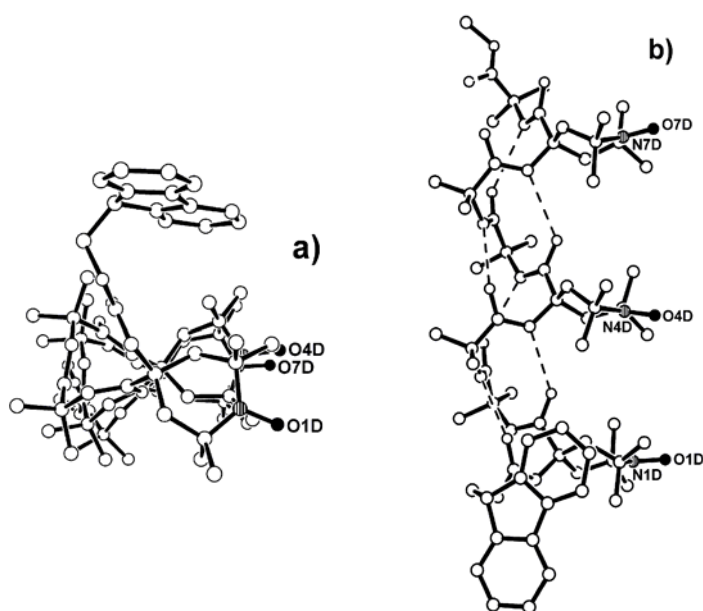


Fig. 1. X-Ray diffraction structure of Fmoc-TOAC-(Aib)₂-TOAC-(Aib)₂-TOAC-Aib-OMe with labelling of the nitroxyl side-chain nitrogen and oxygen atoms. (a) View along the helix axis (the triangular shape of the ternary helix is clearly visible). (b) View orthogonal to the helix axis. The intramolecular C=O...H-N H-bonds are represented by dashed lines.

A detailed EPR study clearly showed that the 3_{10} -helix is maintained in solvents of low polarity (e.g., MeCN), whereas it is disrupted, albeit reversibly, in highly polar alcohols (e.g., HFIP) (Fig. 2).

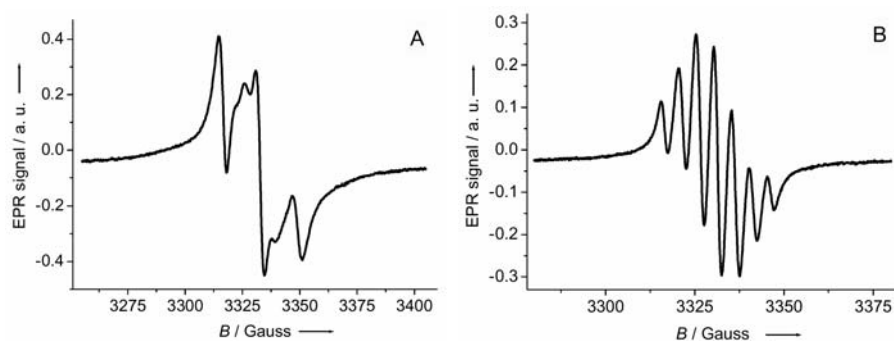


Fig. 2. EPR spectra of the tris-TOAC octapeptide: (A) in HFIP solution, where partial disruption of the 3_{10} -helical structure takes place (multiple conformations in equilibrium); and (B) in MeCN solution after evaporation of HFIP, where the 3_{10} -helical structure is restored (this spectrum is identical to that obtained by directly dissolving the octapeptide in MeCN solution).

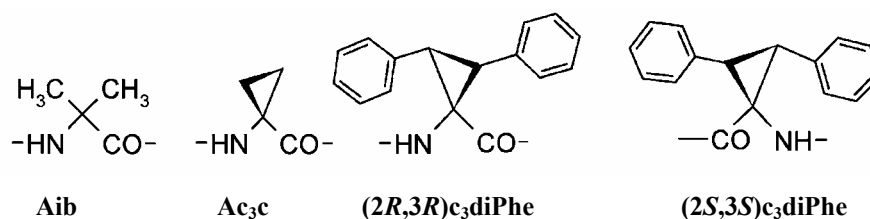
Design, Synthesis, and Preferred Conformation of Peptides Based on a Highly Constrained, β,β' -Diphenyl Substituted Cyclopropane α -Amino Acid

Soledad Royo¹, Wim M. De Borggraeve², Cristina Peggion², Marco Crisma², Ana I. Jiménez¹, Carlos Cativiela¹ and Claudio Toniolo²

¹Department of Organic Chemistry, ICMA, University of Zaragoza-CSIC, 50009 Zaragoza, Spain; ²Institute of Biomolecular Chemistry, CNR, Department of Chemistry, University of Padova, 35131 Padova, Italy

Introduction

To complete our understanding of the 3D-structural properties of the phenyl-substituted, $C^\alpha \leftrightarrow C^\alpha$ cyclized, cyclopropane α -amino acids and to offer new tools to peptide chemists for the control of conformation we embarked on a program directed towards an in-depth 3D-structural characterization of peptides rich in either the (2*R*,3*R*)- or the (2*S*,3*S*)-enantiomer of *c*-2,*t*-3-diphenylcyclopropane-*r*-1-carboxylic acid (*c*₃diPhe), a member of the class of C^α -tetrasubstituted α -amino acids (the prototypes of which are Aib and Ac₃c) bearing two phenyl substituents in a *trans* relative disposition on the β,β' -carbons.



Results and Discussion

Terminally blocked, homo- and hetero-chiral, homo-peptide amides of *c*₃diPhe, from the dimer to the tetramer, and diastereomeric co-oligopeptides of (2*R*,3*R*)- or (2*S*,3*S*)- *c*₃diPhe with (*S*)-Ala residues to the trimer level were prepared in solution and fully characterized. The synthetic effort was extended to terminally-protected co-oligopeptide esters to the hexamer, where *c*₃diPhe residues are combined with achiral Aib or Gly residues.

The preferred conformations of all peptides were assessed in solution by FT-IR absorption and NMR techniques, and for six oligomers in the crystal state (by X-ray diffraction) as well (Fig. 1). Two examples of the latter type of analysis are shown in Figure 1. This study clearly indicates that *c*₃diPhe, a sterically demanding cyclopropane analog of Phe, tends to fold peptides into β -turn and 3_{10} -helix conformations, although less effectively than its side-chain unsubstituted Ac₃c parent compound. However, when *c*₃diPhe is in combination with other chiral residues, the conformation preferred by the resulting peptide is also dictated by the chiral sequence of the amino acid building blocks.

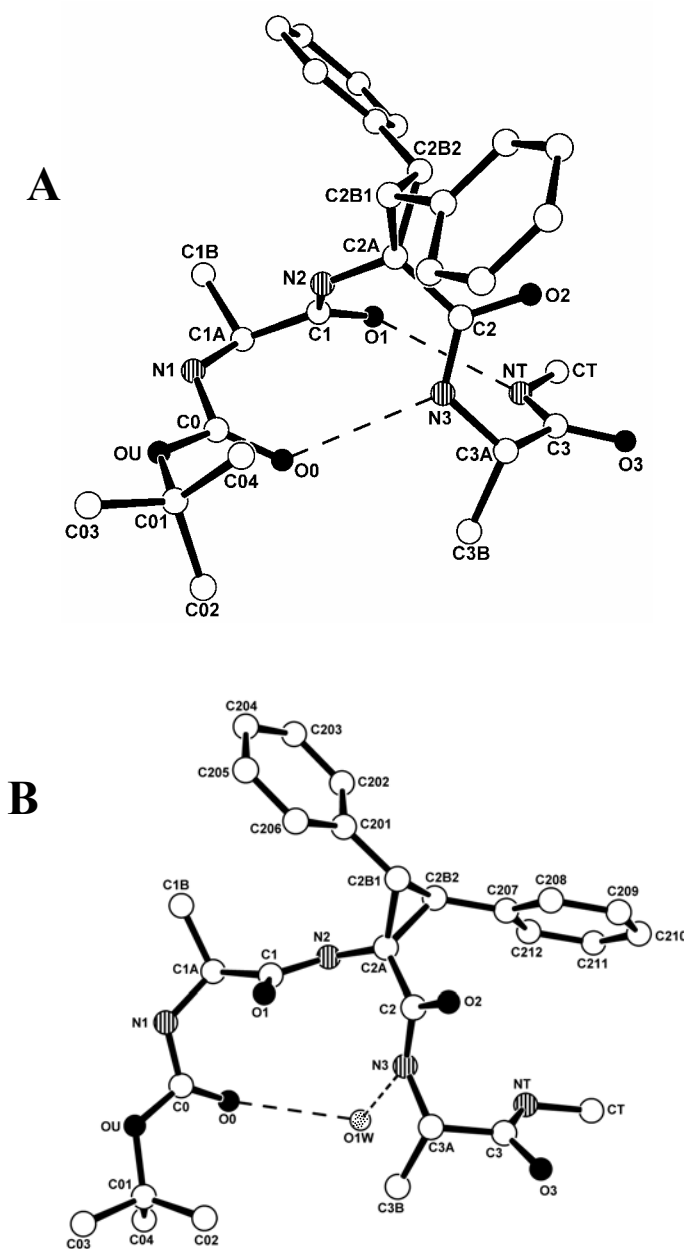


Fig. 1. X-Ray diffraction structures of: (A) the tripeptide Boc-(S)-Ala-(2R,3R)-c₃diPhe-(S)-Ala-NHMe and (B) its Boc-(S)-Ala-(2S,3S)-c₃diPhe-(S)-Ala-NHMe (monohydrate) diastereomer with atom numberings. The two intramolecular H-bonds in (A) and the two intermolecular H-bonds ("water bridge") in (B) are represented by dashed lines.

Identification of a Novel HIV-1 Neutralizing Antibody Using Synthetic Peptides that Mimic a GP41 Fusion Intermediate

Elisabetta Bianchi¹, Michael D. Miller², Romas Geleziunas², Gaetano Barbato¹, Paolo Ingallinella¹, Marco Finotto¹, Renee Hrin², Meiqing Lu², Simon Lennard³, David Lowe³, Gennaro Ciliberto¹, Daria Hazuda², Riccardo Cortese¹, John Shiver² and Antonello Pessi¹

¹IRBM P. Angeletti, 00040 Pomezia (Rome), Italy; ²Merck Research Laboratories, West Point, PA 19486, USA; ³Cambridge Antibody Technology, Cambridge, UK

Introduction

HIV-entry into cells is mediated by the envelope glycoprotein receptor-binding gp120 and fusogenic gp41 subunits. During the fusion process gp41 undergoes a series of conformational changes that culminate in formation of the fusogenic structure: a 6-helix bundle, where three α -helices formed by the heptad repeat region 2 (HR2) pack in an antiparallel manner against a central three-stranded coiled coil formed by the heptad repeat region 1 (HR1). Viral fusion progresses via formation of an intermediate, which transiently exposes the HR1 coiled coil and the HR2 peptides. By targeting these regions with peptides derived from HR1, HR2, it is possible to prevent formation of the 6-helix bundle, and block viral infectivity.

We investigated if antibodies could also block HIV-1 entry by the same mechanism, since this would open the pathway to a vaccine targeting the fusion intermediate.

Results and Discussion

To this purpose, we selected a phage display library of human-derived single-chain antibodies (scFvs) by binding sequentially to 5-helix and IZN36, two peptides designed to mimic the HR1 coiled coil [1,2] (Fig.1). By testing the 5-helix/IZN36-binding scFvs in an HIV entry assay, we identified one scFv, D5 that was able to inhibit HIV fusion. The D5 scFv also blocked HIV infection in a single-cycle infectivity assay. Importantly, the antiviral potency was also maintained after conversion to full-length IgG1, providing proof-of-principle for vaccine development. To identify the D5 binding epitope, we performed binding studies to

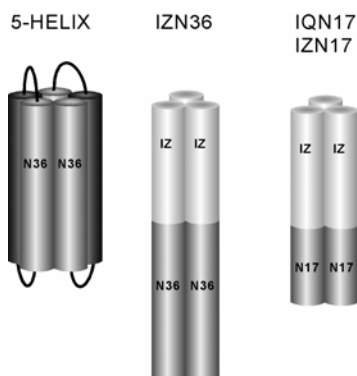


Fig. 1. Schematic models of designed gp41 HR1 coiled coil mimetics.

various synthetic HR1-helix coiled coil peptides (Fig. 1). In addition to binding 5-helix and IZN36, D5 also bound equally well IZN17 and IQN17, which contain only the 17 C-terminal portion of the HR1 region. Within this region, in the groove formed by adjacent N17 helices, lies a hydrophobic pocket, which had been previously identified as a target for antiviral drugs. A helical wheel representation of the N17 coiled coil trimer is shown in Figure 2 with the pocket-forming residues boxed. To identify the amino acids forming the D5 epitope, a series of IZN17 mutant peptides was synthesized using Fmoc chemistry on an APEX396 multi-synthesizer. With the exception of the *a* and *d* heptad repeat positions of the coiled coil trimerization interface, each of the other exposed positions was mutated to alanine. Glycine 572 was mutated to aspartic acid to introduce a bulkier, charged residue in the pocket. Thermal denaturation experiments by CD showed that the coiled coil mutants have comparable stabilities to IZN17. Therefore any decrease in potency by a given mutation could be safely interpreted in terms of loss of a binding contribution. When tested as competitors of IQN17/D5 binding, peptides with alanine at positions L568, W571 and K574 were completely ineffective (Fig. 2, residues in black box, $IC_{50} > 1000$ nM) indicating that these residues are critical components of the D5 epitope. Mutant V570A also competed for D5 binding, but less efficiently (Fig. 2, gray box), suggesting that this residue is a minor contact for D5 IgG. As expected, mutant G572D was unable to compete for D5 binding (Fig. 2, black box).

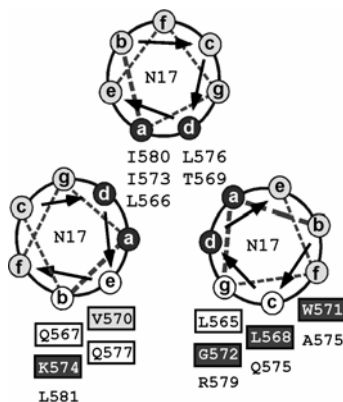


Fig. 2. Helical wheel representation of the trimeric N17 coiled coil.

In conclusion, we identify the binding site of D5, the first neutralizing antibody which binds to a fusion intermediate, as a previously identified hydrophobic pocket in the groove of the HR1 coiled coil. This region therefore represents an attractive novel target for the development of a HIV vaccine.

References

1. Root, M. J., Kay, M. S. and Kim, P. S. *Science* **291**, 884-888 (2001).
2. Eckert, D. M. and Kim, P. S. *Proc. Natl. Acad. Sci. USA* **98**, 11187-11192 (2001).

Covalent Trimeric Coiled Coils of the HIV gp41 HR1 Region are Extremely Potent and Broadly Neutralizing Inhibitors of Viral Infection

Elisabetta Bianchi¹, Marco Finotto¹, Paolo Ingalinella¹, Renee Hrin², Michael D. Miller², Romas Geleziunas² and Antonello Pessi¹

¹IRBM P. Angeletti, 00040 Pomezia (Rome) Italy; ²Merck Research Laboratories, West Point, PA 19486, USA

Introduction

The key players in HIV viral entry are the envelope glycoprotein receptor-binding gp120 and transmembrane fusogenic gp41 subunits. The mechanism of fusion involves two helical regions of gp41, an N-terminal heptad repeat (HR1) and a C-terminal heptad repeat (HR2). The HR1 and HR2 helical regions form a fusogenic structure, a six-helix-bundle, in which three α -helices formed by HR2 peptides pack in an antiparallel manner against a central three stranded coiled coil formed by the HR1 peptides. It is generally accepted that fusion progresses via the formation of a fusion intermediate, in which both the HR1 coiled coil and the HR2 regions are exposed. The fusion intermediate is the target of both synthetic C- and N-peptides, that inhibit viral infection by preventing formation of the 6-helix bundle. HR2 peptides are potent inhibitors of viral fusion, and the peptide DP178 has become the first fusion inhibitor approved as a human therapeutic [1]. Peptides from the HR1 region of gp41 protein can also inhibit viral fusion, but their potency is limited by the low tendency to form a trimeric coil-coil. Accordingly, chimeric peptides, consisting of a designed trimeric coiled coil (IZ) fused to gp41 HR1 sequences are potent inhibitors of fusion as reported for IZN17 [2] (Fig. 1).

Based on the hypothesis that antiviral potency of IZN17 is limited by the self-association equilibrium, we designed a new construct, CCIZN17, with the aim of stabilizing the homotrimeric coiled coil structure to a covalent trimer via formation of intermolecular disulfide bonds. To this purpose, two cysteine residues were introduced at the N-terminus of the IZN17 sequence (Fig. 1). Also, two glycine residues were added between the pair of cysteines and the IZ scaffold sequence to ensure a high conformational freedom of the cysteines from the coiled coil domain and thus to enhance the likelihood of spontaneous formation of the intermolecular disulfide bridges among the three peptide chains.

IZN17 IKKEIEAIKKEQEAIKKKIEAIEKLLQLTVWGIKQLQARIL
CCIZN17 CCGGIKKEIEAIKKEQEAIKKKIEAIEKLLQLTVWGIKQLQARIL

Fig. 1. Sequence of IZN17 and CCIZN17 (the HIV portion is underlined).

Results and Discussion

The peptide CCIZN17 was synthesized using Fmoc chemistry on Fmoc-LinkerAM-Champion on a Pioneer Peptide Synthesizer. When the CCIZN17 peptide is dissolved at neutral pH, the spontaneous association of three CCIZN17 peptide chains into a helical trimeric coiled coil structure brings in close proximity the juxtaposed cysteine residues which form three intermolecular disulfide bonds as confirmed by HPLC-MS analysis, and schematically shown in Figure 2.

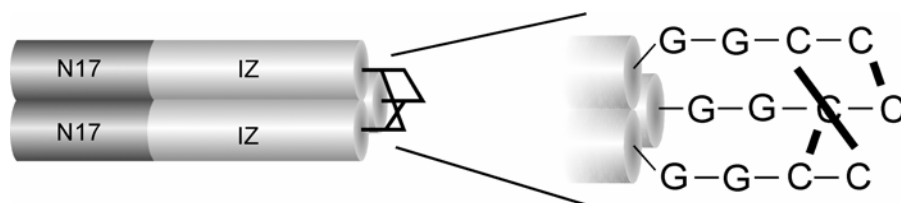


Fig. 2. Schematic representation of the covalent coiled coil trimer (CCIZN17)₃.

The covalent trimer is fully helical by CD. In thermal denaturation experiments, in 2M guanidinium chloride, (CCIZN17)₃ shows a $T_m > 90^\circ\text{C}$ while IZN17 shows a T_m of 61.5°C . Therefore, as expected, covalent stabilization of the IZN17 trimer yields a peptide with a much increased thermodynamic stability.

When tested in a cell-cell fusion assay, (CCIZN17)₃ was found to inhibit viral entry at subnanomolar concentration (IC_{50} , 0.26 nM): in this assay, its potency is 55-fold higher than the human therapeutic DP178 (IC_{50} , 14.5 nM).

Table 1. Inhibition of viral infectivity of various HIV isolates in single-cycle infectivity assay

Peptide	IC_{50} (nM)		
	<i>HIV_{HXB}</i>	<i>HIV_{NL4-3}</i>	<i>HIV_{MN-1}</i>
(CCIZN17) ₃	0.040	0.046	0.38
IZN17	1.3	33.66	394.7
5-Helix	9.9	12.00	159.4
DP178	1.2	1.7	5.5

(CCIZN17)₃ was then tested in a single-cycle infectivity assay against various HIV isolates, and its activity was compared to the parent non-covalent IZN17, to another potent HR1 inhibitor, 5-Helix [3] and to the HR2 inhibitor DP178 [1] (Table 1). The data clearly show that not only (CCIZN17)₃ is one-to-three order of magnitude more potent than IZN17, but it also displays much higher activity than 5-Helix and DP178.

(CCIZN17)₃ was also able to neutralize 100% of a large panel of HIV isolates, including R5, X4, and R5/X4 strains when tested in a commercial phenotypic virus assay (Virologic).

Overall, our data demonstrate that covalent stabilization of HR1 trimers yields extremely potent HIV-1 fusion inhibitors. Moreover, this new class of HR1 peptides are attractive as immunogens to elicit a fusion-blocking neutralizing antibody response targeting the N17 portion of the HR1 coiled coil.

References

1. Matthews, T., *et al.* *Nat. Rev. Drug Discov.* **3**, 215-225 (2004).
2. Eckert, D. M. and Kim, P. S. *Proc. Natl. Acad. Sci. USA* **98**, 11187-11192 (2001).
3. Root, M. J., Kay, M. S. and Kim, P. S. *Science* **291**, 884-888 (2001).

Selective Agonists for the Human Vasopressin V_{1b} Receptor are Potent Antidiuretic Agonists in the Rat

**Stoytcho B. Stoev¹, LingLing Cheng¹, Maurice Manning¹, Nga C. Wo²,
Hazel H. Szeto², Ana Pena³, Brigitte Murat³, Sylvain Derick³, Miguel
Trueba³, Maria A. Ventura⁴ and Gilles Guillon³**

¹Department of Biochemistry and Cancer Biology, Medical University of Ohio, Toledo, OH 43614, USA; ²Department of Pharmacology, Weill Medical College of Cornell University, New York, NY 10021, USA; ³Institut de Génomique Fonctionnelle, UMR5203-CNRS, U661-INSERM, Université Montpellier I & II, 141 rue de la Cardonille, 34094 Montpellier Cedex 5, France; ⁴Institut Cochin Paris, France

Introduction

We recently reported the synthesis and human V_{1a}, V_{1b}, V₂, and OT receptor affinities and selectivities of a broad series of 21 position 4 analogs of [deamino-Cys¹]-arginine vasopressin (dAVP) [1]. Four of these analogs, d[Leu⁴]AVP, d[Orn⁴]AVP, d[Lys⁴]AVP, and d[Har⁴]AVP, peptides 1-4 (Table 1), have high affinities and selectivities for the human V_{1b} receptor and very low affinities for the human V_{1a}, V₂, and OT receptors [1]. In addition, in functional assays they and d[Cha⁴]AVP [2] are the first high affinity selective agonists for the human V_{1b} receptor [1]. This discovery raised the question of whether these four new peptides would possess high selectivity for the rat V_{1b} receptor with respect to the rat V_{1a}, V₂ and OT receptors. We now report the antidiuretic activities in rat bioassays and the binding affinities in rat V_{1a}, V_{1b}, V₂, and OT receptor assays of peptides 1-4 (Table 1). We also report the antidiuretic, vasopressor, and oxytocic activities of 11 additional position 4 analogs of dAVP [1], together with their rat V₂ receptor affinities (peptides 5-15, Table 1).

Results and Discussion

The data in Table 1 show clearly that peptides 1-4 exhibit moderate to highly potent antidiuretic activities in the rat. All four peptides exhibit much higher affinities for the rat V₂ receptor than for the human V₂ receptor (Table 1). With the exception of d[Lys⁴]AVP (No. 3), the remaining three peptides exhibit high affinities for both the rat and the human V_{1b} receptors. Thus, while these three peptides have high affinities for the rat V_{1b} receptor because they exhibit potent antidiuretic activities in the rat and have high affinities for the rat V₂ receptor, they are clearly not selective for the V_{1b} receptor with respect to the V₂ receptor in the rat. All of the remaining position 4-analogs of dAVP in Table 1 [1], with the exception of d[Phe⁴]AVP, exhibit very high antidiuretic potencies, all in the same range as those for the previously reported analogs: d[Abu⁴]AVP, d[Val⁴]AVP, d[Thr⁴]AVP, and d[Arg⁴]AVP (for refs. to these peptides see [1]).

Conclusion

The studies reported here show that peptides 1-4 (Table 1), previously shown to be potent and selective agonists for the human V_{1b} receptor [1], also exhibit high affinities for the rat V_{1b} receptor. Moreover, because they are also potent antidiuretic agonists in the rat, they are not selective V_{1b} agonists in the rat. However, the finding that these peptides exhibit high affinities for the rat V_{1b} and V₂ receptors,

while exhibiting very low affinities for the rat V_{1a} and OT receptors, have provided very promising new leads to the design of the first selective agonists for the rat V_{1b} receptor [3].

Table 1. Rat antidiuretic activities (A) (units/mg), and rat (r) VP and OT human (h) receptor affinities (K_i 's, nM) for position 4 modified analogs and dAVP^a

No	Peptide	Rat (A)	Rat receptors				Human receptors	
			rV ₂ R	rV _{1a} R	rV _{1b} R	rOTR	hV ₂ R	hV _{1b} R
	AVP ^b	332	0.5	2.6	3.3	1.7	1.2	0.7
	dAVP ^b	1745	0.8	1.3	2.2	1.0	5.0	0.4
	d[Cha ⁴]AVP ^b	133	12.7	2297	1.4	1430	750	1.2
1	d[Leu ⁴]AVP ^c	378	3.1	1252	0.02	481	245	0.2
2	d[Orn ⁴]AVP ^c	260	3.4	900	0.4	997	1125	0.5
3	d[Lys ⁴]AVP ^c	35	24.6	1478	9.8	5042	11170	1.8
4	d[Har ⁴]AVP ^c	505	0.6	32	0.3	2996	1386	0.5
5	d[Arg ⁴]AVP ^{b,c}	748	0.2	12.9	0.1	3552	131	0.4
6	d[Val ⁴]AVP ^b	1150	0.3	60	4.5		1.2	0.3
7	d[Ala ⁴]AVP ^c	841	0.6				13.7	6.5
8	d[Abu ⁴]AVP ^{b,c}	1020	0.5				2.1	1.2
9	d[Nva ⁴]AVP ^c	877	1.4				24.1	0.8
10	d[Nle ⁴]AVP ^c	1141	0.2				117	0.4
11	d[Ile ⁴]AVP ^c	819	1.4				9.9	0.4
12	d[Phe ⁴]AVP ^c	11	86				1067	9.5
13	d[Asn ⁴]AVP ^c	996	0.9				50	1.5
14	d[Thr ⁴]AVP ^{b,c}	758	0.3				1.5	1.0
15	d[Dap ⁴]AVP ^c	1053	0.07				36.8	3.4

^aOriginal synthesis of peptides 1-4, 7, 9-14 reported in [1]. Binding data are performed either on rat liver, kidney or pituitary membranes known to naturally express V_{1a} , V_2 or V_{1b} receptor isoforms or on membranes from CHO cells stably transfected with the OT receptor isoform.

^bFor references to original synthesis and antidiuretic activities see [1]. ^cThis publication.

Acknowledgments

We thank Ms. Ann Chlebowski for expert help in the preparation of this manuscript. Supported by NIH Grant GM-25280 and the Institut National de la Santé et de la Recherche Médicale.

References

1. Cheng, L. L., Stoev, S., Manning, M., Derick, S., Pena, A., Ben Mimoun, M. and Guillon, G. *J. Med. Chem.* **47**, 2375-2388 (2004).
2. Derick, S., Cheng, L. L., Voirol, M. J., Stoev, S., Giacomini, M., Wo, N. C., Szeto, H. H., Ben Mimoun, M., Andres, M., Gaillard, R. C., Guillon, G. and Manning, M. *Endocrinology* **143**, 4655-4664 (2002).
3. Manning, M., Cheng, L. L., Stoev, S., Wo, N. C., Szeto, H. H., Pena, A., Murat, B., Trueba, M., Ventura, M. A. and Guillon, G. In *Understanding Biology Using Peptides, Proceedings of the 19th American Peptide Symposium*, this volume, pp. 659-660 (2006).

Prion Protein Misfolding: Conformational Stability of the $\alpha 2$ -Helix

Pasquale Palladino¹, Luisa Ronga¹, Barbara Tizzano¹, Filomena Rossi¹,
Raffaele Ragone², Teodorico Tancredi³, Gabriella Saviano⁴, Angelo
Facchiano⁵, Susan Costantini⁵, Menotti Ruvo¹ and Ettore Benedetti¹

¹Dipartimento delle Scienze Biologiche, Università "Federico II" di Napoli, CIRPeB, and
Istituto di Biostrutture e Bioimmagini Biostrutture e Bioimmagini C.N.R. Napoli, Italy;

²Dipartimento di Biochimica e Biofisica, Seconda Università di Napoli, Italy; ³Istituto di
Chimica Biomolecolare, CNR, Pozzuoli, Napoli, Italy; ⁴DiSTAT, 86170 Isernia, Italy, ⁵
Istituto di Scienze dell'Alimentazione, CNR, Avellino, Italy

Introduction

Cellular prion protein (PrP^c) is a glycoprotein anchored to cell surface. Its structural conversion is related to uncommon diseases known as Spongiform Encephalopathies. PrP^c is highly expressed in neurons, binds copper and has antioxidant properties [1,2]. In a recent thermodynamic study [3], we have shown that the peptide corresponding to the $\alpha 2$ helix of human prion protein [hPrP], which has gained attention because of a possible role in the nucleation and aggregation processes, is structurally ambivalent. We have suggested that this conformational ambivalence could be involved in the modulation process of prion misfolding and is likely focused on the short C-terminal end of the helix. We report here the conformational preferences of synthetic N-acetylated and C-amidated $\alpha 2$ helix, hPrP[173-195], Ac-NNFVHDCVNITIKQHTVTTTCKG-NH₂, as obtained by NMR and molecular dynamic (MD) simulations.

Results and Discussion

In aqueous solution at neutral pH, even at a concentration of 0.1 mM, sample opalescence and NMR spectra are indicative of a time-dependent peptide aggregation. The analysis of NMR spectra has then been performed in neat TFE, a solvent known to favor helical conformation. The preliminary molecular modeling, based on NMR data and DYANA calculations, shows a high helical content in the C-terminal region of peptide in TFE. Figure 1 depicts the stereo view of the superimposition of the backbone of the best 30 Dyana structures of the peptide, obtained by fitting residues from Ile¹⁰ to Thr²¹.

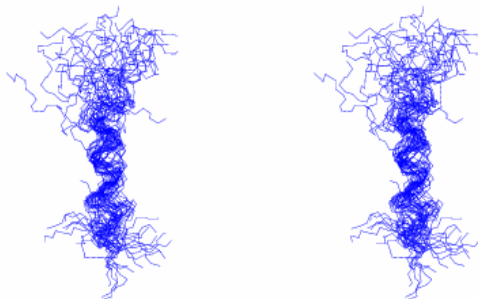


Fig. 1. Stereo view of the best 30 structures as obtained by Dyana calculations of PrP[173-195] peptide in neat TFE (T=300 K).

The molecular structure of the hPrP[173-195] peptide has been created using the tool Builder in Insight, with the C-terminal and N-terminal blocked as amide and acetyl, respectively. The Insight/Discover program with the Consistent Valence Force Field (CVFF) was applied for energy minimizations and MD. The MD was performed *in vacuo* as well as within a fixed-volume box filled with water molecules at 300 K. The initial structure of this peptide was relaxed by energy minimization, followed by 300 ps of MD after the addition of three SDS molecules. Secondary structure has been assigned with the program DSSP. The structural model of hPrP[173-195] has been built by setting the initial structure as an extended conformation. After energy minimization, the interaction of the peptide with three SDS molecules has been simulated by MD runs. The resulting average molecular model of the peptide is represented in Figure 2 as a β -structure consisting of three or two anti-parallel β -strands, as obtained by vacuum or water MD calculations, respectively. These results are in agreement with both secondary structure predictions and previous experimental observations [3]. Although still preliminary, the present results suggest that this region of the prion globular domain may be involved in the anomalous misfolding of the whole protein due to the high instability of its secondary structure.

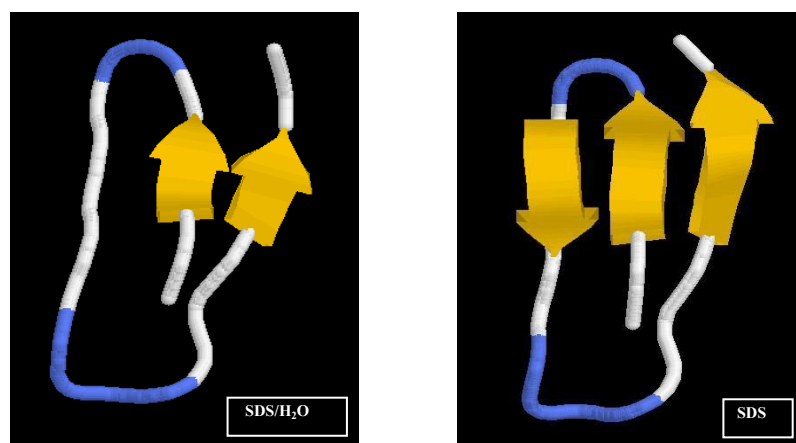


Fig. 2. hPrP[173-195] MD secondary structures *in vacuo* after addition of three SDS molecules (right) and with water molecules at 300 K (left).

Acknowledgments

The work was funded by MIUR COFIN Prot.2003031424 (2003) and RBNE03PX8 (2005).

References

1. Prusiner, S. B. *Proc. Natl. Acad. Sci. USA* **95**, 13363-13383 (1998).
2. Brown, D. R., Guantieri, V., Grasso, G., Impellizzeri, G., Pappalardo, G. and Rizzarelli, E. *J. Inorg. Biochem.* **98**, 133-143 (2004).
3. Tizzano, B., Palladino, P., De Capua, A., Marasco, D., Rossi, F., Benedetti, E., Pedone, C., Ragone, R. and Ruvo M. *Proteins* **59**, 72-79 (2005).

Modeling Flexible Loops in the Dark-Adapted and Activated States of Rhodopsin, a Prototypical G-protein-Coupled Receptor

Gregory V. Nikiforovich and Garland R. Marshall

Department of Biochemistry and Molecular Biophysics, Washington University School of Medicine, St. Louis, MO 63110, USA

Introduction

High flexibility of the intra- and extracellular loops in rhodopsin and other G-protein coupled receptors (GPCRs) introduces specific challenge in determining 3D structures of the dark-adapted (R) and activated (R*) states, since even the most detailed structural information on the dark-adapted rhodopsin provided by X-ray crystallography produces only one snapshot out of many possible loop conformations. This study presents results of modeling of the intra- and extracellular loops in rhodopsin by a *de novo* computational procedure developed for restoring interhelical loops in GPCRs; part of this procedure has been described earlier [1]. To circumvent the conflict between thoroughness of sampling of conformational space available to a particular loop versus the required amount of computer resources, we have decided to sacrifice detailed description of any particular 3D structure of a loop in rhodopsin in favor of less precise description of many structures, which allowed focusing on the major differences among them detectable by experimental procedures.

Results and Discussion

The loops were mounted on the “template”, i.e., on the specific 3D structure of the TM region of rhodopsin. The templates for the R and R* states were the same as developed earlier [2]. The build-up procedure of geometrical conformational sampling was applied first to stepwise elongation of the individual loops from the starting residue to the target residue in TM helices. The procedure covered all combinations of the local minima of the Ramachandran map for the residues in rhodopsin fragments 64-72 (intracellular loop IC1), 139-150 (IC2), 225-246 (IC3), 99-108 (extracellular loop EC1), 172-200 (EC2), and 277-286 (EC3). Distance limitations imposed on the growing peptide chain ensured that the chain (i) is self-avoided; (ii) avoids sterical clashes with the existing template; and (iii) goes not too far from the starting point as well as from the target point. All potentially loop-closing conformations for a specific loop were subjected to energy minimization employing the ECEPP/2 force field. The low-energy conformers selected by results of energy calculations for individual loops were then combined to account for the inter-loop interactions into the IC1+IC2+IC3 and EC1+EC2+EC3 “packages”.

Calculation results showed that the intra- and extracellular loops of rhodopsin may possess sterically consistent structures that correspond to large conformational movements both in the R and R* states. In both states, there were low-energy conformers of the loops that may be considered as the “closed” and “opened” ones. Specifically, the lowest and largest C α -C α distances (the latter in parentheses) between the central residues of the intracellular loops were 12.5 (24.5) Å, 19.7 (34.1) Å and 10.0 (31.6) Å for the R state (distances between residues L68 – S144, L68 – A235 and S144 – A235, respectively) and 9.25 (20.6) Å, 13.8 (33.9) Å, and 5.3 (31.6) Å for the R* state. The corresponding distances found for the extracellular loops were 20.8 (32.2) Å, 12.2 (31.9) Å, and 7.1 (19.2) Å in the R state (distances

between residues F103 – T193, F103 - S281 and T193 – S281), and 18.2 (31.0) Å, 11.0 (24.8) Å, and 5.9 (37.5) Å in the R* state. The global rmsd values (all heavy atoms) for the low-energy conformers of the interacting IC1+IC2+IC3 and EC1+EC2+EC3 loops in the R state that are most close to the X-ray structure (1GZM entry in the PDB) were 4.2 Å and 4.5 Å for 37 and 43 residues, respectively. Combining these conformers with the template previously suggested for the R state of the TM region of rhodopsin [2], the total rms value (C α atoms only) between 1GZM (fragment 35-313) and the resulting structure was of 2.9 Å for total of 279 residues, 80 of them being the loop residues.

The modeling results can be also compared with new emerging experimental data to select the plausible 3D models for the loop structures. For instance, some preliminary data obtained by the novel technique of double electron-electron resonance suggested that the distance between spin labels inserted in positions 63 (close to IC1) and 241 (in IC3) of rhodopsin became larger by *ca.* 6 Å upon transition from R to R* (W.L. Hubbell, personal communication; also see www.bruker-biospin.com/brukerepr/october.html). The sets of calculated low-energy conformers with C α -C α distances 63-241 below *ca.* 26 Å for the R state (maximal distance for the R* state less 6 Å) and above *ca.* 26 Å for the R* state (minimal distance for the R state plus 6 Å) satisfy the above experimental observation. The average C α -C α distances 63 – 241 in the sets are 24.2 Å for the R state and 28.4 Å for the R* state. Distances between spin labels are always larger than the corresponding C α -C α distances by 4 – 9 Å (see [3]); therefore, the average distances between the spin labels in positions 63 and 241 for the selected sets of the low-energy structures would be 28 – 33 Å for the R state, and 32 - 37 Å for the R* state, whereas the experimental estimations were *ca.* 34 Å and *ca.* 40 Å, respectively.

The obtained calculation results may also be used to produce the testable structural hypotheses concerning the plausible 3D models of the loops. As an example, the sets of the low-energy conformers satisfying the observed differences in distances between positions 63 and 241 in the R state can be further divided into two distinct groups as to C α -C α distances between residues 140 and 241. The first group consists of 13 conformers where the distances are from 9.3 Å to 13.4 Å, and the second group involves 20 remaining conformers where the distances are from 25.3 Å and 29.0 Å, according to calculation results. In the R* state, the same distances vary from 16.6 Å to 26.6 Å, but here it is difficult to divide the low-energy conformers into the distinctly different groups. Inserting spin labels or other reporting groups at positions 140 and 241 and estimating distances between them both in the R and R* states of rhodopsin could provide new experimental data to select even more narrow sets of the plausible structures for the rhodopsin loops out of the low-energy conformations suggested by calculations.

Acknowledgments

G.N. was partly supported by the NIH grant GM 22086.

References

1. Galaktionov, S., Nikiforovich, G. V. and Marshall, G. R. *Biopolymers* **60**, 153-168 (2001).
2. Nikiforovich, G. V. and Marshall, G. R. *Biochemistry* **42**, 9110-9120 (2003).
3. Arimoto, R., Kisselev, O. G., Makara, G. M. and Marshall, G. R. *Biophys. J.* **81**, 3285-3293 (2001).

Deducing 3D Models of the Activated States for TM Regions of GPCRs by Modeling Constitutively Active Mutants: The Test Case of Opsin

Gregory V. Nikiforovich and Garland R. Marshall

Department of Biochemistry and Molecular Biophysics, Washington University School of Medicine, St. Louis, MO 63110, USA

Introduction

The activated (R^*) states of constitutively active mutants (CAMs) of G-protein-coupled receptors (GPCRs) are supposedly characterized by lower energies than the resting (R) states. Accordingly, if some specific configuration of TM helices in a GPCR possesses energy lower than that in the R state for most of its CAMs, but not for non-CAMs, this particular mutual orientation of TM helices may be a good candidate 3D model for the R^* state. We have studied this hypothesis for the test case of opsin (the apoprotein of rhodopsin, a prototypical GPCR), where both R and R^* for the TM region should not be different from those previously determined for rhodopsin by experimental techniques [1,2].

Results and Discussion

We have hypothesized that the 3D structures of the R^* states for different CAMs of the same GPCR are geometrically similar to each other. Energy calculations have been simplified to allow fast and efficient estimation of atom-atom interactions in large molecular systems as GPCRs. Specifically, only TM bundle was considered; no molecular environment (lipids, water molecules, etc.) was considered; the ECEPP force field was employed (see also [3]). Packing of TM helices was performed in the space of “global” parameters (related to translations and rotations of individual TM helices as rigid bodies) and the “local” parameters (the dihedral rotational angles of the side chains; the backbone angles were fixed in the values they obtained in energy calculations for the individual TM helices). The study involved 18 opsin receptors, namely K296G, E113Q, A292E, G90D, M257Y, M257N, T94E, T94D, and E113Q/M257Y as the pronounced CAMs; E134Q, M257Q, and T94I as moderate CAMs; and M257L, T94V, D83N, E122Q, R135Q, and the wild type receptor (WT) as non-CAMs.

It appeared that, due to simplifications, the better scoring function to discriminate between R and R^* in pronounced CAMs and non-CAMs of opsin was not the total energy of interactions within TM bundles, but energy of the inter-helical interactions only. The first panel in Figure 1 displays differences in total energy calculated with the ECEPP force field between the two configurations that correspond to the experimentally suggested 3D models of the R and R^* states of the TM bundles of the fifteen opsin receptors; ideally, the differences are expected to be negative for all CAMs and positive for all non-CAMs. The second panel presents the same differences obtained by additional energy minimization performed with the OPLS-AA force field employing the MacroModel package, i.e., without the limiting assumption of the fixed backbone. The third panel contains differences in the ECEPP energies of only inter-helical (but not intra-helical) interactions between TM helices. Only the values in the third panel are negative for most pronounced CAMs (all except E113Q) and positive for most non-CAMs (all except R135Q).

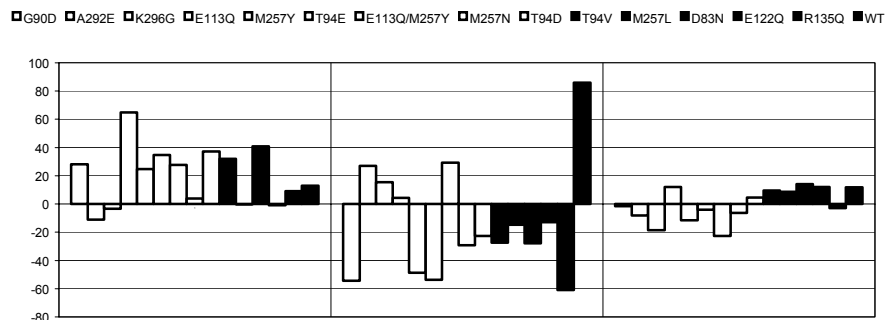


Fig. 1. Energy differences (in kcal/mol) between configurations of the TM bundle corresponding to the R and R* states of opsin for pronounced CAMs (open bars) and for non-CAMs (closed bars). Three panels (left to right) correspond to total energies calculated by the ECEPP force field, by the OPLS-AA force field and to the ECEPP inter-helical energies.

Employing values of inter-helical energies, we were able to distinguish between the pronounced CAMs and non-CAMs of opsin provided that configurations of TM helices corresponding to the R and R* states are known. The next step was to study the reverse problem, namely, whether it is possible to identify all possible configurations that may be the likely candidates for the R* state of opsin by calculations of inter-helical energies. The entire configurational space of packing options for the seven TM helices in several pronounced CAMs of opsin (G90D, A292E, K296G, E113Q, M257Y, and T94E) was sampled by the build-up procedure covering all possible rotations along the long axes of the helices with a grid of 60°. The procedure started from all “triplets” of the contacting TM helices, then expanded to “fourplets”, and so on until all seven TM helices are involved. Sampling delineated six types of configurations differing by orientations of helices TM5 and TM6 with relative inter-helical energies less than in the corresponding R states for each of the receptors.

Energy calculations found that the differences in the values of inter-helical energies between R and the six candidates for the R* state satisfy the main hypothesis (to be negative for most CAMs and positive for most non-CAMs) in two out of the six configurations. However, only one of the two configurations showed correlation between these values and experimentally observed levels of basal activity for the series of the opsin receptors with replacements in positions 257 (M257Y > M257N > M257L [4]) and 94 (T94E > T94D > T94I [5]); this configuration of TM helices corresponded to the R* state of rhodopsin determined by experiment.

Acknowledgments

G.N. was partly supported by the NIH grant GM 22086.

References

1. Palczewski, K., *et al.* *Science* **289**, 739-745 (2000).
2. Hubbell, W. L., Altenbach, C. and Khorana, H. G. *Adv. Protein Chem.* **63**, 243-290 (2003).
3. Nikiforovich, G. V. and Marshall, G. R. *Biochemistry* **42**, 9110-9120 (2003).
4. Han, M., Smith, S. O. and Sakmar, T. P. *Biochemistry* **37**, 8253-8261 (1998).
5. Gross, A. K., Rao, V. R. and Oprian, D. D. *Biochemistry* **42**, 2009-2015 (2003).

Identification of a Unique Stability Propagation Site that Controls Protein Stability of α -Tropomyosin: a Two-Stranded α -Helical Coiled-coil

Janine B. Mills¹, Stanley C. Kwok¹, Lawrence B. Smillie² and Robert S. Hodges¹

¹*Department of Biochemistry & Molecular Genetics, University of Colorado at Denver and Health Sciences Center, Aurora, CO, 80045, USA;* ²*Department of Biochemistry, University of Alberta, Canada*

Introduction

Our laboratory demonstrated the relative contribution of all 19 amino acid residues in the hydrophobic core “a” and “d” positions to coiled-coil stability (excluding Pro which is not found in the core of coiled-coils) [1,2]. These results allowed us to define residues in the hydrophobic core as either stabilizing (Ile, Leu, Val, Met, Phe, and Tyr) or destabilizing residues (remaining). We then showed the importance of hydrophobic clusters of stabilizing residues in the core “a” and “d” positions [3].

Sequence analysis of highly conserved and ubiquitous coiled-coil proteins differing dramatically in sequences, function, and length showed that tropomyosin (284 res.) and myosin heavy chain domain (1086 res.) had remarkable similarity in the following ways: first, the percentage of stabilizing residues or destabilizing residues in the hydrophobic core was 58% and 42%, respectively; second, in both coiled-coils, these residues are organized into stabilizing and destabilizing clusters that are well distributed along the molecules. The stabilizing clusters are generally comprised of 3 to 5 consecutive stabilizing residues in the hydrophobic core [3,4].

It was our hypothesis that there is a region in tropomyosin responsible for initiating and controlling the stability of the native protein which we have referred to as a “stability propagation site”. That is, the stability of the native protein would not be obtained without this region and that all constructs of different lengths of tropomyosin sequence having this region would be of the same stability, while regions lacking this sequence would be significantly less stable.

Results and Discussion

Seven recombinant proteins (1-81, 1-92, 1-99, 1-119, 1-131, 1-260, and 1-284) were prepared and their oligomerization states and thermal stabilities characterized at physiological pH to identify the stability propagation site and the possible non-covalent interactions responsible for the unique properties of this site.

All tropomyosin constructs were fully folded as shown by two representative CD spectra at 5°C in benign conditions (50 mM PO₄ buffer, pH7, containing 100 mM KCl) and in 50% TFE (Fig. 1, top panel). To our surprise, the T_m value (the transition temperature where 50% of the structure is lost) for 1-119 was 42°C, similar to all longer constructs, including the native protein, and 16°C higher than the three shorter constructs 1-81, 1-92, 1-99 (Fig. 1, bottom panel).

These results located the stability propagation site in tropomyosin to the region 100-119. Examination of the sequence in this region suggested that the heptad sequence 112-118 was most likely the site of interest. Figure 2 shows that this sequence contains a series of i to i+3 and i to i+4 intrachain electrostatic attractions and interchain i to i'+5 electrostatic interactions. Even though a destabilizing Ala

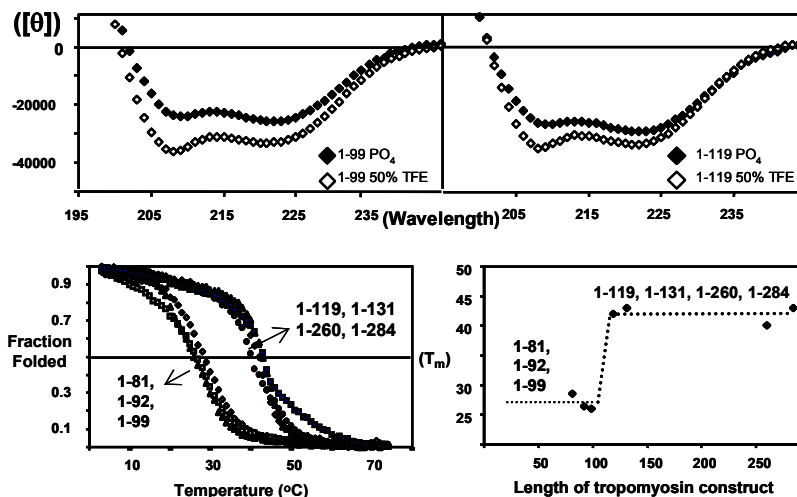


Fig. 1. Secondary structure and stability of Tropomyosin constructs.

residue [2] is observed in the hydrophobic core “d” position, the size of the Ala side-chain could be critical in optimizing the strength of the interchain electrostatic attractions overcoming the loss in stability from the decreased hydrophobicity of Ala. Thus we postulate that this is the critical stability propagation site in tropomyosin (Fig. 2).

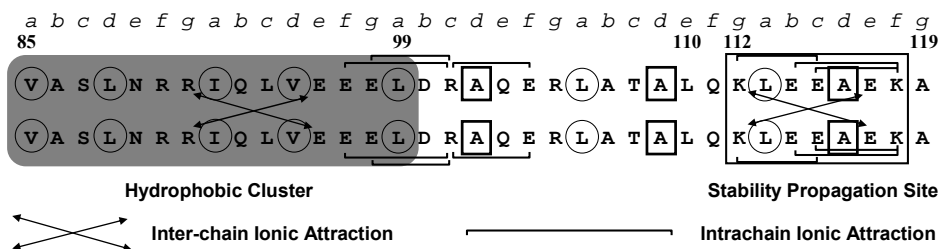


Fig. 2. Position of stabilizing intra- and inter-chain electrostatic interactions.

References

1. Wagschal, K., Tripet, B., Lavigne, P., Mant, C. and Hodges, R. S. *Prot. Sci.* **8**, 2312-2329 (1999).
2. Tripet, B., Wagschal, K., Lavigne, P., Mant, C. and Hodges, R. S. *J. Mol. Biol.* **300**, 377-402 (2000).
3. Kwok, S. C. and Hodges, R. S. *J. Biol. Chem.* **279**, 21576-21588 (2004).
4. Lu, S. M. and Hodges, R. S. *Prot. Sci.* **3**, 714-726 (2004).

The Introduction of Uncharged α -Hydroxymethyl Amino Acid Residues in Substrate Specificity P₁ Position of Trypsin Inhibitor SFTI-1 from Sunflower Seeds Retains its Activity

**Ewa Zablotna¹, Agnieszka Kret¹, Anna Jaśkiewicz¹, Aleksandra Olma²,
Mirosław T. Leplawy² and Krzysztof Rolka¹**

¹*Faculty of Chemistry, University of Gdańsk, Gdańsk, Poland;* ²*Institute of Organic Chemistry, Technical University of Łódź, Łódź, Poland*

Introduction

Isolated in 1999 from sunflower seeds, SFTI-1 is the smallest and the most potent peptidic trypsin inhibitor known so far [1]. This homodetic 14-amino-acid peptide containing a disulfide bridge (Fig. 1) and possessing a well-defined structure became an attractive object for studying enzyme-inhibitor interactions. Residues Lys⁵ and Ser⁶ constitute the inhibitor reactive site P₁-P₁'. In earlier papers we have shown that the acyclic analog of this inhibitor (containing the disulfide bridge only) displays almost the same trypsin inhibitory activity and proteolytic stability as the parent compound [2]. In the case of canonical inhibitors, the inhibitor P₁ position is responsible for up to 50% of contacts with the target enzyme, and therefore it is often referred to as the primary specificity residue. In the case of trypsin canonical inhibitors the P₁ position is occupied by Lys or Arg and the electrostatic interactions of the positively charged side chain of this amino acid residue with the deprotonated β -carboxyl group of trypsin Asp¹⁸⁹ is probably the best known protein-protein interaction. An interesting feature of the inhibitor – serine proteinase complexes is the presence of a hydroxyl group positioned very close to the P₁-P₁' reactive site. In the majority of inhibitors the -OH group is provided by a water molecule trapped in a "cage" constituted by the inhibitor superstructure. In some inhibitors, however, the -OH group is provided by a Ser residue incorporated in an adjacent fragment of the inhibitor backbone. It could be that this hydroxyl group somehow subverts the function of the enzyme catalytic triad.

In order to investigate the role of the -OH group positioned close to the inhibitor P₁-P₁' reactive site in the enzyme-inhibitor interactions a series of acyclic analogs of SFTI-1 modified in position P₁ by α -hydroxymethylvaline (HmVal) and α -hydroxymethylserine (HmSer) were synthesized: [(R)HmVal⁵]SFTI-1, [(S)HmVal⁵]SFTI-1, [(R,S)HmVal⁵]SFTI-1, [HmSer⁵]SFTI-1. As reference compounds, analogs with unmodified, proteinogenic Val and Ser in the discussed position were also obtained. The inhibitory activity of all the synthesized SFTI-1 analogs against bovine β -trypsin was also determined.

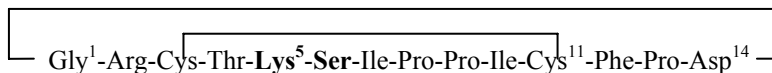


Fig. 1. Primary structure of SFTI-1.

Results and Discussion

All SFTI-1 analogs were synthesized manually by the solid-phase method using Fmoc chemistry as described previously [2]. (R,S)HmVal and HmSer were synthesized by selective α -hydroxymethylation of the respective oxazolone derived from N-BzVal or copper complex of Gly respectively [3]. Racemic HmVal was

Table 1. Association equilibrium constants (K_a) of SFTI-1 analogs with bovine β -trypsin

Inhibitor	K_a [M^{-1}]
SFTI-1	1.1×10^{10}
[(R)HmVal ⁵]SFTI-1	6.5×10^8
[(S)HmVal ⁵]SFTI-1	5.5×10^8
[(R,S)HmVal ⁵]SFTI-1	7.0×10^8
[HmSer ⁵]SFTI-1	1.4×10^9
[Val ⁵]SFTI-1	inactive
[Ser ⁵]SFTI-1	6.0×10^7

resolved into enantiomers by fractional crystallization of diastereomeric salt of its N-benzoyl derivative with (-)-quinine as described previously [4]. In the case of HmSer the hydroxyl groups were protected in form of isopropylidene derivatives [5], whereas the -OH groups of HmVal derivatives remained unprotected during peptide synthesis.

Determined K_a values for the peptides studied (Table 1) clearly indicated that the replacement of Lys⁵ present in position P₁ of the trypsin inhibitor SFTI-1 by uncharged Val and Ser additionally substituted at the α carbon with hydroxymethyl group affects the peptide's trypsin inhibitory activity. In comparison with wild SFTI-1, the analog containing HmSer is only 10 times less active. Moreover, analogs containing in this position both enantiomers of HmVal inhibited trypsin activity only less than two orders of magnitude weaker. The reference compound [Val⁵]SFTI-1 was practically inactive against trypsin, also the K_a value determined for [Ser⁵]SFTI-1 was significantly lower than that obtained for [HmSer⁵]SFTI-1. In the case of SFTI-1 analogs modified in position P₁ with HmVal and HmSer the above-mentioned electrostatic interaction between the inhibitor and the enzyme was probably effectively replaced by additionally formed hydrogen bond(s) between the α -hydroxymethyl group of the amino acid residue present in the inhibitor P₁ position and, most probably, the backbone of the enzyme. Therefore we believe that the SFTI-1 analogs described here belong to a novel class of serine proteinase inhibitors. This hypothesis will be verified by X-ray studies of complexes formed by trypsin with these STTI-1 analogs (analyses in progress).

Acknowledgments

This work was supported by the University of Gdansk under grant BW/8000-5-0281-5 and by the Polish State Committee for Scientific Research (KBN), grant No. 1007/T09/2003/24.

References

1. Luckett, S., *et al.* *J. Mol. Biol.* **290**, 525-533 (1999).
2. Zabłotna, E., *et al.* *Biochem. Biophys. Res. Commun.* **292**, 855-859 (2002).
3. Kamiński, Z. J. and Leplawy, M. T. *Synthesis* 292-293 (1974); Kociolek, K., *et al.* In *Peptides 1986, Proceedings of the 19th European Peptide Symposium* (Theodoropoulos, D., ed) De Gruyter, Berlin, p.251 (1987).
4. Olma, A., Lachwa, M. and Lipkowski, A. W. *J. Peptide Res.* **62**, 45-52 (2003).
5. Stasiak, M., Wolf, W. M. and Leplawy, M. T. *J. Peptide Sci.* **4**, 46-57 (1998).

Molecular Simulation of an α/ϵ -Peptide Dendrimer

Qitao Yu¹, Yuguang Mu², Lars Nordenskiöld² and James P. Tam^{1,2}

¹Department of Biomedical Sciences, The Scripps Research Institute Florida, Jupiter, FL 33458, USA; ²School of Biological Sciences, Nanyang University, Singapore 637551

Introduction

In developing peptide dendrimers as potential therapeutics, we have found that certain α/ϵ -peptide dendrimers such as D4R4 (Fig. 1A) are proteolytic resistant and broadly active with minimum inhibitory concentrations averaging about 1 μ M against 10 test microbes that include bacteria and fungi under both low- and high-salt conditions [1]. D4R4 has an α/ϵ -Lys scaffold that tethers four tetrapeptides RLYR. We reasoned that its antimicrobial activity might have a correlation to form an ordered structure. Because D4R4 contains short peptide strands, we also reasoned that it likely adopted a β -sheet structure mimicking amphipathic antimicrobial peptides such as protegrins or tachypasins. Structure determination of peptide dendrimers containing repeating units is difficult by NMR due to overlapping peaks. Here, we describe the use of Molecular Dynamics (MD) simulation to sample conformation of α/ϵ -peptide dendrimer D4R4.

Results and Discussion

CD measurements of ϵ -dendrimers suggested the presence of β -structure with a weak negative trough around 217 nm, characteristic of a β -sheet structure from poly- ϵ -Lys [2]. To characterize a β -like structure of D4R4, MD simulation was used to sample its conformations using the radius of gyration (Rg), a quantity reflecting the folded state of a molecule. In general, Rg is small in a well folded molecule, but is large in unfolded states [3]. After 40-nanosecond simulation at 400°K, a reasonable sampling was obtained. Comparing the Rg of residues Tyr and Leu that form the hydrophobic LY-core of D4R4 with the whole molecule, we found that its Rg was significantly smaller than that of the whole molecule (Fig. 2).

These results suggest D4R4 is able to fold onto its nonpolar LY-core with the

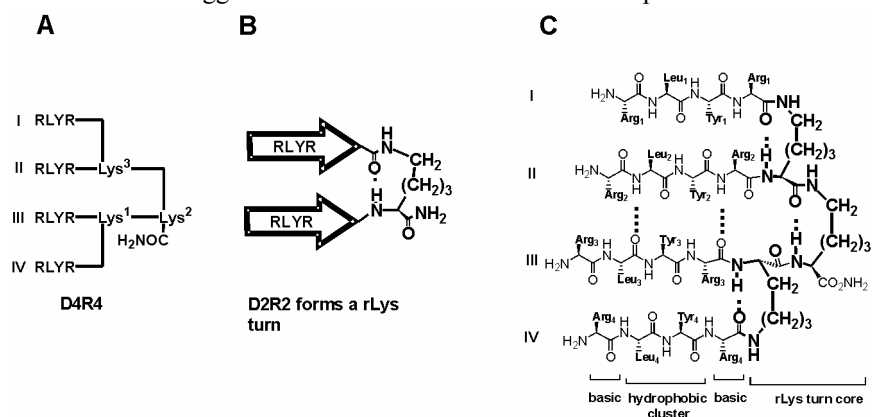


Fig. 1. Schematic representation of dendron D4R4 (A), the putative γ -turn of D2R2 (B), and proposed dimmer-of-dimer structure of dendrons D4R4 (C).

charged residues facing outside. For comparison, MD simulation of D4R4(Orn) replacing Lys by Orn as scaffold showed that the extension of the LY-core was slightly larger than that of the whole molecule, suggesting the inability of D4R4(Orn) to fold properly. Because D4R4 forms a dimer-of-dimer consisting of two halves of D2R2, preliminary NMR study of the dimer D2R2 showed that Lys-scaffold could form a reverse Lys (rLys) turn connecting two parallel strands of RLYR (Fig. 1B) consistent with the findings by Gellman's group [4] whereas Nowick's group found that Orn turn could stabilize only antiparallel strands [5].

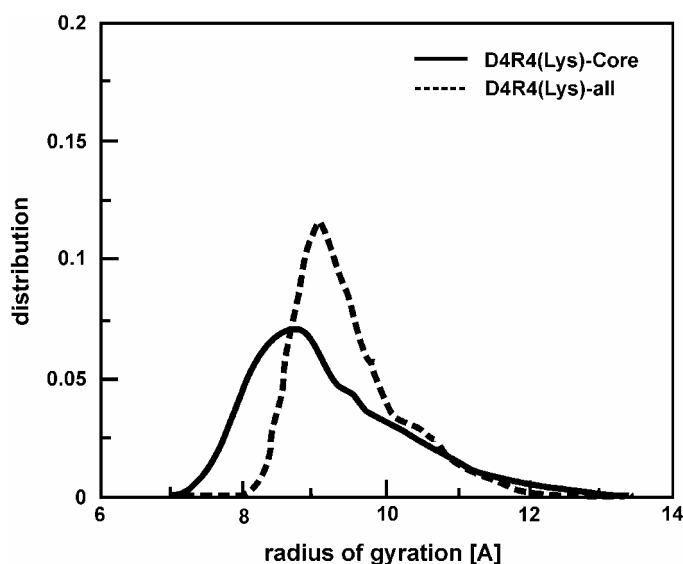


Fig. 2. Radius of gyration of D4R4 molecule and D4R4 Core.

Based on these results, we propose that D4R4 forms a dimer-of-dimer. Each half of this dimer-of-dimer contains two parallel chains connected by a reverse-Lys (rLys) turn (Fig. 1B). Both dimers are then connected by a third rLys turn to produce the dimer-of-dimer of D4R4 that folds into a 4 β -stranded structure (Fig. 1C).

Acknowledgments

This work was supported in part by US public Health Service grant EB001986.

References

1. Tam, J. P., Lu, Y. -A. and Yang, J. -L. *Eur. J. Biochem.* **269**, 923-932 (2002).
2. Shima, S., Matsuoka, H., Iwamoto, T. and Sakai, H. *J. Antibiotics* **37**, 1449-1455 (1984).
3. Duang, Y., Wang, L. and Kollman, P. A. *Proc. Natl. Acad. Sci. USA* **95**, 9897-9902 (1998).
4. Stanger, H. E. and Gellman, S. H. *J. Am. Chem. Soc.* **120**, 4236-4237 (1998).
5. Nowick, J. S. and Brower, J. O. *J. Am. Chem. Soc.* **125**, 876-877 (2003).

A GHS-1a Receptor Agonist that is Highly Effective in Stimulating Body Weight Gain

Jesse Z. Dong, John Eynon, Jundong Zhang, John E. Taylor, Heather A. Halem, Rakesh Datta and Michael D. Culler

IPSEN Group, 27 Maple Street, Milford, MA 01757, USA

Introduction

Ghrelin, a 28 amino acid octanoylated peptide, has been identified as an endogenous ligand for the growth hormone (GH) secretagogue (GHS) receptor [1]. In addition to stimulating GH secretion, ghrelin increases food intake and induces body weight gain [2]. Due to its unique biological effects on appetite and positive energy balance, ghrelin is considered as a viable target for developing therapeutic agents for the treatment of cachexic and anorexic disorders. In an effort to search for ghrelin analogs that are more suitable for therapeutic use, we have discovered a pentapeptide that has higher GHS-1a receptor binding affinity and longer plasma half-life than human ghrelin (h-ghrelin).

Results and Discussion

The initial screening of a series of peptides against the GHS-1a receptor revealed that the pentapeptide Inp-D-Bpa-D-Trp-Phe-Lys-NH₂ binds to the receptor with moderate binding affinity (peptide #1, K_i=93.8nM, Table 1). A significant improvement in the receptor binding was achieved when the second residue D-benzoylphenylalanine (D-Bpa) and the fourth residue Phe in the peptide were replaced with D-2Nal and 2-thienylalanine (Thi), respectively. The resulting peptide Inp-D-2Nal-D-Trp-Thi-Lys-NH₂ has sub-nanomolar binding affinity to the GHS-1a receptor (peptide #2, K_i=0.45nM), which is ~2-fold more potent than h-ghrelin (K_i=0.45nM vs. 0.89nM, respectively).

Table 1. GHS-1a receptor binding affinity

Peptide	Sequence	GHS-1a Receptor Binding Affinity, K _i (nM) ^a
#1	Inp-D-Bpa-D-Trp-Phe-Lys-NH ₂	93.8
#2	Inp-D-2Nal-D-Trp-Thi-Lys-NH ₂	0.45
human ghrelin		0.89

^aMembranes prepared from GHS-1a/CHO-K1 cells were incubated with [¹²⁵I]ghrelin, with or without unlabeled competing test peptides. The membrane-bound radioactivity was counted by gamma spectrometry, which was used in the K_i calculation.

The plasma stability of Inp-D-2Nal-D-Trp-Thi-Lys-NH₂ was studied in comparison with that of h-ghrelin. The *in vitro* half-life of the pentapeptide in rat plasma was ~4.5 hours compared to ~1.9 hours of h-ghrelin. The relatively long plasma half-life of the synthetic pentapeptide is presumably due to the presence of D-amino acids, Thi and isonipecotic acid (Inp) that protect the peptide bonds against enzymatic cleavage.

To examine the ability of Inp-D-2Nal-D-Trp-Thi-Lys-NH₂ in stimulating body weight gain, male, Sprague Dawley rats were injected 3x/day, ip, with the peptide at the dose of 40 nmole/kg or vehicle for 7 days. Treatment with the peptide induced a progressive, dose-related increase in body weight gain that reached ~10g over that of vehicle-treated controls by day 7 (Fig. 1).

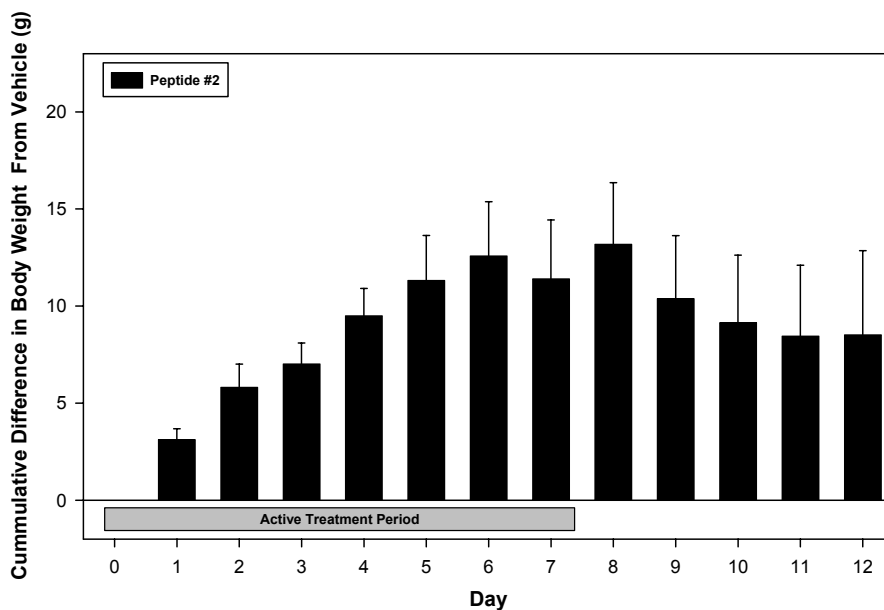


Fig. 1. Body weight gain induced by Inp-D-2Nal-D-Trp-Thi-Lys-NH₂ in male, Sprague Dawley rats.

Taken together, due to its high GHS-1a receptor binding affinity and long plasma half-life, the pentapeptide Inp-D-2Nal-D-Trp-Thi-Lys-NH₂ is highly efficacious in stimulating body weight gain in rats.

References

1. Kojima, M., Hosoda, H., Date, Y., Nakazato, M., Matsuo, H. and Kangawa, K. *Nature* **402**, 656-660 (1999).
2. Nakazato, M., Murakami, N., Date, Y., Kojima, M., Matsuo, H., Kangawa, K. and Matsukura, S. *Nature* **409**, 194-198 (2001).

A Non-Competitive Peptide Agonist of GHSR1a Receptor Stimulates Growth Hormone Secretion and Food Intake

Abdelkrim Habi¹, Patric Delhanty², Daniel Abran¹, Aart Jan van der Lely² and Krishna G. Peri¹

¹Theratechnologies Inc., 2310 Alfred-Nobel Blvd, Montreal (Saint-Laurent), Quebec, H4S 2A4, Canada; ²Department of Internal Medicine, Erasmus MC, Rotterdam, The Netherlands

Introduction

Ghrelin is a 28 amino acid acylated peptide identified as the endogenous ligand for the GHSR-1a receptor. In addition to its central actions of growth hormone (GH) secretion, ghrelin stimulate feeding and weight gain. G protein-coupled receptors (GPCR) undergo conformational changes during activation by the ligand; these changes include the movement of one or more transmembrane domains and intra and extracellular loops. Exopep™ technology comprises selection of small peptides (8-9 aa long) from the putative interacting surfaces of GPCR domains which could participate in the above conformational changes. ExoPep™ peptides are tested in cell-based assays or directly in animals to select agonistic or antagonistic peptide leads. In this report, we describe the characterization of a lead peptide #1 and its optimized derivative #2 which are potent allosteric agonists of GHSR1a.

Ghrelin is a peptide hormone produced mainly in the stomach, which stimulates a strong GH-releasing activity upon activation of the pituitary GHSR-1a receptor. Other major effects of ghrelin include appetite stimulation, positive energy balance, gastric motility and acid secretion, modulation of pancreatic exocrine and endocrine function as well as glucose levels. Binding of ghrelin to the GHSR-1a activates the phospholipase C pathway, leading to increased inositol phosphate turnover and protein kinase C activation, followed by the release of Ca²⁺ from intracellular stores. Compound #1 and its optimized peptide #2 are designed based on the secondary structure of human GHSR1a using ExoPep™ technology. Our results show the characterization of these peptide agonists in *in vitro* and *in vivo* assays.

Results and Discussion

To produce a GHSR1a-selective allosteric modulator, an octa- to decapeptide Exopep™ library based on the primary sequence of the GHSR-1a receptor was screened in *in vitro* assays and in animals. A structure-activity relationship studies, focusing on N-terminus, C-terminus, and amino acid substitution were performed on the dodecapeptide lead compound #1 (EC₅₀ 20 nM) to identify the minimal sequence able to effect GHSR1a agonism, and critical amino acid residues responsible for agonist activity. This optimization resulted in a potent agonist, compound #2 (EC₅₀ 2 nM in Ca²⁺ mobilization assays). Neither of these compounds displaced bound ¹²⁵I-ghrelin in membranes prepared from GHSR1a-expressing cells. Ghrelin and compound #2 (30 µg/kg iv) equipotently stimulated GH (C_{max} 577± 94; 509 ± 222 ng/ml; AUC_{60min} 9784 ± 1519; 8689 ± 3558 ng/ml/h, respectively) in Sprague-Dawley rats and increased GH secretion, cumulative food intake and weight gain in CD-1 mice (Fig. 1). Neither compounds increased basal blood glucose levels in 4hr-fasted rats. Compound #2 is distinct in its interaction with GHSR1a receptor and could be used to discriminate ghrelin's actions arising from other ghrelin receptors.

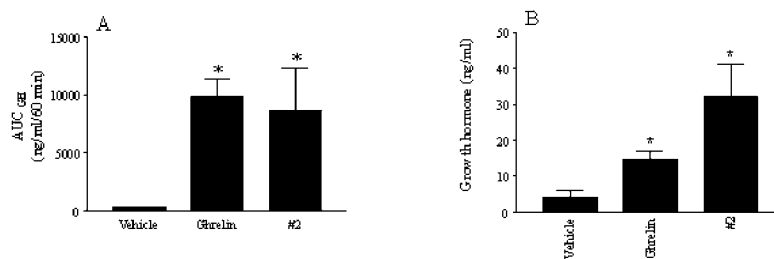


Fig. 1. Effects of ghrelin and #2 on GH secretion in 4 hr fasted Sprague-Dawley rats (A) and overnight fasted CD-1 mice (B). Vehicle, ghrelin or #2 were given to (A) Sprague-Dawley rats (30 μ g/kg iv; GH AUC_{2hr}) and (B) CD-1 mice (400 μ g/kg sc; GH levels at 5 min post-injection). Data are Mean \pm SEM; n=4; * p < 0.05 vs vehicle.

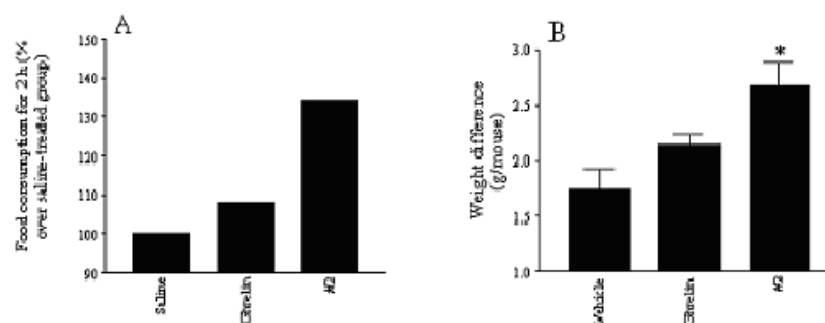


Fig. 2. Effects of Ghrelin and #2 on food intake in CD-1 mice. Ghrelin or #2 (400 μ g/kg sc) were given to overnight fasted CD-1 mice. A). Food consumption for the following 2 hrs is shown as percent of saline-treated group. B). The weight difference of the mice before and 2 hrs after peptide injections. Data are Mean \pm SEM; n=4; * p < 0.05 vs vehicle.

Conclusion

Compound #2 is a potent allosteric agonist of GHSR1a receptor for ghrelin. Similar to its parent compound #1, #2 displayed non-competitive binding to GHSR1a-expressing cells and did not displace bound ¹²⁵I-ghrelin. #2 and #1 increased GH secretion and food consumption (Fig. 2); #2, unlike ghrelin, did not have a significant acute effect on blood glucose levels in fasted mice. #2 appears to be an allosteric agonist of the pituitary ghrelin receptor.

Development of μ Opioid Receptor Selective 4-Anilinidopiperidine Analogs

Yeon Sun Lee¹, Joel Nyberg¹, Sharif Moye¹, Richard Agnes¹, Adriano Mollica¹, Peg Davis², Shou-Wu Ma², Josephin Lai², Frank Porreca², Ruben Vardanyan¹ and Victor J. Hruby¹

¹Department of Chemistry; ²Department of Pharmacology, University of Arizona, Tucson, AZ 85721, USA

Introduction

Since the discovery of fentanyl in 1962 [1], which is a highly potent synthetic analgesic, the 4-anilinidopiperidines have been exploited for developing highly selective μ opioid agonists with specific pharmacological properties. Here, new fentanyl analogs in which the phenethyl group on the piperidine ring was replaced by several aromatic ring-substituted amino acids, *N*-(1-substituted piperidin-4-yl)-*N*-phenyl-propionamide, were designed and synthesized to study the biological effect of these substituents on the opioid receptors. Furthermore we tested the hypothesis that these analogs should show high μ opioid receptor selectivity over δ opioid receptor based on the message-address concept (Fig. 1).

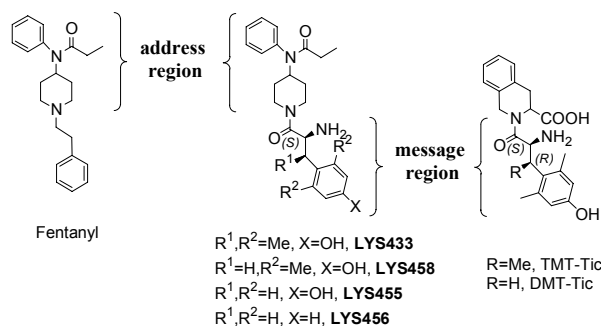


Fig. 1. Opioid ligands.

Results and Discussion

New 4-anilinidopiperidine analogs were prepared by coupling several kinds of aromatic ring substituted amino acids to the *N*-phenyl-*N*-piperidin-4-yl-propionamide using BOP/HOBt/NMM in solution. After deprotection of Boc group with TFA, crude compounds were isolated by RP-HPLC to give pure (more than 98%) 4-anilinidopiperidine analogs. The synthesized analogs except the β -amino acid substituted one showed high selectivity for μ opioid receptor over δ opioid receptor, which was expected from the address region of fentanyl structure.

One of the analogs, **LYS458** in which 2,6-dimethyltyrosine was substituted to 1-position of piperidine ring showed high binding affinities at both μ and δ opioid receptors ($K_i = 49$ and 47 nM, respectively) (Table 1). In addition to bioassays, molecular modeling experiments using MacroModel 8.1 were performed yielding some clues to the determinants of opioid activity and selectivity. The experiment on **LYS433** [2] gave a topographically identical structure to the same part of fentanyl,

Table 1. Binding affinities and functional assays at δ and μ opioid receptors

compd	hDOR(Ki, nM)	rMOR(Ki, nM)	selectivity δ/μ	MVD	GPI
	³ [H]DPDPE	³ [H]DAMGO		IC ₅₀ (nM)	IC ₅₀ (nM)
LYS433	350	400	0.9	13% at 1 μ M	3300
LYS458	49	47	1.0	2% at 1 μ M	45% at 1 μ M
LYS455	16000	7700	2.1	18% at 1 μ M	8% at 1 μ M
LYS456	6900	3900	1.8	0% at 1 μ M	2% at 1 μ M

which is considered to play an important role in opioid selectivity, and gave a longer length between the two ends of the molecule than the other three compounds (Fig. 2). Contrarily, the lowest energy conformer of **LYS458** looked similar to the bioactive conformation of Dmt-Tic [3], even though the two aromatic rings were not oriented parallel. It was interesting that the conformer fully matched the structure which was obtained from X-ray crystallography. **LYS455** and **LYS456** which had no significant differences in these biological activities showed completely superimposed lowest energy conformations with the two aromatic rings perpendicularly oriented, demonstrating that the hydroxyl group is not necessary for μ opioid activity. From these results, it is proposed that the constraint caused by the three methyl groups serve as the most critical factor of determining conformation, and further modification in message region will give increased μ opioid activity in the case of extension of molecular length to the linearity of fentanyl.

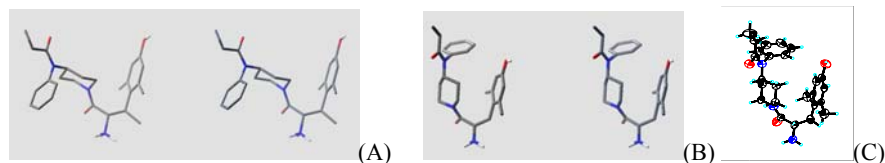


Fig. 2. Stereoviews of the lowest energy conformers of (A) **LYS433** and (B) **LYS458**, and (C) X-ray diffraction structure of **LYS458**.

Acknowledgments

The work was supported by grants from the USPHS and NIDA (VJH).

References

1. Janssen, P. A. J. *Br. J. Anaesth.* **34**, 260-268 (1962).
2. Qian, X., Russel, K. C., Boteju, L. W. and Hruby, V. J. *Tetrahedron* **51**, 1033-1054 (1995).
3. Bryant, S. D., George, C., Flippen-Anderson, J. L., *et al.* *J. Med. Chem.* **45**, 5506-5513 (2002).

A Whole-Cell Binding Assay for Testing the Targeting Potential of Cyclic Peptide Ligands

Sonya Cressman¹, Ning Fang², David D. Y. Chen² and Pieter R. Cullis¹

¹Department of Biochemistry; ²Department of Chemistry, University of British Columbia, Vancouver, BC, Canada

Introduction

The study of membrane surface receptor binding with peptides should be conducted with intact cell membranes because the elements of intercellular communication such as nutrient receptors, adhesion foci, and surface bound enzymes, are then present. The use of whole-cell binding assays is complicated by the variable nature of protein expression *in vitro*, therefore, a relationship between the number of targeted receptors, the number of whole cells, and the amount of targeting peptide needs to be established.

Cyclic RGD-containing pentapeptides and higher conjugates have been shown to bind the $\alpha v \beta 3$ integrin receptor in receptor-immobilized inhibition assays [1-3] and exhibit *in vivo* anti-angiogenic activity [4]. This activity has led to the progression of Cilengitide™(cRGDnmefV) into the clinic, and has also led to higher conjugates being employed with success in tumor imaging [4,5]. Targeting angiogenesis with these sequences could lead to a powerful and generalized anticancer strategy.

In order to develop a whole-cell binding assay, we have designed an experiment where cyclic RGD-containing peptides that bind to $\alpha v \beta 3$ integrin-expressing, human umbilical vein endothelial cells (HUVEC) were compared using flow cytometry (FACS).

Recently, the use of capillary electrophoresis (CE) with laser induced fluorescence detection (LIF) has attracted attention because of the short analysis time and sensitivity [6]. We chose to use this technique to determine the concentration of bound peptide since Scatchard curves require high sensitivity and low concentrations. Our goal is to use this assay to bridge chemistry and biology and to understand how targeted receptor expression and *in vitro* binding of cyclic peptide analogues are related.

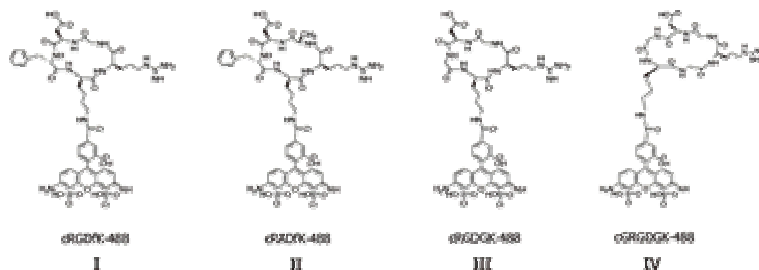


Fig. 1. RGD-containing analogs I, III and IV were tested for binding. I is hypothesized to fix the cycle in a $\beta II/\gamma$ turn arrangement and best antagonizes the $\alpha v \beta 3$ receptor. II exhibits low receptor binding due to steric effects, III exhibits flexibility of R and D side chains and improved solubility, and IV exhibits additional flexibility but decreased specificity [2].

Results and Discussion

Peptides in Figure 1 were synthesized as previously described [7]. Fully protected and cyclic peptides were purified by preparative RP-HPLC. A one-hour deprotection with 90% TFA in DCM, H₂O, and TIS scavengers produced hydrophilic peptides for characterization. Ether precipitated peptides were conjugated to Alexafluor488-TFP(Molecular Probes) in DMF. Purification on a semi-preparative scale resulted in a final product that was validated by MALDI-MS, and CE/LIF.

CE analyses were done on a Beckman Coulter ProteomeLab PA800. LIF detection of 520nm emission upon 488nm excitation produced peak areas that were integrated for peptide quantity. We found that CE/LIF provided a more reliable analysis of final conjugates than analytical RP-HPLC. Peptide analogs III and IV were particularly difficult to purify since they impart a minimal hydrophobic shift.

HUVEC (Cascade Biologics) were grown in the presence of basic Fibroblast Growth Factor (Cascade Biologics), known to promote $\alpha v\beta 3$ -mediated angiogenesis [8]. The same population of cells was assayed for binding of compounds I-IV, with II as a negative control shown in Figure 2.

Binding of II reaches a maximum at a lower concentration than those of the non-hindered analogues. In this experiment, the RGD compounds exhibited increased cell binding with concentration, however a maximum was not achieved. The agreement between replicates is encouraging, lending confidence to the application of this assay for relating targeted receptor expression, peptide concentration and binding affinity.

Future work will examine the effect of water soluble, versus a less hydrophilic, bracket around RGD by competitive kinetic measurement. Long-term application of this strategy may lead to other ligand-target approaches and has the potential for miniaturization.

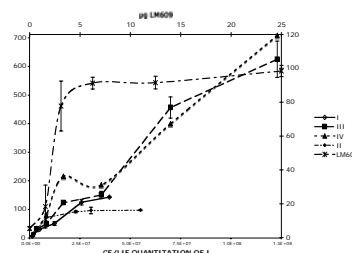


Fig. 2. HUVEC binding curves. The left and right y axes were obtained from FACS data as the mean fluorescence intensity of a fixed number of events. The left and bottom axes describes peptide I-IV binding. The top x axis describes the amount of $\alpha v\beta 3$ specific antibody (LM609, Chemicon) and the right y axis is adjusted to show the full curve from with FITC-goat- α -mouse (Chemicon) secondary labeling.

Acknowledgments

This work was funded by Inex Pharmaceuticals Corporation, the Canadian Institute for Health Research and the Natural Sciences and Engineering Research Council of Canada.

References

1. Marchi-Artzner, V., *et al. Langmuir* **19**, 835-841 (2003).
2. Dechantsreiter, M. A. *J. Med. Chem.* **42**, 3033-3040 (1999).
3. Achilefu, S., *et al. Proc. Natl. Acad. Sci. USA* **102** 7976-7981 (2005).
4. Conti, P. S., *et al. Mol. Imaging and Biology* **6**, 350-359 (2004).
5. Smith, J. W. *Curr. Opin. Investig. Drugs* **6**, 741-5 (2003).
6. Lacroix, M., Poinso, V., Fournier, C. and Couderc, F. *Electrophoresis* **26**, 1-14 (2005).
7. Haubner, R., *et al. J. Amer. Chem. Soc.* **118**, 7461-7472 (1996).
8. Eliceiri, B. P. and Cheresch, D. A., *Cancer J.* **6**, Suppl 3:S245-249 (2000).

Synthesis and Evaluation of Chiral and Achiral α,α -Disubstituted Amino Acids as β -Sheet Stabilizing Factors

Jia Wang and Robert P. Hammer

Department of Chemistry, Louisiana State University, Baton Rouge, LA 70803, USA

Introduction

A number of diseases including Alzheimer's disease and prion disease are caused by protein misfolding into β -sheet structures. An increased understanding of what factors control or stabilize β -sheet structures may lead to insights into the underlying causes of these diseases and suggest possible treatments for such protein misfolding disorders [1]. Modeling studies suggest that $C^{\alpha,\alpha}$ -disubstituted amino acids ($\alpha\alpha$ AAs) with side-chains larger than ethyl (both chiral and achiral) can stabilize β -strand conformations and may also create additional stabilizing intrastrand and interstrand side-chain interactions for sheet-like structures. Synthesis of chiral $\alpha\alpha$ AAs often involves the use of chiral auxiliaries. To streamline the synthesis of highly functionalized $\alpha\alpha$ AAs, we preferred to use a catalytic method which would minimize the need for protection and deprotection chemistries. Herein we report the syntheses of several chiral $\alpha\alpha$ AAs utilizing the method of Maruoka and coworkers which utilized a chiral phase transfer catalyst [2].

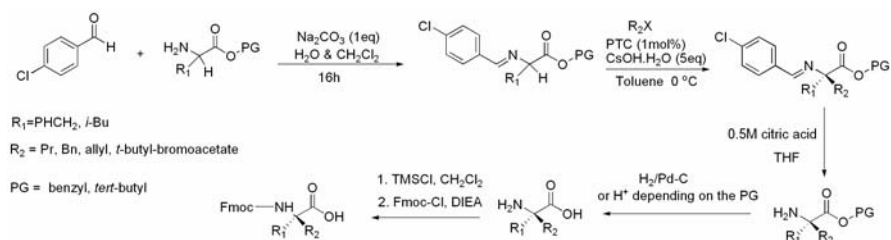
Results and Discussion

Schiff base was formed by a reaction of amino esters with 4-chloro-benzylaldehyde using Na_2CO_3 in H_2O and DCM (Scheme 1). Schiff base has the added bonus of acidifying the α -proton. The resulting carbon-nitrogen double bond stabilized the carbanion which was then reacted with an electrophile to form a new carbon-carbon bond under chiral phase transfer catalytic conditions using a chiral quaternary ammonium salt (PTC). Cleavage of the imine under acidic condition provided chiral amino ester in good yields with high to moderate enantiomeric excess as listed in Table 1.

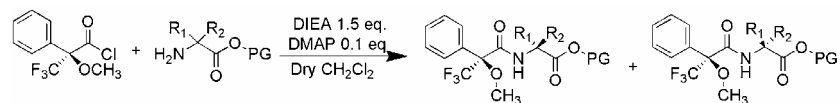
Table 1. Alkylation of Schiff base to form chiral $C^{\alpha,\alpha}$ -dialkylated amino ester

Entry	R_1	R_2X	PG	Chemical yield	% ee	Configuration
1	PhCH_2	allyl bromide	Bn	52%	91	S
2	PhCH_2	1-bromopropane	Bn	60%	89	S
3	<i>i</i> -Bu	benzyl bromide	<i>i</i> -Bu	66%	77.8	R
4	<i>i</i> -Bu	allyl bromide	<i>i</i> -Bu	70%		
5	<i>i</i> -Bu	<i>t</i> -butyl-bromoacetate	Bn	42%		
6	<i>i</i> -Bu	allyl bromide	Bn	68%		

The enantiomeric excess of each $\alpha\alpha$ AA ester was determined by ^{19}F -NMR analysis of the Mosher amide (Fig. 1), which has been prepared from an optically pure compound $\text{R}-(-)\text{-}\alpha\text{-methoxy-}\alpha\text{-trifluoromethylphenylacetyl chloride}$ (MTPACl) and amino ester (Scheme 2) [3].



Scheme 1. Synthesis of chiral amino acids via chiral phase transfer alkylation.



Scheme 2. Preparation of Mosher amide for NMR study.

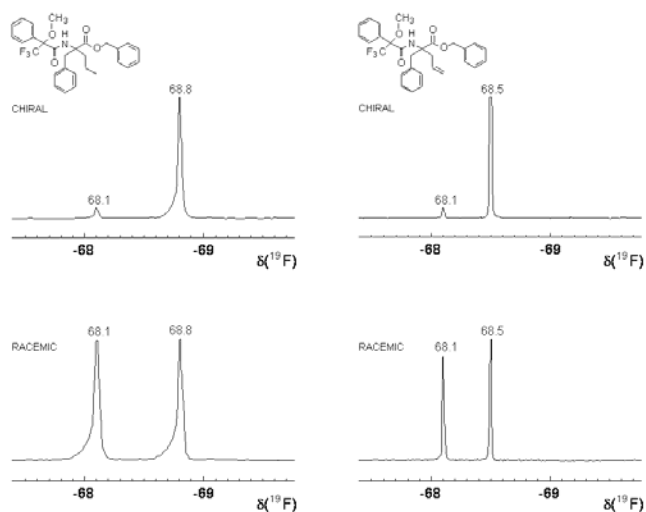


Fig. 1. ^{19}F NMR spectra of Mosher amides of the chiral and racemic amino acids.

Acknowledgments

We would like to acknowledge NIH for funding support.

References

1. Nesloney, C. L. and Kelly, J. W. *Bioorg. Med. Chem.* **125**, 739-766 (1996).
2. Ooi, T., Takeuchi, M., Kameda, M. and Maruoka, K. *J. Am. Chem. Soc.* **122**, 5228-5229 (2000).
3. Dale, J. A. and Mosher, H. S. *J. Org. Chem.* **90**, 3732-3736 (1968).

Evaluation of Malarial Protease Plasmepsin Inhibitors Containing Hydroxymethylcarbonyl Isostere

Koushi Hidaka¹, Tooru Kimura¹, Yumi Tsuchiya¹, Aiko Kiso¹, Yoshio Hayashi¹, Azin Nezami², Ernesto Freire² and Yoshiaki Kiso¹

¹Department of Medicinal Chemistry, Center for Frontier Research in Medicinal Science, 21st Century COE Program, Kyoto Pharmaceutical University, Kyoto 607-8412, Japan;

²Department of Biology, The Johns Hopkins University, Baltimore, Maryland 21218, USA

Introduction

Malaria parasites use hemoglobins of infected victims as a source of nutrients during their growth. In the case of most lethal *Plasmodium falciparum*, aspartic protease plasmepsin (Plm) I and II initiate hemoglobin digestion. These enzymes have become the target for the development of new antimalarial drugs, because their inhibition leads to the starvation of the parasite. Focusing on the similarity of substrate recognitions of Plm and HIV-1 protease, we identified some HIV protease inhibitors containing hydroxymethylcarbonyl as an ideal transition state mimic with potent Plm II inhibitory activities [1]. In the following study, we designed and synthesized a series of dipeptide-type inhibitors containing allophenylnorstatine-dimethylthioprolin scaffold against Plm II [2]. Among these compounds, KNI-10006 which has aminoindanol at the P₂' position was found to be a highly potent Plm II inhibitor with a K_i value of 0.5 nM. Interestingly, KNI-10006 is also a potent inhibitor for Plm I, IV and histo-aspartic protease (HAP), which participates in hemoglobin degradation [2]. To understand the high activity of KNI-10006, we searched for inhibitors fitting the S₂' space of Plm II [3]. From a SAR at the P₂' position, it is concluded that both the hydroxyl group and the indan structure of the aminoindanol of KNI-10006 are important for its tight binding. The activity of KNI-10006, however, attenuated significantly in *P. falciparum*-infected erythrocyte cultures. In an attempt to develop more potent antimalarial compounds, we synthesized inhibitors introducing various P₁ and P₂ ligands (Fig. 1.), and evaluated the Plm II inhibitory and antimalarial activities of the synthesized compounds.

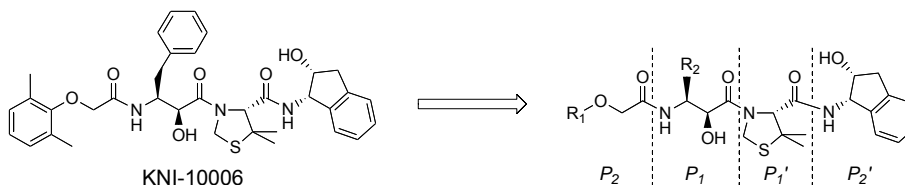


Fig. 1. Modifications at the P₁ and P₂ positions from KNI-10006.

Results and Discussion

Dipeptidic compounds introducing new ligands at the P₁ or P₂ position were prepared by the usual Boc strategy in the solution phase. Boc protected α -hydroxy- β -amino acids used as P₁ residues were synthesized via cyanohydrin intermediates from leucine and cyclohexylalanine. Inhibition constants (K_i) against Plm II and activities against *P. falciparum* in erythrocyte were obtained as described previously [1]. Compound **a**, which has an isobutyl side chain replaced from a benzyl group of KNI-10006 at the P₁ position, showed moderate Plm II inhibitory activity (Table 1).

Table 1. Inhibitory activities of synthetic compounds against Plm II and *P. falciparum*

Compound	R ₁ *	R ₂ *	Plm II	EC ₅₀
			K _i (nM)	(μM)
KNI-10006	2,6-dimethylphenyl	benzyl	0.5	6.8
a	2,6-dimethylphenyl	isobutyl	42	2.6
b	2,6-dimethylphenyl	cyclohexylmethyl	136	1.6
c	4-hydroxymethylphenyl	benzyl	10	1.1

*General structure is shown in Fig. 1.

Compound **b** introducing a larger aliphatic group, cyclohexylmethyl, exhibited low inhibitory activity. From these results, it is suggested that the S₁ pocket of Plm II favors the π -electron interaction or the planar character of phenyl ring. In spite of their low potencies against Plm II, their antimalarial activities were better than KNI-10006. For example, compound **b** showed only a ten-fold decrease in enzyme inhibition.

We also modified the phenoxyacetyl group at the P₂ position with mono- and disubstitutions. KNI-10006 having 2,6-dimethylphenoxyacetyl possessed the most potent Plm II inhibitory activity among the synthesized compounds. Interestingly, compound **c** (KNI-10125, Fig. 2.), which has relatively high Plm II inhibitory activity, exhibited a promising antimalarial activity. These results are useful for further modification of Plm inhibitors with potent antimalarial activity.

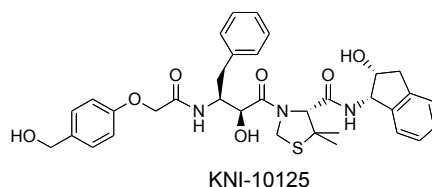


Fig. 2. Structure of KNI-10125.

Acknowledgments

This research was supported in part by the Frontier Research Program and the 21st Century Center of Excellence Program “Development of Drug Discovery Frontier Integrated from Tradition to Proteome” of the Ministry of Education, Culture, Sports, Science and Technology of Japan, and grants from the Ministry of Education, Culture, Sports, Science and Technology of Japan.

References

1. Nezami, A., Luque, I., Kimura, T., Kiso, Y. and Freire E. *Biochemistry* **41**, 2273–2280 (2002).
2. Nezami, A., Kimura, T., Hidaka, K., Kiso, A., Liu, J., Kiso, Y., Goldberg, D. E. and Freire E. *Biochemistry*, **42**, 8459–8464 (2003), highlighted in Editors’ Choice, *Science*, **301**, 143 (2003).
3. Kiso, A., Hidaka, K., Kimura T., Hayashi, Y., Nezami, A., Freire, E., and Kiso, Y. *J. Peptide Sci.* **10**, 641–647 (2004).

Design and Synthesis of β -Secretase Inhibitors: Optimization at the P_4 and P_1' Positions

Yoshio Hamada¹, Daisuke Shuto¹, Naoto Igawa¹, Soko Kasai¹, Ping Liu¹, Koushi Hidaka¹, Tooru Kimura¹, Yoshio Hayashi¹, Shoichi Ishiura² and Yoshiaki Kiso¹

¹Department of Medicinal Chemistry, Center for Frontier Research in Medicinal Science, and 21st Century COE Program, Kyoto Pharmaceutical University, Yamashina-ku, Kyoto 607-8412, Japan; ²Department of Life Sciences, Graduate School of Arts and Sciences, University of Tokyo, Meguro-ku, Tokyo 153-8902, Japan

Introduction

The amyloid β peptide ($A\beta$), which is the main component of senile plaques found in the brains of Alzheimer's disease (AD) patients, is formed by proteolytic processing of amyloid precursor protein (APP). Since BACE1 (β -site APP cleaving enzyme, β -secretase) triggers $A\beta$ formation by cleaving at the N -terminus of the $A\beta$ domain, it is a molecular target for therapeutic intervention in AD.

Recently, we have reported the small-sized BACE1 inhibitors containing phenylnorstatine [Pns: (2*R*,3*S*)-3-amino-2-hydroxy-4-phenylbutyric acid] as a substrate transition-state mimic (Fig. 1) [1]. KMI-358 was designed from the octapeptide BACE1 inhibitor KMI-008 [2] as the lead compound. However, KMI-358 has a labile β - N -oxalyl-DAP residue (DAP: L- α , β -diaminopropionic acid) at the P_4 position [3]. In addition, we optimized the P_4 and P_1' positions of this inhibitor in order to develop a practical AD's drug.

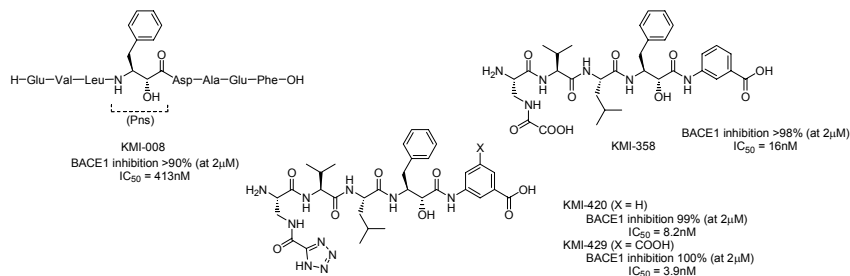


Fig. 1. BACE1 inhibitors containing phenylnorstatine as a substrate transition-state mimic.

Results and Discussion

BACE1 inhibitors **1-21** and KMI-429 were synthesized by the (Fmoc)-based solid phase method or by a traditional solution method as previously reported [1-3].

Previously, we have established that a pentapeptide consisting of P_4 - P_1' is the minimal molecular size for BACE1 inhibition [1]. Hence, we focused the optimization on P_4 and P_1' positions of KMI-358. To study the structure-activity relationship (SAR) at P_4 position, we evaluated compounds **1-9** (Table 1). Compounds **2** and **4** exhibited weak BACE1 inhibitory activity in comparison with **1**, suggesting that the length and a carboxylic acid of side chain at the P_4 position are important for BACE1 inhibitory activity. On the other hand, the modifications of α -amino groups (i.e., **5** and **6**) and α -carbons (i.e., **3** and **6**) reduced drastically BACE1 inhibitory activity, suggesting that the α -amino group and its 3-dimensional structure

Table 1. BACE1 inhibitory activity (P_4 position)

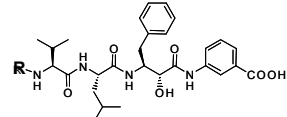
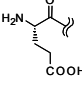
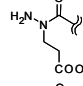
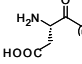
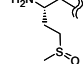
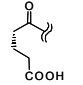
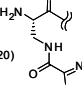
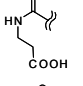
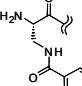
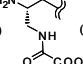
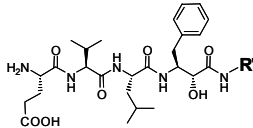
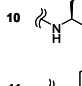
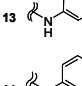
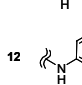
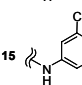
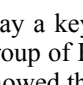
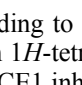
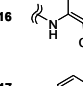
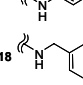
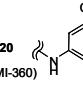
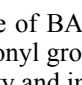
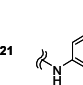
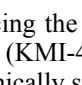
					
Compd	R	BACE1 inhibition (%) at 2μM	Compd	R	BACE1 inhibition (%) at 2μM
1		82	3		<20
2		21	4		<20
5		<20	8		99 (KMI-420) (IC ₅₀ = 8.2nM)
6		55	9		71
7		98 (KMI-358) (IC ₅₀ = 16nM)			

Table 2. BACE1 inhibitory activity (P_1 ' position)

					
Compd	R'	BACE1 inhibition (%) at 2μM	Compd	R'	BACE1 inhibition (%) at 2μM
10		61	13		29
11		53	14		62
12		41	15		84
16		55	17		79
19		82 (KMI-260)	18		64
20		99 (KMI-360) (IC ₅₀ = 55nM)	21		61

play a key role for binding to the active site of BACE1. Replacing the β -N-oxalyl group of KMI-358 with 1*H*-tetrazole-5-carbonyl group afforded **8** (KMI-420), which showed the highest BACE1 inhibitory activity and improved chemically stability.

A SAR study focused on P_1 ' was performed. As shown in Table 2, compound **20** showed the highest BACE1 inhibitory activity, suggesting that aromatic ring and carboxylic acid group are important for BACE1 inhibitory activity. Compounds **14** and **21**, which contained no carboxylic acid at the P_4 position, showed a moderate BACE1 inhibitory activity, suggesting that some polar groups on the benzene ring might be able to bind to S_1 ' site of BACE1.

From the results above, we designed the potent BACE1 inhibitors KMI-420 and KMI-429, containing a tetrazole ring at the P_4 position.

Acknowledgments

This research was supported in part by the Frontier Research Program and the 21st century COE program of the Ministry of Education, Science and Culture of Japan, and grants from the Ministry of Education, Science and Culture of Japan.

References

- Kimura, T., Kiso, Y., *et al.* *Bioorg. Med. Chem. Lett.* **14**, 1527-1531 (2004).
- Shuto, D., Kiso, Y., *et al.* *Bioorg. Med. Chem. Lett.* **13**, 4273-4276 (2003).
- Kimura, T., Kiso, Y., *et al.* *Bioorg. Med. Chem. Lett.* **15**, 211-215 (2005).

Synthesis of Non-linear Potential Vaccines for HSV-1

**Rosalba Mansi¹, Stefania Galdiero¹, Diego Tesauro¹, Ettore Benedetti¹,
Giancarlo Morelli¹ and Massiliano Galdiero²**

¹Department of Biological Sciences & CIRPeB, University of Naples “Federico II”, I-80134 Napoli, Italy; ²Department of Experimental Medicine - Faculty of Medicine of Second University of Naples Napoli I-80127, Italy

Introduction

Herpes Simplex Virus Type I (HSV-1) affects a wide range of population. No vaccine is available for prevention and the main problem is the identification of the immunogenic peptide sequences. HSV-1 encodes a large number of glycoproteins, three of these, gB, gD and gH/gL heterodimer, are essential for the fusion of the viral envelope with the cellular membrane and for the cell-to-cell spread of virions [1]. Our goal is to synthesize a potential vaccine constructed on a lipid core using peptides from the glycoproteins involved in virus entry. This construct is based on a Lipidic Core Peptide (LCP) system and on a Multiple Antigen Peptide (MAP) system. The LCP system incorporates lipoamino acids, presents self-adjuvant properties, elicits the immune responses, and represents a potentially safe option for vaccine delivery in humans [2]. The MAP system, based on branched lysine, is immunogenically inert and allows the incorporation of multiple copies of different glycoprotein peptides [3]. This construct is uniquely designed to incorporate the antigens, the adjuvant, and the carrier in a single molecular entity. The possible B cell and T cell epitopes were chosen comparing different data obtained with several prediction programs.

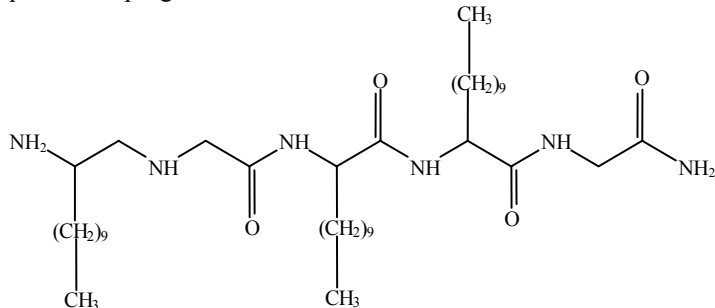


Fig. 1. Lipidic core peptide (LCP) system.

Results and Discussion

The LCP system consists of a sequence of glycine and α -aminododecanoic acid [$\text{H}_2\text{N}-\text{CH}[(\text{CH}_2)_9\text{CH}_3]-\text{OH}$] ($\text{C}_{12}-\text{OH}$) (Fig.1). Synthesis of LCP system was carried out in solid-phase under standard conditions using Pre-loaded Boc-Gly-PAM resin. The next two cycles were carried out with Boc- $\text{C}_{12}-\text{OH}$, those were followed sequentially by the coupling of Boc-Gly-OH and Boc- $\text{C}_{12}-\text{OH}$. In order to obtain the peptide construct with three different epitopes, lysine with orthogonal protection on the α and ϵ amino groups was bound on the N-terminus of the core. After removing protection in sequence with different selective cleavage conditions, two Lys with three protecting groups (Fmoc, Mtt, and Dde) were coupled. These protections can

be removed under three different conditions. Therefore the N-terminus became available to couple fully protected peptides. They were selected between the possible T cell and B cell epitopes chosen by analyzing the glycoproteins gB and gD of HSV-1 with several prediction programs and comparing the results. Possible T cell epitopes were identified using the TEPITOPE [4] program. The TEPITOPE program uses structural data from MHC-peptide complexes and MHC peptide-binding data to predict the potential of peptides or proteins to bind to an MHC molecule. B cell epitopes are located on the surface of proteins and usually at or near γ -turns. Possible B cell epitopes were chosen using the Predict Protein Server [5,6,7] and Chou-Fasman [8] prediction methods. The predicted data of hydrophobicity and solvent accessibility, and the propensity to form surface loops were compared and the hydrophilic sequences with unordered structure or γ -turn were chosen. The peptides gD119-140, gD215-235, gB288-310, gB438-462 (corresponding to T cell epitopes) and gB308-316 gB472-480 (corresponding to B cell epitopes) were synthesized on 2-chlorotriylchloride resin (superacid-labile resin) using Fmoc strategy.

The biotin was coupled at the N-terminus of possible B cell epitopes in order to exam the antigenic integrity of the possible B cell determinants with ELISA tests. *In vitro* and *in vivo* experiments are currently being performed in order to analyze the activity of our synthetic vaccines.

Acknowledgments

We gratefully acknowledge support by EU under contract n° QLK2-CT-2002-00810.

References

1. Turner, A., Bruun, B., Minson, T. and Browne, H. *J. Virol.* **72**, 873-875 (1998).
2. Toth, I., Danton, M., Flinn, N. and Gibbons, W. A. *Tetrahedron Lett.* **34**, 3925-3928 (1993).
3. Olive, C., *et al.* *Infect. Immun.* **70**, 2734-2738 (2002).
4. Manici, S., *et al.* *J. Exp. Med.* **189**, 871-876 (1999).
5. Rost, B. and Sander, C. *Proteins* **19**, 55-72 (1994).
6. Rost, B. *Methods in Enzymology* **266**, 525-539 (1996).
7. Rost, B. and Sander, C. *J. Mol. Biol.* **232**, 584-599 (1993).
8. Prevelige, P. and Fasman, G. *Prediction of protein structure and the principles of protein conformation*, Plenum Press, New York (1990).

Intramolecular Triplet Quenching by Nitroxide Radicals as a Tool for Determining Peptide Secondary Structure in Solution

Lorenzo Stella¹, Gianfranco Bocchinfuso¹, Emanuela Gatto¹, Antonio Palleschi¹, Mariano Venanzi¹, Daniela Zavallone¹, Andrea Bettio², Fernando Formaggio², Claudio Toniolo² and Basilio Pispisa¹

¹Department of Chemical Sciences and Technologies, University of Roma Tor Vergata, 00133 Rome, Italy; ²Department of Chemistry, University of Padua, 35131 Padua, Italy

Introduction

Quenching of the excited states of a chromophore by a suitable moiety can provide important information on the probe-quencher distance. Singlet quenching through Förster energy transfer has been exploited by us in the determination of the structural features of many ordered oligopeptides in solution, by combining experimental data with molecular modeling studies [1]. Quenching of excited triplet states would extend this approach from the nanoseconds time-region of singlet lifetimes to the microseconds, possibly providing new insights on peptide dynamics. To verify the scope of this method, we have investigated the distance dependence of the intramolecular quenching of the benzophenone triplet of the Bpa residue by the nitroxide radical of TOAC in the oligopeptides listed in Figure 1.

BT0	Boc-Aib- Bpa -TOAC-Ala-Aib-Aib-Ala-OtBu
BT1	Boc-Aib- Bpa -Aib-TOAC-Ala-Aib-Ala-OtBu
BT2	Boc-Aib- Bpa -Aib-Ala-TOAC-Aib-Ala-OtBu
BT3	Boc-Aib- Bpa -Aib-Aib-Ala-TOAC-Ala-OtBu
B	Boc- Bpa -Aib-Aib-Aib-Aib-Aib-OtBu

Fig. 1. Primary structures of the synthetic oligopeptides investigated. Bpa = 4'-benzoylphenyl-alanine, TOAC = 4-amino-1-oxyl-2,2,6,6,-tetramethylpiperidine-4-carboxylic acid.

Results and Discussion

IR absorption spectra indicate that these peptides adopt a helical structure, but they do not allow us to discriminate between the α - or the 3_{10} -helical conformation. Furthermore, the presence of the Bpa and TOAC labels makes NMR and CD studies quite difficult. Transient absorption experiments show that the benzophenone triplet is efficiently quenched by TOAC (Fig. 2). The observed rates of this quenching process can not be simply related to the position of the probes along the sequence, thus ruling out a "through bond" mechanism. For instance, the lowest population of the benzophenone triplet state is observed in the **BT2** analog, suggesting a close proximity of the two probes in this peptide. A "through space" quenching mechanism is further confirmed by the viscosity dependence of the quenching rate, which decreases significantly on going from acetonitrile to a glycerol/methanol 8:2 mixture, indicating that some intramolecular diffusional motion does take place during the μ s triplet lifetime and is involved in the quenching process. Considering the relative rigidity bestowed on the peptide chain by the C $^{\alpha}$ -tetrasubstituted residues, these motions can be attributed to internal rotations of the Bpa side chain, bringing the benzophenone moiety in contact with the TOAC quencher. Comparison of the experimental results with preliminary molecular mechanics (MM) calculations confirms this view. In particular, for the **BT3** analog the lowest energy conformer is

a distorted α -helical structure (Fig. 3), while several different orientations are indeed possible for the Bpa side chain. A good correlation is found between the triplet quenching rate in the different analogs and the distance between the Bpa C^β -atom and the center of the TOAC nitroxide bond, as obtained from MM calculations (Fig. 3). Overall, the experimental findings confirm that transient absorption experiments of triplet quenching may provide information on the intramolecular distances.

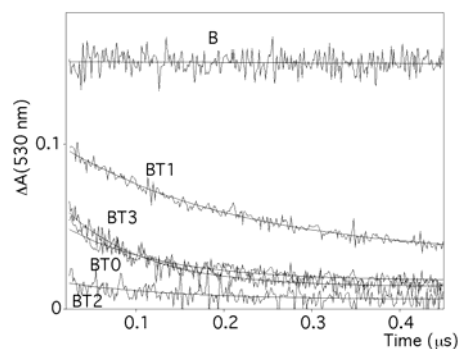


Fig. 2. Transient absorption of benzophenone triplet in deaerated acetonitrile solutions of the different peptides examined (50 μ M). Excitation was obtained with a 266 nm pulse of a Nd:YAG ns laser. In the case of **BT2** the transient absorption is too low for a reproducible determination of the quenching rate.

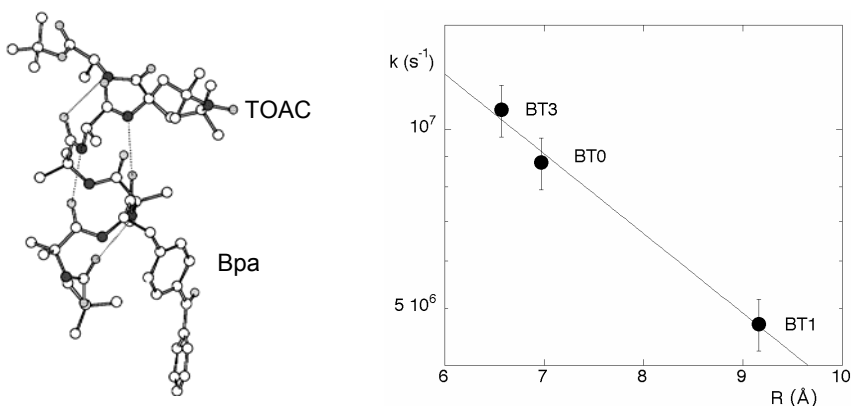


Fig. 3. Minimum energy (distorted α -helical) conformer for analog **BT3** obtained by MM calculations (left). The right panel compares the experimental quenching rate with the distance between the Bpa C^β -atom and the center of the TOAC N-O bond in the minimized conformations for the **BT0**, **BT1**, and **BT3** peptides.

Acknowledgments

This work was funded by MIUR.

References

1. Pispisa, B., Palleschi, A., Mazzuca, C., Stella, L., Valeri, A., Venanzi, M., Formaggio, F., Toniolo, C. and Broxterman, Q. B. *J. Fluoresc.* **12**, 213-217 (2002).

A Time-Resolved Spectroscopic Study on Peptide Folding

Basilio Pispisa¹, Emanuela Gatto¹, Gianfranco Bocchinfuso¹, Antonio Palleschi¹, Lorenzo Stella¹, Mariano Venanzi¹, Fernando Formaggio² and Claudio Toniolo²

¹*Department of Chemical Sciences and Technologies, University of Roma Tor Vergata, 00133 Rome, Italy;* ²*Department of Chemistry, University of Padua, 35131 Padua, Italy*

Introduction

Generation of nucleation centers, such as the helix-turn-helix motif, is one of the possible mechanisms of protein folding. Therefore, knowledge of the kinetics of formation of such locally structured domains may be important for discriminating different folding pathways. To investigate this aspect of the folding process, we employed time-resolved optical spectroscopies, from nanosecond to microsecond time scales, on the analog of trichogin GAIV denoted as F0T8

Fmoc-Aib-Gly-Leu-Aib-Gly-Gly-Leu-Toac-Gly-Ile-Leu-OMe

where Fmoc is fluoren-9-ylmethoxycarbonyl, and Toac is 4-amino-1-oxyl-2,2,6,6-tetramethylpiperidine-4-carboxylic acid. The central -(Gly)₂- sequence is mobile, being thus able to populate different conformational states.

Results and Discussion

CD spectra in methanol show that the peptide investigated adopts a mixed $\alpha/3_{10}$ -helical conformation. Time-resolved fluorescence experiments were carried out to investigate the nature of conformers in solution and their relative populations (α_i) by taking advantage of the presence of an energy transfer donor-acceptor pair in the peptide [1]. The fluorescence time decay of F0T8 in MeOH is accounted for by two lifetimes, as determined by the distribution analysis of the decay curves. The first lifetime is peaked at $\tau_1 = 1.7$ ns ($\alpha_1 = 0.15$) while the second at $\tau_2 = 5.7$ ns ($\alpha_2 = 0.85$). The corresponding quenching efficiencies, as given by $E_i = [1 - (\tau_i/\tau_0)]$, where τ_0 is the lifetime of the reference ($\tau_0 = 9.0$ ns in methanol), are $E_1 = 0.81$ and $E_2 = 0.37$, respectively. In principle, each decay time may arise from a variety of species, all having a similar quenching rate. This property, in turn, implies that these species have similar geometric features. From the results, it appears that F0T8 populates two conformations in methanol solution, characterized by different interchromophoric distances and, possibly, by different orientations of the probes. In this connection, it is worth noting that a quenching efficiency as high as 0.81 can be obtained only when the probes are close to each other, which, in turn, suggests that a bent, ordered structure must be present in solution (besides a linear structure, in which the two probes are far apart). When the same type of measurements was performed in a high viscosity solvent, such as glycerol, the lifetimes were found to be practically unchanged. This result is suggestive of a rate of interconversion between the two conformers significantly slower than that corresponding to a ns fluorescence lifetime.

We then studied the peptide dynamics in the microsecond time scale by performing transient absorption measurements on the Fmoc triplet state that can be *intramolecularly* quenched by Toac through a short-range mechanism. The observation that the triplet decay rate constant is $k_T = 3.5 \cdot 10^6$ s⁻¹ in methanol, as compared to $1.8 \cdot 10^6$ s⁻¹ in glycerol, while those of the reference compound are

$0.4 \cdot 10^6$ and $0.5 \cdot 10^6 \text{ s}^{-1}$, respectively, strongly suggests that, in this case, is the interconversion from the linear to the bent helical structure that is actually measured. This conclusion is based on the fact that the quenching rate was independently found to be much higher than the interconversion rate. To summarize, our results show that a transition from an *extended* helical conformation, characterized by a relatively large Fmoc/Toac distance, to a *compact*, protein-like structure, having a short interchromophoric separation, does take place in the μs time scale. The latter conformation relies on the flexibility of the Gly⁵-Gly⁶ sequence, a hinge central point between the two helical segments located at the N- and C-termini.

A low-energy, linear conformer, having an α -helical arrangement, was built up by molecular mechanics (MM) calculations [2]. As its theoretical efficiency is close to that experimentally determined (E_2) according to the Förster mechanism [1], the structure proposed (Fig. 1) is validated. However, as pointed out above, an additional conformer characterized by a bent, ordered geometry, in which the probes are close together, must be present in solution. This is the only way to account for the other observed quenching efficiency (E_1). MM calculations, carried out with the E_1 constraint, lead, in fact, to the bent structure illustrated in Figure 1, corresponding to the helix-turn-helix motif.

Overall, our results provide a hint for the time scale of a possible elementary step in protein folding.

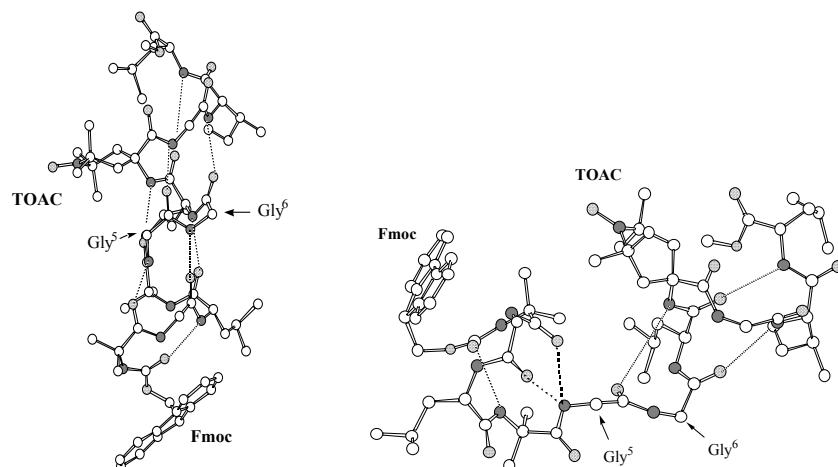


Fig. 1. Theoretical structures of F0T8, as obtained by molecular mechanics calculations. In the bent conformation (right), preserving an ordered arrangement, the probes are close to each other.

References

1. Pispisa, B., Mazzuca, C., Palleschi, A., Stella, L., Venanzi, M., Wakselman, M., Mazaleyra, J. -P., Rainaldi, M., Formaggio, F. and Toniolo, C. *Chem. Eur. J.* **9**, 4084-4093 (2003), and references therein.
2. Pispisa, B., Venanzi, M., Palleschi, A. and Zanotti, G. *Biopolymers* **36**, 497-510 (1995).

Ion Channel Activities and Mechanisms of Ion Conduction about Cyclic Hexapeptides

Junichi Taira¹, Ryo Hayashi¹, Satoshi Osada¹, Tsuguhisa Ehara² and Hiroaki Kodama¹

¹Department of Chemistry and Applied Chemistry, Faculty of Science and Engineering, Saga University, Saga, 840-8502, Japan; ²Department of Physiology, Faculty of Medicine, Saga University, Saga, 849-8501, Japan

Introduction

Cyclic peptides are of interest due to numerous and unique biological activities. Whereas pharmacological properties of natural cyclic peptides have great attentions, functions of artificial cyclic peptides are also widely investigated. Recently, as one of the functions of artificial cyclic peptides, occurrences of ion-channel function have been reported [1]. It has been proposed that these cyclic peptides form self-assembled tube-like assembly with potency to conduct ions in lipid bilayer. Construction of tube-like structures with cyclic peptides has two advantages. The outside surface properties and the internal diameter of the tubes will be controlled simply by adjusting the side chain functional groups and the ring size. However, the relationships between structure and ion channel function of cyclic peptide are not well known. In this study, cyclic hexapeptides with different characters were investigated to explore the ion channel forming abilities and selective ion-conduction of cyclic peptides.

Results and Discussion

The structures of cyclic hexapeptides are shown in Figure 1. The sequence cyclo(Pro-Xxx-D-Yyy)₂ has optimum back-bone structure to form tube architectures by six residues [2]. According to molecular modeling, the diameter of the peptide was expected about 0.4 nm and it can form intermolecular hydrogen bonding.

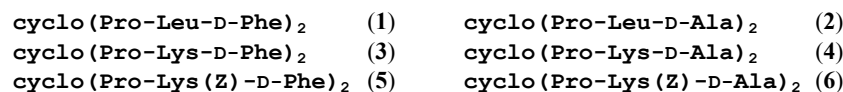


Fig. 1. Structures of cyclic peptides. Two Pro residues promote cyclization of peptide. Xxx and Yyy positions were substituted by Leu or Lys residues and D-Ala or D-Phe residues, respectively.

The designed peptides were prepared according to the reported procedure [3]. Homogeneities and structures of synthetic peptide were confirmed by analytical RP-HPLC, MALDI-TOF MS, and NMR analysis. Ion channel experiments were performed by pipette-dipping technique [4]. Electrolytes were filled by suitable buffers and the composition was symmetrical for both sides of the diphytanoyl phosphatidylcholine (DPhPC) membrane. All peptide concentrations were 1 μ M. Peptide 1-4 showed typical open-close conductance states in the presence of KCl (Fig. 2). The observed conductance values were mainly around 50-100 pS. Considering the ion transport mechanism of cyclic peptide, the observed conductance values were appropriate for an ion channel mechanism (10^7 ions / sec) but not a carrier mechanism. Estimated pore diameters from the bserved

conductance values are about 0.2 nS in each analog [5]. Peptide **1** and **2** showed single state open-close. Transition between open and close state was rapid with an opening duration was about 10 to 100 msec. On the other hand, peptide **3** and **4** showed multi-state conductance patterns and opening durations also tend to expand. These multi-state ion conduction patterns suggested the possibility of existence of different pore diameters [6]. We hypothesize that the side chain of Lys residues contribute to the phenomena. To evaluate the effect of side chain of Lys residues, analogs with blocked Lys side chains, peptide **5** and **6**, were investigated under the same conditions. Large conductance values disappeared for each analog suggesting that the amino groups contribute to the occurring large conductance values.

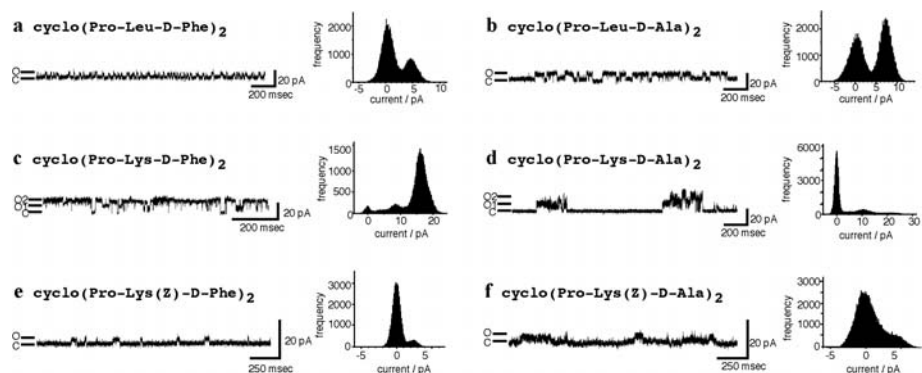


Fig. 2. Conductance pattern and histogram analysis of cyclic hexapeptides in 500 mM KCl 5 mM HEPES buffer. All conductance patterns were observed under +100 mV potentials.

In the presence of KAsp buffer, peptides **1-4** showed typical open-close of ion-channel. This result suggested that these peptides have the ability to conduct cation. To evaluate ion-selecting properties, ion-channel activities were compared under various conditions. Generally, experiments with CsCl and NaCl showed smaller conductance values than that of KCl. Owing to this fact, these peptides conduct more selectively potassium ions than sodium and cesium ions. This result suggest that the pore diameter of the tube structure constructed by cyclic hexapeptides was the optimized size for potassium ion conduction.

Acknowledgments

The work was funded by JSPS Research Fellowships for Young Scientists to J. T.

References

1. Bong, D. T., Clark, T. D., Granja, J. R. and Ghadiri, M. R. *Angew. Chem. Int. Ed. Engl.* **40**, 988-1011 (2001).
2. Gierasch, L. M., Deber, C. M., Madison, V., Niu, C. and Blout, E. R. *Biochemistry* **20**, 4730-4738 (1981).
3. Osada, S., Hayashi, R., Yamashita, T., Yoshiki, M., Okamoto, Y., Ueda, T., Kodama, H. and Kondo, M. *Peptides* 468-469 (2001).
4. Higashimoto, Y., Kodama, H., Jelokhani-Niaraki, M., Kato, F. and Kondo, M. *J. Biochem.* **125**, 705-712 (1999).
5. Sansom, M. S. P. *Eur. Biophys. J.* **22**, 105-124 (1993).
6. Fernandez-Lopez, S., *et al.* *Nature* **412**, 452-455 (2001).

Synthesis and Biological Activities of Proline Rich Cyclic Heptapeptide Hymenamide B Analogs

Yasuhiro Shiki, Junichi Taira, Aya Nakamura, Satoshi Osada and
 Hiroaki Kodama

Department of Chemistry, Faculty of Science and Engineering, Saga University,
 Saga 840-8502, Japan

Introduction

The isolation of a great variety of biological active materials from marine organisms has been reported. Many types of these bioactive compounds are cyclic peptides. Cyclic peptides have metabolic stabilities and restricted conformations. Since these characters play a key role for biological activities, cyclic peptides have been the focus as pharmacological targets. One class of these cyclic peptides, named hymenamides, has been isolated from Okinawan marine sponge *Hymeniacidon* sp. [1,2]. This peptide family contains proline and hydrophobic residues with high frequency and shows high cytotoxic activity, antifungal activity, and occasionally works as enzymatic inhibitor [2]. However, it is difficult to secure enough amounts of natural product for physiological estimation by isolation. Therefore, to further explore these peptides, it is necessary to chemically synthesize them to obtain sufficient amounts to perform structure-function relationships studies.

In this study, hymenamide B and hymenamide B analogs were synthesized in the aim to explore the structure-activity relationships (Fig. 1).

hymenamide B	cyclo(FPPNFVE)	(1)
[Gln⁷]hymenamide B	cyclo(FPPNFVQ)	(2)
hymenamide C	cyclo(LWPFGE)	(3)

Fig. 1. Structures of hymenamide B, [Gln⁷]hymenamide B, and hymenamide C.

Results and Discussion

Peptide synthesis was carried out using solid phase method. Our strategy was to anchor the peptide to the solid support *via* the side chain of one of the residues to allow subsequent cyclization on the resin [3]. The peptides were elongated by standard Fmoc chemistry. The side chain carboxyl group of Fmoc-Glu-OAll was activated by HBTU-HOBt and coupled to Rink amide resin. After deprotection of Fmoc group by 20% piperidine, the condensation of Fmoc protected amino acid was carried out by HBTU-HOBt method. After synthesis completion, the allyl protecting group on the C-terminal was removed by Pd⁰(PPh₃)₄ catalyst, followed by removal of the N-terminal Fmoc protecting group. The cyclization was carried out using the HBTU-HOBt method for 3 hrs. Cleavage was performed with 2% and 90% TFA with suitable scavengers. Cleavage with 2% TFA gave the desired product containing Trt group without detecting oligomeric byproducts (Fig. 2a and b). These byproducts are not cleaved when using high diluted acid because they are anchored by multiple sites on the resin. This confirms that this method is useful for cleaving cyclized peptide from common resins. The Trt group of the cyclic peptide was finally removed with a 30% TFA treatment. Peptide purification was carried out by preparative RP-HPLC. The homogeneities of the peptides were confirmed by analytical RP-HPLC and MALDI-TOF MS analysis.

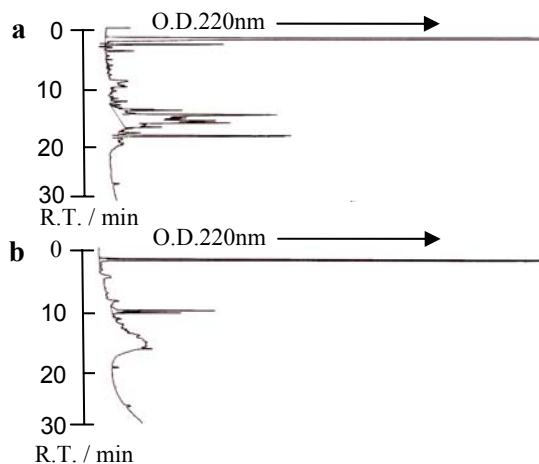


Fig. 2. RP-HPLC analysis of [Gln⁷]hymenamide B cleaved with (a) 2% TFA and (b) 90% TFA.

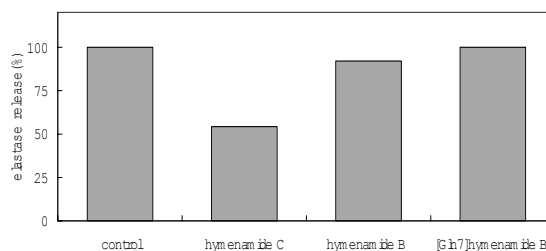


Fig. 3. Inhibition of elastase release from human neutrophils. The activity of hymenamide C quoted a result of previous report [4].

The biological activity of hymenamides was evaluated as inhibition of elastase release from human neutrophils. Elastase activity was evaluated in aliquots of stimulated human neutrophile supernatants incubated with *N*-*tert*-butoxy-carbonyl-L-alanine *p*-nitrophenol ester. In the presence of elastase, *p*-nitrophenol is released resulting in a detectable absorbance at 414 nm. Hymenamide B and its analog did not inhibit elastase release (Fig. 3). Studies toward the exploration of essential structures for the activities of hymenamide are in progress in our laboratory.

References

1. Kobayashi, J., Tsuda, M., Nakamura, T., Mikami, Y. and Shigemori, H. *Tetrahedron* **49**, 2391-2402 (1993).
2. Tsuda, M., Shigemori, H., Mikami, Y. and Kobayashi, J. *Tetrahedron* **49**, 6785-6796 (1993).
3. Nakamura, A., Tatebe, S., Taira, J., Osada, S., Ohba, H., Yasuda, S. and Kodama, H. *Peptide Sci.* **2004**, 535-538 (2005).
4. Napolitano, A., Bruno, I., Rovero, P., Lucas, R., Peris, M. P., Gomez-Paloma, L. and Riccio, R. *Tetrahedron* **57**, 6249-6255 (2001).

Synthesis and Biomaterials Application of Polymers Containing Pentapeptide and/or Hexapeptide Sequences Derived from Elastin

Kouji Okamoto^{1,2}, Shuichiroh Uehara², Kayoko Matsui¹, Maria Portia P. Briones¹, Iori Maeda^{1,2} and Masakazu Furuta³

¹*Department of Bioscience and Bioinformatics, Kyushu Institute of Technology, Iizuka, Fukuoka 820-8502, Japan;* ²*Graduate School of Life Science and Systems Engineering, Kyushu Institute of Technology, Kitakyushu, Fukuoka 805-0196, Japan;* ³*Research Institute for Advanced Science and Technology, Osaka Prefecture University, Sakai, Osaka 599-8570, Japan*

Introduction

Elastin is an insoluble core protein of elastin fiber in elastic tissues such as arterial walls, ligaments, lungs, skin, etc. Soluble elastin molecules, tropoelastin (precursor protein of fibrous elastin) and α -elastin (chemical fragmentation product from fibrous elastin), exhibit an interesting and unique property. That is to say, these soluble elastin molecules form clear homogeneous solution at below room temperature, but on raising the temperature to body temperature or above, the solution becomes turbid in which microcoacervate droplets with diameters of approximately 1000 nm are formed [1]. This process is reversible and called coacervation. Furthermore, these soluble elastin molecules are known to be chemoattractants for fibroblasts [2], monocytes [3], and macrophages [4].

The repeating peptide sequences, Val-Pro-Gly-Val-Gly or simply VPGVG and Val-Ala-Pro-Gly-Val-Gly or simply VAPGVG, are the primary structural features in human, bovine, and porcine elastin molecules. These repeating sequences differ from one another in coacervation and cell migration. For example, the VPGVG sequence coacervates but does not serve as a chemoattractant, while the VAPGVG sequence serves as a chemoattractant but does not coacervate. Here, we synthesized two sequential polymers, poly(VPGVG) and poly(VAPGVG), and a copolymer, poly[10 (VPGVG), (VAPGVG)] by means of a conventional solution method and studied macrophage chemotactic response to these polymers by using a chemotactic chamber, temperature profiles for coacervation of these polymers by monitoring light scattering at 400 nm, and nanoparticle preparation of these polymers cross-linked with cobalt-60 γ -irradiation for drug release devices.

Results and Discussion

The molecular weights of poly(VPGVG), poly(VAPGVG), and poly[10(VPGVG), (VAPGVG)] synthesized by a conventional solution method were distributed in the ranges of 23,000 to 36,000, 22,000 to 34,000, and 20,000 to 45,000, respectively. The onset temperature for coacervation of poly[10(VPGVG), (VAPGVG)] was higher than poly(VPGVG). As coacervation is considered to be the process of an increase in intermolecular and intramolecular hydrophobic associations, the hydrophobic association of poly(VPGVG) in coacervation process seems to be reduced by the addition of VAPGVG sequence into the VPGVG molecule. Two polymers, poly(VPGVG) and poly[10(VPGVG), (VAPGVG)], were dissolved in phosphate buffered saline (pH 7.4), heated to 60°C, and cross-linked by cobalt-60 γ -irradiation for 3 hrs at an irradiation rate of 10 kGy/hr. The nanoparticle sizes of microcoacervate droplets before and after γ -irradiation are shown in Table 1. The

nanoparticles of poly[10(VPGVG), (VAPGVG)] were nearly the same sizes as those of poly(VPGVG). The nanoparticle sizes of both poly(VPGVG) and poly[10(VPGVG), (VAPGVG)] were reduced after γ -irradiation. However, these nanoparticle sizes in the range of 100-200 nm seem to be suitable for drug release devices.

Table 1. Nanoparticle sizes of polymers before and after γ -irradiation

Polymers	Before γ -irradiation diameter (nm) \pm SD (nm)	After γ -irradiation diameter (nm) \pm SD (nm)
Poly(VPGVG)	596 \pm 126	195 \pm 38
Poly[10(VPGVG), (VAPGVG)]	328 \pm 71	150 \pm 27

Concentration of polymers is 0.4 mg/ml.

γ -Irradiation is performed at 60°C for 3 hrs at an irradiation rate of 10 kGy/hr.

Table 2. Macrophage chemotactic response to polymers

Polymers	Chemotactic activity (%)
Formyl-Met-Leu-Phe (fMLP)	100
Poly(VPGVG)	4
Poly(VAPGVG)	72
Poly[10(VPGVG), (VAPGVG)]	65

Concentrations of fMLP (positive control), poly(VPGVG), poly(VAPGVG), poly[10(VPGVG), (VAPGVG)] are 10^{-8} M, 10^{-4} - 10^{-4} μ g/ml, 10^{-3} μ g/ml, and 10 μ g/ml, respectively.

Chemotaxis was determined in a 48-well microchemotaxis chamber using rat macrophage suspension (2×10^6 cells/ml) and the results are shown in Table 2. Poly(VPGVG) did not serve as a chemoattractant but poly[10(VPGVG), (VAPGVG)] was shown to be a chemoattractant. The chemotactic activity of poly[10(VPGVG), (VAPGVG)] was nearly equal to that of poly(VAPGVG). The evidences that poly[10(VPGVG), (VAPGVG)] which is composed of VPGVG and VAPGVG sequences gives nanoparticles in the range of 100-200 nm after γ -irradiation as does poly(VPGVG) and serves as a chemoattractant as does poly(VAPGVG) indicate the potential use of this polymer as a biomaterial for medical application.

References

1. Kaibara, K., Okamoto, K. and Miyakawa, K. In *Handbook of Polyelectrolytes and Their Applications, Volume 3: Application of Polyelectrolytes and Theoretical Models* (Tripathy, S. K., Kumar J. and Nalwa, H. S., eds) American Scientific Publishers, pp.143-194 (2002).
2. Senior, R. M., Griffin, G. L. and Mecham, R. P. *J. Clin. Invest.* **20**, 614-618 (1982).
3. Uemura, Y. and Okamoto, K. *Biochem. Mol. Biol. Int.* **41**, 57-64 (1997).
4. Kamisato, S., Uemura, Y., Takami, N. and Okamoto, K. *J. Biochem.* **121**, 862-867 (1997).

Synthesis and Biological Activities of fMLP Analogs Containing 2,3-Cyclopropane Amino Acid Derivatives

Daisuke Sugiyama¹, Ryo Hayashi¹, Hiroshi Kawasaki¹, Hiroaki Kodama¹, Satoshi Osada¹, Masafumi Zaitu² and Ichiro Fujita²

¹Department of Chemistry, Faculty of Science and Engineering, Saga University, Saga 840-8502, Japan; ²Department of Pediatrics, Faculty of Medicine, Saga University, Saga 849-8501, Japan

Introduction

Neutrophils play an important role in the self-defence mechanisms. The chemotactic peptide, HCO-Met-Leu-Phe-OH (fMLP), has been known as an activator of neutrophils and can promote various biological responses for inflammation, such as chemotaxis, superoxide production and secretion of lysozymes. fMLP has been reported to activate at least two formyl peptide receptor family (FPRs) on human neutrophils [1]. N-protected peptides, Boc-Met-Leu-Phe-OH (Boc-MLF) and Boc-Phe-D-Leu-Phe-D-Phe-OH (Boc-FIFIF) were reported as a competitive antagonist against FPRs [2].

Conformationally constrained amino acid is a useful tool for structure-activities relationship studies of fMLP peptides. Previously we reported the syntheses and biological activities of fMLP analogs containing the restricted amino acid 2,3-cyclopropyl phenylalanine (∇ Phe) [3]. In the present study, Boc-MLF analogs containing E- and Z-isomers of ∇ Phe, Boc-Met-Leu- ∇^E Phe (Boc-ML ∇^E F) and Boc-Met-Leu- ∇^Z Phe (Boc-ML ∇^Z F) were synthesized and their biological activities were evaluated on human neutrophils and differentiated HL-60 (dHL-60).

Results and Discussion

E- and Z-isomers of ∇ Phe were synthesized by the malonate method (Fig. 1). Monoester **4** was utilized as a precursor in preparation of both E- and Z-isomers of ∇ Phe. Monoester **4** was treated with hydrazine monohydrate to give hydrazide **5**.

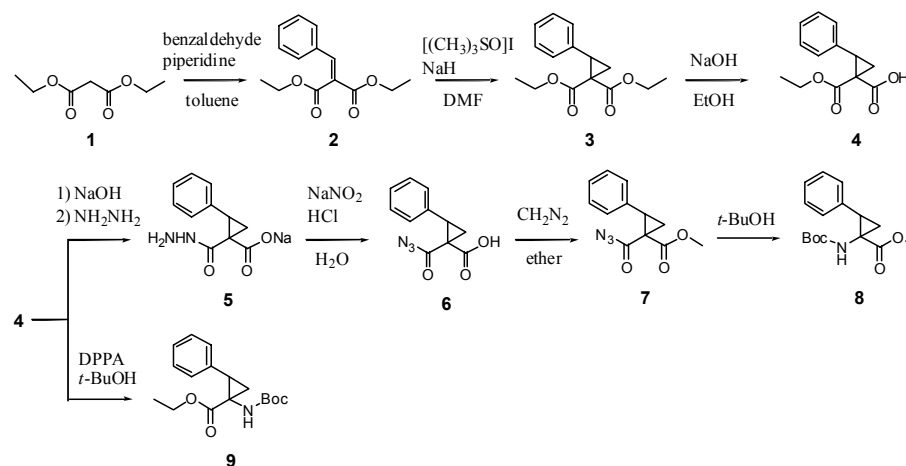


Fig 1. Synthesis of E- and Z-isomers of ∇ Phe.

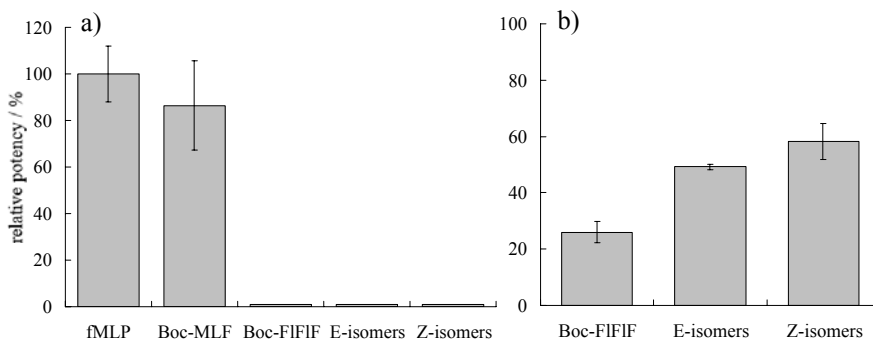


Fig. 2. Biological activities of Boc-MLF and Boc-MLVF analogs in human neutrophils; a) Agonist activities, peptide concentration is 10^{-6} M; b) antagonist activities, neutrophil suspension was stimulated by 10^{-7} M fMLP after pre-incubating with 10^{-6} M synthetic peptides.

The hydrazine group was oxidized to an azide group followed by the esterification of the carboxyl group to prevent side reaction. This azide ester **7** was refluxed in *t*-BuOH to give Z-isomers **8** of ∇ Phe (∇^Z F) by Curtius rearrangement. E-isomers **9** of ∇ Phe (∇^E F) were also synthesized by Curtius rearrangement, by treating with diphenylphosphorylazide (DPPA). ∇ Phe esters were obtained by deprotection of Boc group of isomers **8** and **9**. The synthesis of ∇ Phe-contained peptides was performed by conventional solution procedures. The coupling of ∇ Phe was only achieved using the mixed-anhydride method due to the steric hindrance of ∇ Phe. Synthetic peptides containing ∇ Phe were characterized by HPLC, 1 H-NMR and MALDI-TOF MS.

The biological activities of the synthetic peptides were evaluated as superoxide anion production, measured as superoxide dismutase inhibitable reduction of cytochrome c in human neutrophils and dHL-60 [4]. Human neutrophils were purified using the standard techniques of centrifugation on Ficoll-Paque. HL-60 cells were differentiated into neutrophil-like cells by DMSO. Agonist and antagonist activities of Boc-MLF analogs in human neutrophils are shown in Figure 2. Boc-MLF stimulated superoxide production with an EC_{50} of 0.16 μ M. On the other hand, Boc-MLVF analogs did not exhibit agonist activities. Both E- and Z-isomer analogs of Boc-MLVF inhibited superoxide production stimulated by 10^{-7} M fMLP with IC_{50} values of 1.0 and 1.3 μ M, respectively. In DMSO-differentiated HL-60, the synthetic peptides did not exhibit agonist or antagonist activities. These results suggest that Boc-MLVF analogs have different inhibition mechanism in contrast to that of Boc-MLF. Boc-MLF analogs containing ∇ Phe would be useful ligands to investigate the signal transduction of FPRs in human neutrophils.

References

1. Murphy, P. M., Ozcelik, T., Kenney, R. T., Tiffany, H. F., McDermott D. and Francke, U. *A. J. Biol. Chem.* **267**, 7637-7643 (1992).
2. Le, Y., Murphy, P. M. and Wang, J. M. *Trends Pharmacol. Sci.* **23**, 541-548 (2002).
3. Kodama, H., Hirano, E., Yamaguchi, T., Osada, S., Miyazaki, M., Fujita, I., Miyazaki, S. and Kondo, M. In *Peptides: Frontiers of Peptide Science, Proceedings of the 15th APS* (Kaumaya, P. T. and Tam, J. P., eds.) Kluwer Academic, pp. 623-624 (1997).
4. Miyazaki, M., Kodama, H., Fujita, I., Hamasaki, Y., Miyazaki, S. and Kondo, M. *J. Biochem.* **117**, 489-494 (1995).

***pI*-shifted Basal Insulin Analogs with High Selectivity for Insulin vs IGF-1 Receptor**

Wayne D. Kohn, Radmila Micanovic, Sharon L. Myers, Andrew M. Vick, Steven Kahl, Lianshan Zhang, Beth Striffler, Shun Li, Jing Shang, John M. Beals, John P. Mayer and Richard D. DiMarchi

Lilly Research Laboratories, Eli Lilly & Co., Indianapolis, IN 46285, USA

Introduction

The advent of rapid-acting insulin analogs to cover mealtime glucose excursions has intensified the need for a basal insulin with a peakless activity profile and 24 hr duration to enhance the treatment regimen. A recently introduced basal insulin, insulin glargine (Lantus®) [1], contains one amino acid substitution relative to human insulin (HI) and two additional Arg residues which increase the isoelectric point (*pI*) from 5.6 to 7.0. Glargine is formulated at pH 4 and precipitates upon subcutaneous injection due to low solubility at physiological pH, effectively forming a depot which redissolves slowly. Insulin glargine possesses a peakless PK/PD profile, but it also demonstrates a significantly increased mitogenic potential relative to HI and appreciable intra- and inter-patient variability. There is also evidence that it falls short of providing 24 hr coverage in a number of patients [2]. We have sought to identify other *pI*-shifted basal insulin analogs with a receptor selectivity profile that compares more favorably with HI. Our intention was to identify the ideal number of Arg residues and their optimal placement in the molecule in order to obtain the desirable pharmacological and physical properties. Effects of Arg residues added at the N terminus of the A chain, and/or the C terminus of the B chain were measured in terms of insulin receptor (IR) and IGF-1 receptor (IGF-1R) binding, and stimulation of cell proliferation in human mammary epithelial cells (HMEC). To identify analogs that may have a protracted time-action profile *in vivo*, solubility of the insulin analogs was measured in pH 7 PBS buffer. Summarized here are results of *in vitro* and *in vivo* evaluations of insulin glargine (B31:R,B32:R,A21:G-HI, (**1**)) and three structurally related analogs: A0:R,A(-1):R,A21:G-HI, (**2**); A0:R,A(-1):R,B31:R,A21:G-HI, (**3**); and A0:R,B31:R,B32:R,A21:G-HI, (**4**).

Results and Discussion

Competitive receptor binding was carried out with ¹²⁵I-labelled HI and IGF-1 in SPA mode. Relative to HI, all four analogs had reduced affinity to the IR by roughly 2-3 fold (Table 1). In contrast, their relative affinities for the IGF-1R differed much more significantly. Addition of Arg residues at the C terminus of the B chain increased the relative IGF-1R affinity while Arg residues at the N terminus of the A chain decreased the relative IGF-1R affinity. Thus, the receptor selectivity index of the analogs ranged from 0.06 for **1** to 1.74 for **2** (a 29-fold difference). The mitogenic potency of the analogs was estimated from their effect on proliferation (¹⁴C-thymidine incorporation) of HMECs over a 48 hr period. The relative potencies correlated with the relative IGF-1R affinities for the analogs in Table 1 and numerous additional analogs not shown (linear regression $r^2 = 0.97$).

The insulin analogs were formulated under conditions similar to those for insulin glargine: ~3.64 mg/ml of protein, 30 mg/mL Zn²⁺ (as ZnCl₂), 2.7 mg/mL *m*-cresol,

Table 1: Summary of in vitro evaluation of insulin analogs

Analog	Relative IR ^a Affinity		Relative ^a IGF-1R Affinity		Receptor ^b Selectivity Index	Relative ^c Mitogenic Potency		PBS Solubility (%)
	Mean	SEM	Mean	SEM		Mean	SEM	
HI	1.0	na	1.0	na	1.0	1.0	na	89.5
1	0.33	0.02	5.51	0.14	0.06	4.10	0.23	10.3
2	0.58	0.08	0.34	0.02	1.74	0.32	0.03	23
3	0.63	0.03	0.70	0.09	0.90	0.40	0.04	nd
4	0.32	0.03	1.2	0.12	0.27	0.86	0.05	9.6

^a relative affinity = $IC_{50} \text{ HI} / IC_{50} \text{ analog}$ (HI IC_{50} = 0.35 nM for IR (n = 89) and 172 nM for IGF-1R (n = 88)); ^b receptor selectivity index = relative IR affinity / relative IGF-1R affinity; ^c relative potency = $EC_{50} \text{ HI} / EC_{50} \text{ analog}$ (HI EC_{50} ~ 2 nM).

and 20 mg/ml 85 % glycerol, adjusted to pH 4 with HCl. For the solubility assay an aliquot was diluted 10 fold with PBS and allowed to sit 15 min at r.t., then spun down for 5 min at 14,000 rpm and protein remaining in solution was quantitated from the peak area on RP-HPLC. *In vivo* evaluation was performed in cannulated dogs infused i.v. with cyclic somatostatin to inhibit insulin secretion. A subcutaneous injection of insulin analog (dose 2 nmol/kg) was administered 30 min after the infusion was initiated, and blood samples were drawn over the next 24 hrs for analysis of serum glucose and insulin levels. The four analogs resulted in markedly different PK/PD profiles (Fig. 1) although for each analog the PD (glucose-lowering) effect was correlated to the PK (insulin levels). While insulin glargine (**1**) displayed a maximal glucose lowering effect for up to 16 hrs, analogs **2** and **3** displayed early peaks and little glucose lowering past 4 hrs after injection. Conversely, **4** displayed a glucose-lowering effect that persisted up to 20 hrs and this longer PD effect correlated with a more prolonged PK profile for **4** relative to that of **1**. The bioavailability (AUC_{0-24hr}) of **4** was also 1.5 times higher than that of **1**. These results indicate analog **4** is a promising basal insulin candidate.

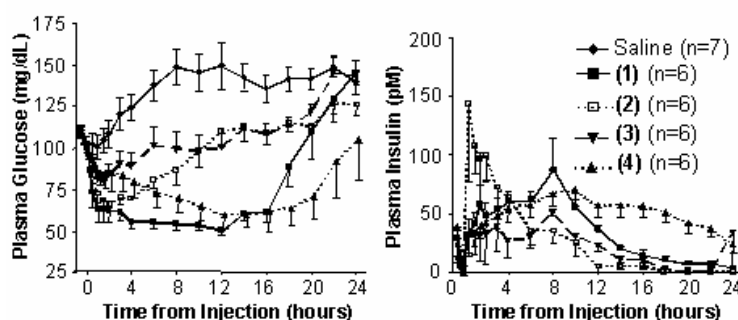


Fig. 1. Glucose-lowering (left) and PK (right) profiles of insulin analogs in dogs.

References

1. Dunn, C. J., Plosker, G. L., Keating, G. M., McKeage, K. and Scott, L. J. *Drugs* **63**, 1743-1778 (2003).
2. Clement, S. and Bowen-Wright, H. *Diabetes Care* **25**, 1479-1480 (2002).

N-Backbone Methylations of Parathyroid Hormone (PTH) C-Terminal Region: Bioactivities and Implications for PTH-Receptor Complex

Zhanna Potetinova¹, Jean-René Barbier¹, Thomas J. Gardella², Thomas Dean², James F. Whitfield¹ and Gordon E. Willick¹

¹Institute for Biological Sciences, National Research Council, Ottawa, ON K1A 0R6, Canada;

²Endocrine Unit, Massachusetts General Hospital, Boston, MA 02114, USA

Introduction

Parathyroid hormone (PTH) is the principal regulator of serum calcium. It acts by stimulating a 7-transmembrane receptor (P1R), mainly found on osteoblasts, renal, and intestinal cells. The principal binding domain is an amphiphilic α -helix between residues 17-29 of hPTH(1-31)NH₂ and this domain has been postulated to bind mainly to the long extracellular N-terminus (EC) of P1R. Although much has been learned about amino acid requirements for this binding, no work has been done on the role of backbone groups, in particular the amides. In this work, we have methylated each residue in turn between Ser17 and Val31, and probed the bioactivities using two receptors, P1R and a mutant receptor lacking the long, extracellular N-terminal sequence (EC) of P1R, delNT-P1R. If the hormone only binds to EC then we expect no or very little activity with delNT-P1R.

Results and Discussion

Backbone N-methylated analogs were prepared by standard Fmoc synthesis protocols. The appropriate N-methyl residue was either introduced as the N- α -Fmoc amino acid (Novabiochem) or by methylation during SPPS by the method of Miller *et al* [1]. The receptor-binding or adenylyl cyclase (AC)-stimulating activities were measured for each analog against either a P1R stably transformed porcine cell line (HKRK-B7) or COS-7 cells transiently transformed with delNT-P1R [2].

The AC-stimulating data is shown in Figure 1, with the data normalized to the natural sequence (WT). When tested against P1R the Val21, Leu24, Arg25, or Leu28 backbone N-methylated analogs, essentially all AC-stimulating activity was

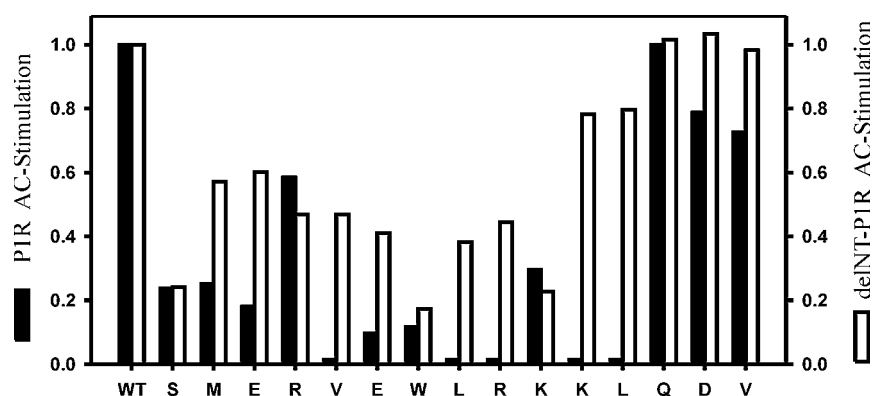


Fig. 1. Relative AC-stimulating activities of hPTH(17-31) N-backbone methylated analogs.

lost. However, the pattern of activities was different when they were assayed against the delNT-P1R receptor. Here, minimum activities were observed with the Ser17, Trp23, and Lys26 N- α -methylated analogs.

This differential pattern of the activities was unexpected if the C-terminal region bound only to the extracellular N-terminal sequence. Rather, the C-terminal α -helix binds to both the extracellular N-terminal sequence and one or more of the extracellular looped-out regions of the receptor (Fig. 2). The distance between Ser17 and Lys26 suggests that this additional binding is better explained by a binding between two of the looped-out sequences.

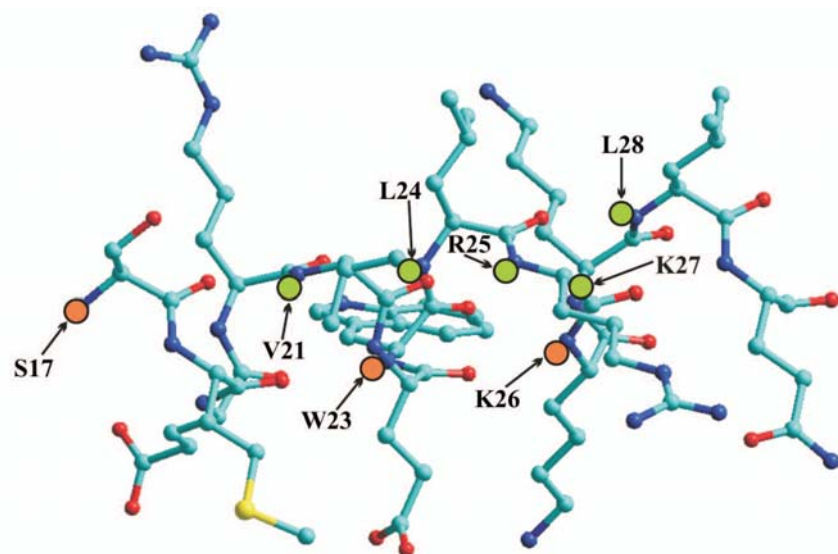


Fig. 2. Side view of C-terminal α -helix with amino acid backbone NHs interacting with EC (green circles) and looped out regions identified (orange circles).

References

1. Miller, S. C. and Scanlan, T. S. *J. Am. Chem. Soc.* **119**, 2301-2302 (1997).
2. Barbier, J. R., *et al.* *J. Biol. Chem.* **280**, 23771-23777 (2005).

N-Backbone Methylations of Parathyroid Hormone (PTH) C-Terminal Region: Effects on Structure

Zhanna Potetinova¹, Feng Ni² and Gordon E. Willick¹

¹Institute for Biological Sciences, National Research Council, Ottawa, ON K1A 0R6, Canada;

²Biotechnology Research Institute, National Research Council, Montréal, QC H4P 2R2, Canada

Introduction

The minimal *in vivo* fully active parathyroid hormone (PTH) is hPTH(1-31)NH₂. In solution at near physiological pH and ionic strength, both CD [1] and NMR [2] have shown this peptide to have two α -helices. The C-terminal α -helix, between Ser17 and Gln29, is well-defined and contributes almost to all of the CD signal, whereas the shorter N-terminal one, between Ser3 and His9, is less well-defined and contributes little to the CD signal. We have prepared backbone N-methylated analogs as part of a recent study of PTH interactions with its receptor. These methylations, when within the helical region, had profound effect on its structure, as indicated by both CD and NMR data.

Results and Discussion

Backbone N-methylated analogs were prepared by standard Fmoc synthesis protocols. The appropriate N-methyl residue was either introduced as the N- α -Fmoc amino acid (Novabiochem) or by methylation during SPPS by the method of Miller and Scanlan [3].

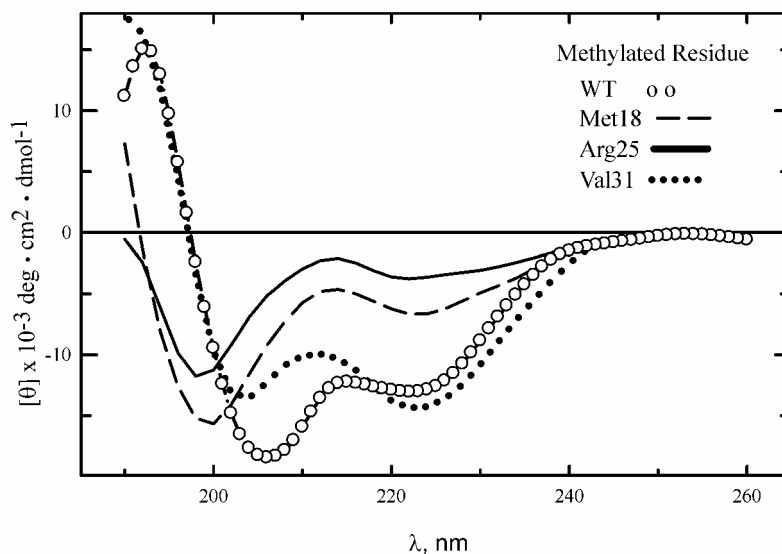


Fig. 1. CD spectra of selected analogs of hPTH(1-31) with (1-17) subtracted.

The impact of backbone N- α -methylation on the secondary structure as measured by CD is shown in Figure 1. The spectrum of hPTH(1-17)NH₂ has been subtracted from the spectra to show more clearly the helical spectrum of hPTH(17-31)NH₂. For example, the spectra of the natural sequence (WT) and N- α -methylated analogs Met18, Arg25, and Leu24 are shown in Figure 1.

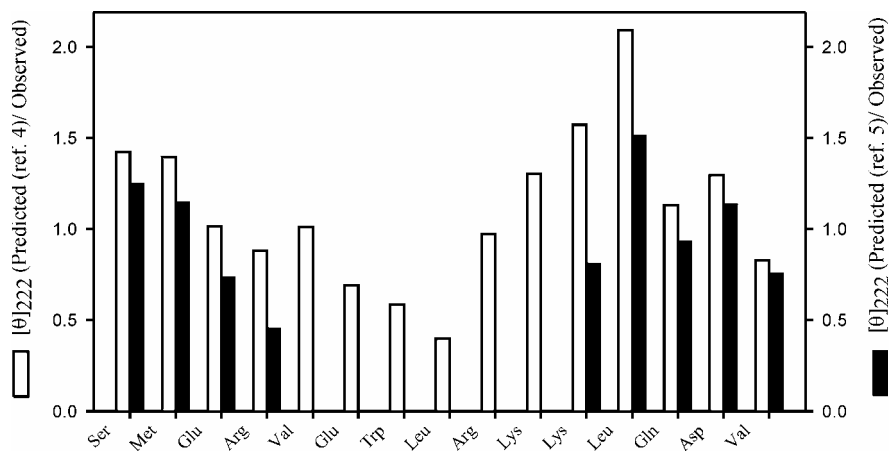


Fig. 2. Predicted [4,5] $[\theta]_{222}$ values for N- α -methylated analogs expressed relative to natural hPTH.

NMR spectra of the N- α -Me-Leu24 analog showed a large disruption of the helical structure of the helix about the point of methylation. This is consistent with the large diminution of the helix-associated $[\theta]_{222}$ that was dependent on the position within the helix, with minimum values where methylation was at the center. The CD signal per residue is dependent on the helix length. We assumed a disruption of helix for 4 residues either side of the methylation (Fig. 2). The $[\theta]_{222}$ were estimated assuming either the dependency of Chin *et al* [4], who showed even short helices have some lessened CD, or that of Yang *et al* [5], where helices less than about 9 residues long have no signal. The Chin *et al* dependency is clearly most consistent with the observations here and given the rough approximations used well-approximated the experimental data.

References

1. Neugebauer, W., *et al. Biochemistry* **31**, 2056-2063 (1992).
2. Chen, Z., *et al. Biochemistry* **39**, 12766-12777 (2000).
3. Miller, S. C. and Scanlan, T. S. *J. Am. Chem. Soc.* **119**, 2301-2302 (1997).
4. Chin, D. H., *et al. Proc. Natl. Acad. Sci. USA* **99**, 15416-15421 (2002).
5. Yang, J. T., Wu, C. S. and Martinez, H. M. *Methods Enzymol.* **130**, 208-269 (1986).

C-Terminal Modified Parathyroid Hormone: Effects on Structure and Activity

Zhanna Potetinova¹, Jean-Rene Barbier¹, Thomas Dean², Thomas J. Gardella² and Gordon E. Willick¹

¹Institute for Biological Sciences, National Research Council, Ottawa, ON K1A 0R6, Canada;

²Endocrine Unit, Massachusetts General Hospital, Boston, MA 02114, USA

Introduction

Parathyroid hormone (PTH) is now used as an anabolic therapy for osteoporosis. The hormone acts through a 7-transmembrane G-protein linked receptor (P1R) [1]. The N-terminal 31 residue analog is the smallest *in vivo* fully functional anabolic analog. An amphiphilic α -helix near the C-terminus is a key region for the receptor binding. An amide C-terminus rather than the natural COOH also is an enhancer of *in vivo* activity but the role of the C-terminus group in both structure and function is poorly understood, with few studies reported [2]. We have constructed C-terminal analogs of hPTH(1-31) and hPTH(1-28) and studied their secondary structure, using CD, and bioactivities in an attempt to clarify the role of the C-terminal functional group.

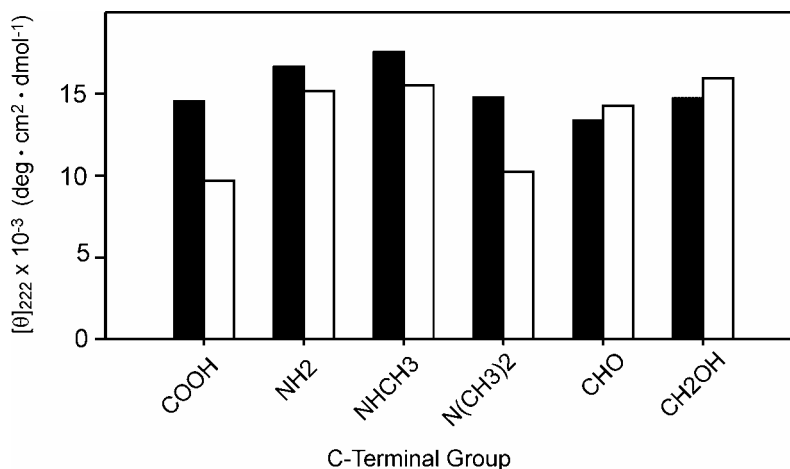


Fig. 1. Effect on C-terminal α -helix of C-terminal modification (1-31 (black), 1-28 (white)).

Results and Discussion

The C-terminal carboxyl and amide for hPTH(1-31) and hPTH(1-28) were synthesized by standard Fmoc protocols. Mono- and dimethylamide analogs were prepared by coupling the fully protected hPTH with either monomethylamine or dimethylamine. Preloaded aldehyde resin, based on the oxazolidine linker, was used to prepare peptide aldehydes. Peptide alcohols were prepared by activating the fully protected peptide with N-hydroxysuccinimide followed by reduction with NaBH₄. Peptides were purified to greater than 90% purity by acetonitrile gradient HPLC, with the MS values confirmed by MALDI-TOF.

The CD and bioactivity values for hPTH(1-31) and hPTH(1-28) were in parallel, with larger effects noted with hPTH(1-28). The CD spectra for the C-terminal α -helix were obtained by subtraction of the spectrum of hPTH(1-17)NH₂. The effect of the C-terminal function on this helix, as represented by $[\theta]_{222}$, is shown in Figure 1. Receptor binding effects are shown for hPTH(1-31) and hPTH(1-28) in Figure 2. Only the carboxyl and dimethylamide analogs had substantially reduced helix levels with about a 30% reduction compared to the amide terminus. In general, effects on helix stability were more pronounced when the C-terminus was at the end of the helix, located at Gln29 in hPTH(1-31) than when external to the end of this helix. The effects on the helix likely result from changes in the helix macrodipole and/or loss of a stabilizing H-bond involving the C-terminal function.

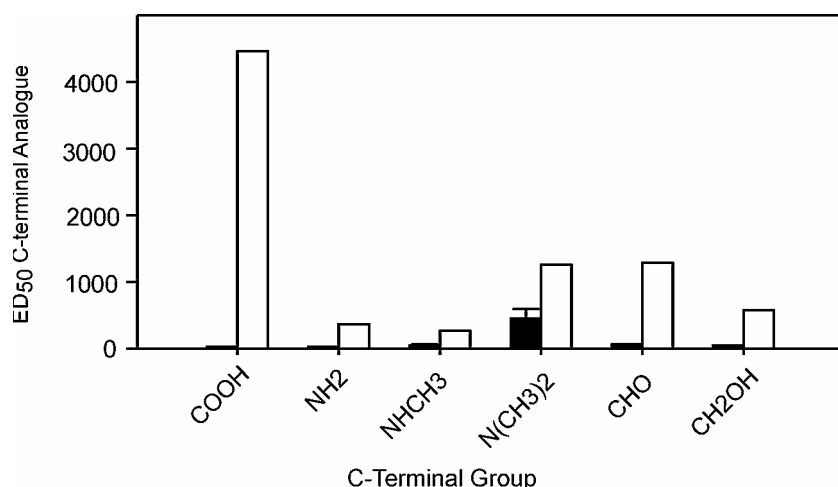


Fig. 2. Effect on receptor binding of C-terminal modification (1-31 (black), 1-28(white)).

There was no dramatic loss of activities on modifying the C-terminal group. However, there was about a 10-fold loss of binding with the carboxyl, and 4-fold loss with dimethylamide or aldehyde C-termini. Retention of binding with the monomethylamide but a loss with the dimethylamide is consistent with H-bond stabilization of the C-terminal helix, as has been suggested by Sforca *et al* [3]. Even though helical structure was retained with the aldehyde C-terminus it is likely that there was a conformational change compared to the amide or methylamide groups and it is possible the aldehyde function of hPTH(1-28) formed a carbinolamine with Arg25 or Lys26. The ethanol C-terminus can act as a H-bond donor or receptor and this may account for its retention of helix.

References

1. Willick, G. E., Morley, P. and Whitfield, J. F. *Curr. Med. Chem.* **11**, 2867-2881 (2004).
2. Geraghty, R. F., Williams, C. H., *et al. Peptides* **15**, 835-841 (1994).
3. Sforca, M. L., Oyama, S. Jr., *et al. Biochemistry* **43**, 5608-5617 (2004).

Spectroscopic Characterization of PEG-Amylin Derivatives

Giuseppe Impellizzeri¹, Diego La Mendola², Antonio Magri², Giuseppe Maccarrone¹, Giuseppe Pappalardo² and Enrico Rizzarelli^{1,2}

¹Università degli Studi di Catania, Dipartimento di Scienze Chimiche, V. le A. Doria 6, 95125 Catania, Italy; ²C. N. R. Istituto di Biostrutture e Bioimmagini Sez. di Catania, V. le A. Doria 6, 95125 Catania, Italy

Introduction

Human islet amyloid polypeptide (hIAPP), a 37-residue hormone, is able to form amyloid aggregates in the extracellular space of the pancreas [1]. These aggregates are assumed to play a key role in type II diabetes by means of a cytotoxic effect towards β -cells [2]. An alteration of the Cu(II) concentration levels during the course of the disease has been observed [3] arguing for the involvement of copper ion in the formation of these fibrils. The conformational study of human amylin and its related amyloidogenic fragments in water solution is limited due to their low solubility; this fact limits also the characterization of corresponding copper(II) complexes. The conjugation at the N-terminus with PEG moiety of a peptide fragment of the human amylin encompassing the 17-29 amino acid sequence, allowed the solubilization of this amyloidogenic peptide.

Human amylin: KCNTATCATQRLANFLVHSSNFGAILSSNTY-NH₂ (hA)

Rat amylin: KCNTATCATQRLANFLVRSSNNLGPVLPPTNVGSNTY-NH₂ (rA)

N-terminus PEG-h-Amylin (17-29) Ac-Peg-VHSSNFGAILSS-NH₂ (1)

Rat amylin modified (17-29) Ac-VHSSNNLGPVLPP-NH₂ (2)

Fig. 1. Sequences of human and rat amylin and the 17-29 fragments studied in this work.

Peptide 1 was characterized by means of spectroscopic techniques in water. The Cu(II) complex of PEG derivative was also studied by means of CD, UV-Vis and potentiometric techniques. The data obtained have been compared with those reported for a soluble rat amylin peptide corresponding to the region 17-29 in which the arginine residue has been replaced by a histidine (peptide 2) [4].

Results and Discussion

In the acidic pH range peptide 1 showed a typical spectra associated with a random coil conformation with a minimum around 198. Between pH 6 and 7, the deprotonation of the histidine's imidazole nitrogen turned the CD curves similar to those reported for a type II β -turn conformation. Peptide 2 showed in the whole pH range studied a random coil conformation [4]. In Table 1 are reported the spectroscopic parameters of copper(II) complexes with the two peptides. Both peptides showed the same Cu (II) complex species in the overall pH range investigated. For both systems we have observed a stepwise deprotonation process starting from CuLH₂ species to give CuLH₃ and CuLH₄ (Fig. 2). At acidic pH the major species is the CuLH₂ in which copper ion is bound to three nitrogens (N_{im}, 3N_{amid}). However the lower energy of d-d transition observed in the absorption spectra in comparison to other analog systems suggests a tetragonal distorted geometry around the metal ion.

Table 1: Spectroscopic and thermodynamic data for both Cu (II) peptide systems

System	Species (CuLH)	log β	λ (nm), ϵ (cm ⁻¹ M ⁻¹)	$g_{ }$	$A_{ }$ (10 ⁴ cm ⁻¹)
Cu (II)-peptide 1	11-2	-7.57 (2)	614 (88)	-	-
	11-3	-16.55 (3)	581 (132)	2.273 (2)	172(5)
	11-4	-26.97 (3)	545 (123)	2.189 (2)	203(4)
Cu (II)-peptide 2	11-2	-8.77 (3)	614 (120)	2.233 (2)	153 (4)
	11-3	-18.05 (3)	562 (103)	2.217 (2)	178 (5)
	11-4	-28.03 (3)	541 (84)	2.195 (2)	201 (4)

This effect is more evident for the Cu (II)-peptide 2 system as indicated by the higher value of ϵ_{\max} . The CuLH₃ species is the most relevant at physiological pH in both systems.

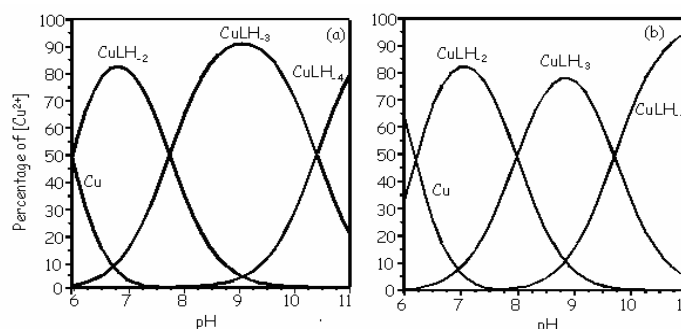


Fig. 2. Species distribution diagrams of the Cu (II) complex species in aqueous solution with (a) Cu-peptide 1 and (b) Cu-peptide 2 present in the pH range 6–11.

The thermodynamic and spectroscopic data suggest a pentacoordinate geometry with a binding mode involving four nitrogens (N_{lm} , $3N_{amid}$) and one oxygen. Above pH 10 the CuLH₄ species is formed and all data indicated a distinct change in coordination with copper ion coordinated by four nitrogens ($4N_{amid}$) in equatorial position.

Acknowledgments

We thank CNR (Rome) and MIUR (Grant 196 D.M. 1105/02) for financial support.

References

1. Opie, E. L. *J. Exp. Med.* **5**, 397-428 (1990).
2. Westermark, P. *Amyloid* **1**, 47-60 (1994).
3. Kogire, M., Ishizuka, J., Thompson, J. C. and Greeley, G. H., Jr. *Pancreas* **6**, 459-463 (1991).
4. Amoresano, A., Flagiello, A., Impellizzeri, G., Magri, A., Pappalardo, G., Pucci, P. and Rizzarelli, E. In *Peptide Revolution: Genomics, Proteomics & Therapeutics, Proceedings of the 18th APS* (Chorev, M. and Sawyer, T. K., eds.), American Peptide Society, pp. 771-772 (2003).

Conformational Properties and Functional Role of VDAC N-Terminal Peptide

Vito De Pinto¹, Angela Messina¹, Rita Aiello¹, Flora Tomasello¹, Diego La Mendola², Antonio Magri², Danilo Milardi² and Giuseppe Pappalardo²

¹Università di Catania, Dipartimento di Scienze Chimiche, V.le A. Doria 6, Catania, Italy;

²C.N.R., Istituto di Biostrutture e Bioimmagini, Sezione di Catania, V.le A. Doria 6, Catania, Italy

Introduction

Eukaryotic porins (or VDACS, Voltage Dependent Anion-selective Channels) are membrane proteins forming an aqueous pore channel in the mitochondrial outer membrane [1]. While bacterial porins structure has been determined by X-Ray diffraction, the structure of eukaryotic porins is still a matter of debate. Bacterial porins can “hole” the outer membrane by a peculiar structure called beta-barrel, since it is formed by 16 (on average) antiparallel amphipathic beta strands lining an aqueous environment [2,3]. Theoretical predictions largely agree in the indication of a predominant content of amphipathic beta strands in the eukaryotic porin structure. In addition to a very structured and compact beta-barrel, every prediction performed so far has highlighted in VDACc the presence of a segment of α -helix, 19-20 amino acids long, with amphipathic features, at the N-terminal of the protein. The bacterial porins do not show such an helical structure and it is thus the most relevant addition to porins in eukaryotic cells. The N-terminal α -helix was claimed to be part of the channel walls, to lie transiently upon one side of the phospholipid bilayer, to allow some motion to the protein during the voltage-gating or to interact specifically with other molecules like cytochrome C and the so called polyanion, a pore-activity inhibitor [4-6]. In this work we report about the physico-chemical characterization of the peptide corresponding to the human porin (VDAC1) sequence 1-19. The biological effects of the deletion of this segment are also shown. The results are discussed on the basis of the known functions of this intriguing membrane protein.

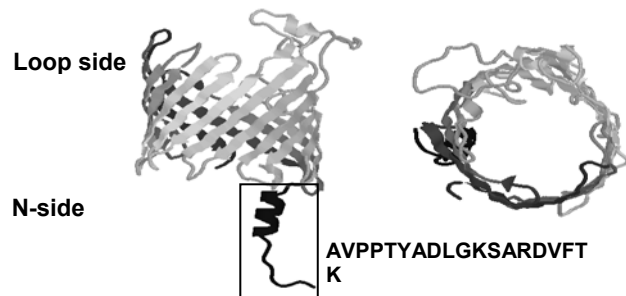


Fig. 1. The predicted 3D structure of *Neurospora crassa* VDAC and the N-terminal peptide studied in this work.

Results and Discussion

To distinguish the function of the α -helix segment from that of the first amino acids in the VDAC sequence, we expressed two mutated porins, deleted of the first 7 or of

the first 19 amino acids. Confocal microscopy revealed that deletion of the N-terminal end of HVDAC1 does not change the mitochondrial targeting of the protein; by contrast its deletion strongly affects the electrophysiological features of the pore as evinced from membrane conductance measurements.

The N-terminal peptide fragment was synthesized using Fmoc chemistry on a PAL-PEG resin in an Applied Biosystem Pioneer peptide synthesizer. CD and NMR experiments were carried out under different experimental conditions to investigate on the conformational preferences of this peptide. CD spectra indicated that the peptide can adopt an α -helical conformation in water/TFE mixed solvent as well as in the presence of SDS micelles conditions mimicking the hydrophobic environment of a membrane (Fig. 2). Notably micellar dodecyl maltoside (DM) did not induce an helical structure. The comparative analysis of the NMR spectra acquired both in water or 5% SDS solutions, gave also evidence of the presence of an helical structure in SDS solution. In particular, the secondary shifts of the H_α protons together with NOE connectivities indicated that the α -helix does not cover the whole sequence but encompasses mainly the C-terminal part of the peptide (Fig.2).

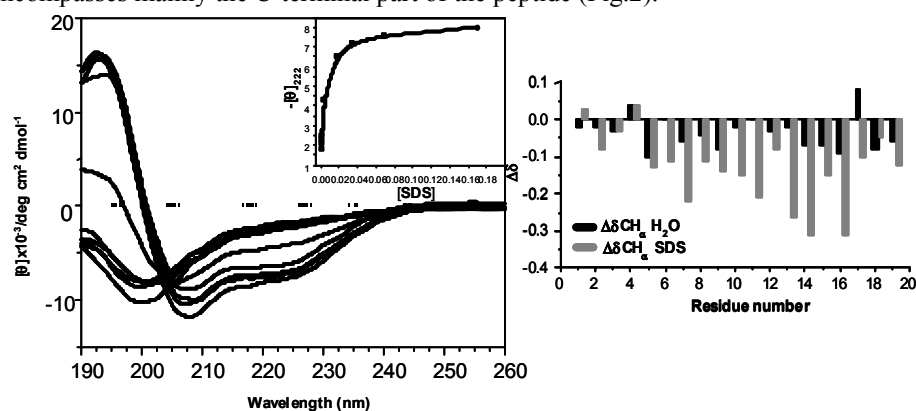


Fig. 2. CD spectra at different [SDS]. Plot of the H_α secondary shifts calculated in SDS.

Finally, preliminary DSC results showed that the peptide was able to interact with DPPS membranes by affecting their thermally-induced gel-liquid crystal transition. Thus our work confirms that the evolutionary addition of this N-terminal sequence to the protein domain responsible of the transmembrane pore-forming unit has a functional/structural meaning peculiar for the eukaryotic porin protein.

Acknowledgments

We thank MIUR and CNR for financial support.

References

1. De Pinto, V., Ludwig, O., Krause, J., *et al. Biochim. Biophys. Acta* **894**, 109-119 (1987).
2. Cowan, S.W., Schirmer, T., Rummel, G., *et al. Nature* **358**, 727-733 (1992).
3. Casadio R., Jacobini I., Messina A., *et al., Febs Lett.*, **520**, 1 (2002).
4. Popp, B., Court, D.A., Benz, R., *et al. J. Biol. Chem.* **271**, 13593-13599 (1996).
5. De Pinto, V., Prezioso, G., Thinner, F., *et al. Biochemistry* **30**, 10191-10200 (1991).
6. Song, J., Midson, C., Blachly-Dyson, E., *et al. J. Biol. Chem.* **273**, 24406-24413 (1998).

Design of Membrane Active Peptides with Regularly Repeating Glycine or D-amino Acid Residues

Jyothi Thundimadathil, Roger W. Roeske and Lili Guo

*Department of Biochemistry and Molecular Biology, Indiana University School of Medicine,
Indianapolis, IN 46202, USA*

Introduction

Design and synthesis of simple protein structures capable of mimicking the complex functional properties of natural ion channels are an active area of research for understanding the basic principles of protein folding and development of novel macromolecular devices. Due to our interest in understanding the role of glycine and D-amino acid residues in designing new type of peptide structures, we are currently pursuing structure-activity studies of synthetic peptides with regularly repeating pattern of glycine or D-amino acid residues. In this direction, we found that N-formyl analog of a D-alanine repeat peptide (VSLGLSLAFSVAVSLAWSFARSRG, where *A* is D-alanine, designated as f-(xSxA/G)₆) forms ion channels in membranes whereas its desformyl analog failed to do so, suggesting the possibility of a β^{12} -helical dimer structure similar to that in gramicidin (gA) [1]. More interestingly, recently we observed the formation of porin-like high-conductance voltage-gated channels by both the N-formyl and desformyl analogs of glycine substituted form of the above peptide (VSLGLSIGFSVGVSIGWSFGRSRG, abbreviated as f/df-(xSxG)₆). The formation of porin-like channels by f/df-(xSxG)₆ indicates organization of β sheets into an ordered β -barrel-like molecular architecture in membranes through peptide assembly [2]. In the present study we compared the ion channel activity of the two types of peptides and tried to correlate the activity with their structural properties. The synthesis, purification and characterization of these peptides have already been reported [1,2].

Results and Discussion

Synthetic peptides were examined for their ability to increase the conductance of a diphytanoylphosphatidyl choline (DPhPC) bilayer membrane formed by painting a 2 % solution of the lipid in n-decane over a small aperture (200 μ m) between two chambers filled with electrolyte (1 M CsCl, unbuffered) solutions. A dilute methanolic solution of the peptide (3 μ l of 0.1 mg/mL) was added to both sides of the bilayer. The current signals were recorded at 1 KHz and sampled at 0.5 KHz using a Bilayer Clamp-525C amplifier and Digidata 1320A digitizer and analyzed using Clampex 8.2 software. Typical channel traces of f-(xSxA/G)₆ and f-(xSxG)₆ are shown in Fig. 1 (A and B). It can be readily seen that f-(xSxA/G)₆ channels constitute low-conductance single channel events without sub-conductance states and flickerings, whereas f-(xSxG)₆ channels are characterized by high-conductance transitions in the nano-Siemens range and several short-lived sub-conductance states. The charge selectivities of peptide channels were determined from zero-current potentials of I-V curves under asymmetric conditions (Fig. 1C & D). The f-(xSxA/G)₆ channel is found to be highly cation selective ($pK^+/pCl^- = 6.9$) whereas f-(xSxG)₆ channel has little preference for cations over anions ($pK^+/pCl^- = 2.1$). High monovalent cation selectivity of f-(xSxA/G)₆ channels support the idea of a β helical

pore lined with seryl hydroxyl groups which can co-ordinate cations effectively. Also, impermeability to cations with a diameter $> 4 \text{ \AA}$ suggests that the diameter of the narrowest portion of the $f\text{-(xSxA/G)}_6$ channel should be $\sim 4 \text{ \AA}$ similar to gA channel. In the proposed β^{12} helical model the $f\text{-(xSxA/G)}_6$ channel comprises three peripheral pores each about the same size as gA channel ($\sim 4.5 \text{ \AA}$, Ref. 1). The $f\text{-(xSxG)}_6$ channel transports a variety of ions such as alkali ions, Ca^{2+} , NH_4^+ , NMe_4^+ , NEt_4^+ , NEt_3Bz^+ and glucosammonium suggesting a pore diameter $> 10.5 \text{ \AA}$. Moreover, the $f\text{-(xSxG)}_6$ channels were inhibited by Congo red suggesting that the peptide aggregates are the active channel species.

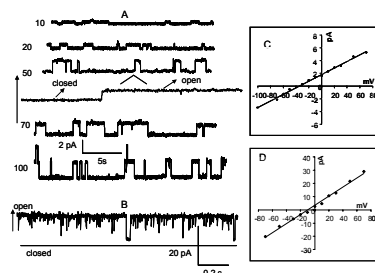


Fig. 1. Ion channels formed by $f\text{-(xSxA/G)}_6$ (A, 10-100 mV) and $f\text{-(xSxG)}_6$ (B, 10 mV) peptides (1 M CsCl, DPhPC) and I-V relationship ($f\text{-(xSxA/G)}_6$: C & $f\text{-(xSxG)}_6$: D) under asymmetric conditions (100 mM:500 mM KCl).

Two distinct bands at -216 and -225 nm along with positive bands around 200 nm in the CD spectrum of $f\text{-(xSxA/G)}_6$ in membranes suggest a novel backbone structure (Fig. 2). Furthermore, IR spectrum indicates a structure stabilized by β sheet type hydrogen bonding pattern (Fig. 2, peaks at 1627 and 1690 cm^{-1}). Both the CD and IR spectra of $f\text{-(xSxG)}_6$ incorporated liposomes indicate a β sheet structure stabilized by anti-parallel hydrogen bonding.

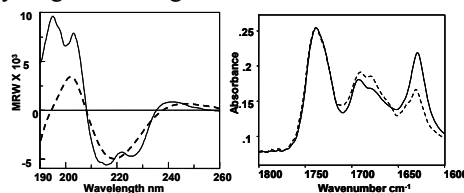


Fig. 2. CD and ATR-IR spectra of $f\text{-(xSxA/G)}_6$ (solid lines) and $f\text{-(xSxG)}_6$ (broken lines) peptides in DMPC (dimyristoylphosphatidylcholine)- D_2O liposomes.

In summary, this work demonstrates the transformation of a simple gramicidin-like channel formed through N-formyl-N-formyl dimerization into a complex porin-like channel formed through β sheet aggregation, by substituting glycines for D-alanines in a $f\text{-(xSxA/G)}_6$ peptide (A is D-alanine).

References

1. Thundimadathil, J., Roeske, R. W. and Guo, L. In *Peptide Revolution: Genomics, Proteomics & Therapeutics, Proceedings of the 18th APS* (Chorev, M. and Sawyer, T. K., eds.), American Peptide Society, pp 689-690 (2003).
2. Thundimadathil, J., Roeske, R. W. and Guo, L. *Biochem. Biophys. Res. Commun.* **330**, 585-590 (2005).

Design and Synthesis of Novel α -MSH Peptide Analogs Highly Selective for the hMC4R

Victor J. Hruby¹, Jinfa Ying¹, Xuyuan Gu¹, Minying Cai¹, Josef Vagner¹,
Dev B. Trivedi¹ and Katalin E. Kövér²

¹Department of Chemistry, University of Arizona, Tucson, AZ 85721 USA; ²Department of Chemistry, University of Debrecen, H-4010 Debrecen, Hungary

Introduction

Recent advances in genomics and proteomics have suggested that highly selective ligands for the melanocortin 4 receptor (hMC4R), both agonists and antagonists, may have applications to a variety of disease states including obesity, anorexia, sexual dysfunction, pain and other problems [1]. The primary ligands for the hMC4R receptor are peptides derived from proopiomelanocortin (POMC) especially α -MSH and γ -MSH [2]. We have been interested in developing such peptide and peptidomimetic ligands for many years and have evaluated several different templates [3]. Many years ago we suggested that the bioactive conformation for α -MSH for what is now the MC1R involved a β -turn, and considerable evidence in support of this hypothesis has been obtained over the years. More recently we have performed extensive NMR and computational chemistry studies to obtain the preferred conformations for MT-II (Ac-Nle-c[Asp-His-D-Phe-Arg-Trp-Lys]-NH₂) a potent non-selective agonist, and SHU-9119 (Ac-Nle-c[Asp-His-D-Nal(2')-Arg-Trp-Lys]-NH₂) [4], and have used these peptides as a template to design and synthesize a number of novel ligands for the hMC4R.

Results and Discussion

Figure 1 shows a stereoview of the bioactive conformation of MT-II. In this model it was found that the β -Hs of Asp⁵ and Arg⁸ were in close proximity, and thus we

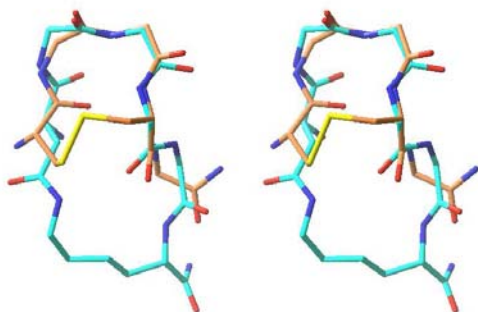


Fig. 1. A stereoview of MT-II conformation derived from NMR and computation studies.

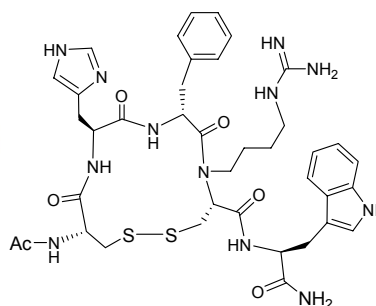


Fig. 2. The structure of peptide 1, Ac-c[Cys-His-D-Phe-N^g-guanidiny]butyl-Cys]-Trp-NH₂.

proposed to replace one of these β Hs from each residue with a sulfur and then made a disulfide bond. Since β -thio-arginine cannot be readily synthesized using available methods, a closely related approach would be to replace the Arg⁸ residue with a Cys residue in which the N ^{α} atom of Cys⁸ would be substituted with a n-butyl-guanidinyll group to mimic the Arg⁸ side chain group as shown in Figure 2. The conformation for this structure as determined by computational methods was similar but not identical to the MT-II conformation, and we felt it was a good model because it provided a novel β -turn, and lent itself to ready modification which would allow us to explore the three dimensional structural requirements for the four melanocortin receptors (hMC1R, hMC3R, hMC4R, and hMC5R), and would lend itself to the synthesis of numerous novel ligands.

A key feature in the synthesis of the designed peptide was the use of the Mitsunobu reaction to alkylate the activated α -amino group of the Cys residue using N,N'-diBoc guanidinyll-butanol [5] and an activated α -amino group, all of which was accomplished on a solid phase support starting with a Rink amide resin. Many alternatives were explored for protection of the Cys-SH and the activation of the α -NH₂ group, many of which led to undesirable side reactions, but an excellent approach was finally developed that led to the synthesis of a number of compounds modified at the α -amino group of the Cys residue and the Trp residue and the D-Phe residue of the structure in Figure 2.

The analog **1** was evaluated for its binding affinity and adenylate cyclase activity for the hMC1R, hMC3R, hMC4R and hMC5R. It was found that **1** has high binding affinity for the hMC4R (1.8 nM), but no binding affinity up to 10⁻⁵M at the other three melanocortin receptors. Interestingly, compound **1** was an antagonist of the hMC4R. This suggests that the conformation obtained for **1**, which is slightly different from MT-II, is sufficiently rigid and different that it recognizes only the hMC4R, but cannot activate the receptor, and hence is an antagonist.

Acknowledgements:

This research was supported by a grant from the U.S. Public Health Service and by an NSF U.S.-Hungary Collaborative Research grant INT-0122172, and by a Fellowship to JY from Merck Research Laboratory.

References

1. Cone, P.D., Ed. The Melanocortin Receptors, Humana Press, 2000.
2. The Melanocortin System, *Ann. N.Y. Acad. Sci.*, **994**, 1-387 (2003).
3. Hruby, V.J., Cai, M., Grieco, P., Han, G., Kavarana, M. and Trivedi, D. *Annals N.Y. Acad. Sci.* **994**, 12-20 (2003).
4. Ying, J., Kövér, K.E., Gu, X., Han, G., Trivedi, D.B., Kavarana, M.J. and Hruby, V.J. *Biopolymers (Peptide Sci.)* **71**, 696-716 (2003).
5. Botta, M., Correlli, F., Maga, G., Manetti, F., Renzulli, M. et al. *Tetrahedron* **57**, 8357-8367 (2001).

Design, Synthesis and Characterization of Conformational Peptides at the Interface of HER-2 Dimerization and Pertuzumab Binding

Joan T. Steele¹, Sharad Rawale² and Pravin T. P. Kaumaya^{1,2,3}

¹*Chemistry-Biology Interface Program;* ²*Department of Obstetrics and Gynecology;* ³*Arthur G. James Comprehensive Cancer Center, The Ohio State University, Columbus, OH 43210, USA*

Introduction

HER-2 is a 185-kDa member of the EGFR family that is expressed in many epithelial tumors. HER-2 positivity is associated with an aggressive disease course and high risk of relapse and death. HER-2 positive tumor cells are potentially good targets for tumor-reactive CTLs. In addition monoclonal antibodies (mAb) against HER-2 protein can inhibit growth of cancer cells that overexpress this receptor on the cell surface. There are several drawbacks associated with passive mAb treatment (insufficient tissue distribution, generation of anti-idiotypic antibodies, and levels necessitating multiple infusions and hence the associated cost [1]). An active specific immunotherapy presents the advantage of generating a long-lasting immune response. We have previously shown the antitumor properties of B-cell epitopes derived from the HER-2 extracellular domain (ECD) [2] using an active immunotherapy approach.

Pertuzumab (recombinant humanized monoclonal antibody 2C4; Omnitarg; Genentech Inc) has been shown to inhibit cancer cell growth [3] and is currently being evaluated in Phase II clinical trials. The crystal structure of HER-2 bound to pertuzumab reveals that the mAb sterically blocks the region necessary for HER-2 dimerization with other members of the EGFR family [4]. We have designed epitopes from this region that makes contact with pertuzumab (MVF HER-2 298-333 and 315-333). In an attempt to elicit conformationally dependent anti-peptide antibodies we have reconstructed this epitope (298-333) by incorporating the native disulfide bonds.

Results and Discussion

The B-cell epitopes were synthesized as a chimeric construct incorporating a T-helper epitope (MVF) using Fmoc chemistry. Regioselective disulfide formation was achieved using differentially protected cysteine residues. Side chain protection for residues 315 and 331 was trityl, which was conveniently removed upon cleavage from the resin. The side chain of cysteine residues at 299 and 311 was protected with Ac, which can be selectively removed and cyclized by oxidation (I₂) after the first cyclization.

We examined the immunogenicity of these peptides in outbred New Zealand White rabbits and inbred FVB/n mice. Both the 298 and 315 epitopes were immunogenic, generating titers greater than 60,000 one week after the third immunization. To test the binding of rabbit peptide antibodies to HER-2, flow cytometry was performed on the SKBR-3 cell line that overexpresses HER-2. Antibodies raised against peptides that contain disulfide bonds (298CYC and 315CYC) have improved binding relative to the linear version of the peptides (Fig. 1). Antibodies raised against the 315CYC showed the most specificity for HER-2,

well within 1 log unit of the mAb herceptin. We next tested the ability of peptide antibodies to mediate antibody dependent cell-mediated cytotoxicity (ADCC) *in vitro*, since it has been documented that *in vivo* the Fc portion of mAbs can be effective in mediating cytotoxicity. Antibodies raised against the cyclized peptide of 315-333 (315 CYC) caused five times the amount of cytotoxicity compared to normal rabbits and 315NC antibodies (49.6% versus 9.1 and 9.3%) at an effector to target ratio of 20:1 (Fig. 2). Taken together these findings confirm the utility of conformational epitopes and have important implications in the development of peptide vaccines for human cancer therapy.

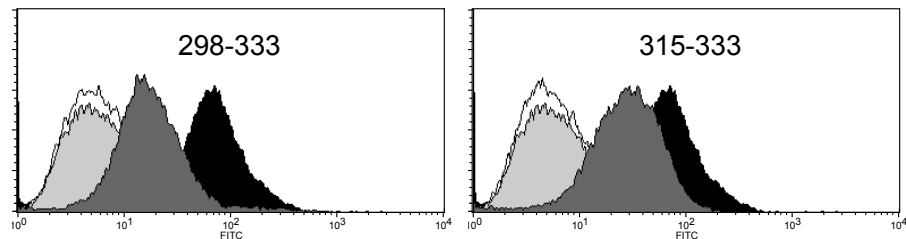


Fig. 1. Flow cytometric analysis of peptide antibodies to breast cancer cells overexpressing HER-2. Histograms indicate linear peptide Abs (white shading), cyclized peptide antibodies (dark gray shading), normal rabbit Ig (negative control, light gray shading), and herceptin (positive control, black shading).

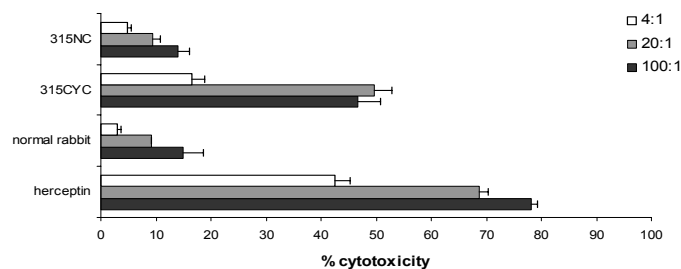


Fig. 2. Peptide antibodies induce ADCC against HER-2 overexpressing cells *in vitro*.

Acknowledgments

The work was supported by a grant from National Cancer Institute (# CA 84356) to P.T.P.K.

References

1. Dakappagari, N.K., Pyles, J., Parihar, R., Carson, W.E., Young, D.C. and Kaumaya, P.T. *J. Immunol.* **170**, 4242-4253 (2003).
2. Dakappagari, N.K., Douglas, D.B., Triozzi, P.L., Stevens, V.C. and Kaumaya, P.T. *Cancer Res.* **60**, 3782-3789 (2000).
3. Agus, D.B., Akita, R.W., Fox, W.D., Lewis, G.D., Higgins, B., Pisacane, P.I., Lofgren, J.A., Tindell, C., Evans, D.P., Maiese, K., Scher, H.I. and Sliwkowski, M.X. *Cancer Cell* **2**, 127-137 (2002).
4. Franklin, M.C., Carey, K.D., Vajdos, F.F., Leahy, D.J., de Vos, A.M. and Sliwkowski, M.X. *Cancer Cell* **5**, 317-328 (2004).
5. Dakappagari, N.K., Lute, K.D., Rawale, S., Steele, J.T., Allen, S.D., Phillips, G., Reilly, R.T. and Kaumaya, P.T. *J. Biol. Chem.* **280**, 54-63 (2005).

Synthesis of a Phosphino Triple Helical Collagen Mimic

John K. Whitehead¹, Shunzi Li¹, LaKeisha N. Myles¹, Robert P. Hammer¹ and Gregg B. Fields²

¹Department of Chemistry, Louisiana State University, Baton Rouge, LA 70803; ²Department of Chemistry and Biochemistry, Florida Atlantic University, Boca Raton, FL, 33431, USA

Introduction

Collagenase is a triple-helical enzyme belonging to the matrix metalloproteinase (MMP) family. This family is mechanistically involved in a variety of diseases such as arthritis, atherosclerosis, and tumor cell metastasis. Several laboratories have investigated phosphorus-based mimics for MMPs and found that phosphinate peptide mimics are effective inhibitors of MMPs [1-3]. To better mimic the natural substrate of MMPs, we have prepared phosphinate containing triple helical peptides. An Fmoc protected phosphino Gly-Val dipeptide mimic has been synthesized and incorporated into the triple helical collagen mimic sequence shown below (Fig. 1).

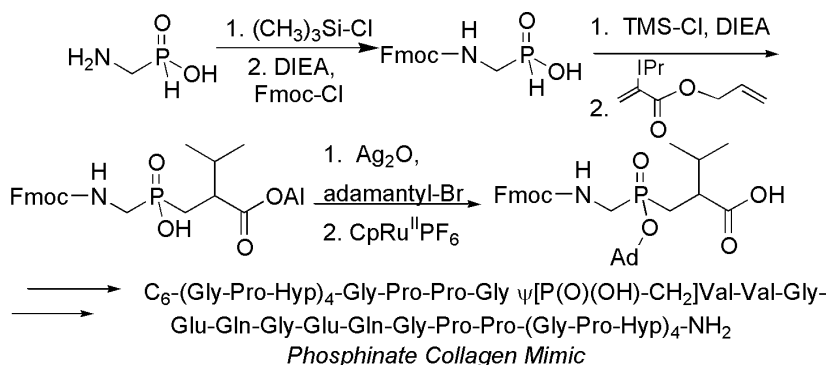


Fig. 1. Top: Synthesis of Fmoc protected phosphino Gly-Val dipeptide mimic. Bottom: Sequence of phosphinate collagen mimic.

Results and Discussion

The peptide mimic was prepared using Fmoc methodology with Fmoc-PAL-PEG-PS resin as a solid support on an Applied Biosystems Pioneer Peptide Synthesizer. The peptide was purified by reverse-phase HPLC and verified by MALDI-MS. The HPLC chromatographs for phosphino triple helical collagen mimics revealed that the diastereomers could be partially separated (Fig. 2).

Each fraction (f1-f4) was collected and analyzed by CD spectroscopy. The fractions containing the C6 tail (f3 and f4) were characteristic of a triple helical structure with the f4 peptide being considerably more triple helical (Fig. 3). Future studies will include determining the absolute configuration of the phosphinopeptides and evaluating their effectiveness as inhibitors of MMPs.

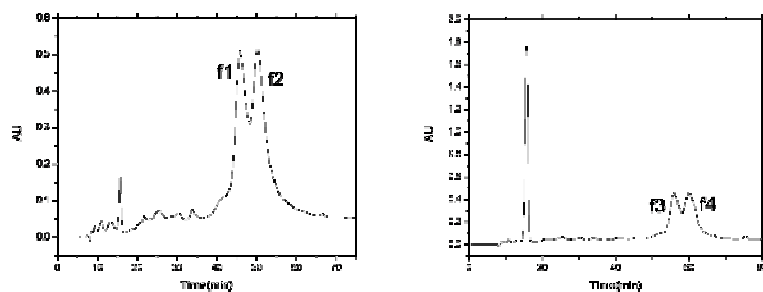


Fig. 2. Left: Chromatograph of phosphinate collagen mimic without C_6 tail. Right: Chromatograph of phosphinate collagen mimic with C_6 tail.

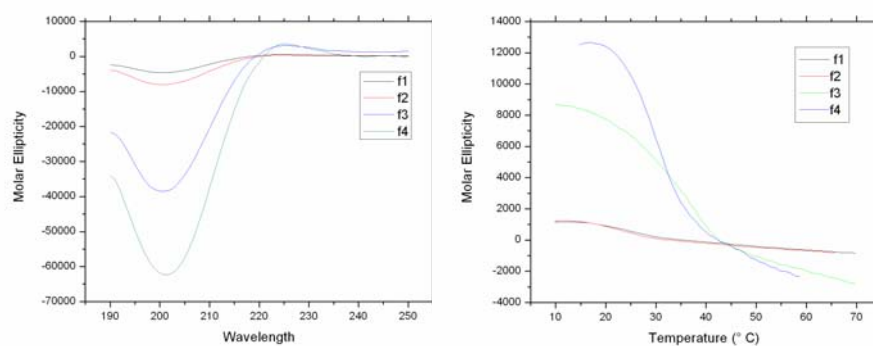


Fig. 3. Left: CD wavelength scans of f1-f4. Right: CD temperature scans of f1-f4.

Acknowledgments

The work was funded by NIH.

References

1. Bartlett, P. A. and Kezer, W. B. *J. Am. Chem. Soc.* **106**, 4282-4283 (1984).
2. Buchardt, J., Ferreras, M., Krog-Jensen, C., Delaisse, J. M., Foged, N. T. and Meldal, M. *Chem. Eur. J.* **5**, 2877-2884 (1999).
3. Gall, A. L., Ruff, M., Kannan, R., Cuniasse, P., Yiotakis, A., Dive, V., Rio, M. C., Basset, P. and Moras, D. *J. Mol. Biol.* **307**, 577-586 (2001).

Steric Hindrance of the HER-2/neu Dimerization Loop by Peptide Mimic Antibodies

Stephanie D. Allen^{1,2}, Sharad Rawale¹ and Pravin T. P. Kaumaya^{1,2,3}

¹*The Ohio State Biochemistry Program, ²Department of Obstetrics and Gynecology, and the*
³*Arthur G. James Comprehensive Cancer Center, The Ohio State University, Columbus, OH*
43210, USA

Introduction

The epidermal growth factor (EGF, ErbB, HER) family is a family of receptor tyrosine kinase receptors, each of which has a cytoplasmic tyrosine-kinase domain, a membrane spanning region, and an extracellular ligand-binding region. There are four receptors in the ErbB family (HER-1, HER-2, HER-3, and HER-4) and multiple ligands that form a diverse, complex signaling system used for development, proliferation, and differentiation [1,2]. HER-2 overexpression is found in 20-30% of all adenocarcinoma breast cancer patients, as well as lung, ovarian, stomach, bladder, salivary, and endometrial cancers. Overexpression of HER-2 has been correlated with a poor clinical prognosis due to increased aggressiveness and resistance to treatment. Increased HER-2 signaling has been implicated in tumor growth and progression of cancer development in patients. Current therapies include humanized monoclonal antibodies such as Herceptin (trastuzumab) and Omnitarg (pertuzumab). Trastuzumab is known to bind extracellular domain IV, while pertuzumab binds the receptor dimerization region in the center of extracellular domain II of HER-2 [3,4].

It has been shown that dimerization in the ErbB family occurs via a ligand-induced structural change. In the “closed” or inactive position, a domain II β hairpin loop interacts with domain IV. When a high-affinity ligand binds the receptor, this loop dissociates from domain IV and extends out from the rest of the receptor into the “open” position and interacts with a binding pocket on domain II of the dimerization partner, allowing transphosphorylation of the intracellular C-terminal tail tyrosines. The HER-2 receptor has the dimerization loop permanently in the “open” or extended conformation, making it the favored dimerization partner for the ErbB family. Pertuzumab binds this dimerization region, blocking the ability of HER-2 to dimerize and inhibiting intracellular signaling.

Monoclonal antibody therapy has several disadvantages including the need for repeated applications, undesirable immunogenicity, and limited duration of action. Based on the recent crystal structure, we have designed a peptide mimic of the dimerization loop (residues 266-296) including the naturally occurring disulfide bond for use in a peptide-based vaccine [4]. Benefits of active immunization with a peptide-based vaccine strategy include immunologic memory as well as preventative and long-term immunity.

Results and Discussion

The B-cell epitope HER-2(266-296) was synthesized co-linearly with the promiscuous T-helper epitope MVF(288-302) on a Milligen/Bioscience 9600 peptide synthesizer (Bedford, MA). The peptide was cleaved from the resin using Reagent B (TFA:Phenol:H₂O:TIS, 90:4:4:2), which also removed the trityl protecting groups on the cysteine residues. The peptide was purified by RP-HPLC, and then exposed to iodine oxidation to allow formation of the naturally occurring disulfide bond

between cysteine residues 268 and 295 [5]. NZW rabbits and wild-type FVB/n mice were immunized with either the cyclized or noncyclized construct and boosted every three weeks. Sera was collected on a weekly basis and tested for antibody titers by direct ELISA. Both constructs were able to elicit high antibody titers in both rabbits and mice (Table 1).

Antibodies were purified from crude sera and used for further diagnostic studies. To determine binding affinity, antibodies were tested for their ability to bind to the native protein on either HER-2 overexpressing human BT474 cells or neu-overexpressing mouse NT2.5 cells. Flow cytometry data indicated that antibodies raised against the cyclized construct bound the native protein better than the noncyclized construct, and noncyclized antibodies had significantly higher binding than control antibodies. These results indicate that the cyclized peptide more closely resembles the native protein. Unlike trastuzumab, the peptide antibodies displayed cross-reactivity with mouse neu as shown by strong binding to the NT2.5 cell line.

Anti-tumor activity was measured using antibody-dependent cell-mediated cytotoxicity. ⁵¹Cr-labeled BT474 cells were incubated with peptide antibodies, then exposed to human PBMCs. The human PBMC recognize the antibody-bound BT474 cells via Fc receptors and produce a lethal hit, killing the BT474 cells and releasing the chromium. Results including high immunogenicity, strong binding affinity, and effective anti-tumor activity indicate that MVF-HER-2(266-296) could be an effective vaccine *in vivo*.

Table 1. Biological characteristics of peptide-mimic antibodies

Peptide Antibody	Immunogenicity ^a	Binding Affinity ^b	Anti-tumor Activity ^c
MVF-HER-2(266-296)NC	+++ ^d	++	+++
MVF-HER-2(266-296)Cyc	+++	+++	+++

^aImmunogenicity determined by direct ELISA from sera of immunized animals;

^bBinding affinity determined by ability of antibodies to bind native protein on HER-2/neu tumor cells;

^cAnti-tumor activity determined by specific lysis of antibody-bound cells;

^d+++ = strong response, ++ = intermediate response.

References

1. Jackson, J. G., St Clair, P., Sliwkowski, M. X. and Brattain, M. G. *Cancer Res.* **64**, 2601-2609 (2004).
2. Olayioye, M. A., Neve, R. M., Lane, H. A. and Hynes, N. E. *Embo J.* **19**, 3159-3167 (2000).
3. Cho, H. S., Mason, K., Ramyar, K. X., Stanley, A. M., Gabelli, S. B., Denney, D. W., Jr. and Leahy, D. J. *Nature* **421**, 756-760 (2003).
4. Franklin, M. C., Carey, K. D., Vajdos, F. F., Leahy, D. J., de Vos, A. M. and Sliwkowski, M. X. *Cancer Cell* **5**, 317-328 (2004).
5. Soll, R. and Beck-Sickinger, A. G. *J. Peptide Sci.* **6**, 387-397 (2000).

Hydrogen/Deuterium Exchange Studies on Helical Peptides in a DMSO/MeOD Solvent System

Erin Daly, Adam Blom and Matt Kubasik

Department of Chemistry, Fairfield University, Fairfield, CT 06824 USA

Introduction

Oligomers of α -aminoisobutyric acid are known to form 3_{10} helices in solution and in the solid state. NMR and IR studies have attempted to establish the minimum length at which reliable 3_{10} helical structures occur. Estimates for the critical length for helix formation have ranged from trimer (with a single intramolecular hydrogen bond) to octamer level.

We have used a hydrogen/deuterium exchange experiment to compare the protection from exchange with solvent deuterons afforded by the 3_{10} helical structure at the tetramer and octamer level. We are using DMSO as solvent and MeOD as a deuteron donor. Oligomers of Aib are known to be helical in DMSO and the literature contains MD studies of Aib oligomers in DMSO for comparison to our experiments.

The structures of the two peptides used in this work are shown below. Dotted lines indicate $i/i+3$ hydrogen bonding of a canonical 3_{10} helical conformation. Within a 3_{10} helical conformation, each structure shows two “solvent-exposed” amide protons. The remaining amide protons might be expected to be protected from exchange through intra-molecular hydrogen bonding.

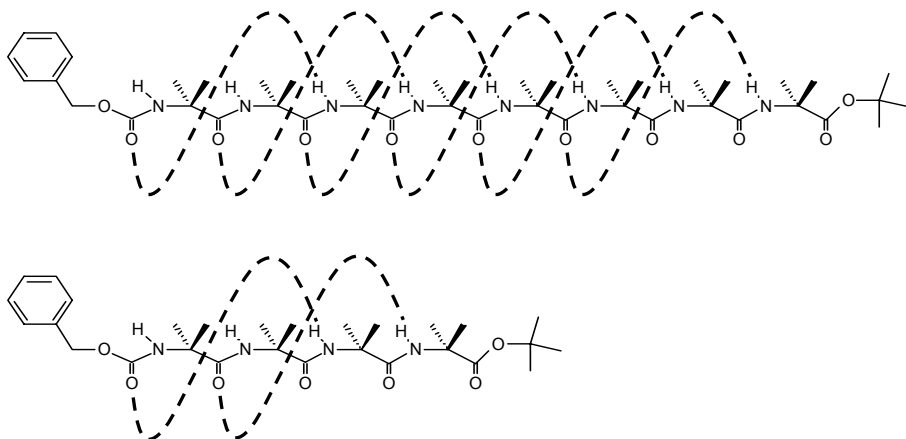


Fig. 1. Structure of octamer and tetramer examined in this work.

Local excursions away from helical structure (e.g., “fraying” of termini) may lead to an opportunity for H/D exchange with solvent. In addition to local conformational fluctuations, oligomers of Aib are known to undergo millisecond-timescale fluctuations between left and right handed helices [1,2]. Because the Aib residue is achiral, oligomers of Aib form isoenergetic left- and right-handed helical structures. When these helices interconvert, the intramolecular hydrogen bonds within the helix are broken, exposing amides to exchange with solvent.

Results and Discussion

Under the conditions of our experiment (~1 mM peptide in 3:1 DMSO/MeOD (v/v), T = 298K), we find that two amide protons on each peptide exchange rapidly (<10 min). These two amide protons most likely correspond to the “solvent exposed” (non-intramolecularly hydrogen bonded) amide protons shown in Figure 1. The remaining amide protons on each peptide exhibit reduced rates of exchange with solvent deuterons. Measured rate constants are listed in Table 1. All four amide protons of the tetramer exchange on the timescale of the experiment, while the octamer has two very fast (solvent-exposed) exchanging amide protons: two amide protons that exchange at roughly the rate of the tetramer’s slowly exchanging amide protons (Table 1), and four remaining amide protons that do not show appreciable exchange within the timescale of the experiment.

Table 1. Rate constants of H/D exchange of Amide protons “NH_A” and “NH_B”

Peptide	Pseudo-first order rate constants		2 nd order rate constants	
	k (hr ⁻¹)		k (M ⁻¹ hr ⁻¹)	
	NH _A	NH _B	NH _A	NH _B
Tetramer	5.1 x 10 ⁻²	1.7 x 10 ⁻¹	8.3 x 10 ⁻³	2.8 x 10 ⁻²
Octamer	3.5 x 10 ⁻²	1.6 x 10 ⁻¹	5.8 x 10 ⁻³	2.6 x 10 ⁻²

Interestingly, the rate constants for exchange for amide protons of the tetramer and the measurably exchanging amide protons of the octamer show very similar exchange rates. Although we have not yet assigned amide protons in our ¹H spectra, it might be reasonable to assume that the unmeasurably slowly exchanging amide protons of the octamer are within the interior of the peptide (e.g., residues 4-7). The similarity of the exchange behavior of the two peptides indicates a remarkable helical stability within the tetramer in DMSO solvent. More kinetics experiments, especially measurement of activation enthalpies for exchange, will be performed to characterize the energetics of amide proton exchange in these two peptides. Assignment of the amide protons will allow for residue-level characterization of the stability of these peptide helices in DMSO.

Peptides were synthesized according to the wet-chemical methods of Toniolo and co-workers [3] and confirmed by MALDI-TOF MS. Rates of exchange were determined via integration of sequential 1-D ¹H NMR spectra collected on a Bruker Avance 300 MHz spectrometer.

Acknowledgments

The work was funded by CCSA 5899 from Research Corporation.

References

1. Hummel, R. -P., Toniolo, C. and Jung, G. *Angew.Chem. Int. Ed. Engl.* **26**, 1150-1152 (1987).
2. Kubasik, M., Kotz, J., Szabo, C., Furlong, T. and Stace, J. *Biopolymers* **78**, 87-89 (2005).
3. Toniolo, C., Bonora, G. M., Barone, V., Bavoso, A., Benedetti, E., Di Blasio, B., Grimaldi, P., Pavone, V. and Pedone, C. *Macromolecules* **18**, 895-902 (1985).

Octapeptide Analogs of Somatostatin Containing α,α -Dialkylated Amino Acids with Potent Anticancer Activity

**Sudhanand Prasad, Archna Mathur, Neena Gupta, Manu Jaggi, Anu
T.Singh and Rama Mukherjee**

Dabur Research Foundation, 22, Site IV, Sahibabad, Ghaziabad 201010, India

Introduction

Somatostatin is a hormonal cyclopeptide produced by normal endocrine, gastrointestinal, immune and neuronal cells, as well as by certain tumours. It inhibits the secretion of growth hormones, glucagon, insulin, gastrin, secretin, intestinal fluid, pancreatic enzymes and plays an important role in neural transmission [1]. Somatostatin receptors have been found to be over-expressed on the surface of a wide range of tumor cells, those arising in the brain, the digestive-pancreatic tract, lung, thyroid, mammary gland, prostate, lymphatic system and ovaries [2]. Because of its wide range of physiological functions, a number of analogs of somatostatin have been synthesized and evaluated for their therapeutic potential [3]. Some of the most potent anticancer octapeptide analogs reported are octreotide, RC-160 and CTOP [4].

Here, we report the synthesis, anticancer activity and solution conformation of octapeptide **I**, and four of its analogs **II-V**. Three peptides, **II**, **III** and **IV** were designed by incorporating α,α -dialkylated amino acids at position 6, replacing Thr of the CTOP peptide **I** (Fig. 1). In peptide **V**, Orn⁵ and Thr⁶ of CTOP were replaced by Lys and Ac5c respectively. α,α -Dialkylated amino acids are known to induce β -turn conformation in small peptides.

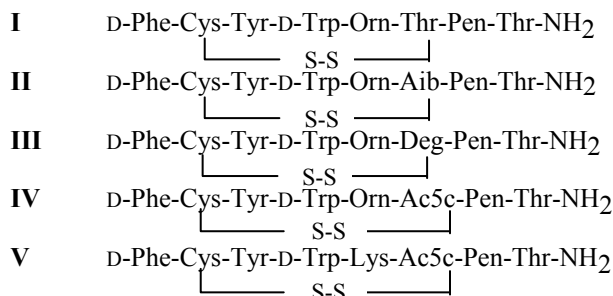


Fig. 1. Peptide sequences.

Results and Discussion

Peptides were synthesized using Fmoc chemistry on Rink amide resin in C.S Bio peptide synthesizer and were purified by HPLC. NMR studies were performed on a Bruker DRX400 NMR spectrometer. *In vitro* anticancer activity on various cancer cells were performed following standard MTT assay and *in vivo* activity in tumor xenografted nude mice.

The conformation of **I** and **IV** was studied by NMR. The appearance of ROE cross peak between NHOrn⁵-NHThr⁶ a small coupling constant for D-Trp⁴ ($J_{\text{NH-C}\alpha\text{H}} = 5.7$ Hz) together with the involvement of NHThr⁶ in hydrogen bond ($d\delta/dT$ for Thr⁶, -0.4ppb/K) suggest the presence of a β -turn around D-Trp⁴-Orn⁵ residues in peptide

I. Furthermore, a strong inter-residue $C^{\alpha}H-NH$ between D-Trp⁴-Orn⁵ and a weak intra-residual $d_{\alpha N}$ Orn⁵ peak indicate a type II β -turn. Peptide **IV** shows sequential NOE peaks of the type d_{NN} between NHOrn⁵-NHAcSc⁶-NHPen⁷-NHThr⁸. Medium-intensity $C^{\alpha}H-NH$ sequential peaks were also seen throughout the peptide sequence. The temperature coefficient of NH Pen⁷ is -1.9 ppb/K, suggesting its involvement in hydrogen bonding. Thus, the peptide assumes a type β -turn centered at Orn⁵-AcSc⁶ residues with NHPen⁷ involved in an intramolecular hydrogen bond with $C=O$ D-Trp⁴.

Antitumor activity. In the case of oral cell line (KB), peptide **III** shows a maximal decrease in cell proliferation at 10 nM. The inhibitory effects of peptides **II** and **IV** are quite comparable at both 10 nM and 100 nM concentrations. All somatostatin peptide analogs show remarkable growth inhibition ($\sim 40\%$) in glioblastoma cell line (U87MG). In the case of the breast cancer (HBL100) cells, peptides **II** and **III** are slightly more effective in inhibiting growth than peptides **IV** and **V** at both the reported concentrations. The laryngeal cells (HeP2) display $\sim 27\%$ growth inhibition when treated with **III** and **IV** peptides at 10 nM. All somatostatin analogs inhibited nearly 25% growth of lung cancer cells (L132). Maximal growth inhibition ($\sim 40\%$) of ovary cells (PA-1) has been demonstrated with **IV**. Peptides **III** and **V** show comparable inhibitory effects while **II** is only marginally less active. In the colon cancer cell line (PTC), little activity is seen for all the peptides. For the endothelial cell line ECV304, all peptides display around 20% growth inhibition.

In vivo activity. The antitumor activity of peptides, **I**, **III** and **IV** was studied in human colon adenocarcinoma (PTC) xenografts in nude mice. Figure 2 shows tumor kinetics till day 25 in the treated and untreated animals. The percentage inhibition of tumor growth caused by peptides **I**, **III** and **IV**, as compared to the untreated tumor on day 21 was 86.3, 57.1 and 54.7% respectively.

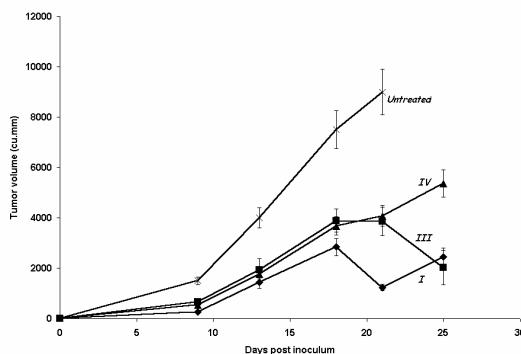


Fig. 2. Tumor kinetics in nude mice.

The designed octapeptide analogs of somatostatin show good antitumor activity both *in vitro* and *in vivo*. In particular these analogs show significant anticancer activity in the glioblastoma cell line. Incorporation of AcSc in peptide **IV** retains β -turn conformation.

References

1. Weckbecker, G., Lewis, I., Albert, R., Schmid, H. A., Hoyer, D. and Bruns, C. *Nat. Rev. Drug Discov.* **12**, 999-1017 (2003).
2. Lamberts, S. W. J., de Herder, W. W. and Hofland, L. J. *Trends Endocrinol. Metabolism* **13**, 451-457 (2002).
3. Janecka, A., Zubrzycka, M. and Janecki, T. *J. Peptide Res.* **58**, 91-107 (2001).
4. Scarpignato, C. and Pelosini, I. *Chemotherapy* **47**, 1-29 (2001).

Backbone Cyclization Improves the Enzymatic Stability of χ -Conotoxin, MrIA, whilst Maintaining its Structure and NET-Modulating Activity

Erica S. Lovelace, Christopher J. Armishaw, Michelle L. Colgrave, Paul F. Alewood, Norelle L. Daly and David J. Craik

Institute for Molecular Bioscience, University of Queensland, Brisbane 4072, Australia

Introduction

Conotoxins, produced by cone snails, have been under investigation in recent years for the treatment of many diseases and conditions including chronic pain, epilepsy, cardiovascular disease, psychiatric disorders, Parkinson's disease, Alzheimer's disease, cancer, and stroke [1-4].

Conotoxins are cysteine-rich peptides that comprise approximately 10-30 amino acids and contain multiple disulfide bonds [5-7]. One recently identified conotoxin, MrIA, a 13 residue peptide of the χ subfamily, has been shown to inhibit the human norepinephrine transporter (NET) and has potential applications in the treatment of pain [8,9]. MrIA contains two disulfide bonds in a "ribbon" connectivity, and the three-dimensional structure of MrIA reveals a structure consisting mainly of a β -hairpin, which places the N- and C-termini in close proximity [10].

The inherent vulnerability to enzymatic cleavage is one major challenge facing all linear peptides that may lead to limitations in their pharmaceutical use. Although conotoxins are generally considered to be relatively stable peptides, we envisaged that their *in vivo* stability could be improved by joining the N- and C-termini of the peptide via "linkers."

Results and Discussion

We synthesized a cyclic version of MrIA, cMrIA(AG), with a two-residue linker by using Boc *in situ* neutralization chemistry and cleaved from the resin using HF / p-cresol (9:1) for 2 hours at 0°C. Cyclization was performed in 6 M guanidine hydrochloride; 100 mM Tris HCl buffer, pH 7.3. Disulfide bonds were formed by stirring the reduced cyclic peptide in 0.1 M NH_4HCO_3 , pH 8.0; 50% isopropanol.

Displacement of radiolabeled ^3H -nisoxetine by the MrIA analogues was conducted to determine their binding to expressed human NET in Cos⁷ cells. The average LogEC₅₀ of MrIA-NH₂ was $-5.74 \text{ M} \pm 0.05$ and the average LogEC₅₀ of cyclic MrIA was $-5.86 \text{ M} \pm 0.28$ ($n = 9$ and $n = 7$, respectively).

cMrIA(AG) gave good quality NMR spectra in aqueous solution at pH 3.5 and temperatures in the range 281-298 K. Residues 3-5 and 10-12 of cMrIA(AG) form an anti-parallel β -sheet. The strands are connected in part by an inverse γ turn between residues 6-8. The overlay of the sheet regions of the representative structures of cMrIA(AG) and MrIA-NH₂ with a RMSD of 0.56 Å indicates highly similar structures as shown in Figure 1. The RMSD of cMrIA is lower than native MrIA, suggesting an increase in the structural stability of the peptide.

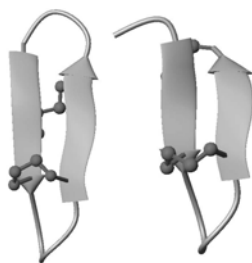


Fig. 1. The ribbon representation of cMrIA(AG) (left) and linear MrIA-NH₂ (right). The overlay of the sheet regions of the representative structures of cMrIA(AG) and MrIA-NH₂ with a RMSD of 0.56 Å indicates highly similar structures.

Enzymatic digestion assays were performed with MrIA-NH₂ and cMrIA(AG) in order to compare the enzymatic stability of the native and cyclized versions. Trypsin successfully digested linear MrIA-NH₂ within 24 hours at a 20:1 ratio. Less than 55% of intact MrIA-NH₂ remained intact after 24 hours compared to 97% of intact cMrIA(AG) remaining, thereby showing an increase in the enzymatic stability of the cyclized version of the peptide.

In summary, MrIA can be backbone cyclized with a two-residue linker whilst maintaining the fold of the native peptide and the activity at the NET. The enzymatic stability of the peptide was significantly improved upon cyclization. This study suggests that cyclization stabilizes the overall structure of MrIA and confers resistance to cleavage to both exoproteases and endoproteases, a property that may enhance its therapeutic potential.

Acknowledgments

DJC and PFA are Senior Research Affiliates of the ARC Special Research Centre for Functional and Applied Genomics, which provided infrastructure support for the work in this project. NLD is an NHMRC Industry Fellow. ESL and CJA acknowledge ARC support.

References

1. Livett, B. G., Gayler, K. R. and Khalil, Z. *Curr. Med. Chem.* **11**, 1715-1723 (2004).
2. Staats, P. S., Yearwood, T., Charapata, S. G., Presley, R. W., Wallace, M. S., Byas-Smith, M., Fisher, R., Bryce, D. A., Mangieri, E. A., Luther, R. R., Mayo, M., McGuire, D. and Ellis, D. *Jama* **291**, 63-70 (2004).
3. Arias, H. R. and Blanton, M. P. *Int. J. Biochem. Cell. Biol.* **32**, 1017-1028 (2000).
4. Nielsen, K. J., Thomas, L., Lewis, R. J., Alewood, P. F. and Craik, D. J. *J. Mol. Biol.* **263**, 297-310 (1996).
5. Terlau, H. and Olivera, B. M. *Physiol. Rev.* **84**, 41-68 (2004).
6. Adams, D. J., Alewood, P. F., Craik, D. J., Drinkwater, R. D. and Lewis, R. J. *Drug Devel. Res.* **46**, 219-234 (1999).
7. Olivera, B. M. and Cruz, L. J. *Toxicon* **39**, 7-14 (2001).
8. Sharpe, I. A., Loughnan, M. L., Thomas, L., Adams, D. A., Atkins, A., Palant, E., Craik, D. J., Alewood, P. F. and Lewis, R. J. *Nat. Neurosci.* **4**, 902-907 (2001).
9. Sharpe, I. A., Palant, E., Schroeder, C. I., Kaye, D. M., Adams, D. J., Alewood, P. F. and Lewis, R. J. *J. Biol. Chem.* **278**, 40317-40323 (2003).
10. Nilsson, K. P. R., Lovelace, E. S., Caesar, C. E., Tynngård, N., Alewood, P. F., Johansson, H. M., Sharpe, I. A., Lewis, R. J., Daly, N. L. and Craik, D. J. *Biopolymers (Peptide Sci.)* **80**, 815-823 (2005).

De novo Design of Peptide Folds of Stereochemically Rationalized Molecular Architecture

Soumendra Rana¹, Bijoy Kundu² and Susheel Durani¹

¹Department of Chemistry; Indian Institute of Technology Bombay, Mumbai-400076

²Medicinal Chemistry Division; Central Drug Research Institute, Lucknow-226001, India

Introduction

Nature extracts phenomenal purchase from an alphabet of stereochemically frozen composition. The bonanza could be extended by artificially restoring the molecular alphabet to stereochemical parity. The homochiral nature of polypeptide stereochemical structure restricts the choice of both residue and motif level conformation in proteins to a handful [1] and therefore the possibility for tertiary structure to $\cong 10^3$ topologically distinct folds [2]. Recruitment of stereochemistry as an additional, higher level, sequence variable promises to multiply the conformational template in polypeptide structure towards *de novo* design, with added bonus that molecular morphologies could be customized stereochemically, by stereospecific folding of polypeptides of heterochiral structure. Illustrating this excursion with Nature's design algorithm, beyond constraints of homochiral alphabet, 14 to 20-residue peptides were recently shown to adopt "bracelet" [3] and "boat" [4] shaped molecular morphologies, along with protein like ordering of conformation. Another variant is now achieved as a "canoe" shaped molecule or as a gramicidin-A channel [5] as if sliced into half. An artificial construct, the "nanotube" [6] was made from building blocks that could be imagined as slabs of gramicidin "channel" sliced horizontally. Performing imaginary longitudinal bisection on gramicidin "channel", we designed molecular "canoe" and our results suggest that indeed a "canoe" type molecular fold exists in water with a double-headed "catgrip" [7] like structure, as observed in proteins. With the lifting of stereochemical degeneracy in Nature's building block alphabet, it may be possible to bridge the gulf between what is possible biologically and what has been accomplished artificially.

Results and Discussion

Stereochemistry is central to polypeptide structure and conformation. The stereochemical degeneracy of building block alphabet of α -amino acids is a severe constraint in the *de novo* design of peptide molecular folds. An isotactic polypeptide chain can either fold into an α -helix, β -sheet or PPII type structures. This restricted diversity of conformation is hardly conducive for the design of customized supramolecular systems useful beyond the realm of biochemical application. The lifting of Nature's constraint on chiral center can, on simple combinatorial reasoning, expand tremendously the architectural diversity of polypeptide folds, providing a novel and untapped potential for *de novo* design. Recently we successfully implemented design of polypeptide folds of stereochemically defined molecular morphology, which suggested that the stereochemical recipe could be applied for large-scale diversification of peptide molecular architecture, with built in prospect for customization of both molecular forms and functions. As a starting point β -hairpin peptides have been taken up for rational stereochemical modification, for creation of customized molecular morphologies. A bracelet [1] shaped fold (Fig. 1a) and a horseshoe shaped fold (Fig. 1b) was generated in 14-residue peptides, whereas a boat [2] shaped molecular fold was accomplished in a 20-residue peptide, making

it the smallest known globular fold with molecular cleft, and suitable template for future development as a molecular receptor (Fig. 1c). We further extended this study by designing “canoe” shaped fold [Ac-Lys(1)-D-Ala(2)-Val(3)-D-Pro(4)-Gly(5)-Leu(6)-D-Val(7)-Glu(8)-D-Val(9)-Pro(10)-Gly(11)-D-Ala(12)-Lys(13)-D-Asp-(14) Ile-(15)-D-Pro(16)-Gly(17)-Val(18)-D-Ala(19)-Ile(20)-NH₂] (Fig. 1d) made of four side-by-side antiparallel strands with main-chain conformation similar to the gramicidin channel-A joined via type II / II' β -turns. The 20-residue “canoe” peptide was synthesized manually in a 10ml syringe by standard solid phase Fmoc-chemistry. The final peptide was obtained as a primary amide group (-CONH₂) at C-terminus and with acetylated (-NCOCH₃) N-terminus. Given its topological cum stereochemical complexity, the peptide was tested for conformational integrity as a molecular canoe by 2D NMR, CD techniques and by molecular dynamics (MD) with gromos-96 43a1 force field in GROMACS package, at 300K in a periodic solvent box filled with water or methanol. The average energy minimized NMR structure of the canoe in water displayed a mean global backbone RMSD of 2Å (Fig. 1d) against the most populated conformer of the peptide in water detected with MD.

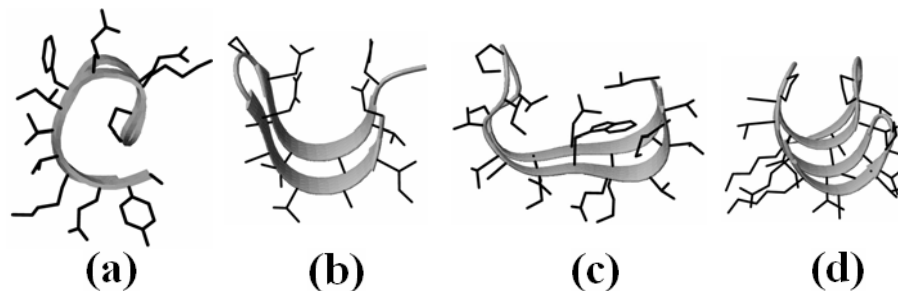


Fig. 1. Ribbon representation of the backbone molecular architecture of the four stereochemically customized peptides of 14 to 20-residues.

Acknowledgments

This work was funded by a research grant from Council of Scientific and Industrial Research (CSIR), New Delhi, India. We acknowledge the use of National High Field NMR Facility at TIFR, Mumbai.

References

1. Pauling, L. and Corey, R. *Proc. Nat. Acad. Sci. U. S. A.* **37**, 282-285 (1951).
2. Chothia, C. *Nature*. **357**, 543-544 (1992).
3. Rana, S., Kundu, B. and Durani, S. *Chem. Commun.* **21**, 2462-2463 (2004).
4. Rana, S., Kundu, B. and Durani, S. *Chem. Commun.* **11**, 207-209 (2005).
5. a) Langs, D. A. *Science*. **241**, 188-191 (1988); b) Ketchum, R. R., Hu, W. and Cross, T. A. *Science*. **261**, 1457-1459 (1993)
6. Khazanovich, N., Granja, J. R., McRee, D. E., Milligan, R. A. and Ghadiri, M. R. *J. Am. Chem. Soc.* **116**, 6011-6012 (1994)
7. Watson, J. D. and Milner-White, E. J. *J. Mol. Biol.* **315**, 183-191 (2002).

Restructuring Artificial Peptide Networks by External Triggering

Gonen Ashkenasy and M. Reza Ghadiri

Departments of Chemistry and Molecular Biology and the Skaggs Institute for Chemical
 Biology, The Scripps Institute, La Jolla, California 92037, USA

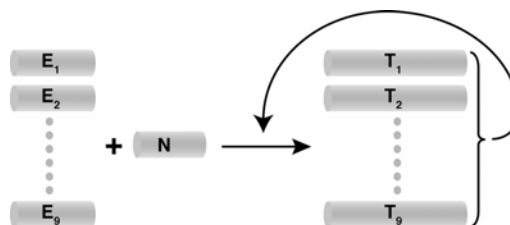
Introduction

Networks appear in numerous aspects of the world we live in, from the large-scale ecological systems, social networks, and World Wide Web, to the microscopic biochemical networks of living cells [1]. Molecular biology and biochemical sciences have and continue to provide a wealth of detailed information about the functional characteristics of biomolecules and their interaction diagrams. Yet, our current inadequate understanding of the influence, transfer, and processing of molecular-level information into the overall dynamic macroscopic behavior remains as a major impediment in the bottom-up approach to systems biology. We reasoned that rationally designed synthetic molecular systems might provide useful model networks for the study and better understanding of complex system behavior. Towards this direction we present here our latest results regarding the *de novo* design, graph prediction, experimental analysis, and characterization of synthetic peptide-based self-organized networks. Similar to natural networks, the generated theoretical graph displays clustered nodes with an overall hierarchical architecture. Furthermore, the experimental molecular array can meaningfully adapt to environmental changes by rewiring different peptides as ‘hubs’ and thus gives rise to different functional sub-networks.

Results and Discussion

The experimental network consists of nine nodes (peptides) that compose a main segment of the theoretical graph [2]. These peptides are formed within the network via auto- and cross-catalytic template-directed coiled-coil condensation reactions [3] from a set of nine thiolester electrophilic mutants (E_{1-9}) and one N-terminal cysteine nucleophile (N) (Scheme 1). The network connectivity and catalytic efficiency were studied in three consecutive sets of experiments.

In the first set, the network was probed by reacting all nine electrophilic peptide fragments, E_{1-9} ($50 \pm 5 \mu\text{M}$ each), and a substoichiometric amount of the nucleophilic peptide fragment, N ($300 \mu\text{M}$) in a single reaction vessel. Quantitative analytical RP-HPLC analysis was used to follow the rate of production of all nine species simultaneously in a given reaction



T_1 : Ar-RVARLEREVSELEKRVACLEXEVARLKKLVGE-CONH₂
 T_2 : Ar-RVARLEREVSELEKRVACLEXEVARLKKLVGE-CONH₂
 T_3 : Ar-RVRQLERKVSELEAKRVACLEXEVARLKKLVGE-CONH₂
 T_4 : Ar-RVARLEKKVSALKKVACLEXEVARLKKLVGE-CONH₂
 T_5 : Ar-RVARLEKKVSALKKVACLEXEVARLKKLVGE-CONH₂
 T_6 : Ar-RVRQLEKEVSALAKKVACLEXEVARLKKLVGE-CONH₂
 T_7 : Ar-RVSALEAAVSELEKRVACLEXEVARLKKLVGE-CONH₂
 T_8 : Ar-RVSALEAAVSELEKRVACLEXEVARLKKLVGE-CONH₂
 T_9 : Ar-RVSKLEAAVSELEKRVACLEXEVARLKKLVGE-CONH₂
 E_1 : Ar-RVARLERZ₁VSELZ₂RKVA-COSR'
 N : H₂N-CLEXEVARLKKLVGE-CONH₂

mixture. These studies confirmed the expectations that it is the assembled, three-dimensional structures in the reaction mechanism that give rise to template-assisted ligation selectivities and specificities, not some inherent differences in reactivity among the peptides.

In the second set of experiment, the most prominent template-assisted catalytic pathways within the network were revealed by repeating the network reaction nine more times, each time seeded with approximately 30 μM of only one of the templates T_{1-9} . Monitoring product formation over time shows that, in the initial stages of the reaction, each added template enhances the formation of not all but only certain products relative to the unseeded, background reaction. Moreover, these initial rate enhancements allow for an overall increased yield of all products in the mixture as noted at later points in the course of the reaction.

The observed product enhancements in the seeded reactions represent operating auto- and cross-catalytic pathways within the network. This network, however, lacks several directed edges and one node as compared to the theoretical predictions. The third set of experiments was thus designed to uncover the latent edges. The additional networking capacity of T_2 , T_5 and T_7 was established by analyzing the rates of product formation in reaction mixtures made up of the nucleophilic fragment (300 μM), and all electrophiles (50 ± 5 μM each) but those that lead to the most efficient processes (e.g., the autocatalytic formation of T_5) in the presence or absence of the relevant template (25 μM) under native conditions.

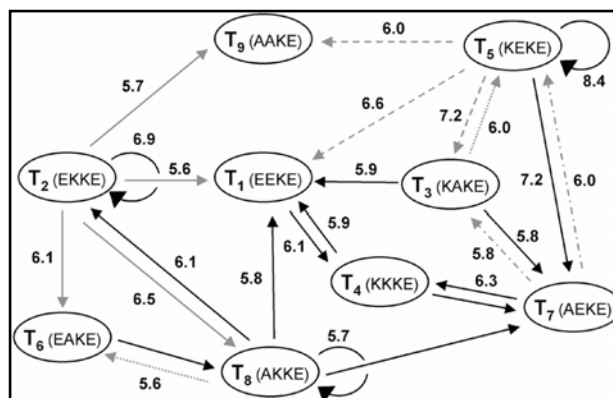


Fig. 1. The experimentally derived network architecture. The arrows (edges) designate template-assisted ligation pathways pointing from the template to the product. Arrows in solid black were generated from data obtained in the second set of experiments and arrows in gray from data from the third set. Numbers along the edges are the estimated $-\Delta\Delta G$ scoring values (kcal.mol^{-1} [3]) for the specified template-directed pathways.

Altogether these studies established that the nine peptide-nodes can participate in the formation of a synthetic, self-organized network composed of 25 edges in good agreement with the estimated graph architecture.

Acknowledgments

GA thanks the Human Frontier Science Program for the post-doctoral fellowship.

References

1. a) Bray, D. *Science* **301**, 1864-1865 (2003); b) Alon, U. *Science* **301**, 1866-1867 (2003).
2. Ashkenasy G., Jagasia R., Yadav M. and Ghadiri M. R. *Proc. Natl. Acad. Sci. USA* **101**, 10872-10877 (2004).
3. a) Lee, D. H., Granja, J. R., Martinez, J. A., Severin, K. and Ghadiri, M. R. *Nature* **382**, 525-528 (1996). b) Severin, K., Lee, D. H., Kennan, A. J. and Ghadiri, M. R. *Nature* **389**, 706-709 (1997).

Development of a Stilbene-type Photoswitchable β -Hairpin Mimetic

Máté Erdélyi^{1,2} and Adolf Gogoll¹

¹Department of Organic Chemistry, Uppsala University, Box 599, S-75124 Uppsala, Sweden;

²Department of Medicinal Chemistry, Uppsala University, Box 574, S-75123 Uppsala, Sweden

Introduction

Molecular switches are units that possess two or more interconvertible conformational states [1]. The development of systems capable of light-triggered conformational change is of outstanding interest since they have a considerable potential for application as new tools in biomedical engineering [2]. Their incorporation into bioactive compounds may allow the external modulation of biological effect.

The β -hairpin motif is involved in various crucial physiological processes and numerous diseases. In addition, the biological activity of some β -hairpins has been shown to be correlated to the thermodynamic stability of their folded conformation [3]. Thus, a β -hairpin mimetic incorporating a photoswitchable moiety would be an attractive candidate for a peptidomimetic allowing externally triggered interconversion between a bioactive β -hairpin and a bioinactive non-hairpin conformation. Compounds containing a switchable azobenzene unit were recently published [4]; however, at present, no attempts for the incorporation of stilbene derivatives into peptides have been reported. Here, we present an investigation of the properties of peptidomimetics incorporating meta-substituted stilbene derivatives (Fig. 1) and compare their conformations with peptides compassing standard, nonswitchable turn mimics.

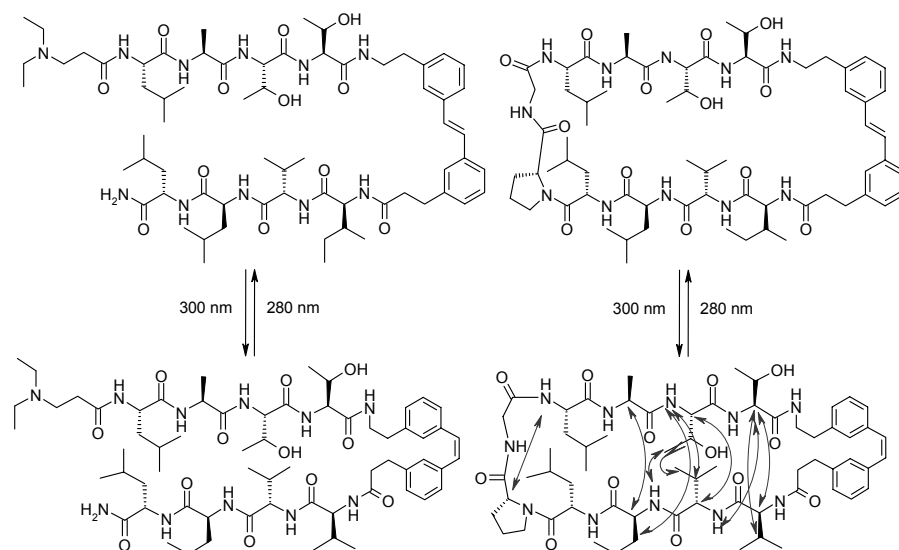


Fig. 1. Photoswitchable model β -turn mimetics in their folded and unfolded states.

Results and Discussion

The cyclic and acyclic peptidomimetics were prepared by combination of solution phase and solid phase methodologies. Conformational switching between the *trans* and *cis* isomers of stilbene type mimetics was obtained by photoisomerisation at 300 or 280 nm, and was confirmed by conformational analysis performed with standard NMR and CD techniques. Interstrand NOEs observed for the solutions of the *cis* isomer of the cyclic pseudopeptide are characteristic of β -hairpin folding (Fig. 1). NOESY spectra obtained for its *trans* isomer revealed its non-folded structure. Moreover, the alternating amide temperature coefficients of the *cis* isomer are consistent with a folded β -hairpin conformation whereas those observed for the *trans* isomer are consistent with a random coil structure. Observed changes in the CD features upon photoirradiation of the compounds was an additional indicator of a conformational alteration upon *cis-trans* isomerization. Monte Carlo Molecular Mechanics computations were then applied for visualization of the solution conformation of the investigated compounds.

Moreover, we have shown that the light induced conformational change is accompanied by a significant alteration of the translational self-diffusion coefficient. Translational self-diffusion coefficients were measured by the LED-PGSE [5] pulse sequence for DMSO- d_6 solutions at 25 °C and were determined as $0.9 \times 10^{-6} \text{ cm}^2 \text{ s}^{-1}$ (nonswitchable analog), $0.7 \times 10^{-6} \text{ cm}^2 \text{ s}^{-1}$ (*cis* and *trans* isomer, acyclic), $1.4 \times 10^{-6} \text{ cm}^2 \text{ s}^{-1}$ (*trans* isomer, cyclic) and $1.8 \times 10^{-6} \text{ cm}^2 \text{ s}^{-1}$ (*cis* isomer, cyclic). The identical diffusion coefficients of the *cis* and *trans* isomers of the acyclic pseudopeptide are in good agreement with our hypothesis as their conformational investigation with standard NMR tools clearly indicated that both isomers were present in solution as an ensemble of interconverting non folded structures. Contrarily, the different coefficients of the isomers of the cyclic analog are an additional indication of the light triggered conformational change of the cyclic stilbene containing peptidomimetic.

In summary we have demonstrated that incorporation of a stilbene-type dipeptide mimic into a cyclic β -hairpin allows for light triggered switching between different peptidomimetic conformations. Structural changes were indicated by standard NMR and CD techniques and suggest folded β -hairpin and non-folded conformations, respectively, for the two isomers. Furthermore, the conformational change was shown to be accompanied by alteration of translational self-diffusion coefficient of oligopeptides.

Acknowledgments

M.E. thanks the University of California, San Diego for providing financial support for participation at the 19th APS.

References

1. Feringa, B. L., *et al. Pure Appl. Chem.* **75**, 563-575 (2003).
2. Dugave, C. and Demange, L. *Chem. Rev.* **103**, 2475-2532 (2003).
3. a) Armitage, B. A. *Annu. Rep. Prog. Chem. Sect. B.* **96**, 187 (2000); (b) Lai, J. R., *et al. Biochemistry* **41**, 12835-12842 (2002).
4. (a) Ulysse, L., Cubillos, J. and Chmielewski, J. *J. Am. Chem. Soc.* **117**, 8466-8467 (1995); (b) Renner, C., *et al. Biopolymers* **54**, 501-514 (2000); (c) Aemissegger, A., *et al. J. Am. Chem. Soc.* **127**, 2929-2936 (2005).
5. Gibbs, S. J. and Johnson, C. S. *J. Magn. Reson.* **93**, 395 (1991).

The Guanidinium Group: A Key Player in Molecular Recognition

Ernest Giralt^{1,2}, Susana Gordo¹, Ignasi Belda¹, Silvia Pujals¹, Marc Martinell¹, Xavier Salvatella¹ and Jimena Fernández-Carneado¹

¹Biomedical Research Institute, Barcelona Science Park; ²Department of Organic Chemistry, University of Barcelona, Spain

Introduction

Protein-protein interactions are paramount in biological processes. As these interactions are primarily mediated through protein surfaces, compounds able to selectively interact with the surface patches of a given protein are of therapeutic interest.

Charged residues, in particular the guanidinium group of the arginine side-chain, are known to be essential to several protein-protein interactions. From the perspective of ligand design, we have previously shown that the interaction of guanidinium groups with bidentate anions such as carboxylate groups can drive highly specific molecular recognition events [1].

The protein p53 is one of the most important natural tumor suppressor factors. The non-covalent tetramer exhibits an anionic, carboxylate-rich surface patch in its tetramerization domain (p53TD), illustrated in Figure 1. p53 is highly mutated in cancers, and in some of these mutants the tetrameric integrity is compromised. Hence molecules that can stabilize the oligomeric structure of these mutants may prove utile for cancer therapy.

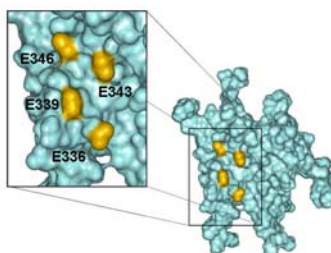
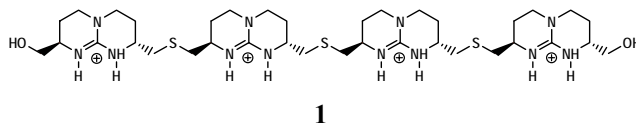


Fig. 1. Anionic surface patch of p53TD composed of the residues E336-E339-E343-E346.

Results and Discussion

In previous work, we reported the recognition of the polyanionic patch of the p53TD surface by the tetraguanidinium compound **1** (Fig. 2).



CAN4 Ac-AGAAGWARGRARSR-NH₂

Fig. 2. Structures of the tetraguanidinium ligand **1** and CAN4.

A peptide ligand with the tetraguanidinium motif was then rationally designed. Several iterations of molecular modeling and molecular dynamics evaluation led to arginine-rich peptides with the general structure ...X-Arg-X-Arg-X-Arg-X-Arg-X... Among the sequences obtained, CAN4 (Fig. 2) was selected for further characterization. Thermodynamic studies of the interaction between p53TD and CAN4 by fluorescence spectroscopy and isothermal titration calorimetry suggested a four sequential binding site model with a first dissociation constant of $\sim 8\mu\text{M}$. Furthermore, differential scanning calorimetry revealed an increase of $\sim 2^\circ\text{C}$ in p53TD transition temperature due to CAN4 binding, and subsequent kinetics evaluation by surface plasmon resonance supported these findings. Finally, NMR experiments confirmed that CAN4 does indeed interact with the polyanionic patch of the p53TD surface.

In the past few years, our group has been working on the design of proline-rich cell penetrating peptides [2,3]. Some of the most active compounds contain several arginine residues and consequently, the corresponding guanidinium group [2,4]. This fact prompted us to determine if our p53TD ligands would be able to translocate the plasma membrane of mammalian cells. Carboxyfluoresceinated versions of CAN4 and analogs of compound **1** were very efficiently internalized in HeLa cells at 37°C . Further experiments with compound **1** analogs strongly suggested that intracellular localization occurred via a mitochondrial mechanism [5].

In conclusion, we have designed, synthesized and evaluated an arginine-rich peptide, CAN4, which recognizes the polyanionic patch of the p53TD surface. Furthermore, CAN4 increases the thermal stability of p53TD due to the strong and specific interaction between the guanidinium groups of the peptide ligand and the carboxylate moieties of the target. Guanidinium-content could be exploited in the discovery of compounds capable of modulating protein stability. Applications for said compounds might include the stabilization of p53TD mutants such as those found in adrenocortical carcinoma (ACC) or Li-Fraumeni and Li-Fraumeni-like syndromes. Finally, cellular uptake experiments demonstrated that two desired properties, molecular recognition and cell penetration, can be designed into a single molecule.

Acknowledgments

S.G, M.M. and X.S. acknowledge the Generalitat de Catalunya for a predoctoral fellowship.

References

1. Salvatella, X., Martinell, M., Gairi, M., Mateu, M. G., Feliz, M., Hamilton, A. D., de Mendoza, J. and Giralt, E. *Angew. Chem. Int. Ed.* **43**, 196–198 (2004).
2. Fernández-Carneado, J., Kogan, M. J., Castell, S. and Giralt, E. *Angew. Chem. Int. Ed.* **43**, 1811–1814 (2004).
3. Crespo, L., Sanclimens, G., Pons, M., Giralt, E., Royo, M. and Albericio, F. *Chem. Rev.* **105**, 1663–1681 (2005).
4. Förg, C., Ziegler, U., Fernández-Carneado, J., Giralt, E., Rennert, R., Berk-Sickinger, A. G. and Merkle, H. P. *Biochemistry* **44**, 72–81 (2005).
5. Fernández-Carneado, J., van Gool, M., Martos, V., Castell, S., Prados, P., de Mendoza, J. and Giralt, E. *J. Am. Chem. Soc.* **127**, 869–874 (2005).

Novel and Highly Selective Antagonist Scaffold for Human Melanocortin 3 Receptor: Computer-Aided Design and Biological Evaluation

Alexander V. Mayorov, Minying Cai, Kevin B. Chandler, Ravil R. Petrov, April R. Van Scoy, Zerui Yu, Dustin K. Tanaka, Dev Trivedi and Victor J. Hruby

Department of Chemistry, University of Arizona, Tucson, AZ 85721, USA

Introduction

The natural melanotropin peptides, which include α -, β -, γ -melanocyte-stimulating hormone (MSH), and adrenocorticotropin (ACTH), are derived by posttranslational processing of the pro-opiomelanocortin (POMC) gene transcript. Each of them possesses a central "core" sequence His-Phe-Arg-Trp, which is essential for their agonist biological activity. It has been discovered that the melanocortin receptors (hMCR) and their ligands control a surprisingly large number of multifaceted biological actions including skin pigmentation, erectile function, blood pressure and heart rate, control of feeding behavior, and effects on memory and learning processes [1,2]. Of particular interest for pharmaceutical research are the hMC3R and the hMC4R, which have been implicated to play complementary roles in weight control [3]. Therefore, selective ligands for these receptors may provide a novel approach in the treatment of obesity, anorexia, weight loss, and related disorders.

Recent reports [4] have shown that some 21-membered or larger cyclic lactam analogs of α - and γ -MSH are potent and hMC4R-selective agonists. At the same time, Kavarana *et al.* [5] have found that enhancing the hydrophobicity of the cyclic peptide combined with the increased ring size resulted in improved hMC3R selectivity. From these observations, we designed a series of novel cyclic γ -MSH analogs with the following general sequence: c[Nle-Xaa-D-Phe/D-Nal(2')-Arg-Trp-Glu]-NH₂. We introduced a bulky hydrophobic residue (Nle⁴) in the close proximity to the pharmacophore (Xaa-D-Phe/D-Nal(2')-Arg-Trp) to investigate the impact of steric hindrance on receptor selectivity. Also, a variety of amino acids with a broad range of hydrophobic/hydrophilic properties were placed in position 5 to further explore their complementary role in receptor selectivity (Fig. 1).

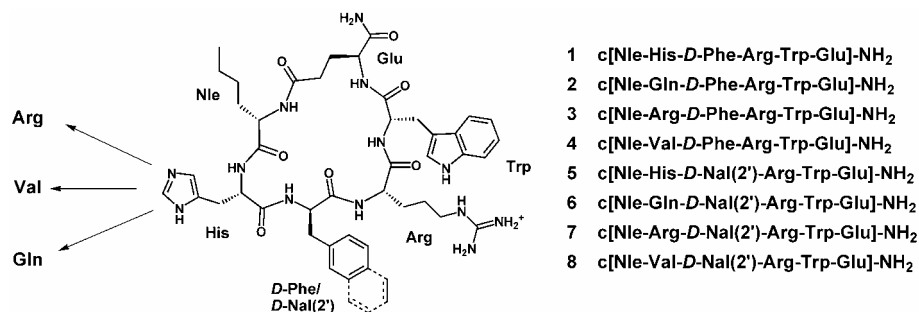


Fig. 1. The novel melanotropin cyclic lactam template c[Nle-Xaa-D-Phe/D-Nal(2')-Arg-Trp-Glu]-NH₂.

Table 1. Biological activity of the cyclic γ -MSH analogs at human melanocortin receptors

	hMC1R			hMC3R			hMC4R			hMC5R		
	IC ₅₀ , nM	EC ₅₀ , nM	% Act	IC ₅₀ , nM	EC ₅₀ , nM	% Act	IC ₅₀ , nM	EC ₅₀ , nM	% Act	IC ₅₀ , nM	EC ₅₀ , nM	% Act
1	>10000	>10000	0	560	37	147	170	2000	48	100	>10000	0
2	1000	1000	20	270	1720	60	>10000	>10000	0	500	300	8
3	1430	>10000	0	144	1.2	112	270	174	63	68	>10000	0
4	>10000	>10000	0	598	27	108	2500	3000	25	110	180	75
5	>10000	>10000	0	12	>10000	0	100	>10000	0	2.3	>10000	0
6	1000	>1000	0	1.4	>10000	0	65	130	50	1.4	>10000	0
7	1,500	>10000	0	2.6	>10000	0	77	530	10	2.3	>10000	0
8	4000	>10000	0	1.7	>10000	0	181	16	13	2.2	>10000	0

IC₅₀=Concentration of peptide at 50% specific binding (N=4); EC₅₀=Effective concentration of peptide that was able to generate 50% maximal intracellular cAMP accumulation (N=4).

Results and Discussion

As evident from Table 1, which summarizes the *in vitro* biological activities of the novel γ -MSH analogs, there is no significant receptor-ligand interaction with hMC1R throughout the series, possibly due to steric interference from Nle⁴. In addition, the peptides in the *D*-Phe⁶ series show moderate binding affinity for the hMC3R (140-600 nM), but high agonist efficacy (analog **3**, EC₅₀=1.2 nM, 112% act). These peptides also show good receptor selectivity against the hMC4R and the hMC5R, where they were found to be weak partial agonists or antagonists.

A higher degree of receptor-ligand interactions for hMC3R (IC₅₀=1.4-12 nM) and hMC5R (IC₅₀=1.4-2.3 nM) in the *D*-Nal(2') series could be due to increased hydrophobicity of these melanotropin analogs. These peptides were found to be potent hMC3R/hMC5R antagonists with good selectivity against the hMC4R, where they showed weak partial agonist or antagonist activities.

A likely cause for the observed receptor selectivity in this series of cyclic γ -MSH analogs is steric and hydrophobic effects of Nle⁴, which would help to discriminate the receptor subtypes based on the size of the receptor binding pocket. In conclusion, we have obtained and evaluated biological properties of several novel cyclic melanotropin peptides, including potent hMC3R agonists and hMC3R/hMC5R antagonists with good selectivity against the hMC1R and the hMC4R, which have a great potential for therapeutic applications in the area of eating disorders/obesity.

Acknowledgments

This work was funded by grants from the U.S. Public Health Service, DK17420 and DA06284.

References

1. Zimanyi, I. A. and Pelleymounter, M. A. *Current Pharm. Design* **9**, 627-641 (2003).
2. Gantz, I., Fong, T. M. *Am. J. Physiol. Endocrinol. Metab.* **284** (3, Pt.1), E468-E474 (2003).
3. Raffin-Sanson, M. L. and Bertherat, J. *Eur. J. Endocrinol.* **144**, 207-208 (2001).
4. Bednarek, M. A., *et al.* *Biochem. Biophys. Res. Comm.* **286**, 641-645 (2001).
5. Kavarana, M. J., *et al.* *J. Med. Chem.* **45**, 2644-2650 (2002).

Transmembrane Peptide Segments of the Uncoupling Protein-1: Chemical Synthesis and Biophysical Properties

Masoud Jelokhani-Niaraki and Marina Ivanova

Department of Chemistry, Wilfrid Laurier University, Waterloo, Ontario N2L 3C5, Canada

Introduction

Mammalian uncoupling proteins (UCPs) are integral membrane proteins located in the inner membrane of mitochondria. UCPs comprise a subfamily within the large family of mitochondrial inner membrane metabolite carriers. The common function among UCPs is their ability to dissipate the proton motive force by inducing proton leakage across the mitochondrial inner membrane, thus *uncoupling* electron transport processes from ATP synthesis. So far, five types of UCPs (UCPs 1-5) have been discovered in mammalian tissues, however, high resolution structures of these proteins are not yet available. Moreover, despite considerable homology in their primary structures, the biological functions of UCPs can be substantially different. Possible involvement of UCPs in several cellular processes such as thermogenesis, oxidative stress, superoxide and ATP level regulation, mechanisms of fever and inflammation, and pathogenesis of type-2 diabetes have been suggested [1,2].

UCP-1 (thermogenin), first discovered in brown adipocytes of hamster, is the prototypic member of the UCP family. UCP-1 is also the most studied uncoupling protein and its major physiological role in thermogenesis in brown adipocytes has been established unambiguously. However, the mechanisms of proton and anion transport in UCP-1 are poorly understood. As a possible approach to comprehend the biophysical properties and topology of UCPs in mitochondrial membranes, we have designed and synthesized the six transmembrane (TM) peptide segments of the golden hamster (*Mesocricetus auratus*) UCP-1 (Table 1) to study their intramembrane conformation, self assembly and ion transport properties.

Table 1. Sequences of UCP-1 transmembrane peptide segments^{a,b}

Peptide (# of AA)	Sequence
MaUCP-1 TM1 (34)	TTSEVHPTMGVKIFSAGVAAS*LADIITFPLDTAK
MaUCP-1 TM2 (35)	TEGLPKLYSGLPAGIQRQISFASLRIGLYDTVQEY
MaUCP-1 TM3 (27)	TLGNRISAGLMTGGVAVFIGQPTDEVK
MaUCP-1 TM4 (28)	WKGTTNLLRNVIINS*VE LVITYDLMKGA
MaUCP-1 TM5 (30)	LADDVPS*HLLSAFVAGFS*TTFLAS PADVVK
MaUCP-1 TM6 (35)	KEGPTAFFKGFVPSFLRLASWNVIMFVS*FEQLKKE
hUCP-1 TM2 (35)	TEGRMKLYSGLPAGLQRQISSASLRIGLYDTVQEF

^a Underlined sequences represent putative intramembrane segments.

^b All Cys residues are replaced by Ser, with their positions marked with “*”. Biological activity of UCP-1 is not affected by replacing Cys residues with Ser.

Results and Discussion

The six TM peptides of MaUCP-1 and the TM2 segment of the human UCP-1 (Table 1) were synthesized by Fmoc solid phase peptide synthesis procedures [3].

The synthetic peptides are longer than their putative intramembrane sequences to promote peptide solubility and represent part of the extramembraneous sequences. Peptides were purified by preparative RP-HPLC (C4 column) and subsequently analyzed using analytical RP-HPLC and ESI mass spectrometry. Conformations of the peptides in aqueous, organic solvent and phospholipid vesicles were analyzed using CD spectroscopy. Electrophysiological properties of the peptides were measured by pipette-dipping patch-clamp technique [3].

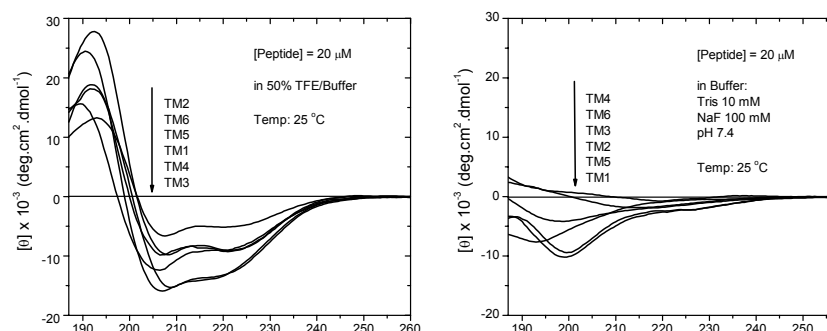


Fig. 1. CD spectra of the TM segments of MaUCP-1.

CD spectra of all TM peptide segments of MaUCP exhibited non-ordered conformations in the buffer solution (Fig. 1, right panel). On the other hand, CD spectra of TM peptides in 50% TFE showed patterns characteristic of α -helical conformations with $n\text{-}\pi^*$ transitions at ~ 222 nm and $\pi\text{-}\pi^*$ transitions at ~ 207 and ~ 192 nm (Fig. 1, left panel). TM peptides also exhibited helical conformations in phospholipid membranes with reduced ellipticities compared to the spectra in 50% TFE (data not shown). Synthetic TM segments of several ion channel proteins such as the sodium channel and acetylcholine receptor have shown electrophysiological properties comparable to those of native proteins and high resolution structural data of these proteins confirmed the participation of TM segments in the channel structures [4]. In comparison, we have shown that assemblies of the TM2 segments of UCP-2 and UCP-1 in phospholipid bilayers form stable multi-state, voltage-dependent ion channels, and inferred that these TM parts of uncoupling proteins can be essential in their ion transport activity [3, and unpublished results]. Further comparative experiments with homomeric and heteromeric TM peptide assemblies of the prototypic MaUCP-1 to investigate their conformational and electrophysiological properties are currently in progress in our laboratory.

Acknowledgments

We would like to thank Junichi Taira for his contribution to this study. The work has been funded by the CFI (6786) and NSERC (250119-02) grants to MJN.

References

1. Klingenberg, M. and Ehtay, K. S. *Biochim. Biophys. Acta* **1504**, 128-143 (2001).
2. Krauss, S., Zhang, C.-U. and Lowell, B. B. *Nature* **249**, 248-261 (2005).
3. Yamaguchi, H., Jelokhani-Niaraki, M. and Kodama, H. *FEBS Letts.* **577**, 299-304 (2004).
4. Betz, H. *Biochemistry* **29**, 3591-3599 (1990).

Discovery and Optimization of β -MSH Derived Melanocortin-4 Selective Agonists

John P. Mayer, Hansen M. Hsiung, David B. Flora, Patrick Edwards, Dennis P. Smith, Xing-Yue Zhang, Robert A. Gadski, Mark L. Heiman, JeAnne L. Hertel, Paul J. Emmerson, Saba Husain, Thomas P. O'Brien, Steven D. Kahl, David L. Smiley, Lianshan Zhang, Richard D. DiMarchi and Liang Zeng Yan

Lilly Research Laboratories, A Division of Eli Lilly & Co., Lilly Corporate Center, Indianapolis, Indiana 46285, USA

Introduction

The pro-opiomelanocortin (POMC) peptides (ACTH, α , β , and γ MSH) are expressed in the arcuate nucleus of the hypothalamus and have been shown to exert control over energy homeostasis. While numerous α -MSH based agonists have been reported in the literature [1], we pursued an SAR strategy based on the β -MSH variant with the goal of developing an effective antiobesity agent.

Table 1. POMC derived peptides

ACTH	SYSMEHFRWGKPVGK..(22AA)..
α -MSH	Ac-SYSMEHFRWGKPVG-NH ₂
β -MSH	AEKKDEPYRMEHFRWGSPPKD
γ -MSH	YVMGHRWDRFG

Results and Discussion

The peptides were evaluated using *in vitro* membrane based receptor binding and cell-based functional assays. The binding data was based on direct competitive inhibition of [¹²⁵I]NDP- α -MSH binding to membranes of human embryonic kidney (HEK) 293 cells stable transfected with cloned melanocortin receptors. The intact cells were utilized to obtain functional data using a standard cAMP assay with NDP- α -MSH (**2**) as the reference agonist. Systematic truncation and N-terminal amidation of the native β -MSH sequence yielded several modestly potent ligands (**3** and **4**) with no selectivity with respect to the four relevant receptor subtypes (Table 2). N-acetylation, and inversion of configuration at Phe⁷, inspired by established SAR precedent [2] gave analog **5** with improved affinity and efficacy, but no improvement in selectivity. The incorporation of the pseudoisosteric [Cys⁴, Cys¹⁰] disulfide constraint originally developed by Sawyer *et.al.* [3] into our series produced analog **6**, which exhibited dramatic loss of binding to the MC-5 receptor subtype. Removal of the C-terminal pentapeptide gave analog **7** which retained >500- fold selectivity versus the MC-5R, gained selectivity against MC-1R, and maintained potent binding and functional activity at MC-4R and MC-3R. The contribution of the D-Phe⁷ residue and the disulfide induced constraint was confirmed through the low potencies of the L-Phe⁷ analog **8**, and the acyclic derivative **9**. Substitution of D-Phe⁷ with D-2'naphthylalanine, analog **10**, resulted in partial agonist at the MC-3R (10.7% relative efficacy) and MC4R (26% relative efficacy).

Table 2. Peptide sequence and in vitro assay data

No.	Sequence	MC1R Ki(nM)	MC3R Ki(nM)	MC4R Ki(nM)	MC5R Ki(nM)	MC4R EC ₅₀ (nM)	MC4R rel.eff.(%)
2	NDP- α -MSH	0.08	0.22	0.31	0.16	0.43	100.00
3	AEKKDEGPYRMEH-FRWGSPPKD-OH	2.98	22.32	14.10	107.1	3.24	104.11
4	GPYRMEH-FRWGSPPKD-NH ₂	0.51	9.23	5.28	24.80	0.67	84.45
5	Ac-YRMEHdFRWGSPPKD-NH ₂	0.09	0.11	0.27	0.26	0.56	99.75
6	Ac-YR[CEHdFRWC]SPPKD-NH ₂	0.57	13.11	0.52	>500	0.24	97.92
7	Ac-YR[CEHdFRWC]-NH ₂	17.82	56.19	0.77	>500	0.27	95.38
8	Ac-YR[CEHFRWC]-NH ₂	147.1	>500	30.51	>500	5.24	99.13
9	Ac-YR(S-Me-Cys)EHdFRW(S-Me-Cys)NH ₂	2.73	166.4	13.25	62.11	0.92	93.25
10	Ac-YR[CEH(d-2'-Nal)RWC]-NH ₂	121.3	6.80	0.30	37.80	0.70	26.40
11	Ac-YR[CEH(p Cl-dF)RWC]-NH ₂	8.22	3.12	0.14	54.67	0.06	95.90
12	Ac-YR[CEH(p F-dF)RWC]-NH ₂	9.91	15.87	0.28	237.6	0.12	104.08
13	Ac-YR[CE(1-Me-His)dFRWC]-NH ₂	>500	>500	6.60	>500	0.54	88.50
14	Ac-[CEHdFRWC]-NH ₂	83.08	478.2	2.46	>500	0.30	95.23
15	Ac-YCit[CEHdFRWC]-NH ₂	49.42	313.5	2.54	>500	0.79	95.55
16	Ac-YK[CEHdFRWC]-NH ₂	15.76	97.97	1.22	>500	0.10	95.35
17	Ac-R[CEHdFRWC]-NH ₂	13.00	39.36	0.44	>500	0.26	95.75
1	Ac-dR[CEHdFRWC]-NH ₂	16.78	56.79	0.55	>500	0.28	94.46

Ki values were determined by a radioligand binding assay using I^{125} -NDP- α -MSH. EC₅₀ values were determined by the concentration of peptide at 50% maximum cAMP release. Relative efficacy was defined as the maximum peptide-induced cAMP release relative to NDP- α -MSH. C(Me) = S-Me-Cysteine.

Substitution of the D-Phe⁷ with D-Phe(pCl)⁷ or D-Phe(pF)⁷ (analogs **11** and **12**, respectively) increased MC-4R potency and MC-4R vs. MC-1R selectivity. A remarkable enhancement in MC-4R selectivity could also be realized through substitution of His⁶ with 1-MeHis⁶ (analog **13**). Deletion of the TyrArg dipeptide gave analog **14** a peptide with an acceptable selectivity profile but significantly reduced binding at MC-4. This finding, along with the diminished potency of the neutrally charged citrulline analog **15** and the improved potency of the lysine analog **16** confirmed our belief that a strong basic charge was essential at this position. This is noteworthy in that the β -MSH isoform is unique in having an arginine at position 3. However, in contrast to the arginine requirement, we noted that the N-terminal tyrosine could be deleted from with no loss of potency or selectivity. This was demonstrated through the synthesis of analog **17** and its D-Arg³ derivative **1**. Accordingly, based on potency, selectivity, as well as additional physico-chemical parameters analog **1** was selected for *in vivo* biological evaluation.

Daily subcutaneous injection of analog **1** to diet-induced obese rats at 0.075 μ moles/kg and 0.299 μ moles/kg for a 14 day period resulted in a dose-dependent decrease in both cumulative body weight gain and food intake. Body composition analysis also demonstrated a statistically significant reduction in fat mass with no change in lean mass.

References

- Holder, J. R. and Haskell-Luevano, C. *Med. Res. Rev.* **24**, 325-326 (2004).
- Sawyer, T. K., et. al. *Proc. Natl. Acad. Sci. USA* **77**, 5754-5758 (1980).
- Sawyer, T. K., et. al. *Proc. Natl. Acad. Sci. USA* **79**, 1751-1755 (1982).

Molecular Mechanisms of Constitutive Activity: Mutations at Position 111 of the Angiotensin AT₁ Receptor

Gregory V. Nikiforovich¹, Balász Mihalik², Kevin J. Catt² and Garland R. Marshall¹

¹*Department of Biochemistry and Molecular Biophysics, Washington University School of Medicine, St. Louis, MO 63110 USA;* ²*Endocrinology and Reproduction Research Branch, National Institute of Child Health and Human Development, Bethesda, MD 20892, USA*

Introduction

The AT₁ receptor, a 359-residue seven-transmembrane domain G-protein coupled receptor (GPCR), is one of the most studied GPCRs by site-directed mutagenesis. Extensive systematic studies on single mutations of residue N111 revealed that replacements with the small-sized residues, Gly and Ala, yielded constitutively active mutants (CAMs) with the most pronounced constitutive activity, whereas mutations with bulkier residues yielded less active CAMs. The order of basal activity for ten AT₁ mutants was: N111G > N111S > N111A, N111C > N111I, N111Q, N111H, N111K, N111F, N111Y, N111W, the wild type (WT) [1,2]. The present study employed molecular modeling to reveal conformational changes occurring in the transmembrane (TM) region of the AT₁ receptor due to mutations of N111. Specifically, we sought conformational differences that may occur in the TM regions of the pronounced CAMs, N111G and N111A, compared to the silent WT and N111W.

Results and Discussion

Modeling involved energy calculations employing the ECEPP force field for the TM region of AT₁ that consisted of seven helical fragments (TM1, M30-I53; TM2, F66-E91; TM3, I103-C121; TM4, L143-A163; TM5, I193-I218; TM6, I242-D263; and TM7, M284-F301, the boundaries of helices defined according to [3]). Each helix was subjected to energy minimization and then aligned to the X-ray structure of rhodopsin. Packing of TM helices was performed in the space of “global” parameters (related to translations and rotations of individual TM helices as rigid bodies) and the “local” parameters (the dihedral rotational angles of the side chains); the backbones angles were fixed in the values they obtained in energy calculations for the individual TM helices.

Energy calculations found two main differences between N111G and N111A, on the one hand, and WT and N111W, on the other. First, they reveal significant steric hindrance in inter-helical interaction of TM4 with other helices in both N111G and N111A, but not in N111W and WT. Second, there was clear distinction in the pattern of low-energy spatial positions of several side chains between WT and either N111G or N111A; no significant differences in side-chain orientations were detected between WT and N111W. More detailed evaluation of the above differences and their energetic consequences is consistent with the following possible pathway of conformational changes that lead to constitutive activity of N111G and N111A. When N111 is mutated to glycine or alanine, the important N111 – N295 and N111 – F77 interactions are broken, so the side chains of F77 and N295 move closer to each other to preserve their favorable interactions. This opens a cavity for the side chain of L112 to move towards F77 and N295. As a consequence, favorable

interactions L112 – Q257 and L112 – Y113 are disrupted, and it becomes energetically more favorable for the side chain of Y113 to move towards F117. In turn, the side chain of F117 changes the spatial orientation and clashes with side chains of I152 and M155 in TM4. The side chain of M155 relieves this potential steric hindrance by changing the value of the χ_2 angle; however, the side chain of I152, despite any possible changes in the χ_1/χ_2 values, is trapped in the closed hindered pocket formed by F111, C149 and N69. The situation relaxes by movement of TM4 away from other TM helices, especially TM3. This mechanism is in good agreement with the 3D model of the complex of the TM region of the AT₁ receptor and angiotensin II proposed by us earlier [4]; the complex contains the same conformational pattern of the side chain arrangements for Y113, F117 and I152 with the same steric hindrance in TM4.

The proposed hypothesis of characteristic conformational changes in the CAMs with mutations of N111 can be verified by making double mutants of the AT₁ receptor that contain the constitutively active mutation N111G together with additional replacement of the residues involved in the above changes, L112, Y113, F117 and I152, by Ala. Such additional mutations will replace the sizable side chains by much less voluminous alanine residues, but presumably will not influence the general helical backbone structure of TM3. Energy calculations performed for the double mutants N111G/L112A, N111G/Y113, N111G/F117 and N111G/I152A showed that the former mutant may fully retain the pattern of side chain rotations characteristic for N111G and N111A, as well as steric hindrance in TM4 and, therefore, might display high constitutive activity comparable to that of N111G. In the other three double mutants, the pattern in question is interrupted, and there is no steric hindrance in TM4; therefore, such mutants are expected to exhibit less constitutive activity than N111G.

Five mutants, namely N111G, N111G/L112A, N111G/Y113, N111G/F117 and N111G/I152A were obtained by site-directed mutagenesis in COS-7 cells; the mutants were characterized by binding with ¹²⁵I-angiotensin and by angiotensin stimulation. The N111G/Y113 mutant was poorly expressed (*ca.* 5% compared to WT). The levels of basal IP2 + IP3 production corrected for expression level were 4.7, 9.2, 3.0 and 6.3 for N111G, N111G/L112A, N111G/F117 and N111G/I152A, respectively (relative to 1.0 for WT). Similar results were also obtained when simulating the mutants with the CGP peptide and Ang3-8 (data not shown). One can conclude that the proposed molecular mechanism for constitutive activity of the mutants of the AT₁ receptor correctly predicted constitutive activity of the double mutants N111G/L112A and N111G/F117A. The basal activity of N111G/I152A was higher than expected, and that of N111G/Y113A was not estimated due to poor expression of the mutant.

Acknowledgments

The work was supported by the NIH grant GM53630 (G.N. and G.M.).

References

1. Feng, Y.-H., Miura, S., Husain, A. and Karnik, S. S. *Biochemistry* **37**, 15791-15798 (1998).
2. Auger-Messier, M., *et al.* *Endocrinology* **144**, 5277-84 (2003).
3. Nikiforovich, G. V. *Protein Engineering* **11**, 279-283 (1998).
4. Nikiforovich, G. V. and Marshall, G. R. *Biochem. Biophys. Res. Commun.* **286**, 1204-1211 (2001).

A Surprise End to 20 Year Search for Selective Agonists for Rat Vasopressin V_{1b} Receptor

**Maurice Manning¹, LingLing Cheng¹, Stoytcho B. Stoev¹, Nga C. Wo²,
Hazel H. Szeto², Ana Pena³, Brigitte Murat³, Miguel Trueba³, Maria A.
Ventura⁴ and Gilles Guillon³**

¹Department of Biochemistry and Cancer Biology, Medical University of Ohio, Toledo, OH 43614, USA; ²Department of Pharmacology, Weill Medical College of Cornell University, New York, NY 10021, USA; ³Institut de Génomique Fonctionnelle, UMR5203-CNRS, U661-INSERM, Université Montpellier I & II, 141 rue de la Cardonille, 34094 Montpellier Cedex 5, France; ⁴Institut Cochin Paris, France

Introduction

The design of selective agonists for the human and rat vasopressin (VP) V_{1b} receptors has proved to be an elusive goal. We recently reported a breakthrough in the discovery of the first selective agonist for the human V_{1b} receptor namely: d[Cha⁴]AVP (A, Table 1) [1]. However, because it retains appreciable antidiuretic activity in the rat it is thus not a selective V_{1b} agonist in the rat. We subsequently reported that d[X⁴]AVP analogs (where X = Leu, Orn, Arg) (peptides B-D, Table 1) are highly selective for the human V_{1b} receptor [2]. However, in a very recent study [3] we report that they are not selective V_{1b} agonists in the rat. In this study, peptides A-D were further modified at position 8 to give the d[X⁴,Y⁸]VP analogs (where X = Cha, Leu, Orn, Arg; Y = Lys, Orn, Dab, Dap) (peptides 1-13, Table 1).

Results and Discussion

The rat V_{1a}, V₂, V_{1a} and OT receptor affinities of peptides 1-13 and A-D [3] are given in Table 1. The antidiuretic activities of peptides 1, 3, 5 and 8, and A-D [3] are also given in Table 1.

Effects of position 8 modifications on rat receptor affinities: Replacement of the Arg⁸ residue in A-D by Lys, Orn, Dab, Dap, with one exception (peptide 4), led to full retention of rat V_{1b} receptor affinity. In fact, 10 of these 13 peptides exhibit subnanomolar affinities for the rat V_{1b} receptor.

With the exception of peptides 12 and 13, the remaining 11 peptides exhibit very weak affinities for the rat V_{1a} receptor. All 13 peptides exhibit substantially reduced affinities for the rat OT receptor.

Analog A-D all exhibit very high affinities for the rat V₂ receptor and high antidiuretic activities (Table 1) [3]. Remarkably, apart from the Arg⁴ analogs (peptides 11-13), the remaining 10 analogs (peptides 1-10) exhibit reductions – some very drastic – in affinities for the rat V₂ receptor. Peptides 1, 3, 5 and 8, exhibit drastic reductions in antidiuretic potencies relative to their respective parents A and B. Over 30 years ago, 10 years prior to the discovery of the VP V_{1b} receptor, one of these peptides d[Leu⁴]LVP (No. 5), had been reported to exhibit weak antidiuretic and vasopressor activities in the rat [4].

Conclusion

Modifications of d[Cha⁴]AVP (A), d[Leu⁴]AVP (B) and d[Orn⁴]AVP (C) [2,3] at position 8 with Lys, Orn, Dab and Dap have uncovered eight peptides: Nos. 1-3, 5-10, (Table 1) which exhibit high affinities and selectivities for the rat V_{1b} receptor.

In functional tests they are full V_{1b} agonists. In a surprise end to the 20 year search for a selective V_{1b} agonist in the rat, one of these peptides is d[Leu⁴]LVP [4]. Because of its weak bioactivities, it elicited very little interest when first reported [4]. We now report its re-emergence as a long sought selective V_{1b} agonist in the rat.

Table 1. Rat receptor affinities and antidiuretic activities of position 4 modified analogs of dAVP

No	Peptide	rV _{1b} R Ki(nM) ^e	rV ₂ R Ki(nM) ^e	Antidiuretic Activity (Units/mg)	rV _{1a} R Ki(nM) ^e	rOTR Ki(nM) ^e
	dAVP ^a	2.2	0.8	1745	10.8	1.0
A	d[Cha ⁴]AVP ^a	1.4	12.8	134	2297	1430
1	d[Cha ⁴]LVP ^d	1.9	596	0.8	9093	585
2	d[Cha ⁴]OVP ^d	3.0	446		2912	546
3	d[Cha ⁴ ,Dab ⁸]VP ^d	0.8	447	1.0	4378	432
4	d[Cha ⁴ ,Dap ⁸]VP ^d	10.3	1044		1804	1191
B	d[Leu ⁴]AVP ^b	0.02	3.1	378	1252	481
5	d[Leu ⁴]LVP ^d	0.07	102	10 (5-6 ^c)	3786	58
6	d[Leu ⁴]OVP ^d	0.3	426		1436	55
7	d[Leu ⁴ ,Dab ⁸]VP ^d	0.3	206		1028	41
8	d[Leu ⁴ ,Dap ⁸]VP ^d	0.4	236	0.7	3269	134
C	d[Orn ⁴]AVP ^b	0.4	3.4	260	900	997
9	d[Orn ⁴]LVP ^d	0.4	50		2801	22
10	d[Orn ⁴]OVP ^d	0.9	67		1285	37
D	d[Arg ⁴]AVP ^b	0.1	0.2	748	12.9	3552
11	d[Arg ⁴]LVP ^d	0.6	3.8		129	125
12	d[Arg ⁴]OVP ^d	0.6	3.1		66	131
13	d[Arg ⁴ ,Dab ⁸]VP ^d	0.2	1.8		24	195

^aData from Ref. 1. ^bSee poster #292 (Ref. 3). ^cData from Ref. 4. ^dThis publication. ^eBinding data are performed either on rat liver or rat kidney membranes known to naturally express V_{1a} or V_2 receptor isoforms or on membranes from CHO or AtT-20 cells stably transfected with OT or V_{1b} receptor isoforms respectively.

Acknowledgments

We thank Ms. Ann Chlebowski and Ms. Karen Kempski for expert help in the preparation of this manuscript. Supported by NIH Grant GM-25280 and the Institut National de la Santé et de la Recherche Médicale.

References

- Derick, S., Cheng, L. L., Voirol, M. J., Stoev, S., Giacomini, M., Wo, N. C., Szeto, H. H., Ben Mimoun, M., Andres, M., Gaillard, R. C., Guillon, G. and Manning, M. *Endocrinology* **143**, 4655-4664 (2002).
- Cheng, L. L., Stoev, S., Manning, M., Derick, S., Pena, A., Ben Mimoun, M. and Guillon, G. *J. Med. Chem.* **47**, 2375-2388 (2004).
- Stoev, S., Cheng, L. L., Manning, M., Wo, N. C., Szeto, H. H., Pena, A., Murat, B., Trueba, M., Ventura, M. A. and Guillon, G. In *Understanding Biology Using Peptides, Proceedings of the 19th American Peptide Symposium*, this volume, pp. 573-574 (2006).
- Dyckes, D. F., Ferger, M. F., du Vigneaud, V. and Chan, W. Y. *J. Med. Chem.* **16**, 843-847 (1973).

Furanoid Sugar Amino Acids in Design of Analogs of VIP Receptor Binding Inhibitor

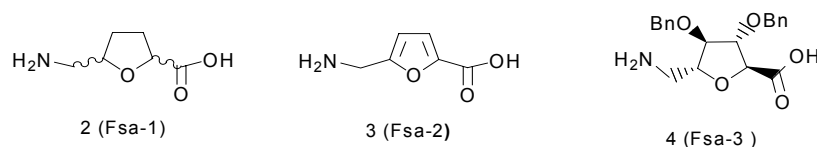
Sudhanand Prasad¹, Archana Mathur¹, Manu Jaggi¹, Rajan Sharma¹,
Neena Gupta¹, Rama Mukherjee¹, Ajit C. Kunwar² and Tushar K.
Chakraborty²

¹Dabur Research Foundation, 22, Site IV, Sahibabad, Ghaziabad 201010, India; ²Indian
Institute of Chemical Technology, Hyderabad 500 017, India

Introduction

The octapeptide sequence Leu¹-Met²-Tyr³-Pro⁴-Thr⁵-Tyr⁶-Leu⁷-Lys⁸-OH (**1**) is reported to be a receptor binding inhibitor of vasoactive intestinal peptide. The anti-cancer activity of octapeptide **1** in combination with other neuropeptide analogs has been reported [1].

Here we report the peptidomimetic analogs of octapeptide **1** by incorporating furanoid sugar amino acids **2-4**. We replaced either Tyr³-Pro⁴ (analogs **5** and **5a**) or Pro⁴-Thr⁵ (analogs **6**, **6a** and **7**) in the sequence by furanoid sugar amino acids as depicted in the following figure. In independent studies in the laboratory, the truncated pentapeptide sequence, Met-Pro-Thr-Tyr-Leu-OH, derived from octapeptide **1**, was also found to be as active as **1**. We also synthesized analogs to this pentapeptide by replacing its Pro-Thr dipeptide segment with sugar amino acids **2** and **3** to get the peptides **8** and **9**, respectively.



- Leu-Met-Fsa1-Thr-Tyr-Leu-Lys-OH (**5** and **5a**)
- Leu-Met-Tyr-Fsa1-Tyr-Leu-Lys-OH (**6** and **6a**)
- Leu-Met-Tyr-Fsa3-Thr-Tyr-Leu-Lys-OH (**7**)
- Met-Fsa1-Tyr-Leu-OH (**8**)
- Met-Fsa2-Tyr-Leu-OH (**9**)

Results and Discussion

The sugar amino acid **3** (Fsa2) was synthesized using D-fructose as starting material [2]. Hydrogenation of **3** furnished the sugar amino acid **2** (Fsa1). Only 2,5-*cis* isomers, (2*S*,5*R*), and (2*R*,5*S*) were obtained as evidenced from the NMR spectra. Sugar amino acid **4** (Fsa3) was synthesized using D-mannitol as starting material. All peptides were synthesized using standard Fmoc chemistry on Wang resin using a peptide synthesizer and were purified by HPLC. Incorporation of racemic **2** into the octapeptide **1** gave diastereomeric mixtures of products **5**, **5a** and **6**, **6a**. These diastereomers were separated by HPLC. NMR studies were performed on a Bruker DRX400 NMR spectrometer.

The solution conformation of **1** using various NMR studies had indicated the presence of a β -turn structure involving the Tyr³-Pro⁴-Thr⁵-Tyr⁶ residues with intra-molecular hydrogen bond between Tyr⁶NH \rightarrow Tyr³CO. From the detailed

structural study by various NMR techniques, it was established that the β -turn structure found in the VIP receptor binding inhibitor **1** was successfully induced by introducing the non-proteinogenic dipeptide isostere **2** (Fsa1) in the molecule, resulting in the development of novel peptidomimetic analogs **5**, **5a**, **6**, **6a**, and **8**. Although all of them showed very similar 10-membered hydrogen bonded structures, the turn structure in those having (2*R*,5*S*) stereochemistry in the tetrahydrofuran ring was more pronounced than those derived from the ones having the (2*S*,5*R*) stereochemistry.

The analogs were tested for *in vitro* anticancer activity on a panel of human cancer cell lines following the standard MTT assay in the 1nM to 100nM concentration range. Of the various analogs tested, analog **6a** showed good anti-proliferative activity in most of the human cancer cell lines tested. It was the most promising analog in cancer cell lines HeP-2 (laryngeal cancer), MiaPaCa.2 (pancreas), KB (oral), and ECV-304 (endothelial) cancer.

The *in vivo* efficacy of peptide **6a** was studied in primary human colon adenocarcinoma (PTC) xenografts grown in Balb/c athymic (nude) mice. Receptors for VIP are expressed in colon cancer and it was envisaged that cell lines prepared from primary colon tumor biopsies would express VIP receptors. Tumors were initiated by subcutaneous inoculation of a single cell suspension of PTC cells (15×10^6 cells/100 μ L). Treatment with analog **6a** was initiated when the average tumor volumes, as measured using a vernier caliper, were between 400 – 800 mm³. Solution of **6a** was intravenously administered to the assigned group of tumor bearing animals at a dose of 0.5 mg/Kg.B.Wt, twice a day, for a period of 21 days. The percentage inhibition of tumor growth was calculated using the formula $[1 - \text{tumor volume}(\text{treated}) / \text{tumor volume}(\text{control})] \times 100$. Analog **6a** showed 57% inhibition of tumor growth in the PTC xenografted *in vivo* nude mouse model.

Our experimental studies suggest that the furanoid sugar amino acids can be used as dipeptide β -turn mimics in the design of biologically active peptides.

References

1. Chakraborty, T.K., et al. *Tetrahedron* **60**, 8329-8339 (2004).
2. Prasad, S., et al. *J. Peptide Res.* **66**, 75-84 (2005).

Two Residues at the Extracellular Face of TM5 and TM6 Interact in the Active State of a G Protein-coupled Receptor

Yong-Hun Lee¹, Fred Naider² and Jeffrey M. Becker¹

¹Department of Microbiology, University of Tennessee, Knoxville, TN 37996, USA;

²Department of Chemistry and Macro-molecular Assemblies Institute, College of Staten Island, CUNY, NY 10314, USA

Introduction

Ste2p is the G protein-coupled receptor for the tridecapeptide pheromone α -factor of the yeast *Saccharomyces cerevisiae*. Previously, we proposed that Y266 in transmembrane six (TM6) of Ste2p was a key residue for transmission of the signal and part of the binding pocket [1]. To find potential Ste2p residues interacting with Y266, a portion of the receptor spanning the junction of TM5 and its contiguous extracellular loop (residues Q200 to I209) was targeted by Ala-scanning mutagenesis.

Results and Discussion

The N205A mutant receptor was biologically inactive but bound α -factor with high affinity indicating that N205 is important for receptor activation (Table 1). Thus the phenotype of N205 is that of a receptor residue critical for signaling but not essential for high-affinity ligand binding. In this respect N205 resembled the phenotype of Y266 previously studied [1].

Using binding assays with a series of Ala-substituted alpha-factor analogs, we showed that the pheromone affinity profile of the N205A mutant receptor was very similar to that of the Y266A mutant receptor (Table 2).

A N205H/Y266H double mutant showed functional recovery in a pH-dependent manner; this mutant was fully functional at pH 6 but not at pH 4 or 8, although N205H and Y266H Ste2ps were non-functional or partially functional at pH 6, respectively, indicating these residues might interact in the active receptor.

Table 1. Ligand binding affinities and biological activities of receptor mutants

Receptor	Affinity of α -factor for receptor	Biological activity (Percent)
Wild-type	5.2 \pm 1.2	(100 \pm 11)
Q200A	3.0 \pm 1.3	92 \pm 8
D201A	4.1 \pm 1.4	95 \pm 10
K202A	5.2 \pm 1.3	95 \pm 7
Y203A	13.3 \pm 3.4	98 \pm 9
F204A	>>100	< 5
N205A	14.5 \pm 4.3	< 5
A206G	10.3 \pm 2.5	114 \pm 13
S207A	2.9 \pm 1.2	108 \pm 9
T208A	10.6 \pm 3.1	105 \pm 9
I209A	2.8 \pm 1.7	104 \pm 9

Table 2. Binding affinities of Ala-scanned α -factor analogs for wild type, N205A, and Y266A

Peptides	Ki - Binding	Fold Change	
	WT	N205A	Y266A
α -factor	6.8 \pm 1.3	-2.13	-6.0
[Ala1]	114.1 \pm 13	+2.51	+2.3
[Ala3]	185.4 \pm 19	+2.34	+4.0
[Ala5]	7.5 \pm 1.2	-10.6	-7.2
[Ala7]	37.7 \pm 7.5	-4.93	-10.4
[Ala9]	683 \pm 58	-2.36	-2.6
[Ala11]	151.7 \pm 14	-2.98	-8.0

To test further the interaction between N205 and Y266 in the active state of receptor, in addition to the genetic analyses of the interaction, we used biochemical analysis to probe the interaction in the activated state using disulfide-crosslinking, as previously applied to establish an interaction between TM5 and TM6 of Ste2p [2]. We introduced the N205C/Y266C double mutation into WT and the P258L/S259L constitutively active receptors. We found that a disulfide-crosslinked fragment of the expected size formed only in the activated receptor.

Based on the results, we built a model to help interpret the findings. The residues composing the transmembrane domains of Ste2p were superimposed upon the rhodopsin model using the Swiss-Prot database generating a model for Ste2p. Though there is no significant sequence homology between rhodopsin and Ste2p, it has been successfully used for the modeling of Ste2p [3]. The model placed residues N205 and Y266 at a distance of ~ 6 Å (corresponding the side-chain O of Asn205 to the C1 of the benzoyl ring of Tyr266) and these atoms come closer together (to ~ 2 Å) if the P258L/S259L mutation (the constitutively active mutant) is introduced. When Cys replaced residues N205 and Y266, the residues are still separated by ~ 6 Å (between the S atoms in 205 and 266), whereas in the active state the residues are close enough to form a disulfide bridge.

The results reported herein suggest that the N205 and Y266 residues are in close proximity in the activated Ste2p and/or that these residues interact during agonist-induced Ste2p activation. To our knowledge this is the first example based on experimental evidence of interaction between specific residues in the active state of a GPCR.

Acknowledgments

The work was funded by NIH grants GM 22086 and GM 22087.

References

1. Lee, B. K., Khare, S., Naider, F. and Becker, J. M. *J. Biol. Chem.* **276**, 37950-37961 (2001).
2. Dube, P., DeConstanzo, A. and Konopka, J. B. *J. Biol. Chem.* **275**, 26492-26499 (2000).
3. Eilers, M., Hornak, V., Smith, S. O. and Konopka, J. B. *Biochemistry* **44**, 8959-8975 (2005).

Molecular Probes for Visualizing Angiogenesis

Alan Cuthbertson¹, Grete Mørk Kindberg¹, Bård Indrevoll¹, Joseph Arukwe¹, Hege Karlsen¹, Alex Gibson², Julie Davis², Marivi Mendizabal², Matthew Morrison² and Matthias Glaser³

¹GE Healthcare Research, NO-0401 Oslo, Norway; ²GE Healthcare Research, The Grove Centre, England, UK; ³Hammersmith Imanet, England, UK

Introduction

The field of molecular imaging aims to provide disease-specific molecular information through non-invasive diagnostic imaging. Both Positron Emission Tomography (PET) and Single Photon Emission Computed Tomography (SPECT) produce tomographic images by detecting radiation emitted from a probe injected into the patient. The probes are designed to bind and accumulate specifically at the site of disease.

Targeting of the integrin receptors associated with angiogenesis using RGD peptides labeled with radionuclides for PET and SPECT has been the focus of this study. The peptide ACDCRGDCFCG (RGD-4C) has been previously reported as being a highly specific inhibitor of $\alpha v\beta 3$ and $\alpha v\beta 5$ -mediated cell attachment to vitronectin [1]. *In vitro* testing of the three disulfide isomers of RGD-4C revealed that the 'nested' peptide had the highest affinity with a K_i of 1 nM [2]. SAR studies showed that the N-terminal Ala could be removed and the Cys²⁻¹⁰ disulfide replaced with a stable thioether bridge. The Asp 3 and the C-terminal Gly could also be replaced by a wide range of amino acids with no significant loss of potency. Peptide 1 (X= H in Fig. 1) was chosen as a key peptide intermediate. A short PEG-like spacer improved the *in vivo* pharmacokinetic profile while the Lys side-chain was employed as the attachment point for conjugation of the imaging moiety.

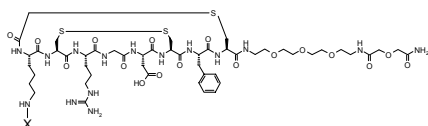
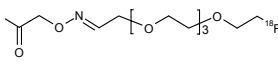
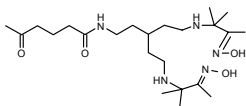


Fig. 1. Peptide scaffold. X=H or is an imaging moiety.

Results and Discussion

Peptide **1** was assembled on Rink Amide resin using Fmoc chemistry and the amino acids O-(N-Fmoc-2-aminoethyl)-O'-(N-diglycolyl-2-aminoethyl)-diethyleneglycol, Cys(Trt), Phe, Cys(tBu), Asp(OtBu), Gly, Arg(Pmc), Cys(tBu), Lys(Boc) on an automated synthesizer with standard HBTU/ HOBt couplings. The terminal Lys residue was capped with chloroacetic acid anhydride prior to cleavage of the product from the resin in TFA containing 5% TIS, 5% water, 2.5% phenol. The crude peptide was dissolved in 20% acetonitrile/ water and the pH adjusted to 7.4 to effect thioether bridge formation. Following lyophilization, the Cys²⁻¹⁰ disulfide was formed by treatment of the Cys(tBu) groups for 10 minutes in 10% DMSO/ TFA [3].

Table 1. RGD peptide K_i 's and structures of the PET and SPECT imaging moieties

	X =	K_i (nM), n=3
Peptide 2		1.7
Peptide 3		1.6

Labeling of peptides for PET imaging with ^{18}F -fluoride still remains a significant challenge for radiochemists and new methods are required if peptide-based probes are to be routinely employed in the clinic setting. To this end our strategy employs ^{18}F -labelled aldehydes suitable for chemoselective oxime formation with an aminoxy-modified peptide. Peptide 1 was reacted with Boc-aminoxyacetic acid pre-activated with HATU. The Boc group was then removed in TFA and the peptide purified by HPLC. The synthon $[\text{}^{18}\text{F}]\text{-CH}_2\text{-CH}_2\text{-(O-CH}_2\text{-CH}_2\text{)}_3\text{-O-CH}_2\text{-CHO}$ was prepared from the mesylate precursor with $[\text{}^{18}\text{F}]\text{fluoride}$, kryptofix [2.2.2.] followed by conjugation to the aminoxy-RGD peptide in acetate buffer pH 4, yielding peptide 2 [4].

The SPECT probe, peptide 3, was prepared by reaction of a diaminodioxime chelate ester with peptide 1. The purified conjugate (0.1 mg) was reconstituted in $\text{Na}^{99\text{m}}\text{TcO}_4$ / SnCl_2 in saline at room temperature, pH 9 [5].

Figure 2 shows the tumor uptake in a PET image of peptide 2 in the mouse Lewis Lung Carcinoma model (transaxial slice) and Figure 3 a clinical SPECT image of the $^{99\text{m}}\text{Tc}$ -peptide 3 in a patient with infiltrating ductal carcinoma of the left breast.

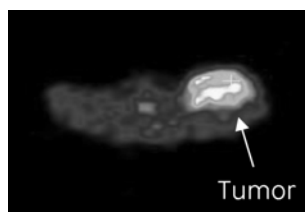


Fig. 2. MicroPET image.

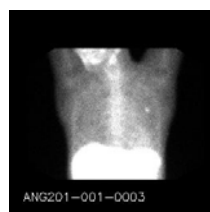


Fig. 3. SPECT image.

References

1. Koivunen, E., Wang, B. and Ruoslahti, E. *Biotechnology* **13**, 265-270 (1995).
2. Binding affinities of peptides were determined using the human adenocarcinoma cell line, EA-Hy926, as a source of receptor. K_i was calculated through competition of peptides with ^{125}I -echistatin.
3. Cuthbertson, A. and Indrevoll, B. *Tetrahedron Lett.* **41**, 3661-3663 (2000).
4. Patent WO 03/006070
5. Patent WO 03/006491

The Two Cysteine-rich Head Domains of Minicollagen from *Hydra* Nematocysts Differ in their Cystine Framework and Overall Fold despite an Identical Cysteine Sequence Pattern

Alexander G. Milbradt, Cyril Boulegue, Luis Moroder and Christian Renner

Max-Planck Institut für Biochemie, Martinsried, Germany

Introduction

Most cysteine-rich bioactive peptides such as hormones, neurotransmitters, growth factors, enzyme inhibitors, and toxins are known to refold in high yields into the native topoisomer under optimized oxidative conditions, although biosynthetically these peptides are products of post-translational processing of larger prefolded precursor forms [1]. Even small subdomains of proteins are capable of refolding correctly when the sequence-encoded structural information in the excised fragments suffices for the thermodynamically controlled correct oxidative refolding. Generally, stabilization of preferred ordered structures such as α -helices or β -sheets by defined disulfide-crossbridgings represents the driving force in such processes. From the sequence composition of minicollagen from *Hydra* nematocysts [2] a larger stretch of collagen-type triple helix followed by a poly-proline II helix can be foreseen, while the N- and C-terminal proline- and cysteine-rich domains are not consistent with known ordered structures.

Results and Discussion

Surprisingly the short synthetic 24-residue C-terminal domain refolds in the presence of a redox buffer (GSH/GSSG, 1:9) mainly into a single isomer whose disulfide connectivities were unambiguously assessed by the NMR structural analysis (Fig. 1 and Fig. 2) [3]. The structure comprises a short helix from residue 4 to 8, followed by an inverse γ -turn (9-11), a type I β -turn (11-14), and a type III β -turn (15-18). The conserved Pro 12 stabilizes the type I β -turn. Reduction of the disulfide bridges renders the molecule unstructured. Even when only a single disulfide bridge is reduced the molecule loses its fold. Also the 21-residue N-terminal domain folds into a single isomer in cysteine/cystine (4:1) buffer with 2 M guanidinium chloride. The isomer shows different disulfide connectivities and a different structure compared to the C-terminal domain (Fig. 1 and Fig. 2). The N-terminal domain comprises a β -II turn from residue 7 to 10, an open type VI β -turn (10-13) with a *cis* peptide bond between residue Ala 11 and Pro 12 followed by a kink at Cys 14 induced by an irregular γ -turn (13-15). The last residues form an α -helical turn (18-21) capped by a 3-10 helix turn (16-18).

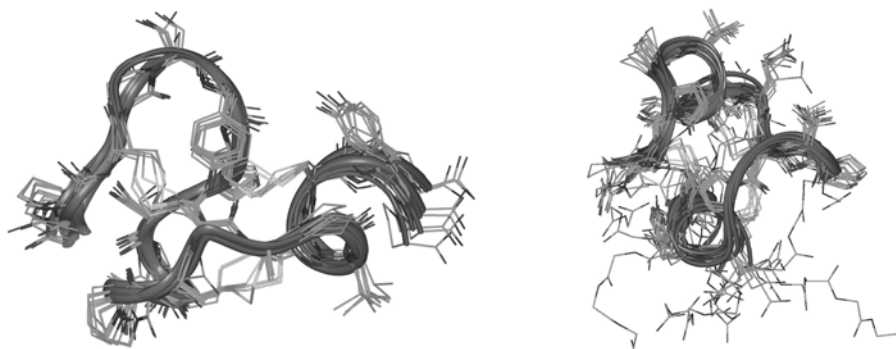


Fig. 1. The energy-lowest structures of the N- (left) and the C-terminal domain (right). The two domains exhibit different disulfide connectivities and folds.

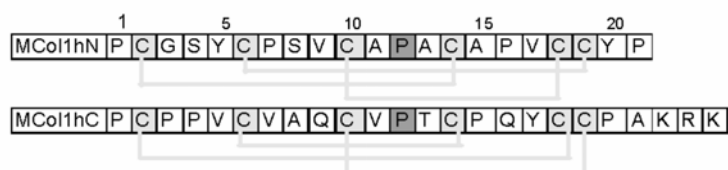


Fig. 2. Sequence alignment of the N- (MCol1hN) and C-terminal (MCol1hC) Cys-rich domains of minicollagen 1. Color coding: light grey = conserved disulfide pattern, and dark grey = conserved Pro-12.

Conclusion

The results of this study clearly show that the cystine connectivities in cysteine-rich peptides and thus the three-dimensional fold are not always dictated by the sequence pattern of cysteine residues, but can vary depending upon the sequence-specific structural preferences. This fact may call for attention in exploiting the robustness of natural scaffolds of cysteine-rich peptides for the design of artificial miniproteins of desired novel bioactivities.

Acknowledgements

The study was supported in part by the Deutsche Forschungsgemeinschaft.

References

1. Kimura, T. In *Houben-Weyl, Methods of Organic Chemistry, Synthesis of Peptides and Peptidomimetics* (Goodman, M., Felix, A., Moroder, L. and Toniolo, C., eds.) Georg Thieme Verlag, Stuttgart, pp. 142-161(2002).
2. Engel, E., Pertz, O., Fauser, C., Engel, J., David, C. N. and Holstein, T. W. *EMBO J.* **20**, 3063-3073 (2001)
3. Pokidysheva, E., Milbradt, A. G., Meier, S., Renner, C., Haussinger, D., Bachinger, H. P., Moroder, L., Grzesiek, S., Holstein, T. W., Ozbek, S. and Engel, J. *J. Biol. Chem.* **279**, 30395-30401 (2004).

Polypeptide Ligands Containing Switchable Flexible Linkers as Retractable Inhibitors of Protein-Protein Interactions

Dmitri Tolkatchev, Anna Vinogradova, Rana Filfil and Feng Ni

Bio-NMR and Protein Research Laboratory, Biotechnology Research Institute, National Research Council of Canada, 6100 Royalmount Avenue, Montreal, Quebec, Canada H4P 2R2

Introduction

The quest for small-molecule therapeutics has become a tremendously-successful venture [1]. However, small-molecule drug discovery has recently met with some difficulties, especially in tackling functionally-important protein-protein interactions. The current biotechnology era has seen the rise of therapeutic antibodies and recombinant proteins [2]. It is predicted that new molecular architectures will not only need to harbor therapeutic intervention elements, but as well will be required to release or contain the intervention action “on demand”.

In meeting these challenges we attempted to create a simple molecular structure (termed as “biomolecular tweezers”), which can couple binding affinity to an on/off-or modulatable switch. Ligands of moderate affinity to the active site and a protein-recognition exosite of thrombin were conjugated using a number of flexible polypeptide linkers. The resulting bivalent molecules displayed affinities in the low- to sub-nanomolar range typical of clinically successful thrombin inhibitors. Reversal of inhibition was achieved through binding of the flexible linker to well-structured protein antidotes. We show that relatively weak linker-antidote interactions can disrupt the molecule’s ability to bind the target in a bivalent high-affinity mode. A number of applications of retractable bivalent inhibitors have been shown, including: (1) development of antidote-reversible therapeutic anticoagulants; (2) site-specific delivery of protein drugs; and (3) design of sensors for small-molecule binding to large protein interaction interfaces.

Results and Discussions

Moiety binding to the fibrinogen-binding exosite I (E) and the active site (A) of thrombin were formed by peptides Hir(55-65) and Bbs-R-(D-Pip), respectively, where Hir(55-65) = DFEEIPEEYLQ, Bbs = 4-*tert*-butyl-benzenesulfonyl, and D-Pip = D-pipecolic acid. The E- and A- monovalent “heads” have comparable affinities to thrombin in the vicinity of 0.5 μ M.

The binding heads were first connected by flexible polypeptide repeats of varying lengths with a general formula of -S-(GS)_n- (inhibitors **TI1-TI6**) (Table 1). The resulting bivalent molecules displayed affinities in the low- to sub-nanomolar range. The poly G-S linkers were then replaced by a c-myc peptide recognizing specifically an antibody 9E10. Linked molecule **TI7** still retained strong bivalent inhibitory activities toward thrombin (Table 1). This potent thrombin inhibitor is responsive to and can be neutralized by the antibody “antidote”. Specifically, we demonstrated that the bivalent inhibitory properties of **TI7** can be reversed by the antibody 9E10 binding to the linker with a relatively large K_d of \sim 0.5 μ M (Fig. 1). Clotting curves [3] were recorded in the presence (\square, \blacksquare) or absence (\circ, \bullet) of 150 nM **TI7**. Addition of \sim 1.2 μ M anti-c-myc antibody 9E10 (Sigma) only slightly slowed clotting of free thrombin (\circ), but reversed the inhibitory effect of **TI7** (\square).

Table 1. Inhibition of the amidolytic activity of thrombin by bivalent thrombin inhibitors of the general formula Bbs-Arg-(D-Pip)-Gly-(linker)-Gly-Hir⁵⁵⁻⁶⁵

Linker	Name	K_i , nM
S-(GS) ₃	T11	0.5±0.2
S-(GS) ₅	T12	0.6±0.1
S-(GS) ₇	T13	1.3±0.3
S-(GS) ₉	T14	2.0±0.3
S-(GS) ₁₁	T15	4.6±0.8
S-(GS) ₁₃	T16	6.7±1.9
EQKLISEEDL	T17	66±13

Additional use of bivalent polypeptide inhibitors with flexible linkers originates from the mechanism of dissociation of bivalent/polyvalent complexes. The slow dissociation of a bivalent ligand can be changed to fast dissociation simply by the inclusion of a monovalent constituent fragment to a certain concentration [4]. This mechanism of action of bivalent polypeptides was characterized by use of surface plasmon resonance experiments. Indeed, the rate of dissociation of a thrombin-binding polypeptide **T11** is increased (Fig. 2) upon incrementation of the concentrations of the peptide Gly-Hir(55-65). This same concentration range reflects the binding affinity of the “monovalent” Gly-Hir(55-65) peptide.

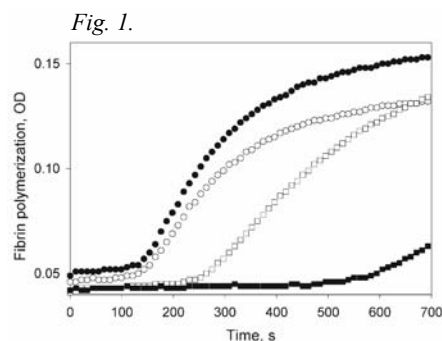


Fig. 1. “Retraction” of tweezer-like inhibitors by a linker-specific antidote in a fibrinogen clotting assay.

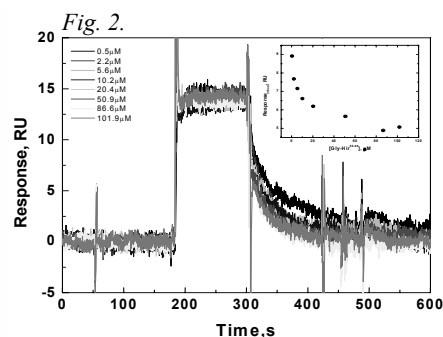


Fig. 2. The effect of Gly-Hir(55-65) on T11 dissociation from immobilized α-human thrombin (428RU immobilized) at 298K.

Acknowledgments

This work was supported by the Genomics and Health Initiative (GHI) of the National Research Council of Canada (NRCC Publication No. 42472).

References

1. Drews, J. *Science* **287**, 1960-1964 (2000).
2. Pavlou, A. K. and Reichert, J. M. *Nat. Biotechnol.* **22**, 1513-1519 (2004).
3. DiMaio, J., et al., *J. Biol. Chem.* **265**, 21698-21703 (1990).
4. Rao, J., et al., *Science* **280**, 708-711 (1998).

Helix Formation in α/β -, α/γ -, and β/γ -Hybrid Peptides

Carsten Baldauf, Robert Günther and Hans-Jörg Hofmann

Institut für Biochemie, Universität Leipzig, Brüderstr. 34, D-04103 Leipzig, Germany

Introduction

The research on oligomers that adopt definite conformations in solution, so called foldamers, has become a field of great interest in the last decade [1]. A lot of inspiration came from the investigation of peptide foldamers. Thus, numerous secondary structure types were found in the homologous α -, β -, γ -, and δ -peptides. Whereas secondary structure formation in homooligomers of amino acids is well-known now, studies on heterooligomers composed of two different homologous amino acid residues arranged in an alternating order are still scarce [2-4]. In particular, knowledge on the folding of such sequences into helices would be of great interest. Here, we provide a complete overview on the basic helix types in oligomers of α/β -, α/γ -, and β/γ -amino acids, respectively. Three basic types of hydrogen-bonded helices could be expected in these classes of hybrid peptides:

- i helices with all hydrogen bonds oriented in backward direction along the sequence,
- ii helices with all hydrogen bonds oriented in forward direction along the sequence, and
- iii helices with the hydrogen bonds changing alternately in backward and forward direction (sometimes named "mixed" or β -helices) [5,6].

Based on the systematic variation of the backbone torsion angles in octamers consisting of four amino acid residues of each type (Fig. 1), the accessible conformational space was screened for hydrogen-bonded helices according to general geometry criteria [7]. Afterwards, geometry optimizations for all potential helix candidates were performed at the HF/6-31G* level of *ab initio* MO theory.

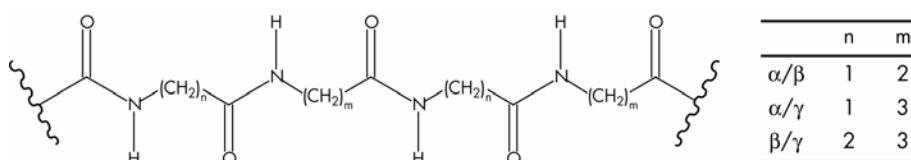


Fig. 1. Schematic representation of the studied models of α/β -, α/γ - or β/γ -hybrid peptides.

Results and Discussion

α/β -Hybrid peptides: In vacuum, most stable among various helix alternatives is a $H_{18/16}$ helix with hydrogen bonds alternating in backward and forward direction (Fig. 2). Considering the solvent water as a polarizable continuum, a mixed helix with smaller hydrogen bonded rings ($H_{11/9}$) becomes most stable (Fig. 2). Another helix conformer (H_{11}) with all hydrogen bonds in backward direction shows also considerable stability in an aqueous environment. This structure corresponds to a helix type suggested by Gellman and coworkers [4]. Another helix arrangement $H_{12/13}$ with all hydrogen bonds in forward direction along the sequence is similar to a helix suggested by Reiser and coworkers [3].

α/γ -Hybrid peptides: The most stable structure in this class of hybrid peptides is a mixed helix with alternating 10- and 12-membered hydrogen-bonded rings (Fig. 2). Since a heterodimer of an α - and γ -amino acid constituent has about the same chain length as a β -amino acid dimer, this hydrogen bonding pattern is similar to a mixed helix described by the Seebach group for the β -Peptides [8]. Obviously, α/γ -hybrid peptides can serve as mimetics for β -peptides.

β/γ -Hybrid peptides: The most stable helix structure in this class of compounds is a mixed helix $H_{11/13}$ (Fig. 2). But, β/γ -hybrid peptides are also peptide mimetics, since a β/γ -dimer has about the same chain length as an α -peptide trimer [2]. Indeed, we found a helix with 13-membered pseudocycles stabilized by hydrogen bonds in backward direction. So, this structure imitates the α -helix of native peptides (Fig. 2).

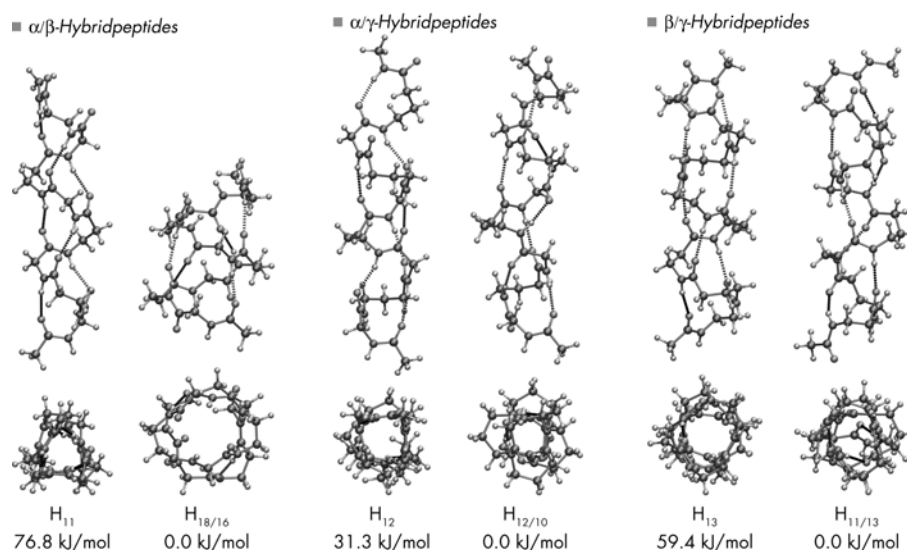


Fig. 2. The most representative helical structures of α/β -, α/γ - or β/γ -hybrid peptide.

Acknowledgments

The work was funded by DFG (Projekt HO-2346/1 and SFB 610).

References

- Gellman, S. H. *Acc. Chem. Res.* **31**, 173-180 (1998).
- Roy, R. S. and Balaram, P. *J. Peptide Res.* **63**, 279-289 (2004).
- De Pol, S., Zorn, C., Klein, C. D., Zerbe, O. and Reiser, O. *Angew. Chem. Int. Edit.* **43**, 511-514 (2004).
- Hayen, A., Schmitt, M. A., Ngassa, F. N., Thomasson, K. A. and Gellman, S. H. *Angew. Chem. Int. Edit.* **43**, 505-510 (2004).
- De Santis, P., Morosetti, S. and Rizzo, R. *Macromolecules* **7**, 52-58 (1974).
- Baldauf, C., Günther, R. and Hofmann, H. -J. *Angew. Chem. Int. Edit.* **43**, 1594-1597 (2004).
- Baldauf, C., Günther, R. and Hofmann, H. -J. *Helv. Chim. Acta* **86**, 2573-2588 (2003).
- Seebach, D., Gademann, K., Schreiber, J. V., Matthews, J. L., Hintermann, T. and Jaun, B. *Helv. Chim. Acta* **80**, 2033-2038 (1997).

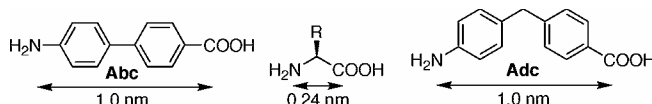
Nanometer-Scale Amino Acids for Biomolecular Nanotechnology

James S. Nowick, Chris M. Gothard, Sang-Woo Kang and Santanu Maitra

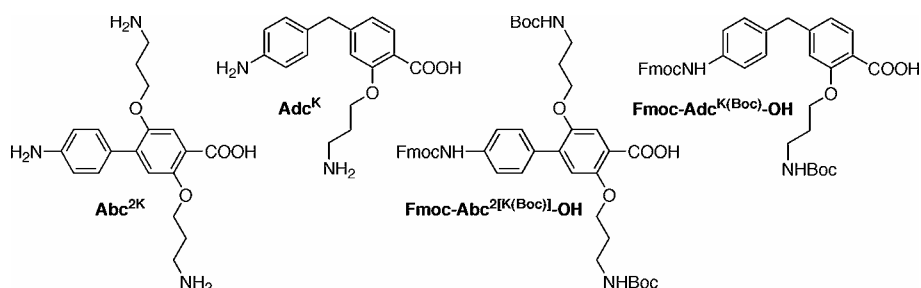
Department of Chemistry, University of California, Irvine, CA 92697-2025, USA

Proteins play the central role in most biological processes both because of their ability to fold into well-defined three-dimensional structures and because of their nanometer-scale size, which allows them to engulf small molecules and to grip other biomacromolecules. Proteins achieve their structures and size by virtue of the dozens or hundreds of α -amino acids that they comprise. Each α -amino acid is only 0.24 nanometers in length. Dozens or more are required to create functional domains that fold into well-defined three-dimensional structures. Still more are required to create the functional multidomain structures that serve as receptors, catalysts, transcription factors, and other species that make up so many of the working parts of living cells.

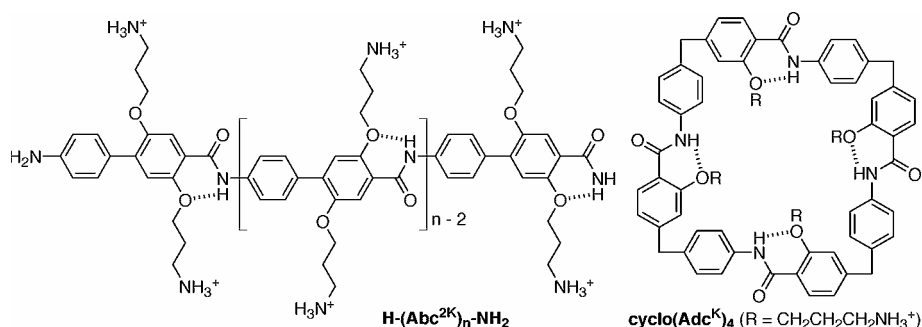
With the goal of mimicking the structure and function of proteins, our research group has begun to create relatively simple molecules that emulate proteins' large size and ability to bind other molecules. Our philosophy is to construct these molecules from amino acid building blocks using standard peptide synthesis technology, both to harness the large range of powerful synthetic, analytical, and purification technologies that have been developed for the synthesis of peptides and to readily allow others to adopt the building blocks and molecules that we develop. This principle of *portability* has already been proven in the elegant work on β -peptides that has been pioneered by the Gellman and Seebach laboratories and has subsequently been widely adopted and commercialized. To achieve large structures without requiring dozens or hundreds of building blocks, we have developed nanometer-scale amino acids based on the *theta*-amino acid aminobiphenylcarboxylic acid (Abc) and the *iota*-amino acid aminodiphenylmethanecarboxylic acid (Adc).



We have created functionalized variants Abc^{2K} and Adc^K, which bear lysine-like side chains designed to impart water solubility, control conformation, and minimize aggregation. We have used the protected forms of these amino acids Fmoc-Abc^{2[K(Boc)]}-OH and Fmoc-Adc^{K(Boc)}-OH to prepare rigid rodlike oligomers of up to 10 nanometers in length and macrocyclic receptors with nanometer-sized cavities.



The Fmoc-Abc^{2K(Boc)}-OH building block is readily synthesized in multigram quantities from 1,4-dibromo-2,5-dimethoxybenzene and 4-(4,4,5,5-tetramethyl-1,3,2-dioxaborolan-2-yl)-aniline by means of the Suzuki cross-coupling reaction. Synthesis of Abc^{2K} oligomers is easily carried out using standard solid-phase peptide synthesis methodologies. Abc^{2K} oligomers are readily purified and analyzed by standard RP-HPLC and ESI-MS techniques. Using these techniques, we have prepared oligomers ranging from trimer H-(Abc^{2K})₃-NH₂ to decamer H-(Abc^{2K})₁₀-NH₂ without difficulty. ¹H NMR dilution studies of the hexamer suggest that little or no aggregation occurs at tenth-millimolar concentrations but that self-association occurs at higher concentrations. Molecular mechanics and dynamics studies of Abc^{2K} oligomers show only minor effects from torsional and bending motions. Fluorescence resonance energy transfer (FRET) experiments are planned to experimentally confirm that Abc^{2K} oligomers behave as rigid molecular rods in solution.



The Fmoc-Adc^{K(Boc)}-OH building block is readily synthesized in gram quantities from 4-methylsalicylic acid and 4,4,5,5-tetramethyl-2-(4-nitrophenyl)-1,3,2-dioxaborolane by means of the Suzuki cross-coupling reaction. Cyclo(Adc^K)₄ is prepared by solid-phase synthesis of H-(Adc^{K(Boc)})₄-OH on 2-chlorotrityl resin, followed by macrocyclization, deprotection, and RP-HPLC purification. ¹H NMR studies suggest that cyclo(Adc^K)₄ adopts two conformations in aqueous solution: a “square” conformer with all *trans*-amide linkages and a “rectangular” conformer with alternating *cis*- and *trans*-amide linkages. ¹H NMR mixing studies show that cyclo(Adc^K)₄ forms a complex with sodium cholate and that complexation shifts the equilibrium toward the “square” conformer. ¹H NMR Job plot and titration experiments show strong ($K \approx 10000 \text{ M}^{-1}$) 1:1 complexation of sodium cholate at tenth-millimolar concentrations. At higher concentrations, precipitation or aggregation occurs. Molecular modeling studies show that cyclo(Adc^K)₄ is complementary in size to cholate and suggest a complex in which the cholate is bound within the macrocycle. These studies also suggest that the ring of the cyclic tetramer is strained. The ring strain, in conjunction with hydrophobic and aromatic interactions, may promote the formation of the “rectangular” conformer, which suffers unfavorable *cis*-amide linkages.

Collectively, these studies establish that nanometer-scale amino acids Abc^{2K} and Adc^K are viable building blocks for the facile construction of large molecules that mimic some of the binding and size properties of proteins.

Acknowledgments

We thank UCI (COR, CORCLR, IGB, and the Institute for Brain Aging and Dementia), UC (BREP), and the American Chemical Society (PRF) for support.

Design and Synthesis of Target-specific Contrast Agents

Anouk Dirksen¹, Sander Langereis¹, Bas F.M. de Waal¹, Marcel H.P. van Genderen¹, E.W. Meijer¹, Wencke Adriaens² and Tilman M. Hackeng²

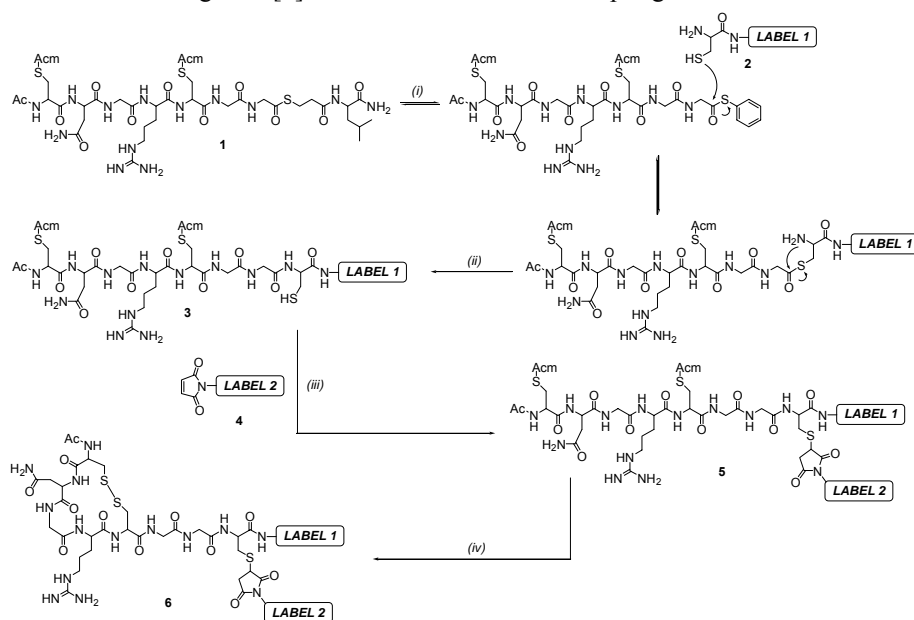
¹Laboratory of Macromolecular and Organic Chemistry, Eindhoven University of Technology, P.O. Box 513, 5600 MB Eindhoven, the Netherlands; ²Cardiovascular Research Institute Maastricht (CARIM), University Maastricht, P.O. Box 616, 6200 MD Maastricht, the Netherlands

Introduction

Contrast agents designed to target a specific event may improve the imaging of this event drastically due the enhancement of contrast at the region of interest. Oligopeptides are widely applied as targeting units for biomedical imaging. Currently, multimodality is at the focus of attention in biomedical imaging, whereas at the same time efforts are made to improve the affinity of target-specific contrast agents for their marker through multivalency[1]. It is of particular interest to develop generally applicable synthetic strategies to address these issues.

Results and Discussion

A synthetic methodology was developed for the double labeling of oligopeptides. This strategy involves a series of highly efficient, chemoselective reactions, namely native chemical ligation [2] and the maleimide-thiol coupling reaction.



Scheme 1. General strategy for the double labeling of oligopeptides. (i) 2 v-% thiophenol, 2 v-% benzylmercaptan, 6 M Guanidine in 0.1 M Tris, 1 hr, pH 7-7.5, 37 °C; (ii) spontaneous rearrangement; (iii) 0.1 M Tris, 1 hr, pH 6.5, RT; (iv) 1-2 eq I₂, 10 v-% acetic acid in 0.1 M Tris, 1 hr, RT.

Its general applicability was demonstrated for the cyclic NGR peptide, which is a ligand for CD13, a protein over-expressed by endothelial cells involved in angiogenesis (Scheme 1) [3,4]. Manual solid phase peptide synthesis using the *in situ* neutralization/HBTU activation procedure for tBoc chemistry on an MBHA resin was applied to synthesize the NGR peptide with a C-terminal thioester (**1**). The thiol groups of the two cysteine residues of the peptide involved in cyclization were protected with Ac₂S groups to avoid reaction with maleimide during the labeling procedure. Peptide **1** was reacted with a cysteine-functionalized label 1 (**2**) under ligation conditions to give **3**. The free thiol of the cysteine residue of **3** involved in the ligation process was used to introduce a maleimide-functionalized label 2 (**4**) to give **5**. Once the reaction went to completion, the reaction mixture was diluted ~ 30 times with 0.1 M Tris (aq) containing 10 v-% of acetic acid and the Ac₂S protecting groups of **5** were removed through the addition of 1-2 equivalents of I₂ to give **6**. The removal of the Ac₂S groups resulted instantaneously in the correct “folding” of the peptide unit into its cyclic form.

The strategy employed for the double labeling of oligopeptides allowed the development of multivalent target-specific contrast agents. By labeling the NGR peptide **1** with both a biotin unit (“label 1”) and a Gd(III)DTPA moiety (MRI “label 2”), a supramolecular contrast agent could be synthesized using the biotin-avidin system [4]. The formation of a 4:1 complex between the biotinylated target-specific contrast agent and avidin was confirmed by the HABA assay and an E-titration.

In addition, a covalent approach was developed to attach in one step multiple labels to a peptide *via* native chemical ligation. This was demonstrated by the reaction of a thioester-functionalized poly(lysine) dendritic wedge[5] with 8 DTPA chelates along its periphery and a cysteine-functionalized A14 peptide, which specifically recognizes fibrin. The multilabeling of the A14 peptide was confirmed by ESI-MS. Subsequent complexation of Gd(III) to the DTPA chelates will provide the corresponding MRI label. Also in this case native chemical ligation can be combined with the maleimide-thiol coupling reaction to introduce multimodality.

In conclusion, the strong combination of native chemical ligation followed by a maleimide-thiol coupling allowed the introduction of multimodality to oligopeptides and the development of well-defined multivalent target-specific contrast agents based on oligopeptides, both in a supramolecular and a covalent fashion.

Currently, we are extending our synthetic strategy to arrive at multivalent target-specific contrast agents with a tunable number of labels and targeting units.

Acknowledgments

The work was funded by the Council for Chemical Sciences of the Netherlands Organization for Scientific Research and by the BSIK-program entitled Molecular Imaging of Ischemic Heart Disease (projectnumber BSIK03033).

References

1. Mammen, M., Choi, S. -K. and Whitesides, G. M. *Angew. Chem. Int. Ed.* **37**, 2754-2794 (1998).
2. Dawson, P. E., Muir, T. W., Clark-Lewis, I. and Kent, S. H. B. *Science* **266**, 776-779 (1994).
3. Dirksen, A., *et al.* *Org. Lett.* **6**, 4857-4860 (2004).
4. Dirksen, A., Langereis, S., de Waal, B. F. M., van Genderen, M. H. P., Hackeng, T. M. and Meijer, E. W. *Chem. Commun.* 2811-2813 (2005).
5. Denkewalter, R. G., Kolc, J. and Lukasavage, W. J. *U.S. Pat.* 4,289,872, *Sept. 15* (1981).

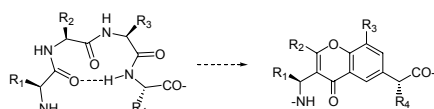
Design and Synthesis of Novel Chromone Based Peptidomimetics

Kristian Dahlén, Morten Grøtli and Kristina Luthman

Department of Chemistry – Medicinal Chemistry, Göteborg University, SE-412 96 Göteborg, Sweden

Introduction

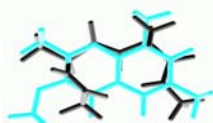
Chromones and flavones (R_2 =phenyl) are widely distributed in nature and have an interesting range of biological activities, including anti-cancer [1], anti-HIV [2], and anti-oxidant [3] properties. They have also been considered as privileged structures in drug discovery [4]. We have been interested in using the chromone ring system as a scaffold for peptidomimetics. The substituents on the chromone scaffold have a possibility to mimic important side chains in target peptides.



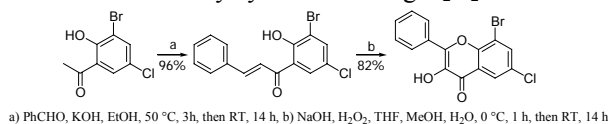
The development of scaffold mimetics of peptides is an interesting strategy to study the bioactive conformation of peptides and to increase the understanding of peptide-receptor interactions [4]. β -Turns are one of the three major secondary structural elements of peptides and proteins and there has been a lot of research devoted to the development of new β -turn mimetics [5].

Results and Discussion

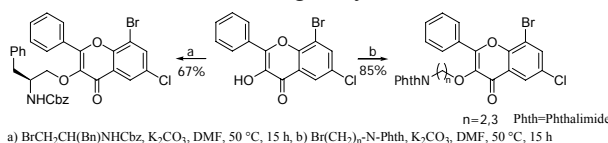
The chromone structure has been compared with a β -turn structure using molecular modeling (MacroModel v.7.1, AMBER force field *in vacuo*). The comparison shows that a chromone scaffold has potential use in β -turn mimetics.



Synthesis of the functionalized scaffold: The functionalized scaffold was obtained by reacting 5-bromo-3-chloro-2-hydroxyacetophenone with benzaldehyde under basic conditions followed by cyclization using H_2O_2 and NaOH.

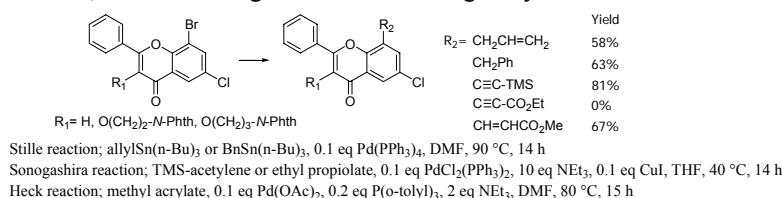


Introduction of substituents in the 3-position: O-Alkylation in the 3-position was performed under basic conditions in good yield.

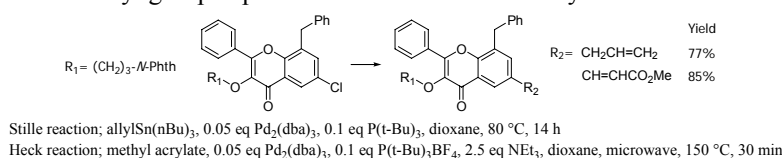


Introduction of substituents in the 8-position: The difference in reactivity between aryl bromides and chlorides in Pd-catalyzed reactions made it possible to

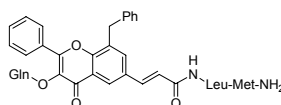
selectively introduce groups in the 8-position. We have shown that it is possible to perform Heck, Stille or Sonogashira reactions in good yields.



Introduction of substituents in the 6-position: It was important to introduce the C-terminal amino acid equivalent in the 6-position. A Heck reaction with methyl acrylate provided such a possibility. An allyl group was introduced using a Stille reaction. The allyl group is possible to oxidize to a carboxylic acid function.



Application to Substance P: Substance P is a neuropeptide consisting of 11 amino acids. It has been proposed that the messenger region, Gln-Phe-Phe-Gly-Leu-Met-NH₂ preferentially adopts a β -turn conformation [6]. Based on our strategy we can synthesize a flavone derivative that has the potential to mimic the sequence Phe-Phe-Gly and we also have the possibility to incorporate the structure in the peptide sequence.



In conclusion, we have devised an efficient synthetic route to 3,6,8-substituted flavone derivatives and molecular modeling indicates that these compounds have potential applications as β -turn mimetics.

Acknowledgement

Financial support was obtained from The Knut and Alice Wallenberg Foundation and The Swedish Research Council.

References

1. Zheng, X., Meng, W. D., Xu, Y. Y., Cao, J. G. and Qing, F. L. *Bioorg. Med. Chem.* **13**, 881-884 (2003); Birt, D. F., Hendrich, S. and Wang, W. *Pharmacol. Therapeutics* **90**, 157-177 (2001).
2. Yu, D., Chen, C. H., Brossi, A. and Lee, K. H. *J. Med. Chem.* **47**, 4072-4082 (2004).
3. Burda, S. and Oleszek, W. *J. Agric. Food Chem.* **49**, 2774-2779 (2001).
4. Horton, D. A., Bourne, G. T. and Smythe, M. L. *Chem. Rev.* **103**, 893-930 (2003).
5. Souers, A. J. and Ellman, J. A. *Tetrahedron* **57**, 7431-7448 (2001).
6. Pawar, V. G., De Borggraeve, W. M., Maes, V., Tourwé, D. A., Compennolle, F. and Hoornaert, G. J. *Tetrahedron Lett.* **46**, 1707-1710 (2005).

Determination of Intrinsic Hydrophilicity/Hydrophobicity Coefficients of Amino Acid Side-Chains using Synthetic Model Peptides

James M. Kovacs, Colin T. Mant and Robert S. Hodges

Department of Biochemistry & Molecular Genetics, University of Colorado at Denver and Health Sciences Center, Aurora, CO, 80045, USA

Introduction

The concept of hydrophobicity has been a topic of much study in all aspects of science [1]. It is most important in the hydrophobic effect, as exemplified by the relative hydrophilicity/hydrophobicity of amino acid side-chains and how they interact, which is the most important factor underlying the hierarchical structure, function, and stability of proteins [2]. The measurement of amino acid side-chain hydrophilicity/hydrophobicity has been carried out by a number of approaches, both chromatographic and non-chromatographic, described in an excellent review by Biswas *et al.* [1]. Despite there being over one hundred scales in the literature, there is not a good consensus in ranking or value for all side-chains. Certainly, we believe that scales to date are useful; however, a definitive “intrinsic” set of coefficients has yet to be determined. “Intrinsic” implies the maximum hydrophilicity/hydrophobicity of side-chains in a peptide chain in the absence of nearest-neighbor effects (i to $i \pm 1$ side-chain interactions) and/or any restriction of rotational freedom of the peptide chain that prevents full expression of the side-chain hydrophilicity/hydrophobicity. Our approach uses reversed-phase high-performance liquid chromatography (RP-HPLC) to separate mixtures of synthetic *de novo* designed model peptides which contain 23 single amino acid substitutions, encompassing the 20 naturally occurring amino acids plus norvaline, norleucine, and ornithine. From the observed retention behavior of these model peptides, we have obtained intrinsic coefficient values at three pH values over six mobile phase conditions.

Results and Discussion

We utilized a model synthetic peptide with the sequence Ac-XGAKGAGVGL-amide, where X is the substitution site. Four Gly residues ensure no defined secondary structure tendencies. The substitution site (X) is adjacent to a Gly residue to allow full rotational freedom about the two bonds (nearest-neighbor effect), C_{α} -C (ψ) and C_{α} -N (ϕ), surrounding the peptide bond, as demonstrated by substituting both D- and L-isomers, and observing identical retention behavior. X was the N-terminal residue to ensure full interaction with the reversed-phase matrix. A single Lys residue was used to ensure good solubility over varying mobile phase conditions and the four hydrophobes were dispersed to prevent a preferred hydrophobic binding domain. Our intrinsic coefficients were determined by using the Gly peptide as a reference. The resulting intrinsic coefficients can be found in Table 1. There is an excellent correlation ($r = 0.999$, Fig. 1) for the 17 peptides substituted at position X with neutral side-chains, demonstrating that pH has no effect on the relative hydrophilicity/hydrophobicity of these side-chains. In stark contrast, the increase of pH from 2 to 7 increases the relative hydrophobicity of Orn, Lys, His, and Arg, likely due to the partial (Orn, Lys, Arg) or complete (His, side chain $pK_a \sim 6$) deprotonation of these residues at the higher pH value, i.e., (1) the positive charge on

these side-chains is diminished or eliminated or (2) an increased neutralization of the positive charge by the increased concentration of the anions H_2PO_4^- and HPO_4^{2-} is occurring as the pH is increased from 2 to 7. In contrast, the relative hydrophobicities of the acidic side-chains of Asp and Glu are decreasing with the increase of pH, due to the deprotonation of these residues at pH 7 (the pKa of these side-chains are ~4). Though not shown, the seventeen neutral side-chain (Gly, Asn, Ser, Gln, Thr, Ala, Cys, Pro, Val, Tyr, n-Val, Met, Ile, Leu, n-Leu, Phe, and Trp) hydrophobicities are independent of pH, mobile phase buffer system (presence or absence of salts and ion-pairing reagents) and hydrophobic column matrix composition (C8 and C18). The potentially charged side-chain hydrophobicities (Orn, Lys, His, Arg, Glu, and Asp), were the only side-chains affected by pH and mobile phase composition. Previous scales have been shown to be affected by pH, mobile phase composition or column functional groups. The fact that our coefficients are unaffected by these parameters strongly suggests that our coefficients are truly intrinsic.

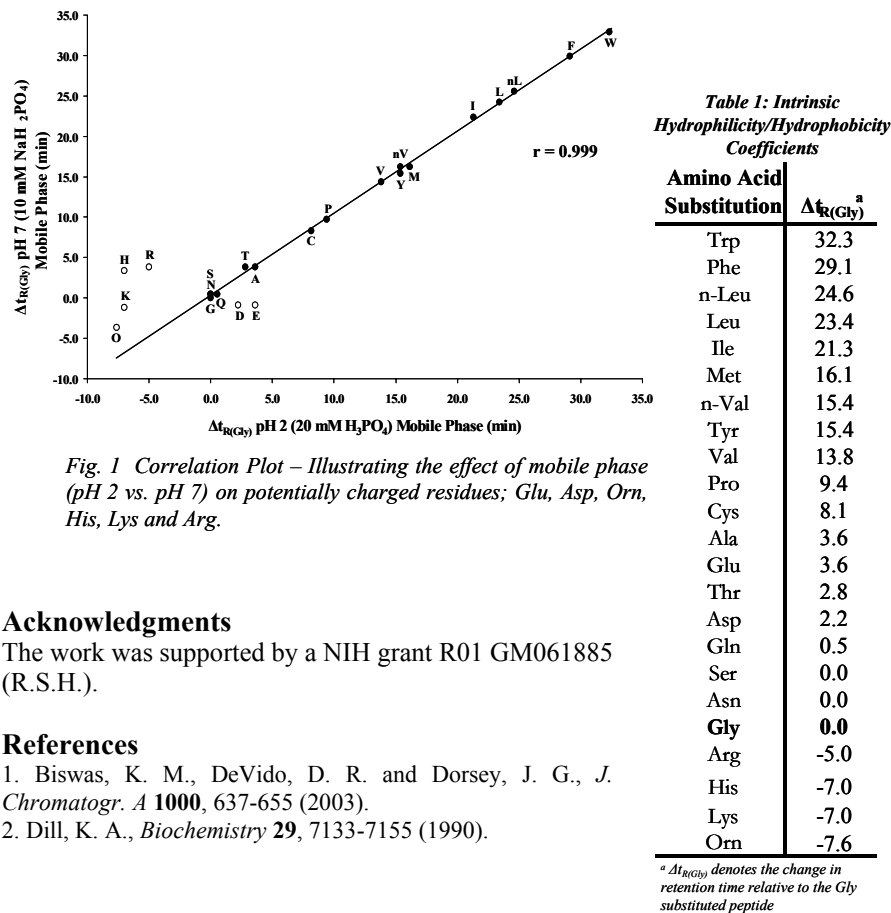


Fig. 1 Correlation Plot – Illustrating the effect of mobile phase (pH 2 vs. pH 7) on potentially charged residues; Glu, Asp, Orn, His, Lys and Arg.

Acknowledgments

The work was supported by a NIH grant R01 GM061885 (R.S.H.).

References

1. Biswas, K. M., DeVido, D. R. and Dorsey, J. G., *J. Chromatogr. A* **1000**, 637-655 (2003).
2. Dill, K. A., *Biochemistry* **29**, 7133-7155 (1990).

Peptide Structures in Material Science and Disease

Peptide Reptation as a Mechanism for Rearrangements within a β -Sheet Aggregate

Sarah A. Petty and Sean M. Decatur

Department of Chemistry, Mount Holyoke College, South Hadley, MA, 01075, USA

Introduction

Many neurodegenerative diseases are characterized by the accumulation of amyloid fibers in the brain, which can occur when a protein misfolds into an extended β -sheet conformation. The nucleation of these β -sheet aggregates is of particular interest, not only because this is the rate determining step towards fiber formation but also because early, soluble aggregate species may be the cytotoxic entities in many diseases. The soluble oligomeric intermediates are difficult to isolate and, due to their large size and dynamic nature, difficult to characterize using traditional biophysical techniques. For these reasons, many studies aimed at studying the aggregation process use small peptides, derived from full length proteins of interest, which also show amyloidogenic behavior. Among the peptides studied extensively include the NFGAIL sequence from the islet amyloid polypeptide, fragments of the prion protein which include the AGAAAAGA amyloidogenic region, and many different fragments of the Alzheimer's $A\beta$ peptide. In simulations of these peptides, ensembles of β -sheet oligomers are initially formed, including species which have a non-native hydrogen bonding registry or mix parallel and antiparallel organization of the strands. Rearrangements from rapidly formed disordered β -sheets to well-ordered oligomers are likely an essential step for forming a template capable of nucleating growth into larger fibrils.

Infrared (IR) spectroscopy is well suited for probing these systems. β -sheet aggregates give distinctive amide I bands in the IR spectrum, and the inclusion of specific isotope labels in the peptide (isotope-edited IR spectroscopy) gives residue-level structural details on the peptide conformation, including the detailed registry of strands within the β -sheet [1,2]. In the case of residues 109-122 of the prion protein (peptide H1; Ac-MKHMAGAAAAGAVV-NH₂), the initial β -sheet aggregates formed in solution lack a regular register between strands, and stable amyloid fibers only form after the β -strands of the peptide have adopted their equilibrium antiparallel β -sheet configuration with residue 117 in register across all strands [2]. Adoption of this register is required for the formation of stable, twisted fibers of aggregates [3]. In this paper, we present the kinetic details of the realignment of these β -strands from their fast-formed non-equilibrium structure with no regular register of the strands into the more ordered β -sheets capable of aggregating into stable fibers. This process is likely the nucleating step towards the formation of stable fibers.

Results and Discussion

A synthetic peptide based on residues 109 – 122 of the Syrian hamster prion protein (H1; Ac-MKHMAGAAAAGAVV-NH₂) was synthesized using Fmoc chemistry on a solid-phase peptide synthesizer and purified using reverse-phase HPLC. A specifically labeled peptide, H1*, was synthesized with a ¹³C carbonyl at residue 117 (Ac-MKHMAGAAAAGAVV-NH₂). Lyophilized peptide was dissolved into 0.1 M DCl/D₂O, left to exchange at room temperature for five hours, then lyophilized

again. The exchanged peptides were dissolved in a 50%D₂O/acetonitrile buffer to a concentration of ~10 mg/mL, then added to a water-jacketed IR cell equipped with CaF₂ windows and a 100 μ m Teflon spacer. FTIR spectra were measured on a Bruker Vector 22 FTIR spectrometer.

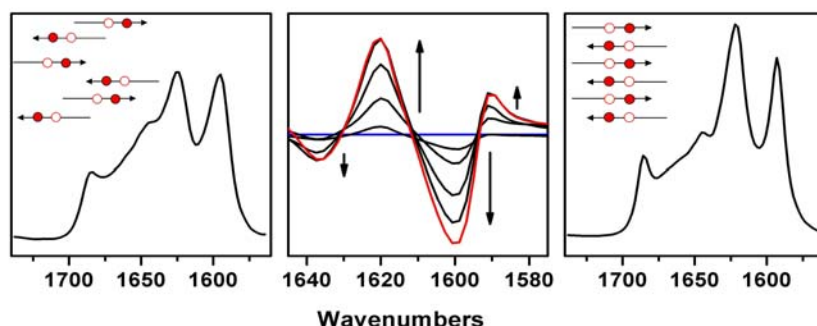


Fig. 1. (A) IR spectra of labeled H1 peptide immediately after sample preparation. The β -sheet is disordered resulting in a ^{13}C amide I' band at $\sim 1601\text{ cm}^{-1}$. (B) Difference spectra obtained by subtracting the initial spectrum from all subsequent spectra, measured each hour over an eight hour period; (C) final spectrum of the peptide in the ordered, aligned β -sheet.

When the H1* peptide is initially dissolved in 50% acetonitrile/D₂O, the ^{13}C amide I' band appears at $\sim 1601\text{ cm}^{-1}$; this frequency corresponds to a disordered β -sheet, lacking any regular strand register. When the sample is allowed to sit at 37°C for several hours, the β -sheets adopt a regular, well-ordered register, with residue 117 aligned in all of the strands, resulting in a shift of the ^{13}C amide I' band to 1591 cm^{-1} . This band shift can be monitored by transient FTIR spectroscopy (Fig. 1). The kinetics of this band shift are best fit by a stretched exponential function ($y = y_0 + A \cdot \exp(-xk)^\alpha$) and show an unusual concentration dependence; the reaction slows as the concentration of peptide increases, but at high concentrations the reaction begins to speed up again (Fig. 2). This behavior suggests that there are two different mechanisms for strand realignment possible – one which dominates at high concentrations, and one which dominates at low concentrations.

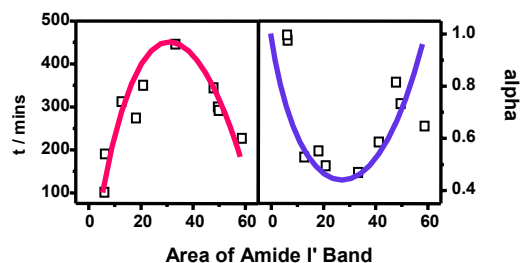


Fig. 2. (A) Time constant for strand rearrangement process as a function of peptide concentration. (B) Stretching constant (α) as a function of concentration.

These two mechanisms were dissected further by using isotope-dilution experiments; samples of labeled and unlabeled peptide were mixed at low and high concentrations, then the kinetics of β -sheet alignment were followed by FTIR spectroscopy. At low concentrations, the ^{13}C amide I' band did not shift with equal amounts of labeled and unlabeled peptide were mixed. This suggests that the labeled and unlabeled strands randomly intermix, preventing the ^{13}C residues from coupling. Thus, at low concentrations, strand alignment must occur via a detachment/re-anneal mechanism, in which strands break away from the β -sheet only to recombine in the equilibrium alignment. However, when labeled and unlabeled peptides are mixed at higher concentrations, the ^{13}C amide I' band does shift to 1591 cm^{-1} , indicating that the labeled and unlabeled strands do not completely intermix (Fig. 3). Under these conditions, the major path for strand realignment must be an intrasheet mechanism such as reptation of neighboring strands.

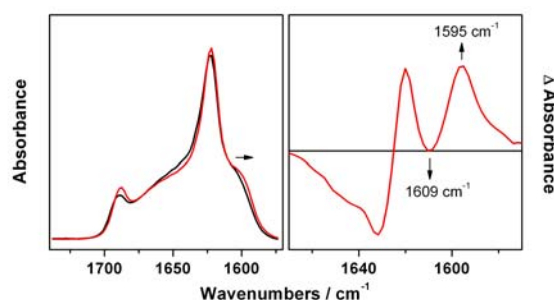


Fig. 3. (A) Initial and final amide I' spectra of a mixture of labeled and unlabeled H1 at high concentration showing the shift of the ^{13}C band to lower frequency. (B) Difference spectrum of final – initial from (A).

The rearrangement of strands within β -sheets may be an essential step in the nucleation of large, fibrillar aggregates. Reptation between strands within β -sheets has been observed in molecular dynamics simulations of several aggregating peptides [4], but this is the first experimental evidence for this phenomenon. We have observed similar behavior for the peptide derived from residues 16–22 of the Alzheimer's A β peptide, and further studies on other systems (such as peptides derived from the islet amyloid polypeptide) are currently underway.

Acknowledgments

The work was funded by an NIH AREA grant to S.M. Decatur.

References

1. Barth, A. and Zscherp, C. Q. *Rev. Biophys.* **35**, 369-430 (2000).
2. Silva, R. A. G. D., Barber-Armstrong, W. and Decatur, S. M. *J. Am. Chem. Soc.* **125**, 13674-13675 (2003).
3. Petty, S. A., Adalsteinsson, T. and Decatur, S. M. *Biochemistry* **44**, 4720-4726 (2005).
4. Santini, S., Mousseau, N. and Derreumaux, P. *J. Am. Chem. Soc.* **126**, 11506-11516 (2004).

The HIV-1 Fusion Peptide has Amyloid Properties

Patrick Mobley¹, Alex Nisthal¹, Jeff Julius¹, Jonathan Kelber¹, Albert Gonzales², Sepehr Eskandari², Alan Waring^{3,4} and Larry Gordon⁴

¹Chemistry Department, ²Biological Sciences Department, Cal Poly Pomona, Pomona, CA 91768; ³Department of Chemistry and Biochemistry, UCLA, Los Angeles, CA 90095; ⁴LA BioMed Research Institute, Torrance, CA 90502, USA

Introduction

The N-terminal domain of HIV-1 glycoprotein 41,000 (gp41) [i.e., FP; residues 1-23; AVGIGALFLGFLGAAGSTMG-ARS-CONH₂] participates in fusion processes underlying virus-cell infection. Given the enriched alanine and glycine levels in HIV-1 FP, Callebaut et al. [1] proposed that this fusion peptide and amyloids (prions) might belong to the same superfamily of proteins. Initial experimental support for this hypothesis has come from both structural and functional studies, which showed that FP and various amyloid peptides each exhibit plaque formation, α -helix to β -sheet interconversion and membrane fusion activity. Here, we test the hypothesis that FP is an amyloid, by studying the structural properties of FP stored in an aqueous-DMSO solvent. We performed transmission electron microscopy (TEM), dynamic light scattering (DLS), and Fourier transform infrared spectroscopy (FTIR) on samples of FP that were made up from a stock solution stored for at least two weeks in DMSO/water (1:1), neutral pH, at -20°C.

Results and Discussion

TEM experiments were conducted on aqueous DMSO-stored FP that was pipetted into phosphate-buffered saline (PBS), to make a peptide solution of 100 μ M. This solution was then transferred to a formvar grid, and the sample allowed to settle for 30 minutes before the PBS was removed and the sample dried and fixed with uranyl acetate. These solutions of DMSO-stored FP in PBS showed large amounts of amorphous tangles in mats (Fig. 1). At the edges of the mats, tangled fibrils are clearly visible, with oligomers in the background. The FP fibrils observed in these electron micrographs are similar to those earlier observed for other amyloid peptides (e.g., β -amyloid), and are consistent with the N-terminal gp41 domain exhibiting 'amyloid-like' properties.

DLS experiments were next performed on aqueous DMSO-stored FP, suspended in PBS, and monitored for 40 min. Figure 2 shows that the mean radius of the FP particles progressively increased over the course of the experiment, from ~ 300

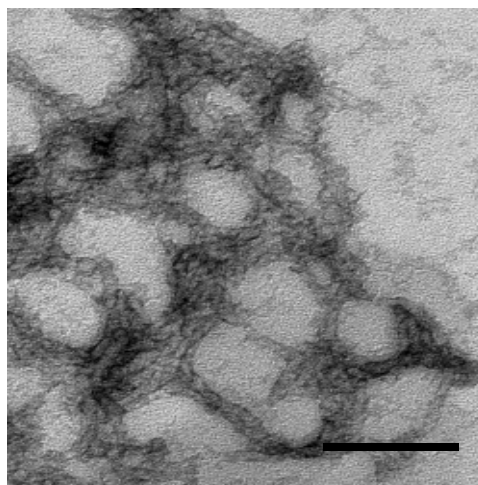


Fig. 1. TEM of HIV-1 FP stored for at least two weeks in aqueous DMSO. The bar is 100nm.

nm to ~700 nm. These findings are consistent with the more aqueous environment (i.e., PBS) promoting an increase in the size/length of the FP fibrils. Since earlier DLS studies indicated that exposure of amyloid peptides to aqueous environments similarly increased particle sizes [2], the results in Figure 2 also suggest that stored FP shares amyloid characteristics.

The secondary structure of aqueous DMSO-stored FP in water was also investigated using FTIR spectroscopy (Fig. 3). The FTIR spectrum of stored FP, first suspended and then dried from 100% D₂O, shows a prominent signature of anti-parallel β -sheets, with a strong peak at $\sim 1630\text{cm}^{-1}$ and a smaller peak at $\sim 1690\text{cm}^{-1}$ [3]. Analogous FTIR spectra have also been observed for amyloid peptides (i.e., β -amyloid, IAPP, PrP) suspended in aqueous solvents, further supporting the hypothesis that FP is amyloid. Note that it appears that 100%-HFIP is unable to dissolve all of the aqueous DMSO-stored FP fibrils. Further studies are planned to examine the relationship between the history of the FP sample and the structural and functional properties of the peptide.

Acknowledgments

This research is supported by NIH MBRS SCORE Grant GM 53933 (PWM and SE).

References

1. Callebaut, I., *et al.* *J. Comput.-Aided Mol. Des.* **8**, 175-191 (1994).
2. Lomakin, A., *et al.* *Proc. Natl. Acad. Sci. USA* **93**, 1125-1129 (1996).
3. Arrondo, J. and Goni, F. *Prog. Biophys. Molec. Biol.* **72**, 367-405 (1999).

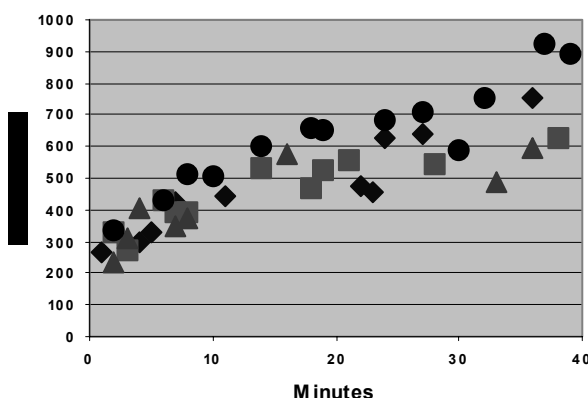


Fig. 2. Radius of FP particles formed in PBS as measured by Dynamic light Scattering. The stored-FP was $50\mu\text{M}$. Four different samples are shown.

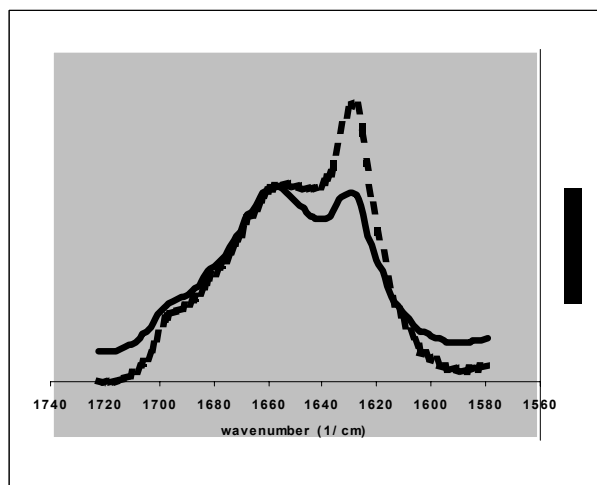


Fig. 3. FTIR spectra of stored FP dried from HFIP (solid line) and D₂O (dotted). Conditions: Ge-ATR, Bruker Vector 22 FTIR, room temperature. 64 scans, MCT detector.

Self-Assembly of Collagen Mimetic Peptides

Frank W. Kotch¹ and Ronald T. Raines^{1,2}

¹Department of Chemistry and ²Department of Biochemistry, University of Wisconsin–Madison, Madison, WI 53706, USA

Introduction

Collagen is a widely used biomaterial, with applications in skin and bone replacement, engineered tissues, and culture media [1,2]. Collagen mimetics have shown promise as biomaterials for cell adhesion and proliferation [3,4], but active structures have been limited to the length of synthetic peptides. Here, we use sticky-end-directed assembly [5] of collagen peptides to generate long synthetically tunable structures that have potential as peptide-based collagen substitutes.

The unique structure of collagen comprises three strands folded into a triple helix [6]. Each strand possesses XaaYaaGly repeats, with ProHypGly (where Hyp is (2*S*,4*R*)-4-hydroxyproline) being the most abundant triplet [6]. For this study, helicogenic collagen sequences (ProProGly)_n and (ProHypGly)_n were tethered through a simplified cystine knot [7] to afford trimers **1** and **2** (Fig. 1a). In these trimers, the identical α1 and α1' strands are constrained to be parallel to the α2 strand by a (ProYaaGly)₃ intramolecular helix. This helix organizes the trimers for intermolecular assembly (Fig. 1b).

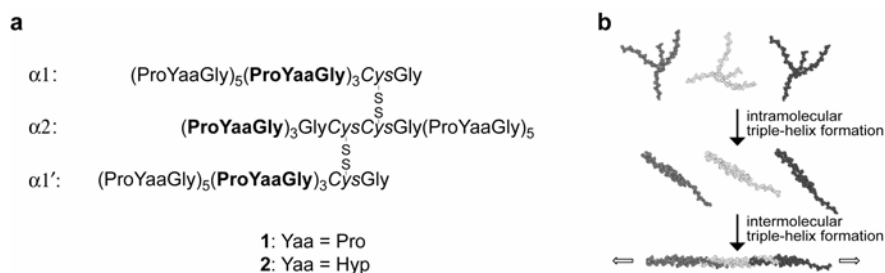


Fig. 1. (a) Trimers **1** and **2**. (b) Representation of the self-assembly process.

Results and Discussion

Circular dichroism (CD) spectra of trimer assemblies in 50 mM HOAc at pH 2.9 were characteristic of a triple helix (Fig. 2a), having a positive peak near 225 nm and a strong negative peak at 200–210 nm. Heat caused a cooperative change in the molar ellipticity at 226 nm (Fig. 2b), which is characteristic of triple-helix denaturation. Assembly (**2**)_n had a larger *T_m* value than did assembly (**1**)_n, as expected from the stability imparted by Hyp in the Yaa position [6]. Both trimers assembled with a concentration-dependent rate (Fig. 2c), indicative of an intermolecular process. Assembly (**2**)_n formed more rapidly than did assembly (**1**)_n, a result likely due to its greater preorganization as well as the rapid *cis*–*trans* isomerization of its Pro–Hyp peptide bonds [6].

The size of assemblies (**1**)_n and (**2**)_n in 50 mM HOAc at 10 °C was estimated by using dynamic light scattering. Hydrodynamic radii were measured to be 3.1 nm for (**1**)_n and 4.0 nm for (**2**)_n. Using the Broersma relations [8], lengths were calculated to be 16 nm for (**1**)_n and 22 nm for (**2**)_n, indicating that the average size of the

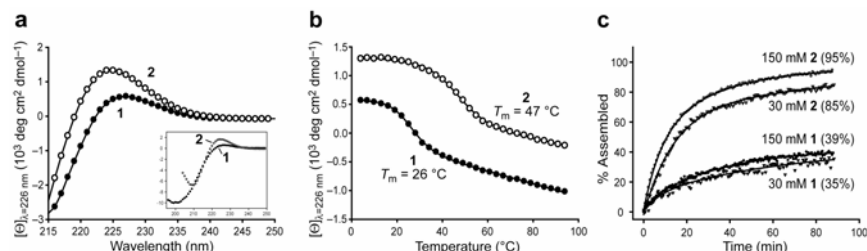


Fig. 2. (a) CD spectra, (b) thermal denaturation curves, and (c) folding rates of $(1)_n$ and $(2)_n$.

assemblies was 2–4 monomer units. This size is consistent with sedimentation equilibrium data (not shown).

The morphology of $(1)_n$ and $(2)_n$ was determined by atomic force microscopy (AFM) and transmission electron microscopy (TEM). AFM images of $(1)_n$ (Fig. 3a,b) and $(2)_n$ showed 20–120 nm long fibrils with diameters of 0.5–1.0 nm, which are similar to those of natural collagen. Rotary-shadowed TEM images of $(1)_n$ (Fig. 3c) and $(2)_n$ showed fibrillar structures 30 nm to >400 nm in length that resemble TEM images of natural collagen. The AFM and TEM data indicate that trimers **1** and **2** can self-assemble into one-dimensional fibrils that are similar in length to natural collagen.

This work is the first step towards the development of synthetic collagen-based biomaterials that could serve as bona fide collagen substitutes as well as templates for a variety of applications in nanotechnology.

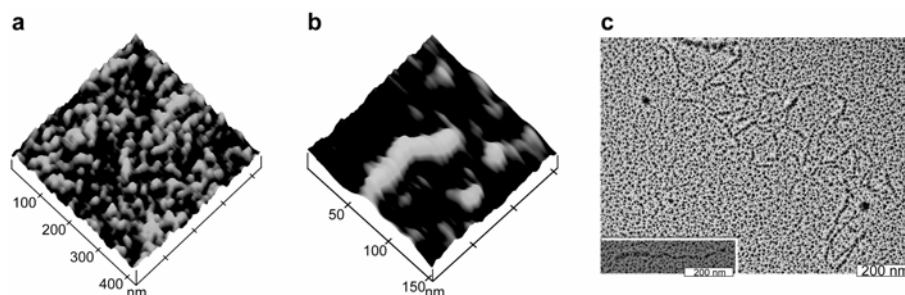


Fig. 3. (a,b) AFM and (c) rotary-shadowed TEM images of $(1)_n$.

Acknowledgments

This work was supported by grant AR44276 (NIH). F.W.K was supported by postdoctoral fellowship AR50881 (NIH).

References

1. Lee, C. H., *et al.* *Int. J. Pharm.* **221**, 1–22 (2001).
2. Ramshaw, J. A. M., *et al.* *Biotechnol. Genet. Eng. Rev.* **13**, 335–382 (1996).
3. Johnson, G., *et al.* *J. Biomed. Mater. Res.* **51**, 612–624 (2000).
4. Fields, G. B., *et al.* *Biopolymers* **47**, 143–151 (1998).
5. MacPhee, C. E. and Woolfson, D. N. *Curr. Opin. Solid State Mater. Sci.* **8**, 141–149 (2004).
6. Jenkins, C. L. and Raines, R. T. *Nat. Prod. Rep.* **19**, 49–59 (2002).
7. Ottl, J. and Moroder, L. *J. Am. Chem. Soc.* **121**, 653–661 (1999).
8. Claire, K. and Pecora, R. *J. Phys. Chem. B* **101**, 746–753 (1997).

Engineered Synthetic Peptide Epitopes from the Extracellular Domain of HER-2/neu are Recognized by Trastuzumab

Joan T. Steele¹, Stephanie D. Allen², Sharad Rawale³ and Pravin T. P. Kaumaya^{1,2,3,4}

¹Chemistry-Biology Interface Program, ²The Ohio State Biochemistry Program, ³Department of Obstetrics and Gynecology, ⁴Arthur G. James Comprehensive Cancer Center, The Ohio State University, Columbus, OH 43210, USA

Introduction

The tumor antigen HER-2/neu is overexpressed in 20-30% of primary breast and prostate cancer and has been linked with a poor prognosis and a high risk of cancer relapse. Trastuzumab (Herceptin®; Genentech, Inc.) a monoclonal antibody to HER-2, has been used successfully to treat cancer patients. Although passive therapy with Trastuzumab has been used successfully, active specific immunotherapy presents the benefit of generating a polyclonal long lasting antitumor immune response. Based on the crystal structure of human HER-2 in complex with the Trastuzumab antigen-binding fragment (Fab) [1] we have designed several synthetic peptides in an attempt to mimic the structure of the extracellular domain (ECD) of HER-2 that makes contact with Trastuzumab. Trastuzumab binds to subdomain IV of HER-2, a disulfide-bond rich region; contact between Trastuzumab and HER-2 occurs through three loops on HER-2 that are formed by disulfide bonds. We have previously shown the utility of incorporating disulfide bonds in synthetic peptide vaccines [2]. Thus we have designed synthetic peptides that incorporate the native disulfide bonds of HER-2 using differentially protected cysteines residues (Fig. 1, disulfide bonds not shown). Conformational peptides with disulfide bonds can elicit antibodies with increased cross-reactivity and antitumor activity.

563-598 NH₂-CHPECQPQNGSVTCFG**PEADQ**CVACA**HYKDPP**FCVA
597-626 NH₂-VARCPSGVKPDLSYMP**IKFPDEEG**ACQPL

Fig. 1. Sequences of peptides derived from the trastuzumab binding region of HER-2. Residues in bold are part of loops that make contact with trastuzumab; residues in italics are a possible N-linked glycosylation site.

Results and Discussion

To examine the ability of Trastuzumab to bind synthetic peptides, a Trastuzumab specificity ELISA was performed. Peptides derived from the Trastuzumab-binding site recognize Trastuzumab whereas an irrelevant peptide (MVF316-339) is not recognized by Trastuzumab (Fig. 2A). Trastuzumab can also bind the synthetic peptide 563-598 that incorporates the natural disulfide pairings of HER-2 and to a lesser extent the linear non-cyclized peptide (Fig. 2B). The 563-598 peptide was also able to block the function of Trastuzumab inhibiting tumor cell proliferation as measured by an MTT assay.

We next examined the immunogenicity of these peptides in FVB/n mice. The 563-598 and 597-626 epitopes proved to be highly immunogenic, generating antibody titers greater than 250,000 three weeks after the third immunization. Flow cytometric analysis was utilized to examine the ability of peptide antibodies to cross-

react with native protein. Antibodies raised against peptide 563-598 do not recognize HER-2, whereas antibodies to 597-626 recognize HER-2 (Fig. 3). The lack of recognition of antibodies raised against 563-598 could be due to the putative N-linked glycosylation site found at amino acid 571 (see Fig. 1). Antibodies to the synthetic peptides may not recognize HER-2 because the presence of a large oligosaccharide in the native protein that could alter the structure of this region. The crystal structure of the HER-2/Trastuzumab complex had been enzymatically deglycosylated, thus no sugar moiety was present. The presence of an oligosaccharide moiety at position 571 could explain the lack of recognition by antibodies elicited to the 563-598 peptide. We are currently examining the potential importance of glycosylation in this region by addition of an N-acetylglucosamine sugar moiety to the peptide.

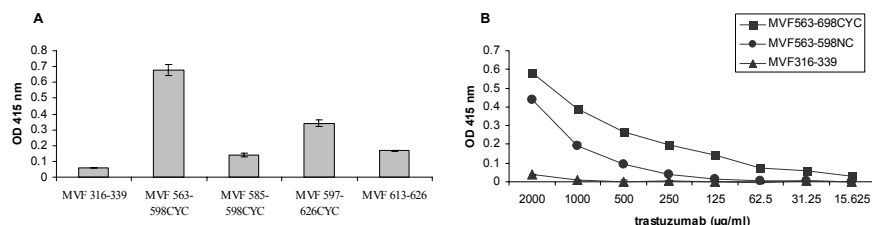


Fig. 2. Binding of trastuzumab to peptides as measured by ELISA. (A) The OD_{415 nm} value for peptides (B) Titration of trastuzumab with the disulfide-bound (CYC) and linear (NC) forms of MVF563-598.

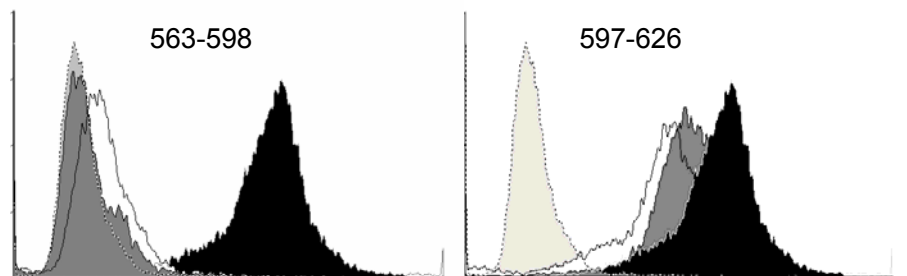


Fig. 3. Flow cytometric analysis of peptide antibodies raised in mice to breast cancer cell line BT474 that overexpresses HER-2. Histograms indicate linear peptide Abs (white shading), cyclized peptide antibodies (dark gray shading), normal mouse Ig (negative control, light gray shading, dashed line), and AB2 (positive control, black shading).

Acknowledgments

The work was supported by a grant from National Cancer Institute (# CA 84356) to P.T.P.K.

References

- 1.Cho, H. S., Mason, K., Ramyar, K. X., Stanley, A. M., Gabelli, S. B., Denney, D. W., Jr. and Leahy, D. J. *Nature* **421**, 756-60 (2003).
- 2.Dakappagari, N. K., Lute, K. D., Rawale, S., Steele, J. T., Allen, S. D., Phillips, G., Reilly, R. T. and Kaumaya, P. T. *J. Biol. Chem.* **280**, 54-63 (2005).

Mapping Protective Epitopes for Anthrax and Plague Vaccine Antigens by LC-MS/MS

Bradford S. Powell¹, Jeffrey T. Enama¹, Stephen F. Little¹, Sylvia Trevino¹ and Tran C. Chanh²

¹Bacteriology Division and ²Headquarters, U.S. Army Medical Research Institute of Infectious Diseases, Fort Detrick, Frederick, Maryland, USA

Introduction

Anthrax and plague, caused by *Bacillus anthracis* and *Yersinia pestis*, are two highly infectious and lethal bacterial diseases that have greatly impacted human history. Effective new medical protections against these diseases are sought for national defense, homeland security, and world wide public health. The present US-licensed vaccine for anthrax contains precipitated formaldehyde-treated bacterial culture supernatant and was engineered four decades ago. Although effective, it has experienced numerous difficulties during the past decade of increased use. New investigational products based on a defined antigen [1] and intended to replace the current vaccine are in clinical testing. Similarly, candidate vaccines against plague are under development [2] because the former US-licensed plague vaccine was ineffective and is no longer manufactured. The active pharmaceutical ingredients for each of these new subunit vaccines are whole-protein antigens [1,2], discovered and vetted over several years time using well-established and conventional research methods. Finished products suitable for human use are anticipated only after several more years of development and testing, as is normal for product development lifetimes. However, recent events underscore the need for improved technologies to detect, treat, and prevent new biological threats that may combine multiple agents or could harbor engineered properties. Therefore, it is important that novel medical countermeasures are discovered and enter development soon for future deployment. Peptide methodologies are being applied as part of a larger effort toward this objective.

We have developed an immunoaffinity LC-MS/MS method to better define the binding sites on protective antigen (PA) from *B. anthracis* and virulence antigen (V) from *Y. pestis* by antibodies previously shown to be protective in animal models against anthrax intoxication and pneumonic plague. Iterative optimization of methods for sample preparation, data collection and results analysis, plus access to protective antigens for two different disease systems and their neutralizing monospecific antibodies were important in developing a reproducible method. Our findings further define the protective elements of these antigens, and indicate that this method is generally applicable for characterizing epitopes of antibody:antigen complexes.

Results and Discussion

Typically, one peptide ion persisted through successive elution washes from each immobilized antibody, establishing these as high-affinity peptides. Concurrence between replicate experiments performed in the absence or presence of BSA as non-specific competitor indicated the antibody:antigen interaction as the source of the observed high affinity and specificity. Some peptides retained specificity and high-affinity binding even on pre-digestion before binding antibody, as was observed for anti-V mAbs 10-1 and 84-1. With one exception, each of the highest-affinity

peptides (primary) mapped onto the amino acid sequences of the cognate protein antigen within a larger region previously shown as important for immunogenicity [3-5]. Together, these results established the antibody:antigen interaction as the source of the observed data. Primary and secondary high affinity peptides were projected onto three-dimensional atomic structures of cognate proteins to model their special relationships, as is shown in Figure 1 for five anti-V mAbs. Since these epitopes derive from antibodies that are known to protect against lethal challenge in animals by antibody transfer experiments, these findings better define structures associated with the induction of protective immunity. This approach may later serve as the foundation for creating peptide and peptide-mimetic targets for the next generation of vaccines, therapeutics, and diagnostics to help protect against anthrax and plague.

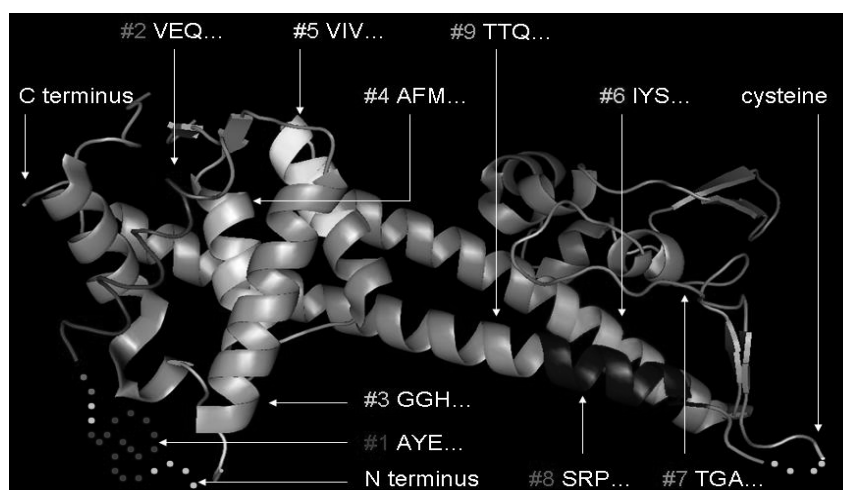


Fig. 1. Projection of 8 tight-binding peptides onto the atomic structure of the V antigen of *Y. pestis*. Peptide # 1 (AYEQNPQHFIEDLEK) showed highest affinity for mAb 84-1 and 10-1, whether digested before or after binding antibody, and in the presence or absence of competitor protein. This region is undefined in the crystal structure.

Acknowledgments

Opinions, interpretations, conclusions, and recommendations are those of the author and are not necessarily endorsed by the U.S. Army. The research described herein was sponsored in part by the Medical Biological Defense Research Program, U.S. Army Medical Research and Materiel Command, Contract DAM17-98-D-0029, Projects 02-4-CC-010 and 02-4-AA-004 to B. Powell.

References

1. Farchaus, J. W., *et al.* *Appl. Environ. Microbiol.* **64**, 982-991 (1998).
2. Powell, B. S., *et al.* *Biotechnol. Prog.* **21**, 1490-1510 (2005).
3. Hill, J., *et al.* *Infect. Immun.* **65**, 4476-4482 (1997).
4. Pullen, J. K., *et al.* *Infect. Immun.* **66**, 521-527 (1998).
5. Little, S. F., *et al.* *Microbiology* **142**, 707-715 (1996).

Co-assembling Peptide based Biomaterials

Sivakumar Ramachandran¹, Yiider Tseng², Peter Flynn³ and
Yihua B. Yu^{1,4}

¹Department of Pharmaceutics & Pharmaceutical Chemistry; ³Department of Chemistry;

⁴Department of Bioengineering, University of Utah, Salt Lake City, UT 84112, USA;

²Department of Chemical & Biomolecular Engineering, Johns Hopkins University, MD 21218, USA

Introduction

Oligopeptide based biomaterial is gaining interest due to its biodegradability and bioresorbability. Furthermore, they can be synthesized with precise control over chain length, sequence and chirality. Previous design of peptide-based hydrogel was based on the concept of self-complementarity, where complementary charge groups were present on the same peptide sequence [1]. To achieve better control over initiation of gelation, a pair of charge complementary but self-repulsive oligopeptide modules with alternating charge and neutral amino acids was designed. This enabled the assembly of peptides only in response to specific trigger like mixing (Scheme 1).

Positively charged peptide module
Acetyl-WK(XK)4-amide
KXW10

Negatively charged peptide module
Acetyl-EW(EX)4-amide
EXW10

Scheme 1. X represents neutral amino acids like valine, alanine and serine. The number represents the chain length of the peptide.

Each sequence had a tryptophan as a spectroscopic probe to monitor gelation. These peptides were synthesized using standard Fmoc-based solid phase peptide synthesis. Each peptide module was purified using reversed-phase HPLC and authenticity verified using mass spectrometry.

Results and Discussion

Each peptide module remained in solution after dialysis in 50mM phosphate buffer (neutral pH). Circular dichroism spectra of peptide solutions revealed their random coil conformation. Upon mixing, charge-complementary peptide pair co-assembled to a viscoelastic hydrogel at a very low total peptide concentration of 0.25wt%. Transmission electron microscopic image showed the presence of nano-fibrillar morphology similar to amyloid fibrils (Fig. 1). In addition, fibrils also bound to congo-red dye, another characteristic of amyloids [2].

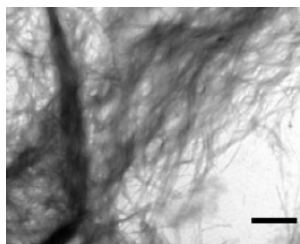


Fig. 1. Transmission Electron Microscopic image of 0.25wt% KVW10:EVW10 hydrogel. The scale bar represents 1μm.

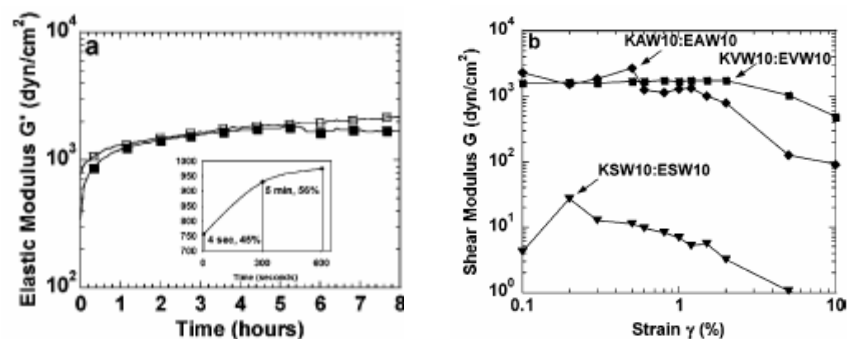


Fig. 2. (a) Time sweep measurement of gelation after mixing (■) & recovery after 100% shear induced breakdown (□) of 0.25wt% KVW10:EVW10 hydrogel. The inset shows the initial burst phase (b) Strain sweep measurement of various decapeptide pairs. Arrows indicate the yield value.

Phase angle in dynamic rheological measurement characterizes the relative viscous and elastic component of the hydrogel. Hydrogels formed were highly elastic or solid like. Increasing the hydrophobicity of the neutral amino acid increased the elastic modulus and the yield value of the hydrogel (Fig. 2b), providing a handle to tune material property. On the other hand, substitution with proline hindered the formation of hydrogel, emphasizing the fact that β -sheet propensity more than hydrophobicity of the neutral amino acid is essential for the co-assembly of this class of novel biomaterials. KVW10:EVW10 hydrogel was capable of recovery from repeated shear induced breakdowns, a property useful in designing injectable biomaterials [2].

Tryptophan, as a spectroscopic probe, was used to monitor the gelation. ^1H resonance of tryptophan's indole-imide, which disappeared as the gelation occurred, acted as a unique downfield signal in NMR to study gelation kinetics. Gelation kinetics was proportional to the total number of charges in the co-assembling peptide pair. Small angle X-ray scattering and fluorescence spectroscopy are currently used to further comprehend the co-assembly process.

For *in vivo* applications, hydrogel should possess molecular biocompatibility, i.e., it should be compatible with the entrapped biomolecule. ^{15}N -enriched ubiquitin was entrapped into the hydrogel and its conformation was monitored using ^1H - ^{15}N HSQC spectrum. Co-assembled hydrogel preserved the native conformation of the entrapped protein. This property is particularly essential for biomedical applications like protein delivery and tissue engineering (growth hormones).

Acknowledgments

The work was funded by National Institutes of Health under grant EB004416.

References

1. Zhang, S., Holmes, T., Lockshin, C. and Rich, A. *Proc. Natl. Acad. Sci. USA* **90**, 3334-3338 (1993).
2. Ramachandran, S., Tseng, Y. and Yu, Y. B. *Biomacromolecules* **6**, 1316-1321 (2005).

Three-Dimensional Solution Structure of the PAS1 Domain of Phytochrome A from Rice

Toshimasa Yamazaki¹, Rintaro Suzuki¹, Paul Reay¹, Nobuya Sakai¹,
Etsuko Katoh¹ and Makoto Takano²

¹Biochemistry Department; ²Plant Physiology Department, National Institute of
Agrobiological Sciences, Tsukuba, Ibaraki 305-8602, Japan

Introduction

Light is one of the most important environmental factors affecting growth and survival of plant. Phytochromes, the red and far-red light-sensing photoreceptors that regulate various aspects of plant growth and development, are encoded by a small gene family (phyA-phyE in *Arabidopsis* and phyA-phyC in rice). All phytochromes exist in two photo-interconvertible forms, an inactive Pr form and an active Pfr form, exchangeable from one form into another upon absorption of light. The phytochrome molecule is divided into two major functional domains. The N-terminal domain with a covalently linked linear tetrapyrrole chromophore is sufficient for light absorption and photoreversibility. The C-terminal domain, which is important for regulatory activity of the protein including dimerization, translocation and downstream signaling, contains two PAS domains and one histidine-kinase-like domain (HKLD) with Ser/Thr kinase activity. The N- and C-terminal domains are connected by a proteolytically-sensitive hinge region that contains a phosphorylatable serine in a Pfr preferential manner. Phytochrome dimerization is essential for its full activity. Previous studies using size-exclusion chromatography experiments and λ repressor-based *in vivo* assays suggest that two regions, residues 599-683 in oat phyA corresponding to 601-685 in rice phyA within the hinge-PAS1 region and/or a large portion of HKLD, are capable of mediating dimerization [1,2]. However, the exact dimerization site has not been identified yet. In addition, majority of loss-of-function missense mutations are observed within the hinge-PAS1 segment [3,4]. To gain insight into the role of the hinge-PAS1 segment (S701-H740) in the rice phyA function, we have determined its three-dimensional solution structure by NMR spectroscopy.

Results and Discussion

Recombinant uniformly ¹⁵N- and ¹⁵N/¹³C-labeled hinge-PAS1 fragments of the rice phyA (phyA⁶⁰¹⁻⁷⁴⁰) were expressed in *E. coli* grown in M9 minimum medium. NMR samples contain a protein (25 μ M – 1.6 mM), 150 mM NaCl and 1 mM DTT in 20 mM Tris-HCl buffer (pH 7.2). All NMR experiments were carried out at 25°C on a Bruker DMX750 spectrometer. NMR signal assignments were obtained by a well-established sequence specific assignment strategy using double- and triple-resonance experiments. Three-dimensional structures of the protein were calculated using the hybrid distance geometry-simulated annealing method as contained in X-PLOR 3.1. Analytical ultracentrifugation experiments were carried out on a sample containing 75 μ M protein, 150 mM NaCl and 6 mM mercaptoethanol in 20 mM Tris-HCl buffer (pH 7.2) using the sedimentation equilibrium method by a Beckman Coulter Optima XL-I instrument. Molecular weight was calculated with a partial specific volume of 0.73 cm³/g.

The self-association property of the phyA hinge-PAS1 fragment in solution was examined in combination with sedimentation equilibrium and NMR spectroscopy. The molecular weight of this fragment was determined by the sedimentation equilibrium experiment to be 16750 ± 300 , indicating that phyA⁶⁰¹⁻⁷⁴⁰ exists as a monomer at the concentration of 75 μ M. In addition, the ¹H-¹⁵N HSQC spectra obtained in the concentration range from 25 μ M to 1.6 mM displayed no changes in signal positions and spectral widths, leading to the conclusion that phyA⁶⁰¹⁻⁷⁴⁰ is unable to dimerize by itself.

A variety of triple-resonance experiments provided essentially complete ¹H, ¹³C and ¹⁵N NMR signal assignments of the protein, revealing that two sets of signals were observed for three regions of the sequence, L654-V659, E672-Q680 and V695-V711. These observations indicate that phyA⁶⁰¹⁻⁷⁴⁰ assumes two distinct structures in a ratio of 3:2 due to *cis-trans* isomerization of P710 that is well conserved in phytochrome sequences. Strong NOEs between G709 H α and P710 H δ and between G709 H α and P710 H α were observed for the major and minor isomers, respectively. These observations indicate that P710 assumes a *trans* configuration in the major isomer and a *cis* configuration in the minor isomer. The structure determination of phyA⁶⁰¹⁻⁷⁴⁰ revealed that the region from V632 to M737 adopts a canonical PAS domain fold comprising a five-stranded antiparallel β -sheet (strand A β , residues 632-639; B β , 642-648; F β , 691-701; G β , 710-721; H β , 729-737) and three α -helices (C α , residues 649-654; D α , 659-662; E α , 676-688). The region from S622 to E629 within the hinge assumes a slightly mobile α -helix while the N-terminal 20 residues are highly flexible.

It has been reported that mutations of R626 with Cys, V633 with Met, P634 with Ser, G709 with Asp, Cys718 with Tyr, and G729 with Glu result in loss of the phytochrome function [3,4]. These residues are located on the solvent exposed surface of the β -sheet, suggesting that this surface is important in regulating the function through protein-protein interactions between subunits of phyA or binding to downstream signaling components.

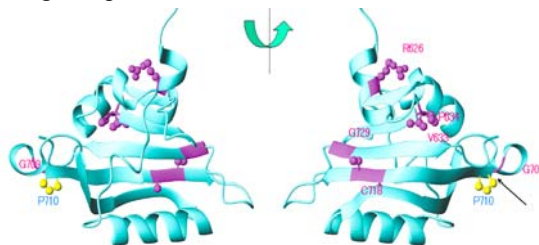


Fig. 1. Ribbon representation of NMR solution structure of the rice phyA⁶⁰¹⁻⁷⁴⁰. P710 and residues whose replacements lead to loss of function are highlighted.

Acknowledgments

The work was funded by a grant for the Rice Genome Project (PR4101) from the Ministry of Agriculture, Forestry, and Fisheries of Japan.

References

1. Cherry, J. R., *et al.* *Plant Cell* **5**, 565-575 (1993).
2. Edgerton, M. D. and Jones, A. M. *Biochemistry* **32**, 8239-8245 (1993).
3. Xu, Y., Parks, B. M., Short, T. W. and Quail, P. H. *Plant Cell* **7**, 1433-1443 (1995).
4. Fry, R. C., Habashi, J., Okamoto, H. and Deng, X. W. *Plant Physiol.* **130**, 457-465 (2002).

Membrane Initiated Gelsolin Amyloid Formation

Inta Liepina¹, Paul A. Janmey², Cezary Czaplewski³ and Adam Liwo³

¹Latvian Institute of Organic Synthesis, Aizkraukles str. 21, Riga, LV1006, Latvia; ²Institute of Medicine and Engineering, University of Pennsylvania, Philadelphia, PA 19104, USA;

³Faculty of Chemistry, University of Gdansk, 80-952 Gdansk, Poland

Introduction

Gelsolin is a six-domain dynamic actin-filament binding, severing and capping protein capable of severing and nucleating of the actin cytoskeleton. Human gelsolin is expressed as a 81 kDa protein in the cytoplasm and a 84 kDa protein in the plasma. Plasma gelsolin is implicated in the familial amyloidosis-Finnish type (FAF) inherited disease. A point mutation in the S2 gelsolin domain causes an amyloidosis with neurological, ophthalmological and dermatological symptoms. Thus, in addition to its role of actin binding, gelsolin domain S2 is involved in the pathogenesis of FAF caused by inherited mutations D187N and D187Y in domain S2 of gelsolin. This makes gelsolin susceptible to aberrant trypsin-like protease cleavage site between residues Arg¹⁷² – Ala¹⁷³ and further cleavage at the Met²⁴³ residue, forming an amyloidogenic 8.1 kDa peptide containing residues 173-243 (G173-243) of gelsolin domain S2. The peptides G173-243 or its sequent cleavage fragment Ala¹⁷³-Gly²⁰², spontaneously associate into amyloid fibrils.

The mechanism of amyloidogenesis is not clear. In our previous work [1] we started to investigate the mechanism of amyloid formation. In this work, using molecular dynamics (MD), we investigated interactions of gelsolin amyloidogenic fragments G173-202 [cleaved from the x-ray structure of gelsolin (1DON)] with dimyristoyl-phosphatidylcholine (DMPC) membrane bilayers.

Results and Discussion

DMPC lipid bilayer containing 6 x 6 arrays of DMPC molecules was taken from a

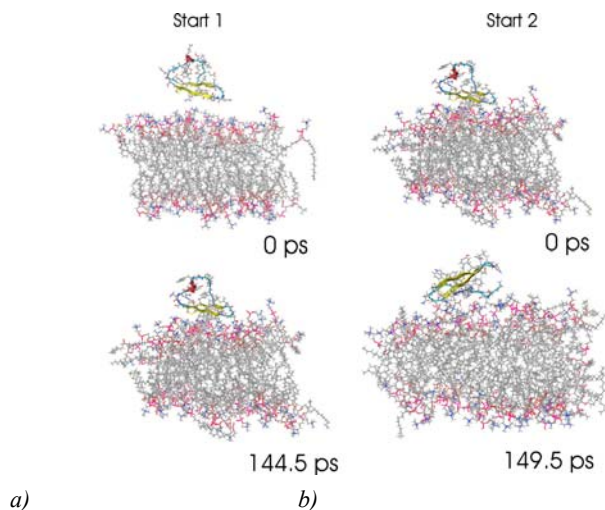


Fig. 1. Molecular dynamics of the DMPC lipid with G173-202, a) start 1 at 0 ps, and 144.5 ps, b) start 2, at 0 ps, and 149.5 ps.

previous study [2]. Mutated gelsolin amyloidogenic fragment 173-202 (G173-202) was cleaved from horse gelsolin crystal structure 1DON. Calculations were carried out with program MOE, AMBER94 force field. The G173-202 fragment was placed 9 Å away from a DMPC bilayer at two different starting orientations (Fig.1 – start 1, start2) and subjected to NTP MD simulations at elevated body temperature $T=312$ K for 150 ps. After 100 ps of MD, the G173-202 fragment at either initial orientation adhered to the DMPC membrane retaining β -sheet structure, suggesting that a lipid membrane could bind G173-202 fragments and serve as a germ for amyloidogenesis (Fig.1).

Afterwards one more amyloidogenic fragment G173-202 was placed in the vicinity of the G173-202 fragment adhered to the DMPC membrane of the previous system “start-2” (Fig. 2), and the new system was subjected to NTP MD simulations at $T=312$ K for 3744 ps. After 700 ps of MD, the newly added amyloidogenic fragment G173-202 was interacting with the membrane attached fragment G173-202 and after 1465 ps they were bound with hydrogen bonds, indicating the possible mechanism of membrane initiated amyloidosis (Fig. 2).

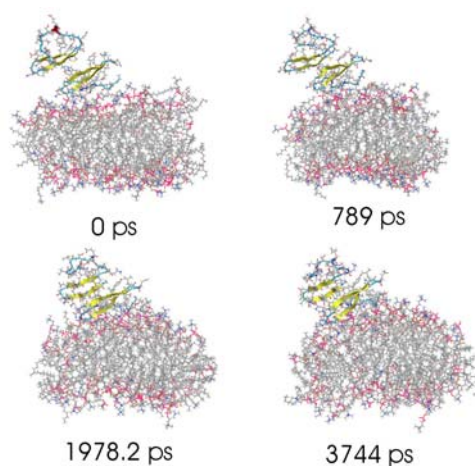


Fig. 2. MD of DMPC lipid with two fragments of G173-202, at the start= 0 ps, 789 ps, 1978 ps, 3744 ps.

In conclusion, the lipid membrane could bind G173-202 fragments and serve as a germ for amyloidogenesis. Gelsolin fragments G173-202 could stick together forming β -structure. The results show that such approach of MD is reasonable to model the mechanism of amyloid formations.

Acknowledgments

This work is supported by NATO Collaborative Linkage Grant LST.CLG.976647, by Fogarty Foundation grant TW006954, by Latvian Science Council Grant 05.1768, by Gdansk Academic Computer Center TASK and by Warsaw ICM Computer Center.

References

1. Liepina, I., Czaplowski, C., Janmey, P. and Liwo, A. *Biopolymers* **76**, 543-548 (2004).
2. Czaplowski, C., Pasenkiewicz-Gierula, M. and Ciarkowski, J. *J. Receptor Signal Transduct. Res.* **19**, 355-367 (1999).

Cooperative Formation, Transformation, and Collapse of Hydrogen-Bonds in Polypeptides

Akihiro Abe¹, Yosuke Imada¹, Toshihiro Hiejima¹ and Hidemine Furuya²

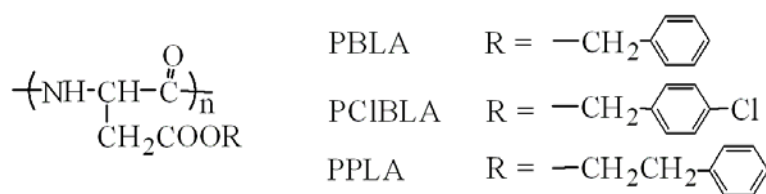
¹Nano-Science Research Center, Tokyo Polytechnic University, 1583 Iiyama, Atsugi 243-0297, Japan; ²Department of Organic and Polymeric Materials, Tokyo Institute of Technology, 2-12-1-H-128 Ookayama, Meguro, Tokyo 152-8552, Japan

Introduction

This is one of a series of studies on the reversal of the helix sense of polyaspartates originated from the pioneering work of Goodman and his associates in 1960's [1,2]. After extensive studies on poly(aspartic acid ester)s in various organic solvents, it has been concluded that these polymers may be in either the right- or left-handed helical form with suitable condition of solvent and temperature [3]. Reversal of the helix sense in binary copolymers including two different characters were found to follow a S-shape curve [1,2]. Around the mid point of the transition, the magnitude of the optical rotation as well as the Moffitt-Yang b_0 changes somewhat steeply. The stereochemical structure of copolymers in this region has been investigated in relation to the mechanism of the helix-sense inversion of polyaspartates.

Effect of the side-chain structure on the α -helical screw sense

Poly(β -p-chlorobenzyl L-aspartate) (PCIBLA) is one of the well-studied polyaspartate derivatives in both solution and the solid state. The chemical structure of PCIBLA differs from those of poly(β -benzyl L-aspartate) (PBLA) and poly(β -phenethyl L-aspartate) (PPLA) only at the terminal of the relatively long side chain (Scheme 1). PBLA takes a left-handed form (L) in conventional helicoidal solvents and does not exhibit any screw-sense inversion. In contrast to PBLA, both PCIBLA and PPLA form a right-handed helix (R) in chlorinated alkane solvents and exhibit a reversal of α -helix sense at higher temperatures [4]. Yet the transition behaviors in the presence of denaturant acid are quite different between these two polymers. While PPLA exhibits transitions such as $R \rightarrow L \rightarrow \text{Coil}$ by lowering temperature, PCIBLA directly goes into the coil state without showing the reentrant L form [5]. The cause of such disparity arising from the difference in the side-chain structure at the terminal has been investigated by constructing the phase diagram. A simplified illustration of the diagram is shown in Figure 1. The examination of the diagrams let us to conclude that the effect of the denaturant acid on the internal bond rotation is subtly controlled by the chemical nature of the side-chain terminals.



Scheme 1

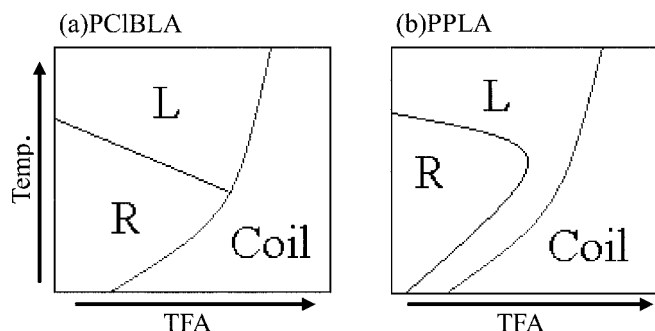


Fig. 1. Schematic illustration of the phase diagrams of PCIBLA and PPLA in mixed solvents, tetrachloroethane- d_2 (TCE) /trifluoroacetic acid (TFA), polymer concentration being kept at 1wt%.^{4,5} Studied by ^1H NMR at room temperature.

Screw-sense reversals observed in copolymers comprising residues of the opposite helical preference

A series of (random) copolymers (PBPLA) consisting of BLA and PLA have been prepared by the NCA method and studied mostly in chlorinated alkane solvents such as chloroform and TCE. The S-shape trend of the b_0 vs. composition curve was confirmed at room temperature [1,2]. The helix content of either the right- or left-handed form can be estimated by following the variation of the ^1H NMR chemical shifts of the amide group. The helix content varies as a function of temperature. The mid-points of the transition curves were plotted against the composition. The extrapolation of the plot suggests that the helix-sense inversion of the PBLA homopolymer would take place at around -40°C , below which the polymer may exist in the right-handed form. This explains the reason why PBLA exists only in the left-handed form at ordinary temperatures.

In the higher concentration range, the solution tends to exhibit cholesteric liquid crystalline texture, suggesting that the backbone of the copolymer maintains the rigid rod-like character even when the polymer contains an equal amount of co-monomer residues having the opposite α -helical screw sense.

Concluding Remarks

In our previous studies, we have proposed a mechanism in which the transition between the two opposite helices takes place while the orientational order of the molecular axis is maintained in the nematic environment [4]. The experimental observations for copolymers are not fully compatible with this molecular scheme. Further investigations are in progress in our laboratory.

Acknowledgements

We wish to dedicate this paper to the memory of Professor Murray Goodman.

References

1. Goodman, M., Deber, C. M., Felix, A. M. *J. Am. Chem. Soc.*, **84**, 3773-3774 (1962).
2. Goodman, M., Felix, A. M., Deber, C. M. *Biopolymers* **1**, 371-400 (1963).
3. Bradbury, E. M., Carpenter, B. G., Goldman, H. *Biopolymers* **6**, 837-850 (1968).
4. Abe, A., Furuya, H., Okamoto, S. *Biopolymers (Peptide Sci.)*, **43**, 405-412 (1997).
5. Abe, A., *et al.* *Biopolymers (Peptide Sci.)*, **80**, 249-257 (2005).

Reversible Insulin Self-Assembly under Carbohydrate Control

Thomas Hoeg-Jensen, Svend Havelund and Jan Markussen

Novo Nordisk A/S, Novo Alle 6B2.54, DK-2880 Bagsvaerd, Denmark

Introduction

Peptide and protein drugs are often administered via subcutaneous injections. The *in vivo* half-life of peptide/protein drug is typically dependent on the rate of diffusion of the drug from the subcutaneous injection site to the circulation. The rate of diffusion in turn correlates with the size of the drug (molecular weight) [1,2].

In diabetes, proper dosing and timing of insulin shots can dramatically improve the long-term prognosis of the disorder [3]. However, since diabetes patients often encounter unexpected fluctuations in blood glucose, perfect dosing and timing of insulin shots are very difficult. Improvements could potentially be gained with self-adjusting release systems, for example release of insulin from polymers that swell in a glucose-dependent manner [4]. The use of external polymers raises however problems with biocompatibility and increase in drug volume. We present here a polymer-free system for carbohydrate-controlled insulin release.

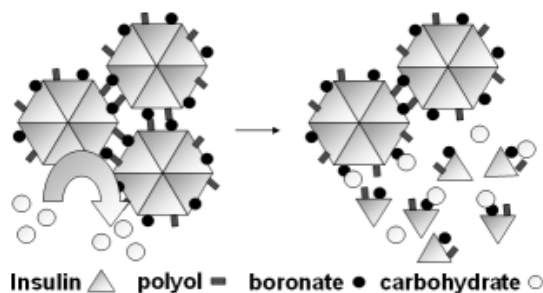
Results and Discussion

Soluble carbohydrate-sensitive insulin self-assemblies have been obtained by equipping insulin with built-in pairs of polyols and boronates [5], the latter acting as carbohydrate sensors. The size of the Zn(II) insulin hexamer self-assemblies were evaluated by use of size-exclusion chromatography (SEC, Fig. 1, left) and dynamic light scattering (DLS, Fig. 1, right), showing assemblies > 1 MDa.

Encouragingly, the size of the insulin self-assemblies could be controlled by addition of carbohydrates, e.g. sorbitol, which eroded the complex with EC₅₀ of 50 mM. Glucose was less effective in the given system.

Interestingly, the self-assemblies were observed only in the presence of phenol (pH buffered at 7.4). The N-terminal of the B-chain of insulin is known to adopt either of two types of folding: Coiled or helical (T or R-fold); R-fold is induced by the presence of phenol (>mM). Accordingly, R-fold seems required for the given insulin to pack into high molecular weight self-assemblies.

In conclusion, soluble carbohydrate-sensitive insulin self-assemblies can be formed from insulins with built-in pairs of polyols and boronates. The system potentially enables autonomous carbohydrate dependent insulin delivery from subcutaneous depots, without employment of external polymers. The illustrated principle is potentially applicable to other peptide and protein drugs.



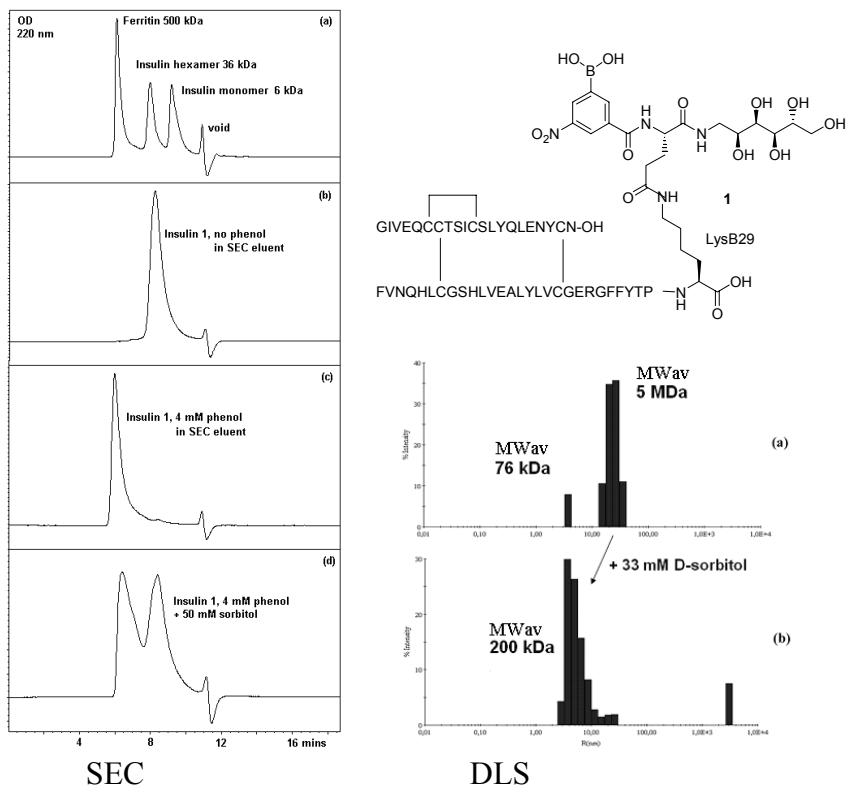


Fig. 1. Insulin 1 with SEC and DLS data from Zn(II) formulations +/- phenol and sorbitol, 100 mM NaCl, 20 mM KCl, 7 mM phosphate, pH 7.4.

Acknowledgments

We thank C. Rischel for instructions on DSL equipment and R. Dyrnesli for expert technical assistance.

References

1. Brange, J., Ribel, U., Hansen, J. F. Dodson, Hansen, M. T., *et al.* *Nature* **333**, 679-682 (1988).
2. Whittingham, J. L., Jonassen, I., Havelund, S., *et al.* *Biochemistry* **43**, 5987-5995 (2004).
3. Steffes, M. W., Chavers, B. M., Molitch, M. E., *et al.* *J. Am. Med. Assoc.* **290**, 2159-2167 (2003).
4. Allen, T.M. and Cullis, P.R. *Science* **303**, 1818-1822 (2004).
5. Hoeg-Jensen, T., Havelund, S., Nielsen, P. K. and Markussen, J. *J. Am. Chem. Soc.* **127**, 6158-6159 (2005).

Influence of the Nucleophilic and Electrophilic Properties of Solvents for Peptide Solubilization: CD Monitoring and the Special Effect of the Water Molecule

Luciana Malavolta and Clóvis R. Nakaie

*Departement of Biophysics, Federal University of Sao Paulo Rua 03 de maio, 100 CEP
04044-020, SP, Brazil*

Introduction

The solvation effect of polymeric material attaching or not peptide chains has been the focus of our effort to better understand the solute-solvent interaction process as a whole [1,2]. As a consequence of these studies, the (1:1) combination of the Gutmann's electrophilic (AN) and nucleophilic (DN) parameters [3] was proposed in order to build an alternative solvent polarity scale (amphoteric constant) [4]. The search for rules which might govern dissociation process of peptides not only bound to a resin but also free in solution was recently initiated [5]. In this context the present report follows with this approach by examining two model aggregated sequences mainly in the light of the acidic or basic character of the solvent system, including water. The strongly aggregated VVLGAAIV peptide, which corresponds to the 291-298 sequence of the murine H-2K protein [6], and the (1-42) β -amyloid segment (DAEFRHDSGYEVHHQKLVFFAEDVGSNKGAIIGLMVGGVVIA) involved in the Alzheimer disease [7] were examined towards the solubility behavior in association with CD investigation.

Results and Discussion

Table 1 shows the results of solubility studies of these two peptides in 15 solvent systems. In general, only solvents involving the strong electron donor DMSO (DN of 29.8) or the strong electron acceptor HFIP (AN of 88.0) and TFE (AN of 53.5) seemed to be able to dissolve partially aggregated sequences such as these peptides. When water, a strong electrophilic solvent (AN = 54.8), was added to other strong polar organic solvents such as DMSO or HFIP and TFE, its solubilization strength is highly dependent upon the type and amount of organic solvent to be cosolvated (electron acceptor or electron donor) and also on the particular characteristic of the peptide sequence (degree of aggregation). For instance, it can be observed in Table 1 that its addition induces significant decrease in the solubilization of peptides when mixed with DMSO and in lesser extent, with HFIP. In contrast, when the cosolvent is TFE, an enhancement of the solubilization of peptides is observed. These findings indicate that there is a neutralization effect between the acidic water molecule and the basic DMSO but this effect does not occur with the acidic TFE which forms a homogeneous solution with water.

On the other hand, due to the similarity between the AN and DN values of some solvents such as MeCN, acetone and iPrOH, a self-neutralizing effect by the solvent molecules has been proposed that reduces their peptide solvation capability [5]. This premise agrees with the data displayed in Table 1 where a complete lack of peptide solubilization was observed with MeCN and acetone. However when water was added, an increase in their solubilization degree occurs, depending on the inter-chain association strength of each peptide sequence. Thus, in contrast to β -amyloid peptide, the solubilization yield of the well known aggregating VVLGAAIV

Table 1: Solvent parameters and solubility of individual peptides

Solvent	Parameter				Solubility of Peptide (%)	
	AN	DN	(AN+DN)	(AN-DN)	A	B
H ₂ O pH 7.4	54.8	18.0	72.8	36.8	0	6
MeCN	18.9	14.1	33.0	4.8	0	0
50% MeCN/H ₂ O	36.9	16.1	53.0	20.8	0	88
Acetone	12.5	17.0	29.5	-4.5	0	0
50% Acetone/H ₂ O	33.7	17.5	51.2	16.2	11	94
iPrOH	33.5	36.0	69.5	-2.5	10	nd
50% iPrOH/H ₂ O	44.2	27.0	71.2	17.2	25	nd
TFE	53.5	0.0	53.5	53.5	20	20
50% TFE/H ₂ O	54.2	9.0	63.2	45.2	60	88
HFIP	88.0	0.0	88.0	88.0	80	95
50% HFIP/H ₂ O	71.4	9.0	80.4	62.4	70	88
DMSO	19.3	29.8	49.1	-10.5	84	83
50% DMSO/H ₂ O	37.1	23.9	60.9	13.2	32	39

Peptide A: VVLGAAIV; Peptide B: β -amyloid; nd = not determined.

sequence does not increase as the water was added to organic solvents. In conclusion, the results depicts that, the greater the difference between electrophilicity and nucleophilicity values of solvent, the higher its solubilization power.

In complement, CD investigation of both peptides in TFE indicated that typical conformational transitions are detected as the amount of this solvent increases, leading to a more α -helix-type structure, mainly in the β -amyloid peptide. Nevertheless this structural change seems to be in close accordance with the solubilization improvement of peptides in this polyfluorinated alcohol. Other model peptides are currently been evaluated in order to better understand the complex physico-chemical factors which might be involved in large amount of solvent-solute interactions.

Acknowledgments

Grants from the Brazilian FAPESP and CNPq agencies are gratefully acknowledged.

References

1. Cilli, E. M., Oliveira, E., Marchetto, R. and Nakaie, C. R. *J. Org. Chem.* **61**, 8992-9000 (1996).
2. Marchetto, R., Cilli, E. M., Jubilut, G. N., Schreier, S. and Nakaie, C. R. *J. Org. Chem.* **70**, 4561-4568 (2005).
3. Gutmann, V. *The Donor-Acceptor Approach to Molecular Interactions*; Plenum: New York, 1978.
4. Malavolta, L., Oliveira, E., Cilli, E. M. and Nakaie, C. R. *Tetrahedron* **58**, 4383-4394 (2002).
5. Malavolta, L. and Nakaie, C. R. *Tetrahedron* **60**, 9417-9424 (2004).
6. Lansbury, Jr. P. T. *Biochemistry* **31**, 6865-6870 (1992).
7. Narita, M., Chen, J. Y., Sato, H. and Kim, Y. *Bull. Chem. Soc. Jpn* **58**, 2494-2501 (1985).

VCD Spectroscopic Analysis of the Exendin-4 Truncated Analog TC5b

Jeffrey Copps, Richard F. Murphy and Sándor Lovas

Department of Biomedical Science, School of Medicine, Creighton University, Omaha, NE 68178, USA

Introduction

Truncation and residue replacements of the peptide exendin-4 with the goal of creating the smallest self-folding protein yielded the 20-residue "miniprotein" TC5b (Asn-Leu-Tyr-Ile-Gln-Trp-Leu-Lys-Asp-Gly-Gly-Pro-Ser-Ser-Gly-Arg-Pro-Pro-Ser) [1]. The folding and resulting tertiary structure of TC5b, unique for a sequence of its length, is a product of its 'Trp-cage' motif [3], which is formed through CH- π interactions between Trp6 and Pro12, 18, and 19, as well as some crucial hydrogen bonds. TC5b has been the subject of much computational analysis and some spectroscopic analysis. Electronic circular dichroism spectroscopy (ECD) has shown that this peptide appears to be primarily α -helical in 30% TFE, as well as in aqueous and phosphate buffer [1]. However, NMR has also shown the existence of a poly-Pro II helix associated with the C-terminal region. The poly-Pro II helix is not apparent in the ECD spectrum [1], but it may be possible to resolve it using vibrational circular dichroism spectroscopy (VCD) [2]. In the present study, VCD spectroscopy was used to examine the conformation of TC5b in a variety of deuterated aqueous and organic solvents. The observed spectra were compared to VCD spectra of poly-L-Pro (av. MW: 8900 Da) in deuterated aqueous and organic solvents.

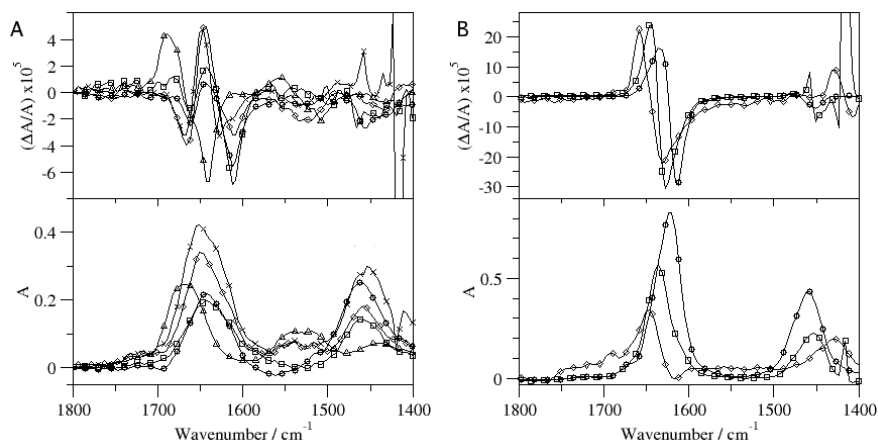


Fig. 1. Normalized VCD and IR spectra of (A) TC5b in (○) D_2O , (□)15 mM Na_2HPO_4 in D_2O , (◇)30% TFE- d_1 /70% 15mM Na_2HPO_4 in D_2O (v/v), (×)5% DMSO- d_6 /95% TFE- d_1 (v/v), (Δ)DMSO- d_6 , and (B) poly-L-Pro (DMSO VCD/4, IR*16) in (○) D_2O , (□)5% DMSO- d_6 /95% TFE- d_1 (v/v), (◇)DMSO- d_6 .

Results and Discussion

VCD spectra for TC5b (Fig. 1A) in the amide I' region ($1600\text{--}1700\text{ cm}^{-1}$) show a triplet form, which is associated with α -helical structure in deuterated solvents [2]. A large bias on the second troughs indicates varying degrees of H-D exchange on backbone amide groups. This effect is clearly related to predeuteration of samples. The amide II and II' regions at $1500\text{--}1600\text{ cm}^{-1}$ and $1400\text{--}1500\text{ cm}^{-1}$, respectively, also show the effect of backbone amide exchange, with the amide II trough growing smaller and the amide II' trough larger with strong exchange, and *vice versa* in the opposite case. The second trough of the amide I' region in the spectra of D_2O and 15 mM Na_2HPO_4 in D_2O are smooth and peak at 1612 cm^{-1} , while the spectra in 30% TFE- d_1 / 70% 15 mM Na_2HPO_4 in D_2O (v/v) and 5% DMSO- d_6 in TFE- d_1 (v/v), respectively, contain a shoulder at 1628 cm^{-1} and a minima at 1612 cm^{-1} and *vice versa*, respectively. Normalized VCD spectra of poly-L-Pro (Fig. 1B) show a shift in the position of its characteristic couplet in the amide I region in all solvents tested. This couplet shift corresponds to the position of the shoulders on the second troughs in the TC5b spectra, indicating that poly-Pro II helical structure is present. The VCD spectrum of TC5b in DMSO- d_6 (Fig. 1A) shows a radically different conformation that is not indicative of α -helix or poly-Pro II helix structure. Titration of TC5b in DMSO- d_6 in D_2O reveals that 75% or greater DMSO- d_6 (v/v) results in a loss of helical conformation (Fig. 2).

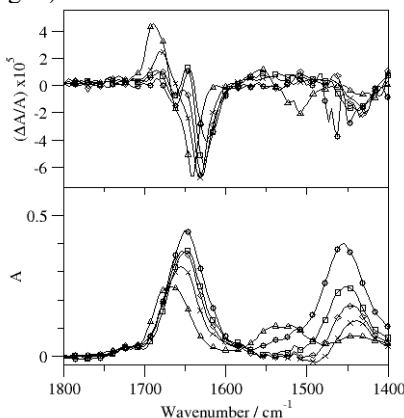


Fig. 2. VCD spectra of TC5b in (○)50% , (□)60% , (◇)70% , (×)75% , (Δ)100% DMSO- d_6 in D_2O (v/v).

Acknowledgments

This work was supported by NIH Grant Number 1 P20 RR16469 from the BRIN program of the National Center of Research Resources and Carpenter Chair in Biochemistry, Creighton University, Omaha, NE.

References

1. Neidigh, J. W., Fesinmeyer, R. M. and Andersen, N. H. *Nature Struct. Biol.* **9**, 425-430 (2002).
2. Polavarapu, P. L. and Zhao, C. *Fresenius J. Anal. Chem.* **366**, 727-734 (2000).
3. Neidigh, J.W., Fesinmeyer, R. M., Prickett, K. S. And Andersen, N. H. *Biochemistry* **40**, 13188-13200 (2001).

Type II β -Turn Formation in Tetrapeptides Evidenced by Vibrational Circular Dichroism Spectroscopy

Attila Borics, Richard F. Murphy and Sándor Lovas

Department of Biomedical Sciences, Creighton University Medical Center, Omaha, NE 68178, USA

Introduction

The vibrational circular dichroism (VCD) features of β -turns were studied previously in cyclic peptides, although a complete set of rules for their characterization has not yet been given [1]. The model peptides (Fig. 1) used in this investigation, Ac-NPGQ-NH₂ [2] and Ac-VPaH-NH₂ [3] were selected on the basis of their high propensity to adopt β -turn structure suggested by previous experimental and theoretical studies [4]. This study is to give more insight to the prototypical VCD spectral properties of turns. In addition, an alternative method, combining theory and experiment, for the conformational analysis of short peptides is proposed.

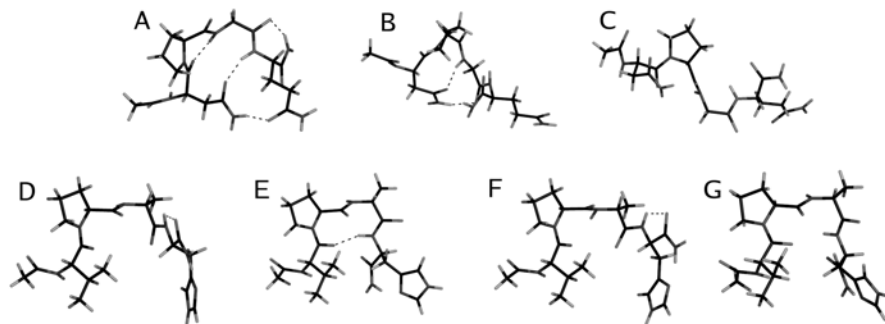


Fig. 1. Representative structures obtained from MD simulations and used for the modelling of IR and VCD spectra of Ac-NPGQ-NH₂ (A, B, C) and Ac-VPaH-NH₂ (D, E, F, G).

Results and Discussion

ECD spectra of Ac-NPGQ-NH₂ and Ac-VPaH-NH₂ in 0-100% TFE in water showed a mixture of type I(III) β -turn and random coil and a mixture of type II β -turn and β -sheet structure, respectively. Excluding the possibility of aggregation at higher concentrations, similar results are expected when peptides are studied using VCD spectroscopy. Figure 2A shows the IR and VCD spectra of model peptides in D₂O, 60%(v/v) TFE in D₂O and DMSO. Both peptides yielded negatively biased negative couplet-type signals in all solvents and the broadness of spectra and occasional shoulders indicate multiple conformations. The high frequency component suggested for β -turns is present in the spectra recorded in DMSO. Previous 25 ns molecular dynamics simulations [4] revealed representative structures (Fig. 1) of which IR and VCD spectra were calculated after geometry optimization at the B3LYP/6-31G(d) level of theory. These calculated spectra multiplied by the following contribution factors: A: 0.730, B: 0.149, C: 0.121 and D: 0.491, E: 0.216, F: 0.161, G: 0.132 were used to construct the model spectra in Figure 2B.

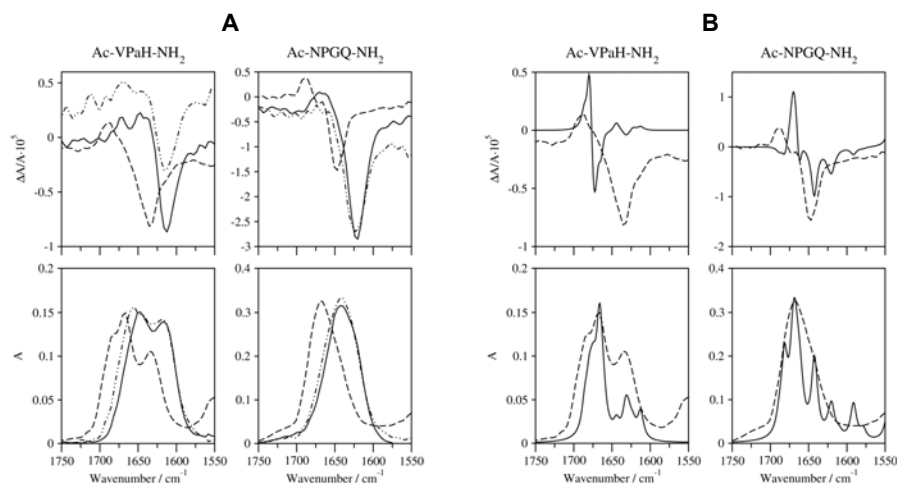


Fig. 2. **A:** IR and VCD spectra of model peptides in D_2O (solid), DMSO (dashed) and 60% TFE in D_2O (dotted-dashed) at 20mM concentration; **B:** Comparison of modelled (solid) and experimental (dashed) IR and VCD spectra of model peptides in the amide I region. Experimental spectra were recorded in DMSO at 20 mM concentration.

Contribution factors representing the population of the dominant structural families in solution were determined by clustering studies. Calculated IR and VCD spectral constructs (Fig. 2B.) are in good agreement with spectra obtained in DMSO. For Ac-VPaH-NH₂ the underestimation of low frequency components in both the IR and VCD spectra suggests that the representative structures obtained from MD simulations are not sufficient to describe the conformational ensemble. The apparent β -character of IR and VCD spectra is possibly due to molecular associations, which take place even at very low concentrations (50 μ M) and are not modeled by MD simulations. Results for Ac-NPGQ-NH₂ indicate that, in DMSO, a significant amount of γ -turn and Asx-turn [5] structure (Fig. 1B) is also present. Creating a direct link between theory and experiment here provides a useful alternative approach to conformational analysis of short flexible peptides. Moreover, this method could help to identify VCD features which are yet unknown.

Acknowledgments

This work was supported by NIH, Grant Number 1 P20 RR16469 from the BRIN program of the National Center of Research Resources and Carpenter Chair in Biochemistry, Creighton University, Omaha, NE.

References

1. Xie, P. and Diem, M. *J. Am. Chem. Soc.* **117**, 429-437 (1995).
2. Carbone, F. R. and Leach, S. J. *Int. J. Peptide Prot. Res.* **26**, 498-508 (1985).
3. Imperiali, B., Fisher, S. L., Moats R. A. and Prins, T. J. *J. Am. Chem. Soc.* **114**, 3182-3188 (1992).
4. Borics, A., Murphy R. F. and Lovas, S. *Biopolymers* **72**, 21-24 (2003).
5. Abbadi, A., Mcharfi, M., Aubry, A., Prémilat, S., Boussard G. and Marraud, M. *J. Am. Chem. Soc.* **113**, 2729-2735 (1991).

The Conformational Preference of C^α-Centered Protein Radicals

Michael Owen, Richard F. Murphy and Sándor Lovas

Department of Biomedical Sciences, Creighton University Medical Center, Omaha, NE
68178, USA

Introduction

C^α protein radicals can have adverse physiological effects. Free-radical damage to proteins and lipids have been implicated in aging [1] and has been shown to initiate β-amyloid(1-42) aggregation. Homolytic bond-dissociation enthalpy for C^α carbons as well as the captodative stability of the resulting C^α radical [2] provide thermodynamic evidence for the stability of the C^α radical structure. Although glycyl radicals have been shown to induce β-sheet formation [3], the full structural implications of C^α radical formation have not been explored.

In this study, the $E = f(\phi, \psi)$ potential energy surface (PES) of *N*-Ac-Gly[•]-NHMe and that of the closed-shell *N*-Ac-Gly-NHMe was calculated using density functional theory. The JAGUAR 5.5[®] software package was used for all calculations. To generate a PES with $0^\circ \leq \phi \leq 360^\circ$ and $0^\circ \leq \psi \leq 360^\circ$, ϕ and ψ angles were independently constrained at 30° intervals and all other variables were fully relaxed. This procedure allows 144 conformers to fit on each PES. Density functional theory, B3LYP/6-31G(d,p), was used to optimize the geometries of *N*-Ac-Gly-NHMe and *N*-Ac-Gly[•]-NHMe and the energy values of these optimizations were plotted on the PES. This procedure allows the effects of C^α radical formation on the secondary structure of an amino acid residue to be determined.

Results and Discussion

The PES of *N*-Ac-Gly-NHMe in the gas phase is predominantly flat, except for a maximum at $\phi = 0^\circ$ and $\psi = 180^\circ$ (Fig. 1A). When $30^\circ < \phi < 120^\circ$, and $150^\circ < \psi < 300^\circ$, the system is in a low energy state as when $90^\circ < \phi < 270^\circ$, $150^\circ < \psi < 210^\circ$, and $270^\circ < \phi < 300^\circ$, $30^\circ < \psi < 180^\circ$.

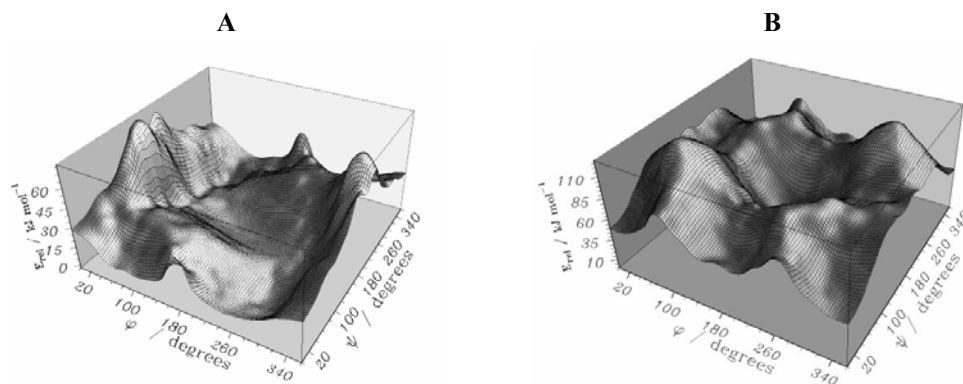


Fig. 1. PES of *N*-Ac-Gly-NHMe (A) and *N*-Ac-Gly[•]-NHMe (B) calculated with B3LYP/6-31G(d,p) in the gas phase.

The three regions are connected and contain low-energy conformers with minima in the γ_D , ϵ_D , β_L , and γ_L conformations. The flat PES in both environments accurately reflects the conformational flexibility of the Gly residue.

In the gas phase, the γ_L and γ_D conformations are stabilized by hydrogen bonds to form a C_7 ring (Fig. 2). Conversely, H-bonds do not stabilize any conformations of closed-shell glycyl model in the aqueous environment.

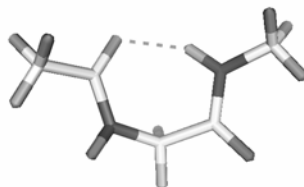


Fig. 2. Chemical structure of *N*-Ac-Gly-NHMe in the γ_D conformation stabilized by H-bond.

N-Ac-Gly \bullet -NHMe lacks the conformational flexibility of the closed-shell model. The PES indicates that the β_L conformation is the global minimum (Fig. 1B). A high-energy barrier of about 80 kJmol⁻¹ extends within an area with a 90° radius from the $\phi = 180^\circ$, $\psi = 180^\circ$ geometry. A $\phi = 180^\circ$, $\psi = 0^\circ$ geometry containing the δ_L , δ_D conformations, and a $\phi = 0^\circ$, $\psi = 0^\circ$ geometry containing the α_D , α_L , γ_D , γ_L conformations are stabilized. By contrast with the flexibility shown in the closed-shell Gly model, the high-energy barriers restrict the Gly \bullet to the β -conformation.

The flat PES of *N*-Ac-Gly-NHMe depicts the conformational flexibility of the glycyl residue. The PES of the *N*-Ac-Gly \bullet -NHMe was constrained in the β_L conformation, indicating its stability in fully extended conformations. The present findings correspond to other observations [4] of β -sheet structures of peptides and amino acids that have undergone radical oxidation at the C $^\alpha$ atom. The β -conformation permits interactions with neighboring β -strands, making subsequent radical propagation and peptide aggregation possible as observed with β -amyloid.

Acknowledgments

This work was supported by NIH-BRIN grant 1 P20 RR16469 and the Carpenter Endowed Chair in Biochemistry, Creighton University.

References

1. Perez-Campo R., Lopez-Torres, M., Cadenas S., Rojas, C. and Barja, G. *J. Comp. Phys. [B]* **168**, 149-158 (1998).
2. Himo, F. *Chem. Phys. Lett.* **328**, 270-276 (2000).
3. Brunelle, P. and Rauk, A. *J. Alzheimers Dis.* **4**, 283-289 (2002).
4. Cotman, C., *et al.* *J. Neurochem.* **64**, 253-265 (1995).

Impact of a Single α,α -Disubstituted Amino Acid on β -Hairpin Folding

Larry R. Masterson¹, Marcus A. Etienne², George Barany¹, Gianluigi Veglia¹ and Robert P. Hammer²

¹Department of Chemistry, University of Minnesota-TC, Minneapolis, MN 55455, USA;

²Department of Chemistry, Louisiana State University, Baton Rouge, LA 7080, USA

Introduction

Conditions warranted for secondary structure formation have been obtained by reducing complex macromolecular configurations to simpler peptide models in order to facilitate the evaluation of parameters such as length, sequence, and side chain effects on the roles of stability and disorder. The development of a number of autonomously folding β -hairpin models has enhanced our understanding of the roles of turn and sheet residues in stabilizing this fundamental protein secondary structure building block [1]. Rooted in the work of Gellman [2] and Balaram [3], we have investigated the capability of an α -aminoisobutyric acid (Aib=B) residue to nucleate β -hairpin formation. The structure of the peptide H-RYVEV**B**GOKILQ-NH₂ (Ω BG) has been characterized by CD and high resolution NMR and compared with a sequence studied by Gellman and associates, H-RYVEV^DPGOKILQ-NH₂ (Ω^D PG).

Results and Discussion

Two-dimensional homonuclear ¹H NMR experiments obtained at 5°C and a peptide concentration of 2.7 mM in 200 mM deuterated sodium acetate buffer (pH 3.5) were used for resonance assignments based on TOCSY and ROESY spectra. Through space dipolar interactions within the structure of the peptide were determined with ROESY spectra obtained at 200-400 ms mixing times, while a DQF-COSY experiment was conducted to calculate the J_(HN-H α)-coupling constants for the determination of ϕ angles of backbone atoms. A significant number of cross-strand NOE interactions were found between the sidechains of Y2, E4, K9, and L11. Interactions of the amide protons of Val3 and Val5 with Ile10 and Orn8, respectively, were also determined. Furthermore, sets of *i*, *i* + 2 sidechain NOE interactions were found between Arg1/Val3, Val3/Val 5, Orn8/Ile10, and Ile10/Gln12.

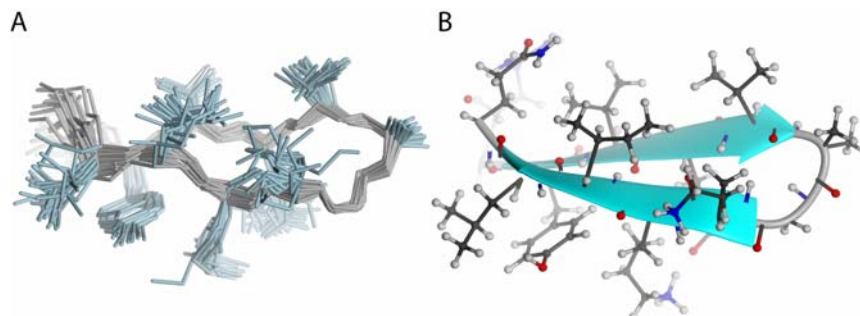


Fig. 1. A) Ensemble of 20 lowest energy structures and B) single average structure from simulated annealing/energy minimization calculation.

A total of 82 inter-residue NOE interactions were used as distance constraints from ROESY data in a simulated annealing/energy minimization calculation of 100 random coil structures of Ω BG with the software XPLOR-NIH. An ensemble of 20 lowest energy structures (Fig. 1A) resulted in a well-defined backbone RMSD of 0.34 ± 0.2 Å (residues 2-11) and a side-chain superposition of 1.5 ± 0.3 Å (residues 2-11, heavy atoms only) from the average of these structures. Back-calculated $^3J_{\text{HN-H}\alpha}$ coupling constants from the average of the structural ensemble (Fig. 1B) were compared with those derived from DQF-COSY data and varied by no more than ~ 2 Hz for residues 2-11 (with the exception of Gly7), thus within the resolution of the spectrum that was obtained.

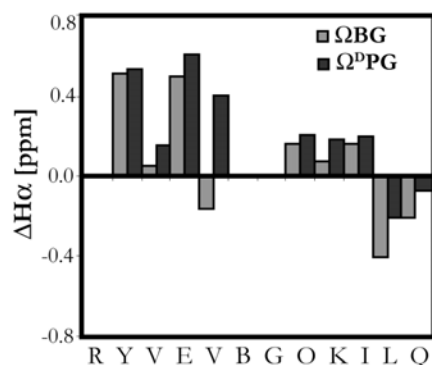


Fig. 2. Chemical shift index of the Aib and ^DPro containing sequences.

In order to compare hairpin structures, we determined the chemical shift deviation (CSD) of H^α resonances for Ω BG and compared them with Ω ^DPG, both at 5°C. Furthermore, we obtained temperature coefficients of the amide protons for both peptides at a 5-28°C. The CSI profile is nearly identical in both peptides (Fig. 2) and indicates that although the turn sequences are different (Type I' for Ω BG and Type II' for Ω ^DPG), the molecules have comparable structures (with the exception of Val 5 in Ω BG which is the first amino acid in the four residue turn). This is further supported by information on the stability of these sequences from temperature coefficient data—both have temperature coefficients that vary by no more $\sim 0.2\%$ (with the exception of the termini and Tyr2 which is proximal to the N-terminus, changing by $\sim 2\%$) under same solvent conditions and concentrations.

Acknowledgment

This work was supported by grants from the Petroleum Research Fund administered by the ACS (RPH) and the NIH (AG17983, RPH; GM 51628, GB) and fellowship support from the Louisiana Board of Regents (MAE). The University of Minnesota High-Field NMR Center in the Department of Biochemistry, Molecular Biology, and Biophysics was funded by the NSF (BIR-961477) and the University of Minnesota Medical School.

References

1. Searle, M. S. and Ciani, B., *Curr. Opin. Struct. Biol.* **14**, 458-464 (2004).
2. Gellman, S. H. *Curr. Opin. Struct. Biol.* **2**, 717-725 (1998).
3. Aravinda, S., Shamala, N., Rajkishore, R., Gopi, H. N. and Balaram, P. *Angew. Chem. Int. Ed.* **41**, 3863-3865 (2002).

RGD-Cy7 Conjugates as Near-Infrared Fluorescence Probes to Image $\alpha_v\beta_3$ Integrin Expression in Brain Tumor Xenografts

Yun Wu and Xiaoyuan Chen

Molecular Imaging Program at Stanford (MIPS), Department of Radiology & Bio-X, Stanford University, Stanford, California, USA

Introduction

Angiogenesis plays an important role during tumor growth and spread. The cell adhesion receptor integrin $\alpha_v\beta_3$, which is highly expressed on both tumor cells and proliferating endothelial cells, is being explored as a logical target for imaging tumor associated angiogenesis [1].

We have previously reported the integrin receptor specificity of a novel peptide-dye conjugate Cy5.5-RGD as a contrast agent *in vitro* and *in vivo* [2]. Herein, we report our progress for noninvasive NIR fluorescence imaging of $\alpha_v\beta_3$ integrin expression in U87MG glioblastoma xenograft using Cy7-RGD and Cy7-PEG-RGD. Since Cy7 has longer wavelength (emission maximum at 767 nm), which can penetrate several centimeters into tissue, Cy7-labeled probes would give higher tumor to background contrast. We also introduced a poly(ethylene glycol) (PEG) linker between the Cy7 and the RGD moiety in order to optimize tumor retention and biodistribution characteristics of an Cy7-labeled RGD fluorescent probes (Fig. 1A).

Results and Discussion

The PEG conjugation of cyclic RGD peptide was accomplished by reacting the active succinimidyl ester (NHS) of PEG-propionate (MW 3400) with the side-chain ϵ -amino group under basic condition (pH = 8.5). The Cy7 and peptide conjugates were performed in 0.1 mol/L sodium borate buffer (pH = 8.3) in the dark at 4°C. After HPLC purification, Cy7-RGD and Cy7-PEG-RGD were obtained in 75% yield.

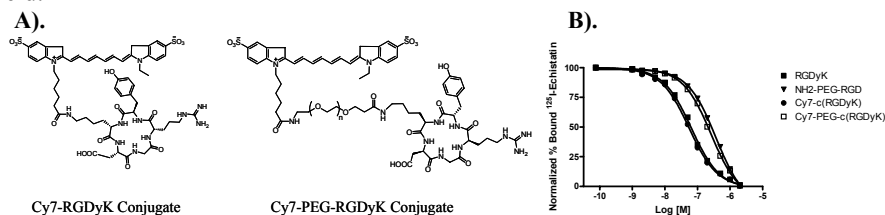


Fig. 1. A) Schematic structure of Cy7-c(RGDyK) and Cy7-PEG-c(RGDyK). PEG (MW, 3,400); B) Inhibition of $[^{125}\text{I}]$ -Echistatin-binding to $\alpha_v\beta_3$ integrin receptor by c(RGDyK), NH₂-PEG-c(RGDyK), Cy7-c(RGDyK) and Cy7-PEG-c(RGDyK) on brain tumor U87MG cells.

The $\alpha_v\beta_3$ integrin receptor binding affinity of the synthesized fluorescent probes was tested using receptor binding assay on $\alpha_v\beta_3$ -integrin positive brain tumor U87MG cells. The experiment was performed in cell binding buffer (20 mM Tris, pH 7.4, 150 mM NaCl, 2 mM CaCl₂, 1 mM MgCl₂, 1 mM MnCl₂, 0.1% BSA) using $[^{125}\text{I}]$ -labeled echistatin as the integrin-specific radioligand. The IC₅₀ values for c(RGDyK), NH₂-PEG-c(RGDyK), Cy7-c(RGDyK) and Cy7-PEG-c(RGDyK) were

64.9 nM, 368.8 nM, 54.8 nM, and 262.4 nM, respectively (Fig. 1B). These two fluorescent probes showed the same binding affinity to integrin receptor on tumor cell line as peptides.

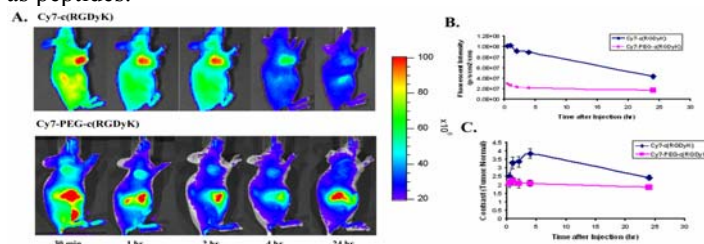


Fig. 2. (A) In vivo fluorescence imaging of mice with intravenous injection of 1 nmol Cy7-c(RGDyK) or Cy7-PEG-c(RGDyK). (B) Quantification and kinetics of in vivo targeting character of two fluorescent probes. (C) Tumor contrast as a function of time.

In vivo near-infrared fluorescent imaging was performed using female athymic Nu/Nu mice bearing subcutaneous U87MG brain tumor after intravenous injection of 1 nmol of Cy7-c(RGDyK) and Cy7-PEG-c(RGDyK). The whole-body images were obtained from 30 min to 24hrs, and the tumor could be clearly delineated from the surrounding background tissue (Fig. 2). Cy7-c(RGDyK) had higher fluorescence intensity in the tumor than the pegylated analog with maximum contrast occurring 4 hrs postinjection.

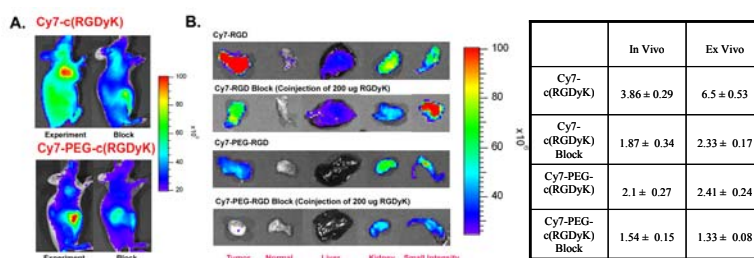


Fig. 3. (A) In vivo fluorescent images of block experiments [coinjection of 10 mg/Kg RGD peptide with probes]. (B) Representative images of dissected organs of mice sacrificed 4hrs p.i.

The fluorescent dye conjugate also indicated integrin-specific tumor uptake (Fig. 3A). Unlabeled RGD peptide successfully reduced tumor contrast from 3.86 ± 0.29 to 1.87 ± 0.34 for Cy7-c(RGDyK), and for peglated probe from 2.1 ± 0.27 to 1.54 ± 0.15 . Figure 3B showed dissected organs of the four mice. No significant difference in tumor contrast was found between in vivo and ex vivo data. All these data demonstrated that Cy7-labeled RGD peptides were appropriate for imaging $\alpha_v\beta_3$ integrin expression in animal models.

Acknowledgments

The work was funded by National Institute of Biomedical Imaging and Bioengineering (NIBIB) Grant R21 EB001785 to X. Chen.

References

1. Folkman, J. *Nat. Med.* **1**, 27–31 (1995).
2. Chen, X., Conti, P. S. and Moats, R. A. *Cancer. Res* **64**, 8009-8014 (2004).

Parameters Influencing Helix Stability of Oligourea Foldamers

Aude Violette¹, Marie-Christine Averlant-Petit², Didier Rognan³, Henri Monteil⁴, Jean-Paul Briand¹ and Gilles Guichard¹

¹UPR 9021 CNRS - ICT, IBMC, 15 rue René Descartes, F-67084 Strasbourg Cedex; ²LCPM, UMR CNRS-INPL 7568, ENSIC-INPL, BP 451, F-54001 Nancy; ³LPCC, UMR CNRS-ULP 7081, 74 route du Rhin, B.P. 24, F-67401 Illkirch; ⁴Institut de bactériologie, 3 rue Koeberlé, 67000 Strasbourg, France

Introduction

In the realm of peptide mimetics, aliphatic and aromatic ω -peptides as folding oligomers, known as “foldamers” [1] have received considerable attention. Interested by secondary structure elucidation and bioactivity investigation of urea-based peptidomimetics, we have shown recently using NMR spectroscopy that the structural information encoded in the γ^4 -peptide backbone is partially retained upon substitution of a nitrogen atom for the α -carbon of γ -amino acid residues [2]. In pyridine-*d*₅, the resulting enantiopure *N,N'*-linked oligoureas adopt a well defined 2.5 helical structure [3], reminiscent of the 2.6₁₄ helical structure of γ^4 peptides. The helix of oligoureas is characterized by a stable (+)-synclinal arrangement around the ethane bond and the structure is held by H-bonds closing 12 and 14 membered rings formed between C=O(*i*) and N'H(*i*-2) and NH(*i*-3), respectively.

Results and Discussion

In an attempt to assess the presence of a regular conformation in protic solvent as well as to correlate far-UV chiroptical properties and conformational preferences of oligoureas, we have undertaken a detailed conformational analysis of enantiopure *N,N'*-linked oligoureas of different length utilizing both CD and NMR spectroscopy in MeOH.⁴ We chose an alternating sequence of Ala, Val and Tyr side chains to prepare oligomers of varying length, from tetramer to nonamer (Fig. 1).

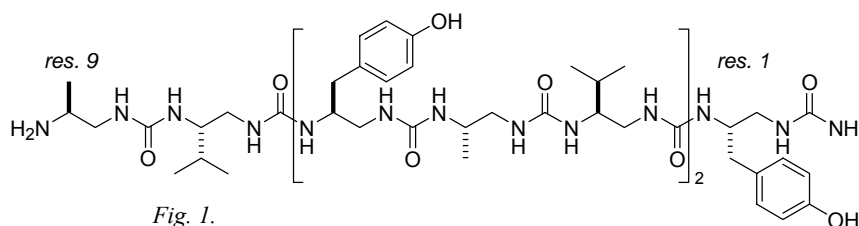


Fig. 1.

The tetramer exhibits a very weak CD spectrum whereas CD spectra for the pentamer to nonamer all display a similar shape with a maximum of positive ellipticity at ca 203 nm. The intensity of the maximum increases dramatically with the oligomer length from four to seven residues and stabilizes between seven and nine residues (Fig. 2). These data are in good agreement with NMR observations of the same oligomers.

However, attempts to define the dominant structure(s) of the heptamer in MeOH from experimentally determined NMR constraints were unsuccessful as most structures presented large NOE violations suggesting that, although it is significantly

populated, the 2.5 helical structure of the studied heptamer in CD₃OH coexists with a certain amount of various partially folded conformations.

Removing unfavorable electrostatic interaction at the amino terminal end of the heptamer and adding one H-bond acceptor by acylation with isopropyl isocyanate was believed to enforce a stable and consistent 2.5 helical folding in MeOH that would allow unambiguous NMR structure determination. Conformational preference of capped heptamer was investigated by NMR spectroscopy in CD₃OH at 293 K and calculations converged well. Although the structure was grossly similar to the helical fold determined for oligomers in pyridine (Fig. 3), evidences for cis/trans isomerisation of the urea bond were observed.

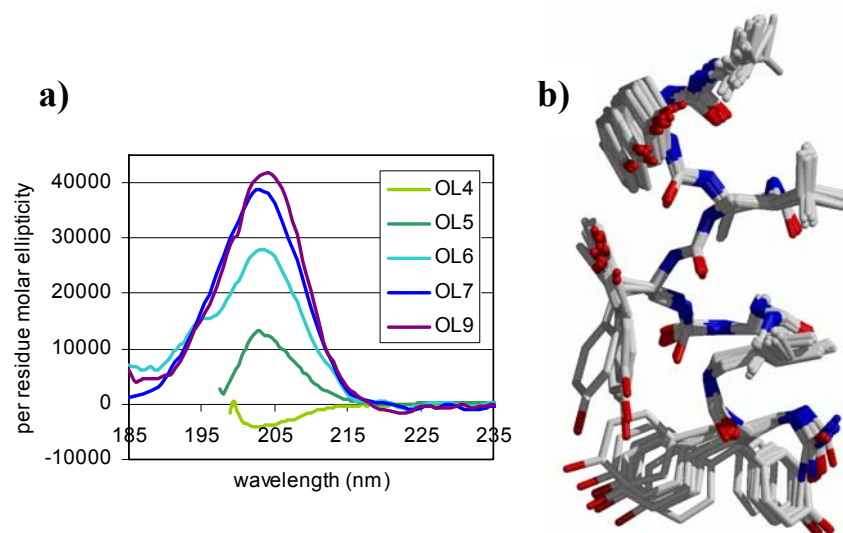


Fig. 2. a) CD spectra, 0.5mM in MeOH.
b) Modeling of capped heptamer under NMR constraints in CD₃OH.

Perspectives

The precise knowledge of the requirements for the 2.5 helix formation of oligoureas now provides a rationale for the design of bioactive molecules, for example antimicrobials.

Acknowledgment

This work received financial support from CNRS, Region Alsace and BIO ImmuPharma France.

References

1. Gellman, S. H. and DeGrado, W. F. *Chem. Rev.* **101**, 3219-3232 (2001).
2. Hanessian, S., Luo, X., Schaum, R. And Minnick, S. *J. Am. Chem. Soc.* **120**, 8569-8570 (1998).
3. Semetey, V., Didierjean, C., Briand, J.-P., Aubry, A. and Guichard, G. *Angew. Chem. Int. Ed.* **41**, 1895-1898 (2002).
4. Violette, A. et al. *J. Am. Chem. Soc.* **127**, 2156-2164 (2005).

The Tertiary Structure of A β 1-40 Determined by Scanning Tunnelling Microscopy

**Dusan Losic^{1,3}, Lisandra L. Martin², Adam Mechler², David H. Small¹
and Marie-Isabel Aguilar¹**

¹*Department of Biochemistry and Molecular Biology, Monash University, Clayton Vic 3800, Australia;* ²*School of Chemistry, Monash University, Clayton Vic 3800, Australia;* ³*SoCPES, Flinders University, SA, 5001, Australia*

Introduction

In Alzheimer's disease, the β -amyloid protein (A β) is deposited in the extracellular compartment of the brain where it accumulates to form amyloid plaques and cerebral amyloid angiopathy. Numerous studies have demonstrated that aggregation of A β monomers into fibrillar structures is associated with neurotoxicity. However, the detailed molecular structure of amyloid fibrils and protofibrils remains uncertain. Scanning probe microscopy provides a powerful approach to molecular structure determination. Amyloid fibrils can be visualized by both scanning tunnelling microscopy (STM) and atomic force microscopy, but resolution has not been sufficient to determine the orientation of monomers within the fibril. In this study, we describe the use of STM to image the tertiary structure of a single molecule of A β .

Results and Discussion

STM has the capacity to image the morphology of molecular structures at subnanometer resolution [1]. However, there have been only a few reported observations of A β fibrils *via* STM [2,3]. These studies have used graphite or mica as a substrate for imaging, under conditions which may not have been optimal for visualising A β . The present study was undertaken to examine the detailed structure of A β monomers and protofibrils by STM using a highly conductive substrate of atomically flat gold.

Previous studies have shown that, at low micromolar concentrations, A β 1-40 is predominantly in monomeric form [4]. Therefore, to image A β monomers, freshly prepared recombinant human A β 1-40 of >95% purity (RPeptides Inc.) was dissolved at a low concentration (0.5 μ M) and the solution applied to a surface of atomically flat gold for STM imaging. High resolution scans of globular structures confirmed that they were monomers, which contained a single chain-like structure approximately 12 nm in length, which was folded into four 3-nm strands (data not shown).

Oligomeric A β forms and protofibril-like structures (Fig. 1) were also evident when the peptide was incubated ("aged") at 37°C prior to imaging, a process that enhances A β aggregation. To age the peptide, a stock solution of A β (10 μ M in PBS, pH 7.4) was incubated at 37°C for 24 h before being diluted to 0.5 μ M with PBS for STM imaging. The protofibrils created this way were 3-nm wide and up to 0.4 nm in height, and appeared to result from the end-to-end fusion of monomers (Fig. 1 A-C). Three-nm wide strands were oriented at 90 degrees to the axis of the fibril. The more compact nature of the protofibril made it more difficult to distinguish individual strands of the polypeptide chain. However, the minimum inter-strand distance was approximately 5 Å, similar to that for the monomers.

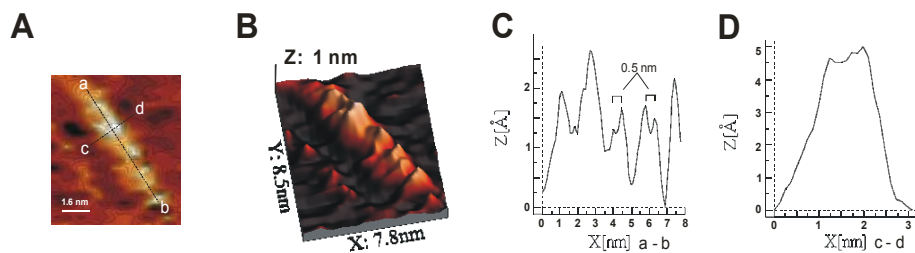


Fig. 1. A. Two-dimensional contour diagram of an A β 1-40 protofibril. B. Three-dimensional representation of the same structure showing that strands of the polypeptide chain are organized at approximately 90° to the axis of the fibril. C., D. Section profiles of the surface topography along the a-b (C) and c-d axes (D).

The data show that A β monomers can align to form oligomeric structures, in which the β strands are perpendicular to the axis of the fibril. This structure is consistent with previous studies that show that fibrillar A β contains a cross- β sheet structure [5]. The protofibrils seen in this study may be structurally similar to a neurotoxic form of A β . While it is now generally accepted that an aggregated form of A β is the pathogenic species that causes neurodegeneration in Alzheimer's disease, the structure of the neurotoxic A β remains unknown. There is increasing evidence that low molecular weight "protofibrillar" A β may be more neurotoxic than high molecular weight fibrils [6]. It is for this reason that the structures described in the present study may be of considerable significance for understanding the mechanism of pathogenesis of Alzheimer's disease.

References

1. Poggi, M. A., Gadsby, E. D., Bottomley, L. A., King, W. P., Oroudjev, E. and Hansma, H., *Anal. Chem.* **76**, 3429-3443 (2004).
2. Shivji, A. P., Brown, F., Davies, M. C., Jennings, K. H., Roberts, C. J., Tendler, S., Wilkinson, M. J. and Williams, P. M. *FEBS Lett.* **371**, 25-28 (1995).
3. Wang, Z., Zhou, C., Wang, C., Wan, L., Fang, X. and Bai, C. *Ultramicroscopy* **97**, 73-79 (2003).
4. Sengupta, P., Garai, K., Shi Y., Callaway, D. G. E. and Maiti, S. *Biochemistry* **42**, 10506-10513 (2003).
5. Malinchik, S. B., Inouye, H., Szumowski, K. E. and Kirschner, D. A. *Biophys. J.* **74**, 537-545 (1998).
6. Walsh, D. M. and Selkoe, D. J. *Neuron*, **44**, 181-193 (2004).

Validation of Active-Site Mapping of Enzymes

Daniel J. Kuster^{1,2} and Garland R. Marshall^{1,2,3}

¹Department of Biomedical Engineering; ²Center for Computational Biology; ³Department of Biochemistry and Molecular Biophysics, Washington University, St. Louis, MO 63110, USA

Introduction

Structure-based drug design presupposes detailed knowledge of the structure of a therapeutic target and/or complex to design potential inhibitors. Yet, despite the increasing number of high-resolution 3D structures publicly available, a distinct knowledge gap remains between the identification of potential disease targets and the generation of accurate structure-based models to drive drug discovery efforts. Methodologies like the active-analog approach aim to bridge this gap, by taking advantage of three-dimensional chemical information implicitly stored in a series of active drug molecules.

The active-analog approach was used to predict the active conformations of angiotensin-converting enzyme (ACE) inhibitors bound at the (C-terminal) active site of ACE in 1987 by Mayer *et al.* [1]. This and previous schematic-type models [2] were the basis for discovery efforts that produced the large family of ACE inhibitors employed as safe, effective, orally-available, anti-hypertensive drugs throughout the last two decades. Since the prediction of the ACE active site in 1987, new inhibitors have been developed for therapeutic application. Computational power has increased dramatically as well. These two parallel developments enabled refinement of the original ACE active site model—the inclusion of structural information from new inhibitors added further constraints to the system, and greater computational power allowed better sampling of conformational space. Likewise, advances in protein engineering and structural determination enabled Natesh *et al.* to solve high-resolution, x-ray crystallography structures of human testicular ACE [3] (EC 3.4.15.1), and ACE complexed with lisinopril [3], captopril [4] and enalapril [4] (potent ACE inhibitors of demonstrated therapeutic relevance).

The active site model proposed by Mayer *et al.* [1] was evaluated with respect to the three crystal structures and found to be accurate within 0.37 to 0.77 Å root mean square deviation (RMSD) across the model distances. Using published information on new ACE inhibitors, the commercial software package Sybyl 6.9.1 and a single-processor workstation, an active site model of higher resolution was developed. This model has been shown to be accurate with respect to the three published x-ray crystallography structures of ACE-inhibitor complexes, within 0.43 to 0.81 Å RMSD. These observations represent the achievement of a significant milestone in the fields of protein science and drug design—this is the earliest known *in silico* prediction shown to be highly accurate with respect to high-resolution experimental data. Further, the methodology for achieving these results is shown to be accessible to anyone with a modern workstation and the appropriate software.

The three x-ray crystal structures with bound inhibitor (lisinopril, enalapril or captopril) were analyzed in the framework of the predicted active site using distance maps. Figure 1 establishes that the distance maps derived from the three experimentally determined structures fit precisely within the active site prediction, allowing for some delocalization (less than 1.1 Å) of the zinc atom. Since the crystal structures show evidence that the coordinated zinc does not have a precisely localized position [4], the zinc delocalization is not a breakdown of the active analog

paradigm, but rather a reinforcement that the predicted model correctly allowed flexibility at the zinc locus. The deviations between the predicted model and the crystal structures for distances involving the zinc are likely due to applying molecular-level modeling assumptions to a zinc atom that requires quantum-level coordination of its *d*-electrons and idealized zinc-coordinated ligand geometry. Clearly, the chemical groups from both the enzyme and the ligand will optimize a binding geometry among all groups involved in zinc coordination, not just the zinc-binding group of the inhibitor, but in the absence of structural data for the enzyme, idealized ligand values for the predicted coordination geometry introduced less bias.

Such results corroborate the feasibility of exploiting the three-dimensional information implicit in a series of chemically diverse inhibitors to accurately predict the bound conformations of ligands at enzyme active sites; in this case, the C-terminal active site of ACE. This study provides the proof of concept that the active-analog approach may be applied for active site mapping with enzymes where no high-resolution structures of the enzyme or enzyme-inhibitor complexes exist.

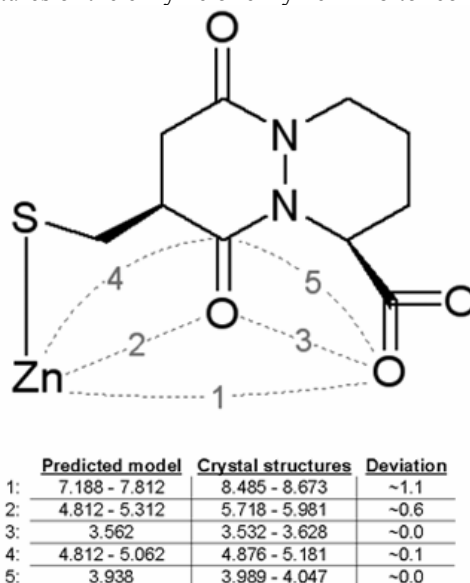


Fig. 1. Comparing distance maps among predicted conformations (of the bound ligands) and crystal structures. Distances are in angstroms.

References

1. Mayer, D., Naylor, C. B., Motoc, I. and Marshall, G. R. *J. Comput. Aided Mol. Des.* **1**, 3-16 (1987).
2. Ondetti, M. A., Rubin, B. and Cushman, D. W. *Science* **196**, 441-4 (1977).
3. Natesh, R., Schwager, S. L., Sturrock, E. D. and Acharya, K. R. *Nature* **421**, 551-4 (2003).
4. Natesh, R., Schwager, S. L., Evans, H. R., Sturrock, E. D. and Acharya, K. R. *Biochemistry* **43**, 8718-24 (2004).

Peptide and Protein Arrays

Protein Arrays as Tools for Detection of Protein-Protein Interactions by Mass Spectrometry

Christian F. W. Becker¹, Ron Wacker², Werner Bouschen³, Ralf P. Seidel¹, Branko Kolaric¹, Pascal Lang¹, Hendrik Schroeder^{2,4}, Christof Niemeyer⁴, Bernhard Spengler³, Roger S. Goody¹ and Martin Engelhard¹

¹Max-Planck-Institut für molekulare Physiologie, Otto-Hahn-Str. 11, 44227 Dortmund;
²Chimera Biotech GmbH, Emil-Figge-Str. 76A, 44227 Dortmund; ³Justus-Liebig Universität
Giessen, Schubertstr. 60, 35392 Giessen; ⁴Universität Dortmund, Otto-Hahn-Str. 6, 44227
Dortmund, Germany

Introduction

DNA-Protein arrays can be developed into tools for the detection of protein-protein interactions and identification of protein binding partners by mass spectrometry. An important advantage of mass spectrometry readout of microarrays is the molecular weight information that is obtained for the analyte. Such a readout system has been successfully used in approaches to determine protein expression levels, to follow enzyme activity, and to observe proteins bound to immobilized ligands [1-4]. Here we describe a microarray that combines the reversible immobilization of proteins with readout by MALDI mass spectrometry in order to study protein-protein interactions and to identify binding partners of immobilized proteins. The immobilization strategy is based on the much further advanced technology of DNA chips, utilizing protein-DNA conjugates to achieve highly specific but non-covalent binding to the surface-attached oligonucleotides [5-7].

The Ras protein and the Ras-binding domain of its effector protein cRaf-1 were chosen as a test system for this approach [8]. The Ras protein plays a vital role in the transduction of extracellular signals from the cell membrane towards the nucleus by cycling between its activated, GTP-bound state in which it interacts with its downstream effectors and its inactive GDP-bound state [9]. Mutations in the Ras protein can lead to constitutive activation of signaling cascades either by deactivation of GTP hydrolysis or by preventing the interaction with Ras GAPs. Such mutations occur in 30% of all solid human cancers [10]. These facts turn the Ras-RBD protein pair into a highly interesting test case where two isoforms of a protein (Ras) with different affinities for the capture protein (RBD) have to be distinguished. A potential diagnostic use can also be deduced.

Results and Discussion

In order to achieve functional immobilization of the protein samples in a controlled manner, protein-DNA fusion proteins were synthesized. The synthesis strategy is based on the expressed protein ligation approach. A protein with a C-terminal thioester and an oligonucleotide that carries a 5'-cysteine modification are linked by an amide bond (Fig. 1A) [11,12]. The protein thioesters were generated from recombinantly produced intein fusion proteins that, upon treatment with mercaptoethanesulfonic acid (Mesna), released Ras- and RBD-thioesters. The cysteine-modified oligonucleotide was synthesized using standard phosphoramidite chemistry and a cysteine-modified thymidine building block.

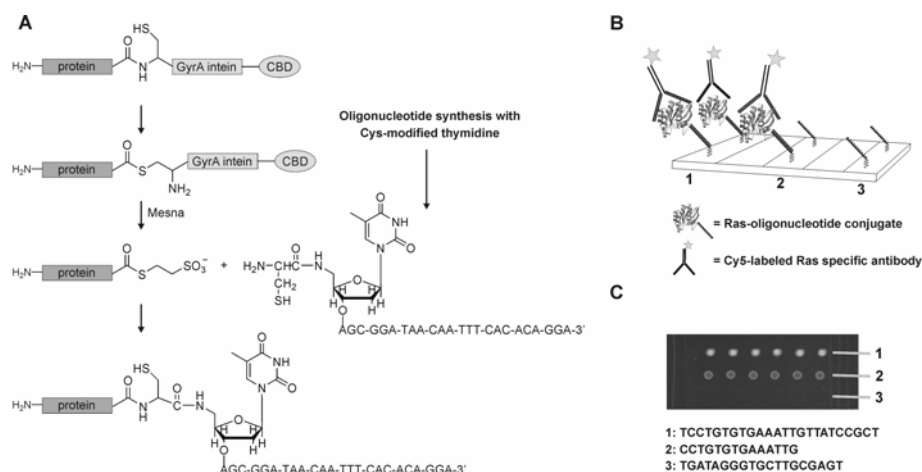


Fig. 1. A) Schematic representation of the ligation reaction of RBD and Ras thioesters with 5'-Cys-modified oligonucleotide to produce the capture proteins RBD-DNA and Ras-DNA. B) Schematic representation of Ras-DNA detection on glass arrays with a fluorescently labeled Ras-specific antibody. C) Fluorescence readout signal of Ras-DNA-antibody complex.

The immobilization strategy was initially tested with Ras- and RBD-DNA conjugates on glass microarrays using conventional fluorescence readout (Fig. 1B). The glass surface was covalently modified with commercially available 5'-amino modified oligonucleotides. Immobilized Ras-DNA was detected after incubation with a Cy5-labeled Ras-specific antibody. Specific interaction between a fully complementary surface-attached oligonucleotide **1** and the Ras-DNA conjugate was clearly demonstrated by the strong fluorescence signal (Fig. 1C). A complementary but truncated oligonucleotide **2** on the surface produced a much weaker signal indicating a lower amount of bound Ras-DNA. A non-complementary oligonucleotide **3** did not produce any signal.

This DNA-directed immobilization (DDI)-based approach was successfully transferred towards silica-based microarrays that were combined with a MALDI readout system. The interaction of the Ras-RBD protein pair was unambiguously detected by using RBD-DNA conjugates as capture molecules on the microarrays and activated Ras:GppNHp (GppNHp is a non-hydrolyzable GTP analog) as the analyte. The incubation with analyte protein was followed by several washing steps and application of a layer of organic matrix (sinapinic acid) in order to allow efficient ionization before insertion into the home-build MALDI spectrometer (Fig. 2A) [13]. Multiple control experiments, e.g., with inactive Ras:GDP, did not produce a MALDI signal (Fig. 2B). However, after incubation with activated Ras, subsequent washing and matrix application, the Ras protein (calculated MW 18853 Da) was easily detected in the mass spectrum (Fig. 2C).

In conclusion, it was shown that MALDI mass spectrometry is a suitable detection method for DDI-based protein microarrays. The presented approach provides highly selective immobilization of capture and analyte molecules as demonstrated for the interacting protein pair Ras and RBD.

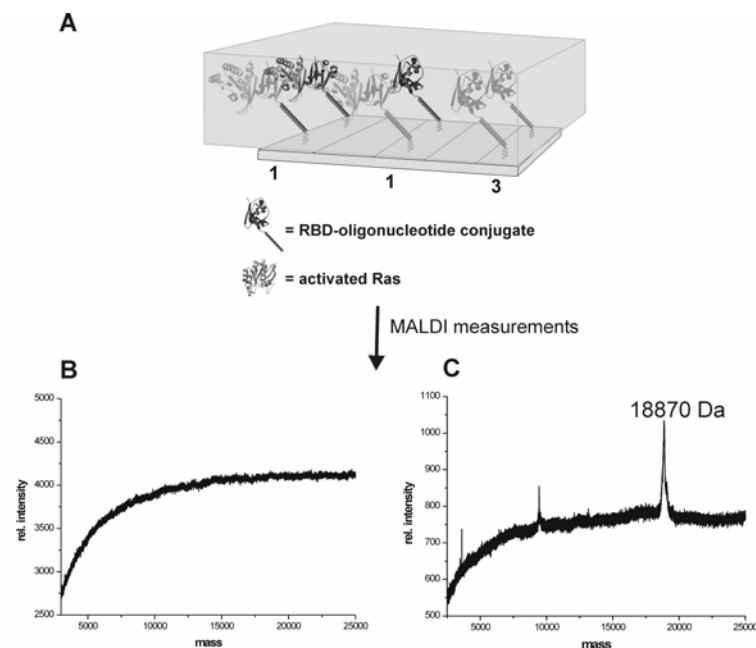


Fig. 2. A) Ras captured by immobilized RBD-DNA on a silica-based array covered with a layer of organic matrix. B) Typical readout signal in control experiments. C) Typical readout after incubation of immobilized RBD-DNA with activated Ras:GppNHp.

Acknowledgement

This work was funded in part by the MPG, DFG, BMBF and VCI.

References

1. Seibert, V., Wiesner, A., Buschmann, T. and Meuer, J. *Pathol. Res. Pract.* **200**, 83-94 (2004).
2. Min, D. H., Su, J. and Mrksich, M. *Angew. Chem. Int. Ed. Engl.* **43**, 5973-5977 (2004).
3. Min D. H. and Mrksich, M. *Curr. Opin. Chem. Biol.* **8**, 554-558 (2004).
4. Yeo, W. S., Min, D. H. R., Hsieh, W., Greene, G. L. and Mrksich, M. *Angew. Chem. Int. Ed. Engl.* **44**, 5480-5483 (2005).
5. Niemeyer, C. M. *Biochem. Soc. Trans.* **32**, 51-53 (2004).
6. Lovrinovic, M., Seidel, R., Wacker, R., Schroeder, H., Seitz, O., Engelhard, M., Goody, R. S. and Niemeyer, C. M. *Chem. Commun.* 822-823 (2003).
7. Wacker, R., Schroder, H. and Niemeyer, C. M. *Anal. Biochem.* **330**, 281-287 (2004).
8. Wittinghofer A. and Waldmann, H. *Angew. Chem. Int. Ed. Engl.* **39**, 4193-4214 (2000).
9. Boguski M. S. and McCormick, F. *Nature* **366**, 643-654 (1993).
10. Barbacid, M. *Annu. Rev. Biochem.* **56**, 779-827 (1987).
11. Muir T. W. *Annu. Rev. Biochem.* **72**, 249-289 (2003).
12. Takeda, S., Tsukiji, S. and Nagamune, T. *Bioorg. Med. Chem. Lett.* **14**, 2407-2410 (2004).
13. Spengler, B. *J. Mass Spectrometry* **32**, 1019-1036 (1997).

New Tools for the Site-Specific Attachment of Proteins to Surface

Youngeun Kwon¹, Matthew A. Coleman² and Julio A. Camarero¹

¹*Chemical Biology and Nuclear Sciences Division; ²Biosciences Directorate, Lawrence Livermore National Laboratory, University of California, Livermore, CA 94550, USA*

Introduction

Protein microarrays in which proteins are immobilized to a solid surface are ideal reagents for high-throughput experiments that require very small amounts of analyte. Such protein microarrays ('protein chips') can be used very efficiently to analyze all kind of protein interactions en masse. Although a variety of methods are available for attaching proteins on solid surfaces, most of them rely on non-specific adsorption methods or on the reaction of chemical groups within proteins (mainly, amino and carboxylic acid groups) with complementary reactive groups. In both cases the protein is attached to the surface in random orientations. The use of recombinant affinity tags addresses the orientation issue, however in most cases the interaction of the tags are reversible (e.g., glutathione S-transferase, maltose binding protein and poly-His) and, hence, are not stable over the course of subsequent assays or require large mediator proteins (e.g., biotin-avidin and antigen antibody). The key for the covalent attachment of a protein to a solid support with a total control over the orientation is to introduce two unique and mutually reactive groups on both the protein and the surface. The reaction between these two groups should be highly selective thus behaving like a molecular 'velcro'.

Results and Discussion

The present work describes the use of protein splicing units (also called inteins) for the selective attachment of proteins to solid surfaces through its C-termini. In our first approach we used "Expressed Protein Ligation" (EPL) [1,2] for the selective immobilization of proteins to a modified glass surface containing an N-terminal Cys poly(ethylene glycol) linker (Fig. 1A). Key to this approach is the use of protein α -thioesters recombinantly generated using an engineered intein expression system. The protein α -thioesters are covalently attached by "Native Chemical Ligation" (NCL) to a glass surface modified with PEGylated thiol linkers **1** and **2** (Fig. 1B). Two fluorescent proteins, EGFP (enhanced green fluorescent protein) and DsRed are used to test the suitability of EPL for selective protein immobilization. DsRed is a tetrameric red fluorescent protein and EGFP is a monomeric version of the green fluorescent protein. In both cases, the proteins are fluorescent only if their tertiary and quaternary structures are kept intact (DsRed shows red fluorescence only as tetramer). Thus, they were used as controls to test if the native architecture of these two proteins was altered during the attachment process. Both protein α -thioesters were readily expressed in *E. coli* using a modified Gyrase intein expression system. In order to facilitate the site-specific ligation of the fluorescent proteins onto a glass surface for the fabrication of protein microrrays, a glass slide was silanized with (3-acryloxypropyl)trimethoxysilane and reacted with a mixture of PEGylated thiols **1** and **2**, in a molar ratio 1:5, respectively. Linker **1** contained a protected N-terminal Cys for the selective attachment of the α -thioester protein through NCL and linker **2** was used as a diluent. Linker **1** also contains a longer PEG moiety than linker **2** (Fig. 1B) to ensure that the reactive Cys residue is available to react with the corresponding protein thioester in solution. After the glass derivatization was

complete the protecting groups (N-Boc and S-Trt) of the Cys residue from linker **1** were removed by brief treatment with trifluoroacetic acid (TFA). The surface was rinsed, neutralized and quickly used for spotting (Fig. 1C). As a control, a solution of EGFP with no α -thioester group was also spotted. The ligation reaction was kept for 36 hrs at room temperature, and the protein-modified slide was then extensively washed with phosphate buffer solution containing 0.2% Tween-20 (PBS). As shown in Figure 1, only specific attachment between the N-terminal Cys-containing surface and the protein α -thioester was observed. No fluorescence signal was detected where the control EGFP with no C-terminal α -thioester function was spotted. We also investigated the minimum protein concentration required for the effective immobilization of protein α -thioesters onto Cys-modified glass surfaces through NCL. Different concentrations of EGFP and DsRed α -thioesters were spotted onto a Cys-containing glass slide and incubated for 36 hrs. After extensive washing with PBS the slides were imaged for fluorescence (Fig. 1C). As expected, the concentration of the protein was critical for efficient attachment of the corresponding protein α -thioester. In both cases, the minimum concentration required for acceptable levels of immobilization was found to be around 50 μ M (\approx 1 mg/mL).

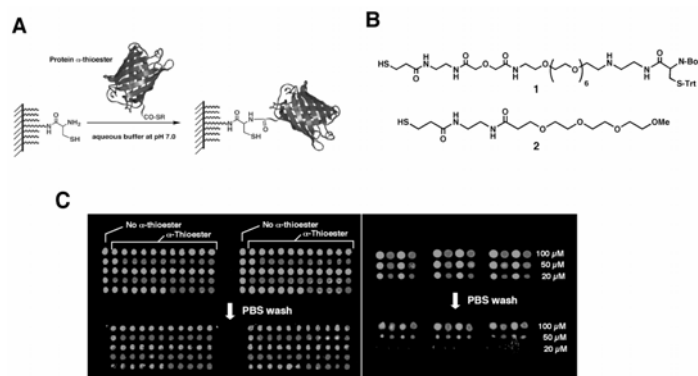


Fig. 1. A. Selective immobilization of proteins onto Cys-containing surfaces through NCL. B. Chemical structures of linkers **1** and **2**. C. Selective attachment of EGFP (lighter grey) and DsRed (darker grey) α -thioesters onto a Cys-containing glass slide. Epifluorescence image of the glass slide after the protein spotting (top) and after PBS washes (bottom). Spotting was carried out using 100 μ M protein solutions (left panel) and with variable concentrations (from 100 μ M to 20 μ M) of protein α -thioesters (right panel).

More recently we have developed a new approach for the more efficient immobilization of proteins onto surfaces through their C-termini [3]. This new method is based on protein trans-splicing (Fig. 2A) [4]. This naturally occurring process is similar to the protein splicing with the only difference that the intein self-processing domain is split in two fragments (called N-intein and C-intein, respectively). These two intein fragments alone are inactive. However, they can bind each other with high affinity under the appropriate conditions yielding a totally functional splicing domain. In our approach, one of the fragments (C-intein) is covalently attached to the surface through a small peptide-linker while the other fragment (N-intein) is fused to the C-terminus of the protein to be attached to surface. When both intein fragments interact, they form the active intein, which ligates the protein of interest to the surface at the same time the split intein is spliced

out into solution. Key to our approach is the use of the naturally split DnaE intein from *Synechocystis* sp. PCC6803. In contrast with other inteins engineered to act as trans-splicing elements, which only work after a refolding step, the C- and N-intein fragments of the DnaE intein are able to self-assemble spontaneously ($K_d \approx 0.7 \mu\text{M}$) not requiring any refolding step.

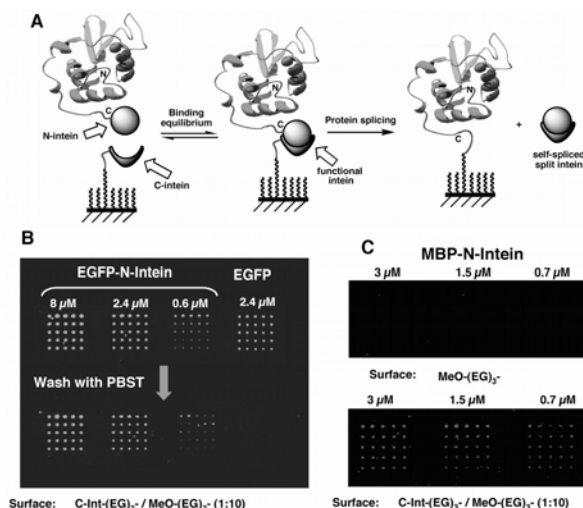


Fig. 2. *A.* Site-specific immobilization of proteins through its C-termini to a solid surface by using protein trans-splicing. *B.* Immobilization and detection of EGFP-DnaE-N-Intein fusion protein. *C.* Immobilization and detection of MBP-DnaE-N-Intein fusion protein. Immobilized MBP was detected by incubating first with anti-MBP monoclonal murine antibody and then with anti-mouse IgG-TRITC conjugate.

We have successfully used this approach for the efficient immobilization of Maltose binding protein (MBP) and EGFP onto a C-Intein-modified glass slide (Fig. 2B and 2C). In both cases the attachment was extremely selective with minimal background. Also, the minimum concentration required for effective protein immobilization was found to be lower than $1 \mu\text{M}$. This result demonstrates that this new method of protein immobilization can be easily interfaced with cell-free protein expression systems thus allowing rapid access to high throughput production of protein chips.

Acknowledgments

The work was performed under the auspices of the U.S. Department of Energy by the University of California, Lawrence Livermore National Laboratory, under Contract W-7405-Eng-48.

References

1. Muir, T.W. *Annu. Rev. Biochem.* **72**, 249-289 (2003).
2. Camarero, J. A., Kwon, Y. and Coleman, M. A. *J. Am. Chem. Soc.* **126**, 14730-14731 (2004).
3. Camarero, J. A. *Biophys. Rev. Lett.* **1**, 1-28 (2006).
4. Wu, H., Hu, Z. and Liu X. Q. *Proc. Natl. Acad. Sci. USA* **95**, 9226-9231 (1998).

Designed Peptide Microarrays for Protein Detection and Characterization

Kenji Usui¹, Kin-ya Tomizaki¹, Kiyoshi Nokihara² and Hisakazu Mihara¹

¹Graduate School of Bioscience and Biotechnology and the COE21 program, Tokyo Institute of Technology, Yokohama 226-8501, Japan; ²HiPep Laboratories, Kyoto 602-8158, Japan

Introduction

As improvement on genome-wide sciences, the development of protein-chips/microarrays [1] has been highly significant for the technology providing a high-throughput parallel detection method of target proteins. To realize a practical protein-chip system, novel peptide arrays have been constructed using designed peptide libraries with loop, α -helix or β -strand structures (Fig. 1) [2-5]. Additionally, we established peptide libraries with functional groups such as phosphorylated and glycosylated amino acids or nucleobase amino acids (NBAs) to increase the diversity of the peptide array system and to apply to focused proteomics. Furthermore, in order to develop more useful and convenient peptide arrays, we have achieved novel detection systems using an anomalous reflection (AR) of gold or a chromism-based assay (CHROBA) technique coupled with a photochromic molecule, and developed new array format procedures using a dry peptide array or a PNA-DNA hybrid array method. Statistic analyses of data obtained from the peptide arrays including the cluster analysis were also applied. The present concept and study, the structure-designed peptide array, promise realization of high-throughput protein nano/micro arrays for focused proteomics and ligand screening.

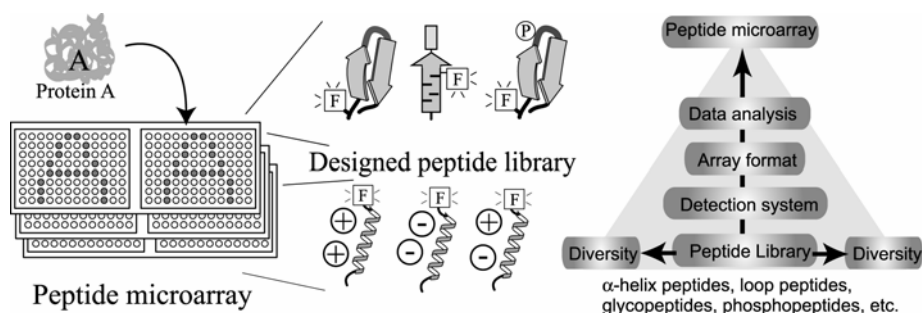


Fig. 1. Microarrays using designed peptide libraries.

Results and Discussion

Construction of a novel protein-detection system was carried out using a designed peptide library with fluorescent labels based on secondary and/or tertiary structures such as α -helix [2], loop [3], and β -strand [4] (Fig. 1). Initially, the fluorescent probes and suitable scaffolds of peptides were examined for the effective detection of proteins using several structured peptides known to interact with model proteins. In the case of α -helix peptides, the response of a peptide with fluorescent resonance energy transfer (FRET) between two probes at both termini was several times higher than that of a peptide with a single probe upon interactions with target proteins. In

the cases of peptides with other structures, however, proteins were effectively detectable even by the fluorescent change of single probe. Furthermore, structurally-focused libraries consisting of totally ca. 300 different peptides based on the model peptides were constructed with systematic replacement of residues and with functional groups such as phosphorylated, glycosylated amino acids or NBAs. Using these libraries, various proteins were characterized effectively to give their own fluorescent 'protein fingerprint (PFP)' patterns (Fig. 2). The resulting PFPs reflected the recognition properties of the proteins.

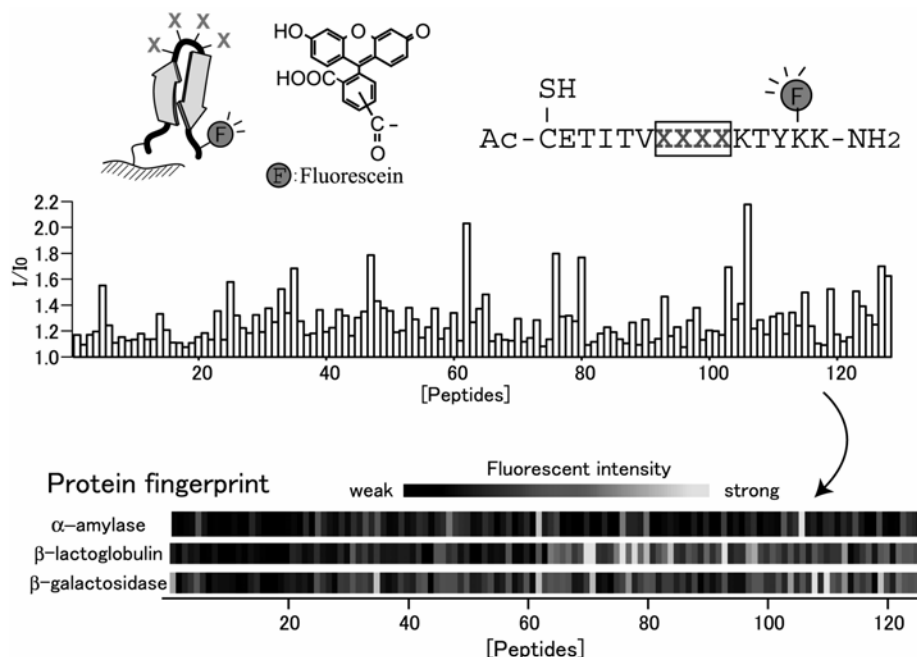


Fig. 2. The loop peptide library and fluorescence responses by addition of various proteins to give their 'protein fingerprints'.

For achievement of more robust and convenient peptide chips, we have also developed novel detection systems, array format procedures and statistic data analyses. In the case of the detection system, a novel gold AR technique was constructed. The system with designed peptides using AR of gold has an advantage that label-free samples are applied to the measurements using simple devices such as an optical fiber and LED within microscale gold spots. In addition, a unique CHROBA technique using photochromic spiropyran-containing peptides has been firstly established for the detection of protein kinase A-catalyzed phosphorylation based on the thermocoloration rates for a discrimination factor [6]. The alternative method has an advantage that isolation and/or immobilization of kinase substrates to remove excess reagents including non-reactive isotope-labeled ATP or fluorescently-labeled anti-phosphoamino acid antibodies from the reaction mixture can be avoided. For development of the array format procedures, we also constructed a new dry peptide array and PNA-DNA hybrid array methods. We describe here the dry

peptide array method. The dry peptide array method is an array preparation and assay procedure with dried samples of peptides and analyte proteins (Fig. 3A). The system has advantages that the dry peptide arrays are portable and that vaporization of sample solution needs not be taken care in a nano-liter solution measurement. In the nano-liter array format, a tiny amount of protein sample (20 pg) was detectable by the dry peptide array method (10 fmol peptide per spot). Finally, statistic data analyses from obtained PFPs including the cluster analysis were prosecuted. Taking the glycopeptide library for examples, it can be clearly described that the PFPs of lectins and those of glycosidases are clustered, respectively, when the Euclidean distance and the cluster analyses of the PFPs of saccharide-related proteins were performed (Fig. 3B). Especially, in the case of the cluster analysis, the PFP of α -amylase, whose substrates are α -anomer saccharides, was discerned from the PFPs of other glycosidases, whose substrates are β -anomer saccharides [5].

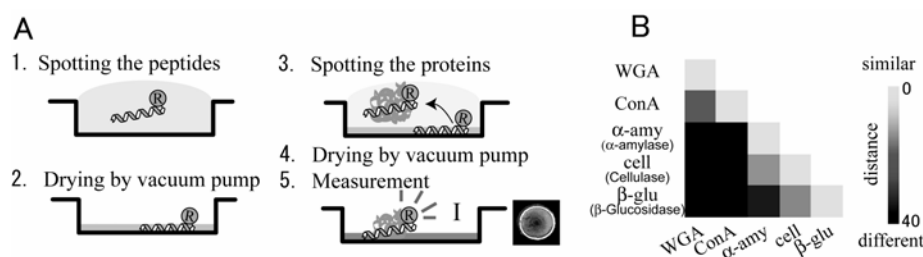


Fig. 3. (A) Illustration of the dry peptide array method. (B) The Euclidean distance matrix between the different sugar-binding PFPs in the glycopeptide library.

These studies demonstrate that the target proteins can be characterized using arrays with peptide libraries based on designed structures. Further improvement of the detection sensitivity and the number of peptides together with robotic handling will provide practical protein detection chips. The peptide chips will be applicable not only for proteomics studies including structure and binding specificity analyses but also for ligand screening assays. This technology could be a promising tool for researches in industrial, medical and/or environmental fields.

Acknowledgments

The authors thank Dr. Eiry Kobatake, Tokyo Institute of Technology, Japan, for array measurements, and Nippon Sheet Glass Foundation for support. The micro-well glass plates were generously provided by Nippon Sheet Glass Co., Ltd.

References

1. Tomizaki, K., Usui, K. and Mihara, H. *ChemBioChem* **6**, 782-799 (2005).
2. Usui, K., *et al.* *Mol. Diversity* **8**, 209-218 (2004).
3. Takahashi, M., Nokihara, K. and Mihara, H. *Chem. Biol.* **10**, 53-60 (2003).
4. Usui, K., Ojima, T., Takahashi, M., Nokihara, K. and Mihara, H. *Biopolymers* **76**, 129-139 (2004).
5. Usui, K., *et al.* *NanoBiotechnology* **1**, 191-200 (2005).
6. Tomizaki, K., Jie, X. and Mihara, H. *Bioorg. Med. Chem. Lett.* **15**, 1731-1735 (2005).

Luminescent Cd Te Quantum Dots/Albumin Conjugates: Preparation, Fluorescence, Characterization and Labeling of *C. Elegans*

Huilian Ma¹, Hanzhi Liu¹, Liping Wang¹, Shukun Xu² and Wei Li¹

¹*College of Life Science, Jilin University, Changchun, 130023, P. R. China;* ²*College of Science, Northeastern University, Shenyang, 110004, P. R. China*

Introduction

Recently, semiconductor quantum dots (QDs) have attracted great interest as new luminescent biological probes [1]. Compared with the conventional fluorophores, QDs have the potential to overcome problems encountered by organic small molecules in certain fluorescent tagging applications, by combining the advantages of high photo-bleaching threshold, good chemical stability, broad excitation spectra, narrow and symmetric emission spectrum in the visible wavelength range, and readily tunable spectral properties [2]. QD-protein conjugates were mostly characterized by UV-Vis spectrophotometer, spectrofluorometer, electrophoresis, etc. [2,3]. But the limitations of these methods such as the inability to get the pure component of the QD-protein conjugates and the detection results, which could also be influenced by other components, make it difficult to apply the conjugates to biological research. Here, we found that high performance liquid chromatography (HPLC) is a more efficient, fast, accurate, and reliable method compared to the published characterization and separation method [4]. Size exclusion chromatography column was used.

Nematode *Caenorhabditis elegans* (*C. elegans*) was used to study the imaging of QDs in the living organism. QDs and QD-BSA conjugates were phagocytized by *C. elegans*, and fluorescence localization of the luminescent particle was explored. This study provides a new method for locating and tracing biological molecules in the living organism.

Results and Discussion

QDs were attached to BSA via the use of coupling reagents. The carboxylic group of mercaptopropyl acid on QDs reacts with the amine groups of BSA to form an amide bond. A reaction mixture containing QDs, NHS, EDC (as the coupling reagent), BSA in pH 9.0 PBS buffer was prepared and kept at 37°C with intense shaking for 2-2.5 hours. After the conjugation was finished, Gly was added to quench the un-conjugated carboxyl group of QDs. The crude compound was purified by HPLC and phosphate buffer solution was used as eluent. The molecular mass of the QDs-BSA was found to be more than 100,000 by SDS-PAGE gel electrophoresis.

C. elegans was used as animal models to phagocytize QDs and QD-BSA conjugates. The locations of QDs and QD-BSA conjugates in *C. elegans* were observed by fluorescence microscopy. The red-emitting QD-BSA can be distinguished from the spontaneous green fluorescence of the worms. The result shows that red-emitting QDs and red-emitting QD-BSA conjugates not only can be easily swallowed by *C. elegans*, but also can be located in the body of the worms obviously because of the nearly transparent body (Fig. 1). Furthermore, the fluorescence intensity of QDs was enhanced when QDs were encapsulated by BSA,

so QD-BSA conjugates which are swallowed by the *C. elegans* are more clearly observed than the free QDs.

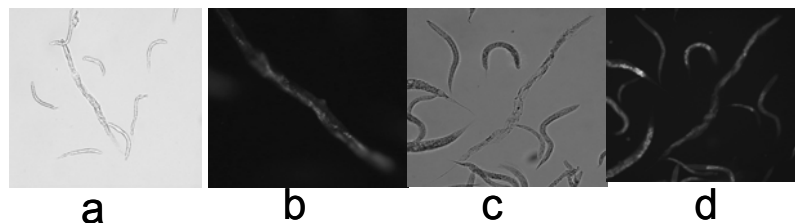


Fig. 1. The C. elegans with QDs and QDs-BSA conjugate at 628nm). The fluorescent images of C. elegans were recorded by using 10×objectives. a, c): the images of C. elegans in the light field; b, d): the corresponding photoluminescence images; C. elegans have swallowed QDs (a, b) and QD-BSA(c, d). The scale bar represents 100 μm.

In summary, the simple conjugation of QDs with BSA is a useful reference for the conjugation of QDs with other proteins and peptides. The separation and characterization of QD-BSA conjugates by using of HPLC is more accurate and reliable. The fluorescence imaging of QDs and QD-BSA conjugate in the organism of *C. elegans* provides a new way for the promising fluorescent QDs to be used in biological imaging.

References

1. Thomas, M. J. *Nature Biotechnol.* **21**, 32-33 (2003).
2. Wang, S. P., Mamedova, N., Kotov, N. A., Chen, W. and Studer, J. *Nano Lett.*, 2817-2822 (2002).
3. Mamedova, N. N., Kotov, N. A., Rogach, A. L. and Jor, S. *Nano. Lett.* 1281-1286 (2001).
4. Schafer, W. R. *et al. Neuropharmacology* **47**, 123 -131 (2004).

SC²: A Novel Process for Manufacturing of High Density Multi-Purpose Chemical Micro-Arrays

Antonius J. Dikmans, Ulrike Beutling, Sabine Thiele and Ronald Frank

Department of Chemical Biology, German Research Centre for Biotechnology, Mascheroder Weg 1, D-38124 Braunschweig, Germany

Introduction

The pivotal role of micro-arrays is emerging as one of the dominant and innovative analytic tools in a variety of research fields in the life sciences, including drug screening, genetics, and biomolecular recognition [1,2]. The manufacture of the array, which can entail immobilization of biomaterial, such as peptides, proteins, DNA or the *in situ* chemical synthesis of small organic molecules certainly plays an important role in its design and application. Novel array concepts still inspire the development of new technologies leading to faster and more accurate production of the desired analytical systems. With respect to the *in situ* synthesis of compound arrays, the SPOT technique is the prototype of the addressable reagent delivery strategy [3]. It is an established, easy, flexible and very economic synthetic procedure designed, originally, for the preparation of peptide repertoires on membrane-type carriers and planar surfaces. One of the drawbacks of the SPOT technology is the limitation of re-usability and multiple testing. Each array must be completely re-synthesised resulting in higher labor and chemical costs as well as time consumption. A second drawback is the size of the array generated, which corresponds with the current definition of a “macro” array, thus requiring large amounts of biological sample.

Results and Discussion

Our current research is particularly concerned with the implementation of a novel process, entitled SC² (Spotting Compound Support Conjugates), for manufacturing and application of peptide libraries (as well as other small molecule libraries) through the advancement of the current macro SPOT technology on cellulose to a micro-array format. The integrated process involves special new surfaces for the synthesis and printing of thousands of array replicates (cellulose-peptide conjugates) from only nmol scaled syntheses in densities up to 1000 spots per cm². The SC² process first involves normal SPOT synthesis of the desired array on a specially prepared cellulose membrane. After synthesis, the peptide-spots are endcapped and punched out into separate wells of 96 deepwell microtiter plates. During the side chain deprotection step with the TFA cocktail, however, the cellulose discs are allowed to fully dissolve, resulting in a clear solution of conjugate in each respective well. Precipitation of the cellulose-peptides with ether followed by several washing steps and re-dissolution in DMSO then provides a stock solution of each cellulose-peptide in its own respective well, which can then be printed by split pin (Microgrid TAS BioRobotics) to a glass microscope slide surface (Fig. 1).

As a proof of principle, the 120 hexapeptide array of NYGKYE (a known binding partner of mouse mAb 1D3), where each position of the peptide hexamer is exchanged for the 20 natural amino acids (6 x 20) in successive order (e.g., pos. 1: AYGKYE → YYGKYE, pos. 2: NAGYKE → NYGYKE, etc.) was synthesized. After application of the SC² process, the stock solutions were diluted 1:20 with DMSO, and printed to a surface-unmodified glass slide. Multiple copies of the 120

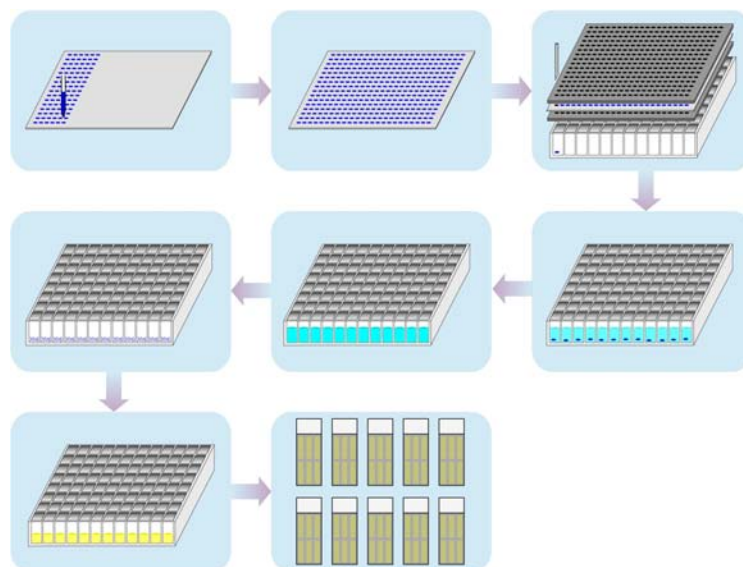


Fig. 1. SC^2 (Spotting Compound Support Conjugates) process for the generation of multiple copies of high-density arrays from SPOT membranes

peptide array fit easily within the borders of the glass slide. Figure 2 shows a comparison of the original 120 hexapeptide macro-array on a cellulose filter (bottom) with the current SC^2 array (top). Both were incubated with mouse mAb 1D3 (1:100 dilution), washed, and incubated a second time with tagged goat-anti-mouse antibody (macro-array tag: AP, micro-array tag: Cy5).



Fig. 2. Comparison of 120 hexapeptide NYGKYE array. Top: micro-array, 0.5 mm spot distance, 1 μ L 1D3 mAb; Bottom: macro-array, 5 mm spot distance, 10 mL 1D3 mAb.

Acknowledgements

This work was funded by German BMBF Grant # 01GR0102 as a subproject of NGFN-1, project KB-P8T01. The authors are solely responsible for the content presented within.

References

1. Freundlieb, S. and Gamer, J. *New Drugs* **3**, 54-60 (2002).
2. Frank, R. *Comb. Chem. High Throughput Screen.* **5**, 429-440 (2002).
3. Frank, R. *Tetrahedron* **48**, 9217-9232 (1992).

High Throughput Preparation of Peptide Arrays Containing Two Fluorescent Dyes Focusing on Practical Protein Detection Systems

Kiyoshi Nokihara^{1,2}, Takafumi Ohyama¹, Koichi Yonemura¹, Yasuo Oka³, Kenji Usui⁴ and Hisakazu Mihara⁴

¹HiPep Laboratories, Kyoto 602-8158, Japan; ²Nanjing Medical University, Nanjing 210029, China; ³Nippon Light Metal Company, Ltd., Shizuoka 421-3291, Japan; ⁴Graduate School of Bioscience and Biotechnology, Tokyo Institute of Technology, Yokohama 226-8501, Japan

Introduction

Novel high-throughput protein-detection systems for proteome studies are urgently required that can replace the classical combination of electrophoresis and mass spectroscopic analysis, as the number of different expressed proteins, including those generated by post-translational modifications, are extremely large in number. For this purpose we have successfully developed a novel concept that incorporates the interaction between proteins and designed peptide arrays (that involves loop, α -helix and β -strand), which are visualized with fluorescent labels to give a "protein fingerprint". This method allows a high-throughput characterization of such proteins [1-4].

The present concept with a bio-chip using designed peptide arrays for protein detection has many advantages. Synthetic peptides for arrays are more easily manufactured than arrays with proteins/antibodies with regard to conformational stability. Peptides can be immobilized in controlled amounts at any position in their sequence. The concept provides the flexible design of molecules for any sequence, any dye, and allows any functional molecule to be attached at any position. Unlike rDNA, oligosaccharides, lipids, spacers, cyclic compounds, and non natural amino acids can be applied. High-quality industrial production is guaranteed.

Key factors in the practical manufacturing process for peptide microarrays are development of chip materials, characterization of the array surface (for quality control), high throughput preparation of labeled peptides (high throughput synthesis), and characterization of arrayed peptides by the improved SPPS without complicated purification, followed by efficient deposition of peptides by an arrayer to afford good production economics. The present study describes some improvements that focus on the construction of a production system for novel bio-chips.

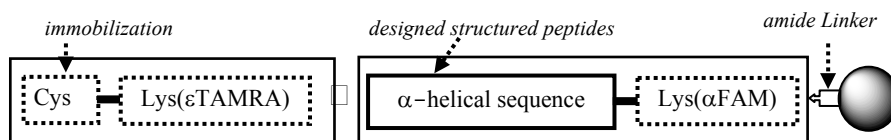


Fig. 1. Construction of arrayed peptides. Two fragments were coupled on solid-supports. The designed sequence has large diversity through replacement of amino acids.

Results and Discussion

To realize the highly efficient construction of labeled peptide libraries, improved protocols have been developed. FAM and TAMRA were selected for their stability

during assembly, storage and costs. The peptides used as sensing elements were designed in two parts. Hence, the segment with Cys for immobilization onto the chip surface and a fluorescent label (common among the diversity) were prepared on a larger scale as a protected fragment. The second unit may contain desired secondary and/or tertiary structures (that interact with proteins) and has a large diversity of possible side chain functions. Figure 1 illustrates the scheme of array construction.

Amorphous carbon was developed as a novel chip material. This has significant advantages over conventional glass or polymers, such as lower costs, mechanically more stable, easy manufacturing (precised and high throughput processing), and no self fluorescents. The surface has been derivatized through carbon radical formation by ammonia irradiation or argon plasma/oxidation with aryl amine treatment to give amino groups. The surface was characterized by X-ray photoelectron spectroscopy (XPS), although XPS data do not directly correlate with reaction stoichiometry. A microtitration method using a commercial automated titration apparatus or ultra microscale ion analysis using electric conductivity detector has been developed. The results revealed that the loading amounts on a chip surface is much smaller compared to polymer support for SPPS. For example a commercial amino-slide glass was 2.6 pmol/mm² and the present amino-carbon plate was 4.4 pmol/mm². The present methods can be used for quality control of bio-chip surface.

The present studies based on the successfully developed method, which uses visualization in a barcode like pattern (the protein finger print) generated by the designed labeled peptide arrays with various proteins, afford a high throughput protein detection and characterization system. Because designed peptide microarrays are more easily manufactured and more stable than those using proteins/antibodies, our strategy has a significant advantage for protein chip-production on an industrial scale.

Acknowledgments

A part of this work was funded by the Millennium Project, MEXT (2000-02), Okinawa-Bio-Project (2004-2006) and NEDO-Grant (2005-2006) to K. Nokihara.

References

1. Takahashi M., Nokihara K. and Mihara H. *Chemistry Biol.*, **10**, 53-60 (2003).
2. Usui K., Ojima T., Takahashi M., Nokihara K. and Mihara H. *Biopolymers*, **76**, 129-139 (2004).
3. Usui K., Takahashi M., Nokihara K. and Mihara H. *Mol. Diversity* **8**, 209-218 (2004).
4. Nokihara K., Ohyama T., Usui K., Yonemura K., Takahashi M. and Mihara H., in *Solid Phase Synthesis and Combinatorial Chemical Libraries 2004* (Epton, R., ed.) Mayflower Worldwide Ltd, Kingswinfold, UK, pp. 83-88 (2004).

Identification of Antioxidant Peptides using SPOT Synthesis

Marloes Schurink^{1,2}, Willem J. H. van Berkel¹, Harry J. Wichers² and
Carmen G. Boeriu²

¹Laboratory of Biochemistry, Wageningen University, Dreijenlaan 3, 6703 HA Wageningen,
the Netherlands; ²Agrotechnology & Food Innovations, Bornsesteeg 59, 6708 PD
Wageningen, the Netherlands

Introduction

Oxidation reactions catalyzed by enzymes such as lipoxygenases and polyphenol oxidases initiate food quality decay. Oxidative enzymes also have a health impact and are involved in certain diseases. Most antioxidants exert their function by scavenging free radicals or by reducing oxidation products formed in enzyme catalyzed oxidation reactions. The oxidative enzyme activity, which is the cause of the formation of these oxidized compounds, is however not removed. In addition, most of the conventional oxidative enzyme inhibitors are synthetic, unstable, difficult to obtain and cannot be used in food, cosmetics or medicines. Hydrolyzed proteins from animal and plant sources have been found to possess antioxidant activity. They have a potential to be used as alternative, natural antioxidants.

Our aim is to identify peptides from industrial proteins that have antioxidant properties and specifically inhibit the enzymes mentioned above (Fig. 1). Protein hydrolysates are complex mixtures of amino acids and peptides of which individual effects most probably will interfere with each other. Moreover, not only the preferred enzyme inhibition, but also several other mechanisms, such as radical scavenging, accumulation of the peptides at the lipid/water interface and changes of the physico-chemical state of the substrate, may account for a decreased oxidation rate. Therefore, we have chosen a novel approach using SPOT synthesis [1] for the selection of potential inhibitory peptides. The principle of this approach lies in the fact that for a peptide being an enzyme inhibitor, it should be able to bind to the enzyme.

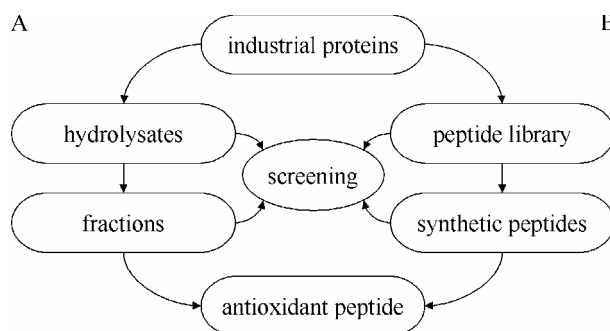


Fig. 1. Two approaches in the search for antioxidant peptides: (A) hydrolysis and (B) SPOT synthesis.

Results and Discussion

Since several peptides derived from β -casein are able to inhibit the lipoxygenase catalyzed oxidation of linoleic acid [2], β -casein was chosen as a starting-point.

Using SPOT synthesis, arrays of β -casein derived peptides comprising the complete β -casein amino acid sequence were synthesized in defined positions on cellulose sheets. In this way, 367 different peptide sequences were prepared at a nmol scale. Incubating the cellulose bound peptide library with fluorescently labeled lipoxxygenase (Fig. 2) resulted in a set of peptides that showed interaction with this enzyme. These peptides were synthesized on a larger scale by solid phase peptide synthesis to obtain the free peptides suitable for enzyme inhibition and radical scavenging assays. Two of the selected peptides showed a true lipoxxygenase inhibition [3], i.e., they specifically inhibit the lipoxxygenase activity. The mode of inhibition is presently addressed in more detail.

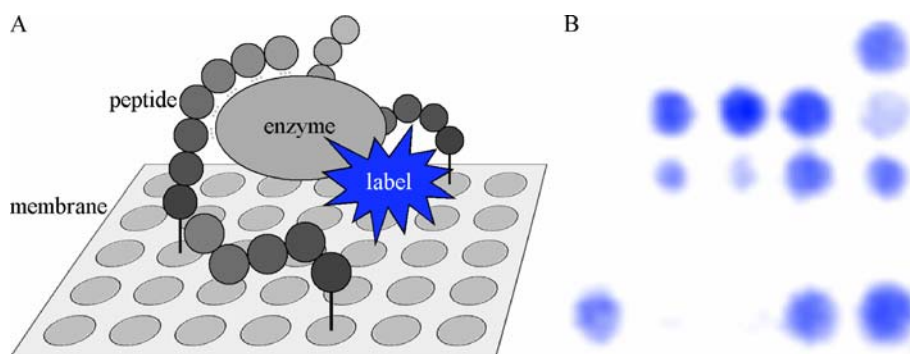


Fig. 2. High-throughput screening of a peptide library: (A) schematic representation and (B) spots containing β -casein peptides that interact with fluorescently labeled lipoxxygenase.

The importance of peptide amino acid constituents in the recognition of lipoxxygenase will be determined by synthesis of mutational analogs of the inhibiting peptides. This might also improve binding interactions and consequently the inhibitory activity of these peptides.

Acknowledgments

This work was supported by the innovation driven program IOP Industrial Proteins (project IIE00022) of the Ministry of Economic Affairs of the Netherlands, and by Cargill, Cebeco Egg Research, Cosmoform BV and DMV International.

References

1. Frank, R. *Tetrahedron* **48**, 9217-9232 (1992).
2. Rival, S. G., Fornaroli, S., Boeriu, C. G. and Wichers, H. J. *J. Agric. Food Chem.* **49**, 287-302 (2001).
3. Schurink, M., Boeriu, C. G., van Berkel, W. J. H. and Wichers, H. J. *European Patent Application* 04077592.6 (filed 2004).

Water Channel (Aquaporin 3) Gene Activation Correlates with Substance P in ARDS

Simon S. Wong, Nina N. Sun and Mark L. Witten

Lung Injury Laboratory, Department of Pediatrics, College of Medicine, University of Arizona, Tucson, AZ 85724, USA

Introduction

Substance P (SP) is an important member of tachykinin and consists of 11 amino-acids: Arg-Pro-Lys-Pro-Gln-Gln-Phe-Phe-Gly-Leu-Met-NH₂ [1]. In the human respiratory tract, SP is synthesized in the ribosome of the primary sensory neurons and neurons intrinsic plexus as a larger protein and then enzymatically converted into the active undecapeptide. SP-immunoreactive nerves are located beneath and within the epithelium, around submucosal bronchial glands, bronchial blood vessels, and to a lesser extent within airway smooth muscle. The effects of SP on target cells are mediated by at least three specific receptors, the neurokinin-1 receptor (NK-1R), NK-2R, and NK-3R. But SP appears to preferentially activate a distinct NK-1R (the relative affinity is 100 and 500-fold higher than for NK-2R and NK-3R, respectively). Although SP is known to be involved in 'neurogenic inflammation' that links to normal physiology and pulmonary diseases such as acute lung injury, its signal transduction pathways in many pathophysiological processes remains unclear. In this regard, we examined transcriptome alterations in the homolized lung tissue in a rat model of smoke inhalation injury [2]. We found that a specific NK-1R antagonist significantly attenuated a water channel (aquaporin 3) gene expression. Our finding revealed that SP, via its NK-1R, could have clinical utilization in a water balance-related pathophysiological process through modulation of water channels.

Results and Discussion

We examined 28,757 genes cDNA microarrays for transcriptome alterations in the inflamed lung tissue. Treatment of rats with SR 140333B (10 mg/kg, i.m.), a specific NK-1R antagonist, fully prevented smoke inhalation and induced 60 gene alterations at 24 h after insult in addition to significantly attenuating another 23 genes. Among them, prominent effects include regulation of water channels (aquaporin 3, 13.02-fold when compared to controls), electron transport (Cyp2e1, 6.67-fold), cytoskeleton (Acta1, 10.51-fold; Myh6, -4.61-fold), and motor activity (Apb1, 5.47-fold) after insults (Table 1). However, NK-1R antagonist significantly

Table 1. Gene modulation of neurokinin-1 receptor antagonist

Gene ID	Name	Activity	Smoke only	Smoke + NK-1R antagonist
NM031703	Aquaporin 3	Water channel	13.02	3.95
NM019212	Actin-alpha	Structural activity	10.51	0
NM031543	Cyp2e1	Cell fraction & monooxygenase	6.67	0
NM053587	Apb1	Phospholipase & motor activities	5.47	0
NM017239	Myh6	Nucleotide binding	-4.61	-1.84

attenuated or prevented these genetic alterations. Therefore, these identified genes reveal that there exists a complex molecular cascade involving SP signal transduction, further influencing water permeability via water channels. This finding may provide new insight into the mechanism of transepithelial water regulation in the lungs because it is known that aquaporin 3 is expressed not only in large airways, but also in bronchioles, and is related to water movement in pulmonary edema.

To confirm the effect of SP on aquaporin 3 expression, we are conducting *in vitro* experiment by using respiratory epithelial cell lines. Hopefully, this and further studies will confirm the role of SP in the regulation of water channels. As we know, water transport across pulmonary epithelia is a vital component of normal physiology and pathophysiological conditions. In proximal airways, transepithelial water movement replaces insensible water loss; in the perinatal period, water is reabsorbed across the alveolar epithelium during the transition from fetal to *ex utero* life; and in all airway regions, transepithelial water flux is responsible for maintenance of an isotonic airway surface liquid [3]. Especially, aquaporin 3 has been an "aquaglyceroporin" because it is capable of transporting glycerol and urea, in addition to transporting water. Its role as a solute channel and the relevance of this function in human bronchial epithelial physiology may be especially important due to aquaporin 3-expressed basal cells that do not face the airway lumen. This structural location may account for the rapid shrinkage and water efflux in this cell type in response to subepithelial osmotic gradients [4]. Most recently, aquaporin 3 was observed to localize on the basolateral membrane of alveolar type II pneumocytes, suggesting its role of water balance in alveoli. Therefore, additional structure functional studies after SP treatment are necessary to understand the role of aquaporin 3 in the human lungs and its contribution to lung disease.

Additionally, aquaporin 3 has been found in the basolateral membrane of principal cells through the renal collecting duct, the meningeal cells at the surface of the brain, the conjunctival epithelial cells of the eye, and on the basolateral membrane of villous epithelial cells of the distal colon. Recent findings also demonstrate that the expression of aquaporin 3 is found in tumor cells and is associated with an early stage of cancer development [5]. Collectively, increasing data support many fundamental roles of water channels in cell migration, angiogenesis, wound healing, carcinogenesis, and organ regeneration. We speculate that SP may have regulatory functional role on water balance in physiology and pathophysiological conditions of these organs or tissues.

Acknowledgments

The work was partially funded by National American Lung Association and U. S. Air Force.

References

1. Chang, M. M. and Leeman, S. E. *J. Biol. Chem.* **245**, 4784-4790 (1970).
2. Wong S. S., *et al. Am. J. Physiol. Lung Cell Mol. Physiol.* **287**, L859-L866 (2004).
3. Kreda, S. M., *et al. Am. J. Respir. Cell Mol. Biol.* **24**, 224-234 (2001).
4. Matsui, H., C. *et al. J. Clin. Invest.* **105**, 1419-1427 (2000).
5. Moon, C., *et al. Oncogene* **22**, 6699-6703 (2003).

Proteomics and Emerging Technologies

RDC as a New NMR-Parameter for Peptides

**Horst Kessler, Burkhard Luy, Kyryl Kobzar, J. Christoph
Freudenberger, Sebastian Knör, Dominik Heckmann and Jochen Klages**

Department Chemie, TU München, Lichtenbergstr. 4, 85747 Garching, Germany

Introduction

The structure determination of peptides by NMR often struggles with the limited information about long-range orientations. These arrangements are highly desirable to monitor e.g. global bends or twists within β -sheets. Classical NMR parameters like NOE intensities and scalar couplings usually only give structural information about the nearest neighbourhood. This problem can be overcome by the use of residual dipolar couplings (RDCs) as they provide relative orientations of internuclear vectors [1]. These couplings are therefore not subjected to any limitations regarding the distance of these vectors and can be used for structural refinement. RDCs have proven to be a beneficial tool for the analysis of protein structures but their application to small molecules like peptides has so far been limited. This is due to the fact that the measurement of RDCs requires partial alignment of the molecules. Although numerous alignment media are known for the partial alignment within aqueous solutions like filamentous phage, phospholipid bicelles, or liquid crystalline phases, only very few had been available for organic solvents. During the past years new alignment media such as cross-linked poly(styrene) (PS) [2], poly(dimethylsiloxane) (PDMS) [3], or poly(vinylacetate) (PVAc) [4] have been designed, applicable for all common NMR solvents like e.g. DMSO and CDCl_3 . These media have the advantage over previously used (e.g., poly- γ -benzyl-L-glutamate (PBLG) [5]) that the observed dipolar coupling can easily be scaled by adjusting the sample temperature or the degree of cross-linking resulting in sharp signals and high resolution spectra.

Residual dipolar couplings (D) can be best observed via their contribution to the scalar coupling (J). As dipolar couplings average to zero in isotropic solutions, RDCs are simply the signed difference in isotropic and aligned couplings. For samples at natural abundance, $^1\text{J}_{\text{CH}}$ couplings are the most easily observed due to good sensitivity and high resolution of heteronuclear correlation experiments.

The application of residual dipolar couplings for the structural refinement of peptides is demonstrated on the well-studied immunosuppressant drug Cyclosporin A (CsA) [6]. The resulting structure is compared to the crystal structure [7] and a structure just based on NOE distance restraints [7,8].

Results and Discussion

In this study we have used a PDMS-gel crosslinked by accelerated electrons [3] to partially align a sample of CsA in chloroform. Conventional sensitivity-enhanced $^{13}\text{C}, ^1\text{H}$ -HSQC-spectra have been acquired without heteronuclear decoupling in the directly detected dimension. Altogether 35 D_{CH} couplings in the range of -22.3 to 27.9 Hz could be extracted.

For the structure calculation all 35 RDCs in concert with 114 NOE distance restraints were used. The calculation was performed with the help of the software package XPLOR-NIH [9] where RDCs can be incorporated as angular restraints. A highly defined set of structures could be obtained where the best 10 out of 20

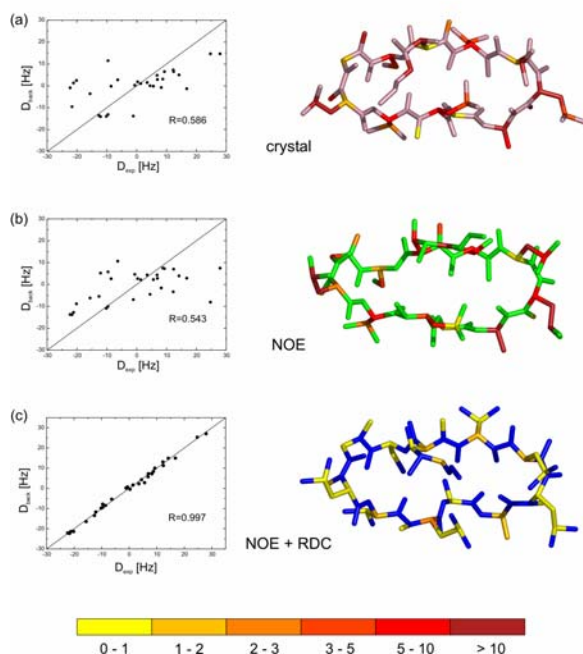


Fig. 1. Experimental vs. back-calculated DCH couplings for the RDC-refined structural model of CsA and visualization of the differences. The correlation factor $R=0.997$ of the RDC-refined structure represents the fact that all RDCs are very close to the experimental error. The color coding is given below with yellow indicating deviations of less than 1 Hz and "hotter" colors indicating stronger deviations.

present inside the PDMS-gel.

For comparison, the backbone of the lowest energy RDC-refined structure of CsA is shown in Figure 2, superimposed with the crystal and NOE-derived structures over the well-defined β II' turn spanning residues 2-5. The difference in backbone planarity is immediately obvious, explaining the poor correlation of experimental vs. back-calculated RDCs in the crystal and NOE-derived structures. While the crystal structure appears to be flattened, presumably due to crystal packing effects, the NOE-derived structure shows a slight bend in the backbone around residues 11-1 and 6-7. In the RDC-refined structure, however, this bend appears to be significantly stronger, caused by the sum of slight changes in backbone angles of

calculated structures showed a very small RMSD value of only 0.12 Å over all heavy atoms. All RDC restraints are very close to being fulfilled within experimental error, as shown in Figure 1c. The correlation between measured and back-calculated RDCs is $R=0.997$. It is worth noting that, in addition to RDC restraints, the structure still fulfills all NOE-derived distance restraints. RDCs were also fitted to the existing crystal and NMR structures based only on NOE restraints using the program PALES [9]. In both cases a scattering of back-calculated vs. measured RDCs was obtained with poor overall correlations of $R=0.586$ and $R=0.543$ for the crystal and NOE-derived structure, respectively (Fig. 1a, b). We therefore conclude that neither one of the structures represents the time-averaged structure

residues 6-11. This clearly indicates that the short-distance NOE-derived restraints alone do not confer this long-range conformational arrangement.

When measuring RDCs in an alignment medium, one always has to be aware that the gel or liquid crystal works as a co-solvent and might influence the structure of the solute to some extent (as was shown previously for oligosaccharides in liquid

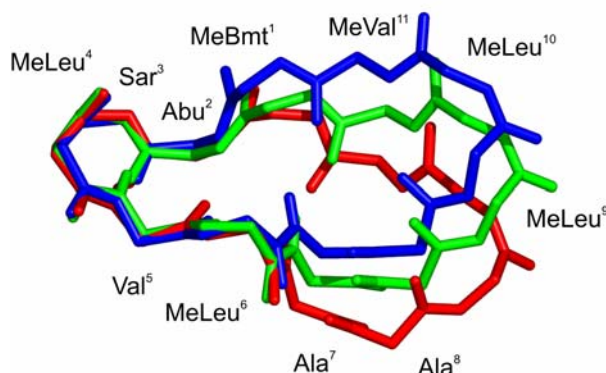


Fig. 2. Superimposition of the highly defined $\beta II'$ turn of the crystal structure (red), the NOE-derived NMR structure (green) and the RDC-refined structure (blue).

the PDMS/chloroform gel we compared the ^1H and ^{13}C chemical shifts of all relevant cross peaks and found only very minor deviations which are generally less than 0.3 ppm for carbons and less than 0.07 ppm for protons. Taking into account that chemical shift changes are expected due to residual chemical shift anisotropy, potential structural changes can be considered to be of minor importance.

Acknowledgments

The work was funded by the Fonds der Chemischen Industrie and the DFG (Emmy-Noether-fellowship LU 835/1-1; Ke 147/37-1).

References

1. Tolman, J. R., Flanagan, J. M., Kenned, M. A. and Prestegard, J. H. *Proc. Natl. Acad. Sci. USA* **92**, 9279-9283 (1995).
2. Luy, B., Kobzar, K. And Kessler, H., *Angew. Chem. Int. Ed.* **43**, 1092-1094 (2004).
3. Freudenberger, J. C., Spiteller, P., Bauer, R., Kessler, H. and Luy, B. *J. Am. Chem. Soc.* **126**, 14690-14691 (2004).
4. Freudenberger, J. C., Knörr, S., Kobzar, K., Heckman, D., Paulutat, B. And Luy, B. *Angew. Chem. Int. Ed.* **44**, 423-426 (2005); Habertz, P., Farjon, J., Griesinger, C. *ibid* 427-429.
5. Thiele, C. M. *J. Org. Chem.* **69**, 7403-7413 (2004).
6. Loosli, H. R., Kessler, H., Oschkinat, H., Weber, H. P., Petcher, T. J. and Widmer, A. *Helv. Chim. Acta* **68**, 682-704 (1985); Kessler, H., Köck, M., Wein, T. and Gehrke, M. *Helv. Chim. Acta* **73**, 1818-1832 (1990).
7. Klages, J. Neubauer, C., Coles, M., Kessler, H. and Luy, B. *Chembiochem.* **6**, 1672-1678 (2005).
8. Tjandra, N., Omichinski, J. G., Gronenborn, A. M., Clore, G. M. and Bax, A. *Nat. Struct. Biol.* **4**, 732-738 (1997).
9. Zweckstetter, M. and Bax, A. *J. Am. Chem. Soc.* **122**, 3791-3792 (2000).
10. Berthault, P., Jeannerat, D., Camerel, F., Salgado, F. A., Boulard, Y., Gabriel, J. -C. P. and Desvaux, H. *Carbohydrate Res.* **338**, 1771-1785 (2003).

Examination of the Role of Lipid Rafts in GPCR Signal Transduction Using Plasmon Waveguide Resonance (PWR) Spectroscopy

Victor J. Hruby^{1,2}, Isabel D. Alves^{1,2}, Savitha Devanathan², Zdzislaw Salamon² and Gordon Tollin^{1,2}

¹*Department of Chemistry;* ²*Department of Biochemistry and Molecular Biophysics;*
University of Arizona, Tucson, Arizona 85721, USA

Introduction

The fluid mosaic model [1] has been the standard view of membrane protein structure for many years. Recent evidence suggests that the standard model is inadequate, and that lateral segregation of membrane components occurs which leads to microdomains (lipid rafts) in the membrane bilayer [2]. These microdomains could play a critical role in receptor transduction. However, it has been difficult to study this phenomena directly because of the highly anisotropic nature of proteolipid bilayers and the need to chemically modify the proteins and/or the lipids with spectral probes that may modulate the intrinsic properties of the system.

We have been developing a new spectroscopic method, plasmon waveguide resonance (PWR) spectroscopy [3,4] which allows the direct examination of the structural properties of proteolipid bilayers containing integral membrane proteins, including GPCRs without using labels. This method can evaluate structural changes accompanying interactions of receptors with their ligands and G-proteins and their modulation of transduction, including GDP/GTP exchange [e.g. 5,6], thereby providing new insights into GPCR properties, and new approaches to drug design. In this report, we have used PWR to examine the partitioning of the delta opioid receptor (DOR) into a solid-supported lipid bilayer system composed of a 1:1 mixture of palmitoylcholine-phosphatidylcholine (POPC), and brain sphingomyelin (SM). This lipid mixture spontaneously forms POPC-rich and SM-rich microdomains that can be directly observed using PWR. We demonstrate ligand-directed partitioning of the DOR into these microdomains, and the effect of microenvironment on G-protein binding and activation of the agonist occupied DOR, which may be critical to signal transduction.

Results and Discussion

The formation of the lipid bilayer on the resonator surface of the PWR spectrometer, the incorporation of the purified DOR into the lipid bilayer, and the further incorporation of the G-proteins into the system were accomplished as previously reported [5,7,8]. PWR spectra were obtained with a Proterion Corp. (Piscataway, N.J.) instrument that had an angular resolution of 1 mdeg. PWR spectra were obtained using light from a polarized CW laser (He-Ne, $\lambda = 632.8$ or 543.5 nm) using both s and p polarized light. This allows determination of two refractive index values (n_s and p_s) as well as the sample thickness t , thus providing information about changes in mass density, structural asymmetry, and molecular orientation resulting from biomolecular interactions at the resonator surface. PWR spectra were simulated for spectra containing more than one resonance by superposition of single resonance curves that were obtained for bilayers composed of single lipid components, and the complex spectrum which was obtained from the bilayer formed

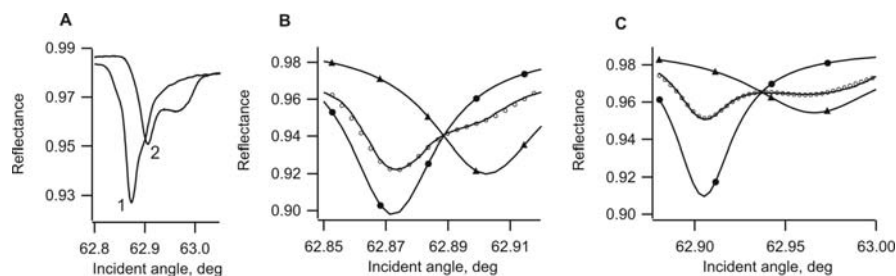


Fig. 1. PWR spectra of a solid-lipid supported bilayer formed from a 1:1 mixture of POPC and SM (panel A, curve 1) and for incorporation of DPDPE-bound hDOR into the lipid bilayer (A, curve 2). Experimental spectra and simulation of the bilayer before (B) and after (C) agonist-liganded hDOR incorporation are shown. In the B and C panels, the solid curves containing the open symbols show the experimental and simulated spectra. The solid curves with the filled symbols represent the deconvoluted single-lipid component spectra for POPC (circles) and SM (triangles) obtained from the simulated fits. The simulated fit to the experimental spectrum is an appropriately weighted sum of the component curves. Data from ref. 10.

from binary lipid mixtures was deconvoluted into a sum of single component spectra [see 9 for details]. The same procedure was for examining lipid bilayers containing the receptor and G-proteins thereby allowing the evaluation of the sorting of such proteins into the separate microdomains. Binding affinities of ligands, G-proteins, and GTP γ S were determined as previously reported [5,7]. The deconvolution shown in panel B of Figure 1 yields a thickness of 5.4 ± 0.1 nm and a surface area per lipid of 0.49 ± 0.01 nm² for the lower angle component, and a thickness of 6.0 ± 0.1 nm and a surface area per lipid of 0.41 ± 0.01 nm² for the higher angle component (separate experiments with a pure POPC bilayer gave values of 5.4 nm and 0.48 nm², respectively, and for a pure SM bilayer 6.1 nm and 0.39 nm², respectively [9]). We conclude from these values that the lower angle component corresponds to a POPC-rich microdomain, and the higher angle component to a SM-rich microdomain. Inspection of the spectra in the left panel reveals that the higher angle component is shifted to a greater amount than the lower angle component by agonist-bound DOR incorporation, indicating that the receptor inserts preferentially into the SM-rich microdomain. Deconvolution of this spectrum into single components (shown in the right hand panel) supports this conclusion. Experiments with the hDOR in the absence of ligand (i.e., the unoccupied receptor), and with the receptor occupied with the receptor antagonist naltrindol (NTI) demonstrated that the unoccupied hDOR prefers the POPC-rich bilayer phase, whereas the antagonist (NTI)-occupied hDOR preferred the SM-rich microdomains, although to a lesser degree than the agonist bound receptor. These results can be explained by reference to our previous observation [5] that the hDOR adopts different conformations upon binding of different classes of ligands. Thus, as shown below, the SM-rich bilayer is thicker than the PC-rich bilayer as a consequence of having longer saturated acid lipid chains. Our previous PWR studies have shown that the DPDPE bound receptor is more elongated than either the unliganded or antagonist-bound receptor. This suggests that hydrophobic matching between the receptor and bilayer provides the basis for different receptor partitioning. Thus, the unliganded hDOR, which is less elongated, prefers the POPC-rich lipid microdomain, with the antagonist intermediate. It also is possible that the agonist occupied receptor is recruiting SM

Table 1. Interactions of the G-protein ($G_{i\alpha 2} + \beta\gamma$) with DPDPE-hDOR and GTP γ S interaction with the ligand-receptor-G protein complex

Polarization	K_D (G-protein), nM ^a		K_D (GTP γ S), nM	
	<i>p</i>	<i>s</i>	<i>p</i>	<i>s</i>
POPC:SM(1:1), POPC rich	6*	19	12*	11
POPC:SM(1:1), SM rich		0.6		10

K_d values were obtained by plotting the resonance minimum position for the PWR spectra as a function of G-protein concentration and fitting them to the following hyperbolic function for binding: $Y = (B_{max} \times X) / (K_d + X)$. *Due to the difficulty of separating the spectral changes upon interaction of G-protein with the PC-rich and SM-rich domains for the p-polarized spectra, only one value is presented which is obtained from the major minimum.

molecules to its immediate environment rather than moving into an SM-rich microdomain. Finally, we examined the interactions of G-proteins with the agonist DPDPE bound to the hDOR using the $G_{i\alpha 2}$ -subunit containing G-protein which we previously showed [6] had the highest affinity for the DPDPE-hDOR complex. As demonstrated in Table 1, this G-protein subtype has a 60-fold higher affinity for the DPDPE-receptor complex that is present in the SM-rich microdomain ($K_D = 0.6$ nM) than for the receptor present in the POPC-rich microdomain ($K_D = 19$ nM). On the other hand, the affinity of GTP γ S for the agonist occupied receptor was not affected by the lipid microenvironment demonstrating that G-protein binding and activation (GTP γ S binding) are influenced differently by the properties of the receptor microenvironment [6].

In conclusion, we have demonstrated that PWR spectroscopy provides a powerful tool to examine lipid segregation into microdomains and allows direct examination of incorporation of GPCRs into bilayers containing such microdomains and its modulation by ligand binding. In addition, it allows quantitation of G-protein binding to the receptor complexes in the microdomains and the effect of microenvironment on activation. In future experiments we will examine directly the effects of other lipid components such as cholesterol, kinases, and phosphatases.

Acknowledgments

This work was supported by grants from the U.S. Public Health Service and NIDA, by NIH and by the V. P. for Research, University of Arizona.

References

1. Singer, S. J. and Nicolson, G. L. *Science* **175**, 720-731 (1972).
2. Simons, K. and Vaz, W. L. C. *Ann. Rev. Biophys. Biomol. Struct.* **33**, 269-295 (2004).
3. Salamon, Z., Macleod, H. A. and Tollin, G. *Biophys. J.* **73**, 2791-2797 (1997).
4. Tollin, G., Salamon, Z. and Hruby, V. J. *Trends Pharma. Sci.* **24**, 655-659 (2003).
5. Salamon, Z., Cowell, S., Varga, E., Yamamura, H. I., Hruby, V. J. and Tollin, G. *Biophys. J.* **79**, 2463-2474 (2000).
6. Alves, I. D., Ciano, K. A., Boguslovsky, V., Varga, E., Salamon, Z., Yamamura, H. I., Hruby, V. J. and Tollin, G. *J. Biol. Chem.* **279**, 44673-44682 (2004).
7. Alves, I. D., Salamon, Z., Varga, E., Yamamura, H. I., Tollin, G. and Hruby, V. J. *J. Biol. Chem.* **278**, 48890-48897 (2003).
8. Alves, I. D., Salgado, G. F. J., Salamon, Z., Brown, M. F., Tollin, G. and Hruby, V. J. *Biophys. J.* **88**, 198-210 (2005).

9. Salamon, Z., Devanathan, S., Alves, I. D. and Tollin, G. *J. Biol. Chem.* **280**, 11175-11184 (2005).
10. Alves, I. D., Salamon, Z., Hruby, V. J. and Tollin, G. *Biochemistry* **44**, 9168-9178 (2005).

Switchable Inteins: New Tools to Control Protein Function by using Regulated Protein Splicing

Steffen Brenzel, Christina Ludwig and Henning D. Mootz

Department of Chemistry/Biochemistry, Philipps-University of Marburg,
 Hans-Meerwein-Str. 35032 Marburg, Germany

Introduction

Inteins are intervening protein elements that autocatalytically excise themselves from their host protein in a post-translational reaction (Fig. 1) [1]. This process is referred to as protein splicing. It leads to the formation of the mature protein by linking the flanking N- and C-terminal sequences, the so-called N- and C-exteins, with a native peptide bond. The excised intein is the second product of the reaction.

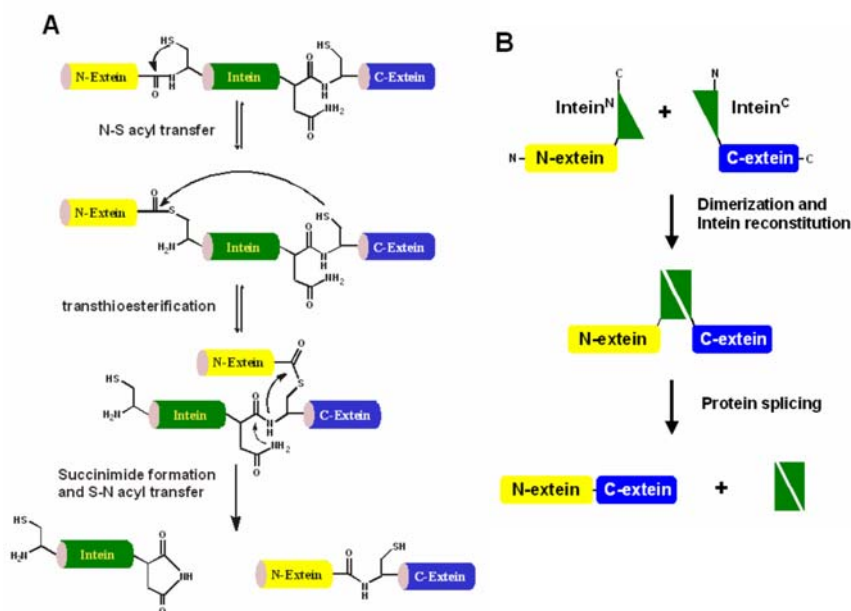


Fig. 1. Protein splicing and protein-trans-splicing. (A) The mechanism of protein splicing highlighting the key amino acids that are conserved in most inteins. The cysteine nucleophiles are frequently found to be replaced by serine or threonine residues. (B) Protein-trans-splicing is mediated by a split intein domain located on separate polypeptides. Once the intein is reconstituted the mechanism of protein splicing is believed to occur as shown in (A).

Protein-trans-splicing is a special form of protein splicing in which the intein domain is split into two parts. These Int^N and Int^C parts first have to reassemble to fold into the active intein and proceed with the reaction of protein splicing. The only characterized intein that is natively found in the split form is the *Ssp* DnaE intein. In contrast, over 200 “cis”-inteins have been identified so far in all three branches of life [2]. While the physiological role of inteins is still a matter of debate, their potential for the protein chemist in protein engineering approaches is eminent and

exploited in many ways. The usefulness of inteins as molecular tools stems from at least three reasons: (i) Inteins are very promiscuous toward their extein sequences and can therefore be inserted into heterologous host proteins by genetic means. (ii) Mutation of key residues can selectively impair one part of the reaction. For example, mutation of the Cys1 nucleophile to Ala will abolish thioester formation but still lead to succinimide formation and thereby C-terminal hydrolysis of the C-extein (compare Fig. 1). (iii) Split intein parts can be separately prepared (e.g., by solid phase synthesis or expression in cells grown in labeled media and allow for the segmental isotopic labelling of proteins for NMR studies. Consequently, inteins have mostly been used for preparative purposes in protein chemistry. The probably best known application is the generation of protein thioesters for subsequent chemical ligation of polypeptides containing an N-terminal cysteine residue (“expressed protein ligation”) [3,4].

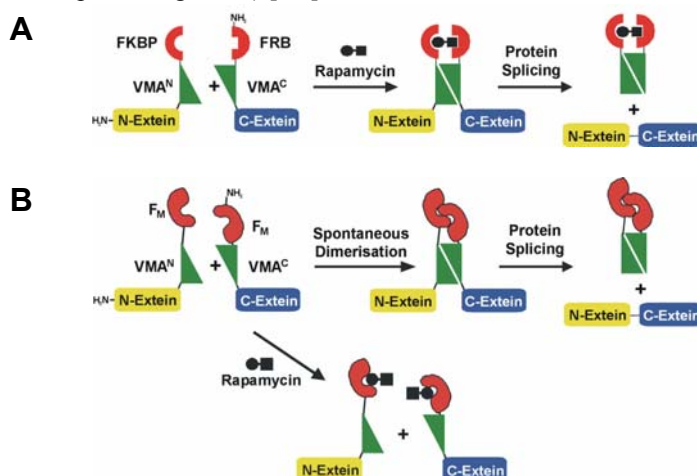


Fig. 2. Conditional protein splicing of the Sce VMA intein. (A) General structure of the intein that is activated with the small molecule rapamycin. (B) Design of an intein that is inhibited by a small molecule ligand like rapamycin.

Important for the present work is another exploration of the benefits of inteins as molecular tools. The goal is to take advantage of the intein’s ability to form a native peptide bond between virtually any two polypeptides for the control of protein activity in living cells. A regulated intein would allow for the defined editing of the primary sequence of a protein of interest, which could be translated into protein function. This represents a new tool to modulate protein function on the posttranslational level. However, all naturally occurring inteins characterized so far seem to be not regulated in their activity. In the following, we will describe how trans-splicing inteins can be generated that are activated or inhibited by the addition of a small molecule ligand.

The initial work was carried out in Tom Muir’s laboratory at The Rockefeller University. The Sce VMA intein was artificially split into two halves (VMA^N and VMA^C) that were found to be inactive for protein-trans-splicing, probably because of improper folding of the two halves. These inactive pieces were then engineered into a conditionally active intein by fusion with the domains FKBP12 and FRB, respectively (Fig. 2A) [5]. FKBP is the human FK506-binding protein and FRB

stands for FKBP-rapamycin binding domain. The small molecule ligand rapamycin binds FKBP and this binary complex then binds to FRB, effecting a high affinity ternary complex. The induced close proximity led to efficient protein-trans-splicing, probably by promoting folding of the intein domain. We refer to this process as Conditional Protein Splicing (CPS). Further work showed that CPS works well in mammalian cell lines [6] and that the system can be arranged in a way suitable to switch on the activity of protein kinase A [7]. Meanwhile, ligand-dependent cis-splicing inteins were also developed in other groups [8,9].

Results and Discussion

In this work, we aimed at the development of an intein whose activity is inhibited by a small molecule ligand [10]. This should be a useful tool for protein knock-out strategies. For the generation of an intein with an incorporated off-switch, we fused the same split *Sce* VMA intein halves as described above with FKBP12(F36M)-domains, or briefly F_M-domains. The F36M mutation leads to a spontaneous dimerization of the F_M-domains [11], which results in a constitutively active intein in the absence of rapamycin. Importantly, binding of rapamycin leads to the dissociation into F_M-domain monomers and, hence, to the inhibition of the protein splicing reaction (Fig. 2B).

As model systems to investigate the protein splicing reactions three sets of constructs were prepared. The N-terminal intein half (VMA^N) was fused with maltose-binding protein (MBP) as the N-extein and the F_M-domain (1), a tandem arrangement of two F_M-domains (3) or FKBP (5), respectively, followed by a hexahistidin tag. The constructs with the C-terminal intein half (VMA^C) contained a hexahistidin tag as the C-extein and one F_M-domain (2), two F_M-domains (4) or FRB (6) with MBP for high expression yields at the N-terminus [10]. The rationale for the tandem arrangement of F_M-domains was the higher affinity mediated compared to just one domain.

As a proof-of-principle of intein inhibition, dose-response experiments were performed with mixtures of proteins 1 and 2 containing only one F_M-domain as well as 3 and 4 with two F_M-domains. Figure 3A shows that both reactions can be inhibited by rapamycin and slightly more effectively by AP21998, a synthetic derivative thereof, in a dose-dependent manner [10].

Kinetic measurements of the protein-splicing reactions in the absence of ligand revealed that constructs 1 and 2 reacted significantly faster than constructs 3 and 4 (Fig. 3B, e.g., 38% vs. 18% completion after 20 min). This might be due to the higher affinity mediated by the two F_M-domains, since homodimers formed before mixing the two proteins have to dissociate to form splicing-competent heterodimers. A higher affinity would slow down the dissociation step. With the addition of rapamycin at different time points an ongoing protein splicing reaction can be stopped at certain levels of product formation (shown for 1 and 2 in Fig. 3C) [10].

Although the protein splicing reaction could be inhibited with rapamycin, a background splicing activity was still observed. As indicated in Figure 3D, the ratio to the uninhibited control reaction with only DMSO (the solvent of the rapamycin stock solution) could be improved at elevated temperatures (after 120 min 3-fold inhibition at 25°C and 10-fold inhibition at 30°C) [10].

The observed background splicing activity might be caused by a residual affinity between the intein halves VMA^N and VMA^C. In order to reduce this affinity a mutant of VMA^N was constructed in which Val27 was changed to Ala in the construct with one F_M-domain (1*). An examination of the crystal structure

suggested that this mutation destroys a hydrophobic core at the interface between the N- and C-terminal intein halves. The mutation indeed affected the protein splicing reaction such that it proceeded significantly slower (Fig. 3E), however, and remarkably, also with a significantly decreased level of background splicing activity in the presence of rapamycin (less than 6% completion over a 70 hr time period).

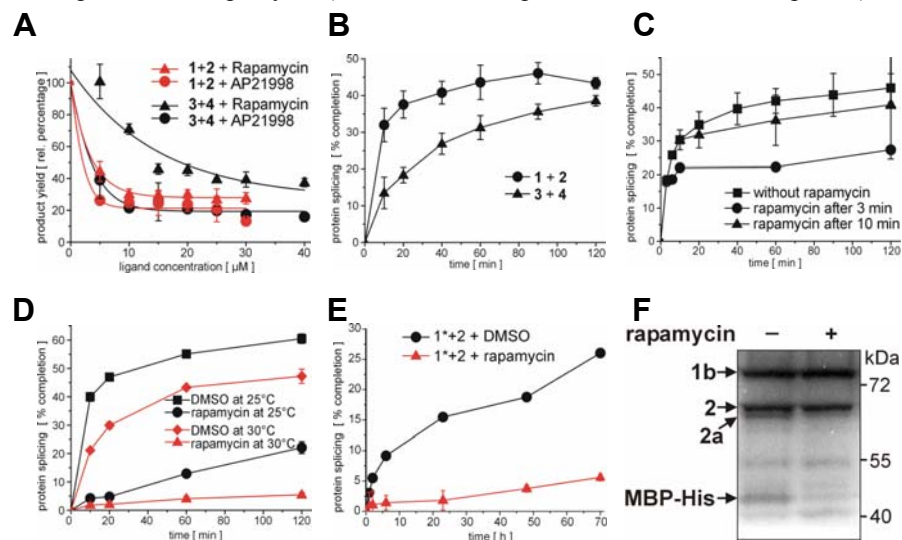


Fig. 3. (A) Dose-response curves of reactions of constructs **1** and **2** as well as **3** and **4** with the two inhibitors rapamycin and AP21998, a synthetic derivative. (B) Kinetic measurements without inhibitor. (C) Addition of rapamycin to an ongoing splicing reaction of **1** and **2**. (D) Effect of different temperatures on the level of ligand-inhibition using **1** and **2**. (E) Kinetics of the intein V27A mutant. (F) Intein inhibition in HEK293 cells. Western blot using an anti-MBP antibody.

To investigate the *in vivo* applicability of the ligand-inhibited intein, HEK293 cells were transfected with plasmids encoding constructs **1b** (**1** lacking the hexahistidin tag) and **2**. Cells were then grown for 24 h at 37°C in the presence or absence of rapamycin in the culture medium. The appearance of the product band of MBP-His₆ indicates that constitutive protein splicing in the absence of rapamycin also works in living cells (Fig. 3F). In contrast, in the presence of ligand this band is weaker suggesting inhibition of the intein to a certain extend.

The two different CPS tools presented can be combined in an interesting fashion that is based on the fact that in both cases rapamycin facilitates the activity-switch. We envisioned a three-piece CPS system, in which the C-terminal intein half VMA^C is either fused to the F_M-domain (construct **4** in Fig. 4A) or to the FRB-domain (construct **6** in Fig. 4A). In this arrangement, VMA^N of construct **1** can react with either one of the two C-terminal partners, depending on the presence or absence of rapamycin. To demonstrate this alternative protein splicing, proteins **1**, **4** and **6** were mixed. After 3 min, the reaction mixture was split and rapamycin was added to one part. Construct **4** was chosen instead of **2** because it has the proper size to distinguish the products on an SDS-PAGE gel. After mixing and in the absence of rapamycin, **1** and **4** spontaneously started to splice, but no product bands for the reaction between **1** and **6** were observed (Fig. 4B). In the presence of rapamycin, however, the reaction between **1** and **4** was turned off and the product bands

corresponding to the reaction between **1** and **6** could be identified. The formation of these distinct products is very specific over the entire reaction time of 5 hrs.

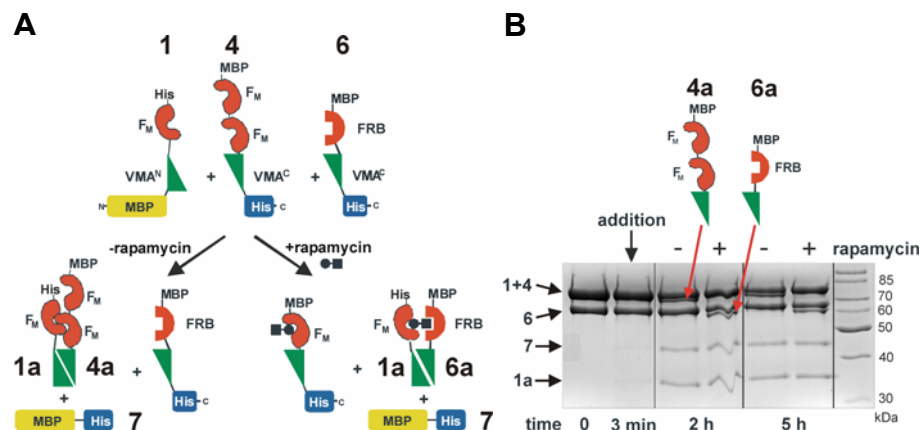


Fig. 4. (A) Reaction scheme of alternative protein splicing. (B) Coomassie blue stained SDS-PAGE gel of the corresponding reactions with or without rapamycin.

We believe that this alternative protein splicing approach might be useful for several applications, for example to switch between the production of two isoforms of a certain protein. In summary, conditional inteins were generated that can be regulated with small molecule ligands. The goal of future studies will be to incorporate these new tools into a suitable context to address biological questions in complex cellular networks by precise modulation of protein function.

Acknowledgments

This work was funded by an Emmy Noether-fellowship of the Deutsche Forschungsgemeinschaft and the Fonds der Chemischen Industrie. ARIAD Pharmaceuticals supplied the rapamycin analog AP21998.

References

1. Noren, C. J., Wang, J. and Perler, F. B. *Angew. Chem. Int. Ed. Engl.* **39**, 450-466 (2000).
2. Perler, F. B. *Nucleic Acids Res.* **30**, 383-384 (2002).
3. Muir, T. W., Sondhi, D. and Cole, P. A. *Proc. Natl. Acad. Sci. USA* **95**, 6705-6710 (1998).
4. Evans, T. C., Jr., Benner, J. and Xu, M. Q. *Protein Sci.* **7**, 2256-2264 (1998).
5. Mootz, H. D. and Muir, T. W. *J. Am. Chem. Soc.* **124**, 9044-9045 (2002).
6. Mootz, H. D., Blum, E. S., Tyszkiewicz, A. B. and Muir, T. W. *J. Am. Chem. Soc.* **125**, 10561-10569 (2003).
7. Mootz, H. D., Blum, E. S. and Muir, T. W. *Angew. Chem. Int. Ed. Engl.* **43**, 5189-5192 (2004).
8. Buskirk, A. R., Ong, Y. C., Gartner, Z. J. and Liu, D. R. *Proc. Natl. Acad. Sci. USA* **101**, 10505-10510 (2004).
9. Skretas, G. and Wood, D. W. *Protein Sci.* **14**, 523-532 (2005).
10. Brenzel, S. and Mootz, H. D. *J. Am. Chem. Soc.* **127**, 4176-4177 (2005).
11. Rollins, C. T., Rivera, V. M., Woolfson, et al. *Proc. Natl. Acad. Sci. USA* **97**, 7096-7101 (2000).

Pin1: Inhibitors and Mechanism

Felicia A. Etzkorn¹, Joseph P. Noel², Yan Zhang² and Xiaodong J. Wang¹

¹Department of Chemistry, Virginia Tech, Blacksburg, VA 24060; ²Jack Skirball Chemical Biology and Proteomics Laboratory, The Salk Institute for Biological Studies, La Jolla, California 92037, USA

Introduction

Peptidyl-prolyl isomerase (PPIase) enzymes are something of an enigma. Part chaperone, part enzyme, they play multiple roles in multiple biological systems. Cyclophilin and FKBP were first discovered in the late 1980's because they bind to distinct natural products, cyclosporine and FK506 respectively, immunosuppressants which act as prodrugs and become activated by their specific PPIase [1]. The PPIase activity is not relevant to the immunosuppressive activity [2]. The PPIases have also been shown to play distinct chaperone roles in protein folding, improving both rate and yield of their folding substrates [3]. So began a story that seems only to grow more interesting with the telling. In 1996, Pin1 was discovered as the first example of a new class of PPIase enzymes, the parvulins that appears to regulate the cell cycle [4]. Pin1 is unique both among PPIases and among cell cycle regulators. Unlike cyclophilin and FKBP, it does not bind an immunosuppressant drug. Among cell cycle regulators, primarily kinases, phosphatases, histone acetyl transferases, and histone deacetylases, Pin1 is the only PPIase, the only enzyme that does not make or break a bond. The activity of Pin1 is to recognize phosphoSer/Thr-Pro amide bonds in other cell cycle proteins, and swiftly interconvert *cis* and *trans* amide isomers (Fig. 1). The reaction is completely reversible and quite rapid. In order to capture snapshots of this enigmatic reaction, we designed conformationally locked isosteres **1** and **2** of each ground state, the *cis* and *trans* amides.

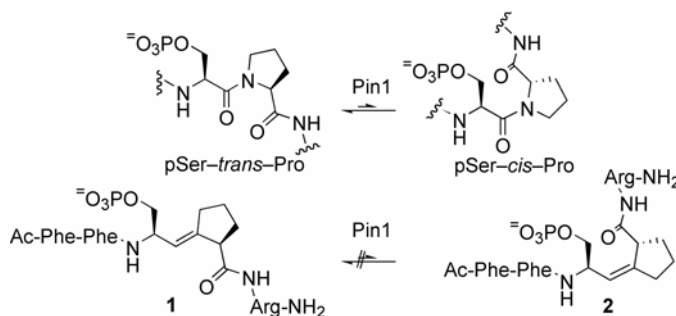


Fig. 1. Isomerization of Pin1 substrates and conformationally locked *cis* and *trans* isosteres.

Results and Discussion

We have previously reported the stereocontrolled synthesis of the *cis* and *trans* Ser-Pro dipeptide isosteres in 13% and 20% overall yields respectively. Our ability to generate large quantities of these key intermediates allowed us to phosphorylate and install the isosteres into pentapeptide substrate analogs. These were shown to be competitive inhibitors with K_i values of 40 μ M and 1.74 μ M respectively [5]. In

addition, each isostere demonstrated antiproliferative activity in A2780 ovarian cancer cells, with IC_{50} values of 140 μ M and 8.3 μ M respectively [5]. In each assay, the cis isostere proved to be the better inhibitor, which is not surprising since in the X-ray crystal structure of Pin1, the cis isomer of Ala-Pro was captured in the active site [6]. In the PPIase enzyme assay, the cis was 23-fold more potent than the trans, while in the cell-based assay the difference was 17-fold [5]. This closely parallel activity for the two isomers provides circumstantial evidence that Pin1 will prove to be the target for antiproliferative activity.

X-ray structures of the cis and trans isosteres **1** and **2** in the Pin1 active site were recently captured by isomorphous replacement methods. The inhibitors were soaked into the crystalline enzyme. The X-ray structures confirm the competitive inhibition data; the inhibitors do indeed bind in the catalytic site in the same orientation as the Ala-Pro ligand, with the phosphate bound in the site where sulfate was first found in the first crystal structure of Pin1 [6]. It was not entirely clear that this would be the case because the WW domain of Pin1 also recognizes pSer/pThr-Pro motifs, but in the trans conformation [7]. The selectivity of the trans isostere for the catalytic domain over the WW domain is curious. We thought that the inclusion of the two aromatic residues at the N-terminus and the Arg at the C-terminus had targeted both inhibitors, but particularly the trans isostere, to the catalytic domain. However, the electron density map is disordered for the two N-terminal Phe residues, and weak for the Arg residue. The structures demonstrate that there are salt bridging Arg and Lys partners for the phosphate and a potential hydrogen bond donor, His59, to the site where the prolyl nitrogen would be. The backbone NH of residue 131 forms a strong hydrogen bond to the Pro carbonyl oxygen in both structures. In addition, we can begin to speculate upon the mechanism of proline isomerization in Pin1 based upon these two structures.

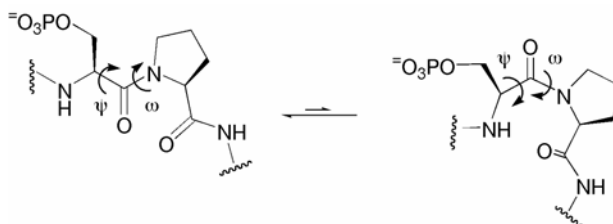


Fig. 2. Proposed mechanism for isomerization by Pin1 based upon X-ray structure of alkene isosteres with the least motion of the substrate. Rotation around both Ψ and ω bonds adjacent to the carbonyl leaves both arms of the substrate in roughly the same general directions.

The minimal motion for proline isomerization catalyzed by PPIases would be for the substrate to undergo simultaneous rotation around the pSer Ψ bond and the pSer-Pro ω bond so that essentially only the C=O rotate would rotate, as shown in Figure 2. Rotation around an entire arm of the substrate might require massive reorganization of the enzyme to accommodate the large substrate conformational change. From the X-ray crystal structures of the cis and trans isosteres bound to Pin1 (Fig. 3), it appears that indeed, the pseudo-Ser phosphate and the pseudo-Pro carbonyl are both held in nearly the same positions, while the atoms in between the pSer α -C and the Pro α -C, including the 5-membered ring, are substantially different

in the two structures. In the crystal structure these atoms are also more disordered, which would be expected for the corresponding amide atoms during catalysis. The low electron density observed for the Arg in each structure would also be expected because the C-terminus must change conformation during catalysis. The Pro carbonyl oxygen, the Pro nitrogen, and the phosphate act as pivot points that are held in place while the rest of the backbone reorganizes. The residues C- and N-terminal of the pSer-Pro core appear to be unimportant for binding or catalysis of either cis or trans substrate. In some sense, we think that we have captured snapshots of both ends of the reaction coordinate, as represented by the cis and trans pSer-Pro isosteres bound to Pin1.

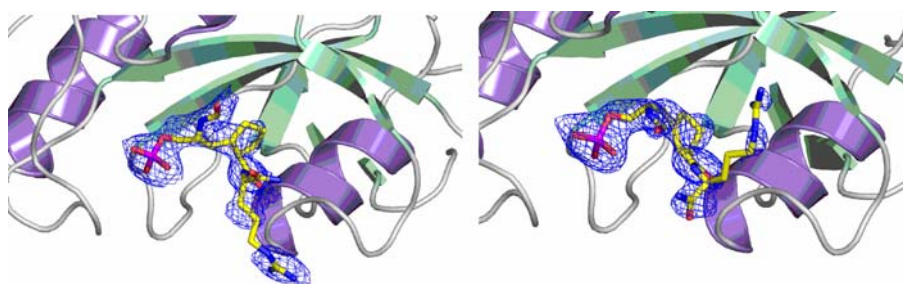


Fig. 3. X-ray crystal structures of trans (left) and cis (right) phosphoSer-Pro peptide isosteres in the catalytic site of Pin1.

The quantitative difference in binding of 1.7 kcal/mol for the cis vs. trans isosteres led us to speculate on the relative rate of the reaction in each direction for the PPIase activity. If we grant that part of the catalytic energy probably arises from transition-state stabilization, according to Linus Pauling's hypothesis[8], and another part arises from substrate destabilization, we can generate a reaction coordinate diagram (Fig. 4). We assume that the desolvation involved in binding cis and trans amide substrates are not different from each other, since they are simply stereoisomers, differing only in the conformation of the alkene. We also assume that the forces involved in substrate binding, such as desolvation are not different from each other. In this case, we are comparing $\Delta\Delta G$ for the alkenes with $\Delta\Delta G$ for the amides. The difference in free energy of binding of isosteres **1** and **2** is 1.7 kcal/mol at 4°C, the temperature of the assay. Thus, we hypothesize that the difference in enzyme-substrate recognition is similar, ca. 1.7 kcal/mol. In short peptides in solution, the trans-Pro isomers are more stable than the cis-Pro isomers, which may also be the case for proteins in solution, whether folded or unfolded, though this is yet unknown for Pin1 substrates. If all these assumptions hold, the reaction coordinate diagram shown in Figure 4 shows that the elevated energy of the trans substrate would give it a shorter way to go to attain the transition state than the energy required for the cis substrate to attain the same transition state. This would imply that the trans to cis direction of the reaction would be faster than the cis to trans direction. With all the assumptions made to reach this conclusion we hesitate to insist upon it, but our results may give an initial glimpse into the mechanism of proline isomerization in Pin1. Certainly we have created tools to investigate the fascinating biology of the Pin1 cell cycle regulator.

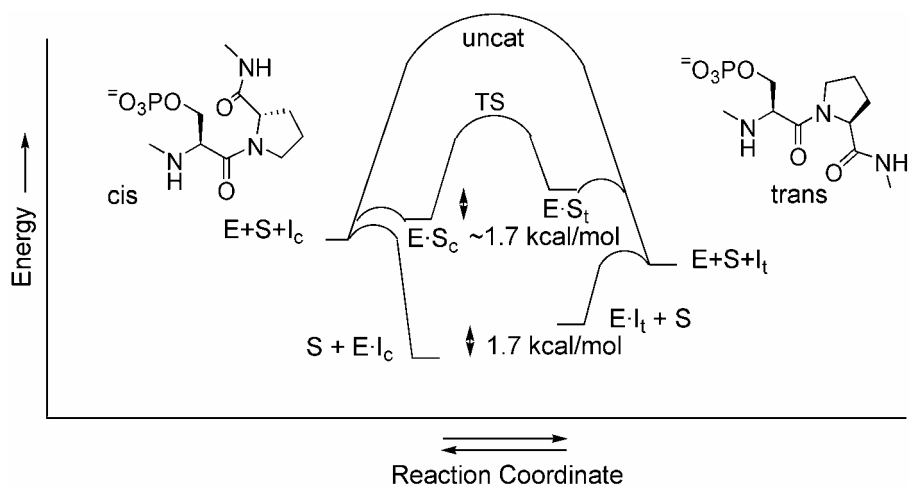


Fig. 4. Possible reaction coordinate diagram for the Pin1 catalyzed isomerization of cis and trans pSer-Pro substrates. E = enzyme (Pin1), S_c = cis substrate, S_t = trans substrate, I_c = cis isostere inhibitor, I_t = trans isostere inhibitor.

Acknowledgments

The work was funded by NIH grant R01 GM63271.

References

1. Liu, J., Farmer, Jr., J. D., Lane, W. S., Friedman, J., Weissman, I. and Schreiber, S. L. *Cell* **66**, 807-815 (1991).
2. Zydowsky, L. D., Etzkorn, F. A., Chang, H., Ferguson, S. B., Stolz, L. A., Ho, S. I. and Walsh, C. T. *Prot. Sci.* **1**, 1092-1099 (1992).
3. Gothel, S. F. and Marahiel, M. A. *Cell. Mol. Life Sci.* **55**, 423-436 (1999).
4. Lu, K. P., Hanes, S. D. and Hunter, T. *Nature* **380**, 544-547 (1996).
5. Wang, X. J., Xu, B., Mullins, A. B., Neiler, F. K. and Etzkorn, F. A. *J. Am. Chem. Soc.* **126**, 15533-15542 (2004).
6. Ranganathan, R., Lu, K. P., Hunter, T. and Noel, J. P. *Cell* **89**, 875-886 (1997).
7. Verdecia, M. A., Bowman, M. E., Lu, K. P., Hunter, T. and Noel, J. P. *Nat. Struct. Biol.* **7**, 639-643 (2000).
8. Pauling, L. *Chem. Eng. News* **24**, 1375 (1946).

Discovery and Structural Optimization of High Affinity Co-Agonists at the Glucagon and GLP-1 Receptors

**Vasily M. Gelfanov, David L. Smiley, Wesleyne Whittaker and
Richard D. DiMarchi**

Department of Chemistry, Indiana University, Bloomington IN 47405, USA

Introduction

Hypoglycemia is a life threatening event that requires immediate medical attention. Glucagon is the most proven medication for treating acute hypoglycemia. It can restore normal glucose concentration within minutes of administration [1]. When glucagon is used in the acute medical treatment of hypoglycemia a crystal is solubilized with a dilute acid buffer and the solution injected intramuscularly. While highly effective, the methodology is cumbersome and dangerous for someone that is semi-conscious. Previous studies have reported that glucagon must maintain its structural integrity for it to retain its full hormonal activity. Histidine at position one and aspartic acid at position nine are two residues of special importance [2,3]. Our goal is to identify a glucagon analog that maintains the biological performance of the native hormone but possesses improved physical properties. Ideally, we desire a sufficiently soluble and stable analog that could be pre-formulated as a solution ready for injection.

Our synthetic approach to discovery of an improved glucagon analog is based upon adding supplemental positive charge to the molecule. Selective addition of lysine residues to glucagon was explored as a possible route to increase the stability and solubility of the hormone. Arginine was substituted for lysine at position twelve to further enhance the alkaline character of each glucagon analog studied. Additionally, we have changed the methionine residue at position 27 to leucine to eliminate oxidative degradation. The last change introduced in each glucagon analog was the use of a C-terminal amide to facilitate chemical synthesis.

Results and Discussion

While the primary objective of this study was the improvement in glucagon pharmaceutical properties, we serendipitously observed an appreciable change in selectivity of biological action. The results demonstrate that native GLP-1 has much reduced ability to bind and signal through the glucagon receptor relative to the inverse ability of glucagon to function at the GLP-1 receptor (Table 1). The simultaneous change to the native glucagon sequence of Arg12, Leu27, and C-terminal amidation yielded a peptide ligand capable of signaling at either the glucagon or GLP-1 receptor with picomolar affinity. Unexpectedly, the relative selectivity in cAMP production at the two receptors diminished from a ratio of nearly twenty-fold for native glucagon to a difference of less than two-fold when all three changes were introduced. The primary basis for the change in selectivity was a much increased potency at the GLP-1 receptor (0.48 vs 3.85 nanomolar EC₅₀) with a more subtle decrease in potency at the glucagon receptor (0.36 vs 0.21 nanomolar EC₅₀). The binding affinity of the Arg12, Leu27 glucagon C29-amide for the glucagon receptor was changed in the same direction as that of cAMP production, but proportionally the change was to a much smaller absolute degree.

The additional selective placement of lysine residues at positions 20, 24, or 29 slightly altered the biological potency at the GLP-1 receptor with two of the analogs demonstrating some reduction in activity. The EC₅₀ values were observed within a range of 0.41-1.25 nM, which places their respective potency approximately equal distance from the two native hormones (glucagon at 3.85 nM and GLP-1 at 0.04 nM). The activity at the glucagon receptor for the three individual lysine-substituted analogs was reduced within a range of approximately 2-3 fold. The substitution of the native glutamine residues at position 20 or 24 with lysine yielded proportional increases in potency at both receptors that were nearly identical. The substitution of the native C-terminal threonine with lysine yielded a greater decrease in potency at the glucagon receptor than that observed at the GLP-receptor. Each of the three lysine substituted glucagon analogs (K20, 24, and 29), as well as the starting triply-substituted peptide nucleus were of similar potency at each of the two receptors. The K20 derivative appeared virtually equipotent in these assays at both sites with sub-nanomolar potency.

Table 1. Binding affinities and bioactivity of glucagon analogs

Peptide	Receptor Binding				cAMP Induction			
	Glucagon Receptor		GLP-1 Receptor		Glucagon Receptor		GLP-1 Receptor	
	IC ₅₀ , nM	n ^a	IC ₅₀ , nM	n	EC ₅₀ , nM	n	EC ₅₀ , nM	n
Glucagon	3.38±1.44	4	250±59	4	0.21±0.11	11	3.85±1.64	10
GLP-1	na ^c	-	0.97±0.28	6	>10000	8	0.04±0.01	13
Glucagon ^b R12	1.85±0.92	4	105±36	4	0.36±0.31	7	0.48±0.11	5
Glucagon ^b R12K20	6.10±1.45	3	73±12	2	0.84±0.40	5	0.82±0.49	5
Glucagon ^b R12K24	2.38±0.29	3	158±12	2	1.00±0.39	4	1.25±0.97	5
Glucagon ^b R12K29	3.53±1.86	4	65±47	3	0.81±0.49	5	0.41±0.24	6
Oxyntomodulin	317±179	3	270±11	2	3.25±1.65	5	2.53±1.74	5

^aNumber of Experiment; ^bL27, T29-amide; ^cna - not active

Oxyntomodulin was prepared and studied since it possesses a C-terminal cationic amino acid extension to native glucagon. Our results demonstrate an appreciable reduction in binding and signaling for it at the glucagon receptor. In contrast, we observed little change in the nature or affinity of oxyntomodulin interaction at the homologous GLP-1 receptor. Clearly these two homologous receptors have a distinct ability to recognize structural changes at the C-terminus of these related peptide hormones with the glucagon receptor being much more discriminating.

References

1. Lefèbvre, P. J. *Diabetes Care* **18**, 715-730 (1995).
2. Unson, C. G. and Merrifield, R. B. *Proc. Natl. Acad. Sci. USA* **91**, 454-458 (1994).
3. Sturm, N. S., et al. *J. Med. Chem* **41**, 2693-2700 (1998).

Development of a Lanthanide-based Assay for δ -Opioid Receptor

Josef Vagner¹, Rajesh Sankaranarayanan¹, Heather Handl², Victor J. Hruby^{1,2} and Robert J. Gillies²

¹Department of Chemistry; ²Department of Biochemistry and Molecular Biophysics and Arizona Cancer Center Sciences, University of Arizona, Tucson, AZ 85721, USA

Introduction

A lanthanide-based assay for ligand-receptor interactions provides an attractive alternative to the traditional radiolabeled determinations in terms of sensitivity, throughput and biohazards. Several recent reports have described the development of such assays [1-3], although to date there has been no assay reported to characterize ligand binding to the δ -opioid receptor (δ OR). The δ OR is widely studied for its role in pain and a reproducible assay that can be performed with ease will prove useful in characterizing ligand binding to the receptor. The lanthanide-based whole-cell assay provides superior results with higher throughput and eliminates the need for radioactive waste disposal. This assay is appropriate for high-throughput screening.

Recently, we have developed a europium-based binding assay for the melanocortin receptors. We have synthesized the labeled ligand, Eu-DTPA-NDP- α -MSH, and verified its use in a competitive ligand-binding assay on whole cells [3]. Herein, we report the synthesis of europium labeled δ OR ligands and their binding affinities to the δ OR.

Results and Discussion

Ligands were synthesized by standard solid-phase technology using a manual synthesizer (Torviq, Niles, MI, USA) with *N*^α-Fmoc/*tert*-butyl chemistry [4]. The DTPA chelator was attached to the ϵ -amino group of lysine directly or via a ϵ -aminocaproic spacer (compound 1). Peptide-Lys(Aloc) was constructed on Rink resin. Deprotection of the ϵ -amino chain of lysine gave free ϵ -amino function while retaining side chain protection groups and *N* α -terminal Boc. DTPA was conjugated to peptides on the solid support using an improved *in-situ* HOBt ester method (Vagner, unpublished data). Similarly, the protected DOTA ligand was prepared by

Table 1. Sequence and calculated K_i values for δ OR ligands.

Compound	Sequence	K_i [nM]	K^*_i [nM]
1	H-Tyr-DAla-Phe-Glu-Phe-Aca-Lys-(Aca ^a -DTPA[Eu ³⁺])-NH ₂	27.0	N.D.
2	H-Tyr-DAla-Phe-Glu-Val-Val-Gly-Lys(DTPA[Eu ³⁺])-NH ₂	81.3	1.1
3	H-Tyr-DAla-Phe-Glu-Val-Val-Gly-Lys(DOTA[Eu ³⁺])-NH ₂	101.4	1.1
4	H-Tyr-DAla-Phe-Glu-Val-Val-(Gly- β Ala) ₂ -Lys(DTPA[Eu ³⁺])-NH ₂	> 1000	N.D.
5	H-Tyr-c[pPen-Gly-Phe-Cys]Phe-Lys(DTPA[Eu ³⁺])-NH ₂	6.2	8.8

The K_i was calculated based on the equation $K_i = EC_{50}/(1 + ([\text{ligand}]/K_d))$ where ligand and K_d refer to ³H-Deltorphin II and $[\text{ligand}] = 20$ nM and $K_d = 0.75$ nM in this experimental system. The K^*_i of the parental (unlabeled ligand) is indicated, where available.

coupling DOTA-Tris(tBu) esters to the resin. The ligands were cleaved from the resin together with protecting groups by the TFA-scavenger cocktail. The linear ligand was cyclized by air oxidation. All compounds were purified by HPLC. Chelate-ligands were labeled with Eu(III) chloride in neutral buffer. The excess of metal salt was removed by SEC. The purity of the products was checked by thin-layer chromatography, analytical HPLC, and high resolution ESI.

In binding to rat brain membranes, the ligand 1 had an $IC_{50} = 310$ nM. In assessing binding to whole CHO cells overexpressing the δ OR, it was determined that the $IC_{50} = 750$ nM. Since this affinity was lower than expected synthesis of analogs 2-4 was initiated. We synthesized a control Deltorphin II analogue (H-Tyr-DAla-Phe-Glu-Val-Val-Gly-NH₂) with the IC_{50} value of 22 nM. The unlabeled ligands derived from the same Deltorphin II (compounds 2 and 3) had a $K_i = 1.1$ nM indicating that the addition of the chelate moieties interferes with ligand binding.

The fifth ligand synthesized, Eu-DTPA-DPLCE (5), bound with an affinity comparable to that of the unlabeled ligand. The binding of this Eu-ligand was verified by specific binding to CHO cells overexpressing the δ OR (Fig. 1). The ligand binds in a specific and saturable manner and can be competed off by unlabeled ligands, thus proving its utility in competitive binding assays. It is not clear why the labeled deltorphin ligands bound with decreased affinity compared to the parent unlabeled compounds. We hypothesize that the linear and somewhat flexible structures of compounds 1-4, coupled with the presence of the highly hydrophobic Tyr and Phe residues, enable the ligand to form a conformation which involves interactions with chelator, thus preventing adequate binding to the receptor. The more rigid and conformationally constrained cyclic analog 5 would potentially prevent this effect, and thus retain its receptor binding capabilities [5].

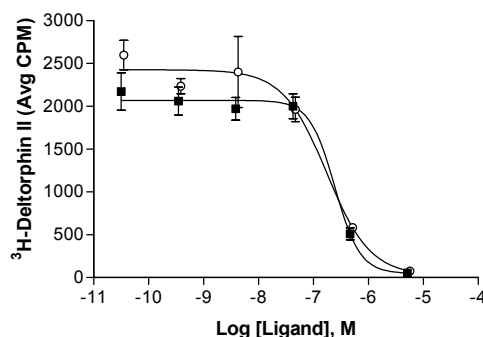


Fig. 1. ³H-Deltorphin II binding assay comparing DPLCE to Eu-DTPA-DPLCE.

Binding was completed on whole CHO/ δ OR cells. ■, DPLCE, $IC_{50} = 240$ nM, $R^2 = 0.94$; ○, Eu-DTPA-DPLCE, $EC_{50} = 170$ nM, $R^2 = 0.91$.

Acknowledgments

The work was funded by NIH grants R33 CA95944 and R01 CA097360.

References

1. Takeuchi, T., Yoshida, M., Kabasawa, Y., Matsukawa, R., Tamiya, E. and Karube, I. *Anal. Letters* **26**, 1535-1545 (1993).
2. Peuralahti, J., Hakala, H., Mikkala, V. M., Loman, K., Hurskainen, P., Mulari, O. and Hovinen, J. *Bioconjugate Chem.* **13**, 876-880 (2002).
3. Handl, H. L., Vagner, J., Yamamura, H. I., Hruby, V. J. and Gillies, R. *Anal. Biochem.* **330**, 242-250 (2004).
4. Vagner, J., Handl, H. L., Gillies, R. J. and Hruby, V. J. *Biorg. Med. Chem. Lett.* **14**, 211-215 (2004).
5. Liao, S., et al. *J. Med. Chem.* **41**, 4767-4776 (1998).

Interaction between a Minimum Hevein Domain and Chitooligosaccharides Studied by NMR and a Novel Surface Plasmon Resonance Method

Miquel Vila-Perelló¹, Nuria Aboitiz², Ricardo Gutierrez Gallego¹,
 Francisco J. Cañada², Jesús Jiménez-Barbero² and David Andreu¹

¹Department of Experimental and Health Sciences, Universitat Pompeu Fabra, 08003 Barcelona, Spain; ²Centro de Investigaciones Biológicas, CSIC, 28040 Madrid, Spain

Introduction

Protein-carbohydrate interactions regulate many biologically relevant processes, from fertilization and tissue maturation to tumor metastasis and immune response, and thus are one of the major topics in current biomedical research. In order to gain a major insight into the thermodynamic, kinetic and structural details of such interactions we have recently started a project aimed at defining minimal sugar-binding protein domains and developing suitable tools for studying their interaction with oligosaccharides.

As a model system we have chosen the hevein or chitin-binding domain (CBD) which specifically recognizes chitooligosaccharides and is found in a wide variety of proteins, from plant lectins and chitinases to some antimicrobial peptides. The structure of hevein bound to chitooligosaccharides was recently described [1]; key residues for the interaction were identified and the C-terminal region seemed not to be directly involved in the recognition process. Accordingly, we decided to study a peptide corresponding to the 32 N-terminal residues of hevein, to ascertain whether it retained the ability to interact specifically with chitooligosaccharides and elucidate the role of the C-terminal region of this important protein domain (Fig. 1).

Hevein	EQCGRQAGGKLCPPNNLCC SQWGW CGSTDE Y CSPDHNCQSNCKD
Acamp-2	VGECVRGR---CPSGMCC SQFGY CGKGPK Y CGR
HEV32	EQCGRQAGGKLCPPNNLCC SQWGW CGSTDE Y CS

Fig. 1. Sequences of two naturally occurring hevein-like peptides (hevein and Acamp-2) and our designed minimal hevein domain (HEV32). In bold are shown the residues known to be key for the interactions with chitooligosaccharides.

Results and Discussion

The HEV-32 hexathiol precursor was efficiently produced by SPPS, purified and submitted to oxidative folding under optimized conditions (14 μ M peptide in 0.1 M Tris-HCl buffer, pH 8.0, under Ar atmosphere in the presence of 1 mM EDTA and 10:100 GSH/GSSG). Cys connectivities of folded HEV32 were assessed by the method of partial reduction and cyanilation [2].

Thermodynamic parameters for HEV32-chitooligosaccharide interaction were obtained from NMR titration data with increasing amounts of ligand. K_a and ΔG° values (Table 1) were in good agreement with those previously reported for full length hevein, thus suggesting the same mode of binding for the truncated peptide. Moreover, the NMR structure of HEV32 bound to chitooligosaccharides is almost identical to that of hevein itself; a slight increase in the flexibility of free HEV32 is

observed which correlates with the increased ΔS° of the binding. Accordingly, we concluded that HEV32 could be considered a minimal CBD [3].

Table 1. Thermodynamic parameters of hevein and HEV32 interaction with GlcNAc₃

	K_a				ΔG° (KJ mol ⁻¹)	ΔH° (KJ mol ⁻¹)	ΔS° (KJ mol ⁻¹)
	298K	303K	308K	313K			
Hevein	11500	8700	6900	5700	-23.1	-36.4	-44.5
HEV32	7700	4200	3400	2200	-21.8	-62.6	-136.0

We were also interested to develop a method for carbohydrate immobilization that would allow monitoring protein-sugar interactions by SPR and would not be sample nor chemically demanding. We designed a peptide module with an aminoxy group to capture carbohydrates through its reducing end [4] and two Lys residues for immobilization onto a carboxyl-containing surface (Fig. 2). As proof of principle we monitored the interaction of wheat germ agglutinin (WGA), a well-known lectin, with immobilized chitopentaose (Fig. 2). The specificity of the interaction was confirmed using a reference cell surface with immobilized lactose (which does not interact with WGA). Values in good agreement with those previously reported were obtained for all kinetic ($k_{on}=3.58\times 10^5\text{ M}^{-1}\text{ s}^{-1}$, $k_{off}=1.27\times 10^{-4}\text{ s}^{-1}$) and thermodynamic ($K_A=2.26\times 10^9\text{ M}^{-1}$) parameters. Finally, we demonstrated the suitability of our method to study by SPR the interaction of chitopentaose with HEV32, a challenging peptide due to its low MW and weak affinity. Although data could not be fitted to any known kinetic model, an affinity constant ($2.31\times 10^4\text{ M}^{-1}$) in good agreement with those previously obtained for HEV32 and hevein was found.

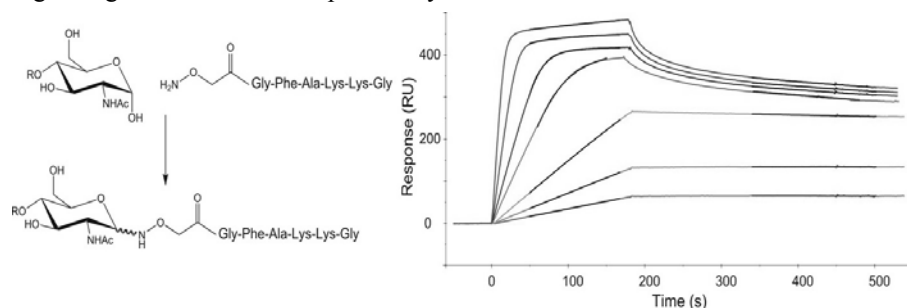


Fig. 2. Left: oxime chemical ligation between our designed peptide module and a sugar (for clarity only the cyclic form of the product is shown). Right: sensorgrams of WGA binding to immobilized chitopentaose at seven (0.49 to 31.25 nM) different concentrations.

References

1. Asensio, J. L., Cañada, F. J., Bruix, M., Rodríguez-Romero, A. and Jiménez-Barbero, J. *Eur. J. Biochem.* **230**, 621-633 (1995).
2. Wu, J. and Watson, J.T. *Prot. Sci.* **6**, 391-398 (1997).
3. Aboitiz, N., Vila-Perello, M., Groves, P., Asensio, J. L., Andreu, D., Canada, F. J. and Jimenez-Barbero, J. *ChemBioChem* **5**, 1245-1255 (2004).
4. Cervigni, S. E., Dumy, P. and Muttter M. *Angew. Chem. Int. Ed. Engl.* **35**, 1230-1232 (1996).

Cross-Reactivity Studies of rMOG_{ED} with Synthetic Putative Autoantigens CSF114(Glc) and [N³¹(Glc)]hMOG(30-50) in Multiple Sclerosis Patients' Sera

Barbara Mulinacci^{1,2}, Constanze Breithaupt², Prajna P. Pal², Nedilko Budisa², Marta Pazzagli¹, Benedetta Mazzanti¹, Paolo Rovero¹, Luis Moroder² and Anna M. Papini¹

¹Laboratory of Peptide & Protein Chemistry & Biology, Polo Scientifico, Università di Firenze, I-50019 Sesto Fiorentino (FI), Italy, ²Max-Planck-Institut für Biochemie, D-82152 Martinsried, Germany

Introduction

Multiple Sclerosis (MS) is supposed to be a group of diseases with distinct pathogenetic mechanisms. In the last years, the role of auto-antibodies (auto-Abs) has been reevaluated, and therefore their identification as specific biomarkers became a relevant target. We demonstrated for the first time that an aberrant N-glycosylation is a fundamental determinant of autoantibody recognition in MS.

In particular, by a reverse approach, we developed a specific probe, termed CSF114(Glc), to detect at the best Abs in sera of MS patients. CSF114(Glc) is a structure-based designed synthetic glycopeptide characterized by a β -hairpin structure with a β -D-glucopyranosyl moiety linked to an Asn residue on the tip of the I' β -turn. The Ab titer correlates with the disease activity. CSF114(Glc) recognized myelin and oligodendrocyte antigens by immunohistochemistry, therefore it may be a mimetic of all aberrantly glucosylated myelin antigens [1-4].

Very recently, several works considered auto-Abs to unglycosylated or unspecifically glycosylated recombinant Myelin Oligodendrocyte Glycoprotein (MOG) as predictors of clinically definite MS even if these results are still subject of debate. Therefore, aberrant glucosylation on Asn residues of myelin proteins may create neoantigens triggering an autoimmune response in which anti-CSF114(Glc) Abs are biomarkers of disease activity. For that reason we focused our attention on the conformation and glycosylation of recombinant MOG. We compared Ab-recognition in MS patients' sera by rMOG (as a putative autoantigen) or by [N³¹(Glc)]hMOG(30-50) [5], and CSF114(Glc), as possible molecular mimotopes, to study the Ab response in solid-phase ELISA and to elucidate the role of MOG in an Ab-mediated MS pattern.

Results and Discussion

For an efficient expression of the extracellular domain of rat MOG(1-125), the pQE-12/rMOG(His)₆ plasmid was transformed into BL21(DE3) cells from *E. coli*. Over-expression of rMOG_{ED}(His)₆ results in the production of inclusion bodies, insoluble aggregates of misfolded protein. The solubilization of the expressed protein was obtained using strongly denaturing conditions and an efficient refolding *in vitro* was achieved. The proper refolding was checked by CD measurements. The Abs affinities of expressed rMOG_{ED}, of glycopeptides CSF114(Glc) and [Asn³¹(Glc)]hMOG(30-50) and of peptide hMOG(30-55) were evaluated by SP-ELISA (Fig. 1).

To obtain glycosylated proteins in prokaryotic cells with a well defined glycosyl moiety, an unnatural amino acid with an alkyne moiety was introduced in

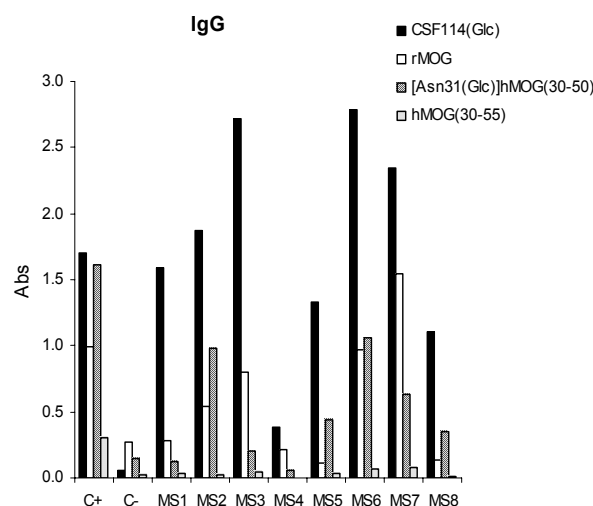


Fig.1. IgG titers of MS patients' sera (MS1 to MS8), positive control (C+), and blood donor sera (C-) to rMOG_{ED}, to the glycopeptides CSF114(Glc), and [Asn³¹(Glc)]hMOG(30-50) and to the unglycosylated peptide hMOG(30-55).

recombinant proteins in order to get a suitable substrate for Huisgen cycloaddition with an azido-sugar. Met is one of the most suitable amino acid for replacement studies in recombinant proteins, and is an attractive target for bioconjugates engineering. We decided to incorporate, after a site directed mutagenesis, 2-amino-5-hexynoic acid (homopropargylglycine), a Met analog, at position 31 of rMOG, native site of glycosylation, under the selective pressure incorporation. Although the expression profiles of rMOG_{ED}(His)₆ N₃₁M in cellular lysates gave us the first insight that homopropargylglycine is incorporated, the isolation and purification of the modified rMOG require further work.

In conclusion, the control of protein conformation is important, since rMOG_{ED} properly folded showed an increased detection of anti-MOG (or anti-myelin) Abs, as biomarkers, of MS. Specifically glucosylated MOG (or other myelin proteins) is a necessary step to understand the role of anti-MOG (or anti-myelin) Abs in MS patients' sera.

Acknowledgments

We thank Fondazione Ente Cassa di Risparmio di Firenze and the Travel Award Committee for the financial support to the participation of B. Mulinacci at 19th APS.

References

1. Papini, A. M. *Nature Medicine* **11**, 1 (2005).
2. Lolli, F., et al. *Proc. Natl. Acad. Sci. USA* **102** 10273-10278 (2005).
3. Lolli, F., et al. *J. Neuroimmunol.* **167**, 131-137 (2005).
4. Papini, A. M., Rovero, P., Chelli, M. and Lolli, F. PCT International application (2003) WO 03000733 A2. Priority Data FI2001A000114.
5. Mazzucco, S., et al. *Bioorg. Med. Chem. Lett.* **9**, 167-172, (1999).

Thiohydantoins – A Technique for Labeling Peptides and Proteins

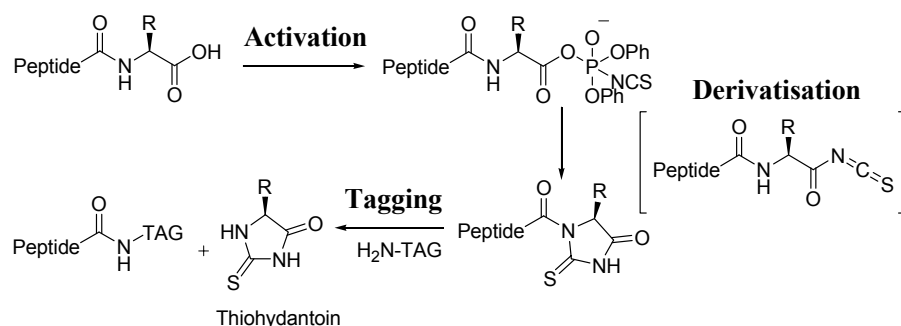
Carole Brückler and Mark Bradley

School of Chemistry, University of Edinburgh, West Mains Road, Edinburgh, EH9 3AF, UK

Introduction

Proteomics relies on 2D comparative electrophoresis of labeled proteomes, allowing protein profiles to be determined in response to cellular stimulation (e.g., the addition of a drug to a specific cell, etc.). A key requirement is to efficiently label the cell proteome population with specific fluorophores in such a way that their mobilities and properties are not altered [1]. The objective of this work was to develop a method to control site specific labeling of proteins and peptides that would enhance current techniques in this field (e.g., 2D difference gel electrophoresis).

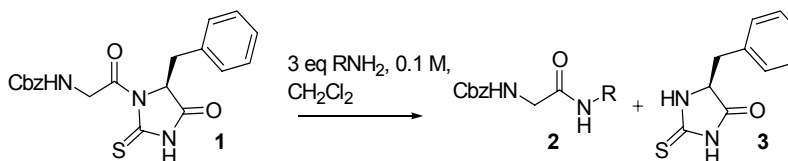
The methodology was based on carboxy terminal sequencing [2], a method complementary to Edman sequencing, but which provides an elegant method of converting a C-terminal amino acid into a good leaving group and thus a handle for attaching a fluorophore or another tag of interest (Scheme 1).



Scheme 1. Mechanism of carboxy terminal activation and introduction of tag.

Results and Discussion

As a proof of principle, a short peptide was converted into its thiohydantoin **1** using diphenylphosphoryl isothiocyanate [2]. Following displacement with primary amines, hydrazines and hydrazides, the corresponding amides **2** were obtained in average isolated yields of ~ 95 %. Solubility problems lowered the yields for hydrazides **2** to 60-70 % (Scheme 2).



Scheme 2. Displacement of peptide thiohydantoin with nucleophiles.

A comparison of reactivities proved that primary amines had the shortest reaction times (conditions: 60 °C, 0.1 M, 3 eq nucleophile, MeCN), thus making amines the most desirable nucleophiles, as shown by complete consumption of **1** in Figure 1a.

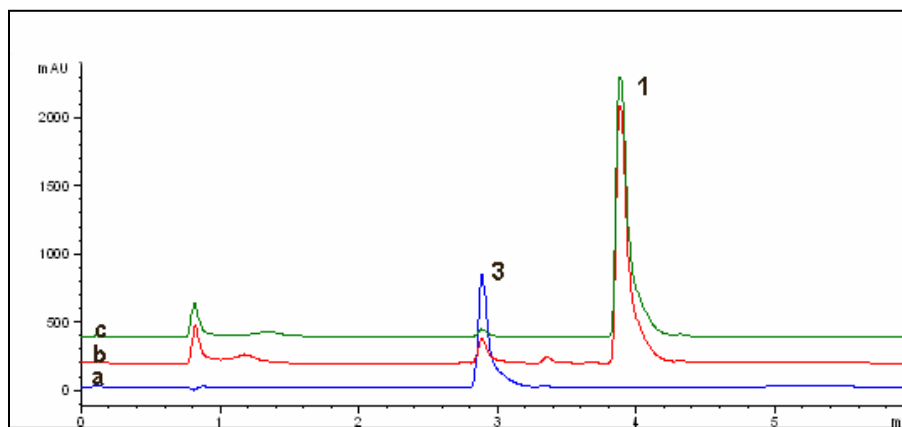
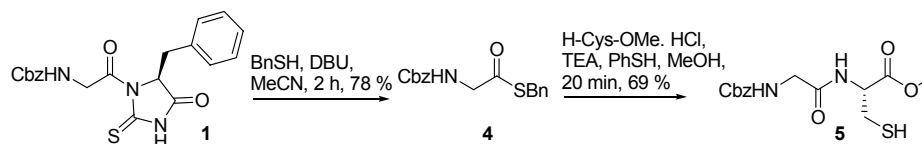


Fig. 1. HPLC Chromatographs for thiohydantoin displacement reactions obtained after 10 min (282 nm, C18, 90 - 10 % 0.1 % TFA/H₂O in 0.04% TFA/MeCN). Nucleophiles used: (a) benzylamine, (b) phenylhydrazine, (c) benzoic hydrazide.

An alternative application of the thiohydantoin technique was found in Native Chemical Ligation, a technique pioneered by Kent *et al.* [3] to condense two peptide fragments. The beauty of this chemistry is that it is chemoselective and operates under mild conditions without protecting groups. However, the synthesis of thioesters is not always straightforward and the thiohydantoin technique was extended to give access to thioesters.

Peptide thiohydantoin **1** was cleaved with thiols as nucleophiles to yield thioester **4** and was thus shown to provide a route to synthesis of thioesters. Native chemical ligation was successfully applied to the synthesis of a small peptide **5** (Scheme 3).



Scheme 3. Synthesis of thioester and application to native chemical ligation.

Acknowledgments

The work was funded by a BBSRC grant to C. Brückler.

References

1. Pandey, A. and Mann, M. *Nature* **405**, 837-846 (2000).
2. Bailey, J. M., Nikfarjam, F., Shenoy, N. R. and Shively, J. E. *Prot. Sci.* **1**, 1622-1633, (1992).
3. Dawson, P. E., Muir, T. W., Clark-Lewis, I. and Kent, S. B. H. *Science* **266**, 776-779 (1994).

Photodimerization in Substituted di- and Oligopeptides by UV-light for Optical Data Storage

Brian Lohse¹, P. S. Ramanujam², Søren Hvilsted³ and Rolf H. Berg¹

¹Polymer Department, Risø National Laboratory, DK-4000 Roskilde, Denmark; ²Department of Optics and Plasma Research, Risø National Laboratory, DK-4000 Roskilde, Denmark;

³Danish Polymer Centre, Department of Chemical Engineering, Technical University of Denmark, DK-2800 Kgs. Lyngby, Denmark

Introduction

DNA is the ultimate data storage molecule, storing in four bases the information to make proteins and, essentially, life. The photodimerization of thymine, discovered long ago upon UV irradiation, is one of the most important reactions in photobiology. It is highly probable that dimerization in irradiated DNA constitutes one of the essential factors responsible for the sensitivity of nucleic acids and cells to the effects of UV-light. The dimerization takes place through the C5-C6 double bond of the pyrimidine and involves the formation of a cyclobutane ring, as shown for our system in Figure 1. Here we describe chromophores attached to a peptide backbone, where the storage of data can be achieved through the principle of photodimerization of neighboring chromophores undergoing $(2\pi + 2\pi)$ cycloaddition, first in solution (H_2O), and then as a film applied onto a quartz plate, if good dimerization efficiency was observed [1-3].

To develop a film of pyrimidine-substituted peptides for digital optical storage requires five important criteria:

1. Large contrast between irradiated and non-irradiated areas of the medium (dimerization efficiency)
2. Fast response for recording
3. Stability during storage ($-30^{\circ}C$ and $50^{\circ}C$)
4. Good optical and mechanical properties
5. Cheap large-scale production.

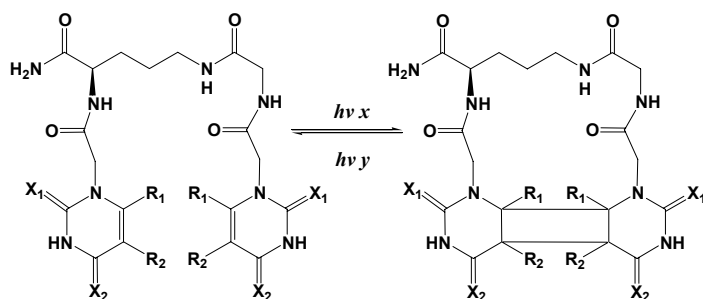


Fig. 1. The photodimerization process shown for a dipeptide (Orn-Gly).

$X = O, S$ and $R = H, CH_3, F, Cl, Br, I$. $h\nu x < h\nu y$.

Results and Discussion

The peptides were synthesized using the stepwise Merrifield SPPS method. The chromophores were synthesized using standard organic chemistry. The compounds were first tested in solution, and irradiated under a UV-lamp for 15, 30 and 60 min (Fig. 2a and 2b). When good dimerization efficiency was observed, the compound

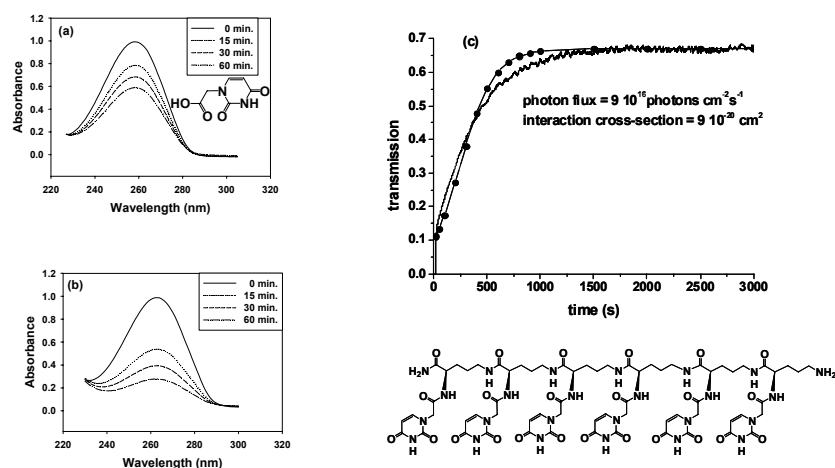


Fig. 2. Experimentally measured absorption of (a) Uracil 1-acetic acid, (b) uracil ornithine hexamer in solution. (c) Transmission through a thin film of uracil ornithine hexamer.

was prepared as a film and tested in our UV-laser setup, in order to test how fast the compound could reach maximum transmission (Fig. 2c).

Overall we observed a significant increase in dimerization efficiency when going from a free chromophore in solution to a chromophore attached to a peptide. Furthermore the peptide films had good optical and mechanical properties, and were completely stable. Good correlation was found between solution and film, making solution testing an effective screening method. Finally, the peptides are environmentally safe and suitable for upgrade to large scale.

Acknowledgments

The work was funded by the Danish Research Council (STVF).

References

1. Lohse, B., Ramanujam, P. S., Hvilsted, S. and Berg, R. H. *J. Peptide Sci.*, 2005; 11: 499-505.
2. Lohse, B., Ramanujam, P. S., Hvilsted, S. and Berg, R. H. *J. Peptide Sci.*, submitted (2006).
3. Lohse, B., Ramanujam, P. S., Hvilsted, S. and Berg, R. H. *J. A. P.*, in press (2005).

Does an Aberrant Glucosylation Trigger Autoimmunity in Multiple Sclerosis?

Francesca Nuti, Ilaria Paolini, Elisa Peroni, Feliciano Real-Fernández, Marta Pazzagli, Maria C. Pozo-Carrero, Francesco Lolli, Mario Chelli, Paolo Rovero and Anna M. Papini

Laboratory of Peptide & Protein Chemistry & Biology, Polo Scientifico, University of Florence, I-50019 Sesto Fiorentino (FI), Italy

Introduction

Glycoproteins are ubiquitous in all forms of life from bacteria to humans and are involved in immune response. In fact the presence of carbohydrates in proteins provides unique epitopes for molecular recognition.

In the literature there are many examples demonstrating that a loss or change in glycosylation of proteins and/or glycolipids (glycosylation defects) are often associated with a large number of autoimmune disorders [1], such as Multiple Sclerosis (MS) [2-4].

Very recently, we reported that auto-antibodies in MS can be recognized as biomarkers only using the glucosylated antigenic probe CSF114(Glc) [4]. The corresponding native antigen has not been yet characterized.

Results and Discussion

It is well known that natural *N*-glycoproteins are heterogeneous, but share the typical core formed by a β -*N*-acetylglucosamine linked to an Asn side chain (β -GlcNAc), that is the putative first glycosylated moiety. Up to now, only one example of novel forms of *N*-glycoproteins have been recognized. In particular a β -D-glucose was unequivocally demonstrated to be linked to the Asn side chain in *Halobacterium halobium* cross-reacting with the laminin glycoprotein [5-6]. Moreover, in our laboratory we demonstrated that Asn(Glc) in the glycopeptide CSF114(Glc) is fundamental for auto-antibody recognition in MS [4,7].

In *N*-glycoproteins, the Asn glycosylation site is always located in the specific amino acid sequence Asn-Xaa-Ser/Thr (sequon). With the aim of identifying the native glycoprotein myelin auto-antigen recognized by CSF114(Glc), and possibly related to the pathogenesis of MS, we undertook a deductive approach to rule out sequons.

As a proof of concept, among the 19 x 2 tripeptides, we started synthesizing the ones containing Xaa = Gly or Lys. In particular, N(Glc)GS (**1**), N(Glc)GT (**2**), N(Glc)KS (**3**), and N(Glc)KT (**4**), as well as N(Glc)GH (**5**), N(Glc)KH (**6**), derived from the original glucosylated core of CSF114(Glc), and N(Glc)AT (**7**), present in [Asn³¹(Glc)]hMOG(30-50) [8]. All tripeptides were acetylated and synthesized as amides, to mimic auto-Ab binding sites (Table 1).

The anti-CSF114(Glc) antibody titer to the glycopeptides was evaluated by inhibition ELISA. Most of the glucosylated sequons inhibit anti-CSF114(Glc) antibodies independently from the Xaa-amino acid. These results let us to formulate a hypothesis on the molecular mechanism of the recently characterized auto-antibody mediated MS pattern: an aberrant glucosylation on Asn residues of myelin proteins creates neoantigens triggering the autoimmune response. Thus, randomly

Table 1. Glucosylated tripeptides

Glucosylated core peptide	Sequence
Glycoprotein consensus sequence	Ac-N(Glc)GS-NH ₂ (1); Ac-N(Glc)GT-NH ₂ (2); Ac-N(Glc)KS-NH ₂ (3); Ac-N(Glc)KT-NH ₂ (4).
CSF114(Glc)	Ac-N(Glc)GH-NH ₂ (5) Ac-N(Glc)KH-NH ₂ (6)
[Asn ³¹ (Glc)]hMOG(30-50)	Ac-N(Glc)AT-NH ₂ (7)

glucosylated myelin proteins will be recognized as non-self antigens, and CSF114(Glc) may be a mimetic of all aberrantly glucosylated myelin proteins.

Acknowledgments

We thank Fondazione Ente Cassa di Risparmio di Firenze and the Travel Award Committee for the financial support to the participation of F. Nuti at 19th APS.

References

1. Saso, L., *et al. Inflammation* **17**, 465-479 (1993).
2. Orlacchio, A., *et al. J. Neurological Sci.* **151**, 177-182 (1997).
3. Demetriou, M., *et al. Nature* **409**, 733-739 (2001).
4. Lolli, F., *et al. Proc. Natl. Acad. Sci. USA* **102**, 10273-10278 (2005).
5. Schreiner, R., *et al. J. Cell. Biol.* **124**, , 1071-1074 (1994).
6. Wieland, F., *et al. Proc. Natl. Acad. Sci. USA* **80**, 5470-5473 (1983).
7. Papini, A. M., *et al. Nat. Med.* **11**, 13 (2005).
8. Mazzucco, S., *et al. Bioorg. Med. Chem. Lett.* **9**, 167-172 (1999).

Phosphopeptide Proteomics with On-Bead Chemical Synthesis and Display on PEGA Support

Malene Brandt^{1,2}, Jens Chr. Madsen³, Steen Gammeltoft² and Knud J. Jensen¹

¹Section for Bioorganic Chemistry, Department of Natural Sciences, KVL, 1871 Frederiksberg, Denmark; ²Department of Clinical Biochemistry, Glostrup Hospital, 2600 Glostrup, Denmark; ³Compound Identification and Purification, H. Lundbeck A/S, Ottiliavej 9, 2500 Valby, Denmark

Introduction

Serine/threonine phosphorylation plays a central role in cellular regulation, either by altering protein activity directly or by inducing specific protein-protein interactions [1]. The development of new methods for phosphopeptide proteomics and their use for identification and characterization of phosphopeptide binding proteins are highly desirable. Immobilized phosphopeptide affinity pull-down experiments have previously been prepared using biotinylated peptides [2]. Here we describe the synthesis of phosphopeptides directly on a solid support compatible with affinity pull-down experiments.

14-3-3 proteins are a family of dimeric pSer/pThr binding proteins present in high abundance in eukaryotic cells [3]. 14-3-3 proteins bind the phosphorylated ligands such as BAD [4] through recognition of the consensus motifs R(S/Ar)XpSXP or RX(Ar/S)XpSXP, where pS denotes pSer/pThr, and Ar denotes aromatic residues [5].

Results and Discussion

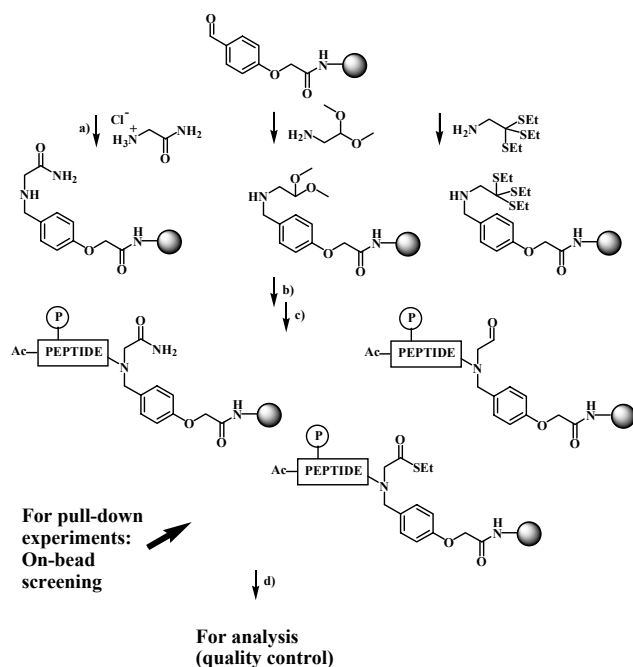
We synthesized short analogs of the BAD₁₃₆ phosphorylation site to use as baits in affinity pull-down experiments [2] to determine their ability to pull-down 14-3-3. Furthermore, we introduced a C-terminal, soft electrophile (aldehyde or thioester) to modulate binding.

We chose poly(ethylene glycol) polyacrylamide (PEGA) resin as solid support due to its superior swelling properties providing access of proteins up to at least 35 kDa [6]. The peptides were synthesized directly on the solid support through a BAL (backbone amide linker)-type handle (scheme 1) [7].

For characterization purposes, small amounts of peptides were cleaved from the solid support and analyzed by RP-HPLC and ESI-MS. The resin-bound peptide with a C-terminal aldehyde was also analyzed by High Resolution-Magic Angle Spinning (HR-MAS) NMR.

HA-tagged 14-3-3 ζ was transfected into COS-7 cells, and the resin-bound peptides (synthesized in phosphorylated [active] and unphosphorylated [control] forms) were incubated overnight with cell lysates. The results of the binding reactions were visualized by Western blotting. The two phosphopeptides with a C-terminal, soft electrophile are able to pull-down 14-3-3 to the same extent as phosphopeptides with a C-terminal amide moiety.

The phosphorylated peptides were able to pull-down 14-3-3 in both transfected and untransfected cells. The bands from a coomassie staining were cut out, digested with trypsin, and analyzed by MS. The bands showed the different isoforms of 14-3-3.



Scheme 1. Phosphopeptide synthesis on solid support. a) $\text{H}_2\text{NCH}_2\text{R}$, NaBH_3CN , 1 % AcOH in MeOH. b) Fmoc-Aaa-OH, HBTU, HOBT, DIEA, NMP. c) TFA/ H_2O /TES or TFA/ H_2O (for C-terminal aldehyde). d) TFA/TFMSA. R: CONH_2 , CH(OMe)_2 , C(SEt)_3 . P: Phosphorylation.

Acknowledgments

We thank Birte Kofoed, Glostrup Hospital, for technical assistance, and Dr. Andrew Coffey, Polymer Laboratories, for a generous supply of PEGA.

References

1. Yaffe, M. B. and Elia, A. E. H. *Curr. Opin. Cell. Biol.* **13**, 131-138 (2001).
2. Schulze, W. X. and Mann, M. *J. Biol. Chem.* **279**, 10756-10764 (2004).
3. a) Fu, H., Subramanian, R. R. and Masters, S. C. *Annu. Rev. Pharmacol. Toxicol.* **40**, 617-647 (2000); b) Yaffe, M. B. *FEBS Letts.* **513**, 53-57 (2002).
4. Petros, A. M., Olejniczak, E. T. and Fesik, S. W. *Biochem. Biophys. Acta* **1644**, 83-94 (2004).
5. Yaffe, M. B., Rittinger, K., Volinia, S., Caron, P. R., Aitken, A., Leffers, H., Gamblin, S. J., Smerdon, S. J. and Cantley, L. C. *Cell* **91**, 961-971 (1997).
6. St. Hilaire, P. M., Willert, M., Juliano, M. A., Juliano, L. and Meldal, M. *J. Comb. Chem.* **1**, 509-523 (1999).
7. a) Jensen, K. J., Alsina, J., Songster, M. F., Vágner, J., Albericio, F. and Barany, G. *J. Am. Chem. Soc.* **120**, 5441-5452 (1998); b) Bourne, G. T., Meutermanns, W. D. F., Alewood, P. F., McGeary, R. P., Scanlon, M., Watson, A. A. and Smyth, M. L. *J. Org. Chem.* **64**, 3095-3101 (1999).

Optimization of Multiple Sclerosis Antigenic Probes by a Combinatorial Approach

Maria C. Alcaro, Francesca Barbetti, Francesca Nuti, Feliciano Real-Fernández, Benedetta Mazzanti, Mario Chelli, Paolo Rovero and Anna M. Papini

Laboratory of Peptide & Protein Chemistry & Biology, Polo Scientifico, Università di Firenze, I-50019 Sesto Fiorentino (FI), Italy

Introduction

Multiple Sclerosis (MS) is a chronic, inflammatory, demyelinating disease of the central nervous system. MS can be considered as a group of diseases, which have not been yet characterized [1]. The Laboratory of Peptide & Protein Chemistry & Biology has been involved for almost a decade in investigating the molecular mechanisms of an antibody-mediated MS pattern. We previously developed the synthetic glycopeptide CSF114(Glc), first generation of antigenic probes, to detect sugar-specific autoantibodies, (auto-Abs), correlating with the disease activity, in a consistent population of MS patients [2-4]. CSF114(Glc) displays a well-defined conformation characterized by a β -hairpin motif with the minimal epitope Asn(Glc), fundamental for the autoantibody recognition, on the tip of a type I' β -turn structure.

Results and Discussion

To improve the autoantibody recognition of CSF114(Glc) by SP-ELISA, we investigated the role of the residues involved in the β -hairpin structure and thus responsible of the optimal exposition of Asn(Glc) at position 7. To optimize the +B1 and +B2 positions of the β -hairpin, we synthesized the [Xaa⁹,Yaa¹⁰]CSF114(Glc) glycopeptide library where diversity is provided by the 19 natural amino acids, excluding Cys. The sublibrary [O⁹,Yaa¹⁰]CSF114(Glc) was synthesized by a split&mix technique following the Fmoc/tBu SPPS strategy, and introducing the glucosylated amino acid by a building-block approach [5].

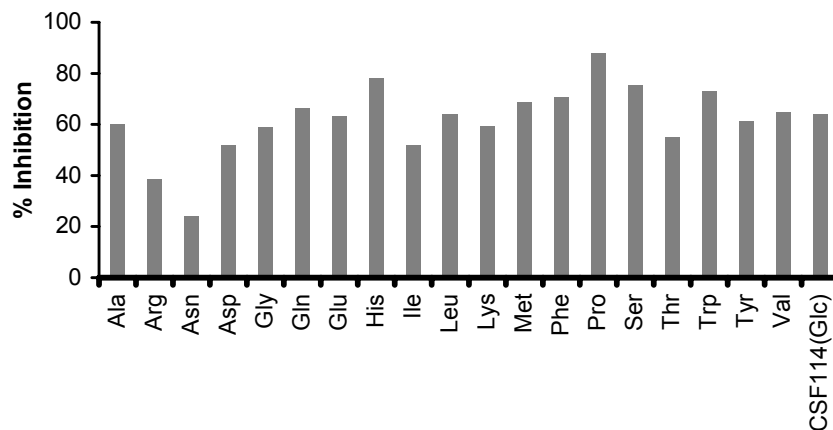


Fig. 1. Inhibition (%) of anti-CSF114(Glc) Abs by the [O⁹,Yaa¹⁰]CSF114(Glc) sublibrary.

In the case of the +B1 position, the $[O^9, Yaa^{10}]CSF114(Glc)$ sublibrary, was screened by inhibition ELISA (Fig. 1). The mixtures of glycopeptides containing Pro, His, or Ser at position +B1 showed a higher affinity for anti-CSF114(Glc) auto-Abs in MS patients' sera. The sublibrary containing Pro at position +B1 showed an $IC_{50} = 0.032 \mu g/ml$, while CSF114(Glc) possesses an $IC_{50} = 0.15 \mu g/ml$.

In a first attempt to optimize the +B2 position, we performed an iterative deconvolution synthesizing the 19 glycopeptides $[Pro^9, O^{10}]CSF114(Glc)$. After screening, all the glycopeptides $[Pro^9, O^{10}]CSF114(Glc)$ showed a comparable biological activity, even if lower than CSF114(Glc) one (Fig. 2).

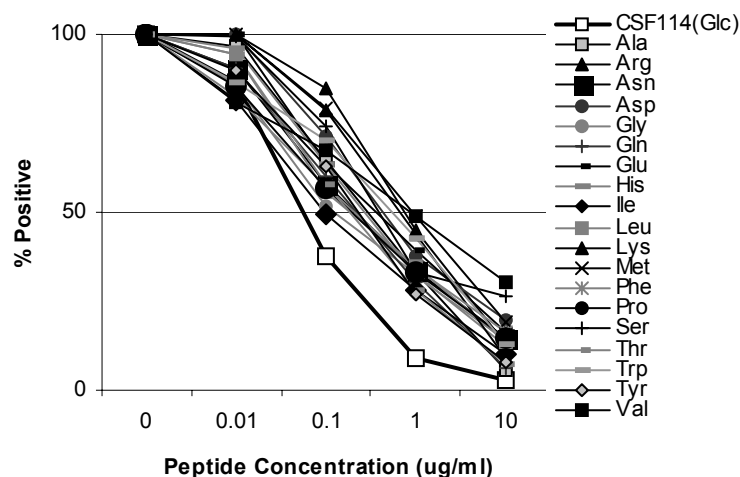


Fig. 2. Inhibition (%) of anti-CSF114(Glc) using $[Pro^9, O^{10}]CSF114(Glc)$ sublibrary.

The positive results obtained with the $[Pro^9, O^{10}]CSF114(Glc)$ sublibrary can be due to the sum of the individual glycopeptide activities.

In the case of optimization of the +B2 position, we synthesized the $[Xaa^9, O^{10}]CSF114(Glc)$ sublibrary introducing the diversity at the +B1 position using equimolar mixtures of amino acids. The screening for the above described sublibrary is in progress.

Acknowledgments

This research was supported in part by PRIN2002. We thank Fondazione Ente Cassa di Risparmio di Firenze.

References

1. Lucchinetti, C., et al. *Brain Pathol.* **6**, 259-274 (1996).
2. Papini, A. M., Rovero, P., Chelli, M. and Lolli, F. PCT International application (2003) WO 03000733 A2. Priority Data FI2001A000114.
3. Lolli, F., et al. *Proc. Natl. Acad. Sci. USA* **102**, 10273-10278 (2005).
4. Lolli, F., et al. *J. Neuroimmunol.* **167**, 131-137 (2005).
5. Christiansen-Brams, I., et al. *J. Chem. Soc., Perkin Trans 1* 1461 (1993).

Antiproliferative Effect of Lamprey Gonadotropin-releasing Hormone III on Cancer Cells from Non-reproductive Organs

Krisztina Herédi-Szabó, Richard F. Murphy and Sándor Lovas

Department of Biomedical Science, School of Medicine, Creighton University, Omaha, NE 68178, USA

Introduction

Receptors for gonadotropin-releasing hormone (GnRH) are expressed in many extra-pituitary tissues and their role and mechanism of action in gynecological tumors are well characterized [1]. GnRH and its analogs utilize the $G_{q/11}$ signaling pathway in the pituitary whereas, in ovarian, endometrial, and prostate cancer cells, the G_i pathway is activated [1].

GnRH receptors were also found in tumors in the liver and the pancreas, not originating in reproductive organs [2]. The mechanism of growth inhibition by GnRH analogs in these tumors has not been studied extensively. These tumors can be targeted through their GnRH receptors, although peptides with high-affinity for the pituitary GnRH receptors can not be used because of their numerous endocrine side effects. An isoform of GnRH from lamprey, lGnRH-III, inhibits the growth of cancer cells which express GnRH receptors but has negligible endocrine activity in mammals, making it a good candidate for targeting such tumors [3,4].

The objective of this study was to compare the signaling pathway utilized by lGnRH-III in cancer cells of different origin.

Competition receptor binding and cell growth experiments were carried out to determine the binding affinity and growth inhibitory action of lGnRH-III on HT-29 colonic, PANC-1 pancreatic, and MDA-MB 231 breast cancer cells. The involvement of the G_i pathway in lGnRH-III signaling was investigated with the help of pertussis toxin (PTX), since this pathway was shown to be activated by GnRH analogs in extra-pituitary tissues [1].

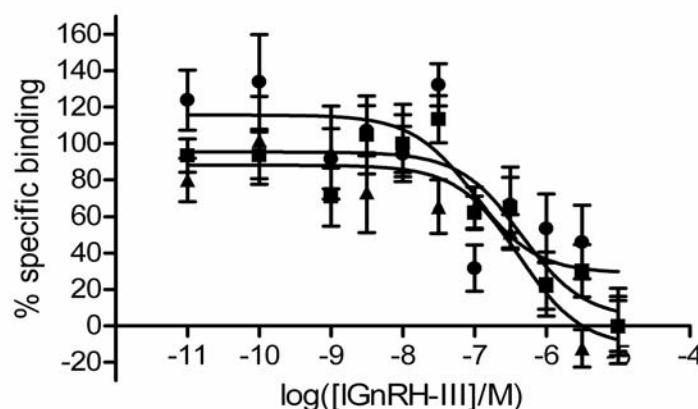


Fig. 1. Displacement of ^{125}I -GnRH by lGnRH-III from (■) MDA-MB 231, (●) HT-29 and (▲) PANC-1 cancer cells.

Table 1. Effect of 1 μ M lGnRH-III on cAMP levels and growth

Cell line	% of control			
	[cAMP]		Cell number	
	lGnRH-III	lGnRH-III + PTX	lGnRH-III	lGnRH-III + PTX
MDA-MB 231	108.46 \pm 12.86	80.08 \pm 7.90	74.94 \pm 7.94 ^b	84.01 \pm 12.84 ^b
HT-29	75.34 \pm 5.94 ^a	81.02 \pm 7.98	71.84 \pm 9.54 ^c	94.79 \pm 13.18
PANC-1	70.57 \pm 2.71 ^a	109.89 \pm 17.5	69.32 \pm 8.46 ^c	93.99 \pm 11.71

^a $p < 0.05$; ^b $p < 0.01$; ^c $p < 0.001$ determined by the Kruskal-Wallis test. Data are presented as mean \pm SEM of at least 6 determinations.

Results and Discussion

lGnRH-III bound with similar affinities to MDA-MB 231 (IC_{50} =455.0 \pm 31.1 nM), HT-29 (IC_{50} =97.6 \pm 33.7 nM), and PANC-1 (IC_{50} =421.4 \pm 29.4 nM) cells (Fig. 1). lGnRH-III inhibited the growth of all three cell lines in a dose-dependent manner in sub-micromolar concentrations. This is in good agreement with the IC_{50} values obtained from the binding experiments.

Table 1 shows the effect of lGnRH-III with or without PTX on cAMP concentrations and cell growth. PTX alone did not influence cell growth. Both these studies showed that lGnRH-III activates the G_i pathway in HT-29 and PANC-1 cells, since a significant decrease in cAMP levels was observed following peptide treatment and PTX completely reversed the growth inhibitory effect of lGnRH-III. On the other hand, the growth inhibitory effect of lGnRH-III on MDA-MB 231 breast cancer cells was not mediated by the G_i pathway. Keri and associates [5] showed that signaling in response to GnRH analogs in breast cancer cells entails the activation of protein kinase C, a possible downstream effector in the $G_{q/11}$ pathway. This study supports the view that the same GnRH receptor can signal through different pathways in cancer cells depending on the tissue.

Acknowledgments

This work was supported by NIH Grant Number 1 P20 RR16469 from the BRIN program of the National Center of Research Resources and Carpenter Chair in Biochemistry, Creighton University, Omaha, NE.

References

1. Imai A., Takagi H., Horibe S., Fuseya T. and Tamaya T. *J. Clin. Endocrinol. Metabol.* **81**, 3249-3253 (1996).
2. Szende B., Srkalovic G., Timar J., Mulchahey J. J., Neill J. D., Lapis K., Csikos A., Szepeshazi K. and Schally A. V. *Proc. Natl. Acad. Sci. USA* **88**, 4153-4156 (1991).
3. Lovas S., et al. *J. Peptide Res.* **52**, 384-389 (1998).
4. Heredi-Szabo K., Lubke J., Toth G., Murphy R. F. and Lovas S. *Peptides* **26**, 419-422 (2005).
5. Keri Gy., Balogh A., Szoke B., Teplan I. and Csuka O. *Tumor Biol.* **12**, 61-67 (1991).

New Cyclotide Precursor Sequences

Lillian Sando, Rekha Bharathi and David J. Craik

Institute for Molecular Bioscience, University of Queensland, Brisbane, QLD 4072, Australia

Introduction

Originally discovered based on their use in native African medicine to accelerate childbirth [1], these fascinating mini-proteins from plants have become the largest family of naturally occurring cyclic proteins. Cyclotides have a range of potentially useful bio-activities including anti-HIV [2], anti-cancer [3], and insecticidal [4] activities. Embedded within their circular peptide backbone is the topologically intriguing cystine knot motif, consisting of a ring formed by two disulfides and their connecting backbone segments, penetrated by a third disulfide bond [5], as shown in Figure 1. Approximately 50 cyclotide sequences have been published to date but the family is estimated to comprise hundreds or thousands of members.

Although the gene structure of cyclotides is known [4] (Fig. 1), the mechanism by which the linear precursors are processed into mature proteins with cyclic backbones is not well understood. A conserved C-terminal Asn or Asp is thought to play a role in the cyclization. The aims of this study were 1) to identify more cyclotide precursors to further the understanding of how cyclotides are processed and cyclized in the plant, and 2) to explore the natural sequence variation of cyclotides in plants to gain knowledge of how the cyclotide framework may be utilized in protein engineering applications.

Results and Discussion

In this study we used PCR-based approaches to determine the cDNA sequences of new cyclotides and cyclotide precursors from *Melicytus* and *Hybanthus* species in the Violaceae family. OneStep RT-PCR (Qiagen) was used with oligo-dT and degenerate primers designed from known cyclotide sequences to amplify partial cyclotide precursor clones. FirstChoice® RLM-RACE (Ambion) was used to isolate the full length clones of three precursors. Further, comparison of the precursors isolated in this study and previously [6,7] identified a conserved element (AAFALPA) in the ER-signal sequence, as shown in Figure 1. This element was targeted in a new approach to the discovery of cyclotide sequences using RT-PCR with oligo-dT and a primer designed to target the newly discovered AAFALPA sequence within the ER-signal. This approach proved successful for the rapid discovery of cyclotide sequences including most of the precursor without the need for cDNA or 5'-RACE library construction. Figure 1 shows the full precursors identified in this study.

There are two main subclasses of cyclotides, Möbius and bracelet. Most of the cyclotides discovered in this study were bracelet peptides. Bracelets usually contain six to seven amino acids in loop 3, forming a short helix (Fig. 1). Many of the new bracelet cyclotides have a shorter loop 3 (four residues). A 3D homology model of one of these showed that loop 3 formed a turn, as in Möbius cyclotides. This has advanced our understanding of the sequence variation allowed in cyclotides, which may be regarded as a natural combinatorial template with a range of potential applications in drug design and crop protection. Our findings suggest that loops 3 and 5 are potentially amenable to grafting of foreign bioactive epitopes.

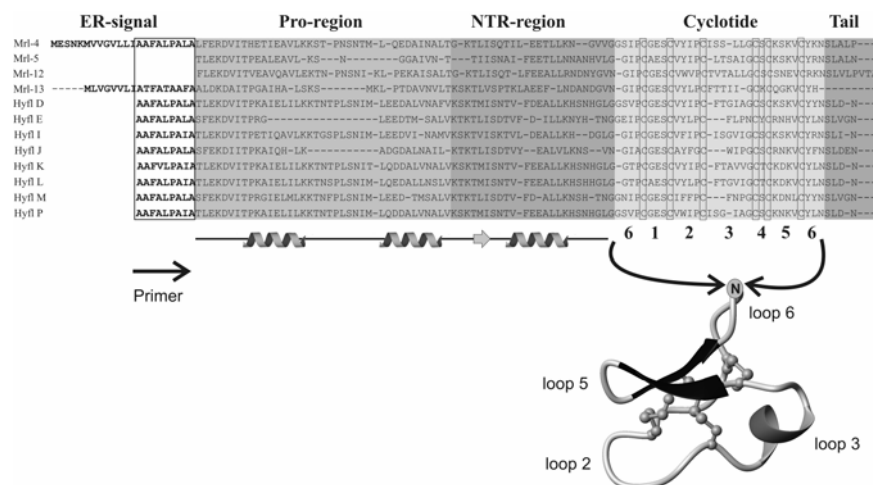


Fig. 1. A selection of the new cyclotide precursors identified in this study. The precursors typically contain an endoplasmic reticulum (ER) signal, a pro-region, 1-3 copies of a cyclotide domain preceded by an N-terminal repeat (NTR) sequence within the pro-region, and a short tail region [4]. The pro-regions typically contain 1-3 helices and a short β -strand, as indicated. In some precursors with multiple copies of the cyclotide domain and NTR, only the helix closest to the cyclotide domain is present. This helix is thought to be important in cyclotide processing or detoxification [6]. The newly discovered consensus sequence AAFALPA within the ER-signal, which was used as a new primer binding site, is boxed. The cyclotide domain is cleaved from the precursor by an as yet unidentified mechanism, cyclized in loop 6, and folded into an extremely stable 3D structure. A ribbon structure of a typical bracelet cyclotide is shown, with disulfides in ball and stick form. The conserved Asn at the cyclization point, which is thought to be important for cyclotide processing, is highlighted. Two of the new sequences identified in this study lack the Asn as well as the tail, and are most likely linear cyclotide homologues.

Acknowledgments

The work was funded by the Australian Research Council (ARC). LS is a recipient of an Australian Postgraduate Award, IMB Travel Funding, and APS Travel Award. DJC is an ARC Professorial Fellow.

References

1. Gran, L. *Acta Pharmacol. Toxicol.* **33**, 400-408 (1973).
2. Gustafson, K. R., et al. *J. Am. Chem. Soc.* **116**, 9337-9338 (1994).
3. Lindholm, P., et al. *Mol. Cancer Ther.* **1**, 365-369. (2002).
4. Jennings, C., West, J., Waite, C., Craik, D. J., and Anderson, M. *Proc. Natl. Acad. Sci. USA* **98**, 10614-10619 (2001).
5. Craik, D. J., Daly, N. L., Bond, T. and Waite, C. *J. Mol. Biol.* **294**, 1327-1336 (1999).
6. Dutton, J. L., et al. *J. Biol. Chem.* **279**, 46858-46867 (2004).
7. Mulvenna, J., Sando, L. and Craik, D. J. *Structure* **13**, 691-701 (2005).

Development of an Efficient Multiple Sclerosis Diagnostic Technology Based on an Optical Glycopeptide Immunosensor

**Emily S. Bulukin¹, Elisa Peroni², Maria Minunni¹, Marta Pazzagli²,
Paolo Rovero², Marco Mascini¹ and Anna M. Papini²**

¹*Department of Chemistry, University of Florence, Via della Lastruccia 3, I-50019, Sesto Fiorentino (FI), Italy;* ²*Laboratory of Peptide & Protein Chemistry and Biology, University of Florence, Via della Lastruccia 13, I-50019 Sesto Fiorentino (FI), Italy*

Introduction

Multiple Sclerosis (MS) is an inflammatory demyelinating disease of the central nervous system and one of the most common causes of neurological disability in young adults in the northern hemisphere. Recent works have been undertaken to characterize an antibody-mediated MS disease pattern [1]. An ELISA-based diagnostic/prognostic kit (MSPepKit), based on the glycopeptide CSF114(Glc) able to recognize specific auto-antibodies (auto-Abs) in sera of MS patient has been developed [2,3,4].

A biosensor technology can offer advantages such as rapid analysis, and high sensitivity. For this purpose the instrument BIAcore XTM, based on surface plasmon resonance was used for real-time, label-free monitoring in sera of MS patients of anti-CSF114(Glc) auto-Abs.

Results and Discussion

CSF114(Glc) was immobilised on a dextran coated gold chip. Two immobilisation strategies were applied: one based on direct amino coupling of the antigen, the other on streptavidin-biotin linkage using a biotin derivative of CSF114(Glc) onto a streptavidin covered surface. Optimisation of the sensor was performed with anti-CSF114(Glc) Abs purified by affinity chromatography from MS patients' sera. The system was tested on MS and healthy blood donors' sera and the analytical parameters such as specificity, sensitivity and matrix effects were evaluated. Calibration curves obtained with the purified anti-CSF114(Glc) Abs in buffer and in commercial healthy blood donors serum (BD, Sigma) are reported in Figure 1, relatively to the two different immobilization procedures. The matrix effect of serum (1:100) was evaluated by adding purified anti-CSF114(Glc) Abs at different concentrations. Higher sensitivity was observed in the case of the streptavidin-biotin immobilization. This difference could be explained by the fact that the antigen may be oriented differently on the sensor surface. Consequently, the minimal epitope Asn(Glc) may not be well exposed for antibody interaction. The immunosensor was tested using positive and negative control sera (Table 1). The positive control, from an MS patients' serum was compared with BD. The results show that the sensor, in both cases, is able to discriminate between MS and BD. The sample analysis time was 15 minutes. Furthermore, a comparison of the antibody titer of longitudinal sera from an MS patient evaluated with the immunosensor and MSPepKit was undertaken (Fig. 2). The results indicate that the BIAcore technology may offer interesting future applications in MS diagnostics.

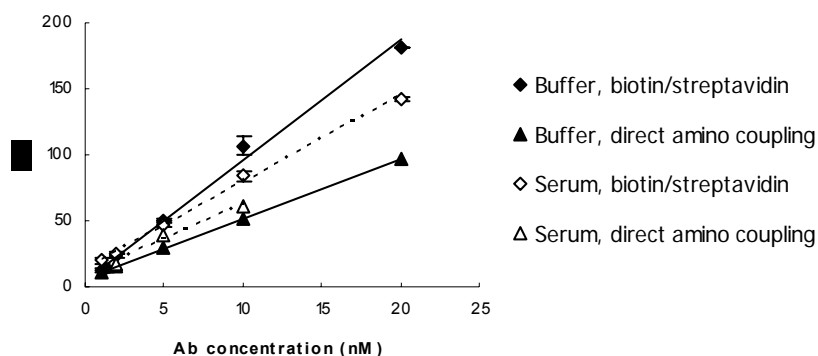


Fig. 1. Calibration curves obtained with purified anti-CSF114(Glc) Abs, in buffer and in BD serum by BIAcore.

Table 1. BIAcore with different immobilization strategies

Sample	Amino coupling (RU)	Streptavidin/biotin (RU)
Abs isolated from one MS patient (10 nM)	52	140
Serum from one MS patient	118	173
BD serum (Sigma)	11	1
BD serum	12	14

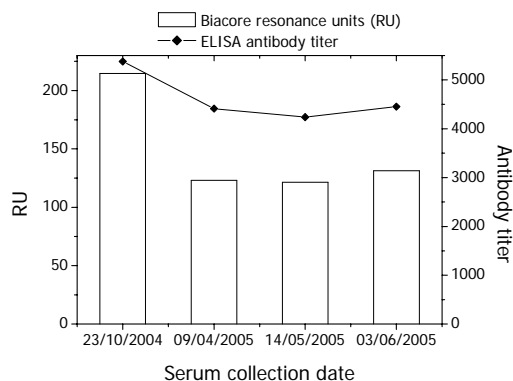


Fig. 2. Comparative analysis (BIAcore/MS PepKit) of longitudinal sera of one MS patient positive to CSF114(Glc) Abs in sera collected at different times from an MS patient.

Acknowledgments

We thank Fondazione Ente Cassa di Risparmio di Firenze, WATERS Corporation and the Travel Award Committee for the financial support.

References

1. Lucchinetti, C. *et al. Brain Pathol.* **6**, 259-274 (1996).
2. Papini, A. M. *Nat. Med.* **11**, 13 (2005).
3. Looli, F., *et al. Proc. Natl. Acad. Sci. USA*, **102**, 10273-10278 (2005).
4. Papini, A. M., Rovero, P., Chelli, M. and Lolli, F. PCT International application (2003) WO 03000733 A2. Priority Data FI2001A000114.

Author Index
Subject Index

Authors

- Abdel-Malek, Z.** 461, 537
Abe, A. 700
Abel-Santos, E. 338
Aboitiz, N. 767
Abran, D. 589
Abrescia, P. 449
Adams, J. 457
Adermann, K. 156
Adriaens, W. 675
Agbaba, D. 433
Agnes, R.S. 361, 591
Aguilar, M.I. 718
Ahmadian, M. 447
Aiello, R. 625
Aimoto, S. 132, 160
Ajmo, T. 471
Alagarsamy, S. 489
Albericio, F. 108, 114, 116, 142, 210, 220
Albrizio, S. 401
Alcaro, M.C. 779
Aldrich, J.V. 162, 523, 525, 533
Aletras, A. 140
Alewood, P.F. 641
Allen, S.D. 635, 690
Aloj, L. 182
Álvarez, M. 116
Alves, I.D. 332, 750
Ambo, A. 507
Amela-Cortés, C. 475
An, J. 377
Anantharamaiah, G.M. 329
Andersen, N.H. 541
Andersen, P. 383
Andrade, G.F.S. 86
Andreu, D. 248, 767
Angell, Y.M. 405
Anglister, J. 118, 172
Ankersen, M. 383
Appella, E. 208
Armishaw, C.J. 641
Arra, C. 182
Arshava, B. 80, 118, 122, 172
Arukwe, J. 665
Arumugam, T.V. 491
Ashkenasy, G. 645
Atkinson, N. 457
Aucoin, J.P. 471
Auriemma, L. 76, 112
Avedanian, L. 120
Averlant-Petit, M.C. 716
Ayzenshtat, I. 118
Baas, D. 144
Babu, V.V.S. 122
Baessler, K. 59
Bakelaar, F.T. 156
Balasubramaniam, A. 419
Baldauf, C. 671
Baldini, C. 265
Ballet, S. 359, 495
Bandoli, G. 349
Barany, G. 134, 144, 146, 192, 194, 196, 297, 712
Barany, M.J. 196
Baratova, L.A. 307
Barazza, A. 385
Barbato, G. 569
Barbetti, F. 779
Barbier, J.R. 617, 621
Barchi, J.J.Jr. 559
Bardroff, M. 429
Barlos, K. 138, 140
Baronas-Lowell, D. 315
Barozzi, N. 407
Basak, A. 341
Basak, S. 341
Bastiras, S. 164
Batistatos, M. 140
Bauzo, R.M. 521, 537
Bayo, N. 114, 220
Beals, J.M. 615
Beaulieu, M.E. 176, 455, 473
Beck, H. 429
Becker, C.F.W. 725
Becker, J.M. 80, 122, 663
Beck-Sickinger, A.G. 544
Behery, A.A. 527
Belda, I. 649
Benedetti, E. 166, 182, 367, 449, 575, 601
Bennett, M.A. 533
Berezowska, I. 31
Berg, R.H. 773
Berg-Cross, S. 465
Bernard, E. 451
Bernstein, S.L. 515
Bertamino, A. 112, 353
Bett, C. 471
Bettio, A. 603

Beutling, U. 736
 Beyermann, M. 168
 Bhandari, A. 405
 Bharathi, R. 783
 Bhuiyan, M.P.I. 391, 393, 499
 Bianchi, E. 267, 569, 571
 Bidlack, J.M. 332
 Bienert, M. 168
 Biesemans, M. 495
 Bilsky, E.J. 332
 Bindu, L.K. 180, 208, 559
 Biondi, B. 417, 479
 Biron, E. 100, 102, 423
 Bitan, G. 515
 Bkaily, G. 120
 Blanchfield, J.T. 511
 Blat, D. 443
 Blishchenko, E.Y. 513
 Blom, A. 637
 Blondelle, S.E. 255, 379
 Boaquan, M. 237
 Bocchinfuso, G. 603, 605
 Bodas, M.S. 47
 Bodestine, T. 78
 Boeglin, D.R. 47, 184
 Boeriu, C.G. 740
 Boggs, J. 297
 Bohling, J. 220
 Bolzati, C. 349
 Borics, A. 708
 Borin, G. 417, 479, 491
 Boros, M. 363
 Bottaro, D.P. 208
 Botti, P. 61, 166
 Boulanger, N. 289
 Boulanger, Y. 225
 Boulegue, C. 667
 Bouschen, W. 725
 Bowers, M.T. 515
 Boyd, J.G. 64
 Bracci, L. 371
 Bradley, M. 771
 Brandt, M. 777
 Braun, K. 136
 Breithaupt, C. 769
 Brenzel, S. 754
 Breveglieri, G. 367
 Briand, J.P. 716
 Brigham-Burke, M. 429
 Briones, M.P.P. 611
 Brodjian, S.J. 154
 Brogan, A.P. 252
 Brophy, S.E. 154
 Brouwer, A.J. 152, 198
 Brower, J.O. 325
 Broxterman, Q.B. 68, 261
 Brückler, C. 771
 Brue, R.J. 457
 Brunel, F.M. 519
 Bryant, S.D. 507
 Buckley, V. 451
 Budisa, N. 769
 Bulet, P. 273, 289
 Bulukin, E.S. 785
 Bunn, P.A.Jr. 459
 Burattini, M. 281
 Burger, K. 108, 142
 Burke, T.R.Jr. 180, 208, 559
 Burns, N. 413
 Burton, D.R. 519
 Busby, S.A. 315
 Byk, G. 150
 Cabello, C. 399
 Cadamuro, S.A. 561
 Cai, M. 399, 535, 550, 629, 651
 Cai, W. 42, 463
 Cain, J.P. 550
 Calderan, A. 417, 479, 491
 Caliendo, G. 401
 Camarero, J.A. 235, 728
 Camperi, S.A. 114
 Campiglia, P. 76, 112, 353, 401, 437, 439
 Camus, M.S. 56
 Cañada, F.J. 767
 Cañedo, L.M. 210
 Cano, P. 172
 Cano-Sanchez, P. 118, 122
 Caporale, A. 38, 349
 Carbin, D.M. 395, 529
 Carenbauer, A.L. 146
 Carlson, J.R. 467
 Carlucci, A. 449
 Carotenuto, A. 76, 112, 401, 437, 439
 Carpino, L.A. 168
 Carrasco, M.R. 300
 Carta, D. 349
 Carton, J. 429
 Cascone, O. 114
 Caso, P. 449
 Cativiela, C. 567
 Catt, K.J. 657
 Cecil, M.R. 146
 Cescato, R. 517
 Chaddha, M. 329

- Chakrabarti, A. 405
 Chakraborty, T.K. 661
 Chalmers, M.J. 315
 Chamberland, C. 473
 Chan, D.C. 459
 Chandler, K.B. 399, 651
 Chandravarkar, A. 56
 Chanh, T.C. 692
 Chastain, M. 267
 Chatterjee, J. 102
 Chelli, M. 190, 775, 779
 Chen, D.D.Y. 593
 Chen, J. 501
 Chen, L. 447
 Chen, X. 463, 714
 Chen, Y. 291, 447
 Cheng, L.L. 573, 659
 Chiyomori, Y. 104, 106
 Chorev, M. 38
 Chung, N.N. 31
 Ciarmiello, A. 182
 Ciliberto, G. 267, 569
 Clapham, B. 252
 Clement, C.C. 553
 Clément, M. 473
 Coast, G.M. 369
 Cofano, L. 349
 Coffey, A.F. 355
 Coin, I. 168
 Coleman, D.R.IV. 53
 Coleman, L. 451
 Coleman, M.A. 728
 Colgrave, M.L. 641
 Condie, B.A. 287
 Copps, J. 706
 Corey, M.M. 196
 Cortese, R. 267, 569
 Corvaja, C. 557, 565
 Costantini, S. 575
 Côté, J. 120
 Côté, S. 114
 Craik, D.J. 243, 641, 783
 Cressman, S. 593
 Crisma, M. 68, 557, 565, 567
 Croston, G. 441, 489
 Cruz, L.J. 114, 210, 220
 Cudic, M. 303
 Cudic, P. 271
 Cui, K. 447
 Culler, M.D. 40, 587
 Cullis, P.R. 593
 Cupido, T. 108
 Cuthbertson, A. 665
 Czaplewski, C. 698
 Czerwinski, A. 146
 D'Alessio, A. 182
 D'Andrea, L.D. 449
 Dafflon, N. 61
 Daffre, S. 86, 273
 Dahlén, K. 677
 Dalla Bona, A. 261
 Daly, E. 637
 Daly, N.L. 641
 Dangoor, D. 443
 Darlak, K. 146
 Darlak, M. 146
 Das, A. 78, 429
 Datta, G. 329
 Datta, R. 587
 Dattilo, J.W. 447
 David, R. 544
 Davis, J. 665
 Davis, P. 361, 535, 591
 Dawson, P.E. 519
 Dayton, B.D. 154
 De Borggraeve, W.M. 567
 De Francisco, M.N. 405
 De Luca, S. 182
 de Oliveira, P.V. 82
 De Pinto, V. 625
 De Stefano, A. 449
 de Waal, B.F.M. 675
 De Wachter, R. 495
 Dean, T. 344, 617, 621
 Deber, C.M. 26, 293
 Decatur, S.M. 683
 Del Gatto, A. 449
 Delhanty, P. 589
 Della Moglie, R. 182
 Demers, A. 188
 Demers, J.P. 184
 Depresle, B. 61
 Derick, S. 573
 Devanathan, S. 750
 Devocelle, M. 451
 Dharmawardana, P.G. 208
 Di Niola, E. 367
 Dick, F. 218
 Dickerson, T.J. 252
 Dickson, R.B. 485
 Dieckelmann, M. 511
 Dikmans, A.J. 736
 DiMarchi, R.D. 88, 229, 237, 305, 311,
 409, 547, 615, 655, 763
 Dirksen, A. 200, 675

Distefano, M.D. 297
 Diurno, M.V. 112, 353
 Diwu, Z. 425
 Dobson, C.M. 194
 Doisy, X. 275, 277, 279
 Dong, J.Z. 40, 587
 Dong, S. 70
 Dong, S.L. 36
 Dos Santos, S. 56
 Ducata, D.D. 429
 Duguay, A.N. 405
 Durani, S. 643
 Dyba, M. 509

Ebbinghaus, S. 363
 Edison, A.S. 381
 Edwards, P. 409, 655
 Eggen, I.F. 156
 Eggleton, R.D. 332
 Egmond, M.R. 212
 Ehara, T. 607
 Eidenschink, L.A. 541
 Eltschinger, V. 517
 Emini, E. 267
 Emmerson, P.J. 409, 655
 Enama, J.T. 692
 Engelhard, M. 725
 Englander, J. 80
 Erchehyi, J. 517
 Erdélyi, M. 647
 Erić, S. 433
 Errachid, A. 114
 Escher, E. 176, 357, 455, 473
 Eskandari, S. 686
 Estephan, R. 80
 Etienne, M.A. 471, 712
 Eto, Y. 497
 Etzkorn, F.A. 759
 Eynon, J. 40
 Eynon, J. 587

Fabbrini, M. 371
 Facchiano, A. 575
 Falciani, C. 371
 Falla, T.J. 285
 Falletta, E. 265
 Fan, J. 267
 Fang, N. 593
 Fang, W.J. 533
 Farber, K.W. 447
 Farndale, R.W. 431
 Farquhar, M. 397
 Fasulo, R. 166

Fázio, M.A. 273
 Feng, Y. 341
 Feriotto, G. 367
 Fernández-Carneado, J. 649
 Fesinmeyer, R.M. 541
 Fields, G.B. 303, 315, 633
 Fierro, O. 401
 Filfil, R. 669
 Fillion, D. 357
 Finotto, M. 267, 569, 571
 Fiori, N. 38
 Fisher, R.J. 180, 208, 559
 Flora, D. 409
 Flora, D.B. 655
 Floreani, M. 417
 Flynn, P. 694
 Fogelman, A.M. 329
 Formaggio, F. 68, 261, 263, 557, 565, 603, 605
 Forssmann, W.G. 156
 Fortier, A. 120
 Fournier, A. 225
 Fowler, J. 395
 Fralick, J. 387
 Frank, H.G. 148
 Frank, R. 736
 Frederick, B.T. 405
 Freed, D. 267
 Freire, E. 597
 Freudenberg, J.C. 747
 Fridkin, M. 443
 Friend, L.A. 419
 Fritzsche, R.W. 377
 Fu, T.M. 267
 Fujii, N. 202, 204, 469
 Fujita, I. 613
 Fukao, F. 106
 Furic, R. 114
 Furuta, M. 611
 Furuya, H. 700

Gadski, R. 409
 Gadski, R.A. 655
 Gaertner, H. 61
 Galaud, F. 47, 188
 Galdiero, M. 601
 Galdiero, S. 601
 Galyean, R. 489
 Gambari, R. 367
 Gammeltoft, S. 777
 Gao, F. 373
 Gao, J.Q. 497
 Garber, D.W. 329

- García-Martín, F. 114, 220
 García-Ramos, Y. 114
 Gardella, T.J. 344, 617, 621
 Gatos, D. 138, 140
 Gatto, E. 603, 605
 Geleziunas, R. 569, 571
 Gelfanov, V.M. 229, 237, 305, 311, 547, 763
 Gera, L. 413, 459
 Gerhardt, J. 218
 Ghadiri, M.R. 283, 645
 Ghalit, N. 50
 Ghosh, I. 214
 Gibson, A. 665
 Gillies, R.J. 373, 765
 Giralt, E. 142, 210, 649
 Glaser, M. 665
 Glukhov, E. 293
 Gobeil, F.Jr. 120
 Gogoll, A. 647
 Gomez-Monterrey, I. 76, 112, 353
 Gonzales, A. 686
 Good, M. 407
 Goodman, M. 42
 Goody, R.S. 725
 Gopisetty-Venkatta, N. 365
 Gordo, S. 649
 Gordon, L. 686
 Gothard, C.M. 673
 Gottipati, K.K. 269
 Götz, M. 385
 Gozes, I. 443
 Grace, C.R.R. 517
 Grieco, P. 76, 112, 353, 401, 437, 439
 Griffin, P.R. 315
 Grötli, M. 677
 Gu, X. 186, 347, 629
 Guarino, D. 401
 Guarnieri, M. 291
 Guasch-Camell, J. 116
 Guichard, G. 716
 Guidelli, R. 265
 Guidolin, A. 164
 Guillemette, G. 357, 473
 Guillon, G. 573, 659
 Guiotto, A. 417, 479, 491
 Günther, R. 671
 Guo, L. 481, 627
 Gupta, N. 639, 661
 Gutierrez Gallego, R. 767
 Habi, A. 589
 Hackeng, T.M. 200, 206, 675
 Halem, H. 40
 Halem, H.A. 587
 Hama, S. 329
 Hamada, Y. 599
 Hamel, E. 509
 Hamill, P. 403
 Hammer, R.P. 196, 471, 595, 633, 712
 Han, J. 229
 Handl, H. 373, 765
 Hanrieder, J. 287
 Hanson, M.C. 196
 Hao, X. 341
 Harris, K.M. 90
 Harris, S.M. 285
 Harvey, M. 457
 Haskell-Luevano, C. 381, 521, 537
 Havelund, S. 702
 Hayakawa, T. 497
 Hayashi, R. 607, 613
 Hayashi, Y. 96, 98, 104, 106, 597, 599
 Hazuda, D. 569
 He, Y. 92
 Heavner, G.A. 78, 429
 Heckmann, D. 747
 Heiman, M.L. 409, 655
 Hemmi, H. 555
 Herber, D. 471
 Herédi-Szabó, K. 781
 Hertel, J. 409
 Hertel, J.L. 655
 Hey, A.W. 164
 Heyl, D.L. 269
 Hidaka, K. 597, 599
 Hiejima, T. 700
 Hiramatsu, K. 469
 Hirashima, Y. 393
 Hodges, R.S. 258, 291, 335, 531, 581, 679
 Hoeg-Jensen, T. 702
 Hoffman, A. 229
 Hoffmann, R. 287
 Hofmann, H.J. 671
 Hojo, H. 309
 Hojo, K. 74, 497
 Holder, J.R. 537
 Holland, R. 78
 Holleran, B.J. 455
 Holmes, C.P. 405
 Hon, P.N. 377
 Hondal, R.J. 90
 Hong, A. 425
 Hong, D.J. 441
 Horton, M. 267

- Horváth, A. 407
 Hough, G. 329
 Houghten, R.A. 3
 Houston, M.E. 447
 Howl, J. 397, 453
 Hoyer, D. 423
 Hrin, R. 569, 571
 Hruby, V.J. 186, 332, 347, 361, 373, 399, 535, 550, 591, 629, 651, 750, 765
 Hsieh, C.Y. 415, 427
 Hsiung, H.M. 409, 655
 Hu, J. 503
 Huang, Z. 377
 Hudleson, W.P. 527
 Hudson, D. 403
 Husain, A. 477
 Husain, S. 409, 655
 Hvilsted, S. 773

Iaccariono, G. 437, 439
 Iannucci, N.B. 114
 Igawa, N. 599
 Imada, Y. 700
 Impellizzeri, G. 623
 Indrevoll, B. 665
 Ingallinella, P. 267, 569, 571
 Inui, K. 202
 Inui, T. 118, 122, 172
 Ionescu, R. 267
 Isaka, S. 72
 Ishiura, S. 599
 Ishizu, T. 72
 Isidro-Llobet, A. 116
 Ivanov, V.T. 513
 Ivanova, M. 653

Jackson, P. 461
 Jacobs, H.J.F. 152
 Jacobson, S. 527
 Jager, U. 429
 Jaggi, M. 639, 661
 Jakobi, B. 218
 James, J.H. 419
 Janda, K.D. 252
 Janmey, P.A. 698
 Jaques, D. 120
 Jaśkiewicz, A. 583
 Jean, F. 403
 Jean-Charles, P.Y. 271
 Jelokhani-Niaraki, M. 653
 Jennings, M.P. 511
 Jensen, K.J. 777
 Jensen, T.J. 471

 Jiang, J. 154
 Jiang, S. 485, 505
 Jiang, Z.X. 126
 Jiménez, A.I. 567
 Jiménez, J.C. 142
 Jiménez-Barbero, J. 767
 Jinsmaa, Y. 507
 Jivani, M. 457
 Jo, D.G. 491
 Johnson, M. 485
 Johnson, P.H. 447
 Johnson, R.M. 26
 Johnstone, K.D. 511
 Jones, D.N.M. 258
 Jones, S. 397, 453
 Josan, J.S. 373
 Joshi, R. 419
 Jost, M. 263
 Jouvensal, L. 273
 Juaristi, E. 369
 Julius, J. 686

Kadekaro, A.L. 461
 Kahl, S. 615
 Kahl, S.D. 409, 655
 Kalashnikov, V.V. 222
 Kaluarachchi, K.K. 53
 Kang, S.U. 180
 Kang, S.W. 673
 Kao, D.J. 531
 Kaptein, B. 68, 261
 Karelin, A.A. 513
 Kariki, R. 180
 Karki, R. 559
 Karlsen, H. 665
 Karpati, L. 407
 Kasai, S. 599
 Kato, T. 391, 393, 499
 Katoh, E. 696
 Kaufmann, G.F. 252
 Kaumaya, P.T.P. 124, 395, 527, 529, 631, 635, 690
 Kavanagh, R. 537
 Kavanagh, R.J. 461
 Kawakami, T. 132, 160
 Kawasaki, H. 613
 Kawasaki, K. 74, 497
 Kelber, J. 686
 Kemmink, J. 158, 198
 Kempe, M. 170
 Kenny, D. 451
 Kessler, H. 100, 102, 423, 747
 Keyari, C.M. 332

- Khachin, D.P. 513
 Khakshoor, O. 325
 Khan, M.S.Y. 477
 Khatri, A. 344
 Kida, S. 497
 Kimura, M. 104, 106
 Kimura, R. 235
 Kimura, T. 72, 96, 104, 106, 597, 599
 Kindberg, G.M. 665
 Kiso, A. 597
 Kiso, Y. 96, 98, 104, 106, 597, 599
 Kitamatsu, M. 375
 Klages, J. 747
 Knapik, E. 164
 Knittel, J.J. 461
 Knör, S. 747
 Kobzar, K. 747
 Kodama, H. 607, 609, 613
 Koerber, S.C. 517
 Kohn, W. 229
 Kohn, W.D. 615
 Koikov, L.N. 461
 Kolaric, B. 725
 Kordyukova, L.V. 307
 Kosakowska-Cholody, T. 509
 Kotake, T. 96
 Kotch, F.W. 688
 Kotnik, M. 433
 Kovacs, J.M. 679
 Kövér, K.E. 629
 Krajewski, K. 411
 Krause, E. 168
 Kret, A. 583
 Krishnan, K. 235
 Kruijtzter, J.A.W. 158
 Kruszynski, M. 78, 429
 Kubasik, M. 637
 Kulkarni, V. 361
 Kumaki, Y. 377
 Kumar, K. 377
 Kumar, V. 525
 Kundu, B. 643
 Kung, H.J. 415, 427
 Kung, J. 415
 Kunwar, A.C. 661
 Kurachi, S. 497
 Kusebauch, U. 561
 Kuster, D.J. 720
 Kwok, S.C. 581
 Kwok, S.W. 42
 Kwon, Y. 728
 La Mendola, D. 623, 625
 Ladefoged Nielsen, S. 279
 Lai, J. 361, 591
 Lai, J.Y. 535
 Lam, K.S. 128, 130, 389, 415, 421, 427, 445, 467
 Lama, T. 76, 112, 353, 401, 437, 439
 Landon, C. 289
 Lang, P. 725
 Langenegger, D. 423
 Langereis, S. 675
 Laporte, R. 489
 Lastoria, S. 182
 Lauer-Fields, J.L. 303, 315
 Lavigne, P. 176
 Lawrence, D.S. 320
 Lazarus, L.H. 507
 Lazo, N.D. 515
 Leduc, R. 357, 455, 473
 Lee, L. 26, 427
 Lee, S.H. 252
 Lee, S.L. 485
 Lee, Y. 59
 Lee, Y.H. 663
 Lee, Y.S. 186, 361, 535, 550, 591
 Leech, T. 208
 Leiva-Leon, J. 255
 Lelli, B. 371
 Lemieux, C. 31
 Lenevich, S. 297
 Lennard, S. 569
 Leplawy, M.T. 583
 Létourneau, M. 225
 Leu, K. 405
 Leung, J.W. 445
 Leuther, K. 405
 Levy, J.J. 547
 Li, P. 485
 Li, S. 615, 633
 Li, T. 507
 Li, W. 481, 501, 503, 734
 Li, W.C. 487
 Li, X. 405
 Liang, X. 267
 Lieblein, J.C. 529
 Liepina, I. 698
 Lin, C.Y. 485
 Lin, F. 287
 Lin, T.H. 174
 Lin, W. 64
 Liou, C.C. 487
 Liskamp, R.M.J. 50, 152, 158, 198, 212
 Little, S.F. 692
 Liu, D. 377

Liu, F. 559
 Liu, G. 467
 Liu, H. 734
 Liu, K. 70
 Liu, L. 347
 Liu, M. 134, 192
 Liu, P. 599
 Liu, R. 389, 421, 427
 Liu, Y. 445
 Live, D. 134, 192
 Liwo, A. 698
 Lloyd, L.L. 355
 Lobel, P. 483
 Lohner, K. 255
 Lohse, B. 773
 Lolli, F. 775
 Lombana, N. 239
 Long, D.W. 146
 Long, Y.Q. 485
 López, P.E. 116
 Losic, D. 718
 Lotfipour, F. 341
 Lou, B.S. 174
 Louassini, M. 338
 Lovas, S. 706, 708, 710, 781
 Lovelace, E.S. 641
 Lowe, D. 569
 Löweneck, M. 36
 Lozzi, L. 371
 Lu, G. 92
 Lu, J. 425
 Lu, M. 569
 Lu, Y.A. 84
 Lubell, W.D. 47, 184, 188
 Ludwig, C. 754
 Lung, F.D.T. 487
 Luo, J. 429
 Luthman, K. 677
 Luy, B. 747
 Lynch, M.P. 527, 529

Ma, H. 734
 Ma, J. 70
 Ma, S.W. 361, 535, 591
 Maccarrone, G. 623
 MacDonald, A. 355
 Maderia, M. 559
 Madsen, J.C. 777
 Madsen, K. 383
 Maeda, I. 611
 Maeda, M. 74, 497
 Maftai, M. 493
 Magri, A. 623, 625

Maitra, S. 673
 Majerle, R.S. 194, 196
 Malavolta, L. 704
 Malda, H. 206
 Mammi, S. 38
 Mandal, B. 56
 Manganiello, S. 61
 Manger, W. 267
 Manning, M. 573, 659
 Mansi, R. 601
 Mant, C.T. 679
 Mapp, K.J. 355
 Marani, M.M. 114
 Marasco, D. 166
 Marchand, C. 411
 Marik, J. 389, 415, 421, 427
 Markos, S. 140
 Markussen, J. 702
 Marshall, G. 465
 Marshall, G.R. 577, 579, 657, 720
 Martello, R.T. 271
 Martin, A. 239
 Martin, L.L. 718
 Martin, S.S. 473
 Martinell, M. 649
 Martínez de Tejada, G. 255
 Martínez, M. 210
 Mascini, M. 785
 Masterson, L.R. 712
 Mathur, A. 639, 661
 Matsui, K. 611
 Matsumoto, Y. 309
 Matsuzaki, R. 375
 Mattson, M.P. 491
 Maxwell, L. 395
 May, J.P. 216
 Mayer, J.P. 229, 409, 615, 655
 Mayer, S.J. 447
 Mayorov, A. 399
 Mayorov, A.V. 550, 651
 Mayumi, T. 497
 Mazaleyrat, J.P. 557
 Mazzanti, B. 769, 779
 Mazzella di Bosco, A. 353
 Mazzoni, O. 112, 353
 Mazzuca, C. 281
 McCarley, R.L. 471
 McMurray, J.S. 53
 Mechler, A. 718
 Meijer, E.W. 206, 675
 Meijler, M.M. 252
 Mendizabal, M. 665
 Merx, R. 152, 198

- Messina, A. 625
 Meudal, H. 289
 Mezzato, S. 239
 Miampamba, M. 489
 Micanovic, R. 229, 615
 Michejda, C.J. 509
 Mierke, D.F. 40, 351
 Mihala, N. 66
 Mihalik, B. 657
 Mihara, H. 731, 738
 Milardi, D. 625
 Milbradt, A.G. 667
 Milhauser, G. 461
 Miller, M.D. 569, 571
 Mills, J.B. 581
 Mimna, R. 56
 Min, B.J. 186
 Minond, D. 315
 Minunni, M. 785
 Miranda, A. 273
 Miranda, M.T.M. 82, 86, 273
 Mitchell, B.F. 94
 Miyazaki, A. 507
 Mizuguchi, H. 497
 Mizumoto, M. 202
 Mobley, P. 686
 Moeller, H. 493
 Mohottalage, D. 341
 Molina, A. 248
 Mollica, A. 591
 Moman, E. 451
 Moncelli, M.R. 265
 Monteil, H. 716
 Monteith, G.R. 365
 Mootz, H.D. 754
 Morelli, G. 182, 601
 Moretto, A. 68
 Morgan, D. 471
 Moriyón, I. 255
 Moroder, L. 17, 36, 385, 561, 667, 769
 Morra, M. 449
 Morrison, C. 395
 Morrison, M. 665
 Moss, J.A. 252
 Motiei, L. 283
 Mountzouris, J. 92
 Moya, R. 379
 Moye, S. 591
 Moyle, P.M. 407
 Mu, Y. 585
 Mukherjee, R. 639, 661
 Mulinacci, B. 769
 Mullen, D.G. 144, 297
 Murat, B. 573, 659
 Murat, K. 56
 Murata, T. 555
 Murphy, R.F. 706, 708, 710, 781
 Murray, T.F. 523, 525, 533
 Muthu, D. 332
 Mutter, M. 56
 Myers, S.L. 615
 Myles, L.N. 633
 Nachman, R.J. 369
 Nagase, H. 315
 Naider, F. 80, 118, 122, 172, 663
 Nakagawa, S. 497
 Nakahara, Y. 309
 Nakaie, C.R. 704
 Nakamura, A. 609
 Nakamura, K. 132, 160
 Nakamura, S. 555
 Nakashima, H. 469
 Navab, M. 329
 Nemeth, J.F. 78, 429
 Neugebauer, W.A. 120
 Nezami, A. 597
 Ni, F. 619, 669
 Nicklaus, M. 180, 559
 Nie, A. 377
 Niemeyer, C. 725
 Niida, A. 202
 Nikiforovich, G.V. 577, 579, 657
 Nikolovska-Coleska, Z. 505
 Nilsson, L.O. 338
 Nishino, N. 391, 393, 499
 Nishino, T. 393
 Nishiuchi, Y. 72
 Nisthal, A. 686
 Noel, J.P. 759
 Nokihara, K. 731, 738
 Nordenskiöld, L. 585
 Novellino, E. 76, 112, 353, 401, 437, 439
 Nowick, J.S. 325, 673
 Nuti, F. 190, 775, 779
 Nyberg, J. 591
 O'Brien, T.P. 409, 655
 Oancea, S. 565
 Oblak, M. 433
 Oda, A. 98
 Ohyama, T. 738
 Oishi, S. 202, 559
 Oka, Y. 738
 Okada, Y. 507
 Okamoto, K. 611

- Okihara, R. 72
 Okuno, Y. 98
 Olive, C. 407
 Olma, A. 583
 Olsen, K.A. 541
 Omiyi, D. 457
 Ong, H. 188
 Ooi, A.T. 214
 Opligger, F. 61
 Osada, S. 607, 609, 613
 Osler, A. 417, 479, 491
 Otaka, A. 202, 204, 469
 Otvos, L. 287
 Owen, M. 710
- Pal**, P.P. 769
 Palgunachari, M.N. 329
 Palladino, P. 575
 Palleschi, A. 281, 603, 605
 Paolini, I. 190, 775
 Paolini, M. 61
 Papa, D. 475
 Papini, A.M. 190, 769, 775, 779, 785
 Pappalardo, G. 623, 625
 Parente, J. 285
 Pascal, J.H. 222
 Patriarca, E. 166
 Pazzagli, M. 769, 775, 785
 Peachey, T. 431
 Peck, A.M. 162, 525
 Pedone, C. 166, 367, 449
 Peggion, C. 68, 261, 263, 265, 281, 557, 567
 Peggion, E. 38, 349
 Peiper, S.C. 469
 Pena, A. 573, 659
 Peng, L. 389, 421, 445
 Pensato, S. 367
 Penta, K. 405
 Perchellet, E. 475
 Perchellet, J.P. 475
 Pérez, J. 210
 Peri, K.G. 589
 Peroni, E. 775, 785
 Perrin, D.M. 216
 Peruzzi, B. 208
 Peschke, B. 383
 Pessi, A. 267, 569, 571
 Peterman, E.E. 457
 Petrov, R.R. 186, 535, 651
 Petty, S.A. 683
 Phan, J. 180
 Philipp, M. 553
- Phillipson, A. 457
 Pieters, R.J. 152, 212
 Pini, A. 371
 Piontek, C. 239
 Pipkorn, R. 136
 Piplani, S. 405
 Piserchio, A. 40
 Pispisa, B. 603, 605
 Pla-Roca, M. 114
 Polt, R. 332
 Pomerantz, S.C. 78
 Pommier, Y. 411
 Porreca, F. 361, 535, 591
 Porter, J.R. 214
 Potetinova, Z. 110, 344, 617, 619, 621
 Powell, B.S. 692
 Pozo-Carrero, M.C. 775
 Prasad, S. 639, 661
 Price, C. 267
 Proti, P.B. 82
 Proulx, C. 455
 Pujals, S. 649
 Purvis, L.J. 447
- Qi**, C. 70
 Qie, J. 70
 Qu, H. 347
 Quan, B. 311
 Quay, S.C. 447
 Quintanar-Audelo, M. 114
 Quintieri, L. 417
- Rabenstein**, D. 435
 Ragone, R. 575
 Raguse, T.L. 78
 Rahimipour, S. 283
 Raichman, D. 150
 Raimondi, S. 61
 Raines, R.T. 688
 Rajesh, S. 96
 Ramachandran, S. 694
 Ramamoorthy, A. 269
 Ramana Rao, M.H.V. 184
 Ramanujam, P.S. 773
 Rana, S. 643
 Rath, A. 26
 Rauchenberger, R. 429
 Rawale, S. 395, 631, 635, 690
 Rawale, S.V. 124, 527, 529
 Rawat, R. 271
 Raynal, N.F. 431
 Real-Fernández, F. 775, 779
 Reay, P. 696

Reddy, S.T. 329
 Reed, J.C. 377
 Refosco, F. 349
 Reid, T.W. 387
 Remuzgo, C. 86
 Renner, C. 17, 36, 385, 561, 667
 Reubi, J.C. 517
 Reutelingsperger, C.P.M. 200
 Reyes-Rangel, G. 369
 Rezende, M. 475
 Richardson, P.L. 154
 Richer, M. 403
 Riek, R. 517
 Rijkers, D.T.S. 50, 152, 198
 Rivier, C. 441
 Rivier, J. 441
 Rivier, J.E. 517
 Riviere, P. 489
 Rizzarelli, E. 623
 Roberts-Thomson, S.J. 365
 Robinson, J.A. 365
 Rochell, L.E. 355
 Rodeheaver, G.T. 285
 Rodríguez, R. 210
 Roeske, R.W. 481, 627
 Rogers, C.J. 252
 Rognan, D. 716
 Rolka, K. 583
 Roller, P.P. 411, 485, 505
 Romanelli, A. 367
 Ronga, L. 575
 Rose, K. 66
 Rosenblatt, M. 351
 Rosengren, K.J. 243
 Rossi, F. 575
 Roth, S.E. 447
 Rovero, P. 437, 439, 769, 775, 779, 785
 Royo, S. 567
 Rubini, C. 491
 Ruíz-Rodríguez, J. 108
 Russu, W.A. 325
 Ruvo, M. 166, 575
 Ruzza, P. 417, 479, 491
 Rybka, A. 148

 Sabatino, G. 190
 Sakai, N. 696
 Salamon, Z. 750
 Salibay, C. 361
 Salvatella, X. 649
 Salvatori, F. 367
 Samant, M.P. 441
 Samitier, J. 114

 Sampson, N.S. 59
 Sana, R. 405
 Sánchez-Gómez, S. 255
 Sánchez-Vallet, A. 248
 Sando, L. 243, 783
 Sankaranarayanan, R. 373, 765
 Saporito, A. 166
 Saravanos, A. 140
 Sarciaux, M. 557
 Sargsyan, H. 172
 Sartori, E. 565
 Sartorio, R. 252
 Sasaki, M. 104
 Sasaki, Y. 202, 507
 Sasikumar, P.G. 170
 Saucède, L. 56
 Saviano, G. 575
 Saviano, M. 367
 Sax, B. 218
 Sazonova, O.V. 513
 Scerbavicius, R. 413
 Schaffrath, M. 239
 Schatz, P.J. 405
 Schievano, E. 38, 349
 Schiller, P.W. 31
 Schmid, F.X. 239
 Schrader, T.E. 36
 Schreier, W.J. 36
 Schroder, K. 379
 Schroeder, H. 725
 Schteingart, C. 489
 Schulz, A. 156
 Schurink, M. 740
 Schwindling, J. 218
 Scott, J.W. 381, 521, 537
 Segal, D.J. 214
 Sehested, B. 383
 Seidel, R.P. 725
 Sekiguchi, F. 497
 Serebryakova, M.V. 307
 Severino, B. 122
 Sferdean, C.D. 168
 Shan, Y. 503
 Shang, J. 615
 Sharma, R. 661
 Sheng, L. 425
 Shi, L. 267
 Shi, Z.D. 180, 208, 559
 Shiki, Y. 609
 Shimizu, K. 555
 Shiotani, K. 507
 Shiver, J. 267, 569
 Shuto, D. 599

- Simkeviciene, V. 459
 Simonsen, S.S. 243
 Singh, A.T. 639
 Sirois, A. 225
 Sisido, M. 375
 Small, D.H. 718
 Smiley, D.L. 237, 311, 409, 655, 763
 Smillie, L.B. 581
 Smith, D.P. 655
 Smith, K. 164
 Snyder, C. 287
 Soerensen, J. 383
 Sohar, I. 483
 Sohma, Y. 104, 106
 Šolmajer, T. 433
 Song, A. 128
 Song, H.C. 267
 Soni, P. 393
 Spagnuolo, M.S. 449
 Spasiano, A. 166
 Spengler, B. 725
 Spengler, J. 108, 142
 Spring, S.M. 515
 Sreekumar, S. 269
 Staehelin, C. 218
 Stains, C.I. 214
 Stankova, L. 363
 Stanley, H.E. 515
 Steele, J.T. 631, 690
 Stella, L. 603, 605, 281
 Stewart, J.M. 413, 459
 Stöcklin, R. 289
 Stoev, S.B. 573, 659
 Stowell, N. 78, 429
 Strey, A. 369
 Striffler, B. 615
 Stymiest, J.L. 94
 Su, C. 419
 Sugiyama, D. 613
 Sumida, M. 160
 Sun, N.N. 742
 Suzuki, A. 309
 Suzuki, M. 309
 Suzuki, R. 696
 Suzuki, Y. 309, 555
 Sweeney, C. 415
 Sweet, R. 429
 Szeto, H.H. 573, 659

T
 Taira, J. 607, 609
 Takada, Y. 421
 Takano, M. 696
 Takenouchi, N. 527

 Taki, H. 489
 Tam, J.P. 84, 585
 Tamamura, H. 202, 204, 469
 Tamura, M. 72
 Tanaka, D. 399
 Tanaka, D.K. 651
 Tancredi, T. 575
 Tang, S.C. 491
 Tang, Y. 222, 425
 Taniguchi, A. 104, 106
 Taormina, P.II. 457
 Tarallo, L. 182
 Taraseviciene-Stewart, L. 413, 459
 Tarasova, N.I. 509
 Taulane, J.P. 42
 Taylor, J.E. 40, 587
 Taylor, J.W. 483, 563
 Tchertchian, S. 61
 Temperini, M.L.A. 86
 Ten Brink, H.T. 50
 Ten Kortenaar, P.B.W. 156
 Teplow, D.B. 515
 Terada, T. 202
 Tesauro, D. 601
 Thennarasu, S. 269
 Thiele, S. 736
 Thomas, B.E. 351
 Thundimadathil, J. 627
 Tian, X. 493
 Tian, Y. 483
 Tieman, B.C. 154
 Tisato, F. 349
 Tizzano, B. 575
 Todorovic, A. 537
 Toffoletti, A. 557
 Tognon, S. 248
 Tois, J. 50
 Tolkatchev, D. 669
 Tollin, G. 750
 Tolmazova, A.G. 513
 Tomasello, F. 625
 Tomita, K. 202
 Tomizaki, K. 731
 Tong, X. 425
 Toniolo, C. 22, 68, 261, 263, 265, 281,
 557, 565, 567, 603, 605
 Toth, I. 365, 407, 511
 Tourwé, D. 359, 495
 Tran, P.L. 387
 Tremmel, S. 168
 Trent, J.O. 469
 Trevino, S. 692
 Tripet, B. 335

- Trivedi, D. 399, 651
 Trivedi, D.B. 629
 Trojnar, J. 489
 Trueba, M. 573, 659
 Trujillo, M. 210
 Tseng, Y. 694
 Tsuchiya, M. 132
 Tsuchiya, Y. 597
 Tsuda, Y. 507
 Tsui, P. 429
 Tuchscherer, G. 56
 Tulla-Puche, J. 114

U
 Ueda, S. 204, 469
 Uehara, S. 611
 Unverzagt, C. 239
 Urbanc, B. 515
 Usui, K. 731, 738

V
 Vagner, J. 373, 629, 765
 Valenzuela, F. 146
 van Berkel, W.J.H. 740
 Van den Eynde, I. 359, 495
 van der Lely, A.J. 589
 van Esse, G.W. 152
 van Genderen, M.H.P. 206, 675
 Van Rompaey, K. 359, 495
 Van Scoy, A.R. 651
 van Zoelen, D.J. 212
 Vanommeslaeghe, K. 495
 Vardanyan, R. 591
 Vardanyan, R.S. 535
 Varon, D. 239
 Vasil, M. 291
 Vasileiou, Z. 138
 Vaskovsky, B.V. 307
 Vederas, J.C. 94
 Veglia, G. 712
 Venanzi, M. 281, 603, 605
 Ventura, M.A. 573, 659
 Viau, M. 225
 Vick, A.M. 615
 Vigil-Cruz, S.C. 162, 475
 Vila-Perelló, M. 248, 767
 Vinogradova, A. 669
 Violette, A. 716
 Voelkel, N.F. 413
 Vorherr, T. 160
 Vovelle, F. 273, 289

W
 Wacker, R. 725
 Wade, J.D. 287

 Wakselman, M. 557
 Waldeck, W. 136
 Wang, C. 501
 Wang, J. 377, 435, 595
 Wang, L. 70, 481, 501, 503, 734
 Wang, S. 505
 Wang, X. 128, 130, 421, 445, 523
 Wang, X.J. 759
 Wang, Z. 469
 Waring, A. 686
 Waser, B. 517
 Watanabe, L.A. 393, 499
 Waugh, D.S. 180
 Weiner, L.M. 443
 Weltrowska, G. 31
 Wen, E. 267
 Wenger, M. 267
 Wenger, S. 517
 Whitehead, J.K. 633
 Whitehorn, E.A. 405
 Whitfield, J.F. 617
 Whittaker, W. 763
 Wichers, H.J. 740
 Wilczynski, A. 381
 Wilczynski, A.M. 521
 Wilkes, B.C. 31
 Willem, M. 385
 Willem, R. 495
 Williams, H.J. 369
 Willick, G. 344
 Willick, G.E. 110, 617, 619, 621
 Wilson, D.B. 379
 Wilson, I.A. 519
 Wilson, K.R. 381, 521
 Wimmer, N. 365, 407
 Wisniewski, K. 489
 Witkowska, R.T. 447
 Wittelsberger, A. 351
 Witten, M.L. 742
 Wo, N.C. 573, 659
 Wong, S. 94
 Wong, S.S. 742
 Wood, J.M. 258
 Wood, S. 363
 Wooden, E. 361
 Woods, R.J. 325
 Worthy, K.M. 180, 208, 559
 Wright, K. 557
 Wu, C. 92
 Wu, L. 128
 Wu, Y. 463, 714

X
 Xu, H. 403

Xu, J. 297	Zweytick, D. 255
Xu, S. 734	Zwick, M.B. 519
Xu, W. 563	
Yakovleva, T. 475	
Yamaguchi, I. 555	
Yamamoto, N. 469	
Yamamura, H.I. 332	
Yamazaki, T. 696	
Yamazaki, Y. 98	
Yan, L. 429	
Yan, L.Z. 409, 655	
Yan, Z. 335	
Yang, B. 88, 305	
Yao, K. 527	
Yao, N. 427	
Yao, N.H. 467	
Yeomans, L. 332	
Yim, C.B. 200	
Yin, K. 405	
Ying, J. 550, 629	
Yokoi, T. 507	
Yonemura, K. 738	
Yoshida, M. 393	
Yoshizawa-Kumagaye, K. 72	
Youdim, M.B.H. 443	
Young, L.H. 457	
Yu, Q. 585	
Yu, Y.B. 126, 694	
Yu, Z. 651	
Zablotna, E. 583	
Zabrocki, J. 369	
Zaccaro, L. 367	
Zaitsu, M. 613	
Zareie, R. 164	
Zavallone, D. 603	
Zhang, J. 40, 587	
Zhang, L. 285, 409, 615, 655	
Zhang, X. 463	
Zhang, X.Y. 655	
Zhang, Y. 759	
Zhao, X. 70, 481	
Zheng, H. 443	
Zheng, J. 70	
Zhilina, Z. 363	
Zhong, X. 425	
Zhou, W. 70	
Zhou, X. 387	
Ziemba, A. 363	
Zinth, W. 36	
Zoetewey, D.L. 258	
Zubrzak, P. 369	

Subject

- Abbreviated nomenclature 142
Ab initio MO theory 671
Acanthoscurrin 86
ACE inhibitor 720
Activation mechanism 176
Active-site mapping 720
Acylhomoserine lactone 252
Acyl migration 56
Acylpeptide 307
Acyl sulfonamide 198
Acyliminium ion cyclization 186
ADAM 59
Address-message 591
Adenovirus vector 497
Aggregation 225, 683
Agonist 311, 413, 547, 659
AGRP 381, 399, 521
Aib 637
Ala scan 275
Alamethicin 281
Albumin 734
Aldehyde scavenger 491
Alkali 355
Alkene 202
Alkylation 88
Alpha 1b-adrenergic antagonist 433
Alpha4 beta1 integrin ligand 389
Alpha, alpha-disubstituted amino acid 712
Alpha-factor 122
Alpha-helix stabilization 248
Alternative protein splicing 754
Aluminium ion 479
Alzheimer's disease 493, 515, 718
Amide bond formation 198
Amide-mimetic 383
Amino acid 325, 595, 673,
Amino acid side chain 679
2-Amino-(n-1)-alkenoic acid 391
Aminobenzazepinone 359
Aminoglycine 517
Amylin 623
Amyloid 515, 686, 698
Amyloid β fibrillogenesis 471
Amyloid self-assembly 56
Analgesia 535
Analog 275, 277
Angiogenesis 665
Angiotensin II 473
Angiotensin converting enzyme 720
Angiotensin II type 1 receptor 357
Angiotensin receptor 657
4-Anilindopiperidine 591
Annexin 200
Antagonist 305, 651
Anti-adhesion 445
Anti-angiogenesis 593
Antiatherogenic peptide 329
Antibacterial activity 283
Antibiotic 271
Antibiotic peptide 248
Antibody 395, 429, 531, 692, 775
Anticancer 661
Anticancer peptide 639
Antidiuretic agonist 573
Antidote 669
Antigene strategy 363
Anti-metastatic 485
Antimicrobial 269, 285, 338, 387, 477
Antimicrobial peptide 255, 273, 275, 277, 279, 291,
293
Antiparallel coiled-coil 258
Antisense 367
Anti- β -substituted γ,δ -unsaturated α -amino acid 347
Antithrombotic 553
Antithrombotic drug 451
Antitumoral agent 353
ApoA-I peptide mimetic 329
Apolipoprotein A-I 449
Aquaporin 742
Aqueous solvent 74
Architecture modification 405
ARDS 742
Arginine aldehyde diethylacetal 218
Aroclor 533
Arsenical 365
Astrocytoma 453
Asymmetric induction 68
Asymmetric reaction 96
Autoantibody 769
Autoantibody recognition 779
Auxiliary 160
Aza-amino acid 47, 184
Aza-peptide 184
Azobenzene 17, 36, 561

BACE1 599

Bacteria 445
 Bacterial membrane 293
 Bacterial resistance 136
 Bactericidal activity 252
 B-cell epitope 124
 Bcl-2 protein 377
 p-Benzoylphenylalanine 351
 Benzyloxymethyl 72
 Beta amino acid 369
 Beta-amyloid 704, 718
 Beta amyloid peptide 104
 Beta amyloid peptide 1-42 mutant 106
 Beta-extended conformation 385
 Beta-hairpin 36
 Beta-hairpin mimetic 451
 Beta-lactam 53
 Beta-lactamase 214
 Beta-MSH 655
 Beta-peptide 557
 Beta-secretase 385
 Beta-sheet 325
 Beta-TOAC 557
 Beta-turn 112, 495
 Beta-turn mimetic 186
 Beta-turn mimic 495
 BH3 domain 377
 Binding affinity 335, 617
 Binding domain 344
 Bioactive peptide 148
 Biological activity 291, 353, 609
 Biomarker 769, 775
 Biomaterial 688, 694
 Biotin 349
 Biotin conjugate 208
 Blood-brain barrier 332
 Boronate 702
 Bradykinin 413, 459
 Bradykinin B2 120
 Brain natriuretic peptide 154
 Branched and cyclic peptide 142
 Branched library 130
 Branched peptide 371
 Breast cancer 631, 635, 690
 Building block 190, 192
 Burn 419

Cachexia 419
 C α,α -disubstituted amino acid 471
 C α,α -tetrasubstituted amino acids 38
 Calcium influx 513
 Calmodulin 479
 Cancer 315, 459, 781
 Cancer imaging 421
 Cancer targeting agents 389
 Carbocyclic peptide 94
 Carnosine 491
 Casein 740
 Catechol 42
 Cathepsin B 417
 CCK receptor 361
 CCR5 118, 172
 CD excitation couplet 541
 CD spectroscopy 653
 Cecropin B2 279
 C. elegans 734
 CE-LIF 593
 Cell 375
 Cell membrane crossing 120
 Cell penetrating peptide 375, 397
 Cellular delivery 341
 Chemical ligation 61, 645
 Chemical protein synthesis 61
 Chemoselective bioconjugation 198
 Chemoselective ligation 300
 Chemotaxis 611
 Chemotherapeutics 365
 Chimera 287, 521
 Chiral aziridine 347
 Chiral synthesis 595
 Chlamydocin 391, 393
 Chromatography 222
 Chromones 677
 Cinchona alkaloid 359
 Circular dichroism 619, 621
 Circular peptides 243
 CLEAR 146, 170
 Co-agonist 763
 Co-assembly 694
 Coiled-coil 581
 Coefficients 679
 Collagen 42, 315, 431, 561, 633, 688
 Combinatorial approach 112
 Combinatorial chemistry 3, 114, 421
 Combinatorial fluorogenic peptide library 483
 Combinatorial library 320
 Conformation 627
 Conformational analysis 184, 263, 567
 Conformational transition 700
 Conjugate 267
 Conotoxin 641
 Consensus sequence 775
 Constitutively active mutant 657
 Constrained amino acid 567
 Contrast agent 675
 Controllable linker 669
 Controlled release 702
 Convergent synthesis 138
 Copper 623
 Covalent capture 66
 Crystallization 134
 C-terminus 547, 621
 CTL epitope 379
 CXCR4 118, 182, 469
 CXCR4 chemokine receptor antagonist 475
 Cy7-RGD conjugate 714
 Cyclic 465, 647
 Cyclic imino acid 499
 Cyclic inhibitor 385
 Cyclic lipopeptides 271
 Cyclic peptide 50, 124, 338, 409, 607, 609
 Cyclic tetrapeptide 393
 Cyclization 98
 Cycloaddition reaction 152
 Cyclopropane amino acid 613

Cyclosporin A 747
 Cyclotide 783
 Cyclotide biosynthesis 235
 Cysteic acid 305
 Cysteine 88
 Cysteine protease 212
 Cystine knot 243
 Cystine peptide 148
 Cytotoxin 453

Delta opioid receptor 523, 525
 Demethylvancomycin derivative 467
 Dendrimer 42, 206, 585
 Deprotection 90
 Depsipeptides 108
 Depsipeptide technique 168
 Depth dependent quenching 281
 Design 731
 Detritylation 216
 Diabetes 229
 Diagnostic 214
 Dialkylated amino acid 639
 Dicarba analog 31
 Dicarboxylic acid 505
 Difficult peptide 92, 114
 Difficult sequence 86
 Difficult synthesis 168
 Diketopiperazine 98
 2',6'-Dimethyl-L-tyrosine 507
 DioRaSSP 156
 Dipeptide 353
 Dipeptide isostere 469
 Disulfide 409
 Disulfide bond 124
 Disulfide macrocyclization 154
 Disulfide rich 667
 Dithiasuccinoyl 196
 Diuretic activity 369
 DnaK binding 287
 Docking 433
 Drug delivery 453
 Dual-labeled affinity ligand 523
 Duration of action 489

Elastin derived polymer 611
 Electrochemistry 265
 Endomorphin 511
 Enzyme inhibition 740
 Epitope 692
 EPR 565
 Esterified peptides 82
 Etk 427
 Europium 765
 Evans' oxazolidinone 96
 Expressed protein ligation 235, 544
 Extended chemical ligation 132

Fatty acid 277, 537
 Fentanyl analog 535
 Fluorescence 731
 Fluorescent dye 738

Fluorinated amino acid 126
 fMLP 613
 Fmoc-Lys(Npa)-OH 128
 Fmoc-Lys(Tfa)-OH 503
 Foldamer 671, 716
 Folding 605
 Fold stability 541
 Food intake 589
 Formaldehyde 72
 Free radical 710
 Freidinger Lactam 47, 76, 188
 FRET 425
 FRET peptides 417
 Furin inhibitor 341
 Fusaricidin A 271
 Fusion 686
 Fusion inhibitors 571
 Fusion intermediate 569

Gelsolin 698
 Ghrelin 40, 419, 587
 Ghrelin agonist 589
 GHRP-6 analog 188
 GHS-1a 587
 Gibberellin 555
 GLP-1 763
 Glucagon 305, 547, 763
 Glutamine synthetase inhibitor 166
 Gluten peptide 401
 Glycine-rich protein 86
 Glycopeptide 134, 192, 283, 309, 332, 511
 Glycopeptide library 779
 Glycoprotein 239, 431, 769
 Glycoprotein epitope 601
 Glycosylated derivative 303
 Glycosyltransferase 511
 Glycyl radical 710
 GnRH antagonist 441
 Gomesin 273
 Goodman oxazolone 22
 Goodman plot 22
 Gp41 563, 569, 571
 GPCR activation molecular mechanism 357
 G-protein coupled receptor 80, 122, 172, 176, 204, 373, 455, 663, 750, 765
 Grb2-SH2 domain 180, 208, 559
 Grb2 SH2 inhibitor 487
 Group A streptococcus 407
 Growth hormone 589
 Growth hormone secretagogue 383, 587
 Growth inhibition 287
 Guanidinium group 649

Hairpin 647, 712
 Handle 194
 Haptoglobin 449
 HCV 425
 HDAC inhibitor 393
 Heck reaction 150
 Helical peptides 285, 519
 Helix 22, 716

Helix bundle 563
 Hemiasterlin 509
 Heparin 435
 Heteroclitic analog 529
 Heterocycle amino acid 100
 Heterocyclic compound 3
 Hexafluoroacetone 108
 Hexafluoroisopropanol 216
 High density lipoprotein 329, 449
 High throughput screening 785
 HIP analog peptide 435
 His tag affinity label 525
 Histone deacetylase 391
 HIV 156, 569, 571, 597, 686
 HIV vaccine 379, 519, 601
 HTLV-1 527, 529
 Human interleukin-8 544
 Human neutrophil 613
 Human papillomavirus 407
 Humanin 493
 Hydrogels 694
 Hydrogen bond 700
 Hydrogen exchange 637
 Hydrogen fluoride 72
 Hydrophilic resin 140
 Hydrophobicity 291
 Hydrophobicity/Hydrophilicity 679
 Hydroxylysine 303
 Hydroxyphenylacetic acid 499
 Hypoxia inducible factor 363

IGF-1 229
 IGnRH-III 781
 Imaging 200, 325, 665
 Immunogenicity 379
 Immunoenhancer 70
 IMPACT system 544
 Infrared 683
 Infection 285
 Influenza 267
 Influenza hemagglutinin 307
 Inhibitor 320, 401, 411, 583, 599, 633, 759
 Insect antimicrobial peptide 289
 Insect kinin 369
 Insulin 229, 237, 311, 615, 702
 Integrase 411
 Integrin 431, 463
 Intein 239, 728
 Intein inhibition 754
 Internally quenched fluorogenic substrate 403
 Inverse agonist 40
In vitro activity 489
 Ion channels 607, 627
 Ion transport 653
 Ipamorelin 383
 Iron chelator 443
 Ischemia/reperfusion 457

Kappa opioid receptor 533
 Kinase inhibitor 427

Lactam bridge 377
 Lactoferricin analog 255
 Library 64
 Ligand 437
 Ligation 84, 144
 Linker 373
 Lipid core peptide 407
 Lipid raft 750
 Lipoamino acid 365
 Lipopeptide 261, 265

Macrocyclic 208, 180, 325, 559, 673
 Magnetic supports 170
 Malaria 597
 MALDI-TOF MS 307
 MAP kinase 397
 Mass spectrometry 692, 725
 Matrilysin 485
 Mdm2 138
 Melanin-concentrating hormone 154
 Melanocortin 381, 461, 521, 537, 550, 651
 Melanocortin agonist 409
 Melanocortin receptor 399, 655
 Membrane activity 261, 265
 Membrane permeabilizing peptide 255
 Metal ion 82
 Methanolysis 82
 Methionine 473
 Methylation 110
 Microarray 736
 Microcine 243
 Microwave 76, 150, 162
 Microwave assisted peptide synthesis 148
 Microwave assisted synthesis 152
 Microwave SPPS 146
 Mild condition 116, 220
 Mimetic peptide 555
 Mimetics 459, 481
 Minimal active domain 248
 MMP 633
 Molecular dynamics 575, 698
 Molecular engineering 643
 Molecular modeling 381, 577, 579, 657
 Molecular probe 665
 Molecular recognition 649
 Molecular simulation 585
 Monocyte chemoattractant protein 1 78, 429
 MSH analog 629
 MS-based sequencing 130
 MTII 399
 Mucin 134, 192, 309
 Multimeric peptide 411
 Multiple sclerosis 779
 Multivalency 200, 206, 675
 Multivalent dendrimeric peptide 152
 Mu-opioid receptor 507

Na⁺ channel 174
 Nalidixic acid 477
 Nanotechnology 673
 NAP 443

Nanoparticle 611
 Native chemical ligation 78, 166, 204, 239, 771
 Neoglycopeptide 300
 Neolipopeptide 300
 Networks 645
 Neuroprotection 443, 491
 Neurotensin 371
 Neutrophil 457
 N-(Fmoc)homoserine-derived cyclic sulfamidate 188
 NIF 714
 Nitroxide 263, 565
 Nitroxide label 557
 Nitroxide radical 603
 N-methylamino acid 102
 N-methylated peptide 102, 423
 N-methylation 102, 423
 NMR 38, 110, 174, 258, 273, 387, 435, 439, 575, 641, 696, 747, 767
 NMR peptide structure 40
 NMR structure 289, 667
 Nociception 361
 Norepinephrine transporter 641
 Novel drug design 629
 N-S acyl shift 160
 Nuclear targeting signal 503
 Nucleation site 26

O-acyl isopeptide method 104, 106
 26-O-acyl isoA β 1–42 104, 106
 Obesity 655
 Oligomer 515
 Oligopeptide 675
 Oligourea 716
 One-bead one-compound 445
 One-bead one-compound peptidomimetic library 389
 One-line text formulae 142
 Opioid 332, 535, 591
 Opioid antagonist 31
 Opioid peptide 31
 Opsin 579
 Optical data storage 773
 Organocopper 202
 Organosulfur 196
 Orthogonal protecting group 116, 220
 Osmosensory protein 258
 Ovarian cancer 395
 Oxazole 100
 Oxidative folding 667
 Oxytocin antagonist 94

P53 tetramerization domain 649
 PAD approach 130
 Pain 361
 Parathyroid hormone 38, 110, 344, 617, 619, 621
 Parathyroid hormone receptor 351
 Patch clamp 607
 PCR 783
 PEG 140, 441
 PEG hybrid 497
 PEGylation 70
 Peptide 605
 Peptide aldehyde 218
 Peptide antibiotic 293
 Peptide array 731, 738
 Peptide conformation 22, 261, 625, 643
 Peptide cyclization 150
 Peptide design 269, 595, 627, 645
 Peptide dynamics 637
 Peptide fragment 80
 Peptide fusion inhibitor 527
 Peptide hormone 663
 Peptide inhibitor 335, 415, 669
 Peptide labeling 771
 Peptide library 481, 736
 Peptide-mediated delivery 447
 Peptide mimetic 180, 550, 559
 Peptide mimic 631, 635, 690
 Peptide nucleic acid 136, 363, 375
 Peptide oxazolone 68
 Peptide-protein interaction 479
 Peptide-siRNA conjugate 447
 Peptide solubilization 704
 Peptide synthesis 64, 90, 92, 94, 126, 128, 158, 206, 222, 263, 601
 Peptide therapeutic 615
 Peptide thioester 309
 Peptide thioester synthesis 160
 Peptide toxin 509
 Peptide vaccine 635, 631, 267, 690
 Peptidomimetic 3, 50, 202, 421, 469, 495, 661, 677
 Peptidyl-prolyl isomerase 759
 Peroxidase 481
 Phenylalanine mimetic 359
 Phenylcysteine 61
 Phenytoin 174
 Phosphopeptide 53, 222, 777
 Phosphoserine phosphatase 395
 Photoaffinity crosslinking 351
 Photoaffinity labeling 357, 455
 Photodamaging 461
 Photodimerization 773
 Photoisomerization 17
 Photolabeling 473
 Photomodulation 561
 Photoreceptor 696
 Photoremovable protecting group 204
 Photoswitchable 647
 Phytochrome 696
 Pin1 759
 Pipecolic acid 499
 Plasmepsin inhibitor 597
 Plasmon waveguide resonance 750
 Platelet adhesion 451
 PNA 367
 Polyamide-polystyrene resin 140
 Polyaspartates 700
 Polyglutamine 225
 Polymer 59
 Polyproline 706
 Porin 625
 Positional scanning 47
 Precursor 783
 Prenylation 297

Pretargeting 349
 Prion 683, 575
 Production 164
 Pro-drug 417, 477
 Prognostic test 785
 Prokineticin 2 169
 Prolactin releasing peptide 750
 Proliferation 513
 Proprotein convertase 341
 Prostate cancer 415, 441
 Protease 315
 Protease substrate specificity 483
 Protein chip 728
 Protein-DNA conjugate 725
 Protein finger print
 Protein folding 17, 26, 36
 Protein kinase C 457, 513
 Protein labeling 297
 Protein loop 577
 Protein microarray 725
 Protein radical 710
 Protein splicing 235, 728
 Protein trans-splicing 754
 Protein-protein interaction 212
 Proteomics 777
 Pseudomonas aeruginosa 531
 Pseudoproline dipeptide 78
 Pull-down experiment 777
 Pulmonary endothelial cells 413
 Purification 355
 Pyrazinone ring-containing analgesic 507
 Pyrimidine 773
 Pyrrolo-indole 216

Quantom dot 463, 501, 503
 Quantom dots labeling 734
 Quartz crystal microbalance 487
 Quorum sensing 252

Racemization 98, 146
 Racemization control 218
 Radiolabeled peptide 182
 Raman spectroscopy 279
 Rational design 550
 Rat V1b receptor 659
 Receptor 344, 617, 633
 Receptor selectivity 615
 Receptor selective analogs 517, 629
 Recombinant 164
 Repair 461
 Residual dipolar coupling 747
 Resin 114
 Retro inverso 527
 RGD 463, 709
 RGD peptide 497
 Rhodopsin 577
 Ring-closing alkene/alkyne metathesis 50
 RING domain 138
 Robotic 64
 ROMP 59

SAR 599
 SARS-CoV 335
 SARS-CoV 3CL protease 403
 Scaffold 212
 Scaffold mimetics 677
 Scanning tunnelling microscopy 718
 Scoring functions 433
 Secondary structure 603, 671
 Selective 573
 Selectivity 355, 651, 659
 Selenocysteine 90
 Selenium labeled peptide 387
 Self assembly 283, 688
 SICLOPPS 338
 Side reaction 116, 533
 Side-chain chirality 567
 Signal transduction 320, 397, 781
 Silicon 194
 Simulated annealing calculation 712
 SiRNA 447
 S,N-acyl migration 84
 Solid phase 88, 128, 220
 Solid phase ligation 66
 Solid phase peptide synthesis 162, 373, 429, 475
 Solid phase synthesis 53, 74, 76, 96, 100, 108, 136, 166, 170, 186, 467, 765
 Solid support 162, 505
 Solubility 704
 Solution phase 156
 Somatostatin 517, 639
 Somatostatin analog 423
 Spectroscopic analysis 22
 Spectroscopy 281, 605, 625
 Spectrum modeling 708
 Spot synthesis 736, 740
 Stability propagation site 581
 Staudinger ligation 297
 STD-NMR 555
 Ste2p 80, 122
 Stereospecific fold 643
 Steroid peptide 120
 Stilbene 647
 Stomoxyn/spinigerin 289
 Structural determinant 176
 Structure 402, 420, 619
 Structure-activity relationship 437, 439, 475, 553
 Structure characterization 467, 493
 Substance P 742
 Substrate 425
 Sugar 190
 Sugar amino acid 661
 Sugar immobilization 767
 Sulfated peptide 118, 158
 Superagonism 237
 Surface plasmon resonance 487, 767, 785
 Switch peptides 56
 Symmetrical dimeric peptides 505
 Synthesis 22, 144, 164, 194, 225, 303, 583, 609
 Synthetic peptide agonist 405
 Synthetic strategy 190

Tachyplesin 269
 Tandem mass spectrometry 483

Targeting 593
 TC5b 706
 Technetium 349
 Template assembly 563
 Terlipressin 489
 Tetrapeptide 465, 553
 Tetra-substituted amino acid 68
 Thalassemia 367
 Thermodynamics 623
 Thiazolidine 66, 112, 132
 Thio-Claisen rearrangement 347
 Thioester 84, 144
 Thioester method 132
 Thiohydantoin 771
 Threonine 126
 Th-T fluorescence 471
 Thymopentin 501
 Thymosin α 1 70, 501
 TIPP 523
 TIPP analog 525
 TRAIL R2 405
 Transglutaminase 2 401
 Transmembrane helix 579
 Transmembrane segment 26
 Triplet quenching 603
 Trithiaglutaroyl 196
 Tropomyosin 581
 Trypsin 583
 Trypsin inhibitor 485

Tryptophan stacking 541
 Tubulin polymerization 509
 Tumor imaging 182, 714
 Tumor targeting 371
 Turn 465, 708
 TyrB26 237
 Tyrosinase 537
 Tyrosine kinase 415, 427
 Tyrosine sulfate ester 158
 Tyrosine sulfated peptide 172

Uncoupling protein 653
 Unnatural amino acid 311
 Urotensin II 437, 439, 455

Vaccine 529, 531
 V1b receptor 573
 VCD spectroscopy 706, 708
 Viral protease 403

X-ray crystallography 565

Water-soluble N-protecting group 74
 WW domain 168

Zinc finger 214